

## Magnetic field and its extrapolations Corona

---

### Space Weather Live

<https://www.spaceweatherlive.com/en.html>

---

**The PFSS model and global photospheric magnetic maps to calculate the magnetic field configuration in the low corona** <http://connect-tool.irap.omp.eu/>

See **Rouillard et al. 2020**, Models and data analysis tools for the Solar Orbiter mission, Astronomy & Astrophysics, Volume 642, id.A2 (Special issue: Solar Orbiter Mission).

<https://www.aanda.org/articles/aa/pdf/2020/10/aa35305-19.pdf>

---

**Topical Issue** Space Since Rev.

Volume 210, Issue 1-4, September 2017

**Solar Magnetic Fields: From Measurements Towards Understanding**

[https://link.springer.com/journal/11214/210/1?wt\\_mc=alerts.TOCjournals](https://link.springer.com/journal/11214/210/1?wt_mc=alerts.TOCjournals)

---

**Coronal Magnetometry.** **Ebook**

**Gibson**, S. E., Rachmeler, L. A., White, S. M., eds. (2017).

Lausanne: Frontiers Media. doi: 10.3389/978-2-88945-220-0

[http://www.frontiersin.org/books/Coronal\\_Magnetometry\\_5/1259#nogo](http://www.frontiersin.org/books/Coronal_Magnetometry_5/1259#nogo)

<http://journal.frontiersin.org/researchtopic/3547/coronal-magnetometry>

---

**Inference of chromospheric magnetic fields in a sunspot derived from spectropolarimetry of Ca II 8542 A**

Ali G. A. **Abdelkawy**, **Abdelrazek M. K. Shaltout**, **M. M. Beheary**, **T. A. Schad**

Al-Azhar Bull. Sci. 2017

<https://arxiv.org/ftp/arxiv/papers/1712/1712.06829.pdf>

We analyze spectropolarimetric observations of the chromospheric Ca II 8542 A line taken by the Interferometric Bidimensional Spectrometer (IBIS) at the Dunn Solar Telescope. The data were observed on **2012 January 29** for the NOAA active region 11408. Adopting the center-of-gravity (COG) approach we obtain the line-of-sight (LOS) field strength for the chromospheric IBIS data of Ca II 8542 A line. The LOS strength of the magnetic field is determined in the target active region inside a field of view 45 x 95 arcsec. The LOS field values were found to be increase up to 800 G inside the umbral region and decrease systematically toward the edges of a sunspot. Under the weak field approximation (WFA), the horizontal, vertical magnetic field components and azimuthal field vector are obtained.

**The chromospheric magnetic field in active regions derived from spectropolarimetry of Ca II 8542**

Ali G. A. [Abdelkawy](#), [Abdelrazek M. K. Shaltout](#), [M. M. Beheary](#)

[Global Journal of Advanced Research \(GJAR\)](#)

2017

<https://arxiv.org/ftp/arxiv/papers/1712/1712.06828.pdf>

We analyze spectropolarimetric observations of the chromospheric Ca II 8542 line taken by the Interferometric Bidimensional Spectrometer (IBIS) at the Dunn Solar Telescope and photospheric Fe I 6302 lines obtained with the Solar Optical Telescope (SOT) of Spectro-polarimeter (SP) on board the Hinode satellite. The data were obtained on 2012 January 29 targeting NOAA active region (AR) 11408 and AR 11410. By using the center-of-gravity (COG) method we compute the line-of-sight (LOS) field strength for observed lines of Fe I 6301.5/6302.5 with SP spacecraft at every places in the active region. Also, we construct a COG map for the chromospheric IBIS data of Ca II 8542 line in comparison with COG maps derived from the SP of field strength. We found the photospheric field strength ranges up to 2 kG in plages and up to 2 kG or higher values inside the umbral region. In the case of chromospheric field strength, the LOS field inside the umbral region increases up to 800 G, and the field strength decreases toward the edges of sunspot. **2012 January 29**

## **Correlation Functions of Photospheric Magnetic Fields in Solar Active Regions**

[Valentina Abramenko](#), [Regina Suleymanova](#)

Solar Physics, **2024**, Volume 299, Issue 3, article id.31

<https://arxiv.org/pdf/2404.06879.pdf>

We used magnetograms acquired with the Helioseismic and Magnetic Imager (HMI) on board the Solar Dynamics Observatory (SDO) to calculate and analyze spatial correlation functions and the multi-fractal spectra in solar active regions (ARs). The analysis was performed for two very different types of ARs: i) simple bipolar magnetic structures with regular orientation (the magneto-morphological class A1), and ii) very complex multi-polar ARs (the magneto-morphological class B3). All ARs were explored at the developed phase during flareless periods. For correlation functions, the power-law and exponential approximations were calculated and compared. It was found that the exponential law holds for the correlation functions of both types of ARs within spatial scales of 1-36~Mm, while the power law failed to approximate the observed correlation functions. The property of multi-fractality was found in all ARs, being better pronounced for the complex B3-class ARs. Our results might imply that photospheric magnetic fields of an AR is a self-organized system, which, however, does not exhibit properties of self-organized criticality (SOC), and its fractal properties are an attribute of more broad (than SOC only) class of non-linear systems.

## **Magnetic fluxes of solar active regions of different magneto-morphological classes: I. Cyclic variations**

[Valentina I. Abramenko](#), [Regina A. Suleymanova](#), [Anastasija V. Zhukova](#)

MNRAS Volume 518, Issue 3, January **2023**, Pages 4746–4754

<https://arxiv.org/pdf/2212.07115.pdf>

<https://doi.org/10.1093/mnras/stac3338>

Data for 3046 solar active regions (ARs) observed since May 12, 1996 to December 27, 2021 were utilized to explore how the magnetic fluxes from ARs of different complexity follow the solar cycle. Magnetograms from the Michelson Doppler Imager instrument on the Solar and Heliospheric Observatory and from the Helioseismic and Magnetic Imager instrument on the Solar Dynamics Observatory were utilized. Each AR was classified as a regular bipolar AR (classes A1 or A2), or as an irregular bipolar AR (class B1), or as a multipolar AR (classes B2 or B3). Unipolar ARs were segregated into a specific class U. We found the following results. Unsigned magnetic fluxes from ARs of different classes evolve synchronously following the cycle, the correlation coefficient between the flux curves varies in a range of (0.70 - 0.99). The deepest solar minimum is observed simultaneously for all classes. Only the most simple ARs were observed during a deepest minimum: A1- and B1-class ARs. The overall shape of a cycle is governed by the regular ARs, whereas the fine structure of a solar maximum is determined by the most complex irregular ARs. Approximately equal amount of flux (45–50% of the total flux) is contributed by the A-class and B-class ARs during a solar maximum. Thus, observations allow us to conclude that the appearance of ARs with the magnetic flux above 1021 Mx is caused by the solar dynamo that operates as a unique process displaying the properties of a non-linear dynamical dissipative system with a cyclic behaviour and unavoidable fluctuations. **April 25, 2001, February 24, 2004**

## **Dispersion of small magnetic elements inside active regions on the Sun**

Valentina I. [Abramenko](#)

MNRAS 480, Issue 2, 21 October **2018**, Pages 1607–1611

<https://arxiv.org/pdf/1812.05469.pdf>

A process of diffusion of small-scale magnetic elements inside four active regions (ARs) was analyzed. Line-of-sight magnetograms acquired by the Helioseismic and Magnetic Imager (HMI) onboard the Solar Dynamic Observatory (SDO) during a two-day time interval around the AR culmination time were utilized. Small magnetic

elements of size of 3-100 squared HMI pixels with the field strength above the detection threshold of  $30 \text{ Mx cm}^{-2}$  were detected and tracked. The turbulent diffusion coefficient was retrieved using the pair-separation technique. Comparison with the previously reported quiet-sun (QS) diffusivity was performed. It was found that: i) dispersion of small-scale magnetic elements inside the AR area occurs in the regime close to normal diffusion, whereas well-pronounced super-diffusion is observed in QS; ii) the diffusivity regime operating in an AR (the magnitude of the spectral index and the range of the diffusion coefficient) does not seem to depend on the individual properties of an AR, such as total unsigned magnetic flux, state of evolution, and flaring activity. We conclude that small-scale magnetic elements inside an AR do not represent an undisturbed photosphere, but they rather are intrinsic part of the whole coherent magnetic structure forming an active region. Moreover, turbulence of small-scale elements in an AR is not closely related to processes above the photosphere, but it rather carries the footprint of the sub-photospheric dynamics. **2011.02.14, 2011.08.03, 2014.06.09, 2016.02.05**

## **Dispersion of the solar magnetic flux in undisturbed photosphere as derived from SDO/HMI data**

Valentina **Abramenko**

Monthly Notices of the Royal Astronomical Society, Volume 471, Issue 4, p.3871-3877 11/2017

<https://arxiv.org/pdf/1709.01724.pdf>

To explore the magnetic flux dispersion in the undisturbed solar photosphere, magnetograms acquired by Helioseismic and Magnetic Imager (HMI) onboard the Solar Dynamic Observatory (SDO) were utilized. Two areas, a coronal hole area (CH) and an area of super-granulation pattern, SG, were analyzed. We explored the displacement and separation spectra and the behavior of the turbulent diffusion coefficient,  $K$ . The displacement and separation spectra are very similar to each other. Small magnetic elements (of size 3-100 squared pixels and the detection threshold of  $20 \text{ Mx sm}^{-2}$ ) in both CH and SG areas disperse in the same way and they are more mobile than the large elements (of size 20-400 squared pixels and the detection threshold of  $130 \text{ Mx sm}^{-2}$ ). The regime of super-diffusivity is found for small elements ( $\gamma \approx 1.3$  and  $K$  growing from  $\sim 100$  to  $\sim 300 \text{ km}^2 \text{ s}^{-1}$ ). Large elements in the CH area are scanty and show super-diffusion with  $\gamma \approx 1.2$  and  $K = (62-96) \text{ km}^2 \text{ s}^{-1}$  on rather narrow range of 500-2200 km. Large elements in the SG area demonstrate two ranges of linearity and two diffusivity regimes: sub-diffusivity on scales (900-2500) km with  $\gamma = 0.88$  and  $K$  decreasing from  $\sim 130$  to  $\sim 100 \text{ km}^2 \text{ s}^{-1}$ , and super-diffusivity on scales (2500-4800) km with  $\gamma \approx 1.3$  and  $K$  growing from  $\sim 140$  to  $\sim 200 \text{ km}^2 \text{ s}^{-1}$ . Comparison of our results with the previously published shows that there is a tendency of saturation of the diffusion coefficient on large scales, i.e., the turbulent regime of super-diffusivity is gradually replaced by normal diffusion.

## **Analysis of the flux growth rate in emerging active regions on the Sun**

V.I. **Abramenko**, A.S. Kutsenko, O.I. Tikhonova, V.B. Yurchyshyn

Solar Phys. April 2017, 292:48 **2017**

<https://arxiv.org/pdf/1703.00739.pdf>

<http://link.springer.com/article/10.1007/s11207-017-1075-6>

We studied the emergence process of 42 active region (ARs) by analyzing the time derivative,  $R(t)$ , of the total unsigned flux. Line-of-sight magnetograms acquired by the Helioseismic and Magnetic Imager (HMI) onboard the Solar Dynamics Observatory (SDO) were used. A continuous piecewise linear fitting to the  $R(t)$ -profile was applied to detect an interval,  $dt_2$ , of nearly-constant  $R(t)$  covering one or several local maxima. The averaged over  $dt_2$  magnitude of  $R(t)$  was accepted as an estimate of the maximal value of the flux growth rate,  $R_{MAX}$ , which varies in a range of  $(0.5-5) \times 10^{20} \text{ Mx hour}^{-1}$  for active regions with the maximal total unsigned flux of  $(0.5-3) \times 10^{22} \text{ Mx}$ . The normalized flux growth rate,  $R_N$ , was defined under an assumption that the saturated total unsigned flux,  $F_{MAX}$ , equals unity. Out of 42 ARs in our initial list, 36 event were successfully fitted and they form two subsets (with a small overlap of 8 events): the ARs with a short ( $< 13$  hours) interval  $dt_2$  and a high ( $> 0.024 \text{ hour}^{-1}$ ) normalized flux emergence rate,  $R_N$ , form the "rapid" emergence event subset. The second subset consists of "gradual" emergence events and it is characterized by a long ( $> 13$  hours) interval  $dt_2$  and a low  $R_N$  ( $< 0.024 \text{ hour}^{-1}$ ). In diagrams of  $R_{MAX}$  plotted versus  $F_{MAX}$ , the events from different subsets are not overlapped and each subset displays an individual power law. The power law index derived from the entire ensemble of 36 events is  $0.69 \pm 0.10$ . The "rapid" emergence is consistent with a "two-step" emergence process of a single twisted flux tube. The "gradual" emergence is possibly related to a consecutive rising of several flux tubes emerging at nearly the same location in the photosphere. **18-19 Feb 2013, 25-28 Feb 2013**

**Table 1.** Active regions under the study and the calculated emergence parameters

## **Magnetic and Kinetic Power Spectra as a Tool to Probe the Turbulent Dynamo**

Valentyna **Abramenko**, Vasyl Yurchyshyn, Philip Googe

E-print, Dec **2011**; accepted in ASP Conference Series

Generation and diffusion of the magnetic field on the Sun is a key mechanism responsible for solar activity on all spatial and temporal scales - from the solar cycle down to the evolution of small-scale magnetic elements in the quiet Sun. The solar dynamo operates as a non-linear dynamical process and is thought to be manifest in two types: as a global dynamo responsible for the solar cycle periodicity, and as a small-scale turbulent dynamo responsible for the formation of magnetic carpet in the quiet Sun. Numerous MHD simulations of the solar turbulence did not yet reach a consensus as to the existence of a turbulent dynamo on the Sun. At the same time, high-resolution observations of the quiet Sun from Hinode instruments suggest possibilities for the turbulent dynamo. Analysis of characteristics of turbulence derived from observations would be beneficial in tackling the problem. We analyze magnetic and velocity energy spectra as derived from Hinode/SOT, SOHO/MDI, SDO/HMI and the New Solar Telescope (NST) of Big Bear Solar Observatory (BBSO) to explore the possibilities for the small-scale turbulent dynamo in the quiet Sun.

## **Effects of Initial Conditions on Magnetic Reconnection in a Solar Transient**

[Satyam Agarwal](#), [Ramit Bhattacharyya](#) & [Thomas Wiegmann](#)

[Solar Physics](#) volume 297, Article number: 91 (2022)

<https://doi.org/10.1007/s11207-022-02016-2>

Coronal magnetic field extrapolations are necessary to understand the magnetic field morphology of the source region in solar coronal transients. The extrapolation models are broadly classified into nonforce-free and force-free, depending on whether the model allows for a Lorentz force or not. Presently, these models are employed to carry out state-of-the-art data-driven and data-constrained magnetohydrodynamics (MHD) simulations to explore magnetic reconnection (MR)—the underlying cause of the transients. It is then imperative to study the influence of different extrapolation models on simulated evolution. For this purpose, the numerical model EULAG-MHD is employed to carry out simulations with different initial magnetic and velocity fields obtained through nonforce-free and force-free extrapolations. The selected active region is NOAA 11977, hosting a C6.6 class eruptive flare. Both extrapolations are found to be in good agreement with the observed line-of-sight and transverse magnetic fields. Further, a morphological comparison on the global scale and particularly for selected topologies, such as a magnetic null point and a hyperbolic flux tube (HFT), suggests that similar magnetic field line structures are reproducible in both models, although the extent of agreement between the two varies. Astoundingly, generation of a three-dimensional null near the HFT is observed in all the simulations, inferring the evolution to be independent of the particular initial field configuration. Moreover, the magnetic field lines (MFLs) undergoing MRs at the null point and HFT evolve similarly, further confirming the near independence of reconnection details on the chosen initial conditions. Consequently, both the extrapolation techniques can be suitable for initiating data-driven and data-constrained simulations.

## **Single spots, unipolar magnetic regions, and pairs of spots**

[Akasofu](#), S.-I.

*Geophysical Research Letters*, Volume 41, Issue 11, pp. 3698-3700, **2014**

McIntosh (1981) noted that sunspot pairs appear preferentially near the boundary of unipolar magnetic (UM) regions of opposite polarity. A large number of solar magnetograms from the Mount Wilson Observatory and the Kitt Peak Observatory during fairly quiet periods are examined to confirm his finding. In this study, it is also found collaterally that positive single spots appear in a positive UM region and vice versa. It is suggested thus that a pair of spots of opposite polarity is formed because two single spots develop in the vicinity of the boundary (the neutral line) of two UM regions of opposite polarity for polarity arrangement appropriate to the Hale law, namely, the Hale boundary. For these reasons, it is suggested that single spots and UM regions have significant meaning in solar magnetism.

## **Variations over time in latitudinal distribution of the large-scale magnetic fields in the solar atmosphere at heights from the photosphere to the source surface**

Z.S. [Akhtemov](#), O.A. Andreyeva, G.V. Rudenko, N.N. Stepanian, V.G. Fainshtein  
*Advances in Space Research*, Volume 55, Issue 3, 1 February **2015**, Pages 968–978

<http://www.sciencedirect.com/science/article/pii/S0273117714006280>

Calculations of magnetic field in the solar atmosphere and the “potential field-source surface” model have been used to study time variations in several parameters of the large-scale magnetic field at various heights during the last four solar cycles...

## **Exploring the Asymmetry of the Solar Corona Electron Density with Very Long Baseline Interferometry**

Dan [Aksim](#), Alexey Melnikov, Dmitry Pavlov, and Sergey Kurdubov

**2019** *ApJ* 885 159

[sci-hub.se/10.3847/1538-4357/ab499a](https://doi.org/10.3847/1538-4357/ab499a)

The Sun's corona has interested researchers for multiple reasons, including the search for a solution to the famous coronal heating problem and a purely practical consideration of predicting geomagnetic storms on Earth. There exist numerous different theories regarding the solar corona; therefore, it is important to be able to perform comparative analysis and validation of those theories. One way that could help us move toward the answers to those problems is the search for observational methods that could obtain information about the physical properties of the solar corona and provide means for comparing different solar corona models. In this work we present evidence that very long baseline interferometry (VLBI) observations are, in certain conditions, sensitive to the electron density of the solar corona and are able to distinguish between different electron density models, which makes the technique of VLBI valuable for solar corona investigations. Recent works on the subject used a symmetric power-law model of the electron density in solar plasma; in this work, an improvement is proposed based on a three-dimensional numerical model. **2017/05/01, 2018/05/01**

### **Filling Factors of Sunspots in SODISM Images**

Amro F. [Alasta](#), [Abdrzag Algamudi](#), [Fatma Almesrati](#), [Mustapha Meftah](#), [Rami Qahwaji](#)

Annals of Emerging Technologies in Computing (AETiC) Vol. 3, No. 2, **2019**

<https://arxiv.org/ftp/arxiv/papers/1904/1904.01133.pdf>

The calculated filling factors (FFs) for a feature reflect the fraction of the solar disc covered by that feature, and the assignment of reference synthetic spectra. In this paper, the FFs, specified as a function of radial position on the solar disc, are computed for each image in a tabular form. The filling factor (FF) is an important parameter and is defined as the fraction of area in a pixel covered with the magnetic field, whereas the rest of the area in the pixel is field-free. However, this does not provide extensive information about the experiments conducted on tens or hundreds of such images. This is the first time that filling factors for SODISM images have been catalogued in tabular formation. This paper presents a new method that provides the means to detect sunspots on full-disk solar images recorded by the Solar Diameter Imager and Surface Mapper (SODISM) on the PICARD satellite. The method is a totally automated detection process that achieves a sunspot recognition rate of 97.6%. The number of sunspots detected by this method strongly agrees with the NOAA catalogue. The sunspot areas calculated by this method have a 99% correlation with SOHO over the same period, and thus help to calculate the filling factor for wavelength (W.L.) 607nm.

### **The temporal and spatial evolution of MHD wave modes in sunspots**

[A. B. Albidah](#), [V. Fedun](#), [A. A. Aldhafeeri](#), [I. Ballai](#), [D. B. Jess](#), [W. Brevis](#), [J. Higham](#), [M. Stangalini](#), [S. S. A. Silva](#), [C. D. MacBride](#), [G. Verth](#)

ApJ **954** 30 **2023**

<https://arxiv.org/pdf/2305.19418.pdf>

<https://iopscience.iop.org/article/10.3847/1538-4357/acd7eb/pdf>

Through their lifetime sunspots undergo a change in their area and shape and, as they decay, they fragment into smaller structures. Here, for the first time we analyze the spatial structure of magnetohydrodynamic (MHD) slow body and fast surface modes in observed umbrae as their cross-sectional shape changes. The Proper Orthogonal Decomposition (POD) and Dynamic Mode Decomposition (DMD) techniques were used to analyze 3 and 6 hours SDO/HMI time series of Doppler velocities at the photospheric level of approximately circular and elliptically shaped sunspots. Each time series were divided equally into time intervals, to evidence the change of the sunspots' shape. To identify physical wave modes, the POD/DMD modes were cross-correlated with a slow body mode model using the exact shape of the umbra, whereas the shape obtained by applying a threshold level of the mean intensity for every time interval. Our results show that the spatial structure of MHD modes are affected, even by apparently small changes of the umbral shape, especially in the case of the higher-order modes. For the datasets used in our study, the optimal time intervals to consider the influence of the change in the shape on the observed MHD modes is 37 - 60 minutes. The choice of these intervals is crucial to properly quantify the energy contribution of each wave mode to the power spectrum. **2011 December 10, 2014 August 24**

### **Magnetohydrodynamic wave mode identification in circular and elliptical sunspot umbrae: evidence for high order modes**

[A. B. Albidah](#), [V. Fedun](#), [A. A. Aldhafeeri](#), [I. Ballai](#), [W. Brevis](#), [D. B. Jess](#), [J. Higham](#), [M. Stangalini](#), [S. S. A. Silva](#), [G. Verth](#)

ApJ **2022**

<https://arxiv.org/pdf/2202.00624.pdf>

In this paper we provide clear direct evidence of multiple concurrent higher order magnetohydrodynamic (MHD) modes in circular and elliptical sunspots by applying both Proper Orthogonal Decomposition (POD) and Dynamic Mode Decomposition (DMD) techniques on solar observational data. These techniques are well documented and validated in the areas of fluid mechanics, hydraulics, and granular flows, yet are relatively new to the field of solar

physics. While POD identifies modes based on orthogonality in space and it provides a clear ranking of modes in terms of their contribution to the variance of the signal, DMD resolves modes that are orthogonal in time. The clear presence of the fundamental slow sausage and kink body modes, as well as higher order slow sausage and kink body modes have been identified using POD and DMD analysis of the chromospheric H $\alpha$  line at 6562.808~Å for both the circular and elliptical sunspots. Additionally, to the various slow body modes, evidence for the presence of the fast surface kink mode was found in the circular sunspot. All the MHD modes patterns were cross-correlated with their theoretically predicted counterparts and we demonstrated that ellipticity cannot be neglected when interpreting MHD wave modes. The higher-order MHD wave modes are even more sensitive to irregularities in umbral cross-sectional shapes, hence this must be taken into account for more accurate modelling of the modes in sunspots and pores. **10 DECEMBER 2011, 24 AUGUST 2014**

### **Proper Orthogonal and Dynamic Mode Decomposition of Sunspot Data**

[A. B. Albidah](#), [W. Brevis](#), [V. Fedun](#), [I. Ballai](#), [D. B. Jess](#), [M. Stangalini](#), [J. Higham](#), [G. Verth](#)

Philosophical Transactions of the Royal Society of London Series A, 379, 20200181, **2021**

doi: 10.1098/rsta.2020.0181

<https://arxiv.org/pdf/2010.08530.pdf>

High resolution solar observations show the complex structure of the magnetohydrodynamic (MHD) wave motion. We apply the techniques of POD and DMD to identify the dominant MHD wave modes in a sunspot using the intensity time series. The POD technique was used to find modes that are spatially orthogonal, whereas the DMD technique identifies temporal orthogonality. Here we show that the combined POD and DMD approaches can successfully identify both sausage and kink modes in a sunspot umbra with an approximately circular cross-sectional shape. **10 December 2011**

### **Comparison of Exact and Approximate MHD Slow Body Mode Solutions in Photospheric Waveguides**

Anwar A. [Aldhafeeri](#)<sup>1</sup>, Gary Verth<sup>2</sup>, Viktor Fedun<sup>3</sup>, Matthew Lennard<sup>3</sup>, and I. Ballai<sup>2</sup>

**2022** ApJ 938 32

<https://iopscience.iop.org/article/10.3847/1538-4357/ac912b/pdf>

In this study, we explore the possibility of simplifying the modeling of magnetohydrodynamic slow body modes observed in photospheric magnetic structures such as the umbrae of sunspots and pores. The simplifying approach assumes that the variation of the eigenvalues of slow body waves can be derived by imposing that the longitudinal component of velocity with respect to the tube axis is zero at the boundary of the magnetic flux tube, which is in good agreement with observations. To justify our approach, we compare the results of our simplified model for slow body modes in cylindrical flux tubes with the model prediction obtained by imposing the continuity of the radial component of the velocity and total pressure at the boundary of the flux tube. Our results show that, to a high accuracy (less than 1% for the considered model), the conditions of continuity of the component of transversal velocity and pressure at the boundary can be neglected when modeling slow body modes under photospheric conditions.

### **The Magnetic Sensitivity of the Resonance and Subordinate Lines of Mg II in the Solar Chromosphere**

T. del Pino [Alemán](#)<sup>1,2</sup>, J. Trujillo Bueno<sup>1,2,3,6</sup>, R. Casini<sup>4,7</sup>, and R. Manso Sainz

**2020** ApJ 891 91

<https://doi.org/10.3847/1538-4357/ab6bc9>

We carry out a theoretical study of the polarization of the solar Mg ii h–k doublet (including its extended wings) and the subordinate ultraviolet (UV) triplet around 280 nm. These lines are of great diagnostic interest, as they encode information on the physical properties of the solar atmosphere from the upper photosphere to the chromosphere–corona transition region. We base our study on radiative transfer calculations of spectral line polarization in one-dimensional models of quiet and plage regions of the solar atmosphere. Our calculations take into account the combined action of atomic polarization, quantum level interference, frequency redistribution, and magnetic fields of arbitrary strength. In particular, we study the sensitivity of the emergent Stokes profiles to changes in the magnetic field through the Zeeman and Hanle effects. We also study the impact of the chromospheric plasma dynamics on the emergent Stokes profiles, taking into account the angle-dependent frequency redistribution in the h–k resonance transitions. The results presented here are of interest for the interpretation of spectropolarimetric observations in this important region of the solar UV spectrum.

### **Evidence for two-loop interaction from IRIS and SDO observations of penumbral brightenings**

C. E. [Alissandrakis](#), A. Koukras, S. Patsourakos, A. Nindos

We analyzed spectral and imaging data from the Interface Region Imaging Spectrograph (IRIS), images from the Atmospheric Imaging Assembly (AIA) aboard the Solar Dynamics Observatory (SDO), and magnetograms from the Helioseismic and Magnetic Imager (HMI) aboard SDO. We report observations of small flaring loops in the penumbra of a large sunspot on **July 19, 2013**. Our main event consisted of a loop spanning  $\sim 15$  arcsec, from the umbral-penumbral boundary to an opposite polarity region outside the penumbra. It lasted approximately 10 minutes with a two minute impulsive peak and was observed in all AIA/SDO channels, while the IRIS slit was located near its penumbral footpoint. Mass motions with an apparent velocity of  $\sim 100$  km/s were detected beyond the brightening, starting in the rise phase of the impulsive peak; these were apparently associated with a higher-lying loop. We interpret these motions in terms of two-loop interaction. IRIS spectra in both the C II and Si IV lines showed very extended wings, up to about 400 km/s, first in the blue (upflows) and subsequently in the red wing. In addition to the strong lines, emission was detected in the weak lines of C I, O I and C I as well as in the Mg II triplet lines. Absorption features in the profiles of the C II doublet, the Si IV doublet and the Mg h and k lines indicate the existence of material with a lower source function between the brightening and the observer. We attribute this absorption to the higher loop and this adds further credibility to the two-loop interaction hypothesis. We conclude that the absorption features in the C II, Si IV and Mg II profiles originate in a higher-lying, descending loop; as this approached the already activated lower-lying loop, their interaction gave rise to the impulsive peak, the very broad line profiles and the mass motions.

### Evolution of the magnetic field and flows of solar active regions with persistent magnetic bipoles before emergence

[Camron S. Alley](#), [Hannah Schunker](#)

Cambridge Large Two 2023

<https://arxiv.org/pdf/2312.04157.pdf>

Magnetic active regions on the Sun are harbingers of space weather events. Understanding the physics of how they form and evolve will improve space weather forecasting. Our aim is to characterise the surface magnetic field and flows for a sample of active regions with persistent magnetic bipoles prior to emergence. We identified 42 emerging active regions (EARs), in the Solar Dynamics Observatory Helioseismic Emerging Active Region survey (Schunker et al. 2016), associated with small magnetic bipoles at least one day before the time of emergence. We then identified a contrasting sample of 42 EARs that emerge more abruptly without bipoles before emergence. We computed the supergranulation scale surface flows using helioseismic holography. We averaged the flow maps and magnetic field maps over all active regions in each sample at each time interval from 2 days before emergence to 1 day after. We found that EARs associated with a persistent pre-emergence bipole evolve to be, on average, lower flux active regions than EARs that emerge more abruptly. Further, we found that the EARs that emerge more abruptly do so with a diverging flow of  $(3 \pm 0.6) \times 10^{-6} \text{ s}^{-1}$  on the order of  $50\text{-}100 \text{ ms}^{-1}$ . Our results suggest that there is a statistical dependence of the surface flow signature throughout the emergence process on the maximum magnetic flux of the active region.

### Hi-C Observations of Sunspot Penumbra Bright Dots

Shane E. [Alpert](#), Sanjiv K. Tiwari, Ronald L. Moore, Amy R. Winebarger, Sabrina L. Savage

ApJ 822 35 2016

<http://arxiv.org/pdf/1603.04968v1.pdf>

We report observations of bright dots (BDs) in a sunspot penumbra using High Resolution Coronal Imager (Hi-C) data in 193 Å and examine their sizes, lifetimes, speeds, and intensities. The sizes of the BDs are on the order of 1 arcsec and are therefore hard to identify in the Atmospheric Imaging Assembly (AIA) 193 Å images, which have 1.2 arcsec spatial resolution, but become readily apparent with Hi-C's five times better spatial resolution. We supplement Hi-C data with data from AIA's 193 Å passband to see the complete lifetime of the BDs that appeared before and/or lasted longer than Hi-C's 3-minute observation period. Most Hi-C BDs show clear lateral movement along penumbral striations, toward or away from the sunspot umbra. Single BDs often interact with other BDs, combining to fade away or brighten. The BDs that do not interact with other BDs tend to have smaller displacements. These BDs are about as numerous but move slower on average than Interface Region Imaging Spectrograph (IRIS) BDs, recently reported by [Tian et al. \(2014\)](#), and the sizes and lifetimes are on the higher end of the distribution of IRIS BDs. Using additional AIA passbands, we compare the lightcurves of the BDs to test whether the Hi-C BDs have transition region (TR) temperature like that of the IRIS BDs. The lightcurves of most Hi-C BDs peak together in different AIA channels indicating that their temperature is likely in the range of the cooler TR ( $1\text{-}4 \times 10^5$  K).

### Dynamics of Large-scale Coronal Structures as Imaged during the 2012 and 2013 Total Solar Eclipses

Nathalia [Alzate](#)<sup>1</sup>, Shadia R. Habbal<sup>2</sup>, Miloslav Druckmüller<sup>3</sup>, Constantinos Emmanouilidis<sup>4</sup>, and Huw Morgan<sup>5</sup>

2017 ApJ 848 84

White light images acquired at the peak of solar activity cycle 24, during the total solar eclipses of **2012 November 13 and 2013 November 3**, serendipitously captured erupting prominences accompanied by CMEs. Application of state-of-the-art image processing techniques revealed the intricate details of two "atypical" large-scale structures, with strikingly sharp boundaries. By complementing the processed white light eclipse images with processed images from co-temporal Solar Dynamics Observatory/AIA and SOHO/LASCO observations, we show how the shape of these atypical structures matches the shape of faint CME shock fronts, which traversed the inner corona a few hours prior to the eclipse observations. The two events were not associated with any prominence eruption but were triggered by sudden brightening events on the solar surface accompanied by sprays and jets. The discovery of the indelible impact that frequent and innocuous transient events in the low corona can have on large-scale coronal structures was enabled by the radial span of the high-resolution white light eclipse images, starting from the solar surface out to several solar radii, currently unmatched by any coronagraphic instrumentation. These findings raise the interesting question as to whether large-scale coronal structures can ever be considered stationary. They also point to the existence of a much larger number of CMEs that goes undetected from the suite of instrumentation currently observing the Sun.

### Large Scale Coronal Structures Imaged During the 2012/2013 Total Solar Eclipses

Nathalia [Alzate](#), Huw Morgan, Shadia R. Habbal, Miloslav Druckmüller, Constantinos Emmanouilidis  
UKSP Nuggets #80, 2017

[www.uksolphys.org/?p=13114](http://www.uksolphys.org/?p=13114)

White light eclipse images underscore the importance of acquiring coronal data over a large FoV to capture and follow the dynamic evolution and expansion of the coronal magnetic fields and plasmas, and to reliably establish their origin as they present themselves in these images. Although limited by the very short observing time, complementing them with space-based observations yields a unique tool, at present, for exploring the dynamics of the corona, in particular the long-lasting imprint of the passage of CMEs on coronal structures, starting from the solar surface. **13 November 2012, 3 November 2013**

### Shock Heating Energy of Umbral Flashes Measured with Integral Field Unit Spectroscopy

Tetsu [Anan](#), [Thomas A. Schad](#), [Sarah A. Jaeggli](#), [Lucas A. Tarr](#)

ApJ **882** 161 **2019**

<https://arxiv.org/pdf/1907.10797.pdf>

Umbral flashes are periodic brightness increases routinely observed in the core of chromospheric lines within sunspot umbrae and are attributed to propagating shock fronts. In this work we quantify the shock heating energy of these umbral flashes using observations in the near infrared He I triplet obtained on **2014 December 7** with the SpectroPolarimetric Imager for the Energetic Sun (SPIES), which is a novel integral field unit spectrograph at the Dunn Solar Telescope. We determine the shock properties (the Mach number and the propagation speed) by fitting the measured He I spectral profiles with a theoretical radiative transfer model consisting of two constant property atmospheric slabs whose temperatures and macroscopic velocities are constrained by the Rankine-Hugoniot relations. From the Mach number, the shock heating energy per unit mass of plasma is derived to be  $2 \times 10^{10} \text{ erg g}^{-1}$ , which is insufficient to maintain the umbral chromosphere. In addition, we find that the shocks propagate upward with the sound speed and the Mach number does not depend on the temperature upstream of the shocks. The latter may imply suppression of the amplification of the Mach number due to energy loss of the shocks.

### Coronal Diagnostics from Narrowband Images Around 30.4 nm

V. [Andretta](#), D. Telloni and G. Del Zanna

Solar Physics, Volume 279, Number 1 (2012), 53-73

Images taken in the band centered at 30.4 nm are routinely used to map the radiance of the He II Ly  $\alpha$  line on the solar disk. That line is one of the strongest, if not the strongest, line in the EUV observed in the solar spectrum, and one of the few lines in that wavelength range providing information on the upper chromosphere or lower transition region. However, when observing the off-limb corona, the contribution from the nearby Si XI 30.3 nm line can become significant. In this work we aim at estimating the relative contribution of those two lines in the solar corona around the minimum of solar activity. We combine measurements from CDS taken in August 2008 with temperature and density profiles from semiempirical models of the corona to compute the radiances of the two lines, and of other representative coronal lines (e.g. Mg X 62.5 nm, Si XII 52.1 nm). Considering both diagnosed quantities from line ratios (temperatures and densities) and line radiances in absolute units, we obtain a good overall match between observations and models. We find that the Si XI line dominates the He II line from just above the limb up to  $\approx 2 R$



◊ in streamers, while its contribution to narrowband imaging in the 30.4 nm band is expected to become smaller, even negligible in the corona beyond  $\approx 2 - 3 R_{\odot}$ , the precise value being strongly dependent on the coronal temperature profile.

## **HELICITY CONDENSATION AS THE ORIGIN OF CORONAL AND SOLAR WIND STRUCTURE**

S. K. [Antiochos](#)

2013 ApJ 772 72

Three of the most important and most puzzling features of the Sun's atmosphere are the smoothness of the closed-field corona (the so-called coronal loops), the accumulation of magnetic shear at photospheric polarity inversion lines (PILs; filament channels), and the complex dynamics of the slow wind. We propose that a single process, helicity condensation, is the physical mechanism giving rise to all three features. A simplified model is presented for how helicity is injected and transported in the closed corona by magnetic reconnection. With this model, we demonstrate that magnetic shear must accumulate at PILs and coronal hole boundaries, and estimate the rate of shear growth at PILs and the loss to the wind. Our results can account for many of the observed properties of the corona and wind.

## **A MODEL FOR THE SOURCES OF THE SLOW SOLAR WIND**

S. K. [Antiochos](#)<sup>1</sup>, Z. Mikić<sup>2</sup>, V. S. Titov<sup>2</sup>, R. Lionello<sup>2</sup> and J. A. Linker

2011 ApJ 731 112

Models for the origin of the slow solar wind must account for two seemingly contradictory observations: the slow wind has the composition of the closed-field corona, implying that it originates from the continuous opening and closing of flux at the boundary between open and closed field. On the other hand, the slow wind also has large angular width, up to  $\sim 60^\circ$ , suggesting that its source extends far from the open-closed boundary. We propose a model that can explain both observations. The key idea is that the source of the slow wind at the Sun is a network of narrow (possibly singular) open-field corridors that map to a web of separatrices and quasi-separatrix layers in the heliosphere. We compute analytically the topology of an open-field corridor and show that it produces a quasi-separatrix layer in the heliosphere that extends to angles far from the heliospheric current sheet. We then use an MHD code and MDI/SOHO observations of the photospheric magnetic field to calculate numerically, with high spatial resolution, the quasi-steady solar wind, and magnetic field for a time period preceding the 2008 August 1 total solar eclipse. Our numerical results imply that, at least for this time period, a web of separatrices (which we term an S-web) forms with sufficient density and extent in the heliosphere to account for the observed properties of the slow wind. We discuss the implications of our S-web model for the structure and dynamics of the corona and heliosphere and propose further tests of the model.

## **Thermal Instability–Induced Fundamental Magnetic Field Strands in the Solar Corona**

Patrick [Antolin](#)<sup>1</sup>, Juan Martínez-Sykora<sup>2,3,4,5</sup>, and Seray Şahin<sup>1</sup>

2022 ApJL 926 L29

<https://iopscience.iop.org/article/10.3847/2041-8213/ac51dd/pdf>

Thermal instability is a fundamental process of astrophysical plasmas. It is expected to occur whenever the cooling is dominated by radiation and cannot be compensated for by heating. In this work, we conduct 2.5D radiation MHD simulations with the Bifrost code of an enhanced activity network in the solar atmosphere. Coronal loops are produced self-consistently, mainly through Joule heating, which is sufficiently stratified and symmetric to produce thermal nonequilibrium. During the cooling and driven by thermal instability, coronal rain is produced along the loops. Due to flux freezing, the catastrophic cooling process leading to a rain clump produces a local enhancement of the magnetic field, thereby generating a distinct magnetic strand within the loop up to a few Gauss stronger than the surrounding coronal field. These strands, which can be considered fundamental, are a few hundred kilometers in width, span most of the loop leg, and emit strongly in the UV and extreme UV (EUV), thereby establishing a link between the commonly seen rain strands in the visible spectrum with the observed EUV coronal strands at high resolution. The compression downstream leads to an increase in temperature that generates a plume-like structure, a strongly emitting spicule-like feature, and short-lived brightening in the UV during the rain impact, providing an explanation for similar phenomena seen with IRIS. Thermal instability and nonequilibrium can therefore be associated with localized and intermittent UV brightening in the transition region and chromosphere, as well as contribute to the characteristic filamentary morphology of the solar corona in the EUV.

## **Fine Strand-like Structure in the Solar Corona from Magnetohydrodynamic Transverse Oscillations**

P. [Antolin](#), T. Yokoyama, and T. Van Doorselaere

2014 ApJ 787 L22

Current analytical and numerical modeling suggest the existence of ubiquitous thin current sheets in the corona that could explain the observed heating requirements. On the other hand, new high resolution observations of the corona indicate that its magnetic field may tend to organize itself in fine strand-like structures of few hundred kilometers widths. The link between small structure in models and the observed widths of strand-like structure several orders of magnitude larger is still not clear. A popular theoretical scenario is the nanoflare model, in which each strand is the product of an ensemble of heating events. Here, we suggest an alternative mechanism for strand generation. Through forward modeling of three-dimensional MHD simulations we show that small amplitude transverse MHD waves can lead in a few periods time to strand-like structure in loops in EUV intensity images. Our model is based on previous numerical work showing that transverse MHD oscillations can lead to Kelvin-Helmholtz instabilities that deform the cross-sectional area of loops. While previous work has focused on large amplitude oscillations, here we show that the instability can occur even for low wave amplitudes for long and thin loops, matching those presently observed in the corona. We show that the vortices generated from the instability are velocity sheared regions with enhanced emissivity hosting current sheets. Strands result as a complex combination of the vortices and the line-of-sight angle, last for timescales of a period, and can be observed for spatial resolutions of a tenth of loop radius.

## **OBSERVING THE FINE STRUCTURE OF LOOPS THROUGH HIGH-RESOLUTION SPECTROSCOPIC OBSERVATIONS OF CORONAL RAIN WITH THE CRISP INSTRUMENT AT THE SWEDISH SOLAR TELESCOPE**

P. Antolin<sup>1</sup> and L. Rouppe van der Voort

2012 ApJ 745 152

Observed in cool chromospheric lines, such as H $\alpha$  or Ca II H, coronal rain corresponds to cool and dense plasma falling from coronal heights. Considered as a peculiar sporadic phenomenon of active regions, it has not received much attention since its discovery more than 40 years ago. Yet, it has been shown recently that a close relationship exists between this phenomenon and the coronal heating mechanism. Indeed, numerical simulations have shown that this phenomenon is most likely due to a loss of thermal equilibrium ensuing from a heating mechanism acting mostly toward the footpoints of loops. We present here one of the first high-resolution spectroscopic observations of coronal rain, performed with the CRisp Imaging Spectro Polarimeter (CRISP) instrument at the Swedish Solar Telescope. This work constitutes the first attempt to assess the importance of coronal rain in the understanding of the coronal magnetic field in active regions. With the present resolution, coronal rain is observed to literally invade the entire field of view. A large statistical set is obtained in which dynamics (total velocities and accelerations), shapes (lengths and widths), trajectories (angles of fall of the blobs), and thermodynamic properties (temperatures) of the condensations are derived. Specifically, we find that coronal rain is composed of small and dense chromospheric cores with average widths and lengths of  $\sim 310$  km and  $\sim 710$  km, respectively, average temperatures below 7000 K, displaying a broad distribution of falling speeds with an average of  $\sim 70$  km s $^{-1}$ , and accelerations largely below the effective gravity along loops. Through estimates of the ion-neutral coupling in the blobs we show that coronal rain acts as a tracer of the coronal magnetic field, thus supporting the multi-strand loop scenario, and acts as a probe of the local thermodynamic conditions in loops. We further elucidate its potential in coronal heating. We find that the cooling in neighboring strands occurs simultaneously in general suggesting a similar thermodynamic evolution among strands, which can be explained by a common footpoint heating process. Constraints for coronal heating models of loops are thus provided. Estimates of the fraction of coronal volume with coronal rain give values between 7% and 30%. Estimates of the occurrence time of the phenomenon in loops set times between 5 and 20 hr, implying that coronal rain may be a common phenomenon, in agreement with the frequent observations of cool downflows in extreme-ultraviolet lines. The coronal mass drain rate in the form of coronal rain is estimated to be on the order of  $5 \times 10^9$  g s $^{-1}$ , a significant quantity compared to the estimate of mass flux into the corona from spicules.

## **Observations of the Solar Corona from Space**

**Review**

[Ester Antonucci](#), [Louise Harra](#), [Roberto Susino](#) & [Daniele Telloni](#)

[Space Science Reviews](#) volume 216, Article number: 117 (2020)

<https://link.springer.com/content/pdf/10.1007/s11214-020-00743-1.pdf>

<https://link.springer.com/article/10.1007/s11214-020-00743-1>

Space observations of the atmosphere of the Sun, obtained in half a century of dedicated space missions, provide a well established picture of the medium and large-scale solar corona, which is highly variable with the level of solar activity through a solar cycle and evolves with the long-term evolution of the magnetic cycles. In this review, we summarize the physical properties and dynamics of the medium and large-scale corona, consisting primarily of *active regions*, *streamers and coronal holes*; describe the dependence of coronal patterns on the magnetic field patterns changing through the solar cycle and the properties of the regions of open magnetic flux channeling the solar wind; the ubiquitous presence of fluctuations in the outer corona; the rotational properties of the large-scale corona; and the persistent hemispheric asymmetries in the emergence of magnetic fields and the distribution of the coronal emission. **August 10, 1996, August 19 and September 1, 1996, August 26, 1996, April 18, 2008, 2011-02-14**

## **Sunspot Numbers and Areas from the Madrid Astronomical Observatory (1876 – 1986)**

A. J. P. [Aparicio](#), J. M. Vaquero, V. M. S. Carrasco, M. C. Gallego

Solar Physics, Volume 289, Issue 11, pp 4335-4349 **2014**

The solar program of the Astronomical Observatory of Madrid started in 1876. Observations were made in this institution to determine sunspot numbers and areas for ten solar cycles. The program was completed in 1986 and the resulting data have been published in various Spanish scientific publications. Four periods of this program (with different observers and instruments) were identified with the aid of the interesting metadata that has been made available. In the present work, the published data were retrieved and digitized. Their subsequent analysis showed that most of these data could be considered reliable given their very high correlation with reference indices (international sunspot number, group sunspot number, and sunspot area). An abrupt change emerged in the sunspots/groups ratio in 1946, which lasted until 1972.

## **EFFECT OF SOLAR CHROMOSPHERIC NEUTRALS ON EQUILIBRIUM FIELD STRUCTURES**

[T. D. Arber](#), [G. J. J. Botha](#) and [C. S. Brady](#)

ApJ 705 1183-1188, **2009**

Solar coronal equilibrium fields are often constructed by nonlinear force-free field (NLFFF) extrapolation from photospheric magnetograms. It is well known that the photospheric field is not force-free and the correct lower boundary for NLFFF construction ought to be the top of the chromosphere. To compensate for this, pre-filtering algorithms are often applied to the photospheric data to remove the non-force-free components. Such pre-filtering models, while physically constrained, do not address the mechanisms that may be responsible for the field becoming force-free. The chromospheric field can change through, for example, field expansion due to gravitational stratification, reconnection, or flux emergence. In this paper, we study and quantify the effect of the chromospheric neutrals on equilibrium field structures. It is shown that, depending on the degree to which the photospheric field is not force-free, the chromosphere will change the structure of the equilibrium field. This is quantified to give an estimate of the change in  $\alpha$  profiles one might expect due to neutrals in the chromosphere. Simple scaling of the decay time of non-force-free components of the magnetic field due to chromospheric neutrals is also derived. This is used to quantify the rate at which, or equivalent at which height, the chromosphere is expected to become force-free.

## **On the structure and evolution of complexity in sigmoids: a flux emergence model**

[Archontis](#), V., Hood, A., Savcheva, A., Golub, L., Deluca, E.

E-print, Oct **2008**, ApJ

Sigmoids are structures with a forward or inverse S-shape, generally observed in the solar corona in soft X-ray emission. It is believed that the appearance of a sigmoid in an active region is an important factor in eruptive activity. The association of sigmoids with dynamic phenomena such as flares and coronal mass ejections (CMEs) make the study of sigmoids important. Recent observations of a coronal sigmoid, obtained with the X-Ray Telescope (XRT) on board Hinode, showed the formation and eruption phase with high spatial resolution. These observations revealed that the topological structure of the sigmoid is complex : it consists of many, differently oriented, loops that all together form two opposite {it J-like} bundles or an overall S-shaped structure. A series of theoretical and numerical models have been proposed, over the past years, to explain the nature of sigmoids but there is no explanation on how the afore-mentioned complexity in sigmoids is build up. In this paper we present a flux emergence model that leads to the formation of a sigmoid, whose structure and evolution of complexity are in good qualitative agreement with the recent observations.

## **Comparison of Coronal Extrapolation Methods for Cycle 24 Using HMI Data**

William M. [Arden](#), Aimee A. Norton, Xudong Sun, Xuepu Zhao

ApJ **2016**

<http://arxiv.org/pdf/1603.04385v1.pdf>

Two extrapolation models of the solar coronal magnetic field are compared using magnetogram data from the SDO/HMI instrument. The two models, a horizontal current-current sheet-source surface (HCCSSS) model and a potential field-source surface (PFSS) model differ in their treatment of coronal currents. Each model has its own critical variable, respectively the radius of a cusp surface and a source surface, and it is found that adjusting these heights over the period studied allows better fit between the models and the solar open flux at 1 AU as calculated from the Interplanetary Magnetic Field (IMF). The HCCSSS model provides the better fit for the overall period from 2010 November to 2015 May as well as for two subsets of the period - the minimum/rising part of the solar

cycle, and the recently-identified peak in the IMF from mid-2014 to mid-2015 just after solar maximum. It is found that a HCCSSS cusp surface height of 1.7 R<sub>sun</sub> provides the best fit to the IMF for the overall period, while 1.7 & 1.9 R<sub>sun</sub> give the best fits for the two subsets. The corresponding values for the PFSS source surface height are 2.1, 2.2 and 2.0 R<sub>sun</sub> respectively. This means that the HCCSSS cusp surface rises as the solar cycle progresses while the PFSS source surface falls.

### **Potential field source surface 'breathes' over the course of the solar cycle**

W. M. Arden<sup>1,\*</sup>, A. A. Norton<sup>2</sup>, X. Sun

HMI Science Nuggets, #15, 2014

<http://hmi.stanford.edu/hminuggets/?p=730>

The potential field source surface (PFSS) model is a well-established method for calculating open solar flux at a "source surface," an imaginary spherical surface above the corona. PFSS is used to represent the large-scale geometry of the solar coronal magnetic fields. It is customary to take the height of the source surface to be 2.5 solar radii (R<sub>s</sub>) in a heliocentric coordinate system<sup>1</sup>. Nothing in the model, however, requires that this height be fixed, either spatially or in time; the height of the source surface can be taken as a free parameter. A non-spherical source surface height has been explored in the past<sup>2</sup>, for instance.

### **A "Breathing" Source Surface for Cycles 23 & 24†**

W. M. Arden<sup>1,\*</sup>, A. A. Norton<sup>2</sup>, X. Sun

JGR, Volume 119, Issue 3, pages 1476–1485, March 2014

The potential field source surface (PFSS) model is used to represent the large-scale geometry of the solar coronal magnetic fields. The height of the source surface in this model can be taken as a free parameter. Previous work suggests that varying the source surface height during periods of solar minimum yields better agreement between PFSS models and the measured magnitude of the IMF open flux at 1 AU – in other words, the source surface "breathes" in and out over the course of the solar cycle. We examine the evolution of open flux during all of cycle 23 and the first part of cycle 24 using photospheric magnetic field maps from the SOHO/MDI and SDO/HMI instruments. We determine the value of source surface height that provides a best fit to the IMF open flux at 1 AU (using the OMNI 2 data set) for the time period 1996–2012. The canonical 2.5 R<sub>s</sub> source surface matches the measured IMF open flux during periods of solar maximum, but needs to be raised by approximately 15-30% in order to match the measured IMF open flux at the periods of solar minimum.

### **Vortex waves in sunspots**

A. López Ariste<sup>1,2</sup>, R. Centeno<sup>3</sup> and E. Khomenko

A&A 591, A63 (2016)

Context. Waves in the magnetized solar atmosphere are one of the favourite means of transferring and depositing energy into the solar corona. The study of waves brings information not just on the dynamics of the magnetized plasma, but also on the possible ways in which the corona is heated.

Aims. The identification and analysis of the phase singularities or dislocations provide us with a complementary approach to the magnetoacoustic and Alfvén waves propagating in the solar atmosphere. They allow us to identify individual wave modes, shedding light on the probability of excitation or the nature of the triggering mechanism.

Methods. We use a time series of Doppler shifts measured in two spectral lines, filtered around the three-minute period region. The data show a propagating magnetoacoustic slow mode with several dislocations and, in particular, a vortex line. We study under what conditions the different wave modes propagating in the umbra can generate the observed dislocations.

Results. The observed dislocations can be fully interpreted as a sequence of sausage and kink modes excited sequentially on average during 15 min. Kink and sausage modes appear to be excited independently and sequentially. The transition from one to the other lasts less than three minutes. During the transition we observe and model the appearance of superoscillations inducing large phase gradients and phase mixing.

Conclusions. The analysis of the observed wave dislocations leads us to the identification of the propagating wave modes in umbrae. The identification in the data of superoscillatory regions during the transition from one mode to the other may be an important indicator of the location of wave dissipation.

### **Scales of the magnetic fields in the quiet Sun**

A. López Ariste<sup>1</sup> and A. Sainz Dalda

A&A 540, A66 (2012)

Context. The presence of a turbulent magnetic field in the quiet Sun has been unveiled observationally using different techniques. The magnetic field is quasi-isotropic and has field strengths weaker than 100 G. It is pervasive and may host a local dynamo.

**Aims.** We aim to determine the length scale of the turbulent magnetic field in the quiet Sun.

**Methods.** The Stokes V area asymmetry is sensitive to minute variations in the magnetic topology along the line of sight. Using data provided by Hinode-SOT/SP instrument, we performed a statistical study of this quantity. We classified the different magnetic regimes and infer properties of the turbulent magnetic regime. In particular we measured the correlation length associated to these fields for the first time.

**Results.** The histograms of Stokes V area asymmetries reveal three different regimes: one organized, quasi-vertical and strong field (flux tubes or other structures of the like); a strongly asymmetric group of profiles found around field concentrations; and a turbulent isotropic field. For the last, we confirm its isotropy and measure correlation lengths from hundreds of kilometers down to 10 km, at which point we lost sensitivity. A crude attempt to measure the power spectra of these turbulent fields is made.

**Conclusions.** In addition to confirming the existence of a turbulent field in the quiet Sun, we give further prove of its isotropy. We also measure correlation lengths down to 10 km. The combined results show magnetic fields with a large span of length scales, as expected from a turbulent cascade.

## **Solar Activity in the Past and the Chaotic Behaviour of the Dynamo**

**Review**

Rainer [Arlt](#), Nigel Weiss

[Space Science Reviews](#), December 2014, Volume 186, [Issue 1-4](#), pp 525-533

The record of solar activity is reviewed here with emphasis on peculiarities. Since sunspot positions tell us a lot more about the solar dynamo than the various global sunspot numbers, we first focus on the records of telescopic observations of sunspots leading to positional information. Then we turn to the proxy record from cosmogenic isotope abundances, which shows recurrent grand minima over the last 9500 years. The apparent distinction between episodes of strong modulation, and intervening episodes with milder modulation and weaker overall activity, hints at the solar dynamo following a variety of solutions, with different symmetries, over the course of millennia.

## **Determination of the cross-field density structuring in coronal waveguides using the damping of transverse waves**

I. [Arregui](#)<sup>1,2</sup> and A. Asensio Ramos

*A&A* 565, A78 (2014)

**Context.** Time and spatial damping of transverse magnetohydrodynamic (MHD) kink oscillations is a source of information on the cross-field variation of the plasma density in coronal waveguides.

**Aims.** We show that a probabilistic approach to the problem of determining the density structuring from the observed damping of transverse oscillations enables us to obtain information on the two parameters that characterise the cross-field density profile.

**Methods.** The inference is performed by computing the marginal posterior distributions for density contrast and transverse inhomogeneity length-scale using Bayesian analysis and damping ratios for transverse oscillations under the assumption that damping is produced by resonant absorption.

**Results.** The obtained distributions show that, for damping times of a few oscillatory periods, low density-contrasts and short inhomogeneity length scales are more plausible to explain observations.

**Conclusions.** This means that valuable information on the cross-field density profile can be obtained even if the inversion problem, with two unknowns and one observable, is a mathematically ill-posed problem.

## **Helical Twisting Number and Braiding Linkage Number of Solar Coronal Loops**

M.J. [Aschwanden](#)

2019

<https://arxiv.org/pdf/1902.10612.pdf>

Coronal loops in active regions are often characterized by quasi-circular and helically twisted (sigmoidal) geometries, which are consistent with dipolar potential field models in the former case, and with nonlinear force-free field models with vertical currents in the latter case. Alternatively, Parker-type nanoflare models of the solar corona hypothesize that a braiding mechanism operates between unresolved loop strands, which is a more complex topological model. In this study we use the vertical-current approximation of a nonpotential magnetic field solution (that fulfills the divergence-free and force-free conditions) to characterize the number of helical turns  $N_{\text{twist}}$  in twisted coronal loops. We measure the helical twist in 15 active regions observed with AIA and HMI/SDO and find a mean nonpotentiality angle (between the potential and nonpotential field directions) of  $\mu_{\text{NP}} = 15^\circ \pm 3^\circ$ . The resulting mean rotational twist angle is  $\phi = 49^\circ \pm 11^\circ$ , which corresponds to  $N_{\text{twist}} = \phi/360^\circ = 0.14 \pm 0.03$  turns with respect to the untwisted potential field, with an absolute upper limit of  $N_{\text{twist}} < \sim 0.5$ , which is far below the kink instability limit of  $|N_{\text{twist}}| \gg 1$ . The number of twist turns  $N_{\text{twist}}$  corresponds to the Gauss linkage number  $N_{\text{link}}$  in braiding topologies. We conclude that any braided topology (with  $|N_{\text{link}}| \geq 1$ ) cannot explain the observed stability of loops in a force-free corona, nor the observed low twist number. Parkertype nanoflaring can thus occur in non-forcefree environments only, such as in the chromosphere and transition region

## Tracing the Chromospheric and Coronal Magnetic Field with AIA, IRIS, IBIS, and ROSA Data

M.J. [Aschwanden](#), K. Reardon, D. Jess

2016 *ApJ* **826** 61

<http://arxiv.org/pdf/1602.02119v1.pdf>

The aim of this study is to explore the suitability of chromospheric images for magnetic modeling of active regions. We use high-resolution images (0.1") from the Interferometric Bidimensional Spectrometer (IBIS) in the Ca II 8542 Å line, the Rapid Oscillations in the Solar Atmosphere (ROSA) instrument in the H-alpha 6563 Å line, the Interface Region Imaging Spectrograph (IRIS) in the 2796 Å line, and compare non-potential magnetic field models obtained from those chromospheric images with those obtained from images of the Atmospheric Imaging Assembly (AIA) in coronal (171 Å, etc.) and in chromospheric (304 Å) wavelengths. Curvi-linear structures are automatically traced in those images with the OCCULT-2 code, to which we forward-fitted magnetic field lines computed with the Vertical-Current Approximation Non-Linear Force Free Field (VCA-NLFFF) code. We find that the chromospheric images: (1) reveal crisp curvi-linear structures (fibrils, loop segments, spicules) that are extremely well-suited for constraining magnetic modeling; (2) that these curvi-linear structures are field-aligned with the best-fit solution by a median misalignment angle of ~4-7 deg; (3) the free energy computed from coronal data may underestimate that obtained from chromospheric data by a factor of ~ 2-4, (4) the height range of chromospheric features is confined to  $h \sim 4000$  km, while coronal features are detected up to  $h \sim 35,000$  km; and (5) the plasma-beta parameter is  $\beta \sim 10^{-5}$ - $10^{-1}$  for all traced features. We conclude that chromospheric images reveal important magnetic structures that are complementary to coronal images and need to be included in comprehensive magnetic field models, a quest that is not accommodated in standard NLFFF codes. **2010 Aug 3; 2014 Aug 24, 2014 Aug 30**

## The Vertical Current Approximation Nonlinear Force-Free Field Code - Description, Performance Tests, and Measurements of Magnetic Energies Dissipated in Solar Flares

Markus J. [Aschwanden](#)

2016

<http://arxiv.org/pdf/1602.00635v1.pdf>

In this work we provide an updated description of the Vertical Current Approximation Nonlinear Force-Free Field (VCA-NLFFF) code, which is designed to measure the evolution of the potential, nonpotential, free energies, and the dissipated magnetic energies during solar flares. This code provides a complementary and alternative method to existing traditional NLFFF codes. The chief advantages of the VCA-NLFFF code over traditional NLFFF codes are the circumvention of the unrealistic assumption of a force-free photosphere in the magnetic field extrapolation method, the capability to minimize the misalignment angles between observed coronal loops (or chromospheric fibril structures) and theoretical model field lines, as well as computational speed. In performance tests of the VCA-NLFFF code, by comparing with the NLFFF code of Wiegelmann (2004), we find agreement in the potential, nonpotential, and free energy within a factor of about 1.3, but the Wiegelmann code yields in the average a factor of 2 lower flare energies. The VCA-NLFFF code is found to detect decreases in flare energies in most X, M, and C-class flares. The successful detection of energy decreases during a variety of flares with the VCA-NLFFF code indicates that current-driven twisting and untwisting of the magnetic field is an adequate model to quantify the storage of magnetic energies in active regions and their dissipation during flares. - The VCA-NLFFF code is also publicly available in the Solar SoftWare (SSW). **2011 Febr 12-17, 2014 Mar 29,**

**Table 2. Data sets used in performance tests of the VCA-NLFFF code in this study: X-class flares**

## Global Energetics of Solar Flares. IX. Refined Magnetic Modeling

Markus J. [Aschwanden](#)

*ApJ* **2019**

[http://www.lmsal.com/~aschwand/eprints/2019\\_global9.pdf](http://www.lmsal.com/~aschwand/eprints/2019_global9.pdf)

A more accurate analytical solution of the vertical-current approximation nonlinear force-free field (VCA3-NLFFF) model is presented that includes besides the radial ( $B_r$ ) and the azimuthal ( $B_\phi$ ) magnetic field components a poloidal component ( $B_\theta \neq 0$ ) also. This new analytical solution is of second-order accuracy in the divergence-freeness condition, and of third-order accuracy in the force-freeness condition. We re-analyze the sample of 173 GOES M- and X-class flares observed with the Atmospheric Imaging Assembly (AIA) and Helioseismic and Magnetic Imager (HMI) onboard the Solar Dynamics Observatory (SDO). The new code reproduces helically twisted loops with a low winding number below the kink instability consistently, avoiding unstable, highly-twisted structures of the Gold-Hoyle flux rope type. The magnetic energies agree within  $E_{VCA3/E_W} = 0.99 \pm 0.21$  with the Wiegelmann (W-NLFFF) code. The time evolution of the magnetic field reveals

multiple, intermittent energy build-up and releases in most flares, contradicting both the Rosner-Vaiana model (with gradual energy storage in the corona) and the principle of time scale separation ( $\tau_{\text{flare}} \ll \tau_{\text{storage}}$ ) postulated in self-organized criticality models. The mean dissipated flare energy is found to amount to  $7\% \pm 3\%$  of the potential energy, or  $60\% \pm 26\%$  of the free energy, a result that can be used for predicting flare magnitudes based on the potential field of active regions. **2010-08-07, 2010-10-16, 2011/02/13-18**

### **Blind Stereoscopy of the Coronal Magnetic Field**

Markus J. [Aschwanden](#), Carolus J. Schrijver, Anna Malanushenko

Solar Phys. Volume 290, Issue 10, pp 2765-2789 **2015**

<http://arxiv.org/pdf/1506.04713v1.pdf>

We test the feasibility of 3D coronal-loop tracing in stereoscopic EUV image pairs, with the ultimate goal of enabling efficient 3D reconstruction of the coronal magnetic field that drives flares and coronal mass ejections (CMEs). We developed an automated code designed to perform triangulation of coronal loops in pairs (or triplets) of EUV images recorded from different perspectives. The automated (or blind) stereoscopy code includes three major tasks: (i) automated pattern recognition of coronal loops in EUV images, (ii) automated pairing of corresponding loop patterns from two different aspect angles, and (iii) stereoscopic triangulation of 3D loop coordinates. We perform tests with simulated stereoscopic EUV images and quantify the accuracy of all three procedures. In addition we test the performance of the blind stereoscopy code as a function of the spacecraft-separation angle and as a function of the spatial resolution. We also test the sensitivity to magnetic non-potentiality. The automated code developed here can be used for analysis of existing  $\{\backslash\text{sl Solar TERrestrial RELationship Observatory (STEREO)}\}$  data, but primarily serves for a design study of a future mission with dedicated diagnostics of non-potential magnetic fields. For a pixel size of  $0.6\backslash\text{arcsec}$  (corresponding to the  $\{\backslash\text{sl Solar Dynamics Observatory (SDO) Atmospheric Imaging Assembly (AIA)}\}$  spatial resolution of  $1.4\backslash\text{arcsec}$ ), we find an optimum spacecraft-separation angle of  $\alpha \approx 5^\circ$ . **15 February 2011**

### **The Magnetic Field of Active Region 11158 During the 2011 February 12-17 Flares : Differences between Photospheric Extrapolation and Coronal Forward-Fitting Methods**

[Aschwanden](#), M.J., Sun, X.D., and Liu, Y.

E-print, Feb **2014**; **2014 ApJ** 785 34.

We developed a  $\{\backslash\text{sl coronal non-linear force-free field (COR-NLFFF)}\}$  forward-fitting code that fits an approximate  $\{\backslash\text{sl non-linear force-free field (NLFFF)}\}$  solution to the observed geometry of automatically traced coronal loops. In contrast to photospheric NLFFF codes, which calculate a magnetic field solution from the constraints of the transverse photospheric field, this new code uses coronal constraints instead, and this way provides important information on systematic errors of each magnetic field calculation method, as well as on the non-forcefreeness in the lower chromosphere. In this study we applied the COR-NLFFF code to active region NOAA 11158, during the time interval of 2011 Feb 12 to 17, which includes an X2.2 GOES-class flare plus 35 M and C-class flares. We calculated the free magnetic energy with a 6-minute cadence over 5 days. We find good agreement between the two types of codes for the total nonpotential  $E_N$  and potential energy  $E_P$ , but find up to a factor of 4 discrepancy in the free energy  $E_{\text{free}} = E_N - E_P$ , and up to a factor of 10 discrepancy in the decrease of the free energy  $\Delta E_{\text{free}}$  during flares. The coronal NLFFF code exhibits a larger time variability, and yields a decrease of free energy during the flare that is sufficient to satisfy the flare energy budget, while the photospheric NLFFF code shows much less time variability and an order of magnitude less free energy decrease during flares. The discrepancy may partly be due to the pre-processing of photospheric vector data, but more likely due to the non-forcefreeness in the lower chromosphere. We conclude that the coronal field cannot be correctly calculated based on photospheric data alone, but requires additional information on coronal loop geometries.

### **NONLINEAR FORCE-FREE MAGNETIC FIELD FITTING TO CORONAL LOOPS WITH AND WITHOUT STEREOSCOPY**

Markus J. [Aschwanden](#)

**2013 ApJ** 763 115

We developed a new nonlinear force-free magnetic field (NLFFF) forward-fitting algorithm based on an analytical approximation of force-free and divergence-free NLFFF solutions, which requires as input a line-of-sight magnetogram and traced two-dimensional (2D) loop coordinates of coronal loops only, in contrast to stereoscopically triangulated three-dimensional loop coordinates used in previous studies. Test results of simulated magnetic configurations and from four active regions observed with STEREO demonstrate that NLFFF solutions can be fitted with equal accuracy with or without stereoscopy, which relinquishes the necessity of STEREO data for magnetic modeling of active regions (on the solar disk). The 2D loop tracing method achieves a 2D misalignment of  $\mu_2 = 27 \pm 13$  between the model field lines and observed loops, and an accuracy of 1.0% for the magnetic energy or free magnetic energy ratio. The three times higher spatial resolution of TRACE or SDO/AIA (compared with STEREO) also yields a proportionally smaller misalignment angle between model fit and observations.

Visual/manual loop tracings are found to produce more accurate magnetic model fits than automated tracing algorithms. The computation time of the new forward-fitting code amounts to a few minutes per active region.

## **A Nonlinear Force-Free Magnetic Field Approximation Suitable for Fast Forward-Fitting to Coronal Loops. III. The Free Energy**

Markus J. [Aschwanden](#)

Solar Physics, October **2013**, Volume 287, Issue 1-2, pp 369-389

An analytical approximation of a nonlinear force-free magnetic field (NLFFF) solution was developed in Paper I, while a numerical code that performs fast forward-fitting of this NLFFF approximation to a line-of-sight magnetogram and coronal 3D loops has been described and tested in Paper II. Here we calculate the free magnetic energy  $E_{\text{free}} = E_N - E_P$ , i.e., the difference of the magnetic energies between the non-potential field and the potential field. A second method to estimate the free energy is obtained from the mean misalignment angle change  $\Delta\mu = \mu_P - \mu_N$  between the potential and non-potential field, which scales as  $E_{\text{free}}/E_P \approx \tan^2(\Delta\mu)$ . For the four active regions observed with STEREO in 2007 we find free energies in the range of  $q_{\text{free}} = (E_{\text{free}}/E_P) \approx 1\% - 10\%$ , with an uncertainty of less than  $\pm 2\%$  between the two methods, while the free energies obtained from 11 other NLFFF codes exhibit a larger scatter of about  $\pm 10\%$ . We also find a correlation between the free magnetic energy and the GOES flux of the largest flare that occurred during the observing period, which can be quantified by an exponential relationship,  $F_{\text{GOES}} \propto \exp(q_{\text{free}}/0.015)$ , implying an exponentiation of the dissipated currents.

## **A Nonlinear Force-Free Magnetic Field Approximation Suitable for Fast Forward-Fitting to Coronal Loops. II. Numeric Code and Tests**

Markus J. [Aschwanden](#)

E-print, July **2012**, Solar Phys. (**2013**) 287:345–367

Based on a second-order approximation of nonlinear force-free magnetic field solutions in terms of uniformly twisted field lines derived in Paper I, we develop here a numeric code that is capable to forward-fit such analytical solutions to arbitrary magnetogram (or vector magnetograph) data combined with (stereoscopically triangulated) coronal loop 3D coordinates. We test the code here by forward-fitting to six potential field and six nonpotential field cases simulated with our analytical model, as well as by forward-fitting to an exactly force-free solution of the Low and Lou (1990) model. The forward-fitting tests demonstrate: (i) a satisfactory convergence behavior (with typical misalignment angles of  $\mu \approx 1^\circ - 10^\circ$ ), (ii) relatively fast computation times (from seconds to a few minutes), and (iii) the high fidelity of retrieved force-free  $\alpha$ -parameters ( $\alpha_{\text{m fit}} \approx \alpha_{\text{m model}} \approx 0.9 - 1.0$  for simulations and  $\alpha_{\text{m fit}} \approx \alpha_{\text{m model}} \approx 0.7 \pm 0.3$  for the Low and Lou model). The salient feature of this numeric code is the relatively fast computation of a quasi-forcefree magnetic field, which closely matches the geometry of coronal loops in active regions, and complements the existing {sl nonlinear force-free field (NLFFF)} codes based on photospheric magnetograms without coronal constraints.

## **A Nonlinear Force-Free Magnetic Field Approximation Suitable for Fast Forward-Fitting to Coronal Loops. I. Theory**

Markus J. [Aschwanden](#)

E-print, July **2012**, Solar Phys. (**2013**) 287:323–344

We derive an analytical approximation of nonlinear force-free magnetic field solutions (NLFFF) that can efficiently be used for fast forward-fitting to solar magnetic data, constrained either by observed line-of-sight magnetograms and stereoscopically triangulated coronal loops, or by 3D vector-magnetograph data. The derived NLFFF solutions provide the magnetic field components  $B_x(x)$ ,  $B_y(x)$ ,  $B_z(x)$ , the force-free parameter  $\alpha(x)$ , the electric current density  $j(x)$ , and are accurate to second-order (of the nonlinear force-free  $\alpha$ -parameter). The explicit expressions of a force-free field can easily be applied to modeling or forward-fitting of many coronal phenomena.

## **THE SPATIAL AND TEMPORAL DEPENDENCE OF CORONAL HEATING BY ALFVÉN WAVE TURBULENCE**

M. [Asgari-Targhi](#), A. A. van Ballegooijen, S. R. Cranmer, and E. E. DeLuca

**2013** ApJ 773 111

The solar atmosphere may be heated by Alfvén waves that propagate up from the convection zone and dissipate their energy in the chromosphere and corona. To further test this theory, we consider wave heating in an active region observed on **2012 March 7**. A potential field model of the region is constructed, and 22 field lines representing observed coronal loops are traced through the model. Using a three-dimensional (3D) reduced magnetohydrodynamics code, we simulate the dynamics of Alfvén waves in and near the observed loops. The results for different loops are combined into a single formula describing the average heating rate  $Q$  as a function of position within the observed active region. We suggest this expression may be approximately valid also for other



active regions, and therefore may be used to construct 3D, time-dependent models of the coronal plasma. Such models are needed to understand the role of thermal non-equilibrium in the structuring and dynamics of the Sun's corona.

### **Identification of photospheric activity features from SOHO/MDI data using the ASAP tool**

Omar **Ashamari**<sup>1\*</sup>, Rami Qahwaji<sup>1</sup>, Stan Ipson<sup>1</sup>, Micha Schöll<sup>2</sup>, Omar Nibouche<sup>3</sup> and Margit Haberreiter

J. Space Weather Space Clim., 5, A15 (2015)

<http://www.swsc-journal.org/articles/swsc/pdf/2015/01/swsc130048.pdf>

The variation of solar irradiance is one of the natural forcing mechanisms of the terrestrial climate. Hence, the time-dependent solar irradiance is an important input parameter for climate modelling. The solar surface magnetic field is a powerful proxy for solar irradiance reconstruction. The analyses of data obtained with the Michelson Doppler Imager (MDI) on board the SOHO mission are therefore useful for the identification of solar surface magnetic features to be used in solar irradiance reconstruction models. However, there is still a need for automated technologies that would enable the identification of solar activity features from large databases. To achieve this we present a series of enhanced segmentation algorithms developed to detect and calculate the area coverages of specific magnetic features from MDI intensitygrams and magnetograms. These algorithms are part of the **Automated Solar Activity Prediction (ASAP) tool**. The segmentation algorithms allow us to identify the areas on the solar disk covered by magnetic elements inside and outside boundaries of active regions. Depending on their contrast properties, magnetic features within an active region boundary are classified as sunspot umbra and penumbra, or faculae. Outside an active region boundary magnetic elements are identified as network. We present the detailed steps involved in the segmentation process and provide the area coverages of the segmented MDI intensitygrams and magnetograms. The feature segmentation was carried out on daily intensitygrams and magnetograms from April 21, 1996 to April 11, 2011. This offers an exciting opportunity to undertake further investigations that benefit from solar features segmentations, such as solar irradiance reconstruction, which we plan to investigate in the future. **May 17, 2000**

*Full-disk 1,024 · 1,024 pixel intensitygrams and line-of-sight magnetograms data sets are both available to download from the SOHO and JSOC archive: <http://soho.nascom.nasa.gov> and <http://jsoc.stanford.edu>*

### **A New Field Line Tracer for the Study of Coronal Magnetic Topologies**

Valentin **Aslanyan**<sup>1</sup>, Roger B. Scott<sup>2</sup>, Chloe P. Wilkins<sup>3</sup>, Karen A. Meyer<sup>1</sup>, David I. Pontin<sup>3</sup>, and Anthony R. Yeates<sup>4</sup>

2024 ApJ 9717 13

<https://iopscience.iop.org/article/10.3847/1538-4357/ad55ca/pdf>

We present a new code for the tracing of magnetic field lines and calculation of related quantities such as the squashing factor in the solar corona. The Universal Fieldline Tracer (UFIT) is an open-source package that can currently take inputs directly from four well-established coronal models, with additional models planned to be made directly accessible in the future. This package contains tools to make use of large-scale three-dimensional field line maps to calculate volumetric quantities, such as the total volume of the open corona, or the fraction that maps to regions on the solar surface within some distance of a coronal hole boundary, which may be relevant to phenomenological models of solar wind speed such as the Wang–Sheeley–Arge model. Synthetic coronagraphs can also be produced rapidly by this package. We have postprocessed long-term magnetofrictional simulations to demonstrate that the separatrix web occupies a larger fraction of the corona during solar maximum than solar minimum.

### **Coronal Models and Detection of the Open Magnetic Field**

Eleanna **Asvestari**<sup>1</sup>, Manuela Temmer<sup>2</sup>, Ronald M. Caplan<sup>3</sup>, Jon A. Linker<sup>3</sup>, Stephan G. Heinemann<sup>2,4</sup>, Rui F. Pinto<sup>5,6</sup>, Carl J. Henney<sup>7</sup>, Charles N. Arge<sup>8</sup>, Mathew J. Owens<sup>9</sup>, Maria S. Madjarska<sup>4,10</sup>Show full author list

2024 ApJ 971 45

<https://iopscience.iop.org/article/10.3847/1538-4357/ad5155/pdf>

A plethora of coronal models, from empirical to more complex magnetohydrodynamic (MHD) ones, are being used for reconstructing the coronal magnetic field topology and estimating the open magnetic flux. However, no individual solution fully agrees with coronal hole observations and in situ measurements of open flux at 1 au, as there is a strong deficit between the model and observations contributing to the known problem of the missing open flux. In this paper, we investigate the possible origin of the discrepancy between modeled and observed magnetic field topology by assessing the effect on the simulation output by the choice of the input boundary conditions and the simulation setup, including the choice of numerical schemes and the parameter initialization. In the frame of this work, we considered four potential field source surface-based models and one fully MHD model, different types of

global magnetic field maps, and model initiation parameters. After assessing the model outputs using a variety of metrics, we conclude that they are highly comparable regardless of the differences set at initiation. When comparing all models to coronal hole boundaries extracted by extreme-ultraviolet filtergrams, we find that they do not compare well. This mismatch between observed and modeled regions of the open field is a candidate contributing to the open flux problem. **2010-09-18-19**

### **Precursors of Magnetic Flux Emergence in the Moat Flows of Active Region AR12673**

R. [Attie](#), [M. S. Kirk](#), [B. J. Thompson](#), [K. Muglach](#), [A. A. Norton](#)

Space Weather [Volume16, Issue8](#) August **2018** Pages 1143-1155

<https://doi.org/10.1029/2018SW001939>

We report on observations of magnetic disturbances in active region AR12673 between **1 and 3 September 2017** seen as a disruption of the moat flow several hours before the onset of strong flux emergence near the main sunspot. The moat flow is commonly known as a radially oriented strong outflow of photospheric plasma surrounding sunspots, which ends abruptly and thus shapes an annular pattern around the penumbra. Using highly accurate methods of tracking this photospheric flow applied to Solar Dynamics Observatory/HelioSeismic and Magnetic Imager data, we are able to describe the evolution of the moat surrounding the main sunspot of AR 12673. We find that several hours before the emergence of strong magnetic flux near the main sunspot, the moat boundaries are broken at these very same locations. This behavior is observed both on 1 and 3 September. There is no such behavior observed in the absence of flux emergence. These observational results pose the question of how often they occur in other active regions and whether the disruption of the moat flow might be, like in this case, an indication of impending enhanced magnetic activity or simply a coincidental event.

### **Magnetic balltracking: Tracking the photospheric magnetic flux**

R. [Attie](#), D. E. Innes

A&A, 574, A106 **2015**

<http://arxiv.org/pdf/1412.8294v1.pdf>

Context: One aspect of understanding the dynamics of the quiet Sun is to quantify the evolution of the flux within small-scale magnetic features. These features are routinely observed in the quiet photosphere and were given various names, such as pores, knots, magnetic patches.

Aims: This work presents a new algorithm for tracking the evolution of the broad variety of small-scale magnetic features in the photosphere, with a precision equal to the instrumental resolution.

Methods: We have developed a new technique to track the evolution of the individual magnetic features from magnetograms, called "magnetic balltracking". It quantifies the flux of the tracked features, and it can track the footpoints of magnetic field lines inferred from magnetic field extrapolation. The algorithm can detect and quantify flux emergence, as well as flux cancellation.

Results: The capabilities of magnetic balltracking are demonstrated with the detection and the tracking of two cases of magnetic flux emergence that lead to the brightening of X-ray loops. The maximum emerged flux ranges from  $10^{18}$  Mx to  $10^{19}$  Mx (unsigned flux) when the X-ray loops are observed.

### **Slip-running reconnection in quasi-separatrix layers**

[Aulanier](#), G.; [Pariat](#), E.; [Demoulin](#), P.; [DeVore](#), C.R.

Solar Phys, **2006**

### **Relationship between the brightness in the coronal green line and magnetic fields on various scales**

O. G. [Badalyan](#)

Astronomy Reports, March **2013**, Volume 57, Issue 3, pp 222-232

Astronomicheskii Zhurnal, **2013**, Vol. 90, No. 3, pp. 253–264.

The relationship between the brightness in the FeXIV 530.3 nm coronal green line and magnetic fields on various scales in the corona is studied quantitatively. The cross-correlations of the corresponding synoptic maps for 1977–2001 have been calculated. Maps of the brightness of the coronal green line are constructed using daily monitoring data. Maps of the magnetic field are constructed separately for fields on large and small spatial scales, based on computations in a potential approximation using photospheric observations for distances of  $1.1R_{\odot}$  carried out at the Wilcox Solar Observatory. The correlations between the brightness in the coronal green line and the magnetic-field strengths on various scales as a function of latitude have a cyclic character. The correlation coefficients in the spot-formation zone are positive. Here, the green-line brightness corresponds mainly to the strength of small-scale fields, corresponding to the sizes of large active regions and activity complexes. The correlation coefficients are sign-variable above  $40^{\circ}$  latitude, and reach their greatest positive and negative values at the cycle maximum and minimum. Larger-scale fields influence the green-line brightness at higher latitudes and near the phase of the cycle

minimum. The results obtained can be used to investigate mechanisms for heating the corona. The relationship between the results obtained and the subsurface and deep solar dynamos are also discussed.

### **Constraining Global Coronal Models with Multiple Independent Observables**

[Samuel T. Badman](#), [David H. Brooks](#), [Nicolas Poirier](#), [Harry P. Warren](#), [Gordon Petrie](#), [Alexis P. Rouillard](#), [C. Nick Arge](#), [Stuart D. Bale](#), [Diego de Pablos Aguero](#), [Louise Harra](#), [Shaela I. Jones](#), [Athanasios Kouloumvakos](#), [Pete Riley](#), [Olga Panasenco](#), [Marco Velli](#), [Samantha Wallace](#)

ApJ 932 135 2022

<https://arxiv.org/pdf/2201.11818.pdf>

<https://iopscience.iop.org/article/10.3847/1538-4357/ac6610/pdf>

Global coronal models seek to produce an accurate physical representation of the Sun's atmosphere which can be used, for example, to drive space weather models. Assessing their accuracy is a complex task and there are multiple observational pathways to provide constraints and tune model parameters. Here, we combine several such independent constraints, defining a model-agnostic framework for standardized comparison. We require models to predict the distribution of coronal holes at the photosphere, and neutral line topology at the model outer boundary. We compare these predictions to extreme ultraviolet (EUV) observations of coronal hole locations, white-light Carrington maps of the streamer belt and the magnetic sector structure measured *in situ* by Parker Solar Probe and 1AU spacecraft. We study these metrics for Potential Field Source Surface (PFSS) models as a function of source surface height and magnetogram choice, as well as comparing to the more physical Wang-Sheeley-Arge (WSA) and the Magnetohydrodynamics Algorithm outside a Sphere (MAS) models. We find that simultaneous optimization of PFSS models to all three metrics is not currently possible, implying a trade-off between the quality of representation of coronal holes and streamer belt topology. WSA and MAS results show the additional physics they include addresses this by flattening the streamer belt while maintaining coronal hole sizes, with MAS also improving coronal hole representation relative to WSA. We conclude that this framework is highly useful for inter- and intra-model comparisons. Integral to the framework is the standardization of observables required of each model, evaluating different model aspects.

### **Measurement of the Open Magnetic Flux in the Inner Heliosphere down to 0.13AU**

[Samuel T. Badman](#), [Stuart D. Bale](#), [Alexis P. Rouillard](#), [Trevor A. Bowen](#), [John W. Bonnell](#), [Keith Goetz](#), [Peter R Harvey](#), [Robert J. MacDowall](#), [David M. Malaspina](#), [Marc Pulupa](#)

A&A 2020

<https://arxiv.org/pdf/2009.06844.pdf>

(Abridged) Aim: We attempt to determine robust estimates of the heliospheric magnetic flux ( $\Phi_H$ ) using Parker Solar Probe (PSP) data, analyze how susceptible this is to overestimation compared to the true open flux ( $\Phi_{open}$ ), assess its dependence on time and space, and compare it to simple estimates from Potential Field Source Surface (PFSS) models. Methods: We compare different methods of computation using data from PSP, STEREO A and Wind. The effects of fluctuations and large scale structure on the estimate are probed by using measured radial trends to produce synthetic data. Best estimates are computed as a function of time and space, and compared to estimates from PFSS models. Results: Radially-varying fluctuations of the HMF vector and variation of the Parker spiral angle cause the standard metrics of the mean and mode to evolve with radius independent of the central value about which the vector fluctuates. This is best mitigated by projecting the vector into the background Parker spiral direction. Nevertheless, we find a small enhancement in flux close to 1AU. The fraction of locally inverted field lines grows with radial distance from the Sun which remains a possible physical reason for this excess, but is negligible at PSP's perihelia. Similarly, the impact of fluctuations in general is much reduced at PSP's perihelia. The overall best estimate is  $\sim 2.5$  nT AU<sup>2</sup>. No strong dependence on latitude or longitude is apparent. The PFSS models predict lower values from 1.2 to 1.8 nT AU<sup>2</sup>. Conclusions: The heliospheric flux is most robustly estimated relative to a mean Parker spiral direction at PSP's perihelia where the decay of fluctuations and weakening importance of local flux inversions means  $\Phi_H \sim \Phi_{open}$ . Despite this, the estimate remains too high to be explained by PFSS models, supporting the idea that coronal models underestimate the open magnetic flux.

### **Calibration and Performance of the Full-Disk Vector MagnetoGraph (FMG) on Board the Advanced Space-Based Solar Observatory (ASO-S).**

[Bai, X.](#), [Deng, Y.](#), [Zhang, H.](#) et al.

Sol Phys 299, 157 (2024).

<https://doi.org/10.1007/s11207-024-02400-0>

We present the ground calibration and on-orbit performance of the Full-disk vector MagnetoGraph (FMG) payload on board the Advanced Space-Based Solar Observatory (ASO-S), which is China's first spaceborne magnetograph. FMG has the ability to acquire the full-disk Stokes I, Q/I, U/I, and V/I maps with a spatial resolution of about 1.5 arcsec. The Lyot filter for the flight model has a full width at half maximum of 0.01 nm. Using two calibration lenses, we measure the non-uniform wavelength drift across the entire field of view, with a maximum value of

0.003 nm. The on-orbit polarization sensitivity is approximately 0.00039 and 0.0009 for the deep integration and routine modes, corresponding to a cadence of 18 and 2 minutes, respectively. The corresponding sensitivity of the longitudinal magnetic field is 8.5 G and 20 G with the current linear calibration coefficient of 21,913. Since 1 April 2023, FMG has released Level 2 filtergram and longitudinal magnetic field data products for active regions. Furthermore, line-of-sight Carrington synoptic magnetograms spanning a 27-day solar rotation can be generated, which have been released to the public since February 2024. The longitudinal magnetic field obtained by FMG is consistent with that of the Helioseismic and Magnetic Imager on board the Solar Dynamic Observatory and the Solar Magnetism and Activity Telescope at Huairou Solar Observing Station for the regions without magnetic saturation.

### **A deep learning method to estimate magnetic fields in solar active regions from photospheric continuum images\***

Xianyong **Bai**<sup>1,2</sup>, Hui Liu<sup>3</sup>, Yuanyong Deng<sup>1,2</sup>, Jie Jiang<sup>4</sup>, Jingjing Guo<sup>1,2</sup>, Yi Bi<sup>3</sup>, Tao Feng<sup>5</sup>, Zhenyu Jin<sup>3</sup>, Wenda Cao<sup>6</sup>, Jiangtao Su<sup>1,2</sup> and Kaifan Ji<sup>3</sup>

A&A 652, A143 (2021)

<https://www.aanda.org/articles/aa/pdf/2021/08/aa40374-21.pdf>

<https://doi.org/10.1051/0004-6361/202140374>

**Context.** The magnetic field is the underlying cause of solar activities. Spectropolarimetric Stokes inversions have been routinely used to extract the vector magnetic field from observations for about 40 years. In contrast, the photospheric continuum images have an observational history of more than 100 years.

**Aims.** We suggest a new method to quickly estimate the unsigned radial component of the magnetic field,  $|Br|$ , and the transverse field,  $Bt$ , just from photospheric continuum images ( $I$ ) using deep convolutional neural networks (CNN).

**Methods.** Two independent models, that is,  $I$  versus  $|Br|$  and  $I$  versus  $Bt$ , are trained by the CNN with a residual architecture. A total of 7800 sets of data ( $I$ ,  $Br$  and  $Bt$ ) covering 17 active region patches from 2011 to 2015 from the Helioseismic and Magnetic Imager are used to train and validate the models.

**Results.** The CNN models can successfully estimate  $|Br|$  as well as  $Bt$  maps in sunspot umbra, penumbra, pore, and strong network regions based on the evaluation of four active regions (test datasets). From a series of continuum images, we can also detect the emergence of a transverse magnetic field quantitatively with the trained CNN model. The three-day evolution of the averaged value of the estimated  $|Br|$  and  $Bt$  from continuum images follows that from Stokes inversions well. Furthermore, our models can reproduce the nonlinear relationships between  $I$  and  $|Br|$  as well as  $Bt$ , explaining why we can estimate these relationships just from continuum images.

**Conclusions.** Our method provides an effective way to quickly estimate  $|Br|$  and  $Bt$  maps from photospheric continuum images. The method can be applied to the reconstruction of the historical magnetic fields and to future observations for providing the quick look data of the magnetic fields.

### **Predicting the Evolution of Photospheric Magnetic Field in Solar Active Regions Using Deep Learning**

[Liang Bai](#), [Yi Bi](#), [Bo Yang](#), [Jun-Chao Hong](#), [Zhe Xu](#), [Zhen-Hong Shang](#), [Hui Liu](#), [Hai-Sheng Ji](#), [Kai-Fan Ji](#)

Research in Astron. Astrophys. (RAA) 2020

<https://arxiv.org/pdf/2012.03584.pdf>

The continuous observation of the magnetic field by Solar Dynamics Observatory (SDO)/Helioseismic and Magnetic Imager (HMI) produces numerous image sequences in time and space. These sequences provide data support for predicting the evolution of photospheric magnetic field. Based on the spatiotemporal long short-term memory (LSTM) network, we use the preprocessed data of photospheric magnetic field in active regions to build a prediction model for magnetic field evolution. Because of the elaborate learning and memory mechanism, the trained model can characterize the inherent relationships contained in spatiotemporal features. The testing results of the prediction model indicate that (1) the prediction pattern learned by the model can be applied to predict the evolution of new magnetic field in the next 6 hour that have not been trained, and predicted results are roughly consistent with real observed magnetic field evolution in terms of large-scale structure and movement speed; (2) the performance of the model is related to the prediction time; the shorter the prediction time, the higher the accuracy of the predicted results; (3) the performance of the model is stable not only for active regions in the north and south but also for data in positive and negative regions. Detailed experimental results and discussions on magnetic flux emergence and magnetic neutral lines finally show that the proposed model could effectively predict the large-scale and short-term evolution of the photospheric magnetic field in active regions. Moreover, our study may provide a reference for the spatiotemporal prediction of other solar activities. 2013.08.18, 2013.10.01, 2014.06.15

### **Signatures of magnetic reconnection at the footpoints of fan shape jets on a light bridge driven by photospheric convective motions**

Xianyong [Bai](#), [Hector Socas-Navarro](#), [Daniel Nóbrega-Siverio](#), [Jiangtao Su](#), [Yuanyong Deng](#), [Dong Li](#), [Wenda Cao](#), [Kaifan Ji](#)

2018

<https://arxiv.org/pdf/1811.03723.pdf>

Dynamical jets are generally found on Light bridges (LBs), which are key to studying sunspots decays. So far, their formation mechanism is not fully understood. In this paper, we used state-of-the-art observations from the Goode Solar Telescope, the Interface Region Imaging Spectrograph, the Spectro-Polarimeter on board Hinode and the Atmospheric Imaging Assembly (AIA) on board the Solar Dynamics Observatory to analyze the fan shape jets on LBs in detail. Continuous upward motion of the jets in ascending phase is found from the  $H\alpha$  velocity, which lasts for 12 minutes and is associated with the  $H\alpha$  line wing enhancements. Two mini jets appear upon the bright fronts of the fan shape jets visible in the AIA 171 Å and 193 Å channels, with a time interval as short as 1 minute. Two kinds of small scale convective motions are identified in the photospheric images, along with the  $H\alpha$  line wing enhancements. One seems to be associated with the formation of a new convection cell and the other manifests as the motion of a dark lane passing through the convection cell. The finding of three lobes Stokes V profiles and their inversion with NICOLE code indicates that there is magnetic field lines with opposite polarities in LBs. From the  $H\alpha$  -0.8 Å images, we found ribbon like brightenings propagating along the LBs, possibly indicating slipping reconnection. Our observation supports that the fan shape jets under study are caused by the magnetic reconnection and photospheric convective motions play an important role in triggering the magnetic reconnection. **2014 August 1**

### Improved magnetogram calibration of SMFT and its comparison with the HMI

Xianyong [Bai](#), Yuanyong Deng, Fei Teng, Jiangtao Su, Xinjie Mao, Guoping Wang

MNRAS, 2014

<http://arxiv.org/pdf/1409.4869v1.pdf>

In this paper, we try to improve the magnetogram calibration method of the Solar Magnetic Field Telescope (SMFT). The improved calibration process fits the observed full Stokes information, using six points on the profile of Fe I 5324.18 Å line, and the analytical Stokes profiles under the Milne-Eddington atmosphere model, adopting the Levenberg-Marquardt least-square fitting algorithm. In Comparison with the linear calibration methods, which employs one point, there is large difference in the strength of longitudinal field  $B_l$  and transverse field  $B_t$ , caused by the non-linear relationship, but the discrepancy is little in the case of inclination and azimuth. We conclude that it is better to deal with the non-linear effects in the calibration of  $B_l$  and  $B_t$  using six points. Moreover, in comparison with SDO/HMI, SMFT has larger stray light and acquires less magnetic field strength. For vector magnetic fields in two sunspot regions, the magnetic field strength, inclination and azimuth angles between SMFT and HMI are roughly in agreement, with the linear fitted slope of 0.73/0.7, 0.95/1.04 and 0.99/1.1. In the case of pores and quiet regions ( $B_l < 600$  G), the fitted slopes of the longitudinal magnetic field strength are 0.78 and 0.87 respectively. **Nov. 12, 2012**

### Alfvenic Perturbations in a Sunspot Chromosphere Linked to Fractionated Plasma in the Corona

[D. Baker](#) , [M. Stangalini](#) , [G. Valori](#) , [D. H. Brooks](#) , [A. S. H. To](#) , [L. van Driel-Gesztelyi](#) (UCL/MSSL), [P. Demoulin](#) (LESIA-Meudon), [D. Stansby](#) (UCL/MSSL), [D. B. Jess](#) (Queen's University Belfast), [S. Jafarzadeh](#) (University of Oslo)

ApJ 2020

<https://arxiv.org/pdf/2012.04308.pdf>

In this study, we investigate the spatial distribution of highly varying plasma composition around one of the largest sunspots of solar cycle 24. Observations of the photosphere, chromosphere, and corona are brought together with magnetic field modelling of the sunspot in order to probe the conditions which regulate the degree of plasma fractionation within loop populations of differing connectivities. We find that in the coronal magnetic field above the sunspot umbra, the plasma has photospheric composition. Coronal loops rooted in the penumbra contain fractionated plasma, with the highest levels observed in the loops that connect within the active region. Tracing field lines from regions of fractionated plasma in the corona to locations of Alfvenic fluctuations detected in the chromosphere shows that they are magnetically linked. These results indicate a connection between sunspot chromospheric activity and observable changes in coronal plasma composition. **20 May 2016**

### Thermal Properties of Coronal Cavities

Urszula [Bak-Stęślicka](#), [Sarah E. Gibson](#), [Marek Stęślicki](#)

[Solar Physics](#) October 2019, 294:164

<https://doi.org/10.1007/s11207-019-1554-z>

We have analyzed 33 cavities observed between 2012 and 2018, from solar activity maximum to minimum. For each cavity we applied a differential emission measure method to obtain both a temperature distribution and a value of the average temperature. We find that cavities are filled with material hotter than the surrounding streamer, with temperatures in the range of 1.67 – 2.15 MK. Differences between temperatures of cavities and surrounding

streamers are in the range of 0.11 – 0.32 MK with an average value of 0.21 MK. We found that temperatures of both, cavities and streamers, vary as a function of different phases of solar activity. During solar maximum the structures are slightly hotter than those observed during solar minimum (1.85 – 2.15 MK vs. 1.67 – 1.88 MK for cavities and streamers, respectively).

## **The FIELDS Instrument Suite for Solar Probe Plus**

### **Measuring the Coronal Plasma and Magnetic Field, Plasma Waves and Turbulence, and Radio Signatures of Solar Transients**

S. D. [Bale](#), K. Goetz, P. R. Harvey, P. Turin, J. W. Bonnell, T. Dudok de Wit, R. E. Ergun, R. J. MacDowall, M. Pulupa and [75 more](#)

Space Science Reviews

2016 Open Access

NASA's Solar Probe Plus (SPP) mission will make the first in situ measurements of the solar corona and the birthplace of the solar wind. The FIELDS instrument suite on SPP will make direct measurements of electric and magnetic fields, the properties of in situ plasma waves, electron density and temperature profiles, and interplanetary radio emissions, amongst other things. Here, we describe the scientific objectives targeted by the SPP/FIELDS instrument, the instrument design itself, and the instrument concept of operations and planned data products.

## **The transfer of polarized radiation in resonance lines with partial frequency redistribution, J-state interference, and arbitrary magnetic fields**

### ***A radiative transfer code and useful approximations***

E. Alsina [Ballester](#)<sup>1,2,3</sup>, L. Belluzzi<sup>1,4,5</sup> and J. Trujillo Bueno<sup>2,3,6</sup>

A&A 664, A76 (2022)

<https://www.aanda.org/articles/aa/pdf/2022/08/aa42934-21.pdf>

**Aims.** We present the theoretical framework and numerical methods we have implemented to solve the problem of the generation and transfer of polarized radiation in spectral lines without assuming local thermodynamical equilibrium, while accounting for scattering polarization, partial frequency redistribution (due to both the Doppler effect and elastic collisions), J-state interference, and hyperfine structure. The resulting radiative transfer code allows one to model the impact of magnetic fields of an arbitrary strength and orientation through the Hanle, incomplete Paschen-Back, and magneto-optical effects. We also evaluate the suitability of a series of approximations for modeling the scattering polarization in the wings of strong resonance lines at a much lower computational cost, which is particularly valuable for the numerically intensive case of three-dimensional radiative transfer.

**Methods.** We examine the suitability of the considered approximations by using our radiative transfer code to model the Stokes profiles of the Mg II h & k lines and of the H I Lyman- $\alpha$  line in magnetized one-dimensional models of the solar atmosphere.

**Results.** Neglecting Doppler redistribution in the scattering processes that are unperturbed by elastic collisions (i.e., treating them as coherent in the observer's frame) produces a negligible error in the scattering polarization wings of the Mg II resonance lines and a minor one in the Lyman- $\alpha$  wings, although it is unsuitable to model the cores of these lines. For both lines, the scattering processes that are perturbed by elastic collisions only give a significant contribution to the intensity component of the emissivity. Neglecting collisional as well as Doppler redistribution (so that all scattering processes are coherent) represents a rough but suitable approximation for the wings of the Mg II resonance lines, but a very poor one for the Lyman- $\alpha$  wings. The magnetic sensitivity in the scattering polarization wings of the considered lines can be modeled by accounting for the magnetic field in only the  $\eta_I$  and  $\rho_V$  coefficients of the Stokes-vector transfer equation (i.e., using the zero-field expression for the emissivity).

## **The magnetic sensitivity of the Mg ii k line to the joint action of Hanle, Zeeman and magneto-optical effects**

Ernest Alsina [Ballester](#), Luca Belluzzi, Javier Trujillo Bueno

ApJL 2016

<https://arxiv.org/pdf/1610.00649v1.pdf>

We highlight the main results of a radiative transfer investigation on the magnetic sensitivity of the solar Mg ii k resonance line at 2795.5 angstrom, accounting for the joint action of the Hanle and Zeeman effects as well as partial frequency redistribution (PRD) phenomena. We confirm that at the line center, the linear polarization signals produced by scattering processes are measurable, and that they are sensitive, via the Hanle effect, to magnetic fields with strengths between 5 and 50 G, approximately. We also show that the Zeeman effect produces conspicuous circular polarization signals, especially for longitudinal fields stronger than 50 G, which can be used to estimate the magnetization of the solar chromosphere via the familiar magnetograph formula. The most novel result is that magneto-optical effects produce, in the wings of the line, a decrease of the Q/I scattering polarization pattern and the appearance of U/I signals (i.e., a rotation of the plane of linear polarization). This sensitivity of the Q/I and U/I wing

signals to both weak (around 5 G) and stronger magnetic fields expands the scientific interest of the Mg ii k line for probing the chromosphere in quiet and active regions of the Sun

### **The problem of the height dependence of magnetic fields in sunspots**

Horst **Balthasar**

Solar Phys. 293:120 2018

<https://arxiv.org/pdf/1808.06426.pdf>

To understand the physics of sunspots, it is important to know the properties of their magnetic field, and especially its height stratification plays a substantial role. There are mainly two methods to assess this stratification, but they yield different magnetic gradients in the photospheric layers. Determinations based on the different origin of several spectral lines and the slope of their profiles result in gradients of -2 to -3G/km, or even steeper. This is similar for the total magnetic field strength and for the vertical component of the magnetic field. The other option is to determine the horizontal partial derivatives of the magnetic field, and with the condition  $\text{div}B=0$ , also the vertical derivative is known. With this method, gradients of -0.5 G/km and shallower are obtained. Obviously, these results do not agree. If chromospheric spectral lines are included, only shallow gradients around -0.5G/km are encountered. Shallow gradients are also found from gyro-resonance measurements in the radio wave range 300 - 2000GHz. Some indirect methods are also considered, but they cannot clarify the total picture. An analysis of a numerical simulation of a sunspot indicates a shallow gradient over a wide height range, but with slightly steeper gradients in deep layers. Several ideas to explain the discrepancy are also discussed. With no doubts cast on Maxwell's equations, the first one is to look at the uncertainties of the formation heights of spectral lines, but a wider range of these heights would require an extension of the solar photosphere that is incompatible with observations and the theory of stellar atmospheres. The problem of the height gradient of the magnetic field in sunspots is still not solved.

### **Editorial: Measuring Solar Magnetic Fields—An Outline of History, Current Status and Challenges**

**Review**

André **Balogh**, Rudolf von Steiger

Space Science Reviews Volume 210, Issue 1–4, pp 1–3 2017

<https://link.springer.com/content/pdf/10.1007%2Fs11214-017-0417-x.pdf>

The collection of review papers, published in this volume of Space Science Reviews and the subsequent publication of the collection in the Space Science Series of ISSI (Vol. 57) provides a highly topical overview of the achievements of solar magnetic field measurements in improving the quantitative observational data base for making further progress in solar physics

### **Comparison of Debrecen and Mount Wilson/Kodaikanal sunspot group tilt angles and the Joy's law**

T. **Baranyi**

MNRAS 2014

<http://arxiv.org/pdf/1412.1355v1.pdf>

The study of active region tilt angles and their variations in different time scales plays an important role in revealing the subsurface dynamics of magnetic flux ropes and in understanding the dynamo mechanism. In order to reveal the exact characteristics of tilt angles, precise long-term tilt angle data bases are needed. However, there are only a few different data sets at present, which are difficult to be compared and cross-calibrate because of their substantial deviations. In this paper, we describe new tilt angle data bases derived from the Debrecen Photoheliographic Data (DPD) (1974-- ) and from the SOHO/MDI-Debrecen Data (SDD) (1996-2010) sunspot catalogues. We compare them with the traditional sunspot group tilt angle data bases of Mount Wilson Observatory (1917-85) and Kodaikanal Solar Observatory (1906-87) and we analyse the deviations. Various methods and filters are investigated which may improve the sample of data and may help deriving better results based on combined data. As a demonstration of the enhanced quality of the improved data set a refined diagram of the Joy's law is presented.

### **Are Electric-field-driven Magnetohydrodynamic Simulations of the Solar Corona Sensitive to the Initial Condition?**

Graham **Barnes**<sup>1</sup>, Keiji Hayashi<sup>2</sup>, and S. A. Gilchrist<sup>3</sup>

2024 ApJ 960 102

<https://iopscience.iop.org/article/10.3847/1538-4357/ad10a7/pdf>

Magnetohydrodynamic (MHD) simulations of the solar corona are often started from a potential field initial condition, which may be far from the true state of the coronal magnetic field. To test the sensitivity of the simulations to the initial condition, an electric-field-driven MHD code was initiated from three different initial conditions: the commonly used potential field, a nonlinear force-free field (NLFFF) extrapolation, which is believed

to be a better representation of the true coronal magnetic field, and a purely vertical field. After relaxation, the magnetic field in the MHD simulations was compared. It was found that there is a tendency for all of the initial conditions to converge to a similar connectivity, particularly in areas of strong fields that are not close to the boundary, suggesting that the final state of the simulation is not particularly sensitive to the initial condition. The relaxed solution more closely resembles the NLFFF initial condition than the other initial conditions, but still exhibits substantial differences from it.

### **Helioseismology of Pre-emerging Active Regions. III. Statistical Analysis**

G. Barnes, A. C. Birch<sup>1</sup>, K. D. Leka, and D. C. Braun

2014 ApJ 786 19

The subsurface properties of active regions (ARs) prior to their appearance at the solar surface may shed light on the process of AR formation. Helioseismic holography has been applied to samples taken from two populations of regions on the Sun (pre-emergence and without emergence), each sample having over 100 members, that were selected to minimize systematic bias, as described in Paper I. Paper II showed that there are statistically significant signatures in the average helioseismic properties that precede the formation of an AR. This paper describes a more detailed analysis of the samples of pre-emergence regions and regions without emergence based on discriminant analysis. The property that is best able to distinguish the populations is found to be the surface magnetic field, even a day before the emergence time. However, after accounting for the correlations between the surface field and the quantities derived from helioseismology, there is still evidence of a helioseismic precursor to AR emergence that is present for at least a day prior to emergence, although the analysis presented cannot definitively determine the subsurface properties prior to emergence due to the small sample sizes.

### **The FitCoPI Code: Iterative Determination of the 3D Density and Temperature Configuration in the Active-Region Corona**

Stephan Barra

[Solar Physics](#) July 2019, 294:101

<https://link.springer.com/content/pdf/10.1007%2Fs11207-019-1482-y.pdf>

For understanding the physical processes in the solar corona, it is helpful to reconstruct the 3D-distribution of plasma density and temperature. We introduce a new iterative method that uses multi-filter observations and an extrapolated coronal magnetic field to fit the physical parameters along the field lines to the observations. Since a model is applied only for the field extrapolation but not to the loops themselves, non-stationary plasma configurations along the loops can be captured. We demonstrate the performance of our code on a self-made model active-region corona and on active region (AR) 11087 observed by the Solar Dynamics Observatory and the Solar Terrestrial Relation Observatory-A in 2010. In the coronal parts of the model AR, the 25% quantile of the deviations of the reconstructed densities relative to the model values is  $-0.5$  to  $-0.6$  below the model values, the 75% quantile being  $0.3$ . Likewise, for the logarithm of the temperature, the same quantiles are at minus and plus  $0.04$ , respectively, relative to the model values. For AR 11087, the seven channels of the Atmospheric Imaging Assembly in the extreme ultraviolet are reproduced very well. For the four channels of the Extreme Ultra Violet Imager in that regime, the synthesised images are slightly brighter than the observations. The structure of the AR can still be identified here. **15 July 2010**

### **Enhancing SDO/HMI Images Using Deep Learning**

C. J. Díaz Baso<sup>1,2</sup> and A. Asensio Ramos<sup>1,2</sup>

**HMI Science Nuggets**, #103, June 2018 <http://hmi.stanford.edu/hminuggets/?p=2552>

The Helioseismic and Magnetic Imager (HMI) is a space-borne observatory that deploys full-disk images (plus magnetograms and dopplergrams) of the Sun every 45 s (or every 720 s for a better signal-to-noise ratio) with a spatial resolution of  $\sim 1.0''$  and a sampling of  $\sim 0.5''/\text{pix}$ . In spite of the enormous advantage of having such a synoptic space telescope without the problematic Earth's atmosphere, the spatial resolution is not enough to track many of the small-scale solar structures of interest. One would desirably prefer images with a better spatial resolution that compensates the telescope PSF, and for that we develop a new method to simultaneously deconvolve and super-resolve HMI images and magnetograms.

### **Modelling solar coronal magnetic fields with physics-informed neural networks**

H Baty, V Vigon

MNRAS, Volume 527, Issue 2, January 2024, Pages 2575–2584,

<https://doi.org/10.1093/mnras/stad3320>

<https://academic.oup.com/mnras/article-pdf/527/2/2575/53452839/stad3320.pdf>

We present a novel numerical approach aiming at computing equilibria and dynamics structures of magnetized plasmas in coronal environments. A technique based on the use of neural networks that integrates the partial differential equations of the model, and called physics-informed neural networks (PINNs), is introduced. The



functionality of PINNs is explored via calculation of different magnetohydrodynamic (MHD) equilibrium configurations, and also obtention of exact two-dimensional steady-state magnetic reconnection solutions. Advantages and drawbacks of PINNs compared to traditional numerical codes are discussed in order to propose future improvements. Interestingly, PINNs is a meshfree method in which the obtained solution and associated different order derivatives are quasi-instantaneously generated at any point of the spatial domain. We believe that our results can help to pave the way for future developments of time dependent MHD codes based on PINNs.

## **Impact of spatially correlated fluctuations in sunspots on metrics related to magnetic twist**

[C. Baumgartner](#), [A. C. Birch](#), [H. Schunker](#), [R.H. Cameron](#), [L. Gizon](#)

A&A 664, A183 2022

<https://arxiv.org/pdf/2207.02135.pdf>

<https://www.aanda.org/articles/aa/pdf/2022/08/aa43357-22.pdf>

The twist of the magnetic field above a sunspot is an important quantity in solar physics. For example, magnetic twist plays a role in the initiation of flares and coronal mass ejections (CMEs). Various proxies for the twist above the photosphere have been found using models of uniformly twisted flux tubes, and are routinely computed from single photospheric vector magnetograms. One class of proxies is based on  $\alpha_z$ , the ratio of the vertical current to the vertical magnetic field. Another class of proxies is based on the so-called twist density,  $q$ , which depends on the ratio of the azimuthal field to the vertical field. However, the sensitivity of these proxies to temporal fluctuations of the magnetic field has not yet been well characterized. We aim to determine the sensitivity of twist proxies to temporal fluctuations in the magnetic field as estimated from time-series of SDO/HMI vector magnetic field maps. To this end, we introduce a model of a sunspot with a peak vertical field of 2370 Gauss at the photosphere and a uniform twist density  $q = -0.024 \text{ Mm}^{-1}$ . We add realizations of the temporal fluctuations of the magnetic field that are consistent with SDO/HMI observations, including the spatial correlations. Using a Monte-Carlo approach, we determine the robustness of the different proxies to the temporal fluctuations. The temporal fluctuations of the three components of the magnetic field are correlated for spatial separations up to 1.4 Mm (more than expected from the point spread function alone). The Monte-Carlo approach enables us to demonstrate that several proxies for the twist of the magnetic field are not biased in each of the individual magnetograms. The associated random errors on the proxies have standard deviations in the range between 0.002 and 0.006  $\text{Mm}^{-1}$ , which is smaller by approximately one order of magnitude than the mean value of  $q$ . 2010.05.25

## **Global Coronal Magnetic Field Estimation Using Bayesian Inference**

[Upasna Baweja](#), [Vaibhav Pant](#), [Iñigo Arregui](#)

ApJ 963 69 2024

<https://arxiv.org/pdf/2401.05022.pdf>

<https://iopscience.iop.org/article/10.3847/1538-4357/ad1b57/pdf>

Estimating the magnetic field strength in the solar corona is crucial for understanding different physical processes happening over diverse spatio-temporal scales. However, the high temperatures and low density of the solar corona make this task challenging. The coronal magnetic field is too weak to produce a measurable splitting of the spectral lines using the Zeeman effect, and high temperature causes spectral lines to become weak and broad, making it difficult to detect the small Zeeman splitting. Coronal magneto-seismology, which combines the theoretical and observed properties of magnetohydrodynamic (MHD) waves, can be used to infer the magnetic field strength of oscillating structures in the solar corona, which are otherwise difficult to estimate. In this work, we use the Doppler velocity and density data obtained from the Coronal Multichannel Polarimeter (CoMP) on **2016 October 14** to obtain the global map of the coronal magnetic field using Bayesian inference. Two priors are used for plasma density, viz Gaussian and uniform distributions. Bayesian inference provides us with the probability distribution for the magnetic field strength at each location from 1.05 to 1.35  $R_{\odot}$ . A comparison between the magnetic field obtained using simple inversion and Bayesian inference is also drawn. We find that the values obtained using simple inversion do not always match the maximum posterior estimates obtained using Bayesian inference. We find that the inferred values follow a power-law function for the radial variation of the coronal magnetic field, with the power-law indices for simple and Bayesian inversion being similar.

## **A Study of the relation between intensity oscillations and magnetic field parameters in a Sunspot: Hinode Observations**

Ankala Raja [Bayanna](#), Shibu K Mathew, Brajesh Kumar, Rohan E Louis, Parameswaran Venkatakrishnan

Research in Astronomy and Astrophysics (RAA), 2014

<http://arxiv.org/pdf/1407.7363v1.pdf>

We present properties of intensity oscillations of a sunspot in the photosphere and chromosphere using G $\sim$ band and CaIIH filtergrams from Hinode. Intensity power maps as function of magnetic field strength and frequency reveal reduction of power in Gband with increase in photospheric magnetic field strength at all frequencies. In CaIIH, however, stronger fields exhibit more power at high frequencies particularly in the 4.5 mHz-8.0 mHz band. Power

distribution in different locations of the active region show that the oscillations in CaIIH exhibit more power in comparison to that of Gband. We also relate the power in intensity oscillations with different components of the photospheric vector magnetic field using near simultaneous spectro-polarimetric observations of the sunspot from the Hinode spectropolarimeter. The photospheric umbral power is strongly anti-correlated with the magnetic field strength and its the line-of-sight component while there is a good correlation with the transverse component. A reversal of this trend is observed in the chromosphere with the exception at low frequencies ( $\nu \leq 1.5$  mHz). The power in sunspot penumbrae is anti-correlated with the magnetic field parameters at all frequencies ( $1.0 \leq \nu \leq 8.0$  mHz) in both the photosphere and chromosphere, except that the chromospheric power shows a strong correlation in the frequency range 3-3.5 mHz.

### **Photometric analysis of the corona during the 20 March 2015 total solar eclipse: density structures, hydrostatic temperatures and magnetic field inference**

C. [Bazin](#), J. Vilinga, R. Wittich, S. Koutchmy, J. Mouette, C. Nitschelm

Proceedings of the SF2A meeting, June 2015

<http://arxiv.org/pdf/1510.06436v1.pdf>

We present some new accurate CCD photometry analysis of the white light solar corona at the time of the last 20 March 2015 total eclipse (airborne observations on a Falcon 7X and at ground-based Svalbard). We measured coronal brightness profiles taken along radial directions from 1.001 to 3 solar radii in the northern, southern and equatorial regions, after removing the F corona and the sky background. These studies allow to evaluate the density gradients, structures and temperature heterogeneity, by considering the Thomson scattering in white light of the K corona and also emissions of the EUV Fe XII 193A (1 to 2 MK) and Fe XI 171/174 (lower temperature) simultaneously observed by SDO/AIA and SWAP Proba2 space missions. Some dispersion between the regions is noticed. The limitation of the hydrostatic equilibrium assumption in the solar atmosphere is discussed as well as the contribution of the magnetic field pressure gradients as illustrated by a comparison with the model stationary magnetic corona from Predictive Sc. Inc. These results are compared with the results of the quieter 2010 total solar eclipse corona analyzed with the same method. This photometric analysis of the inner and intermediate white light corona will contribute to the preparation of the Aspiics/Proba 3 flying formation future coronagraphic mission of ESA for new investigation at time of artificial eclipses produced in Space. Note that Aspiics will also observe in the He I D3 line at 5876 Å, and will record intensities of the Fe XIV line 5303Å simultaneously with the analysis of the orange white- light continuum, including precise polarimetry analysis.

### **Derivation and Application of a Scaling Between Hinode/SP and SDO/HMI Vector Magnetic Fields to Improve Magnetic Field Extrapolations**

C. [Beck](#), [A. Prasad](#), [Q. Hu](#), [M. S. Yalim](#), [S. Gosain](#), [D.P. Choudhary](#)

ApJ 2024

<https://arxiv.org/pdf/2411.17649>

Full-disk measurements of the solar magnetic field by the Helioseismic and Magnetic Imager (HMI) are often used for magnetic field extrapolations, but its limited spatial and spectral resolution can lead to significant errors. We compare HMI data with observations of NOAA 12104 by the Hinode Spectropolarimeter (SP) to derive a scaling curve for the magnetic field strength,  $B$ . The SP data in the  $\text{Fe I}$  lines at 630 nm were inverted with the SIR code. We find that the Milne-Eddington inversion of HMI underestimates  $B$  and the line-of-sight flux,  $\Phi$ , in all granulation surroundings by an average factor of 4.5 in plage and 9.2 in the quiet Sun in comparison to the SP. The deviation is inversely proportional to the magnetic fill factor,  $f$ , in the SP results. We derived a correction curve to match the HMI  $B$  with the effective flux  $B_f$  in the SP data that scaled HMI  $B$  up by 1.3 on average. A comparison of non-force-free field extrapolations over a larger field of view without and with the correction revealed minor changes in connectivity and a proportional scaling of electric currents and Lorentz force ( $\propto B \sim 1.3$ ) and free energy ( $\propto B^2 \sim 2$ ). Magnetic field extrapolations of HMI vector data with large areas of plage and quiet Sun will underestimate the photospheric magnetic field strength by a factor of 5--10 and the coronal magnetic flux by at least 2. An HMI inversion including a fill factor would mitigate the problem. **2014 Jul 03**

### **Temporal Evolution of the Inverse Evershed Flow**

C. [Beck](#) and D. P. Choudhary

2020 ApJ 891 119

<https://doi.org/10.3847/1538-4357/ab75bd>

The inverse Evershed flow (IEF) is an inflow of material into the penumbra of sunspots in the solar chromosphere that occurs along dark, elongated super-penumbral fibrils extending from about the outer edge of the moat cell to the sunspot. The IEF channels exhibit brightenings in the penumbra, where the supersonic IEF descends to the photosphere causing shock fronts with localized heating. We used an 1 hr time series of spectroscopic observations of the chromospheric spectral lines of Ca II IR at 854 nm and H $\alpha$  at 656 nm taken with the Interferometric Bidimensional Spectrometer at the Dunn Solar Telescope to investigate the temporal evolution of IEF channels. Complementary information on the photospheric magnetic field was obtained from observations with the Facility

Infrared Spectropolarimeter at 1083 nm and the Helioseismic and Magnetic Imager. We find that individual IEF channels are long-lived (10–60 minutes) and only show minor changes in position and flow speed during their lifetime. Initiation and termination of IEF channels takes several minutes. The IEF channels with line-of-sight velocities of about  $10 \text{ km s}^{-1}$  show no lasting impact from transient or oscillatory phenomena with maximal velocity amplitudes of only about  $1 \text{ km s}^{-1}$  that run along them. We could not detect any clear correlation of the location and evolution of IEF channels to local magnetic field properties in the photosphere in the penumbra or moving magnetic features in the sunspot moat. Our results support a picture of the IEF as a field-aligned siphon flow along arched loops. From our data we cannot determine if their evolution is controlled by events at the outer end in the moat or at the inner end in the penumbra.

## **Magnetic Properties and Flow Angle of the Inverse Evershed Flow at Its Downflow Points**

C. Beck, D.P. Choudhary

ApJ 2019

<https://arxiv.org/pdf/1902.04660.pdf>

We determined the direction and strength of the photospheric and lower chromospheric magnetic field in the umbra and penumbra of a sunspot from inversions of spectropolarimetric observations of photospheric lines at 617 nm and 1565 nm, and the chromospheric  $\text{Ca II}$  IR line at 854 nm, respectively. We compare the magnetic field vector with the direction of 75 flow channels that harbor the chromospheric inverse Evershed effect (IEF) near their downflow points (DFPs) in the sunspot's penumbra. The azimuth and inclination of the IEF channels to the line of sight (LOS) were derived from spatial maps of the LOS velocity and line-core intensity of the  $\text{Ca II}$  IR line and a thermal inversion of the  $\text{Ca II}$  IR spectra to obtain temperature cubes. We find that the flow direction of the IEF near the DFPs is aligned with the photospheric magnetic field to within about  $\pm 15^\circ$ . The IEF flow fibrils make an angle of  $30\text{--}90^\circ$  to the local vertical with an average value of about  $65^\circ$ . The average field strength at the DFPs is about  $1.3 \text{ kG}$ . Our findings suggest that the IEF in the lower chromosphere is a field-aligned siphon flow, where the larger field strength at the inner footpoints together with the lower temperature in the penumbra causes the necessary gas pressure difference relative to the outer footpoints in the hotter quiet Sun with lower magnetic field strength. The IEF connects to magnetic field lines that are not horizontal like for the regular photospheric Evershed flow, but which continue upwards into the chromosphere indicating an "uncombed" penumbral structure. **03 Aug 2013**

## **The polarization signature of photospheric magnetic fields in 3D MHD simulations and observations at disk center**

C. Beck, D. Fabbian, R. Rezaei, K.G. Puschmann

ApJ 2017

<https://arxiv.org/pdf/1705.06812.pdf>

Before using 3D MHD simulations of the solar photosphere in the determination of elemental abundances, one has to ensure that the correct amount of magnetic flux is present in the simulations. The presence of magnetic flux modifies the thermal structure of the solar photosphere, which affects abundance determinations and the solar spectral irradiance. We compare the polarization signals in disk-center observations of the solar photosphere in quiet-Sun regions with those in Stokes spectra computed on the basis of 3D MHD simulations having average magnetic flux densities of about 20, 56, 112 and 224 G. This approach allows us to find the simulation run that best matches the observations. The observations were taken with the Hinode SP, TIP, POLIS and the GFPI, respectively. We determine characteristic quantities of full Stokes profiles in a few photospheric spectral lines in the visible (630 nm) and near-infrared (1083 and 1565 nm). We find that the appearance of abnormal granulation in intensity maps of degraded simulations can be traced back to an initially regular granulation pattern with numerous bright points in the intergranular lanes before the spatial degradation. The linear polarization signals in the simulations are almost exclusively related to canopies of strong magnetic flux concentrations and not to transient events of magnetic flux emergence. We find that the average vertical magnetic flux density in the simulation should be less than 50 G to reproduce the observed polarization signals in the quiet Sun internetwork. A value of about 35 G gives the best match across the SP, TIP, POLIS and GFPI observations.

## **A three-dimensional view of the thermal structure in a super-penumbral canopy**

C. Beck, D. Prasad Choudhary, R. Rezaei

ApJ, 2014

<http://arxiv.org/pdf/1405.1473v1.pdf>

We investigate the thermal topology in a super-penumbral canopy by determining the 3D thermal structure of an active region. We derive the temperature stratifications in the active region by an inversion of the Ca II IR line at 854.2 nm, assuming LTE. We trace the 3D topology of individual features located in the super-penumbral canopy, mainly radially oriented fibrils. We find that about half of the fibrils form short, arched, low-lying loops in the temperature cube. These closed loops connect from bright grains that are either in or close to the penumbra to the

photosphere a few Mms away from the sunspot. They reach less than 1 Mm in height. The other half of the fibrils rise with distance from the sunspot until they leave the Ca II IR formation height. Many of the fibrils show a central dark core and two lateral brightenings as seen in line-core intensity images. The corresponding velocity image shows fibrils that are as wide as the fibrils seen in intensity without a lateral substructure. Additionally, we study one example of exceptional brightness in more detail. It belongs to a different class of structures without prominent mass flows and with a 3D topology formed by two parallel, closed loops connecting patches of opposite polarity. We present evidence that the inverse Evershed flow into the sunspot in the lower chromosphere is the consequence of siphon flows along short loops that connect photospheric foot points. The dark-cored structure of the chromospheric fibrils cannot have a convective origin because of their location above regular granulation in an optically thin atmosphere. The dark core most likely results from an opacity difference between the central axis and the lateral edges caused by the significant flow speed along the fibrils. **29/07/2013**

## **Coronal Magnetic Fields derived with Images acquired during the 21 August 2017 Total Solar Eclipse**

**Alessandro Bemporad**

ApJ **946** 14 **2023**

<https://arxiv.org/pdf/2302.10647.pdf>

<https://iopscience.iop.org/article/10.3847/1538-4357/acb8b8/pdf>

The coronal magnetic field, despite its overwhelming importance to the physics and dynamics of the corona, has only rarely been measured. Here, the electron density maps derived from images acquired during the total solar eclipse of **August 21st, 2017** are employed to demonstrate a new technique to measure the coronal magnetic fields. The strength of the coronal magnetic fields is derived with a semiempirical formula relating the plasma magnetic energy density to the gravitational potential energy. The resulting values are compared with those provided by more advanced coronal field reconstruction methods based on MHD simulations of the whole corona starting from photospheric field measurements, finding a very good agreement. Other parameters such as the plasma- $\beta$  and Alfvén velocity are also derived and compared with those of MHD simulations. Moreover, the plane-of-sky (POS) orientation of the coronal magnetic fields is derived from the observed inclination of the coronal features in the filtered images, also finding a close agreement with magnetic field reconstructions. Hence, this work demonstrates for the first time that the 2D distribution of coronal electron densities measured during total solar eclipses is sufficient to provide the coronal magnetic field strengths and inclinations projected on the POS. These are among the main missing pieces of information that limited so far our understanding of physical phenomena going on in the solar corona.

## **Measuring coronal magnetic fields with remote sensing observations of shock waves**

### **Review**

Alessandro **Bemporad**, Roberto Susino, Federica Frassati, Silvano Fineschi

Frontiers in Astronomy and Space Sciences, Volume 3, id.17 **2016**

<https://arxiv.org/ftp/arxiv/papers/1608/1608.05536.pdf>

<https://www.frontiersin.org/articles/10.3389/fspas.2016.00017/full>

<https://doi.org/10.3389/fspas.2016.00017>

Recent works demonstrated that remote sensing observations of shock waves propagating into the corona and associated with major solar eruptions can be used to derive the strength of coronal magnetic fields met by the shock over a very large interval of heliocentric distances and latitudes. This opinion article will summarize most recent results obtained on this topic and will discuss the weaknesses and strengths of these techniques to open a constructive discussion with the scientific community.

## **Plasma physical parameters along Coronal Mass Ejection-driven shocks: I observations**

A. **Bemporad**, R. Susino, G. Lapenta

ApJ, **2014**

<http://arxiv.org/pdf/1403.0870v1.pdf>

In this work UV and white light (WL) coronagraphic data are combined to derive the full set of plasma physical parameters along the front of a shock driven by a Coronal Mass Ejection. Pre-shock plasma density, shock compression ratio, speed and inclination angle are estimated from WL data, while pre-shock plasma temperature and outflow velocity are derived from UV data. The Rankine-Hugoniot (RH) equations for the general case of an oblique shock are then applied at three points along the front located between 2.2–2.6  $R_{\odot}$  at the shock nose and at the two flanks. Stronger field deflection (by  $\sim 46^{\circ}$ ), plasma compression (factor  $\sim 2.7$ ) and heating (factor  $\sim 12$ ) occur at the nose, while heating at the flanks is more moderate (factor 1.5–3.0). Starting from a pre-shock corona where protons and electrons have about the same temperature ( $T_p \sim T_e \sim 1.5 \cdot 10^6$  K), temperature increases derived with RH equations could better represent the protons heating (by dissipation across the shock), while the temperature increase implied by adiabatic compression (factor  $\sim 2$  at the nose,  $\sim 1.2$ – $1.5$  at the flanks) could be more

representative of electrons heating: the transit of the shock causes a decoupling between electron and proton temperatures. Derived magnetic field vector rotations imply a draping of field lines around the expanding flux rope. The shock turns out to be super-critical (sub-critical) at the nose (at the flanks), where derived post-shock plasma parameters can be very well approximated with those derived by assuming a parallel (perpendicular) shock.  
**1999 June 11**

## **IDENTIFICATION OF SUPER- AND SUBCRITICAL REGIONS IN SHOCKS DRIVEN BY CORONAL MASS EJECTIONS**

A. [Bemporad](#) and S. Mancuso

**2011 ApJ 739 L64**

<http://arxiv.org/pdf/1108.3783v1.pdf>

In this work, we focus on the analysis of a CME-driven shock observed by SOHO/LASCO. We show that white-light coronagraphic images can be employed to estimate the compression ratio  $X = \rho_d / \rho_u$  all along the front of CME-driven shocks.  $X$  increases from the shock flanks (where  $X \sim 1.2$ ) to the shock center (where  $X \sim 3.0$  is maximum). From the estimated  $X$  values, we infer the Alfvén Mach number for the general case of an oblique shock. It turns out that only a small region around the shock center is supercritical at earlier times, while higher up in the corona the whole shock becomes subcritical. This suggests that CME-driven shocks could be efficient particle accelerators at the initiation phases of the event, while at later times they progressively lose energy, also losing their capability to accelerate high energy particles. This result has important implications on the localization of particle acceleration sites and in the context of predictive space weather studies.

## **Total Solar Eclipse White Light Images as a Benchmark for PFSS Coronal Magnetic Field Models: An In-Depth Analysis over a Solar Cycle**

[Luke Fushimi Benavitz](#), [Benjamin Boe](#), [Shadia Rifai Habbal](#)

**ApJ 974 178 2024**

<https://arxiv.org/pdf/2408.16149>

<https://iopscience.iop.org/article/10.3847/1538-4357/ad71c6/pdf>

Potential Field Source Surface (PFSS) models are widely used to simulate coronal magnetic fields. PFSS models use the observed photospheric magnetic field as the inner boundary condition and assume a perfectly radial field beyond a "Source Surface" ( $R_{ss}$ ). At present, total solar eclipse (TSE) white light images are the only data that delineate the coronal magnetic field from the photosphere out to several solar radii ( $R_{\odot}$ ). We utilize a complete solar cycle span of these images between 2008 and 2020 as a benchmark to assess the reliability of PFSS models. For a quantitative assessment, we apply a rolling Hough transform (RHT) to the eclipse data and corresponding PFSS models to measure the difference,  $\Delta\theta$ , between the data and model magnetic field lines throughout the corona. We find that the average  $\Delta\theta$ ,  $\langle\Delta\theta\rangle$ , can be minimized for a given choice of  $R_{ss}$  depending on the phase within a solar cycle. In particular,  $R_{ss} \approx 1.3 R_{\odot}$  is found to be optimal for solar maximum, while  $R_{ss} \approx 3 R_{\odot}$  yields a better match at solar minimum. However, large ( $\langle\Delta\theta\rangle > 10^\circ$ ) discrepancies between TSE data and PFSS-generated coronal field lines remain regardless of the choice of source surface. Yet, implementation of solar cycle dependent  $R_{ss}$  optimal values do yield more reliable PFSS-generated coronal field lines for use in models and for tracing in-situ measurements back to their sources at the Sun.

## **The dependence of the magnetism of a near-limb sunspot on height**

M. [Benko](#) (1), [H. Balthasar](#) (2), [P. Gömöry](#) (1), [C. Kuckein](#) (3,4,5), [S.J. González Manrique](#)

**A&A 686, A194 2024**

<https://arxiv.org/pdf/2403.14532>

The physical parameters of the sunspot are not fully understood, especially the height dependence of the magnetic field. So far, it is also an open question as to which heights the He I 1083 nm spectral line is formed at. Our aim is to investigate the magnetic and dynamical properties in the atmosphere above a sunspot, from the photosphere to the chromosphere. We analyzed the photospheric and chromospheric magnetic field properties of a stable sunspot in AR 12553 on **June 20, 2016** using spectropolarimetric observations obtained with GRIS at GREGOR. A spectral-line inversion technique was used to infer the magnetic field vector and Doppler velocities from the full Stokes profiles. In total, three spectral lines were inverted and the variation of the magnetic properties was qualified using the average values of the radial circles. The sunspot is located close to the solar limb, and thus this allows us to make a geometrical determination of the height of the spectral line He I 1083 nm. We find the height of helium spectral line to be 970 km above the photospheric spectral lines directly from observation at a stable sunspot. The total magnetic field strength decreases with height over the sunspot; the rates are  $-0.34$  G/km for the umbra and  $-0.28$  G/km for the penumbra. The inclination increases with increasing height in the umbra, but decreases in the penumbra. In the umbra, the vertical component ( $B_z$ ) decreases with height, while the horizontal component ( $B_{hor}$ ) remains almost constant. In the penumbra this is reversed, as  $B_z$  remains nearly constant over height, while  $B_{hor}$  decreases. We also observe fast velocities with 30 km/s in small chromospheric patches on the central side of the spot. The key

parameters depending on height in the sunspot are the Bz component of the magnetic field for the umbra and the Bhor component of the magnetic field for the penumbra.

### **Properties of the inner penumbral boundary and temporal evolution of a decaying sunspot**

M. [Benko](#) (1), [S. J. González Manrique](#) (1), [H. Balthasar](#) (2), [P. Gömöry](#) (1), [C. Kuckein](#) (2), [J. Jurčák](#)  
A&A [620, A191](#) **2018**

<https://arxiv.org/pdf/1810.13185.pdf>

<https://doi.org/10.1051/0004-6361/201834296>

It was empirically determined that the umbra-penumbra boundaries of stable sunspots are characterized by a constant value of the vertical magnetic field. We analyzed the evolution of the photospheric magnetic field properties of a decaying sunspot belonging to NOAA 11277 between **August 28 - September 3, 2011**. The observations were acquired with the spectropolarimeter on-board of the Hinode satellite. We aim to prove the validity of the constant vertical magnetic-field boundary between the umbra and penumbra in decaying sunspots. A spectral-line inversion technique was used to infer the magnetic field vector from the full-Stokes profiles. In total, eight maps were inverted and the variation of the magnetic properties in time were quantified using linear or quadratic fits. We found a linear decay of the umbral vertical magnetic field, magnetic flux, and area. The penumbra showed a linear increase of the vertical magnetic field and a sharp decay of the magnetic flux. In addition, the penumbral area quadratically decayed. The vertical component of the magnetic field is weaker on the umbra-penumbra boundary of the studied decaying sunspot compared to stable sunspots. Its value seem to be steadily decreasing during the decay phase. Moreover, at any time of the shown sunspot decay, the inner penumbra boundary does not match with a constant value of the vertical magnetic field, contrary to what was seen in stable sunspots. During the decaying phase of the studied sunspot, the umbra does not have a sufficiently strong vertical component of the magnetic field and is thus unstable and prone to be disintegrated by convection or magnetic diffusion. No constant value of the vertical magnetic field was found for the inner penumbral boundary.

**Erratum:** A&A 652, C7 (2021)

<https://www.aanda.org/articles/aa/pdf/2021/08/aa34296e-18.pdf>

<https://doi.org/10.1051/0004-6361/201834296>

### **Synoptic Solar Cycle 24 in Corona, Chromosphere, and Photosphere Seen by the Solar Dynamics Observatory**

E. [Benevolenskaya](#), G. Slater, J. Lemen

Solar Phys., Volume 289, Issue 9, pp 3371-3379, **2014**

The Solar Dynamics Observatory provides multiwavelength imagery from extreme ultraviolet (EUV) to visible light as well as magnetic-field measurements. These data enable us to study the nature of solar activity in different regions of the Sun, from the interior to the corona. For solar-cycle studies, synoptic maps provide a useful way to represent global activity and evolution by extracting a central meridian band from sequences of full-disk images over a full solar Carrington rotation ( $\approx 27.3$  days). We present the global evolution during Solar Cycle 24 from 20 May 2010 to 31 August 2013 (CR 2097 – CR 2140), using synoptic maps constructed from full-disk, line-of-sight magnetic-field imagery and EUV imagery (171 Å, 193 Å, 211 Å, 304 Å, and 335 Å). The synoptic maps have a resolution of 0.1 degree in longitude and steps of 0.001 in sine of latitude. We studied the axisymmetric and non-axisymmetric structures of solar activity using these synoptic maps. To visualize the axisymmetric development of Cycle 24, we generated time–latitude (also called butterfly) images of the solar cycle in all of the wavelengths, by averaging each synoptic map over all longitudes, thus compressing it to a single vertical strip, and then assembling these strips in time order. From these time–latitude images we observe that during the ascending phase of Cycle 24 there is a very good relationship between the integrated magnetic flux and the EUV intensity inside the zone of sunspot activities. We observe a North–South asymmetry of the EUV intensity in high-latitudes. The North–South asymmetry of the emerging magnetic flux developed and resulted in a consequential asymmetry in the timing of the polar magnetic-field reversals.

### **Properties of the inner penumbral boundary and temporal evolution of a decaying sunspot**

M. [Benko](#)<sup>1</sup>, [S. J. González Manrique](#)<sup>1</sup>, [H. Balthasar](#)<sup>2</sup>, [P. Gömöry](#)<sup>1</sup>, [C. Kuckein](#)<sup>2</sup> and [J. Jurčák](#)

A&A 620, A191 (**2018**)

[sci-hub.tw/10.1051/0004-6361/201834296](https://arxiv.org/pdf/1810.13185.pdf)

<https://arxiv.org/pdf/1810.13185.pdf>

Context. It has been empirically determined that the umbra-penumbra boundaries of stable sunspots are characterized by a constant value of the vertical magnetic field.

Aims. We analyzed the evolution of the photospheric magnetic field properties of a decaying sunspot belonging to NOAA 11277 between **August 28–September 3, 2011**. The observations were acquired with the spectropolarimeter

on-board of the Hinode satellite. We aim to prove the validity of the constant vertical magnetic-field boundary between the umbra and penumbra in decaying sunspots.

**Methods.** A spectral-line inversion technique was used to infer the magnetic field vector from the full-Stokes profiles. In total, eight maps were inverted and the variation of the magnetic properties in time were quantified using linear or quadratic fits.

**Results.** We find a linear decay of the umbral vertical magnetic field, magnetic flux, and area. The penumbra showed a linear increase of the vertical magnetic field and a sharp decay of the magnetic flux. In addition, the penumbral area quadratically decayed. The vertical component of the magnetic field is weaker on the umbra-penumbra boundary of the studied decaying sunspot compared to stable sunspots. Its value seem to be steadily decreasing during the decay phase. Moreover, at any time of the sunspot decay shown, the inner penumbra boundary does not match with a constant value of the vertical magnetic field, contrary to what is seen in stable sunspots.

**Conclusions.** During the decaying phase of the studied sunspot, the umbra does not have a sufficiently strong vertical component of the magnetic field and is thus unstable and prone to be disintegrated by convection or magnetic diffusion. No constant value of the vertical magnetic field is found for the inner penumbral boundary.

### **Determining the parameter for the linear force-free magnetic field model with multi-dipolar configurations using deep neural networks**

B. [Benson](#)1 [W. David Pan](#)1 [G. Allen Gary](#)2 [Q. Hu](#)2 [T. Staudinger](#)  
[Astronomy and Computing](#) Volume 26, January 2019, Pages 50-60  
<https://www.sciencedirect.com/science/article/pii/S2213133718301148>

Recent advances in the field of [neural networks](#) have made convolutional neural networks (CNNs) a conventional algorithm for many computer vision tasks including image recognition and [object detection](#). Because modeling the coronal [magnetic field](#) of the Sun is an important objective in heliophysics, this study extends the use of CNNs to the application of coronal magnetic field modeling. We employ a simple one-parameter model of linear force-free magnetic fields (LFFFs) to model active regions of multiple dipolar configurations including the Active Region (AR) 11117. We use state-of-the-art architectures such as ResNet and Inception networks, and develop our customized network “SolarNet” to determine the associated LFFF parameter alpha from a set of pseudo-coronal loop images, which are generated using the modeled active regions. Our results show very high accuracy of determining the LFFF parameter alpha, thereby demonstrating the effectiveness of the generic and customized deep CNN architectures to understand the coronal magnetic field.

### **Determination of Linear Force-Free Magnetic Field Constant Alpha Using Deep Learning**

Bernard [Benson](#), Zhuocheng Jiang, W. David Pan, G. Allen Gary and Qiang Hu  
CSCI-ISAI 2017, Las Vegas Conference 2017  
<http://www.ece.uah.edu/~dwpan/papers/CSCI17.pdf>

Modeling the coronal magnetic field of the Sun is an important objective in heliophysics. In this study, we illustrate how to use deep learning to estimate the parameter for a magnetic field model. A linear force-free magnetic field configuration is employed to model, as an initial illustration, an active region by using two magnetic dipoles and to determine the associated linear force-free field (LFFF)  $\alpha$  parameter from a set of pseudocoronal loop images which serve as training and validation sets to existing deep learning algorithms. Our results show very high accuracy of determining the LFFF parameter  $\alpha$  from pseudocoronal loop images. **October 25, 2010.**

### **Magnetic pattern at supergranulation scale: the Void Size Distribution**

Francesco [Berrilli](#), Stefano Scardigli, Dario Del Moro  
[A&A](#), 2014

<http://arxiv.org/pdf/1406.5871v1.pdf>

The large-scale magnetic pattern of the quiet sun is dominated by the magnetic network. This network, created by photospheric magnetic fields swept into convective downflows, delineates the boundaries of large scale cells of overturning plasma and exhibits voids in magnetic organization. Such voids include internetwork fields, a mixed-polarity sparse field that populate the inner part of network cells. To single out voids and to quantify their intrinsic pattern a fast circle packing based algorithm is applied to 511 SOHO/MDI high resolution magnetograms acquired during the outstanding solar activity minimum between 23 and 24 cycles. The computed Void Distribution Function shows a quasi-exponential decay behavior in the range 10-60 Mm. The lack of distinct flow scales in such a range corroborates the hypothesis of multi-scale motion flows at the solar surface. In addition to the quasi-exponential decay we have found that the voids reveal departure from a simple exponential decay around 35 Mm.

### **Multi-height Measurements Of The Solar Vector Magnetic Field:**

**Review**

[L. Bertello](#), [N. Arge](#), [A. G. De Wijn](#), [S. Gosain](#), [C. Henney](#), [K.D. Leka](#), [J. Linker](#), [Y. Liu](#), [J. Luhmann](#), [P.J. Macniece](#), [G. Petrie](#), [A. Pevtsov](#), [A.A. Pevtsov](#)

A White Paper Submitted To The Decadal Survey For Solar And Space Physics (Heliophysics) 2024-2033      2022

<https://arxiv.org/pdf/2209.04453.pdf>

This white paper advocates the importance of multi-height measurements of the vector magnetic field in the solar atmosphere. As briefly described in this document, these measurements are critical for addressing some of the most fundamental questions in solar and heliospheric physics today, including: (1) What is the origin of the magnetic field observed in the solar atmosphere? (2) What is the coupling between magnetic fields and flows throughout the solar atmosphere? Accurate measurements of the photospheric and chromospheric three-dimensional magnetic fields are required for a precise determination of the emergence and evolution of active regions. Newly emerging magnetic flux in pre-existing magnetic regions causes an increase in the topological complexity of the magnetic field, which leads to flares and coronal mass ejections. Measurements of the vector magnetic field constitute also the primary product for space weather operations, research, and modeling of the solar atmosphere and heliosphere. The proposed next generation Ground-based solar Observing Network Group (ngGONG), a coordinated system of multi-platform instruments, will address these questions and provide large datasets for statistical investigations of solar feature behavior and evolution and continuity in monitoring for space-weather focused endeavors both research and operational. It will also enable sun-as-a-star investigations, crucial as we look toward understanding other planet-hosting stars.

### **SOLIS/VSM Polar Magnetic Field Data**

Luca [Bertello](#), Andrew R. Marble

Technical Report No. NSO/NISP-2015-002

<http://arxiv.org/pdf/1507.07976v1.pdf>

The Vector Spectromagnetograph (VSM) instrument on the Synoptic Optical Long-term Investigations of the Sun (SOLIS) telescope is designed to obtain high-quality magnetic field observations in both the photosphere and chromosphere by measuring the Zeeman-induced polarization of spectral lines. With 1'' spatial resolution (1.14'' before 2010) and 0.05\AA spectral resolution, the VSM provides, among other products, chromospheric full-disk magnetograms using the CaII 854.2 nm spectral line and both photospheric full-disk vector and longitudinal magnetograms using the FeI 630.15 nm line. Here we describe the procedure used to compute daily weighted averages of the photospheric radial polar magnetic field at different latitude bands from SOLIS/VSM longitudinal full-disk observations. Time series of these measurements are publicly available from the SOLIS website at [this http URL](#) Future plans include the calculation of the mean polar field strength from SOLIS/VSM chromospheric observations and the determination of the radial polar field from SOLIS/VSM full-Stokes measurements.

### **Spatial-Variance Magnetic Synoptic Maps**

L. [Bertello](#), A. A. Pevtsov, G. J. D. Petrie

HMI Science Nuggets, #16, 2014

<http://hmi.stanford.edu/hminuggets/?p=746>

### **Uncertainties in Solar Synoptic Magnetic Flux Maps**

L. [Bertello](#), A. A. Pevtsov, G. J. D. Petrie, D. Keys

Solar Physics, July 2014, Volume 289, Issue 7, pp 2419-2431

<http://arxiv.org/pdf/1312.0509v1.pdf>

Magnetic flux synoptic charts are critical for a reliable modeling of the corona and heliosphere. Until now, however, these charts were provided without uncertainty estimates. The uncertainties are due to instrumental noise in the measurements and to the spatial variance of the magnetic flux distribution that contributes to each bin in the synoptic chart. We describe here a simple method to compute synoptic magnetic flux maps and their corresponding magnetic flux spatial variance charts that can be used to estimate the uncertainty in the results of coronal models. We have tested this approach by computing a potential-field source-surface model of the coronal field for a Monte Carlo simulation of Carrington synoptic magnetic flux maps generated from the variance map. We show that these uncertainties affect both the locations of source-surface neutral lines and the distributions of coronal holes in the models.

### **Spectropolarimetric observations of the solar atmosphere in the H $\alpha$ 6563 Å line**

[J. Jaime Bestard](#), [J. Trujillo Bueno](#), [M. Bianda](#), [J. Štěpán](#), [R. Ramelli](#)

A&A      2022



<https://arxiv.org/pdf/2201.03815.pdf>

We present novel spectropolarimetric observations of the hydrogen H $\alpha$  line taken with the Zürich Imaging Polarimeter (ZIMPOL) at the Gregory Coudé Telescope of the Istituto Ricerche Solari Locarno (IRSOL). The linear polarization is clearly dominated by the scattering of anisotropic radiation and the Hanle effect, while the circular polarization by the Zeeman effect. The observed linear polarization signals show a rich spatial variability, the interpretation of which would open a new window for probing the solar chromosphere. We study their spatial variation within coronal holes, finding a different behaviour for the U/I signals near the North and South solar poles. We identify some spatial patterns, which may facilitate the interpretation of the observations. In close-to-the-limb regions with sizable circular polarization signals we find similar asymmetric Q/I profiles. We also show examples of net circular polarization profiles (NCP), along with the corresponding linear polarization signals. The application of the weak field approximation to the observed circular polarization signals gives 10G (40–60G) in close to the limb quiet (plage) regions for the average longitudinal field strength over the spatio-temporal resolution element.

## **Opposite polarity magnetic field and convective downflows in a simulated sunspot penumbra**

Lokesh [Bharti](#), [Matthias Rempel](#)

ApJ **884** 94 2019

<https://arxiv.org/pdf/1908.06439.pdf>

<https://doi.org/10.3847/1538-4357/ab3c6b>

Recent numerical simulations and observations of sunspots show a significant amount of opposite polarity magnetic field within the sunspot penumbra. Most of the opposite polarity field is associated with convective downflows. We present an analysis of 3D MHD simulations through forward modeling of synthetic Stokes profiles of the Fe\sci 6301.5 Å~ and Fe\sci 6302.5 Å~ lines). The synthetic Stokes profiles are spatially and spectrally degraded considering typical instrument properties. Line bisector shifts of the Fe\sci 6301.5 Å~ line are used to determine line-of-sight velocities. Far wing magnetograms are constructed from the Stokes V profiles of the Fe\sci 6302.5 Å~ line. While we find an overall good agreement between observations and simulations, the fraction of opposite polarity magnetic field, the downflow filling factor and the opposite polarity-downflow association are strongly affected by spatial smearing and presence of strong gradients in the line-of-sight magnetic field and velocity. A significant fraction of opposite polarity magnetic field and downflows are hidden in the observations due to typical instrumental noise. Comparing simulations that differ by more than a factor of two in grid spacing we find that these quantities are robust within the simulations.

## **Small-Scale Activity Above the Penumbra of a Fast-Rotating Sunspot**

L. [Bharti](#), C. Quintero Noda, S. Rakesh, B. Sobha, A. Pandya, C. Joshi

[Solar Physics](#) March **2018**, 293:46

High-resolution observations of small-scale activity above the filamentary structure of a fast-rotating sunspot of NOAA Active Region 10930 are presented. The penumbral filament that intrudes into the umbra shows a central dark core and substructures. It almost approached another end of the umbra, like a light bridge. The chromospheric Ca ii H images show many jet-like structures with a bright leading edge above it. These bright jets move across the filament tips and show coordinated up and down motions. Transition region images also show brightening at the same location above the intrusion. Coronal 195 Å images suggest that one end of the bright coronal loop footpoints resides in this structure. The intrusion has opposite polarity with respect to the umbra. Strong downflows are observed at the edges along the length of the intrusion where the opposite-polarity field is enhanced. We also observe a counter-Evershed flow in the filamentary structure that also displays brightening and energy dissipation in the upper atmosphere. This scenario suggests that the jets and brightenings are caused by low-altitude reconnection driven by opposite-polarity fields and convective downflows above such structures.

## **Lambda-shaped jets from a penumbral intrusion into a sunspot umbra: a possibility for magnetic reconnection\***

L. [Bharti](#)<sup>1,2</sup>, S. K. Solanki<sup>1,3</sup> and J. Hirzberger

A&A 597, A127 (2017)

[http://www.aanda.org/articles/aa/full\\_html/2017/01/aa29656-16/aa29656-16.html](http://www.aanda.org/articles/aa/full_html/2017/01/aa29656-16/aa29656-16.html)

We present the results of high resolution co-temporal and co-spatial photospheric and chromospheric observations of sunspot penumbral intrusions. The data were taken with the Swedish Solar Telescope (SST) on the Canary Islands. Time series of Ca II H images show a series of transient jets extending roughly 3000 km above a penumbral intrusion into the umbra. For most of the time series, jets were seen along the whole length of the intruding bright filament. Some of these jets develop a clear  $\lambda$ -shaped structure, with a small loop appearing at their footpoint and lasting for around a minute. In the framework of earlier studies, the observed transient  $\lambda$  shape of these jets suggests that they could be caused by magnetic reconnection between a curved arcade-like or flux rope-like field in the lower part of the penumbral intrusion and the more vertical umbral magnetic field forming a cusp-shaped structure above the penumbral intrusion.

2006 August 13

### **Magnetic reconnection as a source of jets from a penumbral intrusion into a sunspot umbra**

L. [Bharti](#), S. K. Solanki, J. Hirzberger

ApJ 2015

<http://arxiv.org/pdf/1509.02123v1.pdf>

We present the results of high resolution co-temporal and co-spatial photospheric and chromospheric observations of sunspot penumbral intrusions. The data was taken with the Swedish Solar Telescope (SST) on the Canary Islands. Time series of Ca\,II H images show a series of transient jets extending roughly 3000 km above a penumbral intrusion into the umbra. For most of the time series jets were seen along the whole length of the intruding bright filament. Some of these jets develop a clear  $\lambda$ -shaped structure, with a small loop appearing at their footpoint and lasting for around a minute. In the framework of earlier studies, the observed transient  $\lambda$  shape of these jets strongly suggests that they are caused by magnetic reconnection between a curved arcade-like or flux-rope like field in the lower part of the penumbral intrusion and the more vertical umbral magnetic field forming a cusp-shaped structure above the penumbral intrusion. **2006 August 13**

### **Fine structures in the atmosphere above a sunspot umbra**

L. [Bharti](#)<sup>1</sup>, J. Hirzberger<sup>1</sup> and S. K. Solanki

A&A 552, L1 (2013)

We present simultaneous photospheric and chromospheric observations of the trailing sunspot in NOAA 10904, obtained with the Swedish Solar Telescope (SST) La Palma, Canary Islands. Time series of high resolution Ca ii H images show transient jet-like structures in sunspot umbrae are elongated, which we call umbral microjets. These jets are directed roughly parallel to nearby penumbral microjets, suggesting that they are aligned with the background magnetic field. In general, first a bright dot-like structure appears, from which a jet later emerges, although some jets appear without an associated chromospheric dot. Bright photospheric umbral dots are associated with umbral microjets arising in the outer umbra. Nevertheless, a one-to-one correspondence between jet-like events and underlying umbral dots is not seen. They are typically less than 1'' long and less than 03 wide. The typical lifetime of umbral microjets is around one minute. The brightness of these structures increases from the center of the umbra toward the umbra-penumbra boundary along with the brightness of the local background.

### **Partial eruption of a filament with twisting nonuniform fields**

Yi [Bi](#), [Yunchun Jiang](#), [Jiayan Yang](#), [Yongyuan Xiang](#), [Yunfang Cai](#), [Weiwei Liu](#)

ApJ 2015

<http://arxiv.org/pdf/1504.03090v1.pdf>

The eruption of the filament with the kink fashion is often regarded as a signature of the kink instability. However, the kink instability threshold for the filament magnetic structure has been not widely understood. Using the H-alpha observation from the New Vacuum Solar Telescope (NVST), we present a partial eruptive filament. In the eruption, a filament thread appeared to split from the middle portion of the filament and to break out in a kinklike fashion. During this period, the left filament material remained below, which erupted without the kinking motion later on. The coronal magnetic field lines associated with the filament are obtained from the nonlinear force-free field (NLFFF) extrapolations using the 12 minutes cadence vector magnetograms of the Helioseismic and Magnetic Imager (HMI) on board the Solar Dynamic Observatory (SDO). We studied the extrapolated field lines passing through the magnetic dips that are in good agreement with the observed filament. The field lines are non-uniformly twisted and appear to be made up by two twisted flux ropes winding about each other. One of them has higher twist than the other, and the highly twisted one has its dips aligned with the kinking eruptive thread at the beginning of its eruption. Before the eruption, moreover, the highly twisted flux rope was found to expand with the approximately constant field twist. In addition, the helicity flux maps deduced from the HMI magnetograms show that some helicity is injected into the overlying magnetic arcade, but no significant helicity is injected into the flux ropes. Accordingly, we suggest that the highly twisted flux rope became kink unstable when the instability threshold declined with the expansion of the flux rope. **2014 Nov 4**

### **Determination of the Coronal and Interplanetary Magnetic-Field Strength and Radial Profiles from the Large-Scale Photospheric Magnetic Fields**

[Irina A. Bilenko](#)

We propose a new model for the magnetic field at different distances from the Sun during different phases of the solar cycle. The model depends on the observed large-scale non-polar ( $\pm 55^\circ \pm 55^\circ$ ) photospheric magnetic field and on the magnetic field measured at polar regions from  $55^\circ 55'$  N to  $90^\circ 90'$  N and from  $55^\circ 55'$  S to  $90^\circ 90'$  S, which are the visible manifestations of cyclic changes in the toroidal and poloidal components of the global magnetic field of the Sun. The modeled magnetic field is determined as the superposition of the non-polar and polar photospheric magnetic field and considers cycle variations. The agreement between the model predictions and magnetic fields derived from direct in situ measurements at different distances from the Sun, obtained with different methods and at different solar activity phases, is quite satisfactory. From a comparison of the magnetic fields as observed and calculated from the model at 1 AU, we conclude that the model magnetic field variations adequately explain the main features of the interplanetary magnetic field (IMF) radial, BxBx, component cycle evolution at Earth's orbit. The modeled magnetic field averaged over a Carrington rotation (CR) correlates with the IMF BxBx component also averaged over a CR at Earth's orbit with a coefficient of 0.691, while for seven CR-averaged data, the correlation reaches 0.81. The radial profiles of the modeled magnetic field are compared with those of already existing models. In contrast to existing models, ours provides realistic magnetic-field radial distributions over a wide range of heliospheric distances at different cycle phases, taking into account the cycle variations of the solar toroidal and poloidal magnetic fields. The model is a good approximation of the cycle behavior of the magnetic field in the heliosphere. In addition, the decrease in the non-polar and polar photospheric magnetic fields is shown. Furthermore, the magnetic field during solar cycle maxima and minima decreased from Cycle 21 to Cycle 24. This implies that both the toroidal and poloidal components, and therefore the solar global magnetic field, decreased from Cycle 21 to Cycle 24.

## **Influence of the Solar Global Magnetic-Field Structure Evolution on CMEs**

Irina A. **Bilenko**

Solar Physics, July 2014

We consider the influence of the solar global magnetic-field structure (GMFS) cycle evolution on the occurrence rate and parameters of coronal mass ejections (CMEs) in Solar Cycles 23 – 24. It has been shown that, over solar cycles, CMEs are not distributed randomly, but they are regulated by evolutionary changes in the GMFS. It is proposed that the generation of magnetic Rossby waves in the solar tachocline results in the GMFS cycle changes. Each Rossby wave period favors a particular GMFS. It is proposed that the changes in wave periods result in GMFS reorganization and consequently in CME location, occurrence rate, and parameter changes. The CME rate and parameters depend on the sharpness of the GMFS changes, the strength of the global magnetic field, and the phase of a cycle

## **Slow Appearance of Sunspots Challenges Theory**

A. C. **Birch**<sup>1</sup>, H. Schunker<sup>1</sup>, D. C. Braun<sup>2</sup>, R. Cameron<sup>1</sup>, L. Gizon<sup>1,3,5,6</sup>, B. Löptien<sup>1</sup>, M. Rempel<sup>4</sup> & E. Guggenberger

HMI Science Nuggets #64 November 2016

<http://hmi.stanford.edu/hminuggets/?p=1770>

A comparison of the surface flow patterns in observation and numerical simulation suggests that the flux tube emerging speed has been overestimated in theories.

## **Solar Flare Forecasting Using HMI Vector Magnetic Field Data with a Support Vector Machine Algorithm**

Monica **Bobra** and Sebastien Couvidat

HMI Science Nuggets, #25, 2014

<http://hmi.stanford.edu/hminuggets/?p=911>

We attempt to forecast M- and X-class flares using a machine-learning algorithm, called Support Vector Machine (SVM), and four years of HMI data.

## **The Helioseismic and Magnetic Imager (HMI) Vector Magnetic Field Pipeline: SHARPs - Space-weather HMI Active Region Patches**

Monica **Bobra**, X. Sun, J.T. Hoeksema, M. Turmon, Y. Liu, K. Hayashi, G. Barnes, K.D. Leka  
E-print, Apr 2014, Solar Phys. Volume 289, Issue 9, pp 3549-3578, 2014

<http://sun.stanford.edu/~todd/SHARP.pdf>

<http://arxiv.org/pdf/1404.1879v1.pdf>

A new data product from the Helioseismic and Magnetic Imager (HMI) onboard the Solar Dynamics Observatory (SDO) called Space-weather HMI Active Region Patches (SHARPs) is now available. SDO/HMI is the first space-based instrument to map the full-disk photospheric vector magnetic field with high cadence and continuity. The SHARP data series provide maps in patches that encompass automatically tracked magnetic concentrations for their entire lifetime; map quantities include the photospheric vector magnetic field and its uncertainty, along with Doppler velocity, continuum intensity, and line-of-sight magnetic field. Furthermore, keywords in the SHARP data series provide several parameters that concisely characterize the magnetic-field distribution and its deviation from a potential-field configuration. These indices may be useful for active region event forecasting and for identifying regions of interest. The indices are calculated per patch and are available on a twelve-minute cadence. Quick-look data are available within approximately three hours of observation; definitive science products are produced approximately five weeks later. SHARP data are available at [jsoc.stanford.edu](http://jsoc.stanford.edu) and maps are available in either of two different coordinate systems. This article describes the SHARP data products and presents examples of SHARP data and parameters.

### **Modeling Non-Potential Magnetic Fields in Solar Active Regions**

M. G. [Bobra](#), A. A. van Ballegoijen, E. E. DeLuca  
E-print, March 2007, ApJ

### **Coronal Magnetic Field Topology From Total Solar Eclipse Observations**

Benjamin [Boe](#), [Shadia Habbal](#), [Miloslav Druckmuller](#)  
ApJ 895 123 2020

<https://arxiv.org/pdf/2004.08970.pdf>

<https://doi.org/10.3847/1538-4357/ab8ae6>

Measuring the global magnetic field of the solar corona remains exceptionally challenging. The fine-scale density structures observed in white light images taken during Total Solar Eclipses (TSEs) are currently the best proxy for inferring the magnetic field direction in the corona from the solar limb out to several solar radii ( $R_s$ ). We present, for the first time, the topology of the coronal magnetic field continuously between 1 and 6  $R_s$ , as quantitatively inferred with the Rolling Hough Transform (RHT) for 14 unique eclipse coronae that span almost two complete solar cycles. We find that the direction of the coronal magnetic field does not become radial until at least 3  $R_s$ , with a high variance between 1.5 and 3  $R_s$  at different latitudes and phases of the solar cycle. We find that the most non-radial coronal field topologies occur above regions with weaker magnetic field strengths in the photosphere, while stronger photospheric fields are associated with highly radial field lines in the corona. In addition, we find an abundance of field lines which extend continuously from the solar surface out to several solar radii at all latitudes, regardless of the presence of coronal holes. These results have implications for testing and constraining coronal magnetic field models, and for linking in situ solar wind measurements to their sources at the Sun.

**Table 1:** Observing dates, locations and observers for the TSE data used in this work (2001-2019)

### **Would the Sun's photosphere be negatively charged and magnetised ?**

Véronique [Bommier](#)  
A&A 2019

<https://arxiv.org/pdf/1907.06476.pdf>

In an observation review published in Solar Physics in 2018, H. Balthasar shows that observations with different telescopes, spectral lines and interpretation methods all agree about a vertical magnetic field gradient in solar active regions on the order of 3 G/km, when the horizontal magnetic field gradient is found of 0.3 G/km only. This represents an inexplicable discrepancy with respect to the  $\text{div}B=0$  law. The objective of this paper is to explain these observations through the law  $B=\mu_0(H+M)$  in magnetised media. Magnetisation is due to the plasma diamagnetism, which results from the spiral motion of free electrons or charges about the magnetic field. Their usual photospheric densities lead to very weak magnetisation  $M$ , four orders of magnitude smaller than  $H$ . It is then assumed that electrons escape from the solar interior, where their thermal velocity is much larger than the escape velocity, and accumulate in the photosphere where they are slowed down by the charge-dipole interaction with the neutral Hydrogen atoms. By evaluating the magnetic energy of the microscopic atom embedded in the magnetised medium obeying the macroscopic law  $B=\mu_0(H+M)$ , it is shown that the Zeeman hamiltonian is due to the effect of  $H$ . Thus, what is measured is  $H$ . The decrease of the density with height is responsible for non-zero divergence of  $M$ , which is compensated for by the divergence of  $H$ , in order to ensure  $\text{div}B=0$ . The behavior of the observed quantities is recovered. The problem of the divergence of the observed magnetic field in solar active regions finally reveals evidence of electron accumulation in the solar photosphere. This is not the case of the heavier protons, which remain in lower layers. Electric field would thus be present in the solar interior, but as the total charge remains negligible, no electric field or effect would result outside the star.

## Milne-Eddington inversion for unresolved magnetic structures in the quiet-Sun photosphere†

Véronique [Bommier](#)

JGR Volume 121, Issue 6 June 2016 Pages 5025–5040 **2016**

This paper is first devoted to present our method for modeling unresolved magnetic structures in the Milne-Eddington inversion of spectropolarimetric data. The related definitions and other approaches and different used inversion algorithms, are recalled for comparison. In a second part, we apply our method to quiet sun data outside active regions. We obtain the quiet sun photospheric magnetic field as comprised of unresolved opening and connected magnetic fluxtubes, which form a loop carpet of field lines. We then analyze the spatial correlation, which we also observed for the magnetic field vector, in terms of fluxtube diameter, distance and field strength. We find that different observations with the ZIMPOL and THEMIS polarimeters mounted on the THEMIS telescope give very close results, and we add results also very close derived from HINODE/SOT/SP observations analyzed with the same method. We obtain a mean fluxtube diameter of 30 km, a mean fluxtube distance of 230 km and a mean fluxtube magnetic field of 1.3 kG.

## Electromagnetism in a strongly stratified plasma showing an unexpected effect of the Debye shielding

Véronique [Bommier](#)

Comptes Rendus Physique, Volume 15, Issue 5, May **2014**, Pages 430–440

<http://www.sciencedirect.com/science/article/pii/S1631070514000462>

In the literature, we found 15 references showing, without exception, that the sunspot photospheric magnetic field vertical gradient is on the order of 3–4 G/km, with field strength decreasing with height, whereas the horizontal gradient is nine times weaker, on the order of 0.4–0.5 G/km. This is confirmed by our recent THÉMIS observations. As a consequence, the vanishing of  $\text{div}\rightarrow\mathbf{B}$  is not realized, and the present paper is devoted to the investigation of this problem. We point out that the photosphere is a strongly stratified plasma, having different horizontal and vertical characteristic lengths of aspect ratio 1/9 as the different terms contributing to the observed  $\text{div}\rightarrow\mathbf{B}$ . The velocities are also anisotropic under the stratification effect. As a consequence, the Debye volume is a flattened sphere. We show that in this case  $\text{div}\rightarrow\mathbf{B}$  may mathematically depart from zero. Anisotropic shielding constitutes an alternative to the existence of monopoles for being responsible for non-zero  $\text{div}\rightarrow\mathbf{B}$ . We evaluate that the solar corona is conversely not a strongly stratified plasma, so that the conditions are very different there.

## A potential magnetic field calculator for solar physics applications using staggered grids

Callum M. [Boocock](#), [David Tsiklauri](#)

A&A **2019**

<https://arxiv.org/pdf/1903.10546.pdf>

A program has been designed for accurately generating a potential magnetic field on a staggered grid by extrapolating the magnetic field normal to the photospheric surface. The code first calculates a magnetic potential using the Green's function method and then uses a finite differencing scheme to calculate the magnetic field from the potential. A new finite differencing formula was derived which accounts for grid staggering, it is shown that this formula gives a numerical approximation that is closest to the real potential field. It is also shown that extending the region over which normal photospheric field is specified can improve the accuracy of the potential field produced. The program is a FORTRAN 90 code that can be used to generate potential magnetic field inputs for Lare3d and other MHD solvers that use a staggered grid for magnetic field components. The program can be parallelised to run quickly over multiple computing cores. The code and supporting description are provided alongside this paper and can also be found at [this https URL](#) \\_Field\\_ Calculator.

## Penumbral thermal structure below the visible surface

J.M. [Borrero](#), M. Franz, R. Schlichenmaier, [M. Collados](#), [A. Asensio Ramos](#)

A&A **2017**

<https://arxiv.org/pdf/1705.02832.pdf>

Context. The thermal structure of the penumbra below its visible surface (i.e.,  $\tau_5 \geq 1$ ) has important implications for our present understanding of sunspots and their penumbrae: their brightness and energy transport, mode conversion of magneto-acoustic waves, sunspot seismology, and so forth. Aims. We aim at determining the thermal stratification in the layers immediately beneath the visible surface of the penumbra:  $\tau_5 \in [1, 3]$  ( $\approx 70$ – $80$  km below the visible continuum-forming layer). Methods. We analyzed spectropolarimetric data (i.e., Stokes profiles) in three Fe  $\lambda_{\text{textsc{i}}$  lines located at 1565 nm observed with the GRIS instrument attached to the 1.5-meter solar telescope GREGOR. The data are corrected for the smearing effects of wide-angle scattered light and then subjected to an inversion code for the radiative transfer equation in order to retrieve, among others, the temperature as a function of optical depth  $T(\tau_5)$ . Results. We find that the temperature gradient below the visible surface of the penumbra is

smaller than in the quiet Sun. This implies that in the region  $\tau_5 \geq 1$  the penumbral temperature diverges from that of the quiet Sun. The same result is obtained when focusing only on the thermal structure below the surface of bright penumbral filaments. We interpret these results as evidence of a thick penumbra, whereby the magnetopause is not located near its visible surface. In addition, we find that the temperature gradient in bright penumbral filaments is lower than in granules. This can be explained in terms of the limited expansion of a hot upflow inside a penumbral filament relative to a granular upflow, as magnetic pressure and tension forces from the surrounding penumbral magnetic field hinder an expansion like this.

## **Deep probing of the photospheric sunspot penumbra: no evidence for magnetic field-free gaps**

J.M. [Borrero](#), A. Asensio Ramos, M. Collados, [R. Schlichenmaier](#), [H. Balthasar](#), [M. Franz](#), [R. Rezaei](#), [C. Kiess](#), [D. Orozco Suarez](#), [A. Pastor](#), [T. Berkefeld](#), [O. von der Luehe](#), [D. Schmidt](#), [W. Schmidt](#), [M. Sigwarth](#), [D. Soltau](#), [R. Volkmer](#), [T. Waldmann](#), [C. Denker](#), [A. Hofmann](#), [J. Staude](#), [K.G. Strassmeier](#), [A. Feller](#), [A. Lagg](#), [S.K. Solanki](#), [M. Sobotka](#), [H. Nicklas](#)

A&A 2016

<http://arxiv.org/pdf/1607.08165.pdf>

Some models for the topology of the magnetic field in sunspot penumbrae predict the existence of field-free or dynamically weak-field regions in the deep Photosphere. To confirm or rule out the existence of weak-field regions in the deepest photospheric layers of the penumbra. The magnetic field at  $\log \tau_5 = 0$  is investigated by means of inversions of spectropolarimetric data of two different sunspots located very close to disk center with a spatial resolution of approximately 0.4-0.45 arcsec. The data have been recorded using the GRIS instrument attached to the 1.5-meters GREGOR solar telescope at El Teide observatory. It includes three Fe I lines around 1565 nm, whose sensitivity to the magnetic field peaks at half a pressure-scale-height deeper than the sensitivity of the widely used Fe I spectral line pair at 630 nm. Prior to the inversion, the data is corrected for the effects of scattered light using a deconvolution method with several point spread functions. At  $\log \tau_5 = 0$  we find no evidence for the existence of regions with dynamically weak ( $B < 500$  Gauss) magnetic fields in sunspot penumbrae. This result is much more reliable than previous investigations done with Fe I lines at 630 nm. Moreover, the result is independent of the number of nodes employed in the inversion, and also independent of the point spread function used to deconvolve the data, and does not depend on the amount of straylight (i.e. wide-angle scattered light) considered.

## **Inferring the magnetic field vector in the quiet Sun**

### **II. Interpreting results from the inversion of Stokes profiles**

J. M. [Borrero](#)<sup>1</sup> and P. Kobel

A&A 547, A89 (2012)

In a previous paper, we argued that the inversion of Stokes profiles applied to spectropolarimetric observations of the solar internetwork yield unrealistically large values of the inclination of the magnetic field vector ( $\gamma$ ). This is because photon noise in Stokes Q and U are interpreted by the inversion code as valid signals, that leads to an overestimation of the transverse component  $B_{\perp}$ , thus the inclination  $\gamma$ . However, our study was based on the analysis of linear polarization signals that featured only uncorrelated noise. In this paper, we develop this idea further and study this effect in Stokes Q and U profiles that also show correlated noise. In addition, we extend our study to the three components of the magnetic field vector, as well as the magnetic filling factor  $\alpha$ . With this, we confirm the tendency to overestimate  $\gamma$  when inverting linear polarization profiles that, although non-zero, are still below the noise level. We also establish that the overestimation occurs mainly for magnetic fields that are nearly vertical  $\gamma \lesssim 20^\circ$ . This indicates that a reliable inference of the inclination of the magnetic field vector cannot be achieved by analyzing only Stokes I and V. In addition, when inverting Stokes Q and U profiles below the noise, the inversion code retrieves a randomly uniform distribution of the azimuth of the magnetic field vector  $\phi$ . To avoid these problems, we propose only inverting Stokes profiles for which the linear polarization signals are sufficiently above the noise level. However, this approach is also biased because, in spite of allowing for a very accurate retrieval of the magnetic field vector from the selected Stokes profiles, it selects only profiles arising from highly inclined magnetic fields.

## **Semi-empirical model atmospheres for the chromosphere of the sunspot penumbra and umbral flashes**

Souvik [Bose](#), [Vasco M. J. Henriques](#), [Luc Rouppe van der Voort](#), [Tiago M.D. Pereira](#)

A&A 627, A46 2019

<https://arxiv.org/pdf/1905.08264.pdf>

Context. The solar chromosphere and the lower transition region is believed to play a crucial role in the heating of the solar corona. Models that describe the chromosphere (and the lower transition region), accounting for its highly

dynamic and structured character are, so far, found to be lacking. This is partly due to the breakdown of complete frequency redistribution in the chromospheric layers and also because of the difficulty in obtaining complete sets of observations that adequately constrain the solar atmosphere at all relevant heights.

**Aims.** We aim to obtain semi-empirical model atmospheres that reproduce the features of the Mg II h&k line profiles that sample the middle chromosphere with focus on a sunspot. **Methods.** We use spectropolarimetric observations of the Ca II 8542 Å spectra obtained with the Swedish 1-m Solar Telescope (SST) and use NICOLE inversions to obtain semi-empirical model atmospheres for different features in and around a sunspot. These are used to synthesize Mg II h&k spectra using RH1.5D code, which we compare with observations taken with the Interface Region Imaging Spectrograph (IRIS).

**Results.** Comparison of the synthetic profiles with IRIS observations reveals that there are several areas, especially in the penumbra of the sunspot, where most of the observed Mg II h&k profiles are very well reproduced. In addition, we find that supersonic hot downflows, present in our collection of models in the umbra, lead to synthetic profiles that agree well with the IRIS Mg II h&k profiles, with the exception of the line core. **Conclusions.** We put forward and make available four semi-empirical model atmospheres. Two for the penumbra, reflecting the range of temperatures obtained for the chromosphere, one for umbral flashes, and a model representative of the quiet surroundings of a sunspot. These are available in electronic as well as in table formats. **29 April 2016**

## **On the variability of the solar mean magnetic field: contributions from various magnetic features on the surface of the Sun**

Souvik [Bose](#), [K. Nagaraju](#)

ApJ **862** 35 **2018**

<https://arxiv.org/pdf/1806.05291.pdf>

<http://sci-hub.tw/http://iopscience.iop.org/0004-637X/862/1/35/>

The solar mean magnetic field (SMMF) is referred to as the disc-averaged line-of-sight (LOS) magnetic field that also reflects the polarity imbalance of the magnetic field on the Sun. The origin of the SMMF has been debated over the past few decades, with one school of thought suggesting that the contribution to the SMMF is mostly due to the large scale magnetic field structure, also termed as the background magnetic field, whereas other and more recent studies have indicated that active regions have a major contribution to the observed SMMF. In this paper, we re-investigate the issue of the origin of the SMMF by decomposing the solar disk into plages, networks, sunspots and background regions, thereby calculating the variation in the observed SMMF due to each of these features. We have used full disk images from SDO/AIA recorded at 1600-Å, for earmarking plages, networks and background regions and 4500-Å, images for separating the sunspots. The LOS fields corresponding to each of these regions are estimated from the co-temporal SDO/HMI full disk magnetograms. The temporal variation of the SMMF shows a near one-to-one correspondence with that of the background field regions suggesting that they constitute the major component of the observed SMMF. A linear regression analysis based on the coefficient of determination shows that the background field dominates, and accounts for 89% of the variation in the SMMF whereas the magnetic field from the other features accounts for the rest 11%.

## **Role of the background regimes towards the Solar Mean Magnetic Field**

Souvik [Bose](#), [K Nagaraju](#)

Proceedings of IAU Symposium No. 340

**2018**

<https://arxiv.org/pdf/1805.11151.pdf>

The Solar Mean Magnetic Field (SMMF) is generally defined as disc-averaged line-of-sight (LOS) magnetic field on the sun. The role of active regions and the large-scale magnetic field structures (also called the background) has been debated over past few decades to understand whether the origin of SMMF is either due to the active regions or the background. In this paper, we have investigated the contribution of sunspots, plages, network regions and the background towards the SMMF using data from the SDO-AIA & HMI, and found that 83% of the SMMF is due to the background whereas the remaining 17% originates from the active and network regions.

## **Solar Active Region Magnetogram Image Dataset for Studies of Space Weather**

[Laura E. Boucheron](#), [Ty Vincent](#), [Jeremy A. Grajeda](#), [Ellery Wuest](#)

**2023**

<https://arxiv.org/pdf/2305.09492.pdf>

In this dataset we provide a comprehensive collection of magnetograms (images quantifying the strength of the magnetic field) from the National Aeronautics and Space Administration's (NASA's) Solar Dynamics Observatory (SDO). The dataset incorporates data from three sources and provides SDO Helioseismic and Magnetic Imager (HMI) magnetograms of solar active regions (regions of large magnetic flux, generally the source of eruptive events) as well as labels of corresponding flaring activity. This dataset will be useful for image analysis or solar physics research related to magnetic structure, its evolution over time, and its relation to solar flares. The dataset will be of interest to those researchers investigating automated solar flare prediction methods, including supervised and unsupervised machine learning (classical and deep), binary and multi-class classification, and regression. This

dataset is a minimally processed, user configurable dataset of consistently sized images of solar active regions that can serve as a benchmark dataset for solar flare prediction research.

See <http://jsoc.stanford.edu/ajax/exportdata.html>

### **Magnetic helicity reversal in the corona at small plasma beta**

[Philippe-A. Bourdin](#) (1), [Nishant K. Singh](#) (2,3), [Axel Brandenburg](#)

ApJ 2018

<https://arxiv.org/pdf/1804.04153.pdf>

Solar and stellar dynamos shed small-scale and large-scale magnetic helicity of opposite signs. However, solar wind observations and simulations have shown that some distance above the dynamo, both the small-scale and large-scale magnetic helicities have reversed signs. With realistic simulations of the solar corona above an active region now being available, we have access to the magnetic field and current density along coronal loops. We show that a sign reversal in the horizontal averages of the magnetic helicity occurs when the local maximum of the plasma beta drops below unity and the field becomes nearly fully force free. Hence, this reversal is expected to occur well within the solar corona and would not directly be accessible to in situ measurements with Parker Solar Probe or SolarOrbiter. We also show that the reversal is associated with subtle changes in the relative dominance of structures with positive and negative magnetic helicity.

### **Magnetic helicity from multipolar regions on the solar surface**

[Philippe-A. Bourdin](#) (1), [Axel Brandenburg](#)

ApJL 2018

<https://arxiv.org/pdf/1804.04160.pdf>

The emergence of dipolar magnetic features on the solar surface is an idealization. Most of the magnetic flux emergence occurs in complex multipolar regions. Here we show that the surface pattern of magnetic structures alone can reveal the sign of the underlying magnetic helicity in the nearly force-free coronal regions above. The sign of the magnetic helicity can be predicted to good accuracy by considering the three-dimensional position vectors of three spots on the sphere ordered by their relative strengths at the surface and compute from them the skew product. This product, which is a pseudo scalar, is shown to be a good proxy for the sign of the coronal magnetic helicity.

### **Plasma Beta Stratification in the Solar Atmosphere: A Possible Explanation for the Penumbra Formation**

Ph.-A. Bourdin

2017 ApJL 850 L29

<https://arxiv.org/pdf/1711.10965.pdf>

Plasma beta is an important and fundamental physical quantity in order to understand plasma dynamics, particularly in the context of magnetically active stars, because it tells about the domination of magnetic versus thermodynamic processes on the plasma motion. We estimate the value ranges of plasma beta in different regions within the solar atmosphere and we describe a possible mechanism that helps forming a penumbra. For that we evaluate data from a 3D magnetohydrodynamic model of the solar corona above a magnetically active region. We compare our results with previously established data that is based on magnetic field extrapolations and that was matched for some observations. Our model data suggest that plasma beta in the photosphere should be considered to be larger than unity outside of sunspots. However, in the corona we also find that the beta value range reaches lower than previously thought, which coincides with a recent observation. We present an idea based on a gravity-driven process in a high-beta regime that might be responsible for the formation of the penumbra around sunspot umbra, where the vertical field strength reaches a given threshold. This process would also explain counter-Evershed flows. Regarding the thermal and magnetic pressure within the mixed-polarity solar atmosphere, including non-vertical magnetic field and quiet regions, plasma beta may reach unity at practically any height from the photosphere to the outer corona.

### **Coronal energy input and dissipation in a solar active region 3D MHD model**

Philippe-A. Bourdin (1 and 2), Sven Bingert (3), Hardi Peter

A&A 2015

<http://arxiv.org/pdf/1507.03573v1.pdf>

Context. We have conducted a 3D MHD simulation of the solar corona above an active region in full scale and high resolution, which shows coronal loops, and plasma flows within them, similar to observations. Aims. We want to find the connection between the photospheric energy input by field-line braiding with the coronal energy conversion by Ohmic dissipation of induced currents. Methods. To this end we compare the coronal energy input and dissipation within our simulation domain above different fields of view, e.g. for a small loops system in the active region (AR) core. We also choose an ensemble of field lines to compare, e.g., the magnetic energy input to the heating per particle along these field lines. Results. We find an enhanced Ohmic dissipation of currents in the corona above areas that also have enhanced upwards-directed Poynting flux. These regions coincide with the regions where hot coronal loops within the AR core are observed. The coronal density plays a role in estimating the coronal



temperature due to the generated heat input. A minimum flux density of about 200 Gauss is needed in the photosphere to heat a field line to coronal temperatures of about 1 MK. Conclusions. This suggests that the field-line braiding mechanism provides the coronal energy input and that the Ohmic dissipation of induced currents dominates the coronal heating mechanism.

### **Compensating Faraday depolarization by magnetic helicity in the solar corona**

Axel [Brandenburg](#), Mohira B. Ashurova, [Sarah Jabbari](#)

ApJL **845** L15 **2017**

<https://arxiv.org/pdf/1706.09540.pdf>

A turbulent dynamo in spherical geometry with an outer corona is simulated to study the sign of magnetic helicity in the outer parts. In agreement with earlier studies, the sign in the outer corona is found to be opposite to that inside the dynamo. Line-of-sight observations of polarized emission are synthesized to explore the feasibility of using the local reduction of Faraday depolarization to infer the sign of helicity of magnetic fields in the solar corona. This approach was previously identified as an observational diagnostic in the context of galactic magnetic fields. Based on our simulations, we show that this method can be successful in the solar context if sufficient statistics is gathered by using averages over ring segments in the corona separately for the regions north and south of the solar equator.

### **On Sunspot and Starspot Lifetimes**

Stephen J. [Bradshaw](#), Patrick Hartigan

**2014** ApJ **795** 79

<http://arxiv.org/pdf/1409.4337v1.pdf>

We consider the lifetimes of spots on the Sun and other stars from the standpoint of magnetic diffusion. While normal magnetic diffusivity predicts lifetimes of sunspots that are too large by at least two orders of magnitude, turbulent magnetic diffusivity accounts for both the functional form of the solar empirical spot-lifetime relation and for the observed sunspot lifetimes, provided that the relevant diffusion length is the supergranule size. Applying this relation to other stars, the value of turbulent diffusivity depends almost entirely on supergranule size, with very weak dependence on other variables such as magnetic field strength and density. Overall, the best observational data for other stars is consistent with the extension of the solar relation provided that stellar supergranule sizes for some stars are significantly larger than they are on the Sun.

### **A global two-scale helicity proxy from $\pi$ -ambiguous solar magnetic fields**

Axel [Brandenburg](#)

ApJ **883** 119 **2019**

<https://arxiv.org/pdf/1906.03877.pdf>

<https://doi.org/10.3847/1538-4357/ab3ec0>

If the alpha effect plays a role in the generation of the Sun's magnetic field, the field should show evidence of magnetic helicity of opposite signs at large and small length scales. Measuring this faces two challenges: (i) in weak-field regions, horizontal field measurements are unreliable because of the  $\pi$  ambiguity, and (ii) one needs a truly global approach to computing helicity spectra in the case where one expects a sign reversal across the equator at all wavenumbers. Here we develop such a method using spin-2 spherical harmonics to decompose the linear polarization in terms of the parity-even and parity-odd E and B polarizations, respectively. Using simple one- and two-dimensional models, we show that the product of the spectral decompositions of E and B, taken at spherical harmonic degrees that are shifted by one, is a good proxy of the magnetic helicity. We then apply this method to the analysis of solar synoptic vector magnetograms, from which we extract a pseudo-polarization corresponding to a " $\pi$ -ambiguous" magnetic field, i.e., a magnetic field vector that has no arrow. We find opposite signs of the global helicity proxy for spherical harmonic degrees larger or smaller than around 10, which corresponds to an effective wavenumber of around  $0.014 \text{ Mm}^{-1}$ . We argue that our global two-scale helicity proxy constitutes a new powerful measure that is worth applying routinely and over many more synoptic vector magnetograms. It might also be applicable to stellar and Galactic polarization data.

### **Mean-field and direct numerical simulations of magnetic flux concentrations from vertical field**

A. [Brandenburg](#)<sup>1,2</sup>, O. Gressel<sup>1,3</sup>, S. Jabbari<sup>1,2</sup>, N. Kleeorin<sup>4,1,5</sup> and I. Rogachevskii

A&A **562**, A53 (**2014**)

<http://arxiv.org/pdf/1309.3547v3.pdf>

Context. Strongly stratified hydromagnetic turbulence has previously been found to produce magnetic flux concentrations if the domain is large enough compared with the size of turbulent eddies. Mean-field simulations (MFS) using parameterizations of the Reynolds and Maxwell stresses show a large-scale negative effective magnetic pressure instability and have been able to reproduce many aspects of direct numerical simulations (DNS) regarding growth rate, shape of the resulting magnetic structures, and their height as a function of magnetic field strength.

Unlike the case of an imposed horizontal field, for a vertical one, magnetic flux concentrations of equipartition strength with the turbulence can be reached, resulting in magnetic spots that are reminiscent of sunspots. Aims. We determine under what conditions magnetic flux concentrations with vertical field occur and what their internal structure is.

Methods. We use a combination of MFS, DNS, and implicit large-eddy simulations (ILES) to characterize the resulting magnetic flux concentrations in forced isothermal turbulence with an imposed vertical magnetic field. Results. Using DNS, we confirm earlier results that in the kinematic stage of the large-scale instability the horizontal wavelength of structures is about 10 times the density scale height. At later times, even larger structures are being produced in a fashion similar to inverse spectral transfer in helically driven turbulence. Using ILES, we find that magnetic flux concentrations occur for Mach numbers between 0.1 and 0.7. They occur also for weaker stratification and larger turbulent eddies if the domain is wide enough. Using MFS, the size and aspect ratio of magnetic structures are determined as functions of two input parameters characterizing the parameterization of the effective magnetic pressure. DNS, ILES, and MFS show magnetic flux tubes with mean-field energies comparable to the turbulent kinetic energy. These tubes can reach a length of about eight density scale heights. Despite being  $\leq 1\%$  equipartition strength, it is important that their lower part is included within the computational domain to achieve the full strength of the instability.

**Conclusions. The resulting vertical magnetic flux tubes are being confined by downflows along the tubes and corresponding inflow from the sides, which keep the field concentrated. Application to sunspots remains a viable possibility.**

## **THE CORONAL SOURCE OF EXTREME-ULTRAVIOLET LINE PROFILE ASYMMETRIES IN SOLAR ACTIVE REGION OUTFLOWS**

David H. [Brooks](#)<sup>1,3</sup> and Harry P. Warren

2012 ApJ 760 L5

High-resolution spectra from the Hinode EUV Imaging Spectrometer have revealed that coronal spectral line profiles are sometimes asymmetric, with a faint enhancement in the blue wing on the order of  $100 \text{ km s}^{-1}$ . These asymmetries could be important since they may be subtle yet diagnostically useful signatures of coronal heating or solar wind acceleration processes. It has also been suggested that they are signatures of chromospheric jets supplying mass and energy to the corona. Until now, however, there have been no studies of the physical properties of the plasma producing the asymmetries. Here we identify regions of asymmetric profiles in the outflows of AR 10978 using an asymmetric Gaussian function and extract the intensities of the faint component using multiple Gaussian fits. We then derive the temperature structure and chemical composition of the plasma producing the asymmetries. We find that the asymmetries are dependent on temperature, and are clearer and stronger in coronal lines. The temperature distribution peaks around 1.4-1.8 MK with an emission measure at least an order of magnitude larger than that at 0.6 MK. The first ionization potential bias is found to be 3-5, implying that the high-speed component of the outflows may also contribute to the slow-speed wind. Observations and models indicate that it takes time for plasma to evolve to a coronal composition, suggesting that the material is trapped on closed loops before escaping, perhaps by interchange reconnection. The results, therefore, identify the plasma producing the asymmetries as having a coronal origin.

## **EUNIS Sees Pervasive Faint Fe XIX Emission: Evidence for Nanoflare Heating**

Jeff [Brosius](#)

RHESSI Science Nugget, No. 233, Aug 2014

[http://sprg.ssl.berkeley.edu/~tohban/wiki/index.php/RHESSI\\_Science\\_Nuggets](http://sprg.ssl.berkeley.edu/~tohban/wiki/index.php/RHESSI_Science_Nuggets)

Observations with the Extreme Ultraviolet Normal Incidence Spectrograph (EUNIS) sounding rocket instrument during its 2013 flight now have provided strong evidence for "nanoflare heating" as the explanation. **23 April 2013**

## **A Semi-Automatic Method to Measure the Rotation of Sunspots**

[Daniel Brown](#) & [Andrew Walker](#)

[Solar Physics](#) volume 296, Article number: 48 (2021)

<https://link.springer.com/content/pdf/10.1007/s11207-021-01787-4.pdf>

Sunspots have been observed to undergo rotation about their umbral centre. This is typically a slow rotation, with even the fastest sunspot rotations only reaching angular velocities of a few degrees per hour. This rotation may inject magnetic energy into the Sun's atmosphere, which can be stored in the coronal magnetic field and later released in eruptive events such as solar flares and coronal mass ejections. To usefully investigate rotating sunspots long periods of data need to be analysed, often of the order of several days, to build up a bulk rotation profile for the sunspot over time. This article outlines a semi-automated approach for analysing series of solar continuum data to extract the rotation profile of a sunspot as it transits across the solar disc. Moving towards an automated approach is vital for generating large, unbiased statistical samples of rotating sunspots in order to understand their contribution

to solar activity. Existing methods typically focus on sunspots near disc centre for short time periods, neglecting much of the rotation history of the sunspot. The method is tested on six sunspots observed in continuum data from the Helioseismic and Magnetic Imager (HMI) instrument on board the Solar Dynamics Observatory (SDO). These have been chosen to test the method for a range of different types of sunspots, including well-behaved sunspots, shape-changing sunspots, fast rotators, non-rotators, and interacting sunspots. The rotation profiles are compared by eye to animations of the sunspot from the data and are in acceptable visual agreement with the observed bulk rotation of the sunspot for all of the cases, except for the one which contains two sunspots in a shared penumbra. The method is also tested against sunspot rotations in active region (AR) 11158 that have been reported in the literature. While the results compare to some degree, the method outlined in this article reports lower rotations than those reported in the literature. Some of this discrepancy can be attributed to selection bias by the approaches in the literature, where only features that undergo larger rotation are tracked in sunspots that exhibit non-uniform rotation. The method also provides uncertainties on the calculated rotation profile which can be broken down to allow the principal sources of error to be identified. For the test sunspots in this article, the dominant source of uncertainty is the resolution of the SDO/HMI instrument. **17-25 Jan-2011, 14-20 Jun-2013, 6-15 Sep-2014, 24-30 Sep-2015**

## **Magnetism, dynamo action and the solar-stellar connection, Review**

**Brun**, A.S. & Browning, M.K.,

Living Rev Sol Phys (2017) 14: 4.

<https://link.springer.com/content/pdf/10.1007%2Fs41116-017-0007-8.pdf>

The Sun and other stars are magnetic: magnetism pervades their interiors and affects their evolution in a variety of ways. In the Sun, both the fields themselves and their influence on other phenomena can be uncovered in exquisite detail, but these observations sample only a moment in a single star's life. By turning to observations of other stars, and to theory and simulation, we may infer other aspects of the magnetism – e.g., its dependence on stellar age, mass, or rotation rate – that would be invisible from close study of the Sun alone. Here, we review observations and theory of magnetism in the Sun and other stars, with a partial focus on the “Solar-stellar connection”: i.e., ways in which studies of other stars have influenced our understanding of the Sun and vice versa. We briefly review techniques by which magnetic fields can be measured (or their presence otherwise inferred) in stars, and then highlight some key observational findings uncovered by such measurements, focusing (in many cases) on those that offer particularly direct constraints on theories of how the fields are built and maintained. We turn then to a discussion of how the fields arise in different objects: first, we summarize some essential elements of convection and dynamo theory, including a very brief discussion of mean-field theory and related concepts. Next we turn to simulations of convection and magnetism in stellar interiors, highlighting both some peculiarities of field generation in different types of stars and some unifying physical processes that likely influence dynamo action in general. We conclude with a brief summary of what we have learned, and a sampling of issues that remain uncertain or unsolved.

## **Recent Advances on Solar Global Magnetism and Variability Review**

A. S. **Brun**, M. K. Browning, M. Dikpati, H. Hotta, A. Strugarek

Space Science Reviews, Volume 196, Issue 1, pp 101-136 **2015**

We discuss recent observational, theoretical and numerical progress made in understanding the solar global magnetism and its short and long term variability. We discuss the physical process thought to be at the origin of the solar magnetic field and its 22-yr cycle, namely dynamo action, and the nonlinear interplay between convection, rotation, radiation and magnetic field, yielding modulations of the solar constant or of the large scale flows such as the torsional oscillations. We also discuss the role of the field parity and dynamo families in explaining the complex multipolar structure of the solar global magnetic field. We then present some key MHD processes acting in the deep radiative interior and discuss the probable topology of a primordial field there. Finally we summarize how helioseismology has contributed to these recent advances and how it could contribute to resolving current unsolved problems in solar global dynamics and magnetism.

## **The Dark Side of Penumbral Microjets: Observations in H $\alpha$**

D. **Buehler**, S. Esteban Pozuelo, J. de la Cruz Rodriguez, and G. B. Scharmer

**2019** ApJ 876 47

<https://arxiv.org/pdf/1905.01245.pdf>

We present data of 10 penumbral microjets (PMJs) observed in a H $\alpha$ , Ca ii 8542 Å, and Fe i 6302 Å line pair with the Swedish 1 m Solar Telescope (SST) with CRISP and Ca ii K with SST/CHROMIS in active region NOAA 12599 on **2016 October 12** at  $\mu = 0.68$ . All four Stokes parameters of the Ca ii 8542 Å and Fe i 6302 Å lines were observed and a series of test pixels were inverted using the Stockholm inversion code. Our analysis revealed for the first time that PMJs are visible in H $\alpha$ , where they appear as dark features with average line-of-sight (LOS) upflows of  $1.1 \pm 0.6$  km s $^{-1}$ , matching the LOS velocities from the inversions. Based on the H $\alpha$  observations we extend the previous average length and lifetime of PMJs to  $2815 \pm 530$  km and  $163 \pm 25$  s, respectively. The plane-of-sky (POS) velocities of our PMJs of up to 17 km s $^{-1}$  tend to give increased velocities with distance traveled.

Furthermore, two of our PMJs with significant Stokes V signal indicate that the PMJs possess an increased LOS magnetic field of up to 100 G compared to the local pre-/post- PMJ magnetic field, which propagates as quickly as the PMJs' POS velocities. Finally, we present evidence that PMJs display an on average 1 minute gradual precursory brightening that only manifests itself in the cores of the Ca II lines. We conclude that PMJs are not ordinary jets but likely are manifestations of heat fronts that propagate at the local Alfvén velocity.

### **Properties of solar plage from a spatially coupled inversion of Hinode SP data**

D. [Buehler](#), A. Lagg, S.K. Solanki, M. van Noort

2015 A&A

<http://arxiv.org/pdf/1501.01151v1.pdf>

The properties of magnetic fields forming an extended plage region in AR 10953 were investigated. Stokes spectra of the Fe I line pair at 6302 Å recorded by the spectropolarimeter aboard the Hinode satellite were inverted using the SPINOR code. The code performed a 2D spatially coupled inversion on the Stokes spectra, allowing the retrieval of gradients in optical depth within the atmosphere of each pixel, whilst accounting for the effects of the instrument's PSF. Consequently, no magnetic filling factor was needed. The inversion results reveal that plage is composed of magnetic flux concentrations (MFCs) with typical field strengths of 1520 G at  $\log(\tau)=-0.9$  and inclinations of 10-15 degrees. The MFCs expand by forming magnetic canopies composed of weaker and more inclined magnetic fields. The expansion and average temperature stratification of isolated MFCs can be approximated well with an empirical plage thin flux-tube model. The highest temperatures of MFCs are located at their edges in all  $\log(\tau)$  layers. Whilst the plasma inside MFCs is nearly at rest, each is surrounded by a ring of downflows of on average 2.4 km/s at  $\log(\tau)=0$  and peak velocities of up to 10 km/s, which are supersonic. The downflow ring of an MFC weakens and shifts outwards with height, tracing the MFC's expansion. Such downflow rings often harbour magnetic patches of opposite polarity to that of the main MFC with typical field strengths below 300 G at  $\log(\tau)=0$ . These opposite polarity patches are situated beneath the canopy of their main MFC. We found evidence of a strong broadening of the Stokes profiles in MFCs and particularly in the downflow rings surrounding MFCs (expressed by a microturbulence in the inversion). This indicates the presence of strong unresolved velocities. Larger magnetic structures such as sunspots cause the field of nearby MFCs to be more inclined. **30th of April 2007**

### **The Physics and Diagnostic Potential of Ultraviolet Spectropolarimetry Review**

Javier Trujillo [Bueno](#), Egidio Landi Degl'Innocenti, Luca Belluzzi

[Space Science Reviews](#) September 2017, Volume 210, [Issue 1-4](#), pp 183-226

The empirical investigation of the magnetic field in the outer solar atmosphere is a very important challenge in astrophysics. To this end, we need to identify, measure and interpret observable quantities sensitive to the magnetism of the upper chromosphere, transition region and corona. This paper provides an overview of the physics and diagnostic potential of spectropolarimetry in permitted spectral lines of the ultraviolet solar spectrum, such as the Mg I<sub>1</sub> and II<sub>1</sub> lines around 2800 Å, the hydrogen Lyman- $\alpha$  line at 1216 Å, and the Lyman- $\alpha$  line of He II at 304 Å. The outer solar atmosphere is an optically pumped vapor and the linear polarization of such spectral lines is dominated by the atomic level polarization produced by the absorption and scattering of anisotropic radiation. Its modification by the action of the Hanle and Zeeman effects in the inhomogeneous and dynamic solar atmosphere needs to be carefully understood because it encodes the magnetic field information. The circular polarization induced by the Zeeman effect in some ultraviolet lines (e.g., Mg I<sub>1</sub> & II<sub>1</sub>) is also of diagnostic interest, especially for probing the outer solar atmosphere in plages and more active regions. The few (pioneering) observational attempts carried out so far to measure the ultraviolet spectral line polarization produced by optically pumped atoms in the upper chromosphere, transition region and corona are also discussed. We emphasize that ultraviolet spectropolarimetry is a key gateway to the outer atmosphere of the Sun and of other stars.

### **THE HANLE EFFECT OF THE HYDROGEN Ly $\alpha$ LINE FOR PROBING THE MAGNETISM OF THE SOLAR TRANSITION REGION**

Javier Trujillo [Bueno](#)<sup>1,2,3</sup>, Jiří Štěpán<sup>1,2,5</sup> and Roberto Casini

2011 ApJ 738 L11

We present some theoretical predictions concerning the amplitude and magnetic sensitivity of the linear-polarization signals produced by scattering processes in the hydrogen Ly $\alpha$  line of the solar transition region. To this end, we have calculated the atomic-level polarization (population imbalances and quantum coherences) induced by anisotropic radiation pumping in semiempirical and hydrodynamical models of the solar atmosphere, taking into account radiative transfer and the Hanle effect caused by the presence of organized and random magnetic fields. The line-center amplitudes of the emergent linear-polarization signals are found to vary typically between 0.1% and 1%, depending on the scattering geometry and the strength and orientation of the magnetic field. The results shown here encourage the development of UV polarimeters for sounding rockets and space telescopes with the aim of opening up a diagnostic window for magnetic field measurements in the upper chromosphere and transition region of the Sun.

## Magnetic Connectivity in the Corona as a Source of Structure in the Solar Wind

B. L. [Burkholder](#) [A. Otto](#) [P. A. Delamere](#) [J. E. Borovsky](#)

JGR [Volume 124, Issue 1](#) January 2019 Pages 32-49

[sci-hub.tw/10.1029/2018JA026132](https://doi.org/10.1029/2018JA026132)

Five decades of satellite data confirm that the solar wind contains many boundaries separating flow with distinct magnetic and plasma properties. Some speculate the boundaries in the solar wind found at Earth originate at the solar surface and are carried along with the expanding solar wind as fossil structures to 1 AU. This begs the question, is it the physics and magnetic structure above the photosphere that creates well-defined boundaries between different magnetic flux regions at 1 AU in the solar wind? Magnetic boundaries in the corona exist all the time as topological features of null points in the field. These topological magnetic boundaries seem to be likely locations for plasma boundaries. It can be expected that these boundaries are typical locations where field line-integrated quantities, such as field-aligned current, experience large and abrupt changes. We perform three-dimensional resistive magnetohydrodynamic simulations of the solar corona driven by photospheric foot point motions. We find that large and abrupt changes occur for field line-integrated quantities across a magnetic topological boundary and the cause for these changes is the discontinuous mapping for magnetic field lines and thus for Alfvén waves across these boundaries. It is also demonstrated via in situ properties that thin layers of field-aligned and perpendicular currents are frequently located at or close to topological boundaries.

## Dynamic Three-Dimensional Tomography of the Solar Corona

M. D. [Butala](#) [✉](#), R. J. Hewett1 [✉](#), R. A. Frazin2 [✉](#) and F. Kamalabadi1

Solar Phys. 262(2), 495-509, 2010

Empirical, three-dimensional electron-density maps of the solar corona can be tomographically reconstructed using polarized-brightness images measured from ground- and space-based observatories. Current methods for computing these reconstructions require the assumption that the structure of the corona is unchanging with time. We present the first global reconstructions that do away with this static assumption and, as a result, allow for a more accurate empirical determination of the dynamic solar corona. We compare the new dynamic reconstructions of the coronal density during February 2008 to a sequence of static reconstructions. We find that the new dynamic reconstructions are less prone to certain computational artifacts that may plague the static reconstructions. In addition, these benefits come without a significant increase in computational cost.

## Relationships Between Physical Parameters of Umbral Dots Measured for 12 Sunspot Umbrae with the Goode Solar Telescope

[M. Ali Calisir](#), [H. Tayfun Yazici](#), [Ali Kilcik](#) & [Vasyl Yurchyshyn](#)

[Solar Physics](#) volume 298, Article number: 103 (2023)

<https://doi.org/10.1007/s11207-023-02198-3>

We present a comprehensive analysis of the physical parameters and relationships of umbral dots (UDs), which assists in our understanding of the physical properties of the Sun. This study is based on a detailed analysis of UD detected in 12 umbrae belonging to 10 different sunspots using high-resolution data recorded by the Goode Solar Telescope at Big Bear Solar Observatory. We obtained the physical parameters (total intensity, diameter, eccentricity, lifetime, and dynamic velocity) of each UD and calculated correlation coefficients using linear and nonlinear approaches to reveal the relationships between these parameters. We found that: i) The diameter of UD vary between 92.2 km and 246.5 km, the eccentricity varies between 0.02 and 0.65, the lifetimes of UD vary from 0.75 to 120.00 min and the dynamic velocities vary from 0.01 km s<sup>-1</sup> to 3.80 km s<sup>-1</sup>. ii) The intensity–diameter and diameter–eccentricity relationships show the highest degree of correlation, while the lowest linear correlation was obtained for the diameter–lifetime relationship and the lowest nonlinear correlation was obtained for the eccentricity–lifetime relationship. iii) In general, the nonlinear correlation coefficients are higher than the linear correlation without exception. iv) The linear and nonlinear correlation coefficients are very close to each other in the case of the diameter–eccentricity relation. v) While the average diameter, intensity, and eccentricity are related to the umbral area, the average lifetime and dynamic velocity of UD are not dependent on the umbral area.

## A semi-automated method to reveal the evolution of each sunspot group in a solar cycle

Hikmet [Çakmak](#)

Astrophysics and Space Science

2018

<https://arxiv.org/pdf/1811.12648.pdf>

Sunspots are the most important indicator of the magnetic activity on the solar surface during a cycle. Every sunspot group is formed and shaped by the magnetic field of the Sun. Hence, the magnetic field intensity shows itself as the size of a sunspot group area on the surface. This shows that getting the development or evolution of sunspot groups over time means getting the change of magnetic field intensity during same interval. Here, to reveal the evolution of sunspot groups in a cycle, a method called Solar Cycle Analyzer Tool (SCAT) is presented. This method was

developed as a part of Computer-Aided Measurements for Sunspots (CAMS) because the same subroutines and subprograms were used for calculations (Cakmak 2014). The developed software tracks sunspot groups every day and gives them the same group number. The confirmation is made by the user to prevent counting re-formations as a continuation of an old group in the same active region. With this method, the evolution of every sunspot group can be listed for each cycle year besides other cycle features like the daily and monthly sunspot relative numbers and distribution frequency of the sunspot group types. Since 2015, SCAT is being used to get data for the annual reports of Istanbul University Observatory.

## **Computer-aided measurement of the heliographic coordinates of sunspot groups**

H. [Cakmak](#)

Experimental Astronomy, 2014

Heliographic coordinates are used to identify the positions of solar features, especially the sunspot groups on the Sun's surface. Tracking the positions of sunspot groups provides information about solar rotation and the movement behavior of sunspot groups over Solar Cycles. Two heliographic coordinates are defined: Carrington and Stonyhurst. The calculations used here depend on three solar parameters, position angle P, latitude angle  $B_0$  and the starting longitude  $L_0$ . These values are calculated by using Astronomical Almanac for the observation time. In this study, a computer program called Computer Aided Measurement for Sunspots (CAMS) is presented. The main aim of the program is to determine the heliographic latitude and longitude of the sunspot groups besides other features like the latitudinal and longitudinal length, rectangular area and the tilt angle. This is accomplished by generating the corresponding Stonyhurst disk for the P and  $B_0$  angles of the time of observation and superimposing it onto the scanned drawing. Since 2009, CAMS is being used to process daily solar drawings at the Istanbul University Observatory.

## **A digital method to calculate the true areas of sunspot groups**

H. [Cakmak](#)

<http://arxiv.org/pdf/1403.7418v1.pdf>

The areas of sunspots are the most prominent feature of the development of sunspot groups. Since the size of sunspot areas depend on the strength of the magnetic field, accurate measurements of these areas are important. In this study, a method which allows to measure true areas of the sunspots is introduced. A Stonyhurst disk is created by using a computer program and is coincided with solar images. By doing this, an accurate heliographic coordinate system is formed. Then, the true area of the whole sunspot group is calculated in square degrees with the aid of the heliographic coordinates of each picture element forming the image of the sunspot group. This technique's use is not limited with sunspot areas only. The areas of the flare and filaments observed on the chromospheric disk can also be calculated with the same method. In addition to this, it is possible to calculate the area of any occurrence on the solar disk, whether it is related to an activity or not.

## **The relationship between flux emergence and subsurface toroidal magnetic flux**

Robert [Cameron](#), [Jie Jiang](#)

A&A 631, A27 2019

<https://arxiv.org/pdf/1909.06828.pdf>

<https://doi.org/10.1051/0004-6361/201834852>

The 1-D mean-field equation describing the evolution of the subsurface toroidal field can be used together with the observed surface radial field to model the subsurface toroidal flux density. We aim to test this model and determine the relationship between the observationally inferred surface toroidal field (as a proxy for flux emergence), and the modelled subsurface toroidal flux density. We use a combination of sunspot area observations, the surface toroidal field inferred from WSO line-of-sight magnetic field observations, and compare with the results of a 1-D mean-field evolution equation for the subsurface toroidal field, driven by the observed radial field from the National Solar Observatory/Kitt Peak and SOLIS observations. We derive calibration curves relating the subsurface toroidal flux density to the observed surface toroidal field strengths and sunspot areas. The calibration curves are for two regimes, one corresponding to ephemeral region emergence outside of the butterfly wings, the other to active region emergence in the butterfly wings. We discuss this in terms of the size and vertical velocity associated with the two types of flux emergence.

## **Magnetic field line tangling and twisting in the corona**

Simon [Candelaresi](#), David Pontin, Gunnar Hornig (Dundee), Anthony Yeates (Durham), Paul Bushby (Newcastle).

**UKSP Nugget: 91, June 2018**

<http://www.uksolphys.org/uksp-nugget/91-magnetic-field-line-tangling-and-twisting-in-the-corona/>

Plasma motions on the Sun's photosphere can lead to tangling of the coronal magnetic field lines that are rooted there. The high tangling can generate thin current layers, potential sites of magnetic field reconnection and energy conversion. Here we study the field line tangling induced by these photospheric motions.

## **Spatiotemporal Evolution of Hanle and Zeeman Synthetic Polarization in a Chromospheric Spectral Line**

E. S. **Carlin** and M. Bianda

2017 ApJ 843 64

<http://sci-hub.cc/10.3847/1538-4357/aa7800>

Due to the quick evolution of the solar chromosphere, its magnetic field cannot be inferred reliably without accounting for the temporal variations of its polarized light. This has been broadly overlooked in the modeling and interpretation of the polarization, due to technical problems (e.g., lack of temporal resolution or of time-dependent MHD solar models) and/or because many polarization measurements can apparently be explained without dynamics. Here, we show that the temporal evolution is critical for explaining the spectral-line scattering polarization because of its sensitivity to rapidly varying physical quantities and the possibility of signal cancellations and attenuation during extended time integration. For studying the combined effect of time-varying magnetic fields and kinematics, we solved the 1.5D non-LTE problem of the second kind in time-dependent 3D R-MHD solar models and synthesized the Hanle and Zeeman polarization in forward scattering for the chromospheric  $\lambda 4227$  line. We find that the quiet-Sun polarization amplitudes depend on the periodicity and spectral coherence of the signal enhancements produced by kinematics, but that substantially larger linear polarization signals should exist all over the solar disk for short integration times. The spectral morphology of the polarization is discussed as a combination of Hanle, Zeeman, partial redistribution and dynamic effects. We give physical references for observations by degrading and characterizing our slit time series in different spatiotemporal resolutions. The implications of our results for the interpretation of the second solar spectrum and for the investigation of the solar atmospheric heatings are discussed.

## **Time evolution of Hanle and Zeeman polarization in MHD models**

E.S. **Carlin**

Solar Workshop Polarization 8

2016

<https://arxiv.org/pdf/1612.05091v1.pdf>

Exposing the polarization signatures of the solar chromosphere requires studying its temporal variations, which is rarely done when modelling and interpreting scattering and Hanle signals. The present contribution sketches the scientific problem of solar polarization diagnosis from the point of view of the temporal dimension, remarking some key aspects for solving it. Our time-dependent calculations expose the need of considering dynamics explicitly when modelling and observing scattering polarization in order to achieve effective diagnosis techniques as well as a deeper knowledge of the second solar spectrum.

## **A New Approach to Calculate Coronal Electron Density: Simplified van de Hulst's Method**

**Hikmet Cakmak**

Physics and Astronomy Reports 2023

<https://arxiv.org/pdf/2310.14903.pdf>

Determining the electron density is a challenging task in solar corona studies, as it requires certain assumptions to be made, such as symmetric, homogeneous and radial distribution, thermal equilibrium, etc. In such studies, the observed K corona brightness is based on the coronal electron density. An important paper on the calculation of electron density was published in 1950 by van de Hulst in an article titled "The Electron Density of the Solar Corona". The author developed a method with some assumptions to calculate the electron density from the observed K corona brightness. We presented here, a new simplified calculation method for the coronal electron density is presented. The integral equation solution given by van de Hulst is interpreted from a different perspective and the K coronal electron density is calculated using only observational data without making any additional adjustments such as successive approximations and multiple attempts.

## **A Curious History of Sunspot Penumbrae: An Update**

V.M.S. **Carrasco**, **J.M. Vaquero**, **R.M. Trigo**, **M.C. Gallego**

Solar Phys.

2018

<https://arxiv.org/ftp/arxiv/papers/1807/1807.03017.pdf>

The ratio of penumbral to umbral area of sunspots is an important topic for solar and geophysical studies. Hathaway (Solar Physics, 286, 347, 2013) found a curious behaviour in this parameter for small sunspot groups (areas smaller than 100 millionths of solar hemisphere, msh) using records from Royal Greenwich Observatory (RGO). Hathaway

showed that penumbra-umbra ratio decreased smoothly from more than 7 in 1905 to lower than 3 by 1930 and then increased to almost 8 in 1961. Thus, Hathaway proposed the existence of a secular variation in the penumbra-umbra area ratio. In order to confirm that secular variation, we employ data of the sunspot catalogue published by the Coimbra Astronomical Observatory (COI) for the period 1929-1941. Our results disagree with the penumbra-umbra ratio found by Hathaway for that period. However, the behaviour of this ratio for large (areas greater or equal than 100 msh) and small groups registered in COI during 1929-1941 is similar to data available from RGO for the periods 1874-1914 and 1950-1976. Nevertheless, while the average values and time evolution of the ratio in large groups is similar to the ratio for small groups according to Coimbra data (1929-1941) it is not analogous for RGO data for the same period. We also found that the behaviour of the penumbra-umbra area ratio for smaller groups in both observatories is significantly different. The main difference between the area measurements made in Coimbra and RGO is associated with the umbra measurements. We would like to stress that the two observatories used different methods of observation and while in COI both methodology and instruments did not change during the study period, some changes were carried out in RGO that could have affected measurements of umbra and penumbra. These facts illustrate the importance of the careful recovery of past solar data.

### **Sunspot Catalogue of the Valencia Observatory (1920-1928)**

V.M.S. [Carrasco](#), J.M. Vaquero, A.J.P. Aparicio, M.C. Gallego

Solar Physics, Volume 289, Issue 11, pp 4351-4364 2014

<http://arxiv.org/pdf/1407.5315v1.pdf>

A sunspot catalogue was maintained by the Astronomical Observatory of Valencia University (Spain) from 1920 to 1928. Here we present a machine-readable version of this catalogue (OV catalog or OVc), including a quality control analysis. Sunspot number (total and hemispheric) and sunspot area series are constructed using this catalogue. The OV catalog's data are compared with other available solar data, demonstrating that the present contribution provides the scientific community with a reliable catalogue of sunspot data.

### **Comparison of automatic methods to detect sunspots in the Coimbra Observatory spectroheliograms**

S. [Carvalho](#), [S. Gomes](#), [T. Barata](#), [A. Lourenco](#), [N. Peixinho](#)

Astronomy and Computing 2020

<https://arxiv.org/pdf/2002.04270.pdf>

The Astronomical Observatory of the University of Coimbra has a huge collection of solar images, acquired daily since 1926. From the beginning, only spectroheliograms in the CaIIK line has been recorded, and since 1989 in the H<sub>α</sub> line also. Such dataset requires efficient tools to detect and analyze solar activity features. The objective of this work is to create a tool that allows to automatic detect sunspots, umbra, and penumbra, that can be applied to the entire dataset. To achieve this, two different approaches have been developed, one based on mathematical morphology and another based on the intensities of the digital levels of the pixels. Both approaches were applied to a subset of images with features identified visually by an experimented solar observer. The performance of both methods was compared through the metrics Precision, Recall and F-score. Another evaluation was made based on the catalogs from Heliophysics Features Catalog and the SILSO catalogue.

### **The polarization angle in the wings of Ca I 4227: A new observable for diagnosing unresolved photospheric magnetic fields**

[Emilia Capozzi](#), [Ernest Alsina Ballester](#), [Luca Belluzzi](#), [Javier Trujillo Bueno](#)

A&A 657, A44 2022

<https://arxiv.org/pdf/2111.08967.pdf>

<https://www.aanda.org/articles/aa/pdf/2022/01/aa40753-21.pdf>

<https://doi.org/10.1051/0004-6361/202140753>

When observed in quiet regions close to the solar limb, many strong resonance lines show conspicuous linear polarization signals, produced by scattering processes, with extended wing lobes. Recent studies indicate that, contrary to what was previously believed, the wing lobes are sensitive to the presence of relatively weak longitudinal magnetic fields through magneto-optical (MO) effects. We theoretically investigate the sensitivity of the scattering polarization wings of the Ca I 4227 Å line to the MO effects, and we explore its diagnostic potential for inferring information on the longitudinal component of the photospheric magnetic field. We calculate the intensity and polarization profiles of the Ca I 4227 Å line by numerically solving the problem of the generation and transfer of polarized radiation under non-local thermodynamic equilibrium conditions in one-dimensional semi-empirical models of the solar atmosphere, taking into account the joint action of the Hanle, Zeeman, and MO effects. We consider volume-filling magnetic fields as well as magnetic fields occupying a fraction of the resolution element. In contrast to the circular polarization signals produced by the Zeeman effect, we find that the linear polarization angle in the scattering polarization wings of Ca I 4227 presents a clear sensitivity, through MO effects,



not only to the flux of the photospheric magnetic field, but also to the fraction of the resolution element that the magnetic field occupies. We identify the linear polarization angle in the wings of strong resonance lines as a valuable observable for diagnosing unresolved magnetic fields. Used in combination with observables that encode information on the magnetic flux and other properties of the observed atmospheric region, it can provide constraints on the filling factor of the magnetic field.

### **Magnetic Diagnostics of the Solar Corona: Synthesizing Optical and Radio Techniques**

R. [Casini](#), S. M. White, P. G. Judge

**Review**

[Space Science Reviews](#)

Volume 210, [Issue 1–4](#), pp 145–181

2017

DOI 10.1007/s11214-017-0400-6

In this contribution we review the current state-of-the-art of coronal magnetometry, in both optical and radio domains. We address the achievable objectives and the challenges of present measurement techniques and interpretation tools. In particular, we focus on the role that these observations can play for constraining and validating numerical models of the global coronal magnetic field. With regard to optical techniques, we mainly focus on the use of M1 diagnostics, further developing the theory of the formation of their polarization signatures in the magnetized corona.

### **Magnetic Energy Powers the Corona: How We Can Understand its 3D Storage & Release**

[Amir Caspi](#), [Daniel B. Seaton](#), [Roberto Casini](#), [Cooper Downs](#), [Sarah E. Gibson](#), [Holly Gilbert](#), [Lindsay Glesener](#), [Silvina E. Guidoni](#), [J. Marcus Hughes](#), [David McKenzie](#), [Joseph Plowman](#), [Katharine K. Reeves](#), [Pascal Saint-Hilaire](#), [Albert Y. Shih](#), [Matthew J. West](#)

White paper to the Decadal Survey for Solar and Space Physics (Heliophysics) 2024-2033 2023

<https://arxiv.org/pdf/2305.17146.pdf>

The coronal magnetic field is the prime driver behind many as-yet unsolved mysteries: solar eruptions, coronal heating, and the solar wind, to name a few. It is, however, still poorly observed and understood. We highlight key questions related to magnetic energy storage, release, and transport in the solar corona, and their relationship to these important problems. We advocate for new and multi-point co-optimized measurements, sensitive to magnetic field and other plasma parameters, spanning from optical to  $\gamma$ -ray wavelengths, to bring closure to these long-standing and fundamental questions. We discuss how our approach can fully describe the 3D magnetic field, embedded plasma, particle energization, and their joint evolution to achieve these objectives.

### **The Helioseismic and Magnetic Imager (HMI) Vector Magnetic Field Pipeline: Optimization of the Spectral Line Inversion Code**

R. [Centeno](#), J. Schou, K. Hayashi, A. Norton, J.T. Hoeksema, Y. Liu, K.D. Leka, G. Barnes

Solar Phys., Volume 289, Issue 9, pp 3531-3547, 2014

<http://arxiv.org/pdf/1403.3677v1.pdf>

The Very Fast Inversion of the Stokes Vector (VFISV) is a Milne-Eddington spectral line inversion code used to determine the magnetic and thermodynamic parameters of the solar photosphere from observations of the Stokes vector in the 6173 Å Fe I line by the Helioseismic and Magnetic Imager (HMI) onboard the Solar Dynamics Observatory (SDO). We report on the modifications made to the original VFISV inversion code in order to optimize its operation within the HMI data pipeline and provide the smoothest solution in active regions. The changes either sped up the computation or reduced the frequency with which the algorithm failed to converge to a satisfactory solution. Additionally, coding bugs which were detected and fixed in the original VFISV release, are reported here.

### **Why Do Chromospheric Oscillations in Sunspot Umbrae Appear to Propagate Downward?**

Jongchul [Chae](#)<sup>3,1</sup>, Eun-Kyung Lim<sup>2</sup>, Kyeore Lee<sup>1</sup>, Hannah Kwak<sup>2</sup>, Kyoung-Sun Lee<sup>1</sup>, Juhyung Kang<sup>1</sup>, and Soosang Kang<sup>1</sup>

2023 ApJL 944 L52

<https://iopscience.iop.org/article/10.3847/2041-8213/acba7d/pdf>

Umbral oscillations constitute the most noticeable chromospheric feature of sunspot umbrae—large-amplitude oscillations of intensity (umbral flashes, if very strong) and line-of-sight velocity, with periods of about 3 minutes. These umbral oscillations are usually interpreted as acoustic waves propagating upward under the effect of gravity. However, there have been observational reports that intensity peaks tend to occur in downflowing phases of umbral oscillations, and this appears to be more compatible with downward propagation. We investigate whether this intensity–velocity correlation occurs persistently or not, by determining the vertical flux of the wave energy, based on H $\alpha$  line measurements of the temperature and velocity. As a result, we find that the wave flux is persistently negative in sunspot umbrae, confirming the discrepancy specified above. We attribute this discrepancy to the nonzero fluctuation of net radiative heating. We find that when this effect is taken into account in the energy equation, the pressure is peaked during upflowing phases, being compatible with the notion of upward propagation.

We conclude that temperature (and intensity) peaks occur during downflowing phases, not because of downward propagation, but because of radiative heat transport. **2014 June 3**

### **Spectroscopic Detection of Alfvénic Waves in the Chromosphere of Sunspot Regions**

Jongchul **Chae**<sup>1</sup>, Kyuhyoun Cho<sup>1</sup>, Valery M. Nakariakov<sup>2,3</sup>, Kyung-Suk Cho<sup>4,5</sup>, and Ryun-Young Kwon<sup>4</sup>

**2021** ApJL 914 L16

<https://doi.org/10.3847/2041-8213/ac052b>

Transverse magnetohydrodynamic waves often called Alfvénic (or kink) waves have been often theoretically put forward to solve the outstanding problems of the solar corona like coronal heating, solar wind acceleration, and chemical abundance enhancement. Here we report the first spectroscopic detection of Alfvénic waves around a sunspot at chromospheric heights. By analyzing the spectra of the H $\alpha$  line and Ca ii 854.2 nm line, we determined line-of-sight velocity and temperature as functions of position and time. As a result, we identified transverse magnetohydrodynamic waves pervading the superpenumbral fibrils. These waves are characterized by the periods of 2.5 to 4.5 minutes, and the propagation direction parallel to the fibrils, the supersonic propagation speeds of 45 to 145 km s<sup>-1</sup>, and the close association with umbral oscillations and running penumbral waves in sunspots. Our results support the notion that the chromosphere around sunspots abounds with Alfvénic waves excited by the mode conversion of the upward-propagating slow magnetoacoustic waves.

### **Linear Acoustic Waves in a Nonisothermal Atmosphere. II. Photospheric Resonator Model of Three-minute Umbral Oscillations**

Jongchul **Chae**<sup>1</sup>, Juhyung Kang<sup>1</sup>, and Yuri E. Litvinenko<sup>2</sup>

**2019** ApJ 883 72

<https://doi.org/10.3847/1538-4357/ab3d2d>

The velocity oscillations observed in the chromosphere of sunspot umbrae resemble a resonance in that their power spectra are sharply peaked around a period of about three minutes. In order to describe the resonance that leads to the observed 3-minute oscillations, we propose the photospheric resonator model of acoustic waves in the solar atmosphere. The acoustic waves are driven by the motion of a piston at the lower boundary, and propagate in a nonisothermal atmosphere that consists of the lower layer (photosphere), where temperature rapidly decreases with height, and the upper layer (chromosphere), where temperature slowly increases with height. We have obtained the following results: (1) The lower layer (photosphere) acts as a leaky resonator of acoustic waves. The bottom end is established by the piston, and the top end by the reflection at the interface between the two layers. (2) The temperature minimum region partially reflects and partially transmits acoustic waves of frequencies around the acoustic cutoff frequency at the temperature minimum. (3) The resonance occurs in the photospheric layer at one frequency around this cutoff frequency. (4) The waves escaping the photospheric layer appear as upward-propagating waves in the chromosphere. The power spectrum of the velocity oscillation observed in the chromosphere can be fairly well reproduced by this model. The photospheric resonator model was compared with the chromospheric resonator model and the propagating wave model.

### **Photospheric Origin of Three-minute Oscillations in a Sunspot**

Jongchul **Chae**<sup>1</sup>, Jeongwoo Lee<sup>1</sup>, Kyuhyoun Cho<sup>1</sup>, Donguk Song<sup>1</sup>, Kyungsuk Cho<sup>2</sup>, and Vasyl Yurchyshyn<sup>2</sup>

**2017** ApJ 836 18

The origin of the three-minute oscillations of intensity and velocity observed in the chromosphere of sunspot umbrae is still unclear. We investigated the spatio-spectral properties of the 3 minute oscillations of velocity in the photosphere of a sunspot umbra as well as those in the low chromosphere using the spectral data of the Ni i  $\lambda$ 5436, Fe i  $\lambda$ 5435, and Na i D2  $\lambda$ 5890 lines taken by the Fast Imaging Solar Spectrograph of the 1.6 m New Solar Telescope at the Big Bear Solar Observatory. As a result, we found a local enhancement of the 3 minute oscillation power in the vicinities of a light bridge (LB) and numerous umbral dots (UDs) in the photosphere. These 3 minute oscillations occurred independently of the 5 minute oscillations. Through wavelet analysis, we determined the amplitudes and phases of the 3 minute oscillations at the formation heights of the spectral lines, and they were found to be consistent with the upwardly propagating slow magnetoacoustic waves in the photosphere with energy flux large enough to explain the chromospheric oscillations. Our results suggest that the 3 minute chromospheric oscillations in this sunspot may have been generated by magnetoconvection occurring in the LB and UD.

### **The Transient Neutral Flux in Plasma: An Explanation of Heating for the Solar Corona?**

Clifford **Chafin**

**2014**

<http://arxiv.org/pdf/1404.3923v1.pdf>

In this short note, we discuss a mechanism for the transport of energy, momentum and dipole moment via transient neutral carriers in plasma. This gives a way to rapidly convert bulk hydrodynamic flow energy into thermal energy over a distance of several mean free paths. In the transition region of the solar corona we estimate various processes and their potential to introduce the high energies needed to reach the  $2 \times 10^6 \text{K}$  observed there. It implies that kinetic methods may be essential for modeling the corona and that there are more gentle but still robust means than reconnection to relax magnetic fields in plasmas.

### **A study of sunspot 3 minute oscillations using ALMA and GST**

[Yi Chai](#), [Dale E. Gary](#), [Kevin P. Reardon](#), [Vasyl Yurchyshyn](#)

ApJ 2021

<https://arxiv.org/pdf/2111.05812.pdf>

Waves and oscillations are important solar phenomena, not only because they can propagate and dissipate energy in the chromosphere, but also because they carry information about the structure of the atmosphere in which they propagate. The nature of the three-minute oscillations observed in the umbral region of sunspots is considered to be an effect of propagation of magnetohydrodynamic (MHD) waves upward from below the photosphere. We present a study of sunspot oscillations and wave propagation in NOAA AR 12470 using an approximately one-hour long data set acquired on **2015 December 17** by the Atacama Large Millimeter/submillimeter Array (ALMA), the Goode Solar Telescope (GST) operating at the Big Bear Solar Observatory (BBSO), the Atmospheric Imaging Assembly (AIA) on board the Solar Dynamics Observatory (SDO), and the Interface Region Imaging Spectrograph (IRIS). The ALMA data are unique in providing a time-series of direct temperature measurements in the sunspot chromosphere. The two-second cadence of ALMA images allows us to well resolve the three-minute periods typical of sunspot oscillations in the chromosphere. Fourier analysis is applied to ALMA Band 3 ( $\sim 100 \text{ GHz}$ ,  $\sim 3 \text{ mm}$ ) and GST  $\text{H}\alpha$  data sets to obtain power spectra as well as oscillation phase information. We analysed properties of the wave propagation by combining multiple wavelengths that probe physical parameters of solar atmosphere at different heights. We find that the ALMA temperature fluctuations are consistent with that expected for a propagating acoustic wave, with a slight asymmetry indicating non-linear steepening.

### **THE THREE-DIMENSIONAL STRUCTURE OF AN ACTIVE REGION FILAMENT AS EXTRAPOLATED FROM PHOTOSPHERIC AND CHROMOSPHERIC OBSERVATIONS**

L. Yelles [Chaouche](#)<sup>1,2</sup>, C. Kuckein<sup>1,2</sup>, V. Martínez Pillet<sup>1,2</sup> and F. Moreno-Insertis

2012 ApJ 748 23

The three-dimensional structure of an active region filament is studied using nonlinear force-free field extrapolations based on simultaneous observations at a photospheric and a chromospheric height. To that end, we used the Si I 10827 Å line and the He I 10830 Å triplet obtained with the Tenerife Infrared Polarimeter at the Vacuum Tower Telescope (Tenerife). The two extrapolations have been carried out independently from each other and their respective spatial domains overlap in a considerable height range. This opens up new possibilities for diagnostics in addition to the usual ones obtained through a single extrapolation from, typically, a photospheric layer. Among those possibilities, this method allows the determination of an average formation height of the He I 10830 Å signal of 2 Mm above the surface of the Sun. It allows, as well, a cross-check of the obtained three-dimensional magnetic structures to verify a possible deviation from the force-free condition, especially at the photosphere. The extrapolations yield a filament formed by a twisted flux rope whose axis is located at about 1.4 Mm above the solar surface. The twisted field lines make slightly more than one turn along the filament within our field of view, which results in 0.055 turns  $\text{Mm}^{-1}$ . The convex part of the field lines (as seen from the solar surface) constitutes dips where the plasma can naturally be supported. The obtained three-dimensional magnetic structure of the filament depends on the choice of the observed horizontal magnetic field as determined from the  $180^\circ$  solution of the azimuth. We derive a method to check for the correctness of the selected  $180^\circ$  ambiguity solution.

### **Three-Minute Oscillations in Sunspot's Penumbrae and Superpenumbrae. Alfvénic or Sound?**

[Andrei Chelpanov](#), [Nikolai Kobanov](#)

Solar Phys. Volume 299, article number 139 2024

<https://arxiv.org/pdf/2409.15701>

In the immediate sunspots' vicinity -- their superpenumbra -- 3-minute line-of-sight (LOS) velocity oscillations dominate in the photosphere and chromosphere. Oscillations of similar periods are also registered in the transition region and lower corona above active regions. The goal of the work is to clarify whether these LOS velocity oscillations are manifestations of Alfvénic waves in the lower solar atmosphere. The study is based on three sunspots with the use of the Solar Dynamics Observatory data. Additional observations of a sunspot were carried out at ground-based Automated Solar Telescope. We use narrow-band frequency filtration (5.6--5.8 mHz) of the LOS velocity, magnetic field, and intensity signals of the Fe I 6173 Å spectral line. For the analysis, we used 90-minute long series. We come to the conclusion that the 3-minute oscillations in the LOS velocity signals result from

magnetoacoustic waves rather than from Alfvénic waves. However, oscillations registered in magnetic field signals indicate that Alfvénic waves may be present already in the photosphere. Further research requires simultaneous observations of LOS velocity, magnetic field strength, spectral line width, and intensity carried out at two heights of the solar atmosphere. **December 27, 2020, October 3, 2022, November 10, 2022**

### **Solar coronal magnetic field measurements using spectral lines available in Hinode/EIS observations: Strong and weak field techniques and temperature diagnostics**

[Yajie Chen](#), [Xianyong Bai](#), [Hui Tian](#), [Wenxian Li](#), [Feng Chen](#), [Zihao Yang](#), [Yang Yang](#)

MNRAS Volume 521, Issue 1, May 2023, Pages 1479–1488,

<https://doi.org/10.1093/mnras/stad583>

<https://arxiv.org/pdf/2302.10596.pdf>

Recently, it has been proposed that the magnetic-field-induced transition (MIT) in Fe X can be used to measure coronal magnetic field strengths. Several techniques, the direct line ratio technique and the weak and strong magnetic field techniques, are developed to apply the MIT theory to spectroscopic observations taken by EUV Imaging Spectrometer (EIS) onboard Hinode. However, the suitability of coronal magnetic field measurements based on the weak and strong magnetic field techniques has not been evaluated. Besides, temperature diagnostics is also important for measuring coronal magnetic field based on the MIT theory, but how to determine the accurate formation temperature of the Fe X lines from EIS observations still needs investigation. In this study, we synthesized emissions of several spectral lines from a 3D radiation magnetohydrodynamic model of a solar active region, and then derived magnetic field strengths using different methods. We first compared the magnetic field strengths derived from the weak and strong magnetic field techniques to the values in the model. Our study suggests that both weak and strong magnetic field techniques underestimate the coronal magnetic field strength. Then we developed two methods to calculate the formation temperature of the Fe X lines. One is based on differential emission measure analyses, and the other is deriving temperature from the Fe IX and Fe XI line pairs. However, neither of the two methods can provide temperature determination for accurate coronal magnetic field measurements as those derived from the Fe X 174/175 and 184/345 Å line ratios. More efforts are still needed for accurate coronal magnetic field measurements using EIS observations.

### **Radio Studies of the Middle Corona: Current State and New Prospects in the Next Decade**

Bin [Chen](#) (1), [Jason E. Kooi](#) (2), [David B. Wexler](#) (3), [Dale E. Gary](#) (1), [Sijie Yu](#) (1), [Surajit Mondal](#) (1), [Adam R. Kobelski](#) (4), [Daniel B. Seaton](#) (5), [Matthew J. West](#) (5), [Stephen M. White](#) (6), [Gregory D. Fleishman](#) (1), [Pascal Saint-Hilaire](#) (7), [Peijin Zhang](#) (8), [Chris R. Gilly](#) (9), [James P. Mason](#) (10), [Hamish Reid](#) (11)

Science white paper submitted to the 2024 Solar and Space Physics Decadal Survey. **2023**

All submitted white papers (including this one) are available at [this https URL](#).

<https://arxiv.org/pdf/2301.12183.pdf>

The "middle corona," defined by West et al. (2022) as the region between ~1.5-6 solar radii, is a critical transition region that connects the highly structured lower corona to the outer corona where the magnetic field becomes predominantly radial. At radio wavelengths, remote-sensing of the middle corona falls in the meter-decameter wavelength range where a critical transition of radio emission mechanisms occurs. In addition, plasma properties of the middle corona can be probed by trans-coronal radio propagation methods including radio scintillation and Faraday rotation techniques. Together they offer a wealth of diagnostic tools for the middle corona, complementing current and planned missions at other wavelengths. These diagnostics include unique means for detecting and measuring the magnetic field and energetic electrons associated with coronal mass ejections, mapping coronal shocks and electron beam trajectories, as well as constraining the plasma density, magnetic field, and turbulence of the "young" solar wind. Following a brief overview of pertinent radio diagnostic methods, this white paper will discuss the current state of radio studies on the middle corona, challenges to obtaining a more comprehensive picture, and recommend an outlook in the next decade. Our specific recommendations for advancing the middle coronal sciences from the radio perspective are: (1) Prioritizing solar-dedicated radio facilities in the ~0.1-1 GHz range with broadband, high-dynamic-range imaging spectropolarimetry capabilities. (2) Developing facilities and techniques to perform multi-perspective, multiple lines-of-sight trans-coronal radio Faraday Rotation measurements.

### **Inferring Maps of the Sun's Far-side Unsigned Magnetic Flux from Far-side Helioseismic Images using Machine Learning Techniques**

[Ruizhu Chen](#), [Junwei Zhao](#), [Shea Hess Webber](#), [Yang Liu](#), [J. Todd Hoeksema](#), [Marc L. Derosa](#)

ApJ **941** 197 **2022**

<https://arxiv.org/pdf/2211.12666.pdf>

<https://iopscience.iop.org/article/10.3847/1538-4357/aca333/pdf>

Accurate modeling of the Sun's coronal magnetic field and solar wind structures require inputs of the solar global magnetic field, including both the near and far sides, but the Sun's far-side magnetic field cannot be directly

observed. However, the Sun's far-side active regions are routinely monitored by helioseismic imaging methods, which only require continuous near-side observations. It is therefore both feasible and useful to estimate the far-side magnetic-flux maps using the far-side helioseismic images despite their relatively low spatial resolution and large uncertainties. In this work, we train two machine-learning models to achieve this goal. The first machine-learning training pairs simultaneous SDO/HMI-observed magnetic-flux maps and SDO/AIA-observed EUV 304Å images, and the resulting model can convert 304Å images into magnetic-flux maps. This model is then applied on the STEREO/EUVI-observed far-side 304Å images, available for about 4.3 years, for the far-side magnetic-flux maps. These EUV-converted magnetic-flux maps are then paired with simultaneous far-side helioseismic images for a second machine-learning training, and the resulting model can convert far-side helioseismic images into magnetic-flux maps. These helioseismically derived far-side magnetic-flux maps, despite their limitations in spatial resolution and accuracy, can be routinely available on a daily basis, providing useful magnetic information on the Sun's far side using only the near-side observations.

## **Variation of Vorticity Gradient and Formation of Sunspots**

[Haibin Chen](#), [Rong Wu](#)

2022

<https://arxiv.org/pdf/2212.03524.pdf>

Based on the rotating turbulent thermal convection model and using the rotating equivalent temperature assumption and new convection criterion, this paper analyzed the repression of the vorticity gradient on the heat transport and explained that the formation of sunspots originated from the variation of the vorticity gradient in the solar troposphere.

## **Application of a magnetic-field-induced transition in Fe X to solar and stellar coronal magnetic field measurements**

[Yajie Chen](#), [Wenxian Li](#), [Hui Tian](#), [Xianyong Bai](#), [Roger Hutton](#), [Tomas Brage](#)

Research in Astronomy and Astrophysics 2022

<https://arxiv.org/pdf/2212.02873>

Magnetic fields play a key role in driving a broad range of dynamic phenomena in the atmospheres of the Sun and other stars. Routine and accurate measurements of the magnetic fields at all the atmospheric layers are of critical importance to understand these magnetic activities, but in the solar and stellar coronae such a measurement is still a challenge due to the weak field strength and the high temperature. Recently, a magnetic-field-induced transition (MIT) of Fe X at 257.26 Å has been proposed for the magnetic field measurements in the solar and stellar coronae. In this review, we present an overview of recent progresses in the application of this method in astrophysics. We start by introducing the theory underlying the MIT method and reviewing the existing atomic data critical for the spectral modeling of Fe X lines. We also discuss the laboratory measurements that verify the potential capability of the MIT technique as a probe for diagnosing the plasma magnetic fields. We then continue by investigating the suitability and accuracy of solar and stellar coronal magnetic field measurements based on the MIT method through forward modeling. Furthermore, we discuss the application of the MIT method to the existing spectroscopic observations obtained by the Extreme-ultraviolet Imaging Spectrometer onboard Hinode. This novel technique provides a possible way for routine measurements of the magnetic fields in the solar and stellar coronae, but still requires further efforts to improve its accuracy. Finally, the challenges and prospects for future research on this topic are discussed.

## **Coronal Condensation as the Source of Transition Region Supersonic Downflows above a Sunspot**

[Hechao Chen](#), [Hui Tian](#), [Leping Li](#), [Hardi Peter](#), [Lakshmi Pradeep Chitta](#), [Zhenyong Hou](#)

A&A 659, A107 2022

<https://arxiv.org/pdf/2112.01354.pdf>

<https://doi.org/10.1051/0004-6361/202142093>

<https://www.aanda.org/articles/aa/pdf/2022/03/aa42093-21.pdf>

Plasma loops or plumes rooted in sunspot umbrae often harbor downflows with speeds of 100 km/s. These downflows are supersonic at transition region temperatures of 0.1 MK. The source of these flows is not well understood. We aim to investigate the source of sunspot supersonic downflows (SSDs) in AR 12740 using simultaneous spectroscopic and imaging observations. We identified SSD events from multiple raster scans of a sunspot by the Interface Region Imaging Spectrograph, and calculated the electron densities, mass fluxes and velocities of these SSDs. The EUV images provided by the AIA onboard the SDO and the EUVI onboard the STEREO were employed to investigate the origin of these SSDs and their associated coronal rain. Almost all the identified SSDs appear at the footpoints of sunspot plumes and are temporally associated with appearance of chromospheric bright dots inside the sunspot umbra. Dual-perspective EUV imaging observations reveal a large-scale closed magnetic loop system spanning the sunspot region and a remote region. We observed that the SSDs are caused by repeated coronal rain that forms and flows along these closed magnetic loops toward the sunspot. One

episode of coronal rain clearly indicates that reconnection near a coronal X-shaped structure first leads to the formation of a magnetic dip. Subsequently, hot coronal plasma catastrophically cools from 2 MK in the dip region via thermal instability. This results in the formation of a transient prominence in the dip, from which the cool gas mostly slides into the sunspot along inclined magnetic fields under the gravity. This drainage process manifests as a continuous rain flow, which lasts for around 2 hrs and concurrently results in a nearly steady SSD event. Our results demonstrate that coronal condensation in magnetic dips can result in the quasi-steady sunspot supersonic downflows. **2019 May 7-8**

**IRIS Nugget**, 15 Apr 2022 [https://iris.lmsal.com/nuggetvideos/2022/03/22/pod\\_polito\\_vanessa\\_2022-03-22T16%3A10%3A52.903Z/new2.png](https://iris.lmsal.com/nuggetvideos/2022/03/22/pod_polito_vanessa_2022-03-22T16%3A10%3A52.903Z/new2.png)

## **Forward Modeling of Solar Coronal Magnetic Field Measurements Based on a Magnetic-field-induced Transition in FeX**

[Yajie Chen](#), [Wenxian Li](#), [Hui Tian](#), [Feng Chen](#), [Xianyong Bai](#), [Yang Yang](#), [Zihao Yang](#), [Xianyu Liu](#), [Yuanyong Deng](#)

ApJ **920** 116 **2021**

<https://arxiv.org/pdf/2107.11783.pdf>

<https://doi.org/10.3847/1538-4357/ac1792>

It was recently proposed that the intensity ratios of several extreme ultraviolet spectral lines from the Fe X ion can be used to measure the solar coronal magnetic field based on the magnetic-field-induced transition (MIT) theory. To verify the suitability of this method, we performed forward modeling with a three-dimensional radiation magnetohydrodynamic model of a solar active region. Intensities of several spectral lines from Fe X were synthesized from the model. Based on the MIT theory, intensity ratios of the MIT line Fe X 257 Å to several other Fe X lines were used to derive the magnetic field strengths, which were then compared with the field strengths in the model. We also developed a new method to simultaneously estimate the coronal density and temperature from the Fe X 174/175 and 184/345 Å line ratios. Using these estimates, we demonstrated that the MIT technique can provide reasonably accurate measurements of the coronal magnetic field in both on-disk and off-limb solar observations. Our investigation suggests that a spectrometer that can simultaneously observe the Fe X 174, 175, 184, 257, and 345 Å lines and allow an accurate radiometric calibration for these lines is highly desired to achieve reliable measurements of the coronal magnetic field. We have also evaluated the impact of the uncertainty in the Fe X 3p4 3d 4D5/2 and 4D7/2 energy difference on the magnetic field measurements.

**Hinode/EIS Nuggets** Nov 2021 [http://solarb.mssl.ucl.ac.uk/SolarB/nuggets/nugget\\_2021nov\\_b.jsp](http://solarb.mssl.ucl.ac.uk/SolarB/nuggets/nugget_2021nov_b.jsp)

## **Emergence of magnetic flux generated in a solar convective dynamo.**

### **I: Formation of Sunspots and Active regions, and Origin of Their Asymmetries**

Feng [Chen](#), Matthias Rempel, Yuhong Fan

ApJ **846** 149 **2017**

<https://arxiv.org/pdf/1704.05999.pdf>

‘ We present a realistic numerical model of sunspot and active region formation through the emergence of flux bundles generated in a solar convective dynamo. The magnetic and velocity fields in a horizontal layer near the top boundary of the solar convective dynamo simulation are used as a time-dependent bottom boundary to drive realistic radiative-magnetohydrodynamic simulations of the upper most layer of the convection zone. The main results are: (1) The emerging flux bundles rise with the mean speed of convective upflows, and fragment into small-scale magnetic elements that further rise to the photosphere, where bipolar sunspot pairs are formed through the coalescence of the small-scale magnetic elements. (2) Filamentary penumbral structures form when the sunspot is still growing through ongoing flux emergence. In contrast to the classical Evershed effect, the inflow seems to prevail over the outflow in a large part of the penumbra. (3) A well formed sunspot is a mostly monolithic magnetic structures that is anchored in a persistent deep-seated downdraft lane. The flow field outside the spot shows a giant vortex ring that comprises of an inflow below 15 Mm depth and an outflow above 15 Mm depth. (4) The sunspots successfully reproduce the fundamental properties of the observed solar active regions, including the more coherent leading spots with a stronger field strength, and the correct tilts of bipolar sunspot pairs. These asymmetries can be linked to the intrinsic asymmetries in the emerging magnetic and flow fields adapted from the convective dynamo simulation.

## **Using coronal seismology to estimate the magnetic field strength in a realistic coronal model**

Feng [Chen](#), Hardi Peter

A&A **2015**

<http://arxiv.org/pdf/1508.00593v1.pdf>

Coronal seismology is extensively used to estimate properties of the corona, e.g. the coronal magnetic field strength are derived from oscillations observed in coronal loops. We present a three-dimensional coronal simulation including a realistic energy balance in which we observe oscillations of a loop in synthesised coronal emission. We

use these results to test the inversions based on coronal seismology.

From the simulation of the corona above an active region we synthesise extreme ultraviolet (EUV) emission from the model corona. From this we derive maps of line intensity and Doppler shift providing synthetic data in the same format as obtained from observations. We fit the (Doppler) oscillation of the loop in the same fashion as done for observations to derive the oscillation period and damping time.

The loop oscillation seen in our model is similar to imaging and spectroscopic observations of the Sun. The velocity disturbance of the kink oscillation shows an oscillation period of 52.5s and a damping time of 125s, both being consistent with the ranges of periods and damping times found in observation. Using standard coronal seismology techniques, we find an average magnetic field strength of  $B_{\text{kink}}=79\text{G}$  for our loop in the simulation, while in the loop the field strength drops from some 300G at the coronal base to 50G at the apex. Using the data from our simulation we can infer what the average magnetic field derived from coronal seismology actually means. It is close to the magnetic field strength in a constant cross-section flux tube that would give the same wave travel time through the loop.

Our model produced not only a realistic looking loop-dominated corona, but also provides realistic information on the oscillation properties that can be used to calibrate and better understand the result from coronal seismology.

### **Magnetic Jam in the Corona of the Sun**

F. **Chen**, H. Peter, S. Bingert, M.C.M. Cheung

Nature Physics, 11, 492 | 2015

<http://arxiv.org/pdf/1505.01174v1.pdf>

The outer solar atmosphere, the corona, contains plasma at temperatures of more than a million K, more than 100 times hotter than solar surface. How this gas is heated is a fundamental question tightly interwoven with the structure of the magnetic field in the upper atmosphere. Conducting numerical experiments based on magnetohydrodynamics we account for both the evolving three-dimensional structure of the atmosphere and the complex interaction of magnetic field and plasma. Together this defines the formation and evolution of coronal loops, the basic building block prominently seen in X-rays and extreme ultraviolet (EUV) images. The structures seen as coronal loops in the EUV can evolve quite differently from the magnetic field. While the magnetic field continuously expands as new magnetic flux emerges through the solar surface, the plasma gets heated on successively emerging fieldlines creating an EUV loop that remains roughly at the same place. For each snapshot the EUV images outline the magnetic field, but in contrast to the traditional view, the temporal evolution of the magnetic field and the EUV loops can be different. Through this we show that the thermal and the magnetic evolution in the outer atmosphere of a cool star has to be treated together, and cannot be simply separated as done mostly so far.

### **Development of Technique to Detect and Classify Small-Scale Magnetic Flux Cancellation and Rapid Blueshifted Excursions**

Xin **Chen**, Na Deng, Derek A. Lamb, [Ju Jing](#), [Chang Liu](#), [Rui Liu](#), [Sung-Hong Park](#), [Haimin Wang](#)

A&A 2015

<http://arxiv.org/pdf/1501.01226v1.pdf>

We present a set of tools for detecting small-scale solar magnetic cancellations and the disk counterpart of type II spicules (the so-called Rapid Blueshifted Excursions (RBEs)), using line-of-sight photospheric magnetograms and chromospheric spectroscopic observations, respectively. For tracking magnetic cancellation, we improve the Southwest Automatic Magnetic Identification Suite (SWAMIS) so that it is able to detect certain obscure cancellations that can be easily missed. For detecting RBEs, we use a normalized reference profile to reduce false-positive detections caused by the non-uniform background and seeing condition. Similar to the magnetic feature tracking in SWAMIS, we apply a dual-threshold method to enhance the accuracy of RBE detection. These tools are employed to analyze our coordinated observations using the Interferometric Bidimensional Spectrometer at Dunn Solar Telescope (DST) of the National Solar Observatory (NSO) and Hinode. We present the statistical properties of magnetic cancellations and RBEs, and explore their correlation using this data set.

### **A model for the formation of the active region corona driven by magnetic flux emergence\***

F. **Chen**, H. Peter<sup>1</sup>, S. Bingert<sup>1</sup> and M. C. M. Cheung

A&A 564, A12 (2014)

**Aims.** We present the first model that couples the formation of the corona of a solar active region to a model of the emergence of a sunspot pair. This allows us to study when, where, and why active region loops form, and how they evolve.

**Methods.** We use a 3D radiation magnetohydrodynamics (MHD) simulation of the emergence of an active region through the upper convection zone and the photosphere as a lower boundary for a 3D MHD coronal model. The coronal model accounts for the braiding of the magnetic fieldlines, which induces currents in the corona to heat up

the plasma. We synthesize the coronal emission for a direct comparison to observations. Starting with a basically field-free atmosphere we follow the filling of the corona with magnetic field and plasma.

Results. Numerous individually identifiable hot coronal loops form, and reach temperatures well above 1 MK with densities comparable to observations. The footpoints of these loops are found where small patches of magnetic flux concentrations move into the sunspots. The loop formation is triggered by an increase in upward-directed Poynting flux at their footpoints in the photosphere. In the synthesized extreme ultraviolet (EUV) emission these loops develop within a few minutes. The first EUV loop appears as a thin tube, then rises and expands significantly in the horizontal direction. Later, the spatially inhomogeneous heat input leads to a fragmented system of multiple loops or strands in a growing envelope.

## **Quantifying solar superactive regions with vector magnetic field observations**

A. Q. [Chen](#), and J. X. Wang

E-print, 29 May 2012; A&A

The vector magnetic field characteristics of superactive regions (SARs) hold the key for understanding why SARs are extremely active and provide the guidance in space weather prediction. We aim to quantify the characteristics of SARs using the vector magnetograms taken by the Solar Magnetic Field Telescope at Huairou Solar Observatory Station. The vector magnetic field characteristics of 14 SARs in solar cycles 22 and 23 were analyzed using the following four parameters: 1) the magnetic flux imbalance between opposite polarities, 2) the total photospheric free magnetic energy, 3) the length of the magnetic neutral line with its steep horizontal magnetic gradient, and 4) the area with strong magnetic shear. Furthermore, we selected another eight large and inactive active regions (ARs), which are called fallow ARs (FARs), to compare them with the SARs. We found that most of the SARs have a net magnetic flux higher than  $7.0 \times 10^{21}$  Mx, a total photospheric free magnetic energy higher than  $1.0 \times 10^{24}$  erg/cm, a magnetic neutral line with a steep horizontal magnetic gradient ( $\geq 300$  G/Mm) longer than 30 Mm, and an area with strong magnetic shear (shear angle  $\geq 80^\circ$ ) greater than  $100 \text{ Mm}^2$ . In contrast, the values of these parameters for the FARs are mostly very low. The Pearson  $\chi^2$  test was used to examine the significance of the difference between the SARs and FARs, and the results indicate that these two types of ARs can be fairly distinguished by each of these parameters. The significance levels are 99.55%, 99.98%, 99.98%, and 99.96%, respectively. However, no single parameter can distinguish them perfectly. Therefore we propose a composite index based on these parameters, and find that the distinction between the two types of ARs is also significant with a significance level of 99.96%. These results are useful for a better physical understanding of the SAR and FAR.

## **A CORONAL SEISMOLOGICAL STUDY WITH STREAMER WAVES**

Y. [Chen](#)<sup>1</sup>, S. W. [Feng](#)<sup>1</sup>, B. [Li](#)<sup>1</sup>, H. Q. [Song](#)<sup>1</sup>, L. D. [Xia](#)<sup>1</sup>, X. L. [Kong](#)<sup>1</sup>, and Xing Li<sup>2</sup>

Astrophysical Journal, 728:147 (6pp), 2011, [File](#)

We present a novel method to evaluate the Alfvén speed and the magnetic field strength along the streamer plasma sheet in the outer corona. The method is based on recent observations of streamer waves, which are regarded as the fast kink body mode carried by the plasma sheet structure and generated upon the impact of a fast coronal mass ejection (CME) on a nearby streamer. The mode propagates outward with a phase speed consisting of two components. One is the phase speed of the mode in the plasma rest frame and the other is the speed of the solar wind streaming along the plasma sheet. The former can be well represented by the Alfvén speed outside the plasma sheet, according to a linear wave dispersion analysis with a simplified slab model of magnetized plasmas. The radial profiles of the Alfvén speed can be deduced with constraints put on the speed of the solar wind, which is done by making use of the measurements of streamer blobs flowing passively in the wind. The radial profiles of the strength of the coronal magnetic field can be depicted once the electron density distribution is specified, this is done by inverting the observed polarized brightness data. Comparing the diagnostic results corresponding to the first wave trough and the following crest, we find that both the Alfvén speed and magnetic field strength at a fixed distance decline with time. This is suggestive of the recovering process of the CME-disturbed corona.

## **DYNAMIC FLARING NON-POTENTIAL FIELDS ON QUIET SUN NETWORK SCALES**

D. L. [Chesny](#)<sup>1,2</sup>, H. M. [Oluseyi](#)<sup>1</sup>, and N. B. [Orange](#)

2016 ApJ 822 72

We report on the identification of dynamic flaring non-potential structures on quiet Sun (QS) supergranular network scales. Data from the Atmospheric Imaging Assembly on board the Solar Dynamics Observatory allow for the high spatial and temporal resolution of this diverse class of compact structures. The rapidly evolving non-potential events presented here, with lifetimes  $< 10$  minutes, are on the order of  $10''$  in length. Thus, they contrast significantly with well-known active region (AR) non-potential structures such as high-temperature X-ray and EUV sigmoids ( $> 100''$ ) and micro-sigmoids ( $> 10''$ ) with lifetimes on the order of hours to days. The photospheric magnetic field environment derived from the Helioseismic and Magnetic Imager shows a lack of evidence for these flaring non-



potential fields being associated with significant concentrations of bipolar magnetic elements. Of much interest to our events is the possibility of establishing them as precursor signatures of eruptive dynamics, similar to notions for AR sigmoids and micro-sigmoids, but associated with uneventful magnetic network regions. We suggest that the mixed network flux of QS-like magnetic environments, though unresolved, can provide sufficient free magnetic energy for flaring non-potential plasma structuring. The appearance of non-potential magnetic fields could be a fundamental process leading to self-organized criticality in the QS-like supergranular network and contribute to coronal heating, as these events undergo rapid helical and vortical relaxations.

## **Non-potential Fields in the Quiet Sun Network: Extreme-ultraviolet and Magnetic Footpoint Observations**

D. L. [Chesny](#), H. M. Oluseyi, and N. B. Orange

2013 ApJ 778 L17

The quiet Sun (QS) magnetic network is known to contain dynamics which are indicative of non-potential fields. Non-potential magnetic fields forming "S-shaped" loop arcades can lead to the breakdown of static activity and have only been observed in high temperature X-ray coronal structures—some of which show eruptive behavior. Thus, analysis of this type of atmospheric structuring has been restricted to large-scale coronal fields. Here we provide the first identification of non-potential loop arcades exclusive to the QS supergranulation network. High-resolution Atmospheric Imaging Assembly data from the Solar Dynamics Observatory have allowed for the first observations of fine-scale "S-shaped" loop arcades spanning the network. We have investigated the magnetic footpoint flux evolution of these arcades from Heliospheric and Magnetic Imager data and find evidence of evolving footpoint flux imbalances accompanying the formation of these non-potential fields. The existence of such non-potentiality confirms that magnetic field dynamics leading to the build up of helicity exist at small scales. QS non-potentiality also suggests a self-similar formation process between the QS network and high temperature corona and the existence of self-organized criticality (SOC) in the form of loop-pair reconnection and helicity dissipation. We argue that this type of behavior could lead to eruptive forms of SOC as seen in active region (AR) and X-ray sigmoids if sufficient free magnetic energy is available. QS magnetic network dynamics may be considered as a coronal proxy at supergranular scales, and events confined to the network can even mimic those in coronal ARs.

## **The Life Cycle of Active Region Magnetic Fields**

**Review**

M. C. M. [Cheung](#), L. van Driel-Gesztelyi, V. Martínez Pillet, M. J. Thompson

Space Science Reviews 2017, Volume 210, [Issue 1–4](#), pp 317–349

We present a contemporary view of how solar active region magnetic fields are understood to be generated, transported and dispersed. Empirical trends of active region properties that guide model development are discussed. Physical principles considered important for active region evolution are introduced and advances in modeling are reviewed.

## **Flux Emergence (Theory)**

**Review**

Mark C. M. [Cheung](#) and Hiroaki Isobe

Living Rev. Solar Phys. 11 (2014), 3

<http://solarphysics.livingreviews.org/Articles/lrsp-2014-3/>

Magnetic flux emergence from the solar convection zone into the overlying atmosphere is the driver of a diverse range of phenomena associated with solar activity. In this article, we introduce theoretical concepts central to the study of flux emergence and discuss how the inclusion of different physical effects (e.g., magnetic buoyancy, magnetoconvection, reconnection, magnetic twist, interaction with ambient field) in models impact the evolution of the emerging field and plasma.

### **4 Flux Emergence and its Relation to Jets and Eruptions**

## **Intensification of magnetic field in merging magnetic flux tubes driven by supergranular vortical flows**

[Abraham C-L Chian](#), [Erico L Rempel](#), [Suzana S A Silva](#), [Luis Bellot Rubio](#), [Milan Gošić](#)

Monthly Notices of the Royal Astronomical Society, 518, Issue 4, February 2023, Pages 4930–4942,

<https://doi.org/10.1093/mnras/stac3352>

<https://watermark.silverchair.com/stac3352.pdf>

The spatiotemporal dynamics of vorticity and magnetic field in the region of a photospheric vortex at a supergranular junction of the quiet Sun is studied, using Hinode's continuum intensity images and longitudinal magnetograms. We show that in a 30-min interval during the vortex lifetime, the magnetic field is intensified at the

centres of two merging magnetic flux tubes trapped inside the vortex boundary. Moreover, we show that the electric current density is intensified at the interface boundary layers of merging tubes, resulting from strong vortical downflows in a supergranular vertex. Evidence of Lagrangian chaos and vortex stretching in the photospheric plasma turbulence responsible for driving the intensification of magnetic fields is analysed. In particular, we report the first solar observation of the intensification of electromagnetic energy flux resulting from the merger of magnetic flux tubes. **2010 November 2**

## **Coronal magnetic field evolution over the cycle 24**

[I. Chifu](#), [B. Inhester](#), [T. Wiegelmann](#)

A&A 659, A174 2022

<https://arxiv.org/pdf/2201.03853.pdf>

<https://www.aanda.org/articles/aa/pdf/2022/03/aa38001-20.pdf>

<https://doi.org/10.1051/0004-6361/202038001>

The photospheric magnetic field vector is continuously derived from measurements, while reconstruction of the three-dimensional (3D) coronal magnetic field requires modelling with photospheric measurements as a boundary condition. For decades the cycle variation of the magnetic field in the photosphere has been investigated. To present, there is no study to show the evolution of the coronal magnetic flux in the corona, nor the evolution of solar cycle magnetic free energy. The paper aims to analyze the temporal variation of the magnetic field and free magnetic energy in the solar corona for the solar cycle 24 and how the magnetic field behaves in the two hemispheres. We investigate if we can obtain better estimates of the magnetic field at Earth using the nonlinear force-free field (NLFFF) extrapolation method. To model the magnetic field over cycle 24 we apply the NLFFF optimization method to the synoptic vector magnetic maps derived from the observations of Heliospheric and Magnetic Imager (HMI) onboard Solar Dynamic Observatory (SDO). We found that during the solar cycle 24, the maximum of the Sun's dynamics is different from the sunspot number (SSN) maximum peak. The major contribution to the total unsigned flux is provided by the flux coming from the magnetic field structures other than sunspots (MSOS) within latitudes between -30 and +30 degrees. The magnetic flux variation during the solar cycle 24 shows a different evolution in the corona than in the photosphere. We found a correlation value of 0.8 between the derived magnetic energy from our model and the flare energy index derived from observations. On average, cycle 24 had a higher number of sunspots in the northern hemisphere (NH) but stronger flux in the southern hemisphere (SH) which could more effectively reach the higher layers of the atmosphere. The coupling between the hemispheres increases with height.

## **3D solar coronal loop reconstructions with machine learning**

[Iulia Chifu](#), [Ricardo Gafeira](#)

ApJL 2021

<https://arxiv.org/pdf/2103.09960.pdf>

The magnetic field plays an essential role in the initiation and evolution of different solar phenomena in the corona. The structure and evolution of the 3D coronal magnetic field are still not very well known. A way to get the 3D structure of the coronal magnetic field is by performing magnetic field extrapolations from the photosphere to the corona. In previous work, it was shown that by prescribing the 3D reconstructed loops' geometry, the magnetic field extrapolation finds a solution with a better agreement between the modeled field and the reconstructed loops. Also, it improves the quality of the field extrapolation. Stereoscopy represents the classical method for performing 3D coronal loop reconstruction. It uses at least two view directions. When only one vantage point of the coronal loops is available, other 3D reconstruction methods must be applied. Within this work, we present a method for the 3D loop reconstruction based on machine learning. Our purpose for developing this method is to use as many observed coronal loops in space and time for the modeling of the coronal magnetic field. Our results show that we can build machine learning models that can retrieve 3D loops based only on their projection information. In the end, the neural network model will be able to use only 2D information of the coronal loops, identified, traced and extracted from the EUV images, for the calculation of their 3D geometry.

## **Nonlinear Force-free Coronal Magnetic Stereoscopy**

[Iulia Chifu](#)<sup>1,2</sup>, [Thomas Wiegelmann](#)<sup>1</sup>, and [Bernd Inhester](#)<sup>1</sup>

2017 ApJ 837 10

<https://arxiv.org/pdf/1709.04177.pdf>

Insights into the 3D structure of the solar coronal magnetic field have been obtained in the past by two completely different approaches. The first approach are nonlinear force-free field (NLFFF) extrapolations, which use photospheric vector magnetograms as boundary condition. The second approach uses stereoscopy of coronal magnetic loops observed in EUV coronal images from different vantage points. Both approaches have their strengths and weaknesses. Extrapolation methods are sensitive to noise and inconsistencies in the boundary data, and the accuracy of stereoscopy is affected by the ability of identifying the same structure in different images and by the separation angle between the view directions. As a consequence, for the same observational data, the 3D coronal

magnetic fields computed with the two methods do not necessarily coincide. In an earlier work (Paper I) we extended our NLFFF optimization code by including stereoscopic constraints. The method was successfully tested with synthetic data, and within this work, we apply the newly developed code to a combined data set from SDO/HMI, SDO/AIA, and the two STEREO spacecraft. The extended method (called S-NLFFF) contains an additional term that monitors and minimizes the angle between the local magnetic field direction and the orientation of the 3D coronal loops reconstructed by stereoscopy. We find that when we prescribe the shape of the 3D stereoscopically reconstructed loops, the S-NLFFF method leads to a much better agreement between the modeled field and the stereoscopically reconstructed loops. We also find an appreciable decrease by a factor of two in the angle between the current and the magnetic field. This indicates the improved quality of the force-free solution obtained by S-NLFFF.

## **Coronal magnetic field modeling using stereoscopy constraints**

I. [Chifu](#), B. Inhester<sup>1</sup> and T. Wiegmann

A&A 577, A123 (2015)

**Aims.** Nonlinear force-free field (NLFFF) extrapolation has been used extensively in the past to extrapolate solar surface magnetograms to stationary coronal field models. In theoretical tests with known boundary conditions, the nonlinear boundary value problem can be solved reliably. However, if the magnetogram is measured with errors, the extrapolation often yields field lines that disagree with the shapes of simultaneously observed and stereoscopically reconstructed coronal loops. We here propose an extension to an NLFFF extrapolation scheme that remedies this deficiency in that it incorporates the loop information in the extrapolation procedure.

**Methods.** We extended the variational formulation of the NLFFF optimization code by an additional term that monitors and minimizes the difference of the local magnetic field direction and the orientation of 3D plasma loops. We tested the performance of the new code with a previously reported semi-analytical force-free solution.

**Results.** We demonstrate that there is a range of force-free and divergence-free solutions that comply with the boundary measurements within some error bound. With our new approach we can obtain the solution out of this set the coronal fields which is well aligned with given loops.

**Conclusions.** We conclude that the shape of coronal loops reconstructed by stereoscopy may lead to an important stabilization of coronal NLFFF field solutions when, as is typically the case, magnetic surface measurements with limited precision do not allow determining the solution solely from photospheric field measurements.

## **RECONSTRUCTING THE SUBSURFACE THREE-DIMENSIONAL MAGNETIC STRUCTURE OF A SOLAR ACTIVE REGION USING SDO/HMI OBSERVATIONS**

Georgios [Chintzoglou](#) and Jie Zhang

2013 ApJ 764 L3

A solar active region (AR) is a three-dimensional (3D) magnetic structure formed in the convection zone, whose property is fundamentally important for determining the coronal structure and solar activity when emerged. However, our knowledge of the detailed 3D structure prior to its emergence is rather poor, largely limited by the low cadence and sensitivity of previous instruments. Here, using the 45 s high-cadence observations from the Helioseismic and Magnetic Imager on board the Solar Dynamics Observatory, we are able for the first time to reconstruct a 3D data cube and infer the detailed subsurface magnetic structure of NOAA AR 11158, and to characterize its magnetic connectivity and topology. This task is accomplished with the aid of the image-stacking method and advanced 3D visualization. We find that the AR consists of two major bipoles or four major polarities. Each polarity in 3D shows interesting tree-like structure, i.e., while the root of the polarity appears as a single tree-trunk-like tube, the top of the polarity has multiple branches consisting of smaller and thinner flux tubes which connect to the branches of the opposite polarity that is similarly fragmented. The roots of the four polarities align well along a straight line, while the top branches are slightly non-coplanar. Our observations suggest that an active region, even appearing highly complicated on the surface, may originate from a simple straight flux tube that undergoes both horizontal and vertical bifurcation processes during its rise through the convection zone.

## **Direct observations of a complex coronal web driving highly structured slow solar wind**

L. P. [Chitta](#), [D. B. Seaton](#), [C. Downs](#), [C. E. DeForest](#), [A. K. Higginson](#)

Nature Astronomy 2022

<https://arxiv.org/ftp/arxiv/papers/2211/2211.13283.pdf>

<https://www.nature.com/articles/s41550-022-01834-5.pdf>

The solar wind consists of continuous streams of charged particles that escape into the heliosphere from the Sun, and is split into fast and slow components, with the fast wind emerging from the interiors of coronal holes. Near the ecliptic plane, the fast wind from low-latitude coronal holes is interspersed with a highly structured slow solar wind, the source regions and drivers of which are poorly understood. Here we report extreme-ultraviolet observations that reveal a spatially complex web of magnetized plasma structures that persistently interact and reconnect in the middle

corona. Coronagraphic white-light images show concurrent emergence of slow wind streams over these coronal web structures. With advanced global MHD coronal models, we demonstrate that the observed coronal web is a direct imprint of the magnetic separatrix web (S-web). By revealing a highly dynamic portion of the S-web, our observations open a window into important middle-coronal processes that appear to play a key role in driving the structured slow solar wind.

### **A closer look at a coronal loop rooted in a sunspot umbra**

L. P. [Chitta](#), H. Peter, P. R. Young

A&A 587, A20 2016

<http://arxiv.org/pdf/1512.03831v1.pdf>

Extreme UV (EUV) and X-ray loops in the solar corona connect regions of enhanced magnetic activity, but usually they are not rooted in the dark umbrae of sunspots. This is because there the strong magnetic field suppresses convection and thus the Poynting flux of magnetic energy into the upper atmosphere is not significant within the umbra, as long as there are no light bridges, umbral dots. Here we report a rare observation of a coronal loop rooted in the dark umbra of a sunspot without any traces of light bridges or umbral dots. We used the slit-jaw images and spectroscopic data from the IRIS and concentrate on the line profiles of O IV and Si IV that show persistent strong redshifted components in the loop rooted in the umbra. Using the ratios of O IV, we can estimate the density and thus investigate the mass flux. The coronal context and temperature diagnostics of these observations is provided through the EUV channels of the AIA. The coronal loop, embedded within cooler downflows, is hosting supersonic downflows. The speed of more than  $100 \text{ km s}^{-1}$  is of the same order of magnitude in the transition region lines of O IV and Si IV, and is even seen at comparable speed in the chromospheric Mg II lines. At a projected distance of within  $1''$  from the footpoint, we see a shock transition to smaller downflow speeds of about  $15 \text{ km s}^{-1}$  being consistent with mass conservation across a stationary isothermal shock. We see no (direct) evidence for energy input into the loop because the loop is rooted in the dark uniform part of the umbra, with no light bridges or umbral dots around. Thus one might conclude that we see a siphon flow driven from the footpoint at the other end of the loop. However, for a final result one would need data of similar quality at the other footpoint, which is too far away to be covered by the field-of-view of IRIS. **9 Jul 2014**

### **Nonlinear Force-Free Field Modeling of the Solar Magnetic Carpet and Comparison with SDO/HMI and Sunrise/IMaX Observations**

L. P. [Chitta](#), R. Kariyappa, A. A. van Ballegoijen, E. E. DeLuca, S. K. Solanki

ApJ, 793 112 2014

<http://arxiv.org/pdf/1408.0497v1.pdf>

In the quiet solar photosphere, the mixed polarity fields form a magnetic carpet, which continuously evolves due to dynamical interaction between the convective motions and magnetic field. This interplay is a viable source to heat the solar atmosphere. In this work, we used the line-of-sight (LOS) magnetograms obtained from the Helioseismic and Magnetic Imager (HMI) on the \textit{Solar Dynamics Observatory} (\textit{SDO}), and the Imaging Magnetograph eXperiment (IMaX) instrument on the \textit{Sunrise} balloon-borne observatory, as time dependent lower boundary conditions, to study the evolution of the coronal magnetic field. We use a magneto-frictional relaxation method, including hyperdiffusion, to produce time series of three-dimensional (3D) nonlinear force-free fields from a sequence of photospheric LOS magnetograms. Vertical flows are added up to a height of  $0.7 \text{ Mm}$  in the modeling to simulate the non-force-freeness at the photosphere-chromosphere layers. Among the derived quantities, we study the spatial and temporal variations of the energy dissipation rate, and energy flux. Our results show that the energy deposited in the solar atmosphere is concentrated within  $2 \text{ Mm}$  of the photosphere and there is not sufficient energy flux at the base of the corona to cover radiative and conductive losses. Possible reasons and implications are discussed. Better observational constraints of the magnetic field in the chromosphere are crucial to understand the role of the magnetic carpet in coronal heating. **2011 January 08,**

### **Investigation of the subsurface structure of a sunspot based on the spatial distribution of oscillation centers inferred from umbral flashes**

[Kyuhyoun Cho](#), [Jongchul Chae](#), [Maria S. Madjarska](#)

A&A 656, A86 2021

<https://arxiv.org/pdf/2109.11185.pdf>

<https://www.aanda.org/articles/aa/pdf/2021/12/aa41500-21.pdf>

<https://doi.org/10.1051/0004-6361/202141500>

The subsurface structure of a solar sunspot is important in the stability of the sunspots and the energy transport therein. Two subsurface structure models have been proposed, the monolithic and cluster models, but no clear observational evidence supporting a particular model has been found so far. To obtain clues about the subsurface structure of sunspots, we analyzed umbral flashes in merging sunspots registered by IRIS Mg II 2796 Angstrom slit-

jaw images (SJIs). Umbral flashes are regarded as an observational manifestation of magnetohydrodynamic (MHD) shock waves originating from convection cells below the photosphere. By tracking the motion of individual umbral flashes, we determined the position of the convection cells that are the oscillation centers located below the umbra. We found that the oscillation centers are preferentially located at dark nuclei in the umbral cores rather than in bright regions such as light bridges or umbral dots. Moreover, the oscillation centers tend to deviate from the convergent interface of the merging sunspots where vigorous convection is expected to occur. We also found that the inferred depths of the convection cells have no noticeable regional dependence. These results suggest that the subsurface of the umbra is an environment where convection can occur more easily than the convergent interface, and hence support the cluster model. For more concrete results, further studies based on umbral velocity oscillations in the lower atmosphere are required.

### Source Depth of Three-minute Umbral Oscillations

Kyuhyouun [Cho](#), [Jongchul Chae](#)

ApJL **892** L31 **2020**

<https://arxiv.org/pdf/2003.10542.pdf>

<https://doi.org/10.3847/2041-8213/ab8295>

We infer the depth of the internal sources giving rise to three-minute umbral oscillations. Recent observations of ripple-like velocity patterns of umbral oscillations supported the notion that there exist internal sources exciting the umbral oscillations. We adopt the hypothesis that the fast magnetohydrodynamic (MHD) waves generated at a source below the photospheric layer propagate along different paths, reach the surface at different times, and excited slow MHD waves by mode conversion. These slow MHD waves are observed as the ripples that apparently propagate horizontally. The propagation distance of the ripple given as a function of time is strongly related to the depth of the source. Using the spectral data of the Fe I 5435A line taken by the Fast Imaging Solar Spectrograph of the Goode Solar Telescope at Big Bear Solar Observatory, we identified five ripples and determined the propagation distance as a function of time in each ripple. From the model fitting to these data, we obtained the depth between 1000 km and 2000 km. Our result will serve as an observational constraint to understanding the detailed processes of magnetoconvection and wave generation in sunspots. **2017 June 15**

HMI Science Nuggets, #141, **2020** <http://hmi.stanford.edu/hminuggets/?p=3287>

### The Observational Evidence for the Internal Excitation of Sunspot Oscillations Inferred from the Fe I 5435 A Line

Kyuhyouun [Cho](#), [Jongchul Chae](#), [Eun-kyung Lim](#), [Heesu Yang](#)

ApJ **879** 67 **2019**

<https://arxiv.org/pdf/1906.01971.pdf>

[sci-hub.se/10.3847/1538-4357/ab2466](https://doi.org/10.3847/1538-4357/ab2466)

The umbral oscillations of velocity are commonly observed in the chromosphere of a sunspot. Their sources are considered to be either the external p-mode driving or the internal excitation by magnetoconvection. Even though the possibility of the p-mode driving has been often considered, the internal excitation has been rarely investigated. We report the identification of the oscillation patterns that may be closely related to the events of internal excitation from the observations of velocity oscillations in the temperature minimum region of two sunspots. The velocities were determined from the spectral data of the Fe I 5435 A line, a magnetically insensitive line, taken with the Fast Imaging Solar Spectrograph of the 1.6 m Goode Solar Telescope at the Big Bear Solar Observatory. As a result, we identified 4 oscillation patterns of  $2.0 \times 10^3$  km coherent size that were clearly identified for about 7.9 minutes with oscillation amplitude of  $9.3 \times 10^{-2}$  km/s. The power of the oscillations in these centers was concentrated in the 3 minute band. All the oscillation centers were located above the umbral dots undergoing noticeable morphological and dynamical changes that may be regarded as an observable signature of small-scale magnetoconvection inside the umbrae. Our results support the notion that magnetoconvection associated with umbral dots inside sunspots can drive the 3 minute umbral oscillations. **16 June 2015 and 15 June 2017**

[HMI Science Nuggets # 130 Sept 2019](http://hmi.stanford.edu/hminuggets/?p=3067) <http://hmi.stanford.edu/hminuggets/?p=3067>

### Determination of the Alfvén Speed and Plasma-beta Using the Seismology of Sunspot Umbra

I.-H. [Cho](#)<sup>1</sup>, K.-S. [Cho](#)<sup>2,3</sup>, S.-C. [Bong](#)<sup>2,3</sup>, Y.-J. [Moon](#)<sup>1,4</sup>, V. M. [Nakariakov](#)<sup>1,5</sup>, J. [Park](#)<sup>1,2</sup>, J.-H. [Baek](#)<sup>2</sup>, S. [Choi](#)<sup>1,2</sup>, Y.-H. [Kim](#)<sup>2,3</sup>, and J. [Lee](#)

**2017** ApJL **837** L11

For 478 centrally located sunspots observed in the optical continuum with Solar Dynamics Observatory/Helioseismic Magnetic Imager, we perform seismological diagnostics of the physical parameters of umbral photospheres. The new technique is based on the theory of slow magnetoacoustic waves in a non-isothermally stratified photosphere with a uniform vertical magnetic field. We construct a map of the weighted

frequency of three-minute oscillations inside the umbra and use it for the estimation of the Alfvén speed, plasma-beta, and mass density within the umbra. We find the umbral mean Alfvén speed ranges between 10.5 and 7.5 km s<sup>-1</sup> and is negatively correlated with magnetic field strength. The umbral mean plasma-beta is found to range approximately between 0.65 and 1.15 and does not vary significantly from pores to mature sunspots. The mean density ranges between  $(1-6) \times 10^{-4}$  kg m<sup>-3</sup> and shows a strong positive correlation with magnetic field strength.

### **STATISTICAL COMPARISON BETWEEN PORES AND SUNSPOTS BY USING SDO/HMI**

I.-H. [Cho](#)<sup>1,2</sup>, K.-S. [Cho](#)<sup>1,2</sup>, S.-C. [Bong](#)<sup>1,2</sup>, E.-K. [Lim](#)<sup>1</sup>, R.-S. [Kim](#)<sup>1,2</sup>, S. [Choi](#)<sup>1</sup>, Y.-H. [Kim](#)<sup>1,2,3</sup>, and V. [Yurchyshyn](#)

2015 ApJ 811 49

We carried out an extensive statistical study of the properties of pores and sunspots, and investigated the relationship among their physical parameters such as size, intensity, magnetic field, and the line-of-sight (LOS) velocity in the umbrae. For this, we classified 9881 samples into three groups of pores, transitional sunspots, and mature sunspots. As a result, (1) we find that the total magnetic flux inside the umbra of pores, transitional sunspots, and mature sunspots increases proportionally to the powers of the area and the power indices in the three groups significantly differ from each other. (2) The umbral area distribution of each group shows a Gaussian distribution and they are clearly separated, displaying three distinct peak values. All of the quantities significantly overlap among the three groups. (3) The umbral intensity shows a rapid decrease with increasing area, and their magnetic field strength shows a rapid increase with decreasing intensity. (4) The LOS velocity in pores is predominantly redshifted and its magnitude decreases with increasing magnetic field strength. The decreasing trend becomes nearly constant with marginal blueshift in the case of mature sunspots. The dispersion of LOS velocities in mature sunspots is significantly suppressed compared to pores. From our results, we conclude that the three groups have different characteristics in their area, intensity, magnetic field, and LOS velocity as well in their relationships.

### **Thermodynamic Properties of the Inverse Evershed Flow at Its Downflow Points**

D. P. [Choudhary](#)<sup>1</sup> and C. Beck

2018 ApJ 859 139

<http://iopscience.iop.org/article/10.3847/1538-4357/aabf36/pdf>

<https://arxiv.org/pdf/1804.07326.pdf>

We used spectropolarimetric observations of a sunspot in the active region NOAA 11809 in the Ca ii line at 854.2 nm taken with the SpectroPolarimeter for Optical and Infrared Regions at the Dunn Solar Telescope to infer thermodynamic parameters along 100 super-penumbral fibrils that harbor the inverse Evershed flow. The fibrils were identified in line-of-sight (LOS) velocity and line-core intensity maps. The chromospheric LOS velocity abruptly decreases from 3 to 15 km s<sup>-1</sup> to zero at the inner footpoints of the fibrils that are located from the mid penumbra to about 1.4 spot radii. The spectra often show multiple absorption components, indicating spatially or vertically unresolved structures. Synthetic spectra with a 100% fill factor of a flow channel in the upper atmosphere yield strongly asymmetric profiles but no multiple separate components. The line-core intensity always peaks slightly closer to the umbra than the LOS velocity. Using the Calcium Inversion using a Spectral ARchive code, we find that the fibrils make an angle of 30°–60° to the local vertical away from the umbra. The temperature near the downflow points is enhanced by 200 K at  $\log \tau \sim -2$  and up to 2000 K at  $\log \tau \sim (-6)$  compared to the quiet Sun, without any signature in the low photosphere. Our results are consistent with a critical, i.e., sonic, or supersonic siphon flow along super-penumbral flux tubes in which accelerating plasma abruptly attains subcritical velocity through a standing shock in or near the penumbra. **2013/08/03**

### **The emergence and growth of the flux transport dynamo model of the sunspot cycle**

#### **Review**

[Arnab Rai Choudhuri](#)

Chandrasekhar Prize [lecture](#), Reviews of Modern Plasma Physics **2023**

<https://arxiv.org/pdf/2212.14617.pdf>

The sunspot cycle is the magnetic cycle of the Sun produced by the dynamo process. A central idea of the solar dynamo is that the toroidal and the poloidal magnetic fields of the Sun sustain each other. We discuss the relevant observational data both for sunspots (which are manifestations of the toroidal field) and for the poloidal field of the Sun. We point out how the differential rotation of the Sun stretches out the poloidal field to produce the toroidal field primarily at the bottom of the convection zone, from where parts of this toroidal field may rise due to magnetic buoyancy to produce sunspots. In the flux transport dynamo model, the decay of tilted bipolar sunspot pairs gives rise to the poloidal field by the Babcock--Leighton mechanism. In this type of model, the meridional circulation of the Sun, which is poleward at the solar surface and equatorward at the bottom of the convection zone, plays a crucial role in the transport of magnetic fluxes. We finally point out that various stochastic fluctuations associated with the dynamo process may play a key role in producing the irregularities of the sunspot cycle.

## **Minimal Magnetic States of the Sun and the Solar Wind: Implications for the Origin of the Slow Solar Wind**

**Review**

E. W. [Cliver](#), R. von Steiger

[Space Science Reviews](#) September 2017, Volume 210, [Issue 1–4](#), pp 227–247

During the last decade it has been proposed that both the Sun and the solar wind have minimum magnetic states, lowest order levels of magnetism that underlie the 11-yr cycle as well as longer-term variability. Here we review the literature on basal magnetic states at the Sun and in the heliosphere and draw a connection between the two based on the recent deep 2008–2009 minimum between cycles 23 and 24. In particular, we consider the implications of the low solar activity during the recent minimum for the origin of the slow solar wind.

## **Quantifying the Difference Between the Flux-Tube Expansion Factor at the Source Surface and at the Alfvén Surface Using A Global MHD Model for the Solar Wind**

Ofer [Cohen](#)

[Solar Phys.](#) Volume 290, Issue 8, pp 2245–2263 2015

<http://arxiv.org/pdf/1507.00572v1.pdf>

The potential field approximation has been providing a fast, and computationally inexpensive estimation for the solar corona's global magnetic field geometry for several decades. In contrast, more physics-based global magnetohydrodynamic (MHD) models have been used for a similar purpose, while being much more computationally expensive. Here, we investigate the difference in the field geometry between a global MHD model and the potential field source surface model (PFSSM) by tracing individual magnetic field lines in the MHD model from the Alfvén surface (AS), through the source surface (SS), all the way to the field line footpoint, and then back to the source surface in the PFSSM. We also compare the flux-tube expansion at two points at the SS and the AS along the same radial line. We study the effect of solar cycle variations, the order of the potential field harmonic expansion, and different magnetogram sources. We find that the flux-tube expansion factor is consistently smaller at the AS than at the SS for solar minimum and the fast solar wind, but it is consistently larger for solar maximum and the slow solar wind. We use the Wang--Sheeley--Arge (WSA) model to calculate the associated wind speed for each field line, and propagate these solar-wind speeds to 1AU. We find a more than five hours deviation in the arrival time between the two models for 20% of the field lines in the solar minimum case, and for 40% of the field lines in the solar maximum case.

## **Understanding the Fe i Line Measurements Returned by the Helioseismic and Magnetic Imager (HMI)**

D. P. [Cohen](#), S. Criscuoli, L. Farris, A. Tritschler

[Solar Phys.](#) 2015

<http://arxiv.org/pdf/1502.02559v1.pdf>

The Helioseismic and Magnetic Imager (HMI) onboard the Solar Dynamics Observatory (SDO) observes the Sun at the Fe i 6173 Å line and returns full-disk maps of line-of-sight (LOS) observables including the magnetic flux density, velocities, Fe I line width, line depth, and continuum intensity. These data are estimated through an algorithm (the MDI-like algorithm, hereafter) that combines observables obtained at six wavelength positions within the Fe i 6173 Å line. To properly interpret such data, it is important to understand any effects of the instrument and of the pipeline that generates these data products. We tested the accuracy of the line width, line depth, and continuum intensity returned by the MDI-like algorithm using various one-dimensional (1D) atmosphere models. It was found that HMI estimates of these quantities are highly dependent on the shape of the line, therefore on the LOS angle and the magnetic flux density associated with the model, and less to line shifts with respect to the central positions of the instrument transmission profiles. In general, the relative difference between synthesized values and HMI estimates increases toward the limb and with the increase of the field; the MDI-like algorithm seems to fail in regions with fields larger than approximately 2000 G. Instrumental effects were investigated by analyzing HMI data obtained at daily intervals for a span of three years at disk center in the quiet Sun and hourly intervals for a span of 200 hours. The analysis revealed periodicities induced by the variation of the orbital velocity of the observatory with respect to the Sun, and long-term trends attributed to instrument adjustments, re-calibrations, and instrumental degradation.

## **CONSTRAINING THREE-DIMENSIONAL MAGNETIC FIELD EXTRAPOLATIONS USING THE TWIN PERSPECTIVES OF *STEREO***

Paul A. [Conlon](#) and Peter T. Gallagher

[Astrophysical Journal](#), 715:59–65, 2010 May

The three-dimensional magnetic topology of a solar active region (NOAA 10956) was reconstructed using a linear force-free field extrapolation constrained using the twin perspectives of *STEREO*. A set of coronal field configurations was initially generated from extrapolations of the photospheric magnetic field observed by the Michelson Doppler Imager on *SOHO*. Using an EUV intensity-based cost function, the extrapolated field lines that were most consistent with 171 Å passband images from the Extreme UltraViolet Imager on *STEREO* were identified. This facilitated quantitative constraints to be placed on the twist ( $\alpha$ ) of the extrapolated field lines, where  $\nabla \times \mathbf{B} = \alpha \mathbf{B}$ . Using the constrained values of  $\alpha$ , the evolution in time of twist, connectivity, and magnetic energy were then studied. A flux emergence event was found to result in significant changes in the magnetic topology and total magnetic energy of the region.

## **The Force-Free Electrodynamics Method for the Extrapolation of Coronal Magnetic Fields from Vector Magnetograms**

### **I. Contopoulos**

Solar Physics, February 2013, Volume 282, Issue 2, pp 419-426

We present a new improved version of our force-free electrodynamics (FFE) numerical code in spherical coordinates that extrapolates the magnetic field in the inner solar corona from a photospheric vector magnetogram. The code satisfies the photospheric boundary condition and the condition  $\nabla \cdot \mathbf{B} = 0$  to machine accuracy. The performance of our method is evaluated with standard convergence parameters, and is found to be comparable to that of other nonlinear force-free extrapolations.

## **Nonlinear Force-Free Reconstruction of the Global Solar Magnetic Field: Methodology<<<**

### **I. Contopoulos, C. Kalapotharakos & M. K. Georgoulis**

Solar Physics, Volume 269, Number 2, 351-365, 2011

We present a novel numerical method that allows the calculation of nonlinear force-free magnetostatic solutions above a boundary surface on which only the distribution of the normal magnetic field component is given. The method relies on the theory of force-free electrodynamics and applies directly to the reconstruction of the solar coronal magnetic field for a given distribution of the photospheric radial field component. The method works as follows: we start with any initial magnetostatic global field configuration (e.g. zero, dipole), and along the boundary surface we create an evolving distribution of tangential (horizontal) electric fields that, via Faraday's equation, give rise to a respective normal-field distribution approaching asymptotically the target distribution. At the same time, these electric fields are used as boundary condition to numerically evolve the resulting electromagnetic field above the boundary surface, modeled as a thin ideal plasma with non-reflecting, perfectly absorbing outer boundaries. The simulation relaxes to a nonlinear force-free configuration that satisfies the given normal-field distribution on the boundary. This is different from existing methods relying on a fixed boundary condition – the boundary evolves toward the a priori given one, at the same time evolving the three-dimensional field solution above it. Moreover, this is the first time that a nonlinear force-free solution is reached by using only the normal field component on the boundary. This solution is not unique, but it depends on the initial magnetic field configuration and on the evolutionary course along the boundary surface. To our knowledge, this is the first time that the formalism of force-free electrodynamics, used very successfully in other astrophysical contexts, is applied to the global solar magnetic field.

## **SOLAR CYCLE VARIATIONS OF CORONAL NULL POINTS: IMPLICATIONS FOR THE MAGNETIC BREAKOUT MODEL OF CORONAL MASS EJECTIONS**

G. R. Cook<sup>1</sup>, D. H. Mackay<sup>1</sup>, and Dibyendu Nandy<sup>2</sup>

Astrophysical Journal, 704:1021–1035, 2009 October

In this paper, we investigate the solar cycle variation of coronal null points and magnetic breakout configurations in spherical geometry, using a combination of magnetic flux transport and potential field source surface models. Within the simulations, a total of 2843 coronal null points and breakout configurations are found over two solar cycles. It is found that the number of coronal nulls present at any time varies cyclically throughout the solar cycle, in phase with the flux emergence rate. At cycle maximum, peak values of 15–17 coronal nulls per day are found. No significant variation in the number of nulls is found from the rising to the declining phase. This indicates that the magnetic breakout model is applicable throughout both phases of the solar cycle. In addition, it is shown that when the simulations are used to construct synoptic data sets, such as those produced by Kitt Peak, the number of coronal nulls drops by a factor of 1/6. The vast majority of the coronal nulls are found to lie above the active latitudes and are the result of the complex nature of the underlying active region fields. Only 8% of the coronal nulls are found to be connected to the global dipole. Another interesting feature is that 18% of coronal nulls are found to lie above the equator due to cross-equatorial interactions between bipoles lying in the northern and southern hemispheres. As the



majority of coronal nulls form above active latitudes, their average radial extent is found to be in the lowcorona below

$1.25 R_{\odot}$  (175,000 km above the photosphere). Through considering the underlying photospheric flux, it is found that 71% of coronal nulls are produced through quadrupolar flux distributions resulting from bipoles in the same hemisphere interacting. When the number of coronal nulls present in each rotation is compared to the number of bipoles emerging, a wide scatter is found. The ratio of coronal nulls to emerging bipoles is found to be approximately 1/3. Overall, the spatio-temporal evolution of coronal nulls is found to follow the typical solar butterfly diagram and is in qualitative agreement with the observed time dependence of coronal mass ejection source-region locations.

### **Designing a New Coronal Magnetic Field Energy Diagnostic**

Marcel F. **Corchado-Albelo**<sup>1</sup>, Kévin Dalmasse<sup>2</sup>, Sarah Gibson<sup>3</sup>, Yuhong Fan<sup>3</sup>, and Anna Malanushenko  
2021 ApJ 907 23

<https://doi.org/10.3847/1538-4357/abc8f0>

In the solar corona, the free energy, i.e., the excess in magnetic energy over a ground-state potential field, forms the reservoir of energy that can be released during solar flares and coronal mass ejections. Such free energy provides a measure of the magnetic field nonpotentiality. Recent theoretical and observational studies indicate that the presence of nonpotential magnetic fields is imprinted into the structures of infrared, off-limb, coronal polarization. In this paper, we investigate the possibility of exploiting such observations for mapping and studying the accumulation and release of coronal free magnetic energy, with the goal of developing a new tool for identifying "hot spots" of coronal free energy such as those associated with twisted and/or sheared coronal magnetic fields. We applied forward modeling of infrared coronal polarimetry to three-dimensional models of nonpotential and potential magnetic fields. From these we defined a quantitative diagnostic of nonpotentiality that in the future could be calculated from a comparison of infrared, off-limb, coronal polarization observations from, e.g., the Coronal Multi-channel Polarimeter or the Daniel K. Inouye Solar Telescope, and the corresponding polarization signal forward-modeled from a potential field extrapolated from photospheric magnetograms. We considered the relative diagnostic potential of linear and circular polarization, and the sensitivities of these diagnostics to coronal density distributions and assumed boundary conditions of the potential field. Our work confirms the capacity of polarization measurements for diagnosing nonpotentiality and free energy in the solar corona.

### **Observables Processing for the Helioseismic and Magnetic Imager Instrument on the Solar Dynamics Observatory**

Sebastien **Couvidat**, Jesper Schou, J. Todd Hoeksema, Rick S. Bogart, Rock I. Bush, Tom L. Duvall, Yang Liu, Aimee A. Norton, Philip H. Scherrer

Solar Phys Volume 291, **Issue 7**, pp 1887–1938 **2016 Open Access**

<http://arxiv.org/pdf/1606.02368v1.pdf>

NASA's Solar Dynamics Observatory (SDO) was launched 11 February 2010 with 3 instruments on board, including the Helioseismic and Magnetic Imager (HMI). Since beginning normal operations on 1 May 2010, HMI has observed the Sun's entire visible disk almost continuously. HMI collects sequences of polarized filtergrams taken at a fixed cadence with two 4096 x 4096 cameras from which are computed arcsecond-resolution maps of photospheric observables: the line-of-sight (LoS) velocity and magnetic field, continuum intensity, line width, line depth, and the Stokes polarization parameters, I Q U V, at 6 wavelengths. Two processing pipelines implemented at the SDO Joint Science Operations Center (JSOC) at Stanford University compute observables from calibrated Level-1 filtergrams. One generates LoS quantities every 45s, and the other, primarily for the vector magnetic field, computes averages on a 720s cadence. Corrections are made for static and temporally changing CCD characteristics, bad pixels, image alignment and distortion, polarization irregularities, filter-element uncertainty and non-uniformity, as well as Sun-spacecraft velocity. This report explains issues affecting the resulting physical quantities, describes the impact of regular updates to the instrument calibration, and shows how the computations are optimized for actual HMI observations. During the 5 years of the SDO prime mission, regular calibration sequences have been used to regularly improve and update the instrument calibration and to monitor instrument changes. The instrument more than satisfies the original specifications for data quality and continuity. The procedures described here still have significant room for improvement. The most significant remaining systematic errors are associated with the spacecraft orbital velocity.

### **Transfer Learning in Spatial-Temporal Forecasting of the Solar Magnetic Field**

Eurico **Covas**

2019

<https://arxiv.org/pdf/1911.03193.pdf>

Machine learning techniques have been widely used in attempts to forecast several solar datasets. Most of these approaches employ supervised machine learning algorithms which are, in general, very data hungry. This hampers the attempts to forecast some of these data series, particularly the ones that depend on (relatively) recent space observations. Here we focus on an attempt to forecast the solar surface longitudinally averaged radial magnetic field

distribution using a form of spatial-temporal neural networks. Given that the recording of these spatial-temporal datasets only started in 1975 and are therefore quite short, the forecasts are predictably quite modest. However, given that there is a potential physical relationship between sunspots and the magnetic field, we employ another machine learning technique called transfer learning which has recently received considerable attention in the literature. Here, this approach consists in first training the source spatial-temporal neural network on the much longer time/latitude sunspot area dataset, which starts in 1874, then transferring the trained set of layers to a target network, and continue training the latter on the magnetic field dataset. The employment of transfer learning in the field of computer vision is known to obtain a generalized set of feature filters that can be reused for other datasets and tasks. Here we obtain a similar result, whereby we first train the network on the spatial-temporal sunspot area data, then the first few layers of the neural network are able to identify the two main features of the solar cycle, i.e. the amplitude variation and the migration to the equator, and therefore can be used to train on the magnetic field dataset and forecast better than a prediction based only on the historical magnetic field data.

## **Spatial-temporal forecasting the sunspot diagram**

Eurico [Covas](#)

A&A 605, A44 (2017)

**Aims.** We attempt to forecast the Sun's sunspot butterfly diagram in both space (i.e. in latitude) and time, instead of the usual one-dimensional time series forecasts prevalent in the scientific literature.

**Methods.** We use a prediction method based on the non-linear embedding of data series in high dimensions. We use this method to forecast both in latitude (space) and in time, using a full spatial-temporal series of the sunspot diagram from 1874 to 2015.

**Results.** The analysis of the results shows that it is indeed possible to reconstruct the overall shape and amplitude of the spatial-temporal pattern of sunspots, but that the method in its current form does not have real predictive power. We also apply a metric called structural similarity to compare the forecasted and the observed butterfly cycles, showing that this metric can be a useful addition to the usual root mean square error metric when analysing the efficiency of different prediction methods.

**Conclusions.** We conclude that it is in principle possible to reconstruct the full sunspot butterfly diagram for at least one cycle using this approach and that this method and others should be explored since just looking at metrics such as sunspot count number or sunspot total area coverage is too reductive given the spatial-temporal dynamical complexity of the sunspot butterfly diagram. However, more data and/or an improved approach is probably necessary to have true predictive power.

## **The Role of Turbulence in Coronal Heating and Solar Wind Expansion** Review

S. R. [Cranmer](#), [M. Asgari-Targhi](#), [M. P. Miralles](#), [J. C. Raymond](#), [L. Strachan](#), [H. Tian](#), [L. N. Woolsey](#)  
Phil. Trans. Royal Soc. A, theme issue on "Dissipation and Heating in Solar Wind Plasma Turbulence,"  
edited by K. Kiyani, K. Osman, and S. Chapman

2014

<http://arxiv.org/pdf/1412.2307v1.pdf>

Plasma in the Sun's hot corona expands into the heliosphere as a supersonic and highly magnetized solar wind. This paper provides an overview of our current understanding of how the corona is heated and how the solar wind is accelerated. Recent models of magnetohydrodynamic turbulence have progressed to the point of successfully predicting many observed properties of this complex, multi-scale system. However, it is not clear whether the heating in open-field regions comes mainly from the dissipation of turbulent fluctuations that are launched from the solar surface, or whether the chaotic "magnetic carpet" in the low corona energizes the system via magnetic reconnection. To help pin down the physics, we also review some key observational results from ultraviolet spectroscopy of the collisionless outer corona.

## **Suprathermal Electrons in the Solar Corona: Can Nonlocal Transport Explain Heliospheric Charge States?**

Steven R. [Cranmer](#)

ApJL, 791 L31, 2014

<http://arxiv.org/pdf/1407.5941v1.pdf>

There have been several ideas proposed to explain how the Sun's corona is heated and how the solar wind is accelerated. Some models assume that open magnetic field lines are heated by Alfvén waves driven by photospheric motions and dissipated after undergoing a turbulent cascade. Other models posit that much of the solar wind's mass and energy is injected via magnetic reconnection from closed coronal loops. The latter idea is motivated by observations of reconnecting jets and also by similarities of ion composition between closed loops and the slow wind. Wave/turbulence models have also succeeded in reproducing observed trends in ion composition signatures versus wind speed. However, the absolute values of the charge-state ratios predicted by those models tended to be too low in comparison with observations. This letter refines these predictions by taking better account of weak

Coulomb collisions for coronal electrons, whose thermodynamic properties determine the ion charge states in the low corona. A perturbative description of nonlocal electron transport is applied to an existing set of wave/turbulence models. The resulting electron velocity distributions in the low corona exhibit mild suprathermal tails characterized by "kappa" exponents between 10 and 25. These suprathermal electrons are found to be sufficiently energetic to enhance the charge states of oxygen ions, while maintaining the same relative trend with wind speed that was found when the distribution was assumed to be Maxwellian. The updated wave/turbulence models are in excellent agreement with solar wind ion composition measurements.

### **LINE SHAPE EFFECTS ON INTENSITY MEASUREMENTS OF SOLAR FEATURES: BRIGHTNESS CORRECTION TO SOHO MDI CONTINUUM IMAGES**

S. [Criscuoli](#)<sup>1</sup>, I. Ermolli<sup>1</sup>, D. Del Moro<sup>2</sup>, F. Giorgi<sup>1</sup>, A. Tritschler<sup>3</sup>, H. Uitenbroek<sup>3</sup> and N. Vitas  
**2011 ApJ 728 92**

Continuum intensity observations obtained with the Michelson Doppler Imager (MDI) on board the SOHO mission provide long time series of filtergrams that are ideal for studying the evolution of large-scale phenomena in the solar atmosphere and their dependence on solar activity. These filtergrams, however, are not taken in a pure continuum spectral band, but are constructed from a proxy, namely a combination of filtergrams sampling the Ni I 6768 Å line. We studied the sensitivity of this continuum proxy to the shape of the nickel line and to the degradation in the instrumental transmission profiles. We compared continuum intensity measurements near the nickel line with MDI proxy values in three sets of high-resolution spectro-polarimetric data obtained with the Interferometric Bidimensional Spectrometer, and in synthetic data, obtained from multi-dimensional simulations of magneto-convection and one-dimensional atmosphere models. We found that MDI continuum measurements require brightness corrections which depend on magnetic field strength, temperature and, to a smaller extent, plasma velocity. The correction ranges from 2% to 25% in sunspots, and is, on average, less than 2% for other features. The brightness correction also varies with position on the disk, with larger variations obtained for sunspots, and smaller variations obtained for quiet Sun, faculae, and micropores. Correction factors derived from observations agree with those deduced from the numerical simulations when observational effects are taken into account. Finally, we found that the investigated potential uncertainties in the transmission characteristics of MDI filters only slightly affect the brightness correction to proxy measurements.

### **Dynamic Properties along the Neutral Line of a Delta Spot Inferred from High-resolution Observations**

A. [Cristaldi](#)<sup>1,7,8</sup>, S. L. Guglielmino<sup>1</sup>, F. Zuccarello<sup>1</sup>, P. Romano<sup>2</sup>, M. Falco<sup>1</sup>, L. Rouppe van der Voort<sup>3</sup>, J. de la Cruz Rodríguez<sup>4</sup>, I. Ermolli<sup>5</sup>, and S. Criscuoli  
**2014 ApJ 789 162**

Delta ( $\delta$ ) spots are complex magnetic configurations of sunspots characterized by umbrae of opposite polarity sharing a common penumbra. In order to investigate the fine structure of the region separating the two magnetic polarities of a  $\delta$  spot, we studied the morphology, the magnetic configuration, and the velocity field in such a region using observations of active region (AR) NOAA 11267 obtained with the CRisp Imaging SpectroPolarimeter (CRISP) at the Swedish Solar Telescope on 2011 August 6. The analysis of CRISP data shows upflows and downflows of  $\sim \pm 3$  km s<sup>-1</sup> in proximity of the  $\delta$  spot polarity inversion line (PIL), and horizontal motions along the PIL of the order of  $\sim 1$  km s<sup>-1</sup>. The results obtained from the SIR inversion of CRISP data also indicate that the transverse magnetic field in the brighter region separating the two opposite magnetic polarities of the  $\delta$  spot is tilted about  $\sim 45^\circ$  with respect to the PIL. Solar Dynamics Observatory/Heliioseismic and Magnetic Imager observations confirm the presence of motions of  $\sim \pm 3$  km s<sup>-1</sup> in proximity of the PIL, which were observed to last 15 hr. From the data analyzed, we conclude that the steady, persistent, and subsonic motions observed along the  $\delta$  spot PIL can be interpreted as being due to Evershed flows occurring in the penumbral filaments that show a curved, wrapped configuration. The fluting of the penumbral filaments and their bending, continuously increased by the approaching motion of the negative umbra toward the positive one, give rise to the complex line-of-sight velocity maps that we observed.

### **Resolving the Azimuthal Ambiguity in Vector Magnetogram Data with the Divergence-Free Condition: Implementations for Disambiguating Each Height Independently**

A. D. [Crouch](#)

Solar Phys. Volume 290, Issue 10, pp 2677-2691 **2015**

We continue the investigation of how to use the divergence-free condition to resolve the azimuthal ambiguity present in vector magnetogram data. In previous articles by Crouch, Barnes, and Leka (Solar Phys. 260, 271, 2009) and Crouch (Solar Phys. 282, 107, 2013), all methods used an expression for the divergence of the magnetic field that involves differentiation of quantities that depend on the choice of azimuthal angle. As a result, all heights used

to approximate line-of-sight derivatives should generally be disambiguated simultaneously. In this article, we investigate a set of methods that use an expression for the divergence that involves differentiation of quantities that do not depend on the choice of azimuthal angle. This results in an expression for the divergence that can be used to disambiguate each height independently. We test two methods using synthetic data and find that the two-step hybrid method, adapted to disambiguate each height independently, generally produces reasonable results. Moreover, the time required to compute solutions is substantially decreased in comparison to the corresponding method that disambiguates all relevant heights simultaneously.

## **Resolving the Azimuthal Ambiguity in Vector Magnetogram Data with the Divergence-Free Condition: The Effects of Noise and Limited Spatial Resolution**

A. D. **Crouch**

Solar Phys., January **2013**, Volume 282, Issue 1, pp 107-131

We investigate how the azimuthal ambiguity in solar vector magnetogram data can be resolved by using the divergence-free property of magnetic fields. In a previous article, by Crouch, Barnes, and Leka (Solar Phys. 260, 271, 2009), error-free synthetic data were used to test several methods that each make a different assumption about how the divergence-free property can be used to resolve the ambiguity. In this paper this testing is continued with an examination of the effects of Poisson photon noise and limited instrumental spatial resolution. We find that all currently available methods based on the divergence-free property can produce undesirable results when photon noise or unresolved structure is present in the data. We perform a series of experiments aimed at improving the performance of the global minimisation method, which is the most promising of the methods. We present a two-step approach that produces reasonable results in tests using synthetic data. The first step of this approach involves the global minimisation of a combination of the absolute value of the approximation for the divergence and a smoothness constraint, which is designed to minimise the difference between the magnetic field in neighbouring pixels. In the second step, pixels with measurements known to be strongly affected by photon noise are revisited with a smoothing algorithm that also seeks to minimise the difference between the magnetic field in neighbouring pixels.

## **Field distribution of magnetograms from simulations of active region formation**

S. **Dacie**<sup>1</sup>, L. van Driel-Gesztelyi<sup>1, 2, 3</sup>, P. Démoulin<sup>2</sup>, M. G. Linton<sup>4</sup>, J. E. Leake<sup>4,5</sup>, D. MacTaggart<sup>6</sup> and M. C. M. Cheung<sup>7</sup>

A&A 606, A34 (**2017**)

<https://www.aanda.org/articles/aa/pdf/2017/10/aa30767-17.pdf>

Context. The evolution of the photospheric magnetic field distributions (probability densities) has previously been derived for a set of active regions. Photospheric field distributions are a consequence of physical processes that are difficult to determine from observations alone.

Aims. We analyse simulated magnetograms from numerical simulations, which model the emergence and decay of active regions. These simulations have different experimental set-ups and include different physical processes, allowing us to investigate the relative importance of convection, magnetic buoyancy, magnetic twist, and braiding for flux emergence.

Methods. We specifically studied the photospheric field distributions (probability densities found with a kernel density estimation analysis) and compared the results with those found from observations.

Results. Simulations including convection most accurately reproduce the observed evolution of the photospheric field distributions during active region evolution.

Conclusions. This indicates that convection may play an important role during the decay phase and also during the formation of active regions, particularly for low flux density values. **2013.06.19-22**

## **Evolution of the Magnetic Field Distribution of Active Regions**

Sally **Dacie**, Pascal Démoulin, Lidia van Driel-Gesztelyi, David Long, Deb Baker, Miho Janvier, Stephanie Yardley, David Pérez-Suárez

A&A 596, A69 **2016**

Aims. Although the temporal evolution of active regions (ARs) is relatively well understood, the processes involved continue to be the subject of investigation. We study how the magnetic field of a series of ARs evolves with time to better characterise how ARs emerge and disperse.

Methods. We examine the temporal variation in the magnetic field distribution of 37 emerging ARs. A kernel density estimation plot of the field distribution was created on a log-log scale for each AR at each time step. We

found that the central portion of the distribution is typically linear and its slope was used to characterise the evolution of the magnetic field.

Results. The slopes were seen to evolve with time, becoming less steep as the fragmented emerging flux coalesces. The slopes reached a maximum value of  $\sim -1.5$  just before the time of maximum flux before becoming steeper during the decay phase towards the quiet Sun value of  $\sim -3$ . This behaviour differs significantly from a classical diffusion model, which produces a slope of  $-1$ . These results suggest that simple classical diffusion is not responsible for the observed changes in field distribution, but that other processes play a significant role in flux dispersion.

Conclusions. We propose that the steep negative slope seen during the late decay phase is due to magnetic flux reprocessing by (super)granular convective cells.

## **EXPLOSIVE INSTABILITY AND CORONAL HEATING**

**R. B. Dahlburg**<sup>1</sup>, **J.-H. Liu**<sup>1</sup>, **J. A. Klimchuk**<sup>2,3</sup> and **G. Nigro**<sup>2</sup>

ApJ 704 1059-1064, 2009

The observed energy-loss rate from the solar corona implies that the coronal magnetic field has a critical angle at which energy is released. It has been hypothesized that at this critical angle an "explosive instability" would occur, leading to an enhanced conversion of magnetic energy into heat. In earlier investigations, we have shown that a shear-dependent magnetohydrodynamic process called "secondary instability" has many of the distinctive features of the hypothetical "explosive instability." In this paper, we give the first demonstration that this "secondary instability" occurs in a system with line-tied magnetic fields and boundary shearing—basically the situation described by Parker. We also show that, as the disturbance due to secondary instability attains finite amplitude, there is a transition to turbulence which leads to enhanced dissipation of magnetic and kinetic energy. These results are obtained from numerical simulations performed with a new parallelized, viscoresistive, three-dimensional code that solves the cold plasma equations. The code employs a Fourier collocation—finite difference spatial discretization, and uses a third-order Runge-Kutta temporal discretization.

## **A Statistical Comparison between Photospheric Vector Magnetograms Obtained by SDO/HMI and Hinode/SP**

Alberto Sainz **Dalda**

2017 ApJ 851 111

<https://arxiv.org/pdf/1801.07374.pdf>

Since 2010 May 1, we have been able to study (almost) continuously the vector magnetic field in the Sun, thanks to two space-based observatories: the Solar Dynamics Observatory (SDO) and Hinode. Both are equipped with instruments able to measure the Stokes parameters of Zeeman-induced polarization of photospheric line radiation. But the observation modes; the spectral lines; the spatial, spectral, and temporal sampling; and even the inversion codes used to recover magnetic and thermodynamic information from the Stokes profiles are different. We compare the vector magnetic fields derived from observations with the HMI instrument on board SDO with those observed by the SP instrument on Hinode. We have obtained relationships between components of magnetic vectors in the umbra, penumbra, and plage observed in 14 maps of NOAA Active Region 11084. Importantly, we have transformed SP data into observables comparable to those of HMI, to explore possible influences of the different modes of operation of the two instruments and the inversion schemes used to infer the magnetic fields. The assumed filling factor (fraction of each pixel containing a Zeeman signature) produces the most significant differences in derived magnetic properties, especially in the plage. The spectral and angular samplings have the next-largest effects. We suggest to treat the disambiguation in the same way in the data provided by HMI and SP. That would make the relationship between the vector magnetic field recovered from these data stronger, which would favor the simultaneous or complementary use of both instruments. **2010/06/29-07/05**

**HMI Science Nuggets #85 Feb 2018** <http://hmi.stanford.edu/hminuggets/?p=2316>

## **Data-Optimized Coronal Field Model: I. Proof of Concept**

K. **Dalmasse**, **A. Savcheva**, **S. E. Gibson**, **Y. Fan**, **D. W. Nychka**, **N. Flyer**, **N. Mathews**, **E. E. DeLuca**

ApJ 877 111 2019

<https://arxiv.org/pdf/1904.06308.pdf>

[sci-hub.se/10.3847/1538-4357/ab1907](https://doi.org/10.3847/1538-4357/ab1907)

Deriving the strength and direction of the three-dimensional (3D) magnetic field in the solar atmosphere is fundamental for understanding its dynamics. Volume information on the magnetic field mostly relies on coupling 3D reconstruction methods with photospheric and/or chromospheric surface vector magnetic fields. Infrared coronal polarimetry could provide additional information to better constrain magnetic field reconstructions. However, combining such data with reconstruction methods is challenging, e.g., because of the optical-thinness of the solar corona and the lack and limitations of stereoscopic polarimetry. To address these issues, we introduce the Data-Optimized Coronal Field Model (DOCFM) framework, a model-data fitting approach that combines a parametrized 3D generative model, e.g., a magnetic field extrapolation or a magnetohydrodynamic model, with forward modeling

of coronal data. We test it with a parametrized flux rope insertion method and infrared coronal polarimetry where synthetic observations are created from a known "ground truth" physical state. We show that this framework allows us to accurately retrieve the ground truth 3D magnetic field of a set of force-free field solutions from the flux rope insertion method. In observational studies, the DOCFM will provide a means to force the solutions derived with different reconstruction methods to satisfy additional, common, coronal constraints. The DOCFM framework therefore opens new perspectives for the exploitation of coronal polarimetry in magnetic field reconstructions and for developing new techniques to more reliably infer the 3D magnetic fields that trigger solar flares and coronal mass ejections.

### **Studying the Transfer of Magnetic Helicity in Solar Active Regions with the Connectivity-based Helicity Flux Density Method**

K. [Dalmasse](#)<sup>1</sup>, É. Pariat<sup>2</sup>, G. Valori<sup>3</sup>, J. Jing<sup>4</sup>, and P. Démoulin

2018 ApJ 852 141

<http://sci-hub.tw/http://iopscience.iop.org/0004-637X/852/2/141/>

In the solar corona, magnetic helicity slowly and continuously accumulates in response to plasma flows tangential to the photosphere and magnetic flux emergence through it. Analyzing this transfer of magnetic helicity is key for identifying its role in the dynamics of active regions (ARs). The connectivity-based helicity flux density method was recently developed for studying the 2D and 3D transfer of magnetic helicity in ARs. The method takes into account the 3D nature of magnetic helicity by explicitly using knowledge of the magnetic field connectivity, which allows it to faithfully track the photospheric flux of magnetic helicity. Because the magnetic field is not measured in the solar corona, modeled 3D solutions obtained from force-free magnetic field extrapolations must be used to derive the magnetic connectivity. Different extrapolation methods can lead to markedly different 3D magnetic field connectivities, thus questioning the reliability of the connectivity-based approach in observational applications. We address these concerns by applying this method to the isolated and internally complex AR 11158 with different magnetic field extrapolation models. We show that the connectivity-based calculations are robust to different extrapolation methods, in particular with regard to identifying regions of opposite magnetic helicity flux. We conclude that the connectivity-based approach can be reliably used in observational analyses and is a promising tool for studying the transfer of magnetic helicity in ARs and relating it to their flaring activity. **2011 February 14**

### **ROAM: a Radial-basis-function Optimization Approximation Method for diagnosing the three-dimensional coronal magnetic field**

K. [Dalmasse](#), D. W. Nychka, S. E. Gibson, [Y. Fan](#), [N. Flyer](#)

Frontiers in Astronomy and Space Sciences **2016**

<http://arxiv.org/pdf/1607.03460v1.pdf>

The Coronal Multichannel Polarimeter (CoMP) routinely performs coronal polarimetric measurements using the Fe XIII 10747 Å and 10798 Å lines, which are sensitive to the coronal magnetic field. However, inverting such polarimetric measurements into magnetic field data is a difficult task because the corona is optically thin at these wavelengths and the observed signal is therefore the integrated emission of all the plasma along the line of sight. To overcome this difficulty, we take on a new approach that combines a parameterized 3D magnetic field model with forward modeling of the polarization signal. For that purpose, we develop a new, fast and efficient, optimization method for model-data fitting: the Radial-basis-functions Optimization Approximation Method (ROAM). Model-data fitting is achieved by optimizing a user-specified log-likelihood function that quantifies the differences between the observed polarization signal and its synthetic/predicted analogue. Speed and efficiency are obtained by combining sparse evaluation of the magnetic model with radial-basis-function (RBF) decomposition of the log-likelihood function. The RBF decomposition provides an analytical expression for the log-likelihood function that is used to inexpensively estimate the set of parameter values optimizing it. We test and validate ROAM on a synthetic test bed of a coronal magnetic flux rope and show that it performs well with a significantly sparse sample of the parameter space. We conclude that our optimization method is well-suited for fast and efficient model-data fitting and can be exploited for converting coronal polarimetric measurements, such as the ones provided by CoMP, into coronal magnetic field data.

### **Internetwork magnetic field as revealed by two-dimensional inversions**

S. [Danilovic](#)<sup>1</sup>, M. van Noort<sup>1</sup> and M. Rempel

A&A 593, A93 (2016)

Context. Properties of magnetic field in the internetwork regions are still fairly unknown because of rather weak spectropolarimetric signals.

Aims. We address the matter by using the two-dimensional (2D) inversion code, which is able to retrieve the information on smallest spatial scales up to the diffraction limit, while being less susceptible to noise than most of the previous methods used.

Methods. Performance of the code and the impact of various effects on the retrieved field distribution is tested first on the realistic magneto-hydrodynamic (MHD) simulations. The best inversion scenario is then applied to the real data obtained by Spectropolarimeter (SP) on board Hinode.

Results. Tests on simulations show that: (1) the best choice of node position ensures a decent retrieval of all parameters; (2) the code performs well for different configurations of magnetic field; (3) slightly different noise levels or slightly different defocus included in the spatial point spread function (PSF) produces no significant effect on the results; and (4) temporal integration shifts the field distribution to a stronger, more horizontally inclined field. Conclusions. Although the contribution of the weak field is slightly overestimated owing to noise, 2D inversions are able to recover well the overall distribution of the magnetic field strength. Application of the 2D inversion code on the Hinode SP internetwork observations reveals a monotonic field strength distribution. The mean field strength at optical depth unity is  $\sim 130$  G. At higher layers, field strength drops as the field becomes more horizontal. Regarding the distribution of the field inclination, tests show that we cannot directly retrieve it with the observations and tools at hand, however, the obtained distributions are consistent with those expected from simulations with a quasi-isotropic field inclination after accounting for observational effects.

## **Simulated Magnetic Flows in the Solar Photosphere**

S. [Danilovic](#), R. H. Cameron, S. K. Solanki

A&A, 2014

<http://arxiv.org/pdf/1408.6159v1.pdf>

Recent Sunrise/IMaX observations have revealed the existence of supersonic magnetic flows. Our aim is to determine the origin of such flows by using realistic MHD simulations. We simulate cancellation and emergence of magnetic flux through the solar photosphere. Our first numerical experiment starts with magnetic field of both polarities. To simulate emergence into a region with pre-existing field, we introduce a large-scale horizontally uniform sheet of horizontal field. We follow the subsequent evolution, creating synthetic polarimetric observations, including known instrumental effects of the Sunrise/IMaX and Hinode/SP instruments. We compare the simulated and observed spectropolarimetric signals. Strongly blue- and redshifted Stokes V signals are produced in locations where strong line-of-sight velocities coincide with the strong line-of-sight component of magnetic field. The size and strength of simulated events is smaller than observed and they are mostly associated with downflows, contrary to observations. In a few cases where they appear above a granule, single blue lobed Stokes V are produced due to strong gradients in magnetic field and velocity. No change of magnetic field sign is detected along the line of sight in these instances. More high-speed magnetized flows occur in the case where emergence is simulated than in the case where no horizontal field was added. The simulations indicate that the observed events result from magnetic flux emergence, where reconnection may take place but does not seem to be necessary.

<http://www2.mps.mpg.de/data/outgoing/danilovic/ss/> - **movies**.

## **The 2019 July 2 Total Solar Eclipse: Prediction of the Coronal Magnetic Field Structure and Polarization Characteristics**

Soumyaranjan [Dash](#), [Prantika Bhowmik](#), [Athira B S](#), [Nirmalya Ghosh](#), [Dibyendu Nandy](#)

2020 *ApJ* 890 37

<https://arxiv.org/pdf/1906.10201.pdf>

<https://doi.org/10.3847/1538-4357/ab6a91>

On **2019 July 2** a total solar eclipse -- visible across some parts of the Southern Pacific Ocean, Chile and Argentina -- will enable observations of the Sun's large-scale coronal structure. The structure of the Sun's corona and their emission characteristics are determined by underlying magnetic fields which also govern coronal heating and solar eruptive events. However, coronal magnetic field measurements remain an outstanding challenge. Computational models of coronal magnetic fields serve an important purpose in this context. Earlier work has demonstrated that the large-scale coronal field is governed by slow surface flux evolution and memory build-up which allows for prediction of the coronal structure on solar rotational timescales. Utilizing this idea and based upon a 51 day forward run of a data-driven solar surface flux transport model and a Potential Field Source Surface model, we predict the Sun's coronal structure for the 2019 July 2 solar eclipse. We also forward model the polarization characteristics of the coronal emission from the predicted magnetic fields. We predict two large-scale streamer structures and their locations on the east and west limbs of the Sun and discuss the possibility of development of a pseudo-streamer based on an analysis of field line topology. This study is relevant for coronal magnetometry initiatives from ground-based facilities such as the Daniel K. Inouye Solar Telescope and Coronal Multichannel Polarimeter, and upcoming space-based instruments such as the Solar Ultraviolet Imaging Telescope and the Variable Emission Line Coronagraph onboard ISRO's Aditya-L1 space mission.

## **Prediction of the Sun's Corona for the Total Solar Eclipse on 2019 July 2**

Soumyaranjan [Dash](#), [Prantika Bhowmik](#), and [Dibyendu Nandy](#)

Res. Notes AAS 3 86 2019

<https://iopscience.iop.org/article/10.3847/2515-5172/ab2ae3>

We utilize the scheme developed by Nandy et al. ([2018](#)) to predict the coronal structure of the 2019 July 2 total solar eclipse which will be visible across a path mostly overlying the Pacific Ocean, Chile and Argentina. Here, we present our primary prediction of the Sun's coronal magnetic field structure and a "synthetic" white light corona generated from the predicted coronal magnetic map. Technical details of the research leading to this prediction, including model descriptions and additional analysis will be presented elsewhere.

## **Projections for measuring the size of the solar core with neutrino-electron scattering**

Jonathan H. [Davis](#)

2016

<http://arxiv.org/pdf/1606.02558v1.pdf>

We quantify the amount of data needed in order to measure the size of the solar core with future experiments looking at elastic scattering between electrons and solar neutrinos. The directions of the electrons immediately after scattering are strongly correlated with the incident directions of the neutrinos, however this is degraded significantly by the subsequent scattering of these electrons in the detector medium. We generate distributions of such electrons for different sizes of the solar core, and use a maximum likelihood analysis to make projections for future experimental sensitivity. We find that after approximately 5 years of data-taking an experiment the size of Hyper Kamiokande could measure the solar core radius with an uncertainty of 20% of the total solar radius at 95% confidence, and could exclude the scenario where the neutrinos are produced throughout the entire sun at  $3\sigma$ .

## **Polarization of the Ly $\alpha$ Lines of H i and He ii as a Tool for Exploring the Solar Corona**

Supriya Hebbur [Dayananda](#)<sup>1,2</sup>, Javier Trujillo Bueno<sup>1,2,3</sup>, Ángel de Vicente<sup>1,2</sup>, and Tanausú del Pino Alemán<sup>1,2</sup>

2021 ApJ 920 140

<https://doi.org/10.3847/1538-4357/ac1068>

The near-Earth space weather is driven by the quick release of magnetic free energy in the solar corona. Probing this extremely hot and rarified region of the extended solar atmosphere requires modeling the polarization of forbidden and permitted coronal lines. To this end, it is important to develop efficient codes to calculate the Stokes profiles that emerge from given three-dimensional (3D) coronal models and this should be done taking into account the symmetry breaking produced by the presence of magnetic fields and non-radial solar wind velocities. We have developed such a tool with the aim of theoretically predicting and interpreting spectropolarimetric observations of the solar corona in permitted and forbidden lines. In this paper, we show the results of a theoretical investigation of the linear polarization signals produced by scattering processes in the H i Ly $\alpha$  line at 1216 Å and in the He ii Ly $\alpha$  line at 304 Å using 3D coronal models by Predictive Science Inc. These spectral lines have very different critical magnetic fields for the onset of the Hanle effect (53 G and 850 G, respectively), as well as different sensitivities to the Doppler effect caused by the solar wind velocities. We study under which circumstances simultaneous observations of the scattering polarization in these Ly $\alpha$  lines can facilitate the determination of magnetic fields and macroscopic velocities in the solar corona.

## **Inbound waves in the solar corona: a direct indicator of Alfvén Surface location**

C.E. [DeForest](#), T.A. Howard, D.J. McComas

ApJ, 787 124, 2014

<http://arxiv.org/pdf/1404.3235v2.pdf>

The tenuous supersonic solar wind that streams from the top of the corona passes through a natural boundary -- the Alfvén surface -- that marks the causal disconnection of individual packets of plasma and magnetic flux from the Sun itself. The Alfvén surface is the locus where the radial motion of the accelerating solar wind passes the radial Alfvén speed, and therefore any displacement of material cannot carry information back down into the corona. It is thus the natural outer boundary of the solar corona, and the inner boundary of interplanetary space. Using a new and unique motion analysis to separate inbound and outbound motions in synoptic visible-light image sequences from the COR2 coronagraph on board the STEREO-A spacecraft, we have identified inbound wave motion in the outer corona beyond 6 solar radii for the first time, and used it to determine that the Alfvén surface is at least 12.5 solar radii from the Sun over the polar coronal holes and 17 solar radii in the streamer belt, well beyond the distance planned for NASA's upcoming Solar Probe Plus mission. To our knowledge this is the first measurement of inbound waves in the outer solar corona, and the first direct measurement of lower bounds for the Alfvén surface.

2007 August 4–14

## **DISCONNECTING OPEN SOLAR MAGNETIC FLUX**

C. E. [DeForest](#)<sup>1</sup>, T. A. Howard<sup>1</sup> and D. J. McComas

2012 ApJ 745 36

Disconnection of open magnetic flux by reconnection is required to balance the injection of open flux by coronal mass ejections and other eruptive events. Making use of recent advances in heliospheric background subtraction, we



have imaged many abrupt disconnection events. These events produce dense plasma clouds whose distinctive shape can now be traced from the corona across the inner solar system via heliospheric imaging. The morphology of each initial event is characteristic of magnetic reconnection across a current sheet, and the newly disconnected flux takes the form of a "U"-shaped loop that moves outward, accreting coronal and solar wind material. We analyzed one such event on **2008 December 18** as it formed and accelerated at  $20 \text{ m s}^{-2}$  to  $320 \text{ km s}^{-1}$ , thereafter expanding self-similarly until it exited our field of view 1.2 AU from the Sun. From acceleration and photometric mass estimates we derive the coronal magnetic field strength to be  $8 \mu\text{T}$ ,  $6 R_{\odot}$  above the photosphere, and the entrained flux to be  $1.6 \times 10^{11} \text{ Wb}$  ( $1.6 \times 10^{19} \text{ Mx}$ ). We model the feature's propagation by balancing inferred magnetic tension force against accretion drag. This model is consistent with the feature's behavior and accepted solar wind parameters. By counting events over a 36 day window, we estimate a global event rate of  $1 \text{ day}^{-1}$  and a global solar minimum unsigned flux disconnection rate of  $6 \times 10^{13} \text{ Wb yr}^{-1}$  ( $6 \times 10^{21} \text{ Mx yr}^{-1}$ ) by this mechanism. That rate corresponds to  $\sim -0.2 \text{ nT yr}^{-1}$  change in the radial heliospheric field at 1 AU, indicating that the mechanism is important to the heliospheric flux balance.

## **The magnetic sensitivity of the (250-278nm) Fe II polarization spectrum**

[David Afonso Delgado](#), [Tanausú del Pino Alemán](#), [Javier Trujillo Bueno](#)

ApJ 2023

<https://arxiv.org/pdf/2303.07066.pdf>

This paper presents a theoretical investigation on the polarization and magnetic sensitivity of the near-ultraviolet (near-UV) solar spectral lines of Fe II between 250 and 278 nm. In recent years, UV spectropolarimetry has become key to uncover the magnetism of the upper layers of the solar chromosphere. The unprecedented data obtained by the CLASP2 suborbital space experiment across the Mg II h and k lines around 280 nm are a clear example of the capabilities of near-UV spectropolarimetry for the magnetic field diagnostics throughout the whole solar chromosphere. Recent works have pointed out the possible complementary diagnostic potential of the many Fe II lines in the unexplored spectral region between 250 and 278 nm, but no quantitative analysis of the polarization and magnetic sensitivity of those spectral lines has been carried out yet. To study the polarization signals in these spectral lines, we create a comprehensive atomic model including all the atomic transitions resulting in strong spectral lines. We then study the magnetic sensitivity of the linear and circular polarization profiles in a semi-empirical model representative of the quiet sun. We present a selection of Fe II spectral lines with significant linear and circular polarization signals and evaluate their diagnostic capabilities by studying their formation heights and magnetic sensitivity through the action of the Hanle and Zeeman effects. We conclude that when combined with the CLASP2 spectral region these Fe II lines are of interest for the inference of magnetic fields throughout the solar chromosphere, up to near the base of the corona.

## **Reconstructing Highly-twisted Magnetic Fields**

[Victor M. Demcsak](#), [Michael S. Wheatland](#), [Alpha Mastrano](#), [Kai E. Yang](#)

Solar Phys. 295, Article number: 116 2020

<https://arxiv.org/pdf/2008.02985.pdf>

<https://link.springer.com/content/pdf/10.1007/s11207-020-01681-5.pdf>

We investigate the ability of a nonlinear force-free code to calculate highly-twisted magnetic field configurations using the Titov and Démoulin (1999) equilibrium field as a test case. The code calculates a force-free field using boundary conditions on the normal component of the field in the lower boundary, and the normal component of the current density over one polarity of the field in the lower boundary. The code can also use the current density over both polarities of the field in the lower boundary as a boundary condition. We investigate the accuracy of the reconstructions with increasing flux-rope surface twist number  $N_t$ , achieved by decreasing the sub-surface line current in the model. We find that the code can approximately reconstruct the Titov-Démoulin field for surface twist numbers up to  $N_t \approx 8.8$ . This includes configurations with bald patches. We investigate the ability to recover bald patches, and more generally identify the limitations of our method for highly-twisted fields. The results have implications for our ability to reconstruct coronal magnetic fields from observational data.

## **Large-Scale Solar Magnetic Fields Observed with the Infrared Spectro-Polarimeter IRmag at the National Astronomical Observatory of Japan: Comparison of Measurements Made in Different Spectral Lines and Observatories**

M. L. [Demidov](#), [Y. Hanaoka](#), [T. Sakurai](#) & [X. F. Wang](#)

[Solar Physics](#) volume 295, Article number: 54 (2020)

<https://link.springer.com/content/pdf/10.1007/s11207-020-01620-4.pdf>

This study presents the results of a quantitative analysis of IRmag (infrared Stokes spectro-polarimeter, National Astronomical Observatory of Japan, (NAOJ)/Mitaka) observations in three spectral lines Fe I 1564.8 nm, Si I 1082.72 nm, He I 1083.0 nm, and comparison between IRmag magnetograms and ones from the Solar Dynamic Observatory/Helioseismic and Magnetic Imager (SDO/HMI), Global Oscillation Network Group (GONG), Wilcox Solar Observatory (WSO), and Solar Telescope for Operative Predictions (STOP). It is shown that there is a good

correlation between observations in all three IRmag spectral lines, but with significant differences in the measured field strengths caused by different depths of formation and, probably, by calibration issues. The correlation of IRmag magnetograms with ones from other observatories, and between different observatories among each other, is as good as 0.70 – 0.95, depending on the combination, but nevertheless there are significant systematic differences (linear-regression coefficients deviating from unity) between different data sets (up to a factor of three or even more). **15 January 2013, 30 October 2015**



## **On the Measurements of Full-Disk Longitudinal Magnetograms at Huairou Solar Observing Station**

M. L. [Demidov](#), X. F. Wang, D. G. Wang, Y. Y. Deng

[Solar Physics](#) October **2018**, 293:146

Reliable information on the distribution of magnetic fields across the whole surface of the Sun is urgently needed to predict conditions in the solar corona, in the interplanetary medium, and in the near-Earth space (space weather). Several space- and ground-based solar instruments currently provide full-disk magnetograms. However, these measurements sometimes differ very significantly, which makes a cross-calibration of different datasets and searching for the reasons for such differences a very crucial task. Here, we analyze the Huairou Solar Observing Station (HSOS) Solar Magnetism and Activity Telescope (SMAT) full-disk line-of-sight magnetograms in comparison with magnetograms taken at the Solar Dynamic Observatory/Helioseismic and Magnetic Imager (SDO/HMI) and Solar Telescope for Operative Predictions (STOP) instruments. We show systematic differences between original SMAT magnetograms and those of other telescopes. The differences are caused by some SMAT instrumental problems, which we investigate. We suggest methods for compensating for these effects that have improved the quality of SMAT magnetograms. These methods will enable us to use SMAT measurements to solve many solar physics problems that are related to studying global solar magnetism and space weather.

## **Spectro-Polarimetric Observations of Solar Magnetic Fields and the SOHO/MDI Calibration Issue**

M. L. [Demidov](#) and H. Balthasar<sup>2</sup>

[Solar Phys.](#), 260(2), 261-270, **2009**

Comparisons of solar magnetic-field measurements made in different spectral lines are very important, especially in those lines in which observations have a long history or (and) specific diagnostic significance. The spectral lines Fe I 523.3 nm and Fe I 525.0 nm belong to this class. Therefore, this study is devoted to a comprehensive analysis using new high-precision Stokes-meter full-disk observations. The disk-averaged magnetic-field strength ratio  $R=B(523.3)/B(525.0)$  equals  $1.97\pm 0.02$ . The center-to-limb variation (CLV) is  $R=1.74-2.43\mu+3.43\mu^2$ , where  $\mu$  is the cosine of the center-to-limb angle. For the disk center, we find  $R=2.74$ , and for near-limb areas with  $\mu=0.3$ ,  $R$  equals 1.32. There is only a small dependence of  $R$  on the spatial resolution. Our results are rather close to those published three decades ago, but differ significantly from recent magnetographic observations. An application of our results to the important SOHO/MDI magnetic data calibration issue is discussed. We conclude that the revision of the SOHO/MDI data, based only on the comparison of magnetic-field measurements in the line pair Fe I 523.3 nm and Fe I 525.0 nm (increasing by a factor of 1.7 or 1.6 on average according to recent publications) is not obvious and new investigations are urgently needed.

## **Extending the concept of separatrices to QSLs for magnetic reconnection**

[Demoulin](#) P.: 2006,

[Advances in Space Research](#), 37, 7, 1269, **2006**.

## **Recent theoretical and observational developments in magnetic helicity studies --**

[Demoulin](#), Pascal, E-print, Dec **2006**

## **PUTTING CORONAL SEISMOLOGY ESTIMATES OF THE MAGNETIC FIELD STRENGTH TO THE TEST**

I. [De Moortel](#), [D. J. Pascoe](#),

[ApJ](#) 699 L72-L75, **2009**

<http://www.iop.org/EJ/abstract/1538-4357/699/2/L72>

Magnetic field strength inside a model coronal loop is "estimated" using coronal seismology, to examine the reliability of magnetic field strengths derived from observed, transverse coronal loop oscillations. Three-dimensional numerical simulations of the interaction of an external pressure pulse with a coronal loop (modeled as a three-dimensional density enhancement inside a two-dimensional magnetic arcade) are analyzed and the "observed" properties of the excited transverse loop oscillations are used to derive the value of the local magnetic field strength,

following the method of Nakariakov & Ofman. Due to the (unexpected) change in periodicity, the magnetic field derived from our "observed" oscillation is substantially different from the actual (input) magnetic field value (approximately 50%). Coronal seismology can derive useful information about the local magnetic field, but the combined effect of the loop curvature, the density ratio, and aspect ratio of the loop appears to be more important than previously expected.

### **The Roles of Reconnected Flux and Overlying Fields in CME Speeds**

Minda **Deng**, Brian T. Welsch

2015

<http://arxiv.org/pdf/1504.02905v1.pdf>

The standard model of eruptive, two-ribbon flares involves reconnection of over-lying magnetic fields beneath a rising ejection. Numerous observers have reported evidence linking this reconnection, indicated by photospheric flux swept out by flare ribbons, to coronal mass ejection (CME) acceleration. This acceleration might be caused by reconnected fields that wrap around the ejection producing an increased outward hoop force. Other observations have linked stronger over-lying fields, measured by the power-law index of the fitted decay rate of field strength overlying eruption sites, to slower CME speeds. This might be caused by greater downward magnetic tension in stronger overlying fields. So overlying fields might both help and hinder the acceleration of CMEs: reconnection that converts overlying fields into flux winding about the ejection might help, but unreconnected overlying fields might hurt. Here, we investigate the roles of both ribbon fluxes and the decay rates of overlying fields in a set of 16 eruptive events. We confirm previous results that higher CME speeds are associated with both larger ribbon fluxes and more rapidly decaying overlying fields. We find the association with ribbon fluxes to be weaker than a previous report, but stronger than the dependence on the decay rate of overlying fields. **1998 Apr 29, 1998 Nov 05, 2000 Jan 18, 2000 Jul 25, 2000 Aug 09, 2000 Nov 24, 2001 Apr 10, 2001 Apr 26, 2001 Sep 28, 2002 Mar 20, 2002 July 26, 2003 Oct 28, 2003 Oct 29, 2003 Nov 18, 2004 Nov 07, 2005 May 13**

### **3D electron density distributions in the solar corona during solar minima: assessment for more realistic solar wind modeling**

Judith **de Patoul**, Claire Foullon, Pete Riley

2015

<http://arxiv.org/pdf/1512.04135v1.pdf>

Knowledge of the electron density distribution in the solar corona put constraints on the magnetic field configurations for coronal modeling and on initial conditions for solar wind modeling. We work with polarized SOHO/LASCO-C2 images from the last two recent minima of solar activity (1996-1997 and 2008-2010), devoid of coronal mass ejections. The goals are to derive the 4D electron density distributions in the corona by applying a newly developed time-dependent tomographic reconstruction method and to compare the results between the two solar minima and with two magnetohydrodynamic models. First, we confirm that the values of the density distribution in thermodynamic models are more realistic than in polytropic ones. The tomography provides more accurate distributions in the polar regions, and we find that the density in tomographic and thermodynamic solutions varies with the solar cycle in both polar and equatorial regions. Second, we find that the highest-density structures do not always correspond to the predicted large-scale heliospheric current sheet or its helmet streamer but can follow the locations of pseudo-streamers. We deduce that tomography offers reliable density distributions in the corona, reproducing the slow time evolution of coronal structures, without prior knowledge of the coronal magnetic field over a full rotation. Finally, we suggest that the highest-density structures show a differential rotation well above the surface depending on how they are magnetically connected to the surface. Such valuable information on the rotation of large-scale structures could help to connect the sources of the solar wind to their in situ counterparts in future missions such as Solar Orbiter and Solar Probe Plus.

See **UKSP Nugget #64, 2016** <http://www.uksolphys.org/?p=10950>

### **Coronal Densities, Temperatures and Abundances During the 2019 Total Solar Eclipse: The Role of Multi-Wavelength Observations in Coronal Plasma Characterization**

[G. Del Zanna](#), [J. Samra](#), [A. Monaghan](#), [C. Madsen](#), [P. Bryans](#), [E. DeLuca](#), [H. Mason](#), [B. Berkey](#), [A. de Wijn](#), [Y. Rivera](#)

ApJ 2022

<https://arxiv.org/pdf/2212.11889.pdf>

The Airborne Infrared Spectrometer (AIR-Spec) offers an unprecedented opportunity to explore the Near Infra-Red (NIR) wavelength range. It has been flown at two total solar eclipses, in 2017 and 2019. The wavelength range of the much improved instrument on the second flight (July 2, 2019) was shifted to cover two density sensitive lines from S XI. In this paper we study detailed diagnostics for temperature, electron density and elemental abundances by comparing results from AIR-Spec slit positions above the east and the west limb with those from Hinode/EIS, the PolarCam detector and SDO/AIA. We find very good agreement in the electron densities obtained from the EIS

EUV line ratios, those from the NIR S XI ratio and those obtained from the polarized brightness PolarCam measurements. Electron densities ranged from  $\text{Log Ne [cm}^{-3}] = 8.4$  near the limb, falling to 7.2 at  $R_0=1.3$ . EIS spectra indicate that the temperature distribution above the west limb is near-isothermal at around 1.3 MK, while that on the east has an additional higher-T component. The AIR-Spec radiances in Si X and S XI as well as the AIA data in the 171, 193, and 211 Angstroms bands are consistent with the EIS results. EIS and AIR-Spec data indicate that the sulphur abundance (relative to silicon) is photospheric in both regions, confirming our previous results of the 2017 eclipse. The AIA data also indicate that the absolute iron abundance is photospheric. Our analysis confirms the importance of the diagnostic potential of the NIR wavelength range, and that this important wavelength range can be used reliably and independently to determine coronal plasma parameters. **2 Jul 2019**

## Probing the Sunspot Atmosphere with Three-Minute Oscillations

A.S. Deres, [S.A. Anfinogentov](#)

[Solar Physics](#) January 2018, 293:2

<https://link.springer.com/content/pdf/10.1007%2Fs11207-017-1222-0.pdf>

<https://arxiv.org/pdf/1710.11552.pdf>

We present a seismological method to probe the solar atmosphere above sunspot umbrae with three-minute oscillations. Our technique allows us to estimate both the vertical distance between atmospheric layers and the wave-propagation speed without specifying any extra parameters, in particular, the phase speed of the wave or the emission formation heights. Our method uses the projected wave paths of slow MHD waves propagating through the atmospheric layers of different heights and guided by the magnetic field. The length of the projected wave path depends upon the distance between the layers and the inclination angle of the magnetic field with respect to the line of sight, allowing us to estimate the distance between the layers from measured projected wave paths and the local magnetic-field vector. In turn, the wave-propagation delay registered at different heights allows for the calculation of the phase speed. We estimated the vertical distance between the emission layers at the temperature minimum (1600 Å) and transition region (304 Å), as well as the average phase speed above the sunspot umbrae, for three active regions. We found that the distance between the 1600 Å emission layer and the transition region above the sunspot umbrae lies in the range of 500 -- 800 km. The average phase speed between these layers was found to be about 30 km/s giving the sound speed of 6 km/s. The temperature between the layers has been roughly estimated as 3000 K and corresponds to the region of the temperature minimum. The results obtained are consistent with the semiempirical model of the sunspot umbrae atmosphere by Fontenla, 2009. **8 December 2010, 2 October 2012, 6 April 2013**

## The Influence of Spatial Resolution on Nonlinear Force-Free Modeling

M. L. DeRosa, M. S. Wheatland, K. D. Leka, G. Barnes, T. Amari, A. Canou, S. A. Gilchrist, J. K. Thalmann, G. Valori, T. Wiegelmann, C. J. Schrijver, A. Malanushenko, X. Sun, S. Rognier

ApJ 811 107 2015

<http://arxiv.org/pdf/1508.05455v1.pdf>

The nonlinear force-free field (NLFFF) model is often used to describe the solar coronal magnetic field, however a series of earlier studies revealed difficulties in the numerical solution of the model in application to photospheric boundary data. We investigate the sensitivity of the modeling to the spatial resolution of the boundary data, by applying multiple codes that numerically solve the NLFFF model to a sequence of vector magnetogram data at different resolutions, prepared from a single Hinode/SOT-SP scan of NOAA Active Region 10978 on **2007 December 13**. We analyze the resulting energies and relative magnetic helicities, employ a Helmholtz decomposition to characterize divergence errors, and quantify changes made by the codes to the vector magnetogram boundary data in order to be compatible with the force-free model. This study shows that NLFFF modeling results depend quantitatively on the spatial resolution of the input boundary data, and that using more highly resolved boundary data yields more self-consistent results. The free energies of the resulting solutions generally trend higher with increasing resolution, while relative magnetic helicity values vary significantly between resolutions for all methods. All methods require changing the horizontal components, and for some methods also the vertical components, of the vector magnetogram boundary field in excess of nominal uncertainties in the data. The solutions produced by the various methods are significantly different at each resolution level. We continue to recommend verifying agreement between the modeled field lines and corresponding coronal loop images before any NLFFF model is used in a scientific setting.

See: HMI Science Nuggets, #45, Nov 2015 <http://hmi.stanford.edu/hminuggets/?p=1323>

## SOLAR MAGNETIC FIELD REVERSALS AND THE ROLE OF DYNAMO FAMILIES

M. L. DeRosa<sup>1</sup>, A. S. Brun<sup>2</sup>, and J. T. Hoeksema

2012 ApJ 757 96

The variable magnetic field of the solar photosphere exhibits periodic reversals as a result of dynamo activity occurring within the solar interior. We decompose the surface field as observed by both the Wilcox Solar Observatory and the Michelson Doppler Imager into its harmonic constituents, and present the time evolution of the mode coefficients for the past three sunspot cycles. The interplay between the various modes is then interpreted from the perspective of general dynamo theory, where the coupling between the primary and secondary families of modes is found to correlate with large-scale polarity reversals for many examples of cyclic dynamos. Mean-field dynamos based on the solar parameter regime are then used to explore how such couplings may result in the various long-term trends in the surface magnetic field observed to occur in the solar case.

### **Notice regarding 'pfss' SolarSoft package**

Marc **DeRosa** & Karel Schrijver

Solar News, 15 Sep 2011

<http://solarnews.nso.edu/2011/20110915.html>

The 'pfss' package in SolarSoft enables access to **potential-field source-surface (PFSS) extrapolations** of the global coronal magnetic field. These extrapolations are computed using evolving surface-flux maps of the full-Sun radial photospheric magnetic field as a lower boundary condition. Such maps are created several times per day by assimilating magnetograms into a surface flux dispersal code (see Schrijver & DeRosa 2003, Sol.Phys., 212, 165) using the most recently available magnetogram data. This database of full-Sun magnetic maps and the associated PFSS extrapolations of the coronal magnetic field now contains over 20,000 entries, spanning 15+ years from July 1996 to the present day.

This software was in part developed to produce up-to-date information about solar conditions for, e.g., coordination with space- and ground-based observatories. Because the data being assimilated are taken from a near-real-time stream, image artifacts and data-flow interruptions occur, and consequently many quality checks are performed on these data prior to assimilation into the surface-flux model. We recently became aware that an unusually high number of magnetograms were being erroneously rejected from inclusion in the surface-flux model from late 2007 through mid 2010, and that some active-region flux may not have been properly accounted for.

Because the 'pfss' SolarSoft package sees increased use as an aid in the analysis and interpretation of observations, we have decided to rerun the assimilation model from 2007/09/01 forward to the present day (as before, using SOHO/MDI Level 1.8 data from 2007/09/01 through 2010/07/14, and transitioning into the SDO/HMI data set on 2010/07/15). This reprocessing started two months ago in July 2011 and, as of this week, is now finished. While in most cases changes to the magnetic maps are not significant and do not drastically affect (for example) field-line connectivity or the amount of open flux in the coronal-field models, nonetheless there are cases where the maps have changed noticeably and we thus advise users of the 'pfss' SolarSoft package to be aware of this reprocessing. We have retained (offline) the earlier version of the models; please e-mail us if such models are needed. Lastly, the open-flux regions determined from the PFSS models during this time period, and stored as coronal-hole events in the Heliophysics Events Knowledgebase, have also been updated.

### **Scattering polarization of the d-states of ions and solar magnetic field: Effects of isotropic collisions**

M. **Derouich**, H. Basurah, B. Badruddin

Publications of the Astronomical Society of Australia (PASA)

2017

<https://arxiv.org/pdf/1703.00802.pdf>

Analysis of solar magnetic fields using observations as well as theoretical interpretations of the scattering polarization is commonly designated as a high priority area of the solar research. The interpretation of the observed polarization raises a serious theoretical challenge to the researchers involved in this field. In fact, realistic interpretations need detailed investigations of the depolarizing role of isotropic collisions with neutral hydrogen. The goal of this paper is to determine new relationships which allow the calculation of any collisional rates of the d-levels of ions by simply determining the value of  $n^*$  and  $E_p$  without the need of determining the interaction potentials and treating the dynamics of collisions. The determination of  $n^*$  and  $E_p$  is easy and based on atomic data usually available online. Accurate collisional rates allow a reliable diagnostics of solar magnetic fields. In this work we applied our collisional FORTRAN code to a large number of cases involving complex and simple ions. After that, the results are utilized and injected in a genetic programming code developed with C++ in order to infer original relationships which will be of great help to solar applications. We discussed the accuracy of our collisional rates in the cases of polarized complex atoms and atoms with hyperfine structure. The relationships are expressed on the tensorial basis and we explain how to include their contributions in the master equation giving the variation of the density matrix elements. As a test, we compared the results obtained through the general relationships provided in this work with the results obtained directly by running our code of collisions. These comparisons show a percentage of error of about 10% in the average value.

### **Inversion of Zeeman polarization for solar magnetic field diagnostics**

M. Derouich

New Astronomy 2016

<https://arxiv.org/pdf/1611.08710v1.pdf>

The topic of magnetic field diagnostics with the Zeeman effect is currently vividly discussed. There are some testable inversion codes available to the spectropolarimetry community and their application allowed for a better understanding of the magnetism of the solar atmosphere. In this context, we propose an inversion technique associated with a new numerical code. The inversion procedure is promising and particularly successful for interpreting the Stokes profiles in quick and sufficiently precise way. In our inversion, we fit a part of each Stokes profile around a target wavelength, and then determine the magnetic field as a function of the wavelength which is equivalent to get the magnetic field as a function of the height of line formation.

To test the performance of the new numerical code, we employed "hare and hound" approach by comparing an exact solution (called input) with the solution obtained by the code (called output). The precision of the code is also checked by comparing our results to the ones obtained with the HAO MERLIN code. The inversion code has been applied to synthetic Stokes profiles of the Na D1 line available in the literature. We investigated the limitations in recovering the input field in case of noisy data. As an application, we applied our inversion code to the polarization profiles of the Fe  $\lambda$  6302.5 Å observed at IRSOL in Locarno.

## Coronal Temperature Maps from Solar EUV Images: A Blind Source Separation Approach

T. Dudok de Wit, S. Moussaoui, C. Guennou, F. Auchère, G. Cessateur, M. Kretzschmar, L. A. Vieira, F. F. Goryaev

Solar Phys., March 2013, Volume 283, Issue 1, pp 31-47

Multi-wavelength solar images in the extreme ultraviolet (EUV) are routinely used for analysing solar features such as coronal holes, filaments, and flares. However, images taken in different bands often look remarkably similar, as each band receives contributions coming from regions with a range of different temperatures. This has motivated the search for empirical techniques that may unmix these contributions and concentrate salient morphological features of the corona in a smaller set of less redundant source images. Blind Source Separation (BSS) does precisely this. Here we show how this novel concept also provides new insight into the physics of the solar corona, using observations made by SDO/AIA. The source images are extracted using a Bayesian positive source-separation technique. We show how observations made in six spectral bands, corresponding to optically thin emissions, can be reconstructed by a linear combination of three sources. These sources have a narrower temperature response and allow for considerable data reduction, since the pertinent information from all six bands can be condensed into a single composite picture. In addition, they give access to empirical temperature maps of the corona. The limitations of the BSS technique and some applications are briefly discussed.

## Application and interpretation of deep learning for identifying pre-emergence magnetic-field patterns

Dattaraj B. Dhuri, Shravan M. Hanasoge, Aaron C. Birch, Hannah Schunker

ApJ 903 27 2020

<https://arxiv.org/pdf/2009.06287.pdf>

<https://doi.org/10.3847/1538-4357/abb771>

Magnetic flux generated within the solar interior emerges to the surface, forming active regions (ARs) and sunspots. Flux emergence may trigger explosive events, such as flares and coronal mass ejections and therefore understanding emergence is useful for space-weather forecasting. Evidence of any pre-emergence signatures will also shed light on sub-surface processes responsible for emergence. In this paper, we present a first analysis of emerging ARs from the Solar Dynamics Observatory/Heliioseismic Emerging Active Regions (SDO/HEAR) dataset (Schunker et al. 2016) using deep convolutional neural networks (CNN) to characterize pre-emergence surface magnetic-field properties. The trained CNN classifies between pre-emergence (PE) line-of-sight magnetograms and a control set of non-emergence (NE) magnetograms with a True Skill Statistic (TSS) score of ~85%, 3h prior to emergence and ~40%, 24h prior to emergence. Our results are better than a baseline classification TSS obtained using discriminant analysis of only the unsigned magnetic flux. We develop a network pruning algorithm to interpret the trained CNN and show that the CNN incorporates filters that respond positively as well as negatively to the unsigned magnetic flux of the magnetograms. Using synthetic magnetograms, we demonstrate that the CNN output is sensitive to the length-scale of the magnetic regions with small-scale and intense fields producing maximum CNN output and possibly a characteristic pre-emergence pattern. Given increasing popularity of deep learning, techniques developed here for interpretation of the trained CNN -- using network pruning and synthetic data -- are relevant for future applications in solar and astrophysical data analysis.

## OBSERVATIONS OF FIVE-MINUTE SOLAR OSCILLATIONS IN THE CORONA USING THE EXTREME ULTRAVIOLET SPECTROPHOTOMETER (ESP) ON BOARD THE SOLAR DYNAMICS OBSERVATORY EXTREME ULTRAVIOLET VARIABILITY EXPERIMENT (SDO/EVE)

L. [Didkovsky](#)<sup>1</sup>, D. Judge<sup>1</sup>, A. G. Kosovichev<sup>2</sup>, S. Wieman<sup>1</sup> and T. Woods

2011 ApJ 738 L7

We report on the detection of oscillations in the corona in the frequency range corresponding to five-minute acoustic modes of the Sun. The oscillations have been observed using soft X-ray measurements from the Extreme Ultraviolet Spectrophotometer (ESP) of the Extreme Ultraviolet Variability Experiment on board the Solar Dynamics Observatory. The ESP zeroth-order channel observes the Sun as a star without spatial resolution in the wavelength range of 0.1-7.0 nm (the energy range is 0.18-12.4 keV). The amplitude spectrum of the oscillations calculated from six-day time series shows a significant increase in the frequency range of 2-4 mHz. We interpret this increase as a response of the corona to solar acoustic (p) modes and attempt to identify p-mode frequencies among the strongest peaks. Due to strong variability of the amplitudes and frequencies of the five-minute oscillations in the corona, we study how the spectrum from two adjacent six-day time series combined together affects the number of peaks associated with the p-mode frequencies and their amplitudes. This study shows that five-minute oscillations of the Sun can be observed in the corona in variations of the soft X-ray emission. Further investigations of these oscillations may improve our understanding of the interaction of the oscillation modes with the solar atmosphere, and the interior-corona coupling, in general.

## Multi-line single point coronal magnetometry

Gabriel I. [Dima](#), [Thomas A. Schad](#)

ApJ

2020

<https://arxiv.org/pdf/2001.06123.pdf>

Polarized magnetic dipole (M1) emission lines provide important diagnostics for the magnetic field dominating the evolution of the solar corona. This paper advances a multi-line technique using specific combinations of M1 lines to infer the full vector magnetic field for regions of optically thin emission that can be localized along a given line of sight. Our analytical formalism is a generalization of the "single-point inversion" approach introduced by Plowman. We show that combinations of M1 transitions for which each is either a  $J=1 \rightarrow 0$  transition or has equal Landé g-factors for the upper and lower levels contain degenerate spectropolarimetric information that prohibits the application of the single-point inversion technique. This may include the pair of infrared Fe XIII lines discussed by Plowman. We identify the Fe XIII 1074.7 nm and Si X 1430.1 nm lines as one alternative combination for implementing this technique. Our sensitivity analysis, based on coronal loop properties, suggests that for photon noise levels around  $10^{-4}$  of the line intensity, which will be achievable with the National Science Foundation's Daniel K. Inouye Solar Telescope, magnetic fields with sufficient strength ( $\sim 10$  G) and not severely inclined to the line-of-sight ( $\lesssim 35^\circ$ ) can be recovered with this method. Degenerate solutions exist; though, we discuss how added constraints may help resolve them or reduce their number.

## Using a New Infrared Si x Coronal Emission Line for Discriminating between Magnetohydrodynamic Models of the Solar Corona During the 2006 Solar Eclipse

Gabriel I. [Dima](#)<sup>1,2</sup>, Jeffrey R. Kuhn<sup>1</sup>, Don Mickey<sup>1</sup>, and Cooper Downs

2018 ApJ 852 23

During the **2006 March 29** total solar eclipse, coronal spectropolarimetric measurements were obtained over a  $6 \times 6 R_\odot$  field of view with a 1–2  $\mu\text{m}$  spectral range. The data yielded linearly polarized measurements of the Fe xiii 1.075  $\mu\text{m}$ , He i 1.083  $\mu\text{m}$ , and for the first time, of the Si x 1.430  $\mu\text{m}$  emission lines. To interpret the measurements, we used forward-integrated synthetic emission from two magnetohydrodynamic models for the same Carrington rotation with different heating functions and magnetic boundary conditions. Observations of the Fe xiii 1.075/Si x 1.430 line ratio allowed us to discriminate between two models of the corona, with the observations strongly favoring the warmer model. The observed polarized amplitudes for the Si x 1.430  $\mu\text{m}$  line are around 7%, which is three times higher than the predicted values from available atomic models for the line. This discrepancy indicates a need for a closer look at some of the model assumptions for the collisional coefficients, as well as new polarized observations of the line to rule out any unknown systematic effect in the present data. All but two near-limb fibers show correlated bright He i 1.083  $\mu\text{m}$  and H i 1.282  $\mu\text{m}$  emission, which likely indicates cool prominence emission that is non-localized by the strongly defocused optics. One of the distant fibers located at 1.5  $R_\odot$  detected a weak He i 1.083  $\mu\text{m}$  intensity signal consistent with previous eclipse measurements around  $3 \times 10^{-7} B_\odot$ . However, given the limitations of these observations, it is not possible to completely remove contamination that is due to emission from prominence material that is not obscured by the lunar limb.

## Evolution of Small-Scale Magnetic Elements in the Vicinity of Granular-Sized Swirl Convective Motions

S. Vargas **Domínguez**, J. Palacios, L. Balmaceda, I. Cabello, V. Domingo  
Solar Phys. February 2015, Volume 290, [Issue 2](#), pp 301-319

Advances in solar instrumentation have led to widespread use of time series to study the dynamics of solar features, especially at small spatial scales and at very fast cadences. Physical processes at such scales are important as building blocks for many other processes occurring from the lower to the upper layers of the solar atmosphere and beyond, ultimately for understanding the larger picture of solar activity. Ground-based (*Swedish Solar Telescope*) and space-borne (*Hinode*) high-resolution solar data are analyzed in a quiet-Sun region that displays negative-polarity small-scale magnetic concentrations and a cluster of bright points observed in G-band. The region is characterized by two granular-sized convective vortex-type plasma motions, one of which appears to be affecting the dynamics of magnetic features and bright points in its vicinity and is therefore the main target of our investigations. We followed the evolution of the bright points, intensity variations at different atmospheric height, and the magnetic evolution for a set of interesting selected regions. We describe the evolution of the photospheric plasma motions in the region near the convective vortex and some plausible cases for convective collapse detected in Stokes profiles.

### **Multi-wavelength high-resolution observations of a small-scale emerging magnetic flux event and the chromospheric and coronal response**

Santiago Vargas **Domínguez**, Alexander Kosovichev, Vasyl Yurchyshyn

ApJ 794 140 2014

<http://arxiv.org/pdf/1405.3550v1.pdf>

State-of-the-art solar instrumentation is revealing magnetic activity of the Sun with unprecedented resolution. Observations with the 1.6m New Solar Telescope of the Big Bear Solar Observatory are making next steps in our understanding of the solar surface structure. Granular-scale magnetic flux emergence and the response of the solar atmosphere are among the key research. As part of a joint observing program with NASA's IRIS mission, the NST observed active region NOAA 11810 in photospheric and chromospheric wavelengths. Complimentary data are provided by SDO and Hinode space-based telescopes. The region displayed a group of solar pores, in the vicinity of which we detect a small-scale buoyant horizontal magnetic flux tube causing abnormal granulation and interacting with the pre-existing ambient field in upper atmospheric layers. Following the expansion of distorted granules at the emergence site, we observed a sudden appearance of an extended surge in the HeI data. IRIS caught ejection of a hot plasma jet associated with the HeI-surge. The SDO/HMI data reveal emerging magnetic looplike structures. Hinode/Ca II H and IRIS filtergrams detail the connectivities of the newly emerged magnetic field in the lower solar chromosphere. From these data we find that the orientation of the emerging flux tube was almost perpendicular to the overlying ambient field. Nevertheless the interaction of emerging magnetic field lines with the pre-existing overlying field generates high-temperature emission regions and boosts the surge/jet production. The localized heating is detected before and after the first signs of the surge/jet ejection. We compare the results with previous observations and theoretical models, and propose a scenario for the activation of plasma jet/surges and confined heating. Such process may play a significant role in the mass and energy flow from the interior to the corona.

August 17, 2013

### **A modified Milne-Eddington approximation for a qualitative interpretation of chromospheric spectral lines**

[A. J. Dorantes-Montenegro](#), [A. L. Siu-Tapia](#), [C. Quintero Noda](#), [D. Orozco Suárez](#)

A&A 2022

<https://arxiv.org/pdf/2112.14536>

The Milne-Eddington approximation provides an analytic and simple solution to the radiative transfer equation. It can be easily implemented in inversion codes that are used to fit spectro-polarimetric observations to infer average values of the magnetic field vector and the line-of-sight velocity of the solar plasma. However, it is in principle restricted to spectral lines formed under local thermodynamic conditions. We show that a simple modification in the linear source function of the Milne-Eddington approximation is sufficient to infer relevant physical parameters from spectral lines that deviate from local thermodynamic equilibrium. This is not a new modification for the solar community but it has been forgotten for quite some time. To check the validity of such approximation we make use of the Mg I b2 and the Ca II lines. We first study the influence of these new terms on the profile shape by means of the response functions. Then, we test the performance of an inversion code including such modification against the presence of noise. The approximation is also tested with realistic spectral lines generated with the RH numerical radiative transfer code. Finally, we confront the code with synthetic profiles generated from magneto-hydrodynamic simulations.

### **Rotation of Some Solar Coronal Bright Features as Derived from the Solar Dynamics Observatory/Atmospheric Imaging Array (SDO/AIA) 21.1 nm Images (for the Years 2011 – 2018)**



[Dorotovič, M. Rybanský](#)

[Solar Physics](#) August 2019, 294:109

[sci-hub.se/10.1007/s11207-019-1501-z](https://doi.org/10.1007/s11207-019-1501-z)

We determine the rotational velocity of solar coronal bright features using the cross-correlation method applied to 21.1 nm EUV images obtained by the Atmospheric Imaging Array (AIA) instrument onboard the Solar Dynamics Observatory (SDO) spacecraft. We reduce the problem to the determination of the maximum of the cross-correlation function constructed from two images with a time lag of about 30 minutes. The spatial resolution is about  $0.6'' \times 0.6''$  per pixel. We have analyzed a total of around 8 million intensity profiles, using about 6 million of them to determine the rotational velocity. We can confirm the results of other authors that the coronal structures are rotating differentially. On the solar Equator, the peripheral rotational velocity is about  $2.02 \text{ km s}^{-1}$ , and it decreases up to a heliographic latitude of  $60^\circ$  to about  $0.8 \text{ km s}^{-1}$ . Coronal bright points rotate about  $20 \text{ m s}^{-1}$  faster. From the dispersion of the rotational velocity, it is possible to estimate the average proper motion velocity of the analyzed coronal structure with a size of about  $50''$  to be roughly  $1 \text{ km s}^{-1}$ . We will use the developed software tool also for data processing of images from SDO/AIA in other wavelengths.

## A multi-diagnostic spectral analysis of penumbral microjets

Ainar [Drews](#), [Luc Rouppe van der Voort](#)

A&A 638, A63 2020

<https://arxiv.org/pdf/2005.02608.pdf>

<https://www.aanda.org/articles/aa/pdf/2020/06/aa37911-20.pdf>

Penumbral microjets (PMJs) are short-lived, jet-like objects found in the penumbra of sunspots. They were first discovered in chromospheric lines and have later also been shown to exhibit signals in transition region (TR) lines. Their origin and manner of evolution is not yet settled. We perform a comprehensive analysis of PMJs through the use of spectral diagnostics that span from photospheric to TR temperatures to constrain PMJ properties. We employed high-spatial-resolution Swedish 1-m Solar Telescope observations in the Ca II 8542 Angstrom and H-alpha lines, IRIS slit-jaw images, and IRIS spectral observations in the Mg II h & k lines, the Mg II 2798.75 Angstrom & 2798.82 Angstrom triplet blend, the C II 1334 Angstrom & 1335 Angstrom lines, and the Si IV 1394 Angstrom & 1403 Angstrom lines. We derived a wide range of spectral diagnostics from these and investigated other secondary phenomena associated with PMJs. We find that PMJs exhibit varying degrees of signal in all of our studied spectral lines. We find low or negligible Doppler velocities and velocity gradients throughout our diagnostics and all layers of the solar atmosphere associated with these. Dark features in the inner wings of H-alpha and Ca II 8542 Angstrom imply that PMJs form along pre-existing fibril structures. We find evidence for upper photospheric heating in a subset of PMJs through emission in the wings of the Mg II triplet lines. There is little evidence for ubiquitous twisting motion in PMJs. There is no marked difference in onset-times for PMJ brightenings in different spectral lines. PMJs most likely exhibit only very modest mass-motions, contrary to earlier suggestions. We posit that PMJs form at upper photospheric or chromospheric heights at pre-existing fibril structures. **April 29 and 30, 2016**

## Microjets in the penumbra of a sunspot

Ainar [Drews](#), [Luc Rouppe van der Voort](#)

A&A 602, A80 2017

<https://arxiv.org/pdf/1702.06078.pdf>

Penumbral Microjets (PMJs) are short-lived jets found in the penumbra of sunspots, first observed in wide-band Ca H-line observations as localized brightenings, and are thought to be caused by magnetic reconnection. Earlier work on PMJs has been focused on smaller samples of by-eye selected events and case studies. It is our goal to present an automated study of a large sample of PMJs to place the basic statistics of PMJs on a sure footing and to study the PMJ Ca II 8542  $\{\AA\}$  spectral profile in detail. High spatial resolution and spectrally well-sampled observations in the Ca II 8542  $\{\AA\}$  line obtained from the Swedish 1-m Solar Telescope (SST) are reduced by a Principle Component Analysis and subsequently used in the automated detection of PMJs using the simple learning algorithm k-Nearest Neighbour. PMJ detections were verified with co-temporal Ca H-line observations. A total of 453 tracked PMJ events were found, or 4253 PMJs detections tallied over all timeframes and a detection rate of 21 events per timestep. From these, an average length, width and lifetime of 640 km, 210 km and 90 s were obtained. The average PMJ Ca II 8542  $\{\AA\}$  line profile is characterized by enhanced inner wings, often in the form of one or two distinct peaks, and a brighter line core as compared to the quiet Sun average. Average blue and red peak positions were determined at  $-10.4 \text{ km s}^{-1}$  and  $+10.2 \text{ km s}^{-1}$  offsets from the Ca II 8542  $\{\AA\}$  line core. We found several clusters of PMJ hotspots within the sunspot penumbra, where PMJ events occur in the same general area repeatedly over time. Our results indicate smaller average PMJs sizes and longer lifetimes compared to previously published values, but with statistics still in the same orders of magnitude. The investigation and analysis of the PMJ line profiles strengthen the proposed heating of PMJs to transition region temperatures. **28-June-2010**

## Discovery of a New Class of Coronal Structures in White Light Eclipse Images

Miloslav [Druckmüller](#)<sup>1</sup>, Shadia Rifai Habbal<sup>2</sup>, and Huw Morgan

2014 ApJ 785 14

White light images of the solar corona, taken during total solar eclipses, capture the complex dynamic relationship between the coronal plasma and the magnetic field. This relationship can be recorded on timescales of seconds to minutes, within a few solar radii above the solar surface. Rays, large-scale loops, and streamers, which are the brightest structures in these images, have shaped current models of the coronal magnetic field and solar wind flow. We show in this work how the application of novel image processing techniques to unique high-resolution white light eclipse images reveals the presence of a new class of structures, reminiscent of smoke rings, faint nested expanding loops, expanding bubbles, and twisted helical structures. These features are interpreted as snapshots of the dynamical evolution of instabilities developing at prominence-corona interfaces and propagating outward with the solar wind.

## ENHANCING CORONAL STRUCTURES WITH THE FOURIER NORMALIZING-RADIAL-GRADED FILTER

Hana [Druckmüllerová](#)<sup>1</sup>, Huw Morgan<sup>2</sup> and Shadia R. Habbal

2011 ApJ 737 88

Images of the corona have a high dynamic range which is excellent for quantitative photometric analysis. To understand the processes governing the solar corona, it is essential to have information about the absolute brightness as well as the underlying structure. However, due to the steep radial gradient of brightness in the images, and to the fact that structures closer to the solar disk have higher contrast than structures further from the disk, human vision cannot view the intricate structure of the corona in such images. The recently developed normalizing-radial-graded filter (NRGF) is an effective way for revealing the coronal structure. In this work, we present a more adaptive filter inspired by the NRGF, which we call the Fourier normalizing-radial-graded filter (FNRGF). It approximates the local average and the local standard deviation by a finite Fourier series. This method enables the enhancement of finer details, especially in regions of lower contrast. We also show how the influence of additive noise is reduced by a modification to the FNRGF. To illustrate the power of the method, the FNRGF is applied to images of emission from coronal forbidden lines observed during the 2010 July 11 total solar eclipse. It is also successfully applied to space-based observations of the low corona in the extreme ultraviolet and to white light coronagraph observations, thus demonstrating the validity of the FNRGF as a new tool that will help the interpretation of the information embedded in most types of coronal images.

## Formation of Large Scale Coronal Loops Interconnecting Two Active Regions Through Gradual Magnetic Reconnection and Associated Heating Process

[Guohui Du](#), [Yao Chen](#), [Chunming Zhu](#), [Chang Liu](#), [Lili Ge](#), [Bing Wang](#), [Chuanyang Li](#), [Haimin Wang](#)

2018 ApJ 860 40

<https://arxiv.org/pdf/1805.04831.pdf>

Coronal loops interconnecting two active regions, called as interconnecting loops (ILs), are prominent large-scale structures in the solar atmosphere. They carry a significant amount of magnetic flux, therefore are considered to be an important element of the solar dynamo process. Earlier observations show that eruptions of ILs are an important source of CMEs. It is generally believed that ILs are formed through magnetic reconnection in the high corona ( $>150$ - $200''$ ), and several scenarios have been proposed to explain their brightening in soft X-rays (SXR). Yet, the detailed IL formation process has not been fully explored and the associated energy release in the corona still remains unresolved. Here we report the complete formation process of a set of ILs connecting two nearby active regions, with successive observations by STEREO-A on the far side of the Sun and SDO and Hinode on the Earth side. We conclude that ILs are formed by gradual reconnection high in the corona, in line with earlier postulations. In addition, we show evidence supporting that ILs become brightened in SXRs and EUVs through heating at or close to the reconnection site in the corona (i.e., through direct heating process of reconnection), a process that has been largely overlooked in earlier studies on ILs. **2015 Dec 06-09, 2015 December 11-12**

## On the Lorentz Force and Torque of Solar Photospheric Emerging Magnetic Fields

[Aiyang Duan](#), [Chaowei Jiang](#), [Shin Toriumi](#), [Petros Syntelis](#)

ApJL 896, L9 2020

<https://arxiv.org/pdf/2005.10532.pdf>

Magnetic flux generated and intensified by the solar dynamo emerges into the solar atmosphere, forming active regions (ARs) including sunspots. Existing theories of flux emergence suggest that the magnetic flux can rise buoyantly through the convection zone but is trapped at the photosphere, while its further rising into the atmosphere resorts to the Parker buoyancy instability. To trigger such an instability, the Lorentz force in the photosphere needs to be as large as the gas pressure gradient to hold up an extra amount of mass against gravity. This naturally results

in a strongly non-force-free photosphere, which is indeed shown in typical idealized numerical simulations of flux tube buoyancy from below the photosphere into the corona. Here we conduct a statistical study of the extents of normalized Lorentz forces and torques in the emerging photospheric magnetic field with a substantially large sample of SDO/HMI vector magnetograms. We found that the photospheric field has a rather small Lorentz force and torque on average, and thus is very close to a force-free state, which is not consistent with theories as well as idealized simulations of flux emergence. Furthermore, the small extents of forces and torques seem not to be influenced by the emerging AR's size, the emergence rate, or the non-potentiality of the field. This result puts an important constraint on future development of theories and simulations of flux emergence.

HMI Science Nuggets, #142, 2020 <http://hmi.stanford.edu/hminuggets/?p=3306>

## Comparison of Two Coronal Magnetic Field Models for Reconstructing a Sigmoidal Solar Active Region With Coronal Loops

Aiyiing [Duan](#), Chaowei Jiang, Qiang Hu, [Huai Zhang](#), [G. Allen Gary](#), [S. T. Wu](#), [Jinbin Cao](#)

ApJ 842 119 2017

<https://arxiv.org/pdf/1706.00595.pdf>

Magnetic field extrapolation is an important tool to study the three-dimensional (3D) solar coronal magnetic field which is difficult to directly measure. Various analytic models and numerical codes exist but their results often drastically differ. Thus a critical comparison of the modeled magnetic field lines with the observed coronal loops is strongly required to establish the credibility of the model. Here we compare two different non-potential extrapolation codes, a non-linear force-free field code (CESE-MHD-NLFFF) and a non-force-free field (NFFF) code in modeling a solar active region (AR) that has a sigmoidal configuration just before a major flare erupted from the region. A 2D coronal-loop tracing and fitting method is employed to study the 3D misalignment angles between the extrapolated magnetic field lines and the EUV loops as imaged by SDO/AIA. It is found that the CESE-MHD-NLFFF code with preprocessed magnetogram performs the best, outputting a field which matches the coronal loops in the AR core imaged in AIA 94 Å with a misalignment angle of ~10 degree. This suggests that the CESE-MHD-NLFFF code, even without using the information of coronal loops in constraining the magnetic field, performs as good as some coronal-loop forward-fitting models. For the loops as imaged by AIA 171 Å in the outskirts of the AR, all the codes including the potential-field give comparable results of mean misalignment angle (~30 degree). Thus further improvement of the codes is needed for a better reconstruction of the long loops enveloping the core region. 2014-09-10

## Wide-band fluctuations of solar active regions probed with SHARP magnetograms

[G. Dumbadze](#), [B.M. Shergelashvili](#), [M.L. Khodachenko](#), [S. Poedts](#)

A&A, 2024

<https://arxiv.org/pdf/2401.07134.pdf>

The power spectra of the fluctuation noise of the solar active region (AR) areas and magnetic fluxes sequentially observed in time contain information about their geometrical features and the related fundamental physical processes. These spectra are analysed for five different ARs with various magnetic field structures. The goal of this work is to detect the characteristic properties of the Fourier and wavelet spectra evaluated for the time series of the fluctuating areas and radial magnetic fluxes of the active regions. Accordingly, this work gathers information on the properties of noise in the different cases considered. The AR area and radial magnetic flux time series were built using SHARP magnetogram datasets that cover nearly the entire time of the ARs' transits over the solar disk. Then we applied Fourier and wavelet analyses to these time series using apodization and detrendization methods for the cross-comparison of the results. These methods allow for the detection and removal of the artefact data edge effects. Finally, we used a linear least-squares fitting method for the obtained spectra on a logarithmic scale to evaluate the power-law slopes of the fluctuation spectral power versus frequency (if any). According to our results, the fluctuation spectra of the areas and radial magnetic fluxes of the considered ARs differ from each other to a certain extent, both in terms of the values of the spectral power-law exponents and their frequency bands. The characteristic properties of the fluctuation spectra for the compact, dispersed, and mixed-type ARs exhibit noticeable discrepancies amongst each other. It is plausible to conclude that this difference might be related to distinct physical mechanisms responsible for the vibrations of the AR areas and/or radial magnetic fluxes.

## Numerical Simulations of the Evolution of Solar Active Regions: the Complex AR12565 and AR12567

Cristiana [Dumitrache](#)

Advances in Astrophysics, vol.2, No.2, 103-116, 2017

[http://www.isaacpub.org/images/PaperPDF/AdAp\\_100060\\_2017051010413989480.pdf](http://www.isaacpub.org/images/PaperPDF/AdAp_100060_2017051010413989480.pdf)

We have performed numerical magnetohydrodynamic (MHD) simulations of two closed active regions (AR). The input magnetic field values were the coronal magnetic field computed as extrapolation coronal from observations of the photospheric magnetic field. The studied active regions, NOAA AR12565 and AR12567, were registered as different bipolar region. Our investigation, the 3D coronal extrapolations, as well as the numerical MHD

experiments, revealed that actually they evolved together as a quadrupolar active region. The second region emerged later under the loops system of AR12565 and separated from this one. A natural current sheet formed between them and it plays an important role in the explosive events (flares and coronal mass ejections) occurrence. **12-24 July 2016.**

### **On twist estimation in active regions**

Cristiana [Dumitrache](#), Liliana Dumitru, Valentina Banciu

*ASP Conference Series, Vol. \*, 2010*

E-print Dec 2010

Our work had two objectives. First, we have extrapolated the 3D coronal magnetic field lines from MDI magnetograms for three active regions, in two different days for each one, and compared with coronal images from XRT/Hinode or EIT/SOHO. Additionally, we computed the force-free field parameter to estimate the twist in these active regions where more explosive events occurred.

### **Expulsion of Counter Evershed Flows from Sunspot Penumbrae**

J. S. Castellanos [Durán](#)<sup>1,2</sup>, A. Korpi-Lagg<sup>1,3</sup>, and S. K. Solanki<sup>1,4</sup>

**2023 ApJ 952 162**

<https://iopscience.iop.org/article/10.3847/1538-4357/acdbc9/pdf>

In addition to the Evershed flow directed from the umbra toward the outer boundary of a sunspot, under special circumstances a counter Evershed flow (CEF) in the opposite direction also occurs. We aim to characterize the proper motions and evolution of three CEFs observed by the Solar Optical Telescope on board the Japanese Hinode spacecraft and the Helioseismic and Magnetic Imager on board the Solar Dynamics Observatory. We use state-of-the-art inversions of the radiative-transfer equation of polarized light applied to spectropolarimetric observations of the Fe I line pair around 630 nm. The three CEFs appeared within the penumbra. Two of the CEF structures, as part of their decay process, were found to move radially outwards through the penumbra parallel to the penumbral filaments with speeds, deduced from their proper motions, ranging between 65 and 117 m s<sup>-1</sup>. In these two cases, a new spot appeared in the moat of the main sunspot after the CEFs reached the outer part of the penumbra. Meanwhile, the CEFs moved away from the umbra, and their magnetic field strengths decreased. The expulsion of these two CEFs seems to be related to the normal Evershed flow. The third CEF appeared to be dragged by the rotation of a satellite spot. Chromospheric brightenings were found to be associated with the CEFs, and those CEFs that reached the umbra–penumbra boundary showed enhanced chromospheric activity. The two CEFs, for which line-of-sight velocity maps were available during their formation phase, appear as intrusions into the penumbra. They may be associated with magnetic flux emergence.. **2006 December 8-15, 2014 February 1-6**

### **How rare are counter Evershed flows?**

[J. Sebastián Castellanos Durán](#), [Andreas Lagg](#), [Sami K. Solanki](#)

**A&A 651, L1 2021**

<https://arxiv.org/pdf/2106.05592.pdf>

<https://www.aanda.org/articles/aa/pdf/2021/07/aa41159-21.pdf>

<https://doi.org/10.1051/0004-6361/202141159>

One of the main characteristics of the penumbra of sunspots is the radially outward-directed Evershed flow. Only recently have penumbral regions been reported with similar characteristics to normal penumbral filaments, but with an opposite direction of the flow. Such flows directed towards the umbra are known as counter Evershed flows (CEFs). We aim to determine the frequency of occurrence of CEFs in active regions (ARs) and to characterize their lifetime and the prevailing conditions in the ARs. We analysed the continuum images, Dopplergrams, and magnetograms recorded by SDO/HMI of 97 ARs that appeared from 2011 to 2017. We followed the ARs for 9.6±1.4 days on average. We found 384 CEFs in total, with a median value of 6 CEFs per AR. CEFs are a rather common feature, they occur in 83.5% of all ARs regardless of the magnetic complexity of the AR. However, CEFs were observed on average only during 5.9% of the mean total duration of all the observations analyzed here. The lifetime of CEFs follows a log-normal distribution with a median value of 10.6+12.4–6.0 hr. In addition, we report two populations of CEFs depending on whether they are associated with light bridges, or not. We explain that the rarity of reports of CEFs in the literature is a result of highly incomplete coverage of ARs with spectropolarimetric data. By using the continuous observations now routinely available from space, we are able to overcome this limitation.

### **Detection of the strongest magnetic field in a sunspot light bridge**

J. S. Castellanos [Durán](#), [A. Lagg](#), [S. K. Solanki](#), [M. van Noort](#)

ApJ 895 129 2020

<https://arxiv.org/pdf/2003.12078.pdf>

<https://doi.org/10.3847/1538-4357/ab83f1>

Traditionally, the strongest magnetic fields on the Sun have been measured in sunspot umbrae. More recently, however, much stronger fields have been measured at the ends of penumbral filaments carrying the Evershed and Counter-Evershed flows. Super-strong fields have also been reported within a light bridge separating two umbrae of opposite polarities. We aim to accurately determine the strengths of the strongest fields in a light bridge using an advanced inversion technique and to investigate their detailed structure. We analyze observations from the spectropolarimeter onboard the Hinode spacecraft of the active region AR11967. The thermodynamic and magnetic configurations are obtained by inverting the Stokes profiles using an inversion scheme that allows multiple height nodes. Both, the traditional 1D inversion technique and the so-called 2D coupled inversions, which take into account the point spread function of the Hinode telescope, are used. We find a compact structure with an area of 32.7 arcsec<sup>2</sup> within a bipolar light bridge with field strengths exceeding 5 kG, confirming the strong fields in this light bridge reported in the literature. Two regions associated with downflows of  $\sim 5$  km s<sup>-1</sup> harbour field strengths larger than 6.5 kG, covering a total area of 2.97 arcsec<sup>2</sup>. The maximum field strength found is 8.2 kG, which is the largest ever observed field in {a bipolar light bridge} up to now. **1-6 February 2014**

## A Statistical Study of Photospheric Magnetic Field Changes During 75 Solar Flares

J. Sebastián Castellanos [Durán](#), [Lucia Kleint](#), [Benjamín Calvo-Mozo](#)

ApJ 2017

<https://arxiv.org/pdf/1711.08631.pdf>

Abrupt and permanent changes of photospheric magnetic fields have been observed during solar flares. The changes seem to be linked to the reconfiguration of magnetic fields, but their origin is still unclear. We carried out a statistical analysis of permanent line-of-sight magnetic field (Blos) changes during 18 X-, 37 M-, 19 C- and 1 B-class flares using data from SDO/HMI. We investigated the properties of permanent changes, such as frequency, areas, and locations. We detected changes of Blos in 59/75 flares. We find that strong flares are more likely to show changes, with all flares  $\geq M1.6$  exhibiting them. For weaker flares, permanent changes are observed in 6/17 C-flares. 34.3% of the permanent changes occurred in the penumbra and 18.9% in the umbra. Parts of the penumbra appeared or disappeared in 23/75 flares. The area where permanent changes occur is larger for stronger flares. Strong flares also show a larger change of flux, but there is no dependence of the magnetic flux change on the heliocentric angle. The mean rate of change of flare-related magnetic field changes is 20.7 Mx cm<sup>-2</sup> min<sup>-1</sup>. The number of permanent changes decays exponentially with distance from the polarity inversion line. The frequency of the strength of permanent changes decreases exponentially, and permanent changes up to 750 Mx cm<sup>-2</sup> were observed. We conclude that permanent magnetic field changes are a common phenomenon during flares, and future studies will clarify their relation to accelerated electrons, white light emission, and sunquakes to further investigate their origin.

**Table 2.** List of flares (2011-2015)

## Probing sunspots with two-skip time–distance helioseismology

Thomas L. [Duvall](#) Jr.1, Paul S. Cally2, Damien Przybylski2,1, Kaori Nagashima1 and Laurent Gizon1,3  
A&A 613, A73 (2018)

<http://sci-hub.tw/https://www.aanda.org/articles/aa/abs/2018/05/aa32424-17/aa32424-17.html>

<https://arxiv.org/pdf/1806.01032.pdf>

Context. Previous helioseismology of sunspots has been sensitive to both the structural and magnetic aspects of sunspot structure.

Aims. We aim to develop a technique that is insensitive to the magnetic component so the two aspects can be more readily separated.

Methods. We study waves reflected almost vertically from the underside of a sunspot. Time–distance helioseismology was used to measure travel times for the waves. Ray theory and a detailed sunspot model were used to calculate travel times for comparison.

Results. It is shown that these large distance waves are insensitive to the magnetic field in the sunspot. The largest travel time differences for any solar phenomena are observed.

Conclusions. With sufficient modeling effort, these should lead to better understanding of sunspot structure.

**Nov. 14–23, 2013**

## MHD waves and instabilities of a temperature-anisotropic plasma in the solar corona as a source of its heating

N. S. [Dzhalilov](#) & V. D. Kuznetsov

Astronomy Letters, Volume 37, Number 9, 649-655, **2011**

Pis'ma v Astronomicheskii Zhurnal, 2011, Vol. 37, No. 9, pp. 706–712.

The MHD instabilities of a temperature-anisotropic coronal plasma are considered. We show that aperiodic mirror instabilities of slow MHD waves can develop under solar coronal conditions for weak magnetic fields ( $B < 1$  G) and periodic ion-acoustic instabilities can develop for strong magnetic fields ( $B > 10$  G). We have found the instability growth rates and estimated the temporal and spatial scales of development and decay of the periodic instability. We show that the instabilities under consideration can play a prominent role in the energy balance of the corona and may be considered as a large-scale energy source of the wave coronal heating mechanism.

## **Solar internetwork magnetic fields: Statistical comparison between observations and MHD simulations**

[Elias Ebert](#), [Ivan Milic](#), [Juan Manuel Borrero](#)

A&A **2024**

<https://arxiv.org/pdf/2410.01613>

Although the magnetic fields in the quiet Sun account for the majority of the magnetic energy in the solar photosphere, inferring their exact spatial distribution, origin, and evolution poses an important challenge because the signals lie at the limit of today's instrumental precision. This severely hinders and biases our interpretations, which are mostly made through nonlinear model-fitting approaches. Our goal is to directly compare simulated and observed polarization signals in the FeI 630.1 nm and 630.2 nm spectral lines in the solar internetwork. This way, we aim to constrain the mechanism responsible for the generation of the quiet Sun magnetism while avoiding the biases that plague other diagnostic methods. We used three different three-dimensional radiative magneto-hydrodynamic simulations representing different scenarios of magnetic field generation in the internetwork: small-scale dynamo, decay of active regions, and horizontal flux emergence. We synthesized Stokes profiles at different viewing angles and degraded them according to the instrumental specifications of the spectro-polarimeter on the Hinode satellite. Finally, we statistically compared the simulated spectra to the observations at the appropriate viewing angles. The small-scale dynamo simulation reproduced best the statistical properties of the observed polarization signals. This is especially prominent for the disk center viewing geometry, where the agreement is excellent. Moving toward more inclined lines of sight, the agreement worsens slightly. The agreement between the small-scale dynamo simulation and observations at the disk center suggests that small-scale dynamo action plays an important role in the generation of quiet Sun magnetism. However, the magnetic field around 50 km above the photosphere in this simulation does not reproduce observations as well as at the very base of the photosphere.

## **Definition of the Spatial Propagator and Implications for Magnetic Field Properties**

Justin K. [Edmondson](#), Pascal Démoulin

[Solar Physics](#) June **2019**, 294:76

<https://link.springer.com/content/pdf/10.1007%2Fs11207-019-1452-4.pdf>

We present a theoretical framework to analyze the 3D coronal vector magnetic-field structure. We assume that the vector magnetic field exists and is a priori smooth. We introduce a generalized connectivity phase space associated with the vector magnetic field in which the basic elements are the field line and its linearized variation: the Spatial Propagator. We provide a direct formulation of these elements in terms of the vector magnetic field and its spatial derivatives, constructed with respect to general curvilinear coordinates and the equivalence class of general affine parameterizations. The Spatial Propagator describes the geometric organization of the local bundle of field lines, equivalent to the kinematic deformation of a propagated volume tied to the bundle. The Spatial Propagator's geometric properties are characterized by dilation, anisotropic stretch, and rotation. Extreme singular values of the Spatial Propagator describe quasi-separatrix layers (QSLs), while true separatrix surfaces and separator lines are identified by the vanishing of one and two singular values, respectively. Finally, we show that, among other possible applications, the squashing factor [QQ] is easily constructed from an analysis of particular sub-matrices of the Spatial Propagator.

## **On the Role of Interchange Reconnection in the Generation of the Slow Solar Wind Review**

J. K. [Edmondson](#)

Space Science Reviews, November **2012**, Volume 172, Issue 1-4, pp 209-225

The heating of the solar corona and therefore the generation of the solar wind, remain an active area of solar and heliophysics research. Several decades of in situ solar wind plasma observations have revealed a rich bimodal solar wind structure, well correlated with coronal magnetic field activity. Therefore, the reconnection processes associated with the large-scale dynamics of the corona likely play a major role in the generation of the slow solar wind flow regime. In order to elucidate the relationship between reconnection-driven coronal magnetic field structure and dynamics and the generation of the slow solar wind, this paper reviews the observations and phenomenology of the solar wind and coronal magnetic field structure. The geometry and topology of nested flux systems, and the

(interchange) reconnection process, in the context of coronal physics is then explained. Once these foundations are laid out, the paper summarizes several fully dynamic, 3D MHD calculations of the global coronal system. Finally, the results of these calculations justify a number of important implications and conclusions on the role of reconnection in the structural dynamics of the coronal magnetic field and the generation of the solar wind.

### **A Comparison of Global Magnetic Field Skeletons and Active-Region Upflows**

S. J. **Edwards**, C. E. Parnell, L. K. Harra, J. L. Culhane, D. H. Brooks

Solar Phys. January 2016, Volume 291, [Issue 1](#), pp 117-142

Plasma upflows have been detected in active regions using Doppler velocity maps. The origin and nature of these upflows is not well known with many of their characteristics determined from the examination of single events. In particular, some studies suggest these upflows occur along open field lines and, hence, are linked to sources of the solar wind. To investigate the relationship these upflows may have with the solar wind, and to probe what may be driving them, this paper considers seven active regions observed on the solar disc using the Extreme ultraviolet Imaging Spectrometer aboard Hinode between August 2011 and September 2012. Plasma upflows are observed in all these active regions. The locations of these upflows are compared to the global potential magnetic field extrapolated from the Solar Dynamics Observatory, Helioseismic and Magnetic Imager daily synoptic magnetogram taken on the day the upflows were observed. The structure of the magnetic field is determined by constructing its magnetic skeleton in order to help identify open-field regions and also sites where magnetic reconnection at global features is likely to occur. As a further comparison, measurements of the temperature, density and composition of the plasma are taken from regions with active-region upflows. In most cases the locations of the upflows in the active regions do not correspond to areas of open field, as predicted by a global coronal potential-field model, and therefore these upflows are not always sources of the slow solar wind. The locations of the upflows are, in general, intersected by separatrix surfaces associated with null points located high in the corona; these could be important sites of reconnection with global consequences.

### **Influence of Non-Potential Coronal Magnetic Topology on Solar-Wind Models**

S. J. **Edwards**, A. R. Yeates, F.-X. Bocquet, D.H. Mackay

Solar Phys. Volume 290, Issue 10, pp 2791-2808 2015

<http://arxiv.org/pdf/1511.00427v1.pdf>

By comparing a magneto-frictional model of the low-coronal magnetic-field to a potential-field source-surface model, we investigate the possible impact of non-potential magnetic structure on empirical solar-wind models. These empirical models (such as Wang–Sheeley–Arge) estimate the distribution of solar-wind speed solely from the magnetic-field structure in the low corona. Our models are computed in a domain between the solar surface and 2.5 solar radii, and they are extended to 0.1 AU using a Schatten current-sheet model. The non-potential field has a more complex magnetic skeleton and quasi-separatrix structures than the potential field, leading to different sub-structure in the solar-wind speed proxies. It contains twisted magnetic structures that can perturb the separatrix surfaces traced down from the base of the heliospheric current sheet. A significant difference between the models is the greater amount of open magnetic flux in the non-potential model. Using existing empirical formulae this leads to higher predicted wind speeds for two reasons: partly because magnetic-flux tubes expand less rapidly with height, but more importantly because more open-field lines are further from coronal-hole boundaries.

### **Null Point Distribution in Global Coronal Potential Field Extrapolations**

S. J. **Edwards**, C. E. Parnell

Solar Physics Volume 290, [Issue 7](#), pp 2055-2076 2015

Magnetic null points are points in space where the magnetic field is zero. Thus, they can be important sites for magnetic reconnection by virtue of the fact that they are weak points in the magnetic field and also because they are associated with topological structures, such as separators, which lie on the boundary between four topologically distinct flux domains and therefore are also locations where reconnection occurs. The number and distribution of nulls in a magnetic field acts as a measure of the complexity of the field.

In this article, the numbers and distributions of null points in global potential field extrapolations from high-resolution synoptic magnetograms are examined. Extrapolations from magnetograms obtained with the Michelson Doppler Imager (MDI) are studied in depth and compared with those from high-resolution Solar Long-time Investigations of the Sun (SOLIS) and Heliospheric Magnetic Imager (HMI).

The fall-off in the density of null points with height is found to follow a power law with a slope that differs depending on whether the data are from solar maximum or solar minimum. The distribution of null points with latitude also varies with the cycle as null points form predominantly over quiet-Sun regions and avoid active-region fields. The exception to this rule are the null points that form high in the solar atmosphere, and these null points tend to form over large areas of strong flux in active regions.

From case studies of data acquired with the MDI, SOLIS, and HMI, it is found that the distribution of null points is very similar between data sets, except, of course, that there are far fewer nulls observed in the SOLIS data than in the cases from MDI and HMI due to its lower resolution.

## **Simulations of 3D Magnetic Merging: Resistive Scalings for Null Point and QSL Reconnection**

Frederic [Effenberger](#), I. J. D. Craig

Solar Phys. January 2016, Volume 291, Issue 1, pp 143-153

Starting from an exact, steady-state, force-free solution of the magnetohydrodynamic (MHD) equations, we investigate how resistive current layers are induced by perturbing line-tied three-dimensional magnetic equilibria. This is achieved by the superposition of a weak perturbation field in the domain, in contrast to studies where the boundary is driven by slow motions, like those present in photospheric active regions. Our aim is to quantify how the current structures are altered by the contribution of so-called quasi-separatrix layers (QSLs) as the null point is shifted outside the computational domain. Previous studies based on magneto-frictional relaxation have indicated that despite the severe field line gradients of the QSL, the presence of a null is vital in maintaining fast reconnection. Here, we explore this notion using highly resolved simulations of the full MHD evolution. We show that for the null-point configuration, the resistive scaling of the peak current density is close to  $J \sim \eta^{-1}$ , while the scaling is much weaker, i.e.  $J \sim \eta^{-0.4}$ , when only the QSL connectivity gradients provide a site for the current accumulation.

## **Vertical magnetic field on boundary of sunspot umbra**

V. [Efremov](#), [L. Parfinenko](#), [A. Soloviev](#)

2021

<https://arxiv.org/ftp/arxiv/papers/2101/2101.11675.pdf>

12 stable single sunspots were investigated in two aspects. The outer boundaries of the sunspots umbra were determined by an independent mathematical method and the vertical component of the magnetic field at these boundaries was found. We analyzed data from the SDO station using the segments of the continuum and magnetic field. It is shown that in a wide range of sunspot fields, the field average along the contour changes weakly, while the vertical component of the magnetic field itself, in a particular spot, changes significantly along the defined contour which reflects the fibrous structure of the penumbral field.

## **Long-Term Oscillations of Sunspots and a Special Class of Artifacts in SOHO(MDI) and SDO(HMI) Data**

V.I. [Efremov](#), [A.A. Soloviev](#), [L.D. Parfinenko](#), [A. Riehoakainen](#), [E. Kirichek](#), [V.V. Smirnova](#), [Y.N. Varun](#), [I. Bakunina](#), [I. Zhivanovich](#)

*Astrophysics and Space Science* March 2018, 363:61

<https://arxiv.org/ftp/arxiv/papers/1802/1802.06379.pdf>

<https://link.springer.com/content/pdf/10.1007%2Fs10509-018-3284-3.pdf>

A specific type of artifacts, that originate due to displacement of the image of a moving object along the digital (pixel) matrix of receiver are analyzed in detail. The criteria of appearance and the influence of these artifacts on the study of long-term oscillations of sunspots are deduced. The obtained criteria suggest us methods for reduction or even elimination of these artifacts. It is shown that the use of integral parameters can be very effective against the artifact distortions. The simultaneous observations of sunspot magnetic field and ultraviolet intensity of the umbra have given the same periods for the long-term oscillations. In this way the real physical nature of the oscillatory process, which is independent of the artifacts have been confirmed again. A number of examples considered here confirm the dependence between the periods of main mode of the sunspot magnetic field long-term oscillations and its strength. The dependence was derived earlier from both the observations and the theoretical model of the shallow sunspot. The anti-phase behavior of time variations of sunspot umbra area and magnetic field of the sunspot demonstrates that the umbra of sunspot moves in long-term oscillations as a whole: all its points oscillate with the same phase. **16/02/1998 , 22-26 September 1999, 26-29 June 2000, 2-7 Desember 2002 , 05 June 2011 , 18 November, 2013**

## **Long-Period Oscillations of Sunspots Observed by SOHO/MDI**

V. I. [Efremov](#), L. D. Parfinenko, A. A. Solov'ev, E. A. Kirichek

Solar Physics, June 2014, Volume 289, Issue 6, pp 1983-1998

<http://arxiv.org/ftp/arxiv/papers/1412/1412.4107.pdf>

We processed magnetograms that were obtained with the Michelson Doppler Imager onboard the Solar and Heliospheric Observatory (SOHO/MDI). The results confirm the basic properties of long-period oscillations of sunspots that have previously been established and also reveal new properties. We show that the limiting (lowest) eigenmode of low-frequency oscillations of a sunspot as a whole is the mode with a period of 10 – 12 up to 32 – 35 hours (depending on the sunspot's magnetic-field strength). This mode is observed consistently throughout an observation period of 5 – 7 days, but its amplitude is subject to quasi-cyclic changes, which are separated by about 1.5 – 2 days. As a result, the lower mode with a period of about 35 – 48 hours appears in the power spectrum of sunspot oscillations. But this lowest mode is apparently not an eigenmode of a sunspot because its period does not



depend on the magnetic field of the sunspot. Perhaps the mode reflects the quasi-periodic sunspot perturbations caused by supergranulation cells that surround it. We also analyzed SOHO/MDI artifacts, which may affect the low-frequency power spectra of sunspots. 24-26 September, 1999, 8 - 10 October 1999), , 10 September 2002), 1 - 5 April 2002 , 5 October 2002,, 21 - 24 July 2004),.

## **Investigation of Long-Period Oscillations of Sunspots with Ground-Based (Pulkovo) and SOHO/MDI Data**

V. I. **Efremov**, L. D. Parfinenko, A. A. Solov'ev, E.  
Solar Physics, Volume 267, Issue 2, pp.279-293, **2010**  
[http://www.pergamentum.com/eprint/Efremov\\_etc.pdf](http://www.pergamentum.com/eprint/Efremov_etc.pdf)

We applied special data-processing algorithms to the study of long-period oscillations of the magnetic-field strength and the line-of-sight velocity in sunspots. The oscillations were investigated with two independent groups of data. First, we used an eight-hour-long series of solar spectrograms, obtained with the solar telescope at the Pulkovo Observatory. We simultaneously measured Doppler shifts of six spectral lines, formed at different heights in the atmosphere. Second, we had a long time series of full-disk magnetograms (10 - 34 hour) from SOHO/MDI for the line-of-sight magnetic-field component. Both ground- and space-based observations revealed long-period modes of oscillations (40 - 45, 60 - 80, and 160 - 180 minutes) in the power spectrum of the sunspots and surrounding magnetic structures. With the SOHO/MDI data, one can study the longer periodicities. We obtained two new significant periods ( $> 3 \sigma$ ) in the power spectra of sunspots: around 250 and 480 minutes. The power of the oscillations in the lower frequencies is always higher than in the higher ones. The amplitude of the long-period magnetic-field modes shows magnitudes of about 200 - 250 G. The amplitude of the line-of-sight velocity periodicities is about 60 - 110 m s<sup>-1</sup>. The absence of low-frequency oscillations in the telluric line proves their solar nature. Moreover, the absence of low-frequency oscillations of the line-of-sight velocity in the quiet photosphere (free of magnetic elements) proves their direct connection to magnetic structures. Long-period modes of oscillation observed in magnetic elements surrounding the sunspot are spread over the meso-granulation scales (10" - 12"), while the sunspot itself oscillates as a whole. The amplitude of the long-period mode of the line-of-sight velocity in a sunspot decreases rapidly with height: these oscillations are clearly visible in the spectral lines originating at heights of approximately 200 km and fade away in lines originating at 500 km. We found a new interesting property: the low-frequency oscillations of a sunspot are strongly reduced when there is a steady temporal trend (strengthening or weakening) of the sunspot's magnetic field. Another important result is that the frequency of long-period oscillations evidently depends on the sunspot's magnetic-field strength.

## **Twist and Writhe of the Magnetic Flux in the Super Active Region NOAA 11429**

A. **Elmhamdi**, P. Romano, A. S. Kordi, H. A. Al-trabulsy  
Solar Physics, March **2014**

We used full-disk line-of-sight magnetograms taken by the Helioseismic and Magnetic Imager (HMI) onboard the Solar Dynamics Observatory (SDO) to study the variation of coronal magnetic helicity in the Active Region (AR) NOAA 11429, where several GOES M- and X-class flares and coronal mass ejections (CMEs) occurred. The magnetic flux, total magnetic-helicity flux, and helicity accumulation over the period of interest, i.e. **6 to 11 March 2012**, were measured and are discussed. We also evaluated the tilt-angle evolution within the standard polarity flux-weighted centroids approach. The AR displays a shearing motion of the magnetic structures along the polarity inversion line, reaching values of about 1.0 km s<sup>-1</sup>. The variations of magnetic helicity flux and the tilt-angle seem to be time-correlated, and both display three-phase evolutionary patterns. We also found that the flare/CME activity is higher during the first observation phase when the tilt-angle decreases and the negative magnetic helicity is accumulated. The main changes in the accumulated helicity curve are observed only after the onset of the two strongest flare/CME events. After the major event (GOES X5.4 class/CME of 7 March) there was a decrease in the occurrence of flares and CMEs. This phase is marked by a decrease of the flux of magnetic helicity from the convection zone to the corona and a change in the orientation of the tilt of the AR. This behavior suggests that the combination of these two quantities might be important in the description of the magnetic complexity accumulated by an AR during its lifetime.

## **The Importance of Long-Term Synoptic Observations and Data Sets for Solar Physics and Helioseismology** **Review**

Yvonne **Elsworth**, Anne-Marie Broomhall, Sanjay Gosain, Markus Roth, Stuart M. Jefferies, Frank Hill  
Space Science Reviews December **2015**, Volume 196, Issue 1, pp 137-166

A casual single glance at the Sun would not lead an observer to conclude that it varies. The discovery of the 11-year sunspot cycle was only made possible through systematic daily observations of the Sun over 150 years and even today historic sunspot drawings are used to study the behavior of past solar cycles. The origin of solar activity is still poorly understood as shown by the number of different models that give widely different predictions for the strength

and timing of future cycles. Our understanding of the rapid transient phenomena related to solar activity, such as flares and coronal mass ejections (CMEs) is also insufficient and making reliable predictions of these events, which can adversely impact technology, remains elusive. There is thus still much to learn about the Sun and its activity that requires observations over many solar cycles. In particular, modern helioseismic observations of the solar interior currently span only 1.5 cycles, which is far too short to adequately sample the characteristics of the plasma flows that govern the dynamo mechanism underlying solar activity. In this paper, we review some of the long-term solar and helioseismic observations and outline some future directions.

### **Plasma flows and magnetic field interplay during the formation of a pore**

I. **Ermolli**, A. Cristaldi, F. Giorgi, F. Giannattasio, M. Stangalini, P. Romano, A. Tritschler, F. Zuccarello  
A&A **2017**

<https://arxiv.org/pdf/1701.06440v1.pdf>

**Aims.** Recent simulations of solar magneto-convection has offered new levels of understanding of the interplay between plasma motions and magnetic fields in evolving active regions. We aim at verifying some aspects of the formation of magnetic regions derived from recent numerical studies in observational data.

**Methods.** We studied the formation of a pore in the active region (AR) NOAA 11462. We analysed data obtained with the Interferometric Bidimensional Spectrometer (IBIS) at the Dunn Solar Telescope on **April 17, 2012**, consisting of full Stokes measurements of the Fe I 617.3 nm lines. Furthermore, we analysed SDO/HMI observations in the continuum and vector magnetograms derived from the Fe I 617.3 nm line data taken from **April 15 to 19, 2012**. We estimated the magnetic field strength and vector components and the line-of-sight (LOS) and horizontal motions in the photospheric region hosting the pore formation. We discuss our results in light of other observational studies and recent advances of numerical simulations.

**Results.** The pore formation occurs in less than 1 hour in the leading region of the AR. We observe that the evolution of the flux patch in the leading part of the AR is faster (. 12 hour) than the evolution (20-30 hour) of the more diffuse and smaller scale flux patches in the trailing region. During the pore formation, the ratio between magnetic and dark area decreases from 5 to 2. We observe strong downflows at the forming pore boundary and diverging proper motions of plasma in the vicinity of the evolving feature that are directed towards the forming pore. The average values and trends of the various quantities estimated in the AR are in agreement with results of former observational studies of steady pores and with their modelled counterparts, as seen in recent numerical simulations of a rising-tube process. The agreement with the outcomes of the numerical studies holds for both the signatures of the flux emergence process (e.g. appearance of small-scale mixed polarity patterns and elongated granules) and the evolution of the region. The processes driving the formation of the pore are identified with the emergence of a magnetic flux concentration and the subsequent reorganization of the emerged flux, by the combined effect of velocity and magnetic field, in and around the evolving structure.

### **CORONAL HEATING BY SURFACE ALFVÉN WAVE DAMPING: IMPLEMENTATION IN A GLOBAL MAGNETOHYDRODYNAMICS MODEL OF THE SOLAR WIND**

R. M. **Evans**<sup>1,2</sup>, M. Opher<sup>2</sup>, R. Oran<sup>3</sup>, B. van der Holst<sup>3</sup>, I. V. Sokolov<sup>3</sup>, R. Frazin<sup>3</sup>, T. I. Gombosi<sup>3</sup>, and A. Vásquez

**2012** ApJ 756 155

The heating and acceleration of the solar wind is an active area of research. Alfvén waves, because of their ability to accelerate and heat the plasma, are a likely candidate in both processes. Many models have explored wave dissipation mechanisms which act either in closed or open magnetic field regions. In this work, we emphasize the boundary between these regions, drawing on observations which indicate unique heating is present there. We utilize a new solar corona component of the Space Weather Modeling Framework, in which Alfvén wave energy transport is self-consistently coupled to the magnetohydrodynamic equations. In this solar wind model, the wave pressure gradient accelerates and wave dissipation heats the plasma. Kolmogorov-like wave dissipation as expressed by Hollweg along open magnetic field lines was presented in van der Holst et al. Here, we introduce an additional dissipation mechanism: surface Alfvén wave (SAW) damping, which occurs in regions with transverse (with respect to the magnetic field) gradients in the local Alfvén speed. For solar minimum conditions, we find that SAW dissipation is weak in the polar regions (where Hollweg dissipation is strong), and strong in subpolar latitudes and the boundaries of open and closed magnetic fields (where Hollweg dissipation is weak). We show that SAW damping reproduces regions of enhanced temperature at the boundaries of open and closed magnetic fields seen in tomographic reconstructions in the low corona. Also, we argue that Ulysses data in the heliosphere show enhanced temperatures at the boundaries of fast and slow solar wind, which is reproduced by SAW dissipation. Therefore, the model's temperature distribution shows best agreement with these observations when both dissipation mechanisms are considered. Lastly, we use observational constraints of shock formation in the low corona to assess the Alfvén speed profile in the model. We find that, compared to a polytropic solar wind model, the wave-driven model with physical dissipation mechanisms presented in this work is more aligned with an empirical Alfvén speed profile. Therefore, a wave-driven model which includes the effects of SAW damping is a better background to simulate coronal-mass-ejection-driven shocks.

## **ALFVE'N PROFILE IN THE LOWER CORONA: IMPLICATIONS FOR SHOCK FORMATION**

R. M. **Evans** and M. Opher, W. B. Manchester IV and T. I. Gombosi

Astrophysical Journal, 687:1355-1362, 2008

<http://www.journals.uchicago.edu/doi/pdf/10.1086/592016>

Observations of type II radio bursts and energetic electron events indicate that shocks can form at 1 Y3 solar radii and are responsible for the GeV nucleon<sub>1</sub> energies observed in ground level solar energetic particle (SEP) events. Here we provide the first study of the lower corona produced from 10 state-of-the-art models. In particular, we look to the Alfvén speed profiles as the criterion for shock formation, independent of exciting agent (e.g., flares and CMEs). Global magnetohydrodynamic models produce Alfvén speed profiles that are in conflict with observations: (1) multiple SEP events are observed with a single exciting agent, but most profiles are missing the “hump” required to form multiple shocks; and (2) few slow CMEs cause large SEP events, but most profiles drop very quickly, allowing all slow CMEs to drive strong shocks to form between 1 and 3 R<sub>⊙</sub>. Simplified Alfvén wave-driven wind models have steeper profiles, but are still in disagreement with multiple shock formation. Only studies that include Alfvén waves with physically based damping are in agreement with observations. This implies the results of these one-dimensional local studies must be included in global models before we can study shock formation in the lower corona.

## **An Observationally Constrained 3D Potential-field Source-surface Model for the Evolution of Longitude-dependent Coronal Structures**

Rosa Wallace **Everson**<sup>1</sup> and Mausumi Dikpati<sup>2</sup>

2017 ApJ 850 152

The improvement of techniques for realistically modeling the solar magnetic field has been a priority in solar physics for decades. The challenge of creating synoptic maps of the photosphere that reliably reflect conditions at all locations concurrently is a major limitation to progress in this area. White-light coronal images, which contain morphological information about the 3D corona at the solar limb, have been largely overlooked as a resource for constraining or correcting synoptic maps. We explore a complementary approach to traditional magnetogram-based coronal field solutions that makes use of these images. Applying a modified 3D potential-field source-surface (PFSS) model, we investigate the use of MLSO white-light coronal images for deriving 3D coronal morphology by empirically fitting model solutions with observations only. Applying an iterative technique to coronal image data from the solar minima preceding Cycles 22, 23, and 24, and the ascending phase of Cycle 23, we obtain model solutions as linear combinations of low order and degree spherical harmonics. We find that the 3D morphology produced by our method agrees qualitatively with traditional magnetogram-based PFSS approaches for coronas that are dipole dominated. For more complex coronas, additional constraints are needed to account for polarity and correct interpretation of coronal structures. Estimates of the relative strength of dipoles versus multipoles in the coronal field also agree with traditional methods, but the contributions of specific multipoles do not, revealing nonuniqueness in our results. Future work will incorporate magnetogram-based solutions prior to applying the iterative technique.

## **Coronal magnetic field value radial distributions obtained by using the information on fast halo coronal mass ejections**

V.G.**Fainshtein**, [Ya.I.Egorov](#)

Solar Phys. 2017

<https://arxiv.org/pdf/1712.09046.pdf>

Based on the method of finding coronal magnetic field value radial profiles  $B(R)$  described in (Gopalswamy and Yashiro, 2011), and applied for the directions close to the sky plane, we determined magnetic field value radial distributions along the directions close to the Sun-Earth axis. For this purpose, by using the method in (Xue, Wang, and Dou, 2005), from the SOHO/LASCO data, we found 3D characteristics for fast halo coronal mass ejections (HCMEs) and for the HCME-related shocks. Through these data, we managed to obtain the  $B(R)$  distributions as far as 43 solar radii from the Sun center, which is approximately by a factor of 2 farther, than those in (Gopalswamy and Yashiro, 2011). We drew a conclusion that, to improve the accuracy of the Gopalswamy-Yashiro method to find the coronal magnetic field, one should develop a technique to detect the CME sites that move in the slow and in the fast solar wind. We propose a technique to select the CMEs, whose central (paraxial) part moves, indeed, in the slow wind. 2003-11-18, 2011-03-08

## **Kinematics and Magnetic Properties of a Light Bridge in a Decaying Sunspot**

M. **Falco**, J. M. Borrero, S. L. Guglielmino, P. Romano, F. Zuccarello, S. Criscuoli, A. Cristaldi, I. Ermolli, S. Jafarzadeh, L. Rouppe van der Voort

Solar Phys. Volume 291, [Issue 7](#), pp 1939–1955

2016

<http://arxiv.org/pdf/1606.07229v1.pdf>

We present the results obtained by analyzing high spatial and spectral resolution data of the solar photosphere acquired by the CRisp Imaging SpectroPolarimeter at the Swedish Solar Telescope on **6 August 2011**, relevant to a large sunspot with a light bridge (LB) observed in NOAA AR 11263. These data are complemented by simultaneous Hinode Spectropolarimeter (SP) observation in the Fe I 630.15 nm and 630.25 nm lines. The continuum intensity map shows a discontinuity of the radial distribution of the penumbral filaments in correspondence with the LB, which shows a dark lane (about 0.3" wide and about 8.0" long) along its main axis. The available data were inverted with the Stokes Inversion based on Response functions (SIR) code and physical parameters maps were obtained. The line-of-sight (LOS) velocity of the plasma along the LB derived from the Doppler effect shows motions towards and away from the observer up to 0.6 km/s, which are lower in value than the LOS velocities observed in the neighbouring penumbral filaments. The noteworthy result is that we find motions toward the observer up to 0.6 km/s in the dark lane where the LB is located between two umbral cores, while the LOS velocity motion toward the observer is strongly reduced where the LB is located between an umbral core at one side and penumbral filaments on the other side. Statistically, the LOS velocities correspond to upflows/downflows and comparing these results with Hinode/SP data, we conclude that the surrounding magnetic field configuration (whether more or less inclined) could have a role in maintaining the conditions for the process of plasma piling up along the dark lane. The results obtained from our study support and confirm outcomes of recent magnetohydro-dynamic simulations showing upflows along the main axis of a LBs.

### **A new method to quantify and reduce projection error in whole-solar-active-region parameters measured from vector magnetograms**

David A. **Falconer**, Sanjiv K. Tiwari, Ronald L. Moore, Igor Khazanov

ApJL 833 L31 2016

<https://arxiv.org/pdf/1612.01948v1.pdf>

Projection error limits the use of vector magnetograms of active regions (ARs) far from disk center. In this Letter, for ARs observed up to 60° from disk center, we demonstrate a method of measuring and reducing the projection error in the magnitude of any whole-AR parameter derived from a vector magnetogram that has been deprojected to disk center. The method assumes that the center-to-limb curve of the average of the parameter's absolute values measured from the disk passage of a large number of ARs and normalized to each AR's absolute value of the parameter at central meridian, gives the average fractional projection error at each radial distance from disk center. To demonstrate the method, we use a large set of large-flux ARs and apply the method to a whole-AR parameter that is among the simplest to measure: whole-AR magnetic flux. We measure 30,845 SDO/HMI vector magnetograms covering the disk passage of 272 large-flux ARs, each having whole-AR flux >1022 Mx. We obtain the center-to-limb radial-distance run of the average projection error in measured whole-AR flux from a Chebyshev fit to the radial-distance plot of the 30,845 normalized measured values. The average projection error in the measured whole-AR flux of an AR at a given radial distance is removed by multiplying the measured flux by the correction factor given by the fit. The correction is important for both the study of evolution of ARs and for improving the accuracy of forecasting an AR's major flare/CME productivity. **2014 January 05-12**

### **MAGNETOGRAM MEASURES OF TOTAL NONPOTENTIALITY FOR PREDICTION OF SOLAR CORONAL MASS EJECTIONS FROM ACTIVE REGIONS OF ANY DEGREE OF MAGNETIC COMPLEXITY**

D. A. **Falconer**, R. L. Moore, and G. A. Gary

Astrophysical Journal, 689:1433–1442, **2008**

For investigating the magnetic causes of coronal mass ejections (CMEs) and for forecasting the CME productivity of active regions, in previous work we have gauged the total nonpotentiality of a whole active region by either of two measures, LSSM and LSGM, two measures of the magnetic field along the main neutral line in a vector magnetogram of the active region. This previous work was therefore restricted to nominally bipolar active regions, active regions that have a clearly identifiable main neutral line. In the present paper, we show that our work can be extended to include multipolar active regions of any degree of magnetic complexity by replacing LSSM and LSGM with their generalized counterparts, WLSS and WLSG, which are corresponding integral measures covering all neutral lines in an active region instead of only the main neutral line. In addition, we show that for active regions within 30 heliocentric degrees of disk center, WLSG can be adequately measured from line-of-sight magnetograms instead of vector magnetograms. This approximate measure of active-region total nonpotentiality, LWLSG, with the extensive set of 96 minute cadence full-disk line-of-sight magnetograms from SOHO MDI, can be used to study the evolution of active-region total nonpotentiality leading to the production of CMEs.

### **MHD Equilibria and Triggers for Prominence Eruption**

Yuhong **Fan**

Chapter 12 of Solar Prominences, Astrophysics and Space Science Library, Volume 415. ISBN 978-3-319-10415-7. Springer International Publishing Switzerland, **2015**, p. 297

<http://arxiv.org/pdf/1512.08044v1.pdf> Magneto-hydrodynamic (MHD) simulations of the emergence of twisted magnetic flux tubes from the solar interior into the corona are discussed to illustrate how twisted and sheared coronal magnetic structures (with free magnetic energy), capable of driving filament eruptions, can form in the corona in emerging active regions. Several basic mechanisms that can disrupt the quasi-equilibrium coronal structures and trigger the release of the stored free magnetic energy are discussed. These include both ideal processes such as the onset of the helical kink instability and the torus instability of a twisted coronal flux rope structure and the non-ideal process of the onset of fast magnetic reconnections in current sheets. Representative MHD simulations of the non-linear evolution involving these mechanisms are presented.

### **A simulation of convective dynamo in the solar convective envelope: maintenance of the solar-like differential rotation and emerging flux**

Yuhong **Fan**, Fang Fang

ApJ, 2014

<http://arxiv.org/pdf/1405.3926v1.pdf>

We report the results of a magneto-hydrodynamic (MHD) simulation of a convective dynamo in a model solar convective envelope driven by the solar radiative diffusive heat flux. The convective dynamo produces a large-scale mean magnetic field that exhibits irregular cyclic behavior with oscillation time scales ranging from about 5 to 15 years and undergoes irregular polarity reversals. The mean axisymmetric toroidal magnetic field is of opposite signs in the two hemispheres and is concentrated at the bottom of the convection zone. The presence of the magnetic fields is found to play an important role in the self-consistent maintenance of a solar-like differential rotation in the convective dynamo model. Without the magnetic fields, the convective flows drive a differential rotation with a faster rotating polar region. In the midst of magneto-convection, we found emergence of strong super-equipartition flux bundles at the surface, exhibiting properties that are similar to emerging solar active regions.

### **$\delta$ -Sunspot Formation in Simulation of Active-Region-Scale Flux Emergence**

Fang **Fang**, Yuhong Fan

2015

<http://arxiv.org/pdf/1504.04393v1.pdf>

$\delta$ -sunspots, with highly complex magnetic structures, are very productive in energetic eruptive events, such as X-class flares and homologous eruptions. We here study the formation of such complex magnetic structures by numerical simulations of magnetic flux emergence from the convection zone into the corona in an active-region-scale domain. In our simulation, two pairs of bipolar sunspots form on the surface, originating from two buoyant segments of a single subsurface twisted flux rope, following the approach of Toriumi et al. (2014). Expansion and rotation of the emerging fields in the two bipoles drive the two opposite polarities into each other with apparent rotating motion, producing a compact  $\delta$ -sunspot with a sharp polarity inversion line. The formation of the  $\delta$ -sunspot in such a realistic-scale domain produces emerging patterns similar to those formed in observations, e.g. the inverted polarity against Hale's law, the curvilinear motion of the spot, strong transverse field with highly sheared magnetic and velocity fields at the PIL. Strong current builds up at the PIL, giving rise to reconnection, which produces a complex coronal magnetic connectivity with non-potential fields in the Delta-spot overlaid by more relaxed fields connecting the two polarities at the two ends.

### **MULTIDIMENSIONAL MODELING OF CORONAL RAIN DYNAMICS**

X. **Fang**, C. Xia, and R. Keppens

2013 ApJ 771 L29

We present the first multidimensional, magnetohydrodynamic simulations that capture the initial formation and long-term sustainment of the enigmatic coronal rain phenomenon. We demonstrate how thermal instability can induce a spectacular display of in situ forming blob-like condensations which then start their intimate ballet on top of initially linear force-free arcades. Our magnetic arcades host a chromospheric, transition region, and coronal plasma. Following coronal rain dynamics for over 80 minutes of physical time, we collect enough statistics to quantify blob widths, lengths, velocity distributions, and other characteristics which directly match modern observational knowledge. Our virtual coronal rain displays the deformation of blobs into V-shaped features, interactions of blobs due to mostly pressure-mediated levitations, and gives the first views of blobs that evaporate in situ or are siphoned over the apex of the background arcade. Our simulations pave the way for systematic surveys of coronal rain showers in true multidimensional settings to connect parameterized heating prescriptions with rain statistics, ultimately allowing us to quantify the coronal heating input.

### **Strongest coronal magnetic fields in solar cycles 23-24: probing, statistics, and implications**

V. V. **Fedenev**, S. A. Anfinogentov, G. D. Fleishman

ApJ 2023

<https://arxiv.org/pdf/2301.08922.pdf>

Strong coronal magnetic field, when present, manifests itself as bright microwave sources at high frequencies produced by gyroresonant (GR) emission mechanism in thermal coronal plasma. The highest frequency at which this emission is observed is proportional to the absolute value of the strongest coronal magnetic field on the line of sight. Although no coronal magnetic field larger than roughly 2,000 G was expected, recently the field at least twice larger has been reported. Here, we report a search for and statistical study of such strong coronal magnetic fields using high-frequency GR emission. A historic record of spatially resolved microwave observations at high frequencies, 17 and 34 GHz, is available from Nobeyama RadioHeliograph for more than 20 years (1995-2018). Here we employ this data set to identify sources of bright GR emission at 34 GHz and perform a statistical analysis of the identified GR cases to quantify the strongest coronal magnetic fields during two solar cycles. We found that although active regions with the strong magnetic field are relatively rare (less than 1% of all active regions), they appear regularly on the Sun. These active regions are associated with prominent manifestations of solar activity.

## Origin of the chromospheric three-minute oscillations in sunspot umbrae

T. Felipe

A&A 2019

<https://arxiv.org/pdf/1906.09797.pdf>

Sunspot umbrae show a change in the dominant period of their oscillations from five minutes in the photosphere to three minutes in the chromosphere. In this paper, we explore the two most popular models proposed to explain the three-minute oscillations: the chromospheric acoustic resonator and the propagation of waves with frequency above the cutoff value directly from lower layers. We employ numerical simulations of wave propagation from the solar interior to the corona. Waves are driven by a piston at the bottom boundary. We have performed a parametric study of the measured chromospheric power spectra in a large number of numerical simulations with differences in the driving method, the height of the transition region (or absence of transition region), the strength of the vertical magnetic field, and the value of the radiative cooling time. We find that both mechanisms require the presence of waves with period in the three-minute band in the photosphere. These waves propagate upward and their amplitude increases due to the drop of the density. Their amplification is stronger than that of evanescent low-frequency waves. This effect is enough to explain the dominant period observed in chromospheric spectral lines. However, waves are partially trapped between the photosphere and the transition region, forming an acoustic resonator. This chromospheric resonant cavity strongly enhances the power in the three-minute band. The chromospheric acoustic resonator model and the propagation of waves in the three-minute band directly from the photosphere can explain the observed chromospheric three-minute oscillations. They are both important in different scenarios. Resonances are produced by waves trapped between the temperature minimum and the transition region. Strong magnetic fields and radiative losses remove energy from the waves inside the cavity, resulting in weaker amplitude resonances.

## Inversions of synthetic umbral flashes: Effects of scanning time on the inferred atmospheres

T. Felipe<sup>1,2</sup>, H. Socas-Navarro<sup>1,2</sup> and D. Przybylski<sup>3</sup>

A&A 614, A73 (2018)

**Context.** The use of instruments that record narrowband images at selected wavelengths is a common approach in solar observations. They allow scanning of a spectral line by sampling the Stokes profiles with two-dimensional images at each line position, but require a compromise between spectral resolution and temporal cadence. The interpretation and inversion of spectropolarimetric data generally neglect changes in the solar atmosphere during the scanning of line profiles.

**Aims.** We evaluate the impact of the time-dependent acquisition of various wavelengths on the inversion of spectropolarimetric profiles from chromospheric lines during umbral flashes.

**Methods.** Numerical simulations of nonlinear wave propagation in a sunspot model were performed with the code MANCHA. Synthetic Stokes parameters in the Ca II 8542 Å line in NLTE were computed for an umbral flash event using the code NICOLE. Artificial profiles with the same wavelength coverage and temporal cadence from reported observations were constructed and inverted. The inferred atmospheric stratifications were compared with the original simulated models.

**Results.** The inferred atmospheres provide a reasonable characterization of the thermodynamic properties of the atmosphere during most of the phases of the umbral flash. The Stokes profiles present apparent wavelength shifts and other spurious deformations at the early stages of the flash, when the shock wave reaches the formation height of the Ca II 8542 Å line. These features are misinterpreted by the inversion code, which can return unrealistic atmospheric models from a good fit of the Stokes profiles. The misguided results include flashed atmospheres with strong downflows, even though the simulation exhibits upflows during the umbral flash, and large variations in the magnetic field strength.

Conclusions. Our analyses validate the inversion of Stokes profiles acquired by sequentially scanning certain selected wavelengths of a line profile, even in the case of rapidly changing chromospheric events such as umbral flashes. However, the inversion results are unreliable during a short period at the development phase of the flash.

### **Magnetic connectivity between the light bridge and penumbra in a sunspot**

Song [Feng](#), [Yuhu Miao](#), [Ding Yuan](#), [Zhongquan Qu](#), [Valery M. Nakariakov](#)

ApJL 2020

<https://arxiv.org/pdf/2003.03976.pdf>

A light bridge is a prominent structure commonly observed within a sunspot. Its presence usually triggers a wealth of dynamics in a sunspot, and has a lasting impact on sunspot evolution. However, the fundamental structure of light bridges is still not well understood. In this study, we used the high-resolution spectropolarimetry data obtained by the Solar Optical Telescope onboard the Hinode satellite to analyze the magnetic and thermal structure of a light bridge at  $\lambda_{\text{AR}}$ . We also combined the high-cadence  $1700\text{\AA}$  channel data provided by the Atmospheric Imaging Assembly onboard the Solar Dynamic Observatory to study the dynamics on this bridge. We found that a pair of blue and red Doppler shift patches at two ends of this bridge, this pattern appears to be the convective motion directed by the horizontal component of the magnetic field aligned with the spine of this bridge. Paired upward and downward motions implies that the light bridge could have a two-legged or undulate magnetic field. Significant four minute oscillations in the emission intensity of the  $1700\text{\AA}$  bandpass were detected at two ends, which had overlap with the paired blue and red shift patches. The oscillatory signals at the light bridge and the penumbra were highly correlated with each other. Although they are separated in space at the photosphere, the periodicity seems to have a common origin from the underneath. Therefore, we infer that the light bridge and penumbra could share a common magnetic source and become fragmented at the photosphere by magneto-convection. **10-15 Apr 2019**

### **Identifying and Tracking of Peripheral and Central Umbral Dots**

Song [Feng](#), Yan Zhao, Yunfei Yang, [Kaifan Ji](#), [Hui Deng](#), [Feng Wang](#)

[Solar Physics](#) April 2015, Volume 290, Issue 4, pp 1119-1133

Umbral dots (UDs) are small isolated brightening observed in sunspot umbrae. They are usually classified into peripheral UD (PUDs) and central UD (CUDs) according to their positions inside an umbra. To accurately investigate the similarities and the distinctions between PUDs and CUDs and better understand their formation mechanisms, we propose a method for identifying and tracking PUDs and CUDs. Firstly, the umbra-penumbra boundary was detected based on morphological reconstruction. Secondly, the UD were identified and tracked based on phase congruency. Finally, the UD were classified into PUDs and CUDs with a new definition of the periphery and the center of an umbra. A data set obtained with the Hinode/Solar Optical Telescope on **2 March 2007** was used to illustrate the procedures. The statistical properties of PUDs and CUDs, including equivalent diameters, ratio of the maximum intensity to the mean photosphere intensity, horizontal velocities, lifetimes, and trajectories were investigated to evaluate the performance of the method.

### **A DATA-DRIVEN MODEL FOR THE GLOBAL CORONAL EVOLUTION**

Xueshang [Feng](#)<sup>1</sup>, Chaowei Jiang<sup>1</sup>, Changqing Xiang<sup>1</sup>, Xuepu Zhao<sup>2</sup>, and S. T. Wu

2012 ApJ 758 62

This work is devoted to the construction of a data-driven model for the study of the dynamic evolution of the global corona that can respond continuously to the changing of the photospheric magnetic field. The data-driven model consists of a surface flux transport (SFT) model and a global three-dimensional (3D) magnetohydrodynamic (MHD) coronal model. The SFT model is employed to produce the global time-varying and self-consistent synchronic snapshots of the photospheric magnetic field as the input to drive our 3D numerical global coronal AMR-CESE-MHD model on an overset grid of Yin-Yang overlapping structure. The SFT model and the 3D global coronal model are coupled through the boundary condition of the projected characteristic method. Numerical results of the coronal evolution from 1996 September 4 to October 29 provide a good comparison with multiply observed coronal images.

### **Observations of umbral flashes in the resonant sunspot chromosphere**

[T. Felipe](#), [S. J. González Manrique](#), [D. Martínez-Gómez](#), [M. M. Gómez-Míguez](#), [E. Khomenko](#), [C. Quintero Noda](#), [H. Socas-Navarro](#)

A&A 2024

<https://arxiv.org/pdf/2411.16467>

In sunspot umbrae, the core of some chromospheric lines exhibits periodic brightness enhancements known as umbral flashes. The consensus is that they are produced by the upward propagation of shock waves. This view has recently been challenged by the detection of downflowing umbral flashes and the confirmation of the existence of a resonant cavity above sunspots. We aim to determine waves' propagating or standing nature in the low umbral chromosphere and confirm or refute the existence of downflowing umbral flashes. Spectroscopic temporal series of

Ca II 8542 Å, Ca II H, and H $\alpha$  in a sunspot were acquired with the Swedish Solar Telescope. The H $\alpha$  velocity was inferred using bisectors. Simultaneous inversions of the Ca II 8542 Å line and the Ca II H core were performed using the NICOLE code. The nature of the oscillations and insights into the resonant oscillatory pattern were determined by analyzing the phase shift between the velocity signals and examining the temporal evolution. Propagating waves in the low chromosphere are more common in regions with frequent umbral flashes, where the transition region is shifted upward, making resonant cavity signatures less noticeable. In contrast, areas with fewer umbral flashes show velocity fluctuations that align with standing oscillations. Evidence suggests dynamic changes in the location of velocity resonant nodes due to variations in transition region height. Downflowing profiles appear at the onset of some umbral flashes, but upflowing motion dominates during most of the flash. These downflowing flashes are more common in standing umbral flashes. We confirm the existence of a chromospheric resonant cavity above sunspot umbrae produced by wave reflections at the transition region. The oscillatory pattern depends on the transition region height, which exhibits spatial and temporal variations due to the impact of the waves. **2022 May 3**

### **Magnetic field fluctuations in the shocked umbral chromosphere**

[T. Felipe](#), [S. J. González Manrique](#), [C. R. Sangeetha](#), [A. Asensio Ramos](#)

A&A 676, A77 **2023**

<https://arxiv.org/pdf/2307.01313.pdf>

<https://www.aanda.org/articles/aa/pdf/2023/08/aa44519-22.pdf>

Several studies have reported magnetic field fluctuations associated with umbral shock waves. We aim to study the properties and origin of magnetic field fluctuations in the umbral chromosphere. Temporal series of spectropolarimetric observations were acquired with the GREGOR telescope. The chromospheric and photospheric conditions were derived from simultaneous inversions of the He I 10830 Å triplet and the Si I 10827 Å line using HAZEL2. The oscillations are interpreted using wavelet analysis and context information from UV observations acquired with SDO/AIA and IRIS. The chromospheric magnetic field shows strong fluctuations in the sunspot umbra, with peak field strengths up to 2900 G. Magnetic field and velocity umbral oscillations exhibit a strong coherence, with the magnetic field lagging the shock fronts detected in the velocity fluctuations. This points to a common origin of the fluctuations in both parameters, whereas the analysis of the phase shift between photospheric and chromospheric velocity is consistent with upwards wave propagation. These results suggest that the strong inferred magnetic field fluctuations are caused by changes in the response height of the He I 10830 Å line to the magnetic field, which is sensitive to high photospheric layers after the shock fronts. The coronal activity seen in EUV data could possibly have some impact on the inferred fluctuations, but it is not the main driver of the magnetic field oscillations since they are found before EUV events take place. Chromospheric magnetic field fluctuations measured with the He I 10830 Å triplet arise due to variations in the opacity of the line. After shocks produced by slow magnetoacoustic waves, the response of the line to the magnetic field can be shifted down to the upper photosphere. This is seen as remarkably large fluctuations in the line of sight magnetic field strength. **2017 June 18**

### **Limitations of the Ca II 8542 Å line for the determination of magnetic field oscillations**

[T. Felipe](#), [H. Socas Navarro](#), [C. R. Sangeetha](#), [I. Milic](#)

ApJ **2021**

<https://arxiv.org/pdf/2107.02160.pdf>

Chromospheric umbral oscillations produce periodic brightenings in the core of some spectral lines, known as umbral flashes. They are also accompanied by fluctuations in velocity, temperature, and, according to several recent works, magnetic field. In this study, we aim to ascertain the accuracy of the magnetic field determined from inversions of the Ca II 8542 Å line. We have developed numerical simulations of wave propagation in a sunspot umbra. Synthetic Stokes profiles emerging from the simulated atmosphere were computed and then inverted using the NICOLE code. The atmospheres inferred from the inversions have been compared with the original parameters from the simulations. Our results show that the inferred chromospheric fluctuations in velocity and temperature match the known oscillations from the numerical simulation. In contrast, the vertical magnetic field obtained from the inversions exhibits an oscillatory pattern with a  $\sim 300$  G peak-to-peak amplitude which is absent in the simulation. We have assessed the error in the inferred parameters by performing numerous inversions with slightly different configurations of the same Stokes profiles. We find that when the atmosphere is approximately at rest, the inversion tends to favor solutions that underestimate the vertical magnetic field strength. On the contrary, during umbral flashes, the values inferred from most of the inversions are concentrated at stronger fields than those from the simulation. Our analysis provides a quantification of the errors associated with the inversions of the Ca II 8542 Å line and suggests caution with the interpretation of the inferred magnetic field fluctuations.

### **Downflowing umbral flashes as an evidence of standing waves in sunspot umbrae**

[T. Felipe](#), [V. M. J. Henriques](#), [J. de la Cruz Rodríguez](#), [H. Socas-Navarro](#)

A&A Let. 645, L12 **2021**

<https://arxiv.org/pdf/2101.04188.pdf>

<https://www.aanda.org/articles/aa/pdf/2021/01/aa39966-20.pdf>



Umbral flashes are sudden brightenings commonly visible in the core of chromospheric lines. Theoretical and numerical modeling suggest that they are produced by the propagation of shock waves. According to these models and early observations, umbral flashes are associated with upflows. However, recent studies have reported umbral flashes in downflowing atmospheres. We aim to understand the origin of downflowing umbral flashes. We explore how the existence of standing waves in the umbral chromosphere impacts the generation of flashed profiles. We performed numerical simulations of wave propagation in a sunspot umbra with the code MANCHA. The Stokes profiles of the Ca II 8542 Å line were synthesized with NICOLE. For freely-propagating waves, the chromospheric temperature enhancements of the oscillations are in phase with velocity upflows. In this case, the intensity core of the Ca II 8542 Å atmosphere is heated during the upflowing stage of the oscillation. If we consider a different scenario with a resonant cavity, the wave reflections at the sharp temperature gradient of the transition region lead to standing oscillations. In this situation, temperature fluctuations are shifted backward and temperature enhancements partially coincide with the downflowing stage of the oscillation. In umbral flashes produced by standing oscillations, the reversal of the emission feature is produced when the oscillation is downflowing. The chromospheric temperature keeps increasing while the atmosphere is changing from a downflow to an upflow. During the appearance of flashed Ca II 8542 Å cores, the atmosphere is upflowing most of the time, and only 38% of the flashed profiles are associated with downflows. We find a scenario that remarkably explains the recent empirical findings of downflowing umbral flashes as a natural consequence of the presence of standing oscillations above sunspot umbrae.

## **Chromospheric resonances above sunspots and potential seismological applications**

[T. Felipe](#), [C. Kuckein](#), [S. J. González Manrique](#), [I. Milic](#), [C. R. Sangeetha](#)

ApJL 900 L29 2020

<https://arxiv.org/pdf/2008.10623.pdf>

<https://doi.org/10.3847/2041-8213/abb1a5>

Oscillations in sunspot umbrae exhibit remarkable differences between the photosphere and chromosphere. We evaluate two competing scenarios proposed for explaining those observations: a chromospheric resonant cavity and waves traveling from the photosphere to upper atmospheric layers. We have employed numerical simulations to analyze the oscillations in both models. They have been compared with observations in the low (Na I D2) and high (He I 10830 Å) chromosphere. The nodes of the resonant cavity can be detected as phase jumps or power dips, although the identification of the latter is not sufficient to claim the existence of resonances. In contrast, phase differences between velocity and temperature fluctuations reveal standing waves and unequivocally prove the presence of an acoustic resonator above umbrae. Our findings offer a new seismic method to probe active region chromospheres through the detection of resonant nodes. **2000 Oct 01, 2001 May 09, 2007 Aug 29, 2017 Jun 17-18, 2018 May 09**

Table 1. Details of the six data sets obtained with VTT and GREGOR telescopes

## **Signatures of sunspot oscillations and the case for chromospheric resonances**

[T. Felipe](#)

2020

<https://arxiv.org/pdf/2007.10471.pdf>

Sunspots host a large variety of oscillatory phenomena, whose properties depend on the nature of the wave modes and the magnetic and thermodynamic structure of the spot. Umbral chromospheric oscillations exhibit significant differences compared to their photospheric counterparts. They show an enhanced power and a shorter dominant period, from waves with an amplitude of a few hundred meters per second in the five-minute band at the photosphere, to amplitudes of several kilometers per second in the three-minute band at the chromosphere. Various models have been proposed to explain this behaviour, including the presence of a chromospheric resonance cavity between the photosphere and the transition region. Jess et al. (2020, Nature Astronomy, 4, 220) claimed the detection of observational evidence supporting this model, obtained from the comparison of spectropolarimetric observations and numerical simulations. Here, it is shown that the observational insight reported by Jess et al. is not a common property of sunspots. More importantly, numerical modelling also shows that it is not an unequivocal signature of an acoustic resonator. **2000 Oct 1, 2001 May 9, 2007 Aug 28, 2017 Jun 17-18**

## **Inversions of synthetic umbral flashes: selection of wavelength sampling**

[T. Felipe](#), [S. Esteban Pozuelo](#)

A&A 632, A75 2019

<https://arxiv.org/pdf/1910.13980.pdf>

<https://doi.org/10.1051/0004-6361/201936679>

Imaging spectrographs are popular instruments used to obtain solar data. They record quasi-monochromatic images at selected wavelength positions. By scanning the spectral range of the line, it is possible to obtain bidimensional maps of the FoV with a moderate spectral resolution. In this work, we evaluate the quality of spectropolarimetric inversions obtained from various wavelength samplings during umbral flashes. We computed numerical simulations

of nonlinear wave propagation in a sunspot and constructed synthetic Stokes profiles in the Ca II 8542 Å line during an umbral flash using the NLTE code NICOLE. The spectral resolution of the Stokes profiles was downgraded to various cases with differences in the wavelength coverage. A large set of wavelength samplings was analyzed and the performance of the inversions was evaluated by comparing the inferred chromospheric temperature, velocity, and magnetic field with the actual values at the chromosphere of the numerical simulation. The errors in the inverted results depend to a large extent on the location of the wavelength points across the profile of the line. The inferred magnetic field improves with the increase of the spectral resolution. In the case of velocity and temperature, low spectral resolution data produce a match of the inverted atmospheres with the actual values comparable to wavelength samplings with finer resolution, while providing a higher temporal cadence in the data acquisition. We validated the NLTE inversions of spectropolarimetric data from the Ca II 8542 Å during umbral flashes, during which the atmosphere undergoes sudden dramatic changes due to the propagation of a shock wave. Our results favor the use of fine spectral resolution for analyses that focus on the inference of the magnetic field, whereas the estimation of temperature and velocity fluctuations can be performed with lower spectral resolution.

## Origin of the chromospheric three-minute oscillations in sunspot umbrae

T. [Felipe](#)

A&A 627, A169 (2019)

Context. Sunspot umbrae show a change in the dominant period of their oscillations from five minutes (3.3 mHz) in the photosphere to three minutes (5.5 mHz) in the chromosphere.

Aims. In this paper, we explore the two most popular models proposed to explain the three-minute oscillations: the chromospheric acoustic resonator and the propagation of waves with frequency above the cutoff value directly from lower layers.

Methods. We employ numerical simulations of wave propagation from the solar interior to the corona. Waves are driven by a piston at the bottom boundary. We have performed a parametric study of the measured chromospheric power spectra in a large number of numerical simulations with differences in the driving method, the height of the transition region (or absence of transition region), the strength of the vertical magnetic field, and the value of the radiative cooling time.

Results. We find that both mechanisms require the presence of waves with periods in the three-minute band at the photosphere. These waves propagate upward and their amplitude increases due to the drop of the density. Their amplification is stronger than that of evanescent low-frequency waves. This effect is enough to explain the dominant period observed in chromospheric spectral lines. However, waves are partially trapped between the photosphere and the transition region, forming an acoustic resonator. This chromospheric resonant cavity strongly enhances the power in the three-minute band.

Conclusions. The chromospheric acoustic resonator model and the propagation of waves in the three-minute band directly from the photosphere can explain the observed chromospheric three-minute oscillations. They are both important in different scenarios. Resonances are produced by waves trapped between the temperature minimum and the transition region. Strong magnetic fields and radiative losses remove energy from the waves inside the cavity, resulting in resonances with weaker amplitude.

## Spiral-shaped wavefronts in a sunspot umbra

T. [Felipe](#), [C. Kuckein](#), [E. Khomenko](#), [I. Thaler](#)

A&A 621, A43 2019

<https://arxiv.org/pdf/1810.11257.pdf>

Solar active regions show a wide variety of oscillatory phenomena. The presence of the magnetic field leads to the appearance of several wave modes, whose behavior is determined by the sunspot thermal and magnetic structure. We aim to study the relation between the umbral and penumbral waves observed at the high photosphere and the magnetic field topology of the sunspot. Observations of the sunspot in active region NOAA 12662 obtained with the GREGOR telescope (Observatorio del Teide, Spain) were acquired on **2017 June 17**. The data set includes a temporal series in the Fe I 5435 Å line obtained with the imaging spectrograph GREGOR Fabry-Pérot Interferometer (GFPI) and a spectropolarimetric raster map acquired with the GREGOR Infrared Spectrograph (GRIS) in the 10830 Å spectral region. The Doppler velocity deduced from the restored Fe I 5435 Å line has been determined, and the magnetic field vector of the sunspot has been inferred from spectropolarimetric inversions of the Ca I 10839 Å and the Si I 10827 Å lines. A two-armed spiral wavefront has been identified in the evolution of the two-dimensional velocity maps from the Fe I 5435 Å line. The wavefronts initially move counterclockwise in the interior of the umbra, and develop into radially outward propagating running penumbral waves when they reach the umbra-penumbra boundary. The horizontal propagation of the wavefronts approximately follows the direction of the magnetic field, which shows changes in the magnetic twist with height and horizontal position. The spiral wavefronts are interpreted as the visual pattern of slow magnetoacoustic waves which propagate upward along magnetic field lines. Their apparent horizontal propagation is due to their sequential arrival to different horizontal positions at the formation height of the Fe I 5435 Å line, as given by the inclination and orientation of the magnetic field.

## Height variation of the cutoff frequency in a sunspot umbra

T. [Felipe](#), [C. Kuckein](#), [I. Thaler](#)

A&A 617, A39 2018

<https://arxiv.org/pdf/1806.05856.pdf>

Context. In the solar atmosphere, the acoustic cutoff frequency is a local quantity which depends on the atmospheric height. It separates the low-frequency evanescent waves from the high-frequency propagating waves. Aims. We measure the cutoff frequency of slow magnetoacoustic waves at various heights of a sunspot umbra and compare the results with the estimations from several analytical formulae.

Methods. We analyzed the oscillations in the umbra of a sunspot belonging to active region NOAA 12662 observed in the 10830 Å spectral region with the GREGOR Infrared Spectrograph and in the Fe I 5435 Å line with the GREGOR Fabry-Pérot Interferometer. Both instruments are attached to the GREGOR telescope at the Observatorio del Teide, Tenerife, Spain. We have computed the phase and amplification spectra between the velocity measured from different pairs of lines that sample various heights of the solar atmosphere. The cutoff frequency and its height variation have been estimated from the inspection of the spectra.

Results. At the deep umbral photosphere the cutoff frequency is around 5 mHz and it increases to 6 mHz at higher photospheric layers. At the chromosphere the cutoff is  $\sim 3.1$  mHz. The comparison of the observationally determined cutoff with the theoretically predicted values reveals an agreement in the general trend and a reasonable match at the chromosphere, but also significant quantitative differences at the photosphere.

Conclusions. Our analyses show strong evidence of the variation of the cutoff frequency with height in a sunspot umbra, which is not fully accounted for by current analytical estimations. This result has implications for our understanding of wave propagation, the seismology of active regions, and the evaluation of heating mechanisms based on compressible waves.

## Inversions of synthetic umbral flashes: effects of the scanning time on the inferred atmospheres

T. [Felipe](#), [H. Socas-Navarro](#), [D. Przybylski](#)

A&A 2018

<https://arxiv.org/pdf/1802.05028.pdf>

The use of instruments that record narrow band images at selected wavelengths is a common approach in solar observations. They allow the scanning of a spectral line by sampling the Stokes profiles with 2D images at each line position, but require a compromise between spectral resolution and temporal cadence. We evaluate the impact of the time-dependent acquisition of different wavelengths on the inversion of spectropolarimetric profiles from chromospheric lines during umbral flashes. Simulations of non-linear wave propagation in a sunspot were performed with the code MANCHA. Synthetic Stokes parameters in the Ca II 8542 Å line in NLTE were computed for an umbral flash using the code NICOLE. Artificial profiles with the same wavelength coverage and temporal cadence from reported observations were constructed and inverted. The inferred atmospheric stratifications were compared with the original models. The inferred atmospheres provide a reasonable characterization of the thermodynamic properties of the atmosphere during most of the phases of the umbral flash. Only at the early stages of the flash, when the shock wave reaches the formation height of the line, the Stokes profiles present apparent wavelength shifts and other spurious deformations. These features are misinterpreted by the inversion code, which can return unrealistic atmospheric models from a good fit of the Stokes profiles. The misguided results include flashed atmospheres with strong downflows, even though the simulation exhibits upflows during the umbral flash, and large variations in the magnetic field strength. Our analyses validate the inversion of Stokes profiles acquired by sequentially scanning certain selected wavelengths of a line profile, even in the case of rapidly-changing events such as umbral flashes. However, the inversions are unreliable during a short period at the development phase of the flash. 2017 June 17

## Signatures of the impact of flare ejected plasma on the photosphere of a sunspot light-bridge

T. [Felipe](#), [M. Collados](#), [E. Khomenko](#), [S. P. Rajaguru](#), [M. Franz](#), [C. Kuckein](#), [A. Asensio Ramos](#)

A&A 608, A97 2017

<https://arxiv.org/pdf/1708.06133.pdf>

We investigate the properties of a sunspot light-bridge, focusing on the changes produced by the impact of a plasma blob ejected from a C-class flare. We observed a sunspot in active region NOAA 12544 using spectropolarimetric raster maps of the four Fe I lines around 15655 Å with the GREGOR Infrared Spectrograph (GRIS), narrow-band intensity images sampling the Fe I 6173 Å line with the GREGOR Fabry-Pérot Interferometer (GFPI), and intensity broad band images in G-band and Ca II H band with the High-resolution Fast Imager (HiFI). All these instruments are located at the GREGOR telescope at the Observatorio del Teide, Tenerife, Spain. The data cover the time before, during, and after the flare event. The analysis is complemented with Atmospheric Imaging Assembly

(AIA) and Helioseismic and Magnetic Imager (HMI) data from the Solar Dynamics Observatory (SDO). The physical parameters of the atmosphere at different heights were inferred using spectral-line inversion techniques. We identify photospheric and chromospheric brightenings, heating events, and changes in the Stokes profiles associated to the flare eruption and the subsequent arrival of the plasma blob to the light bridge, after traveling along an active region loop. The measurements suggest that these phenomena are the result of reconnection events driven by the interaction of the plasma blob with the magnetic field topology of the light bridge. **2016 May 15**

### **Dependence of sunspot photospheric waves on the depth of the source of solar p-modes**

T. **Felipe**, E. Khomenko

A&A **2017**

<https://arxiv.org/pdf/1702.00997.pdf>

Photospheric waves in sunspots moving radially outwards at speeds faster than the characteristic wave velocities have been recently detected. It has been suggested that they are the visual pattern of p-modes excited around 5 Mm beneath the sunspot. Using numerical simulations, we have performed a parametric study of the waves observed at the photosphere and higher layers produced by sources located at different depths. The observational measurements are consistent with waves driven between approximately 1 Mm and 5 Mm below the sunspot surface.

### **Three-dimensional structure of a sunspot light bridge**

T. **Felipe**, M. Collados, E. Khomenko, C. Kuckein, A. Asensio Ramos, H. Balthasar, T. Berkefeld, C. Denker, A. Feller, M. Franz, A. Hofmann, C. Kiess, A. Lagg, H. Nicklas, D. Orozco Suárez, A. Pastor Yabar, R. Rezaei, R. Schlichenmaier, D. Schmidt, W. Schmidt, M. Sigwarth, M. Sobotka, S. K. Solanki, D. Soltau, J. Staude, K. G. Strassmeier, R. Volkmer, O. von der Lühe, T. Waldmann

A&A **2016**

<https://arxiv.org/pdf/1611.04803v1.pdf>

Active regions are the most prominent manifestations of solar magnetic fields; their generation and dissipation are fundamental problems in solar physics. Light bridges are commonly present during sunspot decay, but a comprehensive picture of their role in the removal of photospheric magnetic field is still missing. We study the three dimensional configuration of a sunspot and in particular its light bridge during one of the last stages of its decay. We present the magnetic and thermodynamical stratification inferred from full Stokes inversions of the photospheric Si I 10827 \AA and Ca I 10839 \AA lines obtained with the GREGOR Infrared Spectrograph of the GREGOR telescope at Observatorio del Teide, Tenerife, Spain. The analysis is complemented by a study of continuum images covering the disk passage of the active region, which are provided by the Helioseismic and Magnetic Imager on board the Solar Dynamics Observatory. The sunspot shows a light bridge with penumbral continuum intensity that separates the central umbra from a smaller umbra. We find that in this region the magnetic field lines form a canopy with lower magnetic field strength in the inner part. The photospheric light bridge is dominated by gas pressure (high- $\beta$ ), as opposed to the surrounding umbra where the magnetic pressure is higher. A convective flow is observed in the light bridge. This flow is able to bend the magnetic field lines and to produce field reversals. The field lines close above the light bridge and become as vertical and strong as in the surrounding umbra. We conclude that it develops because of two highly magnetized regions which come closer during the sunspot evolution. **2014 June 27**

### **Helioseismic holography of simulated sunspots: magnetic and thermal contributions to travel times**

T. **Felipe**, D. C. Braun, A. D. Crouch, A. C. Birch

ApJ **2016**

<http://arxiv.org/pdf/1608.04893v1.pdf>

Wave propagation through sunspots involves conversion between waves of acoustic and magnetic character. In addition, the thermal structure of sunspots is very different than that of the quiet Sun. As a consequence, the interpretation of local helioseismic measurements of sunspots has long been a challenge. With the aim of understanding these measurements, we carry out numerical simulations of wave propagation through sunspots. Helioseismic holography measurements made from the resulting simulated wavefields show qualitative agreement with observations of real sunspots. We use additional numerical experiments to determine, separately, the influence of the thermal structure of the sunspot and the direct effect of the sunspot magnetic field. We use the ray approximation to show that the travel-time shifts in the thermal (non-magnetic) sunspot model are primarily produced by changes in the wave path due to the Wilson depression rather than variations in the wave speed. This shows that inversions for the subsurface structure of sunspots must account for local changes in the density. In some ranges of horizontal phase speed and frequency there is agreement (within the noise level in the simulations) between the travel times measured in the full magnetic sunspot model and the thermal model. If this conclusion proves to be robust for a wide range of models, it would suggest a path towards inversions for sunspot structure.

## **Synthetic observations of wave propagation in a sunspot umbra**

T. [Felipe](#), H. Socas-Navarro, E. Khomenko

ApJ, 795 9 2014

<http://arxiv.org/pdf/1408.6565v1.pdf>

Spectropolarimetric temporal series from Fe I  $\lambda$  6301.5 Å and Ca II infrared triplet lines are obtained by applying the Stokes synthesis code NICOLE to a numerical simulation of wave propagation in a sunspot umbra from MANCHA code. The analysis of the phase difference between Doppler velocity and intensity core oscillations of the Fe I  $\lambda$  6301.5 Å line reveals that variations in the intensity are produced by opacity fluctuations rather than intrinsic temperature oscillations, except for frequencies between 5 and 6.5 mHz. On the other hand, the photospheric magnetic field retrieved from the weak field approximation provides the intrinsic magnetic field oscillations associated to wave propagation. Our results suggest that this is due to the low magnetic field gradient of our sunspot model. The Stokes parameters of the chromospheric Ca II infrared triplet lines show striking variations as shock waves travel through the formation height of the lines, including emission self-reversals in the line core and highly abnormal Stokes V profiles. Magnetic field oscillations inferred from the Ca II infrared lines using the weak field approximation appear to be related with the magnetic field strength variation between the photosphere and the chromosphere.

## **Evaluation of the capability of local helioseismology to discern between monolithic and spaghetti sunspot models**

T. [Felipe](#), A. D. Crouch, A. C. Birch

ApJ 788 136., 2014

<http://arxiv.org/pdf/1405.0036v1.pdf>

The helioseismic properties of the wave scattering generated by monolithic and spaghetti sunspots are analyzed by means of numerical simulations. In these computations, an incident f or p1 mode travels through the sunspot model, which produces absorption and phase shift of the waves. The scattering is studied by inspecting the wavefield, computing travel-time shifts, and performing Fourier-Hankel analysis. The comparison between the results obtained for both sunspot models reveals that the differences in the absorption coefficient can be detected above noise level. The spaghetti model produces a steep increase of the phase shift with the degree of the mode at short wavelengths, while mode-mixing is more efficient for the monolithic model. These results provide a clue for what to look for in solar observations to discern the constitution of sunspots between the proposed monolithic and spaghetti models.

## **Magnetic Connectivity between the Light Bridge and Penumbra in a Sunspot**

Song [Feng](#), Yuhu Miao, Ding Yuan, Zhongquan Qu, and Valery M. Nakariakov

2020 ApJL 893 L2

<https://doi.org/10.3847/2041-8213/ab7dc4>

A light bridge is a prominent structure commonly observed within a sunspot. Its presence usually triggers a wealth of dynamics in a sunspot and has a lasting impact on sunspot evolution. However, the fundamental structure of light bridges is still not well understood. In this study, we used the high-resolution spectropolarimetry data obtained by the Solar Optical Telescope on board the Hinode satellite to analyze the magnetic and thermal structure of a light bridge at AR 12838. We also combined the high-cadence channel data provided by the Atmospheric Imaging Assembly on board the Solar Dynamics Observatory to study the dynamics on this bridge. We found a pair of blue and red Doppler shift patches at two ends of this bridge; this pattern appears to be the convective motion directed by the horizontal component of the magnetic field aligned with the spine of the bridge. Paired upward and downward motions imply that the light bridge could have a two-legged or undulating magnetic field. Significant 4 minute oscillations in the emission intensity of the bandpass were detected at two ends, which overlapped the paired blue- and redshift patches. The oscillatory signals at the light bridge and the penumbra were highly correlated with each other. Although they are separated in space at the photosphere, the periodicity seems to have a common origin from underneath the sunspot. Therefore, we infer that the light bridge and penumbra could share a common magnetic source and become fragmented at the photosphere by magnetoconvection.

## **Propagating Slow Sausage Waves in a Sunspot Observed by the New Vacuum Solar Telescope**

Song [Feng](#), [Zheng Deng](#), [Ding Yuan](#), [Zhi Xu](#), [Xiao Yang](#)

Research in Astron. Astrophys. 2020

<https://arxiv.org/pdf/2002.03270.pdf>

A sunspot is an ideal waveguide for a variety of magnetohydrodynamic waves, which carry a significant amount of energy to the upper atmosphere and could be used as a tool to probe magnetic and thermal structure of a sunspot. In this study, we used the New Vacuum Solar Telescope and took high-resolution image sequences simultaneously in

both TiO ( $7058 \pm 10 \text{ \AA}$ ) and H $\alpha$  ( $6562 \pm 2.5 \text{ \AA}$ ) bandpasses. We extracted the area and total emission intensity variations of sunspot umbra and analyzed the signals with synchrosqueezing transform. We found that the area and emission intensity varied with both three and five minute periodicity. Moreover, the area and intensity oscillated in phase with each other, this fact hold in both TiO and H $\alpha$  data. We interpret this oscillatory signal as propagating slow sausage wave. The propagation speed is estimated at about  $8 \text{ km}\cdot\text{s}^{-1}$ . We infer that this sunspot's umbra could have temperature as low as  $2800\text{--}3500 \text{ K}$ .

## **A Comparative Study of Divergence Cleaning Methods of Magnetic Field in the Solar Coronal Numerical Simulation**

Xueshang **Feng**, and Man Zhang

Front. Astron. Space Sci. 3:6, **2016**

This paper presents a comparative study of divergence cleaning methods of magnetic field in the solar coronal three-dimensional numerical simulation. For such purpose, the diffusive method, projection method, generalized Lagrange multiplier method and constrained-transport method are used. All these methods are combined with a finite-volume scheme in spherical coordinates. In order to see the performance between the four divergence cleaning methods, solar coronal numerical simulation for Carrington rotation 2056 has been studied. Numerical results show that the average relative divergence error is around  $10^{-4.5}$  for the constrained-transport method, while about  $10^{-3.1}$ – $10^{-3.6}$  for the other three methods. Although there exist some differences in the average relative divergence errors for the four employed methods, our tests show they can all produce basic structured solar wind.

## **Identifying and Tracking of Peripheral and Central Umbral Dots**

Song **Feng**, Yan Zhao, Yunfei Yang, Kaifan Ji, Hui Deng, Feng Wang

Solar Phys. **2015**

Umbral dots (UDs) are small isolated brightening observed in sunspot umbrae. They are usually classified into peripheral UD (PUDs) and central UD (CUDs) according to their positions inside an umbra. To accurately investigate the similarities and the distinctions between PUDs and CUDs and better understand their formation mechanisms, we propose a method for identifying and tracking PUDs and CUDs. Firstly, the umbra–penumbra boundary was detected based on morphological reconstruction. Secondly, the UD were identified and tracked based on phase congruency. Finally, the UD were classified into PUDs and CUDs with a new definition of the periphery and the center of an umbra. A data set obtained with the Hinode/Solar Optical Telescope on **2 March 2007** was used to illustrate the procedures. The statistical properties of PUDs and CUDs, including equivalent diameters, ratio of the maximum intensity to the mean photosphere intensity, horizontal velocities, lifetimes, and trajectories were investigated to evaluate the performance of the method.

## **Solar coronal loop dynamics near the null point above active region NOAA 2666**

Boris **Filippov**

Publications of the Astronomical Society of Australia (PASA) Vol. 35, e023 **2018**

<https://arxiv.org/ftp/arxiv/papers/1805/1805.08540.pdf>

[sci-hub.tw/10.1017/pasa.2018.20](http://sci-hub.tw/10.1017/pasa.2018.20)

We analyse observations of a saddle-like structure in the corona above the western limb of the Sun on **2017 July 18**. The structure was clearly outlined by coronal loops with typical coronal temperature no more than  $1 \text{ MK}$ . The dynamics of loops showed convergence toward the centre of the saddle in the vertical direction and divergence in the horizontal direction. The event is a clear example of smooth coronal magnetic field reconnection. No heating manifestations in the reconnection region or magnetically connected areas were observed. Potential magnetic field calculations, which use as the boundary condition the SDO/HMI magnetogram taken on July 14, showed the presence of a null point at the height of  $122''$  above the photosphere just at the centre of the saddle structure. The shape of field lines fits the fan-spine magnetic configuration above NOAA 2666.

## **Filament Shape Versus Coronal Potential Magnetic Field Structure**

Boris **Filippov**

MNRAS **2015**

<http://arxiv.org/pdf/1510.04546v1.pdf>

Solar filament shape in projection on disc depends on the structure of the coronal magnetic field. We calculate the position of polarity inversion lines (PILs) of coronal potential magnetic field at different heights above the photosphere, which compose the magnetic neutral surface, and compare with them the distribution of the filament material in H $\alpha$  chromospheric images. We found that the most of the filament material is enclosed between two polarity inversion lines (PILs), one at a lower height close to the chromosphere and one at a higher level, which can be considered as a height of the filament spine. Observations of the same filament on the limb by the *STEREO* spacecraft confirm that the height of the spine is really very close to the value obtained from the PIL and filament border matching. Such matching can be used for filament height estimations in on-disk observations. Filament barbs

are housed within protruding sections of the low-level PIL. On the base of simple model, we show that the similarity of the neutral surfaces in potential and non-potential fields with the same sub-photospheric sources is the reason for the found tendency for the filament material to gather near the potential-field neutral surface. **2012 February 23**

## **Nested active regions anchor the heliospheric current sheet and stall the reversal of the coronal magnetic field**

A. J. **Finley**\*

A&A, 692, A29 (2024)

<https://www.aanda.org/articles/aa/pdf/2024/12/aa51896-24.pdf>

**Context.** During the solar cycle, the Sun's magnetic field polarity reverses due to the emergence, cancellation, and advection of magnetic flux towards the rotational poles. Flux emergence events occasionally cluster together, although it is unclear if this is due to the underlying solar dynamo or simply by chance.

**Aims.** Regardless of the cause, we aim to characterise how the reversal of the Sun's magnetic field and the structure of the solar corona are influenced by nested flux emergence.

**Methods.** From the spherical harmonic decomposition of the Sun's photospheric magnetic field, we identified times when the reversal of the dipole component stalls for several solar rotations. Using observations from sunspot cycle 23 to present, we located the nested active regions responsible for each stalling and explored their impact on the coronal magnetic field using potential field source surface extrapolations.

**Results.** Nested flux emergence has a more significant impact on the topology of the coronal magnetic field than isolated emergences as it produces a coherent (low spherical harmonic order) contribution to the photospheric magnetic field. The heliospheric current sheet, which separates oppositely directed coronal magnetic fields, can become anchored above nested active regions due to the formation of strong opposing magnetic fluxes. Further flux emergence, cancellation, differential rotation, and diffusion, then effectively advects the heliospheric current sheet and shifts the dipole axis.

**Conclusions.** Nested flux emergence can restrict the evolution of the heliospheric current sheet and impede the reversal of the coronal magnetic field. The sources of the solar wind can be more consistently identified around nested active regions because the magnetic field topology remains self-similar for multiple solar rotations. This highlights the importance of identifying and tracking nested active regions to guide the remote-sensing observations of modern heliophysics missions.

## **Observations of solar small-scale magnetic flux-sheet emergence**

C.E. **Fischer**, J.M. **Borrero**, N. **Bello González**, A.J. **Kaithakkal**

A&A **2019**

<https://arxiv.org/pdf/1901.05870.pdf>

**Aims.** Moreno-Insertis et al. (2018) recently discovered two types of flux emergence in their numerical simulations: magnetic loops and magnetic sheet emergence. Whereas magnetic loop emergence has been documented well in the last years, by utilising high-resolution full Stokes data from ground-based telescopes as well as satellites, magnetic sheet emergence is still an understudied process. We report here on the first clear observational evidence of a magnetic sheet emergence and characterise its development.

**Methods.** Full Stokes spectra from the Hinode spectropolarimeter were inverted with the SIR code to obtain solar atmospheric parameters such as temperature, line-of-sight velocities and full magnetic field vector information.

**Results.** We analyse a magnetic flux emergence event observed in the quiet-sun internetwork. After a large scale appearance of linear polarisation, a magnetic sheet with horizontal magnetic flux density of up to 194 Mx/cm<sup>2</sup> hovers in the low photosphere spanning a region of 2 to 3 arcsec. The magnetic field azimuth obtained through Stokes inversions clearly shows an organised structure of transversal magnetic flux density emerging. The granule below the magnetic flux-sheet tears the structure apart leaving the emerged flux to form several magnetic loops at the edges of the granule.

**Conclusions.** A large amount of flux with strong horizontal magnetic fields surfaces through the interplay of buried magnetic flux and convective motions. The magnetic flux emerges within 10 minutes and we find a longitudinal magnetic flux at the foot points of the order of ~1018 Mx. This is one to two orders of magnitude larger than what has been reported for small-scale magnetic loops. The convective flows feed the newly emerged flux into the pre-existing magnetic population on a granular scale. **28 April 2014**

## **The Coronal Global Evolutionary Model (CGEM): Using HMI Vector Magnetogram and Doppler Data to Model the Buildup of Free Magnetic Energy in the Solar Corona**

**Fisher**, George H.; Abbett, William P.; Bercik, David J.; Kazachenko, Maria D.; Lynch, Benjamin J.; Welsch, Brian T.; Hoeksema, J. Todd; Hayashi, Keiji; Liu, Yang; Norton, Aimee A.; Sainz Dalda, Alberto; Sun, Xudong; DeRosa, Marc L.; Cheung, Mark C. M.

Space Weather **2015** Volume 13, Issue 6, pp. 369-373

<http://arxiv.org/ftp/arxiv/papers/1505/1505.06018.pdf>

The most violent space weather events (eruptive solar flares and coronal mass ejections) are driven by the release of free magnetic energy stored in the solar corona. Energy can build up on timescales of hours to days, and then may be suddenly released in the form of a magnetic eruption, which then propagates through interplanetary space, possibly impacting the Earth's space environment. Can we use the observed evolution of the magnetic and velocity fields in the solar photosphere to model the evolution of the overlying solar coronal field, including the storage and release of magnetic energy in such eruptions? The objective of CGEM, the Coronal Global Evolutionary Model, funded by the NASA/NSF Space Weather Modeling program, is to develop and evaluate such a model for the evolution of the coronal magnetic field. The evolving coronal magnetic field can then be used as a starting point for magnetohydrodynamic (MHD) models of the corona, which can then be used to drive models of heliospheric evolution and predictions of magnetic field and plasma density conditions at 1AU. **2011, Feb 14-15**

See Space Weather Quarterly Volume 12, Issue 3, p.12-16 **2015**

<http://onlinelibrary.wiley.com/doi/10.1002/SWQv12i003/pdf>

### **Statistics of convective collapse events in the photosphere and chromosphere observed with the Hinode SOT:**

C. E. **Fischer**, A. G. **deWijn**, R. **Centeno**, B. W. **Lites** and C. U. **Keller**

A&A 504 (2009) 583-588

Convective collapse, a theoretically predicted process that intensifies existing weak magnetic fields in the solar atmosphere, was first directly observed in a single event by Nagata et al. (2008, ApJ, 677, L145) using the high resolution Solar Optical Telescope (SOT) of the Hinode satellite. Using the same space telescope, we observed 49 such events and present a statistical analysis of convective collapse events. Our data sets consist of high resolution time series of polarimetric spectral scans of two iron lines formed in the lower photosphere and filter images in Mg I b<sub>2</sub> and Ca II H, spectral lines that are formed in the high photosphere and the lower chromosphere, respectively. We were thus able to study the implication of convective collapse events on the high photospheric and the chromospheric layers. We found that in all cases, the event was accompanied by a continuum bright point and nearly always by a brightening in the Ca II H images. The magnesium dopplergram exhibits a strong downflow in about three quarters of the events that took place within the field of view of the magnesium dopplergram. The physical parameters from the full Stokes profiles were obtained with the MERLIN Milne-Eddington inversion code. For each of the 49 events we determined the duration, maximum photospheric downflow, field strength increase and size. We found event durations of about 10 min, magnetic element radii of about 0.43'' and 0.35'', before and after the event, respectively, and field strengths of up to 1.65 kG.

### **Force-Free Field Reconstructions Enhanced by Chromospheric Magnetic Field Data**

Gregory **Fleishman**, [Ivan Mysh'yakov](#), [Alexey Stupishin](#), [Maria Loukitcheva](#), [Sergey Anfinogentov](#)

2019 ApJ 870 101

<https://arxiv.org/pdf/1811.02093.pdf>

3D picture of the coronal magnetic field remains an outstanding problem in solar physics, particularly, in active regions. Nonlinear force-free field reconstructions that employ routinely available full-disk photospheric vector magnetograms represent state-of-the-art coronal magnetic field modeling. Such reconstructions, however, suffer from an inconsistency between a force-free coronal magnetic field and non-force-free photospheric boundary condition, from which the coronal reconstruction is performed. In this study we focus on integrating the additional chromospheric and / or coronal magnetic field data with the vector photospheric magnetograms with the goal of improving the reliability of the magnetic field reconstructions. We develop a corresponding modification of the available optimization codes described in Fleishman et al. (2017) and test their performance using a full-fledged MHD model obtained from the Bifrost code by performing a 'voxel-by-voxel' comparison between the reconstructed and the model magnetic fields. We demonstrate that adding even an incomplete set of chromospheric magnetic field data can measurably improve the reconstruction of the coronal magnetic field, greatly improve reconstructions of the magnetic connectivity and of the coronal electric current.

### **Casting the Coronal Magnetic Field Reconstruction Tools in 3D Using MHD Bifrost Model**

Gregory D. **Fleishman**, [Sergey Anfinogentov](#), [Maria Loukitcheva](#), [Ivan Mysh'yakov](#), [Alexey Stupishin](#)

ApJ 839 30 **2017**

<https://arxiv.org/pdf/1703.06360.pdf>

Quantifying coronal magnetic field remains a central problem in solar physics. Nowadays the coronal magnetic field is often modelled using nonlinear force-free field (NLFFF) reconstructions, whose accuracy has not yet been comprehensively assessed. Here we perform a detailed casting of the NLFFF reconstruction tools, such as pi-disambiguation, photospheric field preprocessing, and volume reconstruction methods using a 3D snapshot of the publicly available full-fledged radiative MHD model. Specifically, from the MHD model we know the magnetic field vector in the entire 3D domain, which enables us to perform "voxel-by-voxel" comparison of the restored and the true magnetic field in the 3D model volume. Our tests show that the available pi-disambiguation methods often



fail at the quiet sun areas dominated by small-scale magnetic elements, while they work well at the AR photosphere and (even better) chromosphere. The preprocessing of the photospheric magnetic field, although does produce a more force-free boundary condition, also results in some effective 'elevation' of the magnetic field components. This 'elevation' height is different for the longitudinal and transverse components, which results in a systematic error in absolute heights in the reconstructed magnetic data cube. The extrapolations performed starting from actual AR photospheric magnetogram are free from this systematic error, while have other metrics comparable with those for extrapolations from the preprocessed magnetograms. This finding favors the use of extrapolations from the original photospheric magnetogram without preprocessing. Our tests further suggest that extrapolations from a force-free chromospheric boundary produce measurably better results, than those from the photospheric boundary.

## Time-dependent properties of sunspot groups

### I. Lifetime and asymmetric evolution

Emese **Forgács-Dajka**<sup>1</sup>, László Dobos<sup>2,3</sup> and István Ballai<sup>4</sup>  
A&A 653, A50 (2021)

<https://www.aanda.org/articles/aa/pdf/2021/09/aa40731-21.pdf>

<https://doi.org/10.1051/0004-6361/202140731>

**Aims.** In this paper, we aim to study the time dependence of sunspot group areas in a large sample composed of various databases spanning over 130 years, used state-of-the-art statistical methods.

**Methods.** For a carefully selected but unbiased sample, we use Bayesian modelling to fit the temporal evolution of the combined umbral and penumbral area of spot groups with a skew-normal function to determine the existence of any asymmetry in spot growth or decay. Our primary selection criteria guaranteed that only spot groups with a well-defined maximum area were taken into account. We also analysed the covariance of the resulting model parameters and their correlations with the physical parameters of the sunspots and the ongoing solar cycle.

**Results.** Our results show that the temporal evolution of well-observed sunspot groups that reach at least 50 millionths of a solar hemisphere at their maximum can be fitted surprisingly well with our model. Furthermore, we show significant asymmetry – described by a skew parameter of fitted curves – between the growing and decaying phases of analysed sunspot groups. In addition, we found a weak correlation between the values of skew parameters and the maximum area of sunspot groups and their hemispherical latitude.

## Neglect of Small Spots Remains an Explanation of the Difference Between SOON and RGO Spot Areas

Peter **Foukal**

2024 Res. Notes AAS 8 76

<https://iopscience.iop.org/article/10.3847/2515-5172/ad333a>

I point out that the objection of Györi et al. to my finding that neglect of small spots could explain much of the puzzling difference between Royal Greenwich Observatory and Solar Optical Observation Network spot areas is not valid because their analysis was limited to only 1974–76, when activity was low. The 40%–50% difference occurs only at higher activity levels.

## Magnetic fields of opposite polarity in sunspot penumbrae

M. **Franz**, M. Collados, C. Bethge, [R. Schlichenmaier](#), [J.M. Borrero](#), [W. Schmidt](#), [A. Lagg](#), [S. K. Solanki](#), [T. Berkefeld](#), [C. Kiess](#), [R. Rezaei](#), [D. Schmidt](#), [M. Sigwarth](#), [D. Soltau](#), [R. Volkmer](#), [O. von der Luhe](#), [T. Waldmann](#), [D. Orozco](#), [A. Pastor Yabar](#), [C. Denker](#), [H. Balthasar](#), [J. Staude](#), [A. Hofmann](#), [K. Strassmeier](#), [A. Feller](#), [H. Nicklas](#), [F. Kneer](#), [M. Sobotka](#)

A&A 2016

<http://arxiv.org/pdf/1608.00513v1.pdf>

**Context.** A significant part of the penumbral magnetic field returns below the surface in the very deep photosphere. For lines in the visible, a large fraction of this return field can only be detected indirectly by studying its imprints on strongly asymmetric and 3-lobe Stokes V profiles. Infrared lines probe a narrow layer in the very deep photosphere, providing the possibility to directly measure the orientation of magnetic fields close to the solar surface.

**Aims.** We study the topology of the penumbral magnetic field in the lower photosphere, focussing on regions where it returns below the surface.

**Methods.** We analyze 71 spectropolarimetric datasets from Hinode and from the GREGOR infrared spectrograph. We infer the quality and polarimetric accuracy of the infrared data after applying a number of reduction steps.

Techniques of spectral inversion and forward synthesis are used to test the detection algorithm. We compare the morphology and the fractional penumbral area covered by reversed polarity and 3-lobe Stokes V profiles for sunspots at disk center. We determine the amount of reversed polarity and 3-lobe Stokes V profiles in visible and infrared data of sunspots at various heliocentric angles. From the results, we compute center-to-limb variation curves, which are interpreted in the context of existing penumbral models.

**Results.** Observations in visible and near infrared spectral lines yield a significant difference in the penumbral area covered by magnetic fields of opposite polarity. In the infrared, the number of reversed polarity Stokes V profiles is

smaller by a factor of two than in the visible. In the case of 3-lobe Stokes V profiles the numbers differ up to an order of magnitude.

### **Three-Dimensional Electron Density from Tomographic Analysis of LASCO-C2 Images of the K-Corona Total Brightness**

Richard A. [Frazin](#) · Philippe Lamy · Antoine Llebaria · Alberto M. Vásquez

Solar Phys (2010) 265: 19–30

We present the first quantitative three-dimensional (3D) tomographic reconstructions of electron density from coronagraph measurements of the K-corona's total brightness ( $B$ ) made by LASCO-C2 on SOHO. This is possible because new calibrations of the LASCO-C2 images in both polarized brightness ( $pB$ ) and  $B$  have now been made for the entire mission. The  $B$  and  $pB$  reconstructions are compared, and the differences are explained in terms of line of sight weighting functions in Thomson scattering. We conclude that the LASCO-C2  $B$  archive, which is vastly larger than the  $pB$  archive, will be a very valuable resource for determining the 3D electron density throughout the SOHO mission which started taking data in 1996.

### **QUANTITATIVE, THREE-DIMENSIONAL ANALYSIS OF THE GLOBAL CORONA WITH MULTI-SPACECRAFT DIFFERENTIAL EMISSION MEASURE TOMOGRAPHY**

[Richard A. Frazin](#)<sup>1</sup>, [Alberto M. Vásquez](#)<sup>2</sup> and [Farzad Kamalabadi](#)<sup>3</sup>

ApJ 701 547-560, 2009 doi: [10.1088/0004-637X/701/1/547](https://doi.org/10.1088/0004-637X/701/1/547)

A previous paper (Frazin et al. 2005b) introduced the concept of differential emission measure tomography (DEMT), which is a three-dimensional (3D) extension of the classical differential emission measure technique for determining the distribution of temperatures in a volume of plasma. The information for the reconstruction in the three spatial dimensions is provided by solar rotation and/or multi-spacecraft views. This paper describes, quantitatively, the procedure for implementing DEMT with data from NASA's STEREO/EUVI instrument, including the radiometry, line-of-sight geometry, and image preparation steps. An example of a quantitative, multiband, 3D reconstruction and local differential emission measure curves are given, and it is demonstrated that, when applicable, DEMT is a simple 3D analysis tool that obviates the need for structure-specific modeling.

### **Three-Year Global Survey of Coronal Null Points from Potential-Field-Surface (PFSS) Modeling and Solar Dynamics Observatory (SDO) Observations**

Michael [Freed](#), Dana Longcope, David McKenzie

Solar Physics, February 2015, Volume 290, Issue 2, pp 467-490

<http://arxiv.org/pdf/1410.4493v1.pdf>

This article compiles and examines a comprehensive coronal magnetic-null-point survey created by potential-field-source-surface (PFSS) modeling and Solar Dynamics Observatory/Atmospheric Imaging Assembly (SDO/AIA) observations. The locations of 582 potential magnetic null points in the corona were predicted from the PFSS model between Carrington Rotations (CR) 2098 (June 2010) and 2139 (July 2013). These locations were manually inspected, using contrast-enhanced SDO/AIA images in 171 angstroms at the east and west solar limb, for structures associated with nulls. A Kolmogorov--Smirnov (K--S) test showed a statistically significant difference between observed and predicted latitudinal distributions of null points. This finding is explored further to show that the observability of null points could be affected by the Sun's asymmetric hemisphere activity. Additional K--S tests show no effect on observability related to eigenvalues associated with the fan and spine structure surrounding null points or to the orientation of spine. We find that approximately 31% of nulls obtained from the PFSS model were observed in SDO/AIA images at one of the solar limbs. An observed null on the east solar limb had a 51.6% chance of being observed on the west solar limb. Predicted null points going back to CR 1893 (March 1995) were also used for comparing radial and latitudinal distributions of nulls to previous work and to test for correlation of solar activity to the number of predicted nulls. 2012-05-06, 2012-05-07, 2010-08-29, 2012-01-20, 2012-09-06, 2012-09-16, 2013-01-31, 2013-06-08, 2013-06-23, 2013-02-27. 2011-04-10, 2011-11-30, 2011-11-07

[Table](#)

### **First Observation of Chromospheric Waves in a Sunspot by DKIST/ViSP: The Anatomy of an Umbral Flash**

[Ryan J. French](#), [Thomas J. Bogdan](#), [Roberto Casini](#), [Alfred G. de Wijn](#), [Philip G. Judge](#)

ApJL 945 L27 2023

<https://arxiv.org/pdf/2303.06105.pdf>

<https://iopscience.iop.org/article/10.3847/2041-8213/acb8b5/pdf>

The Visible Spectro-Polarimeter (ViSP) of the NSF Daniel K. Inouye Solar Telescope (DKIST) collected its Science Verification data on **May 7-8, 2021**. The instrument observed multiple layers of a sunspot atmosphere simultaneously, in passbands of Ca-II 397 nm (H-line), Fe-I 630 nm, and Ca-II 854 nm, scanning the region with a spatial sampling of 0.041" and average temporal cadence of 7.76 seconds, for a 38.8 minute duration. The slit moves southward across the plane-of-the-sky at 3.83 km/s. The spectropolarimetric scans exhibit prominent oscillatory 'ridge' structures which lie nearly perpendicular to the direction of slit motion (north to south). These ridges are visible in maps of line intensity, central wavelength, line width, and both linear and circular polarizations. Contemporaneous Atmospheric Imaging Assembly observations indicate these ridges are purely temporal in character and likely attributed to the familiar chromospheric 3-minute umbral oscillations. We observe in detail a steady umbral flash near the center of the sunspot umbra. Although bad seeing limited the spatial resolution, the unique high signal-to-noise enable us to estimate the shock Mach numbers ( $= 2$ ), propagation speeds ( $= 9$  km/s), and their impact on longitudinal magnetic field ( $\Delta B = 50$  G), gas pressure, and temperature ( $\Delta T/T = 0.1$ ) of the subshocks over 30 seconds. We also find evidence for rarefaction waves situated between neighboring wave-train shocks. The Ca-II 854 nm line width is steady throughout the umbral flash except for a sharp 1.5 km/s dip immediately before, and comparable spike immediately after, the passage of the shock front. This zig-zag in line width is centered on the subshock and extends over 0.4".

### **Estimating the Open Solar Flux from In-Situ Measurements**

[Anna Marie Frost](#), [Mathew Owens](#), [Allan Macneil](#) & [Mike Lockwood](#)

[Solar Physics](#) volume 297, Article number: 82 (2022)

<https://link.springer.com/content/pdf/10.1007/s11207-022-02004-6.pdf>

A fraction of the magnetic flux threading the solar photosphere extends to sufficient heliocentric distances that it is dragged out by the solar wind. Understanding this open solar flux (OSF) is central to space weather, as the OSF forms the heliosphere, magnetically connects the Sun to the planets, and dominates the motion of energetic particles. Quantification of OSF is also a key means of verifying global coronal models. However, OSF estimates derived from extrapolating the magnetic field from photospheric observations are consistently smaller than those based on heliospheric magnetic field (HMF) measurements, by around a factor two. It is therefore important to understand the uncertainties in estimating OSF from in-situ HMF measurements. This requires both an assumption of latitudinal invariance in the radial component of the HMF in the heliosphere, and that structures without an immediate connection to the Sun, such as local magnetic field inversions (or 'switchbacks'), can be correctly accounted for. In this study, we investigate the second assumption. Following an established methodology, we use in-situ electron and magnetic data to determine the global topology of the HMF and correct for inversions that would otherwise lead to an overestimation of the OSF. The OSF estimation is applied to the interval 1994 – 2021 and combines measurements from the Wind and ACE spacecraft. This extends the time range over which this methodology has previously been applied from 13 years (1998 – 2011) to 27 years. We find that inversions cannot fully explain the discrepancy between heliospheric and photospheric OSF estimations, with the best heliospheric estimate of OSF still, on average, a factor 1.6 higher than the values extrapolated from photospheric observations.

### **Inter-Correlation Between Sunspot Oscillations and Their Internal Structures**

[Libo Fu](#), [Zizhan Zhu](#), [Ding Yuan](#), [Jiaoyang Wang](#), [Song Feng](#), [Sergey Anfinogentov](#)

Research in Astronomy and Astrophysics 2022

<https://arxiv.org/pdf/2209.05982.pdf>

Three- and five-minute oscillations are commonly found in any sunspot. As they are modulated by the internal thermal and magnetic structures of a sunspot, therefore, they could be used as an effective tool for sunspot seismology. In this paper, we investigate the properties of oscillations in sunspot groups with varying size and magnetic field, and aim to establish the relationships between sunspot oscillations and its internal structure comparatively. We selected three groups of unipolar sunspot with approximately axial-symmetric magnetic field and calculated their Fourier spectra based on the Ultraviolet(UV)/Extreme ultraviolet(EUV) emission intensity variations recorded by the Solar Dynamics Observatory/Atmospheric Imaging Assembly (SDO/AIA). We found that the distribution of three minute oscillation is defined by the joint effect of diverging magnetic field and the stratification of sunspot atmosphere. Its distribution could be modified by any invading magnetic structures in the umbra. Whereas the five minute oscillations are more prominent in small spots, it implies that five minute oscillation is very closely connected with umbral dynamics. **2011-10-10**

**Table 1:** Metrics of selected sunspots 2010-2014

### **The Counter-kink Rotation of a Non-Hale Active Region**

M.C. López [Fuentes](#), P. Démoulin, C.H. Mandrini, L. van Driel-Gesztelyi

ApJ 2014

<http://arxiv.org/pdf/1412.1456v1.pdf>

We describe the long-term evolution of a bipolar non-Hale active region which was observed from **October, 1995, to January, 1996**. Along these four solar rotations the sunspots and subsequent flux concentrations, during the decay phase of the region, were observed to move in such a way that by December their orientation conformed to the Hale-Nicholson polarity law. The sigmoidal shape of the observed soft X-ray coronal loops allows us to determine the sense of the twist in the magnetic configuration. This sense is confirmed by extrapolating the observed photospheric magnetic field, using a linear force-free approach, and comparing the shape of computed field lines to the observed coronal loops. This sense of twist agrees with that of the dominant helicity in the solar hemisphere where the region lies, as well as with the evolution observed in the longitudinal magnetogram during the first rotation. At first sight the relative motions of the spots may be miss-interpreted as the rising of an  $\Omega$ -loop deformed by a kink-instability, but we deduce from the sense of their relative displacements a handedness for the flux-tube axis (writhe) which is opposite to that of the twist in the coronal loops and, therefore, to what is expected for a kink-unstable flux-tube. After excluding the kink instability, we interpret our observations in terms of a magnetic flux-tube deformed by external motions while rising through the convective zone. We compare our results with those of other related studies and we discuss, in particular, whether the kink instability is relevant to explain the peculiar evolution of some active regions.

### **A comparison of preprocessing methods for solar force-free magnetic field extrapolation**

M. **Fuhrmann**<sup>1</sup>, N. Seehafer<sup>1</sup>, G. Valori<sup>2</sup> and T. Wiegelmann<sup>3</sup>

A&A 526, A70 (2011)

**Context.** Extrapolations of solar photospheric vector magnetograms into three-dimensional magnetic fields in the chromosphere and corona are usually done under the assumption that the fields are force-free. This condition is violated in the photosphere itself and a thin layer in the lower atmosphere above. The field calculations can be improved by preprocessing the photospheric magnetograms. The intention here is to remove a non-force-free component from the data.

**Aims.** We compare two preprocessing methods presently in use, namely the methods of Wiegelmann et al. (2006, Sol. Phys., 233, 215) and Fuhrmann et al. (2007, A&A, 476, 349).

**Methods.** The two preprocessing methods were applied to a vector magnetogram of the recently observed active region NOAA AR 10 953. We examine the changes in the magnetogram effected by the two preprocessing algorithms. Furthermore, the original magnetogram and the two preprocessed magnetograms were each used as input data for nonlinear force-free field extrapolations by means of two different methods, and we analyze the resulting fields.

**Results.** Both preprocessing methods managed to significantly decrease the magnetic forces and magnetic torques that act through the magnetogram area and that can cause incompatibilities with the assumption of force-freeness in the solution domain. The force and torque decrease is stronger for the Fuhrmann et al. method. Both methods also reduced the amount of small-scale irregularities in the observed photospheric field, which can sharply worsen the quality of the solutions. For the chosen parameter set, the Wiegelmann et al. method led to greater changes in strong-field areas, leaving weak-field areas mostly unchanged, and thus providing an approximation of the magnetic field vector in the chromosphere, while the Fuhrmann et al. method weakly changed the whole magnetogram, thereby better preserving patterns present in the original magnetogram. Both preprocessing methods raised the magnetic energy content of the extrapolated fields to values above the minimum energy, corresponding to the potential field. Also, the fields calculated from the preprocessed magnetograms fulfill the solenoidal condition better than those calculated without preprocessing.

### **Relationship Between Solar Wind Speed and Coronal Magnetic Field Properties**

Ken'ichi **Fujiki**, Munetoshi Tokumaru, Tomoya Iju, Kazuyuki Hakamada, Masayoshi Kojima

Solar Phys. 2015

<http://arxiv.org/pdf/1507.03301v1.pdf>

We have studied the relationship between the solar-wind speed [ $V$ ] and the coronal magnetic-field properties (a flux expansion factor [ $f$ ] and photospheric magnetic-field strength [ $BS$ ]) at all latitudes using data of interplanetary scintillation and solar magnetic field obtained for 24 years from 1986 to 2009. Using a cross-correlation analyses, we verified that  $V$  is inversely proportional to  $f$  and found that  $V$  tends to increase with  $BS$  if  $f$  is the same. As a consequence, we find that  $V$  has extremely good linear correlation with  $BS/f$ . However, this linear relation of  $V$  and  $BS/f$  cannot be used for predicting the solar-wind velocity without information on the solar-wind mass flux. We discuss why the inverse relation between  $V$  and  $f$  has been successfully used for solar-wind velocity prediction, even though it does not explicitly include the mass flux and magnetic-field strength, which are important physical parameters for solar-wind acceleration.

### **A SURVEY OF CORONAL CAVITY DENSITY PROFILES**

**J. Fuller**<sup>1,2</sup> and **S. E. Gibson**<sup>2</sup>

ApJ 700 1205-1215, 2009 doi: [10.1088/0004-637X/700/2/1205](https://doi.org/10.1088/0004-637X/700/2/1205)

Coronal cavities are common features of the solar corona that appear as darkened regions at the base of coronal helmet streamers in coronagraph images. Their darkened appearance indicates that they are regions of lowered density embedded within the comparatively higher density helmet streamer. Despite interfering projection effects of the surrounding helmet streamer (which we refer to as the cavity rim), Fuller et al. have shown that under certain conditions it is possible to use a Van de Hulst inversion of white-light polarized brightness ( $pB$ ) data to calculate the electron density of both the cavity and cavity rim plasma. In this article, we apply minor modifications to the methods of Fuller et al. in order to improve the accuracy and versatility of the inversion process, and use the new methods to calculate density profiles for both the cavity and cavity rim in 24 cavity systems. We also examine trends in cavity morphology and how departures from the model geometry affect our density calculations. The density calculations reveal that in all 24 cases the cavity plasma has a flatter density profile than the plasma of the cavity rim, meaning that the cavity has a larger density depletion at low altitudes than it does at high altitudes. We find that

the mean cavity density is over four times greater than that of a coronal hole at an altitude of  $1.2 R_{\odot}$  and that every cavity in the sample is over twice as dense as a coronal hole at this altitude. Furthermore, we find that different

cavity systems near solar maximum span a greater range in density at  $1.2 R_{\odot}$  than do cavity systems near solar minimum, with a slight trend toward higher densities for systems nearer to solar maximum. Finally, we found no significant correlation of cavity density properties with cavity height—indeed, cavities show remarkably similar density depletions—except for the two smallest cavities that show significantly greater depletion.

### **Soonspot: Software to Determine Areas and Sunspot Positions**

P. **Galaviz**, V. M. S. Carrasco, F. Sánchez-Bajo, M. C. Gallego, J. M. Vaquero

*Solar Physics* February 2020, 295:17

<https://doi.org/10.1007/s11207-020-1587-3>

A new software (Soonspot) for the determination of the heliographic coordinates and areas of sunspots from solar images is presented. This program is very user-friendly and the accuracy of its results has been checked by using solar images provided by the Debrecen Photoheliographic Data (DPD). Due to its applicability in the studies of historical solar observations, the program has been used to analyze the solar drawings carried out by Hevelius in the 17th century.

### **Generation of Magnetic Structures on the Solar Photosphere**

R. T. **Gangadhara**<sup>1</sup>, V. Krishan<sup>1</sup>, A. K. Bhowmick<sup>2</sup>, and S. M. Chitre

2014 ApJ 788 135

The lower solar atmosphere is a partially ionized plasma consisting of electrons, ions, and neutral atoms. In this, which is essentially a three-fluid system, the Hall effect arises from the treatment of the electrons and ions as two separate fluids and the ambipolar diffusion arises from the inclusion of neutrals as the third fluid. The Hall effect and ambipolar diffusion have been shown to be operational in a region beginning from near the photosphere up to the chromosphere. In a partially ionized plasma, the magnetic induction is subjected to ambipolar diffusion and the Hall drift in addition to the usual resistive dissipation. These nonlinear effects create sharp magnetic structures which then submit themselves to various relaxation mechanisms. A first-principles derivation of these effects in a three-fluid system and an analytic solution to the magnetic induction equation in a stationary state are presented, which in the general case includes the Hall effect, ambipolar diffusion, and ohmic dissipation. The temporal evolution of the magnetic field is then investigated under the combined as well as the individual effects of the Hall drift and ambipolar diffusion to demonstrate the formation of steep magnetic structures and the resultant current sheet formation. These structures have just the right features for the release of magnetic energy into the solar atmosphere.

### **Measurements of the solar coronal magnetic field based on coronal seismology with propagating Alfvénic waves: forward modeling**

**Yuhang Gao**, **Hui Tian**, **Tom Van Doorselaere**, **Zihao Yang**, **Mingzhe Guo**, **Konstantinos Karamelas**

Research in Astron. Astrophys. 2024

<https://arxiv.org/pdf/2411.08310>

Recent observations have demonstrated the capability of mapping the solar coronal magnetic field using the technique of coronal seismology based on the ubiquitous propagating Alfvénic/kink waves through imaging spectroscopy. We established a magnetohydrodynamic (MHD) model of a gravitationally stratified open magnetic flux tube, exciting kink waves propagating upwards along the tube. Forward modeling was performed to synthesize the Fe XIII 1074.7 and 1079.8 nm spectral line profiles, which were then used to determine the wave phase speed, plasma density, and magnetic field with seismology method. A comparison between the seismologically inferred results and the corresponding input values verifies the reliability of the seismology method. In addition, we also identified some factors that could lead to errors during magnetic field measurements. Our results may serve as a

valuable reference for current and future coronal magnetic field measurements based on observations of propagating kink waves.

## **Generating Space-based SDO/HMI-like Solar Magnetograms from Ground-based H $\alpha$ Images by Deep Learning**

Fei Gao<sup>6,1,2</sup>, Tie Liu<sup>6,3,4</sup>, WenQing Sun<sup>1,2</sup>, and Long Xu<sup>1,5</sup>

2023 ApJS 266 19

<https://iopscience.iop.org/article/10.3847/1538-4365/acbb9/pdf>

Recently, the method of estimating magnetic field through monochromatic images by deep learning has been proposed, demonstrating good morphological similarity but somewhat poor magnetic polarity consistency relative to real observation. In this paper, we propose to estimate magnetic field from H $\alpha$  images by using a conditional generative adversarial network (cGAN) as the basic framework. The H $\alpha$  images from the Global Oscillation Network Group are used as the inputs and the line-of-sight magnetograms of the Helioseismic Magnetic Imager (HMI) are used as the targets. First, we train a cGAN model (Model A) with shuffling training data. However, the estimated magnetic polarities are not very consistent with real observations. Second, to improve the accuracy of estimated magnetic polarities, we train a cGAN model (Model B) with the chronological H $\alpha$  and HMI images, which can implicitly exploit the magnetic polarity constraint of time-series observation to generate more accurate magnetic polarities. We compare the generated magnetograms with the target HMI magnetograms to evaluate the two models. It can be observed that Model B has better magnetic polarity consistency than Model A. To quantitatively measure this consistency, we propose a new metric called pixel-to-pixel polarity accuracy (PPA). With respect to PPA, Model B is superior to Model A. This work gives us an insight that the time-series constraint can be implicitly exploited through organizing training data chronologically, and this conclusion also can be applied to other similar tasks related to time-series data.

## **Variations and Regularities in the Hemispheric Distributions in Sunspot Groups of Various Classes**

Peng-Xin Gao

*Solar Physics* May 2018, 293:79

<http://sci-hub.tw/http://link.springer.com/10.1007/s11207-018-1298-1>

The present study investigates the variations and regularities in the distributions in sunspot groups (SGs) of various classes in the northern and southern hemispheres from Solar Cycles (SCs) 12 to 23. Here, we use the separation scheme that was introduced by Gao, Li, and Li (*Solar Phys.* 292, 124, 2017), which is based on A/UA/U (A is the corrected area of the SG, and U is the corrected umbral area of the SG), in order to separate SGs into simple SGs ( $A/U \leq 4.5$ ,  $U \leq 4.5$ ) and complex SGs ( $A/U > 6.2$ ,  $U > 6.2$ ). The time series of Greenwich photoheliographic results from 1875 to 1976 (corresponding to complete SCs 12 – 20) and Debrecen photoheliographic data during the period 1974 – 2015 (corresponding to complete SCs 21 – 23) are used to show the distributions of simple and complex SGs in the northern and southern hemispheres. The main results we obtain are reported as follows: i) the larger of the maximum annual simple SG numbers in the two hemispheres and the larger of the maximum annual complex SG numbers in the two hemispheres occur in different hemispheres during SCs 12, 14, 18, and 19; ii) the relative changing trends of two curves – cumulative SG numbers in the northern and southern hemispheres – for simple SGs are different from those for complex SGs during SCs 12, 14, 18, and 21; and iii) there are discrepancies between the dominant hemispheres of simple and complex SGs for SCs 12, 14, 18, and 21.

## **A Quantity Characterising Variation of Observed Magnetic Twist of Solar Active Regions**

Yu Gao

*Research in Astron. Astrophys* 2017

<https://arxiv.org/pdf/1712.07833.pdf>

An alternative parameter RJz is introduced as the ratio of one of two kinds of opposite-sign current to the total current and investigate the relationship between the quantity and the hemispheric sign rule of helicity (HSR) that is established by a series of previous statistical studies. The classification of current in each hemisphere is according to the following rule: If the product of the current and the corresponding longitudinal field component contributes a consistent sign with reference to the HSR, it is called “HSR-compliant” current, or else it is called “HSR-noncompliant” current. Firstly, the consistence between the butterfly diagram of the RJz and the current helicity was obtained in a statistical study. Active regions with RJz smaller than 0.5 tend to obey the HSR whereas those with RJz greater than 0.5 tend to disobey the HSR. The “HSR-compliant” current systems have 60% probability of realization compared to 40% of “HSR-noncompliant” current systems. Overall, the HSR is violated for active regions in which the “HSR-noncompliant” current is greater than the “HSR-compliant” current. Secondly, the RJz parameter was subsequently used to study the evolution of current systems in the case analyses of flare-productive active regions NOAA AR 11158 and 11283. It is found that there were “RJz -quasi-stationary” phase that is relatively flare quiescent and “RJz -dynamic” phase that is covered by the occurrence of large flares. **13-17 Feb 2011, 3-8 Sept 2011**

## Imbalance of magnetic field observed in vector magnetograms

Yu Gao

Advances in Space Research, Volume 48, Issue 6, 15 September 2011, Pages 1026-1031

The systematic investigation of the three components of the magnetic field is made on 6629 vector magnetograms obtained with the Solar Magnetic Field Telescope at Huairou Solar Observing Station over 18 years 1988–2005. The sign distribution of these values has been analyzed over the solar hemispheres and the solar activity cycle as follows: (1) In the 22nd cycle, Bx in the northern (southern) hemisphere has been 59% (56%) positive (negative); By in the northern (southern) hemisphere has been 66% (65%) negative (negative); while Bz in the northern (southern) hemisphere has been 72% (71%) negative (positive).

(2) In the 23rd cycle, Bx in the southern (northern) hemisphere has been 73% (71%) positive (negative); By in the both northern and southern hemisphere has been 72% (72%) positive (positive); Bz in the southern (northern) hemisphere has been 70% (71%) negative (positive).

The explanation needs further investigation.

## Magnetic properties of the umbral boundary during sunspot decay. Comparative study of multiple datasets

[M. García-Rivas](#), [J. Jurčák](#), [N. Bello González](#)

A&A 2024

<https://arxiv.org/pdf/2406.15272>

The magnetic properties of the umbra-penumbra (UP) boundary of sunspots and the boundary of pores at various evolutionary stages have been characterised using datasets from different instruments. We aim to study the differences between the intensity and vector magnetic field properties derived from Hinode/SP and SDO/HMI observations of a decaying sunspot. We analysed the sunspot embedded in AR 12797 during six days in 30 SP/Hinode scans and 704 HMI/SDO for both regular maps and HMI\_dcon. We studied the correlation of the magnetic properties and continuum intensity in the datasets within the spot, and at the UP boundary. We examined the decaying process using the full temporal resolution of the HMI\_dcon maps. We find a good correspondence between the magnetic properties in the SP and HMI\_dcon maps, but the continuum intensity of the spots in the SP maps is 0.04I<sub>qs</sub> brighter than in the HMI\_dcon maps. The influence of scattered light in the HMI maps makes it the least ideal dataset for studying the boundary of spots without a penumbra. The properties at the UP boundary evolve slowly during the sunspot decay stage, while the penumbra still provides some stability. In contrast, they respond more abruptly to areal changes in the naked-spot stage. During the sunspot decay, we find linear decay in the area and in the magnetic flux. Moreover, the umbra shows two characteristic decaying processes: a slow decay during the first three days, and a sudden fast decay during the final dissipation of the penumbra. We find indications of a 3.5h lag between the dissipation of the vertical fields in the umbral region and the photometric decay of the umbral area. The differences found in the continuum intensity and in the vertical component of the magnetic field, B<sub>ver</sub>, between the analysed datasets explain the discrepancies among the B<sub>ver</sub> values found at the boundaries of umbrae in previous studies. 20-26 Jan 2021

## Onset of penumbra formation

[M. García-Rivas](#), [J. Jurčák](#), [N. Bello González](#), [J.M. Borrero](#), [R. Schlichenmaier](#), [P. Lindner](#)

A&A 2024

<https://arxiv.org/pdf/2403.18455.pdf>

Context. Fully fledged penumbrae have been widely studied both observationally and theoretically. Yet the relatively fast process of penumbra formation has not been studied closely with high spatial resolution. Aims. We investigate the stages previous to and during the formation of penumbral filaments in a developing sunspot. Methods. We analysed Milne-Eddington inversions from spectro-polarimetric data of the leading sunspot of NOAA 11024 during the development of its penumbra. We focused on selected areas of this protospot in which segments of penumbra develop. Results. We find that few types of distinctive flow patterns develop at the protospot limb and centre sides previous to penumbra formation. The flow in the centre side is often characterised by a persistent (>20 min) inflow-outflow pattern extending radially over 4 arcsec at the direct periphery of the protospot umbra. This inflow-outflow system often correlates with elongated granules, as seen in continuum intensity maps, and is also coupled with magnetic bipolar patches at its edges, as seen in magnetograms. The field is close to horizontal between the bipolar patches, which is indicative of its possible loop configuration. All of these aspects are analogous to observations of magnetic flux emergence. In the protospot limb side, however, we observed a mostly regular pattern associated with small granules located near the protospot intensity boundary. Locally, an inflow develops adjacent to an existing penumbral segment, and this inflow is correlated with a single bright penumbral filament that is brighter than filaments containing the Evershed flow. All investigated areas at the centre and limb side eventually develop penumbral filaments with an actual Evershed flow that starts at the umbral boundary and grows outwards radially as the penumbral filaments become longer in time. 9 July 2009

## Magnetic properties on the boundary of an evolving pore

[M. García-Rivas](#), [J. Jurcak](#), [N. Bello González](#)

A&A 2021

<https://arxiv.org/pdf/2102.08459.pdf>

Context. Analyses of magnetic properties on umbrae boundaries have led to the Jurcak criterion, which states that umbra-penumbra boundaries in stable sunspots are equally defined by a constant value of the vertical magnetic field,  $B_{\text{ver\_crit}}$ , and by 0.5 continuum intensity of the quiet Sun,  $I_{\text{qs}}$ . Umbrae with vertical magnetic fields stronger than  $B_{\text{ver\_crit}}$  are stable, whereas umbrae with vertical magnetic fields weaker than  $B_{\text{ver\_crit}}$  are unstable and prone to vanishing. Aims. To investigate the existence of a  $B_{\text{ver\_crit}}$  on a pore boundary and its role in the evolution of the magnetic structure. Methods. We analysed SDO/HMI vector field maps corrected for scattered light with a temporal cadence of 12 minutes during a 28-hour period. An intensity threshold ( $I_{\text{c}} = 0.55 I_{\text{qs}}$ ) is used to define the pore boundary and temporal evolutions of the magnetic properties are studied there. Results. We observe well-defined stages in the pore evolution: (1) during the initial formation phase, total magnetic field strength ( $B$ ) and vertical magnetic field ( $B_{\text{ver}}$ ) increase to their maximum values of 1920 G and 1670 G, respectively; (2) then the pore reaches a stable phase; (3) in a second formation phase, the pore undergoes a rapid growth in size, along with a decrease in  $B$  and  $B_{\text{ver}}$  on its boundary. In the newly formed area of the pore,  $B_{\text{ver}}$  remains below 1665 G and  $B$  below 1921 G; (4) ultimately, pore decay starts. We find overall that pore areas with  $B_{\text{ver}} < 1665$  G, or equivalently  $B < 1921$  G, disintegrate faster than regions that fulfil this criteria. Conclusions. We find that the most stable regions of the pore, similarly to the case of umbral boundaries, are defined by a critical value of the vertical component of the magnetic field that is comparable to that found in stable sunspots. In this case study, the same pore areas can be equivalently well-defined by a critical value of the total magnetic field strength.

HMI Science Nuggets, #158, 2021 <http://hmi.stanford.edu/hminuggets/?p=3553>

## Determining the 3D Structure of the Corona Using Vertical Height Constraints on Observed Active Region Loops

G. Allen [Gary](#), Qiang Hu, Jong Kwan Lee, Markus J. Aschwanden

Solar Phys., Volume 289, Issue 10, pp 3703-3721, 2014

The corona associated with an active region is structured by high-temperature, magnetically dominated closed and open loops. The projected 2D geometry of these loops is captured in EUV filtergrams. In this study using SDO/AIA 171 Å filtergrams, we expand our previous method to derive the 3D structure of these loops, independent of heliostereoscopy. We employ an automated loop recognition scheme (Occult-2) and fit the extracted loops with 2D cubic Bézier splines. Utilizing SDO/HMI magnetograms, we extrapolate the magnetic field to obtain simple field models within a rectangular cuboid. Using these models, we minimize the misalignment angle with respect to Bézier control points to extend the splines to 3D (Gary, Hu, and Lee 2014). The derived Bézier control points give the 3D structure of the fitted loops. We demonstrate the process by deriving the position of 3D coronal loops in three active regions (AR 11117, AR 11158, and AR 11283). The numerical minimization process converges and produces 3D curves which are consistent with the height of the loop structures when the active region is seen on the limb. From this we conclude that the method can be important in both determining estimates of the 3D magnetic field structure and determining the best magnetic model among competing advanced magnetohydrodynamics or force-free magnetic-field computer simulations.

## Evaluation of a Selected Case of the Minimum Dissipative Rate Method for Non-Force-Free Solar Magnetic Field Extrapolation

G. Allen [Gary](#)

E-print, Apr 2009; Solar Phys., 257(2), Page: 271 – 286, 2009

The minimum dissipative rate (MDR) method for deriving a coronal non-force-free magnetic field solution is partially evaluated. These magnetic field solutions employ a combination of three linear (constant- $\alpha$ ) force-free-field solutions with one being a potential field (i.e.,  $\alpha=0$ ). We examine the particular case of the solutions where the other two  $\alpha$ 's are of equal magnitude but of opposite signs. This is motivated by studying the SOLIS vector magnetograms of AR 10987 which show a global  $\alpha$  value consistent with an  $\alpha=0$  value as evaluated by  $(\text{Curl } B)_z/B_z$  over the region. Typical of the current state of the observing technology, there is no definitive twist for input into the general MDR method. This suggests that the special  $\alpha$ -case, of two  $\alpha$ 's with equal magnitudes and opposite signs, is appropriate given the data. Only for an extensively twisted active region does a dominant, non-zero  $\alpha$  normally emerge from a distribution of local values. For a special set of conditions, we find: (i) The resulting magnetic field is a vertically inflated magnetic field resulting from the electric currents being parallel to the photosphere, similar to the results of Gary and Alexander (1999). (ii) For  $\alpha \sim (\alpha_{\text{max}}/2)$ , the Lorentz force per unit volume normalized by the square of the magnetic field is on the order of  $1.4 \times 10^{-10} \text{ cm}^{-1}$ . The Lorentz force ( $L_F$ ) is a factor of ten higher than that of the magnetic force  $d(B^2/8\pi)/dz$ , a component of  $L_F$ . The



calculated photospheric electric current densities are an order smaller than the maximum observed in all active regions. Hence both the Lorentz force density and the generated electric current density seem to be physically consistent with possible solar dynamics. The results imply that the field could be inflated with an over pressure along the neutral line. (iii) However, the implementation of this or any other extrapolation method using the electric current density as a lower boundary condition must be done cautiously, with the current magnetography.

## **Magnetohydrostatic equilibrium. II. Three-dimensional multiple open magnetic flux tubes in the stratified solar atmosphere**

Frederick A. [Gent](#), Viktor Fedun, Rebertus Erd'elyi  
ApJ, 789 42, 2014

<http://arxiv.org/pdf/1405.0613v1.pdf>

A system of multiple open magnetic flux tubes spanning the solar photosphere and lower corona is modelled analytically, within a realistic stratified atmosphere subject to solar gravity. This extends results for a single magnetic flux tube in magnetohydrostatic equilibrium, described in Gent et al. (MNRAS, 435, 689, 2013). Self-similar magnetic flux tubes are combined to form magnetic structures, which are consistent with high-resolution observations. The observational evidence supports the existence of strands of open flux tubes and loops persisting in a relatively steady state. Self-similar magnetic flux tubes, for which an analytic solution to the plasma density and pressure distribution is possible, are combined. We calculate the appropriate balancing forces, applying to the equations of momentum and energy conservation to preserve equilibrium.

Multiplex flux tube configurations are observed to remain relatively stable for up to a day or more, and it is our aim to apply our model as the background condition for numerical studies of energy transport mechanisms from the solar surface to the corona. We apply magnetic field strength, plasma density, pressure and temperature distributions consistent with observational and theoretical estimates for the lower solar atmosphere. Although each flux tube is identical in construction apart from the location of the radial axis, combinations can be applied to generate a non-axisymmetric magnetic field with multiple non-uniform flux tubes. This is a considerable step forward in modelling the realistic magnetized three-dimensional equilibria of the solar atmosphere.

## **MAGNETIC ENERGY AND HELICITY BUDGETS IN THE ACTIVE-REGION SOLAR CORONA. II. NONLINEAR FORCE-FREE APPROXIMATION**

Manolis K. [Georgoulis](#)<sup>1,3</sup>, Kostas Tziotziou<sup>1</sup>, and Nour-Eddine Raouafi  
2012 ApJ 759 1

Expanding on an earlier work that relied on linear force-free (LFF) magnetic fields, we self-consistently derive the instantaneous free magnetic energy and relative magnetic helicity budgets of an unknown three-dimensional nonlinear force-free (NLFF) magnetic structure extending above a single known lower-boundary magnetic field vector. The proposed method does not rely on the detailed knowledge of the three-dimensional field configuration but is general enough to employ only a magnetic connectivity matrix on the lower boundary. The calculation yields a minimum free magnetic energy and a relative magnetic helicity consistent with this free magnetic energy. The method is directly applicable to photospheric or chromospheric vector magnetograms of solar active regions. Upon validation, it basically reproduces magnetic energies and helicities obtained by well known, but computationally more intensive and non-unique, methods relying on the extrapolated three-dimensional magnetic field vector. We apply the method to three active regions, calculating the photospheric connectivity matrices by means of simulated annealing, rather than a model-dependent NLFF extrapolation. For two of these regions we correct for the inherent LFF overestimation in free energy and relative helicity that is larger for larger, more eruptive, active regions. In the third region studied, our calculation can lead to a physical interpretation of observed eruptive manifestations. We conclude that the proposed method, including the proposed inference of the magnetic connectivity matrix, is practical enough to contribute to a physical interpretation of the dynamical evolution of solar active regions.

## **The Origin and Early Evolution of a Bipolar Magnetic Region in the Solar Photosphere**

A. V. [Getling](#)<sup>1</sup> and A. A. Buchnev  
2019 ApJ 871 224

Finding the formation mechanisms for bipolar configurations of a strong local magnetic field under control of the relatively weak global magnetic field of the Sun is a key problem of the physics of solar activity. This study is aimed at discriminating whether the magnetic field or fluid motion plays a primary, active role in this process. The very origin and early development stage of Active Region 12548 are investigated based on Solar Dynamics Observatory/Heliioseismic and Magnetic Imager observations of 2016 May 20–25. Full-vector magnetic and velocity fields are analyzed in parallel. The leading and trailing magnetic polarities are found to grow asymmetrically in terms of their amplitude, magnetic flux, and the time variation of these quantities. The leading-polarity magnetic element originates as a compact feature against the background of a distributed trailing-polarity field, with an already existing trailing-polarity magnetic element. No signs of strong horizontal magnetic fields are detected between the two magnetic poles. No predominant upflow between their future locations precedes the origin of this bipolar magnetic region (BMR); instead, upflows and downflows are mixed, with some prevalence of

downflows. Any signs of a large-scale horizontal divergent flow from the area where the BMR develops are missing; in contrast, a normal supergranulation and mesogranulation pattern is preserved. This scenario of early BMR evolution is in strong contradiction with the expectations based on the model of a rising  $\Omega$ -shaped loop of a flux tube of strong magnetic field, and an in situ mechanism of magnetic-field amplification and structuring should operate in this case.

### **How is a bipolar sunspot group conceived?**

[A. V. Getling](#), [A. A. Buchnev](#)

Solar Phys. **2018**

<https://arxiv.org/pdf/1805.06486.pdf>

The very conception and early development stage of AR 12548 are investigated based on SDO/HMI observations of **20--25 May 2016**. Full-vector magnetic and velocity fields are analysed in parallel. In the growing bipolar magnetic (BMR), the leading-polarity magnetic element nucleates as a compact feature against the background of a distributed trailing-polarity field, in which a germ of the trailing-polarity element is already present. Both magnetic elements give rise to a couple of pores, which then evolves into a bipolar sunspot group. The growth of the leading (negative) polarity sets in abruptly and occurs rapidly while the trailing (positive) polarity grows smoothly and more slowly. There is also similar dissymmetry between the time variations of the negative and positive magnetic fluxes through some area encompassing the BMR. No signs of strong horizontal magnetic fields are detected between the growing leading and trailing magnetic poles of the BMR. No predominant upflow between the future locations of the magnetic poles precedes the origin of the BMR; instead, upflows and downflows are mixed, with some prevalence of downflows. Any signs of a large-scale horizontal divergent flow from the area when the BMR develops are missing; in contrast, a regular supergranulation and mesogranulation pattern remains intact. The observed scenario of early BMR evolution is in strong contradiction with the expectations following from the model of rising  $\Omega$ -shaped loop of a flux tube of strong magnetic field.

### **Development of active regions: flows, magnetic-field patterns and bordering effect**

A. V. [Getling](#), R. Ishikawa, A. A. Buchnev

Solar Phys. Vol. 291, Issue 2 **2016**

<http://arxiv.org/pdf/1506.01848v1.pdf>

A qualitative analysis is given to the data on the full magnetic and velocity vector fields in a growing sunspot group, recorded nearly simultaneously with the Solar Optical Telescope on the Hinode satellite. Observations of a young bipolar subregion developing within AR 11313 were carried out on **9-10 October 2011**. Our aim was to form an idea about the consistency of the observed pattern with the well-known rising-tube model of the formation of bipolar active regions and sunspot groups. We find from our magnetograms that the distributions of the vertical [ $B_v$ ] and the horizontal [ $B_h$ ] component of the magnetic field over the area of the magnetic subregion are spatially well correlated; in contrast, the rise of a flux-tube loop would result in a qualitatively different pattern, with the maxima of the two magnetic-field components spatially separated: the vertical field would be the strongest where either spot emerges, while the maximum horizontal-field strengths would be reached in between them. A specific feature, which we call the bordering effect, is revealed: some local extrema of  $B_v$  are bordered with areas of locally enhanced  $B_h$ . This effect suggests a fountainlike spatial structure of the magnetic field near the  $B_v$  extrema, which is also hardly compatible with the emergence of a flux-tube loop. The vertical-velocity field in the area of the developing active subregion does not exhibit any upflow on the scale of the whole subregion, which should be related to the rising-tube process. Thus, our observational data can hardly be interpreted in the framework of the rising-tube model.

### **Doubts about the crucial role of the rising-tube mechanism in the formation of sunspot groups**

A.V. [Getling](#), , R. Ishikawab, , A.A. Buchnev

Advances in Space Research, Volume 55, Issue 3, 1 February **2015**, Pages 862–870

<http://www.sciencedirect.com/science/article/pii/S0273117714004803>

### **The Complex Nature of Magnetic Element Transport in the Quiet Sun: The Multiscaling Character**

Fabio [Giannattasio](#)<sup>1</sup> and Giuseppe Consolini<sup>2</sup>

**2021** ApJ 908 142

<https://doi.org/10.3847/1538-4357/abd804>

In recent studies the dynamic properties of small-scale magnetic fields (magnetic elements [MEs]) in the quiet Sun were used to investigate peculiar features of turbulent convection and get

insights on the characteristic spatial and temporal scales of evolution of magnetic fields, from granular to supergranular. The aim of this work is to extend previous studies and show that the displacement of MEs is compatible with a multiscaling behavior consistent with a Lévy motion. We tracked over 120,000 MEs in an unprecedented and uninterrupted set of high-resolution magnetograms acquired by the Hinode mission and targeted at quiet-Sun regions in the disk center, and we applied the multifractal diffusion entropy analysis to investigate the multiscaling character of ME transport in the quiet Sun. We found that the displacement of MEs in the quiet Sun exhibits a complex multiscaling behavior that cannot be described by a unique scaling law, as scaling exponents change with the scale considered. This result adds important physical constraints on turbulent convection and diffusion of MEs in the quiet Sun that future models need to account for.

### **Occurrence and persistence of magnetic elements in the quiet Sun**

F. [Giannattasio](#)<sup>1</sup>, F. Berrilli<sup>2</sup>, G. Consolini<sup>1</sup>, D. Del Moro<sup>2</sup>, M. Gošić<sup>3</sup> and L. Bellot Rubio<sup>3</sup>

A&A 611, A56 (2018)

<http://sci-hub.tw/https://www.aanda.org/articles/aa/abs/2018/03/aa30583-17/aa30583-17.html>

Context. Turbulent convection efficiently transports energy up to the solar photosphere, but its multi-scale nature and dynamic properties are still not fully understood. Several works in the literature have investigated the emergence of patterns of convective and magnetic nature in the quiet Sun at spatial and temporal scales from granular to global.

Aims. To shed light on the scales of organisation at which turbulent convection operates, and its relationship with the magnetic flux therein, we studied characteristic spatial and temporal scales of magnetic features in the quiet Sun. Methods. Thanks to an unprecedented data set entirely enclosing a supergranule, occurrence and persistence analysis of magnetogram time series were used to detect spatial and long-lived temporal correlations in the quiet Sun and to investigate their nature.

Results. A relation between occurrence and persistence representative for the quiet Sun was found. In particular, highly recurrent and persistent patterns were detected especially in the boundary of the supergranular cell. These are due to moving magnetic elements undergoing motion that behaves like a random walk together with longer decorrelations (~2 h) with respect to regions inside the supergranule. In the vertices of the supergranular cell the maximum observed occurrence is not associated with the maximum persistence, suggesting that there are different dynamic regimes affecting the magnetic elements. **2 November 2010**

### **Pair separation of magnetic elements in the quiet Sun**

F. [Giannattasio](#)<sup>1</sup>, F. Berrilli<sup>1</sup>, L. Biferale<sup>1</sup>, D. Del Moro<sup>1</sup>, M. Sbragaglia<sup>1</sup>, L. Bellot Rubio<sup>2</sup>, M. Gošić<sup>2</sup> and D. Orozco Suárez<sup>3</sup>

A&A 569, A121 (2014)

The dynamic properties of the quiet Sun photosphere can be investigated by analyzing the pair dispersion of small-scale magnetic fields (i.e., magnetic elements). By using 25 h-long Hinode magnetograms at high spatial resolution ( $\sim 0.1''$ ), we tracked 68 490 magnetic element pairs within a supergranular cell near the disk center. The computed pair separation spectrum, calculated on the whole set of particle pairs independently of their initial separation, points out what is known as a super-diffusive regime with spectral index  $\gamma = 1.55 \pm 0.05$ , in agreement with the most recent literature, but extended to unprecedented spatial and temporal scales (from granular to supergranular). Furthermore, for the first time, we investigated here the spectrum of the mean square displacement of pairs of magnetic elements, depending on their initial separation  $r_0$ . We found that there is a typical initial distance above (below) which the pair separation is faster (slower) than the average. A possible physical interpretation of such a typical spatial scale is also provided.

### **Diffusion of Magnetic Elements in a Supergranular Cell**

F. [Giannattasio](#)<sup>1</sup>, M. Stangalini<sup>2</sup>, F. Berrilli<sup>1</sup>, D. Del Moro<sup>1</sup>, and L. Bellot Rubio

2014 ApJ 788 137

Small scale magnetic fields (magnetic elements) are ubiquitous in the solar photosphere. Their interaction can provide energy to the upper atmospheric layers, and contribute to heat the solar corona. In this work, the dynamic properties of magnetic elements in the quiet Sun are investigated. The high number of magnetic elements detected in a supergranular cell allowed us to compute their displacement spectrum  $(\Delta r)^2 \tau^\gamma$  (with  $\gamma > 0$ , and  $\tau$  the time since the first detection), separating the contribution of the network (NW) and the internetwork (IN) regions. In particular, we found  $\gamma = 1.27 \pm 0.05$  and  $\gamma = 1.08 \pm 0.11$  in NW (at smaller and larger scales, respectively), and  $\gamma = 1.44 \pm 0.08$  in

IN. These results are discussed in light of the literature on the topic, as well as the implications for the build-up of the magnetic network.

### **DIFFUSION OF SOLAR MAGNETIC ELEMENTS UP TO SUPERGRANULAR SPATIAL AND TEMPORAL SCALES**

F. [Giannattasio](#)<sup>1</sup>, D. Del Moro<sup>1</sup>, F. Berrilli<sup>1</sup>, L. Bellot Rubio<sup>2</sup>, M. Gos̃ić<sup>2</sup>, and D. Orozco Suárez  
2013 ApJ 770 L36

The study of spatial and temporal scales on which small magnetic structures (magnetic elements) are organized in the quiet Sun may be approached by determining how they are transported on the solar photosphere by convective motions. The process involved is diffusion. Taking advantage of Hinode high spatial resolution magnetograms of a quiet-Sun region at the disk center, we tracked 20,145 magnetic elements. The large field of view (~50 Mm) and the long duration of the observations (over 25 hr without interruption at a cadence of 90 s) allowed us to investigate the turbulent flows at unprecedented large spatial and temporal scales. In the field of view an entire supergranule is clearly recognizable. The magnetic element displacement spectrum shows a double-regime behavior: superdiffusive ( $\gamma = 1.34 \pm 0.02$ ) up to granular spatial scales (~1500 km) and slightly superdiffusive ( $\gamma = 1.20 \pm 0.05$ ) up to supergranular scales.

### **Simulating the Formation of a Sigmoidal Flux Rope in AR10977 from SOHO/MDI Magnetograms**

G. P. S. [Gibb](#)<sup>1</sup>, D. H. Mackay<sup>1</sup>, L. M. Green<sup>2</sup>, and K. A. Meyer  
2014 ApJ 782 71

The modeling technique of Mackay et al. is applied to simulate the coronal magnetic field of NOAA active region AR10977 over a seven day period (**2007 December 2-10**). The simulation is driven with a sequence of line-of-sight component magnetograms from SOHO/MDI and evolves the coronal magnetic field through a continuous series of non-linear force-free states. Upon comparison with Hinode/XRT observations, results show that the simulation reproduces many features of the active region's evolution. In particular, it describes the formation of a flux rope across the polarity inversion line during flux cancellation. The flux rope forms at the same location as an observed X-ray sigmoid. After five days of evolution, the free magnetic energy contained within the flux rope was found to be  $3.9 \times 10^{30}$  erg. This value is more than sufficient to account for the B1.4 GOES flare observed from the active region on **2007 December 7**. At the time of the observed eruption, the flux rope was found to contain 20% of the active region flux. We conclude that the modeling technique proposed in Mackay et al.—which directly uses observed magnetograms to energize the coronal field—is a viable method to simulate the evolution of the coronal magnetic field.

### **Untangling the global coronal magnetic field with multiwavelength observations**

[S. E. Gibson](#), [A. Malanushenko](#), [G. de Toma](#), [S. Tomczyk](#), [K. Reeves](#), [H. Tian](#), [Z. Yang](#), [B. Chen](#), [G. Fleishman](#), [D. Gary](#), [G. Nita](#), [V. M. Pilet](#), [S. White](#), [U. Bąk-Stęślicka](#), [K. Dalmasse](#), [T. Kucera](#), [L. A. Rachmeler](#), [N. E. Raouafi](#), [J. Zhao](#)

Helio2050 white paper      **2020**

<https://arxiv.org/ftp/arxiv/papers/2012/2012.09992.pdf>

Magnetism defines the complex and dynamic solar corona. Coronal mass ejections (CMEs) are thought to be caused by stresses, twists, and tangles in coronal magnetic fields that build up energy and ultimately erupt, hurling plasma into interplanetary space. Even the ever-present solar wind possesses a three-dimensional morphology shaped by the global coronal magnetic field, forming geoeffective corotating interaction regions. CME evolution and the structure of the solar wind depend intimately on the coronal magnetic field, so comprehensive observations of the global magnetothermal atmosphere are crucial both for scientific progress and space weather predictions. Although some advances have been made in measuring coronal magnetic fields locally, synoptic measurements of the global coronal magnetic field are not yet available.

We conclude that a key goal for 2050 should be comprehensive, ongoing 3D synoptic maps of the global coronal magnetic field. This will require the construction of new telescopes, ground and space-based, to obtain complementary, multiwavelength observations sensitive to the coronal magnetic field. It will also require development of inversion frameworks capable of incorporating multi-wavelength data, and forward analysis tools and simulation testbeds to prioritize and establish observational requirements on the proposed telescopes.

### **Beyond sunspots: Studies using the McIntosh Archive of global solar magnetic field patterns**

Sarah E. [Gibson](#), [David Webb](#), [Ian M. Hewins](#), [Robert H. McFadden](#), [Barbara A. Emery](#), [William Denig](#), [Patrick S. McIntosh](#)

Proceedings IAU Symposium No. 328, p. 93, **2017**, D. Nandi, A. Valio, P. Petit eds      **2018**

<https://arxiv.org/pdf/1808.08215.pdf>

In 1964 (Solar Cycle 20; SC 20), Patrick McIntosh began creating hand-drawn synoptic maps of solar magnetic features, based on H $\alpha$  images. These synoptic maps were unique in that they traced magnetic polarity inversion lines, and connected widely separated filaments, fibril patterns, and plage corridors to reveal the large-scale organization of the solar magnetic field. Coronal hole boundaries were later added to the maps, which were produced, more or less continuously, into 2009 (i.e., the start of SC 24). The result was a record of  $\sim$ 45 years ( $\sim$ 570 Carrington rotations), or nearly four complete solar cycles of synoptic maps. We are currently scanning, digitizing and archiving these maps, with the final, searchable versions publicly available at NOAA's National Centers for Environmental Information. In this paper we present preliminary scientific studies using the archived maps from SC 23. We show the global evolution of closed magnetic structures (e.g., sunspots, plage, and filaments) in relation to open magnetic structures (e.g., coronal holes), and examine how both relate to the shifting patterns of large-scale positive and negative polarity regions.

### **Editorial: Coronal Magnetometry.**

**Gibson** SE, Rachmeler LA and White SM

(2017) Front. Astron. Space Sci. 4:3.

<https://www.frontiersin.org/articles/10.3389/fspas.2017.00003/full>

<https://doi.org/10.3389/fspas.2017.00003>

### **Coronal Magnetometry.**

**Ebook**

**Gibson**, S. E., Rachmeler, L. A., White, S. M., eds. (2017).

Lausanne: Frontiers Media. doi: 10.3389/978-2-88945-220-0

[http://www.frontiersin.org/books/Coronal\\_Magnetometry\\_5/1259#nogo](http://www.frontiersin.org/books/Coronal_Magnetometry_5/1259#nogo)

<http://journal.frontiersin.org/researchtopic/3547/coronal-magnetometry>

### **Magnetic nulls and super-radial expansion in the solar corona**

Sarah E. **Gibson**, Kevin Dalmasse, Laurel A. Rachmeler, Marc L. De Rosa, Steven Tomczyk, Giuliana de Toma, Joan Burkepile, Michael Galloy

2017 *ApJL* **840** L13

<https://arxiv.org/pdf/1704.07470.pdf>

Magnetic fields in the sun's outer atmosphere -- the corona -- control both solar-wind acceleration and the dynamics of solar eruptions. We present the first clear observational evidence of coronal magnetic nulls in off-limb linearly polarized observations of pseudostreamers, taken by the Coronal Multichannel Polarimeter (CoMP) telescope. These nulls represent regions where magnetic reconnection is likely to act as a catalyst for solar activity. CoMP linear-polarization observations also provide an independent, coronal proxy for magnetic expansion into the solar wind, a quantity often used to parameterize and predict the solar wind speed at Earth. We introduce a new method for explicitly calculating expansion factors from CoMP coronal linear-polarization observations, which does not require photospheric extrapolations. We conclude that linearly-polarized light is a powerful new diagnostic of critical coronal magnetic topologies and the expanding magnetic flux tubes that channel the solar wind.

### **Data-model comparison using FORWARD and CoMP**

Sarah **Gibson**

Proceedings of the International Astronomical Union, Volume 305, pp. 245-250, 2015

<http://arxiv.org/pdf/1511.04416v1.pdf>

The FORWARD SolarSoft IDL package is a community resource for model-data comparison, with a particular emphasis on analyzing coronal magnetic fields. FORWARD allows the synthesis of coronal polarimetric signals at visible, infrared, and radio frequencies, and will soon be augmented for ultraviolet polarimetry. In this paper we focus on observations of the infrared (IR) forbidden lines of Fe XIII, and describe how FORWARD may be used to directly access these data from the Mauna Loa Solar Observatory Coronal Multi-channel Polarimeter (MLSO/CoMP), to put them in the context of other space- and ground-based observations, and to compare them to synthetic observables generated from magnetohydrodynamic (MHD) models.

### **On measuring divergence for magnetic field modeling**

**S.A. Gilchrist**, **K.D. Leka**, **G. Barnes**, **M.S. Wheatland**, **M.L. DeRosa**

*ApJ* **900** 136 2020

<https://arxiv.org/pdf/2008.08863.pdf>

<https://doi.org/10.3847/1538-4357/aba752>

A physical magnetic field has a divergence of zero. Numerical error in constructing a model field and computing the divergence, however, introduces a finite divergence into these calculations. A popular metric for measuring divergence is the average fractional flux  $\langle |f_i| \rangle$ . We show that  $\langle |f_i| \rangle$  scales with the size of the computational mesh, and may be a poor measure of divergence because it becomes arbitrarily small for increasing mesh resolution, without the divergence actually decreasing. We define a modified version of this metric that does not scale with mesh size. We apply the new metric to the results of DeRosa et al. (2015), who measured  $\langle |f_i| \rangle$  for a series of Nonlinear Force-Free Field (NLFFF) models of the coronal magnetic field based on solar boundary data binned at different spatial resolutions. We compute a number of divergence metrics for the DeRosa et al. (2015) data and analyze the effect of spatial resolution on these metrics using a non-parametric method. We find that some of the trends reported by DeRosa et al. (2015) are due to the intrinsic scaling of  $\langle |f_i| \rangle$ . We also find that different metrics give different results for the same data set and therefore there is value in measuring divergence via several metrics.

## **Nonlinear Force-Free Modeling of the Corona in Spherical Coordinates**

S. A. [Gilchrist](#), M. S. Wheatland

Solar Physics, April **2014**, Volume 289, Issue 4, pp 1153-1171

We present a code for solving the nonlinear force-free equations in spherical polar geometry, with the motivation of modeling the magnetic field in the corona. The code is an implementation of the Grad–Rubin method. Our method is applicable to a spherical domain of arbitrary angular size. The implementation is based on a global spectral representation for the magnetic field that makes no explicit assumptions about the form of the magnetic field at the transverse boundaries of the domain. We apply the code to a bipolar test case with analytic boundary conditions, and demonstrate the convergence of the Grad–Rubin method and the self-consistency of the resulting numerical solution.

## **A Magnetostatic Grad–Rubin Code for Coronal Magnetic Field Extrapolations**

S. A. [Gilchrist](#), M. S. Wheatland

Solar Physics, January **2013**, Volume 282, Issue 1, pp 283-302

The coronal magnetic field cannot be directly observed, but, in principle, it can be reconstructed from the comparatively well observed photospheric magnetic field. A popular approach uses a nonlinear force-free model. Non-magnetic forces at the photosphere are significant, meaning the photospheric data are inconsistent with the force-free model, and this causes problems with the modeling (De Rosa et al., *Astrophys. J.* 696, 1780, 2009). In this paper we present a numerical implementation of the Grad–Rubin method for reconstructing the coronal magnetic field using a magnetostatic model. This model includes a pressure force and a non-zero magnetic Lorentz force. We demonstrate our implementation on a simple analytic test case and obtain the speed and numerical error scaling as a function of the grid size.

## **The Free Energy of NOAA Solar Active Region AR 11029**

S. A. [Gilchrist](#), M. S. Wheatland and K. D. Leka

Solar Physics, Volume 276, Numbers 1-2, 133-160, **2012**

The NOAA active region (AR) 11029 was a small but highly active sunspot region which produced 73 GOES soft X-ray flares during its transit of the disk in late **October 2009**. The flares appear to show a departure from the well-known power law frequency-size distribution. Specifically, too few GOES C-class and no M-class flares were observed by comparison with a power law distribution (Wheatland, *Astrophys. J.* 710, 1324, 2010). This was conjectured to be due to the region having insufficient magnetic energy to power the missing large events. We construct nonlinear force-free extrapolations of the coronal magnetic field of AR 11029 using data taken on **24 October** by the SOLIS Vector SpectroMagnetograph (SOLIS/VSM) and data taken on **27 October** by the Hinode Solar Optical Telescope SpectroPolarimeter (Hinode/SP). Force-free modeling with photospheric magnetogram data encounters problems, because the magnetogram data are inconsistent with a force-free model. We employ a recently developed “self-consistency” procedure which addresses this problem and accommodates uncertainties in the boundary data (Wheatland and Régnier, *Astrophys. J.* 700, L88, 2009). We calculate the total energy and free energy of the self-consistent solution, which provides a model for the coronal magnetic field of the active region.

The free energy of the region was found to be  $\approx 4 \times 10^{29}$  erg on 24 October and  $\approx 7 \times 10^{31}$  erg on 27 October. An order of magnitude scaling between RHESSI non-thermal energy and GOES peak X-ray flux is established from a sample of flares from the literature and is used to estimate flare energies from the observed GOES peak X-ray flux. Based on the scaling, we conclude that the estimated free energy of AR 11029 on 27 October when the flaring rate peaked was sufficient to power M-class or X-class flares; hence, the modeling does not appear to support the hypothesis that the absence of large flares is due to the region having limited energy.

## **Probabilistic Super-Resolution of Solar Magnetograms: Generating Many Explanations and Measuring Uncertainties**

Xavier [Gitiaux](#), [Shane A. Maloney](#), [Anna Jungbluth](#), [Carl Shneider](#), [Paul J. Wright](#), [Atılım Güneş Baydin](#), [Michel Deudon](#), [Yarin Gal](#), [Alfredo Kalaitzis](#), [Andrés Muñoz-Jaramillo](#)

33rd Conference on Neural Information Processing Systems (NeurIPS 2019), Vancouver, Canada. 2019

<https://arxiv.org/pdf/1911.01486.pdf>

Machine learning techniques have been successfully applied to super-resolution tasks on natural images where visually pleasing results are sufficient. However in many scientific domains this is not adequate and estimations of errors and uncertainties are crucial. To address this issue we propose a Bayesian framework that decomposes uncertainties into epistemic and aleatoric uncertainties. We test the validity of our approach by super-resolving images of the Sun's magnetic field and by generating maps measuring the range of possible high resolution explanations compatible with a given low resolution magnetogram.

## **Comparison of Methods for modelling Coronal Magnetic Fields**

E. E. [Goldstraw](#), [A. W. Hood](#), [P. K. Browning](#), [P. J. Cargill](#)

A&A 610, A48 (2018)

<https://arxiv.org/pdf/1711.07458.pdf>

Four different approximate approaches used to model the stressing of coronal magnetic fields due to an imposed photospheric motion are compared with each other and the results from a full time-dependent magnetohydrodynamic (MHD) code. The assumptions used for each of the approximate methods are tested by considering large photospheric footpoint displacements.

We consider a simple model problem, comparing the full nonlinear magnetohydrodynamic evolution, determined with the Lare2D numerical code, with four approximate approaches. Two of these, magneto-frictional relaxation and a quasi-1D Grad-Shafranov approach, assume sequences of equilibria, whilst the other two methods, a second-order linearisation of the MHD equations and Reduced MHD, are time-dependent.

The relaxation method is very accurate compared to full MHD for force-free equilibria for all footpoint displacements but has significant errors when the plasma  $\beta_0$  is of order unity. The 1D approach gives an extremely accurate description of the equilibria away from the photospheric boundary layers, and agrees well with Lare2D for all parameter values tested. The linearised MHD equations correctly predict the existence of photospheric boundary layers that are present in the full MHD results. As soon as the footpoint displacement becomes a significant fraction of the loop length, the RMHD method fails to model the sequences of equilibria correctly. The full numerical solution is interesting in its own right, and care must be taken for low  $\beta_0$  plasmas if the viscosity is too large.

## **Detecting the solar new magnetic flux regions on the base of vector magnetograms**

A. A. [Golovko](#) & I. I. Salakhutdinova

Journal of Atmospheric and Solar-Terrestrial Physics Volume 179, November 2018, Pages 120-127

<http://sci-hub.tw/http://www.sciencedirect.com/science/article/pii/S1364682617307083>

To understand better the origin of CME and other non-stationary processes, the detailed information about emerging flux regions must be known. The advanced method of mapping emerging magnetic flux regions through the multifractal segmentation of vector photospheric magnetograms, is created. It is free from influence of effects of projection. Maps of the vertical component of the field  $H_z$  and of the two transversal components  $H_x$ ,  $H_y$  are processed separately and the computed segmented images are summarized. As a result, the detailed picture of distribution of new magnetic fluxes at the current time, is obtained. The SOT Hinode magnetograms for 2006-2015 were used. Observations of the flare-productive active regions NOAA 11158 and 11520 were processed. Hills of a new field in case of their birth have the considerable elongation which is possibly related to their rope-like geometry. In the centers of flare activity, in the vicinity of polarity inversion lines, exits of new magnetic flux alternate with processes of "magnetic cancellation".

February 15, 2011, 2012, July 13

## **Variations in Ratio and Correlation of Solar Magnetic Fields in the Fe i 525.02 nm and Na i 589.59 nm Lines According to Mount Wilson Measurements During 2000 – 2012**

Elena [Golubeva](#)

Solar Phys. 291(8) 2213-2241 2016

Variations in the solar magnetic-field ratio over 13 years are analyzed, relying on the comparison of simultaneous measurements in two spectral lines at the Mount Wilson Observatory (MWO). The ratio and correlation coefficient are calculated over the general working range of measured magnetic-field values and in various ranges of the field magnitudes. Variations in both parameters are considered. We found the following tendencies: i) the parameters show changes with the cycle of solar activity in the general case; ii) their dependence on magnetic-field magnitude is a nonlinear function of time, and this is especially pronounced in the ratio behavior; iii) several separate ranges of

the field magnitudes can be distinguished based on the behavioral patterns of the ratio variations. Correspondences between these ranges and the known structural objects of the solar atmosphere are discussed. This permits us to reach the conclusion that the dependence of parameters considered on the magnetic-field magnitude and time is connected with the variety of magnetic structural components and their cyclic rearrangements. The results represented may be useful for solving interpretation problems of solar magnetic-field measurements and for the cross-calibration of applicable instruments. They can also be of interest for tasks related to the creation of a uniform long temporal series of solar magnetic-field data from various sources.

### **Extended MHD modeling of the steady solar corona and the solar wind**

**Review**

Tamas I. **Gombosi**, Bart van der Holst, Ward B. Manchester, Igor V. Sokolov

[Living Reviews in Solar Physics](#) December 2018, 15:4

<https://link.springer.com/content/pdf/10.1007%2Fs41116-018-0014-4.pdf>

<https://arxiv.org/pdf/1807.00417.pdf>

The history and present state of large-scale magnetohydrodynamic modeling of the solar corona and the solar wind with steady or quasi-steady coronal physics is reviewed. We put the evolution of ideas leading to the recognition of the existence of an expanding solar atmosphere into historical context. The development and main features of the first generation of global corona and solar wind models are described in detail. This historical perspective is also applied to the present suite of global corona and solar wind models. We discuss the evolution of new ideas and their implementation into numerical simulation codes. We point out the scientific and computational challenges facing these models and discuss the ways various groups tried to overcome these challenges. Next, we discuss the latest, state-of-the-art models and point to the expected next steps in modeling the corona and the interplanetary medium. **29 March 2006, 2011 March 7**

### **Automatic segmentation of the fine structures of sunspots in high-resolution solar images**

Xiaoying **Gong**<sup>1,2,3,4</sup>, Libo Zhong<sup>1,2</sup> and Changhui Rao<sup>1,2,3</sup>

*A&A* 670, A132 (2023)

<https://www.aanda.org/articles/aa/pdf/2023/02/aa44224-22.pdf>

Context. With the development of large-aperture ground-based solar telescopes and the adaptive optics system, the resolution of the obtained solar images has become increasingly higher. In the high-resolution photospheric images, the fine structures (umbra, penumbra, and light bridge) of sunspots can be observed clearly. The research of the fine structures of sunspots can help us to understand the evolution of solar magnetic fields and to predict eruption phenomena that have significant impacts on the Earth, such as solar flares. Therefore, algorithms for automatically segmenting the fine structures of sunspots in high-resolution solar image will greatly facilitate the study of solar physics.

Aims. This study is aimed at proposing an automatic fine-structure segmentation method for sunspots that is accurate and requires little time.

Methods. We used the superpixel segmentation to preprocess a solar image. Next, the intensity information, texture information, and spatial location information were used as features. Based on these features, the Gaussian mixture model was used to cluster different superpixels. According to different intensity levels of the umbra, penumbra, and quiet photosphere, the clusters were classified into umbra, penumbra, and quiet-photosphere areas. Finally, the morphological method was used to extract the light-bridge area.

Results. The experimental results show that the method we propose can segment the fine structures of sunspots quickly and accurately. In addition, the method can process high-resolution solar images from different solar telescopes and generates a satisfactory segmentation performance.

### **Inference of magnetic fields in the very quiet Sun**

[M. J. Martínez González](#), [A. Pastor Yabar](#), [A. Lagg](#), ...

*A&A* 2018

<https://arxiv.org/pdf/1804.10089.pdf>

We present high-precision spectro-polarimetric data with high spatial resolution (0.4") of the very quiet Sun at 1.56 $\mu\text{m}$  obtained with the GREGOR telescope to shed some light on this complex magnetism. Half of our observed quiet-Sun region is better explained by magnetic substructure within the resolution element. However, we cannot distinguish whether this substructure comes from gradients of the physical parameters along the line of sight or from horizontal gradients (across the surface). In these pixels, a model with two magnetic components is preferred, and we find two distinct magnetic field populations. The population with the larger filling factor has very weak ( $\sim 150$  G) horizontal fields similar to those obtained in previous works. We demonstrate that the field vector of this population is not constrained by the observations, given the spatial resolution and polarimetric accuracy of our data. The topology of the other component with the smaller filling factor is constrained by the observations for field strengths above 250 G: we infer hG fields with inclinations and azimuth values compatible with an isotropic distribution. The filling factors are typically below 30%. We also find that the flux of the two polarities is not



balanced. From the other half of the observed quiet-Sun area  $\sim 50\%$  are two-lobed Stokes V profiles, meaning that 23% of the field of view can be adequately explained with a single constant magnetic field embedded in a non-magnetic atmosphere. The magnetic field vector and filling factor are reliably inferred in only 50% based on the regular profiles. Therefore, 12% of the field of view harbour hG fields with filling factors typically below 30%. At our present spatial resolution, 70% of the pixels apparently are non-magnetised. **2015 September 17**

## **EMERGENCE OF SMALL-SCALE MAGNETIC LOOPS THROUGH THE QUIET SOLAR ATMOSPHERE**

M. J. Martínez [González](#) et al

ApJ 700 1391-1403, **2009** doi: [10.1088/0004-637X/700/2/1391](https://doi.org/10.1088/0004-637X/700/2/1391)

We investigate the emergence of magnetic flux in the quiet Sun at very small spatial scales, focusing on the magnetic connection between the photosphere and chromosphere. The observational data consist of spectropolarimetric measurements and filtergrams taken with the *Hinode* satellite and the Dutch Open Telescope. We find that a significant fraction of the magnetic flux present in internetwork regions appears in the form of  $\Omega$ -shaped loops. The emergence rate is 0.02 loops per hour and  $\text{arcsec}^{-2}$ , which brings  $1.1 \times 10^{12} \text{ Mx s}^{-1} \text{ arcsec}^{-2}$  of new flux to the solar surface. Initially, the loops are observed as small patches of linear polarization above a granular cell. Shortly afterward, two footpoints of opposite polarity become visible in circular polarization within or at the edges of the granule and start moving toward the adjacent intergranular space. The orientation of the footpoints does not seem to obey Hale's polarity rules. The loops are continuously buffeted by convective motions, but they always retain a high degree of coherence. Interestingly, 23% of the loops that emerge in the photosphere reach the chromosphere (16 cases out of 69). They are first detected in Fe I 630 nm magnetograms and 5 minutes later in Mg I b 517.3 nm magnetograms. After about 8 minutes, some of them are also observed in Ca II H line-core images, where the footpoints produce small brightness enhancements.

## **Proper Motions of Sunspots' Umbral Dots at High Temporal and Spatial Resolution**

Hadis [Goodarzi](#)<sup>1,2</sup>, Serge Koutchmy<sup>3</sup>, and Ali Adjabshirizadeh<sup>4</sup>

**2018** ApJ 860 168 DOI [10.3847/1538-4357/aac499](https://doi.org/10.3847/1538-4357/aac499)

<https://arxiv.org/pdf/1807.05531.pdf>

<http://sci-hub.tw/10.3847/1538-4357/aac499>

To deepen the analysis of the photometric properties of the umbra of a sunspot, we study proper motions of small features such as umbral dots (UDs) inside a single sunspot observed by the Solar Optical Telescope of *Hinode* close to the disk center. We consider horizontal flows with high precision and details to study the transient motion behavior of UD in short time intervals. Blue continuum images were first deconvolved with the point-spread function, such that the stray light is precisely removed and the original resolution is improved. Several images were co-added to improve the signal-to-noise ratio, keeping a reasonable temporal resolution and checking that the results are reproducible. The Fourier local correlation tracking technique is applied to the new corrected time sequence of images, and horizontal velocity maps were obtained both for the whole umbra ( $16'' \times 12''$ ) and for a high-resolution small region of the umbra ( $3''.5 \times 3''.5$ ) to study the smallest details of the velocity fields. We used two different Gaussian tracking windows ( $0.8$  and  $0''.2$ ), which reveals two types of horizontal motions for umbral features. First, a global inner penumbra and peripheral umbra inward motion directed to the central parts is revealed as an overall proper motion of bright peripheral fine structures. Second, motions matching small cells inside the darkest parts of the umbra with apparent sink and source areas are revealed, suggesting possible upflows and downflows appearing in different bright and dark locations without a definite answer regarding their brightness identification with a convective or a buoyant cell. **2007 March 1**

## **Improved SOT (Hinode mission) high resolution solar imaging observations: 2— Photometric properties of sunspot umbral dots**

H. [Goodarzi](#), S. Koutchmy, A. Adjabshirizadeh

Astrophysics and Space Science November **2016**, 361:366

[http://link.springer.com/article/10.1007/s10509-016-2896-8?wt\\_mc=alerts.TOCjournals](http://link.springer.com/article/10.1007/s10509-016-2896-8?wt_mc=alerts.TOCjournals)

<https://arxiv.org/pdf/1506.08265v1.pdf>

The origin and evolution of solar sunspots in deep photospheric layers are not yet well understood. The case of a quasi-symmetric single mature sunspot near the solar centre is selected for analysis. We use the best available observations of the partial Sun free of turbulent Earth atmospheric effects from the Solar Optical Telescope (SOT) onboard the *Hinode* spacecraft, after greatly improving the resolution with an optimum Max-likelihood deconvolution with the Point Spread Function (PSF) deduced in a preceding paper. For several different images both the smearing due to the instrumental diffraction effects (PSF core) and the large angle stray light are removed. The selected iterative processing depends on both the signal/noise ratio and on the desired contrast of the ultimate details under examination. The photometric properties of bright umbral dots (BUDs) are deduced from corrected frames. Calibrated isophote maps are provided to show the intensity variations around each UD across the background umbra and the surrounding photospheric field, including the penumbra. We deduce the typical photometrical

properties of bright UD's that populate the whole umbral surface down to sub-pixel scales of  $\sim(0.05448'')$ . The analysis demonstrates the basic heterogeneous nature of the umbra, similar to a network of minute bright and dark round or elongated cells with a spacing of order of  $\sim(0.35'')$ . For the first time a complete and detailed map of the color index and temperature deduced from the analysis of deeply corrected continuum images is provided, showing that tiny bright UD's can reach photospheric temperatures and even higher for the peripheral BUD's. In the umbra, there are some very dark small regions with temperatures as low as 3100 K. Close links seemingly exist with bright UD's. Central BUD's and peripheral BUD's are found to have similar properties but significantly different contrast values. Photometric analysis shows a large dispersion that reflects the broad range of dynamical phenomena involved in the umbra and its periphery, suggesting that the small scale activity observed in the deepest measured photospheric layers of the umbra determines the more impressive rapid phenomena observed in higher layers.

**Febr. 28 – March 1, 2007**

## **Radiating Current Sheets in the Solar Chromosphere**

Michael L. [Goodman](#), Philip G. Judge

**2012**, The Astrophysical Journal, 751, 75

<http://arxiv.org/pdf/1406.1211v1.pdf> **2014**;

An MHD model of a Hydrogen plasma with flow, an energy equation, NLTE ionization and radiative cooling, and an Ohm's law with anisotropic electrical conduction and thermoelectric effects is used to self-consistently generate atmospheric layers over a 50 km height range. A subset of these solutions contain current sheets, and have properties similar to those of the lower and middle chromosphere. The magnetic field profiles are found to be close to Harris sheet profiles, with maximum field strengths  $\sim 25\text{--}150$  G. The radiative flux FR emitted by individual sheets is  $\sim 4.9 \times 10^5\text{--}4.5 \times 10^6$  ergs-cm $^{-2}$ -s $^{-1}$ , to be compared with the observed chromospheric emission rate of  $\sim 107$  ergs-cm $^{-2}$ -s $^{-1}$ . Essentially all emission is from regions with thicknesses  $\sim 0.5\text{--}13$  km containing the neutral sheet. About half of FR comes from sub-regions with thicknesses 10 times smaller. A resolution  $\lesssim 5\text{--}130$  m is needed to resolve the properties of the sheets. The sheets have total H densities  $\sim 10^{13}\text{--}10^{15}$  cm $^{-3}$ . The ionization fraction in the sheets is  $\sim 2\text{--}20$  times larger, and the temperature is  $\sim 2000\text{--}3000$  K higher than in the surrounding plasma. The Joule heating flux FJ exceeds FR by  $\sim 4\text{--}34\%$ , the difference being balanced in the energy equation mainly by a negative compressive heating flux. Proton Pedersen current dissipation generates  $\sim 62\text{--}77\%$  of the positive contribution to FJ. The remainder of this contribution is due to electron current dissipation near the neutral sheet where the plasma is weakly magnetized.

## **Rotation of sunspots in active region NOAA 10930**

O.S. [Gopasyuk](#)

Advances in Space Research, Volume 55, Issue 3, 1 February **2015**, Pages 937–941

<http://www.sciencedirect.com/science/article/pii/S0273117714005699>

The rotation of sunspots of the active region NOAA 10930 has been investigated using a time series of vector magnetic field maps from the Solar Optical Telescope aboard Hinode. The vertical, radial and azimuthal axisymmetrical components of the magnetic field vector have been reconstructed from the magnetic field line-of-sight component for both sunspots of this active region. The existence of an azimuthal field component means that the magnetic field lines are twisted. The azimuthal components of both sunspots are of same sign. The magnetic flux tubes which form the sunspots of the active region on the solar surface are twisted clockwise. The vertical electric currents generated as a result of rotation and twisting of the magnetic flux tubes have the same direction.

## **Using the Stokes V widths of Fe I lines for diagnostics of the intrinsic solar photospheric magnetic field**

M. [Gordovskyy](#), [S. Shelyag](#), [P.K. Browning](#), [V.G. Lozitsky](#)

A&A 633, A136 (**2020**)

<https://arxiv.org/pdf/1912.03340.pdf>

<https://doi.org/10.1051/0004-6361/201937027>

The goal of this study is to explore a novel method for the solar photospheric magnetic field diagnostics using Stokes V widths of different magnetosensitive Fe-I spectral lines. We calculate Stokes I and V profiles of several Fe I lines based on a one-dimensional photospheric model VAL C using the NICOLE radiative transfer code. These profiles are used to produce calibration curves linking the intrinsic magnetic field values with the widths of blue peaks of Stokes V profiles. The obtained calibration curves are then tested using the Stokes profiles calculated for more realistic photospheric models based on MHD models of magneto-convection. It is shown that the developed Stokes V widths (SVW) method can be used with various optical and near-infrared lines. Out of six lines considered in this study, FeI 6301 line appears to be the most effective: it is sensitive to fields over  $\sim 200$ G and does not show any saturation up to  $\sim 2$ kG. Other lines considered can also be used for the photospheric field diagnostics with this method, however, only in narrower field value ranges, typically from about 100G to 700-1000G. The developed method can be a useful alternative to the classical magnetic line ratio method, particularly when the choice of lines is limited.

## **Analysis of unresolved photospheric magnetic field structure using Fe I 6301 and 6302 lines**

M. [Gordovsky](#)., [S. Shelyag](#), [P.K. Browning](#), [V.G. Lozitsky](#)

A&A 619, A164 2018

<https://arxiv.org/pdf/1808.06862.pdf>

Early magnetographic observations indicated that magnetic field in the solar photosphere has unresolved small-scale structure. Near-infrared and optical data with extremely high spatial resolution show that these structures have scales of few tens of kilometres, which are not resolved in the majority of solar observations. The goal of this study is to establish the effect of unresolved photospheric magnetic field structure on Stokes profiles observed with relatively low spatial resolution. Ultimately, we aim to develop methods for fast estimation of the photospheric magnetic filling factor and line-of-sight gradient of the photospheric magnetic field, which can be applied to large observational data sets. We exploit 3D MHD models of magneto-convection developed using MURAM code. Corresponding profiles of Fe I 6301.5 and 6302.5  $\text{\AA}$  spectral lines are calculated using NICOLE radiative transfer code. The resulting I and V Stokes  $[x, y, \lambda]$  cubes with reduced spatial resolution of 150 km are used to calculate magnetic field values as they would be obtained in observations with Hinode/SOT or SDO/HMI. Three different methods of the magnetic filling factor estimation are considered: the magnetic line ratio method, Stokes V width method and a simple statistical method. We find that the statistical method and the Stokes V width method are sufficiently reliable for fast filling factor estimations. Furthermore, we find that Stokes I±V bisector splitting gradient can be used for fast estimation of line-of-sight gradient of the photospheric magnetic field.

## **Stochastic entropy production in the quiet Sun magnetic fields**

Andrei [Gorobets](#), [Svetlana Berdyugina](#)

483, L69–L74 (2019)

<https://arxiv.org/pdf/1812.02561.pdf>

<https://academic.oup.com/mnrasl/article/483/1/L69/5228712>

The second law of thermodynamics imposes an increase of macroscopic entropy with time in an isolated system. Microscopically, however, the entropy production can be negative for a single, microscopic realization of a thermodynamic process. The so-called fluctuation theorems provide exact relations between the stochastic entropy consumption and generation. Here, we analyse pixel-to-pixel fluctuations in time of small-scale magnetic fields (SSMF) in the quiet Sun observed with the SDO/HMI instrument. We demonstrate that entropy generated by SSMF obeys the fluctuation theorems. In particular, the SSMF entropy consumption probability is exactly exponentially smaller than the SSMF entropy generation probability. This may have fundamental implications for the magnetic energy budget of the Sun.

## **Maximum Entropy Limit of Small-scale Magnetic Field Fluctuations in the Quiet Sun**

A. Y. [Gorobets](#), [S.V. Berdyugina](#), [T. L. Riethmüller](#), [J. Blanco Rodríguez](#), [S. K. Solanki](#), [P. Barthol](#), [A. Gandorfer](#), [L. Gizon](#), [J. Hirzberger](#), [M. van Noort](#), [J.C. Del Toro Iniesta](#), [D. Orozco Suárez](#), [W. Schmidt](#), [V. Martínez Pillet](#), [M. Knölker](#)

Astrophysical Journal Supplement Series 233 5 2017

<https://arxiv.org/pdf/1710.08361.pdf>

The observed magnetic field on the solar surface is characterized by a very complex spatial and temporal behavior. Although feature-tracking algorithms have allowed us to deepen our understanding of this behavior, subjectivity plays an important role in the identification and tracking of such features. In this paper, we continue studies Gorobets, A. Y., Borrero, J. M., & Berdyugina, S. 2016, ApJL, 825, L18 of the temporal stochasticity of the magnetic field on the solar surface without relying either on the concept of magnetic features or on subjective assumptions about their identification and interaction. We propose a data analysis method to quantify fluctuations of the line-of-sight magnetic field by means of reducing the temporal field's evolution to the regular Markov process. We build a representative model of fluctuations converging to the unique stationary (equilibrium) distribution in the long time limit with maximum entropy. We obtained different rates of convergence to the equilibrium at fixed noise cutoff for two sets of data. This indicates a strong influence of the data spatial resolution and mixing-polarity fluctuations on the relaxation process. The analysis is applied to observations of magnetic fields of the relatively quiet areas around an active region carried out during the second flight of the Sunrise/IMaX and quiet Sun areas at the disk center from the Helioseismic and Magnetic Imager on board the Solar Dynamics Observatory satellite.  
2013 June 12

## **Markov properties of the magnetic field in the quiet solar photosphere**

A.Y. [Gorobets](#), J.M. Borrero, S. Berdyugina

2016 ApJ 825 L18

<http://arxiv.org/pdf/1605.00074v1.pdf>

The observed magnetic field on the solar surface is characterized by a very complex spatial and temporal behaviour. Although feature-tracking algorithms have allowed us to deepen our understanding of this behaviour, subjectivity plays an important role in the identification, tracking of such features. In this paper we study the temporal stochasticity of the magnetic field on the solar surface without relying on the concept of magnetic feature nor on subjective assumptions about their identification and interaction. The analysis is applied to observations of the magnetic field on the quiet solar photosphere carried out with the IMAx instrument on-board the stratospheric balloon Sunrise. We show that the joint probability distribution functions of the longitudinal ( $B_{\parallel}$ ) and transverse ( $B_{\perp}$ ) components of the magnetic field, as well as of the magnetic pressure ( $B^2=B_{\perp}^2+B_{\parallel}^2$ ), verify the necessary and sufficient condition for the Markov chains. Therefore we establish that the magnetic field, as seen by IMAx with a resolution of  $0.15''$ - $0.18''$  and 33 sec cadence, can be considered as a memoryless temporal fluctuating quantity.

### **Spectral magnetic helicity of solar active regions between 2006 in 2017**

Sanjay [Gosain](#), [Axel Brandenburg](#)

ApJ

2019

<https://arxiv.org/pdf/1902.11273.pdf>

We compute magnetic helicity and energy spectra from about 2500 patches of 100 Mm side length on the solar surface using data from Hinode during 2006--2017. An extensive database is provided where we list magnetic energy and helicity, large- and small-scale magnetic helicity, mean current helicity density, fractional magnetic helicity, and correlation length along with the Hinode map identification number (MapID), as well as Carrington latitude and longitude for each MapID. Significant departures from the hemispheric sign rule are apparent, which is argued to be a physical effect associated with the dominance of individual active regions. In comparison with earlier work, the typical correlation length is found to be between six and eight megameters (Mm), while the length scale relating magnetic and current helicity to each other is found to be around 1.4 Mm. **2006 December 12**

### **Distribution of Electric Currents in Sunspots from Photosphere to Corona**

Sanjay [Gosain](#)<sup>1</sup>, Pascal Démoulin<sup>2</sup>, and Marcelo López Fuentes

2014 ApJ 793 15

We present a study of two regular sunspots that exhibit nearly uniform twist from the photosphere to the corona. We derive the twist parameter in the corona and in the chromosphere by minimizing the difference between the extrapolated linear force-free field model field lines and the observed intensity structures in the extreme-ultraviolet images of the Sun. The chromospheric structures appear more twisted than the coronal structures by a factor of two. Further, we derive the vertical component of electric current density,  $j_z$ , using vector magnetograms from the Hinode Solar Optical Telescope (SOT). The spatial distribution of  $j_z$  has a zebra pattern of strong positive and negative values owing to the penumbral fibril structure resolved by Hinode/SOT. This zebra pattern is due to the derivative of the horizontal magnetic field across the thin fibrils; therefore, it is strong and masks weaker currents that might be present, for example, as a result of the twist of the sunspot. We decompose  $j_z$  into the contribution due to the derivatives along and across the direction of the horizontal field, which follows the fibril orientation closely. The map of the tangential component has more distributed currents that are coherent with the chromospheric and coronal twisted structures. Moreover, it allows us to map and identify the direct and return currents in the sunspots. Finally, this decomposition of  $j_z$  is general and can be applied to any vector magnetogram in order to better identify the weaker large-scale currents that are associated with coronal twisted/sheared structures.

### **FIRST SYNOPTIC MAPS OF PHOTOSPHERIC VECTOR MAGNETIC FIELD FROM SOLIS/VSM: NON-RADIAL MAGNETIC FIELDS AND HEMISPHERIC PATTERN OF HELICITY**

S. [Gosain](#)<sup>1</sup>, A. A. Pevtsov<sup>1</sup>, G. V. Rudenko<sup>2</sup>, and S. A. Anfinogentov

2013 ApJ 772 52

We use daily full-disk vector magnetograms from Vector Spectromagnetograph on Synoptic Optical Long-term Investigations of the Sun system to synthesize the first Carrington maps of the photospheric vector magnetic field. We describe these maps and make a comparison of the observed radial field with the radial field estimate from line-of-sight magnetograms. Furthermore, we employ these maps to study the hemispheric pattern of current helicity density,  $H_c$ , during the rising phase of solar cycle 24. The longitudinal average over the 23 consecutive solar rotations shows a clear signature of the hemispheric helicity rule, i.e.,  $H_c$  is predominantly negative in the north and positive in the south. Although our data include the early phase of cycle 24, there appears to be no evidence for a possible (systematic) reversal of the hemispheric helicity rule at the beginning of the cycle as predicted by some dynamo models. Furthermore, we compute the hemispheric pattern in active region latitudes ( $-30^\circ \leq \theta \leq 30^\circ$ )

separately for weak ( $100 \text{ G} < |\text{Br}| < 500 \text{ G}$ ) and strong ( $|\text{Br}| > 1000 \text{ G}$ ) radial magnetic fields. We find that while the current helicity of strong fields follows the well-known hemispheric rule (i.e.,  $\theta \text{ Hc} < 0$ ), Hc of weak fields exhibits an inverse hemispheric behavior (i.e.,  $\theta \text{ Hc} > 0$ ), albeit with large statistical scatter. We discuss two plausible scenarios to explain the opposite hemispheric trend of helicity in weak and strong field regions.

## **Resolving Azimuth Ambiguity Using Vertical Nature of Solar Quiet-Sun Magnetic Fields**

S. [Gosain](#), A. A. Pevtsov

Solar Physics, March 2013, Volume 283, Issue 1, pp 195-205

The measurement of solar magnetic fields using the Zeeman effect diagnostics has a fundamental  $180^\circ$  ambiguity in the determination of the azimuth angle of the transverse field component. There are several methods that are used in the community and each one has its merits and demerits. Here we present a disambiguation idea that is based on the assumption that most of the magnetic field on the sun is predominantly vertical. While the method is not applicable to penumbra or other features harboring predominantly horizontal fields like the sheared neutral lines, it is useful for regions where fields are predominantly vertical like network and plage areas. The method is tested with the full-disk solar vector magnetograms observed by the SOLIS/VSM instrument. We find that statistically about 60–85 % of the pixels in a typical full-disk magnetogram has a field inclination in the range of  $0–30^\circ$  with respect to the local solar normal, and thus can be successfully disambiguated by the proposed method. Due to its non-iterative nature, the present method is extremely fast and therefore can be used as a good initial guess for iterative schemes like the non-potential field computation (NPFC) method. Furthermore, the method is insensitive to noisy pixels as it does not depend upon the neighboring pixels or derivatives.

## **Emergence of internetwork magnetic fields through the solar atmosphere**

[Milan Gošić](#), [Bart De Pontieu](#), [Luis R. Bellot Rubio](#), [Alberto Sainz Dalda](#), [Sara Esteban Pozuelo](#)

ApJ 2021

<https://arxiv.org/pdf/2103.02213.pdf>

Internetwork (IN) magnetic fields are highly dynamic, short-lived magnetic structures that populate the interior of supergranular cells. Since they emerge all over the Sun, these small-scale fields bring a substantial amount of flux, and therefore energy, to the solar surface. Because of this, IN fields are crucial for understanding the quiet Sun (QS) magnetism. However, they are weak and produce very small polarization signals, which is the reason why their properties and impact on the energetics and dynamics of the solar atmosphere are poorly known. Here we use coordinated, high-resolution, multiwavelength observations obtained with the Swedish 1-m Solar Telescope (SST) and the `Interface Region Imaging Spectrograph` (IRIS) to follow the evolution of IN magnetic loops as they emerge into the photosphere and reach the chromosphere and transition region. We studied in this paper three flux emergence events having total unsigned magnetic fluxes of  $1.9 \times 10^{18}$ ,  $2.5 \times 10^{18}$ , and  $5.3 \times 10^{18}$  Mx. The footpoints of the emerging IN bipoles are clearly seen to appear in the photosphere and to rise up through the solar atmosphere, as observed in  $\text{Fe I } 6173 \text{ \AA}$  and  $\text{Mg I } 4481 \text{ \AA}$  magnetograms, respectively. For the first time, our polarimetric measurements taken in the chromospheric  $\text{Ca II } 8542 \text{ \AA}$  line provide direct observational evidence that IN fields are capable of reaching the chromosphere. Moreover, using IRIS data, we study the effects of these weak fields on the heating of the chromosphere and transition region.

## **THE SOLAR INTERNETWORK. II. FLUX APPEARANCE AND DISAPPEARANCE RATES**

M. [Gošić](#)<sup>1</sup>, L. R. Bellot Rubio<sup>1</sup>, J. C. del Toro Iniesta<sup>1</sup>, D. Orozco Suárez<sup>2</sup>, and Y. Katsukawa

2016 ApJ 820 35

Small-scale internetwork magnetic fields are important ingredients of the quiet Sun. In this paper we analyze how they appear and disappear on the solar surface. Using high resolution Hinode magnetograms, we follow the evolution of individual magnetic elements in the interior of two supergranular cells at the disk center. From up to 38 hr of continuous measurements, we show that magnetic flux appears in internetwork regions at a rate of  $120 \pm 3 \text{ Mx cm}^{-2} \text{ day}^{-1}$  ( $3.7 \pm 0.4 \times 10^{24} \text{ Mx day}^{-1}$  over the entire solar surface). Flux disappears from the internetwork at a rate of  $125 \pm 6 \text{ Mx cm}^{-2} \text{ day}^{-1}$  ( $3.9 \pm 0.5 \times 10^{24} \text{ Mx day}^{-1}$ ) through fading of magnetic elements, cancelation between opposite-polarity features, and interactions with network patches, which converts internetwork elements into network features. Most of the flux is lost through fading and interactions with the network, at nearly the same rate of about  $50 \text{ Mx cm}^{-2} \text{ day}^{-1}$ . Our results demonstrate that the sources and sinks of internetwork magnetic flux are well balanced. Using the instantaneous flux appearance and disappearance rates, we successfully reproduce the time evolution of the total unsigned flux in the two supergranular cells.

## **The Solar Internetwork. I. Contribution to the Network Magnetic Flux**

Milan [Gošić](#), Luis R. Bellot Rubio, David Orozco Suárez, Yukio Katsukawa, Jose Carlos Del Toro Iniesta

ApJ, 2014

The magnetic network observed on the solar surface harbors a sizable fraction of the total quiet Sun flux. However, its origin and maintenance are not well known. Here we investigate the contribution of internetwork magnetic fields to the network flux. Internetwork fields permeate the interior of supergranular cells and show large emergence rates. We use long-duration sequences of magnetograms acquired by Hinode and an automatic feature tracking algorithm to follow the evolution of network and internetwork flux elements. We find that 14% of the quiet Sun flux is in the form of internetwork fields, with little temporal variations. Internetwork elements interact with network patches and modify the flux budget of the network, either by adding flux (through merging processes) or by removing it (through cancellation events). Mergings appear to be dominant, so the net flux contribution of the internetwork is positive. The observed rate of flux transfer to the network is  $1.5 \times 10^{24} \text{ Mx day}^{-1}$  over the entire solar surface. Thus, the internetwork supplies as much flux as is present in the network in only 9-13 hours. Taking into account that not all the transferred flux is incorporated into the network, we find that the internetwork would be able to replace the entire network flux in approximately 18-24 hours. This renders the internetwork the most important contributor to the network, challenging the view that ephemeral regions are the main source of flux in the quiet Sun. About 40% of the total internetwork flux eventually ends up in the network. 2010 Jan 20–21 2010 Nov 02–03

### **The Propagation of Coherent Waves Across Multiple Solar Magnetic Pores**

[S. D. T. Grant](#), [D. B. Jess](#), [M. Stangalini](#), [S. Jafarzadeh](#), [V. Fedun](#), [G. Verth](#), [P. H. Keys](#), [S. P. Rajaguru](#), [H. Uitenbroek](#), [C. D. Macbride](#), [W. Bate](#), [C. A. Gilchrist-Millar](#)

ApJ 938 143 2022

<https://arxiv.org/pdf/2209.06280.pdf>

<https://iopscience.iop.org/article/10.3847/1538-4357/ac91ca/pdf>

Solar pores are efficient magnetic conduits for propagating magnetohydrodynamic wave energy into the outer regions of the solar atmosphere. Pore observations often contain isolated and/or unconnected structures, preventing the statistical examination of wave activity as a function of atmospheric height. Here, using high resolution observations acquired by the Dunn Solar Telescope, we examine photospheric and chromospheric wave signatures from a unique collection of magnetic pores originating from the same decaying sunspot. Wavelet analysis of high cadence photospheric imaging reveals the ubiquitous presence of slow sausage mode oscillations, coherent across all photospheric pores through comparisons of intensity and area fluctuations, producing statistically significant in-phase relationships. The universal nature of these waves allowed an investigation of whether the wave activity remained coherent as they propagate. Utilizing bi-sector Doppler velocity analysis of the Ca II 8542 Å line, alongside comparisons of the modeled spectral response function, we find fine-scale 5 mHz power amplification as the waves propagate into the chromosphere. Phase angles approaching zero degrees between co-spatial bi-sectors spanning different line depths indicate standing sausage modes following reflection against the transition region boundary. Fourier analysis of chromospheric velocities between neighboring pores reveals the annihilation of the wave coherency observed in the photosphere, with examination of the intensity and velocity signals from individual pores indicating they behave as fractured wave guides, rather than monolithic structures. Importantly, this work highlights that wave morphology with atmospheric height is highly complex, with vast differences observed at chromospheric layers, despite equivalent wave modes being introduced into similar pores in the photosphere. 2016 July 12

### **Observation of Differential Rotation Within a Sunspot Umbra During an X-Class Flare**

[Richard Grimes](#), [Balázs Pintér](#) & [Huw Morgan](#)

*Solar Physics* volume 295, Article number: 87 (2020)

<https://link.springer.com/content/pdf/10.1007/s11207-020-01657-5.pdf>

Sunspots and their dynamics dominate the magnetic topology and evolution of both the photosphere and the overlying coronal active regions. Thus a comprehensive understanding of their behaviour is essential to understanding the solar magnetic field. A new technique is presented for applying multiple ellipse fits as a method for rotation tracking of sunspot umbrae. The method is applied to a sunspot in NOAA active region AR 12158 during an X-class flare event and the resulting rotation rate correlates well with other measurements from literature. The method also reveals an apparent difference in rotation rate between the edge and the innermost region of the sunspot umbra of up to 2 degrees per hour. Such differential rotation must lead to the large-scale twisting of sunspot magnetic flux tubes with implications for models of coronal loops and the build-up of instabilities that may lead to eruptions. 10th September 2014

### **Improvement of the Helioseismic and Magnetic Imager (HMI) Vector Magnetic Field Inversion Code**

[Ana Belén Griñón-Marín](#), [Adur Pastor Yabar](#), [Yang Liu](#), [J. Todd Hoeksema](#), [Aimee Norton](#)

2021 ApJ 923 84

<https://arxiv.org/pdf/2109.09131.pdf>

<https://iopscience.iop.org/article/10.3847/1538-4357/ac2aa8/pdf>  
<https://doi.org/10.3847/1538-4357/ac2aa8>

A spectral line inversion code, Very Fast Inversion of the Stokes Vector (VFISV), has been used since May 2010 to infer the solar atmospheric parameters from the spectropolarimetric observations taken by the Helioseismic and Magnetic Imager (HMI) aboard the Solar Dynamics Observatory (SDO). The magnetic filling factor, the fraction of the surface with a resolution element occupied by magnetic field, is set to have a constant value of one in the current version of VFISV. This report describes an improved inversion strategy for the spectropolarimetric data observed with HMI for magnetic field strengths of intermediate values in areas spatially not fully resolved. The VFISV inversion code has been modified to enable inversion of the Stokes profiles with two different components: one magnetic and one non-magnetic. In this scheme, both components share the atmospheric components except for the magnetic field strength, inclination, and azimuth. In order to determine whether the new strategy is useful, we evaluate the inferred parameters inverted with one magnetic component (the original version of the HMI inversion) and with two components (the improved version) using a Bayesian analysis. In pixels with intermediate magnetic field strengths (e.g. plages), the new version provides statistically significant values of filling fraction and magnetic field vector. Not only does the fitting of the Stokes profile improve, but the inference of the magnetic parameters and line-of-sight velocity are obtained uniquely. The new strategy is also proven to be effective for mitigating the anomalous hemispheric bias in the east-west magnetic field component in moderate field regions.

**HMI Science Nuggets** #175 March 2022 <http://hmi.stanford.edu/hminuggets/?p=3850>

## **Long-Term Evolution of Three Light Bridges Developed on the Same Sunspot**

[Ana Belén Griñón-Marín](#), [Adur Pastor Yabar](#), [Rebecca Centeno](#), [Héctor Socas-Navarro](#)

A&A 647, A148 2021

<https://arxiv.org/pdf/2102.04392.pdf>  
<https://www.aanda.org/articles/aa/pdf/2021/03/aa39847-20.pdf>  
<https://doi.org/10.1051/0004-6361/202039847>

One important feature of sunspots is the presence of light bridges. These structures are elongated and bright (as compared to the umbra) features that seem to be related to the formation and evolution of sunspots. In this work, we studied the long-term evolution and the stratification of different atmospheric parameters of three light bridges formed in the same host sunspot by different mechanisms. To accomplish this, we used data taken with the GREGOR Infrared Spectrograph installed at the GREGOR telescope. These data were inverted to infer the physical parameters of the atmosphere where the observed spectral profiles were formed of the three light bridges. We find that, in general, the behaviour of the three light bridges is typical of this kind of structure with the magnetic field strength, inclination, and temperature values between the values at the umbra and the penumbra. We also find that they are of a significantly non-magnetic character (particularly at the axis of the light bridges) as it is deduced from the filling factor. In addition, within the common behaviour of the physical properties of light bridges, we observe that each one exhibits a particular behaviour. Another interesting result is that the light bridge cools down, the magnetic field decreases, and the magnetic field lines get more inclined higher in the atmosphere. Finally, we studied the magnetic and non-magnetic line-of-sight velocities of the light bridges. The former shows that the magnetic component is at rest and, interestingly, its variation with optical depth shows a bi-modal behaviour. For the line-of-sight velocity of the non-magnetic component, we see that the core of the light bridge is at rest or with shallow upflows and clear downflows sinking through the edges. **2014 May 2-5**

## **Discovery of long-period magnetic field oscillations and motions in isolated sunspots**

A. B. [Griñón-Marín](#), [A. Pastor Yabar](#), [H. Socas-Navarro](#), [R. Centeno](#)

2020 A&A 635, A64

<https://arxiv.org/pdf/2001.06030.pdf>  
<https://doi.org/10.1051/0004-6361/201936589>

We analyse the temporal evolution of the inclination component of the magnetic field vector for the penumbral area of 25 isolated sunspots. Compared to previous works, the use of data from the HMI instrument aboard the SDO observatory facilitates the study of very long time series ( $\approx 1$  week), compared to previous works, with a good spatial and temporal resolution. We used the wavelet technique and we found some filamentary-shaped events with large wavelet power. Their distribution of periods is broad, ranging from the lower limit for this study of 48 minutes up to 63 hours. An interesting property of these events is that they do not appear homogeneously all around the penumbra but they seem to concentrate at particular locations. The cross-comparison of these wavelet maps with AIA data shows that the regions where these events appear are visually related to the coronal loops that connect the outer penumbra to one or more neighbouring opposite polarity flux patches.

## **Search for torsional oscillations in isolated sunspots**

A. B. [Griñón-Marín](#)<sup>1,2</sup>, [H. Socas-Navarro](#)<sup>1,2</sup> and [R. Centeno](#)<sup>3</sup>

A&A 604, A36 (2017)

In this work we seek evidence for global torsional oscillations in alpha sunspots. We have used long time series of continuum intensity and magnetic field vector maps from the Helioseismic and Magnetic Imager (HMI) instrument on board the Solar Dynamics Observatory (SDO) spacecraft. The time series analysed here span the total disk passage of 25 isolated sunspots. We found no evidence of global long-term periodic oscillations in the azimuthal angle of the sunspot magnetic field within  $\sim 1$  degree. This study could help us to understand the sunspot dynamics and its internal structure.

### **Active Region Photospheric Magnetic Properties Derived from Line-of-sight and Radial Fields**

Jordan A. [Guerra](#), [Sung-H. Park](#), [Ioannis Kontogiannis](#), [Peter T. Gallagher](#), [Manolis Georgoulis](#), [D. Shaun Bloomfield](#)

Solar Physics January 2018, 293:9

<https://arxiv.org/pdf/1712.06902.pdf>

The effect of using two representations of the normal-to-surface magnetic field to calculate photospheric measures that are related to active region (AR) potential for flaring is presented. Several AR properties were computed using line-of-sight (Blos) and spherical-radial (Br) magnetograms from the Spaceweather HMI Active Region Patch (SHARP) products of the Solar Dynamics Observatory, characterizing the presence and features of magnetic polarity inversion lines, fractality, and magnetic connectivity of the AR photospheric field. The data analyzed corresponds to  $\approx 4,000$  AR observations, achieved by randomly selecting 25% of days between September 2012 and May 2016 for analysis at 6-hr cadence. Results from this statistical study include: i) the Br component results in a slight upwards shift of property values in a manner consistent with a field-strength underestimation by the Blos component; ii) using the Br component results in significantly lower inter-property correlation in one-third of the cases, implying more independent information about the state of the AR photospheric magnetic field; iii) flaring rates for each property vary between the field components in a manner consistent with the differences in property-value ranges resulting from the components; iv) flaring rates generally increase for higher values of properties, except Fourier spectral power index that has flare rates peaking around a value of 5/3. These findings indicate that there may be advantages in using Br rather than Blos in calculating flare-related AR magnetic properties, especially for regions located far from central meridian.

### **Spatio-Temporal Scaling of Turbulent Photospheric Line-of-Sight Magnetic Field in Active Region NOAA 11158**

J. A. [Guerra](#), A. Pulkkinen, V. M. Uritsky, S. Yashiro

Solar Phys. February 2015, Volume 290, Issue 2, pp 335-350

We studied the structure and dynamics of the turbulent photospheric magnetic field in active region NOAA 11158 by characterizing spatial and temporal scaling properties of the line-of-sight (LOS) component. Using high-resolution high-cadence LOS magnetograms from SDO/HMI, we measured the power-law exponents  $\alpha$  and  $\beta$  that describe Fourier power spectra in wavenumber ( $k$ ) and frequency ( $f$ ) domains, and we investigated their evolution during the passage of the active region through the field of view of HMI. The flaring active region NOAA 11158 produces a one-dimensional spatial power spectral density that approximately follows a  $k^{-2}$  power law – a spectrum that suggests parallel MHD fluctuations in an anisotropic turbulent medium. In addition, we found that the values of  $\alpha$  capture systematically change in the configuration of the LOS photospheric magnetic field during flaring activity in the corona. Position-dependent values of the temporal scaling exponent  $\beta$  showed that, on an average, the core of the active region scales with  $\beta > 3$  surrounded by a diffusive region with an approximately  $f^{-2}$ -type spectrum. Our results indicate that only about 1 – 3 % of the studied LOS photospheric magnetic flux displays  $\beta \approx \alpha$ , implying that Taylor's hypothesis of frozen-in-flow turbulence is typically invalid for this scalar field in the presence of turbulent photospheric flows. In consequence, both spatial and temporal variations of the plasma and magnetic field must be included in a complete description of the turbulent evolution of active regions.

### **Persistent Homology analysis for solar magnetograms**

[Pablo Santamarina Guerrero](#), [Yukio Katsukawa](#), [Shin Toriumi](#), [David Orozco Suárez](#)

ApJ 2024

<https://arxiv.org/pdf/2401.16829.pdf>

Understanding the magnetic fields of the Sun is essential for unraveling the underlying mechanisms driving solar activity. Integrating topological data analysis techniques into these investigations can provide valuable insights into the intricate structures of magnetic fields, enhancing our comprehension of solar activity and its implications. In this study, we explore what persistent homology can offer in the analysis of solar magnetograms, with the objective of introducing a novel tool that will serve as the foundation for further studies of magnetic structures at the solar surface. By combining various filtration methods of the persistent homology analysis, we conduct an analysis of solar magnetograms that captures the broad magnetic scene, involving a mixture of positive and negative polarities.



This analysis is applied to observations of both quiet Sun and active regions, taken with Hinode/SOT and SDO/HMI, respectively. Our primary focus is on analyzing the properties of the spatial structures and features of the magnetic fields identified through these techniques. The results show that persistent diagrams can encode the spatial structural complexity of the magnetic flux of active regions by identifying the isolated, connected, and interacting features. They facilitate the classification of active regions based on their morphology and the detection and quantification of interacting structures of opposing polarities, such as  $\delta$ -spots. The small-scale events in the quiet Sun, such as magnetic flux cancellation and emergence, are also revealed in persistent diagrams and can be studied by observing the evolution of the plots and tracking the relevant features.

### **Spectro-Polarimetric Analysis of an Umbral Filament**

S.L. [Guglielmino](#), [P. Romano](#), [B. Ruiz Cobo](#), [F. Zuccarello](#), [M. Murabito](#)

Proceedings of the 9th Solar Polarization Workshop SPW9 **2020**

<https://arxiv.org/pdf/2001.08509.pdf>

High-resolution observations of the solar photosphere have recently revealed the presence of elongated filamentary bright structures inside sunspot umbrae. These features, which have been called umbral filaments (UFs), differ in morphology, evolution, and magnetic configuration from light bridges that are usually observed to intrude in sunspots.

To study an UF observed in the leading sunspot of active region NOAA 12529, we have analyzed spectro-polarimetric observations taken in the photosphere with the spectropolarimeter (SP) aboard the Hinode satellite. High-resolution observations in the upper chromosphere and transition region taken with the IRIS telescope and observations acquired by SDO/HMI and SDO/AIA have been used to complement the spectro-polarimetric analysis. The results obtained from the inversion of the Hinode/SP measurements allow us to discard the hypothesis that UFs are a kind of light bridge. In fact, we find no field-free or low-field strength region cospatial to the observed UF. In contrast, we detect in the structure Stokes profiles that indicate the presence of strong horizontal fields, larger than 2500 G. Furthermore, a significant portion of the UF has opposite polarity with respect to the hosting umbra. In the upper atmospheric layers, we observe filaments being cospatial to the UF in the photosphere. We interpret these findings as suggesting that the UF could be the photospheric manifestation of a flux rope hanging above the sunspot, which triggers the formation of penumbral-like filaments within the umbra via magneto-convection. **April 14, 2016**

### **Properties of the Umbral Filament Observed in Active Region NOAA 12529**

S. L. [Guglielmino](#), [P. Romano](#), [B. Ruiz Cobo](#), [F. Zuccarello](#), [M. Murabito](#)

ApJ **880** 34 **2019**

<https://arxiv.org/pdf/1906.00065.pdf>

[sci-hub.se/10.3847/1538-4357/ab2635](https://doi.org/10.3847/1538-4357/ab2635)

Recent observations of the solar photosphere revealed the presence of elongated filamentary bright structures inside sunspot umbrae, called umbral filaments (UFs). These features differ in morphology, magnetic configuration, and evolution from light bridges that are usually observed to intrude in sunspots. To characterize an UF observed in the umbra of the giant leading sunspot of active region NOAA 12529, we analyze high-resolution observations taken in the photosphere with the spectropolarimeter aboard the Hinode satellite and in the upper chromosphere and transition region with the IRIS telescope. The results of this analysis definitely rule out the hypothesis that the UF might be a kind of light bridge. In fact, we find no field-free or low-field strength region cospatial to the UF. Conversely, we recognize the presence of a strong horizontal field larger than 2500 G, a significant portion of the UF with opposite polarity with respect to the surroundings, and filaments in the upper atmospheric layers corresponding to the UF in the photosphere. These findings suggest that this structure is the photospheric manifestation of a flux rope hanging above the sunspot and forming penumbral-like filaments within the umbra via magneto-convection. This reinforces a previously proposed scenario. **14 April 2016**

### **Satellite observations of reconnection between emerging and pre-existing small-scale magnetic fields**

S.L. [Guglielmino](#), [F. Zuccarello](#), [P.R. Young](#), [P. Romano](#), [M. Murabito](#)

Nuovo Cimento C" as proceeding of the Third Meeting of the Italian Solar and Heliospheric Community **2019**

<https://arxiv.org/pdf/1901.01056.pdf>

We report multi-wavelength ultraviolet observations taken with the IRIS satellite, concerning the emergence phase in the upper chromosphere and transition region of an emerging flux region (EFR) embedded in the unipolar plage of active region NOAA 12529. The photospheric configuration of the EFR is analyzed in detail benefitting from measurements taken with the spectropolarimeter aboard the Hinode satellite, when the EFR was fully developed. In addition, these data are complemented by full-disk, simultaneous observations of the SDO satellite, relevant to the photosphere and the corona. In the photosphere, magnetic flux emergence signatures are recognized in the fuzzy granulation, with dark

alignments between the emerging polarities, cospatial with highly inclined fields. In the upper atmospheric layers, we identify recurrent brightenings that resemble UV bursts, with counterparts in all coronal passbands. These occur at the edges of the EFR and in the region of the arch filament system (AFS) cospatial to the EFR. Jet activity is also found at chromospheric and coronal levels, near the AFS and the observed brightness enhancement sites. The analysis of the IRIS line profiles reveals the heating of dense plasma in the low solar atmosphere and the driving of bi-directional high-velocity flows with speeds up to 100 km/s at the same locations. Furthermore, we detect a correlation between the Doppler velocity and line width of the Si IV 1394 and 1402 Å line profiles in the UV burst pixels and their skewness. Comparing these findings with previous observations and numerical models, we suggest evidence of several long-lasting, small-scale magnetic reconnection episodes between the emerging bipole and the ambient field. This process leads to the cancellation of a pre-existing photospheric flux concentration of the plage with the opposite polarity flux patch of the EFR. The reconnection appears to occur higher in the atmosphere than usually observed. **13 April 2016**

### **Observational Evidence of a Flux Rope within a Sunspot Umbra**

Salvo L. [Guglielmino](#), [Paolo Romano](#), [Francesca Zuccarello](#)

ApJL 846 L16 2017

<https://arxiv.org/pdf/1708.02398.pdf>

<http://iopscience.iop.org/sci-hub.cc/2041-8205/846/2/L16/>

We observed an elongated filamentary bright structure inside the umbra of the big sunspot in active region NOAA 12529, which differs from the light bridges usually observed in sunspots for its morphology, magnetic configuration, and velocity field. We used observations taken with the Solar Dynamic Observatory satellite to characterize this feature. Its lifetime is 5 days, during which it reaches a maximum length of about 30". In the maps of the vertical component of the photospheric magnetic field, a portion of the feature has a polarity opposite to that of the hosting sunspot. At the same time, in the entire feature the horizontal component of the magnetic field is about 2000 G, substantially stronger than in the surrounding penumbral filaments. Doppler velocity maps reveal the presence of both upward and downward plasma motions along the structure at the photospheric level. Moreover, looking at the chromospheric level, we noted that it is located in a region corresponding to the edge of a small filament which seems rooted in the sunspot umbra. Therefore, we interpreted the bright structure as the photospheric counterpart of a flux rope touching the sunspot and giving rise to penumbral-like filaments in the umbra. **2016 April 8-19**

### **A nonlinear solar magnetic field calibration method for the filter-based magnetograph by the residual network**

Jingjing [Guo](#), [Xianyong Bai](#), [Yuanyong Deng](#), [Hui Liu](#), [Jiabao Lin](#), [Jiangtao Su](#), [Xiao Yang](#), [Kaifan Ji](#)

ApJ 646, A41 (2021)

<https://arxiv.org/pdf/2012.07286.pdf>

<https://www.aanda.org/articles/aa/pdf/2021/02/aa38617-20.pdf>

<https://doi.org/10.1051/0004-6361/202038617>

The method of solar magnetic field calibration for the filter-based magnetograph is normally the linear calibration method under weak-field approximation that cannot generate the strong magnetic field region well due to the magnetic saturation effect. We try to provide a new method to carry out the nonlinear magnetic calibration with the help of neural networks to obtain more accurate magnetic fields. We employed the data from Hinode/SP to construct a training, validation and test dataset. The narrow-band Stokes I, Q, U, and V maps at one wavelength point were selected from all the 112 wavelength points observed by SP so as to simulate the single-wavelength observations of the filter-based magnetograph. We used the residual network to model the nonlinear relationship between the Stokes maps and the vector magnetic fields. After an extensive performance analysis, it is found that the trained models could infer the longitudinal magnetic flux density, the transverse magnetic flux density, and the azimuth angle from the narrow-band Stokes maps with a precision comparable to the inversion results using 112 wavelength points. Moreover, the maps that were produced are much cleaner than the inversion results. The method can effectively overcome the magnetic saturation effect and infer the strong magnetic region much better than the linear calibration method. The residual errors of test samples to standard data are mostly about 50 G for both the longitudinal and transverse magnetic flux density. The values are about 100 G with our previous method of multilayer perceptron, indicating that the new method is more accurate in magnetic calibration. **2014 Sep 11**

### **A Non-Linear Magnetic Field Calibration Method for Filter-Based Magnetographs by Multilayer Perceptron**

Jingjing [Guo](#), [Xianyong Bai](#), [Yuanyong Deng](#), [Hui Liu](#), [Jiabao Lin](#)...

[Solar Physics](#) January 2020, 295:5

<https://link.springer.com/content/pdf/10.1007%2Fs11207-019-1573-9.pdf>

For filter-based magnetographs, the linear calibration method under the weak-field assumption is usually adopted; this leads to magnetic saturation effect in the regions with strong magnetic field. This article explores a new method to overcome the above disadvantage using a multilayer perceptron network, which we call MagMLP, based on a back-propagation algorithm with one input layer, five hidden layers, and one output layer. We use the data from the Spectropolarimeter (SP) on board Hinode to simulate single-wavelength observations for the model training, and take into account the influence of the Doppler velocity field and the filling factor. The training results show that the linear fitting coefficient (LFC) of the transverse field reaches above 0.91, and that of the longitudinal field is above 0.98. The generalization of the models is good because the corresponding LFCs are above 0.9 for the test subsets. Compared with the linear calibration method, the MagMLP is much more effective on dealing with the magnetic saturation effect. Analyzing an active region, the results of the linear calibration present an evident magnetic saturation effect in the umbra regions; the corresponding systematic error reaches values greater than 1000 G in most areas, or even exceeds 2000 G at some pixels. However, the results of MagMLP at these locations are very close to the inversion results, and the systematic errors are basically within 300 G. In addition, we find that there are many “bright spots” and “dark spots” on the inclination angle images from the inversion results of Hinode/SP with values of 180 and 0 degrees, respectively, where the inversion is not reliable and does not produce a good result; the MagMLP handles these points well.

## **Origin and Structures of Solar Eruptions II: Magnetic Modeling (Invited Review)**

Yang **Guo**, Xin Cheng, M. D. Ding

SCIENCE CHINA Earth Sciences

2017

<https://arxiv.org/pdf/1706.05769.pdf>

The topology and dynamics of the three-dimensional magnetic field in the solar atmosphere govern various solar eruptive phenomena and activities, such as flares, coronal mass ejections, and filaments/prominences. We have to observe and model the vector magnetic field to understand the structures and physical mechanisms of these solar activities. Vector magnetic fields on the photosphere are routinely observed via the polarized light, and inferred with the inversion of Stokes profiles. To analyze these vector magnetic fields, we need first to remove the 180° ambiguity of the transverse components and correct the projection effect. Then, the vector magnetic field can be served as the boundary conditions for a force-free field modeling after a proper preprocessing. The photospheric velocity field can also be derived from a time sequence of vector magnetic fields. Three-dimensional magnetic field could be derived and studied with theoretical force-free field models, numerical nonlinear force-free field models, magnetohydrostatic models, and magnetohydrodynamic models. Magnetic energy can be computed with three-dimensional magnetic field models or a time series of vector magnetic field. The magnetic topology is analyzed by pinpointing the positions of magnetic null points, bald patches, and quasi-separatrix layers. As a well conserved physical quantity, magnetic helicity can be computed with various methods, such as the finite volume method, discrete flux tube method, and helicity flux integration method. This quantity serves as a promising parameter characterizing the activity level of solar active regions.

## **Magnetic Helicity Estimations in Models and Observations of the Solar Magnetic Field. Part III: Twist Number Method**

Y. **Guo**, E. Pariat , G. Valori , S. Anfinogentov , F. Chen , M. Georgoulis , Y. Liu , K. Moraitis , J. K. Thalmann , S. Yang

ApJ 840 40 2017

[http://www.issibern.ch/teams/magnetic/helicity/guoyang\\_20170326.pdf](http://www.issibern.ch/teams/magnetic/helicity/guoyang_20170326.pdf)

<https://arxiv.org/pdf/1704.02096.pdf>

We study the writhe, twist and magnetic helicity of different magnetic flux ropes, based on models of the solar coronal magnetic field structure. These include an analytical force-free Titov "D" model equilibrium solution, non force-free magnetohydrodynamic simulations, and nonlinear force-free magnetic field models. The geometrical boundary of the magnetic flux rope is determined by the quasi-separatrix layer and the bottom surface, and the axis curve of the flux rope is determined by its overall orientation. The twist is computed by the Berger-Prior formula that is suitable for arbitrary geometry and both force-free and non-force-free models. The magnetic helicity is estimated by the twist multiplied by the square of the axial magnetic flux. We compare the obtained values with those derived by a finite volume helicity estimation method. We find that the magnetic helicity obtained with the twist method agrees with the helicity carried by the purely current-carrying part of the field within uncertainties for most test cases. It is also found that the current-carrying part of the model field is relatively significant at the very location of the magnetic flux rope. This qualitatively explains the agreement between the magnetic helicity computed by the twist method and the helicity contributed purely by the current-carrying magnetic field.

2007 February 12, 20100807

## **MAGNETO-FRICTIONAL MODELING OF CORONAL NONLINEAR FORCE-FREE FIELDS. II. APPLICATION TO OBSERVATIONS**

Y. **Guo**<sup>1,2</sup>, C. Xia<sup>2</sup>, and R. Keppens<sup>1</sup>

2016 ApJ 828 83

A magneto-frictional module has been implemented and tested in the Message Passing Interface Adaptive Mesh Refinement Versatile Advection Code (MPI-AMRVAC) in the first paper of this series. Here, we apply the magneto-frictional method to observations to demonstrate its applicability in both Cartesian and spherical coordinates, and in uniform and block-adaptive octree grids. We first reconstruct a nonlinear force-free field (NLFFF) on a uniform grid of 1803 cells in Cartesian coordinates, with boundary conditions provided by the vector magnetic field observed by the Helioseismic and Magnetic Imager (HMI) on board the Solar Dynamics Observatory (SDO) at 06:00 UT on **2010 November 11** in active region NOAA 11123. The reconstructed NLFFF successfully reproduces the sheared and twisted field lines and magnetic null points. Next, we adopt a three-level block-adaptive grid to model the same active region with a higher spatial resolution on the bottom boundary and a coarser treatment of regions higher up. The force-free and divergence-free metrics obtained are comparable to the run with a uniform grid, and the reconstructed field topology is also very similar. Finally, a group of active regions, including NOAA 11401, 11402, 11405, and 11407, observed at 03:00 UT on **2012 January 23** by SDO/HMI is modeled with a five-level block-adaptive grid in spherical coordinates, where we reach a local resolution of pixel<sup>-1</sup> in an area of 790 Mm × 604 Mm. Local high spatial resolution and a large field of view in NLFFF modeling can be achieved simultaneously in parallel and block-adaptive magneto-frictional relaxations.

## MAGNETO-FRICTIONAL MODELING OF CORONAL NONLINEAR FORCE-FREE FIELDS. I. TESTING WITH ANALYTIC SOLUTIONS

Y. Guo<sup>1,2</sup>, C. Xia<sup>2</sup>, R. Keppens<sup>1,2</sup>, and G. Valori<sup>3</sup>

2016 ApJ 828 82

We report our implementation of the magneto-frictional method in the Message Passing Interface Adaptive Mesh Refinement Versatile Advection Code (MPI-AMRVAC). The method aims at applications where local adaptive mesh refinement (AMR) is essential to make follow-up dynamical modeling affordable. We quantify its performance in both domain-decomposed uniform grids and block-adaptive AMR computations, using all frequently employed force-free, divergence-free, and other vector comparison metrics. As test cases, we revisit the semi-analytic solution of Low and Lou in both Cartesian and spherical geometries, along with the topologically challenging Titov–Démoulin model. We compare different combinations of spatial and temporal discretizations, and find that the fourth-order central difference with a local Lax–Friedrichs dissipation term in a single-step marching scheme is an optimal combination. The initial condition is provided by the potential field, which is the potential field source surface model in spherical geometry. Various boundary conditions are adopted, ranging from fully prescribed cases where all boundaries are assigned with the semi-analytic models, to solar-like cases where only the magnetic field at the bottom is known. Our results demonstrate that all the metrics compare favorably to previous works in both Cartesian and spherical coordinates. Cases with several AMR levels perform in accordance with their effective resolutions. The magneto-frictional method in MPI-AMRVAC allows us to model a region of interest with high spatial resolution and large field of view simultaneously, as required by observation-constrained extrapolations using vector data provided with modern instruments. The applications of the magneto-frictional method to observations are shown in an accompanying paper.

## MODELING MAGNETIC FIELD STRUCTURE OF A SOLAR ACTIVE REGION CORONA USING NONLINEAR FORCE-FREE FIELDS IN SPHERICAL GEOMETRY

Y. Guo<sup>1,2</sup>, M. D. Ding<sup>1,2</sup>, Y. Liu<sup>3</sup>, X. D. Sun<sup>3</sup>, M. L. DeRosa<sup>4</sup>, and T. Wiegelmann

2012 ApJ 760 47

We test a nonlinear force-free field (NLFFF) optimization code in spherical geometry using an analytical solution from Low and Lou. Several tests are run, ranging from idealized cases where exact vector field data are provided on all boundaries, to cases where noisy vector data are provided on only the lower boundary (approximating the solar problem). Analytical tests also show that the NLFFF code in the spherical geometry performs better than that in the Cartesian one when the field of view of the bottom boundary is large, say, 20° × 20°. Additionally, we apply the NLFFF model to an active region observed by the Helioseismic and Magnetic Imager on board the Solar Dynamics Observatory (SDO) both before and after an M8.7 flare. For each observation time, we initialize the models using potential field source surface (PFSS) extrapolations based on either a synoptic chart or a flux-dispersal model, and compare the resulting NLFFF models. The results show that NLFFF extrapolations using the flux-dispersal model as the boundary condition have slightly lower, therefore better, force-free, and divergence-free metrics, and contain larger free magnetic energy. By comparing the extrapolated magnetic field lines with the extreme ultraviolet (EUV) observations by the Atmospheric Imaging Assembly on board SDO, we find that the NLFFF performs better than the PFSS not only for the core field of the flare productive region, but also for large EUV loops higher than 50 Mm.

## Driving Mechanism and Onset Condition of a Confined Eruption

Y. Guo<sup>1,2,3</sup>, M. D. Ding<sup>1,2</sup>, B. Schmieder<sup>3</sup>, H. Li<sup>4</sup>, T. Török<sup>3,5</sup>, T. Wiegelmann<sup>6</sup>

E-print, Nov 2010, ApJL., 725:L38–L42, 2010

We study a confined eruption accompanied by an M1.1 flare in solar active region (AR) NOAA 10767 on **2005 May 27**, where a pre-eruptive magnetic flux rope was reported in a nonlinear force-free field (NLFFF) extrapolation. The observations show a strong writhing motion of the erupting structure, suggesting that a flux rope was indeed present and converted some of its twist into writhe in the course of the eruption. Using the NLFFF extrapolation, we calculate the twist of the pre-eruptive flux rope and find that it is in very good agreement with thresholds of the helical kink instability found in numerical simulations. We conclude that the activation and rise of the flux rope were triggered and driven by the instability. Using a potential field extrapolation, we also estimate the height distribution of the decay index of the external magnetic field in the AR one hour prior to the eruption. We find that the decay index stays below the threshold for the torus instability for a significant height range above the erupting flux rope. This provides a possible explanation for the confinement of the eruption to the low corona.

### **3D MAGNETIC FIELD CONFIGURATION OF THE 2006 DECEMBER 13 FLARE EXTRAPOLATED WITH THE OPTIMIZATION METHOD**

Y. **Guo**, M. D. Ding, T. Wiegelmann, and H. Li

The Astrophysical Journal, 679:1629Y1635, **2008**

<http://www.journals.uchicago.edu/doi/pdf/10.1086/587684>

The photospheric vector magnetic field of the active region NOAA 10930 was obtained with the Solar Optical Telescope (SOT) on board the **Hinode** satellite with a very high spatial resolution (about 0.300). Observations of the two-ribbon flare on **2006 December 13** in this active region provide us a good sample to study the magnetic field configuration related to the occurrence of the flare. Using the optimization method for nonlinear force-free field (NLFFF) extrapolation proposed by Wheatland et al. and recently developed by Wiegelmann, we derive the three-dimensional (3D) vector magnetic field configuration associated with this flare. The general topology can be described as a highly sheared core field and a quasi-potential envelope arch field. The core field clearly shows some dips supposed to sustain a filament. Free energy release in the flare, calculated by subtracting the energy contained in the NLFFF and the corresponding potential field, is  $2.4 \times 10^{31}$  ergs, which is 2% of the preflare potential field energy. We also calculate the shear angles, defined as the angles between the NLFFF and potential field, and find that they become larger at some particular sites in the lower atmosphere, while they become significantly smaller in most places, implying that the whole configuration gets closer to the potential field after the flare. The Ca II H line images obtained with the Broadband Filter Imager (BFI) of the SOT and the 1600 Å images with the Transition Region and Coronal Explorer (TRACE) show that the preflare heating occurs mainly in the core field. These results provide evidence in support of the tether-cutting model of solar flares.

### **Probing the Fundamental Physics of the Solar Corona with Lunar Solar Occultation Observations**

S. Rifai **Habbal**, H. Morgan, M. Druckmüller, A. Ding, J. F. Cooper, A. Daw, E. C. Sittler Jr.

Solar Physics, July **2013**, Volume 285, Issue 1-2, pp 9-24

Imaging and spectroscopy of the solar corona, coupled with polarimetry, are the only tools available at present to capture signatures of physical processes responsible for coronal heating and solar wind acceleration within the first few solar radii above the solar limb. With the recent advent of improved detector technology and image processing techniques, broad-band white light and narrow-band multi-wavelength observations of coronal forbidden lines, made during total solar eclipses, have started to yield new views about the thermodynamic and magnetic properties of coronal structures. This paper outlines these unique capabilities, which until present, have been feasible primarily with observations during natural total solar eclipses. This work also draws attention to the exciting possibility of greatly increasing the frequency and duration of solar eclipse observations with Moon orbiting observatories utilizing lunar limb occultation of the solar disk for coronal measurements.

### **INFERRING THE CORONAL DENSITY IRREGULARITY FROM EUV SPECTRA**

M. **Hahn** and D. W. Savin

**2016** ApJ 829 42

Understanding the density structure of the solar corona is important for modeling both coronal heating and the solar wind. Direct measurements are difficult because of line-of-sight integration and possible unresolved structures. We present a new method for quantifying such structures using density-sensitive extreme ultraviolet line intensities to derive a density irregularity parameter, a relative measure of the amount of structure along the line of sight. We also present a simple model to relate the inferred irregularities to physical quantities, such as the filling factor and density contrast. For quiet-Sun regions and interplume regions of coronal holes, we find a density contrast of at least a factor of 3–10 and corresponding filling factors of about 10%–20%. Our results are in rough agreement with other estimates of the density structures in these regions. The irregularity diagnostic provides a useful relative measure of unresolved structure in various regions of the corona.

## Evidence for Wave Heating of the Quiet Sun Corona

Michael **Hahn**, Daniel Wolf Savin

ApJ, 795 111 2014

<http://arxiv.org/pdf/1407.3250v1.pdf>

We have measured the energy and dissipation of Alfvénic waves in the quiet Sun. A magnetic field was used to infer the location and orientation of the magnetic field lines along which the waves are expected to travel. The waves were measured using spectral lines to infer the wave amplitude. The waves cause a non-thermal broadening of the spectral lines, which can be expressed as a non-thermal velocity  $v_{nt}$ . By combining the spectroscopic measurements with this magnetic field model we were able to trace the variation of  $v_{nt}$  along the magnetic field. At the footpoints of the quiet Sun loops we find that waves inject an energy flux in the range of  $1.2\text{--}5.2 \times 10^5 \text{ erg cm}^{-2} \text{ s}^{-1}$ . At the minimum of this range, this amounts to more than 80% of the energy needed to heat the quiet Sun. We also find that these waves are dissipated over a region centered on the top of the loops. The position along the loop where the damping begins is strongly correlated with the length of the loop, implying that the damping mechanism depends on the global loop properties rather than on local collisional dissipation.

## Comparative Study of a Sunspot at Two Different Instances of Time

Hashem **Hamedivafa**

*Solar Physics* volume 295, Article number: 60 (2020)

<https://link.springer.com/content/pdf/10.1007/s11207-020-01627-x.pdf>

We investigate the evolutionary effects on the brightness of a sunspot as well as on the properties of its fine-structures using two sets of time series of G-band images of a single sunspot in NOAA 10944 recorded at two symmetric locations on the solar disc by Hinode/SOT (Solar Optical Telescope). The second time series (phase W) was recorded 2.5 d after recording the first time series (phase E). Both time series of images were corrected for instrumental stray light; then the p-mode oscillations were removed. Our analysis demonstrates that the spatially and temporally averaged intensities of the umbra as well as the penumbra in both phases are practically the same. Nevertheless, considering only intensities smaller than  $1.0 I_{phIph}$  the penumbra in the phase W is brighter with a contrast of 2 per cent. However, the ratio of the peak intensities of penumbral grains to their background intensities decreases, on average, from 2.9 to 2.6 from phase E to phase W. The penumbra is on average, 6.9 times brighter than the umbra in both phases. The umbra gets smaller in size with a ratio of 0.90 and its magnetic field strength decreases about 200 G after the 2.5 d evolution. Although the central umbral dots (UDs) with lifetimes longer than 2 min are by the factor of 1.6 more frequent in phase E, the most of the physical and kinematic properties of UD do not show considerable changes after the sunspot evolution at this 2.5 d time interval. The registered UD have intensities smaller than  $0.84 I_{phIph}$  with a mean intensity of about  $0.29 I_{phIph}$ . The equivalent diameters of the individual UD have a symmetric distribution around 180 km with a standard deviation about 35 km. The brightest UD show a constant median diameter. The UD registered in both phases have a mean lifetime of 7.4 min. Our results suggest that UD with a certain lifetime have an admissible lower limit for their mean size which grows with lifetime. The proper motions of UD show velocities less than  $1.0 \text{ km s}^{-1}$  with a maximum population around  $0.2 \text{ km s}^{-1}$ . The UD formed in the phase W are faster when the umbral area is smaller and the magnetic field is weaker. **2007 February 27...**

## A study on Ca II 854.2 nm emission in a sunspot umbra using a thin cloud model

H. **Hamedivafa**, M. Sobotka, L. Bellot Rubio, S. Esteban Pozuelo

Iranian Journal of Astronomy and Astrophysics (IJAA) Vol. 3, No. 1, 2016

<https://arxiv.org/pdf/1612.06636v1.pdf>

In the present work, we introduce and explain a method of solution of the radiative transfer equation based on a thin cloud model. The efficiency of this method to retrieve dynamical chromospheric parameters from Stokes I profiles of Ca II 854.2 nm line showing spectral emission is investigated. The analyzed data were recorded with the Crisp Imaging Spectro-Polarimeter (CRISP) at Swedish 1-m Solar Telescope on La Palma on **2012 May 5** between 8:11 - 9:00 UT. The target was a large decaying sunspot (NOAA 11471) at heliocentric position W 15 deg S 19 deg. This sunspot has a large umbra divided into two umbral cores (UCs). One of these UCs shows steady spectral emission in both Ca II 854.2 nm and H-alpha lines, where downflows prevail. The other UC shows intermittent spectral emission only in Ca II 854.2 nm, when umbral flashes are propagating. The statistics of the obtained Doppler velocities in both UCs is discussed.

## Evaluation of Sunspot Areas Derived by Automated Sunspot-Detection Methods

**Yoichiro Hanaoka**

*Solar Phys.* Volume 299, article number 156, (2024)

<https://arxiv.org/pdf/2411.00415>

Sunspot-area measurements using digital images captured by two telescopes at the Mitaka campus of the National Astronomical Observatory of Japan are conducted using automated sunspot detection. A comparison between sunspot areas derived from Mitaka and those from the reference data by Mandal et al. (Astron. Astrophys. 640, A78, 2020), who compiled a cross-calibrated daily sunspot-area catalog, revealed that the correlation coefficients between them are high (0.96–0.97), whereas the areas in the Mitaka data are 70%–83% of those of Mandal et al. The correlation is limited by the differences in observation times and detection capabilities of spots near the limb, with discrepancies in areas arising from different definitions of spot outlines. Given the high correlation and the ease of calibrating area discrepancies with a correction factor, automated sunspot detection appears promising for future sunspot-area measurements. Furthermore, we addressed the measurements of brightness deficit caused by sunspots.

## **Automated Sunspot Detection as an Alternative to Visual Observations**

[Yoichiro Hanaoka](#)

Solar Phys. 297, Article number: 158 2022

<https://arxiv.org/pdf/2211.13552>

<https://doi.org/10.1007/s11207-022-02089-z>

We developed an automated method for sunspot detection using digital white-light solar images to achieve a performance similar to that of visual drawing observations in sunspot counting. To identify down to small, isolated spots correctly, we pay special attention to the accurate derivation of the quiet-disk component of the Sun, which is used as a reference to identify sunspots using a threshold. This threshold is determined using an adaptive method to process images obtained under various conditions. To eliminate the seeing effect, our method can process multiple images taken within a short time. We applied the developed method to digital images captured at three sites and compared the detection results with those of visual observations. We conclude that the proposed sunspot detection method has a similar performance to that of visual observation. This method can be widely used by public observatories and amateurs as well as professional observatories as an alternative to hand-drawn visual observation for sunspot counting.

## **Polarization of the Corona Observed During the 2017 and 2019 Total Solar Eclipses**

[Yoichiro Hanaoka](#), [Yoshiaki Sakai](#), [Koichi Takahashi](#)

Solar Phys. 296, Article number: 158 2021

<https://arxiv.org/pdf/2109.12263.pdf>

<https://link.springer.com/content/pdf/10.1007/s11207-021-01907-0.pdf>

<https://doi.org/10.1007/s11207-021-01907-0>

We carried out polarimetric observations of the white-light corona during the total solar eclipses that occurred on **2017 August 21 and 2019 July 2**, and successfully obtained data at two different sites for both eclipses. After eliminating the sky background, we derived the brightness, polarization brightness, and degree of the polarization of the K+F corona from just above the limb to approximately  $4 R_{\odot}$ . Furthermore, we isolated the K- and F-corona with plausible degree of polarization of the K-corona. The field of view covering up to approximately  $4 R_{\odot}$  enabled us to compare the derived brightness and polarization with a wide range of other observations. The results of the comparison show significant scatter; while some of the observations present very good coincidence with our results, the other ones exhibit systematic discrepancy.

## **HEMISPHERIC HELICITY TREND FOR SOLAR CYCLE 24**

Juan [Hao](#) and Mei Zhang

2011 ApJ 733 L27

Using vector magnetograms obtained with the Spectro-polarimeter (SP) on board Hinode satellite, we studied two helicity parameters (local twist and current helicity) of 64 active regions that occurred in the descending phase of solar cycle 23 and the ascending phase of solar cycle 24. Our analysis gives the following results. (1) The 34 active regions of the solar cycle 24 follow the so-called hemispheric helicity rule, whereas the 30 active regions of the solar cycle 23 do not. (2) When combining all 64 active regions as one sample, they follow the hemispheric helicity sign rule as in most other observations. (3) Despite the so-far most accurate measurement of vector magnetic field given by SP/Hinode, the rule is still weak with large scatters. (4) The data show evidence of different helicity signs between strong and weak fields, confirming previous result from a large sample of ground-based observations. (5) With two example sunspots we show that the helicity parameters change sign from the inner umbra to the outer penumbra, where the sign of penumbra agrees with the sign of the active region as a whole. From these results, we speculate that both the  $\Sigma$ -effect (turbulent convection) and the dynamo have contributed in the generation of helicity, whereas in both cases turbulence in the convection zone has played a significant role.

## **The source of unusual coronal upflows with photospheric abundance in a solar active region★**

L. K. **Harra**<sup>1,2</sup>, C. H. Mandrini<sup>3</sup>, D. H. Brooks<sup>4</sup>, K. Barczynski<sup>1,2</sup>, C. Mac Cormack, +++  
A&A 675, A20 (2023)  
<https://www.aanda.org/articles/aa/pdf/2023/07/aa45747-22.pdf>

*Context.* Upflows in the corona are of importance, as they may contribute to the solar wind. There has been considerable interest in upflows from active regions (ARs). The coronal upflows that are seen at the edges of active regions have coronal elemental composition and can contribute to the slow solar wind. The sources of the upflows have been challenging to determine because they may be multiple, and the spatial resolution of previous observations is not yet high enough.

*Aims.* In this article, we analyse coronal upflows in AR 12960 that are unusually close to the sunspot umbra. We analyse their properties, and we attempt to determine if it is possible that they feed into the slow solar wind.

*Methods.* We analysed the activity in the upflow region in detail using a combination of Solar Orbiter EUV images at high spatial and temporal resolution, Hinode/EUV Imaging Spectrometer data, and observations from instruments on board the Solar Dynamics Observatory. This combined dataset was acquired during the first Solar Orbiter perihelion of the science phase, which provided a spatial resolution of 356 km for two pixels. Doppler velocity, density, and plasma composition determinations, as well as coronal magnetic field modelling, were carried out to understand the source of the upflows.

*Results.* We observed small magnetic fragments, called moving magnetic features (MMFs), moving away from the sunspot in the active region. Specifically, they moved towards the sunspot from the edge of the penumbra where a small positive polarity connects to the umbra via small-scale and very dynamic coronal loops. At this location, small dark grains are evident and flow along penumbral filaments in continuum images. The magnetic field modelling showed small low-lying loops anchored close to the umbral magnetic field. The high-resolution data of the Solar Orbiter EUV Imagers showed the dynamics of these small loops, which last on time scales of only minutes. The edges of these small loops are the location of the coronal upflow that has photospheric abundance. **7 Mar 2022**

## **NON-THERMAL RESPONSE OF THE CORONA TO THE MAGNETIC FLUX DISPERSAL IN THE PHOTOSPHERE OF A DECAYING ACTIVE REGION**

L. K. **Harra**<sup>1</sup> and V. I. Abramenko  
**2012 ApJ 759 104**

We analyzed Solar Dynamics Observatory line-of-sight magnetograms for a decaying NOAA active region (AR) 11451 along with co-temporal Extreme-Ultraviolet Imaging Spectrometer (EIS) data from the Hinode spacecraft. The photosphere was studied via time variations of the turbulent magnetic diffusivity coefficient,  $\eta(t)$ , and the magnetic power spectrum index,  $\alpha$ , through analysis of magnetogram data from the Helioseismic and Magnetic Imager (HMI). These measure the intensity of the random motions of magnetic elements and the state of turbulence of the magnetic field, respectively. The time changes of the non-thermal energy release in the corona was explored via histogram analysis of the non-thermal velocity,  $v_{nt}$ , in order to highlight the largest values at each time, which may indicate an increase in energy release in the corona. We used the 10% upper range of the histogram of  $v_{nt}$  (which we called  $V_{upp\ nt}$ ) of the coronal spectral line of Fe XII 195 Å. A 2 day time interval was analyzed from HMI data, along with the EIS data for the same field of view. Our main findings are the following. (1) The magnetic turbulent diffusion coefficient,  $\eta(t)$ , precedes the upper range of the  $v_{nt}$  with the time lag of approximately 2 hr and the cross-correlation coefficient of 0.76. (2) The power-law index,  $\alpha$ , of the magnetic power spectrum precedes  $V_{upp\ nt}$  with a time lag of approximately 3 hr and the cross-correlation coefficient of 0.5. The data show that the magnetic flux dispersal in the photosphere is relevant to non-thermal energy release dynamics in the above corona. The results are consistent with the nanoflare mechanism of the coronal heating, due to the time lags being consistent with the process of heating and cooling the loops heated by nanoflares.

See EIS Nugget for October 2012 [http://msslxr.mssl.ucl.ac.uk:8080/SolarB/nuggets/nugget\\_2012oct.jsp](http://msslxr.mssl.ucl.ac.uk:8080/SolarB/nuggets/nugget_2012oct.jsp)

## **VARIATIONS IN THE AXISYMMETRIC TRANSPORT OF MAGNETIC ELEMENTS ON THE SUN: 1996-2010**

David H. **Hathaway** and Lisa Rightmire  
**2011 ApJ 729 80**

We measure the axisymmetric transport of magnetic flux on the Sun by cross-correlating narrow strips of data from line-of-sight magnetograms obtained at a 96 minute cadence by the MDI instrument on the ESA/NASA SOHO spacecraft and then averaging the flow measurements over each synodic rotation of the Sun. Our measurements indicate that the axisymmetric flows vary systematically over the solar cycle. The differential rotation is weaker at maximum than at minimum. The meridional flow is faster at minimum and slower at maximum. The meridional flow speed on the approach to the Cycle 23/24 minimum was substantially faster than it was at the Cycle 22/23 minimum. The average latitudinal profile is largely a simple sinusoid that extends to the poles and peaks at about 35° latitude. As the cycle progresses, a pattern of inflows toward the sunspot zones develops and moves



equatorward in step with the sunspot zones. These inflows are accompanied by the torsional oscillations. This association is consistent with the effects of the Coriolis force acting on the inflows. The equatorward motions associated with these inflows are identified as the source of the decrease in net poleward flow at cycle maxima. We also find polar counterflows (equatorward flow at high latitudes) in the south from 1996 to 2000 and in the north from 2002 to 2010. We show that these measurements of the flows are not affected by the nonaxisymmetric diffusive motions produced by supergranulation.

### **The Nonpotentiality of Steady-state Coronal Magnetic Field Derived with Time-relaxation Magnetohydrodynamics Simulations Using Helioseismic and Magnetic Imager Three-component Magnetic Field Data**

Keiji [Hayashi](#)<sup>1</sup>, Chin-Chun Wu<sup>2</sup>, and Kan Liou<sup>3</sup>

2022 ApJ 940 82

<https://iopscience.iop.org/article/10.3847/1538-4357/ac9b25/pdf>

The steady states of the coronal magnetic field obtained with the magnetohydrodynamic (MHD) time-relaxation simulation model are examined. Our electric-field-driven model can introduce the three components of the solar surface magnetic field data maps as the boundary values of an MHD simulation, without violating the divergence-free condition of the magnetic field. The magnetic field in the simulated steady-state solar corona exhibits substantial nonpotentiality in the closed-field streamers. A few choices are allowed in our model, such as the criteria for determining whether or not the horizontal components at the weak-field region are included. The initial magnetic field configuration can be arbitrarily determined. In this work, we examined the differences between the steady states obtained with the information on the horizontal components and with several choices of the simulation setting, and compared the new steady states with those obtained without using the horizontal magnetic field components. We found that nonpotential magnetic structures in the derived steady states well correspond to the observed solar filament structures during a selected period of Carrington Rotation 2106. The difference in the steady state with different boundary treatments is found to be large. The difference caused by the initial magnetic configuration is found to be small. **2011 January 20 - February 16**

### **Comparison of Potential Field Solutions for Carrington Rotation 2144†**

Keiji [Hayashi](#), Shangbin Yang, Yuagyong Deng

JGR Volume 121, Issue 2 Pages 1046–1061 **2016**

We examined differences among the coronal magnetic field structures derived with the PFSS model for Carrington Rotation 2144, from **2013 November 21 to December 19**. We used the synoptic maps of solar photospheric magnetic field from four observatories, the HSOS, GONG, HMI and WSO. We tested two smoothing methods, Gaussian and boxcar averaging, and correction of unbalanced net magnetic flux. The solutions of three-dimensional coronal magnetic field are significantly different each other. An open-field region derived with HSOS data agree best the corresponding coronal hole observed by SDO/AIA, while HMI data yielded best agreements with the near-Earth OMNI database. The GONG data overall gave agreements as good as the HMI. The PFSS calculations using WSO data were least sensitive to the choices we examined in this work. Differences in PFSS solutions using different choices and parameters in smoothing imply that the photospheric magnetic-field distributions with size of several degrees at middle and low latitude regions can be decisive, at least, in the examined period. For better determine the global solar corona, therefore, further evaluation of influences from compact bipolar magnetic field is needed.

### **The Helioseismic and Magnetic Imager (HMI) Vector Magnetic Field Pipeline: Magnetohydrodynamics Simulation Module for the Global Solar Corona**

Keiji [Hayashi](#), [J. Todd Hoeksema](#), [Yang Liu](#), [Monica G. Bobra](#), [Xudong D. Sun](#), [Aimee A. Norton](#)

Solar Phys. May 2015, Volume 290, [Issue 5](#), pp 1507-1529, **2015**

<http://arxiv.org/pdf/1504.05217v1.pdf>

Time-dependent three-dimensional magnetohydrodynamics (MHD) simulation modules are implemented at the Joint Science Operation Center (JSOC) of Solar Dynamics Observatory (SDO). The modules regularly produce three-dimensional data of the time-relaxed minimum-energy state of the solar corona using global solar-surface magnetic-field maps created from Helioseismic Magnetic Imager (HMI) full-disk magnetogram data. With the assumption of polytropic gas with specific heat ratio of 1.05, three types of simulation products are currently generated: i) simulation data with medium spatial resolution using the definitive calibrated synoptic map of the magnetic field with a cadence of one Carrington rotation, ii) data with low spatial resolution using the definitive version of the synchronic frame format of the magnetic field, with a cadence of one day, and iii) low-resolution data using near-real-time (NRT) synchronic format of the magnetic field on daily basis. The MHD data available in the JSOC database are three-dimensional, covering heliocentric distances from 1.025 to 4.975 solar radii, and contain all

eight MHD variables: the plasma density, temperature and three components of motion velocity, and three components of the magnetic field. This article describes details of the MHD simulations as well as the production of the input magnetic-field maps, and details of the products available at the JSOC database interface. In order to assess the merits and limits of the model, we show the simulated data in early 2011 and compare with the actual coronal features observed by the Atmospheric Imaging Assembly (AIA) and the near-Earth in-situ data. **Dec 2010-March 2011 , 1 January 2014.**

### **MHD simulations of the global solar corona around the Halloween event in 2003 using the synchronic frame format of the solar photospheric magnetic field**

Keiji **Hayashi**, Xue Pu Zhao, Yang Liu

JOURNAL OF GEOPHYSICAL RESEARCH, VOL. 113, A07104, doi:10.1029/2007JA012814, **2008**

<http://dx.doi.org/10.1029/2007JA012814>

We performed two time-relaxation magnetohydrodynamics (MHD) simulations of the solar corona: one uses the boundary map representing the solar surface magnetic field distribution before the **Halloween event in 2003**, and the other uses map representing the postevent distribution. The aims of this study are to test a new concept of a solar surface magnetic field map capable of representing a particular time of interest and to examine the coronal responses to the solar photospheric magnetic field changes occurring over a few days. We used a new mapping scheme named “synchronic frame” that can include the longitudinal shift caused by the solar differential rotation and the solar surface variations occurring at the time of interest. These two time-relaxation MHD simulations using the two maps are separately performed to numerically obtain the quasi steady states of the solar corona before and after the Halloween event. Comparisons of the simulated coronal magnetic field structures to the SOHO/EIT measurements show that the combinations of our mapping method and simulation model reproduce the changes of the coronal structures well. We also find that the consequences of solar surface variations can be seen in the plasma quantities in the solar corona. These results show the capability and importance of the solar surface magnetic field mapping scheme for better reconstruction of global coronal structures, parts of which are sensitive to the solar surface magnetic field variations.

### **Exploring the Origin and Dynamics of Solar Magnetic Fields**

Soumitra **Hazra**

PhD Thesis, IISER Kolkata, **2015**

<http://arxiv.org/pdf/1604.00563v1.pdf>

The Sun is a magnetically active star and is the source of the solar wind, electromagnetic radiation and energetic particles which affect the heliosphere and the Earth's atmosphere. The magnetic field of the Sun is responsible for most of the dynamic activity of the Sun. This thesis research seeks to understand solar magnetic field generation and the role that magnetic fields play in the dynamics of the solar atmosphere. Specifically, this thesis focuses on two themes: in the first part, we study the origin and behaviour of solar magnetic fields using magnetohydrodynamic dynamo theory and modelling, and in the second part, utilizing observations and data analysis we study two major problems in solar physics, namely, the coronal heating problem and initiation mechanisms of solar flares.

### **Relationship Between Solar Coronal X-Ray Brightness and Active Region Magnetic Fields: A Study Using High Resolution Observations**

Soumitra **Hazra**, Dibyendu Nandy, B Ravindra

Solar Phys. **2015**

<http://arxiv.org/pdf/1406.1683v1.pdf>

By utilizing high resolution observations of nearly co-temporal and co-spatial SOT spectropolarimeter and XRT coronal X-ray data onboard Hinode, we revisit the contentious issue of the relationship between global magnetic quantities and coronal X-ray intensity. Co-aligned vector magnetogram and X-ray data are used for this study. We find that there is no pixel-to-pixel correlation between the observed loop brightness and magnetic quantities. However, the X-ray brightness is well correlated with the integrated magnetic quantities such as total unsigned magnetic flux, total unsigned vertical current, area integrated square of the vertical magnetic field and horizontal magnetic fields. Comparing all these quantities we find that the total magnetic flux correlates well with the observed integrated X-ray brightness, though there is some differences in the strength of the correlation when we use the X-ray data from different filters. While we get a good correlation between X-ray brightness and total unsigned vertical current when we use the X-ray data sets obtained from the Al-poly filter, we find no correlation between them using data sets obtained from the Ti-poly filter. We confirm that there is no consistent correlation between measures of non-potentiality and coronal X-ray intensity in these high resolution observations; thus earlier results using low resolution observations in this context are validated. We discuss the implications of these observational results for the heating of the solar corona. **30.08.2011, 13.09.2011, 28.09.2011, 28.11.2011, 01.02.2012, 16.08.2012, 25.09.2012, 02.10.2012, 28.10.2012, 17.11.2012.**

## Coronal Magnetic Field Extrapolation and Topological Analysis of Fine-Scale Structures during Solar Flare Precursors

[Wen He](#), [Qiang Hu](#), [Ju Jing](#), [Haimin Wang](#), [Chaowei Jiang](#), [Sushree S. Nayak](#), [Aviyeet Prasad](#)

ApJ **958** 90 **2023**

<https://arxiv.org/pdf/2306.03226.pdf>

<https://iopscience.iop.org/article/10.3847/1538-4357/ad0236/pdf>

Magnetic field plays an important role in various solar eruptions like flares, coronal mass ejections, etc. The formation and evolution of characteristic magnetic field topology in solar eruptions are critical problems that will ultimately help us understand the origination of these eruptions in the solar source regions. With the development of advanced techniques and instruments, observations with higher resolutions in different wavelengths and fields of view have provided more quantitative information for finer structures. So it is essential to improve our method to study the magnetic field topology in the solar source regions by taking advantage of high-resolution observations. In this study, we employ a nonlinear force-free field (NLFFF) extrapolation method based on a nonuniform grid setting for an M-class flare eruption event (SOL2015-06-22T17:39) with embedded magnetograms from the Solar Dynamics Observatory (SDO) and the Goode Solar Telescope (GST). The extrapolation results employing the embedded magnetogram for the bottom boundary are obtained by maintaining the native resolutions of the corresponding GST and SDO magnetograms. We compare the field line connectivity with the simultaneous GST/H $\alpha$  and SDO/AIA observations for fine-scale structures associated with precursor brightenings. Then we perform a topological analysis of the field line connectivity corresponding to fine-scale magnetic field structures based on the extrapolation results. The results indicate that by combining the high-resolution GST magnetogram with a larger HMI magnetogram, the derived magnetic field topology is consistent with a scenario of magnetic reconnection among sheared field lines across the main polarity inversion line during solar flare precursors.

## Variations of the 3-D coronal magnetic field associated with the X3.4-class solar flare event of AR 10930

Han [He](#)<sup>1,2</sup>, Huaning Wang<sup>1</sup>, Yihua Yan<sup>1</sup>, P. F. Chen<sup>2,3</sup> and Cheng Fang

JGR, Volume 119, Issue 5, pages 3286–3315, May 2014

The variations of the 3-D coronal magnetic fields associated with the X3.4-class flare of active region 10930 are studied in this paper. The coronal magnetic field data are reconstructed from the photospheric vector magnetograms obtained by the Hinode satellite and using the nonlinear force-free field extrapolation method developed in our previous work (He et al., 2011). The 3-D force-free factor  $\alpha$ , 3-D current density, and 3-D magnetic energy density are employed to analyze the coronal data. The distributions of  $\alpha$  and current density reveal a prominent magnetic connectivity with strong negative  $\alpha$  values and strong current density before the flare. This magnetic connectivity extends along the main polarity inversion line and is found to be totally broken after the flare. The distribution variation of magnetic energy density reveals the redistribution of magnetic energy before and after the flare. In the lower space of the modeling volume the increase of magnetic energy dominates, and in the higher space the decrease of energy dominates. The comparison with the flare onset imaging observation exhibits that the breaking site of the magnetic connectivity and site with the highest values of energy density increase coincide with the location of flare initial eruption. We conclude that a cramped positive  $\alpha$  region appearing in the photosphere causes the breaking of the magnetic connectivity. A scenario for flare initial eruption is proposed in which the Lorentz force acting on the isolated electric current at the magnetic connectivity breaking site lifts the associated plasmas and causes the initial ejection. **Dec 2006**

## Nonlinear force-free field extrapolation of the coronal magnetic field using the data obtained by the Hinode satellite

[He](#), Han; Wang, Huaning; Yan, Yihua

J. Geophys. Res., Vol. 116, No. A1, A01101, 2011

E-print, Dec 2011

The Hinode satellite can obtain high-quality photospheric vector magnetograms of solar active regions and the simultaneous coronal loop images in soft X-ray and extreme ultraviolet (EUV) bands. In this paper, we continue the work of He and Wang (2008) and apply the newly developed upward boundary integration computational scheme for the nonlinear force-free field (NLFFF) extrapolation of the coronal magnetic field to the photospheric vector magnetograms acquired by the Spectro-Polarimeter of the Solar Optical Telescope aboard Hinode. Three time series vector magnetograms of the same solar active region, NOAA 10930, are selected for the NLFFF extrapolations, which were observed within the time interval of 26 h during 10–11 December 2006 when the active region crossed the central area of the Sun's disk. Parallel computation of the NLFFF extrapolation code was realized through OpenMP multithreaded, shared memory parallelism and Fortran 95 programming language for the extrapolation calculations. The comparison between the extrapolated field lines and the coronal loop images obtained by the X-Ray Telescope and the EUV Imaging Spectrometer of Hinode shows that, in the central area of the active region, the field line configurations generally agree with the coronal images, and the orientations of the field lines basically

coincide with the coronal loop observations for all three successive magnetograms. This result supports the NLFFF model being used for tracing the time series evolution of the 3-D coronal magnetic structures as the responses of the quasi-equilibrium solar atmosphere to the vector magnetic field changes in the photosphere.

## **Reconfiguration of the coronal magnetic field by means of reconnection driven by photospheric magnetic flux convergence**

J.-S. He<sup>1</sup>, E. Marsch<sup>1</sup>, C.-Y. Tu<sup>2</sup>, H. Tian<sup>1,2</sup> and L.-J. Guo

*A&A* 510, A40 (2010)

*Context.* Magnetic reconnection is commonly believed to be responsible for flare-like events and plasma ejections in the solar atmosphere, but the field-line reconfiguration observed in association with magnetic reconnection has rarely been observed before.

*Aims.* We attempt to reconstruct the configuration of the magnetic field during a magnetic reconnection event, estimate the reconnection rate, and analyze the resulting X-ray burst and plasma ejection.

*Methods.* We use the local-correlation-tracking (LCT) method to track the convergence of magnetic fields with opposite polarities using photospheric observations from SOT/Hinode. The magnetic field lines are then extrapolated from the tracked footpoint positions into the corona, and the changes in field-line connections are marked. We estimate the reconnection rate by calculating the convective electric field in the photosphere, which is normalized to the product of the plasma jet speed and the coronal magnetic field strength inside the inflow region. The observed X-ray burst and plasma ejection are analysed with data from XRT/Hinode and TRACE, respectively.

*Results.* We find that in this reconnection event the two sets of approaching closed loops were reconfigured to a set of superimposed large-scale closed loops and another set of small-scale closed loops. Enhanced soft X-ray emission was seen to rapidly fill the reconnected loop after the micro-flare occurred at the reconnection site. Plasma was ejected from that site with a speed between 27 and 40 km s<sup>-1</sup>. The reconnection rate is estimated to range between 0.03 and 0.09.

*Conclusions.* Our work presents a study of the magnetic field reconfiguration owing to magnetic reconnection driven by flux convergence in the photosphere. This observation of the magnetic structure change is helpful for future diagnosis of magnetic reconnection. The results obtained for the reconnection rate, the X-ray emission burst, and the plasma ejection provides new observational evidence, and places constraints on future theoretical study of magnetic reconnection in the Sun.

## **Nonlinear force-free coronal magnetic field extrapolation scheme based on the direct boundary integral formulation**

Han He, Huaning Wang

*JOURNAL OF GEOPHYSICAL RESEARCH*, VOL. 113, A05S90, doi:10.1029/2007JA012441, 2008

The boundary integral equation (BIE) method was first proposed by Yan and Sakurai (2000) and used to extrapolate the nonlinear force-free magnetic field in the solar atmosphere. Recently, Yan and Li (2006) improved the BIE method and proposed the direct boundary integral equation (DBIE) formulation, which represents the nonlinear force-free magnetic field by direct integration of the magnetic field on the bottom boundary surface. On the basis of this new method, we devised a practical calculation scheme for the nonlinear force-free field extrapolation above solar active regions. The code of the scheme was tested by the analytical solutions of Low and Lou (1990) and was applied to the observed vector magnetogram of solar active region NOAA 9077. The results of the calculations show that the improvement of the new computational scheme to the scheme of Yan and Li (2006) is significant, and the force-free and divergence-free constraints are well satisfied in the extrapolated fields. The calculated field lines for NOAA 9077 present the X-shaped structure and can be helpful for understanding the magnetic configuration of the filament channel as well as the magnetic reconnection process during the Bastille Day flare on 14 July 2000.

## **Umbral chromospheric fine structure and umbral flashes modelled as one: the corrugated umbra**

Vasco M. J. Henriques, Chris J. Nelson, Luc H. M. Rouppe van der Voort, Mihalis Mathioudakis

*A&A* 642, A215 2020

<https://arxiv.org/pdf/2008.05482.pdf>

<https://doi.org/10.1051/0004-6361/202038538>

<https://sci-hub.st/https://www.aanda.org/articles/aa/abs/2020/10/aa38538-20/aa38538-20.html>

Small-scale umbral brightenings (SSUBs), umbral microjets, spikes or short dynamic fibrils (SDFs), and umbral dark fibrils are found in any observation of the chromosphere with sufficient spatial resolution. We study the spatial and spectral co-evolution of SDFs, SSUBs, and umbral flashes in Ca II 8542 spectral profiles. We produce models that generate the spectral profiles for all classes of features using non-LTE radiative transfer with a recent version of the NICOLE inversion code. We find that both bright (SSUBs) and dark (SDFs) structures are described with a

continuous feature in the parameter space that is distinct from the surroundings even in pixel-by-pixel inversions. We find a phase difference between such features and umbral flashes in both inverted line-of-sight velocities and timing of the brightenings. For umbral flashes themselves we resolve, for the first time in inversion-based semi-empirical modelling, the pre-flash downflows, post-flash upflows, and the counter-flows present during the umbral flash phase. We further present a simple time-dependent cartoon model that explains the dynamics and spectral profiles of both fine structure, dark and bright, and umbral flashes in umbral chromospheres. Conclusions. The similarity of the profiles between the brightenings and umbral flashes, the pattern of velocities obtained from the inversions, and the phase relationships between the structures all lead us to put forward that all dynamic umbral chromospheric structures observed to this date are a locally delayed or locally early portion of the oscillatory flow pattern that generates flashes, secondary to the steepening large-scale acoustic waves at its source. Essentially, SSUBs are part of the same shock or merely compression front responsible for the spatially larger umbral flash phenomenon, but out of phase with the broader oscillation. **28 July 2014**

## **A Hot Downflowing Model Atmosphere For Umbral Flashes And The Physical Properties Of Their Dark Fibrils**

Vasco M. J. [Henriques](#), Michail Mathioudakis, Hector Socas-Navarro, Jaime de la Cruz Rodriguez

ApJ **845** 102 **2017**

<https://arxiv.org/pdf/1706.05311.pdf>

We perform NLTE inversions in a large set of umbral flashes, including the dark fibrils visible within them, and in the quiescent umbra by using the inversion code NICOLE on a set of full Stokes high-resolution Ca II 8542 Å observations of a sunspot at disk center. We find that the dark structures have Stokes profiles that are distinct from those of the quiescent and flashed regions. They are best reproduced by atmospheres that are more similar to the flashed atmosphere in terms of velocities, even if with reduced amplitudes. We also find two sets of solutions that finely fit the flashed profiles: a set that is upflowing, featuring a transition region that is deeper than in the quiescent case and preceded by a slight dip in temperature, and a second solution with a hotter atmosphere in the chromosphere but featuring downflows close to the speed of sound at such heights. Such downflows may be related, or even dependent, on the presence of coronal loops, rooted in the umbra of sunspots, as is the case in the region analyzed. Similar loops have been recently observed to have supersonic downflows in the transition region and are consistent with the earlier "sunspot plumes" which were invariably found to display strong downflows in sunspots. Finally we find, on average, a magnetic field reduction in the flashed areas, suggesting that the shock pressure is moving field lines in the upper layers.

## **Stable umbral chromospheric structures★**

V. M. J. [Henriques](#)<sup>1</sup>, E. Scullion<sup>2</sup>, M. Mathioudakis<sup>1</sup>, D. Kiselman<sup>3</sup>, P. T. Gallagher<sup>2</sup> and F. P. Keena  
A&A 574, A131 (2015)

**Aims.** We seek to understand the morphology of the chromosphere in sunspot umbra. We investigate if the horizontal structures observed in the spectral core of the Ca ii H line are ephemeral visuals caused by the shock dynamics of more stable structures, and examine their relationship with observables in the H-alpha line.

**Methods.** Filtergrams in the core of the Ca ii H and H-alpha lines as observed with the Swedish 1-m Solar Telescope are employed. We utilise a technique that creates composite images and tracks the flash propagation horizontally.

**Results.** We find 0.15 wide horizontal structures, in all of the three target sunspots, for every flash where the seeing is moderate to good. Discrete dark structures are identified that are stable for at least two umbral flashes, as well as systems of structures that live for up to 24 min. We find cases of extremely extended structures with similar stability, with one such structure showing an extent of 5". Some of these structures have a correspondence in H-alpha, but we were unable to find a one-to-one correspondence for every occurrence. If the dark streaks are formed at the same heights as umbral flashes, there are systems of structures with strong departures from the vertical for all three analysed sunspots.

**Conclusions.** Long-lived Ca ii H filamentary horizontal structures are a common and likely ever-present feature in the umbra of sunspots. If the magnetic field in the chromosphere of the umbra is indeed aligned with the structures, then the present theoretical understanding of the typical umbra needs to be revisited.

## **Data Assimilation in the ADAPT Photospheric Flux Transport Model**

Kyle S. [Hickmann](#), Humberto C. Godinez, Carl J. Henney, C. Nick Arge

[Solar Physics](#) April 2015, Volume 290, [Issue 4](#), pp 1105-1118

Global maps of the solar photospheric magnetic flux are fundamental drivers for simulations of the corona and solar wind and therefore are important predictors of geoeffective events. However, observations of the solar photosphere are only made intermittently over approximately half of the solar surface. The Air Force Data Assimilative Photospheric Flux Transport (ADAPT) model uses localized ensemble Kalman filtering techniques to adjust a set of photospheric simulations to agree with the available observations. At the same time, this information is propagated to areas of the simulation that have not been observed. ADAPT implements a local ensemble transform Kalman

filter (LETKF) to accomplish data assimilation, allowing the covariance structure of the flux-transport model to influence assimilation of photosphere observations while eliminating spurious correlations between ensemble members arising from a limited ensemble size. We give a detailed account of the implementation of the LETKF into ADAPT. Advantages of the LETKF scheme over previously implemented assimilation methods are highlighted.

### **Eigenmodes of three-dimensional magnetic arcades in the Sun's corona**

Bradley W. [Hindman](#), Rekha Jain

2015

<http://arxiv.org/pdf/1511.09411v1.pdf>

We develop a model of coronal-loop oscillations that treats the observed bright loops as an integral part of a larger 3-D magnetic structure comprised of the entire magnetic arcade. We demonstrate that magnetic arcades within the solar corona can trap MHD fast waves in a 3-D waveguide. This is accomplished through the construction of a cylindrically symmetric model of a magnetic arcade with a potential magnetic field. For a magnetically dominated plasma, we derive a governing equation for MHD fast waves and from this equation we show that the magnetic arcade forms a 3-D waveguide if the Alfvén speed increases monotonically beyond a fiducial radius. Both magnetic pressure and tension act as restoring forces, instead of just tension as is generally assumed in 1-D models. Since magnetic pressure plays an important role, the eigenmodes involve propagation both parallel and transverse to the magnetic field. Using an analytic solution, we derive the specific eigenfrequencies and eigenfunctions for an arcade possessing a discontinuous density profile. The discontinuity separates a diffuse cylindrical cavity and an overlying shell of denser plasma that corresponds to the bright loops. We emphasize that all of the eigenfunctions have a discontinuous axial velocity at the density interface; hence, the interface can give rise to the Kelvin-Helmholtz instability. Further, we find that all modes have elliptical polarization with the degree of polarization changing with height. However, depending on the line of sight, only one polarization may be clearly visible.

13-May-2013

### **The Coronal Global Evolutionary Model: Using HMI Vector Magnetogram and Doppler Data to Determine Coronal Magnetic Field Evolution**

[J. Todd Hoeksema](#), [William P. Abbett](#), [David J. Bercik](#), [Mark C. M. Cheung](#), [Marc L. DeRosa](#), [George H. Fisher](#), [Keiji Hayashi](#), [Maria D. Kazachenko](#), [Yang Liu](#), [Erkka Lumme](#), [Benjamin J. Lynch](#), [Xudong Sun](#), [Brian T. Welsch](#)

ApJS **250** 28 2020

<https://arxiv.org/pdf/2006.14579.pdf>

<https://doi.org/10.3847/1538-4365/abb3fb>

The Coronal Global Evolutionary Model (CGEM) provides data-driven simulations of the magnetic field in the solar corona to better understand the build-up of magnetic energy that leads to eruptive events. The CGEM project has developed six capabilities. CGEM modules (1) prepare time series of full-disk vector magnetic field observations to (2) derive the changing electric field in the solar photosphere over active-region scales. This local electric field is (3) incorporated into a surface flux transport model that reconstructs a global electric field that evolves magnetic flux in a consistent way. These electric fields drive a (4) 3D spherical magneto-frictional (SMF) model, either at high-resolution over a restricted range of solid angle or at lower resolution over a global domain, to determine the magnetic field and current density in the low corona. An SMF-generated initial field above an active region and the evolving electric field at the photosphere are used to drive (5) detailed magneto-hydrodynamic (MHD) simulations of active regions in the low corona. SMF or MHD solutions are then used to compute emissivity proxies that can be compared with coronal observations. Finally, a lower-resolution SMF magnetic field is used to initialize (6) a global MHD model that is driven by an SMF electric-field time series to simulate the outer corona and heliosphere, ultimately connecting Sun to Earth. As a demonstration, this report features results of CGEM applied to observations of the evolution of NOAA Active Region 11158 in **February 2011**.

### **Synoptic Q-Maps — Insight into the Topology of the Coronal Magnetic Field**

J. Todd [Hoeksema](#)[1], Yang Liu[1], Xudong Sun[2], Viacheslav Titov[3], & Zoran Mikić[3]

[HMI Science Nuggets](#) #111 Sept 2018

<http://hmi.stanford.edu/hminuggets/?p=2670>

### **SDO/HMI Vector Magnetic Field Observing Mode Changed on 13 April 2016**

Todd [Hoeksema](#)

SolarNews 15 June 2016

<http://solarnews.nso.edu/2016/20160615.html>

On 13 April 2016, a little after 19 UT, the method used to collect HMI vector magnetic field values changed. This new method combines data from two cameras. Since launch, HMI had operated with a framelist that used one

camera (the Vector camera) to collect polarized filtergrams for the determination of the Stokes vector parameters, I Q U and V, every 135 seconds. Every 45 s the other (Doppler) camera collected data for the line-of-sight observables that depend only on Stokes I and V. Overlap in circular-polarization observations can be eliminated by combining the images from the two cameras. The new framelist does not change the sequence for the Doppler camera; however, the Vector camera now collects only linearly polarized filtergrams. The overall effect is to both lower the noise and increase the cadence of the vector measurements, because in 90 seconds the new framelist collects one set of linear-polarized and two sets of circular-polarized images. Analysis described in a forthcoming HMI Nugget shows that images from the two cameras can be successfully combined without introducing significant systematic errors, that the noise in the 720-s Stokes elements is reduced by about 14%, and that the noise-dominated weak-field vector-magnetic-field magnitude is 8% less. Observations that combine data from the two cameras has keyword CAMERA = 3; prior observations had the keyword CAMERA = 1 for 12-minute cadence data.

See Y. Liu's SPD poster for more information.

[http://sun.stanford.edu/~yliu/hmi/modL\\_Summary/YLiu\\_poster2016.pdf](http://sun.stanford.edu/~yliu/hmi/modL_Summary/YLiu_poster2016.pdf)

## **The Helioseismic and Magnetic Imager (HMI) Vector Magnetic Field Pipeline: Overview and Performance**

J.T. [Hoeksema](#), Y. Liu, K. Hayashi, X. Sun, J. Schou, S. Couvidat, A. Norton, M. Bobra, R. Centeno, K.D. Leka, G. Barnes, M. Turmon

E-print, Feb 2014; Solar Phys. Volume 289, Issue 9, pp 3483-3530, 2014

<http://arxiv.org/pdf/1404.1881v1.pdf>

The Helioseismic and Magnetic Imager (HMI) began near-continuous full-disk solar measurements on 1 May 2010 from the Solar Dynamics Observatory (SDO). An automated processing pipeline keeps pace with observations to produce observable quantities, including the photospheric vector magnetic field, from sequences of filtergrams. The basic vector-field frame list cadence is 135 seconds, but to reduce noise the filtergrams are combined to derive data products every 720 seconds. The primary 720s observables were released in mid 2010, including Stokes polarization parameters measured at six wavelengths as well as intensity, Doppler velocity, and the line-of-sight magnetic field. More advanced products, including the full vector magnetic field, are now available. Automatically identified HMI Active Region Patches (HARPs) track the location and shape of magnetic regions throughout their lifetime. The vector field is computed using the Very Fast Inversion of the Stokes Vector (VFISV) code optimized for the HMI pipeline; the remaining 180 degree azimuth ambiguity is resolved with the Minimum Energy (ME0) code. The Milne Eddington inversion is performed on all full-disk HMI observations. The disambiguation, until recently run only on HARP regions, is now implemented for the full disk. Vector and scalar quantities in the patches are used to derive active region indices potentially useful for forecasting; the data maps and indices are collected in the SHARP data series, hmi.sharp\_720s. Definitive SHARP processing is completed only after the region rotates off the visible disk; quick-look products are produced in near real time. Patches are provided in both CCD and heliographic coordinates. HMI provides continuous coverage of the vector field, but has modest spatial, spectral, and temporal resolution. Coupled with limitations of the analysis and interpretation techniques, effects of the orbital velocity, and instrument performance, the resulting measurement have a certain dynamic range and sensitivity and are subject to systematic errors and uncertainties that are characterized in this report.

## **Magnetohydrodynamic Slow Mode with Drifting He<sup>++</sup>: Implications for Coronal Seismology and the Solar Wind**

Joseph V. [Hollweg](#), Daniel Verscharen, Benjamin D. G. Chandran

2014, ApJ 788 35

<http://arxiv.org/pdf/1404.4625v1.pdf>

The MHD slow mode wave has application to coronal seismology, MHD turbulence, and the solar wind where it can be produced by parametric instabilities. We consider analytically how a drifting ion species (e.g. He<sup>++</sup>) affects the linear slow mode wave in a mainly electron-proton plasma, with potential consequences for the aforementioned applications. Our main conclusions are: 1. For wavevectors highly oblique to the magnetic field, we find solutions that are characterized by very small perturbations of total pressure. Thus, our results may help to distinguish the MHD slow mode from kinetic Alfvén waves and non-propagating pressure-balanced structures, which can also have very small total pressure perturbations. 2. For small ion concentrations, there are solutions that are similar to the usual slow mode in an electron-proton plasma, and solutions that are dominated by the drifting ions, but for small drifts the wave modes cannot be simply characterized. 3. Even with zero ion drift, the standard dispersion relation for the highly oblique slow mode cannot be used with the Alfvén speed computed using the summed proton and ion densities, and with the sound speed computed from the summed pressures and densities of all species. 4. The ions can drive a non-resonant instability under certain circumstances. For low plasma beta, the threshold drift can be less than that required to destabilize electromagnetic modes, but damping from the Landau resonance can eliminate this instability altogether, unless  $T_e/T_p \gg 1$ .

## Sausage oscillations of coronal plasma slabs

[Hornsey](#), C., Nakariakov, V.M. and Fludra, A.

E-print, May 2014; A&A, 567, A24 (2014)

[http://www2.warwick.ac.uk/fac/sci/physics/research/cfsa/people/valery/research/eprints/saus\\_paper\\_printer2.pdf](http://www2.warwick.ac.uk/fac/sci/physics/research/cfsa/people/valery/research/eprints/saus_paper_printer2.pdf)

Context. Sausage oscillations are observed in plasma non-uniformities of the solar corona as axisymmetric perturbations of the nonuniformity. Often, these non-uniformities can be modelled as field-aligned slabs of the density enhancement.

Aims. We perform parametric studies of sausage oscillations of plasma slabs, aiming to determine the dependence of the oscillation period on its parameters, and the onset of leaky and trapped regimes of the oscillations.

Methods. Slabs with smooth transverse profiles of the density of a zero-beta plasma are perturbed by an impulsive localised perturbation of the sausage symmetry. In particular, the slab can contain an infinitely thin current sheet in its centre. The initial value problem is then solved numerically. The numerical results are subject to spectral analysis. The results are compared with analytical solutions for a slab with a step-function profile and also with sausage oscillations of a plasma cylinder.

Results. We established that sausage oscillations in slabs generally have the same properties as in plasma cylinders. In the trapped regime, the sausage oscillation period increases with the increase in the longitudinal wavelength. In the leaky regime, the dependence of the period on the wavelength experiences saturation, and the period becomes independent of the wavelength in the long-wavelength limit. In the leaky regime the period is always longer than in the trapped regime. The sausage oscillation period in a slab is always longer than in a cylinder with the same transverse profile. In slabs with steeper transverse profiles, sausage oscillations have longer periods. The leaky regime occurs at shorter wavelengths in slabs with smoother profiles.

## Formation of super-strong horizontal magnetic field in delta-type sunspot in radiation magnetohydrodynamic simulations

[H. Hotta](#), [S. Toriumi](#)

MNRAS 2020

<https://arxiv.org/pdf/2008.07741.pdf>

We perform a series of radiative magnetohydrodynamic simulations to understand the amplification mechanism of the exceptionally strong horizontal magnetic field in delta-type sunspots. In the simulations, we succeed in reproducing the delta-type sunspot and resulting strong magnetic field exceeding 6000 G in a light bridge between the positive and negative polarities. Our conclusions in this study are summarized as follows:

1. The essential amplification mechanism of the strong horizontal magnetic field is the shear motion caused by the rotation of two spots.
2. The strong horizontal magnetic field remains the force-free state.
3. The peak strength of the magnetic fields does not depend on the spatial resolution, top boundary condition, or Alfvén speed limit.

The origin of the rotating motion is rooted in the deep convection zone.

Therefore, the magnetic field in the delta-spot light bridge can be amplified to the superequipartition values in the photosphere.

## On rising magnetic flux tube and formation of sunspots in a deep domain

[H. Hotta](#), [H. Iijima](#)

MNRAS Volume 494, Issue 2, Pages 2523–2537, 2020

<https://arxiv.org/pdf/2003.10583.pdf>

<https://doi.org/10.1093/mnras/staa844>

We investigate the rising flux tube and the formation of sunspots in an unprecedentedly deep computational domain that covers the whole convection zone with a radiative magnetohydrodynamics simulation. Previous calculations had shallow computational boxes (< 30 Mm) and convection zones at a depth of 200 Mm. By using our new numerical code R2D2, we succeed in covering the whole convection zone and reproduce the formation of the sunspot from a simple horizontal flux tube because of the turbulent thermal convection. The main findings are (1) The rising speed of the flux tube is larger than the upward convection velocity because of the low density caused by the magnetic pressure and the suppression of the mixing. (2) The rising speed of the flux tube exceeds 250 m/s at a depth of 18 Mm, while we do not see any clear evidence of the divergent flow 3 hr before the emergence at the solar surface. (3) Initially, the root of the flux tube is filled with the downflows and then the upflow fills the center of the flux tube during the formation of the sunspot. (4) The essential mechanisms for the formation of the sunspot are the coherent inflow and the turbulent transport. (5) The low-temperature region is extended to a depth of at least 40 Mm in the matured sunspot, with the high-temperature region in the center of the flux tube. Some of the findings indicate the importance of the deep computational domain for the flux emergence simulations.



## High-resolution Calculation of the Solar Global Convection with the Reduced Speed of Sound Technique. II. Near Surface Shear Layer with the Rotation

H. [Hotta](#)<sup>1,2</sup>, M. Rempel<sup>1</sup>, and T. Yokoyama

2015 ApJ 798 51

We present a high-resolution, highly stratified numerical simulation of rotating thermal convection in a spherical shell. Our aim is to study in detail the processes that can maintain a near surface shear layer (NSSL) as inferred from helioseismology. Using the reduced speed of sound technique, we can extend our global convection simulation to  $0.99 R_{\odot}$  and include, near the top of our domain, small-scale convection with short timescales that is only weakly influenced by rotation. We find the formation of an NSSL preferentially in high latitudes in the depth range of  $r = 0.95\text{--}0.975 R_{\odot}$ . The maintenance mechanisms are summarized as follows. Convection under the weak influence of rotation leads to Reynolds stresses that transport angular momentum radially inward in all latitudes. This leads to the formation of a strong poleward-directed meridional flow and an NSSL, which is balanced in the meridional plane by forces resulting from the  $\langle v'_r v'_\theta \rangle$  correlation of turbulent velocities. The origin of the required correlations depends to some degree on latitude. In high latitudes, a positive correlation  $\langle v'_r v'_\theta \rangle$  is induced in the NSSL by the poleward meridional flow whose amplitude increases with the radius, while a negative correlation is generated by the Coriolis force in bulk of the convection zone. In low latitudes, a positive correlation  $\langle v'_r v'_\theta \rangle$  results from rotationally aligned convection cells ("banana cells"). The force caused by these Reynolds stresses is in balance with the Coriolis force in the NSSL.

## Various Activities above Sunspot Light Bridges in IRIS Observations: Classification and Comparison

[Yijun Hou](#), [Ting Li](#), [Shuhong Yang](#), [Shin Toriumi](#), [Yilin Guo](#), [Jun Zhang](#)

ApJ 929 12 2022

<https://arxiv.org/pdf/2202.10159.pdf>

<https://iopscience.iop.org/article/10.3847/1538-4357/ac5912/pdf>

Light bridges (LBs) are among the most striking sub-structures in sunspots, where various activities have been revealed by recent high-resolution observations from the Interface Region Imaging Spectrograph (IRIS). According to the variety of physical properties, we classified these activities into four distinct categories: transient brightening (TB), intermittent jet (IJ), type-I light wall (LW-I), and type-II light wall (LW-II). In IRIS 1400/1330 Å observations, TBs are characterized by abrupt emission enhancements, and IJs appear as collimated plasma ejections with a width of 1-2 Mm at some LB sites. Most observed TBs are associated with IJs and show superpositions of some chromosphere absorption lines on enhanced and broadened wings of C II and Si IV lines, which could be driven by intermittent magnetic reconnection in the lower atmosphere. LW-I and LW-II are wall-shaped structures with bright fronts above the whole LB. An LW-I has a continuous oscillating front with a typical height of several Mm and an almost stationary period of 4-5 minutes. On the contrary, an LW-II has a indented front with a height of over 10 Mm, which has no stable period and is accompanied by recurrent TBs in the entire LB. These results support that LW-IIs are driven by frequent reconnection occurring along the whole LB due to large-scale magnetic flux emergence or intrusion, rather than the leakage of waves producing LW-Is. Our observations reveal a highly dynamical scenario of activities above LBs driven by different basic physical processes, including magneto-convection, magnetic reconnection, and wave leakage. 2019 May 12, 2015 January 11, 2014 October 25, and 2014 October 28.

## Sunspot penumbral filaments intruding into a light bridge and the resultant reconnection jets

[Y. J. Hou](#), [T. Li](#), [S. H. Zhong](#), [S. H. Yang](#), [Y. L. Guo](#), [X. H. Li](#), [J. Zhang](#), [Y. Y. Xiang](#)

A&A 642, A44 2020

<https://arxiv.org/pdf/2008.01284.pdf>

<https://doi.org/10.1051/0004-6361/202038668>

Penumbral filaments and light bridges are prominent structures inside sunspots and are important for understanding the nature of sunspot magnetic fields and magneto-convection underneath. We investigate an interesting event where several penumbral filaments intruded into a sunspot light bridge for more insights into magnetic fields of the sunspot penumbral filament and light bridge, as well as their interaction. The emission, kinematic, and magnetic topology characteristics of the penumbral filaments intruding into the light bridge and the resultant jets are studied. At the west part of the light bridge, the intruding penumbral filaments penetrated into the umbrae on both sides of the light bridge, and two groups of jets were also detected. The jets shared the same projected morphology with the intruding filaments and were accompanied by intermittent footpoint brightenings. Simultaneous spectral imaging observations provide convincing evidences for the presences of magnetic reconnection related heating and bidirectional flows near the jet bases and contribute to measuring vector velocities of the jets. Additionally,

nonlinear force-free field extrapolation results reveal strong and highly inclined magnetic fields along the intruding penumbral filaments, consistent well with the results deduced from the vector velocities of the jets. Therefore, we propose that the jets could be caused by magnetic reconnections between emerging fields within the light bridge and the nearly horizontal fields of intruding filaments. They were then ejected outward along the stronger filament fields. Our study indicates that magnetic reconnection could occur between the penumbral filament fields and emerging fields within light bridge and produce jets along the stronger filament fields. These results further complement the study of magnetic reconnection and dynamic activities within the sunspot. **2019 May 13**

## **Observations of Upward Propagating Waves in the Transition Region and Corona above Sunspots**

Zhenyong [Hou](#), Zhenghua Huang, Lidong Xia, Bo Li, and Hui Fu

**2018 ApJ 855 65**

We present observations of persistent oscillations of some bright features in the upper-chromosphere/transition region above sunspots taken by IRIS SJ 1400 Å and upward propagating quasi-periodic disturbances along coronal loops rooted in the same region taken by the AIA 171 Å passband. The oscillations of the features are cyclic oscillatory motions without any obvious damping. The amplitudes of the spatial displacements of the oscillations are about 1". The apparent velocities of the oscillations are comparable to the sound speed in the chromosphere, but the upward motions are slightly larger than that of the downward. The intensity variations can take 24%–53% of the background, suggesting nonlinearity of the oscillations. The FFT power spectra of the oscillations show a dominant peak at a period of about 3 minutes, which is consistent with the omnipresent 3 minute oscillations in sunspots. The amplitudes of the intensity variations of the upward propagating coronal disturbances are 10%–15% of the background. The coronal disturbances have a period of about 3 minutes, and propagate upward along the coronal loops with apparent velocities in a range of 30 ~ 80 km s<sup>-1</sup>. We propose a scenario in which the observed transition region oscillations are powered continuously by upward propagating shocks, and the upward propagating coronal disturbances can be the recurrent plasma flows driven by shocks or responses of degenerated shocks that become slow magnetic-acoustic waves after heating the plasma in the coronal loops at their transition-region bases.

## **Simultaneous Observations of p-mode Light Walls and Magnetic Reconnection Ejections above Sunspot Light Bridges**

Yijun [Hou](#)<sup>1,2</sup>, Jun Zhang<sup>1,2</sup>, Ting Li<sup>1,2</sup>, Shuhong Yang<sup>1,2</sup>, and Xiaohong Li

**2017 ApJL 848 L9**

Recent high-resolution observations from the Interface Region Imaging Spectrograph reveal bright wall-shaped structures in active regions (ARs), especially above sunspot light bridges. Their most prominent feature is the bright oscillating front in the 1400/1330 Å channel. These structures are named light walls and are often interpreted to be driven by p-mode waves. Above the light bridge of AR 12222 on **2014 December 06**, we observed intermittent ejections superimposed on an oscillating light wall in the 1400 Å passband. At the base location of each ejection, the emission enhancement was detected in the Solar Dynamics Observatory 1600 Å channel. Thus, we suggest that in wall bases (light bridges), in addition to the leaked p-mode waves consistently driving the oscillating light wall, magnetic reconnection could happen intermittently at some locations and eject the heated plasma upward. Similarly, in the second event occurring in AR 12371 on 2015 June 16, a jet was simultaneously detected in addition to the light wall with a wave-shaped bright front above the light bridge. At the footpoint of this jet, lasting brightening was observed, implying magnetic reconnection at the base. We propose that in these events, two mechanisms, p-mode waves and magnetic reconnection, simultaneously play roles in the light bridge, and lead to the distinct kinetic features of the light walls and the ejection-like activities, respectively. To illustrate the two mechanisms and their resulting activities above light bridges, in this study we present a cartoon model.

## **Narrow-line-width UV bursts in the transition region above Sunspots observed by IRIS**

Zhenyong [Hou](#), Zhenghua Huang, Lidong Xia, [Bo Li](#), [Maria S. Madjarska](#), [Hui Fu](#), [Chaozhou](#)

[Mou](#), [Haixia Xie](#)

**ApJL 2016**

<http://arxiv.org/pdf/1608.04892v1.pdf>

Various small-scale structures abound in the solar atmosphere above active regions, playing an important role in the dynamics and evolution therein. We report on a new class of small-scale transition region structures in active regions, characterized by strong emissions but extremely narrow Si IV line profiles as found in observations taken with the Interface Region Imaging Spectrograph (IRIS). Tentatively named as Narrow-line-width UV bursts (NUBs), these structures are located above sunspots and comprise of one or multiple compact bright cores at sub-arcsecond scales. We found six NUBs in two datasets (a raster and a sit-and-stare dataset). Among these, four events are short-living with a duration of ~10 mins while two last for more than 36 mins. All NUBs have Doppler shifts of 15--18 km/s, while the NUB found in sit-and-stare data possesses an additional component at ~50 km/s found only in the C II and Mg II lines. Given that these events are found to play a role in the local dynamics, it is important to

further investigate the physical mechanisms that generate these phenomena and their role in the mass transport in sunspots. **2014 February 16, 2014 March 10**

### **Light Walls Around Sunspots Observed by the Interface Region Imaging Spectrograph**

Y. J. [Hou](#), T. Li, S. H. Yang, J. Zhang

A&A Letters **2016**

<http://arxiv.org/pdf/1604.00485v1.pdf>

The Interface Region Imaging Spectrograph (IRIS) mission provides high-resolution observations of the chromosphere and transition region. We try to determine whether the light walls exist somewhere else in active regions besides light bridges. Employing half-year high tempo-spatial data from the IRIS, we find lots of light walls either around sunspots or above light bridges. For the first time, we report one light wall near an umbral-penumbral boundary and another along a neutral line between two small sunspots. These new observations reveal that these light walls are multi-layer and multi-thermal structures which occur along magnetic neutral lines in active regions.

### **Magnetohydrodynamic Nonlinearities in Sunspot Atmospheres: Chromospheric Detections of Intermediate Shocks**

S. J. [Houston](#)<sup>1</sup>, D. B. Jess<sup>1,2</sup>, R. Keppens<sup>3</sup>, M. Stangalini<sup>4,5</sup>, P. H. Keys<sup>1</sup> et al.

**2020** ApJ 892 49

<https://doi.org/10.3847/1538-4357/ab7a90>

The formation of shocks within the solar atmosphere remains one of the few observable signatures of energy dissipation arising from the plethora of magnetohydrodynamic waves generated close to the solar surface. Active region observations offer exceptional views of wave behavior and its impact on the surrounding atmosphere. The stratified plasma gradients present in the lower solar atmosphere allow for the potential formation of many theorized shock phenomena. In this study, using chromospheric Ca ii  $\lambda 8542$  line spectropolarimetric data of a large sunspot, we examine fluctuations in the plasma parameters in the aftermath of powerful shock events that demonstrate polarimetric reversals during their evolution. Modern inversion techniques are employed to uncover perturbations in the temperatures, line-of-sight velocities, and vector magnetic fields occurring across a range of optical depths synonymous with the shock formation. Classification of these nonlinear signatures is carried out by comparing the observationally derived slow, fast, and Alfvén shock solutions with the theoretical Rankine–Hugoniot relations. Employing over 200,000 independent measurements, we reveal that the Alfvén (intermediate) shock solution provides the closest match between theory and observations at optical depths of  $\tau \approx 0.5$ , consistent with a geometric height at the boundary between the upper photosphere and lower chromosphere. This work uncovers first-time evidence of the manifestation of chromospheric intermediate shocks in sunspot umbrae, providing a new method for the potential thermalization of wave energy in a range of magnetic structures, including pores, magnetic flux ropes, and magnetic bright points.

### **The Magnetic Response of the Solar Atmosphere to Umbral Flashes**

S.J. [Houston](#), [D.B. Jess](#), [A. Asensio Ramos](#), [S.D.T. Grant](#), [C. Beck](#), [A.A. Norton](#), [S. Krishna Prasad](#)

ApJ **860** 28 **2018**

<https://arxiv.org/pdf/1803.00018.pdf>

Chromospheric observations of sunspot umbrae offer an exceptional view of magneto-acoustic shock phenomena and the impact they have on the surrounding magnetically-dominated plasma. We employ simultaneous slit-based spectro-polarimetry and spectral imaging observations of the chromospheric He I 10830 Å and Ca II 8542 Å lines to examine fluctuations in the umbral magnetic field caused by the steepening of magneto-acoustic waves into umbral flashes. Following the application of modern inversion routines, we find evidence to support the scenario that umbral shock events cause expansion of the embedded magnetic field lines due to the increased adiabatic pressure. The large number statistics employed allow us to calculate the adiabatic index,  $\gamma = 1.12 \pm 0.01$ , for chromospheric umbral locations. Examination of the vector magnetic field fluctuations perpendicular to the solar normal revealed changes up to  $\sim 200$  G at the locations of umbral flashes. Such transversal magnetic field fluctuations have not been described before. Through comparisons with non-linear force-free field extrapolations, we find that the perturbations of the transverse field components are orientated in the same direction as the quiescent field geometries. This implies that magnetic field enhancements produced by umbral flashes are directed along the motion path of the developing shock, hence producing relatively small changes, up to a maximum of  $\sim 8$  degrees, in the inclination and/or azimuthal directions of the magnetic field. Importantly, this work highlights that umbral flashes are able to modify the full vector magnetic field, with the detection of the weaker transverse magnetic field components made possible by high-resolution data combined with modern inversion routines. **2016 July 14**

**UKSP Nuggets #93 August 2018** [www.uksolphys.org/?p=14804](http://www.uksolphys.org/?p=14804)

### **Comparison of Line-of-Sight Magnetic Field Observed by ASO-S/FMG, SDO/HMI and HSOS/SMAT.**

**Xu, H., Su, J., Liu, S. et al.**

Sol Phys 299, 17 (2024).

<https://doi.org/10.1007/s11207-024-02260-8>

The Full-disk MagnetoGraph (FMG) onboard the Advanced Space based Solar Observatory has obtained a series of line-of-sight magnetic-field measurements since its launch in October 2022. It is important to compare its observational data with other existing solar telescopes. In this paper, we make a detailed comparison of four active regions and a pore region simultaneously observed by FMG, the Helioseismic and Magnetic Imager (HMI) onboard the Solar Dynamic Observatory, and the Solar Magnetism and Activity Telescope (SMAT) at Huairou Solar Observing Station. We find that the magnetic-field structure and spatial distribution are basically consistent among these three instruments. The initial correlation coefficient of magnetic field is approximately 0.90. The coefficient slightly increases when sunspot umbra regions are excluded, and it increases significantly up to 0.98 for the magnetic field in penumbra regions. The magnetic field observed by FMG tends to be weaker than the HMI in strength in sunspot umbra due to saturation effect, whereas larger outside sunspot. The differences are probably due to different noise levels, seeing conditions (SMAT is affected by the Earth's atmosphere) and observational and calibration methods.

### **Non-force-free extrapolation of solar coronal magnetic field using vector magnetograms**

Qiang **Hu**, B. Dasgupta, M. DeRosa, J. Buechner, G.A. Gary

E-print, May 2009

We report our recent improvement in non-force-free extrapolation of coronal magnetic field, using vector magnetograms. Based on the principle of minimum (energy) dissipation rate (MDR), a generally non-force-free magnetic field solution is expressed as the superposition of one potential field and two (constant- $\alpha$ ) linear force-free fields, with distinct  $\alpha$  parameters. With a known potential field, the system is reduced to a second-order one that can be solved using one single-layer vector magnetogram. We devise an iteration procedure to determine the potential field, by achieving satisfactory agreement between the MDR-model computed and measured transverse magnetic field vectors on the bottom boundary. We illustrate this approach by applying it to real magnetograph measurement of solar active region AR10953. We show that the results are satisfactory as judged from the quantitative magnetic field measurement, and the behavior of the derived Lorentz force.

### **A PRACTICAL APPROACH TO CORONAL MAGNETIC FIELD EXTRAPOLATION BASED ON THE PRINCIPLE OF MINIMUM DISSIPATION RATE**

Qiang **Hu**, B. Dasgupta, D. P. Choudhary, and J. Buechner

The Astrophysical Journal, 679:848-853, 2008

<http://www.journals.uchicago.edu/doi/pdf/10.1086/587639>

We present a newly developed approach to solar coronal magnetic field extrapolation from vector magnetograms, based on the principle of minimum dissipation rate (MDR). The MDR system was derived from a variational problem that is more suitable for an open and externally driven system, like the solar corona. The resulting magnetic field equation is more general than force-free. Its solution can be expressed as the superposition of two linear (constant- $\alpha$ ) force-free fields (LFFFs) with distinct  $\alpha$  parameters, and one potential field. Thus, the original extrapolation problem is decomposed into three LFFF extrapolations, utilizing boundary data. The full MDR-based approach requires two layers of vector magnetograph measurements on the solar surface, while a slightly modified practical approach only requires one. We test both approaches against three-dimensional MHD simulation data in a finite volume. Both yield quantitatively good results. The errors in the magnetic energy estimate are within a few percent. In particular, the main features of relatively strong perpendicular current density structures, representative of the non-force-freeness of the solution, are well recovered.

### **AN IMPROVED APPROACH TO NON-FORCE FREE CORONAL MAGNETIC FIELD EXTRAPOLATION --**

QIANG **HU**, and BRAHMANANDA DASGUPTA,

E-print, Nov 2006,

<http://solar.physics.montana.edu/cgi-bin/eprint/index.pl?entry=2105>

Solar Phys (2008) 247: 87–101

<http://www.springerlink.com/content/t07636w0j326633v/fulltext.pdf>

We develop an approach to deriving the three-dimensional non-force-free coronal magnetic field from vector magnetograms. Based on the principle of minimum dissipation rate, a general non-force-free magnetic field is expressed as the superposition of one potential field and two constant- $\alpha$  (linear) force-free fields. Each is extrapolated from its bottom boundary data, providing the normal component only. The constant- $\alpha$  parameters are distinct and determined by minimizing the deviations between the numerically computed and measured transverse magnetic field at the bottom boundary. The boundary conditions required are at least two layers of vector magnetograms, one at the photospheric level and the other at the chromospheric level, presumably. We apply our approach to a few analytic test cases, especially to two

nonlinear force-free cases examined by Schrijver *et al.* (*SolarPhys.* **235**, 161, 2006). We find that for one case with small  $\alpha$  parameters, the quantitative measures of the quality of our result are better than the median values of those from a set of nonlinear force-free methods. The reconstructed magnetic-field configuration is valid up to a vertical height of the transverse scale. For the other cases, the results remain valid to a lower vertical height owing to the limitations of the linear force-free-field solver. Because our method is based on the fast-Fourier-transform algorithm, it is much faster and easy to implement. We discuss the potential usefulness of our method and its limitations.

## Adjusting the Potential Field Source Surface Height Based on Magnetohydrodynamic Simulations

Zhenguang [Huang](#)<sup>1</sup>, Gábor Tóth<sup>1</sup>, Jia Huang<sup>2</sup>, Nishtha Sachdeva<sup>1</sup>, Bart van der Holst<sup>1</sup>, and Ward B. Manchester<sup>1</sup>

2024 ApJL 965 L1

<https://iopscience.iop.org/article/10.3847/2041-8213/ad3547/pdf>

A potential field solution is widely used to extrapolate the coronal magnetic field above the Sun's surface to a certain height. This model applies the current-free approximation and assumes that the magnetic field is entirely radial beyond the source surface height, which is defined as the radial distance from the center of the Sun. Even though the source surface is commonly specified at 2.5 Rs (solar radii), previous studies have suggested that this value is not optimal in all cases. In this study, we propose a novel approach to specify the source surface height by comparing the areas of the open magnetic field regions from the potential field solution with predictions made by a magnetohydrodynamic model, in our case the Alfvén Wave Solar atmosphere Model. We find that the adjusted source surface height is significantly less than 2.5 Rs near solar minimum and slightly larger than 2.5 Rs near solar maximum. We also report that the adjusted source surface height can provide a better open flux agreement with the observations near the solar minimum, while the comparison near the solar maximum is slightly worse.

## Examination of the EUV Intensity in the Open Magnetic Field Regions Associated with Coronal Holes

Guan-Han [Huang](#)<sup>1</sup>, Chia-Hsien Lin<sup>1</sup>, and Lou-Chuang Lee<sup>1</sup>

2019 ApJ 874 45

<https://doi.org/10.3847/1538-4357/ab06f0>

Coronal holes can be identified as the regions with magnetic field lines extending far away from the Sun, or the darkest regions in EUV/X-ray images with predominantly unipolar magnetic fields. A comparison between the locations of our determined regions with open magnetic field lines (OMF) and regions with low EUV intensity (LIR) reveals that only 12% of the OMF regions coincide with the LIRs. The aim of this study is to investigate the conditions leading to the different brightnesses of OMF regions, and to provide a means to predict whether an OMF region would be bright or dark. Examining the statistical distribution profiles of the magnetic field expansion factor ( $f_s$ ) and Atmospheric Imaging Assembly 193 Å intensity ( $I_{193}$ ) reveals that both profiles are approximately log-normal. The analysis of the spatial and temporal distributions of  $f_s$  and  $I_{193}$  indicates that the bright OMF regions often are inside or next to regions with closed field lines, including quiet-Sun regions and regions with strong magnetic fields. Examining the relationship between  $I_{193}$  and  $f_s$  reveals a weak positive correlation between  $\log I_{193}$  and  $\log f_s$ , with a correlation coefficient  $\approx 0.39$ . As a first-order approximation, the positive relationship is determined to be  $\log I_{193} = 0.62 \log f_s + 1.51$  based on the principle of the whitening/dewhitening transformation. This linear relationship is demonstrated to increase the consistency between the OMF regions and LIRs from 12% to 23%.

## Magnetic loops above a small flux-emerging region observed by IRIS, Hinode and SDO

Zhenghua [Huang](#)

ApJ **869** 175 2018

<https://arxiv.org/pdf/1811.03219.pdf>

I report on observations of a set of magnetic loops above a region with late-phase flux emergence taken by IRIS, Hinode and SDO. The loop system consists of many transition region loop threads with size of 5--12 arcsec in length and  $\sim 0.5$  arcsec in width and coronal loops with similar length and  $\sim 2$  arcsec width. Although the loop system consists of threads with different temperatures, most individual loop thread have temperature in a narrow range. In the middle of the loop system, it shows clear systematic blue-shifts of about 10 km/s in the transition region that is consistent with a flux emerging picture, while red-shifts of about 10 km/s in the corona is observed. The nonthermal velocity of the loop system are smaller than the surrounding region in the transition region but are comparable in the corona. The electron densities of the coronal counterpart of the loop system range from  $1 \times 10^9 \text{ cm}^{-3}$  to  $4 \times 10^9 \text{ cm}^{-3}$ . Electron density of a transition region loop is also measured and found to be about  $5 \times 10^{10} \text{ cm}^{-3}$ , a magnitude larger than that in the coronal loops. In agreement with imaging data, the temperature profiles derived from the differential emission measurement technique confirms that some of the loops have been heated to corona. Our observations indicate that the flux emergence in its late phase is much different from that at the early stage. While the observed transition region is dominated by emerging flux, these emerging

loops could be heated to corona and the heatings (if via nonthermal processes) most likely take place only after they reaching the transition region or lower corona. **August 26 2017**

## **Tracking Back the Solar Wind to Its Photospheric Footpoints from Wind Observations – A Statistical Study**

Chong **Huang**, Yihua Yan, Gang Li, Yuanyong Deng, Baolin Tan  
Solar Physics, August **2014**, Volume 289, Issue 8, pp 3109-3119

It is of great importance to track the solar wind back to its photospheric source region and identify the related current sheets; this will provide key information for investigating the origin and predictions of the solar wind. We report a statistical study relating the photospheric footpoint motion and in-situ observation of current sheets in the solar wind. We used the potential force-free source–surface (PFSS) model and the daily synoptic charts to trace the solar wind back from 1 AU, as observed by the Wind spacecraft, to the solar surface. As the footpoints move along the solar surface we obtain a time series of the jump times between different points. These jumps can be within a cell and between adjacent cells. We obtained the distribution of the jump times and the distribution for a subset of the jump times in which only jumps between adjacent cells were counted. For both cases, the distributions clearly show two populations. These distributions are compared with the distribution of in-situ current sheets reported in an earlier work of Miao, Peng, and Li (Ann. Geophys. 29, 237, 2011). Its implications on the origin of the current sheets are discussed.

## **NEWLY DISCOVERED GLOBAL TEMPERATURE STRUCTURES IN THE QUIET SUN AT SOLAR MINIMUM**

Zhenguang **Huang**<sup>1</sup>, Richard A. Frazin<sup>1</sup>, Enrico Landi<sup>1</sup>, Ward B. Manchester<sup>1</sup>, Alberto M. Vásquez<sup>2</sup>, and Tamas I. Gombosi

**2012** ApJ 755 86

Magnetic loops are building blocks of the closed-field corona. While active region loops are readily seen in images taken at EUV and X-ray wavelengths, quiet-Sun (QS) loops are seldom identifiable and are therefore difficult to study on an individual basis. The first analysis of solar minimum (Carrington Rotation 2077) QS coronal loops utilizing a novel technique called the Michigan Loop Diagnostic Technique (MLDT) is presented. This technique combines Differential Emission Measure Tomography and a potential field source surface (PFSS) model, and consists of tracing PFSS field lines through the tomographic grid on which the local differential emission measure is determined. As a result, the electron temperature  $T_e$  and density  $N_e$  at each point along each individual field line can be obtained. Using data from STEREO/EUVI and SOHO/MDI, the MLDT identifies two types of QS loops in the corona: so-called up loops in which the temperature increases with height and so-called down loops in which the temperature decreases with height. Up loops are expected, however, down loops are a surprise, and furthermore, they are ubiquitous in the low-latitude corona. Up loops dominate the QS at higher latitudes. The MLDT allows independent determination of the empirical pressure and density scale heights, and the differences between the two remain to be explained. The down loops appear to be a newly discovered property of the solar minimum corona that may shed light on the physics of coronal heating. The results are shown to be robust to the calibration uncertainties of the EUVI instrument.

## **Solar Sector Structure**

**Review**

Hugh S. **Hudson**, Leif Svalgaard, Iain G. Hannah

[Space Science Reviews](#), December **2014**, Volume 186, [Issue 1-4](#), pp 17-34

<http://arxiv.org/pdf/1503.04477v1.pdf>

The interplanetary magnetic field near 1 AU has a characteristic “sector” structure that reflects its polarity relative to the solar direction. Typically we observe large-scale coherence in these directions, with two or four “away” or “towards” sectors per solar rotation, from any platform in deep space and near the ecliptic plane. In a simple picture, this morphology simply reflects the idea that the sources of the interplanetary field lie mainly in or near the Sun, and that the solar-wind flow enforces a radial component in this field. The sector boundaries are sharply defined in the interplanetary field near one AU, but have more complicated sources within the Sun itself. Recent evidence confirms that the origins of this pattern also appear statistically at the level of the photosphere, with signatures found in the highly concentrated fields of sunspots and even solar flares. This complements the associations already known between the interplanetary sectors and large-scale coronal structures (i.e., the streamers). This association with small-scale fields strengthens at the Hale sector boundary, defining the Hale boundary as the one for which the polarity switch matches that of the leading-to-following polarity alternation in the sunspots of a given hemisphere. Surface features that appear 4.5 days prior to the sector crossings observed at 1 AU correlate with this sense of polarity reversal. **2008 August 1**

## **CORONAL RADIATION BELTS**

H. S. [Hudson](#)<sup>1</sup>, A. L. MacKinnon<sup>2</sup>, M. L. DeRosa<sup>3</sup>, and S. F. N. Frewen<sup>1</sup>

*Astrophysical Journal*, 698:L86–L89, 2009

<http://www.iop.org:80/EJ/toc/-alert=43191/1538-4357/698/2>

The magnetic field of the solar corona has a large-scale dipole character, which maps into the bipolar field in the solar wind. Using standard representations of the coronal field, we show that high-energy ions can be trapped stably in these large-scale closed fields. The drift shells that describe the conservation of the third adiabatic invariant may have complicated geometries. Particles trapped in these zones would resemble the Van Allen belts and could have detectable consequences. We discuss potential sources of trapped particles.

### **HMI Synoptic Maps Produced by NSO/NISP**

Anna L. H. [Hughes](#), Luca Bertello, Andrew R. Marble, [Niles A. Oien](#), [Gordon Petrie](#), [Alexei A. Pevtsov](#)

Report number: NSO/NISP-2016-002

<http://arxiv.org/pdf/1605.03500v1.pdf>

Recently, the National Solar Observatory (NSO) Solar-atmosphere Pipeline Working Group has undertaken the production of synoptic maps from Helioseismic and Magnetic Imager (HMI) magnetograms. A set of maps has been processed spanning the data available for 2010–2015 using twice daily images (taken at UT midnight and noon) and running them through the same algorithms used to produce SOLIS/VSM 63021 mean-magnetic and spatial-variance maps. The contents of this document provide an overview of what these maps look like, and the processing steps used to generate them from the original HMI input data.

### **Multiwavelength Imaging and Spectral Analysis of Jet-like Phenomena in a Solar Active Region Using IRIS and AIA**

Llŷr Dafydd [Humphries](#)<sup>1</sup>, Erwin Verwichte<sup>2</sup>, David Kuridz el, and Huw Morgan<sup>1</sup>

2020 ApJ 898 17

<https://doi.org/10.3847/1538-4357/ab974d>

<https://sci-hub.tw/https://iopscience.iop.org/article/10.3847/1538-4357/ab974d>

<https://arxiv.org/pdf/2010.04042.pdf>

High-resolution observations of dynamic phenomena give insights into the properties and processes that govern the low solar atmosphere. We present an analysis of jet-like phenomena emanating from a penumbral footpoint in active region (AR) 12192 using imaging and spectral observations from the Interface Region Imaging Spectrograph (IRIS) and the Atmospheric Imaging Assembly (AIA) on board the Solar Dynamics Observatory. These jets are associated with line-of-sight Doppler speeds of  $\pm 10$ – $22$  km s<sup>-1</sup> and bright fronts that seem to move across the plane-of-sky at speeds of 23–130 km s<sup>-1</sup>. Such speeds are considerably higher than the expected sound speed in the chromosphere. The jets have signatures that are visible both in the cool and hot channels of IRIS and AIA. Each jet lasts on average 15 minutes and occurs 5–7 times over a period of 2 hr. Possible mechanisms to explain this phenomenon are suggested, the most likely of which involve p-mode or Alfvén wave shock trains impinging on the transition region and corona as a result of steepening photospheric wavefronts or gravity waves. **2014 October 25**

### **Chapter 5.3 - Spectropolarimetry and Magnetic Structures**

**Review**

[Kiyoshi Ichimoto](#)

In: *The Sun as a Guide to Stellar Physics* **Book**

Eds. Oddbjørn Engvold, Jean-Claude Vial, and Andrew Skumanich

Elsevier, November 2018

<https://www.sciencedirect.com/book/9780128143346/the-sun-as-a-guide-to-stellar-physics>

Spectropolarimetry is a powerful tool used to diagnose magnetic fields in the solar atmosphere. Zeeman and Hanlé effects provide the foundation for retrieving information about the magnetic field from the polarization observed in spectral lines. We described the basic concepts of spectropolarimetry in current solar observations and present an overview of the nature of magnetic fields in the photosphere and chromosphere and in prominences. We discuss structures such as sunspots and small-scale photospheric magnetic flux tubes and their distribution.

### **Investigation of Decaying $\beta$ -Configuration Sunspot in Active Region NOAA 13229.**

[Idrees](#), S., [Su](#), J., [Chen](#), J. et al.

*Sol Phys* 299, 91 (2024).

<https://doi.org/10.1007/s11207-024-02322-x>

In this study, we investigate the decay of sunspots in the active region NOAA 13229 using data from the ASO-S/FMG and SDO/HMI. We closely examine the decay patterns of sunspots S1 and S2, which reveal different decay rates and features due to the mechanisms of magnetic cancellation, dispersion, and the role of horizontal flows. Our analysis highlights the significant impact of magnetic flux changes, including the decrease of both the sunspot area and magnetic flux over time, which adheres to distinct decay laws. This study elucidates the complex interplay

between magnetic submergence, cancellation, and dispersion in the sunspot decay process, contributing to our understanding of the underlying mechanisms driving these phenomena. Our results emphasize the importance of horizontal flow dynamics in shaping the decay characteristics of sunspots, providing insights for the role played by the magnetic and plasma processes in solar active regions.

## **Detection of Flux Emergence, Splitting, Merging, and Cancellation of Network Fields. II Apparent Unipolar Flux Change and Cancellation**

Y. Iida, H. Hagenaar, T. Yokoyama

ApJ 2015

<http://arxiv.org/pdf/1510.04764v1.pdf>

In this second paper in the series, we investigate occurrence frequencies of apparent unipolar processes, cancellation, and emergence of patch structures in quiet regions. Apparent unipolar events are considerably more frequent than cancellation and emergence as per our definition, which is consistent with Lamb et al. (2013). Furthermore, we investigate the frequency distributions of changes in flux during apparent unipolar processes and found that they concentrate around the detection limit of the analysis. Combining these findings with the results of our previous paper, Iida et al. (2012), that merging and splitting are more dominant than emergence and cancellation, these results support the understanding that apparent unipolar processes are actually interactions with and among patches below the detection limit and that there still are numerous flux interactions between the flux range in this analysis and below the detection limit. We also investigate occurrence frequency distributions of flux decrease during cancellation. We found a relatively strong dependence,  $2.48 \pm 0.26$  as a power-law index. This strong dependence on flux is consistent with the model, which is suggested in the previous paper.

## **The ion-atom absorption processes as one of the factors of the influence on the sunspot opacity**

Lj. M. Ignjatovic, A. A. Mihajlov, V. A. Sreckovic, M. S. Dimitrijevic

MNRAS, 2014

<http://arxiv.org/pdf/1404.0688v1.pdf>

As a continuation of the previous investigations of the symmetric and strongly non-symmetric ion-atom absorption processes in the far UV region within the models of the quiet Sun photosphere, these processes are studied here within a model of the sunspot. Here we mean the absorption processes in the  $H(1s)+H^+$  and  $H(1s)+X^+$  collisions and the processes of the photo-dissociation of the  $H^+ 2$  and  $HX^+$  molecular ions, where  $X$  is one of the metal atoms:  $X=Na, Ca, Mg, Si$  and  $Al$ . Obtained results show that the influence of the considered ion-atom absorption processes on the opacity of sunspots in the considered spectral region ( $110 \text{ nm} \lesssim \lambda \lesssim 230 \text{ nm}$ ) is not less and in some parts even larger than the influence of the referent electron-atom processes. In such a way, it is shown that the considered ion-atom absorption processes should be included *ab initio* in the corresponding models of sunspots of solar-type and near solar-type stars. Apart of that, the spectral characteristics of the considered non-symmetric ion-atom absorption processes (including here the case  $X = Li$ ), which can be used in some further applications, have been determined and presented within this work.

## **DETECTION OF FLUX EMERGENCE, SPLITTING, MERGING, AND CANCELLATION OF NETWORK FIELD. I. SPLITTING AND MERGING**

Y. Iida<sup>1</sup>, H. J. Hagenaar<sup>2</sup>, and T. Yokoyama

2012 ApJ 752 149

Frequencies of magnetic patch processes on the supergranule boundary, namely, flux emergence, splitting, merging, and cancellation, are investigated through automatic detection. We use a set of line-of-sight magnetograms taken by the Solar Optical Telescope (SOT) on board the Hinode satellite. We found 1636 positive patches and 1637 negative patches in the data set, whose time duration is 3.5 hr and field of view is  $112'' \times 112''$ . The total numbers of magnetic processes are as follows: 493 positive and 482 negative splittings, 536 positive and 535 negative mergings, 86 cancellations, and 3 emergences. The total numbers of emergence and cancellation are significantly smaller than those of splitting and merging. Further, the frequency dependence of the merging and splitting processes on the flux content are investigated. Merging has a weak dependence on the flux content with a power-law index of only 0.28. The timescale for splitting is found to be independent of the parent flux content before splitting, which corresponds to  $\sim 33$  minutes. It is also found that patches split into any flux contents with the same probability. This splitting has a power-law distribution of the flux content with an index of  $-2$  as a time-independent solution. These results support that the frequency distribution of the flux content in the analyzed flux range is rapidly maintained by merging and splitting, namely, surface processes. We suggest a model for frequency distributions of cancellation and emergence based on this idea.



## Parametrization of sunspot groups based on machine learning approach

[E. Illarionov](#), [A. Tlatov](#)

Solar Phys. **297**, Article number: 19 2022

<https://arxiv.org/pdf/2201.05840.pdf>

<https://link.springer.com/content/pdf/10.1007/s11207-022-01955-0.pdf>

Sunspot groups observed in white-light appear as complex structures. Analysis of these structures is usually based on simple morphological descriptors which capture only generic properties and miss information about fine details. We present a machine learning approach to introduce a complete yet compact description of sunspot groups. The idea is to map sunspot group images into an appropriate lower-dimensional (latent) space. We apply a combination of Variational Autoencoder and Principal Component Analysis to obtain a set of 285 latent descriptors. We demonstrate that the standard descriptors are embedded into the latent ones. Thus, latent features can be considered as an extended description of sunspot groups and, in our opinion, can expand the possibilities for the research on sunspot groups. In particular, we demonstrate an application for estimation of the sunspot group complexity. The proposed parametrization model is generic and can be applied to investigation of other traces of solar activity observed in various spectrum lines. Key components of this work, which are the parametrization model, dataset of sunspot groups and latent vectors, are available in the public GitHub repository [this https URL](#) groups and can be used to reproduce the results and for further research. **2016 July 18**

## Helioseismic Detection of Emerging Magnetic Flux

Stathis [Iionidis](#), Junwei Zhao, Alexander G. Kosovichev

E-print, March **2012**,

Proc. of the 61st Fujihara Seminar: Progress in solar/stellar physics with helio- and asteroseismology  
Investigating the properties of magnetic flux emergence is one of the most important problems of solar physics. In this study we present a newly developed deep-focus time-distance measurement scheme which is able to detect strong emerging flux events in the deep solar interior, before the flux becomes visible on the surface. We discuss in detail the differences between our method and previous methods, and demonstrate step-by-step how the signal-to-noise (S/N) ratio is increased. The method is based on detection of perturbations in acoustic phase travel times determined from cross-covariances of solar oscillations observed on the surface. We detect strong acoustic travel-time reductions of an order of 12 - 16 seconds at a depth of 42 - 75 Mm. These acoustic anomalies are detected 1 - 2 days before high peaks in the photospheric magnetic flux rate implying that the average emerging speed is 0.3 - 0.6 km/s. The results of this work contribute to our understanding of solar magnetism and benefit space weather forecasting.

## Statistical Analysis of Asymmetric Sunspot Decay Observed by Hinode

[Shinsuke Imada](#), [Shota Kato](#) & [Masashi Fujiyama](#)

*Solar Physics* volume 295, Article number: 154 (2020)

<https://link.springer.com/content/pdf/10.1007/s11207-020-01724-x.pdf>

We statistically studied the transport of magnetic flux in and around sunspots using a magnetic-element tracking technique to investigate whether sunspot-decay processes are isotropic. Using this method, we detected moving magnetic features (MMFs). The observed radius of an MMFs region was approximately 1.7 times the sunspot radius; furthermore, the average apparent velocity of MMFs was statistically estimated to be approximately 350 ms<sup>-1</sup>–1350 ms<sup>-1</sup>. We determined that the leading sunspots transport approximately 5% more magnetic flux to the Equator side than to the Pole side of the sunspots. In addition, the leading sunspots transport approximately 3% more magnetic flux to the back (East) than to the front (West) of the sunspots. On the other hand, the following sunspots do not show the magnetic-flux transport asymmetry. The statistics might not be sufficient for the analysis of the following sunspots. These asymmetries of magnetic flux transport might contribute to the cross-equatorial transport of net magnetic flux, which is an important physical quantity of polar magnetic-field reversal. **31 December 2009, 20 February 2012**

## Outflow structure of the quiet Sun corona probed by spacecraft radio scintillations in strong scattering

Takeshi [Imamura](#), Munetoshi Tokumaru, Hiroaki Isobe, Daikou Shiota, Hiroki Ando, Mayu Miyamoto, Tomoaki Toda, Bernd H<sup>?</sup>usler, Martin P<sup>?</sup>tzold, Alexander Nabatov, Ayumi Asai, Kentaro Yaji, Manabu Yamada, Masato Nakamura

**2014 ApJ 788 117**

[http://iopscience.iop.org/0004-637X/788/2/117/pdf/0004-637X\\_788\\_2\\_117.pdf](http://iopscience.iop.org/0004-637X/788/2/117/pdf/0004-637X_788_2_117.pdf)

Radio scintillation observations have been unable to probe flow speeds in the low corona where the scattering of radio waves is exceedingly strong. Here we estimate outflow speeds continuously from the vicinity of the Sun to the outer corona (heliocentric distances of 1.5-20.5 solar radii) by applying the strong scattering theory to radio scintillations for the first time, using the Akatsuki spacecraft as the radio source. Small, nonzero outflow speeds

were observed over a wide latitudinal range in the quiet-Sun low corona, suggesting that the supply of plasma from closed loops to the solar wind occurs over an extended area. The existence of power-law density fluctuations down to the scale of 100 m was suggested, being indicative of well-developed turbulence which can play a key role in heating the corona. At higher altitudes a rapid acceleration typical of radial open fields is observed, and the temperatures derived from the speed profile show a distinct maximum in the outer corona. This study opened up a possibility of observing detailed flow structures near the Sun from existing vast amount of interplanetary scintillation data.

## **Coronal turbulence and the angular broadening of radio sources - the role of the structure function**

M. **Ingale**, Prasad Subramaian, Iver Cairns  
MNRAS, 2015

<http://arxiv.org/pdf/1412.6620v1.pdf>

The amplitude of density turbulence in the extended solar corona, especially near the dissipation scale, impinges on several problems of current interest. Radio sources observed through the turbulent solar wind are broadened due to refraction by and scattering off density inhomogeneities, and observations of scatter broadening are often employed to constrain the turbulence amplitude. The extent of such scatter broadening is usually computed using the structure function, which gives a measure of the spatial correlation measured by an interferometer. Most such treatments have employed analytical approximations to the structure function that are valid in the asymptotic limits  $s \gg l_i$  or  $s \ll l_i$ , where  $s$  is the interferometer spacing and  $l_i$  is the inner scale of the density turbulence spectrum. We instead use a general structure function (GSF) that straddles these regimes, and quantify the errors introduced by the use of these approximations. We have included the effects of anisotropic scattering for distant cosmic sources viewed through the solar wind at small elongations. We show that the regimes where the GSF predictions are more accurate than those of the asymptotic expressions are not only of practical relevance, but are where inner scale effects influence estimates of scatter broadening. Taken together, we argue that the GSF should henceforth be used for scatter broadening calculations and estimates of turbulence amplitudes in the solar corona and solar wind.

## **An Evolution and Eruption of the Coronal Magnetic Field through a Data-Driven MHD Simulation**

**Satoshi Inoue**, **Keiji Hayashi**, **Takahiro Miyoshi**

ApJ 2022

<https://arxiv.org/pdf/2210.07492>

We present a newly developed data-driven magnetohydrodynamics (MHD) simulation code under a zero-beta approximation based on a method proposed by Hayashi et al. 2018 and 2019. Although many data-driven MHD simulations have been developed and conducted, there are not many studies on how accurately those simulations can reproduce the phenomena observed in the solar corona. In this study, we investigated the performance of our data-driven simulation quantitatively using ground-truth data. The ground-truth data was produced by an MHD simulation in which the magnetic field is twisted by the sunspot motions. A magnetic flux rope (MFR) is created by the cancellation of the magnetic flux at the polarity inversion line due to the converging flow on the sunspot, which eventually leads the eruption of the MFR. We attempted to reproduce these dynamics using the data-driven MHD simulation. The coronal magnetic fields are driven by the electric fields, which are obtained from a time-series of the photospheric magnetic field that is extracted from the ground-truth data, on the surface. As a result, the data-driven simulation could capture the subsequent MHD processes, the twisted coronal magnetic field and formation of the MFR, and also its eruption. We report these results and compare with the ground-truth data, and discuss how to improve the accuracy and optimize numerical method.

## **Magnetohydrodynamics modeling of coronal magnetic field and solar eruptions based on the photospheric magnetic field**

**Review**

**Satoshi Inoue**

Progress in Earth and Planetary Science 2016 3:19

<http://progearthplanetasci.springeropen.com/articles/10.1186/s40645-016-0084-7>

E-print, 4 July 2016

In this paper, we summarize current progress on using the observed magnetic fields for magnetohydrodynamics (MHD) modeling of the coronal magnetic field and of solar eruptions, including solar flares and coronal mass ejections (CMEs). Unfortunately, even with the existing state-of-the-art solar physics satellites, only the photospheric magnetic field can be measured. We first review the 3D extrapolation of the coronal magnetic fields from measurements of the photospheric field. Specifically, we focus on the nonlinear force-free field (NLFFF) approximation extrapolated from the three components of the photospheric magnetic field. On the other hand, because in the force-free approximation the NLFFF is reconstructed for equilibrium states, the onset and dynamics

of solar flares and CMEs cannot be obtained from these calculations. Recently, MHD simulations using the NLFFF as an initial condition have been proposed for understanding these dynamics in a more realistic scenario. These results have begun to reveal complex dynamics, some of which have not been inferred from previous simulations of hypothetical situations, and they have also successfully reproduced some observed phenomena. Although MHD simulations play a vital role in explaining a number of observed phenomena, there still remains much to be understood. Herein, we review the results obtained by state-of-the-art MHD modeling combined with the NLFFF. **13 February 2011, 15 February 2011, 11 September 2011, 29 March 2014**

## **Structure and Stability of Magnetic Fields in Solar Active Region 12192 Based on Nonlinear Force-Free Field Modeling**

S. [Inoue](#), [K. Hayashi](#), [K. Kusano](#)

ApJ 818 168 **2016**

<http://arxiv.org/pdf/1601.00791v1.pdf>

We analyze a three-dimensional (3D) magnetic structure and its stability in large solar active region (AR) 12192, using the 3D coronal magnetic field constructed under a nonlinear force-free field (NLFFF) approximation. In particular, we focus on the magnetic structure that produced an X3.1-class flare which is one of the X-class flares observed in AR 12192. According to our analysis, the AR contains multiple-flux-tube system, {it e.g.}, a large flux tube, both of whose footpoints are anchored to the large bipole field, under which other tubes exist close to a polarity inversion line (PIL). These various flux tubes of different sizes and shapes coexist there. In particular, the later are embedded along the PIL, which produces a favorable shape for the tether-cutting reconnection and is related to the X-class solar flare. We further found that most of magnetic twists are not released even after the flare, which is consistent with the fact that no observational evidence for major eruptions was found. On the other hand, the upper part of the flux tube is beyond a critical decay index, essential for the excitation of torus instability before the flare, even though no coronal mass ejections (CMEs) were observed. We discuss the stability of the complicated flux tube system and suggest the reason for the existence of the stable flux tube. In addition, we further point out a possibility for tracing the shape of flare ribbons, on the basis of a detailed structural analysis of the NLFFF before a flare. **October 24, 2014**

## **Nonlinear Force-Free Extrapolation of the Coronal Magnetic Field Based on the MHD Relaxation Method**

S. [Inoue](#), T. Magara, V. S. Pandey, D. Shiota, K. Kusano, G. S. Choe and K. S. Kim

E-print, Nov **2013**; **2014** ApJ 780 101

We develop a nonlinear force-free field (NLFFF) extrapolation code based on the magnetohydrodynamic (MHD) relaxation method. We extend the classical MHD relaxation method in two important ways. First, we introduce an algorithm initially proposed by [?cite{2002JCoPh.175..645D}](#) to effectively clean the numerical errors associated with  $\nabla \cdot \vec{B}$ . Second, the multi-grid type method is implemented in our NLFFF to perform direct analysis of the high-resolution magnetogram data. As a result of these two implementations, we successfully extrapolated the high resolution force-free field introduced by [?cite{1990ApJ...352..343L}](#) with better accuracy in a drastically shorter time. We also applied our extrapolation method to the MHD solution obtained from the flux-emergence simulation by [?cite{2012ApJ...748...53M}](#). We found that NLFFF extrapolation may be less effective for reproducing areas higher than a half-domain, where some magnetic loops are found in a state of continuous upward expansion. However, an inverse S shaped structure consisting of the sheared and twisted loops formed in the lower region can be captured well through our NLFFF extrapolation method. We further discuss how well these sheared and twisted fields are reconstructed by estimating the magnetic topology and twist quantitatively.

## **NONLINEAR FORCE-FREE MODELING OF A THREE-DIMENSIONAL SIGMOID OBSERVED ON THE SUN**

S. [Inoue](#)<sup>1,2</sup>, T. Magara<sup>2</sup>, S. Watari<sup>1</sup> and G. S. Choe

**2012** ApJ 747 65, **File**

In this work, we analyze the characteristics of the three-dimensional magnetic structure of a sigmoid observed over an active region (AR 10930) and followed by X-class flares. This is accomplished by combining a nonlinear force-free field (NLFFF) model of a coronal magnetic field and the high-resolution vector-field measurement of a photospheric magnetic field by Hinode. The key findings of our analysis reveal that the value of the X-ray intensity associated with the sigmoid is more sensitive to the strength of the electric current rather than the twist of the field lines. The strong electric current flows along the magnetic field lines and composes the central part of the sigmoid, even though the twist of the field lines is weak in that region. On the other hand, the outer region (i.e., the elbow part) of the sigmoid is basically occupied by field lines of strong twist and weak current density. Consequently, weak X-ray emission is observed. As the initial Ca II illumination basically occurs from the central part of the sigmoid, this region plays an important role in determining the onset mechanism of the flare despite its weak twisted

field-line configuration. We also compare our results with the magnetohydrodynamic simulation for the formation of a sigmoid. Although the estimated values of the twist from the simulation are found to be a little higher than the values obtained from the NLFFF, we find that the field-line configurations generated by the simulation and NLFFF are remarkably analogous as long as we deal with the lower coronal region. **2006 December 13**

### **TWIST AND CONNECTIVITY OF MAGNETIC FIELD LINES IN THE SOLAR ACTIVE REGION NOAA 10930**

S. **Inoue**<sup>1</sup>, K. Kusano<sup>2,5</sup>, T. Magara<sup>3</sup>, D. Shiota<sup>4</sup> and T. T. Yamamoto

**2011 ApJ 738 161**

Twist and connectivity of magnetic field lines in the flare-productive active region NOAA 10930 are investigated in terms of the vector magnetograms observed by the Solar Optical Telescope on board the Hinode satellite and the nonlinear force-free field (NLFFF) extrapolation. First, we show that the footpoints of magnetic field lines reconstructed by the NLFFF correspond well to the conjugate pair of highly sheared flare ribbons on the Ca II images, which were observed by Hinode as an X3.4 class flare on **2006 December 13**. This demonstrates that the NLFFF extrapolation may be used to analyze the magnetic field connectivity. Second, we find that the twist of magnetic field lines anchored on the flare ribbons increased as the ribbons moved away from the magnetic polarity inversion line in the early phase of the flare. This suggests that magnetic reconnection might commence from a region located below the most strongly twisted field. Third, we reveal that the magnetic flux twisted more than a half turn and gradually increased during the last one day prior to the onset of the flare, and that it quickly decreased for two hours after the flare. This is consistent with the store-and-release scenario of magnetic helicity. However, within this active region, only a small fraction of the flux was twisted by more than one full turn and the field lines that reconnected first were twisted less than one turn. These results imply that the kink mode instability could hardly occur, at least before the onset of flare. Based on our results, we discuss the trigger process of solar flares.

### **Coronal Fourier power spectra: implications for coronal seismology and coronal heating**

Jack **Ireland**, R. T. James McAteer, Andrew R. Inglis

**2015 ApJ 798 1**

<http://arxiv.org/pdf/1410.2171v1.pdf>

The dynamics of regions of the solar corona are investigated using Atmospheric Imaging Assembly (AIA) 171\AA and 193\AA data. The coronal emission from the quiet Sun, coronal loop footprints, coronal moss, and from above a sunspot is studied. It is shown that the mean Fourier power spectra in these regions can be described by a power law at lower frequencies that tails to flat spectrum at higher frequencies, plus a Gaussian-shaped contribution that varies depending on the region studied. This Fourier spectral shape is in contrast to the commonly-held assumption that coronal time-series are well described by the sum of a long time-scale background trend plus Gaussian-distributed noise, with some specific locations also showing an oscillatory signal. The implications of this discovery to the field of coronal seismology and the automated detections of oscillations are discussed. The power law contribution to the shape of the Fourier power spectrum is interpreted as being due to the summation of a distribution of exponentially decaying emission events along the line of sight. This is consistent with the idea that the solar atmosphere is heated everywhere by small energy deposition events.

### **Mapping Solar Magnetic Fields from the Photosphere to the Base of the Corona**

[Ryohko Ishikawa](#), [Javier Trujillo Bueno](#), [Tanausu del Pino Aleman](#), [Takenori J. Okamoto](#), [David E. McKenzie](#), [Frederic Auchere](#), [Ryouhei Kano](#), [Donguk Song](#), [Masaki Yoshida](#), [Laurel A. Rachmeler](#), [Ken Kobayashi](#), [Hirohisa Hara](#), [Masahito Kubo](#), [Noriyuki Narukage](#), [Taro Sakao](#), [Toshifumi Shimizu](#), [Yoshinori Suematsu](#), [Christian Bethge](#), [Bart De Pontieu](#), [Alberto Sainz Dalda](#), [Genevieve D. Vigil](#), [Amy Winebarger](#), [Ernest Alsina Ballester](#), [Luca Belluzzi](#), [Jiri Stepan](#), [Andres Asensio Ramos](#), [Mats Carlsson](#), [Jorrit Leenaarts](#)

Science Advances, Vol. 7, no. 8, eabe8406, **2021**

DOI: 10.1126/sciadv.abe8406

<https://arxiv.org/pdf/2103.01583.pdf>

<https://advances.sciencemag.org/content/7/8/eabe8406>

Routine ultraviolet imaging of the Sun's upper atmosphere shows the spectacular manifestation of solar activity; yet we remain blind to its main driver, the magnetic field. Here we report unprecedented spectropolarimetric observations of an active region plage and its surrounding enhanced network, showing circular polarization in ultraviolet (Mg II h & k and Mn I) and visible (Fe I) lines. We infer the longitudinal magnetic field from the photosphere to the very upper chromosphere. At the top of the plage chromosphere the field strengths reach more than 300 gauss, strongly correlated with the Mg II k line core intensity and the electron pressure. This unique mapping shows how the magnetic field couples the different atmospheric layers and reveals the magnetic origin of the heating in the plage chromosphere.

### **Influence of the Atmospheric Model on Hanle Diagnostics**

Ryohko **Ishikawa**, Han Uitenbroek, Motoshi Goto, Yusuke Iida, Saku Tsuneta

*Solar Physics* May 2018, 293:74

<https://link.springer.com/content/pdf/10.1007%2Fs11207-018-1293-6.pdf>

We clarify the uncertainty in the inferred magnetic field vector via the Hanle diagnostics of the hydrogen Lyman- $\alpha$  line when the stratification of the underlying atmosphere is unknown. We calculate the anisotropy of the radiation field with plane-parallel semi-empirical models under the nonlocal thermal equilibrium condition and derive linear polarization signals for all possible parameters of magnetic field vectors based on an analytical solution of the atomic polarization and Hanle effect. We find that the semi-empirical models of the inter-network region (FAL-A) and network region (FAL-F) show similar degrees of anisotropy in the radiation field, and this similarity results in an acceptable inversion error (e.g.,  $\sim 40^\circ$  instead of  $50^\circ$  in field strength and  $\sim 100^\circ$  instead of  $90^\circ$  in inclination) when FAL-A and FAL-F are swapped. However, the semi-empirical models of FAL-C (averaged quiet-Sun model including both inter-network and network regions) and FAL-P (plage regions) yield an atomic polarization that deviates from all other models, which makes it difficult to precisely determine the magnetic field vector if the correct atmospheric model is not known (e.g., the inversion error is much larger than 40% of the field strength;  $> 70^\circ$  instead of  $50^\circ$ ). These results clearly demonstrate that the choice of model atmosphere is important for Hanle diagnostics. As is well known, one way to constrain the average atmospheric stratification is to measure the center-to-limb variation of the linear polarization signals. The dependence of the center-to-limb variations on the atmospheric model is also presented in this paper.

### **ALMA Discovery of Solar Umbral Brightness Enhancement at $\lambda=3$ mm**

Kazumasa **Iwai**, Maria Loukitcheva, Masumi Shimojo, Sami K. Solanki, Stephen M. White

*ApJL* 2017

<https://arxiv.org/pdf/1705.03147.pdf>

We report the discovery of a brightness enhancement in the center of a large sunspot umbra at a wavelength of 3 mm using the Atacama Large Millimeter/sub-millimeter Array (ALMA). Sunspots are amongst the most prominent features on the solar surface, but many of their aspects are surprisingly poorly understood. We analyzed a  $\lambda=3$  mm (100 GHz) mosaic image obtained by ALMA, which includes a large sunspot within the active region AR12470 on **December 16, 2015**. The 3 mm map has a field-of-view and spatial resolution, which is the highest spatial-resolution map of an entire sunspot in this frequency range. We find a gradient of 3 mm brightness from a high value in the outer penumbra to a low value in the inner penumbra/outer umbra. Within the inner umbra, there is a marked increase in 3mm brightness temperature, which we call an umbral brightness enhancement. This enhanced emission corresponds to a temperature excess of 800 K relative to the surrounding inner penumbral region and coincides with excess brightness in the 1330 and 1400  $\text{\AA}$  slitjaw images of the Interface Region Imaging Spectrograph (IRIS), adjacent to a partial lightbridge. This  $\lambda=3$  mm brightness enhancement may be an intrinsic feature of the sunspot umbra at chromospheric heights, such as a manifestation of umbral flashes, or it could be related to a coronal plume since the brightness enhancement was coincident with the footpoint of a coronal loop observed at 171  $\text{\AA}$ .

### **Bipolar magnetic spots from dynamos in stratified spherical shell turbulence**

Sarah **Jabbari**, Axel Brandenburg, Nathan Kleeorin, Dhruvadya Mitra, Igor Rogachevskii

2014

<http://arxiv.org/pdf/1411.4912v2.pdf>

Recent work by Mitra et al. (2014) has shown that in strongly stratified forced two-layer turbulence with helicity and corresponding large-scale dynamo action in the lower layer, a magnetic field occurs in the upper layer in the form of sharply bounded bipolar magnetic spots. Here we extend this model to spherical wedge geometry covering the northern hemisphere up to  $75^\circ$  latitude and an azimuthal extent of  $180^\circ$ . The kinetic helicity and therefore also the large-scale magnetic field are strongest at low latitudes. For moderately strong stratification, several bipolar spots form that fill eventually the full longitudinal extent. At early times, the polarity of spots reflects the orientation of the underlying azimuthal field, as expected from  $\Omega$ -shaped flux loops. At late times their tilt changes such that there is a radial field of opposite orientation at different latitudes separated by about  $10^\circ$ . Our model demonstrates for the first time the spontaneous formation of spots of sizes much larger than the pressure scale height. Their tendency to produce filling factors close to unity is argued to be reminiscent of highly active stars. We confirm that strong stratification is an essential ingredient behind magnetic spot formation, which appears to be associated with downflows at larger depths.

### **Exploration of solar photospheric magnetic field data sets using the UCSD tomography**

B. V. **Jackson**, H.-S. Yu, A. Buffington, P. P. Hick, N. Nishimura, N. Nozaki, M. Tokumaru, K. Fujiki, K. Hayashi

*Space Weather* Volume 14, Issue 12 December 2016 Pages 1107–1124

This article investigates the use of two different types of National Solar Observatory magnetograms and two different coronal field modeling techniques over 10 years. Both the “open-field” Current Sheet Source Surface

(CSSS) and a “closed-field” technique using CSSS modeling are compared. The University of California, San Diego, tomographic modeling, using interplanetary scintillation data from Japan, provides the global velocities to extrapolate these fields outward, which are then compared with fields measured in situ near Earth. Although the open-field technique generally gives a better result for radial and tangential fields, we find that a portion of the closed extrapolated fields measured in situ near Earth comes from the direct outward mapping of these fields in the low solar corona. All three closed-field components are nonzero at 1 AU and are compared with the appropriate magnetometer values. A significant positive correlation exists between these closed-field components and the in situ measurements over the last 10 years. We determine that a small fraction of the static low-coronal component flux, which includes the B<sub>n</sub> (north-south) component, regularly escapes from closed-field regions. The closed-field flux fraction varies by about a factor of 3 from a mean value during this period, relative to the magnitude of the field components measured in situ near Earth, and maximizes in 2014. This implies that a relatively more efficient process for closed-flux escape occurs near solar maximum. We also compare and find that the popular Potential Field Source Surface and CSSS model closed fields are nearly identical in sign and strength.

## **The Magnetic Classification of Solar Active Regions 1992 - 2015**

Sarah A. [Jaeggli](#), Aimee A. Norton

ApJL 820 L11 2016

<http://arxiv.org/pdf/1603.02552v1.pdf>

The purpose of this letter is to address a blind-spot in our knowledge of solar active region statistics. To the best of our knowledge there are no published results showing the variation of the Mount Wilson magnetic classifications as a function of solar cycle based on modern observations. We show statistics for all active regions reported in the daily Solar Region Summary from 1992 January 1 to 2015 December 31. We find that the  $\alpha$  and  $\beta$  class active regions (including all sub-groups e.g.  $\beta\gamma$ ,  $\beta\delta$ ) make up fractions of approximately 20% and 80% of the sample respectively. This fraction is relatively constant during high levels of activity, however, an increase in the  $\alpha$  fraction to about 35% and a decrease in the  $\beta$  fraction to about 65% can be seen near each solar minimum and is statistically significant at the 2- $\sigma$  level. Over 30% of all active regions observed during the years of solar maxima were appended with the classifications  $\gamma$  and/or  $\delta$ , while these classifications account for only a fraction of a percent during the years near the solar minima. This variation in the active region types indicates that the formation of complex active regions may be due to the pileup of frequent emergence of magnetic flux during solar maximum, rather than the emergence of complex, monolithic flux structures.

## **Multi-wavelength study of a delta-spot I: A region of very strong, horizontal magnetic field**

Sarah A. [Jaeggli](#)

ApJ 818 81 2016

<http://arxiv.org/pdf/1512.08463v1.pdf>

Active region NOAA 11035 appeared in December 2009, early in the new solar activity cycle. This region achieved a delta sunspot ( $\delta$ -spot) configuration when parasitic flux emerged near the rotationally leading magnetic polarity and traveled through the penumbra of the largest sunspot in the group. Both visible and infrared imaging spectropolarimetry of the magnetically sensitive Fe I line pairs at 6302 Å and 15650 Å show large Zeeman splitting in the penumbra between the parasitic umbra and the main sunspot umbra. The polarized Stokes spectra in the strongest field region display anomalous profiles, and strong blueshifts are seen in an adjacent region. Analysis of the profiles is carried out using a Milne-Eddington inversion code capable of fitting either a single magnetic component with stray light or two independent magnetic components to verify the field strength. The inversion results show that the anomalous profiles cannot be produced by the combination of two profiles with moderate magnetic fields. The largest field strengths are 3500-3800 G in close proximity to blueshifts as strong as 3.8 km s<sup>-1</sup>. The strong, nearly horizontal magnetic field seen near the polarity inversion line in this region is difficult to understand in the context of a standard model of sunspot magnetohydrostatic equilibrium. Dec 17, 2009.

## **Sausage, kink, and fluting MHD wave modes identified in solar magnetic pores by Solar Orbiter/PHI**

[S. Jafarzadeh](#), [L.A.C. Schiavo](#), [V. Fedun](#), [S.K. Solanki](#), [M. Stangalini](#), +++

A&A 2024

<https://arxiv.org/pdf/2404.18717>

Solar pores are intense concentrations of magnetic flux that emerge through the Sun's photosphere. When compared to sunspots, they are much smaller in diameter and hence can be impacted and buffeted by neighbouring granular activity to generate significant magnetohydrodynamic (MHD) wave energy flux within their confines. However, observations of solar pores from ground-based telescope facilities may struggle to capture subtle motions synonymous with higher-order MHD wave signatures due to seeing effects produced in the Earth's atmosphere. Hence, we have exploited timely seeing-free and high-quality observations of four small magnetic pores from the Polarimetric and Helioseismic Imager (PHI) on board the Solar Orbiter spacecraft. Through acquisition of data

under stable observing conditions, we have been able to measure the area fluctuations and horizontal displacements of the solar pores. Cross correlations between perturbations in intensity, area, line-of-sight velocity, and magnetic fields, coupled with the first-time application of novel Proper Orthogonal Decomposition (POD) techniques on the boundary oscillations, provide a comprehensive diagnosis of the embedded MHD waves as sausage and kink modes. Additionally, the previously elusive  $m = 2$  fluting mode is identified in the most magnetically isolated of the four pores. An important consideration lies in how the identified wave modes contribute towards the transfer of energy into the upper solar atmosphere. We find that the four pores examined have approximately 56%, 72%, 52%, and 34% of their total wave energy associated with the identified sausage modes, and around 23%, 17%, 39%, and 49% to their kink modes, respectively, while the first pore also has around an 11% contribution linked to the fluting mode. This study marks the first-time identification of concurrent sausage, kink, and fluting MHD wave modes in solar magnetic pores. **2022 March 7**

### **Inclinations of small quiet-Sun magnetic features based on a new geometric approach**

S. [Jafarzadeh](#), S. K. Solanki, A. Lagg, L. R. Bellot Rubio, M. van Noort, A. Feller, S. Danilovic  
A&A, 569, A105 **2014**

<http://arxiv.org/pdf/1408.2443v1.pdf>

High levels of horizontal magnetic flux have been reported in the quiet-Sun internetwork, often based on Stokes profile inversions. Here we introduce a new method for deducing the inclination of magnetic elements and use it to test magnetic field inclinations from inversions. We determine accurate positions of a set of small, bright magnetic elements in high spatial resolution images sampling different photospheric heights obtained by the Sunrise balloon-borne solar observatory. Together with estimates of the formation heights of the employed spectral bands, these provide us with the inclinations of the magnetic features. We also compute the magnetic inclination angle of the same magnetic features from the inversion of simultaneously recorded Stokes parameters. Our new, geometric method returns nearly vertical fields (average inclination of around 14 deg with a relatively narrow distribution having a standard deviation of 6 deg). In strong contrast to this, the traditionally used inversions give almost horizontal fields (average inclination of  $75 \pm 8$  deg) for the same small magnetic features, whose linearly polarised Stokes profiles are adversely affected by noise. The almost vertical field of bright magnetic features from our geometric method is clearly incompatible with the nearly horizontal magnetic fields obtained from the inversions. This indicates that the amount of magnetic flux in horizontal fields deduced from inversions is overestimated in the presence of weak Stokes signals, in particular if Stokes Q and U are close to or under the noise level. By combining the proposed method with inversions we are not just improving the inclination, but also the field strength. This technique allows us to analyse features that are not reliably treated by inversions, thus greatly extending our capability to study the complete magnetic field of the quiet Sun.

### **Five-minute Oscillation Power within Magnetic Elements in the Solar Atmosphere**

Rekha [Jain](#)<sup>1</sup>, Andrew Gascoyne<sup>1</sup>, Bradley W. Hindman<sup>2</sup>, and Benjamin Gree  
**2014** ApJ 796 72

It has long been known that magnetic plage and sunspots are regions in which the power of acoustic waves is reduced within the photospheric layers. Recent observations now suggest that this suppression of power extends into the low chromosphere and is also present in small magnetic elements far from active regions. In this paper we investigate the observed power suppression in plage and magnetic elements, by modeling each as a collection of vertically aligned magnetic fibrils and presuming that the velocity within each fibril is the response to buffeting by incident p modes in the surrounding field-free atmosphere. We restrict our attention to modeling observations made near the solar disk center, where the line-of-sight velocity is nearly vertical and hence, only the longitudinal component of the motion within the fibril contributes. Therefore, we only consider the excitation of axisymmetric sausage waves and ignore kink oscillations as their motions are primarily horizontal. We compare the vertical motion within the fibril with the vertical motion of the incident p mode by constructing the ratio of their powers. In agreement with observational measurements we find that the total power is suppressed within strong magnetic elements for frequencies below the acoustic cut-off frequency. However, further physical effects need to be examined for understanding the observed power ratios for stronger magnetic field strengths and higher frequencies. We also find that the magnitude of the power deficit increases with the height above the photosphere at which the measurement is made. Furthermore, we argue that the area of the solar disk over which the power suppression extends increases as a function of height.

### **A Twenty Year Decline in Solar Photospheric Magnetic Fields: Inner-Heliospheric Signatures and Possible Implications?**

P. [Janardhan](#), Susanta Kumar Bisoi, S. Ananthakrishnan, [M. Tokumaru](#), [K. Fujiki](#), [L. Jose](#), [R. Sridharan](#)  
JGR **2015**

<http://arxiv.org/pdf/1506.03589v1.pdf>

We report observations of a steady 20 year decline of solar photospheric fields at latitudes  $\geq 45^\circ$  starting from  $\sim 1995$ . This prolonged and continuing decline, combined with the fact that Cycle 24 is already past its peak,

implies that magnetic fields are likely to continue to decline until  $\sim 2020$ , the expected minimum of the ongoing solar Cycle 24. In addition, interplanetary scintillation (IPS) observations of the inner heliosphere for the period 1983–2013 and in the distance range 0.2–0.8 AU, have also shown a similar and steady decline in solar wind micro-turbulence levels, in sync with the declining photospheric fields. Using the correlation between the polar field and heliospheric magnetic field (HMF) at solar minimum, we have estimated the value of the HMF in 2020 to be 3.9 ( $\pm 0.6$ ) and a floor value of the HMF of  $\sim 3.2$  ( $\pm 0.4$ ) nT. Given this floor value for the HMF, our analysis suggests that the estimated peak sunspot number for solar Cycle 25 is likely to be  $\sim 62$  ( $\pm 12$ ).

### Self-organization of solar magnetic fields

**Review**

T.R. [Jarboe](#), [T.E. Benedett](#), [C.J. Everson](#), [C.J. Hansen](#), [A.C. Hossack](#), [K.D. Morgan](#), [B.A. Nelson](#), [J.M. Penna](#), [D.A. Sutherland](#)

2018

<https://arxiv.org/pdf/1807.09593.pdf>

Self-organization properties of sustained magnetized plasma are applied to selected solar data to understand solar magnetic fields. Torsional oscillations are speed-up and slow-down bands of the azimuthal flow that correlate with the solar cycle, and they imply the existence of a symmetric solar dynamo with a measured polar flux of  $3 \times 10^{14}$  Wb. It is shown that the solar dynamo is thin ( $\sim 0.1$  Mm gradient scale size) and powerful ( $\sim 10^{23}$  W). These properties are found from the amplitude of the torsional oscillations and the relationship of their velocity contours to solar magnetograms supports the result. The dynamo has enough power to heat the chromosphere and to power the corona and the solar wind. The dynamo also causes a rigid rotation of the heliosphere out to at least the corona and the relationship of the rotation of the corona to solar magnetograms supports this result as well. The thin solar dynamo sustains a thin stable minimum energy state that seems to be covering most of the solar surface just below the photosphere. The magnetic field lines of the minimum energy state should be parallel to the solar surface and rotate with distance from the surface with  $2\pi$  radians of rotation in  $\sim 1$  Mm Resistive diffusion helps to push the magnetic fields to the surface and the global magnetic structure (GMS) seems to lose  $\pi$  radians every 11 years, causing the observed 180 degree flipping of the solar magnetic field. The thin sheets of magnetized plasma in solar prominences may be the lost thin sheets of the GMS. For completeness, the formation of sunspots, CMEs and flares is discussed.

### Magnetic Field Evolution of the Solar Active Region 13664

[Robert Jarolim](#), [Astrid Veronig](#), [Stefan Purkhart](#), [Peijin Zhang](#), [Matthias Rempel](#)

ApJ 2024

<https://arxiv.org/pdf/2409.08124>

On 2024 May 10/11, the strongest geomagnetic storm since November 2003 has occurred, with a peak Dst index of  $-412$  nT. The storm was caused by NOAA Active Region (AR) 13664, which was the source of a large number of coronal mass ejections and flares, including 12 X-class flares. Starting from about May 7, AR 13664 showed a steep increase in its size and (free) magnetic energy, along with increased flare activity. In this study, we perform 3D magnetic field extrapolations with the NF2 nonlinear-force free code based on physics informed neural networks (Jarolim et al. 2023). In addition, we introduce the computation of the vector potential to achieve divergence-free solutions. We extrapolate vector magnetograms from SDO/HMI at the full 12 minute cadence from 2024 May 5-00:00 to 11-04:36 UT, in order to understand the active regions magnetic evolution and the large eruptions it produced. The computed change in magnetic energy and free magnetic energy shows a clear correspondence to the flaring activity. Regions of free magnetic energy and depleted magnetic energy indicate the flare origin and are in good correspondence with observations in Extreme Ultraviolet. Our results suggest that the modeled solar flares are related to significant topological reconfigurations. We provide a detailed analysis of the X4.0-class flare on May 10, where we show that the interaction between separated magnetic domains is directly linked to major flaring events. With this study, we provide a comprehensive data set of the magnetic evolution of AR 13664 and make it publicly available for further analysis. **May 2024: 5-11, 8, 10, 11**

### Advancing solar magnetic field extrapolations through multi-height magnetic field measurements

[Robert Jarolim](#), [Benoit Tremblay](#), [Matthias Rempel](#), [Momchil Molnar](#), [Astrid M. Veronig](#), [Julia K. Thalmann](#), [Tatiana Podladchikova](#)

ApJ 963 L21 2024

<https://arxiv.org/pdf/2312.06823.pdf>

Non-linear force-free extrapolations are a common approach to estimate the 3D topology of coronal magnetic fields based on photospheric vector magnetograms. The force-free assumption is a valid approximation at coronal heights, but for the dense plasma conditions in the lower atmosphere, this assumption is not satisfied. In this study, we utilize multi-height magnetic field measurements in combination with physics-informed neural networks to advance solar magnetic field extrapolations. We include a flexible height-mapping, which allows us to account for the different formation heights of the observed magnetic field measurements. The comparison to analytical and simulated



magnetic fields demonstrates that including chromospheric magnetic field measurements leads to a significant improvement of our magnetic field extrapolations. We also apply our method to chromospheric line-of-sight magnetograms, from the Vector Spectromagnetograph (VSM) on the Synoptic Optical Long-term Investigations of the Sun (SOLIS) observatory, in combination with photospheric vector magnetograms, from the Helioseismic Magnetic Imager (HMI) onboard the Solar Dynamic Observatory (SDO). The comparison to observations in extreme ultraviolet wavelengths shows that the additional chromospheric information leads to a better agreement with the observed coronal structures. In addition, our method intrinsically provides an estimate of the corrugation of the observed magnetograms. With this new approach, we make efficient use of multi-height magnetic field measurements and advance the realism of coronal magnetic field simulations.

### **Statistical Properties of Photospheric Magnetic Elements Observed by SDO/HMI**

Mohsen [Javaherian](#), [Hossein Safari](#), [Neda Dadashi](#), [Markus Josef Aschwanden](#)

Solar Phys. 292:164 2017

<https://arxiv.org/pdf/1707.09291.pdf>

<https://link.springer.com/content/pdf/10.1007%2Fs11207-017-1189-x.pdf>

Magnetic elements of the solar surface are studied in magnetograms recorded with the high-resolution Solar Dynamics Observatory / Helioseismic and Magnetic Imager . To extract some statistical and physical properties of these elements (e.g., filling factors, magnetic flux, size, lifetimes), the Yet Another Feature Tracking Algorithm (YAFTA), a region-based method, is employed. An area with  $400'' \times 400''$  was selected to investigate the magnetic characteristics during the year 2011. The correlation coefficient between filling factors of negative and positive polarities is 0.51. A broken power law fit was applied to the frequency distribution of size and flux. Exponents of the power-law distributions for sizes smaller and greater than  $16 \text{ arcsec}^2$  were found to be -2.24 and -4.04, respectively. The exponents of power-law distributions for fluxes smaller and greater than  $2.63 \times 10^{19} \text{ Mx}$  were found to be -2.11 and -2.51, respectively. The relationship between the size (S) and flux (F) of elements can be expressed by a power-law behavior in the form of  $S \propto F^{0.69}$ . The lifetime and its relationship with the flux and size of quiet-Sun (QS) elements are studied during three days. The code detected patches with lifetimes of about 15 hours, which we call long-duration events. It is found that more than 95% of the magnetic elements have lifetimes of less than 100 minutes. About 0.05% of the elements were found with lifetimes of more than 6 hours. The relationships between the size (S), lifetime (T), and the flux (F) for patches in the QS, indicate the power-law relationships  $S \propto T^{0.25}$  and  $F \propto T^{0.38}$ , respectively. Executing a detrended fluctuation analysis of the time series of new emerged magnetic elements, we find a Hurst exponent of 0.82, which implies long-range temporal correlation in the system. **14 February 2011,**

### **A Study of Variations in Correlation Between Rotation Residual and Meridional Velocity of Sunspot Groups**

[J. Javaraiah](#)

Solar Phys. 2021

<https://arxiv.org/pdf/2109.09987.pdf>

We analyzed the combined 142 years sunspot-group data from Greenwich Photoheliographic Results (GPR) and Debrecen Photoheliographic Data (DPD) and determined the yearly mean residual rotation rate and the meridional velocity of sunspot groups in different 5-degree latitude intervals. The residual rotation rate is found to be -120 m/s to 80 m/s. In a large number of solar cycles the rotation is to some extent weaker during maxima than that of during minima. There exist alternate bands of equatorward and poleward meridional motions. The equatorward motion is dominant mostly around the maxima of solar cycles with velocity 8-12 m/s, whereas the poleward motion is dominant mostly around the minima but with a relatively weak velocity, only 4-6 m/s. This analysis suggests the existence of equatorward migrating alternate bands of slower and faster than average rotation within the activity belt and no clear equatorward or poleward migrating bands of meridional motions. A statistically significant anticorrelation exists between the meridional motion and residual rotation. The corresponding linear-least-squares best-fit is found to be reasonably good (slope,  $-0.028 \pm 0.008$ , is about 3.5 times larger than its standard deviation). The significant negative value of the slope indicates the existence of a strong angular momentum transport toward equator. The slope leads sunspot number (SN) by about 4 and 9 years. The Morlet wavelet spectrum of the slope suggests the existence of approximate 11-year periodicity in the slope almost throughout the data window, but it was very weak during 1920-1940. Overall the results suggest there exists a strong relationship between the slope and amount of activity during a solar cycle. However, no relationship is found between the slope and strength of activity on a long-time scale (longer than 11-year period).

### **Numerical Simulations of Oscillations in Solar Corona Excited by Vortex Shedding**

Petr [Jelínek](#)<sup>1</sup>, Sofya Belov<sup>1</sup>, and Marian Karlický<sup>2</sup>

2022 ApJ 941 124

<https://iopscience.iop.org/article/10.3847/1538-4357/aca40d/pdf>

We study transverse oscillations of plasma structures in the solar corona excited by vortex shedding solving the full set of the 3D ideal time-dependent magnetohydrodynamic equations. To present how the creation of vortices and excited oscillations depend on the initial flow speed and various values of the magnetic field, we performed a parametric study for two cases, an interaction of a steady flow with a rigid and spatially fixed cylindrical obstacle, and with a cylinder fixed at the boundaries. We show that generated vortices can excite oscillations, e.g., transverse (kink), in the solar corona, for example in coronal loops, filaments, flux ropes, or similar magnetic structures. It has been found that the oscillation period is close to the theoretically predicted value. Moreover, we study the dependence of the Strouhal number with respect to the magnetic field under the conditions of the solar atmosphere.

### **The Comparison of Total Electron Content Between Radio and Thompson Scattering**

E. A. **Jensen**, R. Frazin, C. Heiles, P. Lamy, A. Llebaria, J. D. Anderson, M. M. Bisi, R. A. Fallows  
Solar Phys. Vol. 291, Issue 2 **2016**

The total electron content (TEC) of the solar corona in June 2002 is calculated by three observational techniques and the results are compared. The first technique is solar rotational tomography (SRT) applied to a 14-day time series of LASCO-C2 polarized brightness images, and the other two techniques use the Cassini spacecraft radio beacon for Doppler tracking (phase delay) and ranging (group delay). While the Doppler-tracking technique has an arbitrary zero-point, it is otherwise found that the three methods produce consistent estimates of the TEC to within established uncertainties, providing an independent check on the calibrations. The verification of the accuracy of the Doppler-tracking technique enables a significant improvement to the use of spacecraft data sets in studying the heliosphere: the density component to Faraday rotation can be separated from the magnetic-field component as variable structures cross, such as coronal mass ejections and magnetohydrodynamic waves. Furthermore, we show that the unique frequency-time variable characteristics of the hydrodynamic components of waves can be studied. Based on this work, future Faraday rotation studies of variable solar phenomena will isolate the electron density changes from the magnetic-field contribution. This capability will enable advanced research into variable heliospheric magnetic fields.

### **Improved AI-generated Solar Farside Magnetograms by STEREO and SDO Data Sets and Their Release**

Hyun-Jin **Jeong**<sup>1</sup>, Yong-Jae Moon<sup>1,2</sup>, Eunsu Park<sup>3</sup>, Harim Lee<sup>2</sup>, and Ji-Hye Baek<sup>3,4</sup>  
**2022** ApJS 262 50

<https://iopscience.iop.org/article/10.3847/1538-4365/ac8d66/pdf>

Here we greatly improve artificial intelligence (AI)-generated solar farside magnetograms using data sets from the Solar Terrestrial Relations Observatory (STEREO) and Solar Dynamics Observatory (SDO). We modify our previous deep-learning model and configuration of input data sets to generate more realistic magnetograms than before. First, our model, which is called Pix2PixCC, uses updated objective functions, which include correlation coefficients (CCs) between the real and generated data. Second, we construct input data sets of our model: solar farside STEREO extreme-ultraviolet (EUV) observations together with nearest frontside SDO data pairs of EUV observations and magnetograms. We expect that the frontside data pairs provide historic information on magnetic field polarity distributions. We demonstrate that magnetic field distributions generated by our model are more consistent with the real ones than previously, in consideration of several metrics. The averaged pixel-to-pixel CC for full disk, active regions, and quiet regions between real and AI-generated magnetograms with  $8 \times 8$  binning are 0.88, 0.91, and 0.70, respectively. Total unsigned magnetic flux and net magnetic flux of the AI-generated magnetograms are consistent with those of real ones for the test data sets. It is interesting to note that our farside magnetograms produce polar field strengths and magnetic field polarities consistent with those of nearby frontside magnetograms for solar cycles 24 and 25. Now we can monitor the temporal evolution of active regions using solar farside magnetograms by the model together with the frontside ones. Our AI-generated solar farside magnetograms are now publicly available at the Korean Data Center for SDO (<http://sdo.kasi.re.kr>). **2011 March 5, 2013 October 13, 2021 May 20**

### **Solar coronal magnetic field extrapolation from synchronic data with AI-generated farside**

[Hyunjin Jeong](#), [Yong-Jae Moon](#), [Eunsu Park](#), [Harim Lee](#)

ApJ **903** L25 **2020**

<https://arxiv.org/pdf/2010.07553.pdf>

<https://doi.org/10.3847/2041-8213/abc255>

Solar magnetic fields play a key role in understanding the nature of the coronal phenomena. Global coronal magnetic fields are usually extrapolated from photospheric fields for which farside data were taken about two weeks ago when it was at the frontside. For the first time we have constructed the extrapolations of global magnetic fields using frontside and AI-generated farside magnetic fields at a near-real time basis. We generate the farside magnetograms from three channel farside observations of Solar Terrestrial Relations Observatory (STEREO) –Ahead (A) and –Behind (B) by our deep learning model trained with frontside Solar Dynamics

Observatory (SDO) EUV images and magnetograms. For frontside testing data sets, we demonstrate that the generated magnetic field distributions are consistent with the real ones; not only active regions (ARs), but also quiet regions of the Sun. We make global magnetic field synchronic maps in which conventional farside data are replaced by farside ones generated by our model. The synchronic maps show much better not only the appearance of ARs but also the disappearance of others on the solar surface than before. We use these synchronized magnetic data to extrapolate the global coronal fields using Potential Field Source Surface (PFSS) model. We show that our results are much more consistent with coronal observations than those of the conventional method in view of solar active regions and coronal holes. We present several positive prospects of our new methodology for the study of solar corona, heliosphere, and space weather. **1 June 2011, 14-21 June 2011, 11 and 21 January 2012, 1 April 2014**

### **An Inside Look at Sunspot Oscillations with Higher Azimuthal Wavenumbers**

David B. **Jess**, Tom Van Doorselaere, Gary Verth, Viktor Fedun, S. Krishna Prasad, Robert Erdélyi, Peter H. Keys, Samuel D. T. Grant, Han Uitenbroek, Damian J. Christian

ApJ **842** 59 **2017**

<https://arxiv.org/pdf/1705.06282.pdf>

<http://iopscience.iop.org/article/10.3847/1538-4357/aa73d6/pdf>

Solar chromospheric observations of sunspot umbrae offer an exceptional view of magneto-hydrodynamic wave phenomena. In recent years, a wealth of wave signatures related to propagating magneto-acoustic modes have been presented, which demonstrate complex spatial and temporal structuring of the wave components. Theoretical modelling has demonstrated how these ubiquitous waves are consistent with an  $m=0$  slow magneto-acoustic mode, which are excited by trapped sub-photospheric acoustic ( $p$ -mode) waves. However, the spectrum of umbral waves is broad, suggesting that the observed signatures represent the superposition of numerous frequencies and/or modes. We apply Fourier filtering, in both spatial and temporal domains, to extract chromospheric umbral wave characteristics consistent with an  $m=1$  slow magneto-acoustic mode. This identification has not been described before. Angular frequencies of  $0.037 \pm 0.007$  rad/s ( $2.1 \pm 0.4$  deg/s), corresponding to a period approximately 170 s for the  $m=1$  mode are uncovered for spatial wavenumbers in the range of  $0.45 < k < 0.90$  arcsec<sup>-1</sup> (5000-9000 km). Theoretical dispersion relations are solved, with corresponding eigenfunctions computed, which allows the density perturbations to be investigated and compared with our observations. Such magnetohydrodynamic modelling confirms our interpretation that the identified wave signatures are the first direct observations of an  $m=1$  slow magneto-acoustic mode in the chromospheric umbra of a sunspot.

### **Solar coronal magnetic fields derived using seismology techniques applied to omnipresent sunspot waves**

D.B. **Jess**, V.E. Reznikova, R.S.I. Ryans, D.J. Christian, P.H. Keys, M. Mathioudakis, D.H. Mackay, S. Krishna Prasad, D. Banerjee, S.D.T. Grant, S. Yau, C. Diamond

Nature Physics, 12, 179 (2016; DOI:10.1038/nphys3544)

<http://arxiv.org/pdf/1605.06112v1.pdf>

Sunspots on the surface of the Sun are the observational signatures of intense manifestations of tightly packed magnetic field lines, with near-vertical field strengths exceeding 6,000 G in extreme cases. It is well accepted that both the plasma density and the magnitude of the magnetic field strength decrease rapidly away from the solar surface, making high-cadence coronal measurements through traditional Zeeman and Hanle effects difficult since the observational signatures are fraught with low-amplitude signals that can become swamped with instrumental noise. Magneto-hydrodynamic (MHD) techniques have previously been applied to coronal structures, with single and spatially isolated magnetic field strengths estimated as 9-55 G. A drawback with previous MHD approaches is that they rely on particular wave modes alongside the detectability of harmonic overtones. Here we show, for the first time, how omnipresent magneto-acoustic waves, originating from within the underlying sunspot and propagating radially outwards, allow the spatial variation of the local coronal magnetic field to be mapped with high precision. We find coronal magnetic field strengths of  $32 \pm 5$  G above the sunspot, which decrease rapidly to values of approximately 1 G over a lateral distance of 7000 km, consistent with previous isolated and unresolved estimations. Our results demonstrate a new, powerful technique that harnesses the omnipresent nature of sunspot oscillations to provide magnetic field mapping capabilities close to a magnetic source in the solar corona.

**2011 December 10**

### **Spatially Resolved Coronal Magnetic Fields Derived Using Seismology Techniques Applied to Omnipresent Sunspot Waves**

D. B. **Jess**<sup>1,2</sup>, V. E. Reznikova<sup>3</sup>, R. S. I. Ryans<sup>1</sup>, D. J. Christian<sup>2</sup>, P. H. Keys<sup>1,4</sup>, M. Mathioudakis<sup>1</sup>, D. H. Mackay<sup>5</sup>, S. Krishna Prasad<sup>1</sup>, D. Banerjee<sup>6</sup>, S. D. T. Grant<sup>1</sup>, S. Yau<sup>1</sup> & C. Diamond

HMI Science Nuggets #46 Nov 2015

<http://hmi.stanford.edu/hminuggets/?p=1337>

2011 December 10

### **Extending the Sunspot Area Series from Kodaikanal Solar Observatory**

Bibhuti **Jha**, Manjunath Hegde, Manjunath Hegde, +++

Front. Astron. Space Sci. 9:1019751. 2022

<https://www.frontiersin.org/articles/10.3389/fspas.2022.1019751/pdf>

Kodaikanal Solar Observatory (KoSO) possesses one of world's longest and homogeneous records of sunspot observations that span more than a century (1904–2017). Interestingly, these observations (originally recorded in photographic plates/films) were taken with the same setup over this entire time period which makes this data unique and best suitable for long-term solar variability studies. A large part of this data, between 1921–2011, were digitized earlier and a catalog containing the detected sunspot parameters (e.g., area and location) was published in Mandal et al. (2017). In this article, we extend the earlier catalog by including new sets of data between 1904–1921 and 2011–2017. To this end, we digitize and calibrate these new datasets which include resolving the issue of random image orientation. We fix this by comparing the KoSO images with co-temporal data from Royal Greenwich Observatory. Following that, a semi-automated sunspot detection and automated umbra detection algorithm are implemented onto these calibrated images to detect sunspots and umbra. Additionally, during this catalog update, we also filled data gaps in the existing KoSO sunspot catalog (1921–2011) by virtue of re-calibrating the “rouge” plates. This updated sunspot area series covering nearly 115 years (1904–2017) are being made available to the community and will be a unique source to study the long term variability of the Sun.

### **Magnetic field dependence of bipolar magnetic region tilts on the Sun: Indication of tilt quenching**

Bibhuti Kumar **Jha**, [Bidya Binay Karak](#), [Sudip Mandal](#), [Dipankar Banerjee](#)

ApJL 2020

<https://arxiv.org/pdf/1912.13223.pdf>

The tilt of bipolar magnetic region (BMR) is crucial in the Babcock--Leighton process for the generation of the poloidal magnetic field in Sun. Based on the thin flux tube model of the BMR formation, the tilt is believed to be caused by the Coriolis force acting on the rising flux tube of the strong toroidal magnetic field from the base of the convection zone (BCZ). We analyze the magnetic field dependence of BMR tilts using the magnetograms of Michelson Doppler Imager (MDI) (1996-2011) and Helioseismic and Magnetic Imager (HMI) (2010-2018). We observe that the distribution of the maximum magnetic field ( $B_{\max}$ ) of BMRs is bimodal. Its first peak at the low field corresponds to BMRs which do not have sunspots as counterparts in the white light images, whereas the second peak corresponds to sunspots as recorded in both types of images. We find that the slope of Joy's law ( $\gamma_0$ ) initially increases slowly with the increase of  $B_{\max}$ . However, when  $B_{\max} \geq 2$  kG,  $\gamma_0$  decreases. Scatter of BMR tilt around Joy's law systematically decreases with the increase of  $B_{\max}$ . The decrease of observed  $\gamma_0$  with  $B_{\max}$  provides a hint to a nonlinear tilt quenching in the Babcock--Leighton process. We finally discuss how our results may be used to make a connection with the thin flux tube model.

### **Study of Sunspot Penumbra to Umbra Area Ratio using Kodaikanal White-light Digitized Data**

Bibhuti Kumar **Jha**, [Sudip Mandal](#), [Dipankar Banerjee](#)

Solar Phys. 294:72 2019

<https://arxiv.org/pdf/1905.06888.pdf>

We study the long-term behaviour of sunspot penumbra to umbra area ratio by analyzing the recently digitized Kodaikanal white-light data (1923-2011). We implement an automatic umbra extraction method and compute the ratio over eight solar cycles (Cycles 16-23). Although the average ratio doesn't show any variation with spot latitudes, cycle phases and strengths, it increases from 5.5 to 6 as the sunspot size increases from 100  $\mu\text{hem}$  to 2000  $\mu\text{hem}$ . Interestingly, our analysis also reveals that this ratio for smaller sunspots (area < 100  $\mu\text{hem}$ ) does not have any long-term systematic trend which was earlier reported from the Royal Observatory, Greenwich (RGO) photographic results. To verify the same, we apply our automated extraction technique on Solar and Heliospheric Observatory (SOHO)/Michelson Doppler Imager (MDI) continuum images (1996-2010). Results from this data not only confirm our previous findings, but also show the robustness of our analysis method.

### **Long-term variation of sunspot penumbra to umbra area ratio: A study using Kodaikanal white-light Digitized Data**

[Bibhuti Kumar Jha](#), [Sudip Mandal](#), [Dipankar Banerjee](#)

IAU Proceedings series (IAUS340) 2018

<https://arxiv.org/pdf/1805.06307.pdf>

A typical sunspot, as seen in white-light intensity images, has a two part structure: a dark umbra and a lighter penumbra. Such distinction primarily arises due to the different orientations of magnetic fields in these two regions. In this study, we use the Kodaikanal white-light digitized data archive to analyze the long-term evolution of umbral and penumbral area. We developed an 'automated algorithm' to uniquely identify the sunspot umbra (including the calculation of penumbra to umbra ratio) from these digitized intensity images. Our analysis reveals that the ratio increases slightly with the increase of sunspot area upto 100 msh but eventually settles down to a constant value after that. This study, not only allows us to better understand the evolution of an individual spot and its corresponding magnetic field but this is also beneficial for solar dynamo studies which aim to reproduce such structures using a MHD theory.

### **Investigation of Umbral Dots with the New Vacuum Solar Telescope**

Kaifan [Ji](#), Xia Jiang, Song Feng, Yunfei Yang, Hui Deng, Feng Wang

Solar Phys. Volume 291, Issue 2, pp 357-369 2016

<http://arxiv.org/pdf/1509.00312v3.pdf>

Umbral dots (UDs) are small isolated brightenings observed in sunspot umbrae. They are convective phenomena existing inside umbrae. UD are usually divided into central UD (CUDs) and peripheral UD (PUDs) according to their positions inside an umbra. Our purpose is to investigate UD properties and analyze their relationships, and further to find whether or not the properties depend on the umbral magnetic field variation. For this purpose, we selected the high-resolution TiO images of four active regions (ARs) obtained under the best seeing conditions with the New Vacuum Solar Telescope in the Fuxian Solar Observatory of the Yunnan Astronomical Observatory, China. The four ARs (NOAA 11598, 11801, 12158, and 12178) include six sunspots. A total of 1220 CUDs were identified in six sunspots, and 603 PUDs in three sunspots. Meanwhile, the radial component of the magnetic field of the sunspots obtained with the Helioseismic and Magnetic Imager onboard the Solar Dynamics Observatory was used to analyze the relationship between UD properties and the magnetic field. The diameters and lifetimes of CUDs exhibit an increasing trend with brightness, whereas their horizontal velocities exhibit an inverse trend. Moreover, the diameter, intensity and velocity depend on the magnetic field variation. The diameter of a CUD becomes larger and brighter, and its motion slower in a weak magnetic field than in a strong field. Similar trends are also found for PUDs. Moreover, we also find that the lifetimes of UD located in different sunspots are not obviously different, implying that they are unrelated to the magnetic flux density in which they live. 29-10-2012, 01-08-2013, 13 September 2014, 03-10-2014

### **OBSERVATION OF ULTRAFINE CHANNELS OF SOLAR CORONA HEATING**

Haisheng [Ji](#)<sup>1,2</sup>, Wenda Cao<sup>2,3</sup>, and Philip R. Goode

2012 ApJ 750 L25

We report the first direct observations of dynamical events originating in the Sun's photosphere and subsequently lighting up the corona. Continuous small-scale, impulsive events have been tracked from their origin in the photosphere on through to their brightening of the local corona. We achieve this by combining high-resolution ground-based data from the 1.6 m aperture New Solar Telescope (NST) at Big Bear Solar Observatory (BBSO), and satellite data from the Atmospheric Imaging Assembly (AIA) on board the Solar Dynamics Observatory (SDO). The NST imaging observations in helium I 10830 Å reveal unexpected complexes of ultrafine, hot magnetic loops seen to be reaching from the photosphere to the base of the corona. Most of these ultrafine loops are characterized by an apparently constant, but surprisingly narrow diameter of about 100 km all along each loop, and the loops originate on the solar surface from intense, compact magnetic field elements. The NST observations detect the signature of upward injections of hot plasma that excite the ultrafine loops from the photosphere to the base of the corona. The ejecta have their individual footpoints in the intergranular lanes between the Sun's ubiquitous, convectively driven granules. In many cases, AIA/SDO detects cospatial and cotemporal brightenings in the overlying, million degree coronal loops in conjunction with the upward injections along the ultrafine loops. Segments of some of the more intense upward injections are seen as rapid blueshifted events in simultaneous H $\alpha$  blue wing images observed at BBSO. In sum, the observations unambiguously show impulsive coronal heating events from upward energy flows originating from intergranular lanes on the solar surface accompanied by cospatial mass flows.

### **Generating Photospheric Vector Magnetograms of Solar Active Regions for SOHO/MDI Using SDO/HMI and BBSO Data with Deep Learning**

[Haodi Jiang](#), [Qin Li](#), [Zhihang Hu](#), [Nian Liu](#), [Yasser Abdullallah](#), [Ju Jing](#), [Genwei Zhang](#), [Yan Xu](#), [Wynne Hsu](#), [Jason T. L. Wang](#), [Haimin Wang](#)

*Solar Physics* volume 298, Article number: 87 2023

<https://arxiv.org/pdf/2211.02278.pdf>

<https://doi.org/10.1007/s11207-023-02180-z>

Solar activity is usually caused by the evolution of solar magnetic fields. Magnetic field parameters derived from photospheric vector magnetograms of solar active regions have been used to analyze and forecast eruptive events such as solar flares and coronal mass ejections. Unfortunately, the most recent solar cycle 24 was relatively weak

with few large flares, though it is the only solar cycle in which consistent time-sequence vector magnetograms have been available through the Helioseismic and Magnetic Imager (HMI) on board the Solar Dynamics Observatory (SDO) since its launch in 2010. In this paper, we look into another major instrument, namely the Michelson Doppler Imager (MDI) on board the Solar and Heliospheric Observatory (SOHO) from 1996 to 2010. The data archive of SOHO/MDI covers more active solar cycle 23 with many large flares. However, SOHO/MDI data only has line-of-sight (LOS) magnetograms. We propose a new deep learning method, named MagNet, to learn from combined LOS magnetograms,  $B_x$  and  $B_y$  taken by SDO/HMI along with H-alpha observations collected by the Big Bear Solar Observatory (BBSO), and to generate vector components  $B_x'$  and  $B_y'$ , which would form vector magnetograms with observed LOS data. In this way, we can expand the availability of vector magnetograms to the period from 1996 to present. Experimental results demonstrate the good performance of the proposed method. To our knowledge, this is the first time that deep learning has been used to generate photospheric vector magnetograms of solar active regions for SOHO/MDI using SDO/HMI and H-alpha data. **2010 August 30, 2010 October 27, 2017 September 6, 2017 October 2**

## **MHD Modeling of Solar Coronal Magnetic Evolution Driven by Photospheric Flow**

[Chaowei Jiang](#), [Xinkai Bian](#), [Tingting Sun](#), [Xueshang Feng](#)

Frontiers in Physics **2021**

<https://arxiv.org/pdf/2104.07229.pdf>

It is well known that magnetic fields dominate the dynamics in the solar corona, and new generation of numerical modelling of the evolution of coronal magnetic fields, as featured with boundary conditions driven directly by observation data, are being developed. This paper describes a new approach of data-driven magnetohydrodynamic (MHD) simulation of solar active region (AR) magnetic field evolution, which is for the first time that a data-driven full-MHD model utilizes directly the photospheric velocity field from DAVE4VM. We constructed a well-established MHD equilibrium based on a single vector magnetogram by employing an MHD-relaxation approach with sufficiently small kinetic viscosity, and used this MHD equilibrium as the initial conditions for subsequent data-driven evolution. Then we derived the photospheric surface flows from a time series of observed magnetograms based on the DAVE4VM method. The surface flows are finally inputted in time sequence to the bottom boundary of the MHD model to self-consistently update the magnetic field at every time step by solving directly the magnetic induction equation at the bottom boundary. We applied this data-driven model to study the magnetic field evolution of AR 12158 with SDO/HMI vector magnetograms. Our model reproduced a quasi-static stress of the field lines through mainly the rotational flow of the AR's leading sunspot, which makes the core field lines to form a coherent S shape consistent with the sigmoid structure as seen in the SDO/AIA images. The total magnetic energy obtained in the simulation matches closely the accumulated magnetic energy as calculated directly from the original vector magnetogram with the DAVE4VM derived flow field. Such a data-driven model will be used to study how the coronal field, as driven by the slow photospheric motions, reaches a unstable state and runs into eruptions. **2014 September 8-10**

## **Testing a Data-driven Active Region Evolution Model with Boundary Data at Different Heights from a Solar Magnetic Flux Emergence Simulation**

[Chaowei Jiang](#), [Shin Toriumi](#)

ApJ **903** 11 **2020**

<https://arxiv.org/pdf/2010.02497.pdf>

<https://doi.org/10.3847/1538-4357/abb5ac>

A data-driven active region evolution (DARE) model has been developed to study the complex structures and dynamics of solar coronal magnetic fields. The model is configured with typical coronal environment of tenuous gas governed by strong magnetic field, and thus its lower boundary is set at the base of the corona, but driven by magnetic fields observed in the photosphere. A previous assessment of the model using data from a flux emergence simulation (FES) showed that the DARE failed to reproduce the coronal magnetic field in the FES, which is attributed to the fact that the photospheric data in the FES has a very strong Lorentz force and therefore spurious flows are generated in the DARE model. Here we further test the DARE by using three sets of data from the FES sliced at incremental heights, which correspond to the photosphere, the chromosphere and the base of the corona. It is found that the key difference in the three sets of data is the extent of the Lorentz force, which makes the data-driven model perform very differently. At the two higher levels above the photosphere, the Lorentz force decreases substantially, and the DARE model attains results in much better agreement with the FES, confirming that the Lorentz force in the boundary data is a key issue affecting the results of the DARE model. However, unlike the FES data, the photospheric field from SDO/HMI observations has recently been found to be very close to force-free. Therefore, we suggest that it is still reasonable to use the photospheric magnetic field as approximation of the field at the coronal base to drive the DARE model.

## **Identifying and Tracking Solar Magnetic Flux Elements with Deep Learning**

Haodi **Jiang**<sup>1,2</sup>, Jiasheng Wang<sup>1,3,4</sup>, Chang Liu<sup>1,3,4</sup>, Ju Jing<sup>1,3,4</sup>, Hao Liu<sup>1,2</sup>, Jason T. L. Wang<sup>1,2</sup>, and Haimin Wang<sup>1,3,4</sup>

2020 ApJS 250 5

<https://doi.org/10.3847/1538-4365/aba4aa>

<https://arxiv.org/pdf/2008.12080.pdf>

Deep learning has drawn significant interest in recent years due to its effectiveness in processing big and complex observational data gathered from diverse instruments. Here we propose a new deep learning method, called SolarUnet, to identify and track solar magnetic flux elements or features in observed vector magnetograms based on the Southwest Automatic Magnetic Identification Suite (SWAMIS). Our method consists of a data preprocessing component that prepares training data from the SWAMIS tool, a deep learning model implemented as a U-shaped convolutional neural network for fast and accurate image segmentation, and a postprocessing component that prepares tracking results. SolarUnet is applied to data from the 1.6 m Goode Solar Telescope at the Big Bear Solar Observatory. When compared to the widely used SWAMIS tool, SolarUnet is faster while agreeing mostly with SWAMIS on feature size and flux distributions and complementing SWAMIS in tracking long-lifetime features. Thus, the proposed physics-guided deep learning-based tool can be considered as an alternative method for solar magnetic tracking. **2017 July 13**

### **Decipher the Three-Dimensional Magnetic Topology of a Great Solar Flare**

Chaowei **Jiang**, [Peng Zou](#), [Xueshang Feng](#), [Qiang Hu](#), [Aiyang Duan](#), [Pingbing Zuo](#), [Yi Wang](#), [Fengsi Wei](#)

2018

<https://arxiv.org/pdf/1802.02759.pdf>

Three-dimensional magnetic topology of solar flare plays a crucial role in understanding its explosive release of magnetic energy in the corona. However, such three-dimensional coronal magnetic field is still elusive in direct observation. Here we realistically simulate the magnetic evolution during the eruptive process of a great flare, using a numerical magnetohydrodynamic model constrained by observed solar vector magnetogram. The numerical results reveal that the pre-flare corona contains multi-set twisted magnetic flux, which forms a coherent rope during the eruption. The rising flux rope is wrapped by a quasi-separatrix layer, which intersects itself below the rope, forming a hyperbolic flux tube and magnetic reconnection is triggered there. By tracing the footprint of the newly-reconnected field lines, we reproduce both the spatial location and its temporal evolution of flare ribbons with an expected accuracy in comparison of observed images. This scenario strongly confirms the three-dimensional version of standard flare model. **September 6 and 10, 2017**

### **Predicting solar surface large-scale magnetic field of Cycle 24**

Jie **Jiang**, Jinbin Cao

JASTP 2017

<https://arxiv.org/pdf/1707.00268.pdf>

The Sun's surface field, especially the polar field, sets the boundary condition for the coronal and heliospheric magnetic fields, but also provides us insight into the dynamo process. The evolution of the polar fields results from the emergence and subsequent evolution of magnetic flux through the solar surface. In this paper we use a Monte Carlo approach to investigate the evolution of the fields during the decay phase of cycle 24. Our simulations include the emergence of flux through the solar surface with statistical properties derived from previous cycles. The well-calibrated surface flux transport model is used to follow the evolution of the large-scale field. We find the polar field can be well reproduced one year in advance using the observed synoptic magnetograms as the initial condition. The temporary variation of the polar field measured by Wilcox Solar Observatory (WSO), e.g., the strong decrease of the south polar field during 2016-2017 which is not shown by SDO/HMI and NSO/SOLIS data usually is not well reproduced. We suggest observational effects, such as the effect of the large gradient of the magnetic field around the southern polar cap and the low resolution of WSO might be responsible. The northern hemisphere polar field is predicted to increase during 2017. The southern polar field is predicted to be stable during 2017-2018. At the end of 2017, the magnetic field in two poles is predicted to be similar (although of opposite polarities). The expected value for the dipole moment around 2020 is  $1.76 \pm 0.68$  G and  $2.11 \pm 0.69$  G based on the initial conditions from SDO/HMI and NSO/SOLIS synoptic magnetograms, respectively. It is comparable to that observed one at the end of Cycle 23 (about 1.6G based on SOHO/MDI).

### **A Magnetic Bald-Patch Flare in Solar Active Region 11117**

Chaowei **Jiang**, Xueshang Feng, S. T. Wu, Qiang Hu

RAA 2017

<https://arxiv.org/pdf/1705.10493.pdf>

With SDO observations and a data-constrained MHD model, we identify a confined multi-ribbon flare occurred on **2010 October 25** in solar active region 11117 as a magnetic bald patch (BP) flare with strong evidences. From the photospheric magnetic field observed by SDO/HMI, we find there is indeed magnetic BPs on the PILs which match parts of the flare ribbons. From the 3D coronal magnetic field derived from a MHD relaxation model constrained by the vector magnetograms, we find strikingly good agreement of the BP separatrix surface (BPSS) footpoints with the flare ribbons, and the BPSS itself with the hot flaring loop system. Moreover, the triggering of the BP flare can be attributed to a small flux emergence under the lobe of the BPSS, and the relevant change of the coronal magnetic field through the flare is well reproduced by the pre-flare and post-flare MHD solutions, which match the corresponding pre and post-flare AIA observations, respectively. Our work contributes to the study of non-typical flares that constitute the majority of solar flares but cannot be explained by the standard flare model.

## **Testing a Solar Coronal Magnetic Field Extrapolation Code with the Titov-Demoulin Magnetic Flux Rope Model**

Chaowei **Jiang**, Xueshang Feng

RAA **2015**

<http://arxiv.org/pdf/1507.01910v1.pdf>

In the solar corona, magnetic flux rope is believed to be a fundamental structure accounts for magnetic free energy storage and solar eruptions. Up to the present, the extrapolation of magnetic field from boundary data is the primary way to obtain fully three-dimensional magnetic information of the corona. As a result, the ability of reliable recovering coronal magnetic flux rope is important for coronal field extrapolation. In this paper, our coronal field extrapolation code (CESE-MHD-NLFFF, Jiang & Feng 2012) is examined with an analytical magnetic flux rope model proposed by Titov & Demoulin (1999), which consists of a bipolar magnetic configuration holding an semi-circular line-tied flux rope in force-free equilibrium. By using only the vector field in the bottom boundary as input, we test our code with the model in a representative range of parameter space and find that the model field is reconstructed with high accuracy. Especially, the magnetic topological interfaces formed between the flux rope and the surrounding arcade, i.e., the "hyperbolic flux tube" and "bald patch separatrix surface", are also reliably reproduced. By this test, we demonstrate that our CESE-MHD-NLFFF code can be applied to recovering magnetic flux rope in the solar corona as long as the vector magnetogram satisfies the force-free constraints.

## **Magnetic Flux Transport at the Solar Surface** Review

J. **Jiang**, D. H. Hathaway, R. H. Cameron, S. K. Solanki, L. Gizon, L. Upton

Space Sci. Rev., Volume 186, [Issue 1-4](#), pp 491-523, Dec **2014**

<http://arxiv.org/pdf/1408.3186v1.pdf>

After emerging to the solar surface, the Sun's magnetic field displays a complex and intricate evolution. The evolution of the surface field is important for several reasons. One is that the surface field, and its dynamics, sets the boundary condition for the coronal and heliospheric magnetic fields. Another is that the surface evolution gives us insight into the dynamo process. In particular, it plays an essential role in the Babcock-Leighton model of the solar dynamo. Describing this evolution is the aim of the surface flux transport model. The model starts from the emergence of magnetic bipoles. Thereafter, the model is based on the induction equation and the fact that after emergence the magnetic field is observed to evolve as if it were purely radial. The induction equation then describes how the surface flows -- differential rotation, meridional circulation, granular, supergranular flows, and active region inflows -- determine the evolution of the field (now taken to be purely radial). In this paper, we review the modeling of the various processes that determine the evolution of the surface field. We restrict our attention to their role in the surface flux transport model. We also discuss the success of the model and some of the results that have been obtained using this model.

## **Effects of the scatter in sunspot group tilt angles on the large-scale magnetic field at the solar surface**

J. **Jiang**, R.H. Cameron, M. Schuessler

**2014**, ApJ 791, 5

<http://arxiv.org/pdf/1406.5564v1.pdf>

The tilt angles of sunspot groups represent the poloidal field source in Babcock-Leighton-type models of the solar dynamo and are crucial for the build-up and reversals of the polar fields in Surface Flux Transport (SFT) simulations. The evolution of the polar field is a consequence of Hale's polarity rules, together with the tilt angle distribution which has a systematic component (Joy's law) and a random component (tilt-angle scatter). We determine the scatter using the observed tilt angle data and study the effects of this scatter on the evolution of the solar surface field using SFT simulations with flux input based upon the recorded sunspot groups. The tilt angle scatter is described in our simulations by a random component according to the observed distributions for different ranges of sunspot group size (total umbral area). By performing simulations with a number of different realizations of the scatter we study the effect of the tilt angle scatter on the global magnetic field, especially on the evolution of the axial dipole moment. The average axial dipole moment at the end of cycle 17 (a medium-amplitude cycle) from



our simulations was 2.73G. The tilt angle scatter leads to an uncertainty of 0.78 G (standard deviation). We also considered cycle 14 (a weak cycle) and cycle 19 (a strong cycle) and show that the standard deviation of the axial dipole moment is similar for all three cycles. The uncertainty mainly results from the big sunspot groups which emerge near the equator. In the framework of Babcock-Leighton dynamo models, the tilt angle scatter therefore constitutes a significant random factor in the cycle-to-cycle amplitude variability, which strongly limits the predictability of solar activity.

## **Nonlinear Force-Free Field Extrapolation of a Coronal Magnetic Flux Rope Supporting a Large-Scale Filament from Photospheric Vector Magnetogram**

Chaowei **Jiang**, S. T. Wu, Xueshang Feng, Qiang Hu

ApJL 786 L16 2014

<http://arxiv.org/pdf/1403.7807v1.pdf>

Solar filament are commonly thought to be supported in magnetic dips, in particular, of magnetic flux ropes (FRs). In this Letter, from the observed photospheric vector magnetogram, we implement a nonlinear force-free field (NLFFF) extrapolation of a coronal magnetic FR that supports a large-scale intermediate filament between an active region and a weak polarity region. This result is the first in that current NLFFF extrapolations with presence of FRs are limited to relatively small-scale filaments that are close to sunspots and along main polarity inversion line (PIL) with strong transverse field and magnetic shear, and the existence of a FR is usually predictable. In contrast, the present filament lies along the weak-field region (photospheric field strength  $\lesssim 100$  G), where the PIL is very fragmented due to small parasitic polarities on both side of the PIL and the transverse field has a low value of signal-to-noise ratio. Thus it represents a far more difficult challenge to extrapolate a large-scale FR in such case. We demonstrate that our CESE--MHD--NLFFF code is competent for the challenge. The numerically reproduced magnetic dips of the extrapolated FR match observations of the filament and its barbs very well, which supports strongly the FR-dip model for filaments. The filament is stably sustained because the FR is weakly twisted and strongly confined by the overlying closed arcades.

## **EXTRAPOLATION OF THE SOLAR CORONAL MAGNETIC FIELD FROM SDO/HMI MAGNETOGRAM BY A CESE-MHD-NLFFF CODE**

Chaowei **Jiang** and Xueshang Feng

2013 ApJ 769 144

Due to the absence of direct measurement, the magnetic field in the solar corona is usually extrapolated from the photosphere in a numerical way. At the moment, the nonlinear force-free field (NLFFF) model dominates the physical models for field extrapolation in the low corona. Recently, we have developed a new NLFFF model with MHD relaxation to reconstruct the coronal magnetic field. This method is based on CESE-MHD model with the conservation-element/solution-element (CESE) spacetime scheme. In this paper, we report the application of the CESE-MHD-NLFFF code to Solar Dynamics Observatory/Helioseismic and Magnetic Imager (SDO/HMI) data with magnetograms sampled for two active regions (ARs), NOAA AR 11158 and 11283, both of which were very non-potential, producing X-class flares and eruptions. The raw magnetograms are preprocessed to remove the force and then inputted into the extrapolation code. Qualitative comparison of the results with the SDO/AIA images shows that our code can reconstruct magnetic field lines resembling the EUV-observed coronal loops. Most important structures of the ARs are reproduced excellently, like the highly sheared field lines that suspend filaments in AR 11158 and twisted flux rope which corresponds to a sigmoid in AR 11283. Quantitative assessment of the results shows that the force-free constraint is fulfilled very well in the strong-field regions but apparently not that well in the weak-field regions because of data noise and numerical errors in the small currents.

## **A Unified and Very Fast Way for Computing the Global Potential and Linear Force-Free Fields**

Chaowei **Jiang**, Xueshang Feng

Solar Physics, December 2012, Volume 281, Issue 2, pp 621-637

We present a fast solver for computing potential and linear force-free fields (LFFF) above the full solar disk with a synoptic magnetic map as input. The global potential field and the LFFF are dealt with in a unified way by solving a three-dimensional Helmholtz equation in a spherical shell and a two-dimensional Poisson equation on the solar surface. The solver is based on a combination of the spectral method and the finite-difference scheme. In the longitudinal direction the equation is transformed into the Fourier spectral space, and the resulting two-dimensional equations in the  $r$ - $\theta$  plane for the Fourier coefficients are solved by finite differencing. The solver shows an extremely fast computing speed, e.g., the computation for a magnetogram with a resolution of  $180(\theta) \times 360(\phi)$  is completed in less than 2 s. Even on a high-resolution  $600 \times 1200$  grid, the solution can be obtained within only about

one minute on a single CPU. The solver can potentially be applied directly to the original resolution of observed magnetograms from SDO/HMI for routinely analyzing daily full-disk data.

## **A NEW CODE FOR NONLINEAR FORCE-FREE FIELD EXTRAPOLATION OF THE GLOBAL CORONA**

Chaowei [Jiang](#), Xueshang Feng, and Changqing Xiang

**2012** ApJ 755 62

Reliable measurements of the solar magnetic field are still restricted to the photosphere, and our present knowledge of the three-dimensional coronal magnetic field is largely based on extrapolations from photospheric magnetograms using physical models, e.g., the nonlinear force-free field (NLFFF) model that is usually adopted. Most of the currently available NLFFF codes have been developed with computational volume such as a Cartesian box or a spherical wedge, while a global full-sphere extrapolation is still under development. A high-performance global extrapolation code is in particular urgently needed considering that the Solar Dynamics Observatory can provide a full-disk magnetogram with resolution up to  $4096 \times 4096$ . In this work, we present a new parallelized code for global NLFFF extrapolation with the photosphere magnetogram as input. The method is based on the magnetohydrodynamics relaxation approach, the CESE-MHD numerical scheme, and a Yin-Yang spherical grid that is used to overcome the polar problems of the standard spherical grid. The code is validated by two full-sphere force-free solutions from Low & Lou's semi-analytic force-free field model. The code shows high accuracy and fast convergence, and can be ready for future practical application if combined with an adaptive mesh refinement technique.

## **A NEW IMPLEMENTATION OF THE MAGNETOHYDRODYNAMICS-RELAXATION METHOD FOR NONLINEAR FORCE-FREE FIELD EXTRAPOLATION IN THE SOLAR CORONA**

Chaowei [Jiang](#) and Xueshang Feng

**2012** ApJ 749 135

The magnetic field in the solar corona is usually extrapolated from a photospheric vector magnetogram using a nonlinear force-free field (NLFFF) model. NLFFF extrapolation needs considerable effort to be devoted to its numerical realization. In this paper, we present a new implementation of the magnetohydrodynamics (MHD) relaxation method for NLFFF extrapolation. The magnetofrictional approach, which is introduced for speeding the relaxation of the MHD system, is realized for the first time by the spacetime conservation-element and solution-element scheme. A magnetic field splitting method is used to further improve the computational accuracy. The bottom boundary condition is prescribed by incrementally changing the transverse field to match the magnetogram, and all other artificial boundaries of the computational box are simply fixed. We examine the code using two types of NLFFF benchmark tests, the Low & Lou semi-analytic force-free solutions and a more realistic solar-like case constructed by van Ballegoijen et al. The results show that our implementation is successful and versatile for extrapolations of either the relatively simple cases or the rather complex cases that need significant rebuilding of the magnetic topology, e.g., a flux rope. We also compute a suite of metrics to quantitatively analyze the results and demonstrate that the performance of our code in extrapolation accuracy basically reaches the same level of the present best-performing code, i.e., that developed by Wiegmann.

## **RECONSTRUCTION OF THE CORONAL MAGNETIC FIELD USING THE CESE-MHD METHOD**

Chaowei [Jiang](#)<sup>1,2</sup>, Xueshang Feng<sup>1</sup>, Yuliang Fan<sup>3,4</sup> and Changqing Xiang<sup>1</sup>

**2011** ApJ 727 101

We present a new implementation of the MHD relaxation method for reconstruction of the nearly force-free coronal magnetic field from a photospheric vector magnetogram. A new numerical MHD scheme is proposed to solve the full MHD equations by using the spacetime conservation-element and solution-element method. The bottom boundary condition is prescribed in a similar way as in the stress-and-relax method, by changing the transverse field incrementally to match the magnetogram, and other boundaries of the computational box are set by the nonreflecting boundary conditions. Applications to the well-known benchmarks for nonlinear force-free-field reconstruction, the Low & Lou force-free equilibria, validate the method and confirm its capability for future practical application, with observed magnetograms as inputs

## MODELING THE SUN'S OPEN MAGNETIC FLUX AND THE HELIOSPHERIC CURRENT SHEET

[J. Jiang](#), [R. Cameron](#), [D. Schmitt](#) and [M. Schüssler](#)

ApJ 709 301-307, 2010

By coupling a solar surface flux transport model with an extrapolation of the heliospheric field, we simulate the evolution of the Sun's open magnetic flux and the heliospheric current sheet (HCS) based on observational data of sunspot groups since 1976. The results are consistent with measurements of the interplanetary magnetic field near Earth and with the tilt angle of the HCS as derived from extrapolation of the observed solar surface field. This opens the possibility for an improved reconstruction of the Sun's open flux and the HCS into the past on the basis of empirical sunspot data.

## Magnetic Outbreak Associated with Exploding Granulations

Chunlan [Jin](#)<sup>1</sup>, Guiping Zhou<sup>1</sup>, Guiping Ruan<sup>2</sup>, T. Baildon<sup>3,4</sup>, Wenda Cao<sup>3,4</sup>, and Jingxiu Wang<sup>1,5</sup>  
2023 ApJL 942 L3

<https://iopscience.iop.org/article/10.3847/2041-8213/aca97c/pdf>

Diagnosing the spatiotemporal pattern of magnetic flux on the Sun is vital for understanding the origin of solar magnetism and activity. Here, we report a new form of flux appearance, magnetic outbreak, using observations with an extremely high spatial resolution of  $0''.16$  from the 1.6 m Goode Solar Telescope at the Big Bear Solar Observatory. Magnetic outbreak refers to an early growth of unipolar magnetic flux and its later explosion into fragments, in association with plasma upflow and exploding granulations; each individual fragment has flux of 1016–1017 Mx, moving apart with a velocity of 0.5–2.2 km s<sup>-1</sup>. The magnetic outbreak takes place in the hecto-Gauss region of pore moats. In this study, we identify six events of magnetic outbreak during 6 hr observations over an approximately 40" × 40" field of view. The newly discovered magnetic outbreak might be the first evidence of the long-anticipated convective blowup. **2016 August 25**

## Assessing the Influence of Input Magnetic Maps on Global Modeling of the Solar Wind and CME-driven Shock in the 2013 April 11 Event

Meng [Jin](#), [Nariaki V. Nitta](#), [Christina M. S. Cohen](#)

Space Weather 2022

<https://arxiv.org/pdf/2202.07214.pdf>

In the past decade, significant efforts have been made in developing physics-based solar wind and coronal mass ejection (CME) models, which have been or are being transferred to national centers (e.g., SWPC, CCMC) to enable space weather predictive capability. However, the input data coverage for space weather forecasting is extremely limited. One major limitation is the solar magnetic field measurements, which are used to specify the inner boundary conditions of the global magnetohydrodynamic (MHD) models. In this study, using the Alfvén wave solar model (AWSOM), we quantitatively assess the influence of the magnetic field map input (synoptic/diachronic vs. synchronic magnetic maps) on the global modeling of the solar wind and the CME-driven shock in the **2013 April 11** solar energetic particle (SEP) event. Our study shows that due to the inhomogeneous background solar wind and dynamical evolution of the CME, the CME-driven shock parameters change significantly both spatially and temporally as the CME propagates through the heliosphere. The input magnetic map has a great impact on the shock connectivity and shock properties in the global MHD simulation. Therefore this study illustrates the importance of taking into account the model uncertainty due to the imperfect magnetic field measurements when using the model to provide space weather predictions.

## The Bipolar Magnetic Emergence in the Solar Polar Region

Chunlan [Jin](#)<sup>1</sup>, Guiping Zhou<sup>1</sup>, Yuzong Zhang<sup>1</sup>, and Jingxiu Wang<sup>1,2</sup>

2020 ApJL 889 L26

<https://iopscience.iop.org/article/10.3847/2041-8213/ab65bf/pdf>

Due to projection effect and polarization sensitivity, it is still unknown whether the bipolar magnetic emergence (BME) exists in the solar polar region. In this study, combining the magnetic observations from the Helioseismic and Magnetic Imager and imaging observations of the 211 Å waveband from the Atmospheric Imaging Assembly, we try to identify and diagnose the BME. Considering the magnetic evolution and the corresponding intensity variation in the extreme ultraviolet waveband, we find definite events of the BMEs in the solar polar region. In total, we identify more than 300 BMEs in the solar polar region in the whole year from 2010 June to 2011 May. We find that whether on the southern or northern polar region, the leading polarity of the BMEs is almost half-positive and half-negative, and the BMEs' magnetic axes show random distribution in that direction. These results imply the possible existence of local dynamo in the solar polar region. **23 Nov 2010, 12 May 2011,**

## Solar Cycle Variation of the Inter-network Magnetic Field

Chunlan **Jin** and Jingxiu Wang

2015 ApJ 806 174

The solar inter-network magnetic field is the weakest component of solar magnetism, but it contributes most of the solar surface magnetic flux. The study of its origin has been constrained by the inadequate temporospatial resolution and sensitivity of polarization observations. With dramatic advances in spatial resolution and detecting sensitivity, the solar spectropolarimetry provided by the Solar Optical Telescope on board Hinode in an interval from the solar minimum to maximum of cycle 24 opens an unprecedented opportunity to study the cyclic behavior of the solar inter-network magnetic field. More than 1000 Hinode magnetograms observed from 2007 January to 2014 August are selected in the study. It has been found that there is a very slight correlation between sunspot number and magnetic field at the inter-network flux spectrum. From solar minimum to maximum of cycle 24, the flux density of the solar inter-network field is invariant, at  $10 \pm 1$  G. The observations suggest that the inter-network magnetic field does not arise from flux diffusion or flux recycling of solar active regions, thereby indicating the existence of a local small-scale dynamo. Combining the full-disk magnetograms observed by the Solar and Heliospheric Observatory/Michelson Doppler Imager and the Solar Dynamics Observatory/Heliographic Imager and Magnetic Imager in the same period, we find that the area ratio of the inter-network region to the full disk of the Sun apparently decreases from solar minimum to maximum but always exceeds 60%, even in the phase of solar maximum.

See HMI Science Nuggets, #39, June 2015

<http://hmi.stanford.edu/hminuggets/?p=1188>

### Variation of the solar magnetic flux spectrum during solar cycle 23†

C. L. **Jin**, J. X. Wang

E-print, Dec 2013; JGR, Volume 119, Issue 1, pages 11–17, January 2014

<http://onlinelibrary.wiley.com/doi/10.1002/2013JA019291/pdf>

By using the unique database of SOHO/MDI full disk magnetograms from 1996 September to 2011 January, covering the entire solar cycle 23, we analyze the time-variability of the solar magnetic flux spectrum and study the properties of extended minimum of cycle 23. We totally identify 11.5 million magnetic structures. It has been revealed that magnetic features with different magnetic fluxes exhibit different cycle behaviors. The magnetic features with flux larger than  $4.0 \times 10^{19}$  Mx, which cover solar active regions and strong network features, show exactly the same variation as sunspots; However, the remaining 82% magnetic features which cover the majority of network elements show anti-phase variation with sunspots. We select a criterion that the monthly sunspot number is less than 20 to represent the Sun's low activity status. Then we find the extended minimum of cycle 23 is characterized by the long duration of low activity status, but the magnitude of magnetic flux in this period is not lower than previous cycle. Both the duration of low activity status and the minimum activity level defined by minimum sunspot number show a century period approximately. The extended minimum of cycle 23 shows similarities with solar cycle 11, which preceded the mini-maxima in later solar cycles. This similarity is suggestive that the solar cycles following cycle 23 are likely to have low activity.

### SYNOPTIC MAPPING OF CHROMOSPHERIC MAGNETIC FLUX

C. L. **Jin**<sup>1,3</sup>, J. W. Harvey<sup>2</sup>, and A. Pietarila

2013 ApJ 765 79

We used daily full-disk Ca II 854.2 nm magnetograms from the Synoptic Optical Long Term Investigations of the Sun (SOLIS) facility to study the chromospheric magnetic field from 2006 April through 2009 November. We determined and corrected previously unidentified zero offsets in the SOLIS magnetograms. By tracking the disk passages of stable unipolar regions, the measured net flux densities were found to systematically decrease from the disk center to the limb by a factor of about two. This decrease was modeled using a thin flux tube model with a difference in signal formation height between the center and limb sides. Comparison of photospheric and chromospheric observations shows that their differences are largely due to horizontal spreading of magnetic flux with increasing height. The north polar magnetic field decreased nearly linearly with time during our study period while the south polar field was nearly constant. We used the annual change in the viewing angle of the polar regions to estimate the radial and meridional components of the polar fields and found that the south polar fields were tilted away from the pole. Synoptic maps of the chromospheric radial flux density distribution were used as boundary conditions for extrapolation of the field from the chromosphere into the corona. A comparison of modeled and observed coronal hole boundaries and coronal streamer positions showed better agreement when using the chromospheric rather than the photospheric synoptic maps.

## **A GLOBAL TWO-TEMPERATURE CORONA AND INNER HELIOSPHERE MODEL: A COMPREHENSIVE VALIDATION STUDY**

M. **Jin**<sup>1</sup>, W. B. Manchester<sup>1</sup>, B. van der Holst<sup>1</sup>, J. R. Gruesbeck<sup>1</sup>, R. A. Frazin<sup>1</sup>, E. Landi<sup>1</sup>, A. M. Vasquez<sup>2</sup>, P. L. Lamy<sup>3</sup>, A. Llebaria<sup>3</sup>, A. Fedorov<sup>3</sup>, G. Toth<sup>1</sup> and T. I. Gombosi  
**2012 ApJ 745 6**

The recent solar minimum with very low activity provides us a unique opportunity for validating solar wind models. During CR2077 (**2008 November 20 through December 17**), the number of sunspots was near the absolute minimum of solar cycle 23. For this solar rotation, we perform a multi-spacecraft validation study for the recently developed three-dimensional, two-temperature, Alfvén-wave-driven global solar wind model (a component within the Space Weather Modeling Framework). By using in situ observations from the Solar Terrestrial Relations Observatory (STEREO) A and B, Advanced Composition Explorer (ACE), and Venus Express, we compare the observed proton state (density, temperature, and velocity) and magnetic field of the heliosphere with that predicted by the model. Near the Sun, we validate the numerical model with the electron density obtained from the solar rotational tomography of Solar and Heliospheric Observatory/Large Angle and Spectrometric Coronagraph C2 data in the range of 2.4 to 6 solar radii. Electron temperature and density are determined from differential emission measure tomography (DEMT) of STEREO A and B Extreme Ultraviolet Imager data in the range of 1.035 to 1.225 solar radii. The electron density and temperature derived from the Hinode/Extreme Ultraviolet Imaging Spectrometer data are also used to compare with the DEMT as well as the model output. Moreover, for the first time, we compare ionic charge states of carbon, oxygen, silicon, and iron observed in situ with the ACE/Solar Wind Ion Composition Spectrometer with those predicted by our model. The validation results suggest that most of the model outputs for CR2077 can fit the observations very well. Based on this encouraging result, we therefore expect great improvement for the future modeling of coronal mass ejections (CMEs) and CME-driven shocks

## **VECTOR MAGNETIC FIELDS OF A SOLAR POLAR REGION**

Chunlan **Jin** and Jingxiu Wang

**2011 ApJ 732 4**

We study the vector magnetic fields of a solar polar region (PR) based on Solar Optical Telescope/Spectro-Polarimeter measurements. To better understand the polar magnetic properties, we compare the observed polar field with that in two solar quiet regions at the limb (QRL) and the disk center (QRD), and with that in a region of a low-latitude coronal hole (CHR). The following results are discussed: (1) The average vertical flux density of PR is 16 G, while the average horizontal flux density is 91 G. If we assume that the observed polar field suffers the same amount of limb weakening in polarization measurements as the Sun's quiet region, the average unsigned flux density in the pole would be 54 G, 60% stronger than that in the CHR. (2) The kG field in the PR occupies 6.7% of the region. The magnetic filling factor in the PR is characterized by a two-peak distribution, which appears at a field strength close to 100 G and 1000 G, respectively. (3) For the network elements, a correlation holds between the vertical and horizontal flux densities, suggesting the same physical entity is manifested by the observed stronger vertical and horizontal components. (4) The ratio of the magnetic flux in the minority polarity to that in the dominant polarity is approximately 0.5, implying that only 1/3 of the magnetic flux in the PR opens to the interplanetary space. Exemplified with CHR by a quasi-linear force-free extrapolation of the observed magnetic field, we find that the photospheric open flux is not always associated with strong vertical magnetic elements.

## **THE SUN'S SMALL-SCALE MAGNETIC ELEMENTS IN SOLAR CYCLE 23**

C. L. **Jin**, J. X. Wang, Q. Song and H. Zhao

**2011 ApJ 731 37**

With the unique database from the Michelson Doppler Imager on board the Solar and Heliospheric Observatory in an interval embodying solar cycle 23, the cyclic behavior of solar small-scale magnetic elements is studied. More than 13 million small-scale magnetic elements are selected, and the following results are found. (1) The quiet regions dominated the Sun's magnetic flux for about 8 years in the 12.25 year duration of cycle 23. They contributed  $(0.94-1.44) \times 10^{23}$  Mx flux to the Sun from the solar minimum to maximum. The monthly average magnetic flux of the quiet regions is 1.12 times that of the active regions in the cycle. (2) The ratio of quiet region flux to that of the total Sun equally characterizes the course of a solar cycle. The 6 month running average flux ratio of the quiet regions was larger than 90.0% for 28 continuous months from July 2007 to October 2009, which very well characterizes the grand solar minima of cycles 23-24. (3) From the small to the large end of the flux spectrum, the variations of numbers and total flux of the network elements show no correlation, anti-correlation, and correlation with sunspots, respectively. The anti-correlated elements, covering the flux of  $(2.9-32.0) \times 10^{18}$  Mx, occupy 77.2% of the total element number and 37.4% of the quiet-Sun flux. These results provide insight into the reason for anti-correlations of small-scale magnetic activity during the solar cycle.

## **Characterizing 3D Magnetic Structures in Sunspot Light Bridges**

Ju **Jing**<sup>1,2</sup>, Nian Liu<sup>1,2</sup>, Jeongwoo Lee<sup>1,2</sup>, Yan Xu<sup>1,2</sup>, Wenda Cao<sup>1,2</sup>, and Haimin Wang<sup>1,2</sup>

2023 ApJ 952 40

<https://iopscience.iop.org/article/10.3847/1538-4357/acd44f/pdf>

Light bridges (LBs) are narrow structures dividing sunspot umbra, and their role in active region evolution is yet to be explored. We investigated the magnetic structure of the two LBs: a narrow LB (with width  $\sim 810$  km) and a considerably wider LB (2475 km) in the active region NOAA 12371. We employed: (1) the high-spatial-resolution spectropolarimetric data obtained by the Near InfraRed Imaging Spectropolarimeter (NIRIS) of the 1.6 m Goode Solar Telescope (GST) for studying the magnetic structure at the photosphere, and (2) the nonlinear force-free field (NLFFF) models, extrapolated from both the photospheric magnetogram from GST/NIRIS and from the Helioseismic and Magnetic Imager on board the Solar Dynamics Observatory, for studying the three-dimensional (3D) magnetic structure on a larger scale. Our observations reveal the presence of a field-free (or, more precisely, weak-field) region and the different velocity structures inside the two LBs. Analysis of the 3D NLFFF model shows a low-lying magnetic canopy as well as the enhanced current system above the LBs. The substantial difference between the LBs and the umbrae is found in the overall magnetic topology in that the field lines emanating from the two LBs are more twisted than that from the neighboring umbrae. **2015 June 22**

### High-resolution Observations of Dynamics of Superpenumbral $H\alpha$ Fibrils

Ju **Jing**<sup>1,2</sup>, Qin Li<sup>1,2</sup>, Chang Liu<sup>1,2</sup>, Jeongwoo Lee<sup>1</sup>, Yan Xu<sup>1,2</sup>, Wenda Cao<sup>1,2</sup>, and Haimin Wang<sup>1,2</sup>  
2019 ApJ 880 143

[sci-hub.se/10.3847/1538-4357/ab2b44](https://sci-hub.se/10.3847/1538-4357/ab2b44)

We present high-resolution  $H\alpha$  observations of a small solar pore in NOAA active region 12661, using the 1.6 m Goode Solar Telescope equipped with high-order adaptive optics at Big Bear Solar Observatory. The observations reveal copious fine-scale chromospheric superpenumbral fibrils (with an average cross-sectional width of  $\sim 0''.17 \pm 0''.03$ ), along with associated transit and intermittent flows with apparent speeds of 5–14 km s<sup>-1</sup>. Wavelet analysis and the spatio-temporal pattern of superpenumbral fibrils suggest that the observed flows along fibrils are not likely an oscillation/wave phenomenon. Based on our pseudo-Dopplergrams, we suggest that the observed flows may be a phenomenon similar to inverse Evershed flows in the chromosphere. The three-dimensional potential field model indicates that the pore and the surrounding fibrils are enclosed by fan-field lines forming a separatrix dome configuration. Such a magnetically confined configuration may help to maintain the steadfastness of the superpenumbral fibril dynamics. **2017 June 4**

### Evolution of a Magnetic Flux Rope and its Overlying Arcade Based on Nonlinear Force-free Field Extrapolations

Ju **Jing**, Chang Liu, Jeongwoo Lee, Shuo Wang, Thomas Wiegelmann, Yan Xu, and Haimin Wang  
ApJ 784 L13, **2014**

Dynamic phenomena indicative of slipping reconnection and magnetic implosion were found in a time series of nonlinear force-free field (NLFFF) extrapolations for the active region 11515, which underwent significant changes in the photospheric fields and produced five C-class flares and one M-class flare over five hours on **2012 July 2**. NLFFF extrapolation was performed for the uninterrupted 5 hour period from the 12 minute cadence vector magnetograms of the Helioseismic and Magnetic Imager on board the Solar Dynamic Observatory. According to the time-dependent NLFFF model, there was an elongated, highly sheared magnetic flux rope structure that aligns well with an  $H\alpha$  filament. This long filament splits sideways into two shorter segments, which further separate from each other over time at a speed of 1–4 km s<sup>-1</sup>, much faster than that of the footpoint motion of the magnetic field. During the separation, the magnetic arcade arching over the initial flux rope significantly decreases in height from  $\sim 4.5$  Mm to less than 0.5 Mm. We discuss the reality of this modeled magnetic restructuring by relating it to the observations of the magnetic cancellation, flares, a filament eruption, a penumbra formation, and magnetic flows around the magnetic polarity inversion line.

### NONPOTENTIALITY OF CHROMOSPHERIC FIBRILS IN NOAA ACTIVE REGIONS 11092 AND 9661

Ju **Jing**<sup>1</sup>, Yuan Yuan<sup>1</sup>, Kevin Reardon<sup>2,3</sup>, Thomas Wiegelmann<sup>4</sup>, Yan Xu<sup>1</sup> and Haimin Wang  
2011 ApJ 739 67, **File**

In this paper, we present a method to automatically segment chromospheric fibrils from  $H\alpha$  observations and further identify their orientation. We assume that chromospheric fibrils are aligned with the magnetic field. By comparing the orientation of the fibrils with the azimuth of the embedding chromospheric magnetic field extrapolated from a potential field model, the shear angle, a measure of nonpotentiality, along the fibrils is readily deduced. Following this approach, we make a quantitative assessment of the nonpotentiality of fibrils in two NOAA active regions (ARs): (1) the relatively simple AR 11092, observed with very high resolution by Interferometric Bidimensional Spectrometer, and (2) a  $\beta$ - $\gamma$ - $\delta$  AR 9661, observed with median resolution by Big Bear Solar Observatory before and after an X1.6 flare.

## Free Magnetic Energy and Flare Productivity of Active Regions

Ju **Jing**, Changyi Tan, Yuan Yuan, Benjamin Wang, Thomas Wiegelmann, Yan Xu, and Haimin Wang  
*ApJ* **713** 440, 2010

In this study, the photospheric vector magnetograms, obtained with the Spectro-Polarimeter of the Solar Optical Telescope on board *Hinode*, are used as the boundary conditions to extrapolate the three-dimensional nonlinear force-free (NLFF) coronal magnetic fields. The observed non-force-free photospheric magnetic fields are preprocessed toward the nearly force-free chromospheric magnetic fields. The performance of the preprocessing procedure is evaluated by comparing with chromospheric magnetic fields obtained by the Vector SpectroMagnetograph instrument located on the Synoptic Optical Long-term Investigations of the Sun Tower. Then, the weighted optimization method is applied to the preprocessed boundary data to extrapolate the NLFF fields with which we are able to estimate the free magnetic energy stored in the active regions. The magnitude scaling correlation between the free magnetic energy and the soft X-ray flare index (FI) of active regions is then studied. The latter quantifies the impending flare production of active regions over the subsequent 1, 2, and 3 day time windows. Based on 75 samples, we find a positive correlation between the free energy and the FI. We also study the temporal variation of free magnetic energy for three active regions, of which two are flare-active and one is flare-quiet during the observation over a period of several days. While the magnitude of free magnetic energy unambiguously differentiates between the flare-active and the flare-quiet regions, the temporal variation of free magnetic energy does not exhibit a clear and consistent pre-flare pattern. This may indicate that the trigger mechanism of flares is as important as the energy storage in active regions

## Quantitative Evaluation of Coronal Magnetic Field Models Using Tomographic Reconstructions of Electron Density

Shaella I. **Jones**<sup>1,2</sup>, T. J. Wang<sup>1,2</sup>, C. N. Arge<sup>1</sup>, C. J. Henney<sup>3</sup>, V. M. Uritsky<sup>1,2</sup>, and C. Rura<sup>1,2</sup>  
*2022 ApJ* 928 131

<https://iopscience.iop.org/article/10.3847/1538-4357/ac5751/pdf>

We introduce a new quantitative approach for assessing the quality of coronal magnetic field models. The method compares the location of the magnetic neutral line at a specified height in the magnetic field model with the locations of localized density peaks in the coronal electron density, as measured using coronal rotational tomography. This approach is flexible to the presence of pseudostreamers in the coronal magnetic field, as well as folds in the streamer belt. We present an example application during mid-2010 when the white-light streamer-belt structure is complex and the emergence of a large active region on the far side of the Sun presents a challenge for modeling the coronal magnetic structure. **CR 2098 June 2010**

## Improving Coronal Magnetic Field Models Using Image Optimization

Shaella I. **Jones**<sup>1,2</sup>, Vadim M. Uritsky<sup>1,2</sup>, Joseph M. Davila<sup>1</sup>, and Vladimir N. Troyan<sup>3</sup>  
*2020 ApJ* 896 57

<https://doi.org/10.3847/1538-4357/ab8cb9>

We have reported previously on our development and testing of a new method for using coronal images to improve coronal magnetic field models. In this technique, which we call image-optimization, coronal magnetic field models are extrapolated from synoptic photospheric magnetograms. The resulting models are then compared to morphological constraints derived from images of the solar corona, and the photospheric magnetograms are perturbed iteratively via an optimization algorithm to achieve optimal agreement with the image-based constraints. Here we present results from the first application of this technique using Mauna Loa Solar Observatory K-Coronagraph images and Global Oscillation Network Group synoptic magnetograms to create optimized models for two time periods, **2014 November 16–29 and 2016 May 16–29**. We find that for both time periods the optimization algorithm converges well and results in better agreement between the model and the images, relatively small changes to the synoptic magnetogram, and an overall increase in the amount of open magnetic flux.

## Image-Optimized Coronal Magnetic Field Models

Shaella I. **Jones**, Joseph M. Davila, Vadim M. Uritsky  
*2017 ApJ* 844 93

<https://arxiv.org/pdf/1706.07316.pdf>

We have reported previously on a new method we are developing for using image-based information to improve global coronal magnetic field models. In that work we presented early tests of the method which proved its capability to improve global models based on flawed synoptic magnetograms, given excellent constraints on the field in the model volume. In this follow-up paper we present the results of similar tests given field constraints of a nature that could realistically be obtained from quality white-light coronagraph images of the lower corona. We pay particular attention to difficulties associated with the line-of-sight projection of features outside of the assumed

coronagraph image plane, and the effect on the outcome of the optimization of errors in localization of constraints. We find that substantial improvement in the model field can be achieved with this type of constraints, even when magnetic features in the images are located outside of the image plane.

### **Optimizing Global Coronal Magnetic Field Models Using Image-Based Constraints**

Shaella I. **Jones**, Joseph M. Davila, Vadim M. Uritsky

2016 *ApJ* **820** 113

<http://arxiv.org/pdf/1511.03994v1.pdf>

The coronal magnetic field directly or indirectly affects a majority of the phenomena studied in space physics. It provides energy for coronal heating, controls the release of coronal mass ejections (CMEs), and drives heliospheric and magnetospheric activity, yet the coronal magnetic field itself has proven difficult to measure. This difficulty has prompted a decades-long effort to develop accurate, timely, models of the field - an effort that continues today. We have developed a method for improving global coronal magnetic field models by incorporating the type of morphological constraints which could be derived from coronal images. Here we report promising initial tests of this approach on two theoretical problems, and discuss opportunities for application.

### **Christian Horrebow's Sunspot Observations – I. Life and Published Writings**

Carsten Sønderskov **Jørgensen**, Christoffer Karoff, V. Senthamizh Pavaai, Rainer Arlt

*Solar Physics* June 2019, 294:77

<https://link.springer.com/content/pdf/10.1007%2Fs11207-019-1465-z.pdf>

Between 1761 and 1776, Christian Horrebow made regular observations of sunspots from Rundetårn in Copenhagen. Based on these observations he writes in 1775 that “it appears that after the course of a certain number of years, the appearance of the Sun repeats itself with respect to the number and size of the spots”. Thus, Horrebow hypothesized the idea of a cyclic Sun several decades before Heinrich Schwabe discovered the solar cycle and estimated its period. This proves the ability of Horrebow as a sunspot observer. In this article, we present a general overview of the work of Christian Horrebow, including a brief biography and a complete bibliography. We also present a translation from Danish to English of his writings on sunspots in the *Dansk Historisk Almanak*. These writings include tables of daily sunspot measurements of which we discuss the completeness.

### **Magnetic field variations associated with umbral flashes and penumbral waves**

Jayant **Joshi**, Jaime de la Cruz Rodríguez

*A&A* 619, A63 2018

<https://arxiv.org/pdf/1803.01737.pdf>

**Context.** Oscillations in sunspots are extensively studied phenomenon for last several decades. These studies mostly concentrate on variations in the intensity and Doppler velocities. Fewer observational studies focused on variations in the magnetic field in the photosphere, report contradicting results. Recently, variations in the magnetic field strength associated to umbral flashes (UFs) running penumbral waves (RPWs) in the chromosphere has been reported.

**Aims.** We studied variations in the magnetic field associated to UFs and RPWs. **Methods.** We obtained stratified atmospheric parameters by performing inversions of the photospheric Fe i 6301.5 & 6302.5 Å and chromospheric Ca ii 8542 Å spectral lines observed with CRisp Imaging SpectroPolarimeter (CRISP) mounted at Swedish 1-m Solar Telescope (SST). We used non-LTE inversion code NICOLE.

**Results.** Our results do not show any significant variations in the magnetic field strength in the photosphere. At chromospheric heights, UFs indicate peak-to-peak variation of ~ 275 G, whereas in the RPWs, variations in the magnetic field strength are reduced to ~ 100 G. Variations in the magnetic field in the UFs and RPWs are correlated to the variations in the temperature. We analyzed the changes in the chromospheric magnetic field and geometrical height (assuming hydrostatic equilibrium) at which the chromospheric magnetic field is inferred. These variations in the geometrical height are caused by the oscillations in the thermodynamical parameters.

**Conclusions.** Our results suggest that observed variations in the magnetic field in the umbra and penumbra can not be explained by opacity changes caused by the oscillations. **22 July 2013**

### **Three-dimensional magnetic structure of a sunspot: comparison of the photosphere and upper chromosphere**

Jayant **Joshi**, Andreas Lagg, Johann Hirzberger, Sami K. Solanki

*A&A* 604, A98 2017

<https://arxiv.org/pdf/1705.08404.pdf>

We investigate the magnetic field of a sunspot in the upper chromosphere and compare it to the field's photospheric properties. We observed the main leading sunspot of the active region NOAA 11124 on two days with the Tenerife Infrared Polarimeter-2 (TIP-2) mounted at the German Vacuum Tower Telescope (VTT). Through inversion of



Stokes spectra of the He I triplet at 1083.0 nm, we obtained the magnetic field vector of the upper chromosphere. For comparison with the photosphere we applied height-dependend inversions of the Si I 1082.71 nm and Ca I 1083.34 nm lines. We found that the umbral magnetic field strength in the upper chromosphere is lower by a factor of 1.30-1.65 compared to the photosphere. The magnetic field strength of the umbra decreases from the photosphere towards the upper chromosphere by an average rate of 0.5-0.9 G km<sup>-1</sup>. The difference in the magnetic field strength between both atmospheric layers steadily decreases from the sunspot center to the outer boundary of the sunspot, with the field (in particular its horizontal component) being stronger in the chromosphere outside the spot, suggestive of a magnetic canopy. The sunspot displays a twist that on average is similar in the two layers. However, the differential twist between photosphere and chromosphere increases rapidly towards the outer penumbral boundary. The magnetic field vector is more horizontal with respect to the solar surface by roughly 5-20° in the photosphere compared to the upper chromosphere. Above a lightbridge, the chromospheric magnetic field is equally strong as that in the umbra, whereas the lightbridge's field is weaker than its surroundings in the photosphere by roughly 1 kG. This suggests a cusp-like magnetic field structure above the lightbridge. **14-16 November, 2010**

### **Vertical magnetic field gradient in the photospheric layers of sunspots**

Jayant **Joshi**, Andreas Lagg, Johann Hirzberger, Sami K. Solanki, Sanjiv K. Tiwari

A&A 599, A35 **2017**

<https://arxiv.org/pdf/1610.00500v1.pdf>

We investigate the vertical gradient of the magnetic field of sunspots in the photospheric layer. Independent observations were obtained with the SOT/SP onboard the Hinode spacecraft and with the TIP-2 mounted at the VTT. We apply state-of-the-art inversion techniques to both data sets to retrieve the magnetic field and the corresponding vertical gradient. In the sunspot penumbrae we detected patches of negative vertical gradients of the magnetic field strength, i.e., the magnetic field strength decreases with optical depth in the photosphere. The negative gradient patches are located in the inner and partly in the middle penumbrae in both data sets. From the SOT/SP observations, we found that the negative gradient patches are restricted mainly to the deep photospheric layers and are concentrated near the edges of the penumbral filaments. MHD simulations also show negative gradients in the inner penumbrae, also at the locations of filaments. Both in the observations and simulation negative gradients of the magnetic field vs. optical depth dominate at some radial distances in the penumbra. The negative gradient with respect to optical depth in the inner penumbrae persists even after averaging in the azimuthal direction, both in the observations and, to a lesser extent, also in MHD simulations. We interpret the observed localized presence of the negative vertical gradient of the magnetic field strength in the observations as a consequence of stronger field from spines expanding with height and closing above the weaker field inter-spines. The presence of the negative gradients with respect to optical depth after azimuthal averaging can be explained by two different mechanisms: the high corrugation of equal optical depth surfaces and the cancellation of polarized signal due to the presence of unresolved opposite polarity patches in the deeper layers of the penumbra.

### **Upper Chromospheric Magnetic Field of a Sunspot Penumbra: Observations of Fine Structure**

J. **Joshi**, A. Lagg, S. K. Solanki, [A. Feller](#), [M. Collados](#), [D. Orozco Suárez](#), [R. Schlichenmaier](#), [M. Franz](#), [H. Balthasar](#), [C. Denker](#), [T. Berkefeld](#), [A. Hofmann](#), [C. Kiess](#), [H. Nicklas](#), [A. Pastor Yabar](#), [R. Rezaei](#), [D. Schmidt](#), [W. Schmidt](#), [M. Sobotka](#), [D. Soltau](#), [J. Staude](#), [K. G. Strassmeier](#), [R. Volkmer](#), [O. von der Lühe](#), [T. Waldmann](#)

A&A **2016**

<http://arxiv.org/pdf/1608.01988v1.pdf>

The fine-structure of magnetic field of a sunspot penumbra in the upper chromosphere is to be explored and compared to that in the photosphere. High spatial resolution spectropolarimetric observations were recorded with the 1.5-meter GREGOR telescope using the GREGOR Infrared Spectrograph (GRIS). The observed spectral domain includes the upper chromospheric He I triplet at 1083.0 nm and the photospheric Si I 1082.7 nm and Ca I 1083.3 nm spectral lines. The upper chromospheric magnetic field is obtained by inverting the He I triplet assuming a Milne-Eddington type model atmosphere. A height dependent inversion was applied to the Si I 1082.7 nm and Ca I 1083.3 nm lines to obtain the photospheric magnetic field. We find that the inclination of the magnetic field shows variations in the azimuthal direction both in the photosphere, but also in the upper chromosphere. The chromospheric variations remarkably well coincide with the variations in the inclination of the photospheric field and resemble the well-known spine and inter-spine structure in the photospheric layers of penumbrae. The typical peak-to-peak variations in the inclination of the magnetic field in the upper chromosphere is found to be 10-15 degree, i.e., roughly half the variation in the photosphere. In contrast, the magnetic field strength of the observed penumbra does not show variations on small spatial scales in the upper chromosphere. Thanks to the high spatial resolution observations possible with the GREGOR telescope at 1.08 microns, we find that the prominent small-scale fluctuations in the magnetic field inclination, which are a salient part of the property of sunspot penumbral photospheres, also persist in the chromosphere, although at somewhat reduced amplitudes. Such a complex

magnetic configuration may facilitate penumbral chromospheric dynamic phenomena, such as penumbral micro-jets or transient bright dots. **25 June 2014**

### **Optimal Spectral Lines for Measuring Chromospheric Magnetic Fields**

P. **Judge**<sup>1</sup>, P. Bryans<sup>1</sup>, R. Casini<sup>1</sup>, L. Kleint<sup>2</sup>, D. Lacatus<sup>1</sup>, A. Paraschiv<sup>1</sup>, and D. Schmit<sup>3</sup>  
**2022** ApJ 941 159

<https://iopscience.iop.org/article/10.3847/1538-4357/aca2a5/pdf>

This paper identifies spectral lines from X-ray to IR wavelengths which are optimally suited to measuring vector magnetic fields as high as possible in the solar atmosphere. Instrumental and Earth's atmospheric properties, as well as solar abundances, atmospheric properties, and elementary atomic physics are considered without bias toward particular wavelengths or diagnostic techniques. While narrowly focused investigations of individual lines have been reported in detail, no assessment of the comparative merits of all lines has ever been published. Although in the UV, on balance the Mg+ h and k lines near 2800 Å are optimally suited to polarimetry of plasma near the base of the solar corona. This result was unanticipated, given that longer-wavelength lines offer greater sensitivity to the Zeeman effect. While these lines sample optical depths photosphere to the coronal base, we argue that cores of multiple spectral lines provide a far more discriminating probe of magnetic structure as a function of optical depth than the core and inner wings of a strong line. Thus, together with many chromospheric lines of Fe+ between 2585 Å and the h line at 2803 Å, this UV region promises new discoveries concerning how the magnetic fields emerge, heat, and accelerate plasma as they battle to dominate the force and energy balance within the poorly understood chromosphere.

### **Magnetic connections across the chromosphere-corona transition region**

[Philip G. Judge](#)

ApJ **2021**

<https://arxiv.org/pdf/2104.07753.pdf>

The plasma contributing to emission from the Sun between the cool chromosphere ( $\leq 104\text{K}$ ) and hot corona ( $\geq 106\text{K}$ ) has been subjected to many different interpretations. Here we look at the magnetic structure of this transition region (TR) plasma, based upon the implications of CLASP2 data of an active region recently published by Ishikawa et al., and earlier IRIS and SDO data of quiet regions. Ishikawa et al. found that large areas of sunspot plages are magnetically unipolar as measured in the cores of  $\text{Mg}\{2\}$  resonance lines, formed in the lower transition region under low plasma- $\beta$  conditions. Here we show that IRIS images in the line cores have fibrils which well aligned with the overlying coronal loop segments seen in the 171 Å channel of SDO. When the TR emission in active regions arise from plasma magnetically and thermally connected to the corona, then the line cores can provide the first credible magnetic boundary conditions for force-free calculations extended to the corona. We also re-examine IRIS images of dynamic TR cool loops previously reported as a major contributor to transition region emission from the quiet Sun. Dynamic cool loops contribute only a small fraction of the total TR emission from the quiet Sun. **2013-09-13, December 1 2013, 2019 April 11, 2019-07-08**

### **From Forbidden Coronal Lines to Meaningful Coronal Magnetic Fields** Review

P. G. **Judge**, S. Habbal, E. Landi

Solar Physics,

December **2013**, Volume 288, Issue 2, pp 467-480,

We review methods to measure magnetic fields within the corona using the polarized light in magnetic-dipole (M1) lines. We are particularly interested in both the global magnetic-field evolution over a solar cycle, and the local storage of magnetic free energy within coronal plasmas. We address commonly held skepticisms concerning angular ambiguities and line-of-sight confusion. We argue that ambiguities are, in principle, no worse than more familiar remotely sensed photospheric vector fields, and that the diagnosis of M1 line data would benefit from simultaneous observations of EUV lines. Based on calculations and data from eclipses, we discuss the most promising lines and different approaches that might be used. We point to the S-like [Fe xi] line ( $J=2$  to  $J=1$ ) at 789.2 nm as a prime target line (for the Advanced Technology Solar Telescope (ATST) for example) to augment the hotter 1074.7 and 1079.8 nm Si-like lines of [Fe xiii] currently observed by the Coronal Multi-channel Polarimeter (CoMP). Significant breakthroughs will be made possible with the new generation of coronagraphs, in three distinct ways: i) through single-point inversions (which encompasses also the analysis of MHD wave modes), ii) using direct comparisons of synthetic MHD or force-free models with polarization data, and iii) using tomographic techniques.

### **Single-Frame Super-Resolution of Solar Magnetograms: Investigating Physics-Based Metrics & Losses**

Anna **Jungbluth**, [Xavier Gitiaux](#), [Shane A. Maloney](#), [Carl Shneider](#), [Paul J. Wright](#), [Alfredo Kalaitzis](#), [Michel Deudon](#), [Atılım Güneş Baydın](#), [Yarin Gal](#), [Andrés Muñoz-Jaramillo](#)

Second Workshop on Machine Learning and the Physical Sciences (NeurIPS 2019), Vancouver, Canada, 2019

<https://arxiv.org/pdf/1911.01490.pdf>

Breakthroughs in our understanding of physical phenomena have traditionally followed improvements in instrumentation. Studies of the magnetic field of the Sun, and its influence on the solar dynamo and space weather events, have benefited from improvements in resolution and measurement frequency of new instruments. However, in order to fully understand the solar cycle, high-quality data across time-scales longer than the typical lifespan of a solar instrument are required. At the moment, discrepancies between measurement surveys prevent the combined use of all available data. In this work, we show that machine learning can help bridge the gap between measurement surveys by learning to  $\text{super-resolve}$  low-resolution magnetic field images and  $\text{translate}$  between characteristics of contemporary instruments in orbit. We also introduce the notion of physics-based metrics and losses for super-resolution to preserve underlying physics and constrain the solution space of possible super-resolution outputs.

## Evaluating the reliability of a simple method to map the magnetic field azimuth in the solar chromosphere

[Jan Jurcak](#), [Jiri Stepan](#), [Javier Trujillo Bueno](#)

ApJ **911** 23 2021

<https://arxiv.org/pdf/2102.02880.pdf>

<https://iopscience.iop.org/article/10.3847/1538-4357/abe402/pdf>

<https://doi.org/10.3847/1538-4357/abe402>

The Zeeman effect is of limited utility for probing the magnetism of the quiet solar chromosphere. The Hanle effect in some spectral lines is sensitive to such magnetism, but the interpretation of the scattering polarization signals requires taking into account that the chromospheric plasma is highly inhomogeneous and dynamic (i.e., that the magnetic field is not the only cause of symmetry breaking). Here we investigate the reliability of a well-known formula for mapping the azimuth of chromospheric magnetic fields directly from the scattering polarization observed in the  $\text{Ca II } 8542\text{\AA}$  line, which is typically in the saturation regime of the Hanle effect. To this end, we use the Stokes profiles of the  $\text{Ca II } 8542\text{\AA}$  line computed with the PORTA radiative transfer code in a three-dimensional (3D) model of the solar chromosphere, degrading them to mimic spectropolarimetric observations for a range of telescope apertures and noise levels. The simulated observations are used to obtain the magnetic field azimuth at each point of the field of view, which we compare with the actual values within the 3D model. We show that, apart from intrinsic ambiguities, the method provides solid results. Their accuracy depends more on the noise level than on the telescope diameter. Large-aperture solar telescopes, like DKIST and EST, are needed to achieve the required noise-to-signal ratios using reasonable exposure times.

## A distinct magnetic property of the inner penumbral boundary

### III. Analysis of simulated sunspots

Jan [Jurčák](#)<sup>1</sup>, Markus Schmassmann<sup>2</sup>, Matthias Rempel<sup>3</sup>, Nazaret Bello González<sup>2</sup> and Rolf Schlichenmaier<sup>2</sup>

A&A 638, A28 (2020)

<https://www.aanda.org/articles/aa/pdf/2020/06/aa37852-20.pdf>

Context. Analyses of sunspot observations revealed a fundamental magnetic property of the umbral boundary: the invariance of the vertical component of the magnetic field.

Aims. We analyse the magnetic properties of the umbra-penumbra boundary in simulated sunspots and thus assess their similarity to observed sunspots. We also aim to investigate the role of the plasma  $\beta$  and the ratio of kinetic to magnetic energy in simulated sunspots in the convective motions because these quantities cannot be reliably determined from observations.

Methods. We used a set of non-gray simulation runs of sunspots with the MURaM code. The setups differed in terms of subsurface magnetic field structure and magnetic field boundary imposed at the top of the simulation domain. These data were used to synthesize the Stokes profiles, which were then degraded to the Hinode spectropolarimeter-like observations. Then, the data were treated like real Hinode observations of a sunspot, and magnetic properties at the umbral boundaries were determined.

Results. Simulations with potential field extrapolation produce a realistic magnetic field configuration on the umbral boundaries of the sunspots. Two simulations with a potential field upper boundary, but different subsurface magnetic field structures, differ significantly in the extent of their penumbrae. Increasing the penumbra width by forcing more horizontal magnetic fields at the upper boundary results in magnetic properties that are not consistent with observations. This implies that the size of the penumbra is given by the subsurface structure of the magnetic field, that is, by the depth and inclination of the magnetopause, which is shaped by the expansion of the sunspot flux rope with height. None of the sunspot simulations is consistent with the observed properties of the magnetic field and the direction of the Evershed flow at the same time. Strong outward-directed Evershed flows are only found in setups with an artificially enhanced horizontal component of the magnetic field at the top boundary that are not

consistent with the observed magnetic field properties at the umbra-penumbra boundary. We stress that the photospheric boundary of simulated sunspots is defined by a magnetic field strength of equipartition field value.

### **The magnetic nature of umbra-penumbra boundary in sunspots**

Jan [Jurčák](#), [Reza Rezaei](#), [Nazaret Bello González](#), [Rolf Schlichenmaier](#), [Jiří Vomlel](#)

A&A Letter 611, L4 2018

<https://arxiv.org/pdf/1801.08983.pdf>

Sunspots are the longest-known manifestation of solar activity, and their magnetic nature has been known for more than a century. Despite this, the boundary between umbrae and penumbrae, the two fundamental sunspot regions, has hitherto been solely defined by an intensity threshold. Here, we aim at studying the magnetic nature of umbra-penumbra boundaries in sunspots of different sizes, morphologies, evolutionary stages, and phases of the solar cycle. We used a sample of 88 scans of the Hinode/SOT spectropolarimeter to infer the magnetic field properties in at the umbral boundaries. We defined these umbra-penumbra boundaries by an intensity threshold and performed a statistical analysis of the magnetic field properties on these boundaries. We statistically prove that the umbra-penumbra boundary in stable sunspots is characterised by an invariant value of the vertical magnetic field component: the vertical component of the magnetic field strength does not depend on the umbra size, its morphology, and phase of the solar cycle. With the statistical Bayesian inference, we find that the strength of the vertical magnetic field component is, with a likelihood of 99%, in the range of 1849-1885 G with the most probable value of 1867 G. In contrast, the magnetic field strength and inclination averaged along individual boundaries are found to be dependent on the umbral size: the larger the umbra, the stronger and more horizontal the magnetic field at its boundary. The umbra and penumbra of sunspots are separated by a boundary that has hitherto been defined by an intensity threshold. We now unveil the empirical law of the magnetic nature of the umbra-penumbra boundary in stable sunspots: it is an invariant vertical component of the magnetic field.

### **A distinct magnetic property of the inner penumbral boundary. II. Formation of a penumbra at the expense of a pore**

Jan [Jurcak](#), [Nazaret Bello Gonzalez](#), [Rolf Schlichenmaier](#), [Reza Rezaei](#)

A&A 597, A60 2017

<https://arxiv.org/pdf/1612.01745v1.pdf>

We recently presented evidence that stable umbra-penumbra boundaries are characterised by a distinct canonical value of the vertical component of the magnetic field,  $B_{\text{stable\_ver}}$ . In order to trigger the formation of a penumbra, large inclinations in the magnetic field are necessary. In sunspots, the penumbra develops and establishes by colonising both umbral areas and granulation, that is, penumbral magneto-convection takes over in umbral regions with  $B_{\text{ver}} < B_{\text{stable\_ver}}$ , as well as in granular convective areas. Eventually, a stable umbra-penumbra boundary settles at  $B_{\text{stable\_ver}}$ .

Here, we aim to study the development of a penumbra initiated at the boundary of a pore, where the penumbra colonises the entire pore ultimately. We have used Hinode/SOT G-band images to study the evolution of the penumbra. Hinode/SOT spectropolarimetric data were used to infer the magnetic field properties in the studied region. The penumbra forms at the boundary of a pore located close to the polarity inversion line of NOAA\,10960. As the penumbral bright grains protrude into the pore, the magnetic flux in the forming penumbra increases at the expense of the pore magnetic flux. Consequently, the pore disappears completely giving rise to an orphan penumbra. At all times, the vertical component of the magnetic field in the pore is smaller than  $B_{\text{stable\_ver}} \approx 1.8$  kG. Our findings are in an agreement with the need of  $B_{\text{stable\_ver}}$  for establishing a stable umbra-penumbra boundary: while  $B_{\text{ver}}$  in the pore is smaller than  $B_{\text{stable\_ver}}$ , the protrusion of penumbral grains into the pore area is not blocked, a stable pore-penumbra boundary does not establish, and the pore is fully overtaken by the penumbral magneto-convective mode. This scenario could also be one of the mechanisms giving rise to orphan penumbrae. **8 June 2007.**

### **A distinct magnetic property of the inner penumbral boundary**

Jan [Jurčák](#), [Nazaret Bello Gonzalez](#), [Rolf Schlichenmaier](#), [Reza Rezaei](#)

A&A 2015

<http://arxiv.org/pdf/1506.08574v1.pdf>

A sunspot emanates from a growing pore or protospot. In order to trigger the formation of a penumbra, large inclinations at the outskirts of the protospot are necessary. The penumbra develops and establishes by colonising both umbral areas and granulation. Evidence for a unique stable boundary value for the vertical component of the magnetic field strength,  $B_{\text{stable\_ver}}$ , was found along the umbra-penumbra boundary of developed sunspots. We use broadband G-band images and spectropolarimetric GFPI/VTT data to study the evolution of and the vertical component of the magnetic field on a forming umbra-penumbra boundary. For comparison with stable sunspots, we also analyse the two maps observed by Hinode/SP on the same spot after the penumbra formed. The vertical component of the magnetic field,  $B_{\text{ver}}$ , at the umbra-penumbra boundary increases during penumbra formation owing to the incursion of the penumbra into umbral areas. After 2.5 hours, the penumbra reaches a stable state as

shown by the GFPI data. At this stable stage, the simultaneous Hinode/SP observations show a  $B_{\text{ver}}$  value comparable to that of umbra-penumbra boundaries of fully fledged sunspots. We confirm that the umbra-penumbra boundary, traditionally defined by an intensity threshold, is also characterised by a distinct canonical magnetic property, namely by  $B_{\text{stablever}}$ . During the penumbra formation process, the inner penumbra extends into regions where the umbra previously prevailed. Hence, in areas where  $B_{\text{ver}} < B_{\text{stablever}}$ , the magneto-convection mode operating in the umbra turns into a penumbral mode. Eventually, the inner penumbra boundary settles at  $B_{\text{stablever}}$ , which hints toward the role of  $B_{\text{stablever}}$  as inhibitor of the penumbral mode of magneto-convection. **July 4, 2009**

### **Orphan penumbrae: Submerging horizontal fields\***

J. [Jurčák](#)<sup>1</sup>, L. R. Bellot Rubio<sup>2</sup> and M. Sobotka<sup>1</sup>

A&A 564, A91 (2014)

**Aims.** We investigate the properties of orphan penumbrae, which are photospheric filamentary structures observed in active regions near polarity inversion lines that resemble the penumbra of regular sunspots but are not connected to any umbra.

**Methods.** We use Hinode data from the Solar Optical Telescope to determine the properties of orphan penumbrae. Spectropolarimetric data are employed to obtain the vector magnetic field and line-of-sight velocities in the photosphere. Magnetograms are used to study the overall evolution of these structures, and G-band and Ca ii H filtergrams are used to investigate their brightness and apparent horizontal motions.

**Results.** Orphan penumbrae form between regions of opposite polarity in places with horizontal magnetic fields. Their magnetic configuration is that of  $\Omega$ -shaped flux ropes. In the two cases studied here, the opposite-polarity regions approach each other with time and the whole structure submerges as the penumbral filaments disappear. Orphan penumbrae are very similar to regular penumbrae, including the existence of strong gas flows. Therefore, they could have a similar origin. The main difference between them is the absence of a “background” magnetic field in orphan penumbrae. This could explain most of the observed differences.

**Conclusions.** The fast flows we detect in orphan penumbrae may be caused by the siphon flow mechanism. Based on the similarities between orphan and regular penumbrae, we propose that the Evershed flow is also a manifestation of siphon flows.

### **Intensity contrast of solar plage as a function of magnetic flux at high spatial resolution**

F. [Kahil](#), [T. L. Riethmüller](#), [S. K. Solanki](#)

A&A 2018

<https://arxiv.org/pdf/1811.05759.pdf>

Magnetic elements have an intensity contrast that depends on the type of region they are located in (e.g. quiet Sun, or active region plage). Observed values also depend on the spatial resolution of the data. Here we investigate the contrast-magnetic field dependence in active region plage observed near disk center with Sunrise during its second flight in 2013. The wavelengths under study range from the visible at 525 nm to the near ultraviolet (NUV) at 300 nm and 397 nm. We use quasi-simultaneous spectropolarimetric and photometric data from the Imaging Magnetograph eXperiment (IMaX) and the Sunrise Filter Imager (SuFI), respectively. We find that in all wavelength bands, the contrast exhibits a qualitatively similar dependence on the line-of-sight magnetic field, BLOS, as found in the quiet Sun, with the exception of the continuum at 525 nm. There, the contrast of plage magnetic elements peaks for intermediate values of BLOS and decreases at higher field strengths. By comparison, the contrast of magnetic elements in the quiet Sun saturates at its maximum value at large BLOS. We find that the explanation of the turnover in contrast in terms of the effect of finite spatial resolution of the data is incorrect with the evidence provided by the high-spatial resolution Sunrise data, as the plage magnetic elements are larger than the quiet Sun magnetic elements and are well-resolved. The turnover comes from the fact that the core pixels of these larger magnetic elements are darker than the quiet Sun. We find that plages reach lower contrast than the quiet Sun at disk center at wavelength bands formed deep in the photosphere, such as the visible continuum and the 300 nm band. This difference decreases with formation height and disappears in the Ca II H core, in agreement with empirical models of magnetic element atmospheres. **2013 June 12**

### **Investigation of Umbral Dots with the New Vacuum Solar Telescope**

Ji [Kaifan](#), Jiang Xia, Feng Song, Yang Yunfei, Deng Hui, Wang Feng

Solar Phys. 2015

<http://arxiv.org/pdf/1509.00312v1.pdf>

Umbral dots (UDs) are small isolated brightenings observed in sunspot umbrae. They are convective phenomena existing inside umbrae. UD are usually divided into central UD (CUDs) and peripheral UD (PUDs) with respect to their positions inside an umbra. Our purpose is to investigate UD properties and analyze their relationships, and further to find whether or not the properties depend on the umbral magnetic field variation. For the purpose, we selected the high-resolution TiO images of four active regions (ARs) obtained under the best seeing conditions with

the \emph{New Vacuum Solar Telescope} (NVST) in Fuxian Solar Observatory of Yunnan Astronomical Observatory, China. The four ARs (NOAA 11598, 11801, 12158, and 12178) include six sunspots. A total of 1220 CUDs were extracted from six sunspots, and 603 PUDs from three sunspots. Meanwhile, the radial component of the magnetic field of the sunspots obtained with the \emph{Helioseismic and Magnetic Imager} onboard the \emph{Solar Dynamics Observatory} was used to analyze the influence to UD properties. To CUDs, their diameters and lifetimes exhibit an increasing trend with brightness, whereas their horizontal velocities exhibit an inverse trend. Moreover, the properties: diameter, intensity and velocity depend on magnetic field variation. To a CUD, its diameter becomes larger and brighter, and its motion shows slower in a weak magnetic field than in a strong field. To PUDs, the similar trends are also found. Moreover, we also find that the lifetimes of UDs located in different sunspots are not obviously different, implying that they are unrelated to the magnetic flux density in which they lived. **2012-10-29, 2013-08-01, 2014-09-13, 2014-10-03**

### **Cancellation of Small-Scale Magnetic Features**

Anjali J. [Kaithakkal](#), [Sami K. Solanki](#)

A&A 622, A200 2019

<https://arxiv.org/pdf/1812.11496.pdf>

We investigate small-scale flux cancellations in a young active region observed with the high-resolution imaging magnetograph IMAx on the Sunrise balloon-borne solar observatory. We identified 11 opposite-polarity cancelling pairs using an automatic detection code, and derived their statistical properties. We classified the cancellations into two groups. Class I events are those for which cancellation happens between a pre-existing large magnetic feature of one polarity and a smaller feature of the other polarity that emerged/appeared nearby. For Class II events cancellations occur between two pre-existing, previously unconnected features that converge toward each other. All studied events have an apparent cancellation time less than 10 minutes and display a significant transient linear polarization signal along the polarity inversion line. The cancellation events are characterized by a flux decay rate of about  $10^{15} \sim Mx s^{-1}$ . Horizontal convergence speeds of Class II pairs fall between 0.3 and  $1.22 \sim km s^{-1}$ . The elements often do not converge directly towards each other, so that the proper motion speeds of the individual elements is higher, in the range of  $1 - 2.7 \sim km s^{-1}$ . We propose that these cancellation events result from either field-line submergence (Class I), or reconnection followed by submergence (Class II and/or Class I). Ohmic dissipation of magnetic energy could also play a role for both classes. We propose that, at least for the Class II events, the granular motions could possibly be driving magnetic reconnection, rather than the supergranular motions proposed for the larger cancellation events studied earlier. Specific flux cancellation rates of the Class II events seem to indicate that they belong to somewhat different category of cancellations when compared with those studied in SOT/Hinode and MDI/SOHO data. **12 June 2013**

### **Moving Magnetic Features around a Pore**

A. J. [Kaithakkal](#), T. L. Riethmüller, S. K. Solanki, A. Lagg, P. Barthol, A. Gandorfer, L. Gizon, J. Hirzberger, M. vanNoort, J. Blanco Rodríguez, J. C. Del Toro Iniesta, D. Orozco Suárez, W. Schmidt, V. Martínez Pillet, M. Knölker

ApJS 2016

<http://arxiv.org/pdf/1609.05664v1.pdf>

Spectropolarimetric observations from Sunrise II/IMaX obtained in June 2013 are used for a statistical analysis to determine the physical properties of moving magnetic features (MMFs) observed near a pore. MMFs of the same and opposite polarity with respect to the pore are found to stream from its border at an average speed of  $1.3 km s^{-1}$  and  $1.2 km s^{-1}$  respectively, with mainly same-polarity MMFs found further away from the pore. MMFs of both polarities are found to harbor rather weak, inclined magnetic fields. Opposite-polarity MMFs are blue-shifted, while same-polarity MMFs do not show any preference for up- or downflows. Most of the MMFs are found to be of sub-arcsecond size and carry a mean flux of  $\sim 1.2 \times 10^{17} Mx$ .

### **Photospheric Flow Field Related to the Evolution of the Sun's Polar Magnetic Patches Observed by Hinode SOT**

Anjali John [Kaithakkal](#), [Y. Suematsu](#), [M. Kubo](#), [Y. Iida](#), [D. Shiota](#), [S. Tsuneta](#)

ApJ, 799 139 2015

<http://arxiv.org/pdf/1412.8023v1.pdf>

We investigated the role of photospheric plasma motions in the formation and evolution of polar magnetic patches using time-sequence observations with high spatial resolution. The observations were obtained with the spectropolarimeter on board the Hinode satellite. From the statistical analysis using 75 magnetic patches, we found that they are surrounded by strong converging, supergranulation associated flows during their apparent life time and that the converging flow around the patch boundary is better observed in the Doppler velocity profile in the deeper photosphere. Based on our analysis we suggest that the like-polarity magnetic fragments in the polar region are advected and clustered by photospheric converging flows thereby resulting in the formation of polar magnetic patches. Our observations show that, in addition to direct cancellation magnetic patches decay by fragmentation

followed by unipolar disappearance or unipolar disappearance without fragmentation. It is possible that the magnetic patches of existing polarity fragment or diffuse away into smaller elements and eventually cancel out with opposite polarity fragments that reach the polar region around solar cycle maximum. This could be one of the possible mechanisms by which the existing polarity decay during the reversal of the polar magnetic field.

2013 Nov 11–13, 2013 Dec 08 and 11, 2014 Jan 17 and 23, 2014 Mar 08

## **Impact of Magnetic and Flow Fields on Penumbrae and Light Bridges of Three Leading Sunspots in an Active Region.**

**Kamlah**, R., Verma, M., Denker, C. et al.

Sol Phys 299, 144 (2024).

<https://doi.org/10.1007/s11207-024-02386-9>

This study investigates penumbrae and light bridges based on photospheric and chromospheric flow fields and photospheric magnetic fields in active region NOAA 13096. The improved High-resolution Fast Imager (HiFi+) and the GREGOR Infrared Spectrograph (GRIS) acquired high-resolution imaging and spectropolarimetric data at the 1.5-meter GREGOR solar telescope at the Observatorio del Teide, Izaña, Tenerife, Spain. Background-Subtracted Activity Maps (BaSAMs) have been used to locate areas of enhanced activity, Local Correlation Tracking (LCT) provides horizontal proper motions, and near-infrared full-Stokes polarimetry offers access to magnetic fields and line-of-sight velocities. The results show that the decaying active region is characterized by a triangular region between the three leading, positive-polarity sunspots with unfavorable conditions for penumbra formation. This region has a spongy appearance in narrow-band H $\alpha$  images, shows signs of enhanced activity on small spatial scales, is free of divergence centers and exploding granules, lacks well-ordered horizontal flows, has low flow speeds, and is dominated by horizontal magnetic fields. Umbral cores are inactive, but the interface between pores and penumbral filaments often shows enhanced activity. Moat flows and superpenumbrae are almost always observed, when penumbral filaments are present, even in very small penumbral sectors. However, evidence of the moat flow can also be seen around pores, surviving longer than the decaying penumbral filaments. Light bridges have mainly umbral temperatures, reaching quiet-Sun temperatures in some places, show strong intensity variations, and exhibit weak photospheric horizontal flows, while narrow-band H $\alpha$  flow maps show substantial inflows.

## **High-resolution imaging of solar pores★**

R. **Kamlah**<sup>1,2</sup>, M. Verma<sup>1</sup>, C. Denker<sup>1</sup> and H. Wang<sup>3</sup>

A&A 675, A182 (2023)

<https://www.aanda.org/articles/aa/pdf/2023/07/aa45410-22.pdf>

Context. Light bridges are bright, long, and narrow features that are typically connected to the formation or decay processes of sunspots and pores.

Aims. The interaction of magnetic fields and plasma flows is investigated in the trailing part of an active region, where pores and magnetic knots evolve into a complex sunspot. The goal is to identify the photospheric and chromospheric processes, which transform the mainly vertical magnetic fields of pores into a sunspot with multiple umbral cores, light bridges, and rudimentary penumbrae.

Methods. Conducting observations with a broad variety of telescopes and instruments provides access to different atmospheric layers and the changing morphology of features connected to strong magnetic fields. While the Helioseismic and Magnetic Imager (HMI) of the Solar Dynamics Observatory (SDO) provides full-disk continuum images and line-of-sight magnetograms, the fine structure and flows around a pore can be deduced from high-resolution observations in various wavelengths as provided by the Goode Solar Telescope (GST) at the Big Bear Solar Observatory (BBSO). Horizontal proper motions are evaluated applying local correlation tracking (LCT) to the available time series, whereas the connectivity of sunspot features can be established using the background-subtracted activity maps (BaSAMs).

Results. Photospheric flow maps indicate radial outflows, where the light bridge connects to the surrounding granulation, whereas inflows are present at the border of the pores. In contrast, the chromospheric flow maps show strong radial outflows at superpenumbral scales, even in the absence of a penumbra in the photosphere. The region in between the two polarities is characterized by expanding granules creating strong divergence centers. Variations in BaSAMs follow locations of significant and persistent changes in and around pores. The resulting maps indicate low variations along the light bridge, as well as thin hairlines connecting the light bridge to the pores and strong variations at the border of pores. Various BaSAMs demonstrate the interaction of pores with the surrounding supergranular cell. The H $\alpha$  line-of-sight velocity maps provide further insights into the flow structure, with twisted motions along some of the radial filaments around the pore with the light bridge. Furthermore, flows along filaments connecting the two polarities of the active region are pronounced in the line-of-sight velocity maps.

Conclusions. The present observations reveal that even small-scale changes of plasma motions in and around pores are conducive to transform pores into sunspots. In addition, chromospheric counterparts of penumbral filaments appear much earlier than the penumbral filaments in the photosphere. Penumbra formation is aided by a stable magnetic feature that anchors the advection of magnetic flux and provides a connection to the surrounding supergranular cell, whereas continuously emerging flux and strong light bridges are counteragents that affect the appearance and complexity of sunspots and their penumbrae.

## Impact of subsurface convective flows on the formation of sunspot magnetic field and energy build-up

[Takafumi Kaneko](#), [Hideyuki Hotta](#), [Shin Toriumi](#), [Kanya Kusano](#)

MNRAS **2022**

<https://arxiv.org/pdf/2209.06311.pdf>

Sunspot formation via flux emergence from the convection zone to the photosphere can be strongly affected by convective turbulent flows. It has not yet been shown how crucial convective flows are for the formation of  $\delta$ -spots. The aim of this study is to reveal the impact of convective flows in the convection zone on the formation and evolution of sunspot magnetic fields. We simulated the emergence and transport of magnetic flux tubes in the convection zone using radiative magnetohydrodynamics code R2D2. We carried out 93 simulations by allocating the twisted flux tubes to different positions in the convection zone. As a result, both  $\delta$ -type and  $\beta$ -type magnetic distributions were reproduced only by the differences in the convective flows surrounding the flux tubes. The  $\delta$ -spots were formed by the collision of positive and negative magnetic fluxes on the photosphere. The unipolar and bipolar rotations of the  $\delta$ -spots were driven by magnetic twist and writhe, transporting magnetic helicity from the convection zone to the corona. We detected a strong correlation between the distribution of the nonpotential magnetic field in the photosphere and the position of the downflow plume in the convection zone. The correlation could be detected 20-30 h before the flux emergence. The results suggest that high free energy regions in the photosphere can be predicted even before the magnetic flux appears in the photosphere by detecting the downflow profile in the convection zone.

## Data-driven MHD simulation of successive solar plasma eruptions

[Takafumi Kaneko](#), [Sung-Hong Park](#), [Kanya Kusano](#)

ApJ **2021**

<https://arxiv.org/pdf/2101.12395.pdf>

Solar flares and plasma eruptions are sudden releases of magnetic energy stored in the plasma atmosphere. To understand the physical mechanisms governing their occurrences, three-dimensional magnetic fields from the photosphere up to the corona must be studied. The solar photospheric magnetic fields are observable, whereas the coronal magnetic fields cannot be measured. One method for inferring coronal magnetic fields is performing data-driven simulations, which involves time-series observational data of the photospheric magnetic fields with the bottom boundary of magnetohydrodynamic simulations. We developed a data-driven method in which temporal evolutions of the observational vector magnetic field can be reproduced at the bottom boundary in the simulation by introducing an inverted velocity field. This velocity field is obtained by inversely solving the induction equation and applying an appropriate gauge transformation. Using this method, we performed a data-driven simulation of successive small eruptions observed by the Solar Dynamics Observatory and the Solar Magnetic Activity Telescope in November 2017. The simulation well reproduced the converging motion between opposite-polarity magnetic patches, demonstrating successive formation and eruptions of helical flux ropes. **2017 November 4-5**

## A model of umbral oscillations inherited from subphotospheric fast-body modes

Juhyung [Kang](#)<sup>1</sup>, Jongchul Chae<sup>1</sup>, Kyuhyoun Cho<sup>2,3</sup>, Soosang Kang<sup>1</sup> and Eun-Kyung Lim<sup>4</sup>  
A&A, 686, A293 (2024)

<https://www.aanda.org/articles/aa/pdf/2024/06/aa49887-24.pdf>

Recently, complex horizontal patterns of umbral oscillations have been reported, but their physical nature and origin are still not fully understood. Here we show that the two-dimensional patterns of umbral oscillations of slow waves are inherited from the subphotospheric fast-body modes. Using a simple analytic model, we successfully reproduced the temporal evolution of oscillation patterns with a finite number of fast-body modes. In this model, the radial apparent propagation of the pattern is associated with the appropriate combination of the amplitudes in radial modes. We also find that the oscillation patterns are dependent on the oscillation period. This result indicates that there is a cutoff radial mode, which is a unique characteristic of the model of fast-body modes. In principle, both internal and external sources can excite these fast-body modes and produce horizontal patterns of umbral oscillations.

## A Statistical Analysis of Spiral-shaped Wave Patterns in Sunspot Umbrae

Juhyung [Kang](#)<sup>1</sup>, Jongchul Chae<sup>1</sup>, and Jooyeon Geem<sup>1</sup>

2024 ApJ 960 115

<https://iopscience.iop.org/article/10.3847/1538-4357/ad12c3/pdf>

Spiral-shaped wave patterns (SWPs) observed in sunspot umbrae represent the superposition of axisymmetric patterns and nonaxisymmetric patterns of umbral oscillations. These patterns give us physical information about the source of oscillations below the surface. Here we present the statistics of their observational properties determined from the 304 Å line-intensity data obtained with the Atmospheric Imaging Assembly onboard the Solar Dynamics Observatory. From the 2013 to 2018 data set, we examined each of the 496 sunspots near the disk center for 2 hr. As a result, we identified 241 SWPs from 140 sunspots, which corresponds to the detection rate of 0.24 per hour in each



sunspot. Most of the SWPs had one spiral arm, 48 SWPs had two arms, and only one had three. The oscillation period was estimated at  $151 \pm 27$  s and the lifetime, at  $770 \pm 250$  s, being comparable to those of conventional umbral oscillations. The rotation period of the SWPs was estimated at  $190 \pm 69$  s for the one-armed SWPs and  $299 \pm 115$  s for the two-armed SWPs. We found that the properties of the SWPs have no dependence on hemisphere, latitude, and sunspot size. From the apparent radial speeds of the SWPs and a simple model of wave propagation, we infer that the SWPs may be generated between 2 and 11 Mm below the photosphere with a mean value of about 6 Mm.

### **The Physical Nature of Spiral Wave Patterns in Sunspots**

Juhyung **Kang**<sup>1</sup>, Jongchul Chae<sup>1</sup>, Valery M. Nakariakov<sup>2,3</sup>, Kyuhyoun Cho<sup>1</sup>, Hannah Kwak<sup>1</sup>, and Kyeore Lee<sup>1</sup>

2019 ApJL 877 L9

[sci-hub.se/10.3847/2041-8213/ab1f6c](https://sci-hub.se/10.3847/2041-8213/ab1f6c)

<https://arxiv.org/pdf/1905.08908.pdf>

Recently, spiral wave patterns (SWPs) have been detected in 3 minute oscillations of sunspot umbrae, but the nature of this phenomenon has remained elusive. We present a theoretical model that interprets the observed SWPs as the superposition of two different azimuthal modes of slow magnetoacoustic waves driven below the surface in an untwisted and non-rotating magnetic cylinder. We apply this model to SWPs of the line-of-sight (LOS) velocity in a pore observed by the Fast Imaging Solar Spectrograph installed at the 1.6 m Goode Solar Telescope. One- and two-armed SWPs were identified in instantaneous amplitudes of LOS Doppler velocity maps of 3 minute oscillations. The associated oscillation periods are about 160 s, and the durations are about 5 minutes. In our theoretical model, the observed spiral structures are explained by the superposition of non-zero azimuthal modes driven 1600 km below the photosphere in the pore. The one-armed SWP is produced by the slow-body sausage ( $m = 0$ ) and kink ( $m = 1$ ) modes, and the two-armed SWP is formed by the slow-body sausage ( $m = 0$ ) and fluting ( $m = 2$ ) modes of the magnetic flux tube forming the pore. **2014 June 3**

### **Investigation of Force-Freeness of Solar Emerging Magnetic Field via Application of the Virial Theorem to MHD Simulations**

Jihye **Kang**, Tetsuya Magara

2014

<http://arxiv.org/pdf/1410.5542v1.pdf>

Force-freeness of a solar magnetic field is a key to reconstructing invisible coronal magnetic structure of an emerging flux region on the Sun where active phenomena such as flares and coronal mass ejections frequently occur. We have performed magnetohydrodynamic (MHD) simulations which are adjusted to investigate force-freeness of an emerging magnetic field by using the virial theorem. Our focus is on how the force-free range of an emerging flux region develops and how it depends on the twist of a pre-emerged magnetic field. As an emerging flux region evolves, the upper limit of the force-free range continuously increases while the lower limit is asymptotically reduced to the order of a photospheric pressure scale height above the solar surface. As the twist becomes small the lower limit increases and then seems to be saturated. We also discuss the applicability of the virial theorem to an evolving magnetic structure on the Sun.

### **Coronal Tomography**

**Kankelborg**, Charles C.

E-print, June 2008.

A simple, yet powerful, algorithm for computed tomography of the solar corona is demonstrated using synthetic EUV data. A minimum of three perspectives are required. These may be obtained from STEREO/EUVI plus an instrument near Earth, e.g. TRACE or SOHO/EIT.

### **Vortex Dynamics in Various Solar Magnetic Field Configurations**

**Arjun Kannan**, **Nitin Yadav**

MNRAS Volume 533, Issue 3 Pages 3611–3622, **2024**

<https://arxiv.org/pdf/2408.08225>

<https://doi.org/10.1093/mnras/stae1990>

We investigate vortex dynamics in three magnetic regions, viz., Quiet Sun, Weak Plage, and Strong Plage, using realistic three-dimensional simulations from a comprehensive radiation-MHD code, MURaM. We find that the spatial extents and spatial distribution of vortices vary for different setups even though the photospheric turbulence responsible for generating vortices has similar profiles for all three regions. We investigate kinetic and magnetic swirling strength and find them consistent with the Alfvén wave propagation. Using a flux tube expansion model and linear magnetohydrodynamics (MHD) wave theory, we find that the deviation in kinetic swirling strength from the theoretically expected value is the highest for the Strong Plage, least for the Weak Plage, and intermediate for the Quiet Sun at chromospheric heights. It suggests that Weak Plage is the most favoured region for chromospheric

swirls, though they are of smaller spatial extents than in Quiet Sun. We also conjecture that vortex interactions within a single flux tube in Strong Plage lead to an energy cascade from larger to smaller vortices that further result in much lower values of kinetic swirling strength than other regions. Fourier spectra of horizontal magnetic fields at 1 Mm height also show the steep cascade from large to smaller scales for Strong Plage. These findings indicate the potential of vortex-induced torsional Alfvén waves to travel higher in the atmosphere without damping for weaker magnetic regions such as the Quiet Sun, whereas vortices would result in dissipation and heating due to the vortex interactions in narrow flux tubes for the strongly magnetized regions such as Strong Plage.

## **Hinode and IRIS observations of the magnetohydrodynamic waves propagating from the photosphere to the chromosphere in a sunspot**

Ryuichi [Kanoh](#), Toshifumi Shimizu, Shinsuke Imada

ApJ 831 24 2016

<http://arxiv.org/pdf/1608.03910v1.pdf>

Magnetohydrodynamic (MHD) waves have been considered as energy sources for heating the solar chromosphere and the corona. Although MHD waves have been observed in the solar atmosphere, there are lack of quantitative estimates on the energy transfer and dissipation in the atmosphere. We performed simultaneous Hinode and IRIS observations of a sunspot umbra to derive the upward energy fluxes at two different atmospheric layers (photosphere and lower transition region) and estimate the energy dissipation. The observations revealed some properties of the observed periodic oscillations in physical quantities, such as their phase relations, temporal behaviors, and power spectra, making a conclusion that standing slow-mode waves are dominant at the photosphere with their high frequency leakage, which is observed as upward waves at the chromosphere and the lower transition region. Our estimate of upward energy fluxes are  $2.0 \times 10^7$  erg cm<sup>-2</sup> s<sup>-1</sup> at the photospheric level and  $8.3 \times 10^4$  erg cm<sup>-2</sup> s<sup>-1</sup> at the lower transition region level. The difference between the energy fluxes is larger than the energy required to maintain the chromosphere in the sunspot umbrae, suggesting that the observed waves can make a crucial contribution to the heating of the chromosphere in the sunspot umbrae. In contrast, the upward energy flux derived at the lower transition region level is smaller than the energy flux required for heating the corona, implying that we may need another heating mechanisms. We should, however, note a possibility that the energy dissipated at the chromosphere might be overestimated because of the opacity effect.

## **A novel algorithm for high fidelity spectro-polarimetric snapshot imaging of the low-frequency radio Sun using SKA-low precursor**

Devojyoti [Kansabanik](#), [Divya Oberoi](#), [Surajit Mondal](#)

2022 3rd URSI Atlantic and Asia Pacific Radio Science Meeting (AT-AP-RASC)

<https://arxiv.org/pdf/2207.11924.pdf>

Magnetic field couples the solar interior to the solar atmosphere, known as the corona. The coronal magnetic field is one of the crucial parameters which determines the coronal structures and regulates the space weather phenomena like flares, coronal mass ejections, energetic particle events, and solar winds. Measuring the magnetic field at middle and higher coronal heights are extremely difficult problem and to date there is no single measurement technique available to measure the higher coronal magnetic fields routinely. polarization measurements of the low-frequency radio emissions are an ideal tool to probe the coronal magnetic fields at higher coronal heights (>1R<sub>☉</sub>). To date, most of the low-frequency polarization observations of the Sun were limited to bright solar radio bursts. Here we developed a novel algorithm for performing precise polarization calibration of the solar observations done with the Murchison Widefield Array, a future Square Kilometer Array (SKA) precursor. We have brought down the instrumental polarization <1%. We anticipate this method will allow us to detect very low-level polarised emissions from coronal thermal emissions, which will become a tool for routine measurements of the global coronal magnetic fields at higher coronal heights. This method can be easily adapted for future SKA and open a window of new discoveries using high fidelity spectro-polarimetric snapshot imaging of the Sun at low radio frequencies. **28 Sep, 24 Oct, 3 Nov 2014**

## **Magnetic flux concentrations from turbulent stratified convection**

P. J. [Käpylä](#) (1,2,3), A. Brandenburg (3,4,5,6), N. Kleeorin (7,3), M. J. Käpylä (1), I. Rogachevskii

A&A 2016

<http://arxiv.org/pdf/1511.03718v1.pdf>

Context: The mechanisms that cause the formation of sunspots are still unclear. Aims: We study the self-organisation of initially uniform sub-equipartition magnetic fields by highly stratified turbulent convection. Methods: We perform simulations of magnetoconvection in Cartesian domains that are 8.5-24 Mm deep and 34-96 Mm wide. We impose either a vertical or a horizontal uniform magnetic field in a convection-driven turbulent flow. Results: We find that super-equipartition magnetic flux concentrations are formed near the surface with domain depths of 12.5 and 24 Mm. The size of the concentrations increases as the box size increases and the largest structures (20 Mm horizontally) are obtained in the 24 Mm deep models. The field strength in the concentrations is in the range of 3-5 kG. The concentrations grow approximately linearly in time. The effective magnetic pressure

measured in the simulations is positive near the surface and negative in the bulk of the convection zone. Its derivative with respect to the mean magnetic field, however, is positive in the majority of the domain, which is unfavourable for the negative effective magnetic pressure instability (NEMPI). Furthermore, we find that magnetic flux is concentrated in regions of converging flow corresponding to large-scale supergranulation convection pattern. Conclusions: The linear growth of large-scale flux concentrations implies that their dominant formation process is tangling of the large-scale field rather than an instability. One plausible mechanism explaining both the linear growth and the concentration of the flux in the regions of converging flow pattern is flux expulsion. Possible reasons for the absence of NEMPI are that the derivative of the effective magnetic pressure with respect to the mean magnetic field has an unfavourable sign and that there may not be sufficient scale separation.

## Properties of Magnetic Neutral Line Gradients and Formation of Filaments

Nina V. **Karachik**, Alexei A. Pevtsov

Solar Physics, March 2014, Volume 289, Issue 3, pp 821-830

<http://arxiv.org/pdf/1307.3317v1.pdf>

We investigate the gradients of magnetic fields across neutral lines (NLs) and compare their properties for NLs with and without chromospheric filaments. Our results show that there is a range of preferred magnetic field gradients where the filament formation is enhanced. On the other hand, a horizontal gradient of the magnetic field across an NL alone does not appear to be a single factor that determines if a filament will form (or not) in a given location.

## Flux Transport Dynamos: From Kinematics to Dynamics

**Review**

Bidya Binay **Karak**, Jie Jiang, [Mark S. Miesch](#), [Paul Charbonneau](#), [Arnab Rai Choudhuri](#)  
[Space Science Reviews](#), December 2014, Volume 186, [Issue 1-4](#), pp 561-602

Over the past several decades, Flux-Transport Dynamo (FTD) models have emerged as a popular paradigm for explaining the cyclic nature of solar magnetic activity. Their defining characteristic is the key role played by the mean meridional circulation in transporting magnetic flux and thereby regulating the cycle period. Most FTD models also incorporate the so-called Babcock-Leighton (BL) mechanism in which the mean poloidal field is produced by the emergence and subsequent dispersal of bipolar active regions. This feature is well grounded in solar observations and provides a means for assimilating observed surface flows and fields into the models in order to forecast future solar activity, to identify model biases, and to clarify the underlying physical processes. Furthermore, interpreting historical sunspot records within the context of FTD models can potentially provide insight into why cycle features such as amplitude and duration vary and what causes extreme events such as Grand Minima. Though they are generally robust in a modeling sense and make good contact with observed cycle features, FTD models rely on input physics that is only partially constrained by observation and that neglects the subtleties of convective transport, convective field generation, and nonlinear feedbacks. Here we review the formulation and application of FTD models and assess our current understanding of the input physics based largely on complementary 3D MHD simulations of solar convection, dynamo action, and flux emergence.

## Christian Horrebow's Sunspot Observations – II. Construction of a Record of Sunspot Positions

Christoffer **Karoff**, Carsten Sønderskov Jørgensen, V. Senthamizh Pavai, Rainer Arlt

[Solar Physics](#) June 2019, 294:78

<https://link.springer.com/content/pdf/10.1007%2Fs11207-019-1466-y.pdf>

The number of spots on the surface of the Sun is one of the best tracers of solar variability we have. The sunspot number is not only known to change in phase with the 11-year solar cycles, but also to show variability on longer time scales. It is, however, not only the sunspot number that changes in connection with solar variability. The location of the spots on the solar surface is also known to change in phase with the 11-year solar cycle. This has traditionally been visualised in the so-called butterfly diagram, but this is only well constrained from the beginning of the 19th century. This is unfortunate, as knowledge about the butterfly diagram could aid our understanding of the variability and the Sun–Earth connection.

As part of a larger review of the work done on sunspots by the Danish astronomer Christian Horrebow, we here present a reanalysis of Christian Horrebow's notebooks covering the years 1761 and 1764 – 1777. These notebooks have been analysed in at least three earlier studies by Thiele (*Astron. Nachr.* 50, 257, [1859](#)), d'Arrest (published in Wolf, *Astron. Mitt. Eidgenöss. Sternwarte Zür.* 4, 77, [1873](#)) and Hoyt and Schatten (*Solar Phys.* 160, 387, [1995](#)). In this article, we construct a complete record of sunspot positions covering the years 1761 and 1764 – 1777. The resulting butterfly diagram shows the characteristic structure known from observations in the 19th and 20th century. We do see some indications of equatorial sunspots in the observations we have from Cycle 1. However, in Cycle 2, which has much better coverage, we do not see such indications.

## **Solar Active Regions Emergence Prediction Using Long Short-Term Memory Networks**

[Spiridon Kasapis](#), [Irina N. Kitiashvili](#), [Alexander G. Kosovichev](#), [John T. Stefan](#)

ApJ 2024

<https://arxiv.org/pdf/2409.17421>

We developed Long Short-Term Memory (LSTM) models to predict the formation of active regions (ARs) on the solar surface. Using the Doppler shift velocity, the continuum intensity, and the magnetic field observations from the Solar Dynamics Observatory (SDO) Helioseismic and Magnetic Imager (HMI), we have created time-series datasets of acoustic power and magnetic flux, which are used to train LSTM models on predicting continuum intensity, 12 hours in advance. These novel machine learning (ML) models are able to capture variations of the acoustic power density associated with upcoming magnetic flux emergence and continuum intensity decrease. Testing of the models' performance was done on data for 5 ARs, unseen from the models during training. Model 8, the best performing model trained, was able to make a successful prediction of emergence for all testing active regions in an experimental setting and three of them in an operational. The model predicted the emergence of AR11726, AR13165, and AR13179 respectively 10, 29, and 5 hours in advance, and variations of this model achieved average RMSE values of 0.11 for both active and quiet areas on the solar disc. This work sets the foundations for ML-aided prediction of solar ARs. **2013.03.15-19, 2013.04.20-27, 2022.12.12-18, 2022.12.30-01.05, 2023.01.06-12**

## **Extrapolation of Three-dimensional Magnetic Field Structure in Flare-productive Active Regions with Different Initial Conditions**

Y. [Kawabata](#)<sup>1</sup>, S. Inoue<sup>2</sup>, and T. Shimizu<sup>3,4</sup>

2020 ApJ 895 105

<https://sci-hub.tw/https://iopscience.iop.org/article/10.3847/1538-4357/ab8ea9>

Nonlinear force-free field (NLFFF) modeling has been extensively used as a tool to infer three-dimensional (3D) magnetic field structure. In this study, the dependency of the NLFFF calculation with respect to the initial guess of the 3D magnetic field is investigated. While major parts of the previous studies used the potential field as the initial guess in NLFFF modeling, we adopt linear force-free fields with different constant force-free alpha as the initial guesses. This method enables us to investigate the uniqueness of the magnetic field obtained by the NLFFF extrapolation with respect to the initial guess. The dependence of the initial conditions on NLFFF extrapolation is smaller in the strong magnetic field region. Therefore, the magnetic field at lower heights (<10 Mm) tends to be less affected by the initial conditions (correlation coefficient  $C > 0.9$  with different initial conditions); although, the Lorentz force is concentrated at lower heights. **2013 March 15. 2014 February 3**

## **Chromospheric magnetic field: A comparison of He I 10830 A observations with nonlinear force-free field extrapolation**

[Yusuke Kawabata](#), [Andrés Asensio Ramos](#), [Satoshi Inoue](#), [Toshifumi Shimizu](#)

ApJ 898 32 2020

<https://arxiv.org/pdf/2006.00179.pdf>

<https://doi.org/10.3847/1538-4357/ab9816>

The nonlinear force-free field (NLFFF) modeling has been extensively used to infer the three-dimensional (3D) magnetic field in the solar corona. One of the assumptions in the NLFFF extrapolation is that the plasma beta is low, but this condition is considered to be incorrect in the photosphere. We examine direct measurements of the chromospheric magnetic field in two active regions through spectropolarimetric observations at He I 10830 A, which are compared with the potential fields and NLFFFs extrapolated from the photosphere. The comparisons allow quantitative estimation of the uncertainty in the NLFFF extrapolation from the photosphere. Our analysis shows that observed chromospheric magnetic field may have larger non-potentiality compared to the photospheric magnetic field. Moreover, the large non-potentiality in the chromospheric height may not be reproduced by the NLFFF extrapolation from the photospheric magnetic field. The magnitude of the underestimation of the non-potentiality at chromospheric heights may reach 30-40 degree in shear signed angle in some locations. This deviation may be caused by the non-force-freeness in the photosphere. Our study suggests the importance of the inclusion of measured chromospheric magnetic fields in the NLFFF modeling for the improvement of the coronal extrapolation. **28 Aug 2007, 12 Oct 2013**

## **Extrapolation of Three Dimensional Magnetic Field Structure in Flare-Productive Active Regions with Different Initial Condition**

Y. [Kawabata](#), [S. Inoue](#), [T. Shimizu](#)

ApJ 2020

<https://arxiv.org/pdf/2005.00177.pdf>

The nonlinear force-free field (NLFFF) modeling has been extensively used as a tool to infer three-dimensional (3D) magnetic field structure. In this study, the dependency of the NLFFF calculation with respect to the initial guess of the 3D magnetic field is investigated. While major part of the previous studies used potential field as the initial guess in the NLFFF modeling, we adopt the linear force-free fields with different constant force-free alpha as the initial guesses. This method enables us to investigate how unique the magnetic field obtained by the NLFFF extrapolation with respect to the initial guess is. The dependence of the initial condition of the NLFFF extrapolation is smaller in the strong magnetic field region. Therefore, the magnetic field at the lower height (<10 Mm) tends to be less affected by the initial condition (correlation coefficient  $C > 0.9$  with different initial condition), although the Lorentz force is concentrated at the lower height. **12-22 Mar 2013, 31 January-9 February 2014**

## **Non-potential field formation in the X-shaped quadrupole magnetic field configuration**

**Kawabata**, Yusuke; Inoue, Satoshi; Shimizu, Toshifumi

ApJ 2017

<https://arxiv.org/pdf/1705.02560.pdf>

Some types of solar flares are observed in X-shaped quadrupolar field configuration. To understand the magnetic energy storage in such a region, we studied non-potential field formation in an X-shaped quadrupolar field region formed in the active region NOAA 11967, which produced three X-shaped M-class flares on **February 2, 2014**. Nonlinear force-free field modeling was applied to a time series of vector magnetic field maps from the Solar Optical Telescope on board Hinode and Helioseismic and Magnetic Imager on board Solar Dynamics Observatory. Our analysis of the temporal three-dimensional magnetic field evolution shows that the sufficient free energy had already been stored more than 10 hours before the occurrence of the first M-class flare and that the storage was observed in a localized region. In this localized region, quasi-separatrix layers (QSLs) started to develop gradually from 9 hours before the first M-class flare. One of the flare ribbons that appeared in the first M-class flare was co-spatial with the location of the QSLs, suggesting that the formation of the QSLs is important in the process of energy release. These QSLs do not appear in the potential field calculation, indicating that they were created by the non-potential field. The formation of the QSLs was associated with the transverse photospheric motion of the pre-emerged flux and the emergence of a new flux. This observation indicates that the occurrence of the flares requires the formation of QSLs in the non-potential field in which free magnetic energy is stored in advance.

## **Dynamics of Sunspot Shock Waves in the Chromosphere and Transition Region**

**Pradeep Kayshap**, **Durgesh Tripathi**, **P. Jelinek**

2021 ApJ 906 121

<https://arxiv.org/pdf/2011.10192.pdf>

<https://doi.org/10.3847/1538-4357/abcc6f>

We study the dynamics of shock waves observed in the umbra of a sunspot using the spectroscopic observations from the Interface Region Imaging Spectrometer (IRIS). The presence of the shock significantly deforms the shape of the spectral lines of Mg II, C II, and Si IV. We found that C II 1335.66 Å and Si IV 1393.75 Å show double-peaked profiles that change to a single peak later on. However, the Mg II h 2803.53 Å line first shows flat-top profiles that change into double-peaked followed by the single peak. To study the shock dynamics, we isolate the shock component from the spectra by fitting two Gaussians. We find that the lifetime of the shock is largest in Mg II h 2803.53 Å line. Moreover, the plasma motion shows both acceleration and deceleration phase of the shock. Yet, in C II 1335.66 Å and Si IV 1393.75 Å, only deceleration phase is observed. We observe a strong correlation between the largest blueshift of the shock and deceleration for all three spectral lines. We find a positive (negative) correlation between intensities contributed due to the shocks in Mg II and C II (Si IV). This is suggestive that the shocks are first amplified in C II, followed by a decline in the height range corresponding to Si IV. These results may indicate the dissipation of shocks above the formation height of C II, and the shocks may have important roles in the dynamics of the upper chromosphere and transition region above sunspots.

## **A Comprehensive Method of Estimating Electric Fields from Vector Magnetic Field and Doppler Measurements**

Maria D. **Kazachenko**, George H. Fisher, Brian T. Welsch

2014 ApJ 795 17

<http://arxiv.org/pdf/1404.4027v1.pdf>

Photospheric electric fields, estimated from sequences of vector magnetic field and Doppler measurements, can be used to estimate the flux of magnetic energy (the Poynting flux) into the corona and as time-dependent boundary conditions for dynamic models of the coronal magnetic field. We have modified and extended an existing method to estimate photospheric electric fields that combines a poloidal-toroidal (PTD) decomposition of the evolving magnetic field vector with Doppler and horizontal plasma velocities. Our current, more comprehensive method, which we dub the "PTD-Doppler-LCT deal" (PDFI) technique, can now incorporate Doppler velocities from non-normal viewing angles. It uses the `FISHPACK` software package to solve

several two-dimensional Poisson equations, a faster and more robust approach than our previous implementations. Here, we describe systematic, quantitative tests of the accuracy and robustness of the PDFI technique using synthetic data from anelastic MHD (ANMHD) simulations, which have been used in similar tests in the past. We find that the PDFI method has less than 1 error in the total Poynting flux and a 10 error in the helicity flux rate at a normal viewing angle ( $\theta=0$ ) and less than 25 and 10 errors respectively at large viewing angles ( $\theta<60^\circ$ ). We compare our results with other inversion methods at zero viewing angle, and find that our method's estimates of the fluxes of magnetic energy and helicity are comparable to or more accurate than other methods. We also discuss the limitations of the PDFI method and its uncertainties.

## Spontaneous Formation of Magnetic Flux Concentrations in Stratified Turbulence

Koen [Kemel](#), Axel Brandenburg, Nathan Kleeorin, Dhruvadya Mitra, Igor Rogachevskii

Solar Physics, October 2012, Volume 280, Issue 2, pp 321-333

<http://arxiv.org/pdf/1112.0279v1.pdf>

The negative effective magnetic pressure instability discovered recently in direct numerical simulations (DNSs) may play a crucial role in the formation of sunspots and active regions in the Sun and stars. This instability is caused by a negative contribution of turbulence to the effective mean Lorentz force (the sum of turbulent and non-turbulent contributions) and results in the formation of large-scale inhomogeneous magnetic structures from an initially uniform magnetic field. Earlier investigations of this instability in DNSs of stably stratified, externally forced, isothermal hydromagnetic turbulence in the regime of large plasma  $\beta$  are now extended into the regime of larger scale separation ratios where the number of turbulent eddies in the computational domain is about 30. Strong spontaneous formation of large-scale magnetic structures is seen even without performing any spatial averaging. These structures encompass many turbulent eddies. The characteristic time of the instability is comparable to the turbulent diffusion time,  $L^2/\eta t$ , where  $\eta t$  is the turbulent diffusivity and  $L$  is the scale of the domain. DNSs are used to confirm that the effective magnetic pressure does indeed become negative for magnetic field strengths below the equipartition field. The dependence of the effective magnetic pressure on the field strength is characterized by fit parameters that seem to show convergence for larger values of the magnetic Reynolds number.

## Photospheric observations of surface and body modes in solar magnetic pores

Peter H. [Keys](#), [Richard J. Morton](#), [David B. Jess](#), [Gary Verth](#), [Samuel D. T. Grant](#), [Mihalis Mathioudakis](#), [Duncan H. Mackay](#), [John G. Doyle](#), [Damian J. Christian](#), [Francis P. Keenan](#), [Robertus Erdelyi](#)

ApJ 857 28 2018

<https://arxiv.org/pdf/1803.01859.pdf>

Over the past number of years, great strides have been made in identifying the various low-order magnetohydrodynamic wave modes observable in a number of magnetic structures found within the solar atmosphere. However, one aspect of these modes that has remained elusive, until now, is their designation as either surface or body modes. This property has significant implications on how these modes transfer energy from the waveguide to the surrounding plasma. Here, for the first time to our knowledge, we present conclusive, direct evidence of these wave characteristics in numerous pores which were observed to support sausage modes. As well as outlining methods to detect these modes in observations, we make estimates of the energies associated with each mode. We find surface modes more frequently in the data, and also that surface modes appear to carry more energy than those displaying signatures of body modes. We find frequencies in the range of  $\sim 2$  to 12 mHz with body modes as high as 11 mHz, but we do not find surface modes above 10 mHz. It is expected that the techniques we have applied will help researchers search for surface and body signatures in other modes and in differing structures to those presented here.

**Table 1.** Summary of observations for the sample of pores studied.

## Spectral lines in FUV and EUV for diagnosing coronal magnetic field

[Raveena Khan](#), [K. Nagaraju](#)

Solar Phys. 297, Article number: 96 2022

<https://arxiv.org/pdf/2205.11844.pdf>

<https://doi.org/10.1007/s11207-022-02024-2>

The diagnostic capabilities of spectral lines in far ultraviolet (FUV) and extreme ultraviolet (EUV) wavelength range are explored in terms of their Hanle and Zeeman sensitivity to probe vector magnetic field in the solar corona. The temperature range covered is  $\log_{10}(T)=5.5-6.3$ . The circular polarization signal due to longitudinal Zeeman effect is estimated for spectral lines in the wavelength range of 500 to 1600 Å. The Stokes V/I signal for a FUV line is found to be in the order of  $10^{-4}$  for a longitudinal field strength of 10 Gauss, which further reduces to  $10^{-5}$  for wavelengths below 1200 Å. Due to such low signals, the present study aims to find combination of spectral lines having different Hanle sensitivity but with identical peak formation temperature to probe coronal magnetic field vector. The combination of Hanle sensitive lines is better suited because the Hanle signals are stronger by at least an

order of magnitude compared to Zeeman signals. The linear polarization signals due to Hanle effect from at least two spectral lines are required to derive information on the full vector. It is found from this study that there is always a pair of Hanle sensitive lines for a given temperature range suitable for probing coronal vector magnetic field and they are located in close proximity with each other in terms of their wavelength.

## **Testing spectropolarimetry in the extreme ultraviolet to infer the solar coronal magnetic field**

A. [Khan](#)

A&A 545, A52 (2012)

Context. Spectropolarimetry has the potential to provide us with important coronal plasma parameters.

Aims. We test spectropolarimetric forward modelling by investigating whether it is possible to reproduce the only linear polarisation measurement made for the optically thin 1032 Å UV O vi line detected by the Solar Ultraviolet Measurements of Emitted Radiation (SUMER) instrument, operating aboard the SOLar and Heliospheric Observatory (SOHO) spacecraft located 1.29 R<sub>☉</sub> above the southern solar rotation axis.

Methods. Through the realistic synthesis of line-of-sight integrated emission coefficients in the four Stokes parameters, we explore subsets of the ten-dimensional parameter space, ( $n_e$ ,  $n_{O^5+}$ ,  $\alpha_c$ ,  $I_{chr}$ ,  $T$ ,  $B$ ,  $v$ ,  $w_{\perp}$ ,  $w_{\parallel}$ ,  $\delta$ ), i.e., the number density of electrons and O<sup>5+</sup> ions, respectively, the electronic collision rate, the chromospheric intensity of the O vi line, the electronic temperature, the magnetic and solar outflow-velocity vectors, the perpendicular and parallel (with respect to the magnetic field) parameters of the anisotropic velocity-distribution functions, and finally the tilt of the solar rotation axis, non-rigorously in search for agreement between the forward-modelled linear polarisation parameters and the observed values.

Results. The most interesting result is that the tilt of the solar rotation axis creates non-radial fields, for both the magnetic field and velocity, above the Sun in the plane of the sky, thus transforming this previously rather uninteresting area from the polarimetric point of view into a highly exciting one. Our findings show that if the magnetic field intensity lies in the range 10–45 G and the solar outflow velocity in the range 20–100 km s<sup>-1</sup>, we are able to reproduce the full range of observed values plus uncertainties in the rotation angle of  $9^{\circ} \pm 6^{\circ}$ . The second observable, i.e., the fractional linear polarisation is somewhat harder to bring into alignment with our forward modelling efforts in that one has to decrease the electron density in most current models by an order of magnitude.

Conclusions. It is indeed very encouraging to note how this single measurement of the linear polarisation parameters in the ultraviolet virtually steers the forward modeller in the right direction of reproducing the physical environment that gave rise to the observed values. This bodes well for spectropolarimetry because it provides the basis for the hope that these observations will aid the forward modeller in determining how and where to start searching in the possibly terribly complicated maze of parameter space.

## **Solar coronal magnetic field diagnostics through polarimetric forward modelling of the Hanle effect**

A. [Khan](#) and E. Landi Degl'Innocenti

A&A 532, A70 (2011)

Context. Progress in the solution to some of the most outstanding open problems of solar physics, such as coronal heating, solar wind acceleration, the generation and triggering of explosive events like flares and CMEs, hinges on the provision of a more stringent estimate of the solar magnetic field coordinates.

Aims. We seek a way to infer the magnetic field of the solar atmosphere. A very promising way of doing this is by using the Hanle effect in resonance scattering in the L $\alpha$  line of the solar atmosphere.

Methods. By forward modelling the known scattering effects in the presence of magnetic fields, i.e. rotation of the plane of polarisation and depolarisation of the linear polarisation parameters, and by comparing them to observations, one could potentially uncover the magnetic morphology and restrict its intensity range. We simulate the effects of simple dipole configurations along the coordinate axes and analyse the outcome through two kinds of graphs (i.e. the difference in angle of the plane of linear polarisation with respect to the field-free case, and the relative depolarisation).

Results. The graphs are either symmetric, anti-symmetric or asymmetric with respect to the (y,z) plane. This is explained by invoking two symmetry operations and taking into account that the magnetic field is a pseudovector. We also show the polarimetric effects of active regions and use them pairwise with the magnetic field due to dipoles to analyse the polarimetric signatures of magnetic field line loops. Inspired by the famous TRACE image, we finally show what one could expect from polarimetry performed on the region of the solar atmosphere displayed in the image.

Conclusions. By combining the two complementary remote sensing techniques, i.e. the Zeeman and the Hanle effect, in all thinkable ways with tracers such as the images revealed by TRACE, SOHO, STEREO, etc., we hope

one day to be able to infer the solar magnetic field coordinates. Much theoretical and instrumental work still lies ahead, however.

## Oscillations and Waves in Sunspots

Review

Elena [Khomenko](#) and Manuel Collados Vera

Living Reviews in Solar Physics PUB.NO. IrsP-2015-6

<http://solarphysics.livingreviews.org/Articles/IrsP-2015-6/download/IrsP-2015-6Color.pdf>

A magnetic field modifies the properties of waves in a complex way. Significant advances have been made recently in our understanding of the physics of sunspot waves with the help of high-resolution observations, analytical theories, as well as numerical simulations. We review the current ideas in the field, providing the most coherent picture of sunspot oscillations as by present understanding. 20-28 Jan 2002

## Evershed flow observed in neutral and singly ionized iron lines

E. [Khomenko](#), M. Collados, N. Shchukina, A. Diaz

A&A 2015

<http://arxiv.org/pdf/1510.00334v1.pdf>

The amplitudes of the Evershed flow are measured using pairs of carefully selected FeI and FeII spectral lines located close in wavelength and registered simultaneously. A sunspot belonging to the NOAA 11582 group was scanned using the spectrograph of the German Vacuum Tower Telescope (Observatorio del Teide, Tenerife). Velocities were extracted from intensity profiles using the lambda-meter technique. The formation heights of the observed spectral lines were calculated using semi-empirical models of a bright and dark penumbral filament taking into account the sunspot location at the limb. Our objective is to compare azimuthally averaged amplitudes of the Evershed flow extracted from neutral and ion lines. We find measurable differences in the radial component of the flow. All five pairs of lines show the same tendency, with a few hundred m/s larger amplitude of the flow measured from FeI lines compared to FeII lines. This tendency is preserved at all photospheric heights and radial distances in the penumbra. We discuss the possible origin of this effect. 7th of October, 2012

## Properties of sunspot umbrae observed in cycle 24

Christoph [Kiess](#), Reza Rezaei and Wolfgang Schmidt

A&A 565, A52 (2014)

**Aims.** There is an ongoing debate whether the solar activity cycle is overlaid with a long-term decline that may lead to another grand minimum in the near future. We used the size, intensity, and magnetic field strength of sunspot umbrae to compare the present cycle 24 with the previous one.

**Methods.** We used data of the Helioseismic and Magnetic Imager on board the Solar Dynamics Observatory and selected all sunspots between May 2010 and October 2012, using one image per day. We created two subsets of this dataset with a manual tracking algorithm, both without duplication. One contains each sunspot (910 umbrae within 488 spots) and was used to analyze the distribution of umbral areas, selected with an automated thresholding method. The other subset contains 205 fully evolved sunspots. We estimated their magnetic field and the total magnetic flux and discuss the relations between umbral size, minimum continuum intensity, maximum field strength, and total magnetic flux.

**Results.** We find non-linear relations between umbral minimum intensity and size and between maximum magnetic field strength and size. The field strength scales linearly with the intensity and the umbral size scales roughly linearly with the total magnetic flux, while the size and field strength level off with stronger flux. When separated into hemispheres and averaged temporally, the southern umbrae show a temporal increase in size and the northern umbrae remain constant. We detected no temporal variation in the umbral mean intensity. The probability density function of the umbral area in the ascending phase of the current solar cycle is similar to that of the last solar cycle.

**Conclusions.** From our investigation of umbral area, magnetic field, magnetic flux, and umbral intensity of the sunspots of the rising phase of cycle 24, we do not find a significant difference to the previous cycle, and hence no indication for a long-term decline of solar activity.

## Physical Characteristics of Umbral Dots Derived from a High-Resolution Observations

Ali [Kilcik](#), [Volkan Sarp](#), [Vasyl Yurchyshyn](#), [Jean-Pierre Rozelot](#) & [Atila Ozguc](#)

*Solar Physics* volume 295, Article number: 58 (2020)

<https://link.springer.com/content/pdf/10.1007/s11207-020-01618-y.pdf>

The aim of this study is to revisit the physical parameters of umbral dots (UDs) with the latest high-resolution observations and contribute to the scientific understanding of their formation and evolution. In this study, we applied a particle tracking algorithm for detecting UD in NOAA AR 12384 observed on **June 14, 2015** by the Goode Solar Telescope (GST). We analyzed average position distributions, location dependencies, and general properties of the



detected total 2892 UD separately during their life time and the periodic behavior of ten selected long-lived UDs. We found: i) the brightest, largest, fastest and most elliptic UDs tend to be located at the umbra–penumbra boundary while their lifetime does not display any meaningful location dependency, ii) average dynamic velocity of all detected UDs is about twice ( $0.76 \text{ km s}^{-1}$ ) of the previously reported average values, iii) obtained trajectories from the longest-lived 354 UDs show that they have generally inward motion, iv) chosen 10 long-lived UDs generally have similar periodic behavior showing 8.5 – 32, 3.5 – 4.1, 1.5 – 1.9, and 1.1 – 1.3 minutes periodicities, v) generally, detected UDs have an elliptical shape with the averaged eccentricity of 0.29, with a 0.11 standard deviation, vi) larger UDs tend to be more elliptic and more dynamic.

### **Sunspot Count Periodicities in Different Zurich Sunspot Group Classes since 1986**

A. **Kilcik**, A. Ozguc, V.B. Yurchyshyn, J.P. Rozelot  
Solar Physics, Volume 289, Issue 11, pp 4365-4376 2014  
<http://arxiv.org/pdf/1407.5895v1.pdf>

In this study, we used two methods to investigate the periodic behavior of sunspot counts in four categories for the time period January 1986-October 2013. These categories include the counts from simple (A and B), medium (C), large (D, E, and F), and final (H) sunspot groups. We used: i) the Multi-taper Method with red noise approximation, and ii) the Morlet wavelet transform for periodicity analysis. Our main findings are: (1) the solar rotation periodicity of about 25 to 37 days, which is of obvious significance, is found in all groups with at least a 95% significance level; (2) the periodic behavior of a cycle is strongly related to its amplitude and group distribution during the cycle; (3) the appearance of periods follow the amplitude of the investigated solar cycles, (4) meaningful periods do not appear during the minimum phases of the investigated cycles. We would like to underline that the cyclic behavior of all categories is not completely the same; there are some differences between these groups. This result can provide a clue for the better understanding of solar cycles.

### **TIME DISTRIBUTIONS OF LARGE AND SMALL SUNSPOT GROUPS OVER FOUR SOLAR CYCLES**

A. **Kilcik**, V. B. Yurchyshyn, V. Abramenko, P. R. Goode, A. Ozguc, J. P. Rozelot and W. Cao  
2011 ApJ 731 30

Here we analyze solar activity by focusing on time variations of the number of sunspot groups (SGs) as a function of their modified Zurich class. We analyzed data for solar cycles 20-23 by using Rome (cycles 20 and 21) and Learmonth Solar Observatory (cycles 22 and 23) SG numbers. All SGs recorded during these time intervals were separated into two groups. The first group includes small SGs (A, B, C, H, and J classes by Zurich classification), and the second group consists of large SGs (D, E, F, and G classes). We then calculated small and large SG numbers from their daily mean numbers as observed on the solar disk during a given month. We report that the time variations of small and large SG numbers are asymmetric except for solar cycle 22. In general, large SG numbers appear to reach their maximum in the middle of the solar cycle (phases 0.45-0.5), while the international sunspot numbers and the small SG numbers generally peak much earlier (solar cycle phases 0.29-0.35). Moreover, the 10.7 cm solar radio flux, the facular area, and the maximum coronal mass ejection speed show better agreement with the large SG numbers than they do with the small SG numbers. Our results suggest that the large SG numbers are more likely to shed light on solar activity and its geophysical implications. Our findings may also influence our understanding of long-term variations of the total solar irradiance, which is thought to be an important factor in the Sun-Earth climate relationship.

### **Solar Farside Magnetograms from Deep Learning Analysis of STEREO/EUVI Data**

**Kim**, T., Park, E., Lee, H., et al.  
2019, Nature Astronomy, 3: 397–400, doi: 10.1038/s41550-019-0711-5  
<http://sci-hub.se/10.1038/s41550-019-0711-5>

Solar magnetograms are important for studying solar activity and predicting space weather disturbances<sup>1</sup>. Farside magnetograms can be constructed from local helioseismology without any farside data<sup>2-4</sup>, but their quality is lower than that of typical frontside magnetograms. Here we generate farside solar magnetograms from STEREO/Extreme UltraViolet Imager (EUVI) 304-Å images using a deep learning model based on conditional generative adversarial networks (cGANs). We train the model using pairs of Solar Dynamics Observatory (SDO)/Atmospheric Imaging Assembly (AIA) 304-Å images and SDO/Helioseismic and Magnetic Imager (HMI) magnetograms taken from 2011 to 2017 except for September and October each year. We evaluate the model by comparing pairs of SDO/HMI magnetograms and cGAN-generated magnetograms in September and October. Our method successfully generates frontside solar magnetograms from SDO/AIA 304-Å images and these are similar to those of the SDO/HMI, with Hale-patterned active regions being well replicated. Thus we can monitor the temporal evolution of magnetic fields

from the farside to the frontside of the Sun using SDO/HMI and farside magnetograms generated by our model when farside extreme-ultraviolet data are available. This study presents an application of image-to-image translation based on cGANs to scientific data. **4-13 June 2014, 1-7 September 2017,**  
[HMI Science Nuggets #125 Apr 2019](#) <http://hmi.stanford.edu/hminuggets/?p=2890>

### **Vertical Kink Oscillation of a Magnetic Flux Rope Structure in the Solar Corona**

S. **Kim**<sup>1</sup>, V. M. Nakariakov<sup>2,3,4</sup>, and K.-S. Cho

**2014** *ApJ* 797 L22

Vertical transverse oscillations of a coronal magnetic rope, observed simultaneously in the 171 Å and 304 Å bandpasses of the Atmospheric Imaging Assembly on board the *Solar Dynamics Observatory* (SDO), are detected. The oscillation period is about 700 s and the displacement amplitude is about 1 Mm. The oscillation amplitude remains constant during the observation. Simultaneous observation of the rope in the bandpasses corresponding to the coronal and chromospheric temperatures suggests that it has a multi-thermal structure. Oscillatory patterns in 171 Å and 304 Å are coherent, which indicates that the observed kink oscillation is collective, in which the rope moves as a single entity. We interpret the oscillation as a fundamental standing vertically polarized kink mode of the rope, while the interpretation in terms of a perpendicular fast wave could not be entirely ruled out. In addition, the arcade situated above the rope and seen in the 171 Å bandpass shows an oscillatory motion with the period of about 1000 s.

### **Machine Learning for Reconstruction of Polarity Inversion Lines from Solar Filaments.**

**Kisielius**, V., Illarionov, E.

*Sol Phys* 299, 69 (**2024**).

<https://doi.org/10.1007/s11207-024-02324-9>

Solar filaments are well-known tracers of polarity inversion lines that separate two opposite magnetic polarities on the solar photosphere. Because observations of filaments began long before the systematic observations of solar magnetic fields, historical filament catalogs can facilitate the reconstruction of magnetic polarity maps at times when direct magnetic observations were not yet available. In practice, this reconstruction is often ambiguous and typically performed manually. We propose an automatic approach based on a machine-learning model that generates a variety of magnetic polarity maps consistent with filament observations. To evaluate the model and discuss the results, we use the catalog of solar filaments and polarity maps compiled by McIntosh. We realize that the process of manual compilation of polarity maps includes not only information on filaments, but also a large amount of prior information, which is difficult to formalize. To compensate for the lack of prior knowledge for the machine-learning model, we provide it with polarity information at several reference points. We demonstrate that this process, which can be considered as the user-guided reconstruction or superresolution, leads to polarity maps that are reasonably close to hand-drawn ones and additionally allows for uncertainty estimation.

### **Morphological study of penumbral formation**

Reizaburo **Kitai**, Hiroko Watanabe, Ken'ichi Otsuji

*PASJ*, **2014**

<http://arxiv.org/pdf/1407.4573v1.pdf>

Penumbrae are known to be area of mainly horizontal magnetic field surrounding umbrae of relatively large and mature sunspots. In this paper, we observationally studied the formation of penumbrae in NOAA10978, where several penumbral formations were observed in G-band images of SOT/Hinode. Thanks to the continuous observation by Hinode, we could morphologically follow the evolution of sunspots and found that there are several paths to the penumbral formation: (1) Active accumulation of magnetic flux, (2) Rapid emergence of magnetic field, and (3) Appearance of twisted or rotating magnetic tubes. In all of these cases, magnetic fields are expected to sustain high inclination at the edges of flux tube concentration longer than the characteristic growth time of downward magnetic pumping.

### **The solar dynamo: inferences from observations and modeling**

L. L. **Kitchatinov**

*Geomagnetism & Aeronomy* (a **review**), **2014**

<http://arxiv.org/pdf/1404.4126v1.pdf>

It can be shown on observational grounds that two basic effects of dynamo theory for solar activity - production of the toroidal field from the poloidal one by differential rotation and reverse conversion of the toroidal field to the poloidal configuration by helical motions - are operating in the Sun. These two effects, however, do not suffice for constructing a realistic model for the solar dynamo. Only when a non-local version of the alpha-effect is applied, is downward diamagnetic pumping included and field advection by the equatorward meridional flow near the base of the convection zone allowed for, can the observed activity cycles be closely reproduced. Fluctuations in the alpha-

effect can be estimated from sunspot data. Dynamo models with fluctuating parameters reproduce irregularities of solar cycles including the grand activity minima. The physics of parametric excitation of irregularities remains, however, to be understood.

### **Open magnetic flux tubes in the corona and the transport of solar energetic particles**

Karl-Ludwig [Klein](#)<sup>1</sup>, S'am Krucker<sup>2</sup>, Guillaume Lointier<sup>1,3</sup>, and Alain Kerdraon<sup>1</sup>

File 2008, A&A

In a quasi-static situation coronal magnetic field lines can be traced by extrapolating photospheric field measurements. It is common to use a current free (potential) field model to identify large-scale coronal structures. While such models are clearly insufficient to represent the sheared and twisted magnetic field configurations in active regions, they have been successful in connecting coronal and interplanetary structures on larger scales. For example, Schrijver & DeRosa (2003) and Wang & Sheeley (2003) used such models to identify the origin of the heliospheric magnetic field, while Wang et al. (2006) showed that they represent the large-scale open magnetic flux tubes which guide SEP through the corona.

Like Nitta et al. (2006), we use the **PFSS (potential field-source surface) code of Schrijver & DeRosa (Sol. Phys., 212, 165, 2003) which is available in the *idl*-based *SolarSoft* data analysis package (<http://www.lmsal.com/derosa/pfsspack/>)**. The extrapolation is based on evolving synoptic maps assembled from measurements of the line-of-sight component of the magnetic field in the photosphere by the Michelson Doppler imager (MDI) aboard the Solar and Heliospheric Observatory (SoHO; Scherrer et al. 1995), assuming the magnetic field to be orthogonal to the photosphere. The model is updated by directly inserting MDI magnetogram data as it becomes available. After flux rotates out of the assimilation window (which extends out to about 60° from disc centre), it continues to evolve subject to transport processes based on the observed effects of differential rotation, meridional flows, convective dispersal, and the merging and fragmentation of flux.

### **Nonlinear force-free modeling of flare-related magnetic field changes at the photosphere and chromosphere**

Lucia [Kleint](#), [Michael S. Wheatland](#), [Alpha Mastrano](#), [Patrick I. McCauley](#)

ApJ **865** 146 **2018**

<https://arxiv.org/pdf/1808.07079.pdf>

[sci-hub.tw/10.3847/1538-4357/aadc5c](http://sci-hub.tw/10.3847/1538-4357/aadc5c)

Rapid and stepwise changes of the magnetic field are often observed during flares but cannot be explained by models yet. Using a 45 min sequence of SDO/HMI 135 s fast-cadence vector magnetograms of the X1 flare on **2014-03-29** we construct, at each timestep, nonlinear force-free models for the coronal magnetic field. Observed flare-related changes in the line-of-sight magnetic field BLOS at the photosphere and chromosphere are compared with changes in the magnetic fields in the models. We find a moderate agreement at the photospheric layer (the basis for the models), but no agreement at chromospheric layers. The observed changes at the photosphere and chromosphere are surprisingly different, and are unlikely to be reproduced by a force-free model. The observed changes are likely to require a change in the magnitude of the field, not just in its direction.

### **Prospects of solar magnetometry - from ground and in space**

**Review**

Lucia [Kleint](#), Achim Gandorfer

Space Science Reviews **2017**, Volume 210, [Issue 1-4](#), pp 397-426

<http://arxiv.org/pdf/1510.03763v1.pdf>

In this review we present an overview of observing facilities for solar research, which are planned or will come to operation in near future. We concentrate on facilities, which harbor specific potential for solar magnetometry. We describe the challenges and science goals of future magnetic measurements, the status of magnetic field measurements at different major solar observatories, and provide an outlook on possible upgrades of future instrumentation.

### **Nanoflare Heating: Observations and Theory**

**Review**

James A. [Klimchuk](#)

"Achievements of Hinode in the First Ten Years," PASJ, **2017**

<https://arxiv.org/ftp/arxiv/papers/1709/1709.07320.pdf>

This is a review of the observational and theoretical evidence for nanoflare heating of the magnetically-closed corona.

### **Key Aspects of Coronal Heating**

**Review**

James A. [Klimchuk](#)

Royal Society Philosophical Transactions A, 2015

<http://arxiv.org/ftp/arxiv/papers/1410/1410.5660.pdf>

We highlight ten key aspects of coronal heating that must be understood before we can consider the problem to be solved. (1) All coronal heating is impulsive. (2) The details of coronal heating matter. (3) The corona is filled with elemental magnetic strands. (4) The corona is densely populated with current sheets. (5) The strands must reconnect to prevent an infinite buildup of stress. (6) What determines the nanoflare frequency? (7) What is the quantum of energy release? (8) What causes the collective behavior responsible for loops? (9) What are the onset conditions for energy release? (10) Chromospheric nanoflares are not a primary source of coronal plasma. Significant progress in solving the coronal heating problem will require a coordination of approaches: observational studies, 1D hydro simulations, large-scale and localized 3D MHD simulations, and possibly also kinetic simulations. There is a unique value to each of these approaches, and the community must strive to coordinate better.

## **Chromospheric Nanoflares as the Source of Coronal Plasma Are Chromospheric Nanoflares a Primary Source of Coronal Plasma?**

J. A. [Klimchuk](#), S. J. Bradshaw

ApJ, 2014

<http://arxiv.org/pdf/1405.1708v1.pdf>

<http://lanl.arxiv.org/pdf/1405.1708v2.pdf>

It has been suggested that the hot plasma of the solar corona comes primarily from impulsive heating events, or nanoflares, that occur in the lower atmosphere, either in the upper part of the ordinary chromosphere or at the tips of type II spicules. We test this idea with a series of hydrodynamic simulations. We find that synthetic Fe XII (195) and Fe XIV (274) line profiles generated from the simulations disagree dramatically with actual observations. The integrated line intensities are much too faint; the blue shifts are much too fast; the blue-red asymmetries are much too large; and the emission is confined to low altitudes. We conclude that chromospheric nanoflares are not a primary source of hot coronal plasma. Such events may play an important role in producing the chromosphere and powering its intense radiation, but they do not, in general, raise the temperature of the plasma to coronal values. Those cases where coronal temperatures are reached must be relatively uncommon. The observed profiles of Fe XII and Fe XIV come primarily from plasma that is heated in the corona itself, either by coronal nanoflares or a quasi-steady coronal heating process. Chromospheric nanoflares might play a role in generating waves that provide this coronal heating.

## **The Emergence of Toroidal Flux Ropes with Different Twist Rising at the Same Speed**

Kalman J. [Knizhnik](#)<sup>1</sup>, Mark G. Linton<sup>1</sup>, and James E. Leake<sup>2</sup>

2022 ApJ 939 54

<https://iopscience.iop.org/article/10.3847/1538-4357/ac90c5/pdf>

The role of twist in the emergence of magnetic flux ropes into the solar atmosphere has remained unclear for some time. Although many studies have investigated how the photospheric properties of active regions resulting from the simulated emergence of magnetic flux ropes from the convection zone with different twists compare to the observed properties of active regions, these simulations have a wide range of magnetic flux rope radii, depths, and initial configurations, making it challenging to form a complete picture of the role of any one variable in the emergence process. Twist, in particular, has been difficult to analyze because isothermally buoyant magnetic flux ropes with different twists also experience different accelerations. In this paper, we develop an analytical model of a toroidal magnetic flux rope in approximate vertical force balance in the convection zone. We numerically implement this model in a stratified atmosphere, and then subtract off a twist-independent density to make magnetic flux ropes buoyant in a twist-independent way, ensuring that the initial acceleration of each magnetic flux rope is approximately the same. We perform numerical simulations to obtain a parameter study of toroidal magnetic flux ropes with different twist rising at the same speed. We analyze the photospheric and coronal properties of the active regions resulting from the emergence of these magnetic flux ropes, and argue that the Parker instability is responsible for many of the features observed in the simulations.

## **The Role of Twist in Kinked Flux Rope Emergence and Delta-Spot Formation**

Kalman J. [Knizhnik](#), [Mark G. Linton](#), [C. Richard DeVore](#)

ApJ 864 89 2018

<https://arxiv.org/pdf/1808.05562.pdf>

<https://doi.org/10.3847/1538-4357/aad68c>

It has been observationally well established that the magnetic configurations most favorable for producing energetic flaring events reside in delta-spots, a class of sunspots defined as having opposite polarity umbrae sharing a common penumbra. They are frequently characterized by extreme compactness, strong rotation and anti-Hale orientation. Numerous studies have shown that nearly all of the largest solar flares originate in delta-spots, making the understanding of these structures a fundamental step in predicting space weather. Despite their important

influence on the space environment, surprisingly little is understood about the origin and behavior of delta-spots. In this paper, we perform a systematic study of the behavior of emerging flux ropes to test a theoretical model for the formation of delta-spots: the kink instability of emerging flux ropes. We simulated the emergence of highly twisted, kink-unstable flux ropes from the convection zone into the corona, and compared their photospheric properties to those of emerged weakly twisted, kink-stable flux ropes. We show that the photospheric manifestations of the emergence of highly twisted flux ropes closely match the observed properties of delta-spots, and we discuss the resulting implications for observations. Our results strongly support and extend previous theoretical work that suggested that the kink instability of emerging flux ropes is a promising candidate to explain delta-spot formation, as it reproduces their key characteristics very well.

## **The Role of Magnetic Helicity in Structuring the Solar Corona**

Kalman J. **Knizhnik**, Spiro K. Antiochos, C. Richard DeVore

ApJ 2016

<http://arxiv.org/pdf/1607.06756v1.pdf>

Two of the most widely observed and yet most puzzling features of the Sun's magnetic field are coronal loops that are smooth and laminar and prominences/filaments that are strongly sheared. These two features would seem to be quite unrelated in that the loops are near their minimum-energy current-free state, whereas filaments are regions of high magnetic stress and intense electric currents. We argue that, in fact, these two features are inextricably linked in that both are due to a single process: the injection of magnetic helicity into the corona by photospheric motions and the subsequent evolution of this helicity by coronal reconnection. In this paper, we present numerical simulations of the response of a \cite{Parker72} corona to photospheric driving motions that have varying degrees of helicity preference. We obtain four main conclusions: 1) in agreement with the helicity condensation model of \cite{Antiochos13}, the inverse cascade of helicity by magnetic reconnection results in the formation of prominences/filaments localized about polarity inversion lines (PILs); 2) this same process removes most structure from the rest of the corona, resulting in smooth and laminar coronal loops; 3) the amount of remnant tangling in coronal loops is inversely dependent on the net helicity injected by the driving motions; and 4) the structure of the solar corona depends only on the helicity preference of the driving motions and not on their detailed time dependence. We discuss the implications of our results for high-resolution observations of the corona.

## **Detection of new emerging magnetic flux from the topology of SOHO/MDI magnetograms<<<**

I. S. **Knязева**, N. G. Makarenko & M. A. Livshits

Astronomy Reports, Volume 55, Number 5, 463-471, 2011

A topological method for detecting the new emergence of magnetic flux using SOHO/MDI magnetograms of the full solar disk is proposed. This method uses the number of pixels in the image that can be distinguished from a specified value to within a predetermined threshold (the number of disconnected components). We study more than ten very powerful active regions (ARs) with very high flare activity and show that the number of disconnected components increases directly before the development of a series of M and X flares, or accompanies this process. This behaviour is evident not only when there is an explicit emergence of a new flux and a series of fast flares, such as in AR 9236 (November 2000), but also in groups with many non-stationary processes developing along a neutral line of the large-scale magnetic field. We also discuss the possibility of using the obtained results for flare prediction.

## **Fine Structures of the Inner Solar Corona and the Associated Magnetic Topology**

Yuan-Kuen **Ko**<sup>1</sup>, Guillermo Stenborg<sup>2,3</sup>, Jon Linker<sup>4</sup>, Micah J. Weberg<sup>5,6</sup>, Roberto Lionello<sup>4</sup>, and Viacheslav Titov<sup>4</sup>

2022 ApJ 933 95

<https://iopscience.iop.org/article/10.3847/1538-4357/ac722c/pdf>

We present the fine structure of the inner solar corona between 1.65 and 3.0 solar radii as revealed by the STEREO-A COR1 white-light coronagraph from **2008 June 20 to July 31**. The COR1 imaging data were wavelet processed to enhance the intensity contrast of coronal features. The constructed limb synoptic maps at a range of altitudes show the evolution in time and altitude of these fine structures within the streamer belt, and equatorial and polar coronal holes during this period near the solar minimum. Distinct streamer-stalk structures are seen embedded within a diffuse background of the helmet streamer belt, which are preserved as they extend to higher heights. Pseudostreamers are also seen as multiple stalk structures, which also continue to higher heights. Various polar plume structures are seen to last from hours to days. Similar plume structures are also seen within the corona subtended by equatorial coronal holes. We compare the COR1 maps to that of the magnetic topology revealed by the modeled squashing factors, and discuss the relation between the two types of maps and its implications in the context of solar wind formation. **2008-06-25**

## **Waves and Magnetism in the Solar Atmosphere (WAMIS)**

Yuan-Kuen **Ko**<sup>1\*</sup>, John D. Moses<sup>2</sup>, John M. Laming<sup>1</sup>, Samuel Tun Beltran<sup>1</sup>, Steven Tomczyk<sup>3</sup>, et al.

Front. Astron. Space Sci., 16 February 2016

[sci-hub.se/10.3389/fspas.2016.00001](http://sci-hub.se/10.3389/fspas.2016.00001)

Comprehensive measurements of magnetic fields in the solar corona have a long history as an important scientific goal. Besides being crucial to understanding coronal structures and the Sun's generation of space weather, direct measurements of their strength and direction are also crucial steps in understanding observed wave motions. In this regard, the remote sensing instrumentation used to make coronal magnetic field measurements is well suited to measuring the Doppler signature of waves in the solar structures. In this paper, we describe the design and scientific values of the Waves and Magnetism in the Solar Atmosphere (WAMIS) investigation. WAMIS, taking advantage of greatly improved infrared filters and detectors, forward models, advanced diagnostic tools and inversion codes, is a long-duration high-altitude balloon payload designed to obtain a breakthrough in the measurement of coronal magnetic fields and in advancing the understanding of the interaction of these fields with space plasmas. It consists of a 20 cm aperture coronagraph with a visible-IR spectro-polarimeter focal plane assembly. The balloon altitude would provide minimum sky background and atmospheric scattering at the wavelengths in which these observations are made. It would also enable continuous measurements of the strength and direction of coronal magnetic fields without interruptions from the day–night cycle and weather. These measurements will be made over a large field-of-view allowing one to distinguish the magnetic signatures of different coronal structures, and at the spatial and temporal resolutions required to address outstanding problems in coronal physics. Additionally, WAMIS could obtain near simultaneous observations of the electron scattered K-corona for context and to obtain the electron density. These comprehensive observations are not provided by any current single ground-based or space observatory. The fundamental advancements achieved by the near-space observations of WAMIS on coronal field would point the way for future ground based and orbital instrumentation.

## **Oscillations Above Sunspots and Faculae: Height Stratification and Relation to Coronal Fan Structure**

N.I. **Kobanov**, D.Y. Kolobov, A.A. Chelpanov

2014

<http://arxiv.org/pdf/1411.6258v1.pdf>

Oscillation properties in two sunspots and two facular regions are studied using Solar Dynamics Observatory (SDO) data and ground-based observations in the SiI 10827 and HeI 10830 lines. The aim is to study different-frequency spatial distribution characteristics above sunspots and faculae and their dependence on magnetic-field features and to detect the oscillations that reach the corona from the deep photosphere most effectively. We used Fast-Fourier-Transform and frequency filtration of the intensity and Doppler-velocity variations with Morlet wavelet to trace the wave propagating from the photosphere to the chromosphere and corona. Spatial distribution of low-frequency (1-2 mHz) oscillations outlines well the fan-loop structures in the corona (the Fe IX 171 line) above sunspots and faculae. High-frequency oscillations (5-7 mHz) are concentrated in fragments inside the photospheric umbra boundaries and close to facular-region centers. This implies that the upper parts of most coronal loops, which transfer low-frequency oscillations from the photosphere, sit in the Fe IX 171 line-formation layer. We used dominant frequency vs. distance from barycenter relations to estimate magnetic-tube inclination angle in the higher layers, which poses difficulties for direct magnetic-field measurements. According to our calculations, this angle is about 40 degrees in the transition region around umbra borders. Phase velocities measured in the coronal loops' upper parts in the Fe IX 171 line-formation layer reach 100-150 km/s for sunspots and 50-100 km/s for faculae. Active regions NOAA [11311](#) and [11479](#)

## **The High-Resolution Coronal Imager (Hi-C)**

Ken **Kobayashi**, Jonathan Cirtain, Amy R. Winebarger, Kelly Korreck, Leon Golub, Robert W. Walsh, Bart De Pontieu, Craig DeForest, Alan Title, Sergey Kuzin, ... show all 24

Solar Phys., Volume 289, Issue 11, pp 4393-4412, 2014

The High-Resolution Coronal Imager (Hi-C) was flown on a NASA sounding rocket on **11 July 2012**. The goal of the Hi-C mission was to obtain high-resolution ( $\approx 0.3 - 0.4''$ ), high-cadence ( $\approx 5$  seconds) images of a solar active region to investigate the dynamics of solar coronal structures at small spatial scales. The instrument consists of a normal-incidence telescope with the optics coated with multilayers to reflect a narrow wavelength range around 19.3 nm (including the Fe xii 19.5-nm spectral line) and a 4096×4096 camera with a plate scale of 0.1'' pixel<sup>-1</sup>. The target of the Hi-C rocket flight was Active Region 11520. Hi-C obtained 37 full-frame images and 86 partial-frame images during the rocket flight. Analysis of the Hi-C data indicates the corona is structured on scales smaller than currently resolved by existing satellite missions.

## **Peculiarity of the oscillation stratification in sunspot penumbrae**

D.Y. **Kolobov**, A.A. Chelpanov, N.I. Kobanov

*Solar Physics* November **2016**, Volume 291, [Issue 11](#), pp 3339–3347

<http://arxiv.org/pdf/1607.06175v1.pdf>

Spatial distributions of the dominant oscillation frequency obtained for four sunspots show a feature shared by all the analysed levels of the solar atmosphere in these sunspots. This feature located in the inner penumbrae indicates that this region has favourable conditions for 2.5–4 mHz oscillation propagation. This agrees with the fact that the spectral composition of the oscillations at three atmospheric heights (Fe I 6173{\AA}, 1700{\AA}, and He II 304{\AA}) in this region are similar. There have been previous evidence of particular similarities along height of photospheric magnetic field strength, line-of-sight velocity, and temperature profile in the inner penumbra, where the internal boundary of the Evershed flow is located. The finding of the same dominant oscillation frequency at a range of altitudes from the chromosphere up to the transition region extends the height range, suggesting similarities in physical conditions. **6 Oct 2011, 16 May 2012, 6 Apr 2013, 27 Aug 2014**

## **Hemispheric Distribution of Subsurface Kinetic Helicity and Its Variation with Magnetic Activity**

R. **Komm**, S. Gosain, A. A. Pevtsov

*Solar Phys.*, July **2014**, Volume 289, Issue 7, pp 2399–2418

We study the hemispheric distribution of the kinetic helicity of subsurface flows in the near-surface layers of the solar convection zone and its variation with magnetic activity. We determine subsurface flows with a ring-diagram analysis applied to Global Oscillation Network Group (GONG) Dopplergrams and Dynamics Program data from the Michelson Doppler Imager (MDI) instrument onboard the Solar and Heliospheric Observatory (SOHO). We determine the average kinetic helicity density as a function of Carrington rotation and latitude. The average kinetic helicity density at all depths and the kinetic helicity, integrated over 2–7 Mm, follow the same hemispheric rule as the current/magnetic helicity proxies with predominantly positive values in the southern and negative ones in the northern hemisphere. This holds true for all levels of magnetic activity from quiet to active regions. However, this is a statistical result; only about 55 % of all locations follow the hemispheric rule. But these locations have larger helicity values than those that do not follow the rule. The average values of helicity density increase with depth for all levels of activity, which might reflect an increase of the characteristic size of convective motions with greater depth. The average helicity of subsets of high magnetic activity is about five times larger than that of subsets of low activity. The solar-cycle variation of helicity is thus mainly due to the presence or absence of active regions. During the rising phase of cycle 24, locations of high magnetic activity at low latitudes show a weaker hemispheric behavior compared to the rising phase of cycle 23.

## **Observational Evidence of Interchange Reconnection between a Solar Coronal Hole and a Small Emerging Active Region**

D. F. **Kong**<sup>1</sup>, G. M. Pan<sup>2</sup>, X. L. Yan<sup>1,3</sup>, J. C. Wang<sup>1,3</sup>, and Q. L. Li

**2018** *ApJL* 863 L22

<http://sci-hub.tw/http://iopscience.iop.org/article/10.3847/2041-8213/aad777/meta>

In this Letter, we present a case study of interchange reconnection between a coronal hole (CH) and a small emerging active region. The small active region emerges at the edge of the CH. Following the emergence of the small active region, the expansion of the arcade loops connecting the negative and the positive polarities of the active region can be clearly seen in 211 and 171 Å observations. During the emergence, the active region develops loop connections to the boundary of the CH, leading to its retreat. The latter has fast and slow phases at speeds of about 2.3 km s<sup>-1</sup> and 0.4 km s<sup>-1</sup>, respectively. By the end, these newly formed closed loops occupy most of the pre-emergence CH. From the line-of-sight magnetograms observed by Solar Dynamics Observatory/Heliioseismic and Magnetic Imager, the magnetic polarity in the CH is mainly positive and the leading sunspot of the active region has negative polarity. It is consistent with the condition of interchange reconnection. Moreover, the potential field source surface model is used to extrapolate the coronal magnetic fields. From a sequence of extrapolation potential fields, it is clear that the open fields in the CH close down, and the closed field at the east of the active region becomes an open field. These observations and the extrapolations of the potential fields suggest that interchange reconnection occurs between the CH and the small emerging active region and is driven by the flux emergence process. **2016 December 17**

## **Measurements of Coronal Faraday Rotation at 4.6 R ☉**

Jason E. **Kooi**, Patrick D. Fischer, Jacob J. Buffo, and Steven R. Spangler

**2014** *ApJ* 784 68

Many competing models for the coronal heating and acceleration mechanisms of the high-speed solar wind depend on the solar magnetic field and plasma structure in the corona within heliocentric distances of 5 R ☉. We report on sensitive Very Large Array (VLA) full-polarization observations made in 2011 August, at 5.0 and 6.1 GHz (each

with a bandwidth of 128 MHz) of the radio galaxy 3C 228 through the solar corona at heliocentric distances of 4.6–5.0  $R_{\odot}$ . Observations at 5.0 GHz permit measurements deeper in the corona than previous VLA observations at 1.4 and 1.7 GHz. These Faraday rotation observations provide unique information on the magnetic field in this region of the corona. The measured Faraday rotation on this day was lower than our a priori expectations, but we have successfully modeled the measurement in terms of observed properties of the corona on the day of observation. Our data on 3C 228 provide two lines of sight (separated by 46", 33,000 km in the corona). We detected three periods during which there appeared to be a difference in the Faraday rotation measure between these two closely spaced lines of sight. These measurements (termed differential Faraday rotation) yield an estimate of 2.6–4.1 GA for coronal currents. Our data also allow us to impose upper limits on rotation measure fluctuations caused by coronal waves; the observed upper limits were 3.3 and 6.4  $\text{rad m}^{-2}$  along the two lines of sight. The implications of these results for Joule heating and wave heating are briefly discussed.

## **First Insights into the Applicability and Importance of Different 3D Magnetic Field Extrapolation Approaches for Studying the Preeruptive Conditions of Solar Active Regions**

Marianna B. **Korsós**<sup>1,2,3</sup>, Robert Jarolim<sup>4</sup>, Robertus Erdélyi<sup>2,3,5</sup>, Astrid M. Veronig<sup>4,6</sup>, Huw Morgan<sup>7</sup>, and Francesca Zuccarello<sup>1,8</sup>

2024 ApJ 962 171

<https://iopscience.iop.org/article/10.3847/1538-4357/ad18bd/pdf>

The three-dimensional (3D) coronal magnetic field has not yet been directly observed. However, for a better understanding and prediction of magnetically driven solar eruptions, 3D models of solar active regions are required. This work aims to provide insight into the significance of different extrapolation models for analyzing the preeruptive conditions of active regions with morphological parameters in 3D. Here, we employed potential field (PF), linear force-free field (LFFF), and nonlinear force-free field (NLFFF) models and a neural network-based method integrating observational data and NLFFF physics (NF2). The 3D coronal magnetic field structure of a "flaring" (AR11166) and "flare-quiet" (AR12645) active region, in terms of their flare productivity, is constructed via the four extrapolation methods. To analyze the evolution of the field, six prediction parameters were employed throughout, from the photosphere up to the base of the lower corona. First, we find that the evolution of the adopted morphological parameters exhibits similarity across the investigated time period when considering the four types of extrapolations. Second, all the parameters exhibited preeruptive conditions not only at the photosphere but also at higher altitudes in the case of active region (AR) 11166, while three out of the six proxies also exhibited preeruptive conditions in the case of AR12645. We conclude that: (i) the combined application of several different precursor parameters is important in the lower solar atmosphere to improve eruption predictions, and (ii) to gain a quick yet reliable insight into the preflare evolution of active regions in 3D, the PF and LFFF are acceptable; however, the NF2 method is likely the more suitable option. **2011/03/02-14, 2011-03-09, 2017/03/28-04/07, 2017-04-02**

## **Revisiting the coronal current sheet model: Parameter range analysis and comparison with the potential field model**

Jennimari **Koskela**, Ilpo Virtanen and Kalevi Mursula

A&A 631, A17 (2019)

<https://doi.org/10.1051/0004-6361/201935967>

**Aims.** We study the properties of the coronal magnetic field according to the current sheet source surface (CSSS) model in 1976–2017 for all physically reasonable values of the three model parameters (cusp surface radius  $R_{cs}$ , source surface radius  $R_{ss}$ , and current parameter  $a$ ), and compare the CSSS field with the potential field source surface (PFSS) model field.

**Methods.** We used the synoptic maps of the photospheric magnetic field from the Wilcox Solar Observatory (WSO), National Solar Observatory/Kitt Peak (NSO/KP), and the NSO Synoptic Optical Long-term Investigations of the Sun Vector Spectromagnetograph (SOLIS/VSM) in order to calculate the coronal magnetic field according to the CSSS and PFSS models. We calculated the coronal field strength, its latitudinal variation and neutral line location, as well as its polarity match with the heliospheric magnetic field.

**Results.** The CSSS model can correct the erroneous latitudinal variation of the PFSS model if the source surface is sufficiently far out with respect to the cusp surface ( $R_{ss} \geq 3 \cdot R_{cs}$ ). The topology of the neutral line only slightly depends on source surface radius or current parameter, but excludes very low values of the cusp surface ( $R_{cs} \leq 1.5$ ). A comparison of the polarities gives an optimum cusp surface radius that varies in time between 2 and 5; a stronger current yields a larger optimum  $R_{cs}$ . Interestingly, the optimum polarity match percentages and optimum radii vary very similarly in the two models over the four solar cycles we studied.

**Conclusions.** The CSSS model can produce a stronger total coronal flux than the PFSS model and correct its latitudinal variation. However, the topology of the CSSS model is rather independent of horizontal currents and remains very similar to that of the PFSS model. Therefore, the CSSS model cannot improve the match of field polarities between corona and heliosphere.



## COMPARING CORONAL AND HELIOSPHERIC MAGNETIC FIELDS OVER SEVERAL SOLAR CYCLES

J. S. [Koskela](#)<sup>1</sup>, I. I. Virtanen<sup>1</sup>, and K. Mursula<sup>1</sup>

2017 ApJ 835 63

DOI 10.3847/1538-4357/835/1/63

Here we use the PFSS model and photospheric data from Wilcox Solar Observatory, SOHO/MDI, SDO/HMI, and SOLIS to compare the coronal field with heliospheric magnetic field measured at 1 au, compiled in the NASA/NSSDC OMNI 2 data set. We calculate their mutual polarity match and the power of the radial decay,  $p$ , of the radial field using different source surface distances and different number of harmonic multipoles. We find the average polarity match of 82% for the declining phase, 78%–79% for maxima, 76%–78% for the ascending phase, and 74%–76% for minima. On an average, the source surface of 3.25 R<sub>S</sub> gives the best polarity match. We also find strong evidence for solar cycle variation of the optimal source surface distance, with highest values (3.3 R<sub>S</sub>) during solar minima and lowest values (2.6 R<sub>S</sub>–2.7 R<sub>S</sub>) during the other three solar cycle phases. Raising the number of harmonic terms beyond 2 rarely improves the polarity match, showing that the structure of the HMF at 1 au is most of the time rather simple. All four data sets yield fairly similar polarity matches. Thus, polarity comparison is not affected by photospheric field scaling, unlike comparisons of the field intensity.

## A New Global Nonlinear Force-Free Coronal Magnetic-Field Extrapolation Code Implemented on a Yin–Yang Grid

Argyrios [Koumtzis](#) & [Thomas Wiegelmann](#)

[Solar Physics](#) volume 298, Article number: 20 (2023)

<https://link.springer.com/content/pdf/10.1007/s11207-023-02109-6.pdf>

The solar magnetic field dominates and structures the solar coronal plasma. Detailed insights into the coronal magnetic field are important to understand most physical phenomena there. While direct, routine measurements of the coronal magnetic field are not available, field extrapolation of the photospheric vector-field measurements into the corona is the only way to study the structure and dynamics of the coronal field. Here we focus on global coronal structures traditionally modeled using spherical grids and synoptic vector magnetograms as boundary conditions. We developed a new code that performs nonlinear force-free magnetic-field extrapolations in spherical geometry. Our new implementation is based on a well-established optimization principle on a Cartesian grid and a single spherical finite-difference grid. In the present work, for the first time, the algorithm is able to reconstruct the magnetic field in the entire corona, including the polar regions. The finite-difference numerical scheme that was employed in previous spherical-code versions suffered from numerical inefficiencies because of the convergence of those grids on the poles. In our new code, we implement the so-called Yin–Yang overhead grid, the structure of which addresses this difficulty. Consequently, both the speed and accuracy of the optimization algorithm are improved compared to the previous implementations. We tested our new code using the well known semi-analytical model (Low and Lou solution). This is a commonly used benchmark for nonlinear force-free extrapolation codes.

## New deep coronal spectra from the 2017 total solar eclipse

S. [Koutchmy](#), [F. Baudin](#), [Sh. Abdi](#), [L. Golub](#), [F. Sèvre](#)

A&A 632, A86 2019

<https://arxiv.org/pdf/1910.01372.pdf>

<https://www.aanda.org/articles/aa/pdf/2019/12/aa35681-19.pdf>

Total eclipses permit a deep analysis of both the inner and the outer parts of the corona using the continuum White-Light (W-L) radiations from electrons (K-corona), the superposed spectrum of forbidden emission lines from ions (E-corona) and the dust component with F-lines (F-corona). By sufficiently dispersing the W-L spectrum, the Fraunhofer (F) spectrum of the dust component of the corona appears and the continuum Thomson radiation can be evaluated. The superposed emission lines of ions with different degrees of ionization are studied to allow the measurement of temperatures, non-thermal velocities, Doppler shifts and abundances. We describe a slit spectroscopic experiment of high spectral resolution for providing an analysis of the most typical parts of the quasi-minimum type corona observed during the total solar eclipse of **Aug. 21, 2017** observed from Idaho, USA. Streamers, active region enhancements and polar coronal holes (CHs) are well measured using deep spectra. 60 spectra are obtained during the totality with a long slit, covering  $\pm 3$  solar radii in the range of 510 to 590nm. The K+F continuum corona is well exposed up to 2 solar radius. The F-corona can be measured even at the solar limb. New weak emission lines were discovered or confirmed. The rarely observed high FIP ArX line is recorded almost everywhere; the FeXIV and NiXIII lines are well recorded everywhere. For the first time hot lines are also measured inside the CH regions. The radial variations of the non-thermal turbulent velocities of the lines do not show a great departure from the average values. No significantly large Doppler shifts are seen anywhere in the inner and the middle corona. The wings of the FeXIV line show some non-Gaussianity.

## Justification of the use of Stokes-V Cryo-NIRSP/DKIST observations for the 3D Reconstruction of the Coronal Magnetic Field

[Maxim Kramar](#), [Haosheng Lin](#)

2022

<https://arxiv.org/pdf/2208.03840.pdf>

This study presents a justification of the use of Stokes-V Cryo-NIRSP/DKIST observations for the 3D Reconstruction of the Coronal Magnetic Field. A magnetohydrodynamic (MHD) model of the solar corona during solar minimum generated by Predictive Science Inc. was used to synthesize spectropolarimetric measurements of the Fe XIII 1075 nm coronal emission line as observed from the Earth. Stokes-Q,U data is "taken" for half a solar rotation period (about two weeks) by Upgraded Coronal Multichannel Polarimeter (UCoMP) with field of view (FOV) up to  $2 R_{\odot}$ . Stokes-V data is "taken" once a day for two days by Cryo-NIRSP/DKIST with a total FOV equal to the two Cryo-NIRSP FOVs. We demonstrated that even this amount Stokes-V observations with Cryo-NIRSP FOV coverage can remarkably improve the 3D coronal magnetic field reconstruction over an active region compared with tomography reconstruction based only on UCoMP linear polarization data.

### 3D Global Coronal Density Structure and Associated Magnetic Field near Solar Maximum

Maxim [Kramar](#), Vladimir Airapetian, Haosheng Lin

*Front. Astron. Space Sci.* 3:25 2016

<http://arxiv.org/pdf/1604.00535v1.pdf>

<https://doi.org/10.3389/fspas.2016.00025>

Measurement of the coronal magnetic field is a crucial ingredient in understanding the nature of solar coronal dynamic phenomena at all scales. We employ STEREO/COR1 data obtained near maximum of solar activity in December 2012 (Carrington rotation, CR 2131) to retrieve and analyze the three-dimensional (3D) coronal electron density in the range of heights from  $1.5$  to  $4 R_{\odot}$  using a tomography method and qualitatively deduce structures of the coronal magnetic field. The 3D electron density analysis is complemented by the 3D STEREO/EUVI emissivity in 195 Å band obtained by tomography for the same CR period. We find that the magnetic field configuration during CR 2131 has a tendency to become radially open at heliocentric distances below  $\sim 2.5 R_{\odot}$ . We compared the reconstructed 3D coronal structures over the CR near the solar maximum to the one at deep solar minimum. Results of our 3D density reconstruction will help to constrain solar coronal field models and test the accuracy of the magnetic field approximations for coronal modeling.

substantial text overlap with arXiv:1405.0951

### Direct Observation of Coronal Magnetic Fields by Vector Tomography of the Coronal Emission Line Polarizations

M. [Kramar](#), H. Lin, S. Tomczyk

2016 *ApJ* 819 L36

<http://arxiv.org/pdf/1502.07200v1.pdf>

This article presents the first direct "observation" of the global-scale, 3D coronal magnetic fields of Carrington Rotation (CR) Cycle 2112 using vector tomographic inversion techniques. The Vector tomographic inversion uses observational measurements of the Fe  $\{\text{sc}\{\text{xiii}\}\}$  10747 Å Hanle effect polarization signals by the Coronal Multichannel Polarimeter (CoMP) and coronal density and temperature structures derived from scalar tomographic inversion of STEREO/EUVI coronal emission lines (CELs) intensity images as inputs to derive a coronal magnetic field model that best reproduces the observed polarization signals. While independent verifications of the vector tomography results cannot be performed, we compared the tomography inverted coronal magnetic fields with those constructed by MagnetoHydroDynamic (MHD) simulation based on observed photospheric magnetic fields of CR 2112 and 2113. We found that the MHD model for CR 2112 is qualitatively consistent with the tomography inverted result for most of the reconstruction domain except for a couple of regions. Particularly for one of the most noticeable exception region, we found that the MHD simulation for CR 2113 predicted a model that more closely resemble the vector tomography inverted magnetic fields. We discuss the utilities and limitations of the tomographic inversion technique, and present ideas for future developments.

### 3D Coronal Density Reconstruction and Retrieving the Magnetic Field Structure during Solar Minimum

M. [Kramar](#), V. Airapetian, Z. Mikić, J. Davila

E-print, May 2014; *Solar Phys.*, Volume 289, Issue 8, pp 2927-2944, 2014

<http://arxiv.org/pdf/1405.0951v1.pdf>

Measurement of the coronal magnetic field is a crucial ingredient in understanding the nature of solar coronal phenomena at all scales. We employed STEREO/COR1 data obtained during a deep minimum of solar activity in February 2008 (Carrington Rotation CR 2066) to retrieve and analyze the three-dimensional (3D) coronal electron

density in the range of heights from  $1.5$  to  $4 R_{\odot}$  using a tomography method. With this, we qualitatively deduced structures of the coronal magnetic field. The 3D electron-density analysis is complemented by the 3D STEREO/EUVI emissivity in the  $195 \text{ \AA}$  band obtained by tomography for the same CR. A global 3D MHD model of the solar corona was used to relate the reconstructed 3D density and emissivity to open/closed magnetic-field structures. We show that the density-maximum locations can serve as an indicator of current-sheet position, while the locations of the density-gradient maximum can be a reliable indicator of coronal-hole boundaries. We find that the magnetic-field configuration during CR 2066 has a tendency to become radially open at heliocentric distances greater than  $2.5 R_{\odot}$ . We also find that the potential-field model with a fixed source surface is inconsistent with the boundaries between the regions with open and closed magnetic-field structures. This indicates that the assumption of the potential nature of the coronal global magnetic field is not satisfied even during the deep solar minimum. Results of our 3D density reconstruction will help to constrain solar coronal-field models and test the accuracy of the magnetic-field approximations for coronal modeling.

## **VECTOR TOMOGRAPHY FOR THE CORONAL MAGNETIC FIELD. II. HANLE EFFECT MEASUREMENTS**

M. [Kramar](#)<sup>1,2</sup>, B. Inhester<sup>3</sup>, H. Lin<sup>4</sup>, and J. Davila

2013 ApJ 775 25

In this paper, we investigate the feasibility of saturated coronal Hanle effect vector tomography or the application of vector tomographic inversion techniques to reconstruct the three-dimensional magnetic field configuration of the solar corona using linear polarization measurements of coronal emission lines. We applied Hanle effect vector tomographic inversion to artificial data produced from analytical coronal magnetic field models with equatorial and meridional currents and global coronal magnetic field models constructed by extrapolation of real photospheric magnetic field measurements. We tested tomographic inversion with only Stokes Q, U, electron density, and temperature inputs to simulate observations over large limb distances where the Stokes I parameters are difficult to obtain with ground-based coronagraphs. We synthesized the coronal linear polarization maps by inputting realistic noise appropriate for ground-based observations over a period of two weeks into the inversion algorithm. We found that our Hanle effect vector tomographic inversion can partially recover the coronal field with a poloidal field configuration, but that it is insensitive to a corona with a toroidal field. This result demonstrates that Hanle effect vector tomography is an effective tool for studying the solar corona and that it is complementary to Zeeman effect vector tomography for the reconstruction of the coronal magnetic field.

## **On the Tomographic Reconstruction of the 3D Electron Density for the Solar Corona from STEREO COR1 Data**

M. [Kramar](#) · S. Jones · J. Davila · B. Inhester · M. Mierla

Solar Phys (2009) 259: 109–121

We present for the first time a three-dimensional reconstruction of the electron

density in the corona at distances from  $1.5R_{\odot}$  to  $4R_{\odot}$  using COR1 STEREO observations.

The reconstruction is performed using a regularized tomography inversion method for two biweekly periods corresponding to Carrington Rotations 2058 and 2066. Images from the two STEREO spacecraft are used to compare the reconstructed density structures with coronal features located by triangulation. We find that the location of a bright tip of a helmet streamer obtained from the tomographic reconstruction is in good agreement with the location obtained by triangulation. The reconstructed density structure of the equatorial streamer belt is largely consistent with the variation of the current sheet derived from a potential magnetic field extrapolation for most of the equatorial region and for an MHD model of the corona. A zero-value density region in the reconstruction is identified with a low-density region seen in an EUVI image below the reconstruction domain.

## **Inversion of coronal Zeeman and Hanle Observations to reconstruct the coronal magnetic field -- M. [Kramar](#) and B. Inhester, E-print, Dec 2006**

## **Modelling the evolution of the Sun's open and total magnetic flux**

[N. A. Krivova](#), [S. K. Solanki](#), [B. Hofer](#), [C.-J. Wu](#), [I. G. Usoskin](#), [R. Cameron](#)

A&A 2021

<https://arxiv.org/pdf/2103.15603.pdf>

Solar activity in all its varied manifestations is driven by the magnetic field. Particularly important for many purposes are two global quantities, the Sun's total and open magnetic flux, which can be computed from sunspot number records using models. Such sunspot-driven models, however, do not take into account the presence of magnetic flux during grand minima, such as the Maunder minimum. Here we present a major update of a widely used simple model, which now takes into account the observation that the distribution of all magnetic features on the Sun follows a single power law. The exponent of the power law changes over the solar cycle. This allows for the emergence of small-scale magnetic flux even when no sunspots are present for multiple decades and leads to non-zero total and open magnetic flux also in the deepest grand minima, such as the Maunder minimum, thus overcoming a major shortcoming of the earlier models. The results of the updated model compare well with the available observations and reconstructions of the solar total and open magnetic flux. This opens up the possibility of improved reconstructions of sunspot number from time series of cosmogenic isotope production rate.

### **Evaluation of a potential field source surface model with elliptical source surfaces via ballistic back mapping of in situ spacecraft data**

M. [Kruse](#), V. Heidrich-Meisner and R. F. Wimmer-Schweingruber

A&A 645, A83 (2021)

<https://www.aanda.org/articles/aa/pdf/2021/01/aa39120-20.pdf>

<https://doi.org/10.1051/0004-6361/202039120>

**Context.** The potential field source surface (PFSS) model is an important tool that helps link the solar coronal magnetic field to the solar wind. Due to its simplicity, it allows for predictions to be computed rapidly and requires little input data, though at the cost of reduced accuracy compared to more complex models. So far, PFSS models have almost exclusively been computed for a spherical outer boundary or “source surface”. Changing this to an elliptical source surface holds promise to increase its prediction accuracy without the necessity of incorporating complex computations or additional model assumptions.

**Aims.** The main goal of this work is to evaluate the merit of adding another parameter, namely the ellipticity of the source surface, to the PFSS model. In addition, the applicability of the PFSS model during different periods of the solar activity cycle as well as the impact of the source surface radius are analyzed.

**Methods.** To evaluate the model, in situ spacecraft data are mapped back to the source surface via a ballistic approach. The in situ magnetic field polarity is compared to the magnetic field polarity predicted by the model at the source surface. This method is based on the assumption that better performing models provide better agreements between the prediction and the measured magnetic field polarity. We employ data from the Advanced Composition Explorer and the twin Solar Terrestrial Relations Observatory (STEREO) for this analysis.

**Results.** We show that the PFSS model performs slightly better with oblate elliptical source surfaces elongated along the solar equatorial plane, although the best found ellipticity varies for different spacecraft and periods. In addition, it is demonstrated that the performance of the presented analysis degrades during the active times of the solar activity cycle.

### **An elliptic expansion of the potential field source surface model**

[Martin Kruse](#), [Verena Heidrich-Meisner](#), [R.F. Wimmer-Schweingruber](#), [Michael Hauptmann](#)

A&A 638, A109 2020

<https://arxiv.org/pdf/2005.12843.pdf>

<https://www.aanda.org/articles/aa/pdf/2020/06/aa37734-20.pdf>

**Context.** The potential field source surface model is frequently used as a basis for further scientific investigations where a comprehensive coronal magnetic field is of importance. Its parameters, especially the position and shape of the source surface, are crucial for the interpretation of the state of the interplanetary medium. Improvements have been suggested that introduce one or more additional free parameters to the model, for example, the current sheet source surface (CSSS) model.

**Aims.** Relaxing the spherical constraint of the source surface and allowing it to be elliptical gives modelers the option of deforming it to more accurately match the physical environment of the specific period or location to be analyzed.

**Methods.** A numerical solver is presented that solves Laplace's equation on a three-dimensional grid using finite differences. The solver is capable of working on structured spherical grids that can be deformed to create elliptical source surfaces.

**Results.** The configurations of the coronal magnetic field are presented using this new solver. Three-dimensional renderings are complemented by Carrington-like synoptic maps of the magnetic configuration at different heights in the solar corona. Differences in the magnetic configuration computed by the spherical and elliptical models are illustrated.

### **Unresolved Mixed Polarity Magnetic Fields at Flux Cancellation Site in Solar Photosphere at 0".3 Spatial Resolution**

Masahito [Kubo](#), Boon Chye Low, Bruce W. Lites

ApJL, 793 L9 2014

<http://arxiv.org/pdf/1408.5796v1.pdf>

This is a follow-up investigation of a magnetic-flux cancellation event at a polarity inversion line (PIL) on the Sun observed with the spectropolarimeter on board Hinode. Anomalous circular polarization (Stokes V) profiles are observed in the photosphere along the PIL at the cancellation sites. Kubo et al. (2010) previously reported that the theoretically expected horizontal fields between the canceling opposite-polarity magnetic elements in this event are not detected at granular scales. We show that the observed anomalous Stokes V profiles are reproduced successfully by adding the nearly symmetric Stokes V profiles observed at pixels immediately adjacent to the PIL. This result suggests that these observed anomalous Stokes V profiles are not indications of a flux removal process, but are the result of either a mixture of unresolved, opposite-polarity magnetic elements or the unresolved width of the PIL, at an estimated resolution element of about  $0''.3$ . The hitherto undetected flux removal process accounting for the larger-scale disappearance of magnetic flux during the observing period is likely to also fall below resolution.

### Comparison of Two Methods for Deriving the Magnetic Field in a Filament Channel

T. A. [Kucera](#)<sup>1</sup>, M. Luna<sup>2</sup>, T. Török<sup>3</sup>, K. Muglach<sup>1,4</sup>, J. T. Karpen<sup>1</sup>, C. Downs<sup>3</sup>, X. Sun<sup>5</sup>, B. J. Thompson<sup>1</sup>, and H. R. Gilbert<sup>6</sup>

2022 ApJ 940 34

<https://iopscience.iop.org/article/10.3847/1538-4357/ac9377/pdf>

Understanding the magnetic structure of filament channels is difficult but essential for identifying the mechanism (s) responsible for solar eruptions. In this paper we characterize the magnetic field in a well-observed filament channel with two independent methods, prominence seismology and magnetohydrodynamics flux-rope modeling, and compare the results. In 2014 May and June, active region 12076 exhibited a complex of filaments undergoing repeated oscillations over the course of 12 days. We measure the oscillation periods in the region with both Global Oscillation Network Group H $\alpha$  and Solar Dynamics Observatory (SDO) Advanced Imaging Assembly EUV images, and then utilize the pendulum model of large-amplitude longitudinal oscillations to calculate the radius of curvature of the fields supporting the oscillating plasma from the derived periods. We also employ the regularized Biot–Savart laws formalism to construct a flux-rope model of the field of the central filament in the region based on an SDO Helioseismic and Magnetic Imager magnetogram. We compare the estimated radius of curvature, location, and angle of the magnetic field in the plane of the sky derived from the observed oscillations with the corresponding magnetic-field properties extracted from the flux-rope model. We find that the two models are broadly consistent, but detailed comparisons of the model and specific oscillations often differ. Model observation comparisons such as these are important for advancing our understanding of the structure of filament channels. **26 May–1 Jun 2014**

### Magnetohydrodynamics evolution of three-dimensional magnetic null in NOAA active region 11515 initiated using non-force-free field extrapolation

Sanjay [Kumar](#), Avijeet Prasad, Ranadeep Sarkar, and Ramit Bhattacharyya

Front. Astron. Space Sci. 9:1039061. 2022

<https://arxiv.org/pdf/2210.03957.pdf>

doi: 10.3389/fspas.2022.1039061

<https://www.frontiersin.org/articles/10.3389/fspas.2022.1039061/pdf>

Magnetohydrodynamics simulation of active region NOAA 11515 is performed to examine the initiation of the M5.6 flaring event that starts around 10:43 UT on **2 July 2012**. The simulation is conducted using an extrapolated non-force-free magnetic field generated from the photospheric vector magnetogram of the active region as the initial magnetic field. The magnetic field shows the presence of a three-dimensional (3D) magnetic null with the corresponding dome overlying a filament and a low-lying magnetic flux rope, observed in 304 Å and 131 Å respectively. The simulated dynamics, triggered by the initial Lorentz force, lead to the bifurcations of the flux rope, which is similar to the observed bifurcation in the 131 Å brightenings. Additionally, the rope exhibits a rise and reconnects at the 3D null. These reconnections convert field lines of the rope into the anchored outer spine of the 3D null—explaining the occurrence of a nearby confined C-class flare. Further, the results show that the field lines of the flux rope reach the vicinity of the filament and become non-parallel to the field lines of the filament. This initiates the reconnections between the rope and the field lines of the filament—activating the filament for the eruption. This interesting interaction of the flux rope and filament seems to contribute to the onset of the M-class flare.

### Direct Estimates of the Solar Coronal Magnetic Field Using Contemporaneous Extreme-ultraviolet, Radio, and White-light Observations

Anshu [Kumari](#), [R. Ramesh](#), [C. Kathiravan](#), [T. J. Wang](#), [N. Gopalswamy](#)

ApJ 881 24 2019

<https://arxiv.org/pdf/1907.09721.pdf>  
[sci-hub.se/10.3847/1538-4357/ab2adf](https://sci-hub.se/10.3847/1538-4357/ab2adf)

We report a solar coronal split-band type II radio burst that was observed on **2016 March 16** with the Gauribidanur Radio Spectro-Polarimeter (GRASP) in the frequency range  $\approx 90$ – $50$  MHz, and the Gauribidanur Radioheliograph (GRAPH) at two discrete frequencies, viz. 80 MHz and 53.3 MHz. Observations around the same epoch in extreme-ultraviolet (EUV) and white-light show that the above burst was associated with a flux rope structure and a coronal mass ejection (CME), respectively. The combined height-time plot generated using EUV, radio, and whitelight data suggest that the different observed features (i.e. the flux rope, type II burst and the CME) are all closely associated. We constructed an empirical model for the coronal electron density distribution ( $N_e(r)$ , where  $r$  is the heliocentric distance) from the above set of observations themselves and used it to estimate the coronal magnetic field strength ( $B$ ) over the range of  $r$  values in which the respective events were observed. The  $B$  values are consistent with each other. They vary as  $B(r) = 2.61 \times r^{-2.21}$  (in units of G) in the range  $r \approx 1.1$ – $2.2 R_\odot$ . As far as we know, similar 'direct' estimates of  $B$  in the near-Sun corona without assuming a model for  $N_e(r)$ , and by combining co-temporal set of observations in two different regions (radio and whitelight) of the electromagnetic spectrum, have rarely been reported. Further, the present work is a novel attempt where the characteristics of a propagating EUV flux rope structure, considered to be the signature of a CME close the Sun, have been used to estimate  $B(r)$  in the corresponding distance range.

### **Addendum to: Strength of the Solar Coronal Magnetic Field – A Comparison of Independent Estimates Using Contemporaneous Radio and White-Light Observations**

Anshu [Kumari](#), R. Ramesh, C. Kathiravan, T. J. Wang

[Solar Physics](#) December 2017, 292:177

<https://link.springer.com/content/pdf/10.1007%2Fs11207-017-1203-3.pdf>

### **Strength of the Solar Coronal Magnetic Field – A Comparison of Independent Estimates Using Contemporaneous Radio and White-Light Observations**

Anshu [Kumari](#), R. Ramesh, C. Kathiravan, T. J. Wang

[Solar Physics](#) November 2017, 292:161

<https://arxiv.org/pdf/1711.02307.pdf>

We estimated the coronal magnetic field strength ( $B$ ) during the **23 July 2016** coronal mass ejection (CME) event using i) the flux rope structure of the CME in the white-light coronagraph images and ii) the band-splitting in the associated type II burst. No models were assumed for the coronal electron density ( $N_e(r)$ ) we used in the estimation. The results obtained with these two independent methods correspond to different heliocentric distances ( $r$ ) in the range  $\approx 2.5$ – $4.5 R_\odot$ , but they show excellent consistency and could be fit with a single power-law distribution of the type  $B(r) = 5.7 r^{-2.6}$  G, which is applicable in that distance range. The power-law index (i.e.  $-2.6$ ) is in good agreement with the results obtained in previous studies by different methods.

### **The rotation rate of solar active and ephemeral regions -- II. Temporal variations of the rotation rates**

[Alexander S. Kutsenko](#), [Valentina I. Abramenko](#), [Daria V. Litvishko](#)

MNRAS 2023

<https://arxiv.org/pdf/2212.14740.pdf>

Systematic studies of the rotation rate of sunspot groups using white-light images yield controversial results on the variations of the rotation rate: sunspot groups were found to either accelerate or decelerate systematically. This disagreement might be related to shortcomings of the method used to probe the rotation rate of sunspot groups. In contrast to previous works, in this study we use magnetic field maps to analyse the variations of the rotation rate of active regions. We found that an active region may exhibit either acceleration or deceleration during the emergence while the rotation rate remains almost unchanged during decay. Hence, we suppose that there is no systematic geometrical inclination to the radial direction of the apex of the subsurface magnetic flux loop forming an active region. A thorough comparison of the rotation rate of unipolar and bi/multipolar active regions revealed no significant changes in the rotation rate of decaying active regions. In contrast to previous works, we presume the rotation rate to keep constant (within the expected uncertainties) during the evolution of an active region after emergence.

### **The rotation rate of solar active and ephemeral regions -- I. Dependence on morphology and peak magnetic flux**

[Alexander S. Kutsenko](#)

MNRAS 2020

<https://arxiv.org/pdf/2011.12060.pdf>

DOI: [10.1093/mnras/staa3616](https://doi.org/10.1093/mnras/staa3616)

Using magnetic field maps acquired by the Helioseismic and Magnetic Imager on board the Solar Dynamics Observatory we measured rotation rates of 864 active and 322 ephemeral regions observed between 2010 and 2016. We found smaller magnetic tracers to show a tendency to rotate faster as compared to larger ones. Thus, ephemeral regions exhibit on average the fastest rotation rate. We further divided active regions into three classes. Class A comprised magnetic bipoles obeying Hale's polarity law, Joy's law, and exhibiting more coherent leading polarity in comparison with the following one. The second class B included active regions violating at least one of the aforementioned empirical laws. The third class U comprised unipolar active regions. We found no significant difference between the rotation rates of active regions of classes A and B. In contrast, unipolar active regions exhibited on average lower rotation rate and narrower distribution of the rotation rate differences. Assuming the rotation rate to indicate the anchoring depth of the magnetic structure within the convection zone, we supposed that active regions of classes A and B might be anchored throughout the entire convective envelope while unipolar active regions are rooted within a thin layer located either near the base of the convection zone or at a shallow near-surface depth. **2010 May 03-05**

### Extended statistical analysis of emerging solar active regions

Alexander S [Kutsenko](#) [Valentina I Abramenko](#) [Alexei A Pevtsov](#)  
MNRAS Volume 484, Issue 3, 11 April 2019, Pages 4393–4400,  
<http://sci-hub.tw/10.1093/mnras/stz308>

We use observations of line-of-sight magnetograms from Helioseismic and Magnetic Imager onboard of Solar Dynamics Observatory to investigate polarity separation, magnetic flux, flux emergence rate, twist and tilt of solar emerging active regions. Functional dependence of polarity separation and maximum magnetic flux of an active region is in agreement with a simple model of flux emergence as the result of buoyancy forces. Our investigation did not reveal any strong dependence of emergence rate on twist properties of active regions. **16-19 Jan 2015**

### Contribution to the Solar Mean Magnetic Field from Different Solar Regions

A.S. [Kutsenko](#), [V.I. Abramenko](#), [V.B. Yurchyshyn](#)  
Solar Phys. 292:121 **2017**  
<https://arxiv.org/pdf/1707.05971.pdf>

Seven-year long seeing-free observations of solar magnetic fields with the Helioseismic and Magnetic Imager (HMI) on board the Solar Dynamics Observatory (SDO) were used to study the sources of the solar mean magnetic field, SMMF, defined as the net line-of-sight magnetic flux divided over the solar disk area. To evaluate the contribution of different regions to the SMMF, we separated all the pixels of each SDO/HMI magnetogram into three subsets: weak (B\_W), intermediate (B\_I), and strong (B\_S) fields. The B\_W component represents areas with magnetic flux densities below the chosen threshold; the B\_I component is mainly represented by network fields, remains of decayed active regions (ARs), and ephemeral regions. The B\_S component consists of magnetic elements in ARs. To derive the contribution of a subset to the total SMMF, the linear regression coefficients between the corresponding component and the SMMF were calculated. We found that: i) when the threshold level of 30 Mx cm<sup>-2</sup> is applied, the B\_I and B\_S components together contribute from 65% to 95% of the SMMF, while the fraction of the occupied area varies in a range of 2-6% of the disk area; ii) as the threshold magnitude is lowered to 6 Mx cm<sup>-2</sup>, the contribution from B\_I+B\_S grows to 98%, and the fraction of the occupied area reaches the value of about 40% of the solar disk. In summary, we found that regardless of the threshold level, only a small part of the solar disk area contributes to the SMMF. This means that the photospheric magnetic structure is an intermittent, inherently porous medium, resembling a percolation cluster. These findings suggest that the long-standing concept that continuous vast unipolar areas on the solar surface are the source of the SMMF may need to be reconsidered.

### Using SDO/HMI magnetograms as a source of the solar mean magnetic field data

A.S. [Kutsenko](#), V.I. Abramenko  
Solar Phys. Volume 291, [Issue 6](#), pp 1613–1623 **2016**  
<http://arxiv.org/pdf/1606.03710v1.pdf>

The solar mean magnetic field (SMMF) provided by the Wilcox Solar Observatory (WSO) is compared with the SMMF acquired by the Helioseismic and Magnetic Imager (HMI) onboard the Solar Dynamic Observatory (SDO). We found that despite the different spectral lines and measurement techniques used in both instruments the Pearson correlation coefficient between these two datasets equals 0.86 while the conversion factor is very close to unity:  $B(\text{HMI}) = 0.99(2)B(\text{WSO})$ . We also discuss artifacts of the SDO/HMI magnetic field measurements, namely the 12 and 24-hour oscillations in SMMF and in sunspots magnetic fields that might be caused by orbital motions of the spacecraft. The artificial harmonics of SMMF reveal significant changes in amplitude and the nearly stable phase. The connection between the 24-hour harmonic amplitude of SMMF and the presence of sunspots is examined. We also found that opposite phase artificial 12 and/or 24-hour oscillations exist in sunspots of opposite polarities.

## **SPIRAL STRUCTURE OF SUNSPOT OSCILLATIONS AS A TRACER OF SOLAR HELICITY**

K. **Kuzanyan**, R. Sych, S. Yang, Y. Yan

ИКИ, 2014 Сессия: Солнце

<http://plasma2014.cosmos.ru/presentations>

## **COCONUT, a Novel Fast-converging MHD Model for Solar Corona Simulations.**

### **III. Impact of the Preprocessing of the Magnetic Map on the Modeling of the Solar Cycle Activity and Comparison with Observations**

Błażej **Kuźma**<sup>1</sup>, Michaela Brchnelova<sup>1</sup>, Barbara Perri<sup>1</sup>, Tinatin Baratashvili<sup>1</sup>, Fan Zhang<sup>1</sup>, Andrea Lani<sup>1</sup>, and Stefaan Poedts<sup>1,2</sup>

2023 ApJ 942 31

<https://iopscience.iop.org/article/10.3847/1538-4357/aca483/pdf>

We developed a novel global coronal COCONUT (Coolfluid Corona Unstructured) model based on the COOLFluiD code. The steady-state model is predetermined by magnetograms set as boundary conditions, while inside the numerical domain the corona is described by MHD equations. This set of equations is solved with the use of an implicit solver on unstructured grids. Here we present numerically obtained results for two extremes of the solar activity cycle represented by CR 2161 and CR 2219 for solar maximum and minimum, respectively. We discuss the impact of reconstruction level on representative solar corona solutions and thus also the impact of small magnetic structures on the overall structure of the solar wind. Moreover, both cases correspond to particular solar eclipses, namely those in **2015 March and 2019 July**, to allow us the direct comparison of simulations with observed coronal features. We use a validation scheme proposed by Wagner et al. (from less to more sophisticated methods, i.e., visual classification, feature matching, streamer direction and width, brute force matching, topology classification). The detailed comparison with observations reveals that our model recreates relevant features such as the position, direction, and shape of the streamers (by comparison with white-light images) and the coronal holes (by comparison with extreme ultraviolet images) for both cases of minimum and maximum solar activity. We conclude that an unprecedented combination of accuracy, computational speed and robustness even in the case of maximum activity is accomplished at this stage, with possible further improvements in a foreseeable perspective.

### **Numerical simulations of sheared magnetic lines at the solar null line★**

B. **Kuźma**<sup>1</sup>, K. Murawski<sup>1</sup> and A. Solov'ev<sup>2</sup>

A&A 577, A138 (2015)

**Aims.** We perform numerical simulations of sheared magnetic lines at the magnetic null line configuration of two magnetic arcades that are settled in a gravitationally stratified and magnetically confined solar corona.

**Methods.** We developed a general analytical model of a 2.5D solar atmospheric structure. As a particular application of this model, we adopted it for the curved magnetic field lines with an inverted Y shape that compose the null line above two magnetic arcades, which are embedded in the solar atmosphere that is specified by the realistic temperature distribution. The physical system is described by 2.5D magnetohydrodynamic equations that are numerically solved by the FLASH code.

**Results.** The magnetic field line shearing, implemented about 200 km below the transition region, results in Alfvén and magnetoacoustic waves that are able to penetrate solar coronal regions above the magnetic null line. As a result of the coupling of these waves, partial reflection from the transition region and scattering from inhomogeneous regions the Alfvén waves experience fast attenuation on time scales comparable to their wave periods, and the physical system relaxes in time. The attenuation time grows with the large amplitude and characteristic growing time of the shearing.

**Conclusions.** By having chosen a different magnetic flux function, the analytical model we devised can be adopted to derive equilibrium conditions for a diversity of 2.5D magnetic structures in the solar atmosphere.

## **Global Coronal Seismology in the Extended Solar Corona through Fast Magnetosonic Waves Observed by STEREO SECCHI COR1**

Ryun-Young **Kwon**<sup>1,2,3</sup>, Maxim Kramar<sup>1,2</sup>, Tongjiang Wang<sup>1,2</sup>, Leon Ofman<sup>1,2,4</sup>, Joseph M. Davila<sup>2</sup>, Jongchul Chae<sup>5</sup>, and Jie Zhang

2013 ApJ 776 55

We present global coronal seismology for the first time, which allows us to determine inhomogeneous magnetic field strength in the extended corona. From the measurements of the propagation speed of a fast magnetosonic wave associated with a coronal mass ejection (CME) and the coronal background density distribution derived from the polarized radiances observed by the STEREO SECCHI COR1, we determined the magnetic field strengths along the trajectories of the wave at different heliocentric distances. We found that the results have an uncertainty less than



40%, and are consistent with values determined with a potential field model and reported in previous works. The characteristics of the coronal medium we found are that (1) the density, magnetic field strength, and plasma  $\beta$  are lower in the coronal hole region than in streamers; (2) the magnetic field strength decreases slowly with height but the electron density decreases rapidly so that the local fast magnetosonic speed increases while plasma  $\beta$  falls off with height; and (3) the variations of the local fast magnetosonic speed and plasma  $\beta$  are dominated by variations in the electron density rather than the magnetic field strength. These results imply that Moreton and EIT waves are downward-reflected fast magnetosonic waves from the upper solar corona, rather than freely propagating fast magnetosonic waves in a certain atmospheric layer. In addition, the azimuthal components of CMEs and the driven waves may play an important role in various manifestations of shocks, such as type II radio bursts and solar energetic particle events.

## Measurements of Photospheric and Chromospheric Magnetic Fields

Review

Andreas **Lagg**, Bruce Lites, Jack Harvey, Sanjay Gosain, Rebecca Centeno

Space Science Reviews September 2017, Volume 210, [Issue 1–4](#), pp 37–76

<http://arxiv.org/pdf/1510.06865v1.pdf>

The Sun is replete with magnetic fields, with sunspots, pores and plage regions being their most prominent representatives on the solar surface. But even far away from these active regions, magnetic fields are ubiquitous. To a large extent, their importance for the thermodynamics in the solar photosphere is determined by the total magnetic flux. Whereas in low-flux quiet Sun regions, magnetic structures are shuffled around by the motion of granules, the high-flux areas like sunspots or pores effectively suppress convection, leading to a temperature decrease of up to 3000 K. The importance of magnetic fields to the conditions in higher atmospheric layers, the chromosphere and corona, is indisputable. Magnetic fields in both active and quiet regions are the main coupling agent between the outer layers of the solar atmosphere, and are therefore not only involved in the structuring of these layers, but also for the transport of energy from the solar surface through the corona to the interplanetary space.

Consequently, inference of magnetic fields in the photosphere, and especially in the chromosphere, is crucial to deepen our understanding not only for solar phenomena such as chromospheric and coronal heating, flares or coronal mass ejections, but also for fundamental physical topics like dynamo theory or atomic physics. In this review, we present an overview of significant advances during the last decades in measurement techniques, analysis methods, and the availability of observatories, together with some selected results. We discuss the problems of determining magnetic fields at smallest spatial scales, connected with increasing demands on polarimetric sensitivity and temporal resolution, and highlight some promising future developments for their solution.

## Vigorous convection in a sunspot granular light bridge

Andreas **Lagg** (1), Sami K. Solanki (1 and 2), Michiel van Noort (1), Sanja Danilovic

A&A, 568, A60, 2014

<http://arxiv.org/pdf/1407.1202v1.pdf>

Light bridges are the most prominent manifestation of convection in sunspots. The brightest representatives are granular light bridges composed of features that appear to be similar to granules. An in-depth study of the convective motions, temperature stratification, and magnetic field vector in and around light bridge granules is presented with the aim of identifying similarities and differences to typical quiet-Sun granules. Spectropolarimetric data from the Hinode Solar Optical Telescope were analyzed using a spatially coupled inversion technique to retrieve the stratified atmospheric parameters of light bridge and quiet-Sun granules. Central hot upflows surrounded by cooler fast downflows reaching 10 km/s clearly establish the convective nature of the light bridge granules. The inner part of these granules in the near surface layers is field free and is covered by a cusp-like magnetic field configuration. We observe hints of field reversals at the location of the fast downflows. The quiet-Sun granules in the vicinity of the sunspot are covered by a low-lying canopy field extending radially outward from the spot. The similarities between quiet-Sun and light bridge granules point to the deep anchoring of granular light bridges in the underlying convection zone. The fast, supersonic downflows are most likely a result of a combination of invigorated convection in the light bridge granule due to radiative cooling into the neighboring umbra and the fact that we sample deeper layers, since the downflows are immediately adjacent to the slanted walls of the Wilson depression.

November 30 2006

## Spatial Nonlocality of the Small-Scale Solar Dynamo

Derek A. **Lamb**, Timothy A. Howard, Craig E. DeForest

ApJ 788 7 2014

<http://arxiv.org/pdf/1404.3259v1.pdf>

We explore the nature of the small-scale solar dynamo by tracking magnetic features. We investigate two previously-explored categories of the small-scale solar dynamo: shallow and deep. Recent modeling work on the shallow dynamo has produced a number of scenarios for how a strong network concentration can influence the formation and polarity of nearby small-scale magnetic features. These scenarios have measurable signatures, which we test for here using magnetograms from the Narrowband Filter Imager (NFI) on Hinode. We find no statistical

tendency for newly-formed magnetic features to cluster around or away from network concentrations, nor do we find any statistical relationship between their polarities. We conclude that there is no shallow or "surface" dynamo on the spatial scales observable by Hinode/NFI. In light of these results, we offer a scenario in which the sub-surface field in a deep solar dynamo is stretched and distorted via turbulence, allowing the field to emerge at random locations on the photosphere.

## **Hinode/EIS measurements of active region magnetic fields**

[E. Landi](#), [R. Hutton](#), [T. Brage](#), [W. Li](#)

2020 *ApJ* 904 87

<https://arxiv.org/pdf/2008.03532.pdf>

<https://doi.org/10.3847/1538-4357/abbf54>

The present work illustrates the potential of a new diagnostic technique that allows the measurement of the coronal magnetic field strength in solar active regions utilizing a handful of bright  $\text{Fe X}$  and  $\text{Fe XI}$  lines commonly observed by the Hinode/EIS high-resolution spectrometer. The importance of this new diagnostic technique lies in two basic facts: 1) the coronal magnetic field is probably the most important quantity in coronal physics, as it is at the heart of the processes regulating Space Weather and the properties of the solar corona, and 2) this technique can be applied to the existing EIS archive spanning from 2007 to 2020, including more than one full solar cycle and covering a large number of active regions, flares, and even coronal mass ejections. This new diagnostic technique opens the door to a whole new field of studies, complementing the magnetic field measurements from the upcoming DKIST and UCoMP ground based observatories, and extending our reach to active regions observed on the disk and until now only sampled by radio measurements. In this work we present a few examples of the application of this technique to EIS observations taken at different times during the EIS mission, discuss its current limitations and the steps to improve its accuracy. We also present a list of EIS observing sequences whose data include all the lines necessary for the application of this diagnostic technique, to help the solar community navigate the immense set of EIS data and to find observations suitable to measure the coronal magnetic field. **June 2, 2007, 2007 December 10-18, January 10-15, 2008, 16 March 2014, 25 October 2016**

**Table 4:** Hinode/EIS observations used in the present work (2007-2018).

**Hinode/ EIS Nugget, Oct 2020** [http://solarb.mssl.ucl.ac.uk/SolarB/nuggets/nugget\\_2020oct.jsp](http://solarb.mssl.ucl.ac.uk/SolarB/nuggets/nugget_2020oct.jsp)

## **Coronal plasma diagnostics from ground-based observations** **Review**

E. [Landi](#), S. R. Habbal, S. Tomczyk

JGR Volume 121, Issue 9 September 2016 Pages 8237–8249

<http://sci-hub.cc/doi/10.1002/2016JA022598>

In this paper we discuss the potential of ground-based visible observations of the solar corona to address the key open problems in the physics of the solar atmosphere and of solar activity. We first compare the diagnostic potential of visible observations with those of high-resolution spectrometers and narrowband imagers working in the EUV and X-ray wavelength ranges. We then review the main diagnostic techniques (and introduce a few new ones) that can be applied to line and continuum emission in the solar atmosphere, and the physical problems that they enable us to address. Finally, we briefly review the main features of ground-based coronagraphic instrumentation currently being developed and planned.

## **Observations of the Solar F-Corona from Space**

**Review**

[P. L. Lamy](#), [H. Gilardy](#) & [A. Llebaria](#)

*Space Science Reviews* volume 218, Article number: 53 (2022)

<https://link.springer.com/content/pdf/10.1007/s11214-022-00918-y.pdf>

We present a review of the observations of the solar F-corona from space with a special emphasis of the 25 years of continuous monitoring achieved by the LASCO-C2 and C3 coronagraphs. Our work includes images obtained by the navigation cameras of the Clementine spacecraft, the SECCHI/HI-1A heliospheric imager onboard STEREO-A, and the Wide Field Imager for Solar Probe onboard the Parker Solar Probe. The connection to the zodiacal light is considered based on ground- and space-based observations, prominently from the past Helios, IRAS, COBE, and IRAKI missions. The characteristic radiance profiles along the two symmetry axis of the "elliptically" shaped F-corona (aka equatorial and polar directions) follow power laws in the  $5 \cdot 5^\circ - 50 \cdot 50^\circ$  range of elongation, with constant power exponents of  $-2.33$  and  $-2.55$ . Both profiles connect extremely well to the corresponding standard profiles of the zodiacal light. The LASCO equatorial profile exhibits a shoulder implying a  $\approx 17\%$  decrease of the radiance within  $\approx 10 R_\odot$  that may be explained by the disappearance of organic materials within  $0.3$  AU. LASCO detected for the first time a secular variation of the F-corona, an increase at a rate of  $0.46\%$  per year of the integrated radiance in the LASCO-C3 field of view. This is likely the first observational evidence of the role of collisions in the inner zodiacal cloud. The temporal evolution of the integrated radiance in the LASCO-C2 field of view is more complex suggesting possible additional processes. Whereas it is well established that the F-corona is slightly redder than the Sun, the spectral variation of its color index is not yet well established.

A composite of C2 and C3 images produced the LASCO reference map of the radiance of the F-corona from 2 to  $30 R_{\odot}$  and, by combining with ground-based measurements, the LASCO extended map from 1 to  $6 R_{\odot}$ . An upper limit of  $0.03 R_{\odot}$  is obtained for the offset between the center of the Sun and that of the F-corona with a most likely value of zero. The flattening index of the F-corona starts from zero at an elongation of  $0.5 \pm 0.01$  and increases linearly with the logarithm of the elongation to connect to that of the zodiacal light with however a small hump related to the shoulder in the equatorial profile. The shape of the isophotes is best described by super-ellipses with an exponent linked to the flattening index. An ellipsoid model of the spatial density of interplanetary dust is solely capable of reproducing this shape, thus rejecting other classical models such as fan, and cosine. The plane of symmetry of the inner zodiacal cloud is strongly warped, its inclination increasing towards the planes of the inner planets and ultimately the solar equator. In contrast, its longitude of ascending node is found to be constant and equal to  $87.6^{\circ}$ . LASCO did not detect any small scale structures such as putative rings occasionally reported during solar eclipses. The outer border of the depletion zone where interplanetary dust particles start to be affected by sublimation appears well constrained at  $\approx 19 R_{\odot}$ . This zone extends down to  $\approx 5 R_{\odot}$ , thus defining the boundary of the dust-free zone where the most refractory materials – likely moderately absorbing silicates – disappear.

## Validation of MHD Model Predictions of the Corona with LASCO-C2 Polarized Brightness Images

Philippe Lamy, Olivier Floyd, Zoran Mikić, Pete Riley

*Solar Physics* October 2019, 294:162

<https://doi.org/10.1007/s11207-019-1549-9>

Progress in our understanding of the solar corona requires that the results of advanced magnetohydrodynamic models driven by measured magnetic fields, and particularly the underlying heating models, be thoroughly compared with coronal observations. The comparison has so far mainly concerned the global morphology of the corona, synthetic images calculated from the models being compared with observed images. We go one step further by performing detailed quantitative comparisons between the calculated polarized radiance pBpB using the three-dimensional electron density produced by MHD models and well calibrated polarized images obtained by the Large Angle Spectrometric Coronagraph LASCO-C2 coronagraph complemented by ground-based images when available from the Mauna Loa Solar Observatory Mark IV and K-Cor instruments to extend the comparison to the inner coronal region  $1.0 - 2.5 R_{\odot}$ , which is inaccessible to C2. We take advantage of the high-resolution and high-quality MHD predictions performed for several solar eclipses (1 August 2008, 11 July 2010, 13 November 2012, and 21 August 2017) and for the first perihelion passage of the Parker Solar Probe (5 November 2018) using two different three-dimensional MHD models relying on either a thermodynamic or a wave-turbulence-driven methodologies to heat the corona. Both models are generally able to match the observed structure and photometry of the corona albeit with various degrees of fidelity for which there is no obvious explanation. However, two limitations emerge, the complexity of coronae of the maximum type and the time lapse between the completion of the magnetograph measurements and the prediction.

## Coronal spectral diagnostics: The coronal solar magnetism observatory (COSMO).

Landi E, Gibson SE, Tomczyk S, Burkepile J, de Toma G, Zhang J, Schad T, Kucera TA, Reeves KK and Cremades H

(2022) *Front. Astron. Space Sci.* 9 :1059716.

doi: 10.3389/fspas.2022.1059716

<https://www.frontiersin.org/articles/10.3389/fspas.2022.1059716/pdf>

**The Need:** Understanding and predicting the major phenomena taking place in the solar corona, such as flares and Coronal Mass Ejections (CMEs), the heating and evolution of the solar atmosphere, and the acceleration of the solar wind, are fundamental challenges to predict our own star. These challenges are related to the solar magnetism and to the physical properties of solar plasmas: meeting them requires two types of measurements: (A) Spectrally resolved, simultaneous observations of the entire corona in multiple spectral lines emitted by chromospheric to hot coronal plasmas at high spatial resolution and cadence for long periods of time; and (B) Coronal magnetic field measurements.

**The Problem:** The current fleet of space instruments suffers from three main limitations: (A) EUV narrow-band imagers provide simultaneous 2D images of the corona, but lack adequate plasma diagnostic capabilities; (B) High-resolution EUV spectrometers have the required diagnostic potential, but their narrow field of view prevents a continuous and simultaneous coverage of the entire corona. (C) No current instrument can measure the global coronal magnetic field.

**The Solution:** Visible to near-IR coronagraphs coupled to tunable filters combine the strengths of both EUV high resolution spectrometers and EUV imagers in one single instrument by 1) providing 2D images of the whole field of view at a single wavelength; 2) spectrally resolving individual lines near-simultaneously across the entire field of view, and 3) measuring the magnetic field through polarimetry. The proposed Coronal Solar Magnetism Observatory (COSMO) visible to near-IR coronagraph would allow the measurement of: (A) simultaneous plasma

thermal structure of the whole solar corona and CMEs; (B) plasma velocity vector; and (C) coronal magnetic field. The technology behind visible/near-IR coronagraphs coupled to tunable filters is mature; ground-based implementation of such instruments would provide long-term, easily-upgradable data sets.

### **ON THE ISOTHERMALITY OF SOLAR PLASMAS**

E. Landi<sup>1,2</sup> and J. A. Klimchuk<sup>3</sup>

*Astrophysical Journal*, 723:320–328, 2010

Recent measurements have shown that the quiet unstructured solar corona observed at the solar limb is close to isothermal, at a temperature that does not appear to change over wide areas or with time. Some individual active region loop structures have also been found to be nearly isothermal both along their axis and across their cross section. Even a complex active region observed at the solar limb has been found to be composed of three distinct isothermal plasmas. If confirmed, these results would pose formidable challenges to the current theoretical understanding of the thermal structure and heating of the solar corona. For example, no current theoretical model can explain the excess densities and lifetimes of many observed loops if the loops are in fact isothermal. All of these measurements are based on the so-called emission measure (EM) diagnostic technique that is applied to a set of optically thin lines under the assumption of isothermal plasma. It provides simultaneous measurement of both the temperature and EM. In this work, we develop a new method to quantify the uncertainties in the technique and to rigorously assess its ability to discriminate between isothermal and multithermal plasmas. We define a formal measure of the uncertainty in the EM diagnostic technique that can easily be applied to real data. We here apply it to synthetic data based on a variety of assumed plasma thermal distributions and develop a method to quantitatively assess the degree of multithermality of a plasma.

### **Testing the Accuracy of Data Driven MHD Simulations of Active Region Evolution**

James E. Leake, Mark G. Linton, Peter W. Schuck

2017 *ApJ* 838 113

<https://arxiv.org/pdf/1702.06808.pdf>

<http://iopscience.iop.org/article/10.3847/1538-4357/aa6578/pdf>

Models for the evolution of the solar coronal magnetic field are vital for understanding solar activity, yet the best measurements of magnetic field lie at the photosphere, necessitating the development of coronal models which are "data-driven" at the photosphere. We present an investigation to determine the feasibility and accuracy of such methods. Our validation framework uses a simulation of active region (AR) formation, modeling the emergence of magnetic flux from the convection zone to the corona, as a ground-truth dataset, to supply both the photospheric information, and to perform the validation of the data-driven method. We focus our investigation on how the data-driven model accuracy depends on the temporal frequency of the driving data. The Helioseismic and Magnetic Imager on NASA's Solar Dynamics Observatory produces full-disk vector magnetic field measurements at a 12 minute cadence. Using our framework we show that ARs that emerge over 25 hours can be modeled by the data-driving method with only ~1% error in the free magnetic energy, assuming the photospheric information is specified every 12 minutes. However, for rapidly evolving features, under-sampling of the dynamics at this cadence leads to a strobe effect, generating large electric currents and incorrect coronal morphology and energies. We derive a sampling condition for the driving cadence based on the evolution of these small-scale features, and show that higher-cadence driving can lead to acceptable errors. Future work will investigate the source of errors associated with deriving plasma variables from the photospheric magnetograms as well as other sources of errors such as reduced resolution and instrument bias and noise.

### **Diagnostics of the Solar Corona from Comparison between Faraday Rotation Measurements and Magnetohydrodynamic Simulations**

G. Le Chat<sup>1,4</sup>, J. C. Kasper<sup>2,4,5</sup>, O. Cohen<sup>1</sup>, and S. R. Spangler

2014 *ApJ* 789 163

Polarized natural radio sources passing behind the Sun experience Faraday rotation as a consequence of the electron density and magnetic field strength in coronal plasma. Since Faraday rotation is proportional to the product of the density and the component of the magnetic field along the line of sight of the observer, a model is required to interpret the observations and infer coronal structures. Faraday rotation observations have been compared with relatively ad hoc models of the corona. Here for the first time we compare these observations with magnetohydrodynamic (MHD) models of the solar corona driven by measurements of the photospheric magnetic field. We use observations made with the NRAO Very Large Array of 34 polarized radio sources occulted by the solar corona between 5 and 14 solar radii. The measurements were made during 1997 May, and 2005 March and April. We compare the observed Faraday rotation values with values extracted from MHD steady-state simulations of the solar corona. We find that (1) using a synoptic map of the solar magnetic field just one Carrington rotation off produces poorer agreements, meaning that the outer corona changes in the course of one month, even in solar minimum; (2) global MHD models of the solar corona driven by photospheric magnetic field measurements are

generally able to reproduce Faraday rotation observations; and (3) some sources show significant disagreement between the model and the observations, which appears to be a function of the proximity of the line of sight to the large-scale heliospheric current sheet.

## **Quantifying Properties of Photospheric Magnetic Cancellations in the Quiet Sun Internetwork**

Vincent E. [Ledvina](#)<sup>1,2</sup>, Maria D. Kazachenko<sup>2,3</sup>, Serena Criscuoli<sup>2</sup>, Dennis Tilipman<sup>2,3</sup>, Ilaria Ermolli<sup>4</sup>, Mariachiara Falco<sup>5</sup>, Salvatore Guglielmino<sup>5</sup>, Shahin Jafarzadeh<sup>6,7</sup>, Luc Rouppe van der Voort<sup>7,8</sup>, and Francesca Zuccarello<sup>9</sup>

2022 ApJ 934 38

<https://iopscience.iop.org/article/10.3847/1538-4357/ac7785/pdf>

We analyzed spectropolarimetric data from the Swedish 1 m Solar Telescope to investigate the physical properties of small-scale magnetic cancellations in the quiet Sun photosphere. Specifically, we looked at the full Stokes polarization profiles along the Fe i 557.6 nm and of the Fe i 630.1 nm lines measured by the CRisp Imaging SpectroPolarimeter to study the temporal evolution of the line-of-sight magnetic field during 42.5 minutes of quiet Sun evolution. From this magnetogram sequence, we visually identified 38 cancellation events. We then used the Yet Another Feature Tracking Algorithm to characterize the physical properties of these magnetic cancellations. We found on average  $1.6 \times 10^{16}$  Mx of magnetic flux canceled in each event with an average cancellation rate of  $3.8 \times 10^{14}$  Mx s<sup>-1</sup>. The derived canceled flux is associated with strong downflows, with an average speed of VLOS  $\approx 1.1$  km s<sup>-1</sup>. Our results show that the average lifetime of each event is 9.2 minutes with an average of 44.8% of initial magnetic flux being canceled. Our estimates of magnetic fluxes provide a lower limit since studied magnetic cancellation events have magnetic field values that are very close to the instrument noise level. We observed no horizontal magnetic fields at the cancellation sites and therefore cannot conclude whether the events are associated with structures that could cause magnetic reconnection. **6-18 Aug 2011**

## **Topology of Coronal Magnetic Fields: Extending the Magnetic Skeleton Using Null-like Points**

[D. T. Lee](#), [D. S. Brown](#)

Solar Phys. **295**, Article number: 168 **2020**

<https://arxiv.org/pdf/2011.10272.pdf>

<https://link.springer.com/content/pdf/10.1007/s11207-020-01729-6.pdf>

Many phenomena in the Sun's atmosphere are magnetic in nature and study of the atmospheric magnetic field plays an important part in understanding these phenomena. Tools to study solar magnetic fields include magnetic topology and features such as magnetic null points, separatrix surfaces, and separators. The theory of these has most robustly been developed under magnetic charge topology, where the sources of the magnetic field are taken to be discrete, but observed magnetic fields are continuously distributed, and reconstructions and numerical simulations typically use continuously distributed magnetic boundary conditions. This article investigates the pitfalls in using continuous source descriptions, particularly when null points on the  $z=0$  plane are obscured by the continuous flux distribution through, e.g., the overlap of non-point sources. The idea of null-like points on the boundary is introduced where the parallel requirement on the field  $B_{\parallel}=0$  is retained but the requirement on the perpendicular component is relaxed, i.e.,  $B_{\perp} \neq 0$ . These allow the definition of separatrix-like surfaces which are shown (through use of a squashing factor) to be a class of quasi-separatrix layer, and separator-like lines which retain the x-line structure of separators. Examples are given that demonstrate that the use of null-like points can reinstate topological features that are eliminated in the transition from discrete to continuous sources, and that their inclusion in more involved cases can enhance understanding of the magnetic structure and even change the resulting conclusions. While the examples in this article use the potential approximation, the definition of null-like points is more general and may be employed in other cases such as force-free field extrapolations and MHD simulations.

## **Magnetic Configurations Related to the Coronal Heating and Solar Wind Generation I. Twist and Expansion Profiles of Magnetic Loops Produced by Flux Emergence**

Hwanhee [Lee](#), Tetsuya Magara

E-print, Jan 2014

The generation of outflows from the Sun known as solar winds is coupled with the heating of the solar corona, and both processes are operated in magnetic structures formed on the Sun. To study the magnetic configuration responsible for these processes, we use three-dimensional magnetohydrodynamic simulations to reproduce magnetic structures via flux emergence and investigate their configurations. We focus on two key quantities characterizing a magnetic configuration: the force-free parameter  $\alpha$  and the flux expansion rate  $f_{ex}$ , the former of which represents how much a magnetic field is twisted while the latter represents how sharply a magnetic field expands. We derive distributions of these quantities in an emerging flux region. Our result shows that an emerging flux region consists of outer part where a magnetic loop takes a large flux expansion rate but a small value of  $\alpha$  at their photospheric footpoints, and inner part occupied by those loops where a strong electric current flows. We also investigate the

expansion profile of a magnetic loop composing an emerging flux region. The profile is given by an exponential expansion type near the solar surface while it is given by a quadratic expansion type in an outer atmosphere. These detailed magnetic configurations obtained by this study contribute to developing a realistic model for the coronal heating and solar wind generation.

### **Coronal Field Opens at Lower Height During the Solar Cycles 22 and 23 Minimum Periods: IMF Comparison Suggests the Source Surface Should Be Lowered<<<**

C. O. [Lee](#), J. G. Luhmann, J. T. Hoeksema, X. Sun, C. N. Arge & I. Pater  
Solar Physics, Volume 269, Number 2, 367-388, 2011

The solar cycle 23 minimum period has been characterized by a weaker solar and interplanetary magnetic field. This provides an ideal time to study how the strength of the photospheric field affects the interplanetary magnetic flux and, in particular, how much the observed interplanetary fields of different cycle minima can be understood simply from differences in the areas of the coronal holes, as opposed to differences in the surface fields within them. In this study, we invoke smaller source surface radii in the potential-field source-surface (PFSS) model to construct a consistent picture of the observed coronal holes and the near-Earth interplanetary field strength as well as polarity measurements for the cycles 23 and 22 minimum periods. Although the source surface value of  $2.5 R_{\odot}$  is typically used in PFSS applications, earlier studies have shown that using smaller source surface heights generates results that better match observations during low solar activity periods. We use photospheric field synoptic maps from Mount Wilson Observatory (MWO) and find that the values of  $\approx 1.9 R_{\odot}$  and  $\approx 1.8 R_{\odot}$  for the cycles 22 and 23 minimum periods, respectively, produce the best results. The larger coronal holes obtained for the smaller source surface radius of cycle 23 somewhat offsets the interplanetary consequences of the lower magnetic field at their photospheric footpoints. For comparison, we also use observations from the Michelson Doppler Imager (MDI) and find that the source surface radius of  $\approx 1.5 R_{\odot}$  produces better results for cycle 23, rather than  $\approx 1.8 R_{\odot}$  as suggested from MWO observations. Despite this difference, our results obtained from MWO and MDI observations show a qualitative consistency regarding the origins of the interplanetary field and suggest that users of PFSS models may want to consider using these smaller values for their source surface heights as long as the solar activity is low.

### **On Identifying and Mitigating Bias in Inferred Measurements for Solar Vector Magnetic-Field Data**

[K. D. Leka](#), [Eric L. Wagner](#), [Ana Belén Griñón-Marín](#), [Véronique Bommier](#) & [Richard E. L. Higgins](#)  
Solar Physics volume 297, Article number: 121 (2022)

<https://link.springer.com/content/pdf/10.1007/s11207-022-02039-9.pdf>

The problem of bias, meaning over- or under-estimation, of the component perpendicular to the line-of-sight [ $B_{\perp}$ ] in vector magnetic-field maps is discussed. Previous works on this topic have illustrated that the problem exists; here we perform novel investigations to quantify the bias, fully understand its source(s), and provide mitigation strategies. First, we develop quantitative metrics to measure the  $B_{\perp}$  bias and quantify the effect in both local (physical) and native image-plane components. Second, we test and evaluate different options available to inversions and different data sources, to systematically characterize the impacts of these choices, including explicitly accounting for the magnetic fill fraction [ff]. Third, we deploy a simple model to test how noise and different models of the bias may manifest. From these three investigations we find that while the bias is dominantly present in under-resolved structures, it is also present in strong-field, pixel-filling structures. Noise in the spectropolarimetric data can exacerbate the problem, but it is not the primary cause of the bias. We show that fitting ff explicitly provides significant mitigation, but that other considerations such as the choice of  $\chi^2$ -weights and optimization algorithms can impact the results as well. Finally, we demonstrate a straightforward “quick fix” that can be applied post facto but prior to solving the  $180^{\circ}$  ambiguity in  $B_{\perp}$ , and which may be useful when global-scale structures are, e.g., used for model boundary input. The conclusions of this work support the deployment of inversion codes that explicitly fit ff or, as with the new SynthIA neural-net, that are trained on data that did so. **04 – 12 Dec 2010, 22-27 Nov 2015, 13 – 21 May 2016, 17 – 25 May 2016**

**Correction:** Solar Physics volume 297, Article number: 146 (2022)

<https://link.springer.com/content/pdf/10.1007/s11207-022-02079-1.pdf>

### **Evaluating (and Improving) Estimates of the Solar Radial Magnetic Field Component from Line-of-Sight Magnetograms**

K.D. [Leka](#), G. Barnes, E. L. Wagner

Solar Phys. February 2017, 292:36 2017

<https://arxiv.org/pdf/1701.04836v1.pdf>

Although for many solar physics problems the desirable or meaningful boundary is the radial component of the magnetic field  $B_r$ , the most readily available measurement is the component of the magnetic field along the line-of-sight to the observer,  $B_{\text{los}}$ . As this component is only equal to the radial component where the viewing angle is exactly zero, some approximation is required to estimate  $B_r$  at all other observed locations. In this study, a common approximation known as the " $\mu$ -correction", which assumes all photospheric field to be radial, is compared to a method which invokes computing a potential field that matches the observed  $B_{\text{los}}$ , from which the potential field radial component,  $B_{\text{pot}r}$  is recovered. We demonstrate that in regions that are truly dominated by radially-oriented field at the resolution of the data employed, the  $\mu$ -correction performs acceptably if not better than the potential-field approach. However, it is also shown that for any solar structure which includes horizontal fields, i.e. active regions, the potential-field method better recovers both the strength of the radial field and the location of magnetic neutral line. 2011. 03. 06, 2014. 03. 15

## **Modeling and Interpreting the Effects of Spatial Resolution on Solar Magnetic Field Maps**

K. D. [Leka](#) and G. Barnes

Solar Physics, Volume 277, Number 1, 89-118, 2012

Different methods for simulating the effects of spatial resolution on magnetic field maps are compared, including those commonly used for inter-instrument comparisons. The investigation first uses synthetic data, and the results are confirmed with Hinode/SpectroPolarimeter data. Four methods are examined, one which manipulates the Stokes spectra to simulate spatial-resolution degradation, and three "post-facto" methods where the magnetic field maps are manipulated directly. Throughout, statistical comparisons of the degraded maps with the originals serve to quantify the outcomes. Overall, we find that areas with inferred magnetic fill fractions close to unity may be insensitive to optical spatial resolution; areas of sub-unity fill fractions are very sensitive. Trends with worsening spatial resolution can include increased average field strength, lower total flux, and a field vector oriented closer to the line of sight. Further-derived quantities such as vertical current density show variations even in areas of high average magnetic fill fraction. In short, unresolved maps fail to represent the distribution of the underlying unresolved fields, and the "post-facto" methods generally do not reproduce the effects of a smaller telescope aperture. It is argued that selecting a method in order to reconcile disparate spatial resolution effects should depend on the goal, as one method may better preserve the field distribution, while another can reproduce spatial resolution degradation. The results presented should help direct future inter-instrument comparisons.

## **Improved Determination of the Location of the Temperature Maximum in the Corona**

J. F. [Lemaire](#), K. Stegen

Solar Phys. Volume 291, [Issue 12](#), pp 3659–3683 2016

The most used method to calculate the coronal electron temperature  $[T_e(r)/T_e(r)]$  from a coronal density distribution  $[n_e(r)/n_e(r)]$  is the scale-height method (SHM). We introduce a novel method that is a generalization of a method introduced by Alfvén (Ark. Mat. Astron. Fys.27, 1, [1941](#)) to calculate  $T_e(r)/T_e(r)$  for a corona in hydrostatic equilibrium: the "HST" method. All of the methods discussed here require given electron-density distributions  $[n_e(r)/n_e(r)]$  which can be derived from white-light (WL) eclipse observations. The new "DYN" method determines the unique solution of  $T_e(r)/T_e(r)$  for which  $T_e(r \rightarrow \infty) \rightarrow 0$  when the solar corona expands radially as realized in hydrodynamical solar-wind models. The applications of the SHM method and DYN method give comparable distributions for  $T_e(r)/T_e(r)$ . Both have a maximum  $[T_{\text{max}}/T_{\text{max}}]$  whose value ranges between 1 – 3 MK. However, the peak of temperature is located at a different altitude in both cases. Close to the Sun where the expansion velocity is subsonic ( $r < 1.3R_{\odot}$ ) the DYN method gives the same results as the HST method. The effects of the other free parameters on the DYN temperature distribution are presented in the last part of this study. Our DYN method is a new tool to evaluate the range of altitudes where the heating rate is maximum in the solar corona when the electron-density distribution is obtained from WL coronal observations.

## **Dark halos around solar active regions**

### **I. Emission properties of the dark halo around NOAA 12706**

S. M. [Lezzi](#)<sup>1,2</sup>, V. Andretta<sup>1</sup>, M. Murabito<sup>1</sup> and G. Del Zanna<sup>3</sup>

A&A 680, A61 (2023)

<https://www.aanda.org/articles/aa/pdf/2023/12/aa47414-23.pdf>

<https://arxiv.org/pdf/2309.11956.pdf>

Context. Dark areas around active regions (ARs) were first observed in chromospheric lines more than a century ago and are now associated with the  $H\alpha$  fibril vortex around ARs. Nowadays, large areas surrounding ARs with reduced emission relative to the quiet Sun (QS) are also observed in spectral lines emitted in the transition region (TR) and the low corona. For example, they are clearly seen in the SDO/AIA 171 Å images. We name these chromospheric and TR-coronal dark regions "dark halos" (DHs). Coronal DHs are poorly studied and, because their origin is still

unknown, to date it is not clear if they are related to the chromospheric fibrillar ones. Furthermore, they are often mistaken for coronal holes (CHs).

**Aims.** Our goal is to characterize the emission properties of a DH by combining, for the first time, chromospheric, TR, and coronal observations in order to provide observational constraints for future studies on the origin of DHs. This study also aims to investigate the different properties of DHs and CHs and provide a quick-look recipe to distinguish between them.

**Methods.** We studied the DH around AR NOAA 12706 and the southern CH that were on the disk on **April 22, 2018** by analyzing IRIS full-disk mosaics and SDO/AIA filtergrams to evaluate their average intensities, normalized to the QS. In addition, we used the AIA images to derive the DH and CH emission measure (EM) and the IRIS Si IV 1393.7 Å line to estimate the nonthermal velocities of plasma in the TR. We also employed SDO/HMI magnetograms to study the average magnetic field strength inside the DH and the CH.

**Results.** Fibrils are observed all around the AR core in the chromospheric Mg II h&k IRIS mosaics, most clearly in the h3 and k3 features. The TR emission in the DH is much lower than in the QS area, unlike in the CH. Moreover, the DH is much more extended in the low corona than in the chromospheric Mg II h3 and k3 images. Finally, the intensities, EM, spectral profile, nonthermal velocity, and average magnetic field strength measurements clearly show that DHs and CHs exhibit different characteristics, and therefore should be considered as distinct types of structures on the Sun.

## **Mapping the Longitudinal Magnetic Field in the Atmosphere of an Active Region Plage from the Inversion of the Near-ultraviolet CLASP2.1 Spectropolarimetric Data**

Hao **Li**<sup>1,2</sup>, Tanausú del Pino Alemán<sup>1,2</sup>, Javier Trujillo Bueno<sup>1,2,3</sup>, Ryohko Ishikawa<sup>4</sup> +++  
**2024** ApJ 974 154

<https://iopscience.iop.org/article/10.3847/1538-4357/ad6dfb/pdf>

We apply the HanleRT Tenerife Inversion Code to the spectropolarimetric observations obtained by the Chromospheric Layer Spectropolarimeter. This suborbital space experiment measured the variation with wavelength of the four Stokes parameters in the near-ultraviolet spectral region of the Mg ii h and k lines over a solar disk area containing part of an active region plage and the edge of a sunspot penumbra. We infer the stratification of the temperature, the electron density, the line-of-sight velocity, the microturbulent velocity, and the longitudinal component of the magnetic field from the observed intensity and circular polarization profiles. The inferred model atmosphere shows larger temperature and electron density in the plage and the superpenumbra regions than in the quiet regions. The shape of the plage region in terms of its brightness is similar to the pattern of the inferred longitudinal component of the magnetic field in the chromosphere, as well as to that of the overlying moss observed by the Atmospheric Imaging Assembly in the 171 Å band, which suggests a similar magnetic origin for the heating in both the plage and the moss region. Moreover, this heating is particularly significant in the regions with larger inferred magnetic flux. In contrast, in the superpenumbra, the regions with larger electron density and temperature are usually found in between these regions with larger magnetic flux, suggesting that the details of the heating mechanism in the chromosphere of the superpenumbra may be different from those in the plage, but with the magnetic field still playing a key role. **2021 October 8**

## **Light Bridges and Solar Active Region Evolution Processes**

[Fuyu Li](#), [Changhui Rao](#), [Xinhua Zhao](#), [Yang Guo](#), [Xiaoying Gong](#), [Yuhao Chen](#), [Nanbin Xiang](#), [Huaning Wang](#)

ApJ **271** 34 **2024**

<https://arxiv.org/ftp/arxiv/papers/2402/2402.13455.pdf>

<https://iopscience.iop.org/article/10.3847/1538-4365/ad2515/pdf>

The formation mechanism of light bridges (LBs) is strongly related to the dynamic evolution of solar active regions (ARs). To study the relationship between LB formation and AR evolution phases, we employ 109 LB samples from 69 ARs in 2014 using observational data from the Helioseismic and Magnetic Imager on board the Solar Dynamics Observatory (HMI/SDO). LBs are well matched with the weak field lanes (WFLs), except that aligned on the polarity inversion line of  $\{\delta\}$  sunspots. For penumbral intrusion (type-A) and umbral-dot emergence (type-C) LBs, the WFLs represent the splitting of magnetic flux systems. The sunspots tend to decay and split into several parts after type-A and type-C LBs formed. For sunspot/umbra merging (type-B) LBs, the WFLs declining are caused by collisions of flux systems. The sunspots merge and keep stable after type-B LBs formed. We conclude that type-B LBs are formed by collisions of flux systems, while type-A and type-C LBs are generated by splits. The time differences ( $\{\delta\}T$ ) between LBs appearing and ARs peaking have average value of 1.06, -1.60, 1.82 for type-A, B, C LBs, with the standard deviation of 3.27, 2.17, 1.89, respectively. A positive value of  $\{\delta\}T$  means that the LB appear after AR peaking, whereas a minus  $\{\delta\}T$  before the peak. Type-A LBs trend to form in the decaying phase or around the peak time. Type-B LBs are more likely to be formed in the developing phase. Type-C LBs mostly take shape in the decaying phase of ARs. **Jan 3-10 2014, 2014.01.29-02.05, 2014.05.12-17, 2014.09.26-10.02, 2014.12.15-19**



## **Rapid Decay of a Penumbra Sector Associated with a Strong Light Bridge in Active Region NOAA 12680**

Qiaoling Li<sup>1,2</sup>, Li Zhang<sup>2</sup>, Xiaoli Yan<sup>3,4</sup>, Jingcheng Wang<sup>3,4</sup>, Liheng Yang<sup>3,4</sup>, and Zhike Xue<sup>3,4</sup>  
2023 ApJ 942 61

<https://iopscience.iop.org/article/10.3847/1538-4357/aca667/pdf>

We present observations of the rapid decay of a penumbra sector associated with a strong light bridge (LB) in the active region NOAA 12680 by analyzing the scattered light-corrected Solar Dynamics Observatory/Helioseismic and Magnetic Imager data. At the beginning of penumbra decay, some dark structures gradually broke away from the umbra to which they were attached. The intensity, vertical field strength, and magnetic inclination of the dark structures are intermediate between those of the umbra and penumbra. And a strong LB formed in the umbra, which originated from the intrusion of neighboring penumbral filaments. With the formation of an LB, the total magnetic flux in the whole penumbra decreased, and a penumbra sector of the sunspot rapidly disappeared on one side of the LB. After performing a partition analysis of the penumbra, it was found that the decay rate in this region of the penumbra sector is significantly accelerated after the appearance of an outward motion of magnetic flux along the LB. The area of this penumbra sector decreased from 21–16 MSH in 4 hr. The reduction in area in this penumbra sector is accompanied by a large decay rate of the magnetic flux,  $2.5 \times 10^{19} \text{ Mx hr}^{-1}$ . These results suggest that the rapid decay of the penumbra sector is associated with the LB. The appearance of dark structures in the penumbra and the strong LB in the umbra may offer a hint that the origin of massive flux migration from the sunspot umbra may have accelerated the decay of the sunspot. **15-17 Sep 2017**

## **Coronal Rain in Randomly Heated Arcades**

Xiaohong Li<sup>1</sup>, Rony Keppens<sup>1</sup>, and Yuhao Zhou<sup>1</sup>  
2022 ApJ 926 216

<https://iopscience.iop.org/article/10.3847/1538-4357/ac41cd/pdf>

Adopting the MPI-AMRVAC code, we present a 2.5-dimensional magnetohydrodynamic simulation, which includes thermal conduction and radiative cooling, to investigate the formation and evolution of the coronal rain phenomenon. We perform the simulation in initially linear force-free magnetic fields that host chromospheric, transition-region, and coronal plasma, with turbulent heating localized on their footpoints. Due to thermal instability, condensations start to occur at the loop top, and rebound shocks are generated by the siphon inflows. Condensations fragment into smaller blobs moving downwards, and as they hit the lower atmosphere, concurrent upflows are triggered. Larger clumps show us clear coronal rain showers as dark structures in synthetic EUV hot channels and as bright blobs with cool cores in the 304 Å channel, well resembling real observations. Following coronal rain dynamics for more than 10 hr, we carry out a statistical study of all coronal rain blobs to quantify their widths, lengths, areas, velocity distributions, and other properties. The coronal rain shows us continuous heating–condensation cycles, as well as cycles in EUV emissions. Compared to the previous studies adopting steady heating, the rain happens faster and in more erratic cycles. Although most blobs are falling downward, upward-moving blobs exist at basically every moment. We also track the movement of individual blobs to study their dynamics and the forces driving their movements. The blobs have a prominence–corona transition-region-like structure surrounding them, and their movements are dominated by the pressure evolution in the very dynamic loop system.

## **The Decay of $\alpha$ -configuration Sunspots**

Qiaoling Li<sup>1,2</sup>, Li Zhang<sup>2</sup>, Xiaoli Yan<sup>3,4</sup>, Jincheng Wang<sup>3,4,5</sup>, Defang Kong<sup>3,4</sup>, Liheng Yang<sup>3,4</sup>, and Zhike Xue<sup>3,4</sup>  
2021 ApJ 913 147

<https://doi.org/10.3847/1538-4357/abfa1b>

To better understand the decay of different types of sunspots, we studied the decay of eight  $\alpha$ -configuration sunspots by using the data that were acquired by the Helioseismic and Magnetic Imager on board the Solar Dynamic Observatory. We followed their decay for about four days and analyzed the evolution of their photospheric area and magnetic field parameters. We found that the area and total magnetic flux of  $\alpha$  sunspots show a near-linear decrease during their decay. Meanwhile, the area decay rate of an individual sunspot is not constant. The area decay of a sunspot can be divided into two stages, a slow and a rapid decay process. Moreover, according to the difference of the area decay of the penumbra and umbra, the  $\alpha$  sunspots decay can be classified in three ways: the penumbra and umbra decay synchronously, the penumbra decays first, and the umbra decays first. In addition, the flux decay of the penumbra is lagging behind the decay of the penumbral area. This finding suggests that the vertical magnetic field of the sunspot penumbra increases significantly in the early stage of sunspot decay.

## **Comparison of Synoptic Maps and PFSS Solutions for The Declining Phase of Solar Cycle 24**

Huichao Li , Xueshang Feng , Fengsi Wei

JGR Volume126, Issue3 March 2021 e2020JA028870

<https://doi.org/10.1029/2020JA028870>

<https://agupubs.onlinelibrary.wiley.com/doi/epdf/10.1029/2020JA028870>

The global distributions of photospheric magnetic field are routinely provided by synoptic maps, which often serve as fundamental observational input for coronal and heliospheric models. In this paper, we compare synoptic maps and PFSS-derived magnetic field results obtained during 2017/12/06–2018/12/06, a period at the declining phase of solar cycle 24. We use four kinds of synoptic maps, the Helioseismic and Magnetic Imager (HMI) maps, the Air Force Data Assimilative Photospheric Flux Transport (ADAPT) maps, the Global Oscillation Network Group (GONG) maps with their zero-point uncertainty corrected (GONGz maps) or uncorrected (GONGb maps). Qualitatively similarity among the four maps are found in the low-latitude region, but the polar fields have notable differences. While the polar fields of HMI, ADAPT and GONGz maps are unipolar and relative stable in large scale, those of the GONGb maps are variable. The PFSS results of HMI, ADAPT, and GONGz compare reasonably with coronal remote observations and near-Earth in situ data, and the HMI maps perform slightly better. There is generally no significant difference among results of the 12 ADAPT ensemble maps, but exceptions are also found. The PFSS results of GONGb maps deviate from observation significantly. The deviations are attributed to the problematic polar field, and the source of the problem may be the zero-point uncertainty of the magnetograms. As GONGb maps perform well in the declining phase of solar cycle 23, results in this study highlight the importance of continuous assessment of synoptic map data quality.

### Small-scale Bright Blobs Ejected from a Sunspot Light Bridge

Fuyu Li<sup>1</sup>, Yajie Chen<sup>1,2</sup>, Yijun Hou<sup>3</sup>, Hui Tian<sup>1,3</sup>, Xianyong Bai

2021 ApJ 908 201

<https://doi.org/10.3847/1538-4357/abd322>

<https://arxiv.org/pdf/2102.13545>

Light bridges (LBs) are bright lanes that divide an umbra into multiple parts in some sunspots. Persistent oscillatory bright fronts at a temperature of  $\sim 105$  K are commonly observed above LBs in the 1400/1330 Å passbands of the Interface Region Imaging Spectrograph (IRIS). Based on IRIS observations, we report small-scale bright blobs ejected from the oscillating bright front above a light bridge. Some of these blobs reveal a clear acceleration, whereas the others do not. The average speed of these blobs projected onto the plane of sky is  $71.7 \pm 14.7$  km s<sup>-1</sup>, with an initial acceleration of  $1.9 \pm 1.3$  km s<sup>-2</sup>. These blobs normally reach a projected distance of 3–7 Mm from their origin sites. They have an average projected area of  $0.57 \pm 0.37$  Mm<sup>2</sup>. The blobs were also detected in multiple extreme-ultraviolet passbands of the Atmospheric Imaging Assembly on board the Solar Dynamics Observatory, but not in the H $\alpha$  images taken by the New Vacuum Solar Telescope. The typical temperature and electron density of these blobs are around  $10^{5.47}$  K and  $10^{9.7}$  cm<sup>-3</sup>, respectively. The estimated kinetic and thermal energies are on the order of  $10^{22.8}$  erg and  $10^{23.3}$  erg, respectively. These small-scale blobs appear to show three different types of formation processes. They are possibly triggered by induced reconnection or release of enhanced magnetic tension due to interaction of adjacent shocks, local magnetic reconnection between emerging magnetic bipoles on the light bridge and surrounding unipolar umbral fields, and plasma acceleration or instability caused by upward shocks, respectively. **15 Oct 2014**

### Infrared diagnostics of the solar magnetic field with Mg I 12 μm lines: forward-model results

[Xin Li](#), [YongLiang Song](#), [H. Uitenbroek](#), [Xiao Yang](#), [XianYong Bai](#), [YuanYong Deng](#)

A&A 646, A79 2020

<https://arxiv.org/pdf/2012.08912.pdf>

<https://doi.org/10.1051/0004-6361/202039365>

<https://www.aanda.org/articles/aa/pdf/2021/02/aa39365-20.pdf>

The Mg I 12.32 and 12.22 μm lines are a pair of emission lines that present a great advantage for accurate solar magnetic field measurement. They potentially contribute to the diagnosis of solar atmospheric parameters through their high magnetic sensitivity. The goal of this study is to understand the radiation transfer process of these lines in detail and explore the ability of magnetic field diagnosis in the infrared. We calculated the Stokes profiles and response functions of the two Mg I 12 μm lines based on one-dimensional solar atmospheric models using the Rybicki-Hummer (RH) radiative transfer code. The integration of these profiles with respect to the wavelength was used to generate calibration curves related to the longitudinal and transverse fields. The traditional single-wavelength calibration curve based on the weak-field approximation was also tested to determine if it is suitable for the infrared. The 12.32 μm line is more suitable for a magnetic field diagnosis because its relative emission intensity and polarization signal are stronger than that of the 12.22 μm line. The result from the response functions illustrates that the derived magnetic field and velocity with 12.32 μm line mainly originate from the height of 450 km, while that for the temperature is about 490 km. The calibration curves obtained by the wavelength-integrated method show a nonlinear distribution. For the Mg I 12.32 μm line, the longitudinal (transverse) field can be effectively inferred from Stokes V/I (Q/I and U/I) in the linear range below  $\sim 600$  G ( $\sim 3000$  G) in quiet regions and below  $\sim 400$  G ( $\sim 1200$  G) in penumbrae. Within the given linear range, the method is a supplement to the magnetic field calibration when the Zeeman components are incompletely split.

## Doppler shift oscillations of a sunspot detected by CYRA and IRIS

[D. Li](#), [X. Yang](#), [X. Y. Bai](#), [J. T. Su](#), [Z. J. Ning](#), [W. Cao](#), [Y. Y. Deng](#)

A&A 642, A231 2020

<https://arxiv.org/pdf/2009.06942.pdf>

<https://doi.org/10.1051/0004-6361/202039007>

<https://sci-hub.st/https://www.aanda.org/articles/aa/abs/2020/10/aa39007-20/aa39007-20.html>

Context. The carbon monoxide (CO) molecular line at around 46655 Å in solar infrared spectra is often used to investigate the dynamic behavior of the cold heart of the solar atmosphere, i.e., sunspot oscillation, especially at the sunspot umbra. Aims. We investigated sunspot oscillation at Doppler velocities of the CO 7-6 R67 and 3-2 R14 lines that were measured by the Cryogenic Infrared Spectrograph (CYRA), as well as the line profile of Mg II k line that was detected by the Interface Region Imaging Spectrograph (IRIS). Methods. A single Gaussian function is applied to each CO line profile to extract the line shift, while the moment analysis method is used for the Mg II k line. Then the sunspot oscillation can be found in the time-distance image of Doppler velocities, and the quasi-periodicity at the sunspot umbra are determined from the wavelet power spectrum. Finally, the cross-correlation method is used to analyze the phase relation between different atmospheric levels. Results. At the sunspot umbra, a periodicity of roughly 5 min is detected at the Doppler velocity range of the CO 7-6 R67 line that formed in the photosphere, while a periodicity of around 3 min is discovered at the Doppler velocities of CO 3-2 R14 and Mg II k lines that formed in the upper photosphere or the temperature minimum region and the chromosphere. A time delay of about 2 min is measured between the strong CO 3-2 R14 line and the Mg II k line. Conclusions. Based on the spectroscopic observations from the CYRA and IRIS, the 3 min sunspot oscillation can be spatially resolved in the Doppler shifts. It may come from the upper photosphere or the temperature minimum region and then propagate to the chromosphere, which might be regarded as a propagating slow magnetoacoustic wave. **2017 September 15**

## The formation and decay of sunspot penumbra in Active Region NOAA 12673

Qiaoling [Li](#), [Xiaoli Yan](#), [Jincheng Wang](#), [Defang Kong](#), [Zhike Xue](#), [Liheng Yang](#)

ApJ 886 149 2019

<https://arxiv.org/pdf/1910.10394.pdf>

<https://doi.org/10.3847/1538-4357/ab4f84>

To better understand the formation and decay of sunspot penumbra, we studied the evolution of sunspots in the three regions of the active-region NOAA 12673 in detail. The evolution of sunspots in the three regions were all involved in the interaction of two magnetic field systems: the pre-existing magnetic field system and the later emerging magnetic field system. Through analyzing the photospheric magnetic field properties, it is found that the formation of the penumbra originated from the newly emerging magnetic bipole that were trapped in the photosphere. The change of magnetic fields in penumbra from horizontal to vertical can cause the disappearance of penumbra. The transformation of the magnetic field between the umbra and the penumbra is found and the outward moat flow around sunspot gradually decreased and vanished during the decay of sunspot. In addition, we found that the mean longitudinal magnetic strength in penumbra decreased and the mean transverse magnetic strength in penumbra increased with the increasing penumbral area during the formation of sunspots. However, during the decay of sunspots, the mean longitudinal magnetic strength in penumbra increased and the mean transverse magnetic strength in penumbra decreased with the decreasing penumbral area. Comparatively, the dependence of the area and the mean transverse/longitudinal magnetic field strength in umbra is not remarkable. These results reveal that the formation and decay process of umbra are different with penumbra. **2-6 Sept 2017**

## Repeated Coronal Condensations Caused by Magnetic Reconnection between Solar Coronal Loops

Leping [Li](#)<sup>1,2,3</sup>, Hardi Peter<sup>4</sup>, Lakshmi Pradeep Chitta<sup>4</sup>, Jun Zhang<sup>1,3</sup>, Jiangtao Su<sup>1,3</sup>, Hongqiang Song<sup>2</sup>, Yijun Hou<sup>1,3</sup>, and Chun Xia<sup>5</sup>

2019 ApJ 884 34

<https://doi.org/10.3847/1538-4357/ab4134>

We recently presented coronal condensations, caused by magnetic reconnection (MR) between coronal loops from extreme ultraviolet observations, over the course of one day, on **2012 January 19**. In this paper, by investigating the loops over an extended period of time from January 16 to 20, we present a case for repeated coronal condensations caused by repeated MR between them. In these five days, MR between higher-lying open loops and lower-lying closed loops occurs repeatedly, forming magnetic dips in the higher-lying open loops. During the MR process, cooling and condensation of coronal plasma occur repeatedly. Early on January 16, cooling, but not condensation, of coronal plasma happens. Later, condensation appears at the edge of the dips and falls down along the loops as coronal rains. On January 17, a similar condensation happens at the edge of the higher-lying dips and falls down along the loops. However, another condensation appears in the lower-lying dips and rains down across them. From January 18 to 19, multiple condensations mostly occur at the edge of the dips and fall down both along the loops and across the dips. On January 20, five condensations sequentially appear and rain down across the dips. Overall, 15

condensation events occur in five days, lasting from 0.5 to 15.6 hr. We suggest that the formation of coronal condensations by MR between loops is common in the solar corona. The repeated MR between loops thus plays an essential role in the mass cycle of coronal plasma by initiating repeated catastrophic cooling and condensation.

### **High-resolution Observation of Moving Magnetic Features**

Qin [Li](#)<sup>1</sup>, Na Deng<sup>1,2</sup>, Ju Jing<sup>1,2</sup>, Chang Liu<sup>1,2</sup>, and Haimin Wang

2019 ApJ 876 129

[sci-hub.se/10.3847/1538-4357/ab18aa](https://doi.org/10.3847/1538-4357/ab18aa)

Moving magnetic features (MMFs) are small magnetic elements moving almost radially away from sunspots toward the boundary of moat regions. They are mostly seen during the decay phase of a sunspot. Here we present a high-resolution observation of MMFs around a sunspot in NOAA AR 12565 on **2016 July 14** using the the 1.6 m Goode Solar Telescope (GST) at Big Bear Solar Observatory. The spectropolarimetric measurements of photospheric magnetic field are obtained from GST's newly commissioned Near Infra-Red Imaging Spectropolarimeter at the Fe i 1.56  $\mu\text{m}$  line. The statistical study of physical properties of identified fine-scale MMFs (i.e., size, lifetime, inclination, horizontal velocity, and flux) is presented. The origin of the minority polarity flux in the sunspot is determined. Same as the majority polarity flux, the minority polarity flux can originate from mid-penumbra with highly inclined fields. The role of MMFs in both polarities in the flux evolution of the sunspot is speculated, as they can both contribute to the sunspot evolution.

### **A Systematic Study of Hale and Anti-Hale Sunspot Physical Parameters**

Jing [Li](#)

2018 ApJ 867 89

[sci-hub.tw/10.3847/1538-4357/aae31a](https://doi.org/10.3847/1538-4357/aae31a)

We present a systematic study of sunspot physical parameters using full-disk magnetograms from the Michelson Doppler Imager/Solar and Heliospheric Observatory and the Helioseismic and Magnetic Imager/Solar Dynamic Observatory. Our aim is to use uniform data sets and analysis procedures to characterize the sunspots, paying particular attention to the differences and similarities between "Hale" and "anti-Hale" spots. Included are measurements of the magnetic tilt angles, areas, fluxes, and polarity pole separations for 4385 sunspot groups in Cycles 23 and 24 each measured, on average, at  $\sim 66$  epochs centered on meridian crossing. The sunspots are classified as either "Hale" or "anti-Hale," depending on whether their polarities align or anti-align with Hale's hemispheric polarity rule. We find that (1) the "anti-Hale" sunspots constitute a fraction  $(8.1 \pm 0.4)\%$  of all sunspots, and this fraction is the same in both hemispheres and cycles; (2) "Hale" sunspots obey Joy's law in both hemispheres and cycles but "anti-Hale" sunspots do not—three equivalent forms of Joy's law are derived:  $\gamma = (0.39 \pm 0.06) \phi$ , and  $\gamma = (0.39 \pm 0.06) \phi$ , where  $\gamma$  is the tilt angle and  $\phi$  is the heliospheric latitude; (3) the average Hale sunspot tilt angle is  $11.5^\circ$  and (4) the tilt angles, magnetic fluxes, and pole separations of sunspots are interrelated, with larger fluxes correlated with larger pole separations and smaller tilt angles. We present empirical relations between these quantities. Cycle 24 is a much weaker cycle than Cycle 23 in sunspot numbers, cumulative magnetic flux, and average sunspot magnetic flux. The "anti-Hale" sunspots are also much weaker than "Hale" sunspots in those parameters, but they share similar magnetic flux distributions and average latitudes. We characterize the two populations, and aim to shed light on the origin of "anti-Hale" sunspots.

### **Solar Coronal Modeling by Path-conservative HLLEM Riemann Solver**

Caixia [Li](#)<sup>1,2</sup>, Xueshang Feng<sup>1,2,3</sup>, Changqing Xiang<sup>1</sup>, Man Zhang<sup>1</sup>, Huichao Li<sup>1,2</sup>, and Fengsi Wei<sup>1</sup>,

2018 ApJ 867 42

In this paper, we employ a path-conservative HLLEM finite-volume method (FVM) to solve the solar wind magnetohydrodynamics (MHD) systems of extended generalized Lagrange multiplier (EGLM) formulation with Galilean invariance (G-EGLM MHD equations). The governing equations of single-fluid solar wind plasma MHD are advanced by using a one-step MUSCL-type time integration with the logarithmic spacetime reconstruction. The code is programmed in FORTRAN language with Message Passing Interface parallelization in spherical coordinates with a six-component grid system. Then, the large-scale solar coronal structures during Carrington rotations (CRs) 2048, 2069, 2097, and 2121 are simulated by inputting the line-of-sight magnetic field provided by the Global Oscillation Network Group (GONG). These four CRs belong to the declining, minimum, rising, and maximum phases of solar activity. Numerical results basically generate the observed characteristics of structured solar wind and thus show the code's capability of simulating solar corona with complex magnetic topology.

### **The Formation of a Sunspot Penumbra Sector in Active Region NOAA 12574**

Qiaoling [Li](#)<sup>1,2</sup>, Xiaoli Yan<sup>1,3</sup>, Jincheng Wang<sup>1,2</sup>, DeFang Kong<sup>1,3</sup>, Zhike Xue<sup>1,3</sup>, Liheng Yang<sup>1,3</sup>, and Wenda Cao<sup>4</sup>

2018 ApJ 857 21

<http://sci-hub.tw/http://iopscience.iop.org/0004-637X/857/1/21/>

We present a particular case of the formation of a penumbra sector around a developing sunspot in the active region NOAA 12574 on **2016 August 11** by using the high-resolution data observed by the New Solar Telescope at the Big Bear Solar Observatory and the data acquired by the Helioseismic and Magnetic Imager and the Atmospheric Imaging Assembly on board the Solar Dynamics Observatory satellite. Before the new penumbra sector formed, the developing sunspot already had two umbrae with some penumbral filaments. The penumbra sector gradually formed at the junction of two umbrae. We found that the formation of the penumbra sector can be divided into two stages. First, during the initial stage of penumbral formation, the region where the penumbra sector formed always appeared blueshifted in a Dopplergram. The area, mean transverse magnetic field strength, and total magnetic flux of the umbra and penumbra sector all increased with time. The initial penumbral formation was associated with magnetic emergence. Second, when the penumbra sector appeared, the magnetic flux and area of the penumbra sector increased after the umbra's magnetic flux and area decreased. These results indicate that the umbra provided magnetic flux for penumbral development after the penumbra sector appeared. We also found that the newly formed penumbra sector was associated with sunspot rotation. Based on these findings, we suggest that the penumbra sector was the result of the emerging flux that was trapped in the photosphere at the initial stage of penumbral formation, and when the rudimentary penumbra formed, the penumbra sector developed at the cost of the umbra.

### **Polarization of Coronal Forbidden Lines**

Hao **Li**<sup>1,2</sup>, Egidio Landi Degl'Innocenti<sup>3</sup>, and Zhongquan Qu<sup>1</sup>

2017 ApJ 838 69

Since the magnetic field is responsible for most manifestations of solar activity, one of the most challenging problems in solar physics is the diagnostics of solar magnetic fields, particularly in the outer atmosphere. To this end, it is important to develop rigorous diagnostic tools to interpret polarimetric observations in suitable spectral lines. This paper is devoted to analyzing the diagnostic content of linear polarization imaging observations in coronal forbidden lines. Although this technique is restricted to off-limb observations, it represents a significant tool to diagnose the magnetic field structure in the solar corona, where the magnetic field is intrinsically weak and still poorly known. We adopt the quantum theory of polarized line formation developed in the framework of the density matrix formalism, and synthesize images of the emergent linear polarization signal in coronal forbidden lines using potential-field source-surface magnetic field models. The influence of electronic collisions, active regions, and Thomson scattering on the linear polarization of coronal forbidden lines is also examined. It is found that active regions and Thomson scattering are capable of conspicuously influencing the orientation of the linear polarization. These effects have to be carefully taken into account to increase the accuracy of the field diagnostics. We also found that linear polarization observation in suitable lines can give valuable information on the long-term evolution of the magnetic field in the solar corona.

### **Mapping magnetic field lines between the Sun and Earth†**

B. **Li**, Iver H. Cairns, J.T. Gosling, G. Steward, M. Francis, D. Neudegg, H. Schulte in den Bäumen, P.R. Player, A.R. Milne

JGR 2016

Magnetic field topologies between the Sun and Earth are important for the connectivity to Earth of solar suprathermal particles, e.g., solar energetic particles and beam electrons in type III solar radio bursts. An approach is developed for mapping large-scale magnetic field lines near the solar equatorial plane, using near-Earth observations and a solar wind model with nonzero azimuthal magnetic field at the source surface. Unlike Parker's spiral model, which restricts the in-ecliptic angle  $\Phi_B$  in the Geocentric Solar Ecliptic coordinates to  $(90^\circ - 180^\circ, 270^\circ - 360^\circ)$ , and so is unable to predict field configurations for the other  $\Phi_B$  values frequently observed in the solar wind, our approach can account for all the observed  $\Phi_B$  values. A set of predicted maps show that near both minimal and maximal solar activity the field lines are typically open and that loops with both ends either connected to or disconnected from the Sun are relatively rare. The open field lines, nonetheless, often do not closely follow the Parker spiral, being less or more tightly wound, or strongly azimuthally or radially oriented, or inverted. The time-varying classes, e.g., bidirectional electrons, of suprathermal electron pitch angle distributions (PADs) at 1 AU are predicted from the mapped field line configurations and compared with Wind observations for two solar rotations, one each near solar minimum and solar maximum. PAD predictions by our approach agree quantitatively ( $\approx 90\%$ ) with the PAD observations and outperform (by  $\approx 20\%$ ) PAD predictions using Parker's model.

### **Statistical properties of the Bipolar Magnetic Regions**

Dong **Li**

Research in Astron. Astrophys. 2016

<https://arxiv.org/pdf/1612.02610v1.pdf>

Using the observations from Michelson Doppler Imager (MDI) onboard Solar and Heliospheric Observatory (SOHO), we develop a computational algorithm to automatically identify the bipolar magnetic regions (BMRs) in the active regions, and then study their statistical properties. The individual magnetic (positive or negative) pole of the BMR is determined from the region with an absolute strength above 55 G and with an area above 250 pixel<sup>2</sup> (495 Mm<sup>2</sup>), while a BMR is identified as a pair of positive and negative poles with a shortest area-weight distance between them. Based on this method, 2234 BMRs are identified from the MDI synoptic magnetograms between the Carrington Rotation 1909 (1996 May 06) and 2104 (2010 December 10). 1005 of them are located in the northern hemisphere, while the other 1229 are in the southern hemisphere. We find that the BMR parameters (e.g., latitudes, separations, fragments, and strength) are similar to those of active regions (ARs). Moreover, based on the maximum likelihood estimation (MLE) method, the frequency distributions of these BMRs occurrence as functions of area size and magnetic flux exhibit a power-law behavior. We also find that their orientation angles follow the Hale's Polarity Laws and deviate slightly to the solar equator direction. Consistent with the previous findings, we obtain the orientation angles dependence on the latitudes for the normal BMRs during the 23rd solar cycle. The north-south asymmetry of these BMRs is also detected here.

## Formation of Pores Associated with the Inflow of Moving Magnetic Features

Xiaobo Li<sup>1,2</sup>, Zhiliang Yang<sup>1</sup>, and Hongqi Zhang

2015 ApJ 807 160

We investigate the formation of pores in NOAA AR 10930 associated with the inflow of moving magnetic features (MMFs) using simultaneous Hinode/Solar Optical Telescope filtergrams and magnetograms. The main results are outlined as follows: (1) the existence of MMFs around pores is a fairly common phenomenon. Around the four innate and one residue pores investigated, there are obvious inflows of MMFs during the pores' growth phase. (2) The observed magnetic flux transport conveyed by MMFs is strongly correlated with the change in the pore's flux content, and therefore reflects the pore's growth and decay. The concentration and dissolution of the pores are direct results of the local convergence and convection of sunspots' magnetic outflow. (3) The most common source of MMF flows into pores are produced near sunspots and move along the connection lines between the sunspots' penumbrae and the pores. These monopolar and bipolar magnetic elements are either fragments from the penumbra or continuations of penumbral fibrils. Pores also merge dissociated elements and receive flows produced by small-scale bipolar emergence. MMF inflows that diminish a pore's magnetic flux often trigger chromospheric bright points. (4) In their decay phase, the pores release outflows of magnetic elements. The distribution of flows around pores is asymmetrical: the inflow is concentrated on the side facing the parent sunspot, while the outflow is generally concentrated on the opposite side. A pore's outflow is also part of the process of decomposing and removing of the active region's magnetic field.

## Diagnostics of Ellerman Bombs with High-resolution Spectral Data

Z. Li, C. Fang, Y. Guo, P. F. Chen, Z. Xu, W. Cao

RAA 2015

<http://arxiv.org/pdf/1504.02538v1.pdf>

Ellerman bombs (EBs) are tiny brightenings often observed near sunspots. The most impressive characteristic of the EB spectra is the two emission bumps in both wings of the H $\alpha$  and  $\text{Ca II}$  8542  $\text{\AA}$  lines. High-resolution spectral data of three small EBs were obtained on **2013 June 6** with the largest solar telescope, the 1.6 meter New Solar Telescope (NST), at the Big Bear Solar Observatory. The characteristics of these EBs are analyzed. The sizes of the EBs are in the range of 0.3 $\text{arcsec}$ –0.8 $\text{arcsec}$  and their durations are only 3–5 minutes. Our semi-empirical atmospheric models indicate that the heating occurs around the temperature minimum region with a temperature increase of 2700–3000 K, which is surprisingly higher than previously thought. The radiative and kinetic energies are estimated to be as high as  $5 \times 10^{25}$ – $3.0 \times 10^{26}$  ergs despite the small size of these EBs. Observations of the magnetic field show that the EBs appeared just in a parasitic region with mixed polarities and accompanied by mass motions. Nonlinear force-free field extrapolation reveals that the three EBs are connected with a series of magnetic field lines associated with bald patches, which strongly implies that these EBs should be produced by magnetic reconnection in the solar lower atmosphere. According to the lightcurves and the estimated magnetic reconnection rate, we propose that there is a three phase process in EBs: pre-heating, flaring and cooling phases.

## Conversion from mutual helicity to self-helicity observed with IRIS

Leping Li, Hardi Peter, Feng Chen, Jun Zhang

A&A, 570, A93 2014

<http://arxiv.org/pdf/1410.5597v1.pdf>

Context. In the upper atmosphere of the Sun observations show convincing evidence for crossing and twisted structures, which are interpreted as mutual helicity and self-helicity.

**Aims.** We use observations with the new Interface Region Imaging Spectrograph (IRIS) to show the conversion of mutual helicity into self-helicity in coronal structures on the Sun.

**Methods.** Using far UV spectra and slit-jaw images from IRIS and coronal images and magnetograms from SDO, we investigated the evolution of two crossing loops in an active region, in particular, the properties of the Si IV line profile in cool loops.

**Results.** In the early stage two cool loops cross each other and accordingly have mutual helicity. The Doppler shifts in the loops indicate that they wind around each other. As a consequence, near the crossing point of the loops (interchange) reconnection sets in, which heats the plasma. This is consistent with the observed increase of the line width and of the appearance of the loops at higher temperatures. After this interaction, the two new loops run in parallel, and in one of them shows a clear spectral tilt of the Si IV line profile. This is indicative of a helical (twisting) motion, which is the same as to say that the loop has self-helicity.

**Conclusions.** The high spatial and spectral resolution of IRIS allowed us to see the conversion of mutual helicity to self-helicity in the (interchange) reconnection of two loops. This is observational evidence for earlier theoretical speculations. **2013-09-27**

## **FINE-SCALE STRUCTURES OF FLUX ROPES TRACKED BY ERUPTING MATERIAL**

Ting [Li](#) and Jun Zhang

**2013** ApJ 770 L25

We present Solar Dynamics Observatory observations of two flux ropes tracked out by material from a surge and a failed filament eruption on **2012 July 29 and August 4**, respectively. For the first event, the interaction between the erupting surge and a loop-shaped filament in the east seems to "peel off" the filament and add bright mass into the flux rope body. The second event is associated with a C-class flare that occurs several minutes before the filament activation. The two flux ropes are, respectively, composed of  $85 \pm 12$  and  $102 \pm 15$  fine-scale structures, with an average width of about  $1.''6$ . Our observations show that two extreme ends of the flux rope are rooted in opposite polarity fields and each end is composed of multiple footpoints (FPs) of fine-scale structures. The FPs of the fine-scale structures are located at network magnetic fields, with magnetic fluxes from  $5.6 \times 10^{18}$  Mx to  $8.6 \times 10^{19}$  Mx. Moreover, almost half of the FPs show converging motion of smaller magnetic structures over 10 hr before the appearance of the flux rope. By calculating the magnetic fields of the FPs, we deduce that the two flux ropes occupy at least  $4.3 \times 10^{20}$  Mx and  $7.6 \times 10^{20}$  Mx magnetic fluxes, respectively.

## **A Test on Two Codes for Extrapolating Solar Linear Force-free Magnetic Fields**

Yiwei [Li](#) · Guoxiang Song · Junlin Li

Solar Phys (2009) 260: 109–124

We evaluate the performances of two newly-implemented codes for extrapolating the solar linear force-free magnetic fields, by measuring their quantified responses to the lower boundary vector field data on a finite region using analytical models. The codes are based on two boundary integral formulas with different mechanisms in utilizing the transverse boundary field: the first one only utilizes the transverse boundary field to derive the value of the force-free parameter, while the other one explicitly utilizes the whole transverse boundary field, in addition to the vertical field component. Studies on the test cases show that both of the codes could reproduce the analytical model fields with reasonable accuracy within the valid domain, provided a sufficient amount of data is available at the lower boundary. The code utilizing explicitly all three components of the boundary field shows generally better performances and requires a smaller boundary-data area in order to achieve the same degree of accuracy in the metric quantities such as the normalized vector error, vector correlation, vector angular difference, and magnetic energy; however, the accuracy in the divergence-free metric and especially the force-free metric are less ideal.

## **Imaging-polarimetric properties of the white-light inner corona during the 2017 total solar eclipse**

[Yu Liang](#), [Zhongquan Qu](#), [Lei Hao](#), [Zhi Xu](#), [Yue Zhong](#)

Monthly Notices of the Royal Astronomical Society, 518, Issue 2, January **2023**, Pages 1776–1788,

<https://doi.org/10.1093/mnras/stac3183>

<https://watermark.silverchair.com/stac3183.pdf>

We carried out the polarimetric observation of the white-light inner corona during the 2017 total solar eclipse in the United States. Degree of linear polarization (DLP) of the inner corona is obtained by the modulated polarized data. The electron density is inferred from the normalized white-light polarization brightness data. According to the observational results, we find that: (1) The DLP of the white-light corona increases with the height, peaking at

approximately  $1.3\sim 1.35R_{\odot}$  and then slightly decreases. In the coronal streamer region, DLP peaks at approximately  $1.35 R_{\odot}$  and its value is about 40 per cent, whereas in the coronal hole region, DLP peaks at approximately  $1.3 R_{\odot}$  and its value is about 35 per cent. (2) The azimuth angle of polarization  $\sin(2\chi)$  is symmetrical around the solar disk center. It can be easily found that the gradients of the angle of polarization, representing the direction of oscillations of the electric vector  $E$ , are tangential. Above the active region, the DLP distribution changes significantly, whereas the azimuth distribution is stable. This proves that the polarization of white-light corona is mainly caused by scattering polarization. (3) The electron density and the K-corona have similar distributions of properties. Electron density decreases from  $6 \times 10^7 \text{cm}^{-3}$  to  $2 \times 10^6 \text{cm}^{-3}$ , whereas the height increases from  $1.1R_{\odot}$  to  $1.85R_{\odot}$ . (4) An interesting finding is that, in the cavity region, there may be other polarization-induced mechanisms besides scattering, which can affect the value of the white-light DLP.

## **Probing Magnetic Fields at the Base of the Solar Convection Zone with Meridional Flows**

Zhi-Chao [Liang](#) and Dean-Yi Chou

2015 ApJ 809 150

Solar magnetic fields are responsible for most of the activities on the Sun. Many theories predict that it is generated by a dynamo near the base of the convection zone (BCZ), located at  $0.71R_{\odot}$ . In this study, we use the solar-cycle variations of the meridional flow to probe magnetic field variations near the BCZ. A helioseismic time-distance method is used to measure the travel-time difference between opposite directions in meridional planes, which reflects the meridional flow at different depths. Two systematic effects, the surface magnetic effect and the center-to-limb effect, are removed. Using Solar and Heliospheric Observatory/Michelson Doppler Imager data, we measure the latitudinal distribution of travel-time difference for different travel distances, corresponding to meridional flow signals in the solar interior down to  $0.54R_{\odot}$ , over 15 years, including two solar minima and one maximum. The travel-time differences at the maximum and the minimum behave differently in three different depth ranges. The travel-time difference at the maximum is greater than that at the minimum above the BCZ, while it is smaller around the BCZ; both are close to zero below the BCZ. The difference in the travel-time difference between the maximum and the minimum changes about 0.1 s from the region above the BCZ to the region around the BCZ, corresponding to a change in flow velocity of about  $10 \text{ m s}^{-1}$  around the BCZ. We tend to attribute this change in the meridional flow to the variation in the magnetic field from the minimum to the maximum near the BCZ.

## **Simulating White Light Images of Coronal Structures for WISPR/Parker Solar Probe: Effects of the Near-Sun Elliptical Orbit**

P. [Liewer](#), A. Vourlidas, A. Thernisien, J. Qiu, P. Penteadó, G. Nisticò, R. Howard, V. Bothmer

[Solar Physics](#) July 2019, 294:93

[sci-hub.se/10.1007/s11207-019-1489-4](https://doi.org/10.1007/s11207-019-1489-4)

The three-to-five-month elliptical orbit of Parker Solar Probe (PSP), approaching within 10 solar radii of the Sun, will allow the Wide-field Imager for Solar Probe (WISPR) to view the corona with unprecedented spatial resolution from multiple viewpoints. WISPR has a wide fixed angular field of view, extending from  $13.5^{\circ}$  to  $108^{\circ}$  from the Sun and approximately  $50^{\circ} \times 50^{\circ}$  in the transverse direction, but the physical extent of the imaged coronal region varies directly with the distance of the spacecraft from the Sun. In a solar encounter period of approximately 10 days around perihelion, PSP covers over  $100 - 200^{\circ}$  of heliographic longitude and the distance from the Sun varies by a factor of two to five. In this paper, we use synthetic white-light images to study the effects of the rapid elliptical orbit on the images that can be anticipated for WISPR's observations. We find that sequences of images can help identify coronal density features that will be sampled by in-situ instruments. We also find that the multiple viewpoints, provided by the rapid motion near perihelion, can be used to obtain three-dimensional information on the coronal density features.

## **Testing the Reliability of Predictions of Far-Side Active Regions from Helioseismology Using STEREO Far-Side Observations of Solar Activity**

P. C. [Liewer](#), I. González Hernández, J. R. Hall, C. Lindsey, X. Lin

[Solar Physics](#), October 2014, Volume 289, Issue 10, pp 3617-3640

We test the reliability of helioseismic far-side active-region predictions, made using Dopplergrams from both the Helioseismic and Magnetic Imager (HMI) onboard the Solar Dynamics Observatory (SDO) and the Global Oscillation Network Group (GONG), by comparison with far-side observation of solar activity from the Solar TERrestrial RELations Observatory (STEREO). Both GONG and HMI produce seismic Carrington maps that show strong magnetic-field regions, labeling predictions of far-side active regions that have a probability  $\geq 70\%$ . By visual comparison of these prediction maps with STEREO extreme ultraviolet (EUV) Carrington maps, we determine whether or not solar activity, as evidenced as brightness in EUV, is observed at the predicted locations. We analyzed nine months of data from 2011 and 2012. For both GONG and HMI, we find that for approximately 90% of the active-region predictions, activity/brightness is observed in EUV at the predicted location. We also



investigated the success of GONG and HMI at predicting large active regions before they appear at the east limb as viewed from Earth. Of the 27 identified large east-limb active regions in the nine months of data analyzed, GONG predicted 15 (55 %) at least once within the week prior to Earth-side appearance and HMI predicted 13 (48 %). Based on the STEREO far-side EUV observations, we suggest that 9 of the 27 active regions were probably too weak to be predicted while on the far side. Overall, we conclude that HMI and GONG have similar reliability using the current data-processing procedures.

### **Detection of Opposite Magnetic Polarity in a Light Bridge: Its Emergence and Cancellation in Association with LB Fan-shaped Jets**

Eun-Kyung [Lim](#)<sup>1</sup>, Heesu Yang<sup>1</sup>, Vasył Yurchyshyn<sup>2</sup>, Jongchul Chae<sup>3</sup>, Donguk Song<sup>4</sup>, and Maria S. Madjarska<sup>3,5</sup>

2020 ApJ 904 84

<https://doi.org/10.3847/1538-4357/abc1e0>

Light bridges (LBs) are relatively bright structures that divide sunspot umbrae into two or more parts. Chromospheric LBs are known to be associated with various activities including fan-shaped jet-like ejections and brightenings. Although magnetic reconnection is frequently suggested to be responsible for such activities, not many studies present firm evidence to support the scenario. We carry out magnetic field measurements and imaging spectroscopy of an LB where fan-shaped jet-like ejections occur with co-spatial brightenings at their footpoints. We study LB fine structure and magnetic field changes using TiO images, Near-InfraRed Imaging Spectropolarimeter, and H $\alpha$  data taken by the 1.6 m Goode Solar Telescope. We detect magnetic flux emergence in the LB that is of opposite polarity to that of the sunspot. The new magnetic flux cancels with the pre-existing flux at a rate of  $5.6 \times 10^{18} \text{ Mx hr}^{-1}$ . Both the recurrent jet-like ejections and their base brightenings are initiated at the vicinity of the magnetic flux cancellation, and show apparent horizontal extension along the LB at a projected speed of up to  $18.4 \text{ km s}^{-1}$  to form a fan-shaped appearance. Based on these observations, we suggest that the fan-shaped ejections may have resulted from slipping reconnection between the new flux emerging in the LB and the ambient sunspot field.

### **FIRST SIMULTANEOUS DETECTION OF MOVING MAGNETIC FEATURES IN PHOTOSPHERIC INTENSITY AND MAGNETIC FIELD DATA**

Eun-Kyung [Lim](#), Vasył Yurchyshyn, and Philip Goode

2012 ApJ 753 89

The formation and the temporal evolution of a bipolar moving magnetic feature (MMF) was studied with high-spatial and temporal resolution. The photometric properties were observed with the New Solar Telescope at Big Bear Solar Observatory using a broadband TiO filter (705.7 nm), while the magnetic field was analyzed using the spectropolarimetric data obtained by Hinode. For the first time, we observed a bipolar MMF simultaneously in intensity images and magnetic field data, and studied the details of its structure. The vector magnetic field and the Doppler velocity of the MMF were also studied. A bipolar MMF with its positive polarity closer to the negative penumbra formed, accompanied by a bright, filamentary structure in the TiO data connecting the MMF and a dark penumbral filament. A fast downflow ( $\leq 2 \text{ km s}^{-1}$ ) was detected at the positive polarity. The vector magnetic field obtained from the full Stokes inversion revealed that a bipolar MMF has a U-shaped magnetic field configuration. Our observations provide a clear intensity counterpart of the observed MMF in the photosphere, and strong evidence of the connection between the MMF and the penumbral filament as a serpentine field.

### **Examining the Magnetic Field Strength and the Horizontal and Vertical Motions in an Emerging Active Region**

Chia-Hsien [Lin](#), Yu-Che Chen

Solar Phys. Volume 291, [Issue 3](#), pp 751-777 2016

<http://arxiv.org/pdf/1606.03811v1.pdf>

Earlier observational studies have used the time evolution of emerging magnetic flux regions at the photosphere to infer their subsurface structures, assuming that the flux structure does not change significantly over the near-surface layer. In this study, we test the validity of this assumption by comparing the horizontal and vertical motions of an emerging active region. The two motions would be correlated if the emerging structure is rigid. The selected active region (AR) NOAA 11645 is not embedded in detectable preexisting magnetic field. The observed horizontal motion is quantified by the separation of the two AR polarities and the width of the region. The vertical motion is derived from the magnetic buoyancy theory. Our results show that the separation of the polarities is fastest at the beginning with a velocity of  $\approx 4 \text{ Mmhr}^{-1}$  and decreases to  $\leq 1 \text{ Mmhr}^{-1}$  after the main growing phase of flux emergence. The derived thick flux-tube buoyant velocity is between 1 and 3  $\text{Mmhr}^{-1}$ , while the thin flux-tube approximation results in an unreasonably high buoyant velocity, consistent with the expectation that the approximation is inappropriate at the surface layer. The observed horizontal motion is not found to directly correlate with either the magnetic field strength or the derived buoyant velocities. However, the percentage of the horizontally oriented fields and the temporal derivatives of the field strength and the buoyant velocity show some positive

correlations with the separation velocity. The results of this study imply that the assumption that the emerging active region is the cross section of a rising flux tube whose structure can be considered rigid as it rises through the near-surface layer should be taken with caution.

### **Time variations of the non-potential and volume-threading magnetic helicities**

Luis [Linan](#), [Étienne Pariat](#), [Kostas Moraitis](#), [Gherardo Valori](#), [James E. Leake](#)

ApJ 2018

<https://arxiv.org/pdf/1809.03765.pdf>

[https://sites.lesia.obspm.fr/helisol/files/2018/09/Flux\\_Hj\\_Hpj.pdf](https://sites.lesia.obspm.fr/helisol/files/2018/09/Flux_Hj_Hpj.pdf)

Relative magnetic helicity is a gauge invariant quantity suitable for the study of the magnetic helicity content of heliospheric plasmas. Relative magnetic helicity can be decomposed uniquely into two gauge invariant quantities, the magnetic helicity of the non-potential component of the field, and a complementary volume-threading helicity. Recent analysis of numerical experiments simulating the generation of solar eruptions have shown that the ratio of the non-potential helicity to the total relative helicity is a clear marker of the eruptivity of the magnetic system, and that the high value of that quantity could be a sufficient condition for the onset of the instability generating the eruptions. The present study introduces the first analytical examination of the time variations of these non-potential and volume-threading helicities. The validity of the analytical formulas derived are confirmed with analysis of three-dimensional (3D) magnetohydrodynamics (MHD) simulations of solar coronal dynamics. Both the analytical investigation, and the numerical application show that, unlike magnetic helicity, the non-potential and the volume-threading helicities are not conserved quantities, even in the ideal MHD regime. A term corresponding to the transformation between the non-potential and volume-threading helicities frequently dominates their dynamics. This finding has an important consequence for their estimation in the solar corona: unlike with relative helicity, their volume coronal evolution cannot be ascertained by the flux of these quantities through the volume's boundaries. Only techniques extrapolating the 3D coronal field will enable both the proper study of the non-potential and volume-threading helicities, and the observational analysis of helicity-based solar-eruptivity proxies.

### **The role of the chromospheric magnetic canopy in the formation of a sunspot penumbra**

[P. Lindner](#), [C. Kuckein](#), [S.J. González Manrique](#), [N. Bello González](#), [L. Kleint](#), [T. Berkefeld](#)

A&A 673, A64 2023

<https://arxiv.org/pdf/2303.07112.pdf>

<https://www.aanda.org/articles/aa/pdf/2023/05/aa45702-22.pdf>

While it is being conjectured that a chromospheric canopy plays a role in penumbra formation, it has been difficult to find observational evidence of the connectivity between the photosphere and the chromosphere. We investigate the existence of a chromospheric canopy as a necessary condition for the formation of a penumbra and aim to find the origin of the inclined magnetic fields. Spectropolarimetric observations of NOAA AR 12776 from the GRIS@GREGOR instrument were analyzed. Atmospheric parameters were obtained from the deep photospheric Ca I 10839 Å line (VFISV inversion code), the mostly photospheric Si I 10827 Å line (SIR inversion code) and the chromospheric He I 10830 Å triplet (HAZEL inversion code). In the deepest atmospheric layers, we find that the magnetic properties (inclination and field strength distribution) measured on the sunspot sector with fully fledged penumbra are similar to those measured on the sector without penumbra. Yet, in higher layers, magnetic properties are different. In the region showing no penumbra, almost vertical chromospheric magnetic fields are observed. Additionally, thin filamentary structures with a maximum width of 0.1 arcsec are seen in photospheric high-resolution TiO-band images in this region. The existence of a penumbra is found to be discriminated by the conditions in the chromosphere. This indicates that a chromospheric canopy is a necessary condition for the formation of a penumbra. However, our results demonstrate that inclined fields in the chromospheric canopy are not needed for the development of inclined fields in the photosphere. We question the 'fallen-magnetic-flux-tubes' penumbra formation scenario and favor a scenario, in which inclined fields emerge from below the surface and are blocked by the overlying chromospheric canopy. 2020-10-16

### **Decay of a photospheric transient filament at the boundary of a pore and the chromospheric response**

[Philip Lindner](#), [Rolf Schlichenmaier](#), [Nazaret Bello González](#), [Jaime de la Cruz Rodríguez](#)

A&A 673, A65 2023

<https://arxiv.org/pdf/2303.03072.pdf>

<https://www.aanda.org/articles/aa/pdf/2023/05/aa45703-22.pdf>

Intermediate stages between pores and sunspots are a rare phenomenon and can manifest with the formation of transient photospheric penumbral-like filaments. Although the magnetic field changes rapidly during the evolution of such filaments, they have not been shown to be connected to magnetic reconnection events yet. We analyzed observations of a pore in NOAA AR 12739 from the Swedish Solar Telescope including spectropolarimetric data of the Fe I 6173 Å and the Ca II 8542 Å line and spectroscopic data of the Ca II K 3934 Å line. The VFISV Milne-Eddington inversion code and the multi-line Non-LTE inversion code STiC were utilized to obtain atmospheric

parameters in the photosphere and the chromosphere. Multiple filamentary structures of inclined magnetic fields are found in photospheric inclination maps at the boundary of the pore, although the pore never developed a penumbra. One of the filaments shows a clear counterpart in continuum intensity maps in addition to photospheric blueshifts. During its decay, a brightening in the blue wing of the Ca II 8542 Å line is observed. The Ca II K 3934 Å and the Ca II 8542 Å lines show complex spectral profiles in this region. Depth-dependent STiC inversion results using data from all available lines yield a temperature increase (roughly 1000 Kelvin) and bidirectional flows (magnitudes up to 8 km/s) at  $\log \tau = -3.5$ . The temporal and spatial correlation of the decaying filament (observed in the photosphere) to the temperature increase and the bidirectional flows in the high photosphere/low chromosphere suggests that they are connected. We propose scenarios in which magnetic reconnection happens at the edge of a rising magnetic flux tube in the photosphere. This leads to both the decay of the filament in the photosphere and the observed temperature increase and the bidirectional flows in the high photosphere/low chromosphere. **2019- 04-19**

## **Characterization of the umbra-penumbra boundary by the vertical component of the magnetic field -- Analysis of ground-based data from the GREGOR Infrared Spectrograph**

P. Lindner, R. Schlichenmaier, N. Bello González

A&A 638, A25 2020

<https://arxiv.org/pdf/2004.09956.pdf>

<https://www.aanda.org/articles/aa/pdf/2020/06/aa37716-20.pdf>

Context. The vertical component of the magnetic field was found to reach a constant value at the boundary between penumbra and umbra of stable sunspots in a recent statistical study of Hinode/SP data. This finding has profound implications as it can serve as a criterion to distinguish between fundamentally different magneto-convective modes operating in the sun. Aims. The objective of this work is to verify the existence of a constant value for the vertical component of the magnetic field ( $B_{\perp}$ ) at the boundary between umbra and penumbra from ground-based data in the near-infrared wavelengths and to determine its value for the GREGOR Infrared Spectrograph (GRIS@GREGOR) data. This is the first statistical study on the Jurčák criterion with ground-based data, and we compare it with the results from space-based data (Hinode/SP and SDO/HMI).

Methods. Eleven spectropolarimetric data sets from the GRIS@GREGOR slit-spectrograph containing fully-fledged stable sunspots were selected from the GRIS archive (sdc.leibniz-kis.de). SIR inversions including a polarimetric straylight correction are used to produce maps of the magnetic field vector using the Fe I 15 648 Å and 15 662 Å lines. Averages of  $B_{\perp}$  along the contours between penumbra and umbra are analyzed for the 11 data sets. In addition, contours at the resulting  $B_{\text{const } \perp}$  are drawn onto maps and compared to intensity contours. The geometric difference between these contours,  $\Delta P$ , is calculated for each data set.

Results. Averaged over the 11 sunspots, we find a value of  $B_{\text{const } \perp} = (1787 \pm 100)$  gauss. The difference from the values previously derived from Hinode/SP and SDO/HMI data is explained by instrumental differences and by the formation characteristics of the respective lines that were used. Contours at  $B_{\perp} = B_{\text{const } \perp}$  and contours calculated in intensity maps match from a visual inspection and the geometric distance  $\Delta P$  was found to be on the order of 2 pixels. Furthermore, the standard deviation between different data sets of averages along umbra–penumbra contours is smaller for  $B_{\perp}$  than for  $B_k$  by a factor of 2.4.

Conclusions. Our results provide further support to the Jurčák criterion with the existence of an invariable value  $B_{\text{const } \perp}$  at the umbra–penumbra boundary. This fundamental property of sunspots can act as a constraining parameter in the calibration of analysis techniques that calculate magnetic fields. It also serves as a requirement for numerical simulations to be realistic. Furthermore, it is found that the geometric difference,  $\Delta P$ , between intensity contours and contours at  $B_{\perp} = B_{\text{const } \perp}$  acts as an index of stability for sunspots.

**19 Sep 2015, 29 Aug 2016, 2 Sep 2017**

**Table 1.** List of GRIS@GREGOR data sets that were used in this study

## **The Open Flux Problem**

J. A. Linker, R. M. Caplan, C. Downs, P. Riley, Z. Mikic, R. Lionello, C. J. Henney, C. N. Arge, Y. Liu, M. L. Derosa, A. Yeates, M. J. Owens

2017 ApJ 848 70

<https://arxiv.org/pdf/1708.02342.pdf>

The heliospheric magnetic field is of pivotal importance in solar and space physics. The field is rooted in the Sun's photosphere, where it has been observed from ground- and space-based observatories for over four decades. Global maps of the solar magnetic field based on full disk magnetograms are commonly used as boundary conditions for coronal and solar wind models. Two primary observational constraints on the models are (1) the open field regions in the model should approximately correspond to coronal holes observed in emission, and (2) the magnitude of the open magnetic flux in the model should match that inferred from in situ spacecraft measurements. In this study, we calculate both MHD and PFSS solutions using fourteen different magnetic maps produced from five different types of observatory magnetograms, for the time period surrounding July, 2010. We have found that for all of the model/map combinations, models that have coronal hole areas close to observations underestimate the interplanetary magnetic flux, or, conversely, for models to match the interplanetary flux, the modeled open field regions are larger

than coronal holes observed in EUV emission. In an alternative approach, we estimate the open magnetic flux entirely from solar observations by combining automatically detected coronal holes for Carrington rotation 2098 with observatory synoptic magnetic maps for this time period. We show that this method also underestimates the interplanetary magnetic flux. Our results imply that either typical observatory maps underestimate the Sun's magnetic flux, or a significant portion of the open magnetic flux is not rooted in regions that are obviously dark in EUV and X-ray emission. **July 8, 2010, 16 June-13 July 2010**

## **Slip-Back Mapping as a Tracker of Topological Changes in Evolving Magnetic Configurations**

R. [Lionello](#), [V. S. Titov](#), [Z. Mikić](#), [J. A. Linker](#)

2020 *ApJ* 891 14

<https://arxiv.org/pdf/1905.01384.pdf>

<https://doi.org/10.3847/1538-4357/ab68d9>

The topology of the coronal magnetic field produces a strong impact on the properties of the solar corona and presumably on the origin of the slow solar wind. To advance our understanding of this impact, we revisit the concept of so-called slip-back mapping (Titov et al. 2009) and adapt it for determining open, closed, and disconnected flux systems that are formed in the solar corona by magnetic reconnection during a given time interval. The developed method allows us, in particular, to describe the magnetic flux transfer between open and closed flux regions via so-called interchange reconnection with unprecedented level of details. We illustrate the application of this method to the analysis of a global MHD evolution of the solar corona that is driven by an idealized differential rotation of the photospheric plasma.

## **ARE INTERNETWORK MAGNETIC FIELDS IN THE SOLAR PHOTOSPHERE HORIZONTAL OR VERTICAL?**

B. W. [Lites](#)<sup>1,4</sup>, M. Rempel<sup>1</sup>, J. M. Borrero<sup>2</sup>, and S. Danilovic<sup>3</sup>

2017 *ApJ* 835 14

Using many observations obtained during 2007 with the Spectro-Polarimeter of the HinodeSolar Optical Telescope, we explore the angular distribution of magnetic fields in the quiet internetwork regions of the solar photosphere. Our work follows from the insight of Stenflo, who examined only linear polarization signals in photospheric lines, thereby avoiding complications of the analysis arising from the differing responses to linear and circular polarization. We identify and isolate regions of a strong polarization signal that occupy only a few percent of the observed quiet Sun area yet contribute most to the net linear polarization signal. The center-to-limb variation of the orientation of linear polarization in these strong signal regions indicates that the associated magnetic fields have a dominant vertical orientation. In contrast, the great majority of the solar disk is occupied by much weaker linear polarization signals. The orientation of the linear polarization in these regions demonstrates that the field orientation is dominantly horizontal throughout the photosphere. We also apply our analysis to Stokes profiles synthesized from the numerical MHD simulations of Rempel as viewed at various oblique angles. The analysis of the synthetic data closely follows that of the observations, lending confidence to using the simulations as a guide for understanding the physical origins of the center-to-limb variation of linear polarization in the quiet Sun area.

## **Modeling sunspot and starspot decay by turbulent erosion**

Yuri E. [Litvinenko](#), M. S. Wheatland

*ApJ*, 2015

<http://arxiv.org/pdf/1501.01699v1.pdf>

Disintegration of sunspots (and starspots) by fluxtube erosion, originally proposed by Simon and Leighton, is considered. A moving boundary problem is formulated for a nonlinear diffusion equation that describes the sunspot magnetic field profile. Explicit expressions for the sunspot decay rate and lifetime by turbulent erosion are derived analytically and verified numerically. A parabolic decay law for the sunspot area is obtained. For moderate sunspot magnetic field strengths, the predicted decay rate agrees with the results obtained by Petrovay and Moreno-Inertis. The new analytical and numerical solutions significantly improve the quantitative description of sunspot and starspot decay by turbulent erosion.

## **What Can DKIST/DL-NIRSP Tell Us About Quiet-Sun Magnetism?**

Jiayi [Liu](#) (1), [Xudong Sun](#) (1), [Peter W. Schuck](#) (2), [Sarah A. Jaeggli](#) (3)

*ApJ* 2024

<https://arxiv.org/pdf/2411.18735>

Quiet-Sun regions cover most of the Sun's surface; its magnetic fields contribute significantly to the solar chromospheric and coronal heating. However, characterizing the magnetic fields of the quiet Sun is challenging due to their weak polarization signal. The 4-m (textit{Daniel K. Inouye Solar Telescope}) (textit{DKIST}) is expected

to improve our understanding of the quiet-Sun magnetism. In this paper, we assess the diagnostic capability of the Diffraction-Limited Near Infrared Spectropolarimeter (DL-NIRSP) instrument on \textit{DKIST} on the energy transport processes in the quiet-Sun photosphere. To this end, we synthesize high-resolution, high-cadence Stokes profiles of the  $\text{Fe I}$  630-nm lines using a realistic magnetohydrodynamic simulation, degrade them to emulate the \textit{DKIST}/DL-NIRSP observations, and subsequently infer the vector magnetic and velocity fields. For the assessment, we first verify that a widely used flow-tracking algorithm, Differential Affine Velocity Estimator for Vector Magnetograms, works well for estimating the large-scale ( $>200$  km) photospheric velocity fields with these high-resolution data. We then examine how the accuracy of inferred velocity depends on the temporal resolution. Finally, we investigate the reliability of the Poynting flux estimate and its dependence on the model assumptions. The results suggest that the unsigned Poynting flux, estimated with existing schemes, can account for about 71.4% and 52.6% of the reference ground truth at  $\log\tau=0.0$  and  $\log\tau=-1$ . However, the net Poynting flux tends to be significantly underestimated. The error mainly arises from the underestimated contribution of the horizontal motion. We discuss the implications on \textit{DKIST} observations.

## **A New Approach of Data-driven Simulation and Its Application to Solar Active Region 12673**

[Zhi-Peng Liu](#), [Chao-Wei Jiang](#), [Xin-Kai Bian](#), [Qing-Jun Liu](#), [Peng Zou](#), [Xue-Shang Feng](#)

Research in Astronomy and Astrophysics **2024**

<https://arxiv.org/pdf/2410.09433>

The solar coronal magnetic field is a pivotal element in the study of eruptive phenomena, and understanding its dynamic evolution has long been a focal point in solar physics. Numerical models, driven directly by observation data, serve as indispensable tools in investigating the dynamics of the coronal magnetic field. This paper presents a new approach to electric field inversion, which involves modifying the electric field derived from the DAVE4VM velocity field using ideal Ohm's law. The time series of the modified electric field is used as a boundary condition to drive a MHD model, which is applied to simulate the magnetic field evolution of active region 12673. The simulation results demonstrate that our method enhances the magnetic energy injection through the bottom boundary, as compared with energy injection calculated directly from the DAVE4VM code, and reproduce of the evolution of the photospheric magnetic flux. The coronal magnetic field structure is also in morphological similarity to the coronal loops. This new approach will be applied to the high-accuracy simulation of eruption phenomena and provide more details on the dynamical evolution of the coronal magnetic field. **2017-09-06**

## **The Magnetic Field Calibration of the Full-Disk Magnetograph onboard the Advanced Space based Solar Observatory (ASO-S/FMG)**

[S. Liu](#), [J.T. Su](#), [X.Y. Bai](#), [Y.Y. Deng](#), [J. Chen](#), [Y.L. Song](#), [X.F. Wang](#), [H.Q. Xu](#), [X. Yang](#)

Solar Phys. 298, Article number: 141 (2023)

<https://arxiv.org/pdf/2312.00319.pdf>

The Full-disk magnetograph is a main scientific payload onboard the Advanced Space based Solar Observatory (ASO-S/FMG) that through Stokes parameter observation to measures the vector magnetic field. The accuracy of magnetic-field values is an important aspect of checking the quality of the FMG magnetic-field measurement. According to the design of the FMG, the linear calibration method under the weak-field approximation is the preferred scheme for magnetic-field calibration. However, the spacecraft orbital velocity can affect the position of observed spectral lines, then result in a change of the polarization-signal strength. Thus, the magnetic field is modulated by the orbit velocity of the spacecraft. In this article, through cross calibration between FMG and HMI (Helioseismic and Magnetic Imager onboard the Solar Dynamic Observatory), the effects of spacecraft orbital velocity on the coefficient of magnetic-field calibration are investigated. By comparing the magnetic field of FMG and HMI with spacecraft orbital velocity as an auxiliary reference, the revised linear-calibration coefficients that depend on spacecraft orbital velocity are obtained. Magnetic field of FMG corrected by the revised calibration coefficients removing the effect of spacecraft orbital velocity will be more accurate and suitable for scientific research. **04 April 2023, 25 Feb 2023**

## **On the Hemispheric Bias Seen in Vector Magnetic Field Data**

[Yang Liu](#), [Ana Belén Griñón-Marín](#), [Jon T. Hoeksema](#), [Aimee A. Norton](#) & [Xudong Sun](#)

*Solar Physics* volume 297, Article number: 17 (2022)

<https://link.springer.com/content/pdf/10.1007/s11207-022-01949-y.pdf>

The east–west component of the magnetic field,  $B_{\phi}$ , as observed in solar magnetograms containing quiet regions, is found to change its sign when the regions cross the central meridian. It is seen in both HMI/SDO and VSM/SOLIS full disk vector magnetograms. A mismatch between the calibrated line-of-sight and transverse fields is the reason for this hemispheric bias problem. Here mismatch means that one of the fields is either over-estimated or under-estimated. For HMI data, the transverse field is over-estimated. This mismatch is caused ultimately by a filling factor that is not precisely determined when unresolved structures are present. An updated inversion procedure for HMI observations, developed recently, is able to derive the filling factor with reasonable accuracy. The new data

show that the hemispheric bias problem has been mitigated substantially. 2010 June 29-July 4, 2015 November 17-22

[HMI Science Nuggets](http://hmi.stanford.edu/hminuggets/?p=3863) #176 March 2022 <http://hmi.stanford.edu/hminuggets/?p=3863>

## **A Study on Correcting the Effect of Polarization Crosstalk in Full-Disk Solar Photospheric Magnetic Fields Observations**

[S. Liu](#), [J.T. Su](#), [X.Y. Bai](#), [Y.Y. Deng](#), [J. Chen](#), [Y.L. Song](#), [X.F. Wang](#), [H.Q. Xu](#), [X. Yang](#)

Solar Phys. 297, Article number: 6 2022

<https://arxiv.org/pdf/2112.04135.pdf>

<https://link.springer.com/content/pdf/10.1007/s11207-021-01933-y.pdf>

<https://doi.org/10.1007/s11207-021-01933-y>

Magnetography using magnetic sensitive lines is regarded traditionally as the main instrument for measuring the magnetic field of the whole Sun. Full polarized Stokes parameters (I, Q, U, V) observed can be used to deduce the magnetic field under specific theoretical model or inversion algorithms. Due to various reasons, there are often cross-talk effects among Stokes signals observed directly by magnetographs. Especially, the circular polarized signal V usually affects the linear polarized ones Q and U seriously, which is one of the main errors of the value of the transverse magnetic field (parallel to the solar surface) that is related to Q and U. The full-disk magnetograph onboard the Advanced Space based Solar Observatory (ASO-S/FMG) is designed to observe Stokes parameters to deduce the vector magnetic field. In this paper, the methods correcting the effects of cross-talk V to Q and U are based on the assumption of perfectly symmetric Q and U and anti-symmetric Stokes V profiles and a new method to reduce the crosstalk effect under observation mode of FMG is developed. Through the test, it is found that the two methods have better effect in cross-talk removal in the sunspot region, and have better consistency. Additionally, the developed method can be applied to remove the cross-talk effect using only one group of Q, U and V images observed at one wavelength position. 2017-09-07

## **Inferring Vector Magnetic Fields from Stokes Profiles of GST/NIRIS Using a Convolutional Neural Network**

Hao [Liu](#)<sup>1,2</sup>, Yan Xu<sup>1,3,4</sup>, Jiasheng Wang<sup>1,3,4</sup>, Ju Jing<sup>1,3,4</sup>, Chang Liu<sup>1,3,4</sup>, Jason T. L. Wang<sup>1,2</sup>, and Haimin Wang<sup>1,3,4</sup>

2020 ApJ 894 70

<https://doi.org/10.3847/1538-4357/ab8818>

We propose a new machine-learning approach to Stokes inversion based on a convolutional neural network (CNN) and the Milne–Eddington (ME) method. The Stokes measurements used in this study were taken by the Near InfraRed Imaging Spectropolarimeter (NIRIS) on the 1.6 m Goode Solar Telescope (GST) at the Big Bear Solar Observatory. By learning the latent patterns in the training data prepared by the physics-based ME tool, the proposed CNN method is able to infer vector magnetic fields from the Stokes profiles of GST/NIRIS. Experimental results show that our CNN method produces smoother and cleaner magnetic maps than the widely used ME method. Furthermore, the CNN method is four to six times faster than the ME method and able to produce vector magnetic fields in nearly real time, which is essential to space weather forecasting. Specifically, it takes ~50 s for the CNN method to process an image of  $720 \times 720$  pixels comprising Stokes profiles of GST/NIRIS. Finally, the CNN-inferred results are highly correlated to the ME-calculated results and closer to the ME's results with the Pearson product-moment correlation coefficient (PPMCC) being closer to 1, on average, than those from other machine-learning algorithms, such as multiple support vector regression and multilayer perceptrons (MLP). In particular, the CNN method outperforms the current best machine-learning method (MLP) by 2.6%, on average, in PPMCC according to our experimental study. Thus, the proposed physics-assisted deep learning-based CNN tool can be considered as an alternative, efficient method for Stokes inversion for high-resolution polarimetric observations obtained by GST/NIRIS.

## **SOTE: A Nonlinear Method for Magnetic Topology Reconstruction in Space Plasmas**

Y. Y. [Liu](#)<sup>1</sup>, H. S. Fu<sup>1</sup>, V. Olshevsky<sup>2</sup>, D. I. Pontin<sup>3</sup>, C. M. Liu<sup>1</sup>, Z. Wang<sup>1</sup>, G. Chen<sup>4,5</sup>, L. Dai<sup>6</sup>, and A. Retino<sup>7</sup>

2019 ApJS 244 31

<https://doi.org/10.3847/1538-4365/ab391a>

Complex magnetic structures are ubiquitous in turbulent astrophysical plasmas. Such structures can be host to many dynamic processes, such as magnetic reconnection and energy dissipation. Thus, revealing the 3D topologies of these structures is necessary. In this study, we propose a new method to reconstruct complex magnetic topologies in quasi-steady space plasmas, by utilizing eight-point measurements of magnetic fields and particles. Such a method, based on the Second-Order Taylor Expansion (SOTE) of a magnetic field, is nonlinear; it is constrained by  $\nabla \cdot \mathbf{B} = 0$  and  $\nabla \cdot \mathbf{j} = -\nabla^2 \phi$ , where  $\mathbf{j}$  is from particle moments. A benchmark test of this method, using the simulation data, shows that the method

can give accurate reconstruction results within an area about three times the size of a spacecraft tetrahedron. By comparing to the previous First-Order Taylor Expansion (FOTE) method, this method (SOTE) gives similar results for reconstructing quasilinear structures but exhibits better accuracy in reconstructing nonlinear structures. Such a method will be useful to the multi-scale missions, such as the future European Space Agency's "cross-scale" mission and China's "self-adaptive" mission. Also, it can be applied to four-point missions, such as Cluster and the Magnetospheric Multiscale Mission. We demonstrated how to apply this method to the four-point missions. In principle, this method will be useful to study shocks, magnetic holes, dipolarization fronts, and other nonlinear structures in space plasmas.

## **Vector Magnetic Field Synoptic Charts from the Helioseismic and Magnetic Imager (HMI)**

Yang **Liu**, J. T. Hoeksema, Xudong Sun, Keiji Hayashi

Solar Phys. 292:29 2017

[http://sun.stanford.edu/~yliu/papers/hmisynop\\_v03.pdf](http://sun.stanford.edu/~yliu/papers/hmisynop_v03.pdf)

Vector magnetic field synoptic charts from the Helioseismic and Magnetic Imager (HMI) are now available for each Carrington Rotation (CR) starting from CR 2097 in May 2010. Synoptic charts are produced using 720-second cadence full-disk vector magnetograms remapped to Carrington coordinates. The vector field is derived from the Stokes parameters (I, Q, U, V) using a Milne-Eddington based inversion model. The 180° azimuth ambiguity is resolved using the Minimum Energy algorithm for pixels in active regions and for strong-field pixels (the field is greater than about 150 G) in quiet Sun regions. Three other methods are used for the rest of the pixels: the potential-field method, the radial-acute angle method, and the random method. The vector field synoptic charts computed using these three disambiguation methods are evaluated. The noise in the three components of vector magnetic field is generally much higher in the potential-field method charts. The component noise levels are significantly different in the radial-acute charts. However, the noise levels in the random-method charts are lower and comparable. The assumptions used in the potential-field and radial-acute methods to disambiguate the weak transverse field introduce bias that propagates differently into the three vector-field components, leading to unreasonable pattern and artifacts, whereas the random method appears not to introduce any systematic bias. The computed current sheet on the source surface, computed using the potential-field source-surface model applied to random-method charts, agrees with the best solution (the result computed from the synoptic charts with the minimum energy algorithm applied to each and every pixel in the vector magnetograms) much better than the other two. Differences in the synoptic charts determined with the best method and the random method are much smaller than those from the best method and the other two. This comparison indicates that the random method is better for vector field synoptic maps computed from near-central meridian data. Thus, the vector field synoptic charts provided by the Joint Science Operations Center (JSOC) are produced with the random method.

## **A New Observing Scheme for HMI Vector Field Measurements: Mod-L**

Y. **Liu**<sup>1</sup>, C. Baldner<sup>1</sup>, R. Bogart<sup>1</sup>, R. Bush<sup>1</sup>, T. Duvall<sup>2</sup>, J. T. Hoeksema<sup>1</sup>, A. Norton<sup>1</sup>, P. Scherrer<sup>1</sup>, J. Schou

HMI Science Nuggets #56, June 2016

<http://hmi.stanford.edu/hminuggets/?p=1596>

HMI/SDO changed the scheme for collecting vector magnetic field measurements on 13 April 2016. Because we are now confident that data from the two HMI cameras can be successfully combined, the noise in the vector observations can be reduced by using all of the filtergrams from both HMI cameras.

## **Fine magnetic characteristics of a light bridge observed by Hinode**

S. **Liu**, D. Liu

Advances in Space Research [Volume 55, Issue 12](#), 15 June 2015, Pages 2931–2939

<https://arxiv.org/pdf/1902.00348.pdf>

Light bridge (LB) is bright structure crossing the umbra of sunspots and associated to the breakup or assembly of sunspots. In this paper, a LB is presented and studied using the observatory data obtained by Hinode satellites. Force-free factor ( $\alpha$ ) and the z -component of current (Jz) and tension force (Tz) are calculated basing on the vector magnetograms observed by Spectro-Polarimeter (SP) of the Solar Optical Telescope (SOT) on board Hinode . It is found that the amplitudes of  $\alpha$  and Jz of LB are generally larger than those of umbra. It is found that there are two signs of Jz along LB, which are divided at near the middle position of LB. It is found that the amplitudes of Tz of LB are smaller than those of umbra and there are changes of sign of Tz between the boundary of LB and umbra. Through comparisons and investigations, it suggest that LB and umbra maybe two different magnetic systems, which is a necessary condition for interaction magnetic reconnection. **19 Aug 2011**,

## **A research on the force-freeness of photosphere magnetic field**

S. Liu, J. Hao

Advances in Space Research Volume 55, Issue 6, 15 March 2015, Pages 1563–1575

<http://www.sciencedirect.com/science/article/pii/S0273117715000241>

<https://arxiv.org/pdf/1902.00308.pdf>

In this paper, the statistical studies on the force-freeness of photosphere magnetic fields are given. The studies are based on the vector magnetic fields observed by Solar Optical Telescope/Spectro-Polarimeter (SOT/SP) on board Hinode. Three parameters ( $F_x/F_p$ ,  $F_y/F_p$ , and  $F_z/F_p$ ) are introduced to investigate the force-freeness of active regions photosphere magnetic field. Various thresholds and reductions of original resolutions are selected to calculated parameters. As for the resolutions, the reductions of original resolution data by a factor of 2, 4 and 8 are applied. While for thresholds, they are calculated from individual active region with the average of 75/77/57 G for  $B_x/B_y/B_z$  for all original data. When the resolution are reduced by 2, 4 and 8, the corresponding averages are 72/75/55, 66/68/49 and 57/59/41 G for  $B_x/B_y/B_z$ , respectively. It is found that the forces indicated by  $F_x/F_p$  and  $F_y/F_p$  increase as thresholds/resolutions increase/decrease. While for  $F_z/F_p$  the trends become more complex. For low threshold, when the resolution decrease the trends of  $F_z/F_p$  are similar as those of  $F_x/F_p$  and  $F_y/F_p$ , while for high threshold the trends of  $F_z/F_p$  are different from those of  $F_x/F_p$  and  $F_y/F_p$ . For original resolution, the forces indicated by  $F_y/F_p$  increase as thresholds increase, while for others resolution they decrease as the thresholds increase contrarily.

## **Three-dimensional Magnetic Restructuring in Two Homologous Solar Flares in the Seismically**

### **Active NOAA AR 11283**

Chang Liu, Na Deng, Jeongwoo Lee, Thomas Wiegmann, Chaowei Jiang, Brian R. Dennis, Yang Su, Alina Donea, Haimin Wang

ApJ, 2014

<http://arxiv.org/pdf/1409.6391v1.pdf>

We carry out a comprehensive investigation comparing the three-dimensional magnetic field restructuring, flare energy release, and the helioseismic response, of two homologous flares, the **2011 September 6 X2.1 (FL1)** and **September 7 X1.8 (FL2)** flares in NOAA AR 11283. In our analysis, (1) a twisted flux rope (FR) collapses onto the surface at a speed of 1.5 km/s after a partial eruption in FL1. The FR then gradually grows to reach a higher altitude and collapses again at 3 km/s after a fuller eruption in FL2. Also, FL2 shows a larger decrease of the flux-weighted centroid separation of opposite magnetic polarities and a greater change of the horizontal field on the surface. These imply a more violent coronal implosion with corresponding more intense surface signatures in FL2. (2) The FR is inclined northward, and together with the ambient fields, it undergoes a southward turning after both events. This agrees with the asymmetric decay of the penumbra observed in the peripheral regions. (3) The amounts of free magnetic energy and nonthermal electron energy released during FL1 are comparable to those of FL2 within the uncertainties of the measurements. (4) No sunquake was detected in FL1; in contrast, FL2 produced two seismic emission sources S1 and S2 both lying in the penumbral regions. Interestingly, S1 and S2 are connected by magnetic loops, and the stronger source S2 has weaker vertical magnetic field. We discuss these results in relation to the implosion process in the low corona and the sunquake generation.

## **Multi-channel Observations of Plasma Outflows and the Associated Small-Scale Magnetic Field Cancellations on the Edges of an Active Region**

S. Liu, J.T. Su

Ap&ss 2014

<http://arxiv.org/pdf/1405.3648v1.pdf>

With the SDO/AIA instrument, continuous and intermittent plasma outflows are observed on the boundaries of an active region along two distinct open coronal loops. %with the speed of 30~200 km s<sup>-1</sup>. By investigating the temporal sequence magnetograms obtained from HMI/SDO, it is found that small-scale magnetic reconnection probably plays an important role in the generation of the plasma outflows in the coronal loops. It is found that the origin of the plasma outflows coincides with the locations of the small-scale magnetic fields with mixed polarities, which suggests that the plasma outflows along coronal loops probably results from the magnetic reconnection between the small-scale close emerging loops and the large-scale open active region coronal loops. **June 14 2012.**

## **A Statistical Study on Property of Spatial Magnetic Field for Solar Active Region**

Liu Suo

Ap&ss 2014

<http://arxiv.org/pdf/1405.2149v1.pdf>



Magnetic fields dominate most solar activities, there exist direct relations between solar flare and the distributions of magnetic field, and also its corresponding magnetic energy. In this paper, the statistical results about the relationships between the spatial magnetic field and solar flare are given basing on vector magnetic field observed by the Solar Magnetic Field Telescope (SMFT) at Huairou Solar Observing Station (HSOS). The spatial magnetic fields are obtained by extrapolated photosphere vector magnetic field observed by SMFT. There are 23 active regions with flare eruption are chosen as data samples, which were observed from 1997 to 2007. The results are as follows: 1. Magnetic field lines become lower after flare for 16(69%) active regions; 2. The free energy are decreased after flare for 17 (74%) active regions. It can conclude that for most active regions the changes of magnetic field after solar flare are coincident with the previous observations and studies. **1997-05-21, 1998-02-15, 1998-05-12, 1998-08-28, 1998-10-28, 1999-10-07, 1999-10-16, 1999-10-21, 2000-03-30, 2000-06-16, 2000-09-06, 2001-06-16, 2001-05-25, 2001-07-11, 2002-08-09, 2002-09-20, 2002-10-03, 2003-10-27, 2005-05-27, 2005-07-05, 2005-12-03, 2007-5-02, 2007-06-05**

## **Study on two Methods for Nonlinear Force-free Extrapolation Based on Semi-Analytical Field**

**Liu S.**, Zhang H.Q., Su J.T. Song M.T.

Solar Phys., **2014**

<http://arxiv.org/pdf/1405.2158v1.pdf>

In this paper, two semi-analytical solutions of force free fields (\citeauthor{low90}, \citeyear{low90}) have been used to test two nonlinear force-free extrapolation methods. One is the boundary integral equation (BIE) method developed by \citeauthor{yan00} (\citeyear{yan00}), and another is the approximate vertical integration (AVI) method developed by \citeauthor{son06} (\citeyear{son06}). Some improvements for the AVI method have been taken to avoid the singular points in the process of calculation. It is found that the correlation coefficients between the first semi-analytical field and extrapolated field by BIE, and also that by improved AVI, are greater than 90% below a height 10 of the 64×64 lower boundary. While for the second semi-analytical field, these correlation coefficients are greater than 80% below the same relative height. Although the differences between the semi-analytical solutions and the extrapolated fields exist for both BIE and AVI methods, these two methods can give reliable results for the height of about 15% of the extent of the lower boundary.

## **Comparison of Nonlinear Force-free Field and Potential Field in the Quiet Sun**

**Liu S.**, Zhang H.Q., Su J.T

Solar Phys., **2014**

<http://arxiv.org/pdf/1405.2159v1.pdf>

In this paper, a potential field extrapolation and three nonlinear force-free (NLFF) field extrapolations (optimization, direct boundary integral (DBIE) and approximate vertical integration (AVI) methods) are used to study the spatial configuration of magnetic field in the quiet Sun. It is found that the strength differences between the three NLFF and potential fields exist in the low layers. However, they tend to disappear as the height increases, which are of the order of 0.1 G when the height exceeds ~ 2000 km above the photosphere. The absolute azimuth difference between one NLFF field and the potential field is as follows: for the optimization field, it decreases evidently as the height increases; for the DBIE field, it almost keeps constant and shows no significant change as the height increases; for the AVI field, it increases slowly as the height increases. The analysis shows that the reconstructed NLFF fields deviate significantly from the potential field in the quiet Sun.

## **Magnetic Helicity in Emerging Solar Active Regions**

Y. **Liu**, J. T. Hoeksema, M. Bobra, K. Hayashi, P. W. Schuck, X. Sun

E-print, Feb **2014**; **2014** ApJ 785 13

Using vector magnetic field data from the Helioseismic and Magnetic Imager (HMI) instrument aboard the Solar Dynamics Observatory (SDO), we study magnetic helicity injection into the corona in emerging active regions and examine the hemispheric helicity rule. In every region studied, photospheric shearing motion contributes most of the helicity accumulated in the corona. In a sample of 28 emerging active regions, 17 active regions follow the hemisphere rule (61% ? 18% at a 95% confidence interval). Magnetic helicity and twist in 25 active regions (89% ? 11%) have the same sign. The maximum magnetic twist, which depends on the size of an active region, is inferred in a sample of 23 emerging active regions with a bipolar magnetic field configuration.

## Testing Hemispheric Rule of Helicity with HMI Data

Y. Liu, J. T. Hoeksema, X. Sun

HMI Science Nuggets, No. 2, Jan 2014

<http://hmi.stanford.edu/hminuggets/?p=361>

Hemispheric helicity preference in groups of active regions with different properties suggests different origins of magnetic twist.

## Test of the Hemisphere Rule of Magnetic Twist in Solar Active Regions Using the Helioseismic and Magnetic Imager (HMI) Vector Magnetic Field Data

Y. Liu, J. T. Hoeksema, X. Sun

E-print, Jan 2014; 2014 ApJ 783 L1

<http://soi.stanford.edu/~yliu/papers/testofHemRule.pdf>

Magnetic twist in solar active regions has been found to have a hemispheric preference in sign (hemisphere rule): negative in the northern hemisphere and positive in the southern. The preference reported in previous studies ranges greatly, from ~ 58% to 82%. In this study, we examine this hemispheric preference using vector magnetic field data taken by HMI and find that 75%  $\pm$  7% of 151 active regions studied obey the hemisphere rule, well within the preference range in previous studies. If the sample is divided into two groups, --, active regions having magnetic twist and writhe of the same sign and having opposite signs, --, the strength of the hemispheric preference differs substantially: ( 64%  $\pm$  11% ) for the former group and ( 87%  $\pm$  8% ) for the latter. This difference becomes even more significant in a sub-sample of 82 active regions having a simple bipole magnetic configuration: ( 56%  $\pm$  16% ) for the active regions having the same signs of twist and writhe, and 93% with lower and upper confidence bounds of 80% and 98% for the active regions having the opposite signs. The error reported here is a 95% confidence interval. This may suggest that, prior to emergence of magnetic tubes, either the sign of twist does not have a hemispheric preference or the twist is relatively weak.

## Comparison of Line-of-Sight Magnetograms Taken by the Solar Dynamics Observatory/Helioseismic and Magnetic Imager and Solar and Heliospheric Observatory/Michelson Doppler Imager

Y. Liu, J.T. Hoeksema, P.H. Scherrer, J. Schou, S. Couvidat, R.I. Bush, T.L. Duvall Jr, K. Hayashi, X. Sun, X. Zhao

E-print, March 2012, **File**; Solar Phys. Volume 279, Number 1 (2012), 295-316

We compare line-of-sight magnetograms from the {it Helioseismic and Magnetic Imager} (HMI) onboard the {it Solar Dynamics Observatory} (SDO) and the {it Michelson Doppler Imager} (MDI) onboard the {it Solar and Heliospheric Observatory} (SOHO). The line-of-sight magnetic signal inferred from the calibrated MDI data is greater than that derived from the HMI data by a factor of 1.40. This factor varies somewhat with center-to-limb distance. An upper bound to the random noise for the 1primeprime resolution HMI 720-second magnetograms is 6.3 Mx cm<sup>-2</sup>, and 10.2 Mx cm<sup>-2</sup> for the 45-second magnetograms. Virtually no {it p}-mode leakage is seen in the HMI magnetograms, but it is significant in the MDI magnetograms. 12-hour and 24-hour periodicities are detected in strong fields in the HMI magnetograms. The newly calibrated MDI full-disk magnetograms have been corrected for the zero-point offset and underestimation of the flux density. The noise is 26.4 Mx cm<sup>-2</sup> for the MDI one-minute full-disk magnetograms and 16.2 Mx cm<sup>-2</sup> for the five-minute full-disk magnetograms observed with four-arcsecond resolution. The variation of the noise over the Sun's disk found in MDI magnetograms is likely due to the different optical distortions in the left- and right-circular analyzers, which allows the granulation and {it p}-mode to leak in as noise. Saturation sometimes seen in sunspot umbrae in MDI magnetograms is caused by the low intensity and the limitation of the onboard computation. The noise in the HMI and MDI line-of-sight magnetic-field synoptic charts appears to be fairly uniform over the entire map. The noise is 2.3 Mx cm<sup>-2</sup> for HMI charts and 5.0 Mx cm<sup>-2</sup> for MDI charts. No evident periodicity is found in the HMI synoptic charts.

## Comparison of Nonlinear Force-Free Field and Potential Field in the Quiet Sun

S. Liu, H. Q. Zhang and J. T. Su

Solar Physics, Volume 270, Number 1, 89-107, 2011

In this paper, a potential field extrapolation and three nonlinear force-free (NLFF) field extrapolations (optimization, direct boundary integral (DBIE), and approximate vertical integration (AVI) methods) are used to study the spatial configuration of magnetic field in the quiet Sun. It is found that differences in the computed field strengths among the three NLFF and potential fields exist in the low layers. However, they tend to disappear as the height increases,

and the differences are of the order of 0.1 gauss when the height exceeds  $\approx 2000$  km above the photosphere. The difference in azimuth angles between each NLFF field model and the potential field is as follows: for the optimization field, it decreases evidently as the height increases; for the DBIE field, it almost stays constant and shows no significant change as the height increases; for the AVI field, it increases slowly as the height increases. Our analysis shows that the reconstructed NLFF fields deviate significantly from the potential field in the quiet Sun.

## Study on Two Methods for Nonlinear Force-Free Extrapolation Based on Semi-Analytical Field

S. Liu · H.Q. Zhang · J.T. Su · M.T. Song

Solar Phys (2011) 269: 41–57

In this paper, two semi-analytical solutions of force-free fields (Low and Lou, *Astrophys. J.* **352**, 343, 1990) have been used to test two nonlinear force-free extrapolation methods. One is the boundary integral equation (BIE) method developed by Yan and Sakurai (*Solar Phys.* **195**, 89, 2000), and the other is the approximate vertical integration (AVI) method developed by Song *et al.* (*Astrophys. J.* **649**, 1084, 2006). Some improvements have been made to the AVI method to avoid the singular points in the process of calculation. It is found that the correlation coefficients between the first semi-analytical field and extrapolated field using the BIE method, and also that obtained by the improved AVI method, are greater than 90% below a height 10 of the 64  $\times$  64 lower boundary. For the second semi-analytical field, these correlation coefficients are greater than 80% below the same relative height. Although differences between the semi-analytical solutions and the extrapolated fields exist for both the BIE and AVI methods, these two methods can give reliable results for heights of about 15% of the extent of the lower boundary.

## Coronal magnetic fields inferred from IR wavelength and comparison with EUV observations

Y. Liu

Ann. Geophys., 27, 2771-2777, 2009

<http://www.ann-geophys.net/27/2771/2009/angeo-27-2771-2009.html>

Spectropolarimetry using IR wavelength of 1075 nm has been proved to be a powerful tool for directly mapping solar coronal magnetic fields including transverse component directions and line-of-sight component intensities. Solar tomography, or stereoscopy based on EUV observations, can supply 3-D information for some magnetic field lines in bright EUV loops. In a previous paper (Liu08) the locations of the IR emission sources in the 3-D coordinate system were inferred from the comparison between the polarization data and the potential-field-source-surface (PFSS) model, for one of five west limb regions in the corona (Lin et al., 2004). The paper shows that the region with the loop system in the active region over the photospheric area with strong magnetic field intensity is the region with a dominant contribution to the observed Stokes signals. So, the inversion of the measured Stokes parameters could be done assuming that most of the signals come from a relatively thin layer over the area with a large photospheric magnetic field strength. Here, the five limb coronal regions are studied together in order to study the spatial correlation between the bright EUV loop features and the inferred IR emission sources. It is found that, for the coronal regions above the stronger photospheric magnetic fields, the locations of the IR emission sources are closer to or more consistent with the bright EUV loop locations than those above weaker photospheric fields. This result suggests that the structures of the coronal magnetic fields observed at IR and EUV wavelengths may be different when weak magnetic fields present there.

## Coronal magnetic fields from the inversion of linear polarization measurements

Yu Liu<sup>1,2</sup>, Haosheng Lin<sup>2</sup> and Jeff Kuhn<sup>2</sup>

Solar and Stellar Variability: Impact on Earth and Planets, Proceedings IAU Symposium No. 264, 2009, p. 96-98, A.G. Kosovichev, A.H. Andrei & J.-P. Rozelot, eds.

Y:\obridko\otchet09

Real 3-D coronal magnetic field reconstruction is expected to be made based on the technologies of IR spectrometry and tomography, in which the data from other wavelengths can be used as critical reference. Our recent studies focused on this issue are briefly reviewed in this paper. Liu & Lin (2008) first evaluated the validity of potential field source surface model applied to one of five limb regions in the corona by comparing the theoretical polarization

maps with SOLARC observations in the IR Fe XIII 10747 Å forbidden coronal emission line (CEL). The five limb coronal regions were then studied together in order to study the spatial relation between the bright EUV features on the solar disk and the inferred IR emission sources, which were obtained from the inversion of the SOLARC linear polarization (LP) measurements (Liu 2009). The inversion for each fiber data in the field of view was made by finding the best location where the difference between the synthesized and the observed polarizations reaches the minimum in the integration path along the line of sight. We found a close relationship between the inferred IR emission source locations and the EUV strong emission positions.

## **Coronal magnetic fields inferred from IR wavelength and comparison with EUV observations**

Y. [Liu](#)

Ann. Geophys., 27, 2771-2777, 2009

<http://www.ann-geophys.net/27/2771/2009/angeo-27-2771-2009.pdf>

Spectropolarimetry using IR wavelength of 1075 nm has been proved to be a powerful tool for directly mapping solar coronal magnetic fields including transverse component directions and line-of-sight component intensities. Solar tomography, or stereoscopy based on EUV observations, can supply 3-D information for some magnetic field lines in bright EUV loops. In a previous paper \citep{liu08} the locations of the IR emission sources in the 3-D coordinate system were inferred from the comparison between the polarization data and the potential-field-source-surface (PFSS) model, for one of five west limb regions in the corona (Lin et al., 2004). The paper shows that the region with the loop system in the active region over the photospheric area with strong magnetic field intensity is the region with a dominant contribution to the observed Stokes signals. So, the inversion of the measured Stokes parameters could be done assuming that most of the signals come from a relatively thin layer over the area with a large photospheric magnetic field strength. Here, the five limb coronal regions are studied together in order to study the spatial correlation between the bright EUV loop features and the inferred IR emission sources. It is found that, for the coronal regions above the stronger photospheric magnetic fields, the locations of the IR emission sources are closer to or more consistent with the bright EUV loop locations than those above weaker photospheric fields. This result suggests that the structures of the coronal magnetic fields observed at IR and EUV wavelengths may be different when weak magnetic fields present there.

## **OBSERVATIONAL TEST OF CORONAL MAGNETIC FIELD MODELS.**

### **I. COMPARISON WITH POTENTIAL FIELD MODEL**

Yu [Liu](#) and Haosheng Lin

The Astrophysical Journal, 680:1496–1507, 2008

<http://www.journals.uchicago.edu/doi/pdf/10.1086/588645>

Recent advances have made it possible to obtain two-dimensional line-of-sight magnetic field maps of the solar corona from spectropolarimetric observations of the Fe xiii 1075 nm forbidden coronal emission line. Together with the linear polarization measurements that map the azimuthal direction of the coronal magnetic field projected in the plane of the sky containing Sun center, these coronal vector magnetograms allow for direct and quantitative observational testing of theoretical coronal magnetic field models. This paper presents a study testing the validity of potential-field coronal magnetic field models. We constructed a theoretical coronal magnetic field model of active region AR 10582 observed by the SOLARC coronagraph in 2004 by using a global potential field extrapolation of the synoptic map of Carrington Rotation 2104. Synthesized linear and circular polarization maps from thin layers of the coronal magnetic field model above the active region along the line of sight are compared with the observed maps. We found that the observed linear and circular polarization signals are consistent with the synthesized ones from layers located just above the sunspot of AR 10582 near the plane of the sky containing the Sun center.

## **A NOTE ON SATURATION SEEN IN THE MDI/SOHO MAGNETOGRAMS**

Y. [Liu](#), A.A. Norton, P.H. Scherrer

Solar Phys., 241 (1), 185-193, 2007.

## **A new solar signal: Average maximum sunspot magnetic fields independent of activity cycle**

William [Livingston](#), Fraser Watson

Geophys. Res. Lett. **2015**, 42, 9185-9188

<http://arxiv.org/pdf/1604.03050v1.pdf>

Over the past five years, 2010-2015, we have observed, in the near infrared (IR), the maximum magnetic field strengths for 4145 sunspot umbrae. Herein we distinguish field strengths from field flux. (Most solar magnetographs measure flux). Maximum field strength in umbrae is co-spatial with the position of umbral minimum brightness (Norton and Gilman, 2004). We measure field strength by the Zeeman splitting of the Fe 15648.5 Å spectral line. We show that in the IR no cycle dependence on average maximum field strength (2050 G) has been found  $\pm 20$  Gauss. A similar analysis of 17,450 spots observed by the Helioseismic and Magnetic Imager onboard the Solar Dynamics Observatory reveal the same cycle independence  $\pm 0.18$  G., or a variance of 0.01%. This is found not to change over the ongoing 2010-2015 minimum to maximum cycle. Conclude the average maximum umbral fields on the Sun are constant with time.

## **DECREASING SUNSPOT MAGNETIC FIELDS EXPLAIN UNIQUE 10.7 cm RADIO FLUX**

W. [Livingston](#)<sup>1</sup>, M. J. Penn<sup>1</sup>, and L. Svalgaard

**2012** ApJ 757 L8

Infrared spectral observations of sunspots from 1998 to 2011 have shown that on average sunspots changed, the magnetic fields weakened, and the temperatures rose. The data also show that sunspots or dark pores can only form at the solar surface if the magnetic field strength exceeds about 1500 G. Sunspots appear at the solar surface with a variety of field strengths, and during the period from 1998 to 2002 a histogram of the sunspot magnetic fields shows a normal distribution with a mean of  $2436 \pm 26$  G and a width of  $323 \pm 20$  G. During this observing period the mean of the magnetic field distribution decreased by  $46 \pm 6$  G per year, and we assume that as the 1500 G threshold was approached, magnetic fields appeared at the solar surface which could not form dark sunspots or pores. With this assumption we propose a quantity called the sunspot formation fraction and give an analytical form derived from the magnetic field distribution. We show that this fraction can quantitatively explain the changing relationship between sunspot number and solar radio flux measured at 10.7 cm wavelengths.

## **Three-Dimensional Structure of the Corona During WHPI Campaign Rotations CR-2219 and CR-2223**

D. G. [Lloveras](#), [A. M. Vásquez](#), [F. A. Nuevo](#), [R. A. Frazin](#), [W. Manchester IV](#), [N. Sachdeva](#), [B. Van der Holst](#), [P. Lamy](#), [H. Gilardy](#)

JGR [Volume127, Issue6](#) **2022** e2022JA030406

<https://agupubs.onlinelibrary.wiley.com/doi/epdf/10.1029/2022JA030406>

<https://doi.org/10.1029/2022JA030406>

Differential emission measure tomography (DEMT) and white light (WL) tomography were applied to study the three-dimensional (3D) structure of the global solar corona for two Whole Heliosphere and Planetary Interactions campaign periods, Carrington rotations 2219 and 2223. With DEMT, Solar Dynamics Observatory/Atmospheric Imaging Assembly images were used to reconstruct the 3D coronal electron density and temperature in the range of heliocentric distance 1.02–1.25  $R_{\odot}$ . With WL tomography, Solar and Heliospheric Observatory/Large Angle and Spectrometric CORonagraph-C2 images were used to reconstruct the 3D electron density in the range of heliocentric distance 2.5–6.0  $R_{\odot}$ . The two periods were also simulated with the 3D-magneto-hydrodynamic Alfvén Wave Solar Model (AWSoM), and its results compared in detail with the reconstructions. The DEMT analysis reveals a 20% less dense and 20% hotter corona than for rotations corresponding to the solar cycle 23/24 deep minimum. The electron density and temperature of the AWSoM model agree with DEMT results within 10% and 20%, respectively, while its electron density overestimates results of WL tomography up to 75%. The slow (fast) component of the terminal wind speed of the model is found to be associated with field lines characterized by larger (smaller) values of the tomographic density and temperature at the coronal base. DEMT reconstructions reveal the coronal plasma to be ubiquitously characterized by temperature variability of up to  $\approx 45\%$  over spatial scales of order  $\sim 104$  km. Taking into account this level of fine-structure by global models may be consequential for their predictions on wave propagation in the corona.

## **Thermodynamic Structure of the Solar Corona: Tomographic Reconstructions and MHD Modeling**

D. G. [Lloveras](#), [A. M. Vásquez](#), [F. A. Nuevo](#), [C. Mac Cormack](#), [N. Sachdeva](#), [W. Manchester IV](#), [B. Van der Holst](#), [R. A. Frazin](#)

Solar Phys. **2020**

<https://arxiv.org/pdf/2004.06815.pdf>

We carry out a study of the global three-dimensional (3D) structure of the electron density and temperature of the quiescent inner solar corona ( $r < 1.25 R_{\odot}$ ) by means of tomographic reconstructions and magnetohydrodynamic

simulations. We use differential emission measure tomography (DEMT) and the Alfvén Wave Solar Model (AWSoM), in their latest versions. Two target rotations were selected from the solar minimum between solar cycles (SCs) 23 and 24 and the declining phase of SC 24. We report in quantitative detail on the 3D thermodynamic structure of the core and outer layers of the streamer belt, and of the high latitude coronal holes (CH), as revealed by the DEMT analysis. We report on the presence of two types of structures within the streamer belt, loops with temperature decreasing/increasing with height (dubbed down/up loops), as reported first in previous DEMT studies. We also estimate the heating energy flux required at the coronal base to keep these structures stable, found to be on order  $10^5 \text{ erg cm}^{-2} \text{ s}^{-1}$ , consistently with previous DEMT and spectroscopic studies. We discuss how these findings are consistent with coronal dissipation of Alfvén waves. We compare the 3D results of DEMT and AWSoM in distinct magnetic structures. We show that the agreement between the products of both techniques is the best so far, with an overall agreement  $\lesssim 20\%$ , depending on the target rotation and the specific coronal region. In its current implementation the AWSoM model can not reproduce down loops though. Also, in the source region of the fast and slow components of the solar wind, the electron density of the AWSoM model increases with latitude, opposite to the trend observed in DEMT reconstructions.

## **Excess open solar magnetic flux from satellite data:**

### **2. A survey of kinematic effects**

**Lockwood, M.;** Owens, M.; Rouillard, A. P.

J. Geophys. Res., Vol. 114, No. A11, A11104, 2009

<http://dx.doi.org/10.1029/2009JA014450>

We investigate the “flux excess” effect, whereby open solar flux estimates from spacecraft increase with increasing heliocentric distance. We analyze the kinematic effect on these open solar flux estimates of large-scale longitudinal structure in the solar wind flow, with particular emphasis on correcting estimates made using data from near-Earth satellites. We show that scatter, but no net bias, is introduced by the kinematic “bunching effect” on sampling and that this is true for both compression and rarefaction regions. The observed flux excesses, as a function of heliocentric distance, are shown to be consistent with open solar flux estimates from solar magnetograms made using the potential field source surface method and are well explained by the kinematic effect of solar wind speed variations on the frozen-in heliospheric field. Applying this kinematic correction to the Omni-2 interplanetary data set shows that the open solar flux at solar minimum fell from an annual mean of  $3.82 \times 10^{16}$  Wb in 1987 to close to half that value ( $1.98 \times 10^{16}$  Wb) in 2007, making the fall in the minimum value over the last two solar cycles considerably faster than the rise inferred from geomagnetic activity observations over four solar cycles in the first half of the 20th century.

## **Excess open solar magnetic flux from satellite data:**

### **1. Analysis of the third perihelion Ulysses pass**

**Lockwood, M.;** Owens, M.; Rouillard, A. P.

J. Geophys. Res., Vol. 114, No. A11, A11103, 2009

<http://dx.doi.org/10.1029/2009JA014449>

We use the third perihelion pass by the Ulysses spacecraft to illustrate and investigate the “flux excess” effect, whereby open solar flux estimates from spacecraft increase with increasing heliocentric distance. We analyze the potential effects of small-scale structure in the heliospheric field (giving fluctuations in the radial component on timescales smaller than 1 h) and kinematic time-of-flight effects of longitudinal structure in the solar wind flow. We show that the flux excess is explained by neither very small-scale structure (timescales  $< 1$  h) nor by the kinematic “bunching effect” on spacecraft sampling. The observed flux excesses is, however, well explained by the kinematic effect of larger-scale ( $> 1$  day) solar wind speed variations on the frozen-in heliospheric field. We show that averaging over an interval  $T$  (that is long enough to eliminate structure originating in the heliosphere yet small enough to avoid cancelling opposite polarity radial field that originates from genuine sector structure in the coronal source field) is only an approximately valid way of allowing for these effects and does not adequately explain or account for differences between the streamer belt and the polar coronal holes.

## **Absolute velocity measurements in sunspot umbrae**

**J. Löhner-Böttcher, W. Schmidt, R. Schlichenmaier, H.-P. Doerr, T. Steinmetz, R. Holzwarth**

A&A 617, A19 2018

<https://arxiv.org/pdf/1804.08304.pdf>

In sunspot umbrae, convection is largely suppressed by the strong magnetic field. Previous measurements reported on negligible convective flows in umbral cores. Based on this, numerous studies have taken the umbra as zero reference to calculate Doppler velocities of the ambient active region. To clarify the amount of convective motion in the darkest part of umbrae, we directly measured Doppler velocities with an unprecedented accuracy and precision. We performed spectroscopic observations of sunspot umbrae with the Laser Absolute Reference Spectrograph

(LARS) at the German Vacuum Tower Telescope. A laser frequency comb enabled the calibration of the high-resolution spectrograph and absolute wavelength positions. A thorough spectral calibration, including the measurement of the reference wavelength, yielded Doppler shifts of the spectral line Ti i 5713.9 Å with an uncertainty of around 5 m s<sup>-1</sup>. The measured Doppler shifts are a composition of umbral convection and magneto-acoustic waves. For the analysis of convective shifts, we temporally average each sequence to reduce the superimposed wave signal. Compared to convective blueshifts of up to -350 m s<sup>-1</sup> in the quiet Sun, sunspot umbrae yield a strongly reduced convective blueshifts around -30 m s<sup>-1</sup>. We find that the velocity in a sunspot umbra correlates significantly with the magnetic field strength, but also with the umbral temperature defining the depth of the titanium line. The vertical upward motion decreases with increasing field strength. Extrapolating the linear approximation to zero magnetic field reproduces the measured quiet Sun blueshift. Simply taking the sunspot umbra as a zero velocity reference for the calculation of photospheric Dopplergrams can imply a systematic velocity error. **2014 / 07 / 12-13, 2014 / 08 / 21-29**

## **Magnetic field reconstruction based on sunspot oscillations**

J. **Löhner-Böttcher**, N. Bello González, W. Schmidt

Astron. Nachrichten **2016**

<http://arxiv.org/pdf/1601.05925v1.pdf>

The magnetic field of a sunspot guides magnetohydrodynamic waves toward higher atmospheric layers. In the upper photosphere and lower chromosphere, wave modes with periods longer than the acoustic cut-off period become evanescent. The cut-off period essentially changes due to the atmospheric properties, e.g., increases for larger zenith inclinations of the magnetic field. In this work, we aim at introducing a novel technique of reconstructing the magnetic field inclination on the basis of the dominating wave periods in the sunspot chromosphere and upper photosphere. On 2013 August 21st, we observed an isolated, circular sunspot (NOAA11823) for 58 min in a purely spectroscopic multi-wavelength mode with the Interferometric Bidimensional Spectro-polarimeter (IBIS) at the Dunn Solar Telescope. By means of a wavelet power analysis, we retrieved the dominating wave periods and reconstructed the zenith inclinations in the chromosphere and upper photosphere. The results are in good agreement with the lower photospheric HMI magnetograms. The sunspot's magnetic field in the chromosphere inclines from almost vertical (0°) in the umbra to around 60° in the outer penumbra. With increasing altitude in the sunspot atmosphere, the magnetic field of the penumbra becomes less inclined. We conclude that the reconstruction of the magnetic field topology on the basis of sunspot oscillations yields consistent and conclusive results. The technique opens up a new possibility to infer the magnetic field inclination in the solar chromosphere.

See **HMI Science Nuggets #51, Apr 2016**

<http://hmi.stanford.edu/hminuggets/?p=1457>

## **Signatures of running penumbral waves in sunspot photospheres**

Johannes **Löhner-Böttcher**, Nazaret Bello González

A&A 580, A53 **2015**

<http://arxiv.org/pdf/1503.09106v1.pdf>

The highly dynamic atmosphere above sunspots exhibits a wealth of magnetohydrodynamic (MHD) waves. Recent studies suggest a coupled nature of the most prominent phenomena: umbral flashes (UFs) and running penumbral waves (RPWs). From an observational point of view, we perform a height-dependent study of RPWs, compare their wave characteristics and aim to track down these so far only chromospherically observed phenomena to photospheric layers to prove the upward propagating field-guided nature of RPWs. We analyze a time series (58 min) of multi-wavelength observations of an isolated circular sunspot (NOAA11823) taken at high spatial and temporal resolution in spectroscopic mode with the Interferometric Bidimensional Spectro-polarimeter (IBIS/DST). By means of a multi-layer intensity sampling, velocity comparisons, wavelet power analysis and sectorial studies of time-slices, we retrieve the power distribution, characteristic periodicities and propagation characteristics of sunspot waves at photospheric and chromospheric levels. Signatures of RPWs are found at photospheric layers. Those continuous oscillations occur preferably at periods between 4-6 min starting at the inner penumbral boundary. The photospheric oscillations all have a slightly delayed, more defined chromospheric counterpart with larger relative velocities (which are linked to preceding UF events). In all layers the power of RPWs follows a filamentary fine-structure and shows a typical ring-shaped power distribution increasing in radius for larger wave periods. The analysis of time-slices reveals apparent horizontal velocities for RPWs at photospheric layers of ≈50 km/s which decrease to ≈30 km/s at chromospheric heights. The observations strongly support the scenario of RPWs being upward propagating slow-mode waves guided by the magnetic field lines. **August 21st 2013**

See **HMI Science Nuggets #44, Oct 2015**

<http://hmi.stanford.edu/hminuggets/?p=1304>

## **Using EIS to measure the coronal magnetic field**

David **Long**, David Williams, Stéphane Régnier, Louise Harra

EIS Nugget, May 2013

[http://solarb.mssl.ucl.ac.uk/SolarB/nuggets/nugget\\_2013may.jsp](http://solarb.mssl.ucl.ac.uk/SolarB/nuggets/nugget_2013may.jsp)

Although the Sun's magnetic field is responsible for much of the activity that makes the Sun such an interesting star, it continues to be difficult to accurately estimate its strength in the low corona. This can be done using Zeeman splitting (cf. Lin et al., 2004) or the Hanle effect (cf. Raouafi et al., 2002), but this is generally only possible near active regions where the magnetic field strength is high. In quieter regions, the lower magnetic field strength can be inferred by examining variations in how global coronal waves (commonly called "EIT Waves") propagate through the corona, a technique called coronal seismology (e.g., Uchida, 1970, Roberts et al., 1984, West et al., 2011).

"EIT Waves" are large-scale global perturbations travelling at velocities of up to 1000 km/s that can traverse the Sun in less than an hour. Originally discovered using SOHO/EIT (Thompson et al., 1998), they have been variously interpreted as fast-mode magnetohydrodynamic waves or the signature of magnetic reconnection as a CME erupts into the heliosphere. Recent results by Warmuth & Mann, (2011) have suggested that the pulse velocity may indicate its physical nature, with faster pulses consistent with a MHD wave interpretation while pulses exhibiting irregular kinematics are more consistent with the "pseudo-wave" interpretation.

In Long et al. (2013) we estimate the magnetic field strength of the quiet solar corona by combining high cadence images from SDO/AIA with high-resolution spectra from Hinode/EIS. These results are then compared to magnetic field extrapolations to determine the height-range of the feature. **12-June-2010, 16-February-2011**

## Topological Methods for the Analysis of Solar Magnetic Fields

Dana W. [Longcope](#)

Living **Rev. Solar Phys.**, 2, (2005), 7

<http://www.livingreviews.org/lrsp-2005-7>

The solar coronal magnetic field is anchored to a complex distribution of photospheric flux consisting of sunspots and magnetic elements. Coronal activity such as flares, eruptions and general heating is often attributed to the manner in which the coronal field responds to photospheric motions. A number of powerful techniques have been developed to characterize the response of the coronal field by describing its topology. According to such analyses, activity will be concentrated around topological features in the coronal field such as separatrices, null points or bald patches. Such topological properties are insensitive to the detailed geometry of the magnetic field and thereby create an analytic tool powerful and robust enough to be useful on complex observations with limited resolution. This article reviews those topological techniques, their developments and applications to observations.

## Similarities of magnetoconvection in the umbra and in the penumbra of sunspots

[B. Löptien](#), [A. Lagg](#), [M. van Noort](#), [S. K. Solanki](#)

A&A **2021**

<https://arxiv.org/pdf/2110.01352.pdf>

Context. It is unclear why there is a rather sharp boundary in sunspots between the umbra and the penumbra. Both regions exhibit magnetoconvection, manifesting in penumbral filaments in the penumbra and in umbral dots in the umbra.

Aims. Here we compare the physical properties of umbral dots and penumbral filaments. Our goal is to understand how the properties of these convective features change across the boundary between the umbra and the penumbra and how this is related to the rapid increase in brightness at the umbra-penumbra boundary.

Methods. We derived ensemble averages of the physical properties of different types of convective features based on observations of two sunspots with Hinode.

Results. There are strong similarities between the convective features in the outer parts of the umbra and the ones in the penumbra, with most physical parameters being smooth and continuous functions of the length of the features.

Conclusions. Our results indicate that the transition in brightness from the umbra to the penumbra is solely caused by an increased effectiveness of magnetoconvection within individual convective cells. There is no significant difference in the number density of convective elements between the outer umbra and the inner penumbra.

Penumbral filaments exhibit a larger area and a higher brightness compared to umbral dots. It is still unclear, how exactly the underlying magnetic field causes the increase in size and brightness of convective features in the penumbra. **14 November 2006, 6 January 2007**

## Oscillator Models of the Solar Cycle

**Review**

Ilídio [Lopes](#), [Dário Passos](#), [Melinda Nagy](#), [Kristof Petrovay](#)

[Space Science Reviews](#), December 2014, Volume 186, [Issue 1-4](#), pp 535-559

This article reviews some of the leading results obtained in solar dynamo physics by using temporal oscillator models as a tool to interpret observational data and dynamo model predictions. We discuss how solar observational



data such as the sunspot number is used to infer the leading quantities responsible for the solar variability during the last few centuries. Moreover, we discuss the advantages and difficulties of using inversion methods (or backward methods) over forward methods to interpret the solar dynamo data. We argue that this approach could help us to have a better insight about the leading physical processes responsible for solar dynamo, in a similar manner as helioseismology has helped to achieve a better insight on the thermodynamic structure and flow dynamics in the Sun's interior.

### **Similarities of magnetoconvection in the umbra and in the penumbra of sunspots**

B. Löptien<sup>1</sup>, A. Lagg<sup>1,3</sup>, M. van Noort<sup>1</sup> and S. K. Solanki<sup>1,2</sup>

A&A 655, A61 (2021)

<https://www.aanda.org/articles/aa/pdf/2021/11/aa41440-21.pdf>

<https://doi.org/10.1051/0004-6361/202141440>

<https://arxiv.org/pdf/2110.01352.pdf>

Context. It is unclear why there is a rather sharp boundary in sunspots between the umbra and the penumbra. Both regions exhibit magnetoconvection, which manifests in penumbral filaments in the penumbra and in umbral dots in the umbra.

Aims. Here we compare the physical properties of umbral dots and penumbral filaments. Our goal is to understand how the properties of these convective features change across the boundary between the umbra and the penumbra and how this is related to the rapid increase in brightness at the umbra-penumbra boundary.

Methods. We derived ensemble averages of the physical properties of different types of convective features based on observations of two sunspots with Hinode.

Results. There are strong similarities between the convective features in the outer parts of the umbra and the ones in the penumbra, with most physical parameters being smooth and continuous functions of the length of the features.

Conclusions. Our results indicate that the transition in brightness from the umbra to the penumbra is solely caused by an increased effectiveness of magnetoconvection within individual convective cells. There is no significant difference in the number density of convective elements between the outer umbra and the inner penumbra.

Penumbral filaments exhibit a larger area and a higher brightness compared to umbral dots. It is still unclear how exactly the underlying magnetic field causes the increase in the size and brightness of convective features in the penumbra. **14 November 2006**

### **No universal connection between the vertical magnetic field and the umbra-penumbra boundary in sunspots**

B. Löptien, A. Lagg, M. van Noort, S. K. Solanki

A&A 639, A106 2020

<https://arxiv.org/pdf/2006.02346.pdf>

<https://www.aanda.org/articles/aa/pdf/2020/07/aa37974-20.pdf>

Context. It has been reported that the boundary between the umbra and the penumbra of sunspots occurs at a canonical value of the strength of the vertical magnetic field, independently of the size of the spot. This critical field strength is interpreted as to be the threshold for the onset of magnetoconvection.

Aims. Here we investigate the reasons why this criterion, also called the Jurčák criterion in the literature, does not always identify the boundary between umbra and penumbra.

Methods. We perform a statistical analysis of 23 sunspots observed with Hinode/SOT. We compare the properties of the continuum intensity and the vertical magnetic field between filaments and spines and how they vary between spots of different sizes.

Results. We find that the inner boundary of the penumbra is not related to a universal value of the vertical magnetic field. The properties of spines and filaments vary between spots of different sizes. Both components are darker in larger spots and the spines exhibit stronger vertical magnetic field. These variations of the properties of filaments and spines with spot size are also the reason for the reported invariance of the averaged vertical magnetic field at 50% of the mean continuum intensity.

Conclusions. The formation of filaments and the onset of magnetoconvection are not related to a canonical value of the strength of the vertical magnetic field. Such a seemingly unique magnetic field strength is rather an effect of the filling factor of spines and penumbral filaments. **2006.11.14, 2007.04.30, 2007.05.01-04, 2007.08.27, 2010.01.26**

**Table 1.** Overview of the sunspot observations used in this study (2006-2012)

### **Connecting the Wilson depression to the magnetic field of sunspots**

B. Löptien, A. Lagg, M. van Noort, S. K. Solanki

A&A 635, A202 2020

<https://arxiv.org/pdf/2002.07484.pdf>

<https://www.aanda.org/articles/aa/pdf/2020/03/aa36975-19.pdf>

Context: In sunspots, the geometric height of continuum optical depth unity is depressed compared to the quiet Sun. This so-called Wilson depression is caused by the Lorentz force of the strong magnetic field inside the spots.

However, it is not understood in detail yet, how the Wilson depression is related to the strength and geometry of the magnetic field or to other properties of the sunspot.

**Aims:** We aim to study the dependence of the Wilson depression on the properties of the magnetic field of the sunspots and how exactly the magnetic field contributes to balancing the Wilson depression with respect to the gas pressure of the surroundings of the spots.

**Methods:** Our study is based on 24 spectropolarimetric scans of 12 individual sunspots performed with Hinode. We derived the Wilson depression for each spot using both, a recently developed method that is based on minimizing the divergence of the magnetic field, and an approach developed earlier that enforces an equilibrium between the gas pressure and the magnetic pressure inside the spot and the gas pressure in the quiet Sun, thus neglecting the influence of the curvature force. We then performed a statistical analysis by comparing the Wilson depression resulting from the two techniques with each other and by relating them to various parameters of the sunspots, such as their size or the strength of the magnetic field.

**Results:** We find that the Wilson depression becomes larger for spots with a stronger magnetic field, but not as much as one would expect from the increased magnetic pressure. This suggests that the curvature integral provides an important contribution to the Wilson depression, particularly for spots with a weak magnetic field. Our results indicate that the geometry of the magnetic field in the penumbra is different between spots with different strengths of the average umbral magnetic field. **31 July 2012**

**Table 1.** Overview of the investigated spots and the derived Wilson depressions

## Measuring the Wilson depression of sunspots using the divergence-free condition of the magnetic field vector

B. Löptien, A. Lagg, M. van Noort, S. K. Solanki

A&A 619, A42 2018

<https://arxiv.org/pdf/1808.06867.pdf>

**Context:** The Wilson depression is the difference in geometric height of unit continuum optical depth between the sunspot umbra and the quiet Sun. Measuring the Wilson depression is important for understanding the geometry of sunspots. Current methods suffer from systematic effects or need to make assumptions on the geometry of the magnetic field. This leads to large systematic uncertainties of the derived Wilson depressions.

**Aims:** We aim at developing a robust method for deriving the Wilson depression that only requires the information about the magnetic field that is accessible from spectropolarimetry, and that does not rely on assumptions on the geometry of sunspots or on their magnetic field.

**Methods:** Our method is based on minimizing the divergence of the magnetic field vector derived from spectropolarimetric observations. We focus on large spatial scales only in order to reduce the number of free parameters.

**Results:** We test the performance of our method using synthetic Hinode data derived from two sunspot simulations. We find that the maximum and the umbral averaged Wilson depression for both spots determined with our method typically lies within 100 km of the true value obtained from the simulations. In addition, we apply the method to Hinode observations of a sunspot. The derived Wilson depression (about 600 km) is consistent with results typically obtained from the Wilson effect. We also find that the Wilson depression obtained from using horizontal force balance gives 110 - 180 km smaller Wilson depressions than both, what we find and what we deduce directly from the simulations. This suggests that the magnetic pressure and the magnetic curvature force contribute to the Wilson depression by a similar amount.

## A new look at sunspot formation using theory and observations

Illa R. Losada, Jörn Warnecke, Kolja Glogowski, Markus Roth, Axel Brandenburg, Nathan Kleorin, Igor Rogachevskii

proceeding series IAUS327 2016

<https://arxiv.org/pdf/1704.04062.pdf>

Sunspots are of basic interest in the study of the Sun. Their relevance ranges from them being an activity indicator of magnetic fields to being the place where coronal mass ejections and flares erupt. They are therefore also an important ingredient of space weather. Their formation, however, is still an unresolved problem in solar physics. Observations utilize just 2D surface information near the spot, but it is debatable how to infer deep structures and properties from local helioseismology. For a long time, it was believed that flux tubes rising from the bottom of the convection zone are the origin of the bipolar sunspot structure seen on the solar surface. However, this theory has been challenged, in particular recently by new surface observation, helioseismic inversions, and numerical models of convective dynamos. In this article we discuss another theoretical approach to the formation of sunspots: the negative effective magnetic pressure instability. This is a large-scale instability, in which the total (kinetic plus magnetic) turbulent pressure can be suppressed in the presence of a weak large-scale magnetic field, leading to a converging downflow, which eventually concentrates the magnetic field within it. Numerical simulations of forced stratified turbulence have been able to produce strong super-equipartition flux concentrations, similar to sunspots at the solar surface. In this framework, sunspots would only form close to the surface due to the instability constraints on stratification and rotation. Additionally, we present some ideas from local helioseismology, where we plan to use

the Hankel analysis to study the pre-emergence phase of a sunspot and to constrain its deep structure and formation mechanism.

### **Magnetic flux concentrations in a polytropic atmosphere**

I. R. [Losada](#)<sup>1,2</sup>, A. Brandenburg<sup>1,2</sup>, N. Kleeorin<sup>3,1,4</sup> and I. Rogachevskii

A&A 564, A2 (2014)

<http://arxiv.org/pdf/1307.4945v4.pdf>

Context. Strongly stratified hydromagnetic turbulence has recently been identified as a candidate for explaining the spontaneous formation of magnetic flux concentrations by the negative effective magnetic pressure instability (NEMPI). Much of this work has been done for isothermal layers, in which the density scale height is constant throughout.

Aims. We now want to know whether earlier conclusions regarding the size of magnetic structures and their growth rates carry over to the case of polytropic layers, in which the scale height decreases sharply as one approaches the surface.

Methods. To allow for a continuous transition from isothermal to polytropic layers, we employ a generalization of the exponential function known as the  $q$ -exponential. This implies that the top of the polytropic layer shifts with changing polytropic index such that the scale height is always the same at some reference height. We used both mean-field simulations (MFS) and direct numerical simulations (DNS) of forced stratified turbulence to determine the resulting flux concentrations in polytropic layers. Cases of both horizontal and vertical applied magnetic fields were considered.

Results. Magnetic structures begin to form at a depth where the magnetic field strength is a small fraction of the local equipartition field strength with respect to the turbulent kinetic energy. Unlike the isothermal case where stronger fields can give rise to magnetic flux concentrations at larger depths, in the polytropic case the growth rate of NEMPI decreases for structures deeper down. Moreover, the structures that form higher up have a smaller horizontal scale of about four times their local depth. For vertical fields, magnetic structures of super-equipartition strengths are formed, because such fields survive downward advection that causes NEMPI with horizontal magnetic fields to reach premature nonlinear saturation by what is called the “potato-sack” effect. The horizontal cross-section of such structures found in DNS is approximately circular, which is reproduced with MFS of NEMPI using a vertical magnetic field.

Conclusions. Results based on isothermal models can be applied locally to polytropic layers. For vertical fields, magnetic flux concentrations of super-equipartition strengths form, which supports suggestions that sunspot formation might be a shallow phenomenon.

, which was proposed earlier to explain other asymmetries in bipolar ARs.

### **Sustained heating of the chromosphere and transition region over a sunspot light bridge**

[Rohan E. Louis](#), [Shibu K. Mathew](#), [A. Raja Bayanna](#), [Christian Beck](#), [Debi P. Choudhary](#)

ApJ 942 62 2023

<https://arxiv.org/pdf/2301.00608.pdf>

<https://iopscience.iop.org/article/10.3847/1538-4357/aca612/pdf>

Sunspot light bridges (LBs) exhibit a wide range of short-lived phenomena in the chromosphere and transition region. In contrast, we use here data from the Multi-Application Solar Telescope (MAST), the Interface Region Imaging Spectrograph (IRIS), Hinode, the Atmospheric Imaging Assembly (AIA), and the Helioseismic and Magnetic Imager (HMI) to analyze the sustained heating over days in an LB in a regular sunspot. Chromospheric temperatures were retrieved from the the MAST Ca II and IRIS Mg II lines by nonlocal thermodynamic equilibrium inversions. Line widths, Doppler shifts, and intensities were derived from the IRIS lines using Gaussian fits. Coronal temperatures were estimated through the differential emission measure, while the coronal magnetic field was obtained from an extrapolation of the HMI vector field. At the photosphere, the LB exhibits a granular morphology with field strengths of about 400 G and no significant electric currents. The sunspot does not fragment, and the LB remains stable for several days. The chromospheric temperature, IRIS line intensities and widths, and AIA 171 Å and 211 Å intensities are all enhanced in the LB with temperatures from 8000 K to 2.5 MK. Photospheric plasma motions remain small, while the chromosphere and transition region indicate predominantly red-shifts of 5-20 km/s with occasional supersonic downflows exceeding 100 km/s. The excess thermal energy over the LB is about  $3.2 \times 10^{26}$  erg and matches the radiative losses. It could be supplied by magnetic flux loss of the sunspot ( $7.5 \times 10^{27}$  erg), kinetic energy from the increase in the LB width ( $4 \times 10^{28}$  erg), or freefall of mass along the coronal loops ( $6.3 \times 10^{26}$  erg). **2019 May 14**

### **Heating of the solar chromosphere in a sunspot light bridge by electric currents**

[Rohan E. Louis](#), [Avijeeet Prasad](#), [Christian Beck](#), [Debi Prasad Choudhary](#), [Mehmet S. Yalim](#)

A&A Lett 652, L4 2021

<https://arxiv.org/pdf/2107.12066.pdf>

<https://doi.org/10.1051/0004-6361/202141456>

<https://www.aanda.org/articles/aa/pdf/2021/08/aa41456-21.pdf>

Context: Resistive Ohmic dissipation has been suggested as a mechanism for heating the solar chromosphere, but few studies have established this association. Aim: We aim to determine how Ohmic dissipation by electric currents can heat the solar chromosphere. Methods: We combine high-resolution spectroscopic Ca II data from the Dunn Solar Telescope and vector magnetic field observations from the Helioseismic and Magnetic Imager (HMI) to investigate thermal enhancements in a sunspot light bridge. The photospheric magnetic field from HMI was extrapolated to the corona using a non-force-free field technique that provided the three-dimensional distribution of electric currents, while an inversion of the chromospheric Ca II line with a local thermodynamic equilibrium and a nonlocal thermodynamic equilibrium spectral archive delivered the temperature stratifications from the photosphere to the chromosphere. Results: We find that the light bridge is a site of strong electric currents, of about  $0.3 \text{ A/m}^2$  at the bottom boundary, which extend to about 0.7 Mm while decreasing monotonically with height. These currents produce a chromospheric temperature excess of about 600-800 K relative to the umbra. Only the light bridge, where relatively weak and highly inclined magnetic fields emerge over a duration of 13 hr, shows a spatial coincidence of thermal enhancements and electric currents. The temperature enhancements and the Cowling heating are primarily confined to a height range of 0.4-0.7 Mm above the light bridge. The corresponding increase in internal energy of  $200 \text{ J/m}^3$  can be supplied by the heating in about 10 min. Conclusions: Our results provide direct evidence for currents heating the lower solar chromosphere through Ohmic dissipation. **2014 March 13**

IRIS Nugget 14 Apr 2023 <https://iris.lmsal.com/nugget>

## Homologous flaring activity over a sunspot light bridge in an emerging active region

[Rohan E. Louis](#), [Julia K. Thalmann](#)

2021 ApJL 907 L4

<https://arxiv.org/pdf/2012.07454.pdf>

<https://doi.org/10.3847/2041-8213/abd478>

Sunspot light bridges are known to exhibit a variety of dynamic and persistent phenomena such as surges, small-scale jets etc. in the chromosphere and transition region. While it has generally been proposed that magnetic reconnection is responsible for this small-scale dynamism, persistent flaring activity lasting several hours from the same spatial location on a sunspot light bridge, has rarely been reported. We combine observations from the Atmospheric Imaging Assembly and the Helioseismic Magnetic Imager on board the Solar Dynamics Observatory to investigate homologous flaring activity over a small sunspot light bridge in an emerging flux region. The homologous flares all produced broad, collimated jets, including a B6.4 class flare. The jets rise at a speed of about 200 km/s, reach projected heights of about 98 Mm, and emerge from the same spatial location for nearly 14 hrs, after which they cease completely. A non-linear force free extrapolation of the photospheric magnetic field shows a low-lying flux rope connecting the light bridge to a remote opposite-polarity network. The persistent flares occur as a result of the rapid horizontal motion of the leading sunspot that causes the relatively vertical magnetic fields in the adjacent umbra to reconnect with the low-lying flux rope in the light bridge. Our results indicate that the flaring ceases once the flux rope has lost sufficient twist through repeated reconnections. **1 July 2012**

## The formation of an atypical sunspot light bridge as a result of large-scale flux emergence

[Rohan E. Louis](#), [Christian Beck](#), [Debi P. Choudhary](#)

ApJ 905 153 2020

<https://arxiv.org/pdf/2010.14085.pdf>

<https://doi.org/10.3847/1538-4357/abc618>

We use a combination of full-disk data from the Solar Dynamics Observatory and high-resolution data from the Dunn Solar Telescope (DST) to study the formation, structure, and evolution of an atypical light bridge (LB) in a regular sunspot. The LB results from the emergence of magnetic flux with one footpoint rooted in a pore outside the parent sunspot that appears about 17 hrs before the LB. The pore has a polarity opposite to that of the sunspot and recedes away from it at a speed of about 0.4 km/s. This is accompanied by the development of an elongated magnetic channel in the outer penumbra which triggers the formation of the LB when it reaches the inner penumbral boundary. The LB is a nearly horizontal structure with a field strength of about 1.2 kG that exhibits long-lived photospheric blue-shifts of about 0.85 km/s along its entire length. The emergence of the LB leads to dynamic surges in the chromosphere and transition region about 13 min later. We derived the photospheric and chromospheric structure of the LB in the DST data from spectral line parameters and inversions of He I at 1083 nm, Si I at 1082.7 nm, Ca II IR at 854 nm and H $\alpha$  at 656 nm, and speckle-reconstructed imaging at 700 nm and 430 nm. The LB shows an elongated filamentary shape in the photosphere without lateral extrusions. The thermal inversion of Ca II IR reveals the LB to be about 600-800 K hotter than the umbra. Different sections of the LB are elevated to heights between 400 and 700 km. Our results indicate that the LB formation is part of a flux emergence event with the LB envelope reaching a height of about 29 Mm before dissolving after about 13 hr. We suggest that the existence of

persistent, large-scale photospheric blue-shifts in LBs is the most likely criterion to distinguish between flux emergence events and overturning convection in field-free umbral intrusions. **2014 March 12-14**

### **Design of an adaptable Stokes polarimeter for exploring chromospheric magnetism**

Rohan E. **Louis**, A. Raja Bayanna, Héctor Socas Navarro

[Advances in Space Research](#) **Volume 60, Issue 7**, 1 October **2017**, Pages 1547-1556

The chromosphere is a highly complex and dynamic layer of the Sun, that serves as a conduit for mass and energy supply between two, very distinct regions of the solar atmosphere, namely, the photosphere and corona. Inferring magnetic fields in the chromosphere, has thus become an important topic, that can be addressed with large-aperture solar telescopes to carry out highly sensitive polarimetric measurements. In this article, we present a design of a polarimeter for investigating the chromospheric magnetic field. The instrument consists of a number of lenses, two ferro-electric liquid crystals, a Wollaston prism, and a CCD camera. The optical design is similar to that of a commercial zoom lens which allows a variable  $f\#$  while maintaining focus and aberrations well within the Airy disc. The optical design of the Adaptable Chromospheric Polarimeter (ACROPOL) makes use of off-the-shelf components and is described for the 70 cm Vacuum Tower Telescope and the 1.5 m GREGOR telescope at Observatorio del Teide, Tenerife, Spain. Our design shows that the optical train can be separated into two units where the first unit, consisting of a single lens, has to be changed while going from the VTT to the GREGOR configuration. We also discuss the tolerances within which, diffraction limited performance can be achieved with our design.

### **Small-scale magnetic flux emergence in a sunspot light bridge**

Rohan E. **Louis**, Luis R. Bellot Rubio, Jaime de la Cruz Rodriguez, Hector Socas-Navarro, Ada Ortiz  
A&A **584**, A1 **2015**

<http://arxiv.org/pdf/1509.00741v1.pdf>

We analyse a sequence of high-resolution spectropolarimetric observations of a sunspot taken at the 1-m SST, to determine the nature of flux emergence in a light bridge and the processes related to its evolution in the photosphere and chromosphere. Blueshifts of about 2 km/s are seen near the entrance of a granular light bridge on the limbward side of the spot. They lie next to a strongly redshifted patch that appeared 6 mins earlier. Both patches are seen for 25 mins until the end of the sequence. The blueshifts coincide with an elongated emerging granule, while the redshifts appear at the end of it. In the photosphere, the development of the blueshifts is accompanied by a simultaneous increase in field strength and inclination, with the field becoming nearly horizontal. In the redshifted patch, the magnetic field is equally horizontal but of opposite polarity. An intense brightening is seen in the Ca filtergrams over these features, 17 mins after they emerge in the photosphere. The brightening is due to emission in the blue wing of the Ca line, close to its knee. Non-LTE inversions reveal that the asymmetric emission is caused by a temperature enhancement of about 700 K between  $-5.0 < \log \tau < -3.0$  and a blueshift of 3 km/s at  $\log \tau = -2.3$ . The photospheric blueshifts and redshifts seem to be caused by the emergence of a small-scale, flat Omega-loop with highly inclined footpoints of opposite polarity. The gas motions detected in the two footpoints are reminiscent of a siphon flow. The rising loop is probably confined to the lower atmosphere by the overlying sunspot magnetic field and the subsequent interaction may be responsible for temperature enhancements in the upper photosphere/lower chromosphere. This is the first time that magnetic flux is observed to emerge in the strongly magnetised environment of sunspots, pushed upward by the convective flows of a granular light bridge. **2009 July 5**

### **Small-scale magnetic and velocity inhomogeneities in a sunspot light bridge**

Rohan E. **Louis**

*Advances in Space Research* **2015**

<http://arxiv.org/pdf/1509.00761v1.pdf>

High resolution spectro-polarimetric observations of a sunspot light bridge by Hinode, reveal small-scale inhomogeneities in the magnetic field and velocity. These inhomogeneities arise as a consequence of a weak, secondary lobe in the Stokes V profile which have a polarity opposite that of the sunspot and very large ( $>5$  km/s) Doppler velocities of both signs, suggesting two distinct types of magnetic anomalies. These two sets of inhomogeneities are highly time-dependent and appear exclusively in the upper half of the light bridge and only after the light bridge is completely formed. Both sets of inhomogeneities appear as patches and can be present independent of the other, next to one another, or spatially separated in a single scan. A two-component inversion of the corresponding spectral profiles indicate that the inhomogeneities occupy a very small fraction, amounting to less than 10 %, of the resolution element. These structures are likely driven by small-scale magneto-convection where they could further interact with the overlying sunspot magnetic field to produce reconnection jets in the chromosphere.

**2011 August 18 and 19.**

## **Anomalous flows in a sunspot penumbra**

Rohan E. [Louis](#), Christian Beck, Shibu K. Mathew, P. Venkatakrishnan

A&A, 570, A92 2014

<http://arxiv.org/pdf/1408.6690v1.pdf>

High-resolution spectropolarimetric observations of active region NOAA 11271 were obtained with the spectropolarimeter on board Hinode to analyze the properties of an anomalous flow in the photosphere in a sunspot penumbra. We detect a blue-shifted feature that appeared on the limb-side penumbra of a sunspot and that was present intermittently during the next two hours. It exhibited a maximum blue-shift of 1.6 km/s, an area of 5.2 arcsec<sup>2</sup>, and an uninterrupted lifetime of 1 hr. The blue-shifted feature, when present, lies parallel to red-shifts. Both blue and red shifts flank a highly inclined/horizontal magnetic structure that is radially oriented in the penumbra. The low-cadence SP maps reveal changes in size, radial position in the penumbra and line-of-sight velocity of the blue-shifted feature, from one scan to the other. There was an increase of nearly 500 G in the field strength and a marginal reduction in the field inclination of about 10 deg with the onset of the blue-shifts. In the chromosphere, intense, arc-shaped brightenings were observed close to the location of the blue-shifts, that extend from the edge of the umbral core to the penumbra-quiet Sun boundary. The strongest and largest brightenings were observed about 30 min after the strongest blue-shifts were detected at the photosphere. The close spatial proximity of the two phenomenon strongly suggests a causal relationship. The blue-shifted feature represents plasma motion that could be related to a magnetic structure that rises in the solar atmosphere and subsequently reconnects with the ambient chromospheric magnetic field of the sunspot or an inverse Evershed flow, which would be unique in the photosphere. This transient phenomena is presumably related to the dynamic stability of the sunspot because the corresponding umbral core separated two days later at the location of the blue-shifts and fragmented subsequently.

2011 August 19

## **Solar ALMA observations: constraining the chromosphere above sunspots**

Maria [Loukitcheva](#), [Kazumasa Iwai](#), [Sami K. Solanki](#), [Stephen M. White](#), [Masumi Shimojo](#)

ApJ 2017

<https://arxiv.org/pdf/1710.03812.pdf>

We present the first high-resolution Atacama Large Millimeter/Submillimeter Array (ALMA) observations of a sunspot at wavelengths of 1.3 mm and 3 mm, obtained during the solar ALMA Science Verification campaign in 2015, and compare them with the predictions of semi-empirical sunspot umbral/penumbral atmosphere models. For the first time millimeter observations of sunspots have resolved umbral/penumbral brightness structure at the chromospheric heights, where the emission at these wavelengths is formed. We find that the sunspot umbra exhibits a radically different appearance at 1.3 mm and 3 mm, whereas the penumbral brightness structure is similar at the two wavelengths. The inner part of the umbra is ~600 K brighter than the surrounding quiet Sun (QS) at 3 mm and is ~700 K cooler than the QS at 1.3 mm, being the coolest part of sunspot at this wavelength. On average, the brightness of the penumbra at 3 mm is comparable to the QS brightness, while at 1.3 mm it is ~1000 K brighter than the QS. Penumbral brightness increases towards the outer boundary in both ALMA bands. Among the tested umbral models, that of Severino et al. (1994) provides the best fit to the observational data, including both the ALMA data analyzed in this study and data from earlier works. No penumbral model amongst those considered here gives a satisfactory fit to the currently available measurements. ALMA observations at multiple mm wavelengths can be used for testing existing sunspot models, and serve as an important input to constrain new empirical models.

2015 December 16

## **Millimeter radiation from a 3D model of the solar atmosphere II. Chromospheric magnetic field**

Maria [Loukitcheva](#), Stephen M. White, Sami K. Solanki, Gregory D. Fleishman, Mats Carlsson

A&A 2017

<https://arxiv.org/pdf/1702.06018.pdf>

We use state-of-the-art, three-dimensional non-local thermodynamic equilibrium (non-LTE) radiative magnetohydrodynamic simulations of the quiet solar atmosphere to carry out detailed tests of chromospheric magnetic field diagnostics from free-free radiation at millimeter and submillimeter wavelengths (mm/submm). The vertical component of the magnetic field was deduced from the mm/submm brightness spectra and the degree of circular polarization synthesized at millimeter frequencies. We used the frequency bands observed by the Atacama Large Millimeter/Submillimeter Array (ALMA) as a convenient reference. The magnetic field maps obtained describe the longitudinal magnetic field at the effective formation heights of the relevant wavelengths in the solar chromosphere. The comparison of the deduced and model chromospheric magnetic fields at the spatial resolution of both the model and current observations demonstrates a good correlation, but has a tendency to underestimate the model field. The systematic discrepancy of about 10 percent is probably due to averaging of the restored field over the heights contributing to the radiation, weighted by the strength of the contribution. On the whole, the method of probing the longitudinal component of the magnetic field with free-free emission at mm/submm wavelengths is found to be applicable to measurements of the weak quiet-Sun magnetic fields. However, successful exploitation of

this technique requires very accurate measurements of the polarization properties (primary beam and receiver polarization response) of the antennas, which will be the principal factor that determines the level to which chromospheric magnetic fields can be measured. Consequently, high-resolution and high-precision observations of circularly polarized radiation at millimeter wavelengths can be a powerful tool for producing chromospheric longitudinal magnetograms.

## **The association of the Hale Sector Boundary with RHESSI solar flares and active longitudes**

K. [Loumou](#), [I. G. Hannah](#), [H. S. Hudson](#)

A&A 2018

<https://arxiv.org/pdf/1808.05866.pdf>

The heliospheric magnetic field (HMF) is structured into large sectors of positive and negative polarity. The parts of the boundary between these sectors where the change in polarity matches that of the leading-to-following sunspot polarity in that solar hemisphere, are called Hale Sector Boundaries (HSB). We investigate the flare occurrence rate near HSBs and the association between HSBs and active longitudes. Previous work determined the times HSBs were at solar central meridian, using the detection of the HMF sector boundary crossing at the Earth. In addition to this, we use a new approach which finds the HSB locations at all times by determining them from Potential Field Source Surface (PFSS) extrapolations of photospheric magnetograms. We use the RHESSI X-ray flare list for comparison to the HSB as it provides accurate flare locations over 14 years, from February 2002 to February 2016, covering both Cycles 23 and 24. For the active longitude positions we use previously published work based on sunspot observations. We find that the two methods of determining the HSB generally agree and that 41% (Cycle 23) and 47% (Cycle 24) of RHESSI flares occur within  $30^\circ$  of the PFSS determined-HSB. The behaviour of the HSBs varies over the two Cycles studied, and as expected they swap in hemisphere as the Cycles change. The HSBs and active longitudes do overlap but not consistently. They often move at different rates relative to each other (and the Carrington solar rotation rate) and these vary over each Cycle. The HSBs provide a useful additional activity indicator, particularly during periods when active longitudes are difficult to determine.

## **Field Line Universal relaXer (FLUX): A Fluxon Approach to Coronal Magnetic Field Modeling**

[Chris Lowder](#), [Chris Gilly](#), [Craig DeForest](#)

ApJ 2024

<https://arxiv.org/pdf/2402.10370.pdf>

We describe a novel method for modeling the global, steady solar wind using photospheric magnetic fields as a driving boundary condition. Prior wind models in this class include both rapid heuristic methods that use potential field extrapolation and variants thereof, trading rigor for computation speed, and detailed 3D magnetohydrodynamic (MHD) models that attempt to simulate the entire solar corona with a degree of physical rigor, but require large amounts of computation. The Field Line Universal relaXer (FLUX), an open-source numerical code which implements the 'fluxon' semi-lagrangian approach to MHD modeling, provides an intermediate approach between these two general classes. In particular, the fluxon approach to MHD describes the magnetic field through discrete analogues of magnetic field lines, relaxing these structures to a stationary state of force balance. In this work we introduce a one-dimensional solar wind solution along each fieldline, providing an ensemble of solutions that are interpolated back onto a uniform grid at an outer boundary surface. This provides advantages in physical rigor over heuristic semi-analytic techniques, and in computational efficiency over full 3D MHD techniques. Here we describe the underlying methodology and the FLUXPipe modeling pipeline process.

## **Optimization of Photospheric Electric Field Estimates for Accurate Retrieval of Total Magnetic Energy Injection**

E. [Lumme](#), J. Pomoell, E. K. J. Kilpua

[Solar Physics](#) December 2017, 292:191

<https://link.springer.com/content/pdf/10.1007%2Fs11207-017-1214-0.pdf>

<https://arxiv.org/pdf/1712.05757.pdf>

Estimates of the photospheric magnetic, electric, and plasma velocity fields are essential for studying the dynamics of the solar atmosphere, for example through the derivative quantities of Poynting and relative helicity flux and using the fields to obtain the lower boundary condition for data-driven coronal simulations. In this paper we study the performance of a data processing and electric field inversion approach that requires only high-resolution and high-cadence line-of-sight or vector magnetograms, which we obtain from the Helioseismic and Magnetic Imager (HMI) onboard Solar Dynamics Observatory (SDO). The approach does not require any photospheric velocity estimates, and the lacking velocity information is compensated for using ad hoc assumptions. We show that the free parameters of these assumptions can be optimized to reproduce the time evolution of the total magnetic energy injection through the photosphere in NOAA AR 11158, when compared to recent state-of-the-art estimates for this active region. However, we find that the relative magnetic helicity injection is reproduced poorly, reaching

at best a modest underestimation. We also discuss the effect of some of the data processing details on the results, including the masking of the noise-dominated pixels and the tracking method of the active region, neither of which has received much attention in the literature so far. In most cases the effect of these details is small, but when the optimization of the free parameters of the ad hoc assumptions is considered, a consistent use of the noise mask is required. The results found in this paper imply that the data processing and electric field inversion approach that uses only the photospheric magnetic field information offers a flexible and straightforward way to obtain photospheric magnetic and electric field estimates suitable for practical applications such as coronal modeling studies.

### **Fundamental transverse vibrations of the active region solar corona★**

M. Luna<sup>1,2</sup>, R. Oliver<sup>3,4</sup>, P. Antolin<sup>5</sup> and I. Arregui

A&A 629, A20 (2019)

<https://sci-hub.se/10.0000/www.aanda.org/articles/aa/abs/2019/09/aa35850-19/aa35850-19.html>

**Context.** Some high-resolution observations have revealed that the active region solar corona is filled with a myriad of thin strands even in apparently uniform regions with no resolved loops. This fine structure can host collective oscillations involving a large portion of the corona due to the coupling of the motions of the neighbouring strands.

**Aims.** We study these vibrations and the possible observational effects.

**Methods.** We theoretically investigated the collective oscillations inherent to the fine structure of the corona. We have called them fundamental vibrations because they cannot exist in a uniform medium. We used the T-matrix technique to find the normal modes of random arrangements of parallel strands. We considered an increasing number of tubes to understand the vibrations of a huge number of tubes of a large portion of the corona. We additionally generated synthetic time-distance Doppler and line-broadening diagrams of the vibrations of a coronal region to compare with observations.

**Results.** We have found that the fundamental vibrations are in the form of clusters of tubes where not all the tubes participate in the collective mode. The periods are distributed over a wide band of values. The width of the band increases with the number of strands but rapidly reaches an approximately constant value. We have found an analytic approximate expression for the minimum and maximum periods of the band. The frequency band associated with the fine structure of the corona depends on the minimum separation between strands. We have found that the coupling between the strands is on a large extent and the motion of one strand is influenced by the motions of distant tubes. The synthetic Dopplergrams and line-broadening maps show signatures of collective vibrations, not present in the case of purely random individual kink vibrations.

**Conclusions.** We conclude that the fundamental vibrations of the corona can contribute to the energy budget of the corona and they may have an observational signature.

### **Twisted Flux Tube Emergence Evidenced in Longitudinal Magnetograms: Magnetic Tongues**

M. L. Luoni, P. Démoulin, C. H. Mandrini and L. van Driel-Gesztelyi

Solar Physics, Volume 270, Number 1, 45-74, 2011

Bipolar active regions (ARs) are thought to be formed by twisted flux tubes, as the presence of such twist is theoretically required for a cohesive rise through the whole convective zone. We use longitudinal magnetograms to demonstrate that a clear signature of a global magnetic twist is present, particularly, during the emergence phase when the AR is forming in a much weaker pre-existing magnetic field environment. The twist is characterised by the presence of elongated polarities, called “magnetic tongues”, which originate from the azimuthal magnetic field component. The tongues first extend in size before retracting when the maximum magnetic flux is reached. This implies an apparent rotation of the magnetic bipole. Using a simple half-torus model of an emerging twisted flux tube having a uniform twist profile, we derive how the direction of the polarity inversion line and the elongation of the tongues depend on the global twist in the flux rope. Using a sample of 40 ARs, we verify that the helicity sign, determined from the magnetic polarity distribution pattern, is consistent with the sign derived from the photospheric helicity flux computed from magnetogram time series, as well as from other proxies such as sheared coronal loops, sigmoids, flare ribbons and/or the associated magnetic cloud observed in situ at 1 AU. The evolution of the tongues observed in emerging ARs is also closely similar to the evolution found in recent MHD numerical simulations. We also found that the elongation of the tongue formed by the leading magnetic polarity is significantly larger than that of the following polarity. This newly discovered asymmetry is consistent with an asymmetric  $\Omega$ -loop emergence, trailing the solar rotation

### **Chapter 6 - Coronal Magnetism as a Universal Phenomenon**

**Review**

B.C. Low

In: *The Sun as a Guide to Stellar Physics* Book

Eds. Oddbjørn Engvold, Jean-Claude Vial, and Andrew Skumanich

Elsevier, November 2018



<https://www.sciencedirect.com/book/9780128143346/the-sun-as-a-guide-to-stellar-physics>

In the 60 years after E. N. Parker's prediction of the existence of the solar wind and the magnetic origin of coronal heating, space-borne and ground-based observations have built a conceptually complete phenomenology of the corona as a fully ionized hydromagnetic atmosphere responding in step to the global magnetic reversals of the Sun in 11-year cycles. This phenomenology is reviewed with the theoretical ideas it motivated, describing the photospheric emergence of new-cycle magnetic fluxes of a reversed polarity into the corona, ubiquitous coronal heating, hydromagnetic self-organization, explosive energy release, and the breaking of self-confinement into flows of expansion winds and episodic ejections of magnetic structures. High electrical and thermal conductivities at coronal million-degree temperatures have central roles. The corona obeys a hemispherical rule independent of magnetic cycle, that self-organized structures have a statistical preference for left- and right-handed magnetic twists, respectively, in the northern and southern hemispheres relative to the rotational axis. It is pointed out, perhaps for the first time, that this hemispherical rule is a hydromagnetic implication of the Parker (1955a,b) dynamo, straightforward to deduce graphically from his book *Cosmical Magnetic Fields* (1979). Solar physics has reached a broad-brush physical understanding of the corona solar-wind system as the prototype of a universal astrophysical phenomenon.

### **Methodical problems of magnetic field measurements in umbra of sunspots**

N.I. **Lozitska**, V.G. Lozitskya, O.A. Andryeyevab, Z.S. Akhtemovb, V.M. Malashchukb, V.A. Perebeynosb, N.N. Stepanyanb, N.I. Shtertser

Advances in Space Research, Volume 55, Issue 3, 1 February 2015, Pages 897–907

<http://www.sciencedirect.com/science/article/pii/S027311771400502X>

Visual measurements of magnetic field strengths in sunspot umbra provide data on magnetic field strength modulus directly, i.e., irrespective from any solar atmosphere model assumptions. In order to increase the accuracy of calculation of the solar magnetic indexes, such as  $\tau B_{\max}$  or  $B_{\text{sp}}$ , the inclusion of all available data from different observatories is needed. In such measurements some methodical problems arise, which bring about inconsistency of the data samples combined from different sources; this work describes the problems at hand and proposes solutions on how to eliminate the inconsistencies. Data sets of sunspot magnetic field strength visual measurements from Mt. Wilson, Crimea and Kyiv observatories in 2010–2012 have been processed. It is found that two measurement modes of Zeeman split,  $\sigma \rightarrow \sigma$  and  $\sigma \rightarrow \pi$ , yield almost the same results, if data rows are long enough (over  $\sim 100$  sunspots in central area of Sun,  $r < 0.7 R$ ). It is generally held that the most reliable measurement results are obtained for magnetic fields that exceed 2400 G. However, the empirical comparison of the internal data consistency of the samples produced by different observers shows that for reliable results this limit can be lowered down to 1100 G. To increase the precision of measurements, empirical calibration of the line-shifter is required by using closely positioned telluric lines. Such calibrations have been performed at Kyiv and Crimea, but as far as we know, it has not been carried out at Mt. Wilson observatory after its diffraction grate was replaced in 1994. Taking into consideration the highest quality and coverage of Mt. Wilson sunspot observational data, the authors are convinced that reliable calibration of its instrument by narrow telluric lines is definitely required.

### **Spectral manifestations of extremely strong magnetic fields in the sunspot umbra**

V.G. **Lozitsky**

Advances in Space Research Volume 59, Issue 5, 1 March 2017, Pages 1416–1424

Fine peculiarities of the Zeeman effect in two big sunspots of **October 29, 2003, and October 25, 2014**, are analyzed. In order to search spectral evidences of very strong spatially unresolved magnetic fields, the Stokes  $I \pm V$  and  $V$  profiles of the Fe I 6301.5 and 6302.5 Å lines are studied in detail. Confirmed are two effects discovered earlier by Lozitsky (2016): (a) non-parallelism of bisectors in the Fe I 6301.5 line at a distance of about  $\pm 250$  mÅ from the line center and (b) the existence of weak secondary peaks in Stokes  $V$  of the Fe I 6302.5 line placed at a distance of, on the average,  $\pm 375$  mÅ from the line center. Close correlation ( $r = 0.77 \pm 0.06$ ) was found between (a) and (b) effects indicating the reality of very strong ( $\approx 8$  kG) unresolved magnetic fields. For the first sunspot, the presence of the abovementioned 8-kG fields is traced along 12 Mm of the sunspot umbra. The filling factor is 0.2–0.3 here, and the relative Doppler velocities (without Evershed's effect) are from  $-1.7$  to  $-3.1$  km/s (plasma lifting). Similar parameters were also obtained for the second sunspot.

### **The Sun's Magnetic Power Spectra Over Two Solar Cycles. I. Calibration Between SDO/HMI And SOHO/MDI Magnetograms**

[Yukun Luo](#), [Jie Jiang](#), [Ruihui Wang](#)

ApJ 954 199 2023

<https://arxiv.org/pdf/2308.07530.pdf>

<https://iopscience.iop.org/article/10.3847/1538-4357/acec77/pdf>

The Sun's magnetic field is strongly structured over a broad range of scales. The magnetic spatial power spectral analysis provides a powerful tool to understand the various scales of magnetic fields and their interaction with plasma motion. We aim to investigate the power spectra using spherical harmonic decomposition of high-resolution

SOHO/MDI and SDO/HMI synoptic magnetograms covering three consecutive solar cycle minima in a series of papers. As the first of the series, we calibrate and analyze the power spectra based on co-temporal SDO/HMI and SOHO/MDI data in this paper. For the first time, we find that the calibration factor  $r$  between SOHO/MDI and SDO/HMI varies with the spatial scale  $l$  of the magnetic field, where  $l$  is the degree of a spherical harmonics. The calibration factor satisfies  $r(l) = -0.02110.64 + 2 \sqrt{5 < l \leq 539}$ . With the calibration function, most contemporaneous SOHO/MDI and SDO/HMI magnetograms show consistent power spectra from about 8 Mm to the global scales over about 3 orders of magnitudes. Moreover, magnetic power spectra from SOHO/MDI and SDO/HMI maps show peaks/knees at  $l \approx 120$  corresponding to the typical supergranular scale (about 35 Mm) constrained from direct velocimetric measurements. This study paves the way for investigating the solar-cycle dependence of supergranulation and magnetic power spectra in subsequent studies.

### Where and how does a decay-index profile become saddle-like?

[Runbin Luo](#), [Rui Liu](#)

ApJ **929** 2 **2022**

<https://arxiv.org/pdf/2203.03913>

<https://iopscience.iop.org/article/10.3847/1538-4357/ac5b06/pdf>

The decay index of solar magnetic fields is known as an important parameter in regulating solar eruptions from the standpoint of the torus instability. In particular, a saddle-like profile of decay index, which hosts a local torus-stable regime at higher altitudes than where the decay index first exceeds the instability threshold, is found to be associated with some confined or two-step eruptions. To understand the occurrence of such a profile, we employed dipoles to emulate different kinds of photospheric flux distributions. Corroborated by observations of representative active regions (ARs), our major results are: 1) in bipolar configurations the critical height increases away from the AR center along the polarity inversion line (PIL) and its average is roughly half of the centroid distance between opposite polarities; 2) in quadrupolar configurations saddle-like profiles appear above the PIL when the two dipoles oriented in the same direction are significantly more separated in this direction than in the perpendicular direction, and when the two dipoles are oriented differently or have unequal fluxes; 3) saddle-like profiles in quadrupolar configurations are associated with magnetic skeletons such as a null point or a hyperbolic flux tube, and the role of such profiles in eruptions is anticipated to be double-edged if magnetic reconnection is involved.

### The S-Web Origin of Composition Enhancement in the Slow-to-Moderate Speed Solar Wind

[B. J. Lynch](#), [N. M. Viall](#), [A. K. Higginson](#), [L. Zhao](#), [S. T. Lepri](#), [X. Sun](#)

ApJ **2023**

<https://arxiv.org/pdf/2303.06465.pdf>

Connecting the solar wind observed throughout the heliosphere to its origins in the solar corona is one of the central aims of heliophysics. The variability in the magnetic field, bulk plasma, and heavy ion composition properties of the slow wind are thought to result from magnetic reconnection processes in the solar corona. We identify regions of enhanced variability and composition in the solar wind from **2003 April 15 to May 13** (Carrington Rotation 2002), observed by the Wind and Advanced Composition Explorer spacecraft, and demonstrate their relationship to the Separatrix-Web (S-Web) structures describing the corona's large-scale magnetic topology. There are four pseudostreamer (PS) wind intervals and two helmet streamer (HS) heliospheric current sheet/plasma sheet crossings (and an ICME) which all exhibit enhanced alpha-to-proton ratios and/or elevated ionic charge states of carbon, oxygen, and iron. We apply the magnetic helicity-partial variance of increments (Hm-PVI) procedure to identify coherent magnetic structures and quantify their properties during each interval. The mean duration of these structures are  $\sim 1$  hr in both the HS and PS wind. We find a modest enhancement above the power-law fit to the PVI waiting time distribution in the HS-associated wind at the 1.5-2 hr timescales that is absent from the PS intervals. We discuss our results in context of previous observations of the  $\sim 90$  min periodic density structures in the slow solar wind, further development of the dynamic S-Web model, and future Parker Solar Probe and Solar Orbiter joint observational campaigns.

### A Model for Coronal Inflows and In/Out Pairs

[Benjamin J. Lynch](#)

**2020** ApJ 905 139

<https://arxiv.org/pdf/2010.13959.pdf>

<https://doi.org/10.3847/1538-4357/abc5b3>

This report presents a three-dimensional (3D) numerical magnetohydrodynamics (MHD) model of the white-light coronagraph observational phenomena known as coronal inflows and in/out pairs. Coronal inflows in the Large Angle and Spectrometric Coronagraph/C2 field of view (approximately  $2-6 R_{\odot}$ ) were thought to arise from the dynamic and intermittent release of solar wind plasma associated with the helmet streamer belt as the counterpart to outward-propagating streamer blobs, formed by magnetic reconnection. This interpretation was essentially confirmed with the subsequent identification of in/out pairs and the multispacecraft observations of their 3D

structure. The MHD simulation results show relatively narrow lanes of density depletion form high in the corona and propagate inward with sinuous motion that has been characterized as "tadpole-like" in coronagraph imagery. The height–time evolution and velocity profiles of the simulation inflows and in/out pairs are compared to their corresponding observations and a detailed analysis of the underlying magnetic field structure associated with the synthetic white-light and mass density evolution is presented. Understanding the physical origin of this structured component of the slow solar wind's intrinsic variability could make a significant contribution to solar wind modeling and the interpretation of remote and in situ observations from Parker Solar Probe and Solar Orbiter. **2015 July 10**

### **The evolution of arch filament systems and moving magnetic features around a sunspot**\*

Li [Ma](#)1,2, Wangping Zhou1,2, Guiping Zhou2 and Jun Zhang

A&A 583, A110 (2015)

**Context.** Arch filament systems (AFSs) are usually considered as the chromospheric manifestations of the emerging flux regions (EFRs) seen in H $\alpha$  observations. Moving magnetic features (MMFs) look similar to EFRs in magnetograms, but often appear in the decaying phase of an active region (AR) and behave differently from EFRs. A possible relation between AFS and MMF would be important for revealing a common mechanism for building up basic structures on the Sun.

**Aims.** Based on H $\alpha$  and magnetic field observations with high spatial resolution, we study the evolution of MMFs around a sunspot, as well as their related AFSs from birth to death.

**Methods.** The multiwavelength observations from the New Vacuum Solar Telescope (NVST) and the Solar Dynamic Observatories (SDO) are co-aligned in the spatial and the temporal sense. MMFs appeared near the northern end of a light bridge (LB). Their related AFSs were carefully identified and traced from their appearance to disappearance based on H $\alpha$ , EUV data, and magnetograms.

**Results.** In the main sunspot of AR NOAA 11711 during **April 1–4, 2013**, many slow-speed MMFs with a polarity opposite to that of the sunspot appeared from the close vicinity of the northern end of a LB. Different from other smaller MMFs around the sunspot, these MMFs were always related to arch filaments and eventually formed AFSs with three twisting branches. The total flux involved in the AFSs was estimated to be about  $2.7 \times 10^{21}$  Mx. The largest MMF "M1" evolved into a small pore that led to an intensity reduction in the continuum intensity images. The appearance and evolution of the AFSs near the sunspot seems to be controlled by MMFs emanating from the penumbra. Owing to continual magnetic cancellation between the MMFs and their surrounding opposite flux, the AFSs gradually disintegrated and finally disappeared.

**Conclusions.** The appearance and evolution of the AFSs near the sunspot seem to be controlled by these MMFs emanating from the penumbra.

### **Ambipolar Diffusion in the Lower Solar Atmosphere: MHD Simulations of a Sunspot**

[Conor D. MacBride](#), [David B. Jess](#), [Elena Khomenko](#), [Samuel D. T. Grant](#)

ApJ 2022

<https://arxiv.org/pdf/2209.14366.pdf>

Magnetohydrodynamic (MHD) simulations of the solar atmosphere are often performed under the assumption that the plasma is fully ionized. However, in the lower solar atmosphere a reduced temperature often results in only the partial ionization of the plasma. The interaction between the decoupled neutral and ionized components of such a partially ionized plasma produces ambipolar diffusion. To investigate the role of ambipolar diffusion in propagating wave characteristics in the photosphere and chromosphere, we employ the Mancha3D numerical code to model magnetoacoustic waves propagating through the atmosphere immediately above the umbra of a sunspot. We solve the non-ideal MHD equations for data-driven perturbations to the magnetostatic equilibrium and the effect of ambipolar diffusion is investigated by varying the simulation to include additional terms in the MHD equations that account for this process. Analyzing the energy spectral densities for simulations with/without ambipolar diffusion, we find evidence to suggest that ambipolar diffusion plays a pivotal role in wave characteristics in the weakly ionized low density regions, hence maximizing the local ambipolar diffusion coefficient. As a result, we propose that ambipolar diffusion is an important mechanism that requires careful consideration into whether it should be included in simulations, and whether it should be utilized in the analysis and interpretation of particular observations of the lower solar atmosphere.

### **Accurately constraining velocity information from spectral imaging observations using machine learning techniques**

[Conor D. MacBride](#), [David B. Jess](#), [Samuel D. T. Grant](#), [Elena Khomenko](#), [Peter H. Keys](#), [Marco Stangalini](#)

Philosophical Transactions of the Royal Society A 2020

<https://arxiv.org/pdf/2007.07904.pdf>

Determining accurate plasma Doppler (line-of-sight) velocities from spectroscopic measurements is a challenging endeavour, especially when weak chromospheric absorption lines are often rapidly evolving and, hence, contain multiple spectral components in their constituent line profiles. Here, we present a novel method that employs

machine learning techniques to identify the underlying components present within observed spectral lines, before subsequently constraining the constituent profiles through single or multiple Voigt fits. Our method allows active and quiescent components present in spectra to be identified and isolated for subsequent study. Lastly, we employ a Ca II 8542 Å spectral imaging dataset as a proof-of-concept study to benchmark the suitability of our code for extracting two-component atmospheric profiles that are commonly present in sunspot chromospheres. Minimisation tests are employed to validate the reliability of the results, achieving median reduced  $\chi^2$  values equal to 1.03 between the observed and synthesised umbral line profiles.

### **Active Region Morphologies Selected from Near-side Helioseismic Data**

G. A. [MacDonald](#)<sup>1</sup>, C. J. Henney<sup>2</sup>, M. Díaz Alfaro<sup>3,4</sup>, I. González Hernández<sup>5</sup>, C. N. Arge<sup>2</sup>, C. Lindsey<sup>6</sup>, and R. T. J. McAtee

2015 ApJ 807 21.

We estimate the morphology of near-side active regions using near-side helioseismology. Active regions from two data sets, Air Force Data Assimilative Photospheric flux Transport synchronic maps and Global Oscillation Network Group near-side helioseismic maps, were matched and their morphologies compared. Our algorithm recognizes 382 helioseismic active regions between 2002 April 25 and 2005 December 31 and matches them to their corresponding magnetic active regions with 100% success. A magnetic active region occupies 30% of the area of its helioseismic signature. Recovered helioseismic tilt angles are in good agreement with magnetic tilt angles. Approximately 20% of helioseismic active regions can be decomposed into leading and trailing polarity. Leading polarity components show no discernible scaling relationship, but trailing magnetic polarity components occupy approximately 25% of the area of the trailing helioseismic component. A nearside phase-magnetic calibration is in close agreement with a previous far-side helioseismic calibration and provides confidence that these morphological relationships can be used with far-side helioseismic data. Including far-side active region morphology in synchronic maps will have implications for coronal magnetic topology predictions and solar wind forecasts.

### **A Comparison of Global Magnetofrictional Simulations of the 2015 March 20 Solar Eclipse**

Duncan H. [Mackay](#)<sup>1</sup> and L. A. Upton<sup>2</sup>

2022 ApJ 939 9

<https://iopscience.iop.org/article/10.3847/1538-4357/ac94c7/pdf>

The solar corona exhibits a wide range of phenomena, from highly non-potential objects such as solar filaments to near-potential structures such as the open magnetic flux. For any global model to be useful in space weather applications, the model must on a single day reproduce all of these phenomena in the same simulation, using the same set of coronal physics and parameters. The purpose of the present paper is to evaluate whether the evolving magnetofrictional model can achieve this goal. Twenty-eight separate simulations are analyzed, where each tries to reproduce both highly non-potential and near-potential phenomena observed in the solar corona on the same day. This day is chosen to be **2015 March 20**, the date of the solar eclipse. The study evaluates how the cadence of bipole data, ideal or nonideal coronal physics, and the variety of helicity injection mechanisms affect the accuracy of the simulations. Results show that significantly better agreement arises when using Advective Flux Transport (AFT) synoptic maps to drive the simulations, as compared to 27-day Carrington rotation synoptic maps. Using the nonideal effect of hyperdiffusion leads to the worst agreement with all coronal phenomena. Alternatively, when running either ideal or ohmic diffusion simulations with helicity condensation or bipoles with a self-helicity, a good agreement with both on-disk and limb structures can be found. This suggests that future studies aiming to simulate the corona and reproduce multiple phenomena on a given day should use data products such as AFT and avoid using the nonideal physics of hyperdiffusion.

### **A Comparison of Sparse and Non-sparse Techniques for Electric-Field Inversion from Normal-Component Magnetograms**

Duncan H. [Mackay](#) & [Anthony R. Yeates](#)

[Solar Physics](#) volume 296, Article number: 178 (2021)

<https://link.springer.com/content/pdf/10.1007/s11207-021-01924-z.pdf>

<https://doi.org/10.1007/s11207-021-01924-z>

An important element of 3D data-driven simulations of solar magnetic fields is the determination of the horizontal electric field at the solar photosphere. This electric field is used to drive the 3D simulations and inject energy and helicity into the solar corona. One outstanding problem is the localisation of the horizontal electric field such that it is consistent with Ohm's law. Yeates (*Astrophys. J.* 836(1), 131, [2017](#)) put forward a new "sparse" technique for computing the horizontal electric field from normal-component magnetograms that minimises the number of non-zero values. This aims to produce a better representation of Ohm's law compared to previously used "non-sparse" techniques. To test this new approach we apply it to active region (AR) 10977, along with the previously developed non-sparse technique of Mackay, Green, and van Ballegooijen (*Astrophys. J.* 729(2), 97, [2011](#)). A detailed comparison of the two techniques with coronal observations is used to determine which is the most successful. Results show that the non-sparse technique of Mackay, Green, and van Ballegooijen ([2011](#)) produces the best

representation for the formation and structure of the sigmoid above AR 10977. In contrast, the Yeates (2017) approach injects strong horizontal fields between spatially separated, evolving magnetic polarities. This injection produces highly twisted unphysical field lines with significantly higher magnetic energy and helicity. It is also demonstrated that the Yeates (2017) approach produces significantly different results that can be inconsistent with the observations depending on whether the horizontal electric field is solved directly or indirectly through the magnetic vector potential. In contrast, the Mackay, Green, and van Ballegooijen (2011) method produces consistent results using either approach. The sparse technique of Yeates (2017) has significant pitfalls when applied to spatially resolved solar data, where future studies need to investigate why these problems arise. **2-10 Dec 2007**

## **IMPACT OF AN L5 MAGNETOGRAPH ON NONPOTENTIAL SOLAR GLOBAL MAGNETIC FIELD MODELING**

Duncan H. Mackay<sup>1</sup>, Anthony R. Yeates<sup>2</sup>, and Francois-Xavier Bocquet  
ApJ 825 131 2016

We present the first theoretical study to consider what improvement could be obtained in global nonpotential modeling of the solar corona if magnetograph data were available from the L5 Lagrange point, in addition to from the direction of Earth. To consider this, we first carry out a "reference Sun" simulation over two solar cycles. An important property of this simulation is that random bipole emergences are allowed across the entire solar surface at any given time (such as can occur on the Sun). Next, we construct two "limited data" simulations, where bipoles are only included when they could be seen from (i) an Earth-based magnetograph and (ii) either Earth- or L5-based magnetographs. The improvement in reproducing the reference Sun simulation when an L5 view is available is quantified through considering global quantities in the limited data simulations. These include surface and polar flux, total magnetic energy, volume electric current, open flux, and the number of flux ropes. Results show that when an L5 observational viewpoint is included, the accuracy of the global quantities in the limited data simulations can increase by 26%–40%. This clearly shows that a magnetograph at the L5 point could significantly increase the accuracy of global nonpotential modeling and with this the accuracy of future space weather forecasts.

## **Global-scale Consequences of Magnetic-helicity Injection and Condensation on the Sun**

Duncan H. Mackay<sup>1</sup>, C. Richard DeVore<sup>2,3</sup>, and Spiro K. Antiochos  
2014 ApJ 784 164

In the recent paper of Antiochos, a new concept for the injection of magnetic helicity into the solar corona by small-scale convective motions and its condensation onto polarity inversion lines (PILs) was developed. We investigate this concept through global simulations of the Sun's photospheric and coronal magnetic fields, and compare the results with the hemispheric pattern of solar filaments. Assuming that the vorticity of the cells is predominantly counterclockwise/clockwise in the northern/southern hemisphere, the convective motions inject negative/positive helicity into each hemisphere. The simulations show that: (1) on a north-south oriented PIL, both differential rotation and convective motions inject the same sign of helicity, which matches that required to reproduce the hemispheric pattern of filaments. (2) On a high-latitude east-west oriented polar crown or subpolar crown PIL, the vorticity of the cells has to be approximately 2-3 times greater than the local differential-rotation gradient in order to overcome the incorrect sign of helicity injection from differential rotation. (3) In the declining phase of the cycle, as a bipole interacts with the polar field, in some cases, helicity condensation can reverse the effect of differential rotation along the east-west lead arm but not in all cases. The results show that this newly developed concept of magnetic helicity injection and condensation, in conjunction with the mechanisms used in Yeates et al., is a viable explanation for the hemispheric pattern of filaments. Future observational studies should focus on examining the vorticity component within convective motions to determine both its magnitude and latitudinal variation relative to the differential-rotation gradient on the Sun.

## **The Sun's Global Photospheric and Coronal Magnetic Fields: Observations and Models** **A Review**

D. H. Mackay, A. R. Yeates

E-print, Nov 2012, Living Rev. Solar Phys., 9 (2012) 6

<http://www.livingreviews.org/lrsp-2012-6>

In this review, our present day understanding of the Sun's global photospheric and coronal magnetic fields is discussed from both observational and theoretical viewpoints. Firstly, the large-scale properties of photospheric magnetic fields are described, along with recent advances in photospheric magnetic flux transport models. Following this, the wide variety of theoretical models used to simulate global coronal magnetic fields are described. From this, the combined application of both magnetic flux transport simulations and coronal modeling techniques to describe the phenomena of **coronal holes, the Sun's open magnetic flux and the hemispheric pattern of solar filaments** is discussed. Finally, recent advances in non-eruptive global MHD models are described. While the review focuses mainly on solar magnetic fields, recent advances in measuring and modeling stellar magnetic fields are described where appropriate. In the final section key areas of future research are identified.

## MODELING THE DISPERSAL OF AN ACTIVE REGION: QUANTIFYING ENERGY INPUT INTO THE CORONA

Duncan H. Mackay<sup>1</sup>, L. M. Green<sup>2</sup>, and Aad van Ballegooijen<sup>3</sup>

*Astrophysical Journal*, 729:97 (11pp), 2011

In this paper, a new technique for modeling nonlinear force-free fields directly from line-of-sight magnetogram observations is presented. The technique uses sequences of magnetograms directly as lower boundary conditions to drive the evolution of coronal magnetic fields between successive force-free equilibria over long periods of time. It is illustrated by applying it to *SOHO*:MDI observations of a decaying active region, NOAA AR 8005. The active region is modeled during a four-day period around its central meridian passage. Over this time, the dispersal of the active region is dominated by random motions due to small-scale convective cells. Through studying the buildup of magnetic energy in the model, it is found that such small-scale motions may inject anywhere from  $(2.5-3) \times 10^{25}$  erg s<sup>-1</sup> of free magnetic energy into the coronal field. Most of this energy is stored within the center of the active region in the low corona, below 30 Mm. After four days, the buildup of free energy is 10% that of the corresponding potential field. This energy buildup is sufficient to explain the radiative losses at coronal temperatures within the active region. Small-scale convective motions therefore play an integral part in the energy balance of the corona. This new technique has wide ranging applications with the new high-resolution, high-cadence observations from the *SDO*:HMI and *SDO*:AIA instruments.

## A Non-Linear Force-Free Field Model for the Evolving Magnetic Structure of Solar Filaments

Duncan H. Mackay<sup>1</sup>  and A. A. van Ballegooijen

*Solar Phys.*, 260(2), 321-346, 2009

In this paper the effect of a small magnetic element approaching the main body of a solar filament is considered through non-linear force-free field modeling. The filament is represented by a series of magnetic dipoles. Once the dipoles are calculated, a simple hydrostatic atmosphere model is applied to determine which structures have sufficient column mass depth to be visible in H $\alpha$ . Two orientations of the bipole are considered, either parallel or anti-parallel to the overlying arcade. The magnetic polarity that lies closest to the filament is then advected towards the filament. Initially for both the dominant and minority polarity advected elements, right/left bearing barbs are produced for dextral/sinistral filaments. The production of barbs due to dominant polarity elements is a new feature. In later stages the filament breaks into two dipped sections and takes a highly irregular, non-symmetrical form with multiple pillars. The two sections are connected by field lines with double dips even though the twist of the field is less than one turn. Reconnection is not found to play a key role in the break up of the filament. The non-linear force-free fields produce very different results to extrapolated linear-force free fields. For the cases considered here the linear force-free field does not produce the break up of the filament nor the production of barbs as a result of dominant polarity elements.

## MODELS OF THE LARGE-SCALE CORONA. II. MAGNETIC CONNECTIVITY AND OPEN FLUX VARIATION

D. H. Mackay and A. A. van Ballegooijen

*Astrophysical Journal*, 642:1193-1204, 2006 May, File

In this paper the changing connectivity of the coronal magnetic field during the formation and ejection of magnetic flux ropes is considered. Using recent simulations of the coronal field, it is shown that reconnection may occur both above and below the flux ropes. Those occurring above slowly strip away coronal arcades overlying the flux ropes and allow the flux ropes to be ejected. In contrast, those below help to push the flux ropes out. It is found that the reconnection occurring below each flux rope may result in significant skew being maintained within the coronal field above the PIL after the flux rope is ejected. In addition, after the eruption, as the coronal field closes down, the large-scale transport of open flux across the bipoles takes place through the process of "interchange reconnection." As a result, new photospheric domains of open flux are created within the centers of the bipoles, where field lines were previously closed. The net open flux in the simulation may be split into two distinct contributions. The first contribution is due to the nonpotential equilibrium coronal fields of the bipoles. The second contribution is a temporary enhancement to this during the ejection of the flux ropes, where previously closed field lines become open. It is shown that the nonpotential equilibrium contribution to the open flux is significantly higher than that due to a potential field deduced

from the same photospheric boundary conditions. These results suggest that the nonpotential nature of coronal magnetic fields may affect the variation of the Sun's open flux during periods of high solar activity and should be considered in future simulations.

### **Validation of community models: 3. Tracing field lines in heliospheric models**

**MacNeice**, Peter; Elliott, Brian; Acebal, Ariel

Space Weather, Vol. 9, No. 10, S10003, 2011

Forecasting hazardous gradual solar energetic particle (SEP) bursts at Earth requires accurately modeling field line connections between Earth and the locations of coronal or interplanetary shocks that accelerate the particles. We test the accuracy of field lines reconstructed using four different models of the ambient coronal and inner heliospheric magnetic field, through which these shocks must propagate, including the coupled Wang-Sheeley-Argge (WSA)/ENLIL model. Evaluating the WSA/ENLIL model performance is important since it is the most sophisticated model currently available to space weather forecasters which can model interplanetary coronal mass ejections and, when coupled with particle acceleration and transport models, will provide a complete model for gradual SEP bursts. Previous studies using a simpler Archimedean spiral approach above 2.5 solar radii have reported poor performance. We test the accuracy of the model field lines connecting Earth to the Sun at the onset times of 15 impulsive SEP bursts, comparing the foot points of these field lines with the locations of surface events believed to be responsible for the SEP bursts. We find the WSA/ENLIL model performance is no better than the simplest spiral model, and the principal source of error is the model's inability to reproduce sufficient low-latitude open flux. This may be due to the model's use of static synoptic magnetograms, which fail to account for transient activity in the low corona, during which reconnection events believed to initiate the SEP acceleration may contribute short-lived open flux at low latitudes. Time-dependent coronal models incorporating these transient events may be needed to significantly improve Earth/Sun field line forecasting.

### **The pre-penumbral magnetic canopy in the solar atmosphere**

David **MacTaggart**, Salvo Guglielmino, Francesca Zuccarello

ApJL 831 L4 2016

<https://arxiv.org/pdf/1610.05554v1.pdf>

Penumbrae are the manifestation of magnetoconvection in highly inclined (to the vertical direction) magnetic field. The penumbra of a sunspot tends to form, initially, along the arc of the umbra antipodal to the main region of flux emergence. The question of how highly inclined magnetic field can concentrate along the antipodal curves of umbrae, at least initially, remains to be answered. Previous observational studies have suggested the existence of some form of overlying magnetic canopy which acts as the progenitor for penumbrae. We propose that such overlying magnetic canopies are a consequence of how the magnetic field emerges into the atmosphere and are, therefore, part of the emerging region. We show, through simulations of twisted flux tube emergence, that canopies of highly inclined magnetic field form preferentially at the required locations above the photosphere.

### **On the emergence of toroidal flux tubes: general dynamics and comparisons with the cylinder model**

D. **MacTaggart** and A. W. Hood

A&A 507, 995-1004 (2009)

In this paper we study the dynamics of toroidal flux tubes emerging from the solar interior, through the photosphere and into the corona. Many previous theoretical studies of flux emergence use a twisted cylindrical tube in the solar interior as the initial condition. Important insights can be gained from this model, however, it does have shortcomings. The axis of the tube never fully emerges as dense plasma becomes trapped in magnetic dips and restrains its ascent. Also, since the entire tube is buoyant, the main photospheric footpoints (sunspots) continually drift apart. These problems make it difficult to produce a convincing sunspot pair. We aim to address these problems by considering a different initial condition, namely a toroidal flux tube.

*Methods.* We perform numerical experiments and solve the 3D MHD equations. The dynamics are investigated through a range of initial field strengths and twists.

*Results.* The experiments demonstrate that the emergence of toroidal flux tubes is highly dynamic and exhibits a rich variety of behaviour. In answer to the aims, however, if the initial field strength is strong enough, the axis of the tube can fully emerge. Also, the sunspot pair does not continually drift apart. Instead, its maximum separation is the diameter of the original toroidal tube.

### **Coronal Plasma Characterization via Coordinated Infrared and Extreme Ultraviolet Observations of a Total Solar Eclipse**

Chad A. **Madsen**<sup>1</sup>, Jenna E. Samra<sup>1</sup>, Giulio Del Zanna<sup>2</sup>, and Edward E. DeLuca<sup>1</sup>

2019 ApJ 880 102

[sci-hub.se/10.3847/1538-4357/ab2b3c](https://doi.org/10.3847/1538-4357/ab2b3c)

We present coordinated coronal observations of the **2017 August 21** total solar eclipse with the Extreme-ultraviolet Imaging Spectrometer (EIS) and the Airborne Infrared Spectrometer (AIR-Spec). These instruments provide an unprecedented view of the solar corona in two disparate wavelength regimes, the extreme ultraviolet (EUV) and the near- to mid-infrared (IR), opening new pathways for characterizing the complex coronal plasma environment. During totality, AIR-Spec sampled coronal IR spectra near the equatorial west limb, detecting strong sources of Mg viii, S xi, Si ix, and Si x in two passbands encompassing 1.4–4  $\mu\text{m}$ . We apply an intensity-ratio diagnostic to a strong resonant Fe xii line pair arising from the coordinated EIS observations. This results in a high-resolution map of electron density throughout the shared EIS/AIR-Spec field of view. Electron density measurements allow us to produce a similar map of plasma temperature using emission measure (EM) loci analysis as applied to 27 EIS emission lines, providing temperatures of  $106.12 \pm 103.5$  K along the limb and  $106.19 \pm 103.5$  K at about 100" outward. Applying EM loci analysis to AIR-Spec IR spectra coadded over two 31" wide ranges centered at two locations, 30" and 100" from the limb, produces temperatures consistent with the EIS data, albeit suffering from moderate uncertainties. Regardless, we demonstrate that EUV spectral data are valuable constraints to coronal IR emission models, and will be powerful supplements for future IR solar observatories, particularly DKIST.

### Scaling laws of free magnetic energy stored in a solar emerging flux region

Tetsuya **Magara**

2014, Publ. Astron. Soc. Japan

<http://arxiv.org/pdf/1405.4587v1.pdf>

This Letter reports scaling laws of free magnetic energy stored in a solar emerging flux region which is a key to understanding the energetics of solar active phenomena such as solar flares and coronal mass ejections. By performing 3-dimensional magnetohydrodynamic simulations that reproduce several emerging flux regions of different magnetic configurations, we derive power law relationships among emerged magnetic flux, free magnetic energy and relative magnetic helicity in these emerging flux regions. Since magnetic flux is an observable quantity, the scaling law between magnetic flux and free magnetic energy may give a way to estimate invisible free magnetic energy responsible for solar active phenomena.

<http://web.khu.ac.kr/~magara/index.html>

### HOW MUCH DOES A MAGNETIC FLUX TUBE EMERGE INTO THE SOLAR ATMOSPHERE?

T. **Magara**

2012 ApJ 748 53

The emergence process of the magnetic field into the solar atmosphere plays an essential role in determining the configuration of the magnetic field and its activity on the Sun. This paper focuses on how much the magnetic flux contained by a flux tube emerges into the solar atmosphere, which is the key to understanding the physical mechanism of solar eruptions. By comparing a kinematic model of an emerging flux tube to a series of magnetohydrodynamic simulations, we derive the characteristics of the emergence process, showing how the process depends on the pre-emerged state of the magnetic field such as the radius of a flux tube, field strength, field-line twist, and wavelength of undulation assumed by the flux tube. We also discuss the relationship between magnetic configurations and their stability on the Sun.

### Assessing the Capabilities of Dynamic Coronal Seismology of Alfvénic Waves through Forward Modeling

N. **Magyar**<sup>1</sup> and T. Van Doorselaere

2018 ApJ 856 144

<http://sci-hub.tw/http://iopscience.iop.org/0004-637X/856/2/144/>

Coronal seismology is a diagnostic tool used in solar physics for measuring parameters that are otherwise hard to measure; of these parameters, magnetic field values are arguably the most important. The parameters are inferred by combining observations of waves with magnetohydrodynamic (MHD) wave theory. To date, coronal seismology has successfully been applied to various single-oscillation events. Such events are relatively rare, resulting in rare occasions to use diagnostics. Ubiquitous waves in the solar atmosphere might, however, allow for the possibility of dynamic coronal seismology, which involves the continuous inversions of coronal parameters and would constitute a huge leap forward in many areas of solar physics. In this paper, we investigate the robustness and accuracy of magnetic field diagnostics applied to forward-modeled 3D MHD simulations of propagating Alfvénic waves. We find that the seismologically measured magnetic field values are reassuringly close to the input value (within  $\approx 20\%$ ) for a range of setups studied, providing encouragement and confidence for the further development of dynamic coronal seismology.



## **ON THE ANISOTROPY IN EXPANSION OF MAGNETIC FLUX TUBES IN THE SOLAR CORONA**

A. [Malanushenko](#)<sup>1,2</sup> and C. J. Schrijve

2013 ApJ 775 120

Most one-dimensional hydrodynamic models of plasma confined to magnetic flux tubes assume circular tube cross sections. We use potential field models to show that flux tubes in circumstances relevant to the solar corona do not, in general, maintain the same cross-sectional shape through their length and therefore the assumption of a circular cross section is rarely true. We support our hypothesis with mathematical reasoning and numerical experiments. We demonstrate that lifting this assumption in favor of realistic, non-circular loops makes the apparent expansion of magnetic flux tubes consistent with that of observed coronal loops. We propose that in a bundle of ribbon-like loops, those that are viewed along the wide direction would stand out against those that are viewed across the wide direction due to the difference in their column depths. That result would impose a bias toward selecting loops that appear not to be expanding, seen projected in the plane of sky. An implication of this selection bias is that the preferentially selected non-circular loops would appear to have increased pressure scale heights even if they are resolved by current instruments.

## **GUIDING NONLINEAR FORCE-FREE MODELING USING CORONAL OBSERVATIONS: FIRST RESULTS USING A QUASI-GRAD-RUBIN SCHEME**

A. [Malanushenko](#)<sup>1,2</sup>, C. J. Schrijver<sup>2</sup>, M. L. DeRosa<sup>2</sup>, M. S. Wheatland<sup>3</sup>, and S. A. Gilchrist

2012 ApJ 756 153

At present, many models of the coronal magnetic field rely on photospheric vector magnetograms, but these data have been shown to be problematic as the sole boundary information for nonlinear force-free field extrapolations. Magnetic fields in the corona manifest themselves in high-energy images (X-rays and EUV) in the shapes of coronal loops, providing an additional constraint that is not at present used as constraints in the computational domain, directly influencing the evolution of the model. This is in part due to the mathematical complications of incorporating such input into numerical models. Projection effects, confusion due to overlapping loops (the coronal plasma is optically thin), and the limited number of usable loops further complicate the use of information from coronal images. We develop and test a new algorithm to use images of coronal loops in the modeling of the solar coronal magnetic field. We first fit projected field lines with those of constant- $\alpha$  force-free fields to approximate the three-dimensional distribution of currents in the corona along a sparse set of trajectories. We then apply a Grad-Rubin-like iterative technique, which uses these trajectories as volume constraints on the values of  $\alpha$ , to obtain a volume-filling nonlinear force-free model of the magnetic field, modifying a code and method presented by Wheatland. We thoroughly test the technique on known analytical and solar-like model magnetic fields previously used for comparing different extrapolation techniques and compare the results with those obtained by currently available methods relying only on the photospheric data. We conclude that we have developed a functioning method of modeling the coronal magnetic field by combining the line-of-sight component of the photospheric magnetic field with information from coronal images. Whereas we focus on the use of coronal loop information in combination with line-of-sight magnetograms, the method is readily extended to incorporate vector-magnetic data over any part of the photospheric boundary.

## **RECONSTRUCTING THE LOCAL TWIST OF CORONAL MAGNETIC FIELDS AND THE THREE-DIMENSIONAL SHAPE OF THE FIELD LINES FROM CORONAL LOOPS IN EXTREME-ULTRAVIOLET AND X-RAY IMAGES**

A. [Malanushenko](#) et al

2009 ApJ 707 1044-1063

Nonlinear force-free fields are the most general case of force-free fields, but the hardest to model as well. There are numerous methods of computing such fields by extrapolating vector magnetograms from the photosphere, but very few attempts have so far made quantitative use of coronal morphology. We present a method to make such quantitative use of X-ray and EUV images of coronal loops. Each individual loop is fit to a field line of a linear force-free field, allowing the estimation of the field line's twist, three-dimensional geometry, and the field strength along it. We assess the validity of such a reconstruction since the actual corona is probably not a linear force-free field, and that the superposition of linear force-free fields is generally not itself a force-free field. To do so, we perform a series of tests on nonlinear force-free fields, described in Low & Lou. For model loops we project field lines onto the photosphere. We compare several results of the method with the original field, in particular the three-dimensional loop shapes, local twist (coronal  $\alpha$ ), distribution of twist in the model photosphere, and strength of the magnetic field. We find that (1) for these trial fields, the method reconstructs twist with a mean absolute deviation of at most 15% of the range of photospheric twist, (2) heights of the loops are reconstructed with a mean absolute

deviation of at most 5% of the range of trial heights, and (3) the magnitude of non-potential contribution to a photospheric field is reconstructed with a mean absolute deviation of at most 10% of the maximal value.

### **The Digital Fields Board for the FIELDS Instrument Suite on the Solar Probe Plus Mission: Analog and Digital Signal Processing†**

David M. [Malaspina](#), Robert E. Ergun, Mary Bolton, Mark Kien, David Summers, Ken Stevens, Alan Yehle, Magnus Karlsson

JGR Volume 121, Issue 6 June 2016 Pages 5088–5096 **2016**

The first in-situ measurements of electric and magnetic fields in the near-Sun environment ( $< 0.25$  AU from the Sun) will be made by the FIELDS instrument suite on the Solar Probe Plus mission. The Digital Fields Board (DFB) is an electronics board within FIELDS that performs analog and digital signal processing, as well as digitization, for signals between DC and 60 kHz from five voltage sensors and four search coil magnetometer (SCM) channels. These nine input signals are processed on the DFB into 26 analog data streams. A specialized application-specific integrated circuit (ASIC) performs analog to digital conversion on all 26 analog channels simultaneously. The DFB then processes the digital data using a field programmable gate array (FPGA), generating a variety of data products, including digitally filtered continuous waveforms, high-rate burst capture waveforms, power spectra, cross-spectra, band pass filter data, and several ancillary products. While the data products are optimized for encounter-based mission operations, they are also highly configurable, a key design aspect for a mission of exploration. This paper describes the analog and digital signal processing used to ensure that the DFB produces high quality science data, using minimal resources, in the challenging near-Sun environment.

### **Radial profile of the inner heliospheric magnetic field as deduced from Faraday rotation observations**

S. [Mancuso](#)<sup>1</sup> and M. V. Garzelli

A&A 553, A100 (2013)

Faraday rotation measures (RMs) of the polarized emission from extragalactic radio sources occulted by the coronal plasma were used to infer the radial profile of the inner heliospheric magnetic field near the solar minimum. By inverting LASCO/SOHO polarized brightness (pB) data taken during the observations in May 1997, we retrieved the electron density distribution along the lines of sight to the sources, which allowed us to separate the two plasma properties that contribute to the observed RMs. By comparing the observed RM values with those theoretically predicted by a power law model of the radial component of the coronal magnetic field using a best-fitting procedure, we found that the radial component of the inner heliospheric magnetic field can be nicely approximated by a power law of the form  $B_r = 3.76 r^{-2.29}$  G in a range of heights from about **5 to 14  $R_\odot$** . Finally, our analysis suggests that the radial computation of the potential field source surface model from the Wilcox Solar Observatory is the preferred choice near solar minimum assuming a radial field in the photosphere and a source surface located at  $R_{ss} = 2.5 R_\odot$ .

### **Doppler-shift oscillations in the H I Ly $\alpha$ coronal emission line: spectroscopic signature of propagating kink waves?**

S. [Mancuso](#)<sup>1</sup> and J. C. Raymond

A&A 573, A33 (2015)

We report the first detection of long-period, slowly decaying Doppler-shift oscillations in the H I Ly $\alpha$  (1215.67 Å) coronal emission line with the Ultraviolet Coronagraph Spectrometer (UVCS) onboard the Solar and Heliospheric Observatory (SOHO) satellite. The UV spectral data were collected at 1.43  $R_\odot$  above the eastern limb of the Sun during a special high-cadence sit-and-stare observation on 1997 December 14. Time-series analyses with different spectral techniques clearly show highly significant Doppler-shift oscillations in a portion with a size of 154'' of the UVCS slit that lasted for several cycles. A period of  $P = 14.3 \pm 0.4$  min was established with a confidence of better than 99.9% in the Lomb-Scargle periodogram. On average, the Doppler-shift amplitude of  $3.7 \pm 0.7$  km s<sup>-1</sup> was estimated for the most significant oscillations, roughly corresponding to a displacement of  $800 \pm 150$  km. The origin of the regular H I Ly $\alpha$  Doppler-shift oscillations is most probably due to the excitation of propagating fast magnetoacoustic kink waves along a narrow, jet-like ejection observed higher up in the white-light corona. However, different mechanisms, such as low-amplitude coherent kink oscillations of a bundle of loops along the line of sight or quasi-periodic outflows caused by oscillatory magnetic reconnection in the low corona cannot be ruled out.

### **DIFFERENTIAL ROTATION OF THE ULTRAVIOLET CORONA AT SOLAR MAXIMUM**

Salvatore [Mancuso](#) and Silvio Giordano

2011 ApJ 729 79

Synoptic observations of the O VI 1032 Å spectral line from the UltraViolet Coronagraph Spectrometer (UVCS) telescope on board the Solar and Heliospheric Observatory (SOHO) have been analyzed in order to establish the rotational characteristics of the solar corona in the time interval from 1999 March 18 to 2002 December 31, corresponding to the maximum phase of solar cycle 23. By using autocorrelation analysis techniques, we determined the latitude and time dependence of the coronal rotation rate at a heliocentric distance of 1.6 R<sub>☉</sub> from the solar equator up to about 15° from the poles. Although the equatorial rotation rate is initially consistent with the coronal synodic rotation period (~27.5 days) inferred in a previous study by Giordano & Mancuso around solar minimum, a systematic and substantial acceleration is observed to occur during the second part of the year 2000, with the equatorial coronal synodic rotation period settling to an average value of 25.7 days in the time interval extending from 2001 August to 2002 April, corresponding to a ~7% increase in coronal rotation rate. It is shown that the coronal magnetic structures rotate much faster at all latitudes, and less differentially, than the underlying small-scale magnetic structures linked to the photospheric plasma. The rotation rate of sunspots is however compatible, at least within ~20° from the solar equator, with the one estimated in the middle corona.

### **On the size distribution of spots within sunspot groups**

[Sudip Mandal](#), [Natalie A. Krivova](#), [Robert Cameron](#), [Sami K. Solanki](#)

A&A 652, A9 2021

<https://arxiv.org/pdf/2104.03534.pdf>

<https://www.aanda.org/articles/aa/pdf/2021/08/aa40621-21.pdf>

<https://doi.org/10.1051/0004-6361/202140621>

Size distribution of sunspots provides key information about the generation and emergence processes of the solar magnetic field. Previous studies on the size distribution have primarily focused on either the whole group or individual spot areas. In this paper, we investigate the organization of spot areas within sunspot groups. In particular, we analyze the ratio,  $R$ , of the area of the biggest spot ( $A_{\text{big\_spot}}$ ) inside a group, to the total area of that group ( $A_{\text{group}}$ ). We use sunspot observations from Kislovodsk, Pulkovo and Debrecen observatories, together covering solar cycles 17 to 24. We find that at the time when the group area reaches its maximum, the single biggest spot in a group typically occupies about 60% of the group area. For half of all groups,  $R$  lies in the range between roughly 50% and 70%. We also find  $R$  to change with the group area,  $A_{\text{group}}$ , such that  $R$  reaches a maximum of about 0.65 for groups with  $A_{\text{group}} \approx 200 \mu\text{Hem}$  and then remains at about 0.6 for larger groups. Our findings imply a scale invariant emergence pattern, providing an observational constraint on the emergence process. Furthermore, extrapolation of our results to larger sunspot groups may have a bearing on the giant unresolved starspot features found in Doppler images of highly active sun-like stars. Our results suggest that such giant features are composed of multiple spots, with the largest spot occupying roughly 55--75% of the total group area (i.e. of the area of the giant starspots seen in Doppler images).

### **Sunspot area catalogue revisited: Daily cross-calibrated areas since 1874**

[Sudip Mandal](#), [Natalie A. Krivova](#), [Sami K. Solanki](#), [Nimesh Sinha](#), [Dipankar Banerjee](#)

A&A 2020

<https://arxiv.org/pdf/2004.14618.pdf>

Long and consistent sunspot area records are important for understanding the long-term solar activity and variability. Multiple observatories around the globe have regularly recorded sunspot areas, but such individual records only cover restricted periods of time. Furthermore, there are also systematic differences between them, so that these records need to be cross-calibrated before they can be reliably used for further studies. We produce a cross-calibrated and homogeneous record of total daily sunspot areas, both projected and corrected, covering the period between 1874 and 2019. A catalogue of calibrated individual group areas is also generated for the same period. We have compared the data from nine archives: Royal Greenwich Observatory (RGO), Kislovodsk, Pulkovo, Debrecen, Kodaikanal, Solar Optical Observing Network (SOON), Rome, Catania, and Yunnan Observatories, covering the period between 1874 and 2019. Mutual comparisons of the individual records have been employed to produce homogeneous and inter-calibrated records of daily projected and corrected areas. As in earlier studies, the basis of the composite is formed by the data from RGO. After 1976, the only datasets used are those from Kislovodsk, Pulkovo and Debrecen observatories. This choice was made based on the temporal coverage and the quality of the data. In contrast to the SOON data used in previous area composites for the post-RGO period, the properties of the data from Kislovodsk and Pulkovo are very similar to those from the RGO series. They also directly overlap the RGO data in time, which makes their cross-calibration with RGO much more reliable. We have also computed and provide the daily Photometric Sunspot Index (PSI) widely used, e.g., in empirical reconstructions of solar irradiance.

### **Parallel Evolution of Quasi-separatrix Layers and Active Region Upflows**

C.H. [Mandrini](#), D. Baker, P. Démoulin, [G.D. Cristiani](#), [L. van Driel-Gesztelyi](#), [S. Vargas Domínguez](#), [F.A. Nuevo](#), [A.M. Vásquez](#), [M. Pick](#)

ApJ 809 73 2015

<http://arxiv.org/pdf/1507.01264v1.pdf>

Persistent plasma upflows were observed with Hinode's EUV Imaging Spectrometer (EIS) at the edges of active region (AR) 10978 as it crossed the solar disk. We analyze the evolution of the photospheric magnetic and velocity fields of the AR, model its coronal magnetic field, and compute the location of magnetic null-points and quasi-separatrix layers (QSLs) searching for the origin of EIS upflows. Magnetic reconnection at the computed null points cannot explain all of the observed EIS upflow regions. However, EIS upflows and QSLs are found to evolve in parallel, both temporarily and spatially. Sections of two sets of QSLs, called outer and inner, are found associated to EIS upflow streams having different characteristics. The reconnection process in the outer QSLs is forced by a large-scale photospheric flow pattern which is present in the AR for several days. We propose a scenario in which upflows are observed provided a large enough asymmetry in plasma pressure exists between the pre-reconnection loops and for as long as a photospheric forcing is at work. A similar mechanism operates in the inner QSLs, in this case, it is forced by the emergence and evolution of the bipoles between the two main AR polarities. Our findings provide strong support to the results from previous individual case studies investigating the role of magnetic reconnection at QSLs as the origin of the upflowing plasma. Furthermore, we propose that persistent reconnection along QSLs does not only drive the EIS upflows, but it is also responsible for a continuous metric radio noise-storm observed in AR 10978 along its disk transit by the Nan\{c\}ay Radio Heliograph. **9 to 14 December 2007**

### **Topological and statistical properties of nonlinear force-free fields**

A. [Mangalam](#) (1), [A. Prasad](#) (2)

[Advances in Space Research](#) **Volume 61, Issue 2**, 15 January 2018, Pages 738-748

<https://arxiv.org/pdf/1711.02881.pdf>

We use our semi-analytic solution of the nonlinear force-free field equation to construct three-dimensional magnetic fields that are applicable to the solar corona and study their statistical properties for estimating the degree of braiding exhibited by these fields. We present a new formula for calculating the winding number and compare it with the formula for the crossing number. The comparison is shown for a toy model of two helices and for realistic cases of nonlinear force-free fields; conceptually the formulae are nearly the same but the resulting distributions calculated for a given topology can be different. We also calculate linkages, which are useful topological quantities that are independent measures of the contribution of magnetic braiding to the total free energy and relative helicity of the field. Finally, we derive new analytical bounds for the free energy and relative helicity for the field configurations in terms of the linking number. These bounds will be of utility in estimating the braided energy available for nano-flares or for eruptions.

### **High-resolution imaging spectroscopy of two micro-pores and an arch filament system in a small emerging-flux region**

S. J. González [Manrique](#)<sup>1,2</sup>, N. Bello González<sup>3</sup> and C. Denker

*A&A* 600, A38 (2017)

<https://arxiv.org/pdf/1703.10140.pdf>

**Context.** Emerging flux regions mark the first stage in the accumulation of magnetic flux eventually leading to pores, sunspots, and (complex) active regions. These flux regions are highly dynamic, show a variety of fine structure, and in many cases live only for a short time (less than a day) before dissolving quickly into the ubiquitous quiet-Sun magnetic field.

**Aims.** The purpose of this investigation is to characterize the temporal evolution of a minute emerging flux region, the associated photospheric and chromospheric flow fields, and the properties of the accompanying arch filament system. We aim to explore flux emergence and decay processes and investigate if they scale with structure size and magnetic flux contents.

**Methods.** This study is based on imaging spectroscopy with the Göttingen Fabry-Pérot Interferometer at the Vacuum Tower Telescope, Observatorio del Teide, Tenerife, Spain on **2008 August 7**. Photospheric horizontal proper motions were measured with Local correlation tracking using broadband images restored with multi-object multi-frame blind deconvolution. Cloud model (CM) inversions of line scans in the strong chromospheric absorption  $H\alpha$ 656.28 nm line yielded CM parameters (Doppler velocity, Doppler width, optical thickness, and source function), which describe the cool plasma contained in the arch filament system.

**Results.** The high-resolution observations cover the decay and convergence of two micro-pores with diameters of less than one arcsecond and provide decay rates for intensity and area. The photospheric horizontal flow speed is suppressed near the two micro-pores indicating that the magnetic field is already sufficiently strong to affect the convective energy transport. The micro-pores are accompanied by a small arch filament system as seen in  $H\alpha$ , where small-scale loops connect two regions with  $H\alpha$  line-core brightenings containing an emerging flux region with opposite polarities. The Doppler width, optical thickness, and source function reach the largest values near the  $H\alpha$  line-core brightenings. The chromospheric velocity of the cloud material is predominantly directed downwards near the footpoints of the loops with velocities of up to 12 km s<sup>-1</sup>, whereas loop tops show upward motions of about 3 km s<sup>-1</sup>. Some of the loops exhibit signs of twisting motions along the loop axis.

Conclusions. Micro-pores are the smallest magnetic field concentrations leaving a photometric signature in the photosphere. In the observed case, they are accompanied by a miniature arch filament system indicative of newly emerging flux in the form of  $\Omega$ -loops. Flux emergence and decay take place on a time-scale of about two days, whereas the photometric decay of the micro-pores is much more rapid (a few hours), which is consistent with the incipient submergence of  $\Omega$ -loops. Considering lifetime and evolution timescales, impact on the surrounding photospheric proper motions, and flow speed of the chromospheric plasma at the loop tops and footpoints, the results are representative for the smallest emerging flux regions still recognizable as such.

## Relationship between Total Solar Irradiance and Magnetic Flux during Solar Minima

Sergey V. [Marchenko](#)<sup>1,2</sup>, Judith L. Lean<sup>3</sup>, and Matthew T. DeLand<sup>1,2</sup>

2022 ApJ 936 158

<https://iopscience.iop.org/article/10.3847/1538-4357/ac8a98/pdf>

What drives the small total solar irradiance (TSI) changes of  $\sim 50$ – $100$  parts per million (compared with  $>1000$  ppm solar-cycle amplitudes) during a deep solar minimum, i.e., in the practical absence of detectable sunspots and long-lasting active regions? We consider the epoch 2008 June–October and investigate multiple data sets (TSI; various Mg ii line-activity indices, extreme ultraviolet fluxes, and full-disk magnetograms) to show that variations in TSI closely follow changes in total magnetic flux from sources with  $|B| > 80$  G (up to  $\sim 600$  G) that persist even during extended periods with no detectable sunspots. These sources comprise the populations of (a) short-lived ( $<20$  minutes), small-scale (predominantly a single 2" MDI pixel),  $\sim$ evenly distributed regions, and (b) on average, more extended (a few MDI pixels) and longer-lived (140–260 minutes median lifetimes) magnetic areas. We ascribe the latter to ephemeral regions, finding them clustering on  $\sim 200$  Mm scales. We speculate that the short-lived MDI sources are linked to the ubiquitous magnetic bright points. Our analysis of magnetic flux variations during solar cycle 23 shows that the magnetic regions present during this deep solar minimum elevate the total magnetic flux above the total flux in just the Gaussian "cores," fitted to histogram distributions of the full-disk flux. This suggests that solar irradiance during more extended, even deeper minima, such as the Maunder Minimum, may be lower than in 2008.

## Formation of Penumbra in a Sample of Active Regions Observed by the SDO Satellite

Murabito [Mariarita](#)<sup>1</sup>, Francesca Zuccarello<sup>1</sup>, Salvo L. Guglielmino<sup>1</sup>, and Paolo Romano<sup>2</sup>

2018 ApJ 855 58

<http://sci-hub.tw/http://iopscience.iop.org/0004-637X/855/1/58/>

Recently, high-resolution observations improved our understanding of the penumbra formation process around sunspots. In particular, two aspects have been carefully investigated: whether the settlement of the penumbra can occur between the main opposite magnetic polarities where new magnetic flux is still emerging, and the establishment of the Evershed flow. In this paper, we present the analysis of twelve active regions (ARs) where both the penumbra formation and the onset of the Evershed flow were observed. We used data acquired by the Helioseismic and Magnetic Imager (HMI) instrument on board the Solar Dynamic Observatory (SDO) satellite analyzing continuum images, magnetograms, and Dopplergrams of the selected ARs. The results obtained in our sample provided the following information about the stable settlement of the penumbra: eight spots formed the first stable penumbral sector in the region between the two opposite polarities, and nine spots formed on the opposite side. Moreover, eleven sunspots showed an inverse Evershed flow (i.e., a plasma motion directed toward the protospot border) before the penumbra formation, which changes within 1–6 hr into the classical Evershed flow as soon as the penumbra forms. Comparing our results with recent observations, we are able to discriminate between the different ways of penumbra formation. Moreover, we suggest that the change from inverse Evershed flow, visible before the penumbra appears, into the classical Evershed flow may be a signature of the formation of penumbral filaments.

Table 1 Selected ARs (2011–2012)

## Turbulent magnetic energy spectrum and the cancellation function of solar photospheric magnetic fields

G. [Marschalkó](#), K. Petrovay

Astron.Nachr.334:952-955, 2013

<http://arxiv.org/pdf/1404.1772v1.pdf>

A simple analytical relation of form  $\{\alpha\} = 2 \{\kappa\} - 1$  between the magnetic energy spectral exponent  $\{\alpha\}$  of the turbulent magnetic field in the solar photosphere and its magnetic flux cancellation exponent  $\{\kappa\}$ , valid under certain restrictive assumptions, is tested and extended outside its range of validity in a series of Monte Carlo simulations. In these numerical tests artificial "magnetograms" are constructed in 1D and 2D by superposing a discrete set of Fourier modes of the magnetic field distribution with amplitudes following a power law spectrum and measuring the cancellation function on these simulated magnetograms. Our results confirm the validity of the analytical relation and extend it to the domain  $\{\alpha\} < -1$  where  $\{\kappa\} \rightarrow 0$  as  $\{\alpha\} \rightarrow -$

infinity. The observationally derived upper limit of 0.38 on  $\{\kappa\}$  implies  $\{\alpha\} < -0.24$  in the granular size range, apparently at odds with a small scale dynamo driven in the inertial range.

## **A novel inversion method to determine the coronal magnetic field including the impact of bound-free absorption**

[Juan Martinez-Sykora](#), [Viggo H. Hansteen](#), [Bart De Pontieu](#), [Enrico Landi](#)

ApJ 938 60 2022

<https://arxiv.org/pdf/2208.13984.pdf>

<https://iopscience.iop.org/article/10.3847/1538-4357/ac8d5b/pdf>

The magnetic field governs the corona; hence it is a crucial parameter to measure. Unfortunately, existing techniques for estimating its strength are limited by strong assumptions and limitations. These techniques include photospheric or chromospheric field extrapolation using potential or non-linear-force-free methods, estimates based on coronal seismology, or by direct observations via, e.g., the Cryo-NIRSP instrument on DKIST which will measure the coronal magnetic field, but only off the limb. Alternately, in this work we investigate a recently developed approach based on the magnetic-field-induced (MIT) transition of the  $\lambda_{\text{FeX}} \sim 257.261 \text{ \AA}$ . In order to examine this approach, we have synthesized several  $\lambda_{\text{FeX}}$  lines from two 3D magnetohydrodynamic simulations, one modeling an emerging flux region and the second an established mature active region. In addition, we take bound-free absorption from neutral hydrogen and helium and singly ionised helium into account. The absorption from cool plasma that occurs at coronal heights has a significant impact on determining the magnetic field. We investigate in detail the challenges of using these  $\lambda_{\text{FeX}}$  lines to measure the field, considering their density and temperature dependence. We present a novel approach to deriving the magnetic field from the MIT using inversions of the differential emission measure as a function of the temperature, density, and magnetic field. This approach successfully estimates the magnetic field strength (up to  $\sim 18\%$  relative error) in regions that do not suffer from significant absorption and that have relatively strong coronal magnetic fields ( $>250 \text{ G}$ ). This method allows the masking of regions where absorption is significant.

## **Hemispheric Patterns in Filament Chirality and Sigmoid Shape over the Solar Cycle,**

**(Invited Review)**

Petrus C. [Martens](#), Anthony R. Yeates, and Karthik G. Pillai, Proceedings of IAU Symposium 300, 122-125, 2014

"Nature of solar prominences and their role in Space Weather", Paris, France, June 10-14, 2013,

B. B. Schmieder, J.-M. Malherbe & S. T. Wu, eds.

<http://solar.physics.montana.edu/martens/papers/IAU300-Martens-proofs.pdf>

The motivation for our research was to study the correlation between the chirality of filaments and the handedness (S- or Z-shape) of sigmoids. It was assumed that sigmoids would mostly coincide with filaments and that the S-shaped sigmoids would correlate well with filaments of sinistral chirality, which we found that to be at best a very weak relation. Since we had a full solar cycle of filament metadata at hand it was easy to verify the supposedly known hemispheric preference of filament chirality. We discovered that the hemispheric chirality rule was confirmed for the epoch where a thorough manual study had been performed, but that at other phases of the solar cycle the rule seems to disappear and sometimes even reverse.

## **The Solar Corona: What Are The Remaining Fundamental Physical Questions?**

**(Invited Review)**

Petrus C. [Martens](#)

Proceedings of the International Symposium on Solar-Terrestrial Physics, November 2012, Pune, India Bull. Astron. Soc. India, 2013-2014, in press.

<http://solar.physics.montana.edu/martens/papers/martens-draft3.pdf>; **File**

The two key unresolved physical questions in our knowledge of the solar corona are: (1) **How is the corona heated** to a temperature of several MK, and, directly related to that, why is the coronal emission structured in nearly constant cross-section loops? And, (2) **what is the mechanism that determines the onset of solar flares and eruptions**, and, again directly related, **can flares be predicted**? I will introduce these questions, discuss some proposed solutions that are not complete, and my view on getting to the full solutions.

## **Surface flux transport simulations: Effect of inflows toward active regions and random velocities on the evolution of the Sun's large-scale magnetic field**

David [Martin-Belda](#), Robert H. Cameron

A&A 586, A73 2016

<http://arxiv.org/pdf/1512.02541v1.pdf>

**Aims:** We aim to determine the effect of converging flows on the evolution of a bipolar magnetic region (BMR), and to investigate the role of these inflows in the generation of poloidal flux. We also discuss whether the flux dispersal due to turbulent flows can be described as a diffusion process.

**Methods:** We developed a simple surface flux transport model based on point-like magnetic concentrations. We tracked the tilt angle, the magnetic flux and the axial dipole moment of a BMR in simulations with and without inflows and compared the results. To test the diffusion approximation, simulations of random walk dispersal of magnetic features were compared against the predictions of the diffusion treatment.

**Results:** We confirm the validity of the diffusion approximation to describe flux dispersal on large scales. We find that the inflows enhance flux cancellation, but at the same time affect the latitudinal separation of the polarities of the bipolar region. In most cases the latitudinal separation is limited by the inflows, resulting in a reduction of the axial dipole moment of the BMR. However, when the initial tilt angle of the BMR is small, the inflows produce an increase in latitudinal separation that leads to an increase in the axial dipole moment in spite of the enhanced flux destruction. This can give rise to a tilt of the BMR even when the BMR was originally aligned parallel to the equator.

## **Dynamics of the Transition Corona**

Sophie **Masson**<sup>1,2</sup>, Patrick McCauley<sup>3</sup>, Leon Golub<sup>3</sup>, Katharine K. Reeves<sup>3</sup>, and Edward E. DeLuca  
**2014 ApJ 787 145**

<http://arxiv.org/pdf/1301.0740v2.pdf>

Magnetic reconnection between the open and closed magnetic fields in the corona is believed to play a crucial role in the corona/heliosphere coupling. At large scale, the exchange of open/closed connectivity is expected to occur in pseudo-streamer (PS) structures. However, there is neither clear observational evidence of how such coupling occurs in PSs, nor evidence for how the magnetic reconnection evolves. Using a newly developed technique, we enhance the off-limb magnetic fine structures observed with the Atmospheric Imaging Assembly and identify a PS-like feature located close to the northern coronal hole. We first identify that the magnetic topology associated with the observation is a PS, null-point (NP) related topology bounded by the open field. By comparing the magnetic field configuration with the EUV emission regions, we determined that most of the magnetic flux associated with plasma emission are small loops below the PS basic NP and open field bounding the PS topology. In order to interpret the evolution of the PS, we referred to a three-dimensional MHD interchange reconnection modeling the exchange of connectivity between small closed loops and the open field. The observed PS fine structures follow the dynamics of the magnetic field before and after reconnecting at the NP obtained by the interchange model. Moreover, the pattern of the EUV plasma emission is the same as the shape of the expected plasma emission location derived from the simulation. These morphological and dynamical similarities between the PS observations and the results from the simulation strongly suggest that the evolution of the PS, and in particular the opening/closing of the field, occurs via interchange/slipping reconnection at the basic NP of the PS. Besides identifying the mechanism at work in the large-scale coupling between the open and closed fields, our results highlight that interchange reconnection in PSs is a gradual physical process that differs from the impulsive reconnection of the solar-jet model. **2012-01-19**

## **Self-consistent Nonlinear Force-free Field Reconstruction from Weighted Boundary Conditions**

Alpha **Mastrano**, [Kai E. Yang](#), [Michael S. Wheatland](#)

*Solar Phys.* **295**, Article number: 97 **2020**

<https://arxiv.org/pdf/2004.12510.pdf>

<https://link.springer.com/content/pdf/10.1007/s11207-020-01663-7.pdf>

Vector magnetogram data are often used as photospheric boundary conditions for force-free coronal magnetic field extrapolations. In general, however, vector magnetogram data are not consistent with the force-free assumption. In this article, we demonstrate a way to deal with inconsistent boundary data, by generalizing the "self-consistency procedure" of Wheatland & Regnier (2009). In that procedure, the inconsistency is resolved by an iterative process of constructing two solutions based on the values of the force-free parameter alpha on the two polarities of the field in the boundary (the P and N polarities), and taking uncertainty-weighted averages of the boundary alpha values in the P and N solutions. When the alpha values in the P and N regions are very different, the self-consistent solution may lose high alpha values from the boundary conditions. We show how, by altering the weighting of the uncertainties in the P or N boundary conditions, we can preserve high alpha values in the self-consistent solution. The weighted self-consistent extrapolation method is demonstrated on an analytic bipole field and applied to vector magnetogram data taken by the Helioseismic and Magnetic Imager (HMI) instrument for NOAA active region AR 12017 on **2014 March 29**.

## **A Check on the Validity of Magnetic Field Reconstructions**

A. **Mastrano**, M. S. Wheatland, S. A. Gilchrist

*Solar Physics* September **2018**, 293:130

<https://link.springer.com/article/10.1007/s11207-018-1351-0>

We investigate a method to test whether a numerically computed model coronal magnetic field  $B_B$  departs from the divergence-free condition (also known as the solenoidality condition). The test requires a potential field  $B_{B0}$  to be calculated, subject to Neumann boundary conditions, given by the normal components of the model field  $B_B$  at the boundaries. The free energy of the model field may be calculated using  $12\mu_0\int(B-B_0)^2dV$ , where the integral is over the computational volume of the model field. A second estimate of the free energy is provided by calculating  $12\mu_0\int B^2dV - 12\mu_0\int B_0^2dV$ . If  $B_B$  is divergence free, the two estimates of the free energy should be the same. A difference between the two estimates indicates a departure from  $\nabla\cdot B=0$  in the volume. The test is an implementation of a procedure proposed by Moraitis et al. (Solar Phys. 289, 4453, 2014) and is a simpler version of the Helmholtz decomposition procedure presented by Valori et al. (Astron. Astrophys. 553, A38, 2013). We demonstrate the test in application to previously published nonlinear force-free model fields, and also investigate the influence on the results of the test of a departure from flux balance over the boundaries of the model field. Our results underline the fact that, to make meaningful statements about magnetic free energy in the corona, it is necessary to have model magnetic fields that satisfy the divergence-free condition to a good approximation.

## **The Plasma-prescribed Active Region Static Extrapolation (PARSE) Dataset: A Machine-Learning-Ready Collection of Magnetohydrostatic Coronal Active Regions**

[Nat H. Mathews](#), [Barbara J. Thompson](#)

ApJ 2023

<https://arxiv.org/pdf/2308.02138.pdf>

As Physics-Informed Neural Networks and other methods for full-vector-field construction or analysis become more prominent, a need has developed for a large set of simulated active regions for training, validation and testing purposes. We use a state-of-the-art magnetohydrostatic extrapolation method to develop a public dataset of over five thousand data cubes based on the Spaceweather HMI Active Region Patch (SHARP) library of active region magnetogram images. Each cube resolves the magnetic field vector and plasma forcing at approximately 100,000 scattered points that are adaptively clustered near the high-flux regions of the domain. This paper describes the methodology of construction of the Plasma-prescribed Active Region Static Extrapolation (PARSE) dataset, as well as its structure and how to access it.

## **Reconstructing the Coronal Magnetic Field: The Role of Cross-field Currents in Solution Uniqueness**

Nathaniel H. [Mathews](#)<sup>1</sup>, Natasha Flyer<sup>1</sup>, and Sarah E. Gibson<sup>2</sup>

2020 ApJ 898 70

<https://iopscience.iop.org/article/10.3847/1538-4357/ab9dfd/pdf>

We present a new 3D magnetohydrostatic (MHS) direct elliptic solver for extrapolating the coronal magnetic field from photospheric boundary conditions in a manner consistent with an assumed plasma distribution. We use it to study the uniqueness of the reconstructed magnetic field as a function of how significant the plasma forcing is on the force balance of the magnetic field. To this end, we consider an analytic MHS model as ground truth. The model uses two free parameters to decompose the current into two parts: a magnetic-field-aligned component and a cross-field component. We perform a comprehensive study of the 2D parameter space to understand under what conditions the ground truth can be reproduced uniquely. We find that current oriented perpendicular to the magnetic field has a smaller solution space than the same amount of current oriented parallel to the magnetic field, and so MHS regimes with larger proportions of plasma-related forcing may be a promising avenue toward finding unique magnetic field reconstructions.

## **Uncertainty quantification in sunspot counts**

[Sophie Mathieu](#), [Véronique Delouille](#), [Laure Lefèvre](#), [Christian Ritter](#), [Rainer von Sachs](#)

The Astrophysical Journal 886(1):7 2019

<https://sci-hub.st/10.3847/1538-4357/ab4990>

<https://arxiv.org/pdf/2009.09810.pdf>

Observing and counting sunspots constitutes one of the longest-running scientific experiment, with first observations dating back to Galileo and the invention of the telescope around 1610. Today the sunspot number (SN) time series acts as a benchmark of solar activity in a large range of physical models. An appropriate statistical modelling, adapted to the time series' complex nature, is however still lacking. In this work, we provide the first comprehensive uncertainty quantification analysis of sunspot counts. Our interest lies in the following three components: the number of spots ( $N_s$ ), the number of sunspot groups ( $N_g$ ), and the composite  $N_c$ , defined as  $N_c = N_s + 10N_g$ . Those are reported by a network of observatories around the world, and are corrupted by errors of various types. We use a multiplicative framework to provide, for each of the three components, an estimation of their error distribution in various regimes (short-term, long-term, minima of solar activity). We also propose a robust estimator for the underlying solar signal and fit a density distribution that takes into account intrinsic characteristics such as over-dispersion, excess of zeros, and multiple modes. The estimation of the solar signal underlying the composite  $N_c$  may



be seen as a robust version of the International Sunspot Number (ISN), a quantity widely used as a proxy of solar activity. Therefore our results on  $N_c$  may serve to characterize the uncertainty on ISN as well. Our results paves the way for a future monitoring of the observatories in quasi-real time, with the aim to alert the observers when they start deviating from the network and prevent large drifts from occurring in the network.

## **Does $H\alpha$ Stokes-V profiles probe the chromospheric magnetic field? An observational perspective**

[Harsh Mathur](#), [K. Nagaraju](#), [Jayant Joshi](#), [Jaime de la Cruz Rodríguez](#)

ApJ **946** 38 **2023**

<https://arxiv.org/pdf/2302.13118.pdf>

<https://iopscience.iop.org/article/10.3847/1538-4357/acbf49/pdf>

We investigated the diagnostic potential of the Stokes V profile of the  $H\alpha$  line to probe the chromospheric line-of-sight (LOS) magnetic field (BLOS) by comparing the BLOS inferred from the weak field approximation (WFA) with that of inferred from the multi-line inversions of the Ca II 8542 Å, Si I 8536 Å and Fe I 8538 Å lines using the STiC inversion code. Simultaneous spectropolarimetric observations of a pore in the Ca II 8542 Å and  $H\alpha$  spectral lines obtained from the SPINOR at the Dunn Solar Telescope on the 4th of December, 2008 are used in this study. The WFA was applied on the Stokes I and V profiles of  $H\alpha$  line over three wavelength ranges viz.: around line core ( $\Delta\lambda=\pm 0.35$  Å), line wings ( $\Delta\lambda=[-1.5, -0.6]$  and  $[+0.6, +1.5]$  Å) and full spectral range of the line ( $\Delta\lambda=\pm 1.5$  Å) to derive the BLOS. We found the maximum BLOS strengths of  $\sim +800$  and  $\sim +600$  G at  $\log\tau_{500} = -1$  and  $-4.5$ , respectively in the pore. The morphological map of the BLOS inferred from the  $H\alpha$  line core is similar to the BLOS map at  $\log\tau_{500} = -4.5$  inferred from multi-line inversions. The BLOS map inferred from the  $H\alpha$  line wings and full spectral range have a similar morphological structure to the BLOS map inferred at  $\log\tau_{500} = -1$ . The BLOS estimated from  $H\alpha$  using WFA is weaker by a factor of  $\approx 0.53$  than that of inferred from the multi-line inversions. **December 4, 2008**

## **Frozen-in Fractals All Around: Inferring the Large-Scale Effects of Small-Scale Magnetic Structure**

R. T. James [McAteer](#)

Solar Phys. Volume 290, [Issue 7](#), pp 1897-1907 **2015**

The large-scale structure of the magnetic field in the solar corona provides the energy to power large-scale solar eruptive events. Our physical understanding of this structure, and hence our ability to predict these events, is limited by the type of data currently available. It is shown that the multifractal spectrum is a powerful tool to study this structure, by providing a physical connection between the details of photospheric magnetic gradients and current density at all size scales. This uses concepts associated with geometric measure theory and the theory of weakly differentiable functions to compare Ampère's law to the wavelet-transform modulus maximum method. The Hölder exponent provides a direct measure of the rate of change of current density across spatial size scales. As this measure is independent of many features of the data (pixel resolution, data size, data type, presence of quiet-Sun data), it provides a unique approach to studying magnetic-field complexity and hence a potentially powerful tool for a statistical prediction of solar-flare activity. Three specific predictions are provided to test this theory: the multifractal spectra will not be dependent on the data type or quality; quiet-Sun gradients will not persist with time; structures with high current densities at large size scales will be the source of energy storage for solar eruptive events.

## **TILT ANGLE AND FOOTPOINT SEPARATION OF SMALL AND LARGE BIPOLAR SUNSPOT REGIONS OBSERVED WITH HMI**

B. H. [McClintock](#)<sup>1</sup> and A. A. Norton

**2016** ApJ 818 7

<http://arxiv.org/pdf/1602.04154v1.pdf>

We investigate bipolar sunspot regions and how tilt angle and footpoint separation vary during emergence and decay. The Helioseismic and Magnetic Imager on board the Solar Dynamic Observatory collects data at a higher cadence than historical records and allows for a detailed analysis of regions over their lifetimes. We sample the umbral tilt angle, footpoint separation, and umbral area of 235 bipolar sunspot regions in Helioseismic and Magnetic Imager—Debrecen Data with an hourly cadence. We use the time when the umbral area peaks as time zero to distinguish between the emergence and decay periods of each region and we limit our analysis of tilt and separation behavior over time to within  $\pm 96$  hr of time zero. Tilt angle evolution is distinctly different for regions with small ( $\approx 30$  MSH), midsize ( $\approx 50$  MSH), and large ( $\approx 110$  MSH) maximum umbral areas, with 45 and 90 MSH being useful divisions for separating the groups. At the peak umbral area, we determine median tilt angles for small (76), midsize (59), and large (93) regions. Within  $\pm 48$  hr of the time of peak umbral area, large regions steadily increase in tilt angle, midsize regions are nearly constant, and small regions show evidence of negative tilt during emergence. A period of growth in footpoint separation occurs over a 72-hr period for all of the regions from roughly 40 to 70 Mm.

The smallest bipoles (<9 MSH) are outliers in that they do not obey Joy's law and have a much smaller footpoint separation. We confirm the Muñoz-Jaramillo et al. results that the sunspots appear to be two distinct populations.

### **Re-examining Sunspot Tilt Angle to Include Anti-Hale Statistics**

B. H. [McClintock](#)<sup>1</sup>, A. A. Norton<sup>2</sup>, and J. Li

2014 ApJ 797 130

<http://arxiv.org/pdf/1412.5094v1.pdf>

Sunspot groups and bipolar magnetic regions (BMRs) serve as an observational diagnostic of the solar cycle. We use Debrecen Photoheliographic Data (DPD) from 1974-2014 that determined sunspot tilt angles from daily white light observations, and data provided by Li & Ulrich that determined sunspot magnetic tilt angle using Mount Wilson magnetograms from 1974-2012. The magnetograms allowed for BMR tilt angles that were anti-Hale in configuration, so tilt values ranged from 0 to 360° rather than the more common 90°. We explore the visual representation of magnetic tilt angles on a traditional butterfly diagram by plotting the mean area-weighted latitude of umbral activity in each bipolar sunspot group, including tilt information. The large scatter of tilt angles over the course of a single cycle and hemisphere prevents Joy's law from being visually identified in the tilt-butterfly diagram without further binning. The average latitude of anti-Hale regions does not differ from the average latitude of all regions in both hemispheres. The distribution of anti-Hale sunspot tilt angles are broadly distributed between 0 and 360° with a weak preference for east-west alignment 180° from their expected Joy's law angle. The anti-Hale sunspots display a log-normal size distribution similar to that of all sunspots, indicating no preferred size for anti-Hale sunspots. We report that 8.4% ± 0.8% of all bipolar sunspot regions are misclassified as Hale in traditional catalogs. This percentage is slightly higher for groups within 5° of the equator due to the misalignment of the magnetic and heliographic equators.

### **Analysis of the magnetic field discontinuity at the potential field source surface and Schatten Current Sheet interface in the WangSheeleyArge model,**

[McGregor](#), S. L., W. J. Hughes, C. N. Arge, and M. J. Owens

J. Geophys. Res., 113, A08112, (2008),

<http://dx.doi.org/10.1029/2007JA012330>

The Wang–Sheeley–Arge solar wind model makes use of coupled potential field source surface (PFSS) and Schatten Current Sheet (SCS) models to reconstruct the coronal magnetic field on the basis of the observed line-of-sight photospheric magnetic field and a 1D kinematic code to propagate the solar wind to 1 AU. The source surface serves as the outer boundary of the PFSS model and the inner boundary of the SCS model. Known discontinuities arise in the tangential components of the magnetic field across this surface owing to differences in the imposed boundary conditions (Wang et al., 1998). Here we introduce a more flexible coupling between the two models, which considerably reduces the discontinuous behavior of the magnetic field across the model interface surface, to investigate the effects and importance of these kinks on the accuracy of the model's solar wind speed predictions at 1 AU. A detailed analysis of select Carrington rotations shows that removing the kinks can lead to changes in connectivity, creating different source regions for the solar wind. These changes lead to significantly improved predictions of solar wind structures at 1 AU some of the time, but most of the time, the kinks do not affect the predicted solar wind speed. This improvement is born out statistically by increases in the prediction skill scores of both solar wind velocity (1.7%) and interplanetary magnetic field polarity (1.4%) at 1 AU.

### **On Magnetic Activity Band Overlap, Interaction, and the Formation of Complex Solar Active Regions**

Scott W. [McIntosh](#), Robert J. Leamon

ApJL 2014

<http://arxiv.org/pdf/1410.6411v1.pdf>

Recent work has revealed a phenomenological picture of the how the ~11-year sunspot cycle of Sun arises. The production and destruction of sunspots is a consequence of the latitudinal-temporal overlap and interaction of the toroidal magnetic flux systems that belong to the 22-year magnetic activity cycle and are rooted deep in the Sun's convective interior. We present a conceptually simple extension of this work, presenting a hypothesis on how complex active regions can form as a direct consequence of the intra- and extra-hemispheric interaction taking place in the solar interior. Furthermore, during specific portions of the sunspot cycle we anticipate that those complex active regions may be particularly susceptible to profoundly catastrophic breakdown---producing flares and coronal mass ejections of most severe magnitude.

### **Deciphering Solar Magnetic Activity I: On The Relationship Between The Sunspot Cycle And The Evolution Of Small Magnetic Features**

Scott W. [McIntosh](#), Xin Wang, Robert J. Leamon, Alisdair R. Davey, Rachel Howe, Larisza D. Krista, Anna V. Malanushenko, Jonathan W. Cirtain, Joseph B. Gurman, Michael J. E-print, March 2014; ApJ

Sunspots are a canonical marker of the Sun's internal magnetic field which flips polarity every ~22-years. The principal variation of sunspots, an ~11-year variation in number, modulates the amount of magnetic field that pierces the solar surface and drives significant variations in our Star's radiative, particulate and eruptive output over that period. This paper presents observations from the Solar and Heliospheric Observatory and Solar Dynamics Observatory indicating that the 11-year sunspot variation is intrinsically tied to the spatio-temporal overlap of the activity bands belonging to the 22-year magnetic activity cycle. Using a systematic analysis of ubiquitous coronal brightpoints, and the magnetic scale on which they appear to form, we show that the landmarks of sunspot cycle 23 can be explained by considering the evolution and interaction of the overlapping activity bands of the longer scale variability.

### **Identifying Potential Markers of the Sun's Giant Convective Scale**

Scott W. [McIntosh](#), Xin Wang, Robert J. Leamon, Philip H. Scherrer  
ApJL, 2014, 784 L32

<http://arxiv.org/pdf/1403.0692v1.pdf>

Line-of-sight magnetograms from the Helioseismic and Magnetic Imager (HMI) of the Solar Dynamics Observatory (SDO) are analyzed using a diagnostic known as the "Magnetic Range of Influence," or MRoI. The MRoI is a measure of the length over which a photospheric magnetogram is balanced and so its application gives the user a sense of the connective length scales in the outer solar atmosphere. The MRoI maps and histograms inferred from the SDO/HMI magnetograms primarily exhibit four scales: a scale of a few megameters that can be associated with granulation, a scale of a few tens of megameters that can be associated with super-granulation, a scale of many hundreds to thousands of megameters that can be associated with coronal holes and active regions, and a hitherto unnoticed scale that ranges from 100 to 250 megameters. We infer that this final scale is an imprint of the (rotationally-driven) giant convective scale on photospheric magnetism. This scale appears in MRoI maps as well-defined, spatially distributed, concentrations that we have dubbed "g-nodes." Furthermore, using coronal observations from the Atmospheric Imaging Assembly (AIA) on SDO, we see that the vicinity of these g-nodes appears to be a preferred location for the formation of extreme ultraviolet (EUV, and likely X-Ray) brightpoints. These observations and straightforward diagnostics offer the potential of a near-real-time mapping of the Sun's largest convective scale, a scale that possibly reaches to the very bottom of the convective zone.

### **ESTIMATING THE "DARK" ENERGY CONTENT OF THE SOLAR CORONA**

Scott W. [McIntosh](#)<sup>1</sup> and Bart De Pontieu

2012 ApJ 761 138

The discovery of ubiquitous low-frequency (3-5 mHz) Alfvénic waves in the solar chromosphere (with Hinode/Solar Optical Telescope) and corona (with CoMP and SDO) has provided some insight into the non-thermal energy content of the outer solar atmosphere. However, many questions remain about the true magnitude of the energy flux carried by these waves. Here we explore the apparent discrepancy in the resolved coronal Alfvénic wave amplitude (~0.5 km s<sup>-1</sup>) measured by the Coronal Multi-channel Polarimeter (CoMP) compared to those of the Hinode and the Solar Dynamics Observatory (SDO) near the limb (~20 km s<sup>-1</sup>). We use a blend of observational data and a simple forward model of Alfvénic wave propagation to resolve this discrepancy and determine the Alfvénic wave energy content of the corona. Our results indicate that enormous line-of-sight superposition within the coarse spatio-temporal sampling of CoMP hides the strong wave flux observed by Hinode and SDO and leads to the large non-thermal line broadening observed. While this scenario has been assumed in the past, our observations with CoMP of a strong correlation between the non-thermal line broadening with the low-amplitude, low-frequency Alfvénic waves observed in the corona provide the first direct evidence of a wave-related non-thermal line broadening. By reconciling the diverse measurements of Alfvénic waves, we establish large coronal non-thermal line widths as direct signatures of the hidden, or "dark," energy content in the corona and provide preliminary constraints on the energy content of the wave motions observed.

### **OBSERVING EPISODIC CORONAL HEATING EVENTS ROOTED IN CHROMOSPHERIC ACTIVITY**

[S. W. McIntosh](#)<sup>1</sup> and [Bart De Pontieu](#)<sup>2</sup>

2009 ApJ 706 L80-L85

We present the results of a multi-wavelength study of episodic plasma injection into the corona of active region (AR) 10942. We exploit long-exposure images of the *Hinode* and *Transition Region and Coronal Explorer* spacecraft to study the properties of faint, episodic, "blobs" of plasma that are propelled upward along coronal loops

that are rooted in the AR plage. We find that the source location and characteristic velocities of these episodic upflow events match those expected from recent spectroscopic observations of faint coronal upflows that are associated with upper chromospheric activity, in the form of highly dynamic spicules. The analysis presented ties together observations from coronal and chromospheric spectrographs and imagers, providing more evidence of the connection of discrete coronal mass heating and injection events with their source, dynamic spicules, in the chromosphere.

## **The Great Solar Active Region NOAA 12192: Helicity Transport, Filament Formation, and Impact on the Polar Field**

Tyler C. [McMaken](#)<sup>1,2</sup> and Gordon J. D. Petrie

2017 ApJ 840 100

<http://sci-hub.cc/10.3847/1538-4357/aa6d0b>

The solar active region (AR), NOAA 12192, appeared in **2014 October** as the largest AR in 24 years. Here we examine the counterintuitive nature of two diffusion-driven processes in the region: the role of helicity buildup in the formation of a major filament, and the relationship between the effects of supergranular diffusion and meridional flow on the AR and on the polar field. Quantitatively, calculations of current helicity and magnetic twist from Helioseismic and Magnetic Imager (HMI) vector magnetograms indicate that, though AR 12192 emerged with negative helicity, positive helicity from subsequent flux emergence, consistent with the hemispheric sign-preference of helicity, increased over time within large-scale, weak-field regions such as those near the polarity inversion line (PIL). Morphologically, Atmospheric Imaging Assembly observations of filament barbs, sigmoidal patterns, and bases of Fe xii stalks initially exhibited signatures of negative helicity, and the long filament that subsequently formed had a strong positive helicity consistent with the helicity buildup along the PIL. We find from full-disk HMI magnetograms that AR 12192's leading positive flux was initially closer to the equator but, owing either to the region's magnetic surroundings or to its asymmetric flux density distribution, was transported poleward more quickly on average than its trailing negative flux, contrary to the canonical pattern of bipole flux transport. This behavior caused the AR to have a smaller effect on the polar fields than expected and enabled the formation of the very long neutral line where the filament formed.

## **Data Assimilative Optimization of WSA Source Surface and Interface Radii using Particle Filtering**

[Grant David Meadors](#) , [Shaela I. Jones](#) , [Kyle S. Hickmann](#) , [Charles N. Arge](#) , [Humberto C. Godinez-Vasquez](#) , [Carl J. Henney](#)

Space Weather [Volume18, Issue5](#) May 2020 e2020SW002464

<https://agupubs.onlinelibrary.wiley.com/doi/epdf/10.1029/2020SW002464>

The Wang-Sheeley-Arge (WSA) model estimates solar wind speed and interplanetary magnetic field polarity in the inner heliosphere using global photospheric magnetic field maps. WSA employs the Potential Field Source Surface (PFSS) and Schatten Current Sheet (SCS) models to determine the Sun's global coronal magnetic field. The PFSS and SCS models are connected through two radial parameters, the source surface and interface radii, which specify the overlap region between the inner SCS and outer PFSS models. Though both radii values are adjustable, they have typically been fixed to 2.5 solar radii. Our work highlights how solar wind predictions improve when the radii are allowed to vary over time. Data assimilation using particle filtering (sequential Monte Carlo) is used to infer optimal values over a fixed time window. Solar wind model predictions and satellite observations are compared with a newly developed quality-of-agreement prediction metric. The agreement metric between the model and observations is assumed to correspond to the probability of the two key WSA model parameters, the source surface and interface radii, where the highest metric value implies the optimal radii. We find that the optimal particle filter values of solar radii can perform twice as well as standard values for an exploratory period during Carrington Rotation 1901, with these values also reducing nonphysical kinking effects seen in solar magnetic field lines. Data assimilation choices of input realization and time frame have implications for variation in the solar wind over time. We present this work's theoretical context and practical applications for prediction accuracy.

## **Remeasurement of Solar Observing Optical Network sunspot areas**

P J [Meadows](#)

Monthly Notices of the Royal Astronomical Society, Volume 497, Issue 1, September 2020, Pages 1110–1114,

<https://doi.org/10.1093/mnras/staa2007>

The United States Air Force solar observing optical network (SOON) sunspot areas have been reported by several researchers over many years to be underestimated by as much as 50 per cent. Here, the areas of sunspots from scanned SOON disc drawings have been accurately remeasured for a period of two months from **2014 October and November** – this being near the peak of Solar Cycle 24 and which includes the largest sunspot group of that cycle. The remeasured sunspot areas are now comparable with areas in sunspot catalogues.

## Fast inversion of Zeeman line profiles using central moments

### II. Stokes V moments and determination of vector magnetic fields

P. Mein<sup>1</sup>, H. Uitenbroek<sup>2</sup>, N. Mein<sup>3</sup>, V. Bommier<sup>1</sup> and M. Faurobert<sup>4</sup>

A&A 591, A64 (2016)

Context. In the case of unresolved solar structures or stray light contamination, inversion techniques using four Stokes parameters of Zeeman profiles cannot disentangle the combined contributions of magnetic and nonmagnetic areas to the observed Stokes I.

Aims. In the framework of a two-component model atmosphere with filling factor  $f$ , we propose an inversion method restricting input data to Q, U, and V profiles, thus overcoming ambiguities from stray light and spatial mixing.

Methods. The V-moments inversion (VMI) method uses shifts  $SV$  derived from moments of V-profiles and integrals of  $Q_2$ ,  $U_2$ , and  $V_2$  to determine the strength  $B$  and inclination  $\psi$  of a magnetic field vector through least-squares polynomial fits and with very few iterations. Moment calculations are optimized to reduce data noise effects. To specify the model atmosphere of the magnetic component, an additional parameter  $\delta$ , deduced from the shape of V-profiles, is used to interpolate between expansions corresponding to two basic models.

Results. We perform inversions of HINODE SOT/SP data for inclination ranges  $0 < \psi < 60^\circ$  and  $120 < \psi < 180^\circ$  for the 630.2 nm Fe I line. A damping coefficient is fitted to take instrumental line broadening into account. We estimate errors from data noise. Magnetic field strengths and inclinations deduced from VMI inversion are compared with results from the inversion codes UNNOFIT and MERLIN.

Conclusions. The VMI inversion method is insensitive to the dependence of Stokes I profiles on the thermodynamic structure in nonmagnetic areas. In the range of  $Bf$  products larger than 200 G, mean field strengths exceed 1000 G and there is not a very significant departure from the UNNOFIT results because of differences between magnetic and nonmagnetic model atmospheres. Further improvements might include additional parameters deduced from the shape of Stokes V profiles and from large sets of 3D-MHD simulations, especially for unresolved magnetic flux tubes.

## Fast inversion of Zeeman line profiles using central moments

P. Mein<sup>1</sup>, H. Uitenbroek<sup>2</sup>, N. Mein<sup>1</sup>, V. Bommier<sup>1</sup> and M. Faurobert<sup>3</sup>

A&A 535, A45 (2011)

Context. Many inversion techniques derive vector magnetic fields and other parameters of the solar atmosphere from Stokes profiles with an iterative process.

Aims. We propose a new inversion method, using functions derived from central moments (ICM), to determine magnetic field vectors with very few iterations.

Methods. Two quantities  $A_1$  and  $A_2$  that combine moments of profiles  $I \pm S$  ( $S = Q, U, V$ ) are proposed. They are nearly linear functions of the longitudinal and transverse components of the magnetic field, and lead to estimates of the field components through a least-squares polynomial fit. A third quantity  $AD$  can be used to interpolate between expansions that correspond to two basic models. Exponents  $\beta_1$  and  $\beta_2$  in the moment expressions are adjusted to minimize the sensitivity to data noise.

Results. Inversion coefficients are computed for magnetic fields up to 3000 G in the case of the 630.2 Fe I line by forward modeling in two selected 1D model atmospheres (FALC and MALT<sub>M</sub>). After inversion of synthetic profiles computed with four models at disk center (FALA, FALC, FALF, MALT<sub>M</sub>), the mean standard deviations with respect to the input fields do not exceed 5 G for both components over the full range 0–3000 G. A comparison of ICM results with inversion by the UNNOFIT code of profiles observed with THEMIS/MTR shows good agreement. The typical computing time for a solar map of 100 000 points is less than 30 s.

Conclusions. The ICM inversions are almost insensitive to thermodynamic properties and solve for vector magnetic fields in a wide range of solar conditions, ranging from plage to spot, with very little computational effort. They are, therefore, extremely suitable for large data sets. Further improvements should take into account instrumental profiles and effects of limited spatial resolution by using filling factors. Extensions using more parameters and models with large departures from the Milne Eddington approximation could also be considered.

## Association Between Magnetic Pressure Difference and the Movement of Solar Pores

Merlin M. Mendoza & Chia-Hsien Lin

2023 ApJ 946 9

<https://iopscience.iop.org/article/10.3847/1538-4357/acbe43/pdf>

Solar pores are closely related to the concentration, dissipation, and transportation of solar magnetic flux. Their observable characteristics can provide constraints on models and simulations of magnetic flux emergence and formation. The specific property investigated in this study is their horizontal movement. The aim is to investigate whether the movement is correlated with any observable quantities. Our statistical analysis of 61 compact pores identified from the Spaceweather HMI Active Region Patches (SHARP) from 2011 to 2018 indicates that the

direction of movement is often either parallel or antiparallel to the direction of maximum magnetic pressure difference ( $dP_{\text{mag}}$ ) at the opposite sides of the edges of the pores. The correlation coefficients for both the parallel and antiparallel cases are higher than 0.74. Despite the high correlation, our analysis using the transfer entropy indicates no significant causal relationship between the direction of motion and the direction of maximum  $dP_{\text{mag}}$ .

2011-01-19, 2015-04-12

[HMI Science Nuggets](http://hmi.stanford.edu/hminuggets/?p=4129) # 193 2023 <http://hmi.stanford.edu/hminuggets/?p=4129>

## **Nonlinear Force-Free Modeling of Coronal Magnetic Fields.**

### **II. Modeling a Filament Arcade and Simulated Chromospheric and Photospheric Vector Fields**

Thomas R. [Metcalf](#) · Marc L. DeRosa · Carolus J. Schrijver · Graham Barnes · Adriaan A. van Ballegooijen · Thomas Wiegmann · Michael S. Wheatland · Gherardo Valori · James M. McTiernan  
*Solar Phys* (2008) 247: 269–299

## **Investigation of the Middle Corona with SWAP and a Data-Driven Non-Potential Coronal Magnetic Field Model**

[Karen A. Meyer](#), [Duncan H. Mackay](#), [Dana-Camelia Talpeanu](#), [Lisa A. Upton](#) & [Matthew J. West](#)  
*Solar Physics* volume 295, Article number: 101 (2020)

<https://link.springer.com/content/pdf/10.1007/s11207-020-01668-2.pdf>

The large field-of-view of the Sun Watcher using Active Pixel System detector and Image Processing (SWAP) instrument onboard the PROject for Onboard Autonomy 2 (PROBA2) spacecraft provides a unique opportunity to study extended coronal structures observed in the EUV in conjunction with global coronal magnetic field simulations. A global non-potential magnetic field model is used to simulate the evolution of the global corona from 1 September 2014 to 31 March 2015, driven by newly emerging bipolar active regions determined from Helioseismic and Magnetic Imager (HMI) magnetograms. We compare the large-scale structure of the simulated magnetic field with structures seen off-limb in SWAP EUV observations. In particular, we investigate how successful the model is in reproducing regions of closed and open structures, the scale of structures, and compare the evolution of a coronal fan observed over several rotations. The model is found to accurately reproduce observed large-scale, off-limb structures. When discrepancies do arise they mainly occur off the east solar limb due to active regions emerging on the far side of the Sun, which cannot be incorporated into the model until they are observed on the Earth-facing side. When such “late” active region emergences are incorporated into the model, we find that the simulated corona self-corrects within a few days, so that simulated structures off the west limb more closely match what is observed. Where the model is less successful, we consider how this may be addressed, through model developments or additional observational products. **11-15 October 2014, 27 October 2014, 4 November 2014, 8 November 2014, 24-28 November 2014, 6 December 2014, 20 December 2014, 1 January 2015, 7 January 2015, 15 January 2015**

## **MODELING THE SUN'S SMALL-SCALE GLOBAL PHOTOSPHERIC MAGNETIC FIELD**

K. A. [Meyer](#)<sup>1</sup> and D. H. Mackay

2016 *ApJ* 830 160

We present a new model for the Sun's global photospheric magnetic field during a deep minimum of activity, in which no active regions emerge. The emergence and subsequent evolution of small-scale magnetic features across the full solar surface is simulated, subject to the influence of a global supergranular flow pattern. Visually, the resulting simulated magnetograms reproduce the typical structure and scale observed in quiet Sun magnetograms. Quantitatively, the simulation quickly reaches a steady state, resulting in a mean field and flux distribution that are in good agreement with those determined from observations. A potential coronal magnetic field is extrapolated from the simulated full Sun magnetograms to consider the implications of such a quiet photospheric magnetic field on the corona and inner heliosphere. The bulk of the coronal magnetic field closes very low down, in short connections between small-scale features in the simulated magnetic network. Just 0.1% of the photospheric magnetic flux is found to be open at  $2.5 R_{\odot}$ , around 10–100 times less than that determined for typical Helioseismic and Magnetic Imager synoptic map observations. If such conditions were to exist on the Sun, this would lead to a significantly weaker interplanetary magnetic field than is currently observed, and hence a much higher cosmic ray flux at Earth.

## **THE STORAGE AND DISSIPATION OF MAGNETIC ENERGY IN THE QUIET SUN CORONA DETERMINED FROM SDO/HMI MAGNETOGRAMS**

K. A. [Meyer](#)<sup>1</sup>, J. Sabol<sup>1</sup>, D. H. Mackay<sup>1</sup>, and A. A. van Ballegooijen

2013 *ApJ* 770 L18

In recent years, higher cadence, higher resolution observations have revealed the quiet-Sun photosphere to be complex and rapidly evolving. Since magnetic fields anchored in the photosphere extend up into the solar corona, it

is expected that the small-scale coronal magnetic field exhibits similar complexity. For the first time, the quiet-Sun coronal magnetic field is continuously evolved through a series of non-potential, quasi-static equilibria, deduced from magnetograms observed by the Helioseismic and Magnetic Imager on board the Solar Dynamics Observatory, where the photospheric boundary condition which drives the coronal evolution exactly reproduces the observed magnetograms. The build-up, storage, and dissipation of magnetic energy within the simulations is studied. We find that the free magnetic energy built up and stored within the field is sufficient to explain small-scale, impulsive events such as nanoflares. On comparing with coronal images of the same region, the energy storage and dissipation visually reproduces many of the observed features. The results indicate that the complex small-scale magnetic evolution of a large number of magnetic features is a key element in explaining the nature of the solar corona.

### **Solar Magnetic Carpet I: Simulation of Synthetic Magnetograms**

K. A. [Meyer](#), D. H. Mackay, A. A. van Ballegooijen and C. E. Parnell  
Solar Physics, Volume 272, Number 1, 29-58, 2011

This paper describes a new 2D model for the photospheric evolution of the magnetic carpet. It is the first in a series of papers working towards constructing a realistic 3D non-potential model for the interaction of small-scale solar magnetic fields. In the model, the basic evolution of the magnetic elements is governed by a supergranular flow profile. In addition, magnetic elements may evolve through the processes of emergence, cancellation, coalescence and fragmentation. Model parameters for the emergence of bipoles are based upon the results of observational studies. Using this model, several simulations are considered, where the range of flux with which bipoles may emerge is varied. In all cases the model quickly reaches a steady state where the rates of emergence and cancellation balance. Analysis of the resulting magnetic field shows that we reproduce observed quantities such as the flux distribution, mean field, cancellation rates, photospheric recycle time and a magnetic network. As expected, the simulation matches observations more closely when a larger, and consequently more realistic, range of emerging flux values is allowed ( $4 \times 10^{16} - 10^{19}$  Mx). The model best reproduces the current observed properties of the magnetic carpet when we take the minimum absolute flux for emerging bipoles to be  $4 \times 10^{16}$  Mx. In future, this 2D model will be used as an evolving photospheric boundary condition for 3D non-potential modeling.

### **Light Bridges Can Suppress the Formation of Coronal Loops**

[Yuhu Miao](#), [Libo Fu](#), [Xian Du](#), [Ding Yuan](#), [Chaowei Jiang](#), [Jiangtao Su](#), [Mingyu Zhao](#), [Sergey Anfinogentov](#)

MNRAS 2021

<https://arxiv.org/pdf/2106.12833.pdf>

A light bridge is a magnetic intrusion into a sunspot, it interacts with the main magnetic field and excites a variety of dynamical processes. In the letter, we studied magnetic connectivity between a light bridge and coronal loops rooted at the sunspot. We used the data of the Atmospheric Imaging Assembly onboard the Solar Dynamics Observatory (SDO) to study the features of sunspots with light bridges. It is found that if a light bridge anchors at the umbra-penumbra boundary, the coronal loops could not be formed around the anchoring point. If the a light bridge become detached from the penumbra, the coronal loop starts to form again. The vector magnetogram provided by the Helioseismic Magnetic Imager onboard SDO shows that the anchoring region of a light bridge usually have an accompanying opposite minor-polarities. We conjugate that the magnetic field line could connect to these opposite polarities and form short-range magnetic loops, and therefore, coronal loops that extend to long-range could not be formed. A model of light bridge is proposed to explain the magnetic connectivity between a light bridge and the coronal loops. This model could explain many physical processes associated with light bridges. **6 October 2011, 29 July 2012, and 10 April 2019**

### **A Three-dimensional Babcock-Leighton Solar Dynamo Model**

Mark S. [Miesch](#) and Mausumi Dikpati

2014 ApJ 785 L8

We present a three-dimensional (3D) kinematic solar dynamo model in which poloidal field is generated by the emergence and dispersal of tilted sunspot pairs (more generally bipolar magnetic regions, or BMRs). The axisymmetric component of this model functions similarly to previous 2.5 dimensional (2.5D, axisymmetric) Babcock-Leighton (BL) dynamo models that employ a double-ring prescription for poloidal field generation but we generalize this prescription into a 3D flux emergence algorithm that places BMRs on the surface in response to the dynamo-generated toroidal field. In this way, the model can be regarded as a unification of BL dynamo models (2.5D in radius/latitude) and surface flux transport models (2.5D in latitude/longitude) into a more self-consistent framework that builds on the successes of each while capturing the full 3D structure of the evolving magnetic field. The model reproduces some basic features of the solar cycle including an 11 yr periodicity, equatorward migration of toroidal flux in the deep convection zone, and poleward propagation of poloidal flux at the surface. The poleward-propagating surface flux originates as trailing flux in BMRs, migrates poleward in multiple non-axisymmetric streams (made axisymmetric by differential rotation and turbulent diffusion), and eventually reverses

the polar field, thus sustaining the dynamo. In this Letter we briefly describe the model, initial results, and future plans.

### **Some properties of latitude-time evolution of local and background solar magnetic fields**

E.V. **Miletsky**, V.G. Ivanov, Yu.A. Nagovitsyn

Advances in Space Research, Volume 55, Issue 3, 1 February 2015, Pages 780–786

<http://www.sciencedirect.com/science/article/pii/S0273117714002828>

A comparative analysis of evolution of latitude distributions of solar magnetic fields of various scales is presented. Using the local photospheric magnetic fields (LMF) represented by the magnetic fields of sunspots for cycles 12–23 it is found that the width of the sunspot generating zone is closely related to the magnitude of the total magnetic flux of sunspots. It is demonstrated that latitude-time distributions of the LMF and absolute strengths of the background magnetic field (BMF) in the latitude range  $\pm 40^\circ \pm 40^\circ$  are very similar and the time variations of power indices of the BMF and LMF are highly correlated. It is found that power characteristics of the BMF and LMF in cycles 21–23 are in close relation to the size of the low-latitude zone of solar activity. It is shown that the speed of the polar drift of the BMF of a given polarity tends to increase in epochs of solar cycle maximums.

The obtained regularities can be used as diagnostic criteria for determination of adequate physical models of solar cyclicity.

### **Radial Distribution of Compressive Waves in the Solar Corona Revealed by Akatsuki Radio Occultation Observations**

Mayu **Miyamoto**, Takeshi Imamura, Munetoshi Tokumaru, Hiroki Ando, Hiroaki Isobe, Ayumi Asai, Daikou Shiota, Tomoaki Toda, Bernd H<sup>?</sup>usler, Martin P<sup>?</sup>tzold, Alexander Nabatov, and Masato Nakamura

2014 *ApJ* 797 51

Radial variations of the amplitude and the energy flux of compressive waves in the solar corona were explored for the first time using a spacecraft radio occultation technique. By applying wavelet analysis to the frequency time series taken at heliocentric distances of 1.5–20.5 Rs (solar radii), quasi-periodic density disturbances were detected at almost all distances. The period ranges from 100 to 2000 s. The amplitude of the fractional density fluctuation increases with distance and reaches ~30% around 5 Rs, implying that nonlinearity of the wave field is potentially important. We further estimate the wave energy flux on the assumption that the observed periodical fluctuations are manifestations of acoustic waves. The energy flux increases with distance below ~6 Rs and seems to saturate above this height, suggesting that the acoustic waves do not propagate from the low corona but are generated in the extended corona, probably through nonlinear dissipation of Alfvén waves. The compressive waves should eventually dissipate through shock generation to heat the corona.

### **Coronal Magnetic Fields Derived from Simultaneous Microwave and EUV Observations and Comparison with the Potential Field Model**

Shun **Miyawaki**, Kazumasa Iwai, Kiyoto Shibasaki, Daikou Shiota, Satoshi Nozawa

*ApJ* 2015

<http://arxiv.org/pdf/1512.04198v1.pdf>

We estimated the accuracy of coronal magnetic fields derived from radio observations by comparing them to potential field calculations and the DEM measurements using EUV observations. We derived line of sight component of the coronal magnetic field from polarization observations of the thermal bremsstrahlung in the NOAA active region 11150, observed around 3:00 UT on **February 3, 2011** using the Nobeyama Radioheliograph at 17 GHz. Because the thermal bremsstrahlung intensity at 17 GHz includes both chromospheric and coronal components, we extracted only the coronal component by measuring the coronal emission measure in EUV observations. In addition, we derived only the radio polarization component of the corona by selecting the region of coronal loops and weak magnetic field strength in the chromosphere along the line of sight. The upper limit of the coronal longitudinal magnetic fields were determined as 100 - 210 G. We also calculated the coronal longitudinal magnetic fields from the potential field extrapolation using the photospheric magnetic field obtained from the Helioseismic and Magnetic Imager (HMI). However, the calculated potential fields were certainly smaller than the observed coronal longitudinal magnetic field. This discrepancy between the potential and the observed magnetic field strengths can be explained consistently by two reasons; (a) the underestimation of the coronal emission measure resulting from the limitation of the temperature range of the EUV observations, (b) the underestimation of the coronal magnetic field resulting from the potential field assumption.



## A Magnetohydrodynamic Relaxation Method for Non-Force-Free Magnetic Field in Magnetohydrostatic Equilibrium

Takahiro [Miyoshi](#), [Kanya Kusano](#), [Satoshi Inoue](#)

The Astrophysical Journal Supplement Series, 247:6 2020

DOI: 10.3847/1538-4365/ab64f2

<https://iopscience.iop.org/article/10.3847/1538-4365/ab64f2>

<https://arxiv.org/pdf/1912.10626.pdf>

A nonlinear force-free field (NLFFF) extrapolation is widely used to reconstruct the three-dimensional magnetic field in the solar corona from the observed photospheric magnetic field. However, the pressure gradient and gravitational forces are ignored in the NLFFF model, even though the photospheric and chromospheric magnetic fields are not in general force-free. Here we develop a magnetohydrodynamic (MHD) relaxation method that reconstructs the solar atmospheric (chromospheric and coronal) magnetic field as a non-force-free magnetic field (NFFF) in magnetohydrostatic equilibrium where the Lorentz, pressure gradient, and gravitational forces are balanced. The system of basic equations for the MHD relaxation method is derived, and mathematical properties of the system are investigated. A robust numerical solver for the system is constructed based on the modern high-order shock capturing scheme. Two-dimensional numerical experiments that include the pressure gradient and gravitational forces are also demonstrated.

See Nuggets No. 27

[https://www.pstep.jp/news\\_en/20200304.html](https://www.pstep.jp/news_en/20200304.html)

## Image patch analysis of sunspots and active regions

### II. Clustering via matrix factorization

Kevin R. [Moon](#)<sup>1\*</sup>, Véronique Delouille<sup>2</sup>, Jimmy J. Li<sup>1</sup>, Ruben De Visscher<sup>2</sup>, Fraser Watson<sup>3</sup> and Alfred O. Hero

J. Space Weather Space Clim., 6, A3 (2016)

**Open Access**

<http://www.swsc-journal.org/articles/swsc/pdf/2016/01/swsc150030.pdf>

<http://arxiv.org/pdf/1504.02762v1.pdf>

**Context.** Separating active regions that are quiet from potentially eruptive ones is a key issue in Space Weather applications. Traditional classification schemes such as Mount Wilson and McIntosh have been effective in relating an active region large scale magnetic configuration to its ability to produce eruptive events. However, their qualitative nature prevents systematic studies of an active region's evolution for example.

**Aims.** We introduce a new clustering of active regions that is based on the local geometry observed in Line of Sight magnetogram and continuum images.

**Methods.** We use a reduced-dimension representation of an active region that is obtained by factoring the corresponding data matrix comprised of local image patches. Two factorizations can be compared via the definition of appropriate metrics on the resulting factors. The distances obtained from these metrics are then used to cluster the active regions.

**Results.** We find that these metrics result in natural clusterings of active regions. The clusterings are related to large scale descriptors of an active region such as its size, its local magnetic field distribution, and its complexity as measured by the Mount Wilson classification scheme. We also find that including data focused on the neutral line of an active region can result in an increased correspondence between our clustering results and other active region descriptors such as the Mount Wilson classifications and the R-value.

**Conclusions.** Matrix factorization of image patches is a promising new way of characterizing active regions. We provide some recommendations for which metrics, matrix factorization techniques, and regions of interest to use to study active regions.

## Image patch analysis of sunspots and active regions

### I. Intrinsic dimension and correlation analysis

Kevin R. [Moon](#)<sup>1\*</sup>, Jimmy J. Li<sup>1</sup>, Véronique Delouille<sup>2</sup>, Ruben De Visscher<sup>2</sup>, Fraser Watson<sup>3</sup> and Alfred O. Hero

J. Space Weather Space Clim., 6, A2 (2016)

**Open Access**

<http://www.swsc-journal.org/articles/swsc/pdf/2016/01/swsc150023.pdf>

<http://arxiv.org/pdf/1503.04127v1.pdf>

**Context.** The flare productivity of an active region is observed to be related to its spatial complexity. Mount Wilson or McIntosh sunspot classifications measure such complexity but in a categorical way, and may therefore not use all the information present in the observations. Moreover, such categorical schemes hinder a systematic study of an active region's evolution for example.

**Aims.** We propose fine-scale quantitative descriptors for an active region's complexity and relate them to the Mount Wilson classification. We analyze the local correlation structure within continuum and magnetogram data, as well as the cross-correlation between continuum and magnetogram data.

Methods. We compute the intrinsic dimension, partial correlation, and canonical correlation analysis (CCA) of image patches of continuum and magnetogram active region images taken from the SOHO-MDI instrument. We use masks of sunspots derived from continuum as well as larger masks of magnetic active regions derived from magnetogram to analyze separately the core part of an active region from its surrounding part.

Results. We find relationships between the complexity of an active region as measured by its Mount Wilson classification and the intrinsic dimension of its image patches. Partial correlation patterns exhibit approximately a third-order Markov structure. CCA reveals different patterns of correlation between continuum and magnetogram within the sunspots and in the region surrounding the sunspots.

Conclusions. Intrinsic dimension has the potential to distinguish simple from complex active regions. These results also pave the way for patch-based dictionary learning with a view toward automatic clustering of active regions.

## **Image patch analysis and clustering of sunspots: a dimensionality reduction approach**

Kevin R. **Moon**, Jimmy J. Li, Veronique Delouille, Fraser Watson, Alfred O. Hero III

ICIP 2014

<http://arxiv.org/pdf/1406.6390v1.pdf>

Sunspots, as seen in white light or continuum images, are associated with regions of high magnetic activity on the Sun, visible on magnetogram images. Their complexity is correlated with explosive solar activity and so classifying these active regions is useful for predicting future solar activity. Current classification of sunspot groups is visually based and suffers from bias. Supervised learning methods can reduce human bias but fail to optimally capitalize on the information present in sunspot images. This paper uses two image modalities (continuum and magnetogram) to characterize the spatial and modal interactions of sunspot and magnetic active region images and presents a new approach to cluster the images. Specifically, in the framework of image patch analysis, we estimate the number of intrinsic parameters required to describe the spatial and modal dependencies, the correlation between the two modalities and the corresponding spatial patterns, and examine the phenomena at different scales within the images. To do this, we use linear and nonlinear intrinsic dimension estimators, canonical correlation analysis, and multiresolution analysis of intrinsic dimension.

## **Bipolar Ephemeral Active Regions, Magnetic Flux Cancellation, and Solar Magnetic Explosions**

Ronald L. **Moore**<sup>1,2</sup>, Navdeep K. Panesar<sup>3,4</sup>, Alphonse C. Sterling<sup>2</sup>, and Sanjiv K. Tiwari<sup>3,4</sup>

2022 ApJ 933 12

<https://iopscience.iop.org/article/10.3847/1538-4357/ac6181/pdf>

We examine the cradle-to-grave magnetic evolution of 10 bipolar ephemeral active regions (BEARs) in solar coronal holes, especially aspects of the magnetic evolution leading to each of 43 obvious microflare events. The data are from the Solar Dynamics Observatory: 211 Å coronal EUV images and line-of-sight photospheric magnetograms. We find evidence that (1) each microflare event is a magnetic explosion that results in a miniature flare arcade astride the polarity inversion line (PIL) of the explosive lobe of the BEAR's anemone magnetic field; (2) relative to the BEAR's emerged flux-rope  $\Omega$  loop, the anemone's explosive lobe can be an inside lobe, an outside lobe, or an inside-and-outside lobe; (3) 5 events are confined explosions, 20 events are mostly confined explosions, and 18 events are blowout explosions, which are miniatures of the magnetic explosions that make coronal mass ejections (CMEs); (4) contrary to the expectation of Moore et al., none of the 18 blowout events explode from inside the BEAR's  $\Omega$  loop during the  $\Omega$  loop's emergence; and (5) before and during each of the 43 microflare events, there is magnetic flux cancellation at the PIL of the anemone's explosive lobe. From finding evident flux cancellation at the underlying PIL before and during all 43 microflare events—together with BEARs evidently being miniatures of all larger solar bipolar active regions—we expect that in essentially the same way, flux cancellation in sunspot active regions prepares and triggers the magnetic explosions for many major flares and CMEs. **2012 04/09, 2012 06/30, 2012 July 1, 2012 08/13, 2013 01/31, 2013 02/05, 2013 02/13, 2013 02/27, 2013 03/01, 2013 05/02, 2014 02/23**

**Table 1** 10 Coronal-hole Cradle-to-grave Bipolar Ephemeral Active Regions (BEARs) and Their 43 Microflare Events 2012-2014

## **SOLAR X-RAY JETS, TYPE-II SPICULES, GRANULE-SIZE EMERGING BIPOLES, AND THE GENESIS OF THE HELIOSPHERE**

Ronald L. **Moore**<sup>1</sup>, Alphonse C. Sterling<sup>1</sup>, Jonathan W. Cirtain<sup>1</sup> and David A. Falconer

2011 ApJ 731 L18

From Hinode observations of solar X-ray jets, Type-II spicules, and granule-size emerging bipolar magnetic fields in quiet regions and coronal holes, we advocate a scenario for powering coronal heating and the solar wind. In this scenario, Type-II spicules and Alfvén waves are generated by the granule-size emerging bipoles (EBs) in the manner of the generation of X-ray jets by larger magnetic bipoles. From observations and this scenario, we estimate that Type-II spicules and their co-generated Alfvén waves carry into the corona an area-average flux of mechanical energy of  $\sim 7 \times 10^5$  erg cm<sup>-2</sup> s<sup>-1</sup>. This is enough to power the corona and solar wind in quiet regions and coronal

holes, and therefore indicates that the granule-size EBs are the main engines that generate and sustain the entire heliosphere.

### **Magnetic helicity and eruptivity in active region 12673**

K. [Moraitis](#), [X. Sun](#), [E. Pariat](#), [L. Linan](#)

A&A 628, A50 2019

<https://arxiv.org/abs/1907.06365>

<https://www.aanda.org/articles/aa/pdf/2019/08/aa35870-19.pdf>

Context. In **September 2017** the largest X-class flare of Solar Cycle 24 occurred from the most active region (AR) of this cycle, AR 12673. The AR attracted much interest because of its unique morphological and evolution characteristics. Among the parameters examined in the AR was magnetic helicity, but either only approximately, and/or intermittently. Aims. This work is interested in studying the evolution of the relative magnetic helicity and of the two components of its decomposition, the non-potential, and the volume-threading one, in the time interval around the highest activity of AR 12673. Special emphasis is given on the study of the ratio of the non-potential to total helicity, that was recently proposed as an indicator of ARs eruptivity. Methods. For these, we first approximate the coronal magnetic field of the AR with two different optimization-based extrapolation procedures, and choose the one that produces the most reliable helicity value at each instant. Moreover, in one of these methods, we weight the optimization by the uncertainty estimates derived from the Helioseismic and Magnetic Imager (HMI) instrument, for the first time. We then follow an accurate method to compute all quantities of interest. Results. The first observational determination of the evolution of the non-potential to total helicity ratio seems to confirm the quality it has in indicating eruptivity. This ratio increases before the major flares of AR 12673, and afterwards it relaxes to smaller values. Additionally, the evolution patterns of the various helicity, and energy budgets of AR 12673 are discussed and compared with other works. **6 Sept 2017**

### **Relative magnetic field line helicity**

K. [Moraitis](#), [E. Pariat](#), [G. Valori](#), [K. Dalmasse](#)

A&A 624, A51 2019

<https://arxiv.org/pdf/1902.10410.pdf>

Context. Magnetic helicity is an important quantity in studies of magnetized plasmas as it provides a measure of the geometrical complexity of the magnetic field in a given volume. A more detailed description of the spatial distribution of magnetic helicity is given by the field line helicity that expresses the amount of helicity associated to individual field lines, rather than in the full analysed volume. Aims. Magnetic helicity is not a gauge-invariant quantity in general, unless it is computed with respect to a reference field, yielding the so called relative magnetic helicity. The field line helicity corresponding to the relative magnetic helicity has only been examined under specific conditions so far. This work aims to define the field line helicity corresponding to relative magnetic helicity in the most general way. In addition to its general form, we provide the expression for the relative magnetic field line helicity in a few commonly used gauges, and reproduce known results as a limit of our general formulation. Methods. By starting from the definition of relative magnetic helicity, we derive the corresponding field line helicity, and we note the assumptions it is based on. Results. We check that the developed quantity reproduces relative magnetic helicity by using three different numerical simulations. For these cases we also show the morphology of field line helicity in the volume, and on the photospheric plane. As an application to solar situations, we compare the morphology of field line helicity on the photosphere with that of the connectivity-based helicity flux density in two reconstructions of an active region's magnetic field. We discuss how the derived relative magnetic field line helicity has a wide range of applications, notably in solar physics and magnetic reconnection studies.

### **Computation of Relative Magnetic Helicity in Spherical Coordinates**

K. [Moraitis](#), [É. Pariat](#), [A. Savcheva](#), [G. Valori](#)

Solar Phys. 2018

<https://arxiv.org/pdf/1806.03011.pdf>

Magnetic helicity is a quantity of great importance in solar studies because it is conserved in ideal magneto-hydrodynamics. While many methods to compute magnetic helicity in Cartesian finite volumes exist, in spherical coordinates, the natural coordinate system for solar applications, helicity is only treated approximately. We present here a method to properly compute relative magnetic helicity in spherical geometry. The volumes considered are finite, of shell or wedge shape, and the three-dimensional magnetic field is considered fully known throughout the studied domain. Testing of the method with well-known, semi-analytic, force-free magnetic-field models reveals that it has excellent accuracy. Further application to a set of nonlinear force-free reconstructions of the magnetic field of solar active regions, and comparison with an approximate method used in the past, indicates that the proposed methodology can be significantly more accurate, thus making our method a promising tool in helicity studies that employ the spherical geometry. Additionally, the range of applicability of the approximate method is determined and discussed.

## Validation and Benchmarking of a Practical Free Magnetic Energy and Relative Magnetic Helicity Budget Calculation in Solar Magnetic Structures

K. [Moraitis](#), K. Tziotziou, M.K. Georgoulis, V. Archontis

Solar Phys., 2014

<http://arxiv.org/pdf/1406.5381v1.pdf>

In earlier works we introduced and tested a nonlinear force-free (NLFF) method designed to self-consistently calculate the free magnetic energy and the relative magnetic helicity budgets of the corona of observed solar magnetic structures. The method requires, in principle, only a single, photospheric or low-chromospheric, vector magnetogram of a quiet-Sun patch or an active region and performs calculations in the absence of three-dimensional magnetic and velocity-field information. In this work we strictly validate this method using three-dimensional coronal magnetic fields. Benchmarking employs both synthetic, three-dimensional magnetohydrodynamic simulations and nonlinear force-free field extrapolations of the active-region solar corona. We find that our time-efficient NLFF method provides budgets that differ from those of more demanding semi-analytical methods by a factor of  $\sim 3$ , at most. This difference is expected from the physical concept and the construction of the method. Temporal correlations show more discrepancies that, however, are soundly improved for more complex, massive active regions, reaching correlation coefficients of the order of, or exceeding, 0.9. In conclusion, we argue that our NLFF method can be reliably used for a routine and fast calculation of free magnetic energy and relative magnetic helicity budgets in targeted parts of the solar magnetized corona. As explained here and in previous works, this is an asset that can lead to valuable insight into the physics and the triggering of solar eruptions.

## Long-Term Evolution of the Sun's magnetic field during Cycles 15--19 based on their proxies from Kodaikanal Solar Observatory

[Alexander V. Mordvinov](#), [Bidya Binay Karak](#), [Dipankar Banerjee](#), [Subhamoy Chatterjee](#), [Elena M. Golubeva](#), [Anna I. Khlystova](#)

ApJL 2020

<https://arxiv.org/pdf/2009.11174.pdf>

The regular observation of the solar magnetic field is available only for about last five cycles. Thus, to understand the origin of the variation of the solar magnetic field, it is essential to reconstruct the magnetic field for the past cycles, utilizing other datasets. Long-term uniform observations for the past 100 years as recorded at the Kodaikanal Solar Observatory (KoSO) provide such opportunity. We develop a method for the reconstruction of the solar magnetic field using the synoptic observations of the Sun's emission in the Ca II K and H $\alpha$  lines from KoSO for the first time. The reconstruction method is based on the facts that the Ca II K intensity correlates well with the unsigned magnetic flux, while the sign of the flux is derived from the corresponding H $\alpha$  map which provides the information of the dominant polarities. Based on this reconstructed magnetic map, we study the evolution of the magnetic field in Cycles 15--19. We also study bipolar magnetic regions (BMRs) and their remnant flux surges in their causal relation. Time-latitude analysis of the reconstructed magnetic flux provides an overall view of magnetic field evolution: emergent magnetic flux, its further transformations with the formation of unipolar magnetic regions (UMRs) and remnant flux surges. We identify the reversals of the polar field and critical surges of following and leading polarities. We found that the poleward transport of opposite polarities led to multiple changes of the dominant magnetic polarities in poles. Furthermore, the remnant flux surges that occur between adjacent 11-year cycles reveal physical connections between them.

## The reversal of the Sun's magnetic field in cycle 24

Alexander V. [Mordvinov](#), Alexei A. Pevtsov, Luca Bertello, Gordon J.D. Petrie

JASTP 2016

<http://arxiv.org/pdf/1602.02460v1.pdf>

Analysis of synoptic data from the Vector Stokes Magnetograph (VSM) of the Synoptic Optical Long-term Investigations of the Sun (SOLIS) and the NASA/NSO Spectromagnetograph (SPM) at the NSO/Kitt Peak Vacuum Telescope facility shows that the reversals of solar polar magnetic fields exhibit elements of a stochastic process, which may include the development of specific patterns of emerging magnetic flux, and the asymmetry in activity between northern and southern hemispheres. The presence of such irregularities makes the modeling and prediction of polar field reversals extremely hard if possible. In a classical model of solar activity cycle, the unipolar magnetic regions (UMRs) of predominantly following polarity fields are transported polewards due to meridional flows and diffusion. The UMRs gradually cancel out the polar magnetic field of the previous cycle, and re-build the polar field of opposite polarity setting the stage for the next cycle. We show, however, that this deterministic picture can be easily altered by the developing of a strong center of activity, or by the emergence of an extremely large active region, or by a "strategically placed" coronal hole. We demonstrate that the activity occurring during the current cycle 24 may be the result of this randomness in the evolution of the solar surface magnetic field. 2010/07/20-30

## Large-Scale Magnetic Field of the Sun and Evolution of Sunspot Activity

A. V. **Mordvinov**, V. M. Grigoryev, V. S. Peshcherov

Solar Physics, October **2012**, Volume 280, Issue 2, pp 379-387

The evolution of the large-scale magnetic field of the Sun has been studied using an algorithm of tomographic inversion. By analyzing line-of-sight magnetograms, we mapped the radial and toroidal components of the Sun's large-scale magnetic field. The evolution of the radial and toroidal magnetic field components in the 11-year solar cycle has been studied in a time–latitude aspect. It is shown that the toroidal magnetic field of the Sun is causally related to sunspot activity; i.e., the sunspot formation zones drift in latitude and follow the toroidal magnetic fields. The results of our analysis support the idea that the high-latitude toroidal magnetic fields can serve as precursors of sunspot activity. The toroidal fields in the current cycle are anomalously weak and also show a barely noticeable equatorward drift. This behavior of the toroidal magnetic field suggests low activity levels in the current cycle and in the foreseeable future.

## Small-scale Magnetic Flux Emergence in the Quiet Sun

F. **Moreno-Insertis**<sup>1,2</sup>, J. Martinez-Sykora<sup>3,4</sup>, V. H. Hansteen<sup>5,3</sup>, and D. Muñoz<sup>6</sup>

**2018** ApJL 859 L26

<https://arxiv.org/pdf/1806.00489.pdf>

Small bipolar magnetic features are observed to appear in the interior of individual granules in the quiet Sun, signaling the emergence of tiny magnetic loops from the solar interior. We study the origin of those features as part of the magnetoconvection process in the top layers of the convection zone. Two quiet-Sun magnetoconvection models, calculated with the radiation-magnetohydrodynamic (MHD) Bifrost code and with domain stretching from the top layers of the convection zone to the corona, are analyzed. Using 3D visualization as well as a posteriori spectral synthesis of Stokes parameters, we detect the repeated emergence of small magnetic elements in the interior of granules, as in the observations. Additionally, we identify the formation of organized horizontal magnetic sheets covering whole granules. Our approach is twofold, calculating statistical properties of the system, like joint probability density functions (JPDFs), and pursuing individual events via visualization tools. We conclude that the small magnetic loops surfacing within individual granules in the observations may originate from sites at or near the downflows in the granular and mesogranular levels, probably in the first 1 or 1.5 Mm below the surface. We also document the creation of granule-covering magnetic sheet-like structures through the sideways expansion of a small subphotospheric magnetic concentration picked up and pulled out of the interior by a nascent granule. The sheet-like structures that we found in the models may match the recent observations of Centeno et al.

## Measuring the Compactness of Active Regions”,

Kelvin H. **Moresi**<sup>1</sup>, Sung-Hong Park<sup>2</sup>, Aimee A. Norton<sup>2</sup>

**HMI Science Nuggets** №184 Aug **2022**

<http://hmi.stanford.edu/hminuggets/?p=3968>

Here we develop a simple but practical way of measuring the compactness of ARs and apply the developed method to a set of  $\beta$ - and  $\delta$ -spots to examine their difference in compactness and to find any relations of compactness with AR magnetic properties.

## Tracing the Magnetic Field Topology of the Quiet Corona Using Propagating Disturbances

Huw **Morgan**<sup>1</sup> and Marianna B. Korsós<sup>1</sup>

**2022** ApJL 933 L27

<https://iopscience.iop.org/article/10.3847/2041-8213/ac7b7e/pdf>

The motion of faint propagating disturbances (PDs) in the solar corona reveals an intricate structure that must be defined by the magnetic field. Applied to quiet Sun observations by the Atmospheric Imaging Assembly (AIA)/Solar Dynamics Observatory (SDO), a novel method reveals a cellular network, with cells of typical diameters 50" in the cool 304 Å channel and 100" in the coronal 193 Å channel. The 193 Å cells can overlie several 304 Å cells, although both channels share common source and sink regions. The sources are points, or narrow corridors, of divergence that occupy the centers of cells. They are significantly aligned with photospheric network features and enhanced magnetic elements. This shows that the bright network is important to the production of PDs and confirms that the network is host to the source footpoint of quiet coronal loops. The other footpoint, or the sinks of the PDs, form the boundaries of the coronal cells. These are not significantly aligned with the photospheric network—they are generally situated above the dark internetwork photosphere. They form compact points or corridors, often without an obvious signature in the underlying photosphere. We argue that these sink points can either be concentrations of closed field footpoints associated with minor magnetic elements in the internetwork or concentrations of an upward-aligned open field. The link between the coronal velocity and magnetic fields is strengthened by comparison with a magnetic extrapolation, which shows several general and specific similarities, thus the velocity maps offer a valuable additional constraint on models. **2018 October 27**

## **An Atlas of Coronal Electron Density at 5R $\odot$ . II. A Spherical Harmonic Method for Density Reconstruction**

Huw [Morgan](#)

2019 ApJS 242 3

<https://iopscience.iop.org/article/10.3847/1538-4365/ab125d/pdf>

<https://arxiv.org/pdf/1908.07866.pdf>

This is the second of a series of three papers that present a methodology with the aim of creating a set of maps of the coronal density over a period of many years. This paper describes a method for reconstructing the coronal electron density based on spherical harmonics. By assuming a radial structure to the corona at the height of interest, line-of-sight integrations can be made individually on each harmonic basis prior to determining coefficients, i.e., the computationally expensive integrations are calculated only once during initialization. This approach reduces the problem to finding the set of coefficients that best match the observed brightness using a regularized least-squares approach and is very efficient. The method is demonstrated on synthetic data created from both a simple and an intricate coronal density model. The quality of reconstruction is found to be reasonable in the presence of noise and large gaps in the data. The method is applied to both Large Angle and Spectrometric Coronagraph Experiment C2 and SolarTerrestrial Relations Observatory Cor2 coronagraph observations from 2009 March 20, and the results from both spacecraft compared. Future work will apply the method to large data sets.

## **LONGITUDINAL DRIFTS OF STREAMERS ACROSS THE HELIOSPHERIC CURRENT SHEET**

Huw [Morgan](#)

2011 ApJ 738 190

Potential field source surface (PFSS) extrapolations of the photospheric magnetic field provide a qualitatively correct model of the coronal magnetic structure. We show that the magnetic structure provided by PFSS describes a framework within which high-density coronal streamers are distributed. However, the density structures have considerable freedom to drift longitudinally along the magnetic structure. Some caution must therefore be taken when using PFSS models as proxies for the coronal density structure. In particular, while measurements of coronal rotation using PFSS models provide an estimate of the large-scale magnetic structure rotation, they are not valid measurements of the density rotation. Furthermore, attempts to assign a consistent rate of rotation to the electron corona over long time periods are not always valid since the movement is dominated by structural reconfiguration. These conclusions are reached by the application of solar rotational tomography to LASCO C2/Solar and Heliospheric Observatory observations during solar minimum (1996-1997), revealing the changing density structure of the equatorial streamer belt at a height of 4 R .

## **THE ROTATION OF THE WHITE LIGHT SOLAR CORONA AT HEIGHT 4 R FROM 1996 TO 2010: A TOMOGRAPHICAL STUDY OF LARGE ANGLE AND SPECTROMETRIC CORONAGRAPH C2 OBSERVATIONS**

Huw [Morgan](#)

2011 ApJ 738 189

Solar rotational tomography is applied to Large Angle and Spectrometric Coronagraph (LASCO) C2/Solar and Heliospheric Observatory (SOHO) observations covering the period 1996-2010, resulting in a set of electron density maps at a height of 4 R from which rotation rates can be calculated. Large variation of rotation rates is measured. Rates are dominated by the Carrington rotation rate (14.18 deg d<sup>-1</sup> sidereal), but at times over the solar cycle, rates are measured between -3 and 3 deg d<sup>-1</sup> relative to the Carrington rotation rate. Rotation rates can vary considerably between latitudes, even between neighboring latitudes. They can remain relatively stable or change smoothly over long periods of times, or can change rather abruptly. There are periods for certain latitudes (for example, the equator at solar maximum) when the movement is dominated by rapid structural reconfiguration, not a coherent rotation. These results raise new questions regarding the link between the Sun and the corona, and provide fresh challenges to interpretations of the coronal structural evolution and the development of large-scale coronal models. In particular, can interchange reconnection provide an explanation of the considerable latitudinal differences in rotation rates, and what mechanism can explain abrupt changes in rotation rates?

## **Observational Aspects of the Three-dimensional Coronal Structure Over a Solar Activity Cycle**

Huw [Morgan](#) and Shadia Rifai Habbal

2010 ApJ 710 1-15

Solar rotational tomography is applied to almost eleven years of Large Angle Spectrometric Coronagraph C2/*Solar and Heliospheric Observatory* data, revealing for the first time the behavior of the large-scale coronal density structures, also known as streamers, over almost a full solar activity cycle. This study gives an overview of the main results of this project. (1) Streamers are most often shaped as extended, narrow plasma sheets. The sheets can be

extremely narrow at times ( $\leq 0.14 \times 10^6$  km at  $4 R_{\odot}$ ). This is over twice their heliocentric angular thickness at 1 AU. (2) At most times outside the height of solar maximum, there are two separate stable large helmet streamer belts extending from mid-latitudes (in both north and south). At solar minimum, the streamers converge and join near the equator, giving the impression of a single large helmet streamer. Outside of solar minimum, the two streamers do not join, forming separate high-density sheets in the extended corona (one in the north, another in the south). At solar maximum, streamers rise radially from their source regions, while during the ascending and descending activity phases, streamers are skewed toward the equator. (3) For most of the activity cycle, streamers share the same latitudinal extent as filaments on the disk, showing that large-scale stable streamers are closely linked to the same large-scale photospheric magnetic configuration, which give rise to large filaments. (4) The poleward footpoints of the streamers are often above crown polar filaments and the equatorial footpoints are above filaments or active regions (or above the photospheric neutral lines which underlie these structures). The high-density structures arising from the equatorial active regions either rise and form the equatorial footpoints of mid-latitude quiescent streamers, or form unstable streamers at the equator, not connected to the quiescent streamer structure at higher latitude (so there are often three streamer sheets sharing the same extended longitudinal region). (5) Comparison between the tomography results and a potential field source surface model shows that streamers are not necessarily associated with a magnetic polarity reversal, but rather are regions containing field lines arising from widely separated sources at the Sun. We call these convergence sheets. (6) There is considerable differential rotation of streamers at high latitudes, which makes comparison between disk and coronal structure complicated. The presence of differential rotation has implications for many areas of coronal and heliospheric research.

### **Exploring Coronal Dynamics: A Next Generation Solar Physics Mission white paper**

R. J. [Morton](#), E. Scullion, D. S. Bloomfield, J. A. McLaughlin, S. Regnier, S. W. McIntosh, S. Tomczyk, P. Young

2016

<https://arxiv.org/pdf/1611.06149v1.pdf>

Determining the mechanisms responsible for the heating of the coronal plasma and maintaining and accelerating the solar wind are long standing goals in solar physics. There is a clear need to constrain the energy, mass and momentum flux through the solar corona and advance our knowledge of the physical process contributing to these fluxes. Furthermore, the accurate forecasting of Space Weather conditions at the near-Earth environment and, more generally, the plasma conditions of the solar wind throughout the heliosphere, require detailed knowledge of these fluxes in the near-Sun corona. Here we present a short case for a space-based imaging-spectrometer coronagraph, which will have the ability to provide synoptic information on the coronal environment and provide strict constraints on the mass, energy, and momentum flux through the corona. The instrument would ideally achieve cadences of  $\sim 10$ -s, spatial resolution of 1" and observe the corona out to  $2-3 R_{\odot}$ . Such an instrument will enable significant progress in our understanding of MHD waves throughout complex plasmas, as well as potentially providing routine data products to aid Space Weather forecasting.

### **Estimating the coronal and chromospheric magnetic fields of solar active regions as observed with the Nobeyama Radioheliograph Compared with the Extrapolated Linear Force-Free Field**

A. [Mouner](#), [Abdelrazek M. K. Shaltout](#), [M. M. Beheary](#), [K.A.K. Gadallah](#), [K. A. Edris](#)

2018

<https://arxiv.org/ftp/arxiv/papers/1802/1802.04598.pdf>

Adopting the thermal free-free emission mechanism, the coronal and chromospheric magnetic fields are derived from the polarization and spectral observations with the Nobeyama Radioheliograph at 1.76 cm. The solar active regions (AR) located near the disk center observed on January 8, 2015 (AR 12257) and December 4, 2016 (AR 12615) are used for the estimate of the chromospheric and coronal magnetic fields with the microwave radio observations. We compare solar radio maps of active regions for both intensity and circularly polarized component with the optical maps from observations with the Helioseismic and Magnetic Imager and the chromosphere and corona transition region images obtained with the Atmospheric Imaging Assembly instrument, on board the Solar Dynamic Observatory. We notice from the comparison between radio maps of both AR that the circular polarization degree in the AR 12257 is about 2 percent, but the AR 12615 has a higher existent value by 3 percent. Radio observations provide us for direct measurements of magnetic fields in the chromospheric and coronal layers. We estimate the coronal magnetic fields using the Atmospheric Imaging Assembly observations by adopting magnetic loops in the corona over some patches with weak photospheric magnetic fields. The coronal magnetic field derived

from the Atmospheric Imaging Assembly data was from 90 to 240 Gauss. We also study the coronal magnetic fields based on the structure of the extrapolated field, where the result of the magnetic fields was in the range from 35 to 145 Gauss, showing that the difference in the coronal magnetic fields between both results is attributed to the assumption of the force-free approximation.

## **Switchbacks in the solar magnetic field: their evolution, their content, and their effects on the plasma, V2**

F.S. [Mozer](#)<sup>1</sup>, [O.V. Agapitov](#)<sup>1</sup>, [S.D. Bale](#)<sup>1</sup>, [J.W. Bonnell](#)<sup>1</sup>, [T. Case](#)<sup>4</sup>, ....

First results from the Parker Solar Probe **2020**

<https://arxiv.org/ftp/arxiv/papers/1912/1912.09252.pdf>

Switchbacks (rotations of the magnetic field) are observed on the Parker Solar Probe. Their evolution, content, and plasma effects are studied in this paper. The solar wind does not receive a net acceleration from switchbacks that it encountered upstream of the observation point. The typical switchback rotation angle increased with radial distance. Significant Poynting fluxes existed inside, but not outside, switchbacks and they are related to the increased EXB/B2 flow caused by the magnetic field rotating to become more perpendicular to the flow direction. (Outside the switchbacks, the magnetic field and solar wind flow were generally radial.) The solar wind flow inside switchbacks was faster than that outside due to the frozen-in ions moving with the magnetic structure at the Alfvén speed. This energy gain results from the divergence of the Poynting flux from outside to inside the switchback, which produces a loss of electromagnetic energy on switchback entry and recovery of that energy on exit, with the lost energy appearing in the plasma flow. Switchbacks contain 0.3-10 Hz waves that may result from currents and the Kelvin-Helmholtz instability that occurs at the switchback boundaries. These waves may combine with lower frequency MHD waves to heat the plasma. The radial decreases of the Poynting flux and solar wind speed inside switchbacks are due to a geometrical effect. **April 2019**

## **The umbral--penumbral boundary in sunspots in the context of magneto-convection**

D. J. [Mullan](#), [J. MacDonald](#)

**2019** ApJL 873 L10

<https://arxiv.org/ftp/arxiv/papers/1902/1902.09431.pdf>

Jurcak et al (2018) have reported that, in a sample of more than 100 umbral cores in sunspots, the umbral-penumbral boundary (UPB) is characterized by a remarkably narrowly-defined numerical value (1867 G) of the vertical component of the magnetic field. Gough and Tayler (1966), in their study of magneto-convection, showed that the onset of convection in the presence of a magnetic field is controlled by a parameter  $\{\delta\}$  which also depends on the vertical component of the field. Combining the Jurcak et al result with various empirical models of sunspots leads us to propose the following hypothesis: the UPB occurs where the vertical field is strong enough to increase the effective adiabatic temperature gradient by at least 100% above its non-magnetic value.

## **Multi-wavelength Fibril Dynamics and Oscillations Above Sunspot - I. Morphological Signature**

Emanuel Sungging [Mumpuni](#), [Dhani Herdiwijaya](#), [Mitra Djamaal](#), [Thomas Djamaaluddin](#)

A&A **2015**

<http://arxiv.org/pdf/1504.03533v1.pdf>

In this work we selected one particular fibril from a high resolution solar chromosphere observation from the Dutch Open Telescope, and tried to obtain a broad picture of the intricate mechanism that might be incorporated in the multiple layer of the Solar atmosphere in high cadence multi-wavelength observation. We analyzed the changing fibril pattern using multi-wavelength tomography, which consists of both H $\alpha$  line center & the blue wing, Doppler-signal, Ca II H, and the G-band. We have found that the intermittent ejected material through fibril from Doppler images has clearly shown oscillation mode, as seen in the H $\alpha$  blue wing. The oscillations in the umbrae and penumbrae magnetic field lines that are above the sunspot cause a broadening and forms the area like a ring shape from 3 to 15-minute oscillations as function of height. These made a distinct boundary of umbrae and penumbrae which suggest the comb structure, and indicate that the oscillations could propagate along the inclined magnetic flux tubes from below. The 3-minute strongly appeared in the broadly inclined penumbrae magnetic field lines and gave the clear light-bridge. The well known 5-minute was dominated in the umbrae-penumbrae region boundary, the long 7-minute one was transparent in the H $\alpha$  blue wing, but this was the same with 10 and 15-minute, it was concentrated in the inner-penumbrae, as seen in the H $\alpha$  line center. From these findings we propose a picture on the role of fibril as the fabric of interaction between the layers, also the related activities around the active region under investigation. **July 13, 2005**



## Physically Motivated Deep Learning to Superresolve and Cross Calibrate Solar Magnetograms

Andrés **Muñoz-Jaramillo**<sup>10,1</sup>, Anna Jungbluth<sup>10,2</sup>, Xavier Gitiaux<sup>10,3</sup>, Paul J. Wright<sup>10,4,5</sup>, Carl Shneider<sup>6</sup>, Shane A. Maloney<sup>4,7</sup>, Atılım Güneş Baydin<sup>8</sup>, Yarin Gal<sup>8</sup>, Michel Deudon<sup>9</sup>, and Freddie Kalaitzis<sup>8</sup>

2024 ApJS 271 46

<https://iopscience.iop.org/article/10.3847/1538-4365/ad12c2/pdf>

Superresolution (SR) aims to increase the resolution of images by recovering detail. Compared to standard interpolation, deep learning-based approaches learn features and their relationships to leverage prior knowledge of what low-resolution patterns look like in higher resolution. Deep neural networks can also perform image cross-calibration by learning the systematic properties of the target images. While SR for natural images aims to create perceptually convincing results, SR of scientific data requires careful quantitative evaluation. In this work, we demonstrate that deep learning can increase the resolution and calibrate solar imagers belonging to different instrumental generations. We convert solar magnetic field images taken by the Michelson Doppler Imager (resolution  $\sim 2''$  pixel<sup>-1</sup>; space based) and the Global Oscillation Network Group (resolution  $\sim 2''.5$  pixel<sup>-1</sup>; ground based) to the characteristics of the Helioseismic and Magnetic Imager (resolution  $\sim 0''.5$  pixel<sup>-1</sup>; space based). We also establish a set of performance measurements to benchmark deep-learning-based SR and calibration for scientific applications.

## Small-scale and Global Dynamos and Area and Flux Distributions of Active Regions, Sunspot Groups, and Sunspots: A Multi-Database Study

Andrés **Muñoz-Jaramillo**, Ryan R. Senkpeil, John C. Windmueller, Ernest C. Amouzou, Dana W. Longcope, Andrey G. Tlatov, Yury A. Nagovitsyn, Alexei A. Pevtsov, Gary A. Chapman, Angela M. Cookson, Anthony R. Yeates, Fraser T. Watson, Laura A. Balmaceda, Edward E. DeLuca, Petrus C. H. Martens

ApJ 800 48 2015

<http://arxiv.org/pdf/1410.6281v1.pdf>

In this work, we take advantage of 11 different sunspot group, sunspot, and active region databases to characterize the area and flux distributions of photospheric magnetic structures. We find that, when taken separately, different databases are better fitted by different distributions (as has been reported previously in the literature). However, we find that all our databases can be reconciled by the simple application of a proportionality constant, and that, in reality, different databases are sampling different parts of a composite distribution. This composite distribution is made up by linear combination of Weibull and log-normal distributions—where a pure Weibull (log-normal) characterizes the distribution of structures with fluxes below (above) 1021Mx (1022Mx). Additionally, we demonstrate that the Weibull distribution shows the expected linear behavior of a power-law distribution (when extended to smaller fluxes), making our results compatible with the results of Parnell et al. We propose that this is evidence of two separate mechanisms giving rise to visible structures on the photosphere: one directly connected to the global component of the dynamo (and the generation of bipolar active regions), and the other with the small-scale component of the dynamo (and the fragmentation of magnetic structures due to their interaction with turbulent convection).

## Penumbral decay observed in active region NOAA 12585★

M. **Murabito**<sup>1</sup>, S. L. Guglielmino<sup>2</sup>, I. Ermolli<sup>1</sup>, P. Romano<sup>2</sup>, S. Jafarzadeh<sup>3,4</sup> and L. H. M. Rouppe van der Voort<sup>3,4</sup>

A&A 653, A93 (2021)

<https://www.aanda.org/articles/aa/pdf/2021/09/aa41034-21.pdf>

<https://doi.org/10.1051/0004-6361/202141034>

Context. The physical conditions leading the sunspot penumbra decay are poorly understood so far.

Aims. We investigate the photospheric magnetic and velocity properties of a sunspot penumbra during the decay phase to advance the current knowledge of the conditions leading to this process.

Methods. A penumbral decay was observed with the CRISP instrument at the Swedish 1 m Solar Telescope on **2016 September 4 and 5** in the active region NOAA 12585. During these days, full-Stokes spectropolarimetric scans along the Fe I 630 nm line pair were acquired over more than one hour. We inverted these observations with the VFISV code to obtain the evolution of the magnetic and velocity properties. We complement the study with data from instruments on board the Solar Dynamics Observatory and Hinode space missions.

Results. The studied penumbra disappears progressively in time and space. The magnetic flux evolution seems to be linked to the presence of moving magnetic features (MMFs). Decreasing Stokes V signals are observed. Evershed flows and horizontal fields were detected even after the disappearance of the penumbral sector.

## Penumbral brightening events observed in AR NOAA 12546

M. Murabito, S. L. Guglielmino, I. Ermolli, M. Stangalini, F. Giorgi

ApJ 890 96 2020

<https://arxiv.org/pdf/1912.06002.pdf>

<https://doi.org/10.3847/1538-4357/ab6664>

Penumbral transient brightening events have been attributed to magnetic reconnection episodes occurring in the low corona. We investigated the trigger mechanism of these events in active region NOAA 12546 by using multi-wavelength observations obtained with the Interferometric Bidimensional Spectrometer (IBIS), by the \textit{Solar Dynamics Observatory} (SDO), the \textit{Interface Region Imaging Spectrograph} (IRIS), and the \textit{Hinode} satellites. We focused on the evolution of an area of the penumbra adjacent to two small-scale emerging flux regions (EFRs), which manifested three brightening events detected from the chromosphere to the corona. Two of these events correspond to B-class flares. The same region showed short-lived moving magnetic features (MMFs) that streamed out from the penumbra. In the photosphere, the EFRs led to small-scale penumbral changes associated with a counter-Evershed flow and to a reconfiguration of the magnetic fields in the moat. The brightening events had one of the footpoints embedded in the penumbra and seemed to result from the distinctive interplay between the pre-existing penumbral fields, MMFs, and the EFRs. The \textit{IRIS} spectra measured therein reveal enhanced temperature and asymmetries in spectral lines, suggestive of event triggering at different height in the atmosphere. Specifically, the blue asymmetry noted in  $\text{ion}\{C\}_{2}$  and  $\text{ion}\{Mg\}_{2}$  h&k lines suggests the occurrence of chromospheric evaporation at the footpoint located in the penumbra as a consequence of magnetic reconnection process at higher atmospheric heights. **2016 May 20**

### Height dependence of the penumbral fine-scale structure in the inner solar atmosphere

Mariarita Murabito, I. Ermolli, F. Giorgi, M. Stangalini, S.L. Guglielmino, S. Jafarzadeh, H. Socas-Navarro, P. Romano, F. Zuccarello

ApJ 873 126 2019

<https://arxiv.org/pdf/1812.09029.pdf>

<https://doi.org/10.3847/1538-4357/aaf727>

We studied the physical parameters of the penumbra in a large and fully-developed sunspot, one of the largest over the last two solar cycles, by using full-Stokes measurements taken at the photospheric Fe I 617.3 nm and chromospheric Ca II 854.2 nm lines with the Interferometric Bidimensional Spectrometer. Inverting measurements with the NICOLE code, we obtained the three-dimensional structure of the magnetic field in the penumbra from the bottom of the photosphere up to the middle chromosphere. We analyzed the azimuthal and vertical gradient of the magnetic field strength and inclination. Our results provide new insights on the properties of the penumbral magnetic fields in the chromosphere at atmospheric heights unexplored in previous studies. We found signatures of the small-scale spine and intra-spine structure of both the magnetic field strength and inclination at all investigated atmospheric heights. In particular, we report typical peak-to-peak variations of the field strength and inclination of  $\approx 300$  G and  $\approx 20^\circ$ , respectively, in the photosphere, and of  $\approx 200$  G and  $\approx 10^\circ$  in the chromosphere. Besides, we estimated the vertical gradient of the magnetic field strength in the studied penumbra: we find a value of  $\approx 0.3$  G  $\text{km}^{-1}$  between the photosphere and the middle chromosphere. Interestingly, the photospheric magnetic field gradient changes sign from negative in the inner to positive in the outer penumbra. **2016 May 20**

### On the formation of a stable penumbra in a region of flux emergence in the Sun

M. Murabito, P. Romano, S. L. Guglielmino, F. Zuccarello

2017 ApJ 834 76

<https://arxiv.org/pdf/1611.04749v1.pdf>

We studied the formation of the first penumbral sector around a pore in the following polarity of the Active Region (AR) NOAA 11490. We used a high spatial, spectral, and temporal resolution data set acquired by the Interferometric Bidimensional Spectrometer operating at the NSO/Dunn Solar Telescope as well as data taken by the Helioseismic and Magnetic Imager onboard the Solar Dynamics Observatory satellite. On the side towards the leading polarity, elongated granules in the photosphere and an arch filament system (AFS) in the chromosphere are present, while the magnetic field shows a sea-serpent configuration, indicating a region of magnetic flux emergence. We found that the formation of a stable penumbra in the following polarity of the AR begins in the area facing the opposite polarity located below the AFS in the flux emergence region, differently from what found by Schlichenmaier and colleagues. Moreover, during the formation of the first penumbral sector, the area characterized by magnetic flux density larger than 900 G and the area of the umbra increase. **2012 May 28**

HMI Science Nuggets, # 93 March 2018 <http://hmi.stanford.edu/hminuggets/?p=2395>

### FORMATION OF THE PENUMBRA AND START OF THE EVERSHERD FLOW

M. Murabito<sup>1</sup>, P. Romano<sup>2</sup>, S. L. Guglielmino<sup>1</sup>, F. Zuccarello<sup>1</sup>, and S. K. Solanki<sup>3</sup>

2016 ApJ 825 75

We studied the variations of line of sight photospheric plasma flows during the formation phase of the penumbra around a pore in active region NOAA 11490. We used a high spatial, spectral, and temporal resolution data set acquired by the Interferometric Bidimensional Spectrometer operating at the NSO/Dunn Solar Telescope as well as data taken by the Helioseismic and Magnetic Imager on board the Solar Dynamics Observatory satellite (SDO/HMI). Before the penumbra formed we observed a redshift of the spectral line in the inner part of the annular zone surrounding the pore as well as a blueshift of material associated with opposite magnetic polarity farther away from the pore. We found that the onset of the classical Evershed flow occurs on a very short timescale (1 to 3 hr) while the penumbra is forming. During the same time interval we found changes in the magnetic field inclination in the penumbra, with the vertical field actually changing sign near the penumbral edge, while the total magnetic field showed a significant increase, about 400 G. To explain these and other observations related to the formation of the penumbra and the onset of the Evershed flow we propose a scenario in which the penumbra is formed by magnetic flux dragged down from the canopy surrounding the initial pore. The Evershed flow starts when the sinking magnetic field dips below the solar surface and magnetoconvection sets in.

### **Recent insights on the penumbra formation process**

M. [Murabito](#), P. [Romano](#), F. [Zuccarello](#), S.L. [Guglielmino](#)

"Nuovo Cimento C" as proceeding of the Third Meeting of the Italian Solar and Heliospheric Community 2019

<https://arxiv.org/pdf/1901.05207.pdf>

Using high-resolution spectropolarimetric data acquired by `\textit{IBIS}`, as well as `\textit{SDO}/HMI` observations, we studied the penumbra formation in AR NOAA 11490 and in a sample of twelve ARs appeared on the solar disk on 2011 and 2012, which were characterized by  $\beta$ -type magnetic field configuration. The results show that the onset of the classical Evershed flow occurs in a very short time scale, 1-3 hours. Studying the formation of the first penumbral sector around the following proto-spot, we found that a stable penumbra forms in the area facing the opposite polarity, which appears to be co-spatial with an AFS, i.e. in a flux emergence region, in contrast with the results of `\cite{Schlichenmaier2010}` concerning the leading polarity of AR NOAA 11490. Conversely, analyzing the sample of twelve ARs, we noticed that there is not a preferred location for the formation of the first penumbral sector. We also observed before the penumbra formation an inverse Evershed flow, which changes its sign when the penumbra appears. This confirms the observational evidence that the appearance of the penumbral filaments is correlated with the transition from the inverse Evershed to the classical Evershed flow. Furthermore, the analysis suggests that the time needed to form the penumbra may be related to the location where the penumbra first appears. New high-resolution observations, like those that will be provided by the European Solar Telescope, are expected to increase our understanding of the penumbra formation process. **2012 May 28-29**

### **Variation of sunspot groups' polarity separation during their evolution**

[Judit Muraközy](#)

A&A 690, A257 2024

<https://arxiv.org/pdf/2408.12213>

<https://www.aanda.org/articles/aa/pdf/2024/10/aa50194-24.pdf>

During the emergence of sunspot groups the footpoints of their leading and following parts move apart. This diverging motion results in the stretching of the active regions, which continues during the decay phase. The aim of the present work is to study the separation distance variations during the active region evolution on a large statistical sample. Altogether more than 2000 individual sunspot groups were taken into account. The investigation is mainly based on data of the SoHO/MDI - Debrecen Sunspot Data (SDD) catalog which covers the time span 1996-2010, practically the whole solar cycle 23. For check of the possible cyclical variation the Debrecen Photoheliographic Data (DPD) is used which contains data for solar cycles 20-24. The separation distance is calculated between the leading and following centers of mass and starts to increase after the emergence and shows a plateau around the peak flux. The polarity separation reaches its maximum in the decay phase and then starts to decrease in the cases of the largest and medium size groups, but continues its increase in the case of the smallest groups. This decrease is caused by the eastward motion of the leading part, while the following part continues its backward motion. The separation distance is size dependent, i. e., the larger the sunspot group the greater its extent. Cycle and cycle phase dependencies as well as hemispheric connection can also be observed.

### **Variations of the Internal Asymmetries of Sunspot Groups During their Decay**

[Judit Muraközy](#)

ApJ 925 87 2022

<https://arxiv.org/pdf/2111.14221>

<https://iopscience.iop.org/article/10.3847/1538-4357/ac3de6/pdf>

The aim of the present study is to show the varying asymmetries during the decay of sunspot groups. The source of input data is the SoHO/MDI-Debrecen Database (SDD) sunspot catalog that contains the magnetic polarity data for

time interval 1996-2010. Several types of asymmetries were examined on the selected sample of 142 sunspot groups. The leading-following asymmetry increases in three phases during the decay and exhibits anticorrelation with size. It is also related to a hemispheric asymmetry, during the decay the area asymmetry index has higher values in the southern hemisphere which may be due to the higher activity level in the southern hemisphere in cycle 23. The total umbral area is inversely proportional to the umbra/penumbra ratio but it is directly proportional to the umbral decay rate. During the decay the umbra/penumbra (U/P) ratio decreases unambiguously in the trailing parts but in most cases in the leading parts as well. The U/P variation is a consequence of the different depths of umbral and penumbral fields.

## **On the Decay of Sunspot Groups and Their Internal Parts in Detail**

[Judit Muraközy](#)

ApJ **908** 133 **2021**

<https://arxiv.org/pdf/2012.00446.pdf>

<https://doi.org/10.3847/1538-4357/abcfb>

The decay of sunspot groups is a relatively unknown field since most studies have focused mainly on the decay of sunspots or sunspot groups, but only on small samples. As an extension of the recent work of \cite{2020ApJ...892..107M} which is based on a large verified sample, this study investigates not only the long-term behavior of the decay of sunspot groups but also the dynamics of their parts. The aim of the present work is to search for dependencies of the decay process in order to find physical conditions that modify or contribute to the decay. The investigations are based on the catalog of SoHO Debrecen Sunspot Database (SDD) and the Greenwich Photoheliographic Results (GPR) as well as the Debrecen Photoheliographic Data (DPD). Altogether more than 750 sunspot groups were considered. The decay rates have been calculated for the total, umbral and penumbral area of the groups and in the case of the SDD's groups they have been calculated for both the leading and the following parts. The decay rates depend linearly on the maximum areas and ranged from 30-50 MSH/day for the sunspot groups and penumbrae and 5-10 MSH/day for the umbrae throughout the cycle. The decay rates fall significantly during the Gnevyshev gap and show 4+4 Schwabe cyclical variations in the ascending/descending phases, but it is always higher in the northern hemisphere. There is a slight decrease of the decay rates in the activity range toward higher latitudes. **4-12 Apr 1998**

## **Study of the decay rates of the umbral area of sunspot groups by using a high resolution database**

[Judit Muraközy](#)

ApJ **892** 107 **2020**

<https://arxiv.org/pdf/2002.08997.pdf>

<https://doi.org/10.3847/1538-4357/ab7898>

The emergence and decay of the sunspot groups are important components of the solar dynamo models. There are two different types of studies on the evolution of active regions. One of them is based on fewer data with higher spatial resolution, the other one uses more data with lower spatial resolution. The input data of the present study allow the investigation with high-resolution both spatially and temporally. The temporal resolution of the SoHO Debrecen Sunspot Database (SDD) is one and a half hours, and it also makes possible to identify all individual sunspots with the position, area, and magnetic polarity. More than 200 sunspot groups have been selected, which have clear maxima on the solar disc, and the decrease of their umbral area is observable during at least four days. The decay rates were calculated by using two data: the umbral area and the number of contained sunspots -- these decay rates were computed for the total umbral area of sunspot groups and their leading and following parts. The decay rate has a linear area dependency, and it is higher for the following part than for the leading one. **10-16 March 2010,**

## **Connection Between Solar Hemispheric Toroidal Cycles and Geomagnetic Variations**

[Judit Muraközy](#)

[Solar Physics](#) April **2019**, 294:46

[sci-hub.se/10.1007/s11207-019-1438-2](https://doi.org/10.1007/s11207-019-1438-2)

The solar activity has hemispheric asymmetries. The levels of activity are different on the two hemispheres on intermediate and longer time scales. During four Schwabe cycles the progress of the northern hemispheric activity precedes the southern one, while in the next four cycles the southern cycle takes over the preceding role (Muraközy and Ludmány, Mon. Not. Roy. Astron. Soc.419, 3624, [2012](#); Muraközy, Astrophys. J.826, 145, [2016](#)). The interplanetary magnetic field is formed by the distribution of the solar magnetic fields and the outward-streaming solar wind. The present study intends to show how the solar-hemispheric predominance affects the interplanetary and geophysical magnetic field. The interplanetary and geophysical data sets have been chosen from various sources such as the components of the interplanetary magnetic field [BB], cosmic-ray data, Ap, aa, and Dst geomagnetic indices, while the solar-hemispheric asymmetry has been examined by using sunspot data from Greenwich Photoheliographic Results (GPR) and Debrecen Photoheliographic Data (DPD).

## Magnetic swirls and associated fast magnetoacoustic kink waves in a solar chromospheric flux tube

K. [Murawski](#), [P. Kayshap](#), [A. K. Srivastava](#), [D. J. Pascoe](#), [P. Jelínek](#), [B. Kuźma](#), [V. Fedun](#)

MNRAS

2017

<https://arxiv.org/pdf/1710.08179.pdf>

We perform numerical simulations of impulsively generated magnetic swirls in an isolated flux tube which is rooted in the solar photosphere. These swirls are triggered by an initial pulse in a horizontal component of the velocity. The initial pulse is launched either: (a) centrally, within the localized magnetic flux tube; or (b) off-central, in the ambient medium. The evolution and dynamics of the flux tube is described by three-dimensional, ideal magnetohydrodynamic equations. These equations are numerically solved to reveal that in case (a) dipole-like swirls associated with the fast magnetoacoustic kink and  $m=1$  Alfvén waves are generated. In case (b), the fast magnetoacoustic kink and  $m=0$  Alfvén modes are excited. In both these cases, the excited fast magnetoacoustic kink and Alfvén waves consist of similar flow pattern and magnetic shells are also generated with clockwise and counter-clockwise rotating plasma within them, which can be the proxy of dipole-shaped chromospheric swirls. The complex dynamics of vortices and wave perturbations reveals the channelling of sufficient amount of energy to fulfill energy losses in the chromosphere ( $\sim 104 \text{ W m}^{-1}$ ) and in the corona ( $\sim 102 \text{ W m}^{-1}$ ). Some of these numerical findings are reminiscent of signatures in recent observational data.

## A Numerical Model of MHD Waves in a 3D Twisted Solar Flux Tube

K. [Murawski](#), A. Solov'ev, J. Kraśkiewicz

Solar Phys.

2015

We generalize our analytical and numerical models of the solar flux tube on twisted magnetic-field lines. The basic equations and numerical methods have much in common with those of [Murawski et al. \(Astron. Astrophys. 577, A126, 2015\)](#); the new and important issue is the twisted magnetic-field component that couples explored torsional Alfvén and magnetoacoustic waves. In these models we specify a magnetic-flux function and derive general analytical formulas for the equilibrium mass density and a gas pressure. We use the developed models, which can be adopted for any axisymmetric structure with twisted and untwisted magnetic lines, to simulate the MHD waves. These waves are excited by a localized pulse in the azimuthal velocity component that is launched at the top of the solar photosphere. Their propagation through the solar chromosphere and transition region to the solar corona reveals a complex scenario of twisted magnetic-field lines and flows associated with torsional Alfvén and magnetoacoustic waves.

## Torsional Alfvén waves in solar magnetic flux tubes of axial symmetry

K. [Murawski](#)<sup>1</sup>, A. Solov'ev<sup>2</sup>, Z. E. Musielak<sup>3,4</sup>, A. K. Srivastava<sup>5</sup> and J. Kraśkiewicz

A&A 577, A126 (2015)

Aims. Propagation and energy transfer of torsional Alfvén waves in solar magnetic flux tubes of axial symmetry is studied.

Methods. An analytical model of a solar magnetic flux tube of axial symmetry is developed by specifying a magnetic flux and deriving general analytical formulas for the equilibrium mass density and gas pressure. The main advantage of this model is that it can be easily adopted to any axisymmetric magnetic structure. The model is used to numerically simulate the propagation of nonlinear Alfvén waves in such 2D flux tubes of axial symmetry embedded in the solar atmosphere. The waves are excited by a localized pulse in the azimuthal component of velocity and launched at the top of the solar photosphere, and they propagate through the solar chromosphere, the transition region, and into the solar corona.

Results. The results of our numerical simulations reveal a complex scenario of twisted magnetic field lines and flows associated with torsional Alfvén waves, as well as energy transfer to the magnetoacoustic waves that are triggered by the Alfvén waves and are akin to the vertical jet flows. Alfvén waves experience about 5% amplitude reflection at the transition region. Magnetic (velocity) field perturbations that experience attenuation (growth) with height agree with analytical findings. The kinetic energy of magnetoacoustic waves consists of 25% of the total energy of Alfvén waves. The energy transfer may lead to localized mass transport in the form of vertical jets, as well as to localized heating because slow magnetoacoustic waves are prone to dissipation in the inner corona.

## Fast Magnetic Twister and Plasma Perturbations in a 3-D Coronal Arcade

K. [Murawski](#), A.K. Srivastava, Z. E. Musielak

ApJ 788 8 2014

<http://arxiv.org/pdf/1404.4176v1.pdf>

We present results of 3-D numerical simulations of a fast magnetic twister excited above a foot-point of the potential solar coronal arcade that is embedded in the solar atmosphere with the initial VAL-IIIC temperature profile, which is smoothly extended into the solar corona. With the use of the FLASH code, we solve 3-D ideal magnetohydrodynamic equations by specifying a twist in the azimuthal component of magnetic field in the solar chromosphere. The imposed perturbation generates torsional Alfvén waves as well as plasma swirls that reach the other foot-point of the arcade and partially reflect back from the transition region. The two vortex channels are evident in the generated twisted flux-tube with a fragmentation near its apex that results from the initial twist as well as from the morphology of the tube. The numerical results are compared to observational data of plasma motions in a solar prominence. The comparison shows that the numerical results and the data qualitatively agree even though the observed plasma motions occur over comparatively large spatio-temporal scales in the prominence.

4-Aug-2012

### **SDO/HMI Multi-height Dopplergrams**

Kaori [Nagashima](#)<sup>1</sup>, Björn Löptien<sup>2</sup>, Laurent Gizon<sup>1,2</sup>, Aaron C. Birch<sup>1</sup>, Robert Cameron<sup>1</sup>, Sebastien Couvidat<sup>3</sup>, Sanja Danilovic<sup>1</sup>, Bernhard Fleck<sup>4</sup>, Robert Stein

HMI Science Nuggets, #26, 2014

<http://hmi.stanford.edu/hminuggets/?p=932>

Both numerical simulations and observations indicate that the plasma velocity varies with height within the solar photosphere. Mapping the velocity simultaneously at several different heights would give us insight into, for example, how waves are affected by radiative transfer above the surface. Multi-height Doppler velocity maps are also important for many other types of studies, e.g. to learn about how energy is transported in the atmosphere.

### **Interpreting the Helioseismic and Magnetic Imager (HMI) Multi-Height Velocity Measurements**

Kaori [Nagashima](#), Björn Löptien, Laurent Gizon, Aaron C. Birch, Robert Cameron, Sebastien Couvidat, Sanja Danilovic, Bernhard Fleck, Robert Stein

Solar Phys., Volume 289, Issue 9, pp 3457-3481, 2014

<http://arxiv.org/pdf/1404.3569v1.pdf>

The Solar Dynamics Observatory/Helioseismic and Magnetic Imager (SDO/HMI) filtergrams, taken at six wavelengths around the Fe I 6173.3 Å line, contain information about the line-of-sight velocity over a range of heights in the solar atmosphere. Multi-height velocity inferences from these observations can be exploited to study wave motions and energy transport in the atmosphere. Using realistic convection simulation datasets provided by the STAGGER and MURaM codes, we generate synthetic filtergrams and explore several methods for estimating Dopplergrams. We investigate at which height each synthetic Dopplergram correlates most strongly with the vertical velocity in the model atmospheres. On the basis of the investigation, we propose two Dopplergrams other than the standard HMI-algorithm Dopplergram produced from HMI filtergrams: a line-center Dopplergram and an average-wing Dopplergram. These two Dopplergrams correlate most strongly with vertical velocities at the heights of 30 - 40 km above (line-center) and 30 - 40 km below (average-wing) the effective height of the HMI-algorithm Dopplergram. Therefore, we can obtain velocity information from two layers separated by about a half of a scale height in the atmosphere, at best. The phase shifts between these multi-height Dopplergrams from observational data as well as those from the simulated data are also consistent with the height-difference estimates in the frequency range above the photospheric acoustic cutoff frequency.

### **Two Populations of Sunspot Groups and Their Meridional Motions**

[Yury Nagovitsyn](#), [Alexei Pevtsov](#) & [Aleksandra Osipova](#)

[Solar Physics](#) volume 298, Article number: 108 (2023)

<https://doi.org/10.1007/s11207-023-02204-8>

It is shown that the average meridional velocities of sunspot groups linearly depend on their average longitudinal velocities (solar rotation) with a high correlation coefficient of -0.95. The relationship differs for small, short-lived and large, long-lived groups. The meridional motions of sunspots do not have any pronounced global distribution law with latitude, but depend on their individual longitudinal velocities in a rotating coordinate system close to the Carrington one. The found relations indicate that the Coriolis force may play a role in driving the meridional motions of sunspot groups.

### **Tilt angle and lifetime of sunspot groups**

[Yury A Nagovitsyn](#), [Aleksandra A Osipova](#), [Alexei A Pevtsov](#)

<https://doi.org/10.1093/mnras/staa3848>

We use the Catalogue of Solar Activity (CSA) to study the latitudinal variations of tilt of solar active regions. The tilt angles  $\beta$  are computed taking into account changes of the heliographic grid with latitude  $\varphi$ . We show that when sunspot groups of different sizes and lifetimes are included, a classical representation of the Joy's law as a linear function of latitude ( $\beta \propto \varphi$ ) is only the first approximation valid within a limited range of latitudes ( $-25^\circ \leq \varphi \leq +25^\circ$ ). Outside this range, the functional dependence  $\beta = f(\varphi)$  becomes non-linear. Separating the data set on large long-living groups (LLG) and small short-living groups (SSG) reveals two quite different dependencies in  $\beta = f(\varphi)$ : non-linearity in tilt is only present in LLGs and the steepness of linear section of  $\beta = f(\varphi)$  fit is higher for LLGs. This suggests a difference in the physical properties of two populations of solar groups, which could be hypothesized as an indication of different localization of subsurface zones of their formation in the framework of a distributed dynamo. However, since CSA contains the coordinates of sunspots averaged over the lifetime (or disc passage) of each group, one cannot rule out that the difference in tilts of SSG and LLG groups may be affected by the evolution of tilt angles during the lifetime/disc passage of the groups.

### **Bi-lognormal Distribution of Sunspot Group Areas**

Yury A. Nagovitsyn<sup>1,2</sup> and Alexei A. Pevtsov<sup>3</sup>

2021 ApJ 906 27

<https://doi.org/10.3847/1538-4357/abc82d>

We use daily observations from the Royal Greenwich Observatory and Kislovodsk Mountain Astronomical Station of Pulkovo Observatory to study the distribution properties of sunspot areas. To mitigate the poor statistics in the distribution of small areas, we introduce a "precision randomization" approach based on the assumption that all measured areas have a random component within the measurement uncertainty of 1 millionth of the solar hemisphere (M.S.H.). We confirm the presence of two distinct components in the distribution of sunspots previously reported by several authors, and show that the area distribution is described by the sum of two lognormal distributions responsible for small and large groups (sunspots), respectively. We also demonstrate that the area of the main spots in the groups correlates well with the total area of the group, and, thus, the findings derived for the total group areas are equally applicable to the main spots of groups.

### **Long-term variations in sunspot magnetic field - area relation**

Yury A. Nagovitsyn, Alexei A. Pevtsov, Aleksandra A. Osipova

Astron. Nachrichten **2016**

<http://arxiv.org/pdf/1608.01132v1.pdf>

Using observations of sunspot magnetic field strengths ( $H$ ) from the Crimean Astrophysical Observatory (CrAO) and area ( $S$ ) of sunspots from the Kislovodsk Mountain Astronomical Station of Pulkovo Observatory, we investigate the changes in the relation between  $H$  and  $S$  over the period of about two solar cycles (1994-2013). The data were fitted by  $H = A + B \log S$ , where  $A = (778 \pm 46)$  and  $B = (778 \pm 25)$ . We show that the correlation between  $H$  and  $S$  varies with the phase of solar cycle, and  $A$  coefficient decreases significantly after year 2001, while  $B$  coefficient does not change significantly. Furthermore, our data confirm the presence of two distinct populations in distribution of sunspots (small sunspots with weaker field strength and large sunspots with stronger field). We show that relative contribution of each component to the distribution of sunspots by their area changes with the phase of solar cycle and on longer-than-cycle periods. We interpret these changes as a signature of a long-term (centennial) variations in properties of sunspots.

### **ON A POSSIBLE EXPLANATION OF THE LONG-TERM DECREASE IN SUNSPOT FIELD STRENGTH**

Yury A. Nagovitsyn<sup>1</sup>, Alexei A. Pevtsov<sup>2</sup>, and William C. Livingston

2012 ApJ 758 L20

Recent studies revealed a controversy in long-term variations in sunspot field strengths. On one hand, the sunspot field strengths computed by averaging both large and small sunspots and pores show a gradual decrease over the declining phase of solar Cycle 23 and the rising phase of Cycle 24. On the other hand, the strongest sunspot field strengths demonstrate only solar cycle variations with no long-term decline. Here, we investigate the field strength and area properties of sunspots in an attempt to reconcile the presence of both tendencies in recent sunspot field strength measurements. First, we analyze the data set from Penn & Livingston, and we show that in addition to the

previously reported long-term decline, the data show the solar cycle variation when only sunspots with the strongest magnetic fields are included. Next, we investigate the variations in the number of sunspots of different sizes, and we find a negative correlation between the numbers of small and large sunspots. Finally, we show that during the period of 1998-2011, the number of large sunspots gradually decreased, while the number of small sunspots steadily increased. We suggest that this change in the fraction of small and large sunspots (perhaps, due to changes in the solar dynamo) can explain the gradual decline in average sunspot field strength as observed by Penn & Livingston.

### **Magnetohydrodynamic Oscillations in the Solar Corona and Earth's Magnetosphere: Towards Consolidated Understanding** **Review**

V. M. [Nakariakov](#), V. Pilipenko, B. Heilig, P. Jelínek, M. Karlický, D. Y. Klimushkin, D. Y. Kolotkov, D.-H. Lee, G. Nisticò and 3 more

Space Science Reviews April 2016, Volume 200, Issue 1, pp 75-203

<http://www2.warwick.ac.uk/fac/sci/physics/research/cfsa/people/valery/research/eprints/s11214-015-0233-0.pdf>

Magnetohydrodynamic (MHD) oscillatory processes in different plasma systems, such as the corona of the Sun and the Earth's magnetosphere, show interesting similarities and differences, which so far received little attention and remain under-exploited. The successful commissioning within the past ten years of THEMIS, Hinode, STEREO and SDO spacecraft, in combination with matured analysis of data from earlier spacecraft (Wind, SOHO, ACE, Cluster, TRACE and RHESSI) makes it very timely to survey the breadth of observations giving evidence for MHD oscillatory processes in solar and space plasmas, and state-of-the-art theoretical modelling. The paper reviews several important topics, such as Alfvénic resonances and mode conversion; MHD waveguides, such as the magnetotail, coronal loops, coronal streamers; mechanisms for periodicities produced in energy releases during substorms and solar flares, possibility of Alfvénic resonators along open field lines; possible drivers of MHD waves; diagnostics of plasmas with MHD waves; interaction of MHD waves with partly-ionised boundaries (ionosphere and chromosphere). The review is mainly oriented to specialists in magnetospheric physics and solar physics, but not familiar with specifics of the adjacent research fields.

### **The possible role of vortex shedding in the excitation of kink-mode oscillations in the solar corona**

V. M. [Nakariakov](#)<sup>1</sup>, M. J. Aschwanden<sup>2</sup>, and T. Van Doorselaere<sup>1</sup>  
A&A 502, 661-664 (2009)

We propose a model for the excitation of horizontally polarised transverse (kink) magnetoacoustic oscillations of solar coronal loops by upflows associated with coronal mass ejections. If the magnetic field in the plasma that is dragged in the vertical direction by the flow is parallel to the loop, the phenomenon of vortex shedding causes the appearance of a quasi-periodic horizontal force that is applied to alternating sides of the loop. The period of the force is determined by the flow speed and the loop's minor radius. The oscillations are excited the most effectively when the force is in resonance with the natural frequency of the kink oscillations. This model can explain the selectivity of the excitation of the oscillations and the initial growth of the oscillation amplitude.

### **"Coronal Waves and Oscillations"** **Review**

Valery M. [Nakariakov](#) and Erwin Verwichte

<http://www.livingreviews.org/lrsp-2005-3>

Wave and oscillatory activity of the solar corona is confidently observed with modern imaging and spectral instruments in the visible light, EUV, X-ray and radio bands, and interpreted in terms of magnetohydrodynamic (MHD) wave theory. The **review** reflects the current trends in the observational study of coronal waves and oscillations (standing kink, sausage and longitudinal modes, propagating slow waves and fast wave trains, the search for torsional waves), theoretical modelling of interaction of MHD waves with plasma structures, and implementation of the theoretical results for the mode identification. Also the use of MHD waves for remote diagnostics of coronal plasma - MHD coronal seismology - is discussed and the applicability of this method for the estimation of coronal magnetic field, transport coefficients, fine structuring and heating function is demonstrated.

### **The Large-scale Coronal Structure of the 2017 August 21 Great American Eclipse: An Assessment of Solar Surface Flux Transport Model Enabled Predictions and Observations**

Dibyendu [Nandy](#)<sup>1,2</sup>, Prantika Bhowmik<sup>1</sup>, Anthony R. Yeates<sup>3</sup>, Suman Panda<sup>1,2</sup>, Rajashik Tarafder<sup>1</sup>, and Soumyaranjan Dash<sup>1</sup>

2018 ApJ 853 72

[10.3847/1538-4357/aaa1eb](https://doi.org/10.3847/1538-4357/aaa1eb)

On 2017 August 21, a total solar eclipse swept across the contiguous United States, providing excellent opportunities for diagnostics of the Sun's corona. The Sun's coronal structure is notoriously difficult to observe except during solar eclipses; thus, theoretical models must be relied upon for inferring the underlying magnetic structure of the Sun's outer atmosphere. These models are necessary for understanding the role of magnetic fields in



the heating of the corona to a million degrees and the generation of severe space weather. Here we present a methodology for predicting the structure of the coronal field based on model forward runs of a solar surface flux transport model, whose predicted surface field is utilized to extrapolate future coronal magnetic field structures. This prescription was applied to the 2017 August 21 solar eclipse. A post-eclipse analysis shows good agreement between model simulated and observed coronal structures and their locations on the limb. We demonstrate that slow changes in the Sun's surface magnetic field distribution driven by long-term flux emergence and its evolution governs large-scale coronal structures with a (plausibly cycle-phase dependent) dynamical memory timescale on the order of a few solar rotations, opening up the possibility for large-scale, global corona predictions at least a month in advance.

### **A Prediction of the Coronal Structure of the 21 August 2017 Great American Solar Eclipse**

Dibyendu [Nandy](#), [Prantika Bhowmik](#), [Anthony R. Yeates](#), [Suman Panda](#), [Rajashik Tarafder](#), [Soumyaranjan Dash](#)

ApJL 2017

<https://arxiv.org/pdf/1708.05996.pdf>

In what is being dubbed as the great American solar eclipse, on 21 August 2017, a total solar eclipse will sweep across the continental United States. Given the path of the eclipse and the length of totality available for eclipse observations, this eclipse will offer unprecedented opportunities for observations of the Sun's coronal structure and diagnostics of the coronal magnetic field. The Sun's coronal magnetic field is notoriously difficult to constrain and theoretical computational models must be relied upon for gaining insight on the coronal structure. Well-constrained solar coronal field models are crucial for understanding the origin of, and predicting solar storms that generate severe space weather. Here we present a technique for predicting and inferring the structure of the coronal field based on a data driven solar surface flux transport model which is forward run to 21 August 2017 to predict the Sun's surface field distribution. The predicted solar surface field is subsequently used as input in a potential field source surface model to generate the coronal structure during the imminent solar eclipse. Our results -- which can be verified during the 21 August 2017 eclipse observations -- indicate the presence of two helmet streamers, one each in the eastern and western limb on the southern solar hemisphere and significant radial open-flux at the poles indicating the accumulation of unipolar, polar fields in the build-up to the minimum of sunspot cycle 24. The South (open) polar flux appears to be stronger indicating an asymmetric sunspot cycle 25 with stronger activity in the southern hemisphere. The CESSI prediction of the coronal field expected during the 21 August, 2017 great American solar eclipse, accompanying images and data is available at the CESSI prediction website: [this http URL](#)

### **Calibration of Spectropolarimetry channel of Visible Emission Line Coronagraph onboard Aditya-L1**

[Venkata Suresh Narra](#), [K. Sasikumar Raja](#), [Raghavendra Prasad B](#), [Jagdev Singh](#), [Shalabh Mishra](#), [Sanal Krishnan V U](#), [Bhavana Hegde S](#), [Utkarsha D.](#), [Natarajan V](#), [Pawan Kumar S](#), [Muthu Priyal V](#), [Savarimuthu P](#), [Priya Gavshinde](#), [Umesh Kamath P](#)

Journal of Experimental Astronomy 2024

<https://arxiv.org/pdf/2409.12793>

The magnetic field strength and its topology play an important role in understanding the formation, evolution, and dynamics of the solar corona. Also, it plays a significant role in addressing long-standing mysteries such as coronal heating problem, origin and propagation of coronal mass ejections, drivers of space weather, origin and acceleration of solar wind, and so on. Despite having photospheric magnetograms for decades, we do not have reliable observations of coronal magnetic field strengths today. To measure the coronal magnetic field precisely, the spectropolarimetry channel of the Visible Emission Line Coronagraph (VELC) on board the Aditya-L1 mission is designed. Using the observations of coronal emission line Fe XIII [10747 Å], it is possible to generate full Stokes maps (I, Q, U, and V) that help in estimating the Line-of-Sight (LOS) magnetic field strength and to derive the magnetic field topology maps of solar corona in the Field of View (FOV) (1.05 -- 1.5-R<sub>☉</sub>). In this article, we summarize the instrumental details of the spectropolarimetry channel and detailed calibration procedures adopted to derive the modulation and demodulation matrices. Furthermore, we have applied the derived demodulation matrices to the observed data in the laboratory and studied their performance.

### **Magnetic field topology from non-force free extrapolation and magnetohydrodynamic simulation of its eventual dynamics**

Sushree S. [Nayak](#), [R. Bhattacharyya](#), [A. Prasad](#), [Qiang Hu](#)

Proc. IAU Symp. 340. 2018

<https://arxiv.org/pdf/1804.04814.pdf>

Magnetic reconnections (MRs) for various magnetic field line (MFL) topologies are believed to be the initiators of various solar eruptive events like flares and coronal mass ejections (CMEs). Consequently, important is a thorough understanding and quantification of the MFL topology and their evolution which leads to MRs. Contemporary standard is to extrapolate the coronal MFLs using equilibrium models where the Lorentz force on the coronal

plasma is zero everywhere, because either there is no current or the current is parallel to the magnetic field. In tandem, a non-force-free-field (NFFF) extrapolation scheme has evolved and allows for a Lorentz force which is non-zero only at the photosphere but asymptotically vanishes with height. The paper reports magnetohydrodynamic (MHD)- simulations initiated by NFFF extrapolation of the coronal MFLs for the active region NOAA 11158. Interestingly, quasi-separatrix layers (QSLs) which facilitate MRs are detected in the extrapolated MFLs. The AR 11158 is flare producing and, the paper makes an attempt to assess the role of QSLs in the flare onsets. **15th February, 2011**

## **Evolution Of Downflows In The Transition Region Above A Sunspot Over Short Time-Scales**

[C. J. Nelson](#), [S. Krishna Prasad](#), [M. Mathioudakis](#)

A&A 640, A120 2020

<https://arxiv.org/pdf/2006.13617.pdf>

<https://www.aanda.org/articles/aa/pdf/2020/08/aa38155-20.pdf>

Downflows with high velocities occur in the transition region above many sunspots; however, how these signatures evolve over short time-scales in both spatial and spectral terms is still unknown. In this article, we investigate the evolution of downflows detected within the transition region on time-scales of the order minutes and search for clues as to their formation mechanisms in co-temporal imaging data. The high-resolution spectral and imaging data used to identify downflows here were sampled by IRIS on the **20th and 21st May 2015**. Imaging data from the Hinode and SDO satellites provided context about the wider solar atmosphere. Four downflows were identified and analysed. The potential super-sonic components of these downflows had widths of around 2" and evolved over time-scales of the order minutes. The measured apparent downflow velocities were structured both in time and space, with the highest apparent velocities occurring above a bright region detected in Si IV 1400 Å images. Downflows with apparent velocities below 50 km s<sup>-1</sup> were observed to extend a few arcsecs away from the foot-points suggesting the potential super-sonic components are linked to larger-scale flows. The electron density and mass flux for these events were within the ranges 10<sup>9.6</sup>-10<sup>10.2</sup> cm<sup>-3</sup> and 10<sup>-6.81</sup>-10<sup>-7.48</sup> g cm<sup>-2</sup> s<sup>-1</sup>, respectively. Each downflow formed at the foot-point of thin 'fingers' extending out around 3-5" in Si IV 1400 Å data with smaller widths (<1") than the super-sonic downflows. Downflows can appear, disappear, and recur within time-scales of less than one hour in sunspots. As potential super-sonic downflow signatures were detected at the foot-points of both extended fingers in Si IV 1400 Å SJI data and sub-sonic downflows in Si IV 1394 Å spectra, it is likely that these events are linked to flows within structures such as coronal loops.

## **Evolution Of Super-Sonic Downflows In A Sunspot**

[C. J. Nelson](#), [S. Krishna Prasad](#), [M. Mathioudakis](#)

A&A 636, A35 2020

<https://arxiv.org/pdf/2003.02489.pdf>

<https://www.aanda.org/articles/aa/pdf/2020/04/aa37357-19.pdf>

Super-sonic downflows have been observed in transition region spectra above numerous sunspots; however, little research has been conducted to date into how persistent these signatures are within sunspots on time-scales longer than a few hours. Here, we analyse the lead sunspot of AR 12526 to infer the properties and evolution of super-sonic downflows occurring within it. Sixteen large, dense raster scans sampled by IRIS are analysed. These rasters tracked the lead sunspot of AR 12526 at discrete times between the 27th March 2016 and the 2nd April 2016. One sit-and-stare observation acquired on the 1st April 2016 is also studied in order to analyse the evolution of super-sonic downflows on shorter time-scales. Super-sonic downflows are variable within this sunspot both in terms of spatial structuring and velocities. 13 of the 16 raster scans display some evidence of super-sonic downflows in the Si IV 1394 Å line co-spatial to a sustained bright structure detected in the 1400 Å slit-jaw imaging channel, with a peak velocity of 112 km s<sup>-1</sup> being recorded on the 29th March 2016. Evidence for super-sonic downflows in the O IV 1401 Å line was found in 14 of these rasters, with the spatial structuring differing from that inferred from the Si IV 1394 Å line. In the sit-and-stare data, no dual flow is initially detected, however, a super-sonic downflow does develop after 60 minutes. This downflow accelerates from 73 km s<sup>-1</sup> to close to 80 km s<sup>-1</sup> in both the Si IV 1394 Å and O IV 1401 Å lines over the course of 20 minutes before the end of the observation. The morphology of these downflows evolved over the course of both hours and days and was often different in the Si IV 1394 Å and O IV 1401 Å lines. These events were found co-spatial to a bright region in the core of the Si IV 1394 Å line which appeared to form at the foot-points of coronal fan loops. **2016.03.27-04.02**

## **The formation of small-scale umbral brightenings in sunspot atmospheres**

[C. J. Nelson](#), [V. M. J. Henriques](#), [M. Mathioudakis](#), [F. P. Keenan](#)

A&A 605, A14 2017

<https://arxiv.org/pdf/1705.05617.pdf>

Sunspot atmospheres are highly inhomogeneous hosting both quasi-stable and transient features, such as 'umbral micro-jets' and dark fibril-like events. We seek to understand the morphological properties and formation

mechanisms of small-scale umbral brightenings (SSUBs; analogous to umbral micro-jets) and to understand whether links between these events and short dynamic fibrils, umbral flashes, and umbral dots can be established. An SST filtergram time-series sampling the Ca II H line and a CRISP full-Stokes 15-point Ca II 8542 Å line scan dataset were used. The average lifetime and lengths of 54 SSUBs identified in the sunspot umbra are found to be 44.2 seconds ( $\sigma=20$  seconds) and 0.56" ( $\sigma=0.14$ "). The spatial positioning and morphological evolution of these events was investigated finding no evidence of parabolic or ballistic profiles nor a preference for co-spatial formation with umbral flashes. The presence of Stokes V profile reversals provided evidence that these events could form through the development of shocks in the chromosphere. The application of the weak-field approximation indicated that changes in the line-of-sight magnetic field were not responsible for the modifications to the line profile and suggested that thermodynamic effects are the actual cause of the increased emission. Finally, a sub-set of SSUBs were observed to form at the foot-points of short dynamic fibrils. Overall, we found no correlation between the spatial locations where these events were observed and the occurrence of umbral dots and umbral flashes. SSUBs, however, have lifetimes and spectral signatures comparable to umbral flashes and are located at the footpoints of short dynamic fibrils, during or at the end of the red-shifted stage. It is possible, therefore, that these features form due to the shocking of fibrillar material in the lower atmosphere upon its return under gravity.

28th July 2014

## **Analytical Three-dimensional Magnetohydrostatic Equilibrium Solutions for Magnetic Field Extrapolation Allowing a Transition from Non-force-free to Force-free Magnetic Fields**

Thomas [Neukirch](#), [Thomas Wiegmann](#)

Solar Phys. **294**, Article number: 171 **2019**

<https://arxiv.org/pdf/1911.11084.pdf>

<https://link.springer.com/content/pdf/10.1007/s11207-019-1561-0.pdf>

For the extrapolation of magnetic fields into the solar corona from measurements taken in the photosphere (or chromosphere) force-free magnetic fields are typically used. This does not take into account that the lower layers of the solar atmosphere are not force-free. While some numerical extrapolation methods using magnetohydrostatic magnetic fields have been suggested, a complementary and numerically comparatively cheap method is to use analytical magnetohydrostatic equilibria to extrapolate the magnetic field. In this paper, we present a new family of solutions for a special class of analytical three-dimensional magnetohydrostatic equilibria, which can be of use for such magnetic field extrapolation. The new solutions allow for the more flexible modelling of a transition from non-force-free to (linear) force-free magnetic fields. In particular, the height and width of the region where this transition takes place can be specified by choosing appropriate model parameters.

## **On solutions of the PFSS model with GONG synoptic maps for 2006-2018**

L. [Nikolić](#)

Space Weather [Volume17, Issue8](#) Pages 1293-1311 **2019**

[sci-hub.se/10.1029/2019SW002205](https://sci-hub.se/10.1029/2019SW002205)

The potential-field source-surface (PFSS) model is widely used to derive the magnetic field of the solar corona. The only free parameter in the PFSS model is the radius of the so-called source-surface, where magnetic field lines are forced to open. The radius of this surface is typically set to 2.5 solar radii in research and operational PFSS numerical models. Here, using Global Oscillation Network Group (GONG) synoptic maps of the photospheric field, solutions of the PFSS model for various heights of the source-surface are investigated for 2006-2018. In particular, numerically derived open solar magnetic flux and coronal holes are examined. Solutions of the PFSS model based on GONG synoptic maps are particularly important since they are often used to drive operational space weather forecast models. Comparisons between observations and numerical results in this paper suggest that the radius of the source-surface is significantly lower than 2.5 solar radii during the active phase of solar cycle 24. The fact that the source-surface location depends on the solar activity, suggests that relations which associate solar wind properties with the coronal magnetic field in the PFSS based solar wind modes should be revisited. Furthermore, although the correction of the polar magnetic field is part of GONG synoptic map production pipeline, the results suggest that better treatment of polar fields is needed to cover observational gaps. The issue with the polar fields in GONG maps is particularly pronounced in recent years.

## **Coronal Partings**

Igor F. [Nikulin](#)

**2015**

<http://arxiv.org/ftp/arxiv/papers/1506/1506.01423.pdf>

The basic observational properties of the 'coronal partings'--the special type of the coronal magnetic structures, identified by a comparison of the coronal X-ray images and solar magnetograms--are considered. They represent channels inside the unipolar large-scale magnetic fields, formed by the rows of magnetic arcs directed to the neighboring fields of opposite polarity. The most important characteristics of the partings are revealed. It is found

that--from the evolutionary and spatial point of view--the partings can transform to the coronal holes and visa versa. The classes of global, intersecting, and complex partings are identified.

### **Simulating White-Light Images of Coronal Structures for Parker Solar Probe/WISPR: Study of the Total Brightness Profiles**

Giuseppe [Nisticò](#), [Volker Bothmer](#), [Angelos Vourlidas](#), [Paulett Liewer](#), [Arnaud Thernisien](#), [Guillermo Stenborg](#), [Russell Howard](#)

Solar Phys. 2020

<https://arxiv.org/pdf/2004.05447.pdf>

The Wide-field Imager for Parker Solar Probe (WISPR) captures unprecedented white-light images of the solar corona and inner heliosphere. Thanks to the uniqueness of Parker Solar Probe's (PSP) orbit, WISPR is able to image "locally" coronal structures at high spatial and time resolutions. The observed plane of sky, however, rapidly changes because of the PSP's high orbital speed. Therefore, the interpretation of the dynamics of the coronal structures recorded by WISPR is not straightforward. A first study, undertaken by [Liewer2019](#), shows how different coronal features (e.g., streamers, flux ropes) appear in the field of view of WISPR by means of raytracing simulations. In particular, they analyze the effects of the spatial resolution changes on both the images and the associated height-time maps, and introduce the fundamentals for geometric triangulation. In this follow-up paper, we focus on the study of the total brightness of a simple, spherical, plasma density structure, to understand how the analysis of Thomson-scattered emission by the electrons in a coronal feature can shed light into the determination of its kinematic properties. We investigate two cases: (a) a density sphere at a constant distance from the Sun for different heliographic longitudes; (b) a density sphere moving outwardly with constant speed. The study allows us to characterize the effects of the varying heliocentric distance of the observer and scattering angle on the total brightness observed, which we exploit to contribute to a better determination of the position and speed of the coronal features observed by WISPR. **2018-11-08**

### **North-South asymmetry in the magnetic deflection of polar coronal hole jets**

[Nisticò G.](#), [Zimbaro G.](#), [Patsourakos S.](#), [Bothmer V.](#), [Nakariakov V. M.](#)

A&A 2015

[http://www2.warwick.ac.uk/fac/sci/physics/research/cfsa/people/nistico/publications/paper\\_ns\\_asymmetry.pdf](http://www2.warwick.ac.uk/fac/sci/physics/research/cfsa/people/nistico/publications/paper_ns_asymmetry.pdf)

Context. Measurements of the magnetic field in the interplanetary medium, of the sunspots area, and of the heliospheric current sheet position, reveal a possible North-South asymmetry in the magnetic field of the Sun. This asymmetry could cause the bending of the heliospheric current sheet of the order of 5--10 deg in the southward direction, and it appears to be a recurrent characteristic of the Sun during the minima of solar activity.

Aims. We study the North-South asymmetry as inferred from measurements of the deflection of polar coronal hole jets when they propagate throughout the corona.

Methods. Since the corona is an environment where the magnetic pressure is greater than the kinetic pressure ( $\beta \ll 1$ ), we can assume that magnetic field controls the dynamics of plasma. On average, jets during their propagation follow the magnetic field lines, highlighting its local direction. The average jet deflection is studied both in the plane perpendicular to the line of sight, and, for a reduced number of jets, in three dimensional space. The observed jet deflection is studied in terms of an axisymmetric magnetic field model comprising dipole ( $g_1$ ), quadrupole ( $g_2$ ), and esapole ( $g_3$ ) moments.

Results. We measured the position angles at  $1 R_{\odot}$  and at  $2 R_{\odot}$  of the 79 jets from the catalogue of [Nistico09](#), based on the STEREO ultraviolet and white-light coronagraph observations during the solar minimum period March 2007-April 2008. We found that the propagation is not radial, in agreement with the deflection due to magnetic field lines. Moreover, the amount of the deflection is different between jets over the north and those from the south pole. Comparison of jet deflections and field line tracing shows that a ratio  $g_2/g_1 \approx -0.5$  for the quadrupole and a ratio  $g_3/g_1 \approx 1.6-2.0$  for the esapole can describe the field. The presence of a non-negligible quadrupole moment confirms the North-South asymmetry of the solar magnetic field for the considered period.

Conclusions. We find that the magnetic deflection of jets is larger in the North than in the South of the order of 25-40%, with an asymmetry which is consistent with a southward deflection of the heliospheric current sheet of the order of 10 deg, consistent with that inferred from other, independent, datasets and instruments. **2007-06-07**

### **Data-Constrained Solar Modeling with GX Simulator**

[Gelu M. Nita](#), [Gregory D. Fleishman](#), [Alexey A. Kuznetsov](#), [Sergey A. Anfinogentov](#), [Alexey G. Stupishin](#), [Eduard P. Kontar](#), [Samuel J. Schonfeld](#), [James A. Klimchuk](#), [Dale E. Gary](#)

ApJ 2023

<https://arxiv.org/pdf/2301.00795.pdf>

To facilitate the study of solar active regions and flaring loops, we have created a modeling framework, the freely distributed GX Simulator IDL package, that combines 3D magnetic and plasma structures with thermal and non-thermal models of the chromosphere, transition region, and corona. The package has integrated tools to visualize the model data cubes, compute multi-wavelength emission maps from them, and quantitatively compare the resulting

maps with observations. Its object-based modular architecture, which runs on Windows, Mac, and Unix/Linux platforms, offers capabilities that include the ability to either import 3D density and temperature distribution models, or to assign numerically defined coronal or chromospheric temperatures and densities, or their distributions to each individual voxel. The application integrates FORTRAN and C++ libraries for fast calculation of radio emission (free-free, gyroresonance, and gyrosynchrotron emission) along with soft and hard X-ray and EUV codes developed in IDL. To facilitate the creation of models, we have developed a fully automatic model production pipeline that downloads the required SDO/HMI vector magnetic field data and (optionally) the contextual SDO/AIA images, performs potential or nonlinear force free field extrapolations, populates the magnetic field skeleton with parameterized heated plasma coronal models that assume either steady-state or impulsive plasma heating, and generates non-LTE density and temperature distribution models of the chromosphere that are constrained by photospheric measurements. The standardized models produced by this pipeline may be further customized through a set of interactive tools provided by the graphical user interface. Here we describe the GX Simulator framework and its applications.

## **Dressing the Coronal Magnetic Extrapolations of Active Regions with a Parameterized Thermal Structure**

Gelu M. [Nita](#)<sup>1</sup>, Nicholeen M. Viall<sup>2</sup>, James A. Klimchuk<sup>2</sup>, Maria A. Loukitcheva<sup>1,3</sup>, Dale E. Gary<sup>1</sup>, Alexey A. Kuznetsov<sup>4</sup>, and Gregory D. Fleishman

2018 ApJ 853 66 [10.3847/1538-4357/aaa4bf](https://doi.org/10.3847/1538-4357/aaa4bf)

<http://sci-hub.tw/10.3847/1538-4357/aaa4bf>

The study of time-dependent solar active region (AR) morphology and its relation to eruptive events requires analysis of imaging data obtained in multiple wavelength domains with differing spatial and time resolution, ideally in combination with 3D physical models. To facilitate this goal, we have undertaken a major enhancement of our IDL-based simulation tool, GX\_Simulator, previously developed for modeling microwave and X-ray emission from flaring loops, to allow it to simulate quiescent emission from solar ARs. The framework includes new tools for building the atmospheric model and enhanced routines for calculating emission that include new wavelengths. In this paper, we use our upgraded tool to model and analyze an AR and compare the synthetic emission maps with observations. We conclude that the modeled magneto-thermal structure is a reasonably good approximation of the real one. **23-May-2010**

**CESRA Highlight** #1798 **2018** <http://cesra.net/?p=1798>

## **A COMPARISON OF SOLAR OPEN FIELD REGIONS FOUND BY TYPE III RADIO BURSTS AND THE POTENTIAL FIELD SOURCE SURFACE MODEL**

Nariaki V. [Nitta](#) and Marc L. DeRosa

<http://www.journals.uchicago.edu/doi/pdf/10.1086/527548>

For heliophysics research and applications, the potential field source surface (PFSS) model is often employed to extrapolate the photospheric magnetic field to the corona. In an attempt to evaluate the performance of the PFSS model, we compare the computed footpoints of the heliospheric magnetic field with the locations of flares associated with type III radio bursts, which are a good indicator of open field lines that extend to interplanetary space. **Consistent with past experiences, the agreement is not satisfactory.** We discuss possible reasons for the discrepancy, including the model's inadequacy to reproduce the coronal magnetic field above evolving active regions and the lack of a simultaneous full-surface magnetic map. It is argued that the performance of the PFSS model needs to be quantified further against solar observations, including type III bursts, before it is applied to heliospheric models.

## **Small-scale magnetic flux emergence preceding a chain of energetic solar atmospheric events**

D. [Nobrega-Siverio](#), I. Cabello, S. Bose, L. H. M. Rouppe van der Voort,

R. Joshi, C. Froment, V. M. J. Henriques

A&A **2024**

<https://arxiv.org/pdf/2403.11652>

Advancements in instrumentation have revealed a multitude of small-scale EUV events in the solar atmosphere. Our aim is to employ high-resolution magnetograms to gain a detailed understanding of the magnetic origin of such phenomena. We have used coordinated observations from SST, IRIS, and SDO to analyze an ephemeral magnetic flux emergence episode and the following chain of small-scale energetic events. These unique observations clearly link these phenomena together. The high-resolution (0."057/pixel) magnetograms obtained with SST/CRISP allows us to reliably measure the magnetic field at the photosphere and detect the emerging bipole that causes the subsequent eruptive atmospheric events. Notably, this small-scale emergence episode remains indiscernible in the

lower resolution SDO/HMI magnetograms (0."5/pixel). We report the appearance of a dark bubble in Ca II K related to the emerging bipole, a sign of the canonical expanding magnetic dome predicted in flux emergence simulations. Evidences of reconnection are also found: first through an Ellerman bomb, and later by the launch of a surge next to a UV burst. The UV burst exhibits a weak EUV counterpart in the coronal SDO/AIA channels. By calculating DEM, its plasma is shown to reach a temperature beyond 1 MK and have densities between the upper chromosphere and transition region. Our study showcases the importance of high-resolution magnetograms to unveil the mechanisms triggering phenomena such as EBs, UV bursts, and surges. This could hold implications for small-scale events akin to those recently reported in EUV using Solar Orbiter. The finding of temperatures beyond 1 MK in the UV burst plasma strongly suggests that we are examining analogous features. Therefore, we signal caution regarding drawing conclusions from full-disk magnetograms that lack the necessary resolution to reveal their true magnetic origin.

### **Chromospheric polarimetry through multi-line observations of the 850 nm spectral region III: Chromospheric jets driven by twisted magnetic fields**

C. Quintero [Noda](#), [H. Iijima](#), [Y. Katsukawa](#), [T. Shimizu](#), [M. Carlsson](#), [J. de la Cruz Rodríguez](#), [B. Ruiz Cobo](#), [D. Orozco Suárez](#), [T. Oba](#), [T. Anan](#), [M. Kubo](#), [Y. Kawabata](#), [K. Ichimoto](#), [Y. Suematsu](#)

MNRAS **2019**

<https://arxiv.org/pdf/1904.09151.pdf>

We investigate the diagnostic potential of the spectral lines at 850 nm for understanding the magnetism of the lower atmosphere. For that purpose, we use a newly developed 3D simulation of a chromospheric jet to check the sensitivity of the spectral lines to this phenomenon as well as our ability to infer the atmospheric information through spectropolarimetric inversions of noisy synthetic data. We start comparing the benefits of inverting the entire spectrum at 850 nm versus only the Ca II 8542 Å spectral line. We found a better match of the input atmosphere for the former case, mainly at lower heights. However, the results at higher layers were not accurate. After several tests, we determined that we need to weight more the chromospheric lines than the photospheric ones in the computation of the goodness of the fit. The new inversion configuration allows us to obtain better fits and consequently more accurate physical parameters. Therefore, to extract the most from multi-line inversions, a proper set of weights needs to be estimated. Besides that, we conclude again that the lines at 850 nm, or a similar arrangement with Ca II 8542 Å plus Zeeman sensitive photospheric lines, poses the best observing configuration for examining the thermal and magnetic properties of the lower solar atmosphere.

### **Study of the polarization produced by the Zeeman effect in the solar Mg I b lines**

C. Quintero [Noda](#), [H. Uitenbroek](#), [M. Carlsson](#), [D. Orozco Suárez](#), [Y. Katsukawa](#), [T. Shimizu](#), [B. Ruiz Cobo](#), [M. Kubo](#), [T. Oba](#), [Y. Kawabata](#), [T. Hasegawa](#), [K. Ichimoto](#), [T. Anan](#), [Y. Suematsu](#)

MNRAS **2018**

<https://arxiv.org/pdf/1810.01067.pdf>

The next generation of solar observatories aim to understand the magnetism of the solar chromosphere. Therefore, it is crucial to understand the polarimetric signatures of chromospheric spectral lines. For this purpose, we here examine the suitability of the three Fraunhofer Mg I b1, b2, and b4 lines at 5183.6, 5172.7, and 5167.3 Å, respectively. We start by describing a simplified atomic model of only 6 levels and 3 line transitions for computing the atomic populations of the 3p-4s (multiplet number 2) levels involved in the Mg I b line transitions assuming non-local thermodynamic conditions and considering only the Zeeman effect using the field-free approximation. We test this simplified atom against more complex ones finding that, although there are differences in the computed profiles, they are small compared with the advantages provided by the simple atom in terms of speed and robustness. After comparing the three Mg I lines, we conclude that the most capable one is the b2 line as b1 forms at similar heights and always show weaker polarization signals while b4 is severely blended with photospheric lines. We also compare Mg I b2 with the K I D1 and Ca II 8542 Å lines finding that the former is sensitive to the atmospheric parameters at heights that are in between those covered by the latter two lines. This makes Mg I b2 an excellent candidate for future multi-line observations that aim to seamlessly infer the thermal and magnetic properties of different features in the lower solar atmosphere.

### **Analysis of a spatially deconvolved solar pore**

C. Quintero [Noda](#), [T. Shimizu](#), [B. Ruiz Cobo](#), [Y. Suematsu](#), [Y. Katsukawa](#), [K. Ichimoto](#)

MNRAS **2016**

<http://arxiv.org/pdf/1605.01796v1.pdf>

Solar pores are active regions with large magnetic field strengths and apparent simple magnetic configurations. Their properties resemble the ones found for the sunspot umbra although pores do not show penumbra. Therefore, solar pores present themselves as an intriguing phenomenon that is not completely understood. We examine in this work a solar pore observed with Hinode/SP using two state of the art techniques. The first one is the spatial deconvolution of the spectropolarimetric data that allows removing the stray light contamination induced by the spatial point spread function of the telescope. The second one is the inversion of the Stokes profiles assuming local

thermodynamic equilibrium that let us to infer the atmospheric physical parameters. After applying these techniques, we found that the spatial deconvolution method does not introduce artefacts, even at the edges of the magnetic structure, where large horizontal gradients are detected on the atmospheric parameters. Moreover, we also describe the physical properties of the magnetic structure at different heights finding that, in the inner part of the solar pore, the temperature is lower than outside, the magnetic field strength is larger than 2 kG and unipolar, and the LOS velocity is almost null. At neighbouring pixels, we found low magnetic field strengths of same polarity and strong downward motions that only occur at the low photosphere, below the continuum optical depth  $\log\tau=-1$ . Finally, we studied the spatial relation between different atmospheric parameters at different heights corroborating the physical properties described before.

## **Spatial deconvolution of spectropolarimetric data: an application to quiet Sun magnetic elements**

C. Quintero [Noda](#), A. Asensio Ramos, D. Orozco Suárez, B. Ruiz Cobo

A&A 579, A3 2015

<http://arxiv.org/pdf/1505.03219v1.pdf>

Observations of the Sun from the Earth are always limited by the presence of the atmosphere, which strongly disturbs the images. A solution to this problem is to place the telescopes in space satellites, which produce observations without any (or limited) atmospheric aberrations. However, even though the images from space are not affected by atmospheric seeing, the optical properties of the instruments still limit the observations. In the case of diffraction limited observations, the PSF establishes the maximum allowed spatial resolution, defined as the distance between two nearby structures that can be properly distinguished. In addition, the shape of the PSF induce a dispersion of the light from different parts of the image, leading to what is commonly termed as stray light or dispersed light. This effect produces that light observed in a spatial location at the focal plane is a combination of the light emitted in the object at relatively distant spatial locations. We aim to correct the effect produced by the telescope's PSF using a deconvolution method, and we decided to apply the code on Hinode/SP quiet Sun observations. We analyze the validity of the deconvolution process with noisy data and we infer the physical properties of quiet Sun magnetic elements after the deconvolution process. **April 21th, 2007**

## **Coronal voids and their magnetic nature**

J. D. Nölke<sup>1</sup>, S. K. Solanki<sup>1</sup>, J. Hirzberger<sup>1</sup>, H. Peter<sup>1</sup>, L. P. Chitta<sup>1</sup>, F. Kahil<sup>1</sup> <sup>+++</sup>

A&A 678, A196 (2023)

<https://www.aanda.org/articles/aa/pdf/2023/10/aa46040-23.pdf>

<https://arxiv.org/pdf/2309.09789.pdf>

Context. Extreme ultraviolet (EUV) observations of the quiet solar atmosphere reveal extended regions of weak emission compared to the ambient quiescent corona. The magnetic nature of these coronal features is not well understood.

Aims. We study the magnetic properties of the weakly emitting extended regions, which we name coronal voids. In particular, we aim to understand whether these voids result from a reduced heat input into the corona or if they are associated with mainly unipolar and possibly open magnetic fields, similar to coronal holes.

Methods. We defined the coronal voids via an intensity threshold of 75% of the mean quiet-Sun (QS) EUV intensity observed by the high-resolution EUV channel (HRIEUV) of the Extreme Ultraviolet Imager on Solar Orbiter. The line-of-sight magnetograms of the same solar region recorded by the High Resolution Telescope of the Polarimetric and Helioseismic Imager allowed us to compare the photospheric magnetic field beneath the coronal voids with that in other parts of the QS.

Results. The coronal voids studied here range in size from a few granules to a few supergranules and on average exhibit a reduced intensity of 67% of the mean value of the entire field of view. The magnetic flux density in the photosphere below the voids is 76% (or more) lower than in the surrounding QS. Specifically, the coronal voids show much weaker or no network structures. The detected flux imbalances fall in the range of imbalances found in QS areas of the same size.

Conclusions. We conclude that coronal voids form because of locally reduced heating of the corona due to reduced magnetic flux density in the photosphere. This makes them a distinct class of (dark) structure, different from coronal holes. **2021 February 23**

## **Characterizing the Umbral Magnetic Knots of $\delta$ -Sunspots**

[A. A. Norton](#), [P. J. Levens](#), [K. J. Knizhnik](#), [M. G. Linton](#), [Y. Liu](#)

ApJ 938 117 2022

<https://arxiv.org/pdf/2209.09381.pdf>

<https://iopscience.iop.org/article/10.3847/1538-4357/ac8eb2/pdf>

Delta ( $\delta$ )-spots are active regions (ARs) in which positive and negative umbrae share a penumbra. They are known to be the source of strong flares. We introduce a new quantity, the degree of  $\delta$  ( $Do\delta$ ), to measure the fraction of umbral flux participating in the  $\delta$ -configuration and to isolate the dynamics of the magnetic knot, i.e. adjacent umbrae in the  $\delta$ -configuration. Using Helioseismic and Magnetic Imager data, we analyze 19  $\delta$ -spots and 11  $\beta$ -spots in detail, and 120  $\delta$ -spots in less detail. We find that  $\delta$ -regions are not in a  $\delta$ -configuration for the entire time but spend 55% of their observed time as  $\delta$ -spots with an average, maximum  $Do\delta$  of 72%. Compared to  $\beta$ -spots,  $\delta$ -spots have  $2.6\times$  the maximum umbral flux,  $1.9\times$  the flux emergence rate,  $2.6\times$  the rotation, and  $72\times$  the flare energy. On average, the magnetic knots rotate  $17^\circ \text{ day}^{-1}$  while the  $\beta$ -spots rotate  $2^\circ \text{ day}^{-1}$ . Approximately 72% of the magnetic knots present anti-Hale or anti-Joy tilts, contrasting starkly with only 9% of the  $\beta$ -spots. A positive correlation exists between  $\phi Do\delta$  and the flare energy emitted by that region. The  $\delta$ -spots obey the hemispheric current helicity rule 64% of the time. 84% of the  $\delta$ -spots are formed by single flux emergence events and 58% have a quadrupolar magnetic configuration. The  $\delta$ -spot characteristics are consistent with the formation mechanism signatures as follows: 42% with the kink instability or Sigma effect, 32% with multi-segment buoyancy, 16% with collisions and two active regions that are unclassified but consistent with a rising O-ring.

## Oscillations observed in Umbra, Plage, Quiet-Sun and the Polarity Inversion Line of Active Region 11158 using HMI/SDO Data

[A. A. Norton](#), [R. B. Stutz](#), [B. T. Welsch](#)

Philosophical Transactions of the Royal Society A, **2021**, 379, 2190

<https://arxiv.org/pdf/2101.01349.pdf>

Using data from the Helioseismic Magnetic Imager, we report on the amplitudes and phase relations of oscillations in quiet-Sun, plage, umbra and the polarity inversion line (PIL) of an active region NOAA#11158. We employ Fourier, wavelet and cross correlation spectra analysis. Waves with 5-minute periods are observed in umbra, PIL and plage with common phase values of  $\phi(v,I)=\pi/2$ ,  $\phi(v,B_{los})=-\pi/2$ . In addition,  $\phi(I,B_{los})=\pi$  in plage are observed. These phase values are consistent with slow standing or fast standing surface sausage wave modes. The line width variations, and their phase relations with intensity and magnetic oscillations, show different values within the plage and PIL regions, which may offer a way to further differentiate wave mode mechanics. Significant Doppler velocity oscillations are present along the PIL, meaning that plasma motion is perpendicular to the magnetic field lines, a signature of Alfvénic waves. A time-distance diagram along a section of the PIL shows Eastward propagating Doppler oscillations converting into magnetic oscillations; the propagation speeds range between 2–6 km s<sup>-1</sup>. Lastly, a 3-minute wave is observed in select regions of the umbra in the magnetogram data. **16 February 2011**

## Magnetic Flux Emergence and Decay Rates for Preceder and Follower Sunspots Observed with HMI

A. A. [Norton](#), E. H. Jones, M. G. Linton, J. E. Leake

ApJ **842** 3 **2017**

<https://arxiv.org/pdf/1705.02053.pdf>

We quantify the emergence and decay rates of preceder (p) and follower (f) sunspots within ten active regions from 2010–2014 using Space-weather Helioseismic Magnetic Imager Active Region Patch data. The sunspots are small- to mid-sized regions and contain a signed flux within a single polarity sunspot of  $(1.1\text{--}6.5)\times 10^{21}$  Mx. The net unsigned flux within the regions, including plage, ranges from  $(5.1\text{--}20)\times 10^{21}$  Mx. Rates are calculated with and without intensity contours to differentiate between sunspot formation and flux emergence. Signed flux emergence rates, calculated with intensity contours, for the p (f) spots average  $6.8$  ( $4.9$ )  $\times 10^{19}$  Mx h<sup>-1</sup>, while decay rates are  $-1.9$  ( $-3.4$ )  $\times 10^{19}$  Mx h<sup>-1</sup>. The mean, signed flux emergence rate of the regions, including plage, is  $7.1 \times 10^{19}$  Mx h<sup>-1</sup> for a mean peak flux of  $5.9 \times 10^{21}$  Mx. Using a synthesis of these results and others reported previously, there is a clear trend for larger flux regions to emerge faster than smaller ones. Observed emergence rates ( $d\phi/dt$ , Mx h<sup>-1</sup>) scale with total signed peak flux,  $\phi_{\text{max}}$ , as a power law with an exponent of 0.36, i.e.,  $d\phi/dt = A\phi_{\text{max}}^{0.36}$ . The observed rates may assist in constraining the boundary and initial conditions in simulations which already demonstrate increased rates for flux tubes with higher buoyancy and twist, or in the presence of a strong upflow. Overall, the observed emergence rates are smaller than those in simulations, which may indicate a slower rise of the flux in the interior than captured in simulations.

HMI Science Nuggets #70 2017 <http://hmi.stanford.edu/hminuggets/?p=1863>

See <https://arxiv.org/pdf/1711.08383.pdf>, by Sun and Norton, Research Notes of the AAS, **1**, 24, **2017**.

## The Biggest Sunspots Produced by Cycle 24

Aimee A. [Norton](#)

HMI Science Nuggets, No. 3, Jan 2014



<http://hmi.stanford.edu/hminuggets/?p=381>

Even though Solar Cycle 24 is weak, it has still produced some large sunspots. **We list the largest sunspots** as observed by HMI and discuss some aspects of the data.

### **Relating photometric and magnetic properties of structures at solar surface**

[V.N. Obridko](#), [D.D. Sokoloff](#), [M.K. Katsova](#)

Journal of Atmospheric and Solar-Terrestrial Physics .2023

<https://arxiv.org/pdf/2310.10748.pdf>

We investigate sharp structures visible in solar magnetic field tracers. It is shown that the sunspot magnetic boundaries do not coincide with the photometric ones. Moreover, there is no clear boundary of the magnetic field in the vicinity of sunspots. Thus, the widely accepted concept of magnetic tubes with sharp edges is not always correct and should be used with caution. It is also shown that even in the moments of complete absence of visible spots on the Sun, there are magnetic fields over 800 Gauss. The nature of these strong magnetic fields remains unclear; they may originate at relatively small depths under the photosphere.

### **Some comments on the matching of photometric and magnetic properties of structures at the solar surface**

[V.N. Obridko](#), [D.D. Sokoloff](#), [M.M. Katsova](#)

Proceedings of the Fifteenth Workshop "Solar Influences on the Magnetosphere, Ionosphere and Atmosphere", Primorsko, Bulgaria, June 2023

<https://arxiv.org/ftp/arxiv/papers/2309/2309.10883.pdf>

We investigate sharply outlined features recorded in solar magnetic field tracers. It is shown that the magnetic boundaries of a sunspot do not coincide with the photometric ones. Moreover, there is no clear magnetic boundary around sunspots. Thus, the widely accepted concept of a magnetic tube with clearly pronounced borders is not always correct and should be used with caution. It is also shown that even in the periods of complete absence of visible spots on the Sun, there are magnetic fields over 800 Gauss. The nature of these strong magnetic fields remains unclear; they may originate at relatively small depths under the photosphere.

### **Clarifying Physical Properties of Magnetic Fields in Sunspots**

[V.N. Obridko](#), [M.M. Katsova](#), [D.D. Sokoloff](#), [B.D. Shelting](#), [I.M. Livshits](#)

Solar Phys. 297, Article number: 131 2022

<https://arxiv.org/pdf/2209.14423.pdf>

<https://doi.org/10.1007/s11207-022-02066-6>

We demonstrate that the radial magnetic-field component at the outer boundary of the sunspot penumbra is about 550 Mx cm<sup>-2</sup> independent of the sunspot area and the maximum magnetic field in the umbra. The mean magnetic-field intensity in sunspots grows slightly as the sunspot area increases up to 500 -- 1000 millionth of visual hemisphere (m.v.h.) and may reach about 900 -- 2000 Mx cm<sup>-2</sup>. The total magnetic flux weakly depends on the maximum field strength in a sunspot and is determined by the spottedness, i.e. the sunspot number and the total sunspot area; however, the relation between the total flux and the sunspot area is substantially nonlinear. We suggest an explicit parametrization for this relation. The contribution of the magnetic flux associated with sunspots to the total magnetic flux is small, not achieving more than 20% even at the maximum of the solar activity.

### **Some Statistical Properties of Magnetic Fields and Sunspots**

V. N. [Obridko](#) and B. D. Shelting

2018 Res. Notes AAS 2 40

We are going to answer the following questions:

- Does the field at the penumbra boundary depend on the spot area or does some universal value exist?
- Does the field at the penumbra boundary depend on the maximum field in the spot umbra or does some universal value exist?

### **Longitude variations of solar magnetic fields of different intensity in cycle 23 as inferred from the SOHO/MDI data**

V. N. [Obridko](#) and V. E. Chertoprud

Astronomy Letters, Volume 37, Number 5, 358-366, 2011

SOHO/MDI magnetograms have been used to analyze the longitude distribution of the squared solar magnetic field  $\langle B^2 \rangle$  in the activity cycle no. 23. The energy of the magnetic field ( $\langle B^2 \rangle$ ) is shown to change with longitude.

However, these variations hardly fit the concept of active longitudes. In the epochs of high solar activity, one can readily see a relationship between longitude variations of the medium-strong ( $|B| > 50$  G or  $|B| > 100$  G) and relatively weak ( $|B| \leq 50$  G or  $|B| \leq 100$  G) fields at all latitudes. In other periods, this relationship is revealed mainly at the latitudes not higher than 30°. The background fields ( $|B| \leq 25$  G) also display longitude variations, which are,

however, not related to those of the strong fields. This makes us think that the fields of solar activity are rather inclusions to the general field than the source of the latter.

### **Three-dimensional multi-fluid model of a coronal streamer belt with a tilted magnetic dipole**

L. **Ofman**, E. Provornikova, L. Abbo, and S. Giordano

Ann. Geophys., 33, 47-53, **2015**

<http://www.ann-geophys.net/33/47/2015/angeo-33-47-2015.html>

Observations of streamers in extreme ultraviolet (EUV) emission with SOHO/UVCS show dramatic differences in line profiles and latitudinal variations in heavy ion emission compared to hydrogen Ly- $\alpha$  emission. In order to use ion emission observations of streamers as the diagnostics of the slow solar wind properties, an adequate model of a streamer including heavy ions is required. We extended a previous 2.5-D multi-species magnetohydrodynamics (MHD) model of a coronal streamer to 3-D spherical geometry, and in the first approach we consider a tilted dipole configuration of the solar magnetic field. The aim of the present study is to test the 3-D results by comparing to previous 2.5-D model result for a 3-D case with moderate departure from azimuthal symmetry. The model includes O5+ ions with preferential empirical heating and allows for calculation of their density, velocity and temperature in coronal streamers. We present the first results of our 3-D multi-fluid model showing the parameters of protons, electrons and heavy ions (O5+) at the steady-state solar corona with a tilted steamer belt. We find that the 3-D results are in qualitative agreement with our previous 2.5-D model, and show longitudinal variation in the variables in accordance with the tilted streamer belt structure. Properties of heavy coronal ions obtained from the 3-D model together with EUV spectroscopic observations of streamers will help understanding the 3-D structures of streamers reducing line-of-sight integration ambiguities and identifying the sources of the slow solar wind in the lower corona. This leads to improved understanding of the physics of the slow solar wind.

### **Super-strong Magnetic Field in Sunspots**

Takenori J. **Okamoto**, **Takashi Sakurai**

**2018** ApJL 852 L16

<https://arxiv.org/pdf/1712.08700.pdf>

<http://sci-hub.tw/10.3847/2041-8213/aaa3d8>

Sunspots are the most notable structure on the solar surface with strong magnetic fields. The field is generally strongest in a dark area (umbra), but sometimes stronger fields are found in non-dark regions such as a penumbra and a light bridge. The formation mechanism of such strong fields outside umbrae is still puzzling. Here we report clear evidence of the magnetic field of 6,250 G, which is the strongest field among Stokes I profiles with clear Zeeman splitting ever observed on the Sun. The field was almost parallel to the solar surface and located in a bright region sandwiched by two opposite-polarity umbrae. Using a time series of spectral datasets, we discussed the formation process of the super-strong field and suggested that this strong field region was generated as a result of compression of one umbra pushed by the horizontal flow from the other umbra, like the subduction of the Earth's crust in plate tectonics. **2014 February 4-6**

### **HMI as “Coronagraph”?**

Juan-Carlos Martínez **Oliveros**

HMI Science Nuggets #9, March **2014**

<http://hmi.stanford.edu/hminuggets/?p=560>

Reports of white-light ejecta above the limb of the Sun and imaged without the aid of a true coronagraph are exceedingly rare. Here we report the successful use of HMI to observe flare effects in the corona by the use of differencing as a substitute for an actual occulter.

### **Solar Atmospheric Magnetic Energy Coupling: Broad Plasma Conditions and Temperature Scales**

N. Brice **Orange**, David L. Chesny, **Bruce Gendre**, **David C. Morris**, **Hakeem M. Oluseyi**

**2016**

<http://arxiv.org/pdf/1601.02986v1.pdf>

Solar variability investigations that include its magnetic energy coupling are paramount to solving many key solar/stellar physics problems. Particularly understanding the temporal variability of magnetic energy redistribution and heating processes. Using three years of observations from the Solar Dynamics Observatory's Atmospheric Imaging Assembly and Helioseismic Magnetic Imager, radiative and magnetic fluxes were measured from coronal hole, quiet Sun, active regions, active region cores (i.e., inter moss), and at full-disk scales, respectively. We present, and mathematically describe, their coupling of radiative fluxes, across broad temperature gradients, to the available photospheric magnetic energy. A comparison of the common linear relationship of radiative to magnetic coupling is

performed against our extended broken power-law description, which reveals a potential entanglement of thermodynamic and magnetic energy contributions in existing literature. As such, our work provides an improved approach to describing magnetic energy redistribution processes of gross feature classes, including both the large scale open and closed field corona. A general solar atmospheric model is presented that centers on an observationally derived self-similar central engine of the large scale closed field corona, with possible extension to the cooler atmospheric layers ( $\log T \leq 6.0$ ) of open field structures. Finally, this work indicates stellar X-ray observations could populate radiation distributions in currently limited and/or undetectable spectral ranges, as well as hold potential for investigations of currently unresolved stellar disk gross feature classes.

## **OBSERVATIONS OF AN ENERGETICALLY ISOLATED QUIET SUN TRANSIENT: EVIDENCE OF QUASI-STEADY CORONAL HEATING**

N. Brice [Orange](#)<sup>1,2</sup>, David L. Chesny<sup>1,3</sup>, and Hakeem M. Oluseyi

2015 ApJ 810 98

Increasing evidence for coronal heating contributions from cooler solar atmospheric layers, notably quiet Sun (QS) conditions, challenges standard solar atmospheric descriptions of bright transition region (TR) emission. As such, questions about the role of dynamic QS transients in contributing to the total coronal energy budget are raised. Using observations from the Atmospheric Imaging Assembly and Helioseismic Magnetic Imager on board the Solar Dynamics Observatory, and numerical model extrapolations of coronal magnetic fields, we investigate a dynamic QS transient that is energetically isolated to the TR and extrudes from a common footpoint shared with two heated loop arcades. A non-causal relationship is established between episodic heating of the QS transient and widespread magnetic field re-organization events, while evidence is found favoring a magnetic topology that is typical of eruptive processes. Quasi-steady interchange reconnection events are implicated as a source of the transient's visibly bright radiative signature. We consider the QS transient's temporally stable ( $\approx 35$  minutes) radiative nature to occur as a result of the large-scale magnetic field geometries of the QS and/or relatively quiet nature of the magnetic photosphere, which possibly act to inhibit energetic build-up processes that are required to initiate a catastrophic eruption phase. This work provides insight into the QS's thermodynamic and magnetic relation to eruptive processes that quasi-steadily heat a small-scale dynamic and TR transient. This work explores arguments of non-negligible coronal heating contributions from cool atmospheric layers in QS conditions and contributes evidence to the notion that solar wind mass feeds off of dynamic transients therein.

## **Emergence of Granular-sized Magnetic Bubbles through the Solar Atmosphere.**

### **I. Spectropolarimetric Observations and Simulations**

Ada [Ortiz](#)<sup>1</sup>, Luis R. Bellot Rubio<sup>2</sup>, Viggo H. Hansteen<sup>1</sup>, Jaime de la Cruz Rodríguez<sup>3,4</sup>, and Luc Rouppe van der Voort

2014 ApJ 781 126

We study a granular-sized magnetic flux emergence event that occurred in NOAA 11024 in 2009 July. The observations were made with the CRISP spectropolarimeter at the Swedish 1 m Solar Telescope achieving a spatial resolution of  $0.''14$ . Simultaneous full Stokes observations of the two photospheric Fe I lines at 630.2 nm and the chromospheric Ca II 854.2 nm line allow us to describe in detail the emergence process across the solar atmosphere. We report here on three-dimensional (3D) semi-spherical bubble events, where instead of simple magnetic footpoints, we observe complex semi-circular feet straddling a few granules. Several phenomena occur simultaneously, namely, abnormal granulation, separation of opposite-polarity legs, and brightenings at chromospheric heights. However, the most characteristic signature in these events is the observation of a dark bubble in filtergrams taken in the wings of the Ca II 854.2 nm line. There is a clear coincidence between the emergence of horizontal magnetic field patches and the formation of the dark bubble. We can infer how the bubble rises through the solar atmosphere as we see it progressing from the wings to the core of Ca II 854.2 nm. In the photosphere, the magnetic bubble shows mean upward Doppler velocities of  $2 \text{ km s}^{-1}$  and expands at a horizontal speed of  $4 \text{ km s}^{-1}$ . In about 3.5 minutes it travels some 1100 km to reach the mid chromosphere, implying an average ascent speed of  $5.2 \text{ km s}^{-1}$ . The maximum separation attained by the magnetic legs is  $6.''6$ . From an inversion of the observed Stokes spectra with the SIR code, we find maximum photospheric field strengths of 480 G and inclinations of nearly  $90^\circ$  in the magnetic bubble interior, along with temperature deficits of up to 250 K at  $\log \tau = -2$  and above. To aid the interpretation of the observations, we carry out 3D numerical simulations of the evolution of a horizontal, untwisted magnetic flux sheet injected in the convection zone, using the Bifrost code. The computational domain spans from the upper convection zone to the lower corona. In the modeled chromosphere, the rising flux sheet produces a large, cool, magnetized bubble. We compare this bubble with the observed ones and find excellent agreement, including similar field strengths and velocity signals in the photosphere and chromosphere, temperature deficits, ascent speeds, expansion velocities, and lifetimes.

## **Automatic Detection of Magnetic delta in Sunspot Groups**

Sreejith [Padinhatteeri](#), Paul A. Higgins, D. Shaun Bloomfield, Peter T. Gallagher

Solar Phys. January 2016, Volume 291, Issue 1, pp 41-53

<http://arxiv.org/pdf/1510.06413v1.pdf>

Large and magnetically complex sunspot groups are known to be associated with flares. To date, the Mount Wilson scheme has been used to classify sunspot groups based on their morphological and magnetic properties. The most flare prolific class, the delta sunspot-group, is characterised by opposite polarity umbrae within a common penumbra, separated by less than 2 degrees. In this article, we present a new system, called the Solar Monitor Active Region Tracker - Delta Finder (SMART-DF), that can be used to automatically detect and classify magnetic deltas in near-realtime. Using continuum images and magnetograms from the Helioseismic and Magnetic Imager (HMI) onboard NASA's Solar Dynamics Observatory (SDO), we first estimate distances between opposite polarity umbrae. Opposite polarity pairs having distances of less than 2 degrees are then identified, and if these pairs are found to share a common penumbra, they are identified as a magnetic delta configuration. The algorithm was compared to manual delta detections reported by the Space Weather Prediction Center (SWPC), operated by the National Oceanic and Atmospheric Administration (NOAA). SMART-DF detected 21 out of 23 active regions (ARs) that were marked as delta spots by NOAA during 2011 - 2012 (within +/- 60 degrees longitude). SMART-DF in addition detected five ARs which were not announced as delta spots by NOAA. The near-realtime operation of SMART-DF resulted in many deltas being identified in advance of NOAA's daily notification. SMART-DF will be integrated with SolarMonitor ([www.solarmonitor.org](http://www.solarmonitor.org)) and the near-realtime information will be available to the public.

2011-09-27, 2012-03-09, 2013-10-11, 2014-10-20

## Impact of Anomalous Active Regions on the Large-scale Magnetic Field of the Sun

[Shaonwita Pal](#), [Prantika Bhowmik](#), [Sushant S. Mahajan](#), [Dibyendu Nandy](#)

ApJ 2023

<https://arxiv.org/pdf/2305.13145.pdf>

One of the major sources of perturbation in the solar cycle amplitude is believed to be the emergence of anomalous active regions which do not obey Hale's polarity law and Joy's law of tilt angles. Anomalous regions containing high magnetic flux that disproportionately impact the polar field are sometimes referred to as "rogue regions". In this study -- utilizing a surface flux transport model -- we analyze the large-scale dipole moment build-up due to the emergence of anomalous active regions on the solar surface. Although these active regions comprise a small fraction of the total sunspot number, they can substantially influence the magnetic dipole moment build-up and subsequent solar cycle amplitude. Our numerical simulations demonstrate that the impact of "Anti-Joy" regions on the solar cycle is similar to those of "Anti-Hale" regions. We also find that the emergence time, emergence latitude, relative number and flux distribution of anomalous regions influence the large-scale magnetic field dynamics in diverse ways. We establish that the results of our numerical study are consistent with the algebraic (analytic) approach to explaining the Sun's dipole moment evolution. Our results are relevant for understanding how anomalous active regions modulate the Sun's large-scale dipole moment build-up and its reversal timing within the framework of the Babcock-Leighton dynamo mechanism -- now believed to be the primary source of solar cycle variations.

## Large-scale Magnetic Funnels in the Solar Corona

Olga [Panasenco](#)<sup>1</sup>, Marco Velli<sup>2</sup>, and Aram Panasenco

2019 ApJ 873 25

<https://doi.org/10.3847/1538-4357/ab017c>

We describe open coronal magnetic fields with a specific geometry—large-scale coronal magnetic funnels—that are found to play an important role in coronal dynamics. Coronal magnetic funnels can be attributed to three main factors: (i) the presence of pseudostreamer(s), (ii) the presence of filament channels, and (iii) the presence of active regions in the close vicinity of a pseudostreamer. The geometry of magnetic funnels displays a strongly nonmonotonic expansion below  $2 R_{\odot}$ . We present a detailed study of a funnel arising from a double pseudostreamer near the equator, formed between a triplet of coronal holes of the same polarity. By following the evolution of these coronal holes we find that the pseudostreamer and, therefore, funnel topology, changes when two coronal holes have merged together. The funnel geometry of the open magnetic field becomes smoother, with a monotonic expansion factor, after this merging. The presence of magnetic funnels is indirectly confirmed by the appearance of coronal cloud prominences in the solar corona, typically in the 304 Å passband, as a result of colder plasma debris falling back toward the Sun in the wake of eruptions in the surrounding atmosphere. The coronal clouds appear suspended at heights of 1.2–1.3  $R_{\odot}$ , coinciding with the region of strongest gradients in the magnetic field. By studying the evolution of funnel open magnetic fields over several solar rotations we find a direct relation between the presence of coronal clouds high in the solar corona and the coincident existence of funnel magnetic fields below them.

## Sunspot simulations: penumbra formation and the fluting instability

[Mayukh Panja](#), [Robert Cameron](#), [Sami K. Solanki](#)

2021 ApJ 907 102

<https://arxiv.org/pdf/2011.11447.pdf>  
<https://doi.org/10.3847/1538-4357/abccbf>

The fluting instability has been suggested as the driver of the subsurface structure of sunspot flux tubes. We conducted a series of numerical experiments where we used flux tubes with different initial curvatures to study the effect of the fluting instability on the subsurface structure of spots. We used the MURaM code, which has previously been used to simulate complete sunspots, to first compute four sunspots in the slab geometry and then two complete circular spots of opposite polarities. We find that the curvature of a flux tube indeed determines the degree of fluting the flux tube will undergo - the more curved a flux tube is, the more fluted it becomes. In addition, sunspots with strong curvature have strong horizontal fields at the surface and therefore readily form penumbral filaments. The fluted sunspots eventually break up from below, with lightbridges appearing at the surface several hours after fluting commences.

## **Flows and Waves in Braided Solar Coronal Magnetic Structures**

V **Pant**, A Datta, Dipankar Banerjee

ApJ Letters **2015**

<http://arxiv.org/pdf/1501.06507v1.pdf>

We study the high frequency dynamics in the braided magnetic structure of an active region (AR 11520) moss as observed by High-Resolution Coronal Imager (Hi-C). We detect quasi periodic flows and waves in these structures. We search for high frequency dynamics while looking at power maps of the observed region. We find that shorter periodicities (30 - 60 s) are associated with small spatial scales which can be resolved by Hi-C only. We detect quasi periodic flows with wide range of velocities from 13 - 185 km/s associated with braided regions. This can be interpreted as plasma outflows from reconnection sites. We also find presence of short period and large amplitude transverse oscillations associated with braided magnetic region. Such oscillations could be triggered by reconnection or such oscillation may trigger reconnection. **11 July 2012**

## **On Solar Recurrent Coronal Jets: Coronal Geysers as Sources of Electron Beams and Interplanetary Type-III Radio Bursts**

Alin Razvan **Paraschiv** and Alina Donea

**2019** ApJ 873 110

<https://doi.org/10.3847/1538-4357/ab04a6>

Coronal jets are transitory small-scale eruptions that are omnipresent in solar observations. Active regions jets produce significant perturbations on the ambient solar atmosphere and are believed to be generated by microflare reconnection. Multiple sets of recurrent jets are identified in extreme-ultraviolet filter imaging. In this work we analyze the long timescale recurrence of coronal jets originating from a unique footpoint structure observed in the lower corona. We report the detection of penumbral magnetic structures in the lower corona. These structures, which we call "coronal geysers," persist through multiple reconnection events that trigger recurrent jets in a quasi-periodical trend. Recurrent jet eruptions have been associated with Type-III radio bursts that are manifestations of traveling non-thermal electron beams. We examine the assumed link, as the coronal sources of interplanetary Type-III bursts are still open for debate. We scrutinized the hypothesized association by temporally correlating a statistically significant sample of six Geysers structures that released at least 50 recurrent jets, with correspondent Type-III radio bursts detected in the interplanetary medium. Data analysis of these phenomena provides new information on small-scale reconnection, non-thermal electron beam acceleration, and energy release. We find that the penumbral Geysers-like flaring structures produce recurring jets. They can be long-lived, quasi-stable, and act as coronal sources for Type-III bursts, and, implicitly, upward accelerated electron beams.

## **Testing magnetic helicity conservation in a solar-like active event**

E. **Pariat**, G. Valori, P. Démoulin, K. Dalmasse

A&A 580, A128 **2015**

<http://arxiv.org/pdf/1506.09013v1.pdf>

Magnetic helicity has the remarkable property of being a conserved quantity of ideal magnetohydrodynamics (MHD). Therefore, it could be used as an effective tracer of the magnetic field evolution of magnetized plasmas. Theoretical estimations indicate that magnetic helicity is also essentially conserved with non-ideal MHD processes, e.g. magnetic reconnection. This conjecture has however been barely tested, either experimentally or numerically. Thanks to recent advances in magnetic helicity estimation methods, it is now possible to test numerically its dissipation level in general three-dimensional datasets. We first revisit the general formulation of the temporal variation of relative magnetic helicity on a fully bounded volume when no hypothesis on the gauge are made. We introduce a method to precisely estimate its dissipation independently of the type of non-ideal MHD processes occurring. In a solar-like eruptive event simulation, using different gauges, we compare its estimation in a finite volume with its time-integrated flux through the boundaries, hence testing the conservation and dissipation of helicity. We provide an upper bound of the real dissipation of magnetic helicity: It is quasi-null during the quasi-ideal MHD phase. Even when magnetic reconnection is acting the relative dissipation of magnetic helicity is also

very small ( $<2.2\%$ ), in particular compared to the relative dissipation of magnetic energy ( $>30$  times larger). We finally illustrate how the helicity-flux terms involving velocity components are gauge dependent, hence limiting their physical meaning.

### **Estimation of the squashing degree within a three-dimensional domain**

E. **Pariat** and P. Démoulin

A&A 541, A78 (2012)

Context. The study of the magnetic topology of magnetic fields aims at determining the key sites for the development of magnetic reconnection. Quasi-separatrix layers (QSLs), regions of strong connectivity gradients, are topological structures where intense electric currents preferentially build-up, and where, later on, magnetic reconnection occurs.

Aims. QSLs are volumes of intense squashing degree,  $Q$ ; the field-line invariant quantifying the deformation of elementary flux tubes. QSL are complex and thin three-dimensional (3D) structures difficult to visualize directly. Therefore  $Q$  maps, i.e. 2D cuts of the 3D magnetic domain, are a more and more common features used to study QSLs.

Methods. We analyze several methods to derive 2D  $Q$  maps and discuss their analytical and numerical properties. These methods can also be used to compute  $Q$  within the 3D domain.

Results. We demonstrate that while analytically equivalent, the numerical implementation of these methods can be significantly different. We derive the analytical formula and the best numerical methodology that should be used to compute  $Q$  inside the 3D domain. We illustrate this method with two twisted magnetic configurations: a theoretical case and a non-linear force free configuration derived from observations.

Conclusions. The representation of QSL through 2D planar cuts is an efficient procedure to derive the geometry of these structures and to relate them with other quantities, e.g. electric currents and plasma flows. It will enforce a more direct comparison of the role of QSL in magnetic reconnection.

### **Examining the Source Regions of Solar Energetic Particles Using an AI-generated Synchronic Potential Field Source Surface Model**

Jinhye **Park**<sup>1</sup>, Hyun-Jin Jeong<sup>1</sup>, and Yong-Jae Moon<sup>1,2</sup>

2023 ApJ 953 159

<https://iopscience.iop.org/article/10.3847/1538-4357/acdd00/pdf>

We study the source regions of six solar energetic particle (SEP) events accelerated near or behind the limbs of the Sun. We use AI-generated farside magnetograms at a near real-time basis developed by Jeong et al. and AIHMI-PFSS extrapolations up to  $2.5R_{\odot}$  computed using the input of the synchronic data combining AI-generated farside and HMI magnetograms. By comparing the AIHMI, HMI, Global Oscillations Network Group (GONG) synoptic magnetograms, and Air force Data Assimilative Photospheric flux Transport synchronic magnetograms, as well as the PFSS extrapolations, we find interesting differences between them in view of SEP source regions and magnetic field configurations. First, the structures and sizes of the source active regions (ARs) are changed. The total unsigned magnetic field fluxes of the ARs are mostly stronger in the AIHMI than in the HMI and GONG magnetograms. Second, newly emerging ARs are observed in the SEP source regions in the AIHMI magnetograms for two events. Third, the alterations in the magnetic flux, the emergence, and the dissipation of ARs lead to modifications in the locations of the global polarity inversion lines (PILs). The EUV wave propagation is typically observed to be oriented nearly perpendicular with respect to the local PIL, suggesting that the AIHMI-PFSS extrapolations around the source region are more realistic. This study shows that the continuous farside evolution of AR magnetic fields, which is accomplished by our AI synchronic magnetograms, can lead to an improved understanding of SEP source ARs. **20110921, 20110922, 20120927, 20130305, 20130621, 20140106**

**Table 1.** The Associated Solar Activities for the Six SEP Events, the SEP Onset Times, and the Peak Times

### **De-noising SDO/HMI Solar Magnetograms by Image Translation Method Based on Deep Learning**

Eunsu **Park**<sup>1,2</sup>, Yong-Jae Moon<sup>1,2</sup>, Daye Lim<sup>1,2</sup>, and Harim Lee<sup>1</sup>

2020 ApJL 891 L4

<https://doi.org/10.3847/2041-8213/ab74d2>

In astronomy, long-exposure observations are one of the important ways to improve signal-to-noise ratios (S/Ns). In this Letter, we apply a deep-learning model to de-noise solar magnetograms. This model is based on a deep convolutional generative adversarial network with a conditional loss for image-to-image translation from a single magnetogram (input) to a stacked magnetogram (target). For the input magnetogram, we use Solar Dynamics Observatory (SDO)/Helioseismic and Magnetic Imager (HMI) line-of-sight magnetograms at the center of the solar disk. For the target magnetogram, we make 21-frame-stacked magnetograms, taking into account solar rotation at the same position. We train a model using 7004 pairs of the input and target magnetograms from 2013 January to

2013 October. We then validate the model using 707 pairs from 2013 November and test the model using 736 pairs from 2013 December. Our results from this study are as follows. First, our model successfully de-noises SDO/HMI magnetograms, and the de-noised magnetograms from our model are mostly consistent with the target magnetograms. Second, the average noise level of the de-noised magnetograms is greatly reduced from 8.66 to 3.21 G, and it is consistent with that of the target magnetograms, 3.21 G. Third, the average pixel-to-pixel correlation coefficient value increases from 0.88 (input) to 0.94 (de-noised), which means that the de-noised magnetograms are more consistent with the target ones than the input ones. Our results can be applied to many scientific fields in which the integration of many frames (or long-exposure observations) are used to improve the S/N.

## **RATES OF PHOTOSPHERIC MAGNETIC FLUX CANCELLATION MEASURED WITH HINODE**

Soyoung [Park](#)<sup>1</sup>, Jongchul Chae<sup>1</sup>, and Yuri E. Litvinenko<sup>2</sup>

Astrophysical Journal, 704:L71–L74, 2009 October

Photospheric magnetic flux cancellation on the Sun is generally believed to be caused by magnetic reconnection occurring in the low solar atmosphere. Individual canceling magnetic features are observationally characterized by the rate of flux cancellation. The specific cancellation rate, defined as the rate of flux cancellation divided by the interface length, gives an accurate estimate of the electric field in the reconnecting current sheet. We have determined the specific cancellation rate using the magnetograms taken by the Solar Optical Telescope (SOT) aboard the *Hinode* satellite. The specific rates determined with SOT turned out to be systematically higher than those based on the data taken by the Michelson Doppler Imager (MDI) aboard the *Solar and Heliospheric Observatory*. The median value of the specific cancellation rate was found to be  $8.4 \times 10^6 \text{ G cm s}^{-1}$ —a value four times that obtained from the MDI data. This big difference is mainly due to a higher angular resolution and better sensitivity of the SOT, resulting in magnetic fluxes up to five times larger than those obtained from the MDI. The higher rates of flux cancellation correspond to either faster inflows or stronger magnetic fields of the reconnection inflow region, which may have important consequences for the physics of photospheric magnetic reconnection.

## **Is Magnetic Topology Important for Heating the Solar Atmosphere?**

**Review**

C. E. [Parnell](#), J. E. H. Stevenson, J. Threlfall, S. J. Edwards

Article submitted to Royal Society 2015

<http://arxiv.org/pdf/1505.05701v1.pdf>

Magnetic fields permeate the entire solar atmosphere weaving an extremely complex pattern on both local and global scales. In order to understand the nature of this tangled web of magnetic fields, its magnetic skeleton, which forms the boundaries between topologically distinct flux domains, may be determined. The magnetic skeleton consists of null points, separatrix surfaces, spines and separators. The skeleton is often used to clearly visualize key elements of the magnetic configuration, but parts of the skeleton are also locations where currents and waves may collect and dissipate.

In this review, the nature of the magnetic skeleton on both global and local scales, over solar cycle time scales, is explained. The behaviour of wave pulses in the vicinity of both nulls and separators is discussed and so too is the formation of current layers and reconnection at the same features. Each of these processes leads to heating of the solar atmosphere, but collectively do they provide enough heat, spread over a wide enough area, to explain the energy losses throughout the solar atmosphere? Here, we consider this question for the three different solar regions: active regions, open-field regions and the quiet Sun.

We find that the heating of active regions and open-field regions is highly unlikely to be due to reconnection or wave dissipation at topological features, but it is possible that these may play a role in the heating of the quiet Sun. In active regions, the absence of a complex topology may play an important role in allowing large energies to build up and then, subsequently, be explosively released in the form of a solar flare. Additionally, knowledge of the intricate boundaries of open-field regions (which the magnetic skeleton provides) could be very important in determining the main acceleration mechanism(s) of the solar wind.

## **A POWER-LAW DISTRIBUTION OF SOLAR MAGNETIC FIELDS OVER MORE THAN FIVE DECADES IN FLUX**

C. E. [Parnell](#) et al 2009 ApJ 698 75-82, 2009 doi: [10.1088/0004-637X/698/1/75](https://doi.org/10.1088/0004-637X/698/1/75)

Solar flares, coronal mass ejections, and indeed phenomena on all scales observed on the Sun, are inextricably linked with the Sun's magnetic field. The solar surface is covered with magnetic features observed on many spatial scales, which evolve on differing timescales: the largest features, sunspots, follow an 11-year cycle; the smallest seem to follow no cycle. Here, we analyze magnetograms from Solar and Heliospheric Observatory (SOHO)/*Michelson Doppler Imager (full disk and high resolution)* and *Hinode/Solar Optical Telescope* to determine the fluxes of all currently observable surface magnetic features. We show that by using a "clumping"

algorithm, which counts a single "flux massif" as one feature, all feature fluxes, regardless of flux strength, follow the same distribution—a power law with slope  $-1.85 \pm 0.14$ —between  $2 \times 10^{17}$  and  $10^{23}$  Mx. A power law suggests that the mechanisms creating surface magnetic features are scale-free. This implies that either all surface magnetic features are generated by the same mechanism, or that they are dominated by surface processes (such as fragmentation, coalescence, and cancellation) in a way which leads to a scale-free distribution.

### **White-Light Coronal Imaging at the 21 August 2017 Total Solar Eclipse**

[Jay M. Pasachoff](#) & [Vojtech Rušin](#)

[Solar Physics](#) volume 297, Article number: 28 (2022)

<https://link.springer.com/content/pdf/10.1007/s11207-022-01964-z.pdf>

We describe the solar corona as imaged in the **21 August 2017** total solar eclipse from sites in Oregon and Illinois, USA separated by nearly one hour. Our composite images, each made from dozens of individual frames, show helmet streamers, nearly radially oriented narrow rays, and polar coronal holes filled with polar plumes. The Ludendorff flattening index of 0.24 is compared with measurements from the last two centuries. We discuss the most remarkable coronal dynamics detected over a nearly one-hour interval between the two observing sites.

### **Structure and Dynamics of the 13/14 November 2012 Eclipse White-Light Corona**

Jay M. [Pasachoff](#), Vojtech Rusin, Metod Saniga, Bryce A. Babcock, Muzhou Lu, Allen B. Davis, Ronald F. Dantowitz, Pavlos Gaintatzis, John H. Seiradakis, Aristeidis Voulgaris, Daniel B. Seaton, Kazuo Shiota  
**2014**

<http://arxiv.org/pdf/1412.1155v1.pdf>

Continuing our series of observations of the motion and dynamics of the solar corona over the solar-activity cycle, we observed the corona from sites in Queensland, Australia, during the 13 (UT)/14 (local time) November 2012 total solar eclipse. The corona took the low-ellipticity shape typical of solar maximum (flattening index  $\{\epsilon\} = 0.01$ ), showing a change from the composite coronal images that we had observed and analyzed in this journal and elsewhere for the 2006, 2008, 2009, and 2010 eclipses. After crossing the northeast Australian coast, the rest of the path of totality was over the ocean, so further totality was seen only by shipborne observers. Our results include measurements of velocities of a coronal mass ejection; during the 36 minutes of passage from the Queensland coast to a ship north of New Zealand, we find a speed of 413 km/s, and we analyze its dynamics. We discuss the shapes and positions of several types of coronal features seen on our higher-resolution composite Queensland images of the solar corona, including, many helmet streamers, very faint bright and dark loops at the base of helmet streamers, voids and radially oriented thin streamers. We compare our eclipse observations with a hairy-ball model of the magnetic field, confirming the validity of the prediction, and we relate the eclipse phenomenology seen with the near-simultaneous images from the Atmospheric Imaging Assembly on the NASA's Solar Dynamics Observatory (SDO/AIA), the Extreme Ultraviolet Imager on NASA's Solar Terrestrial Relations Observatory (STEREO/EUVI), ESA/ROB's PROBA2/SWAP, and NRL's LASCO on ESA's SOHO. For example, the southeastern CME is related to the solar flare whose origin we trace with a SWAP series of images.

### **Numerical simulations for MHD coronal seismology**

**REVIEW**

D. J. [Pascoe](#)

E-print, July **2014**; Research in Astronomy and Astrophysics, **2014** Vol. 14 No. 7, 805–830

<http://www.raa-journal.org/raa/index.php/raa/article/download/1839/1507>

Magnetohydrodynamic (MHD) processes are important for the transfer of energy over large scales in plasmas and so are essential to understanding most forms of dynamical activity in the solar atmosphere. The introduction of transverse structuring into models for the corona modifies the behavior of MHD waves through processes such as dispersion and mode coupling. Exploiting our understanding of MHD waves with the diagnostic tool of coronal seismology relies upon the development of sufficiently detailed models to account for all the features in observations. The development of realistic models appropriate for highly structured and dynamical plasmas is often beyond the domain of simple mathematical analysis and so numerical methods are employed. This paper reviews recent numerical results for seismology of the solar corona using MHD.

### **PROPAGATING COUPLED ALFVÉN AND KINK OSCILLATIONS IN AN ARBITRARY INHOMOGENEOUS CORONA**

D. J. [Pascoe](#), A. N. Wright and I. De Moortel

**2011** ApJ 731 73



Observations have revealed ubiquitous transverse velocity perturbation waves propagating in the solar corona. We perform three-dimensional numerical simulations of footpoint-driven transverse waves propagating in a low  $\beta$  plasma. We consider the cases of distorted cylindrical flux tubes and a randomly generated inhomogeneous medium. When density structuring is present, mode coupling in inhomogeneous regions leads to the coupling of the kink mode to the Alfvén mode. The decay of the propagating kink wave is observed as energy is transferred to the local Alfvén mode. In all cases considered, modest changes in density were capable of efficiently converting energy from the driving footpoint motion to localized Alfvén modes. We have demonstrated that mode coupling efficiently couples propagating kink perturbations to Alfvén modes in an arbitrary inhomogeneous medium. This has the consequence that transverse footpoint motions at the base of the corona will deposit energy to Alfvén modes in the corona.

## **A Chromatic Treatment of Linear Polarization in the Solar Corona at the 2023 Total Solar Eclipse**

Ritesh [Patel](#)<sup>1</sup>, Daniel B. Seaton<sup>1</sup>, Amir Caspi<sup>1</sup>, Sarah A. Kovac<sup>1</sup>, Sarah J. Davis <sup>+++</sup>

**2023** Res. Notes AAS 7 241

DOI 10.3847/2515-5172/ad0b0d

<https://iopscience.iop.org/article/10.3847/2515-5172/ad0b0d>

The broadband solar K-corona is linearly polarized due to Thomson scattering. Various strategies have been used to represent coronal polarization. Here, we present a new way to visualize the polarized corona, using observations from the **2023 April 20** total solar eclipse in Australia in support of the Citizen CATE 2024 project. We convert observations in the common four-polarizer orthogonal basis ( $0^\circ$ ,  $45^\circ$ ,  $90^\circ$ , &  $135^\circ$ ) to  $-60^\circ$ ,  $0^\circ$ , and  $+60^\circ$  (MZP) polarization, which is homologous to R, G, B color channels. The unique image generated provides some sense of how humans might visualize polarization if we could perceive it in the same way we perceive color.

## **Core and Wing Densities of Asymmetric Coronal Spectral Profiles: Implications for the Mass Supply of the Solar Corona**

S. [Patsourakos](#)<sup>1</sup>, J. A. Klimchuk<sup>2</sup>, and P. R. Young

**2014** ApJ 781 58

Recent solar spectroscopic observations have shown that coronal spectral lines can exhibit asymmetric profiles, with enhanced emissions at their blue wings. These asymmetries correspond to rapidly upflowing plasmas at speeds exceeding  $50 \text{ km s}^{-1}$ . Here, we perform a study of the density of the rapidly upflowing material and compare it with that of the line core that corresponds to the bulk of the plasma. For this task, we use spectroscopic observations of several active regions taken by the Extreme Ultraviolet Imaging Spectrometer of the Hinode mission. The density sensitive ratio of the Fe XIV lines at  $264.78$  and  $274.20 \text{ \AA}$  is used to determine wing and core densities. We compute the ratio of the blue wing density to the core density and find that most values are of order unity. This is consistent with the predictions for coronal nanoflares if most of the observed coronal mass is supplied by chromospheric evaporation driven by the nanoflares. However, much larger blue wing-to-core density ratios are predicted if most of the coronal mass is supplied by heated material ejected with type II spicules. Our measurements do not rule out a spicule origin for the blue wing emission, but they argue against spicules being a primary source of the hot plasma in the corona. We note that only about 40% of the pixels where line blends could be safely ignored have blue wing asymmetries in both Fe XIV lines. Anticipated sub-arcsecond spatial resolution spectroscopic observations in future missions could shed more light on the origin of blue, red, and mixed asymmetries.

## **Emerging Dimming as Coronal Heating Episodes**

Anna V. [Payne](#), [Xudong Sun](#)

ApJ **2021**

<https://arxiv.org/pdf/2103.09087.pdf>

Emerging dimming occurs in isolated solar active regions (ARs) during the early stages of magnetic flux emergence. Observed by the Atmospheric Imaging Assembly, it features a rapid decrease in extreme-ultraviolet (EUV) emission in the  $171 \text{ \AA}$  channel images, and a simultaneous increase in the  $211 \text{ \AA}$  images. Here, we analyze the coronal thermodynamic and magnetic properties to probe its physical origin. We calculate the time-dependent differential emission measure for a sample of 18 events between 2010 and 2012. The emission measure (EM) decrease in the temperature range  $5.7 \leq \log_{10} T \leq 5.9$  is well correlated with the EM increase in  $6.2 \leq \log_{10} T \leq 6.4$  over eight orders of magnitude. This suggests that the coronal plasma is being heated from the quiet-Sun, sub-MK temperature to 1-2 MK, more typical for ARs. Potential field extrapolation indicates significant change in the local magnetic connectivity: the dimming region is now linked to the newly emerged flux via longer loops. We conclude that emerging dimming is likely caused by coronal heating episodes, powered by reconnection between the emerging and the ambient magnetic fields. **11-12 Sep 2012**

**Table 1.** Thermodynamic properties of all 18 emerging dimming events analyzed in this work.

## **Statistical Comparison between Pores and Sunspots during the Time Interval 2010–2023**

Yang Peng<sup>1,2</sup>, Yu Fei<sup>3</sup>, Nan-bin Xiang<sup>4</sup>, Lin-hua Deng<sup>5</sup>, Ting-ting Xu<sup>5</sup>, Sheng Zheng<sup>6,7</sup>, Shu-guang Zeng<sup>6,7</sup>, Hai-yang Zhang<sup>5</sup>, and Shi-hu Liu<sup>5</sup>  
2024 ApJ 975 23

<https://iopscience.iop.org/article/10.3847/1538-4357/ad7858/pdf>

To reveal the physical properties of pores and sunspots varying with solar cycle, we carried out a statistical comparison among pores, transitional sunspots, and mature sunspots using Solar Dynamics Observatory/Helioseismic and Magnetic Imager from 2010 April to 2023 July. The OTSU method and region-growing algorithm were combined to detect umbrae of 11,876 sunspots covering solar cycles 24 and 25. The relationships between umbral area, continuum intensity (I), line-of-sight (LOS) magnetic field strength (B<sub>los</sub>), and line-of-sight velocity (V<sub>los</sub>) of umbrae were investigated in detail. The main conclusions are as follows. (1) The steepness between the total magnetic flux and total area of transitional sunspots appears to be flattened in each phase of the observed solar cycles, and does not have a significant variation over the solar cycle. (2) For three groups of sunspots, the umbral physical parameters' means and their correlations show only minor variations with the solar cycle, which are in error ranges. (3) As the mean umbral LOS magnetic field strength increases, the correlation of the umbral I–B<sub>los</sub> increases. The flattening of transitional sunspots in total area–total magnetic flux scatter is related to the evolution of sunspots itself, and may not correspond to the solar cycle. The umbral physical parameters and their correlations do not exhibit a discernible regularity over the solar cycle. Our analysis results contribute to a more comprehensive understanding of the dynamic processes of sunspot magnetic fields and give a new perspective on revealing the physical features of vertical magnetic flux tubes.

### The Decay of Two Adjacent Sunspots Associated with Moving Magnetic Features

Yang Peng<sup>1,2</sup>, Zhike Xue<sup>1,3</sup>, Zhongquan Qu<sup>1,2</sup>, Jincheng Wang<sup>1,3</sup>, Zhe Xu<sup>1,3</sup>, Liheng Yang<sup>1,3</sup>, and Yian Zhou<sup>1</sup>  
2024 ApJ 960 95

<https://iopscience.iop.org/article/10.3847/1538-4357/ad063e/pdf>

<https://arxiv.org/pdf/2401.03405.pdf>

The relationship between the decay of sunspots and moving magnetic features (MMFs) plays an important role in understanding the evolution of active regions. We present observations of two adjacent sunspots, the gap between them, and a lot of MMFs propagating from the gap and the sunspots' outer edges in NOAA Active Region 13023. The MMFs are divided into two types based on their magnetic field inclination angle: vertical ( $0^\circ < \gamma < 45^\circ$ ) and horizontal ( $45^\circ \leq \gamma < 90^\circ$ ) MMFs (V-MMFs and H-MMFs, respectively). The main results are as follows: (1) the mean magnetic flux decay rates of the two sunspots are  $-1.7 \times 10^{20}$  and  $-1.4 \times 10^{20}$  Mx day<sup>-1</sup>; (2) the magnetic flux generation rate of all MMFs is calculated to be  $-1.9 \times 10^{21}$  Mx day<sup>-1</sup>, which is on average 5.6 times higher than the total magnetic flux loss rate of the sunspots; (3) the magnetic flux of V-MMFs (including a pore separated from the sunspots) is 1.4 times larger than the total lost magnetic flux of the two sunspots, and in a later stage when the pore has passed through the reference ellipse, the magnetic flux generation rate of the V-MMFs is almost the same as the magnetic flux loss rate of the sunspots; and (4) within the gap, the magnetic flux of V-MMFs is one-third of the total magnetic flux. Few V-MMFs stream out from the sunspots at the nongap region. All observations suggest that MMFs with vertical magnetic fields are closely related to the disintegration of the sunspot, and most of the MMFs from the gap may originate directly from the sunspot umbra. **2022 May 27-June 2**

### The Structure and Dynamics of a Bright Point as seen with Hinode, SoHO and TRACE

D. Perez-Suarez, R.C. Maclean, J.G. Doyle and M.S. Madjarska

E-print, Oct 2008, A&A

Our aim is to determine the plasma properties of a coronal bright point and compare its magnetic topology extrapolated from magnetogram data with its appearance in X-ray images. We analyse spectroscopic data obtained with EIS/Hinode, Ca II H and G-band images from SOT/Hinode, UV images from TRACE, X-ray images from XRT/Hinode and high-resolution/high-cadence magnetogram data from MDI/SoHO. The BP comprises several coronal loops as seen in the X-ray images, while the chromospheric structure consists of tens of small bright points as seen in Ca II H. An excellent correlation exists between the Ca II BPs and increases in the magnetic field, implying that the Ca II H passband is a good indicator for the concentration of magnetic flux. Doppler velocities between 6 and 15 km/s are derived from the Fe XII and Fe XIII lines for the BP region, while for Fe XIV and Si VII they are in the range from -15 to +15 km/s. The coronal electron density is  $3.7 \times 10^9$  cm<sup>-3</sup>. An excellent correlation is found between the positive magnetic flux and the X-ray light-curves. The remarkable agreement between the extrapolated magnetic field configuration and some of the loops composing the BP as seen in the X-ray images suggests that a large fraction of the magnetic field in the bright point is close to potential. The close correlation between the positive magnetic flux and the X-ray emission suggests that energy released by magnetic reconnection is stimulated by flux emergence or cancellation.

### COCONUT, a novel fast-converging MHD model for solar corona simulations:

## II. Assessing the impact of the input magnetic map on space-weather forecasting at minimum of activity

[Barbara Perri](#), [Blazej Kuzma](#), [Michaela Brchneľova](#), [Tinatin Baratashvili](#), [Fan Zhang](#), [Peter Leitner](#), [Andrea Lani](#), [Stefaan Poedts](#)

ApJ 2022

<https://arxiv.org/pdf/2210.06165.pdf>

This paper is dedicated to the new implicit unstructured coronal code COCONUT, which aims at providing fast and accurate inputs for space weather forecast as an alternative to empirical models. We use all 20 available magnetic maps of the solar photosphere covering the date of the **2nd of July 2019** which corresponds to a solar eclipse on Earth. We use the same standard pre-processing on all maps, then perform coronal MHD simulations with the same numerical and physical parameters. In the end, we quantify the performance for each map using three indicators from remote-sensing observations: white-light total solar eclipse images for the streamers' edges, EUV synoptic maps for coronal holes and white-light coronagraph images for the heliospheric current sheet. We discuss the performance for space weather forecasts and we show that the choice of the input magnetic map has a strong impact. We find performances between 24% to 85% for the streamers' edges, 24% to 88% for the coronal hole boundaries and a mean deviation between 4 to 12 degrees for the heliospheric current sheet position. We find that the HMI runs are globally performing better on all indicators, with the GONG-ADAPT being the second-best choice. HMI runs perform better for the streamers' edges, GONG-ADAPT for polar coronal holes, HMI synchronic for equatorial coronal holes and for the streamer belt. We especially showcase the importance of the filling of the poles. This demonstrates that the solar poles have to be taken into account even for ecliptic plane previsions.

## The Time-dependent Chemistry of Cometary Debris in the Solar Corona

W. D. [Pesnelli](#) and P. Bryan

2014 ApJ 785 50

Recent improvements in solar observations have greatly progressed the study of sungrazing comets. They can now be imaged along the entirety of their perihelion passage through the solar atmosphere, revealing details of their composition and structure not measurable through previous observations in the less volatile region of the orbit further from the solar surface. Such comets are also unique probes of the solar atmosphere. The debris deposited by sungrazers is rapidly ionized and subsequently influenced by the ambient magnetic field. Measuring the spectral signature of the deposited material highlights the topology of the magnetic field and can reveal plasma parameters such as the electron temperature and density. Recovering these variables from the observable data requires a model of the interaction of the cometary species with the atmosphere through which they pass. The present paper offers such a model by considering the time-dependent chemistry of sublimated cometary species as they interact with the solar radiation field and coronal plasma. We expand on a previous simplified model by considering the fully time-dependent solutions of the emitting species' densities. To compare with observations, we consider a spherically symmetric expansion of the sublimated material into the corona and convert the time-dependent ion densities to radial profiles. Using emissivities from the CHIANTI database and plasma parameters derived from a magnetohydrodynamic simulation leads to a spatially dependent emission spectrum that can be directly compared with observations. We find our simulated spectra to be consistent with observation.

## Magnetic Imaging of the Outer Solar Atmosphere (MImOSA): Unlocking the driver of the dynamics in the upper solar atmosphere Review

[H. Peter](#), [E. Alsina Ballester](#), [V. Andretta](#), [F. Auchere](#), [L. Belluzzi](#), [A. Bemporad](#), [D. Berghmans](#), [E. Buchlin](#), [A. Calcines](#), [L.P. Chitta](#), [K. Dalmasse](#), [T. del Pino Aleman](#), [A. Feller](#), [C. Froment](#), [R. Harrison](#), [M. Janvier](#), [S. Matthews](#), [S. Parenti](#), [D. Przybylski](#), [S.K. Solanki](#), [J. Stepan](#), [L. Teriaca](#), [J. Trujillo Bueno](#)

Experimental Astronomy (on 28. Jul. 2020). 2021

Based on a proposal submitted in response to a call for white papers in the Voyage 2050 long-term plan in the ESA science programme.

<https://arxiv.org/pdf/2101.01566.pdf>

The magnetic activity of the Sun directly impacts the Earth and human life. Likewise, other stars will have an impact on the habitability of planets orbiting these host stars. The lack of information on the magnetic field in the higher atmospheric layers hampers our progress in understanding solar magnetic activity. Overcoming this limitation would allow us to address four paramount long-standing questions: (1) How does the magnetic field couple the different layers of the atmosphere, and how does it transport energy? (2) How does the magnetic field structure, drive and interact with the plasma in the chromosphere and upper atmosphere? (3) How does the magnetic field destabilise the outer solar atmosphere and thus affect the interplanetary environment? (4) How do magnetic processes accelerate particles to high energies? New ground-breaking observations are needed to address these science questions. We suggest a suite of three instruments that far exceed current capabilities in terms of spatial resolution, light-gathering power, and polarimetric performance: (a) A large-aperture UV-to-IR telescope of the 1-3

m class aimed mainly to measure the magnetic field in the chromosphere by combining high spatial resolution and high sensitivity. (b) An extreme-UV-to-IR coronagraph that is designed to measure the large-scale magnetic field in the corona with an aperture of about 40 cm. (c) An extreme-UV imaging polarimeter based on a 30 cm telescope that combines high throughput in the extreme UV with polarimetry to connect the magnetic measurements of the other two instruments. This mission to measure the magnetic field will unlock the driver of the dynamics in the outer solar atmosphere and thereby greatly advance our understanding of the Sun and the heliosphere. **31. 8. 2012, 20 March 2015, 3 Sept. 2015**

### **Limitations of force-free magnetic field extrapolations: revisiting basic assumptions**

H. [Peter](#), J. Warnecke, L. P. Chitta, R. H. Cameron

A&A 584, A68 2015

<http://arxiv.org/pdf/1510.04642v1.pdf>

Force-free extrapolations are widely used to study the magnetic field in the solar corona based on surface measurements. The extrapolations assume that the ratio of internal energy of the plasma to magnetic energy, the plasma-beta is negligible. Despite the widespread use of this assumption observations, models, and theoretical considerations show that beta is of the order of a few percent to more than 10%, and thus not small. We investigate what consequences this has for the reliability of extrapolation results. We use basic concepts starting with the force and the energy balance to infer relations between plasma-beta and free magnetic energy, to study the direction of currents in the corona with respect to the magnetic field, and to estimate the errors in the free magnetic energy by neglecting effects of the plasma ( $\beta \ll 1$ ). A comparison with a 3D MHD model supports our basic considerations. If plasma-beta is of the order of the relative free energy (the ratio of the free magnetic energy to the total magnetic energy) then the pressure gradient can balance the Lorentz force. This is the case in the solar corona, and therefore the currents are not properly described. In particular the error in terms of magnetic energy by neglecting the plasma is of the order of the free magnetic energy, so that the latter can not be reliably determined by an extrapolation. While a force-free extrapolation might capture the magnetic structure and connectivity of the coronal magnetic field, the derived currents and free magnetic energy are not reliable. Thus quantitative results of extrapolations on the location and amount of heating in the corona (through current dissipation) and on the energy storage of the magnetic field (e.g. for eruptive events) are limited.

### **Magnetic Field Diagnostics and Spatio-Temporal Variability of the Solar Transition**

#### **Region**

H. [Peter](#)

Solar Physics, December 2013, Volume 288, Issue 2, pp 531-547

Magnetic field diagnostics of the transition region from the chromosphere to the corona faces us with the problem that one has to apply extreme-ultraviolet (EUV) spectro-polarimetry. While for the coronal diagnostics techniques already exist in the form of infrared coronagraphy above the limb and radio observations on the disk, one has to investigate EUV observations for the transition region. However, so far the success of such observations has been limited, but various current projects aim to obtain spectro-polarimetric data in the extreme UV in the near future. Therefore it is timely to study the polarimetric signals we can expect from these observations through realistic forward modeling.

We employ a 3D magneto-hydrodynamic (MHD) forward model of the solar corona and synthesize the Stokes I and Stokes V profiles of C iv (1548 Å). A signal well above 0.001 in Stokes V can be expected even if one integrates for several minutes to reach the required signal-to-noise ratio, and despite the rapidly changing intensity in the model (just as in observations). This variability of the intensity is often used as an argument against transition region magnetic diagnostics, which requires exposure times of minutes. However, the magnetic field is evolving much slower than the intensity, and therefore the degree of (circular) polarization remains rather constant when one integrates in time. Our study shows that it is possible to measure the transition region magnetic field if a polarimetric accuracy on the order of 0.001 can be reached, which we can expect from planned instrumentation.

### **Thermal structure of hot non-flaring corona from Hinode/EIS**

A. [Petralia](#), F. Reale, P. Testa, G. Del Zanna

A&A, 2014

<http://arxiv.org/pdf/1402.6554v1.pdf>

In previous studies a very hot plasma component has been diagnosed in solar active regions through the images in three different narrow-band channels of SDO/AIA. This diagnostic from EUV imaging data has also been supported by the matching morphology of the emission in the hot Ca XVII line, as observed with Hinode/EIS. This evidence is debated because of unknown distribution of the emission measure along the line of sight. Here we investigate in detail the thermal distribution of one of such regions using EUV spectroscopic data. In an active region observed with SDO/AIA, Hinode/EIS and XRT, we select a subregion with a very hot plasma component and another cooler one for comparison. The average spectrum is extracted for both, and 14 intense lines are selected for analysis, that probe the  $5.5 < \log T < 7$  temperature range uniformly. From these lines the emission measure distributions are

reconstructed with the MCMC method. Results are cross-checked with comparison of the two subregions, with a different inversion method, with the morphology of the images, and with the addition of fluxes measured with from narrow and broad-band imagers. We find that, whereas the cool region has a flat and featureless distribution that drops at temperature  $\log T \geq 6.3$ , the distribution of the hot region shows a well-defined peak at  $\log T = 6.6$  and gradually decreasing trends on both sides, thus supporting the very hot nature of the hot component diagnosed with imagers. The other cross-checks are consistent with this result. This study provides a completion of the analysis of active region components, and the resulting scenario supports the presence of a minor very hot plasma component in the core, with temperatures  $\log T > 6.6$ .

## **Solar Polar Magnetic Fields: Comparing Full-disk and High-resolution Spectromagnetograph Data**

Gordon J. D. [Petrie](#)<sup>1</sup>

2022 ApJ 941 142

<https://iopscience.iop.org/article/10.3847/1538-4357/aca1a8/pdf>

This is the first systematic comparison between photospheric polar magnetic field data from a full-disk synoptic observing program, the National Solar Observatory's Synoptic Optical Long-term Investigations of the Sun Vector Spectromagnetograph (SOLIS/VSM), and a high-resolution vector spectromagnetograph, the Hinode Solar Optical Telescope Spectropolarimeter (SOT/SP). Polar magnetic fluxes derived from longitudinal magnetic field measurements from both telescopes and from SOT/SP full-Stokes vector data are all compared in the form of polar synoptic maps. Measurements taken over 35 day periods with advantageous rotation axis tilt angle are used; observations extend to the poles, and no synthetic pole-filling is needed. Polar fluxes are derived from longitudinal data assuming an approximately radial field, whereas those derived from vector data are based on measured vector magnitude and direction. However, the full-vector measurements may have a detection problem: polar fields are observed as mostly transverse from (near) Earth, and Zeeman sensitivity to transverse fields is significantly lower than for longitudinal fields. Accordingly, the SOT/SP vector-based polar fluxes are lower than the longitudinal-based fluxes from both telescopes, a result driven by pixels without sufficient Q and U signals for the full-Stokes inversions to detect significant radial field but with good Stokes V signal implying a significant field. Furthermore, the SOT/SP longitudinal-based fluxes are significantly higher than their VSM counterparts because of superior seeing-free spatial resolution and longer observation time. The SOT/SP longitudinal-based polar fluxes appear large enough to account for radial interplanetary field measurements whereas the SOT/SP vector-based and the VSM ones are generally too low.

## **Modeling the Global Coronal Field with Simulated Synoptic Magnetograms from Earth and the Lagrange Points L3L3, L4L4, and L5**

Gordon [Petrie](#), Alexei Pevtsov, Andrew Schwarz, Marc DeRosa

[Solar Physics](#) June 2018, 293:88

<http://sci-hub.tw/10.1007/s11207-018-1306-5>

The solar photospheric magnetic flux distribution is key to structuring the global solar corona and heliosphere. Regular full-disk photospheric magnetogram data are therefore essential to our ability to model and forecast heliospheric phenomena such as space weather. However, our spatio-temporal coverage of the photospheric field is currently limited by our single vantage point at/near Earth. In particular, the polar fields play a leading role in structuring the large-scale corona and heliosphere, but each pole is unobservable for  $>6$  months per year. Here we model the possible effect of full-disk magnetogram data from the Lagrange points L4L4 and L5L5, each extending longitude coverage by  $60^\circ$ . Adding data also from the more distant point L3L3 extends the longitudinal coverage much further. The additional vantage points also improve the visibility of the globally influential polar fields. Using a flux-transport model for the solar photospheric field, we model full-disk observations from Earth/L1L1, L3L3, L4L4, and L5L5 over a solar cycle, construct synoptic maps using a novel weighting scheme adapted for merging magnetogram data from multiple viewpoints, and compute potential-field models for the global coronal field. Each additional viewpoint brings the maps and models into closer agreement with the reference field from the flux-transport simulation, with particular improvement at polar latitudes, the main source of the fast solar wind.

## **High-Resolution Vector Magnetograms of the Sun's Poles from Hinode: Flux Distributions and Global Coronal Modeling**

Gordon [Petrie](#)

[Solar Physics](#) January 2017, 292:13

The Sun's polar fields play a leading role in structuring the large-scale solar atmosphere and in determining the interplanetary magnetic field. They are also believed to supply the seed field for the subsequent solar activity cycle. However, present-day synoptic observations do not have sufficient spatial resolution or sensitivity to diagnose

accurately the high-latitude magnetic vector field. The high spatial resolution and sensitivity of the full-Stokes observations from the Hinode Solar Optical Telescope Spectro-Polarimeter, observing the poles long-term, allows us to build up a detailed picture of the Cycle 24 polar field reversal, including the changing latitude distribution of the high-latitude flux, and to study the effect on global coronal field models. The Hinode observations provide detailed information on the dominant facular-scale magnetic structure of the polar fields, and their field inclination and flux distribution. Hybrid synoptic magnetograms are constructed from Hinode polar measurements and full-disk magnetograms from the Synoptic Optical Long-term Investigations of the Sun (SOLIS) Vector Spectro-Magnetograph (VSM), and coronal potential field models are calculated. Loss of effective spatial resolution at the highest latitudes presents complications. Possible improvements to synoptic polar data are discussed.

## **Solar Magnetism in the Polar Regions** **Review**

Gordon **Petrie**

Living Reviews in Solar Physics 12 (2015), 5

<http://solarphysics.livingreviews.org/Articles/lrsp-2015-5/>

This review describes observations of the polar magnetic fields, models for the cyclical formation and decay of these fields, and evidence of their great influence in the solar atmosphere. The polar field distribution dominates the global structure of the corona over most of the solar cycle, supplies the bulk of the interplanetary magnetic field via the polar coronal holes, and is believed to provide the seed for the creation of the activity cycle that follows. A broad observational knowledge and theoretical understanding of the polar fields is therefore an essential step towards a global view of solar and heliospheric magnetic fields. Analyses of both high-resolution and long-term synoptic observations of the polar fields are summarized. Models of global flux transport are reviewed, from the initial phenomenological and kinematic models of Babcock and Leighton to present-day attempts to produce time-dependent maps of the surface magnetic field and to explain polar field variations, including the weakness of the cycle 23 polar fields. The relevance of the polar fields to solar physics extends far beyond the surface layers from which the magnetic field measurements usually derive. As well as discussing the polar fields' role in the interior as seed fields for new solar cycles, the review follows their influence outward to the corona and heliosphere. The global coronal magnetic structure is determined by the surface magnetic flux distribution, and is dominated on large scales by the polar fields. We discuss the observed effects of the polar fields on the coronal hole structure, and the solar wind and ejections that travel through the atmosphere. The review concludes by identifying gaps in our knowledge, and by pointing out possible future sources of improved observational information and theoretical understanding of these fields.

## **Polar Field Reversals and Active Region Decay** **Review**

Gordon **Petrie**, Sophie Ettinger

Space Science Reviews September 2017, Volume 210, [Issue 1–4](#), pp 77–108

We study the relationship between polar field reversals and decayed active region magnetic flux. Photospheric active region flux is dispersed by differential rotation and turbulent diffusion, and is transported poleward by meridional flows and diffusion. We summarize the published evidence from observation and modeling of the influence of meridional flow variations and decaying active region flux's spatial distribution, such as the Joy's law tilt angle. Using NSO Kitt Peak synoptic magnetograms covering cycles 21–24, we investigate in detail the relationship between the transport of decayed active region flux to high latitudes and changes in the polar field strength, including reversals in the magnetic polarity at the poles. By means of stack plots of low- and high-latitude slices of the synoptic magnetograms, the dispersal of flux from low to high latitudes is tracked, and the timing of this dispersal is compared to the polar field changes. In the most abrupt cases of polar field reversal, a few activity complexes (systems of active regions) are identified as the main cause. The poleward transport of large quantities of decayed trailing-polarity flux from these complexes is found to correlate well in time with the abrupt polar field changes. In each case, significant latitudinal displacements were found between the positive and negative flux centroids of the complexes, consistent with Joy's law bipole tilt with trailing-polarity flux located poleward of leading-polarity flux. The activity complexes of the cycle 21 and 22 maxima were larger and longer-lived than those of the cycle 23 and 24 maxima, and the poleward surges were stronger and more unipolar and the polar field changes larger and faster. The cycle 21 and 22 polar reversals were dominated by only a few long-lived complexes whereas the cycle 23 and 24 reversals were the cumulative effects of more numerous, shorter-lived regions. We conclude that sizes and lifetimes of activity complexes are key to understanding the diversity of polar reversals.

## **SOLAR MAGNETIC ACTIVITY CYCLES, CORONAL POTENTIAL FIELD MODELS AND ERUPTION RATES**

G. J. D. **Petrie**

2013 ApJ 768 162

We study the evolution of the observed photospheric magnetic field and the modeled global coronal magnetic field during the past 3 1/2 solar activity cycles observed since the mid-1970s. We use synoptic magnetograms and extrapolated potential-field models based on longitudinal full-disk photospheric magnetograms from the National Solar Observatory's three magnetographs at Kitt Peak, the Synoptic Optical Long-term Investigations of the Sun vector spectro-magnetograph, the spectro-magnetograph and the 512-channel magnetograph instruments, and from Stanford University's Wilcox Solar Observatory. The associated multipole field components are used to study the dominant length scales and symmetries of the coronal field. Polar field changes are found to be well correlated with active fields over most of the period studied, except between 2003 and 2006 when the active fields did not produce significant polar field changes. Of the axisymmetric multipoles, only the dipole and octupole follow the poles whereas the higher orders follow the activity cycle. All non-axisymmetric multipole strengths are well correlated with the activity cycle. The tilt of the solar dipole is therefore almost entirely due to active-region fields. The axial dipole and octupole are the largest contributors to the global field except while the polar fields are reversing. This influence of the polar fields extends to modulating eruption rates. According to the Computer Aided CME Tracking, Solar Eruptive Event Detection System, and Nobeyama radioheliograph prominence eruption catalogs, the rate of solar eruptions is found to be systematically higher for active years between 2003 and 2012 than for those between 1997 and 2002. This behavior appears to be connected with the weakness of the late-cycle 23 polar fields as suggested by Luhmann. We see evidence that the process of cycle 24 field reversal is well advanced at both poles.

## **Evolution of Active and Polar Photospheric Magnetic Fields During the Rise of Cycle 24 Compared to Previous Cycles**

G. J. D. [Petrie](#)

Solar Physics, December **2012**, Volume 281, Issue 2, pp 577-598

The evolution of the photospheric magnetic field during the declining phase and minimum of cycle 23 and the recent rise of cycle 24 are compared with the behavior during previous cycles. We used longitudinal full-disk magnetograms from the NSO's three magnetographs at Kitt Peak, the Synoptic Optical Long-term Investigations of the Sun (SOLIS) vector spectro-magnetograph (VSM), the spectro-magnetograph and the 512-channel magnetograph instruments, and longitudinal full-disk magnetograms from the Mt. Wilson 150-foot tower. We analyzed 37 years of observations from these two observatories that have been observing daily, weather permitting, since 1974, offering an opportunity to study the evolving relationship between the active region and polar fields in some detail over several solar cycles. It is found that the annual averages of a proxy for the active region poloidal magnetic field strength, the magnetic field strength of the high-latitude poleward streams, and the time derivative of the polar field strength are all well correlated in each hemisphere. The active region net poloidal fields effectively disappeared in both hemispheres around 2004 and the polar fields have not become significantly stronger since this time. These results are based on statistically significant cyclical patterns in the active region fields and are consistent with the Babcock–Leighton phenomenological model for the solar activity cycle. There was more hemispheric asymmetry in the total and maximum active region flux during late cycle 23 (after around 2004), when the southern hemisphere was more active, and the rise of cycle 24, when the northern hemisphere was more active, than at any other time since 1974. We see evidence that the process of cycle 24 field reversal has begun at both poles.

## **Nonlinear Force-Free and Potential-Field Models of Active-Region and Global Coronal Fields during the Whole Heliosphere Interval**

G. J. D. [Petrie](#), A. Canou und T. Amari

Solar Physics, Volume 274, Numbers 1-2, 163-194, **2011**

Between 24 March 2008 and 2 April 2008, the three active regions (ARs) NOAA 10987, 10988 and 10989 were observed daily by the Synoptic Optical Long-term Investigations of the Sun (SOLIS) Vector Spectro-Magnetograph (VSM) while they traversed the solar disk. We use these measurements and the nonlinear force-free magnetic field code XTRAPOL to reconstruct the coronal magnetic field for each active region and compare model field lines with images from the Solar Terrestrial Relations Observatory (STEREO) and Hinode X-ray Telescope (XRT) telescopes. Synoptic maps made from continuous, round-the-clock Global Oscillations Network Group (GONG) magnetograms provide information on the global photospheric field and potential-field source-surface models based on these maps describe the global coronal field during the Whole Heliosphere Interval (WHI) and its neighboring rotations. Features of the modeled global field, such as the coronal holes and streamer-belt locations, are discussed in comparison with extreme ultra-violet and coronagraph observations from STEREO. The global field is found to be far from a minimum, dipolar state. From the nonlinear models we compute physical quantities for the active regions such as the photospheric magnetic and electric current fluxes, the free magnetic energy and the relative helicity for each region each day where observations permit. The interconnectivity of the three regions is addressed in the context of the potential-field source-surface model. Using local and global quantities derived from the models, we briefly discuss the different observed activity levels of the regions.

## A COMPARATIVE STUDY OF MAGNETIC FIELDS IN THE SOLAR PHOTOSPHERE AND CHROMOSPHERE AT EQUATORIAL AND POLAR LATITUDES

G. J. D. [Petrie](#) et al

ApJ 699 871-884, 2009

Besides their own intrinsic interest, correct interpretation of solar surface magnetic field observations is crucial to our ability to describe the global magnetic structure of the solar atmosphere. Photospheric magnetograms are often used as lower boundary conditions in models of the corona, but not data from the nearly force-free chromosphere. National Solar Observatory's (NSO) Synoptic Optical Long-term Investigations of the Sun VSM (Vector Spectromagnetograph) produces full-disk line-of-sight magnetic flux images deriving from both photospheric and chromospheric layers on a daily basis. In this paper, we investigate key properties of the magnetic field in these two layers using more than five years of VSM data. We find from near-equatorial measurements that the east-west inclination angle of most photospheric fields is less than about  $12^\circ$ , while chromospheric fields expand in all directions to a significant degree. Using a simple stereoscopic inversion, we find evidence that photospheric polar fields are also nearly radial but that during 2008 the chromospheric field in the south pole was expanding superradially. We obtain a spatially resolved polar photospheric flux distribution up to  $80^\circ$  latitude whose strength increases poleward approximately as  $\cos(\text{colatitude})$  to the power 9-10. This distribution would give a polar field strength of 5-6 G. We briefly discuss implications for future synoptic map construction and modeling.

## Optimization of surface flux transport models for the solar polar magnetic field

K. [Petrovay](#) and M. Talafha

A&A 632, A87 (2019)

<https://doi.org/10.1051/0004-6361/201936099>

**Context.** The choice of free parameters in surface flux transport (SFT) models describing the evolution of the large-scale poloidal magnetic field of the Sun is critical for the correct reproduction of the polar magnetic flux built up during a solar cycle, which is known to be a good predictor of the amplitude of the upcoming cycle.

**Aims.** For an informed choice of parameters it is important to understand the effects of and interplay among the various parameters and to optimize the models for the polar magnetic field.

**Methods.** Here we present the results of a large-scale systematic study of the parameter space in an SFT model where the source term representing the net effect of tilted flux emergence was chosen to represent a typical, average solar cycle as described by observations.

**Results.** Comparing the results with observational constraints on the spatiotemporal variation of the polar magnetic field, as seen in magnetograms for the last four solar cycles, we mark allowed and excluded regions in the 3D parameter space defined by the flow amplitude  $u_0$ , the magnetic diffusivity  $\eta$  and the decay time scale  $\tau$ , for three different assumed meridional flow profiles.

**Conclusions.** Without a significant decay term in the SFT equation (i.e., for  $\tau > 10$  yr) the global dipole moment reverses too late in the cycle for all flow profiles and parameters, providing independent supporting evidence for the need of a decay term, even in the case of identical cycles. An allowed domain is found to exist for  $\tau$  values in the 5–10 yr range for all flow profiles considered. Generally higher values of  $\eta$  (500–800 km<sup>2</sup> s<sup>-1</sup>) are preferred though some solutions with lower  $\eta$  are still allowed.

## Helio2024 Science White Paper: Solar and Heliospheric Magnetism in 5D

[Alexei A. Pevtsov](#), [T. Woods](#), [V. Martinez-Pillet](#), [D. Hassler](#), [T. Berger](#), [S. Gosain](#), [T. Hoeksema](#), [A. R. Jones](#), [R. Kohnert](#), [T. Y. Chen](#), [L. Upton](#), [A. Pulkkinen](#)

White paper submitted to Decadal Survey for Solar and Space Physics (Heliophysics) 2024-2033, 2022

<https://arxiv.org/pdf/2211.06715.pdf>

This White Paper argues for the urgent need for the multi-vantage/multi-point observations of the Sun and the heliosphere in the framework of six (6) key science objectives. We further emphasize the critical importance of 5D-`space": three spatial, one temporal and the magnetic field components. The importance of such observations cannot be overstated both for scientific research and the operational space weather forecast.

## Long-term studies of photospheric magnetic fields on the Sun

**Review**

Alexei A. [Pevtsov](#)<sup>1\*</sup>, Luca Bertello<sup>1</sup>, Yury A. Nagovitsyn<sup>2,3</sup>, Andrey G. Tlatov<sup>4</sup> and Valery V. Pipin<sup>5</sup>  
J. Space Weather Space Clim. 2021, 11, 4

<https://doi.org/10.1051/swsc/2020069>

[Long-term studies of photospheric magnetic fields on the Sun \(swsc-journal.org\)](https://doi.org/10.1051/swsc/2020069)

We briefly review the history of observations of magnetic fields on the Sun, and describe early magnetograms for full disk measurements. Changes in instruments and detectors, the cohort of observers, the knowledge base etc may result in non-uniformity of the long-term synoptic datasets. Still, such data are critical for detecting and understanding the long-term trends in solar activity. We demonstrate the value of historical data using studies of



active region tilt (Joy's law) and the evolution of polar field and its reversal. Using the longest dataset of sunspot field strength measurements from Mount Wilson Observatory (1917-present) supplemented by shorter datasets from Pulkovo (1956–1997) and Crimean (1956-present) observatories we demonstrate that the magnetic properties of sunspots did not change over the last hundred years. We also show that the relationship between the sunspot area and its magnetic flux can be used to extend the studies of magnetic field in sunspots to periods with no direct magnetic field measurements. Finally, we show how more recent full disk observations of the vector magnetic field can be used to study the long-term (solar cycle) variations in magnetic helicity on the Sun.

### **On a limitation of Zeeman polarimetry and imperfect instrumentation in representing solar magnetic fields with weaker polarization signal**

Alexei A. [Pevtsov](#) (1), [Yang Liu](#) (2), [Ilpo Virtanen](#) (3), [Luca Bertello](#) (1), [Kalevi Mursula](#) (3), [K.D. Leka](#) (4,5), [Anna L.H. Hughes](#) (1)

Journal of Space Weather and Space Climate, **11**, 14 2021

<https://arxiv.org/pdf/2101.07204.pdf>

<https://www.swsc-journal.org/articles/swsc/pdf/2021/01/swsc200003.pdf>

Full disk vector magnetic fields are used widely for developing better understanding of large-scale structure, morphology, and patterns of the solar magnetic field. The data are also important for modeling various solar phenomena. However, observations of vector magnetic fields have one important limitation that may affect the determination of the true magnetic field orientation. This limitation stems from our ability to interpret the differing character of the Zeeman polarization signals which arise from the photospheric line-of-sight vs. the transverse components of the solar vector magnetic field, and is likely exacerbated by unresolved structure (non-unity fill fraction) as well as the disambiguation of the 180° degeneracy in the transverse-field azimuth. Here we provide a description of this phenomenon, and discuss issues, which require additional investigation.

### **Reconstructing solar magnetic fields from historical observations**

#### **V. Sunspot magnetic field measurements at Mount Wilson Observatory**

Alexei A. [Pevtsov](#), Kseniya A. Tlatova, Alexander A. Pevtsov, Elina Heikkinen, Ilpo Virtanen, Nina V. Karachik, Luca Bertello, Andrey G. Tlatov, Roger Ulrich, and Kalevi Mursula

A&A 628, A103 2019

<https://doi.org/10.1051/0004-6361/201834985>

Context. Systematic observations of magnetic field strength and polarity in sunspots began at Mount Wilson Observatory (MWO), USA in early 1917. Except for a few brief interruptions, this historical dataset has continued until the present.

Aims. Sunspot field strength and polarity observations are critical in our project of reconstructing the solar magnetic field over the last hundred years. We provide a detailed description of the newly digitized dataset of drawings of sunspot magnetic field observations.

Methods. The digitization of MWO drawings is based on a software package that we developed. It includes a semiautomatic selection of solar limbs and other features of the drawing, and a manual entry of the time of observations, measured field strength, and other notes hand written on each drawing. The data are preserved in an MySQL database.

Results. We provide a brief history of the project and describe the results from digitizing this historical dataset. We also provide a summary of the final dataset and describe its known limitations. Finally, we compare the sunspot magnetic field measurements with those from other instruments, and demonstrate that, if needed, the data set could be continued using modern observations such as, for example, the Vector Stokes Magnetograph on the Synoptic Optical Long-term Investigations of the Sun platform.

### **Effect of uncertainties in solar synoptic magnetic flux maps in modeling of solar wind**

Alexei A. [Pevtsov](#), , Luca Bertellob, , Peter MacNeice

Advances in Space Research Volume 56, Issue 12, 15 December 2015, Pages 2719–2726

<http://www.sciencedirect.com/science/article/pii/S0273117715004007>

Recently, the NSO/SOLIS team developed variance (error) maps that represent uncertainties in magnetic flux synoptic charts. These uncertainties are determined by the spatial variances of the magnetic flux distribution from full disk magnetograms that contribute to each bin in the synoptic chart. Here we present a study of the effects of variances on solar wind parameters (wind speed, density, magnetic field, and temperature) derived using the WSA–ENLIL model and ensemble modeling approach. We compare the results of the modeling with near-Earth solar wind magnetic field and plasma data as extracted from NASA/GSFC's OMNI data set. We show that analysis of uncertainties may be useful for understanding the sensitivity of the model predictions to short-term evolution of magnetic field and noise in the synoptic magnetograms.

## Cyclic and Long-Term Variation of Sunspot Magnetic Fields

Alexei A. [Pevtsov](#), Luca Bertello, Andrey G. Tlatov, Ali Kilcik, Yury A. Nagovitsyn, Edward W. Cliver  
Solar Physics February 2014, Volume 289, Issue 2, pp 593–602

Measurements from the Mount Wilson Observatory (MWO) were used to study the long-term variations of sunspot field strengths from 1920 to 1958. Following a modified approach similar to that presented in Pevtsov et al. (Astrophys. J. Lett. 742, L36, 2011), we selected the sunspot with the strongest measured field strength for each observing week and computed monthly averages of these weekly maximum field strengths. The data show the solar cycle variation of the peak field strengths with an amplitude of about 500–700 gauss (G), but no statistically significant long-term trends. Next, we used the sunspot observations from the Royal Greenwich Observatory (RGO) to establish a relationship between the sunspot areas and the sunspot field strengths for cycles 15–19. This relationship was used to create a proxy of the peak magnetic field strength based on sunspot areas from the RGO and the USAF/NOAA network for the period from 1874 to early 2012. Over this interval, the magnetic field proxy shows a clear solar cycle variation with an amplitude of 500–700 G and a weaker long-term trend. From 1874 to around 1920, the mean value of magnetic field proxy increases by about 300–350 G, and, following a broad maximum in 1920–1960, it decreases by about 300 G. Using the proxy for the magnetic field strength as the reference, we scaled the MWO field measurements to the measurements of the magnetic fields in Pevtsov et al. (2011) to construct a combined data set of maximum sunspot field strengths extending from 1920 to early 2012. This combined data set shows strong solar cycle variations and no significant long-term trend (the linear fit to the data yields a slope of  $-0.2 \pm 0.8$  G year $^{-1}$ ). On the other hand, the peak sunspot field strengths observed at the minimum of the solar cycle show a gradual decline over the last three minima (corresponding to cycles 21–23) with a mean downward trend of  $\approx 15$  G year $^{-1}$ .

## Magnetic Helicity, Tilt, and Twist

## Review

Alexei A. [Pevtsov](#), Mitchell A. Berger, Alexander Nindos, Aimee A. Norton, Lidia van Driel-Gesztelyi  
[Space Science Reviews](#), December 2014, Volume 186, [Issue 1-4](#), pp 285-324

Since its introduction to astro- and solar physics, the concept of helicity has proven to be useful in providing critical insights into physics of various processes from astrophysical dynamos, to magnetic reconnection and eruptive phenomena. Signature of helicity was also detected in many solar features, including orientation of solar active regions, or Joy's law. Here we provide a summary of both solar phenomena and consider mutual relationship and its importance for the evolution of solar magnetic fields.

## SOLIS: reconciling disk-integrated and disk-resolved spectra from the Sun

Alexei [Pevtsov](#), Luca Bertello, Brian Harker, Mark Giampapa, Andrew Marble  
18th Cambridge Workshop on Cool Stars, Stellar Systems, and the Sun, Proceedings of Lowell  
Observatory (2014), pp. 871-878

<http://arxiv.org/pdf/1411.7266v1.pdf>

Unlike other stars, the surface of the Sun can be spatially resolved to a high degree of detail. But the Sun can also be observed as if it was a distant star. The availability of solar disk-resolved and disk-integrated spectra offers an opportunity to devise methods to derive information about the spatial distribution of solar features from Sun-as-a-star measurements. Here, we present an update on work done at the National Solar Observatory to reconcile disk-integrated and disk-resolved solar spectra from the Synoptic Optical Long-term Investigation of the Sun (SOLIS) station. The results of this work will lead to a new approach to infer the information about the spatial distribution of features on other stars, from the overall filling factor of active regions to, possibly, the latitude/longitude distribution of features.

## Cyclic and Long-Term Variation of Sunspot Magnetic Fields

Alexei A. [Pevtsov](#), Luca Bertello, Andrey G. Tlatov, Ali Kilcik, Yury A. Nagovitsyn, Edward W. Cliver  
Solar Physics, February 2014, Volume 289, Issue 2, pp 593-602

Measurements from the Mount Wilson Observatory (MWO) were used to study the long-term variations of sunspot field strengths from 1920 to 1958. Following a modified approach similar to that presented in Pevtsov et al. (Astrophys. J. Lett. 742, L36, 2011), we selected the sunspot with the strongest measured field strength for each observing week and computed monthly averages of these weekly maximum field strengths. The data show the solar cycle variation of the peak field strengths with an amplitude of about 500–700 gauss (G), but no statistically significant long-term trends. Next, we used the sunspot observations from the Royal Greenwich Observatory (RGO) to establish a relationship between the sunspot areas and the sunspot field strengths for cycles 15–19. This relationship was used to create a proxy of the peak magnetic field strength based on sunspot areas from the RGO and the USAF/NOAA network for the period from 1874 to early 2012. Over this interval, the magnetic field proxy shows a clear solar cycle variation with an amplitude of 500–700 G and a weaker long-term trend. From 1874 to

around 1920, the mean value of magnetic field proxy increases by about 300–350 G, and, following a broad maximum in 1920–1960, it decreases by about 300 G. Using the proxy for the magnetic field strength as the reference, we scaled the MWO field measurements to the measurements of the magnetic fields in Pevtsov et al. (2011) to construct a combined data set of maximum sunspot field strengths extending from 1920 to early 2012. This combined data set shows strong solar cycle variations and no significant long-term trend (the linear fit to the data yields a slope of  $-0.2 \pm 0.8$  G year<sup>-1</sup>). On the other hand, the peak sunspot field strengths observed at the minimum of the solar cycle show a gradual decline over the last three minima (corresponding to cycles 21–23) with a mean downward trend of  $\approx 15$  G year<sup>-1</sup>.

## What Helicity Can Tell us About Solar Magnetic Fields

Alexei A. [Pevtsov](#)

E-print, Feb 2008; J. Astrophys. Astr.

Concept of magnetic/current helicity was introduced to solar physics about 15 years ago. Earlier studies led to discovery of such fundamental properties as hemispheric helicity rule, and role of helicity in magnetic reconnection and solar eruptions. Later, the concept was successfully applied in studies of different solar processes from solar dynamo to flare and CME phenomena. Although no silver bullet, helicity has proven to be a very useful tool in answering many still puzzling questions about origin and evolution of solar magnetic fields. I present an overview of some helicity studies and briefly analyze their findings.

## Comparison of Ground-Based and Space-Based Longitudinal Magnetograms

A. [Pietarila](#)<sup>1</sup>, L. Bertello<sup>1</sup>, J. W. Harvey<sup>1</sup> and A. A. Pevtsov<sup>2</sup>

Solar Physics, January 2013, Volume 282, Issue 1, pp 91-106, [File](#)

We compare photospheric line-of-sight magnetograms from the Synoptic Optical Long-term Investigations of the Sun (SOLIS) Vector Spectro-Magnetograph (VSM) instrument with observations from the 150-foot Solar Tower at Mt. Wilson Observatory (MWO), the Helioseismic and Magnetic Imager (HMI) on the Solar Dynamics Observatory (SDO), and the Michelson Doppler Imager (MDI) on the Solar and Heliospheric Observatory (SOHO). We find very good agreement between VSM and the other data sources for both disk-averaged flux densities and pixel-by-pixel measurements. We show that the VSM mean flux density time series is of consistently high signal-to-noise ratio with no significant zero offsets. We discuss in detail some of the factors – spatial resolution, flux dependence, and position on the solar disk – affecting the determination of scaling between VSM and SOHO/MDI or SDO/HMI magnetograms. The VSM flux densities agree well with spatially smoothed data from MDI and HMI, although the scaling factors show a clear dependence on flux density. The factor to convert VSM to HMI increases with increasing flux density (from  $\approx 1$  to  $\approx 1.5$ ). The nonlinearity is smaller for the VSM vs. SOHO/MDI scaling factor (from  $\approx 1$  to  $\approx 1.2$ ).

## The Imaging Magnetograph eXperiment (IMaX) for the Sunrise Balloon-Borne Solar Observatory

V. Martínez [Pillet](#) · J.C. del Toro Iniesta · A. Álvarez-Herrero · V. Domingo · J.A. Bonet · L. González Fernández · A. López Jiménez · C. Pastor · J.L. Gasent Blesa · P. Mellado · J. Piqueras · B. Aparicio · M. Balaguer · E. Ballesteros · T. Belenguer · L.R. Bellot Rubio · T. Berkefeld · M. Collados · W. Deutsch · A. Feller · F. Girela · B. Grauf · R.L. Heredero · M. Herranz · J.M. Jerónimo · H. Laguna · R. Meller · M. Menéndez · R. Morales · D. Orozco Suárez · G. Ramos · M. Reina · J.L. Ramos · P. Rodríguez · A. Sánchez · N. Uribe-Patarroyo · P. Barthol · A. Gandorfer · M. Knoelker · W. Schmidt · S.K. Solanki · S. Vargas Domínguez

Solar Phys (2011) 268: 57–102

The Imaging Magnetograph eXperiment (IMaX) is a spectropolarimeter built by four institutions in Spain that flew on board the *Sunrise* balloon-borne solar observatory in June 2009 for almost six days over the Arctic Circle. As a polarimeter, IMaX uses fast polarization modulation (based on the use of two liquid crystal retarders), real-time image accumulation, and dual-beam polarimetry to reach polarization sensitivities of 0.1%. As a spectrograph, the instrument uses a LiNbO<sub>3</sub> etalon in double pass and a narrow band pre-filter to achieve a spectral resolution of 85 mÅ. IMaX uses the high-Zeeman-sensitive line of Fe I at 5250.2 Å and observes all four Stokes parameters at various points inside the spectral line. This allows vector magnetograms, Dopplergrams, and intensity frames to be produced that, after reconstruction, reach spatial resolutions in the 0.15 – 0.18 arcsec

range over a  $50 \times 50$  arcsec field of view. Time cadences vary between 10 and 33 s, although the shortest one only includes longitudinal polarimetry. The spectral line is sampled in various ways depending on the applied observing mode, from just two points inside the line to 11 of them. All observing modes include one extra wavelength point in the nearby continuum. Gauss equivalent sensitivities are 4 G for longitudinal fields and 80 G for transverse fields per wavelength sample. The line-of-sight velocities are estimated with statistical errors of the order of 5 – 40  $\text{ms}^{-1}$ . The design, calibration, and integration phases of the instrument, together with the implemented data reduction scheme, are described in some detail.

## **Reversals of the solar magnetic dipole in the light of observational data and simple dynamo models**

V. V. [Pipin](#)<sup>1</sup>, D. Moss<sup>2</sup>, D. Sokoloff<sup>3</sup> and J. T. Hoeksema  
A&A 567, A90 (2014)

**Context.** Observations show that the photospheric solar magnetic dipole usually does not vanish during the reversal of the solar magnetic field, which occurs in each solar cycle. In contrast, mean-field solar dynamo models predict that the dipole field does become zero. In a recent paper it was suggested that this contradiction could be explained as a large-scale manifestation of small-scale magnetic fluctuations of the surface poloidal field.

**Aims.** Our aim is to confront this interpretation with the available observational data.

**Methods.** Here we compare this interpretation with Wilcox Solar Observatory (WSO) photospheric magnetic field data in order to determine the amplitude of magnetic fluctuations required to explain the phenomenon and to compare the results with predictions from a simple dynamo model which takes these fluctuations into account.

**Results.** We demonstrate that the WSO data concerning the magnetic dipole reversals are very similar to the predictions from our very simple solar dynamo model, which includes both mean magnetic field and fluctuations.

The ratio between the rms value of the magnetic fluctuations and the mean field is estimated to be about 2, in reasonable agreement with estimates from sunspot data. The reversal epoch, during which the fluctuating contribution to the dipole is larger than that from the mean field, is about 4 months. The memory time of the fluctuations is about 2 months. Observations demonstrate that the rms of the magnetic fluctuations is strongly modulated by the phase of the solar cycle. This gives additional support to the concept that the solar magnetic field is generated by a single dynamo mechanism rather than also by independent small-scale dynamo action. A suggestion of a weak nonaxisymmetric magnetic field of a fluctuating nature arises from the analysis, with a lifetime of about 1 year.

**Conclusions.** The behaviour of the magnetic dipole during the reversal epoch gives valuable information about details of solar dynamo action.

## **Effects of Anisotropies in Turbulent Magnetic Diffusion in Mean-field Solar Dynamo Models**

V. V. [Pipin](#)<sup>1,2,3</sup> and A. G. Kosovichev  
2014 ApJ 785 49.

We study how anisotropies of turbulent diffusion affect the evolution of large-scale magnetic fields and the dynamo process on the Sun. The effect of anisotropy is calculated in a mean-field magnetohydrodynamics framework assuming that triple correlations provide relaxation to the turbulent electromotive force (so-called the "minimal  $\tau$ -approximation"). We examine two types of mean-field dynamo models: the well-known benchmark flux-transport model and a distributed-dynamo model with a subsurface rotational shear layer. For both models, we investigate effects of the double- and triple-cell meridional circulation, recently suggested by helioseismology and numerical simulations. To characterize the anisotropy effects, we introduce a parameter of anisotropy as a ratio of the radial and horizontal intensities of turbulent mixing. It is found that the anisotropy affects the distribution of magnetic fields inside the convection zone. The concentration of the magnetic flux near the bottom and top boundaries of the convection zone is greater when the anisotropy is stronger. It is shown that the critical dynamo number and the dynamo period approach to constant values for large values of the anisotropy parameter. The anisotropy reduces the overlap of toroidal magnetic fields generated in subsequent dynamo cycles, in the time-latitude "butterfly" diagram. If we assume that sunspots are formed in the vicinity of the subsurface shear layer, then the distributed dynamo model with the anisotropic diffusivity satisfies the observational constraints from helioseismology and is consistent with the value of effective turbulent diffusion estimated from the dynamics of surface magnetic fields.

## **The solar cycle variation of topological structures in the global solar corona**

S. J. **Platten**, C. E. Parnell, A. L. Haynes, E. R. Priest and D. H. Mackay

A&A 565, A44 (2014)

<http://arxiv.org/pdf/1406.5333v1.pdf>

Context. The complicated distribution of magnetic flux across the solar photosphere results in a complex web of coronal magnetic field structures. To understand this complexity, the magnetic skeleton of the coronal field can be calculated. The skeleton highlights the (separatrix) surfaces that divide the field into topologically distinct regions, allowing open-field regions on the solar surface to be located. Furthermore, separatrix surfaces and their intersections with other separatrix surfaces (i.e., separators) are important likely energy release sites.

Aims. The aim of this paper is to investigate, throughout the solar cycle, the nature of coronal magnetic-field topologies that arise under the potential-field source-surface approximation. In particular, we characterise the typical global fields at solar maximum and minimum.

Methods. Global magnetic fields are extrapolated from observed Kitt Peak and SOLIS synoptic magnetograms, from Carrington rotations 1645 to 2144, using the potential-field source-surface model. This allows the variations in the coronal skeleton to be studied over three solar cycles.

Results. The main building blocks which make up magnetic fields are identified and classified according to the nature of their separatrix surfaces. The magnetic skeleton reveals that, at solar maximum, the global coronal field involves a multitude of topological structures at all latitudes criss-crossing throughout the atmosphere. **Many open-field regions exist originating anywhere on the photosphere.** At solar minimum, the coronal topology is heavily influenced by the solar magnetic dipole. A strong dipole results in a simple large-scale structure involving just two large polar open-field regions, but, at short radial distances between  $\pm 60^\circ$  latitude, the small-scale topology is complex. If the solar magnetic dipole is weak, as in the recent minimum, then the low-latitude quiet-sun magnetic fields may be globally significant enough to create many disconnected open-field regions between  $\pm 60^\circ$  latitude, in addition to the two polar open-field regions.

### **Estimation of the Lifetime of Slow-Decaying Unipolar Active Regions in the Framework of the Turbulent Erosion Model.**

**Plotnikov**, A., Abramenko, V. & Kutsenko, A.

Sol Phys 299, 34 (2024).

<https://doi.org/10.1007/s11207-024-02278-y>

We explore the properties and behavior of slow-decaying unipolar sunspot groups in the framework of the turbulent erosion model suggested by Petrovay and Moreno-Insertis (Astrophys. J. 485, 398, 1997). The basic concept of the model is the suppression of turbulent diffusivity inside a magnetic flux tube by strong magnetic fields. As a result, the outer turbulent plasma detaches magnetic features primarily from the external border of a magnetic flux tube. The radius of the tube exhibits inward progression at a constant rate. The model predicts older sunspots to decay slower, and it seems to be very promising to explain the slow decay of long-living unipolar sunspot groups. By analyzing the magnetic structure associated with a sunspot, we did reveal a gradual decrease in the magnetic structure radius at a constant rate, implying the validity of the model. However, in some cases, the derived velocity of the radius decrease was too low: our calculations provided implausibly high estimations for the lifetime and maximal area of such sunspots. We discuss possible additional mechanisms affecting the decay rate of such peculiar sunspots.

### **Statistical analysis of the total magnetic flux decay rate in solar active regions**

**Andrei A. Plotnikov**, **Valentina I. Abramenko**, **Alexander S. Kutsenko**

MNRAS Volume 521, Issue 2, May 2023, Pages 2187–2195,

<https://doi.org/10.1093/mnras/stad691>

<https://arxiv.org/pdf/2303.01321.pdf>

We used line-of-sight magnetograms acquired by the Helioseismic and Magnetic Imager on board the Solar Dynamics Observatory to derive the decay rate of total unsigned magnetic flux for 910 ephemeral and active regions (ARs) observed between 2010 and 2017. We found that: i) most of the ARs obey the power law dependence between the peak magnetic flux and the magnetic flux decay rate, DR, so that  $DR \sim \Phi^{0.70}$ ; ii) larger ARs lose smaller fraction of their magnetic flux per unit of time than the smaller ARs; iii) there exists a cluster of ARs exhibiting significantly lower decay rate than it would follow from the power law and all of them are unipolar sunspots with total fluxes in the narrow range of  $(2-8) \times 10^{21}$  Mx; iv) a comparison with our previous results shows that the emergence rate is always higher than the decay rate. The emergence rate follows a power law with a shallower slope than the slope of the decay-rate power law. The results allowed us to suggest that not only the maximum total magnetic flux determines the character of the decaying regime of the AR, some of the ARs end up as a slowly decaying unipolar sunspot; there should be certain physical mechanisms to stabilize such a sunspot.

**Correction:** MNRAS Volume 521, Issue 4, June 2023, Pages 6293–6294,

<https://doi.org/10.1093/mnras/stad1031> <https://watermark.silverchair.com/stad1031.pdf>

## Improvements of the Longitudinal Magnetic Field Measurement from the Solar Magnetic Field Telescope at the Huairou Solar Observing Station

[Andrei Plotnikov](#), [Alexander Kutsenko](#), [Shangbin Yang](#), [Haiqing Xu](#), [Xianyong Bai](#), [Hongqi Zhang](#) & [Kirill Kuzanyan](#)

*Solar Physics* volume 296, Article number: 165 (2021)

<https://link.springer.com/content/pdf/10.1007/s11207-021-01901-6.pdf>

<https://doi.org/10.1007/s11207-021-01901-6>

The weak-field approximation, implying a linear relationship between Stokes-V/IV/I and the longitudinal magnetic field  $B_{\parallel}|B|$ , often suffers from saturation observed in strong magnetic-field regions such as sunspot umbrae. In this work, we seek to improve the magnetic-field observations carried out by the Solar Magnetic Field Telescope (SMFT) at the Huairou Solar Observing Station, China. We propose using a non-linear relationship between Stokes-V/IV/I and  $B_{\parallel}|B|$  to derive the magnetic field. To determine the form of the relationship, we perform a cross-calibration of the observed SMFT data and magnetograms provided by the Helioseismic and Magnetic Imager onboard the Solar Dynamics Observatory. The algorithm for the magnetic-field derivation is described in detail. We show that using a non-linear relationship between Stokes-V/IV/I and  $B_{\parallel}|B|$  allows us to eliminate magnetic-field saturation inside the sunspot umbra. The proposed technique enables one to enhance the reliability of the SMFT magnetic-field data obtained even long before the space-based instrumentation era, since 1987.

## High-fidelity 3D Reconstruction of Solar Coronal Physics with the Updated CROBAR Method

Joseph **Plowman** (1), [Daniel B. Seaton](#) (1), [Amir Caspi](#) (1), [J. Marcus Hughes](#) (1), [Matthew J. West](#) (1)  
ApJ 2023

<https://arxiv.org/pdf/2309.08053.pdf>

We present an extension of the Coronal Reconstruction Onto B-Aligned Regions (CROBAR) method to Linear Force Free Field (LFFF) extrapolations, and apply it to the reconstruction of a set of AIA, MDI, and STEREO EUVI data. The results demonstrate that CROBAR can not only reconstruct coronal emission structures, but also that it can help constrain the coronal field extrapolations via the LFFF's helicity  $\alpha$  parameter. They also provide a real-world example of how CROBAR can easily incorporate information from multiple perspectives to improve its reconstructions, and we also use the additional perspectives to help validate the reconstructions. We furthermore touch on the use of real-world emission passbands rather than idealized power-law type ones using DEMs. We conclude with a comparison of CROBAR generated emission to observed emission and those produced with idealized DEM based power-laws. These results further illustrate the promise of CROBAR for real-world applications, and we make available a preliminary release of the software available for download. **2010-07-25**

## Three-dimensional Reconstruction of Coronal Plasma Properties from a Single Perspective

Joseph **Plowman**<sup>1</sup>

2021 ApJ 922 109

<https://doi.org/10.3847/1538-4357/ac2664>

Much of our understanding of the state of coronal plasmas comes from observations that are optically thin. This means that light travels freely through the corona without being materially affected by it, which allows it to be easily seen through, but also results in a line-of-sight degeneracy that has previously thwarted attempts to recover the three-dimensional structure of the coronal plasma. However, although the corona is disorganized in the line-of-sight direction, it is highly organized in the field-aligned direction. This paper demonstrates how to exploit this organization to resolve the line-of-sight degeneracy in the plasma properties using a suitable magnetic field structure. This allows, for the first time, the two-dimensional optically thin plasma observations to directly drive the three-dimensional plasma reconstruction throughout an entire active region (or larger). A preliminary investigation with a potential field is shown, finding a solution which clearly resembles the real solar data, even with a single perspective. The results indicate that there is ample information in the resulting residuals that can be used to refine the magnetic field structure, suggesting that these residuals can in turn be used to directly constrain the magnetic field extrapolations used in the reconstruction. The paper concludes with a discussion of how these residuals can in turn be used to directly drive the magnetic field extrapolations.

## Single-point Inversion of the Coronal Magnetic Field

Joseph **Plowman**

2014 ApJ 792 23.

The Fe XIII 10747 and 10798 Å lines observed in the solar corona are sensitive to the coronal magnetic field in such a way that, in principle, the full vector field at a point on the line of sight can be inferred from their combined polarization signals. This paper presents analytical inversion formulae for the field parameters and analyzes the uncertainty of magnetic field measurements made from such observations, assuming emission dominated by a single region along the line of sight. We consider the case of the current Coronal Multi-channel Polarimeter (CoMP)

instrument as well as the future Coronal Solar Magnetism Observatory (COSMO) and Advanced Technology Solar Telescope (ATST) instruments. Uncertainties are estimated with a direct analytic inverse and with a Markov Chain Monte Carlo algorithm. We find that (in effect) two components of the vector field can be recovered with CoMP, and well recovered with COSMO or ATST, but that the third component can only be recovered when the solar magnetic field is strong and optimally oriented.

## **CORONAL LOOP EXPANSION PROPERTIES EXPLAINED USING SEPARATORS**

Joseph E. [Plowman](#), [Charles C. Kankelborg](#) and [Dana W. Longcope](#)

2009 ApJ 706 108-112

One puzzling observed property of coronal loops is that they are of roughly constant thickness along their length. Various studies have found no consistent pattern of width variation along the length of loops observed by TRACE and *SOHO*. This is at odds with expectations of magnetic flux tube expansion properties, which suggests that loops are widest at their tops, and significantly narrower at their footpoints. Coronal loops correspond to areas of the solar corona which have been preferentially heated by some process, so this observed property might be connected to the mechanisms that heat the corona. One means of energy deposition is magnetic reconnection, which occurs along field lines called *separators*. These field lines begin and end on magnetic null points, and loops forming near them can therefore be relatively wide at their bases. Thus, coronal energization by magnetic reconnection may replicate the puzzling expansion properties observed in coronal loops. We present results of a Monte Carlo survey of separator field line expansion properties, comparing them to the observed properties of coronal loops.

## **Modeling Magnetic Flux Emergence in Bipolar Active Regions**

[Mariano Poisson](#), [Marcelo López Fuentes](#), [Cristina H. Mandrini](#), [Pascal Démoulin](#), [Francisco Grings](#)

Solar Phys. 2024

<https://arxiv.org/pdf/2405.12208>

Active regions (ARs) appear in the solar atmosphere as a consequence of the emergence of magnetic flux-ropes (FR). In this study, we use Bayesian methods to analyze line-of-sight magnetograms of emerging ARs. We employ a FR model consisting of a half-torus field structure based on eight parameters. The goal is to derive constrained physical parameters of the originating FR which are consistent with the observations. Specifically, we aim to obtain a precise estimation of the AR tilt angle and magnetic twist at different stages of the emergence process. To achieve this, we propose four temporal methods that correlate the field parameter evolutions with a single coherent FR. These methods differ from each other in the size of the explored parameter space. We test the methods on four bipolar ARs observed with the Michelson Doppler Imager on board the Solar and Heliospheric Observatory. We find that tilt angles are typically consistent between the temporal methods, improving previous estimations at all stages of the emergence. The twist sign derived from the temporal methods is consistent with previous estimations. The standard errors of all the methods used are similar, indicating that they model the observations equally well. These results indicate that the proposed methods can be used to obtain global magnetic parameters of ARs during their early evolution. The derived parameters contribute to a better understanding of the formation of FRs, and the role of ARs in the magnetic recycling process along the solar cycle.

## **Bayesian approach for modeling global magnetic parameters for the solar active region★**

M. [Poisson](#)<sup>1</sup>, F. Grings<sup>1</sup>, C. H. Mandrini<sup>1</sup>, M. López Fuentes<sup>1</sup> and P. Démoulin<sup>2,3</sup>

A&A 665, A101 (2022)

<https://www.aanda.org/articles/aa/pdf/2022/09/aa44058-22.pdf>

Context. Active regions (ARs) appear in the solar atmosphere as a consequence of the emergence of magnetic flux tubes. The presence of elongated magnetic polarities in line-of-sight (LOS) magnetograms indicates the existence of twist in the flux tubes that form them. These polarity elongations, referred to as magnetic tongues, bias the measurement of AR characteristics obtained during their emergence phase (e.g., their tilt angle and magnetic flux). In particular, obtaining a good estimation of the tilt angle evolution plays a key role in constraining flux-transport dynamo models.

Aims. In this work, we aim to estimate the intrinsic properties of the twisted flux tubes, or flux ropes, that form ARs by quantitatively comparing observed LOS magnetograms with synthetic ones derived from a toroidal magnetic flux tube model.

Methods. We developed a Bayesian inference method to obtain the statistical distributions of the inferred model parameters. As an example, we applied the method to NOAA AR 10268. Next, we tested the results using a synthetic-AR generator to quantify the effect of small-scale perturbations over the inferred parameter distributions. Results. We conclude that this method can significantly remove the effects of magnetic tongues on the derived AR global characteristics, providing a better understanding of the intrinsic properties of the emerging flux rope.

Conclusions. These results provide a framework for future analyses of the physical properties of emerging ARs using Bayesian statistics.

## Active-Region Tilt Angles from White-Light Images and Magnetograms: The Role of Magnetic Tongues

M. [Poisson](#), [P. Démoulin](#), [C.H. Mandrini](#), [M.C. López Fuentes](#)

ApJ 894 131 2020

<https://arxiv.org/pdf/2004.07345.pdf>

<https://doi.org/10.3847/1538-4357/ab8944>

The presence of elongations in active region (AR) polarities, called magnetic tongues, are mostly visible during their emergence phase. AR tilts have been measured thoroughly using long-term white-light (WL) databases, sometimes combined with magnetic field information. Since the influence of magnetic tongues on WL tilt measurements has not been taken into account before, we aim to investigate their role in tilt-angle values and to compare them with those derived from LOS magnetograms. We apply four methods to compute the tilt angle of generally bipolar ARs: one applies the k-means algorithm to WL data, a second one includes the magnetic field sign of the polarities to WL data, and a third one uses the magnetic flux-weighted center of each polarity. The tilt values computed in any of these ways are affected by the presence of magnetic tongues. Therefore, we apply the newly developed Core Field Fit Estimator (CoFFE) method to separate the magnetic flux in the tongues from that in the AR core. We compare the four computed tilt-angle values, as well as these with the ones reported in long-term WL databases. For ARs with low magnetic flux tongues the different methods report consistent tilt-angle values. But for ARs with high flux tongues there are noticeable discrepancies between all methods indicating that magnetic tongues affect differently WL and magnetic data. However, in general, CoFFE achieves a better estimation of the main bipole tilt because it removes both the effect of tongues as well as the emergence of secondary bipoles when it occurs in between the main bipole magnetic polarities. **2001-08-11, 2001-12-22, 2002-04-14, 2006-05-01, 2008-11-01, 2009-09-23**

## Correcting the effect of magnetic tongues on the tilt angle of bipolar active regions

M. [Poisson](#), [M.C. López Fuentes](#), [C.H. Mandrini](#), [P. Démoulin](#), [C. MacCormack](#)

A&A 633, A151 2020

<https://arxiv.org/pdf/1912.12990.pdf>

<https://doi.org/10.1051/0004-6361/201936924>

The magnetic polarities of bipolar active regions (ARs) exhibit elongations in line-of-sight magnetograms during their emergence. These elongations are referred to as magnetic tongues and attributed to the presence of twist in the emerging magnetic flux-ropes (FRs) that form ARs. The presence of magnetic tongues affects the measurement of any AR characteristic that depends on its magnetic flux distribution. The AR tilt-angle is one of them. We aim to develop a method to isolate and remove the flux associated with the tongues to determine the AR tilt-angle with as much precision as possible. As a first approach, we used a simple emergence model of a FR. This allowed us to develop and test our aim based on a method to remove the effects of magnetic tongues. Then, using the experience gained from the analysis of the model, we applied our method to photospheric observations of bipolar ARs that show clear magnetic tongues. Using the developed procedure on the FR model, we can reduce the deviation in the tilt estimation by more than 60%. Next we illustrate the performance of the method with four examples of bipolar ARs selected for their large magnetic tongues. The new method efficiently removes the spurious rotation of the bipole. This correction is mostly independent of the method input parameters and significant since it is larger than all the estimated tilt errors. We have developed a method to isolate the magnetic flux associated with the FR core during the emergence of bipolar ARs. This allows us to compute the AR tilt-angle and its evolution as precisely as possible. We suggest that the high dispersion observed in the determination of AR tilt-angles in studies that massively compute them from line-of sight magnetograms can be partly due to the existence of magnetic tongues whose presence is not sufficiently acknowledged.

## Properties of Magnetic Tongues over a Solar Cycle

Mariano [Poisson](#), Pascal Démoulin, Marcelo López Fuentes, Cristina H. Mandrini

Solar Phys. Volume 291, [Issue 6](#), pp 1625–1646 2016

The photospheric spatial distribution of the main magnetic polarities of bipolar active regions (ARs) present during their emergence deformations are known as magnetic tongues. They are attributed to the presence of twist in the toroidal magnetic-flux tubes that form the ARs. The aim of this article is to study the twist of newly emerged ARs from the evolution of magnetic tongues observed in photospheric line-of-sight magnetograms. We apply the procedure described by Poisson et al. (Solar Phys. 290, 727, [2015a](#)) to ARs observed over the full Solar Cycle 23 and the beginning of Cycle 24. Our results show that the hemispherical rule obtained using the tongues as a proxy of the twist has a weak sign dominance (53 % in the southern hemisphere and 58 % in the northern hemisphere). By defining the variation of the tongue angle, we characterize the strength of the magnetic tongues during different phases of the AR emergence. We find that there is a tendency of the tongues to be stronger during the beginning of the emergence and to become weaker as the AR reaches its maximum magnetic flux. We compare this evolution with the emergence of a toroidal flux-rope model with non-uniform twist. The variety of evolution of the tongues in the analyzed ARs can only be reproduced when using a broad range of twist profiles, in particular having a large variety of twist gradients in the direction vertical to the photosphere. Although the analytical model used is a special



case, selected to minimize the complexity of the problem, the results obtained set new observational constraints to theoretical models of flux-rope emergence that form bipolar ARs.

### **Active-Region Twist Derived from Magnetic Tongues and Linear Force-Free Extrapolations**

Mariano [Poisson](#), Marcelo López Fuentes, Cristina H. Mandrini, Pascal Démoulin  
Solar Phys. Volume 290, [Issue 11](#), pp 3279-3294 **2015**

The main aim of this study is to compare the amount of twist present in emerging active regions (ARs) from photospheric and coronal data. We use linear force-free field models of the observed coronal structure of ARs to determine the global twist. The coronal twist is derived, on one hand, from the force-free parameter [ $\alpha$ ] of the model and, on the other, from the computed coronal magnetic helicity normalized by the magnetic flux squared. We compare our results, for the same set of ARs, with those of Poisson et al. (Solar Phys. 290, 727, [2015](#)), in which the twist was estimated using the so-called magnetic tongues observed in line-of-sight magnetograms during AR emergence. We corroborate the agreement between the photospheric and coronal twist-sign and the presence of magnetic tongues as an early proxy of the AR non-potentiality. We find a globally linear relationship between the coronal twist and the one previously deduced for the emerging AR flux rope at the photospheric level. The coronal-twist value is typically lower by a factor of six than the one deduced for the emerging flux rope. We interpret this result as due to the partial emergence of the flux rope that forms the region.

### **Evidence of Twisted Flux-Tube Emergence in Active Regions**

M. [Poisson](#), C. H. Mandrini, P. Démoulin, M. López Fuentes  
Solar Physics March **2015**, Volume 290, Issue 3, pp 727-751  
<http://arxiv.org/pdf/1505.01805v1.pdf>

Elongated magnetic polarities are observed during the emergence phase of bipolar active regions (ARs). These extended features, called magnetic tongues, are interpreted as a consequence of the azimuthal component of the magnetic flux in the toroidal flux-tubes that form ARs. We develop a new systematic and user-independent method to identify AR tongues. Our method is based on determining and analyzing the evolution of the AR main polarity inversion line (PIL). The effect of the tongues is quantified by measuring the acute angle [ $\tau$ ] between the orientation of the PIL and the direction orthogonal to the AR main bipolar axis. We apply a simple model to simulate the emergence of a bipolar AR. This model lets us interpret the effect of magnetic tongues on parameters that characterize ARs (e.g. the PIL inclination and the tilt angles, and their evolution). In this idealized kinematic emergence model,  $\tau$  is a monotonically increasing function of the twist and has the same sign as the magnetic helicity. We systematically apply our procedure to a set of bipolar ARs (41 ARs) that were observed emerging in line-of-sight magnetograms over eight years. For most of the cases studied, the tongues only have a small influence on the AR tilt angle since tongues have a much lower magnetic flux than the more concentrated main polarities. From the observed evolution of  $\tau$ , corrected for the temporal evolution of the tilt angle and its final value when the AR is fully emerged, we estimate the average number of turns in the subphotospherically emerging flux-rope. These values for the 41 observed ARs are below unity, except for one. This indicates that subphotospheric flux-ropes typically have a low amount of twist, i.e. highly twisted flux-tubes are rare. Our results demonstrate that the evolution of the PIL is a robust indicator of the presence of tongues and constrains the amount of twist in emerging flux-tubes.

### **Modeling line-of-sight magnetograms of active regions**

[M. Poisson](#), [M. López Fuentes](#), [C. H. Mandrini](#), [F. Grings](#), [P. Démoulin](#)  
Proceedings IAU Symposium No. xxx, **2008**  
<https://arxiv.org/pdf/2312.06599.pdf>

Active regions (ARs) appear in the solar atmosphere as a consequence of the emergence of magnetic flux ropes (FRs). Due to the presence of twist, the photospheric line-of-sight (LOS) magnetograms of emerging ARs show an elongation of the polarities known as magnetic tongues. These tongues can affect the estimation of tilt angles during their emergence phase. In this work, we propose a Bayesian method to model LOS magnetograms of emerging ARs using a half-torus twisted FR model. We apply this model to 21 emerging ARs observed during Solar Cycle 23. We find that the Bayesian method corrects the tilt when compared to other methods, removing the spurious rotation of the polarities produced by the retraction of the tongues during the emergence. We find a variation in Joy's law with the stage of the AR emergence and the method used for its estimation.

### **Time-dependent Data-driven Modeling of Active Region Evolution Using Energy-optimized Photospheric Electric Fields**

Jens [Pomoell](#), Erkkka Lumme, Emilia Kilpua

[Solar Physics](#) April 2019, 294:41

<https://link.springer.com/content/pdf/10.1007%2Fs11207-019-1430-x.pdf>

In this work, we present results of a time-dependent data-driven numerical simulation developed to study the dynamics of coronal active region magnetic fields. The evolving boundary condition driving the model, the photospheric electric field, is inverted using a time sequence of vector magnetograms as input. We invert three distinct electric field datasets for a single active region. All three electric fields reproduce the observed evolution of the normal component of the magnetic field. Two of the datasets are constructed so as to match the energy input into the corona to that provided by a reference estimate. Using the three inversions as input to a time-dependent magnetofrictional model, we study the response of the coronal magnetic field to the driving electric fields. The simulations reveal the magnetic field evolution to be sensitive to the input electric field despite the normal component of the magnetic field evolving identically and the total energy injection being largely similar. Thus, we demonstrate that the total energy injection is not sufficient to characterize the evolution of the coronal magnetic field: coronal evolution can be very different despite similar energy injections. We find the relative helicity to be an important additional metric that allows one to distinguish the simulations. In particular, the simulation with the highest relative helicity content produces a coronal flux rope that subsequently erupts, largely in agreement with extreme-ultraviolet imaging observations of the corresponding event. Our results suggest that time-dependent data-driven simulations that employ carefully constructed driving boundary conditions offer a valuable tool for modeling and characterizing the evolution of coronal magnetic fields. **2012.06.11-15**

### **The effect of reconnection on the structure of the Sun's open-closed-flux boundary**

D. I. **Pontin**, P. F. Wyper

ApJ **805** 39 **2015**

<http://arxiv.org/pdf/1502.01311v1.pdf>

Global magnetic field extrapolations are now revealing the huge complexity of the Sun's corona, and in particular the structure of the boundary between open and closed magnetic flux. Moreover, recent developments indicate that magnetic reconnection in the corona likely occurs in highly fragmented current layers, and that this typically leads to a dramatic increase in the topological complexity beyond that of the equilibrium field. In this paper we investigate the consequences of reconnection at the open-closed flux boundary ("interchange reconnection") in a fragmented current layer. We demonstrate that it leads to a situation in which magnetic flux (and therefore plasma) from open and closed field regions is efficiently mixed together. This corresponds to an increase in the length and complexity of the open-closed boundary. Thus, whenever reconnection occurs at a null point or separator of the open-closed boundary, the associated separatrix arc of the so-called "S-web" in the high corona becomes not a single line but a band of finite thickness within which the open-closed flux boundary is highly structured. This has significant implications for the acceleration of the slow solar wind, for which the interaction of open and closed field is thought to be important, and may also explain the coronal origins of certain solar energetic particles. The topological structures examined contain magnetic null points, separatrices and separators, and include a model for a pseudo-streamer. The potential for understanding both the large scale morphology and fine structure observed in flare ribbons associated with coronal nulls is also discussed.

### **Properties of sunspot light bridges on a geometric height scale**

S. Esteban **Pozuelo**<sup>1,2,\*</sup>, A. Asensio Ramos<sup>1,2</sup>, C. J. Díaz Baso<sup>3,4</sup> and B. Ruiz Cobo<sup>1,2</sup>

A&A, 689, A255 (**2024**)

<https://doi.org/10.1051/0004-6361/202348181>

<https://www.aanda.org/articles/aa/pdf/2024/09/aa48181-23.pdf>

Context. Investigating light bridges (LBs) helps us comprehend key aspects of sunspots. However, few studies have analyzed the properties of LBs in terms of the geometric height, which is a more realistic perspective given the corrugation of the solar atmosphere.

Aims. We aim to shed light on LBs by studying the variation in their physical properties with geometric height.

Methods. We used the SICON code to infer the physical quantities in terms of the optical depth and the Wilson depression values of three LBs hosted by a sunspot observed with Hinode/SP in the Fe I 630 nm pair lines. We also used SIR inversions to cross-check the height variation of the field inclination in the LBs. In both output sets, we performed linear interpolation to convert the physical parameters from optical depth into a geometric height scale in each pixel.

Results. Depending on their general appearance, we classified each LB as filamentary, grainy, or umbral. They appear as ridges that reach different maximum heights, with the umbral LB being the deepest. While the filamentary LB hosts a plasma inflow from the penumbra, the results for the grainy LB are compatible with an injection of hot plasma through convective cells of reduced field strength. Only a few positions reveal hints suggesting a cusp-like magnetic canopy. Moreover, strong gradients in the magnetic field strength and inclination usually exhibit enhanced electric currents, with the filamentary LB having remarkably strong currents that appear to be related to chromospheric events.

Conclusions. The height stratification in filamentary and grainy LBs differ, indicating diverse mechanisms at work. Our results are in general incompatible with a magnetic canopy scenario, and further analysis is needed to confirm whether it exists along the entire LB or only at specific locations. Furthermore, this work assesses the usefulness of the SICON code when determining the height stratification of solar structures.

### **Estimating the longitudinal magnetic field in the chromosphere of quiet-Sun magnetic concentrations**

[S. Esteban Pozuelo](#), [A. Asensio Ramos](#), [J. de la Cruz Rodríguez](#), [J. Trujillo Bueno](#), [M. J. Martínez González](#)

A&A **2023**

<https://arxiv.org/pdf/2302.04258>

Details of the magnetic field in the quiet Sun chromosphere are key to our understanding of essential aspects of the solar atmosphere. We aim to determine the longitudinal magnetic field component ( $B_{\text{lon}}$ ) of quiet Sun regions depending on their size. We estimated  $B_{\text{lon}}$  by applying the weak-field approximation (WFA) to high-spatial-resolution Ca II 854.2 nm data taken with the Swedish 1m Solar Telescope. Specifically, we analyzed the estimates inferred for different spectral ranges using the data at the original cadence and temporally integrated signals. The longitudinal magnetic field in each considered plasma structure correlates with its size. Using a spectral range restricted to the line core leads to chromospheric longitudinal fields varying from 50 G at the edges to 150-500 G at the center of the structure. These values increase as the spectral range widens due to the photospheric contribution. However, the difference between this contribution and the chromospheric one is not uniform for all structures. Small and medium-sized concentrations show a steeper height gradient in  $B_{\text{lon}}$  compared to their chromospheric values, so estimates for wider ranges are less trustworthy. Signal addition does not alleviate this situation as the height gradients in  $B_{\text{lon}}$  are consistent with time. Finally, despite the amplified noise levels that deconvolving processes may cause, data restored with the destretching technique show similar results, though are affected by smearing. We obtained  $B_{\text{lon}}$  estimates similar to those previously found, except for large concentrations and wide spectral ranges. In addition, we report a correlation between the height variation of  $B_{\text{lon}}$  compared to the chromospheric estimates and the concentration size. This correlation affects the difference between the photospheric and chromospheric magnetic flux values and the reliability of the estimates for wider spectral ranges.

### **Observationally based models of penumbral microjets**

S. Esteban [Pozuelo](#), [J. de la Cruz Rodríguez](#), [A. Drews](#), [L. Rouppe van der Voort](#), [G.B. Scharmer](#), [M. Carlsson](#)

2019 *ApJ* **870** 88

<https://arxiv.org/pdf/1811.07881.pdf>

[sci-hub.tw/10.3847/1538-4357/aaf28a](https://sci-hub.tw/10.3847/1538-4357/aaf28a)

We study the polarization signals and physical parameters of penumbral microjets (PMJs) by using high spatial resolution data taken in the Fe I 630 nm pair, Ca II 854.2 nm and Ca II K lines with the CRISP and CHROMIS instruments at the Swedish 1-m Solar Telescope. We infer their physical parameters, such as physical observables in the photosphere and chromospheric velocity diagnostics, by different methods, including inversions of the observed Stokes profiles with the STiC code. PMJs harbor overall brighter Ca II K line profiles and conspicuous polarization signals in Ca II 854.2 nm, specifically in circular polarization that often shows multiple lobes mainly due to the shape of Stokes I. They usually overlap photospheric regions with sheared magnetic field configuration, suggesting that magnetic reconnections could play an important role in the origin of PMJs. The discrepancy between their low LOS velocities and the high apparent speeds reported on earlier, as well as the existence of different vertical velocity gradients in the chromosphere, indicate that PMJs might not be entirely related to mass motions. Instead, PMJs could be due to perturbation fronts induced by magnetic reconnections occurring in the deep photosphere that propagate through the chromosphere. This reconnection may be associated with current heating that produces temperature enhancements from the temperature minimum region. Furthermore, enhanced collisions with electrons could also increase the coupling to the local conditions at higher layers during the PMJ phase, giving a possible explanation for the enhanced emission in the overall Ca II K profiles emerging from these transients. **September 5th, 2016**

### **Properties of Supersonic Evershed Downflows**

Sara Esteban [Pozuelo](#), Luis R. Bellot Rubio, Jaime de la Cruz Rodríguez

*ApJ* **832** 170 **2016**

<http://arxiv.org/pdf/1609.01106v1.pdf>

We study supersonic Evershed downflows in a sunspot penumbra by means of high spatial resolution spectropolarimetric data acquired in the Fe I 617.3 nm line with the CRISP instrument at the Swedish 1-m Solar Telescope. Physical observables, such as Dopplergrams calculated from line bisectors and Stokes V zero-crossing wavelengths, and Stokes V maps in the far red wing, are used to find regions where supersonic Evershed downflows may exist. We retrieve the LOS velocity and the magnetic field vector in these regions using two-component

inversions of the observed Stokes profiles with the help of the SIR code. We follow these regions during their lifetime to study their temporal behavior. Finally, we carry out a statistical analysis of the detected supersonic downflows to characterize their physical properties. Supersonic downflows are contained in compact patches moving outward, which are located in the mid and outer penumbra. They are observed as bright, roundish structures at the outer end of penumbral filaments that resemble penumbral grains. The patches may undergo fragmentations and mergings during their lifetime, even some of them are recurrent. Supersonic downflows are associated with strong and rather vertical magnetic fields with a reversed polarity compared to that of the sunspot. Our results suggest that downflows returning back to the solar surface with supersonic velocities are abruptly stopped in dense deep layers and produce a shock. Consequently, this shock enhances the temperature and is detected as a bright grain in the continuum filtergrams, which could explain the existence of outward moving grains in the mid and outer penumbra. 28 September 2011

### **Lateral downflows in sunspot penumbral filaments and their temporal evolution**

S. Esteban [Pozuelo](#), L. R. Bellot Rubio, J. de la Cruz Rodriguez

ApJ **803** 93 **2015**

<http://arxiv.org/pdf/1502.02981v1.pdf>

We study the temporal evolution of downflows observed at the lateral edges of penumbral filaments in a sunspot located very close to the disk center. Our analysis is based on a sequence of nearly diffraction-limited spectropolarimetric scans of the Fe I 6173 Å line taken with the CRISP instrument at the Swedish 1-m Solar Telescope. We compute Dopplergrams from the observed intensity profiles using line bisectors and filter the resulting velocity maps for subsonic oscillations. Lateral downflows appear everywhere in the center-side penumbra as small, weak patches of redshifts next to or along the edges of blueshifted flow channels. These patches have an intermittent life and undergo mergings and fragmentations quite frequently. The lateral downflows move together with the hosting filaments and react to their shape variations, very much resembling the evolution of granular convection in the quiet Sun. There is a good relation between brightness and velocity of the flow structures in the center-side penumbra, with downflows being darker than upflows on average, which is again reminiscent of convection in the quiet Sun. These results point to the existence of overturning convection in sunspot penumbrae, with elongated cells in the radial direction where the flow is upward but very inclined, and weak lateral downward flows. In general, the circular polarization profiles emerging from the lateral downflows do not show sign reversals, although sometimes we detect three-lobed profiles which are suggestive of opposite magnetic polarities in the pixel. **Movies are available at this http URL.** 28 September 2011

### **The magnetic fine structure of the Sun's polar region as revealed by Sunrise**

A. [Prabhu](#)<sup>1</sup>, A. Lagg<sup>1</sup>, J. Hirzberger<sup>1</sup> and S. K. Solanki<sup>1,2</sup>

A&A **644**, A86 (**2020**)

<https://www.aanda.org/articles/aa/pdf/2020/12/aa38704-20.pdf>

Context. Polar magnetic fields play a key role in the solar magnetic cycle and they are the source of a significant portion of the interplanetary magnetic field. However, observations of the poles are challenging and hence our understanding of the polar magnetic environment is incomplete.

Aims. We deduce properties of small-scale magnetic features in the polar region using high-resolution data and specifically aim to determine the flux per patch above which one magnetic polarity starts to dominate over the other.

Methods. We study the high spatial resolution, seeing-free observations of the north solar polar region, obtained with the IMAx instrument on-board the balloon-borne SUNRISE observatory during June 2009, at the solar activity minimum. We performed inversions of the full Stokes vector recorded by IMAx to retrieve atmospheric parameters of the Sun's polar region, mainly the temperature stratification and the magnetic field vector.

Results. We infer kilo-Gauss (kG) magnetic fields in patches harbouring polar faculae, without resorting to a magnetic filling factor. Within these patches we find the maxima of the magnetic field to be near the dark narrow lanes, which are shifted towards the disc centre side in comparison to the maxima in continuum intensity. In contrast, we did not find any fields parallel to the solar surface with kG strengths. In addition to the kG patches, we found the polar region to be covered in patches of both polarities, which have a range of sizes. We find the field strength of these patches to increase with increasing size and flux, with the smaller patches showing a significant dispersion in field strength. The dominating polarity of the north pole during this phase of the solar cycle is found to be maintained by the larger patches with fluxes above  $2.3 \times 10^{17}$  Mx. **16 June 2009**

### **Magnetohydrodynamic simulation of magnetic null-point reconnections in NOAA AR12192 initiated with an extrapolated non-force-free-field**

[A. Prasad](#), [R. Bhattacharyya](#), [Qiang Hu](#), [Sanjay Kumar](#), [Sushree S. Nayak](#)

ApJ **2018**

<https://arxiv.org/pdf/1805.00635.pdf>

Magnetohydrodynamics of the solar corona is simulated numerically. The simulation is initialized with an extrapolated non-force-free magnetic field using the vector magnetogram of the active region (AR) NOAA 12192 obtained on the solar photosphere. Particularly, we focus on the magnetic reconnections occurring close to a magnetic null-point that resulted in appearance of circular chromospheric flare ribbons on **October 24, 2014** around 21:21 UT, after peak of an X3.1 flare. The extrapolated field lines show the presence of the three-dimensional (3D) null near one of the polarity inversion lines---where the flare was observed. In the subsequent numerical simulation, we find magnetic reconnections occurring near the null point, where the magnetic field lines from the fan-plane of the 3D null form a X-type configuration with underlying arcade field lines. The footpoints of the dome-shaped field lines, inherent to the 3D null, show high gradients of the squashing factor. We find slipping reconnections at these quasi-separatrix layers, which are co-located with the post-flare circular brightening observed at the chromospheric heights. This demonstrates the viability of the initial non-force-free field along with the dynamics it initiates. Moreover, the initial field and its simulated evolution is found to be devoid of any flux rope, which is in congruence with the confined nature of the flare.

### **Study of magnetic field topology of active region 12192 using an extrapolated non-force-free magnetic field**

[A. Prasad](#), [R. Bhattacharyya](#), [Q. Hu](#), [S. S. Nayak](#), [Sanjay Kumar](#)

Proc. IAU Symp. 340

2018

<https://arxiv.org/pdf/1804.04354.pdf>

The solar active region (AR) 12192 was one of the most flare productive region of solar cycle 24, which produced many X-class flares; the most energetic being an X3.1 flare on **October 24, 2014** at 21:10 UT. Customarily, such events are believed to be triggered by magnetic reconnection in coronal magnetic fields. Here we use the vector magnetograms from solar photosphere, obtained from Heliospheric Magnetic Imager (HMI) to investigate the magnetic field topology prior to the X3.1 event, and ascertain the conditions that might have caused the flare. To infer the coronal magnetic field, a novel non-force-free field (NFFF) extrapolation technique of the photospheric field is used, which suitably mimics the Lorentz forces present in the photospheric plasma. We also highlight the presence of magnetic null points and quasi-separatrix layers (QSLs) in the magnetic field topology, which are preferred sites for magnetic reconnections and discuss the probable reconnection scenarios.

### **The Frequency-dependent Damping of Slow Magnetoacoustic Waves in a Sunspot Umbral Atmosphere**

S. Krishna [Prasad](#), [D. B. Jess](#), [T. Van Doorselaere](#), [G. Verth](#), [R. J. Morton](#), [V. Fedun](#), [R. Erdelyi](#), [D. J. Christian](#)

ApJ **847** 5      2017

<https://arxiv.org/pdf/1708.04835.pdf>

High spatial and temporal resolution images of a sunspot, obtained simultaneously in multiple optical and UV wavelengths, are employed to study the propagation and damping characteristics of slow magnetoacoustic waves up to transition region heights. Power spectra are generated from intensity oscillations in sunspot umbra, across multiple atmospheric heights, for frequencies up to a few hundred mHz. It is observed that the power spectra display a power-law dependence over the entire frequency range, with a significant enhancement around 5.5 mHz found for the chromospheric channels. The phase-difference spectra reveal a cutoff frequency near 3 mHz, up to which the oscillations are evanescent, while those with higher frequencies propagate upwards. The power-law index appears to increase with atmospheric height. Also, shorter damping lengths are observed for oscillations with higher frequencies suggesting frequency-dependent damping. Using the relative amplitudes of the 5.5 mHz (3 minute) oscillations, we estimate the energy flux at different heights, which seems to decay gradually from the photosphere, in agreement with recent numerical simulations. Furthermore, a comparison of power spectra across the umbral radius highlights an enhancement of high-frequency waves near the umbral center, which does not seem to be related to magnetic field inclination angle effects. **2014 August 30**

### **Magnetohydrodynamic Modeling of Solar Coronal Dynamics with an Initial Non-force-free Magnetic Field**

[A. Prasad](#), [R. Bhattacharyya](#), and [Sanjay Kumar](#)

2017 ApJ 840 37

<http://sci-hub.cc/10.3847/1538-4357/aa6c58>

<https://arxiv.org/pdf/1705.02568.pdf>

The magnetic fields in the solar corona are generally neither force-free nor axisymmetric and have complex dynamics that are difficult to characterize. Here we simulate the topological evolution of solar coronal magnetic

field lines (MFLs) using a magnetohydrodynamic model. The simulation is initialized with a non-axisymmetric non-force-free magnetic field that best correlates with the observed vector magnetograms of solar active regions (ARs). To focus on these ideas, simulations are performed for the flaring AR 11283 noted for its complexity and well-documented dynamics. The simulated dynamics develops as the initial Lorentz force pushes the plasma and facilitates successive magnetic reconnections at the two X-type null lines present in the initial field. Importantly, the simulation allows for the spontaneous development of mass flow, unique among contemporary works, that preferentially reconnects field lines at one of the X-type null lines. Consequently, a flux rope consisting of low-lying twisted MFLs, which approximately traces the major polarity inversion line, undergoes an asymmetric monotonic rise. The rise is attributed to a reduction in the magnetic tension force at the region overlying the rope, resulting from the reconnection. A monotonic rise of the rope is in conformity with the standard scenario of flares. Importantly, the simulated dynamics leads to bifurcations of the flux rope, which, being akin to the observed filament bifurcation in AR 11283, establishes the appropriateness of the initial field in describing ARs.

**2011 September 6**

### **A viable non-axisymmetric non-force-free field to represent solar active regions**

A. **Prasad**, R. Bhattacharyya

Physics of Plasmas **2016**

<https://arxiv.org/pdf/1611.05978v1.pdf>

A combination of analytical calculations and vectormagnetogram data are utilized to develop a non-axisymmetric non-force-free magnetic field and assess its viability in describing solar active regions. For the purpose, we construct a local spherical shell where a planar surface, tangential to the inner sphere, represents a Cartesian cutout of an active region. The magnetic field defined on the surface is then correlated with magnetograms. The analysis finds the non-axisymmetric non-force-free magnetic field, obtained by a superposition of two linear-force-free fields, correlates reasonably well with magnetograms.

### **Time-dependent suppression of oscillatory power in evolving solar magnetic fields**

S. Krishna **Prasad**, D. B. Jess, R. Jain, P. H. Keys

ApJ **823** 45 **2016**

<http://arxiv.org/pdf/1604.05667v1.pdf>

Oscillation amplitudes are generally smaller within magnetically active regions like sunspots and plage, when compared to their surroundings. Such magnetic features, when viewed in spatially-resolved powermaps, appear as regions of suppressed power due to reductions in the oscillation amplitudes. Employing high spatial- and temporal-resolution observations from the Dunn Solar Telescope (DST) in New Mexico, we study the power suppression in a region of evolving magnetic fields adjacent to a pore. By utilising wavelet analysis, we study for the first time, how the oscillatory properties in this region change as the magnetic field evolves with time. Image sequences taken in the blue continuum, G-band, Ca-II-K and H $\alpha$  filters were used in this study. It is observed that the suppression found in the chromosphere occupies a relatively larger area confirming previous findings. Also, the suppression is extended to structures directly connected to the magnetic region and is found to get enhanced as the magnetic field strength increased with time. The dependence of the suppression on the magnetic field strength is greater at longer periods and higher formation heights. Furthermore, the dominant periodicity in the chromosphere was found to be anti-correlated with increases in the magnetic field strength.

### **On the Source of Propagating Slow Magneto-acoustic Waves in Sunspots**

S. Krishna **Prasad**, D. B. Jess, Elena Khomenko

ApJL **812** L15 **2015**

<http://arxiv.org/pdf/1510.03275v1.pdf>

Recent high-resolution observations of sunspot oscillations using simultaneously operated ground- and space-based telescopes reveal the intrinsic connection between different layers of the solar atmosphere. However, it is not clear whether these oscillations are externally driven or generated in-situ. We address this question by using observations of propagating slow magneto-acoustic waves along a coronal fan loop system. In addition to the generally observed decreases in oscillation amplitudes with distance, the observed wave amplitudes are also found to be modulated with time, with similar variations observed throughout the propagation path of the wavetrain. Employing multi-wavelength and multi-instrument data we study the amplitude variations with time as the waves propagate through different layers of the solar atmosphere. By comparing the amplitude-modulation period in different layers, we find that slow magneto-acoustic waves observed in sunspots are externally driven by photospheric p-modes, which propagate upwards into the corona before becoming dissipated. **2011 December 10**

## Separable solutions of force-free spheres and applications to solar active regions

A. **Prasad** (1), A. Mangalam (1), B. Ravindra

Astrophysical Journal, **2014** 786 81

<http://arxiv.org/pdf/1404.0910v1.pdf>

In this paper, we present a systematic study of the force-free field equation for simple axisymmetric configurations in spherical geometry and apply it to the solar active regions. The condition of separability of solutions in the radial and angular variables leads to two classes of solutions: linear and non-linear force-free fields. We have studied these linear solutions Chandrasekhar (1956) and extended the non-linear solutions given in Low & Lou (1990) for the radial power law index to the irreducible rational form  $n=p/q$ , which is allowed for all cases of odd  $p$  and cases of  $q>p$  for even  $p$  (the poloidal flux  $\psi \propto 1/r^n$  and field  $B \propto 1/r^{n+2}$ ). We apply these solutions to simulate photospheric vector magnetograms obtained using the spectro-polarimeter onboard Hinode. The effectiveness of our search strategy is first demonstrated on test inputs of dipolar, axisymmetric and non-axisymmetric linear force-free fields. Using the best fit to these magnetograms, we build 3D axisymmetric field configurations and calculate the energy and relative helicity with two independent methods which are in agreement. We have analyzed 5 magnetograms for AR 10930 spanning a period of 3 days during which two X class flares occurred which allowed us to find the free energy and relative helicity of the active region before and after the flare; our analysis indicates a peak in these quantities before the flare events which is consistent with the results mentioned in literature. We also analyzed single polarity regions AR 10923 and 10933 which showed very good fits with potential fields. This method can provide useful reconstruction of the non-linear force-free (NLFF) fields as well as reasonably good input fields for other numerical techniques.

## Models of force-free spheres and applications to solar active regions

A. **Prasad** (1), A. Mangalam (1)

Bulletin of Astronomical Society of India, ASI conference series, **2013**, vol 10, p 53-59

<http://arxiv.org/pdf/1404.0513v1.pdf>

Here we present a systematic study of force-free field equation for simple axisymmetric configurations in spherical geometry. The condition of separability of solutions in radial and angular variables leads to two classes of solutions: linear and non-linear force-free fields. We have studied these linear solutions Chandrasekhar (1956) and extended the non-linear solutions given in Low & Lou (1990) to the irreducible rational form  $n=p/q$ , which is allowed for all cases of odd  $p$  and to cases of  $q>p$  for even  $p$ . We have further calculated their energies and relative helicities for magnetic field configurations in finite and infinite shell geometries. We demonstrate here a method here to be used to fit observed magnetograms as well as to provide good exact input fields for testing other numerical codes used in reconstruction on the non-linear force-free fields.

## A Life of Fun Playing With Solar Magnetic Fields (Special Historical **Review**)

Eric R **Priest**

E-print, May **2014**; Solar Phys., Volume 289, Issue 10, pp 3579-3615, **2014**

<http://arxiv.org/pdf/1405.3481v1.pdf>

This invited memoir describes my fortunate life, which has been enriched by meeting many wonderful people. The story starts at home and university, and continues with accounts of St Andrews and trips to the USA, together with musings on the book "Solar MHD". The nature and results of collaborations with key people from abroad and with students is mentioned at length. Finally, other important aspects of my life are mentioned briefly before wrapping up.

## Interpreting magnetic helicity flux in solar flux emergence

Chris **Prior**, [David MacTaggart](#)

Journal of Plasma Physics

**2019**

<https://arxiv.org/pdf/1902.07997.pdf>

Magnetic helicity flux gives information about the topology of a magnetic field passing through a boundary. In solar physics applications, this boundary is the photosphere and magnetic helicity flux has become an important quantity in analysing magnetic fields emerging into the solar atmosphere. In this work we investigate the evolution of magnetic helicity flux in magnetohydrodynamic (MHD) simulations of solar flux emergence. We consider emerging magnetic fields with different topologies and investigate how the magnetic helicity flux patterns corresponds to the dynamics of emergence. To investigate how the helicity input is connected to the emergence process, we consider two forms of the helicity flux. The first is the standard form giving topological information weighted by magnetic flux. The second form represents the net winding and can be interpreted as the standard helicity flux less the magnetic flux. Both quantities provide important and distinct information about the structure of the emerging field and these quantities differ significantly for mixed sign helicity fields. A novel aspect of this study is that we account

for the varying morphology of the photosphere due to the motion of the dense plasma lifted into the chromosphere. Our results will prove useful for the interpretation of magnetic helicity flux maps in solar observations.

## **The emergence of braided magnetic fields**

**Prior**, C., MacTaggart, D.

GEOPHYSICAL AND ASTROPHYSICAL FLUID DYNAMICS, 2016

<http://www.maths.gla.ac.uk/~dmactaggart/papers/dmac16b.pdf>

We study the emergence of braided magnetic fields from the top of the solar interior through to the corona. It is widely believed that emerging regions smaller than active regions are formed in the upper convection zone near the photosphere. Here, bundles of braided, rather than twisted, magnetic field can be formed, which then rise upward to emerge into the atmosphere. To test this theory, we investigate the behaviour of braided magnetic fields as they emerge into the solar atmosphere. We compare and contrast our models to previous studies of twisted flux tube emergence and discuss results that can be tested observationally. Although this is just an initial study, our results suggest that the underlying magnetic field structure of small emerging regions need not be twisted and that braided field, formed in the convection zone, could suffice.

## **Twisted versus braided magnetic flux ropes in coronal geometry**

### **I. Construction and relaxation**

C. **Prior** and A. R. Yeates

A&A 587, A125 (2016)

We introduce a technique for generating tubular magnetic fields with arbitrary axial geometry and internal topology. As an initial application, this technique is used to construct two magnetic flux ropes that have the same sigmoidal tubular shape, but have different internal structures. One is twisted, the other has a more complex braided magnetic field. The flux ropes are embedded above the photospheric neutral line in a quadrupolar linear force-free background. Using resistive-magnetohydrodynamic simulations, we show that both fields can relax to stable force-free equilibria whilst maintaining their tubular structure. Both end states are nonlinear force-free; the twisted field contains a single sign of alpha (the force-free parameter), indicating a twisted flux rope of a single dominant chirality, the braided field contains both signs of alpha, indicating a flux rope whose internal twisting has both positive and negative chirality. The electric current structures in these final states differ significantly between the braided field, which has a diffuse structure, and the twisted field, which displays a clear sigmoid. This difference might be observable.

## **On the helicity of open magnetic fields**

C. **Prior** and Yeates, A. R

E-print, April 2014, ApJ

We reconsider the topological interpretation of magnetic helicity for magnetic fields in open domains, and relate this to the relative helicity. Specifically, our domains stretch between two parallel planes, and each of these ends may be magnetically open. It is demonstrated that, while the magnetic helicity is gauge-dependent, its value in any gauge may be physically interpreted as the average winding number among all pairs of field lines with respect to some orthonormal frame field. In fact, the choice of gauge is equivalent to the choice of reference field in the relative helicity, meaning that the magnetic helicity is no less physically meaningful. We prove that a particular gauge always measures the winding with respect to a fixed frame, and propose that this is normally the best choice. For periodic fields, this choice is equivalent to measuring relative helicity with respect to a potential reference field. But for aperiodic fields, we show that the potential field can be twisted. We prove by construction that there always exists a possible untwisted reference field.

## **On the Shape of Force-Free Field Lines in the Solar Corona**

C. **Prior** and M. A. Berger

Solar Physics, Volume 278, Number 2 (2012), 323-345

This paper studies the shape parameters of looped field lines in a linear force-free magnetic field. Loop structures with a sufficient amount of kinking are generally seen to form S or inverse S (Z) shapes in the corona (as viewed in projection). For a single field line, we can ask how much the field line is kinked (as measured by the writhe), and how much neighbouring flux twists about the line (as measured by the twist number). The magnetic helicity of a flux element surrounding the field line can be decomposed into these two quantities. We find that the twist helicity contribution dominates the writhe helicity contribution, for field lines of significant aspect ratio, even when their



structure is highly kinked. These calculations shed light on some popular assumptions of the field. First, we show that the writhe of field lines of significant aspect ratio (the apex height divided by the footpoint width) can sometimes be of opposite sign to the helicity. Secondly, we demonstrate the possibility of field line structures which could be interpreted as Z-shaped, but which have a helicity value sign expected of an S-shaped structure. These results suggest that caution should be exercised in using two-dimensional images to draw conclusions on the helicity value of field lines and flux tubes.

### **Observations of Running Penumbral Waves emerging in a Sunspot**

T.G. [Priya](#), [Wenda Cao](#), [Jiangtao Su](#), [Jie Chen](#), [Xinjie Mao](#), [Yuanyong Deng](#), [Robert Erdélyi](#)

2018 ApJ 852 15

<https://arxiv.org/pdf/1711.07145.pdf>

We present results from the investigation of 5-min umbral oscillations in a single-polarity sunspot of active region NOAA 12132. The spectra of TiO, H $\alpha$ , and 304  $\text{\AA}$  are used for corresponding atmospheric heights from the photosphere to lower corona. Power spectrum analysis at the formation height of H $\alpha$  - 0.6  $\text{\AA}$  to H $\alpha$  center resulted in the detection of 5-min oscillation signals in intensity interpreted as running waves outside the umbral center, mostly with vertical magnetic field inclination  $>15^\circ$ . A phase-speed filter is used to extract the running wave signals with speed  $v_{ph} > 4 \text{ km s}^{-1}$ , from the time series of H $\alpha$  - 0.4  $\text{\AA}$  images, and found twenty-four 3-min umbral oscillatory events in a duration of one hour. Interestingly, the initial emergence of the 3-min umbral oscillatory events are noticed closer to or at umbral boundaries. These 3-min umbral oscillatory events are observed for the first time as propagating from a fraction of preceding Running Penumbral Waves (RPWs). These fractional wavefronts rapidly separates from RPWs and move towards umbral center, wherein they expand radially outwards suggesting the beginning of a new umbral oscillatory event. We found that most of these umbral oscillatory events develop further into RPWs. We speculate that the waveguides of running waves are twisted in spiral structures and hence the wavefronts are first seen at high latitudes of umbral boundaries and later at lower latitudes of the umbral center. **August 5, 2014**

### **Spectropolarimetrically accurate magneto-hydrostatic sunspot model for forward modelling in helioseismology**

D. [Przybylski](#), S. Shelyag, P.S. Cally

2015 *ApJ* 807 20.

<http://arxiv.org/pdf/1504.02189v1.pdf>

We present a technique to construct a spectropolarimetrically accurate magneto-hydrostatic model of a large-scale solar magnetic field concentration, mimicking a sunspot. Using the constructed model we perform a simulation of acoustic wave propagation, conversion and absorption in the solar interior and photosphere with the sunspot embedded into it. With the  $6173 \text{ \AA}$  magnetically sensitive photospheric absorption line of neutral iron, we calculate observable quantities such as continuum intensities, Doppler velocities, as well as full Stokes vector for the simulation at various positions at the solar disk, and analyse the influence of non-locality of radiative transport in the solar photosphere on helioseismic measurements. Bisector shapes were used to perform multi-height observations. The differences in acoustic power at different heights within the line formation region at different positions at the solar disk were simulated and characterised. An increase in acoustic power in the simulated observations of the sunspot umbra away from the solar disk centre was confirmed as the slow magneto-acoustic wave.

### **Analysis of the Effects of Sunspots in Their Quiet Surroundings**

M. Cristina [Rabello-Soares](#)<sup>1</sup>, Richard S. Bogart<sup>2</sup>, and Philip H. Scherrer<sup>2</sup>

HMI Science Nuggets, #104, June 2018 <http://hmi.stanford.edu/hminuggets/?p=2562>

As acoustic waves are modified by magnetic field, helioseismology has the potential to study the structure of sunspots below the solar surface. There have been many observational and theoretical studies that have yielded a wealth of information, but, as basic features of sunspots are still being disputed, more work is needed. We analyze the effect of a sunspot in its quiet surroundings by applying a helioseismic technique on almost three years of Helioseismic and Magnetic Imager (HMI) observations obtained during solar cycle 24 to further study the sunspot structure below the solar surface.

### **STATISTICAL ANALYSIS OF ACOUSTIC WAVE PARAMETERS NEAR SOLAR ACTIVE REGIONS**

M. Cristina [Rabello-Soares](#)<sup>1</sup>, Richard S. Bogart<sup>2</sup>, and Philip H. Scherrer<sup>2</sup>

2016 ApJ 827 140

In order to quantify the influence of magnetic fields on acoustic mode parameters and flows in and around active regions, we analyze the differences in the parameters in magnetically quiet regions nearby an active region (which we call "nearby regions"), compared with those of quiet regions at the same disk locations for which there are no neighboring active regions. We also compare the mode parameters in active regions with those in comparably located quiet regions. Our analysis is based on ring-diagram analysis of all active regions observed by the Helioseismic and Magnetic Imager (HMI) during almost five years. We find that the frequency at which the mode amplitude changes from attenuation to amplification in the quiet nearby regions is around 4.2 mHz, in contrast to the active regions, for which it is about 5.1 mHz. This amplitude enhancement (the "acoustic halo effect") is as large as that observed in the active regions, and has a very weak dependence on the wave propagation direction. The mode energy difference in nearby regions also changes from a deficit to an excess at around 4.2 mHz, but averages to zero over all modes. The frequency difference in nearby regions increases with increasing frequency until a point at which the frequency shifts turn over sharply, as in active regions. However, this turnover occurs around 4.9 mHz, which is significantly below the acoustic cutoff frequency. Inverting the horizontal flow parameters in the direction of the neighboring active regions, we find flows that are consistent with a model of the thermal energy flow being blocked directly below the active region.

### **Fast Reconstruction of 3D Density Distribution around the Sun Based on the MAS by Deep Learning**

Sumiaya [Rahman](#)<sup>1</sup>, Seunghoon Shin<sup>1,2</sup>, Hyun-jin Jeong<sup>3</sup>, Ashraf Siddique<sup>4</sup>, Yong-Jae Moon<sup>1,3</sup>, Eunsu Park<sup>5</sup>, Jihye Kang<sup>3</sup>, and Sung-Ho Bae<sup>6</sup>

2023 ApJ 948 21

<https://iopscience.iop.org/article/10.3847/1538-4357/acbd3c/pdf>

This study is the first attempt to generate a three-dimensional (3D) coronal electron density distribution based on the pix2pixHD model, whose computing time is much shorter than that of the magnetohydrodynamic (MHD) simulation. For this, we consider photospheric solar magnetic fields as input, and electron density distribution simulated with the MHD Algorithm outside a Sphere (MAS) at a given solar radius is taken as output. We consider 155 pairs of Carrington rotations as inputs and outputs from 2010 June to 2022 April for training and testing. We train 152 deep-learning models for 152 solar radii, which are taken up to 30 solar radii. The artificial intelligence (AI) generated 3D electron densities from this study are quite consistent with the simulated ones from lower radii to higher radii, with an average correlation coefficient 0.97. The computing time of testing data sets up to 30 solar radii of 152 deep-learning models is about 45.2 s using the NVIDIA TITAN XP graphics-processing unit, which is much less than the typical simulation time of MAS. We find that the synthetic coronagraphic images estimated from the deep-learning models are similar to the Solar Heliospheric Observatory (SOHO)/Large Angle and Spectroscopic Coronagraph C3 coronagraph data, especially during the solar minimum period. The AI-generated coronal density distribution from this study can be used for space weather models on a near-real-time basis.

### **Super-resolution of SDO/HMI Magnetograms Using Novel Deep Learning Methods**

Sumiaya [Rahman](#)<sup>1</sup>, Yong-Jae Moon<sup>1,2</sup>, Eunsu Park<sup>2</sup>, Ashraf Siddique<sup>3</sup>, Il-Hyun Cho<sup>2</sup>, and Daye Lim<sup>2</sup>

2020 ApJL 897 L32

<https://doi.org/10.3847/2041-8213/ab9d79>

Image super-resolution is a technique of enhancing the resolution of an image where a high-resolution (HR) image is reconstructed from a low-resolution (LR) image. In this Letter, we apply two novel deep learning models (residual attention model and progressive GAN model) for enhancing Solar Dynamics Observatory (SDO)/Helioseismic and Magnetic Imager (HMI) magnetograms. For this, we consider line-of-sight (LOS) magnetograms taken by SDO/HMI as output and their degraded ones with  $4 \times 4$  binning as input. Deep learning networks try to find internal relationships between LR and HR images from the given input and the corresponding output image. We consider SDO/HMI magnetograms from 2014 May to August for training, from 2014 October to December for validation, and 2015 January to March for test. We find that the deep learning models generate higher-quality results than the bicubic interpolation in terms of visual aspects and metrics. We apply this model to a full-resolution SDO/HMI magnetogram and then compare the generated magnetogram with the corresponding Hinode/The Solar Optical Telescope Narrowband Filtergrams (NFI) magnetogram. This comparison shows that the generated magnetogram is consistent with the Hinode one with a high correlation (CC: 0.94) and a high similarity (SSIM: 0.93), which are better than the bicubic method.

### **Global Solar Magnetic-field and Interplanetary Scintillations During the Past Four Solar Cycles**

K. Sasikumar [Raja](#), [P. Janardhan](#), [Susanta Kumar Bisoi](#), [Madhusudan Ingale](#), [Prasad Subramanian](#), [K. Fujiki](#), [Milan Maksimovic](#)

Solar Phys. 2019

<https://arxiv.org/pdf/1908.09134.pdf>

The extended minimum of Solar Cycle 23, the extremely quiet solar-wind conditions prevailing and the mini-maximum of Solar Cycle 24 drew global attention and many authors have since attempted to predict the amplitude of the upcoming Solar Cycle 25, which is predicted to be the third successive weak cycle; it is a unique opportunity to probe the Sun during such quiet periods. Earlier work has established a steady decline, over two decades, in solar photospheric fields at latitudes above  $45^\circ$  and a similar decline in solar-wind micro-turbulence levels as measured by interplanetary scintillation (IPS) observations. However, the relation between the photospheric magnetic fields and those in the low corona/solar-wind are not straightforward. Therefore, in the present article, we have used potential force-free source-surface (PFSS) extrapolations to deduce global magnetic-fields using synoptic magnetograms observed with National Solar Observatory (NSO), Kitt Peak, USA (NSO/KP) and Solar Optical Long-term Investigation of the Sun (NSO/SOLIS) instruments during 1975-2018. Furthermore, we have measured the normalized scintillation index [m] using the IPS observations carried out at the Institute of Space Earth Environment Research (ISEE), Japan during 1983-2017. From these observations, we have found that, since the mid-1990s, the magnetic-field over different latitudes at  $2.5 R_\odot$  and  $10 R_\odot$  (extrapolated using PFSS method) has decreased by  $\approx 11.3$ – $22.2\%$ . In phase with the declining magnetic-fields, the quantity  $m$  also declined by  $\approx 23.6\%$ . These observations emphasize the inter-relationship among the global magnetic-field and various turbulence parameters in the solar corona and solar wind.

### **A Fractal Analysis of Magnetograms within Active Regions**

Brandon [Rajkumar](#), [Shirin Haque](#)

[Solar Physics](#) volume 295,

Article number: 10 (2020) <https://arxiv.org/ftp/arxiv/papers/1911/1911.03675.pdf>  
<https://link.springer.com/content/pdf/10.1007/s11207-019-1578-4.pdf>

The magnetograms of sixteen Active Regions, observed during June - November 2015, were obtained from the Joint Science Operations Center and used to determine the fractal dimensions of various magnetic field groups. The fields were divided into strong (positive and negative) and weak (positive and negative) groupings. The area-perimeter method was used to determine the fractal dimensions for the umbral and penumbral regions of the magnetograms. The fractal dimensions were found to be  $1.79 \pm 0.49$  and  $1.96 \pm 0.29$  for strong and weak magnetic fields respectively. When compared to the umbral and penumbral fractal dimensions determined by (Rajkumar, Haque and Hruday, 2017) using white light images, an inverse relationship was found, with the umbra showing lower fractal dimensions than the penumbra for the magnetic field groups compared to the intensity images. This directly implies that there is greater complexity in the penumbral magnetic field groupings than the umbral region. This has implications for models that constrain how the magnetic field groups are contained in the cooler umbral regions.

**16th June 2015**

### **Fractal dimensions of umbral and penumbral regions of sunspots**

B. [Rajkumar](#) (1), [S. Haque](#) (1), [W. Hruday](#) (2)

*Solar Phys.* 292:170 **2017**

<https://arxiv.org/ftp/arxiv/papers/1709/1709.08042.pdf>

The images of sunspots in sixteen active regions taken at the UCCI Observatory in Grand Cayman during **June - November 2015**, were used to determine their fractal dimensions using the perimeter-area method for the umbral and the penumbral region. Scale free fractal dimensions of  $2.09 \pm 0.42$  and  $1.72 \pm 0.4$  were found respectively. This value was higher than the value determined by Chumak and Chumak (1996) who used a similar method but for the penumbral region only for their sample set. There is a positive correlation  $r = 0.58$  between umbral and the penumbral fractal dimensions for the specific sunspots. Furthermore, a time series analysis was done similarly on eight images of AR 12403, from **21st August 2015 - 28th August 2015** taken from the Debrecen Photoheliographic Data (DPD). The correlation,  $r = 0.623$  between the umbral and penumbral fractal dimensions in the time series indicating that the complexity in morphology indicated by the fractal dimension between the umbra and penumbra followed each other in time as well. **18 Oct 2015, 23 Oct 2015, 3 Nov 2015**

### **Tomographic Reconstruction of the Solar K-Corona Using Neural Fields**

[Andrés Asensio Ramos](#)

*Solar Phys.* volume 298, Article number: 135 (2023)

<https://doi.org/10.1007/s11207-023-02226-2>

We explore the application of neural fields for tomographic reconstructions of the solar corona using data from the Large Angle and Spectrometric Coronagraph (LASCO)-C2 instrument. We first demonstrate their ability to recover the electron-density volume in a synthetic static case, utilizing a simulated 3D model of the corona. Our results show that neural fields provide an efficient and accurate representation of the electron-density data. By comparing the synthesized polarized brightness from the modeled electron densities and the observations, we validate the performance of the method in recovering the electron-density structure accurately. Furthermore, we extend our analysis to the dynamic case, considering time-dependent reconstructions. To this end, we incorporate the temporal dimension into the neural field. The results demonstrate that neural fields can effectively capture the

temporal variability of the coronal electron density. We apply the developed tomographic strategy to real observations from the LASCO-C2 instrument. Using a sequence of LASCO-C2 images, we reconstruct the electron-density distribution of the solar corona for a specific period. The reconstructed electron densities are able to reproduce the observed features of the polarized brightness with fidelity, although some streamers are not properly fitted. The results indicate that neural fields provide a powerful tool for tomographic reconstructions, yielding electron-density maps with minimal artifacts and improved agreement with observations. Neural fields offer several advantages, including efficient interpolation, easy to implement implicit and explicit regularization, and the ability to capture temporal variability. The proposed approach has the potential to enhance our understanding of the complex dynamics and structures of the solar corona, enabling more accurate and detailed analyses of coronal features.

### **Inference of the chromospheric magnetic field orientation in the Ca II 8542 Å line fibrils**

A. Asensio [Ramos](#) (1,2), J. de la Cruz Rodriguez (3), M. J. Martinez Gonzalez (1,2), H. Socas-Navarro  
A&A 2017

<https://arxiv.org/pdf/1612.06088v1.pdf>

Solar chromospheric fibrils, as observed in the core of strong chromospheric spectral lines, extend from photospheric field concentrations suggesting that they trace magnetic field lines. These images have been historically used as proxies of magnetic fields for many purposes. We use a Bayesian hierarchical model to analyze several tens of thousands of pixels in spectro-polarimetric chromospheric images of penumbrae and chromospheric fibrils. We compare the alignment between the field azimuth inferred from the linear polarization signals through the transverse Zeeman effect and the direction of the fibrils in the image. We conclude that, in the analyzed fields of view, fibrils are often well aligned with the magnetic field azimuth. Despite this alignment, the analysis also shows that there is a non-negligible dispersion. In penumbral filaments, we find a dispersion with a standard deviation of ~16 degrees, while this dispersion goes up to ~34 degrees in less magnetized regions. **July 19 and 22, 2013.**

### **Estimating the magnetic field strength from magnetograms**

A. Asensio [Ramos](#)<sup>1</sup>, M. J. Martínez González<sup>1,2</sup> and R. Manso Sainz  
A&A 577, A125 (2015)

A properly calibrated longitudinal magnetograph is an instrument that measures circular polarization and gives an estimation of the magnetic flux density in each observed resolution element. This usually constitutes a lower bound of the field strength in the resolution element, given that it can be made arbitrarily large as long as it occupies a proportionally smaller area of the resolution element and/or becomes more transversal to the observer while still produce the same magnetic signal. However, we know that arbitrarily stronger fields are less likely – hG fields are more probable than kG fields, with fields above several kG virtually absent – and we may even have partial information about their angular distribution. Based on a set of sensible considerations, we derive simple formulae based on a Bayesian analysis to give an improved estimation of the magnetic field strength for magnetographs.

### **Hierarchical analysis of the quiet Sun magnetism**

A. Asensio [Ramos](#) (IAC, ULL), M. J. Martínez González (IAC, ULL)  
A&A, 572, A98 2014

<http://arxiv.org/pdf/1410.5953v1.pdf>

Standard statistical analysis of the magnetic properties of the quiet Sun rely on simple histograms of quantities inferred from maximum-likelihood estimations. Because of the inherent degeneracies, either intrinsic or induced by the noise, this approach is not optimal and can lead to highly biased results. We carry out a meta-analysis of the magnetism of the quiet Sun from Hinode observations using a hierarchical probabilistic method. This model allows us to infer the statistical properties of the magnetic field vector over the observed field-of-view consistently taking into account the uncertainties in each pixel due to noise and degeneracies. Our results point out that the magnetic fields are very weak, below 275 G with 95% credibility, with a slight preference for horizontal fields, although the distribution is not far from a quasi-isotropic distribution.

### **Diagnostics of Coronal Magnetic Fields Through the Hanle Effect in UV and IR Lines**

N. E. [Raouafi](#), P. Riley, S. Gibson, S. Fineschi, S. K. Solanki  
Frontiers in Astronomy and Space Sciences, 2016

<http://arxiv.org/pdf/1606.08493v1.pdf>

The plasma thermodynamics in the solar upper atmosphere, particularly in the corona, are dominated by the magnetic field, which controls the flow and dissipation of energy. The relative lack of knowledge of the coronal vector magnetic field is a major handicap for progress in coronal physics. This makes the development of measurement methods of coronal magnetic fields a high priority in solar physics. The Hanle effect in the UV and IR spectral lines is a largely unexplored diagnostic. We use magnetohydrodynamic (MHD) simulations to study the

magnitude of the signal to be expected for typical coronal magnetic fields for selected spectral lines in the UV and IR wavelength ranges, namely the H I Ly- $\alpha$  and the He I 10830  $\{\AA\}$  lines. We show that the selected lines are useful for reliable diagnosis of coronal magnetic fields. The results show that the combination of polarization measurements of spectral lines with different sensitivities to the Hanle effect may be most appropriate for deducing coronal magnetic properties from future observations.

### **Exploring source region of 3-min slow magnetoacoustic waves observed in coronal fan loops rooted in sunspot umbra**

[Ananya Rawat](#), [Girjesh R. Gupta](#)

MNRAS Volume 525, Issue 4, November 2023, Pages 4815–4831,

<https://doi.org/10.1093/mnras/stad2426>

<https://arxiv.org/pdf/2308.03490.pdf>

Sunspots host various oscillations and wave phenomena like umbral flashes, umbral oscillations, running penumbral waves, and coronal waves. All fan loops rooted in sunspot umbra constantly show a 3-min period propagating slow magnetoacoustic waves in the corona. However, their origin in the lower atmosphere is still unclear. In this work, we studied these oscillations in detail along a clean fan loop system rooted in active region AR12553 for a duration of 4-hour on June 16, 2016 observed by Interface Region Imaging Spectrograph (IRIS) and Solar Dynamics Observatory (SDO). We traced foot-points of several fan loops by identifying their locations at different atmospheric heights from the corona to the photosphere. We found presence of 3-min oscillations at foot-points of all the loops and at all atmospheric heights. We further traced origin of these waves by utilising their amplitude modulation characteristics while propagating in the solar atmosphere. We found several amplitude modulation periods in the range of 9-14 min, 20-24 min, and 30-40 min of these 3-min waves at all heights. Based on our findings, we interpret that 3-min slow magnetoacoustic waves propagating in coronal fan loops are driven by 3-min oscillations observed at the photospheric foot-points of these fan loops in the umbral region. We also explored any connection between 3-min and 5-min oscillations observed at the photospheric foot-points of these loops and found them to be weakly coupled. Results provide clear evidence of magnetic coupling of the solar atmosphere through propagation of 3-min waves along fan loops at different atmospheric heights. **June 16, 2016**

### **Probing Coronal Magnetic Fields with Sungrazing Comets: H i Ly $\alpha$ from Pickup Ions**

J. C. [Raymond](#)<sup>1</sup> and S. Giordano<sup>2</sup>

2019 ApJ 887 45

[sci-hub.se/10.3847/1538-4357/ab4e95](https://arxiv.org/abs/1908.07282)

<https://arxiv.org/pdf/1912.07282.pdf>

Observations of sungrazing comets can be used to probe the solar corona, to study the composition of the comets, and to investigate the plasma processes that govern the interaction between the coronal plasma and cometary gas. UVCS observations of the intensities and line profiles of H i Ly $\alpha$  trace the density, temperature, and outflow speed of the corona. Analysis of H i Ly $\alpha$  observations of comet C/2002 S2 showed a surprising split in the comet's Ly $\alpha$  tail and an asymmetry of redshifted and blueshifted emission across the tail axis. It was suggested that the velocity structure might result from a population of neutrals produced by charge transfer between pickup ions and cometary neutrals. Here we present numerical simulations of the H i Ly $\alpha$  intensity and velocity centroid for sungrazing comets under the assumptions that the magnetic field and solar wind are radial. The models qualitatively reproduce the observations of Comet C/2002 S2 and potentially explain the split tail morphology that was seen in C/2002 S2 and also C/2001 C2. They also match the observed red- and blueshifts, though the solar wind velocity needed to explain the blueshift implies strong Doppler dimming and requires a higher outgassing rate to match the light curve. However, the models do not match the observations in detail, and we discuss the remaining discrepancies and the uncertainties in the model. We briefly discuss the implications for other UVCS comet observations and sungrazing comet observations with the Metis coronagraph. **2002 September 18**

### **The Solar Corona as probed by Comet Lovejoy (C/2011 W3)**

J. C. [Raymond](#) (CfA), P. I. McCauley (CfA), S. R. Cranmer (CfA), C. Downs (PSI)

ApJ, 788 152 2014

<http://arxiv.org/pdf/1405.1639v1.pdf>

EUV images of Comet Lovejoy (C/2011 W3) from the AIA show striations related to the magnetic field structure in both open and closed magnetic regions. The brightness contrast implies coronal density contrasts of at least a factor of 6 between neighboring flux tubes over scales of a few thousand km. These density structures imply variations in the Alfvén speed on a similar scale. They will drastically affect the propagation and dissipation of Alfvén waves, and that should be taken into account in models of coronal heating and solar wind acceleration. In each striation, the cometary emission moves along the magnetic field and broadens with time. The speed and the rate of broadening are related to the parallel and perpendicular components of the velocities of the cometary neutrals when they become ionized. We use an MHD model of the coronal magnetic field and the theory of pickup ions to compare the

measurements with theoretical predictions, in particular with the energy lost to Alfvén waves as the cometary ions isotropize. **16 Dec. 2011**

## Evaluating the Uncertainties in the Electron Temperature and Radial Speed Measurements Using White Light Corona Eclipse Observations

Nelson L. **Reginald**, Joseph M. Davila, O. C. St. Cyr, Lutz Rastätter  
Solar Physics, June **2014**, Volume 289, Issue 6, pp 2021-2039

We examine the uncertainties in two plasma parameters from their true values in a simulated asymmetric corona. We use the Corona Heliosphere (CORHEL) and Magnetohydrodynamics Around the Sphere (MAS) models in the Community Coordinated Modeling Center (CCMC) to investigate the differences between an assumed symmetric corona and a more realistic, asymmetric one. We were able to predict the electron temperatures and electron bulk flow speeds to within  $\pm 0.5$  MK and  $\pm 100$  km s<sup>-1</sup>, respectively, over coronal heights up to  $5.0 R_{\odot}$  from Sun center. We believe that this technique could be incorporated in next-generation white-light coronagraphs to determine these electron plasma parameters in the low solar corona. We have conducted experiments in the past during total solar eclipses to measure the thermal electron temperature and the electron bulk flow speed in the radial direction in the low solar corona. These measurements were made at different altitudes and latitudes in the low solar corona by measuring the shape of the K-coronal spectra between 350 nm and 450 nm and two brightness ratios through filters centered at 385.0 nm/410.0 nm and 398.7 nm/423.3 nm with a bandwidth of  $\approx 4$  nm. Based on symmetric coronal models used for these measurements, the two measured plasma parameters were expected to represent those values at the points where the lines of sight intersected the plane of the solar limb.

## A new approach to the maser emission in the solar corona

Stephane **Regnier**

A&A **2015**

<http://arxiv.org/pdf/1507.07350v1.pdf>

The electron plasma frequency  $\omega_{pe}$  and electron gyrofrequency  $\Omega_e$  are two parameters that allow us to describe the properties of a plasma and to constrain the physical phenomena at play, for instance, whether a maser instability develops. In this paper, we aim to show that the maser instability can exist in the solar corona. We perform an in-depth analysis of the  $\omega_{pe}/\Omega_e$  ratio for simple theoretical and complex solar magnetic field configurations. Using the combination of force-free models for the magnetic field and hydrostatic models for the plasma properties, we determine the ratio of the plasma frequency to the gyrofrequency for electrons. For the sake of comparison, we compute the ratio for bipolar magnetic fields containing a twisted flux bundle, and for four different observed active regions. We also study how  $\omega_{pe}/\Omega_e$  is affected by the potential and non-linear force-free field models. We demonstrate that the ratio of the plasma frequency to the gyrofrequency for electrons can be estimated by this novel method combining magnetic field extrapolation techniques and hydrodynamic models. Even if statistically not significant, values of  $\omega_{pe}/\Omega_e \leq 1$  are present in all examples, and are located in the low corona near to photosphere below one pressure scale-height and/or in the vicinity of twisted flux bundles. The values of  $\omega_{pe}/\Omega_e$  are lower for non-linear force-free fields than potential fields, thus increasing the possibility of maser instability in the corona. From this new approach for estimating  $\omega_{pe}/\Omega_e$ , we conclude that the electron maser instability can exist in the solar corona above active regions. The importance of the maser instability in coronal active regions depends on the complexity and topology of the magnetic field configurations. **AR8151, AR8210, 2000 July 14, October-November 2003**

## Magnetic Field Extrapolations into the Corona: Success and Future Improvements

S. **Régnier**

**Review**

Solar Physics, December **2013**, Volume 288, Issue 2, pp 481-505

[http://download.springer.com/static/pdf/977/art%253A10.1007%252Fs11207-013-0367-8.pdf?auth66=1389935812\\_253226c7713a643c2e2c0c0f3d3d7c1a&ext=.pdf](http://download.springer.com/static/pdf/977/art%253A10.1007%252Fs11207-013-0367-8.pdf?auth66=1389935812_253226c7713a643c2e2c0c0f3d3d7c1a&ext=.pdf)

The solar atmosphere being magnetic in nature, the understanding of the structure and evolution of the magnetic field in different regions of the solar atmosphere has been an important task over the past decades. This task has been made complicated by the difficulties to measure the magnetic field in the corona, while it is currently known with a good accuracy in the photosphere and/or chromosphere. Thus, to determine the coronal magnetic field, a mathematical method has been developed based on the observed magnetic field. This is the so-called magnetic field extrapolation technique. This technique relies on two crucial points: i) the physical assumption leading to the system of differential equations to be solved, ii) the choice and quality of the associated boundary conditions. In this review, I summarise the physical assumptions currently in use and the findings at different scales in the solar atmosphere. I concentrate the discussion on the extrapolation techniques applied to solar magnetic data and the comparison with observations in a broad range of wavelengths (from hard X-rays to radio emission).

## **Magnetic Energy Storage and Current Density Distributions for Different Force-Free Models**

S. **Régnier**

Solar Physics, Volume 277, Number 1, 131-151, 2012

In the last decades, force-free-field modelling has been used extensively to describe the coronal magnetic field and to better understand the physics of solar eruptions at different scales. Especially the evolution of active regions has been studied by successive equilibria in which each computed magnetic configuration is subject to an evolving photospheric distribution of magnetic field and/or electric-current density. This technique of successive equilibria has been successful in describing the rate of change of the energetics for observed active regions. Nevertheless the change in magnetic configuration due to the increase/decrease of electric current for different force-free models (potential, linear and nonlinear force-free fields) has never been studied in detail before. Here we focus especially on the evolution of the free magnetic energy, the location of the excess of energy, and the distribution of electric currents in the corona. For this purpose, we use an idealised active region characterised by four main polarities and a satellite polarity, allowing us to specify a complex topology and sheared arcades to the coronal magnetic field but no twisted flux bundles. We investigate the changes in the geometry and connectivity of field lines, the magnetic energy and current-density content as well as the evolution of null points. Increasing the photospheric current density in the magnetic configuration does not dramatically change the energy-storage processes within the active region even if the magnetic topology is slightly modified. We conclude that for reasonable values of the photospheric current density (the force-free parameter  $\alpha < 0.25 \text{ Mm}^{-1}$ ), the magnetic configurations studied do change but not dramatically: i) the original null point stays nearly at the same location, ii) the field-line geometry and connectivity are slightly modified, iii) even if the free magnetic energy is significantly increased, the energy storage happens at the same location. This extensive study of different force-free models for a simple magnetic configuration shows that some topological elements of an observed active region, such as null points, can be reproduced with confidence only by considering the potential-field approximation. This study is a preliminary work aiming at understanding the effects of electric currents generated by characteristic photospheric motions on the structure and evolution of the coronal magnetic field.

## **Nonlinear force-free extrapolation: numerical methods and applications –**

Stephane **Regnier**

E-print, Jan 2007, Mem. S.A.It. Vol. 75, 282

[http://stephaneregnier.free.fr/Publi/regnier\\_nlff06.pdf](http://stephaneregnier.free.fr/Publi/regnier_nlff06.pdf)

We will summarise the different numerical methods used to determine the coronal magnetic field, and we will review the physical processes and properties derived from the computed magnetic configurations (e.g., magnetic reconnection, energy storage, source of energetic particles).

## **Penumbral Waves driving Solar chromospheric fan-shaped jets**

A. **Reid**, [V. M. J. Henriques](#), [M. Mathioudakis](#), [T. Samanta](#)

ApJL 855 L19 2018

<https://arxiv.org/pdf/1802.07537.pdf>

<http://sci-hub.tw/http://iopscience.iop.org/2041-8205/855/2/L19/>

We use Ha imaging spectroscopy taken via the Swedish 1-m Solar Telescope (SST) to investigate the occurrence of fan-shaped jets at the solar limb. We show evidence for near-simultaneous photospheric reconnection at a sunspot edge leading to the jets appearance, with upward velocities of 30\ks, and extensions up to 8~Mm. The brightening at the base of the jets appears recurrent, with a periodicity matching that of the nearby sunspot penumbra, implying running penumbral waves could be the driver of the jets. The jets' constant extension velocity implies that a driver counteracting solar gravity exists, possibly as a result of the recurrent reconnection erupting material into the chromosphere. These jets also show signatures in higher temperature lines captured from the Solar Dynamics Observatory (SDO), indicating a very hot jet front, leaving behind optically thick cool plasma in its wake.

2014 August 02

## **Numerical simulations of sunspot decay: On the penumbra -- Evershed flow -- moat flow connection**

M. **Rempel**

ApJ 814 125 2015

<http://arxiv.org/pdf/1511.01410v1.pdf>

We present a series of high-resolution sunspot simulations that cover a time span of up to 100 hours. The simulation domain extends about 18 Mm in depth beneath the photosphere and 98 Mm horizontally. We use open boundary conditions that do not maintain the initial field structure against decay driven by convective motions. We consider two setups: A sunspot simulation with penumbra, and a "naked-spot" simulation in which we removed the penumbra

after 20 hours through a change in the magnetic top boundary condition. While the sunspot has an Evershed outflow of 3-4 km/s, the naked spot is surrounded by an inflow of 1-2 km/s in close proximity. However, both spots are surrounded by an outflow on larger scales with a few 100 m/s flow speed in the photosphere. While the sunspot has almost constant magnetic flux content for the simulated time span of 3-4 days, the naked spot decays steadily at a rate of 1021 Mx/day. A region with reduced downflow filling factor, which is more extended for the sunspot, surrounds both spots. The absence of downflows perturbs the upflow/downflow massflux balance and leads to a large-scale radially overturning flow system, the photospheric component of this flow is to the observable moat flow. The reduction of the downflow filling factor also inhibits submergence of magnetic field in the proximity of the spots, which stabilizes them against decay. While this effect is present for both spots, it is more pronounced for the sunspot and explains the almost stationary magnetic flux content.

## Numerical Simulations of Active Region Scale Flux Emergence: From Spot Formation to Decay

M. [Rempel](#) and M. C. M. Cheung

2014 ApJ 785 90

We present numerical simulations of active region scale flux emergence covering a time span of up to 6 days. Flux emergence is driven by a bottom boundary condition that advects a semi-torus of magnetic field with  $1.7 \times 10^{22}$  Mx flux into the computational domain. The simulations show that, even in the absence of twist, the magnetic flux is able to rise through the upper 15.5 Mm of the convection zone and emerge into the photosphere to form spots. We find that spot formation is sensitive to the persistence of upflows at the bottom boundary footpoints, i.e., a continuing upflow would prevent spot formation. In addition, the presence of a torus-aligned flow (such flow into the retrograde direction is expected from angular momentum conservation during the rise of flux ropes through the convection zone) leads to a significant asymmetry between the pair of spots, with the spot corresponding to the leading spot on the Sun being more axisymmetric and coherent, but also forming with a delay relative to the following spot. The spot formation phase transitions directly into a decay phase. Subsurface flows fragment the magnetic field and lead to intrusions of almost field free plasma underneath the photosphere. When such intrusions reach photospheric layers, the spot fragments. The timescale for spot decay is comparable to the longest convective timescales present in the simulation domain. We find that the dispersal of flux from a simulated spot in the first two days of the decay phase is consistent with self-similar decay by turbulent diffusion.

## A High-Efficiency and High-Accuracy Polarimeter for Solar Magnetic Field Measurements

[Deqing Ren](#), [Zijian Han](#) & [Jing Guo](#)

[Solar Physics](#) volume 295, Article number: 109 (2020)

<https://link.springer.com/content/pdf/10.1007/s11207-020-01676-2.pdf>

Solar activity is dominated by the magnetic field. Nowadays, a polarimeter is a mandatory tool to measure solar magnetic fields, which are generally faint and correspond to a polarization of an order of  $10^{-2}$ – $10^{-4}$ . As such, polarization measurements of high efficiency with a high accuracy are crucial to investigate faint magnetic fields. Here we propose a high-efficiency and high-accuracy polarimeter, which is based on a pair of nematic liquid crystal variable retarders (LCVRs) and a Wollaston prism (WP). It uses a dedicated Stokes modulation strategy to achieve high efficiency. A calibration unit (CU) is developed to measure the polarimeter response matrix, which provides a high-precision calibration to correct possible systematic errors. Compared with other traditional polarimeters, the modulation scheme of our polarimeter is flexible. In addition to be able to measure all the three Stokes polarization components (QQ, UU, or VV) simultaneously, it can also measure one or two of these polarization components alone, with high polarization efficiency. Dedicated alignment and calibration techniques optimized for our polarimeter are developed and high measurement accuracy is achieved. In our laboratory experimental test, our two-image based polarization measurement delivers an overall measurement accuracy of the order of  $10^{-4}$ , which is about 10 times better, compared with our previous polarimeters that use the traditional four-image polarization modulation. This work provides a new option for high-efficiency and high-accuracy polarization measurement for future solar synoptic observations.

## Dynamics of multi-cored magnetic structures in the quiet Sun

Iker S. [Requerey](#), Jose Carlos Del Toro Iniesta, Luis R. Bellot Rubio, Valentín Martínez Pillet, Sami K. Solanki, Wolfgang Schmidt

ApJ 810 79 2015

<http://arxiv.org/pdf/1508.06998v1.pdf>

We report on the dynamical interaction of quiet-Sun magnetic fields and granular convection in the solar photosphere as seen by *Sunrise*. We use high spatial resolution ( $0''.15$ – $0''.18$ ) and temporal cadence (33 s) spectropolarimetric Imaging Magnetograph eXperiment data, together with simultaneous CN and Ca<sub>II</sub>H filtergrams from *Sunrise* Filter Imager. We apply the SIR inversion code to the polarimetric data in order to infer the line of sight velocity and vector magnetic field in the photosphere. The



analysis reveals bundles of individual flux tubes evolving as a single entity during the entire 23 minute data set. The group shares a common canopy in the upper photospheric layers, while the individual tubes continually intensify, fragment and merge in the same way that chains of bright points in photometric observations have been reported to do. The evolution of the tube cores are driven by the local granular convection flows. They intensify when they are "compressed" by surrounding granules and split when they are "squeezed" between two moving granules. The resulting fragments are usually later regrouped in intergranular lanes by the granular flows. The continual intensification, fragmentation and coalescence of flux results in magnetic field oscillations of the global entity. From the observations we conclude that the magnetic field oscillations first reported by \cite{2011ApJ...730L..37M} correspond to the forcing by granular motions and not to characteristic oscillatory modes of thin flux tubes. **2009 June 9**

### **The History of a Quiet-Sun Magnetic Element Revealed by IMAx/SUNRISE**

Iker S. [Requerey](#)<sup>1</sup>, Jose Carlos Del Toro Iniesta<sup>1</sup>, Luis R. Bellot Rubio<sup>1</sup>, José A. Bonet<sup>2,3</sup>, Valentín Martínez Pillet<sup>2,4</sup>, Sami K. Solanki<sup>5,6</sup>, and Wolfgang Schmidt<sup>7</sup>  
**2014 ApJ 789 6**

Isolated flux tubes are considered to be fundamental magnetic building blocks of the solar photosphere. Their formation is usually attributed to the concentration of magnetic field to kG strengths by the convective collapse mechanism. However, the small size of the magnetic elements in quiet-Sun areas has prevented this scenario from being studied in fully resolved structures. Here, we report on the formation and subsequent evolution of one such photospheric magnetic flux tube, observed in the quiet Sun with unprecedented spatial resolution (0."15-0."18) and high temporal cadence (33 s). The observations were acquired by the Imaging Magnetograph eXperiment on board the SUNRISE balloon-borne solar observatory. The equipartition field strength magnetic element is the result of the merging of several same polarity magnetic flux patches, including a footpoint of a previously emerged loop. The magnetic structure is then further intensified to kG field strengths by convective collapse. The fine structure found within the flux concentration reveals that the scenario is more complex than can be described by a thin flux tube model with bright points and downflow plumes being established near the edges of the kG magnetic feature. We also observe a daisy-like alignment of surrounding granules and a long-lived inflow toward the magnetic feature. After a subsequent weakening process, the field is again intensified to kG strengths. The area of the magnetic feature is seen to change in anti-phase with the field strength, while the brightness of the bright points and the speed of the downflows varies in phase. We also find a relation between the brightness of the bright point and the presence of upflows within it.

### **How skeletons turn into quasi-separatrix layers in source models:**

A. L. [Restante](#), G. Aulanier and C. E. Parnell  
**A&A 508 (2009) 433-443**

*Context.* In situations where there are no magnetic null points located above a reference photospheric plane, and when the photospheric magnetic field is modeled by discrete flux concentrations, the magnetic connectivity is defined by the magnetic skeleton of the configuration. For a continuous distribution of non-zero photospheric flux, the connectivity is defined by quasi-separatrix layers (QSLs). Both the magnetic skeleton and QSLs can account for current sheet formation and dissipation. Observationally, though, only some portions of the skeleton are found to be related to flare ribbons, which are generally associated with QSL footpoints.

*Aims.* In potential magnetic source models, a transition from the skeleton to QSLs has been shown to occur when the sources are displaced below the photospheric plane. The objective of this paper is to understand the topological and geometrical nature of this transition, and to derive rules to predict which parts of a given skeleton will give rise to QSLs.

*Methods.* We consider magnetic configurations, derived from potential magnetic sources, which possess no coronal null points. We have calculated their skeletons, composed of null points, spine field lines and separatrix (fan) surfaces. Choosing a reference photospheric plane above the sources, we have calculated their QSL footprints.

*Results.* As already known, the latter mostly match with subphotospheric spine field lines since, above these lines, field lines tend to diverge as a result of approaching a null and lying either side of the separatrix surface extending out of from this null. However, many non-spine related QSL footprints are also found, which we call branches. They correspond to the intersection with the photosphere of portions of fan field lines which "branch" away from the sources and result in QSLs due to the inclination of the coronal field lines.

*Conclusions.* Our findings allow a better geometrical understanding of the relations between QSLs and skeletons. We show that in the absence of coronal null points, spines, as well as specific portions of fans as calculated in standard potential source models, are good predictors for the location of QSL footprints and of flare ribbons.

### **Global Solar Magnetic Field Organization in the Outer Corona: Influence on the Solar Wind Speed and Mass Flux Over the Cycle**

Victor Réville<sup>1</sup> and Allan Sacha Brun

2017 ApJ 850 45

<http://sci-hub.cc/http://iopscience.iop.org/0004-637X/850/1/45/>

The dynamics of the solar wind depends intrinsically on the structure of the global solar magnetic field, which undergoes fundamental changes over the 11-year solar cycle. For instance, the wind terminal velocity is thought to be anti-correlated with the expansion factor, a measure of how the magnetic field varies with height in the solar corona, usually computed at a fixed height ( $\approx 2.5 R_{\odot}$ , the source surface radius that approximates the distance at which all magnetic field lines become open). However, the magnetic field expansion affects the solar wind in a more detailed way, its influence on the solar wind properties remaining significant well beyond the source surface. We demonstrate this using 3D global magnetohydrodynamic (MHD) simulations of the solar corona, constrained by surface magnetograms over half a solar cycle (1989–2001). A self-consistent expansion beyond the solar wind critical point (even up to  $10 R_{\odot}$ ) makes our model comply with observed characteristics of the solar wind, namely, that the radial magnetic field intensity becomes latitude independent at some distance from the Sun, and that the mass flux is mostly independent of the terminal wind speed. We also show that near activity minimum, the expansion in the higher corona has more influence on the wind speed than the expansion below  $2.5 R_{\odot}$ .

### From solar to stellar corona: the role of wind, rotation and magnetism

Victor Réville, Allan Sacha Brun, Antoine Strugarek, Sean P. Matt, Jérôme Bouvier, Colin P. Folsom, Pascal Petit

ApJ 2015

<http://arxiv.org/pdf/1509.06982v1.pdf>

Observations of surface magnetic fields are now within reach for many stellar types thanks to the development of Zeeman-Doppler Imaging. These observations are extremely useful for constraining rotational evolution models of stars, as well as for characterizing the generation of magnetic field. We recently demonstrated that the impact of coronal magnetic field topology on the rotational braking of a star can be parametrized with a scalar parameter: the open magnetic flux. However, without running costly numerical simulations of the stellar wind, reconstructing the coronal structure of the large scale magnetic field is not trivial. An alternative -broadly used in solar physics- is to extrapolate the surface magnetic field assuming a potential field in the corona, to describe the opening of the field lines by the magnetized wind. This technique relies on the definition of a so-called source surface radius, which is often fixed to the canonical value of  $2.5R_{\text{sun}}$ . However this value likely varies from star to star. To resolve this issue, we use our extended set of 2.5D wind simulations published in 2015, to provide a criteria for the opening of field lines as well as a simple tool to assess the source surface radius and the open magnetic flux. This allows us to derive the magnetic torque applied to the star by the wind from any spectropolarimetric observation. We conclude by discussing some estimations of spin-down time scales made using our technique, and compare them to observational requirements.

### Structure of sunspot light bridges in the chromosphere and transition region

Reza Rezaei

A&A 609, A73 2018

<https://arxiv.org/pdf/1711.10229.pdf>

Light bridges (LBs) are elongated structures with enhanced intensity embedded in sunspot umbra and pores. We studied the properties of a sample of 60 LBs observed with the Interface Region Imaging Spectrograph (IRIS). Using IRIS near- and far-ultraviolet spectra, we measured the line intensity, width, and Doppler shift; followed traces of LBs in the chromosphere and transition region (TR); and compared LB parameters with umbra and quiet Sun. There is a systematic emission enhancement in LBs compared to nearby umbra from the photosphere up to the TR. Light bridges are systematically displaced toward the solar limb at higher layers: the amount of the displacement at one solar radius compares well with the typical height of the chromosphere and TR. The intensity of the LB sample compared to the umbra sample peaks at the middle/upper chromosphere where they are almost permanently bright. Spectral lines emerging from the LBs are broader than the nearby umbra. The systematic redshift of the Si IV line in the LB sample is reduced compared to the quiet Sun sample. We found a significant correlation between the line width of ions arising at temperatures from  $3 \times 10^4$  to  $1.5 \times 10^5$  K as there is also a strong spatial correlation among the line and continuum intensities. In addition, the intensity-line width relation holds for all spectral lines in this study. The correlations indicate that the cool and hot plasma in LBs are coupled. Light bridges comprise multi-temperature and multi-disciplinary structures extending up to the TR. Diverse heating sources supply the energy and momentum to different layers, resulting in distinct dynamics in the photosphere, chromosphere, and TR.

### Variation in sunspot properties between 1999 and 2014

R. Rezaei<sup>1</sup>, C. Beck<sup>2</sup>, A. Lagg<sup>3</sup>, J. M. Borrero<sup>1</sup>, W. Schmidt<sup>1</sup> and M. Collados

## A&A 578, A43 (2015)

**Aims.** We study the variation in the magnetic field strength, area, and continuum intensity of umbrae in solar cycles 23 and 24.

**Methods.** We analyzed a sample of 374 sunspots observed from 1999 until 2014 with the Tenerife Infrared Polarimeter at the German Vacuum Tower Telescope and the Facility Infrared Spectropolarimeter at the Dunn Solar Telescope. The sample of field strength, area, and intensities was used to trace any long-term or cyclic trend of umbral properties in the last 15 years.

**Results.** Sunspots are systematically weaker, that is, have a weaker field strength and stronger continuum intensity, toward the end of cycle 23 than they had at the maximum of cycle 23. The linear trend reverses with the onset of cycle 24. We find that the field strength decreases in the declining phase of cycle 23 by about  $112 (\pm 16)$  G yr<sup>-1</sup>, while it increases in the rising phase of cycle 24 by about  $138 (\pm 72)$  G yr<sup>-1</sup>. The umbral intensity shows the opposite trend: the intensity increases with a rate of  $0.7 (\pm 0.3)\%$  of  $I_c$  yr<sup>-1</sup> toward the end of cycle 23 and decreases with a rate of  $3.8 (\pm 1.5)\%$  of  $I_c$  yr<sup>-1</sup> toward the maximum of cycle 24. The distribution of the umbral maximum field strength in cycle 24 is similar to that of cycle 23, but is slightly shifted toward lower values by about 80 G, corresponding to a possible long-term gradient in umbral field strength of about  $7 \pm 4$  G yr<sup>-1</sup>. If instead of the maximum umbral field we consider the average value over the entire umbra, the distribution shifts by about 44 Gauss.

**Conclusions.** The umbral brightness decreases in the rising stage of a solar cycle, but increases from maximum toward the end of the cycle. Our results do not indicate a drastic change of the solar cycle toward a grand minimum in the near future.

## Comparison of sunspot properties in cycle 24 and 23

Reza **Rezaei**

HMI Science Nuggets, 2014

<http://hmi.stanford.edu/hminuggets/?p=477>

We analyze umbral area, magnetic field, and umbral intensity of the sunspots during the rising phase of cycle 24. We do not find a significant variation in either sunspot physical properties or distribution of sunspot umbral area from previous cycles.

## SPATIAL STRUCTURE OF SUNSPOT OSCILLATIONS OBSERVED WITH SDO/AIA

V. E. **Reznikova**<sup>1,2</sup> and K. Shibasaki

2012 ApJ 756 35

The spatial structure of sunspot oscillations and its variation with frequency and height have been studied using data from SDO/AIA for two well-developed sunspots observed in 2010. Computation of potential magnetic fields together with line-of-sight and vector magnetograms from SDO/HMI allowed us to interpret discovered features of spatial structure. Namely, we have found that (1) expansion of the magnetic field lines above the sunspot causes a gradual broadening of the area occupied by the 3 minute oscillations with height, and (2) variation of magnetic field inclination across the sunspot causes a decrease in the pulsation frequency with distance from the center of the umbra. We have shown that the transformation from 3 minute umbral oscillations to 5 minute penumbral waves can be explained by variation of the acoustic cutoff frequency across the sunspot.

## Mean-field dynamo action from delayed transport

**Rheinhardt**, M., Devlen, E., Rüdler, K.-H., & Brandenburg, A.

E-print, May 2014; Mon. Not. Roy. Astron. Soc. 441, 116-126 (2014)

<http://arxiv.org/pdf/1401.5026v1.pdf>

We analyse the nature of dynamo action that enables growing horizontally averaged magnetic fields in two particular flows that were studied by Roberts in 1972, namely his flows II and III. They have zero kinetic helicity either pointwise (flow II), or on average (flow III). Using direct numerical simulations, we determine the onset conditions for dynamo action at moderate values of the magnetic Reynolds number. Using the test-field method, we show that the turbulent magnetic diffusivity is then positive for both flows. However, we demonstrate that for both flows large-scale dynamo action occurs through delayed transport. Mathematically speaking, the magnetic field at earlier times contributes to the electromotive force through the off-diagonal components of the  $\alpha$  tensor such that a zero mean magnetic field becomes unstable to dynamo action. This represents a qualitatively new mean-field dynamo mechanism not previously described.

## Global Coronal Equilibria with Solar Wind Outflow

[Oliver E. K. Rice](#), [Anthony R. Yeates](#)

ApJ **923** 57 **2021**

<https://arxiv.org/pdf/2110.01319.pdf>

<https://doi.org/10.3847/1538-4357/ac2c71>

Given a known radial magnetic field distribution on the Sun's photospheric surface, there exist well-established methods for computing a potential magnetic field in the corona above. Such potential fields are routinely used as input to solar wind models, and to initialize magneto-frictional or full magnetohydrodynamic simulations of the coronal and heliospheric magnetic fields. We describe an improved magnetic field model which calculates a magneto-frictional equilibrium with an imposed solar wind profile (which can be Parker's solar wind solution, or any reasonable equivalent). These 'outflow fields' appear to approximate the real coronal magnetic field more closely than a potential field, take a similar time to compute, and avoid the need to impose an artificial source surface. Thus they provide a practical alternative to the potential field model for initializing time-evolving simulations or modeling the heliospheric magnetic field. We give an open-source Python implementation in spherical coordinates and apply the model to data from Solar Cycle 24. The outflow tends to increase the open magnetic flux compared to the potential field model, reducing the well known discrepancy with in situ observations.

**RHESSI Science Nugget**, No. **418**, Nov **2021** [https://sprg.ssl.berkeley.edu/~tohban/wiki/index.php/A\\_Non-PFSS\\_Global\\_Coronal\\_Model](https://sprg.ssl.berkeley.edu/~tohban/wiki/index.php/A_Non-PFSS_Global_Coronal_Model)

### **Sunrise Mission Highlights**

Tino L. [Riethmüller](#), Sami K. Solanki

Proceedings of Science **2015**

<http://arxiv.org/pdf/1511.03487v1.pdf>

Solar activity is controlled by the magnetic field, which also causes the variability of the solar irradiance that in turn is thought to influence the climate on Earth. The magnetic field manifests itself in the form of structures of different sizes, starting with sunspots (10-50 Mm) down to the smallest known magnetic features that often have spatial extents of 100 km or less. The study of the fine scale structure of the Sun's magnetic field has been hampered by the limited spatial resolution of the available observations. This has recently changed thanks to new space and ground-based telescopes. A significant step forward has been taken by the Sunrise observatory, built around the largest solar telescope to leave the ground, and containing two science instruments. Sunrise had two successful long-duration science flights on a stratospheric balloon in June 2009 (solar activity minimum) and in June 2013 (at a high activity level) and a number of scientific results have been obtained that have greatly advanced our understanding of solar magnetism, with data analysis still ongoing. After a brief introduction to the Sunrise mission, an overview of a selection of these results will be given.

### **Can an Unobserved Concentration of Magnetic Flux Above the Poles of the Sun Resolve the Open Flux Problem?**

Pete [Riley](#), Jon A. Linker, Zoran Mikic, Ronald M. Caplan, Cooper Downs, and Jean-Luc Thumm

**2019** ApJ 884 18

<https://doi.org/10.3847/1538-4357/ab3a98>

Global models of the extended solar corona, driven by observed photospheric magnetic fields, generally cannot reproduce the amplitude of the measured interplanetary magnetic field at 1 au (or elsewhere in the heliosphere), often underestimating it by a factor of two or more. Some modelers have attempted to resolve this "open flux" problem by adjusting what they believe to be errors in the estimates of the photospheric field values. Others have simply multiplied interplanetary estimates by some correction factor to match 1 au values. Here, we investigate whether this "missing" flux can be explained by a source of largely unobserved, concentrated bundles of flux in the photosphere at latitudes too high to be adequately resolved by ground-based observatories or Earth-based spacecraft. Using potential field source-surface and magnetohydrodynamic models, we demonstrate that this additional polar flux can (at least partially) resolve the open flux problem, without generating any new observational discrepancies. For example, we show that model solutions without this additional flux systematically produce streams lying at higher helio-latitudes than is inferred from observations. More importantly, adding this polar flux to the models does not substantially change the location or size of computed coronal holes. The upcoming joint ESA/NASA Solar Orbiter mission may be able to support or refute this idea.

### **A Multi-Observatory Inter-Comparison of Line-of-Sight Synoptic Solar Magnetograms**

P. [Riley](#), M. Ben-Nun, J. A. Linker, Z. Mikic, L. Svalgaard, J. Harvey, L. Bertello, T. Hoeksema, Y. Liu, R. Ulrich

Solar Physics, March **2014**, Volume 289, Issue 3, pp 769-792

The observed photospheric magnetic field is a crucial parameter for understanding a range of fundamental solar and heliospheric phenomena. Synoptic maps, in particular, which are derived from the observed line-of-sight photospheric magnetic field and built up over a period of 27 days, are the main driver for global numerical models

of the solar corona and inner heliosphere. Yet, in spite of 60 years of measurements, quantitative estimates remain elusive. In this study, we compare maps from seven solar observatories (Stanford/WSO, NSO/KPVT, NSO/SOLIS, NSO/GONG, SOHO/MDI, UCLA/MWO, and SDO/HMI) to identify consistencies and differences among them. We find that while there is a general qualitative consensus, there are also some significant differences. We compute conversion factors that relate measurements made by one observatory to another using both synoptic map pixel-by-pixel and histogram-equalizing techniques, and we also estimate the correlation between datasets. For example, Wilcox Solar Observatory (WSO) synoptic maps must be multiplied by a factor of 3–4 to match Mount Wilson Observatory (MWO) estimates. Additionally, we find no evidence that the MWO saturation correction factor should be applied to WSO data, as has been done in previous studies. Finally, we explore the relationship between these datasets over more than a solar cycle, demonstrating that, with a few notable exceptions, the conversion factors remain relatively constant. While our study was able to quantitatively describe the relationship between the datasets, it did not uncover any obvious “ground truth.” We offer several suggestions for how this may be addressed in the future.

## **Interplanetary Signatures of Unipolar Streamers and the Origin of the Slow Solar Wind**

P. [Riley](#) and J. G. Luhmann

Solar Physics, Volume 277, Number 2, 355-373, 2012

Unipolar streamers (also known as pseudo-streamers) are coronal structures that, at least in coronagraph images, and when viewed at the correct orientation, are often indistinguishable from dipolar (or “standard”) streamers. When interpreted with the aid of a coronal magnetic field model, however, they are shown to consist of a pair of loop arcades. Whereas dipolar streamers separate coronal holes of the opposite polarity and whose cusp is the origin of the heliospheric current sheet, unipolar streamers separate coronal holes of the same polarity and are therefore not associated with a current sheet. In this study, we investigate the interplanetary signatures of unipolar streamers. Using a global MHD model of the solar corona driven by the observed photospheric magnetic field for Carrington rotation 2060, we map the ACE trajectory back to the Sun. The results suggest that ACE fortuitously traversed through a large and well-defined unipolar streamer. We also compare heliospheric model results at 1 AU with ACE in-situ measurements for Carrington rotation 2060. The results strongly suggest that the solar wind associated with unipolar streamers is slow. We also compare predictions using the original Wang–Sheeley (WS) empirically determined inverse relationship between solar wind speed and expansion factor. Because of the very low expansion factors associated with unipolar streamers, the WS model predicts high speeds, in disagreement with the observations. We discuss the implications of these results in terms of theories for the origin of the slow solar wind. Specifically, premises relying on the expansion factor of coronal flux tubes to modulate the properties of the plasma (and speed, in particular) must address the issue that while the coronal expansion factors are significantly different at dipolar and unipolar streamers, the properties of the measured solar wind are, at least qualitatively, very similar.

## **Improved reconstruction of solar magnetic fields from imaging spectropolarimetry through spatio-temporal regularisation**

[Jaime de la Cruz Rodríguez](#), [Jorrit Leenaarts](#)

A&A 685, A85 2024

<https://arxiv.org/pdf/2402.03440.pdf>

<https://www.aanda.org/articles/aa/pdf/2024/05/aa48810-23.pdf>

Determination of solar magnetic fields with a spatial resolution set by the diffraction limit of a telescope is difficult because the time required to measure the Stokes vector with sufficient signal-to-noise is long compared to the solar evolution timescale. This difficulty gets worse with increasing telescope size as the photon flux per diffraction-limited resolution element remains constant but the evolution timescale decreases linearly with the diffraction-limited resolution. We aim to improve magnetic field reconstruction at the diffraction limit without averaging the observations in time or space, and without applying noise filtering. The magnetic field vector tends to evolve slower than the temperature, velocity and microturbulence. We exploit this by adding temporal regularisation terms for the magnetic field to the linear least-squares fitting used in the weak-field approximation, as well as to the Levenberg-Marquardt algorithm used in inversions. The other model parameters are allowed to change in time without constraints. We infer the chromospheric magnetic field from Ca II 854.2 nm observations using the weak field approximation and the photospheric magnetic field from Fe I 617.3 nm observations using Milne-Eddington inversions, both with and without temporal regularisation. Temporal regularisation reduce the noise in the reconstructed maps of the magnetic field and provides a better coherency in time in both the weak-field approximation and Milne-Eddington inversions. Temporal regularisation markedly improves magnetic field determination from spatially and temporally resolved observations.

## **Radiative diagnostics in the solar photosphere and chromospheres**

**Review**

Jaime de la Cruz [Rodríguez](#), Michiel van Noort

<http://arxiv.org/pdf/1609.08324v1.pdf>

Magnetic fields on the surface of the Sun and stars in general imprint or modify the polarization state of the electromagnetic radiation that is leaving from the star. The inference of solar/stellar magnetic fields is performed by detecting, studying and modeling polarized light from the target star. In this review we present an overview of techniques that are used to study the atmosphere of the Sun, and particularly those that allow to infer magnetic fields. We have combined a small selection of theory on polarized radiative transfer, inversion techniques and we discuss a number of results from chromospheric inversions.

### **Observations of the chromospheric Evershed flow of sunspot penumbra with the Application of the Self-organizing Map Technique**

[Paolo Romano](#), [Francesco Schillirò](#), [Mariachiara Falco](#)

2023 *ApJ* 958 56

<https://arxiv.org/pdf/2309.11186.pdf>

<https://iopscience.iop.org/article/10.3847/1538-4357/acfc20/pdf>

The sunspot penumbra is usually observed in the photosphere and it is of particular interest for its magneto-convection which seems to transport the heat from the top of the convection zone into the solar atmosphere. It is well known that the penumbra magnetic field extends in the upper layers of the solar atmosphere forming the so called super-penumbra. Thanks to the application of the Self Organizing Map technique to a spectral dataset containing monochromatic images acquired along the Ca II 854.2 nm and H $\alpha$  656.28 nm lines, we were able to segment the penumbra and to measure the plasma velocity along the chromospheric portions of penumbral filaments. We found that the head, body and tail of penumbral filaments show vertical flows compatible with the persistence of the Evershed flow. Instead, the inverse Evershed flow has been observed only in the outer portion of the super-penumbra. We found that two opposite Evershed regimes work next to each other, without overlapping and both contribute to the downflow around sunspots. These results confirm the uncombed model of the sunspot penumbra and provide some hints that the downflow around sunspots may be ascribed to the magnetic field dragging the plasma down. **2015, May 18,**

### **Restoring process of sunspot penumbra**

[P. Romano](#), [M. Murabito](#), [S. L. Guglielmino](#), [F. Zuccarello](#), [M. Falco](#)

*ApJ* 899 129 2020

<https://arxiv.org/pdf/2006.09746.pdf>

<https://doi.org/10.3847/1538-4357/aba18b>

We describe the disappearance of a sector of sunspot penumbra and its restoring process observed in the preceding sunspot of active region NOAA 12348. The evolution of the magnetic field and the plasma flows support the idea that the penumbra forms due to a change of inclination of the magnetic field of the canopy. Moving magnetic features have been observed during the disintegration phase of that sector of sunspot penumbra. During the restoring phase we have not observed any magnetic flux emergence around the sunspot. The restoring process of the penumbra sector completed in about 72 hours and it was accompanied by the transition from the counter-Evershed flow to the classical Evershed flow. The inversion of photospheric spectropolarimetric measurements taken by IBIS allowed us to reconstruct how the uncombed configuration of the magnetic field forms during the new settlement of the penumbra, i.e., the vertical component of the magnetic field seems to be progressively replaced by some horizontal field lines, corresponding to the intra-spines. **18-21 May, 2015**

### **A first step to reconstruct the solar corona self-consistently with a magnetohydrostatic model during solar activity minimum**

P. [Ruan](#)<sup>1</sup>, T. Wiegelmann<sup>1</sup>, B. Inhester<sup>1</sup>, T. Neukirch<sup>2</sup>, S. K. Solanki<sup>1</sup> and L. Feng<sup>1</sup>

E-print, Jan 2008; *A&A*, 827-834 (2008)

[http://www.mps.mpg.de/homes/wiegelmann/peng\\_aa.pdf](http://www.mps.mpg.de/homes/wiegelmann/peng_aa.pdf)

**Aims.** We compute the distribution of the magnetic field and the plasma in the global corona with a self-consistent magnetohydrostatic (MHS) model.

**Methods.** We take an analytic magnetohydrostatic model to extrapolate the magnetic field in the corona from photospheric magnetic field measurement. In the model, the electric current density can be decomposed into two components: one component is aligned with the magnetic field lines, whereas the other component flows in spherical shells. The second component of the current produces finite Lorentz forces which are balanced by the pressure gradient and the gravity force. We derive the 3D

distribution of the magnetic field and plasma self-consistently in one model. The boundary conditions are given by a synoptic magnetogram on the inner boundary and by a source surface model at the outer boundary. Results. The density in the model is higher in the equatorial plane than in the polar region. We compare the magnetic field distribution of our model with potential and force-free field models for the same boundary conditions and find that our model differs noticeably from both. We discuss the application of the model and how to improve the model.

### **Quiet Sun magnetic fields: an observational view**

**Review**

Luis Bellot **Rubio**, David Orozco Suárez

[Living Reviews in Solar Physics](#), 2019, 16:1

<https://link.springer.com/content/pdf/10.1007%2Fs41116-018-0017-1.pdf>

The quiet Sun is the region of the solar surface outside of sunspots, pores, and plages. In continuum intensity it appears dominated by granular convection. However, in polarized light the quiet Sun exhibits impressive magnetic activity on a broad range of scales, from the 30,000 km of supergranular cells down to the smallest magnetic features of about 100 km resolvable with current instruments. Quiet Sun fields are observed to evolve in a coherent way, interacting with each other as they are advected by the horizontal photospheric flows. They appear and disappear over surprisingly short time scales, bringing large amounts of magnetic flux to the solar surface. For this reason they may be important contributors to the heating of the chromosphere. Peering into such fields is difficult because of the weak signals they produce, which are easily affected, and even completely hidden, by photon noise. Thus, their evolution and nature remain largely unknown. In recent years the situation has improved thanks to the advent of high-resolution, high-sensitivity spectropolarimetric measurements and the application of state-of-the-art Zeeman and Hanle effect diagnostics. Here we review this important aspect of solar magnetism, paying special attention to the techniques used to observe and characterize the fields, their evolution on the solar surface, and their physical properties as revealed by the most recent analyses. We identify the main open questions that need to be addressed in the future and offer some ideas on how to solve them.

### **Validity of NLFFF Optimization Reconstruction**

G. V. **Rudenko**, [I. S. Dmitrienko](#)

Solar Phys. 295, Article number: 85 2020

<https://arxiv.org/pdf/2001.05660.pdf>

<https://link.springer.com/content/pdf/10.1007/s11207-020-01647-7.pdf>

We evaluate validity of NLFFF extrapolation performed with Optimization class (OPTI) codes. While explaining inevitable for OPTI partial non-solenoidality caused by the gas pressure notable role in pressure balance at photospheric heights and by mathematical aspects related to optimization and BVP (boundary value problem), we justify elimination of the non-solenoidal component (postprocessing) from the OPTI result obtained. In essence, postprocessing converts the entire non-solenoidal part into a solenoidal force part, which possibly reflects factual deviation of magnetic field from its force-free approximation on the photosphere and in the solar corona. Two forms of postprocessing have been analyzed in this paper. Postprocessing I eliminates the non-solenoidal component without changing transverse field at the measurement level, and Postprocessing II leaves the field normal component unchanged. Extrapolation, postprocessing, and then comparison of metric and energy characteristics are performed over AR 11158 active region for a small fragment of its evolution containing the February X-class flare. Our version of OPTI code showed that free energy decreased by  $\sim 1032$  erg within 1 hour, which corresponds to theoretical estimations of the flare-caused magnetic energy loss. This result differs significantly from the one in Sun et al. (2012). Therefore, we also comment on some features of our OPTI code implementation, which may cause significant differences between our results and those obtained using the Wiegelmann (2004) version of OPTI code in study by Sun et al. (2012). 2011/02/-14-15

### **Examination of artifact in vector magnetic field SDO/HMI measurements**

G.V. **Rudenko**, [I.S. Dmitrienko](#)

Solar Phys. 2017

<https://arxiv.org/pdf/1711.08156.pdf>

In this paper, we came to conclusion that there is a significant systematic error in the SDO/HMI vector magnetic data, which reveals itself in a significant deviation of the lines of the knot magnetic fields from the radial direction. The value of this deviation demonstrates a clear dependence on the distance to the disk center. This paper suggests a method for correction of the vector magnetograms that eliminates the detected systematic error.

См. **О наличии систематической ошибки в данных SDO/HMI**

Журнал: [Солнечно-земная физика \(Том 4 № 2, 2018\)](#) стр.3-10

### **Algorithms of the Potential Field Calculation in a Three Dimensional Box**

G.V. **Rudenko**, S.A. Anfinogentov  
Solar Phys. 292:103 2017  
<https://arxiv.org/pdf/1706.04352.pdf>

Calculation of the potential field inside a three-dimensional box with the normal magnetic field component given on all boundaries is needed for estimation of important quantities related to the magnetic field such as free energy and relative helicity. In this work we present an analysis of three methods for calculating potential field inside a three-dimensional box. The accuracy and performance of the methods are tested on artificial models with a priori known solutions.

### **Very Fast and Accurate Azimuth Disambiguation of Vector Magnetograms**

G. V. **Rudenko**, S. A. Anfinogentov

Solar Physics, May 2014, Volume 289, Issue 5, pp 1499-1516

We present a method for fast and accurate azimuth disambiguation of vector magnetogram data regardless of the location of the analyzed region on the solar disk. The direction of the transverse field is determined with the principle of minimum deviation of the field from the reference (potential) field. The new disambiguation (NDA) code is examined on the well-known models of Metcalf et al. (Solar Phys. 237, 267, 2006) and Leka et al. (Solar Phys. 260, 83, 2009), and on an artificial model based on the observed magnetic field of AR 10930 (Rudenko, Myshyakov, and Anfinogentov, Astron. Rep. 57, 622, 2013). We compare Hinode/SOT-SP vector magnetograms of AR 10930 disambiguated with three codes: the NDA code, the nonpotential magnetic-field calculation (NPFC: Georgoulis, Astrophys. J. Lett. 629, L69, 2005), and the spherical minimum-energy method (Rudenko, Myshyakov, and Anfinogentov, Astron. Rep. 57, 622, 2013). We then illustrate the performance of NDA on SDO/HMI full-disk magnetic-field observations. We show that our new algorithm is more than four times faster than the fastest algorithm that provides the disambiguation with a satisfactory accuracy (NPFC). At the same time, its accuracy is similar to that of the minimum-energy method (a very slow algorithm). In contrast to other codes, the NDA code maintains high accuracy when the region to be analyzed is very close to the limb.

### **Super Fast and Quality Azimuth Disambiguation**

G. V. **Rudenko**, S. A. Anfinogentov

Solar Phys., Submitted on 7 Apr 2011

<http://arxiv.org/abs/1104.1228>

The paper presents the possibility of fast and quality azimuth disambiguation of vector magnetogram data regardless of location on the solar disc. The new Super Fast and Quality (SFQ) code of disambiguation is tried out on well-known models of Metcalf et al. (2006), Leka et al. (2009) and artificial model of fixed configuration AR 10930 (Rudenko et al., 2010). We make comparison of Hinode SOT SP vector magnetograms of AR 10930 disambiguated with three codes: SFQ, NPFC (Georgoulis, 2005), and SME (Rudenko et al., 2010). We exemplify the SFQ disambiguation of SDO/HMI measurements of the full disc. The preliminary examination indicates that the SFQ algorithm provides better quality than NPFC and is comparable to SME. In contrast to other codes, SFQ supports relatively high quality of results regardless of the magnetogram proximity to the limb (when being very close to the limb, it is efficient unlike all other algorithms).

### **See Disambiguated Hinode (Sot / SP) Vector Field Data Available for Using as vector magnetograms Bx, By, Bz**

George Rudenko

We provide azimuth-disambiguated vector magnetograms, made from Hinode (Sot / SP) Vector Field Data (the entire period of 2011 Year) for testing and use. The data are available at

[http://bdm.iszf.irk.ru/sfq\\_hinode/SFQ\\_Hinode.htm](http://bdm.iszf.irk.ru/sfq_hinode/SFQ_Hinode.htm).

### **Gauge-Invariant Helicity for Force-Free Magnetic Fields in a Rectangular Box**

G. V. **Rudenko** and I. I. Myshyakov

Solar Physics, Volume 270, Number 1, 165-173, 2011

An algorithm for calculating the gauge-invariant helicity of a magnetic field specified in a rectangular box is described. The algorithm has been tested and confirmed on a well-known semi-analytic force-free-field model of Low and Lou (Astrophys. J. 352, 343, 1990) which we have re-formulated in terms of the vector potential.

### **Analysis of Reconstruction Methods for Nonlinear Force-Free Fields**

G. V. **Rudenko**, I. I. Myshyakov

Solar Phys, 257(2), Page: 287 – 304, 2009

We focus on quantitative evaluation of several methods for the reconstruction of force-free magnetic fields in the solar corona. We have studied two topics. The first is to carry out a comparison test of two approaches to implement



the optimization method: (1) using a boundary layer with a weighting function and (2) involving an optimization algorithm for unknown boundary field vector values. The second approach is shown to provide a better approximation to a desired true solution that is finite in an unlimited semispace. The approximation obtained by the second approach is reasonably close to the true solution up to the boundaries of the reconstruction region. Among the applications of the optimization method to real data, we demonstrate its ability to obtain accurate enough energy estimates and find that the pre- to post-flare energy difference is sufficient in powering the flare.

### **Extrapolation of the solar magnetic field within the potential-field approximation from full-disk magnetograms**

G. V. [Rudenko](#)

Solar Physics, Volume 198, Number 1, 5-30, 2001

This paper is concerned with the Laplace boundary-value problem with the directional derivative, corresponding to the specific nature of measurements of the longitudinal component of the photospheric magnetic field. The boundary conditions are specified by a distribution on the sphere of the projection of the magnetic field vector into a given direction, i.e., they exactly correspond to the data of daily magnetograms distributed across the full solar disk. It is shown that the solution of this problem exists in the form of a spherical harmonic expansion, and uniqueness of this solution is proved. A conceptual sketch of numerical determination of the harmonic series coefficients is given. The field of application of the method is analyzed with regard to the peculiarities of actual data. Results derived from calculating magnetic fields from real magnetograms are presented. Finally, we present differences in results derived from extrapolating the magnetic field from a synoptic map and a full-disk magnetogram.

### **On the Ratio of Periods of the Fundamental Harmonic and First Overtone of Magnetic Tube Kink Oscillations**

M. S. [Ruderman](#), N. S. Petrukhin, E. Pelinovsky

Solar Physics April 2016, Volume 291, Issue 4, pp 1143-1157

We study kink oscillations of thin magnetic tubes. We assume that the density inside and outside the tube (and possibly also the cross-section radius) can vary along the tube. This variation is assumed to be of such a form that the kink speed is symmetric with respect to the tube centre and varies monotonically from the tube ends to the tube centre. Then we prove a theorem stating that the ratio of periods of the fundamental mode and first overtone is a monotonically increasing function of the ratio of the kink speed at the tube centre and the tube ends. In particular, it follows from this theorem that the period ratio is lower than two when the kink speed increases from the tube ends to its centre, while it is higher than two when the kink speed decreases from the tube ends to its centre. The first case is typical for non-expanding coronal magnetic loops, and the second for prominence threads. We apply the general results to particular problems. First we consider kink oscillations of coronal magnetic loops. We prove that, under reasonable assumptions, the ratio of the fundamental period to the first overtone is lower than two and decreases when the loop size increases. The second problem concerns kink oscillations of prominence threads. We consider three internal density profiles: generalised parabolic, Gaussian, and Lorentzian. Each of these profiles contain the parameter  $\alpha$  that is responsible for its sharpness. We calculate the dependence of the period ratio on the ratio of the mean to the maximum density. For all considered values of  $\alpha$  we find that a formula relating the period ratio and the ratio of the mean and maximum density suggested by Soler, Goossens, and Ballester (Astron. Astrophys. 575, A123, 2015) gives a sufficiently good approximation to the exact dependence.

### **Standing kink oscillations of thin twisted magnetic tubes with continuous equilibrium magnetic field**

M. S. [Ruderman](#)<sup>1,2</sup> and J. Terradas<sup>3</sup>

A&A 580, A57 (2015)

In this article we study standing kink waves in twisted magnetic tubes. We use the cold plasma and thin tube approximation. We assume that the plasma density is constant inside and outside the tube. We also assume that the magnetic twist is weak and take the ratio of the azimuthal and axial component of the magnetic field to be of the order of ratio of the tube radius and tube length. The azimuthal component of the magnetic field is proportional to the distance from the tube axis inside the tube, and inversely proportional to this distance outside the tube. Using the method of asymptotic expansions we derived the governing integral equation that determines the eigenfrequencies and eigenmodes of the tube kink oscillations. In the approximation of a very weak twist, we calculated analytically the corrections to the frequencies of the fundamental mode and first overtone of a straight magnetic tube related to the presence of twist. The analytical results are compared with the numerical results obtained using the full set of linear ideal magnetohydrodynamic equations. We also calculated the ratio of frequencies of the first overtone and fundamental mode. We found that the magnetic twist enhances this ratio for moderate values of the density ratio, and reduces this ratio for large values of the density ratio. In general, the deviation of the frequency ratio from 2

caused by the magnetic twist is comparable to that found in simultaneous observations of the fundamental mode and first overtone of the coronal loop kink oscillations. Finally, we studied the eigenmode polarization. We found that, in a particular case of linear polarization, the polarization direction rotates along the tube.

### **Rayleigh-Taylor Instabilities with Sheared Magnetic Fields**

M. S. [Ruderman](#)<sup>1,2</sup>, J. Terradas<sup>3</sup>, and J. L. Ballester

2014 ApJ 785 110

Magnetic Rayleigh-Taylor (MRT) instabilities may play a relevant role in many astrophysical problems. In this work the effect of magnetic shear on the growth rate of the MRT instability is investigated. The eigenmodes of an interface and a slab model under the presence of gravity are analytically calculated assuming that the orientation of the magnetic field changes in the equilibrium, i.e., there is magnetic shear. We solve the linearized magnetohydrodynamic equations in the incompressible regime. We find that the growth rate is bounded under the presence of magnetic shear. We have derived simple analytical expressions for the maximum growth rate, corresponding to the most unstable mode of the system. These expressions provide the explicit dependence of the growth rate on the various equilibrium parameters. For small angles the growth time is linearly proportional to the shear angle, and in this regime the single interface problem and the slab problem tend to the same result. On the contrary, in the limit of large angles and for the interface problem the growth time is essentially independent of the shear angle. In this regime we have also been able to calculate an approximate expression for the growth time for the slab configuration. Magnetic shear can have a strong effect on the growth rates of the instability. As an application of the results found in this paper we have indirectly determined the shear angle in solar prominence threads using their lifetimes and the estimation of the Alfvén speed of the structure.

### **Dynamical Field Line Connectivity in Magnetic Turbulence**

D. [Ruffolo](#)<sup>1</sup> and W. H. Matthaeus

2015 ApJ 806 233

Point-to-point magnetic connectivity has a stochastic character whenever magnetic fluctuations cause a field line random walk, but this can also change due to dynamical activity. Comparing the instantaneous magnetic connectivity from the same point at two different times, we provide a nonperturbative analytic theory for the ensemble average perpendicular displacement of the magnetic field line, given the power spectrum of magnetic fluctuations. For simplicity, the theory is developed in the context of transverse turbulence, and is numerically evaluated for the noisy reduced MHD model. Our formalism accounts for the dynamical decorrelation of magnetic fluctuations due to wave propagation, local nonlinear distortion, random sweeping, and convection by a bulk wind flow relative to the observer. The diffusion coefficient  $DX$  of the time-differenced displacement becomes twice the usual field line diffusion coefficient  $Dx$  at large time displacement  $t$  or large distance  $z$  along the mean field (corresponding to a pair of uncorrelated random walks), though for a low Kubo number (in the quasilinear regime) it can oscillate at intermediate values of  $t$  and  $z$ . At high Kubo number the dynamical decorrelation decays mainly from the nonlinear term and  $DX$  tends monotonically toward  $2Dx$  with increasing  $t$  and  $z$ . The formalism and results presented here are relevant to a variety of astrophysical processes, such as electron transport and heating patterns in coronal loops and the solar transition region, changing magnetic connection to particle sources near the Sun or at a planetary bow shock, and thickening of coronal hole boundaries.

### **Coronal Cavities in CoMP Observations**

Agnieszka [Rumińska](#)<sup>1,2</sup>, Urszula Bąk-Stęślicka<sup>1</sup>, Sarah E. Gibson<sup>3</sup>, and Yuhong Fan<sup>3</sup>

2022 ApJ 926 146

<https://iopscience.iop.org/article/10.3847/1538-4357/ac469c/pdf>

Quiescent coronal cavities can provide insight into solar magnetic fields. They are observed in the coronal emission lines in both polarized and unpolarized light. In the total linear polarization fraction ( $L/I$ ), they often possess a "lagomorphic," or "rabbit-shaped," structure that reflects the underlying magnetic field configuration. We studied quiescent coronal cavities observed between 2012 and 2018 by the Coronal Multichannel Polarimeter (CoMP). The majority of cavities in our study had a characteristic lagomorphic structure in linear polarization. We additionally compared cavity widths as observed in intensity with sizes of their linear polarization signatures for 70 cavities and found that both features are strongly correlated. Our results indicate that chances for observing a lagomorphic structure increase greatly with cavity lifetime, suggesting that the visibility depends on the spatial orientation of the cavity. Forward-modeled observations in linear polarization of flux ropes confirmed this assumption. We conclude that observations of the solar coronal cavities in linear polarization are consistent with the theoretical model of flux rope formation and structure. **17, 20 Mar 2012**

### **Evolution of field line helicity during magnetic reconnection**

Alexander J. B. [Russell](#), Anthony R. Yeates, Gunnar Hornig, Antonia L. Wilmot-Smith

2015

<http://arxiv.org/pdf/1501.04856v1.pdf>

We investigate the evolution of field line helicity for non-zero magnetic fields that connect two boundaries, with emphasis on localized finite-B magnetic reconnection. Total (relative) magnetic helicity is already recognized as an important topological constraint on magnetohydrodynamic processes. Field line helicity offers further advantages because it preserves all topological information and can distinguish between different magnetic fields with the same total helicity. Magnetic reconnection changes field topology and field line helicity reflects these changes; the goal of this paper is to characterize that evolution. We start by deriving the evolution equation for field line helicity and examining its terms, also obtaining a simplified form for cases where dynamics are localized within the domain. The main result, which we support using kinematic examples, is that during localized reconnection in a topologically complex magnetic field, the evolution of field line helicity is dominated by a work-like term that is evaluated at the field line endpoints, namely the scalar product of the generalized field line velocity and the vector potential. Furthermore, the flux integral of this term over certain areas is very small compared to the integral of the unsigned quantity, which indicates that changes of field line helicity happen in a well-organized pairwise manner. It follows that reconnection is very efficient at redistributing helicity in topologically complex magnetic fields despite having little effect on the total helicity.

### **On The Solar Origins of Open Magnetic Fields in the Heliosphere**

**Rust**, D.M., Haggerty, D.K., Georgoulis, M.K., Sheeley, N.R., Wang, Y.-M., DeRosa, M.L., Schriver, C.J.

E-print, Oct 2008; ApJ, v. 687, 635–645, **2008**

<http://www.journals.uchicago.edu/doi/abs/10.1086/592017>

A combination of heliospheric and solar data was used to identify open magnetic fields stretching from the lower corona to Earth orbit. 35 near-relativistic electron beams detected at the ACE spacecraft ??labeled?? the heliospheric segments of the open fields. An X-ray flare occurred <20 minutes before injection of the electrons in 25 events. These flares labeled the solar segment of the open fields. The flares occurred in western-hemisphere active regions (ARs) with coronal holes whose polarity agreed with the polarity of the beam-carrying interplanetary fields in 23 of the 25 events. We conclude that electron beams reach 1 AU from open AR fields adjacent to flare sites. The Wang & Sheeley implementation of the potential-field source-surface model successfully identified the open fields in 36% of cases. Success meant that the open fields reached the source surface within 3 heliographic deg of the interplanetary magnetic field connected to ACE at 1 AU. Inclusion of five near misses improves the success rate to 56%. The success rate for the Schrijver & DeRosa PFSS implementation was 50%. Our results suggest that, even if the input magnetic data are updated frequently, the PFSS models succeed in only 50% of cases to identify the coronal segment of open fields. Development of other techniques is in its infancy.

### **Open-field Coronal Structures Neighbouring the Sunspot of AR 8535**

B. I. **Ryabov** & **A. Vrublevskis**

**Solar Physics** volume 295, Article number: 4 (**2020**)

<https://doi.org/10.1007/s11207-019-1572-x>

We make use of the Potential Field Source Surface (PFSS) model and reveal new details in the strong fields of the dominant sunspot of the active region (AR) 8535. Due to its importance in determining the field line connectivity and topology with resulting consequences for both plasma confinement and dynamics we construct the global magnetic fields with the PFSS model. The coronal emission – observed in the soft X-ray images taken with the Yohkoh Soft X-ray Telescope and 284 Å images taken with the Extreme-ultraviolet Imaging Telescope aboard the Solar and Heliospheric Observatory (SOHO/EIT) – is largely asymmetric owing to two dark coronal lanes, which are traceable across the sunspot. The modelled open-field structures overlap with the observed coronal dark lanes and include two narrow coronal corridors that persist for days in the large sunspot. Since the open-field structures overlap also with the plasma upflow observed in the sunspot as Doppler blue-shifts in a set of EUV emission lines (SOHO/Coronal Diagnostic Spectrometer) on 9 May and 13 May 1999, we examine the plasma outflow from the AR 8535. From near-Earth measurements aboard the Advanced Composition Explorer (ACE) spacecraft we estimate the solar-wind speed  $V_p \approx 400 \text{ km s}^{-1}$  and the charge state ratio  $O7+/O6+ = 0.4$  (corresponding to coronal “freezing-in temperature”  $T_e = 1.7 \times 10^6 \text{ K}$ ). However, the abnormally low proton temperature of solar wind,  $T_p = 3 \times 10^4 \text{ K}$ , implies some impact of the interplanetary coronal mass ejection (ICME) on the plasma flow. The evidence in favour of the outflow from AR 8535 is given by the semi-empirical Wang–Sheeley–Arge model, as it predicts the ACE measurements of solar wind and the relevant features in the tomographic velocity map resulted from the Solar-Terrestrial Environment Laboratory observations of the interplanetary scintillations. Finally, we propose constructing a model atmosphere of the sunspot with the narrow coronal corridors included in order to further elaborate the magnetic-field structure through its effect on the observed microwave radiation.

## Observational evidence for two-component distributions describing solar magnetic bright points

Gerardine Berrios [Saavedra](#)<sup>1</sup>, Dominik Utz<sup>2,3,4</sup>, Santiago Vargas Domínguez<sup>5</sup>, José Iván Campos Rozo<sup>6</sup>, Sergio Javier González Manrique<sup>7,8,9</sup>, Peter Gömöry<sup>9</sup>, Christoph Kuckein<sup>7,8,10</sup>, Horst Balthasar<sup>10</sup> and Peter Zelina<sup>9</sup>

A&A 657, A79 (2022)

<https://www.aanda.org/articles/aa/pdf/2022/01/aa41231-21.pdf>

<https://doi.org/10.1051/0004-6361/202141231>

**Context.** High-resolution observations of the solar photosphere reveal the presence of fine structures, in particular the so-called Magnetic Bright Points (MBPs), which are small-scale features associated with strong magnetic field regions of the order of kilogauss (kG). It is especially relevant to study these magnetic elements, which are extensively detected in all moments during the solar cycle, in order to establish their contribution to the behavior of the solar atmosphere, and ultimately a plausible role within the coronal heating problem.

**Aims.** Characterisation of size and velocity distributions of MBPs in the solar photosphere in two different datasets of quiet Sun images acquired with high-resolution solar instruments i.e. Solar Optical Telescope SOT/Hinode and the High-resolution Fast Imager HiFI/GREGOR, in the G-band (4308 Å).

**Methods.** In order to detect the MBPs, an automatic segmentation and identification algorithm is used. Next, the identified features were tracked to measure their proper motions. Finally, a statistical analysis of hundreds of MBPs is carried out, generating histograms for areas, diameters and horizontal velocities.

**Results.** This work establishes that areas and diameters of MBPs display log-normal distributions that are well-fitted by two different components, whereas the velocity vector components follow Gaussians and the vector magnitude a Rayleigh distribution revealing again for all vector elements a two component composition.

**Conclusions.** The results can be interpreted as due to the presence of two different populations of MBPs in the solar photosphere one likely related to stronger network magnetic flux elements and the other one to weaker intranetwork flux elements. In particular this work concludes on the effect of the different spatial resolution of GREGOR and Hinode telescopes, affecting detections and average values.

## The Effect of Weak Magnetic Twist on Resonant Absorption of Slow Sausage Waves in Magnetic Flux Tubes

Mohammad [Sadeghi](#)<sup>1</sup> and Kayoomars Karami<sup>1,2</sup>

2019 ApJ 879 121

[sci-hub.se/10.3847/1538-4357/ab24c4](https://doi.org/10.3847/1538-4357/ab24c4)

Observations show that twisted magnetic flux tubes are present throughout the Sun's atmosphere. The main aim of this work is to obtain the damping rate of sausage modes in the presence of weak magnetic twist. Using the connection formulae obtained by Sakurai et al., we investigate resonant absorption of the sausage modes in the slow continuum under photospheric conditions. We derive the dispersion relation and solve it numerically, and consequently obtain the frequencies and damping rates of the slow surface sausage modes. We conclude that the magnetic twist can result in strong damping in comparison with the untwisted case.

## Magnetic Field Diagnostics with Strong Chromospheric Lines

R. Manso [Sainz](#), [T. del Pino Alemán](#), [R. Casini](#)

Solar Polarization Workshop 8 2017

<https://arxiv.org/pdf/1710.04155.pdf>

The complex spectropolarimetric patterns around strong chromospheric lines, the result of subtle spectroscopic and transport mechanisms, are sensitive, sometimes in unexpected ways, to the presence of magnetic fields in the chromosphere, which may be exploited for diagnostics. We apply numerical polarization radiative transfer implementing partially coherent scattering by polarized multi-term atoms, in the presence of arbitrary magnetic fields, in planeparallel stellar atmospheres to study a few important spectroscopic features: Mg II h-k doublet; Ca II H-K doublet and IR triplet. We confirm the importance of partial redistribution effects in the formation of the Mg II h-k doublet in magnetized atmospheres, as previously pointed out for the non-magnetic case. Moreover, we show, numerically and analytically, that a magnetic field produces measurable modifications of the broadband linear polarization even for relatively small field strengths, while circular polarization remains well represented by the magnetograph formula. We note that this phenomenon has already (unknowingly) been observed by UVSP/SMM, and the interest and possibility of its observation in stars other than the Sun. The interplay between partial redistribution in the H-K doublet of Ca II and metastable level polarization in its IR triplet allow diagnosing the chromospheric magnetic field at different layers and strengths. Our results suggest several new avenues to investigate empirically the magnetism of the solar and stellar chromospheres.

## Probability Distribution Functions of Sunspot Magnetic Flux

Takashi [Sakurai](#)<sup>1,2</sup> and Shin Toriumi<sup>3</sup>

2023 ApJ 943 10

<https://iopscience.iop.org/article/10.3847/1538-4357/aca28a/pdf>

We investigated the probability distributions of sunspot area and magnetic flux by using data from the Royal Greenwich Observatory and USAF/NOAA. We constructed a sample of 2995 regions with maximum-development areas  $\geq 500$  MSH (millionths of solar hemisphere), covering 146.7 yr (1874–2020). The data were fitted by a power-law distribution and four two-parameter distributions (tapered-power-law, gamma, lognormal, and Weibull distributions). The power-law model was unfavorable compared to the four models in terms of AIC, and was not acceptable according to the classical Kolmogorov–Smirnov test. The lognormal and Weibull distributions were excluded because their behavior extended to smaller regions ( $S \ll 500$  MSH) do not connect to previously published results. Therefore, our choices were tapered-power-law and gamma distributions. The power-law portion of the tapered-power-law and gamma distributions was found to have a power exponent of 1.35–1.9. Due to the exponential falloff of these distributions, the expected frequencies of large sunspots are low. The largest sunspot group observed had an area of 6132 MSH, and the frequency of sunspots larger than 104 MSH was estimated to be every  $3\text{--}8 \times 10^4$  yr. We also estimated the distributions of the Sun-as-a-star total sunspot areas. The largest total area covered by sunspots on record was 1.67% of the visible disk, and can be up to 2.7% by artificially increasing the lifetimes of large sunspots in an area evolution model. These values are still smaller than those found on active Sun-like stars.

## Statistical Investigation of Supersonic Downflows in the Transition Region above Sunspots

[Tanmoy Samanta](#), [Hui Tian](#), [Debi Prasad Choudhary](#)

ApJ 859 158 2018

<https://arxiv.org/pdf/1804.05054.pdf>

Downflows at supersonic speeds have been observed in the transition region (TR) above sunspots for more than three decades. These downflows are often seen in different TR spectral lines above sunspots. We have performed a statistical investigation of these downflows using a large sample which was missing earlier. The Interface Region Imaging Spectrograph (IRIS) has provided a wealth of observational data of sunspots at high spatial and spectral resolution in the past few years. We have identified sixty datasets obtained with IRIS raster scans. Using an automated code, we identified the locations of strong downflows within these sunspots. We found that around eighty percent of our sample show supersonic downflows in the Si IV 1403  $\{\AA\}$  line. These downflows mostly appear in the penumbral regions, though some of them are found in the umbrae. We also found that almost half of these downflows show signatures in chromospheric lines. Furthermore, a detailed spectral analysis was performed by selecting a small spectral window containing the O IV 1400/1401  $\{\AA\}$  and Si IV 1403  $\{\AA\}$  lines. Six Gaussian functions were simultaneously fitted to these three spectral lines and their satellite lines associated with the supersonic downflows. We calculated the intensity, Doppler velocity and line width for these lines. Using the O IV 1400/1401  $\{\AA\}$  line ratio, we find that the downflow components are around one order of magnitude less dense than the regular components. Results from our statistical analysis suggest that these downflows may originate from the corona and that they are independent of the background TR plasma. **2013 October 25**

## Dynamics of subarcsecond bright dots in the transition region above sunspot and their relation to penumbral micro-jets

Tanmoy [Samanta](#), Hui Tian, Dipankar Banerjee, Nicole Schanche

ApJL 835 L19 2017

<https://arxiv.org/pdf/1701.02531v1.pdf>

Recent high-resolution observations reveal that subarcsecond bright dots (BDs) with sub-minute lifetimes appears ubiquitously in the transition region (TR) above sunspot penumbra. The presence of penumbral micro-jets (PMJs) in the chromosphere have also been reported earlier. It was proposed that both the PMJs and BDs are formed due to magnetic reconnection process and may play an important role in heating of the penumbra. Using simultaneous observation of the chromosphere from the Solar Optical Telescope (SOT) aboard Hinode and the TR from the Interface Region Imaging Spectrograph (IRIS), we study the dynamics of BDs and their relation with PMJs. We find two types of BDs, one which is related to PMJs and the others which do not show any visible dynamics in the SOT Ca II H images. From a statistical analysis we show that these two types have different properties. The BDs which are related to PMJs always appear at the top of the PMJs, the vast majority of which show inward motion and originate before the generation of the PMJs. These results may indicate that the reconnection occurs at the lower coronal/TR height and initiates PMJs at the chromosphere. This formation mechanism is in contrast with the currently believed formation of PMJs by reconnection in the (upper) photosphere between differently inclined fields. **19 March 2014**

## **A New Method for Modeling the Coronal Magnetic Field with STEREO and Submerged Dipoles**

A. W. [Sandman](#) and M. J. Aschwanden

Solar Physics

Volume 270, Number 2, 503-522, 2011

Recent magnetic modeling efforts have shown substantial misalignment between theoretical models and observed coronal loop morphology as observed by STEREO/EUVI, regardless of the type of model used. Both potential field and non-linear force-free field (NLFFF) models yielded overall misalignment angles of 20 – 40 degrees, depending on the complexity of the active region (Sandman et al., Solar Phys. 259, 1, 2009; DeRosa et al., Astrophys. J. 696, 1780, 2009) We demonstrate that with new, alternative forward-fitting techniques, we can achieve a significant reduction in the misalignment angles compared with potential field source surface (PFSS) models and NLFFF models. Fitting a series of submerged dipoles to the field directions of stereoscopically triangulated loops in four active regions (30 April, 9 May, 19 May, and 11 December 2007), we find that 3 – 5 dipoles per active region yield misalignment angles of  $\sim 11^\circ - 18^\circ$ , a factor of two smaller than those given by previously established extrapolation methods. We investigate the spatial and temporal variation of misalignment angles with subsets of loops for each active region, as well as loops observed prior to and following a flare and filament eruption, and find that the spatial variation of median misalignment angles within an active region (up to 75%) exceeds the temporal variation associated with the flare (up to 40%). We also examine estimates of the stereoscopic error of our analysis. The corrected values yield a residual misalignment of  $7^\circ - 13^\circ$ , which is attributed to the non-potentiality due to currents in the active regions.

## **Comparison of STEREO/EUVI Loops with Potential Magnetic Field Models**

A. W. [Sandman](#), M. J. Aschwanden<sup>2</sup>, M. L. DeRosa<sup>2</sup>, J. P. Wülser<sup>2</sup> and D. Alexander

E-print, June 2009; Solar Phys.

The *Solar Terrestrial Relations Observatory* (STEREO) provides the first opportunity to triangulate the three-dimensional coordinates of active region loops simultaneously from two different vantage points in space. Three-dimensional coordinates of the coronal magnetic field have been calculated with theoretical magnetic field models for decades, but it is only with the recent availability of STEREO data that a rigorous, quantitative comparison between observed loop geometries and theoretical magnetic field models can be performed. Such a comparison provides a valuable opportunity to assess the validity of theoretical magnetic field models. Here we measure the misalignment angles between model magnetic fields and observed coronal loops in three active regions, as observed with the Extreme Ultraviolet Imager (EUVI) on STEREO on 30 April, 9 May, and 19 May 2007. We perform stereoscopic triangulation of some 100 – 200 EUVI loops in each active region and compute extrapolated magnetic field lines using magnetogram information from the Michelson Doppler Imager (MDI) on the *Solar and Heliospheric Observatory* (SOHO). We examine two different magnetic extrapolation methods: (1) a potential field and (2) a radially stretched potential field that conserves the magnetic divergence. We find considerable disagreement between each theoretical model and the observed loop geometries, with an average misalignment angle on the order of  $20^\circ - 40^\circ$ . We conclude that there is a need for either more suitable (coronal rather than photospheric) magnetic field measurements or more realistic field extrapolation models.

## **Solar Coronal Magnetic Fields and Sensitivity Requirements for Spectropolarimetry Channel of VELC Onboard Aditya-L1**

[K. Sasikumar Raja](#), [Suresh Venkata Jagdev Singh](#), [B. Raghavendra Prasad](#)

Journal of Advances in Space Research 2021

<https://arxiv.org/pdf/2110.14179>

Understanding solar coronal magnetic fields is crucial to address the long-standing mysteries of the solar corona and solar wind. Although routine photospheric magnetic fields (MFs) are available for decades, coronal MFs are rarely reported. Visible Emission Line Coronagraph (VELC) on board Aditya-L1 mission (planned to launch in the near future) can directly measure the MFs in the inner solar corona. This can be achieved with the help of spectropolarimetric observations of the forbidden coronal emission line centered at 1074.7 nm over a field of view  $1.05 R_\odot - 1.5 R_\odot$ . In this article, we summarize various direct and indirect techniques used to estimate the MFs at different wavelength regimes. Further, we summarize the expected accuracies that are required to estimate MFs using VELC's spectropolarimetry channel.

## **Comparing extrapolations of the coronal magnetic field structure at $2.5 R_\odot$ with multi-viewpoint coronagraphic observations**

C. [Sasso](#), R. F. Pinto, V. Andretta, R. A. Howard, A. Vourlidas, A. Bemporad, S. Dolei, D. Spadaro, R. S. usino, E. Antonucci [et al. \(12 more\)](#)

A&A 627, A9 (2019)

DOI: <https://doi.org/10.1051/0004-6361/201834125>

The magnetic field shapes the structure of the solar corona, but we still know little about the interrelationships between the coronal magnetic field configurations and the resulting quasi-stationary structures observed in coronagraphic images (such as streamers, plumes, and coronal holes). One way to obtain information on the large-scale structure of the coronal magnetic field is to extrapolate it from photospheric data and compare the results with coronagraphic images. Our aim is to verify whether this comparison can be a fast method to systematically determine the reliability of the many methods that are available for modeling the coronal magnetic field. Coronal fields are usually extrapolated from photospheric measurements that are typically obtained in a region close to the central meridian on the solar disk and are then compared with coronagraphic images at the limbs, acquired at least seven days before or after to account for solar rotation. This implicitly assumes that no significant changes occurred in the corona during that period. In this work, we combine images from three coronagraphs (SOHO/LASCO-C2 and the two STEREO/SECCHI-COR1) that observe the Sun from different viewing angles to build Carrington maps that cover the entire corona to reduce the effect of temporal evolution to about five days. We then compare the position of the observed streamers in these Carrington maps with that of the neutral lines obtained from four different magnetic field extrapolations to evaluate the performances of the latter in the solar corona. Our results show that the location of coronal streamers can provide important indications to distinguish between different magnetic field extrapolations.

## The Relation between Solar Eruption Topologies and Observed Flare Features I: Flare Ribbons

A. [Savcheva](#), E. Pariat, S. McKillop, [P. McCauley](#), [E. Hanson](#), [Y. Su](#), [E. Werner](#), [E. E. DeLuca](#)  
2015

<http://arxiv.org/pdf/1506.03452v1.pdf>

In this paper we present a topological magnetic field investigation of seven two-ribbon flares in sigmoidal active regions observed with Hinode, STEREO, and SDO. We first derive the 3D coronal magnetic field structure of all regions using marginally unstable 3D coronal magnetic field models created with the flux rope insertion method. The unstable models have been shown to be a good model of the flaring magnetic field configurations. Regions are selected based on their pre-flare configurations along with the appearance and observational coverage of flare ribbons, and the model is constrained using pre-flare features observed in extreme ultraviolet and X-ray passbands. We perform a topology analysis of the models by computing the squashing factor,  $Q$ , in order to determine the locations of prominent quasi-separatrix layers (QSLs). QSLs from these maps are compared to flare ribbons at their full extents. We show that in all cases the straight segments of the two J-shaped ribbons are matched very well by the flux-rope-related QSLs, and the matches to the hooked segments are less consistent but still good for most cases. In addition, we show that these QSLs overlay ridges in the electric current density maps. This study is the largest sample of regions with QSLs derived from 3D coronal magnetic field models, and it shows that the magnetofrictional modeling technique that we employ gives a very good representation of flaring regions, with the power to predict flare ribbon locations in the event of a flare following the time of the model.

SOL2007-02-12T07:30:00L075C297 SOL2007-12-07T04:20:00L085C296 SOL2010-04-08T02:35:00L110C176  
SOL2010-08-07T17:55:00L100C002 SOL2012-05-08T09:21:00L108C232 SOL2013-03-15T05:46:00L116C077  
SOL2013-04-11T06:55:00L110C071

## PHOTOSPHERIC FLUX CANCELLATION AND THE BUILD-UP OF SIGMOIDAL FLUX ROPES ON THE SUN

A. S. [Savcheva](#)<sup>1,2</sup>, L. M. Green<sup>3</sup>, A. A. van Ballegooijen<sup>1</sup>, and E. E. DeLuca  
2012 ApJ 759 105

In this study we explore the scenario of photospheric flux cancellation being the primary formation mechanism of sigmoidal flux ropes in decaying active regions. We analyze magnetogram and X-ray observations together with data-driven non-linear force-free field (NLFFF) models of observed sigmoidal regions to test this idea. We measure the total and canceled fluxes in the regions from MDI magnetograms, as well as the axial and poloidal flux content of the modeled NLFFF flux ropes for three sigmoids—**2007 February, 2007 December, and 2010 February**. We infer that the sum of the poloidal and axial flux in the flux ropes for most models amounts to about 60%-70% of the canceled flux and 30%-50% of the total flux in the regions. The flux measurements and the analysis of the magnetic field structure show that the sigmoids first develop a strong axial field manifested as a sheared arcade and then, as flux cancellation proceeds, form long S-shaped field lines that contribute to the poloidal flux. In addition, the dips in the S-shaped field lines are located at the sites of flux cancellation that have been identified from the MDI magnetograms. We find that the line-of-sight-integrated free energy is also concentrated at these locations for all three regions, which can be liberated in the process of eruption. Flare-associated brightenings and flare loops coincide with the location of the X-line topology that develops at the site of most vigorous flux cancellation.

## FIELD TOPOLOGY ANALYSIS OF A LONG-LASTING CORONAL SIGMOID

A. S. [Savcheva](#)<sup>1,2</sup>, A. A. van Ballegoijen<sup>2</sup> and E. E. DeLuca

2012 ApJ 744 78

[http://www.pergamentum.com/eprint/Savcheva\\_QSL\\_NLFFF.pdf](http://www.pergamentum.com/eprint/Savcheva_QSL_NLFFF.pdf)

We present the first field topology analysis based on nonlinear force-free field (NLFFF) models of a long-lasting coronal sigmoid observed in **2007 February 7-12** with the X-Ray Telescope on Hinode. The NLFFF models are built with the flux rope insertion method and give the three-dimensional coronal magnetic field as constrained by observed coronal loop structures and photospheric magnetograms. Based on these models, we have computed horizontal maps of the current and the squashing factor  $Q$  for 25 different heights in the corona for all six days of the evolution of the region. We use the squashing factor to quantify the degree of change of the field line linkage and to identify prominent quasi-separatrix layers (QSLs). We discuss the major properties of these QSL maps and devise a way to pick out important QSLs since our calculation cannot reach high values of  $Q$ . The complexity in the QSL maps reflects the high degree of fragmentation of the photospheric field. We find main QSLs and current concentrations that outline the flux rope cavity and that become characteristically S-shaped during the evolution of the sigmoid. We note that, although intermittent bald patches exist along the length of the sigmoid during its whole evolution, the flux rope remains stable for several days. However, shortly after the topology of the field exhibits hyperbolic flux tubes (HFT) on February 7 and February 12 the sigmoid loses equilibrium and produces two B-class flares and associated coronal mass ejections (CMEs). The location of the most elevated part of the HFT in our model coincides with the inferred locations of the two flares. Therefore, we suggest that the presence of an HFT in a coronal magnetic configuration may be an indication that the system is ready to erupt. We offer a scenario in which magnetic reconnection at the HFT drives the system toward the marginally stable state. Once this state is reached, loss of equilibrium occurs via the torus instability, producing a CME.

## Non-Linear Force-Free Modeling of a Long-Lasting Coronal Sigmoid

Antonia [Savcheva](#) and Adrian van Ballegoijen

E-print, Sept 2009; ApJ, 703(2), 1766-1777, 2009

A study of the magnetic configuration and evolution of a long-lasting quiescent coronal sigmoid is presented. The sigmoid was observed by {it Hinode}/XRT and TRACE between **2007 Feb 6 and Feb 12** when it finally erupted. We construct non-linear force-free field models for several observations during this period, using the flux rope insertion method. The high spatial and temporal resolution of XRT allows us to finely select best-fit models that match the observations. The modeling shows that a highly sheared field, consisting of a weakly twisted flux rope embedded in a potential field, very well describes the structure of the X-ray sigmoid. The flux rope reaches a stable equilibrium, but its axial flux is close to the stability limit of about  $5 \times 10^{20}$  Mx. The relative magnetic helicity increases with time from Feb 8 until just prior to the eruption on Feb 12. We study the spatial distribution of the torsion parameter  $\alpha$  in the vicinity of the flux rope, and find that it has a hollow-core distribution, i.e., electric currents are concentrated in a current layer at the boundary between the flux rope and its surroundings. The current layer is located near the Bald Patch Separatrix Surface (BPSS) of the magnetic configuration, and the X-ray emission appears to come from this current layer/BPSS, consistent with the Titov & D'eu moulin model. We find that the twist angle  $\Phi$  of the magnetic field increases with time to about  $2\pi$  just prior to the eruption, but never reaches the value necessary for the kink instability.

## SWAP Observations of the Long-term, Large-scale Evolution of the Extreme-ultraviolet Solar Corona

Daniel B. [Seaton](#)<sup>1</sup>, Anik De Groof<sup>1,2</sup>, Paul Shearer<sup>3</sup>, David Berghmans<sup>1</sup>, and Bogdan Nicula

2013 ApJ 777 72

The Sun Watcher with Active Pixels and Image Processing (SWAP) EUV solar telescope on board the Project for On-Board Autonomy 2 spacecraft has been regularly observing the solar corona in a bandpass near 17.4 nm since 2010 February. With a field of view of  $54 \times 54$  arcmin, SWAP provides the widest-field images of the EUV corona available from the perspective of the Earth. By carefully processing and combining multiple SWAP images, it is possible to produce low-noise composites that reveal the structure of the EUV corona at relatively large heights. A particularly important step in this processing was to remove instrumental stray light from the images by determining and deconvolving SWAP's point-spread function from the observations. In this paper, we use the resulting images to conduct the first-ever study of the evolution of the large-scale structure of the corona observed in the EUV over a three year period that includes the complete rise phase of solar cycle 24. Of particular note is the persistence over many solar rotations of bright, diffuse features composed of open magnetic fields that overlie polar crown filaments and extend to large heights above the solar surface. These features appear to be related to coronal fans, which have previously been observed in white-light coronagraph images and, at low heights, in the EUV. We also discuss the evolution of the corona at different heights above the solar surface and the evolution of the corona over the course of the solar cycle by hemisphere.



## **He I spectropolarimetry of a supersonic coronal downflow within a sunspot umbra**

[Thomas A. Schad](#), [Gabriel I. Dima](#), [Tetsu Anan](#)

ApJ **916** 5 **2021**

<https://arxiv.org/pdf/2105.12853.pdf>

<https://doi.org/10.3847/1538-4357/ac01eb>

We report spectropolarimetric observations of a supersonic downflow impacting the lower atmosphere within a large sunspot umbra. This work is an extension of Schad et al. 2016 using observations acquired in the He I 10830 Angstrom triplet by the Facility Infrared Spectropolarimeter. Downflowing material accelerating along a cooled coronal loop reaches peak speeds near  $200 \text{ km s}^{-1}$  and exhibits both high speed emission and absorption within the umbra, which we determine to be a consequence of the strong height dependence of the radiatively-controlled source function above the sunspot umbra. Strong emission profiles close to the rest wavelengths but with long red-shifted tails are also observed at the downflow terminus. From the polarized spectra, we infer longitudinal magnetic field strengths of  $\sim 2.4 \text{ kG}$  in the core portion of the He I strong emission, which we believe is the strongest ever reported in this line. Photospheric field strengths along the same line-of-sight are  $\sim 2.8 \text{ kG}$  as inferred using the Ca I 10839 Angstrom spectral line. The temperatures of the highest speed He I absorption and the near rest emission are similar ( $\sim 10 \text{ kK}$ ), while a differential emission measure analysis using SDO/AIA data indicates significant increases in radiative cooling for temperatures between  $\sim 0.5$  and  $1 \text{ MK}$  plasma associated with the downflow terminus. Combined we interpret these observations in the context of a strong radiative shock induced by the supersonic downflow impacting the low sunspot atmosphere. **19 Sep 2011**

## **He I vector magnetic field maps of a sunspot and its superpenumbral fine-structure**

T.A. [Schad](#), M.J. Penn, H. Lin, A. Tritschler

Solar Phys. Volume 290, [Issue 6](#), pp 1607-1626 **2015**

<http://arxiv.org/pdf/1505.05567v1.pdf>

Advanced inversions of high-resolution spectropolarimetric observations of the He I triplet at 1083 nm are used to generate unique maps of the chromospheric magnetic field vector across a sunspot and its superpenumbral canopy. The observations were acquired by the Facility Infrared Spectropolarimeter (FIRS) at the Dunn Solar Telescope (DST) on **29 January 2012**. Multiple atmospheric models are employed in the inversions, as superpenumbral Stokes profiles are dominated by atomic-level polarization while sunspot profiles are Zeeman-dominated but also exhibit signatures perhaps induced by symmetry breaking effects of the radiation field incident on the chromospheric material. We derive the equilibrium magnetic structure of a sunspot in the chromosphere, and further show that the superpenumbral magnetic field does not appear finely structured, unlike the observed intensity structure. This suggests fibrils are not concentrations of magnetic flux but rather distinguished by individualized thermalization. We also directly compare our inverted values with a current-free extrapolation of the chromospheric field. With improved measurements in the future, the average shear angle between the inferred magnetic field and the potential field may offer a means to quantify the non-potentiality of the chromospheric magnetic field to study the onset of explosive solar phenomena.

## **On the Collective Magnetic Field Strength and Vector Structure of Dark Umbral Cores Measured by the Hinode Spectropolarimeter**

T.A. [Schad](#)

Solar Phys. **2015**

<http://arxiv.org/pdf/1505.05581v1.pdf>

We study 7530 sunspot umbrae and pores measured by the Hinode Spectropolarimeter (SP) between November 2006 and November 2012. We primarily seek confirmation of the long term secular decrease in the mean magnetic field strength of sunspot umbrae found by Penn and Livingston (2011, IAU Symp. 273,126) between 1998 and 2011. The excellent SP photometric properties and full vector magnetic field determinations from full-Stokes Milne-Eddington inversions are used to address the interrelated properties of the magnetic field strength and brightness temperature for all umbral cores. We find non-linear relationships between magnetic field strength and umbral temperature (and continuum contrast), as well as between umbral radius and magnetic field strength. Using disambiguated vector data, we find that the azimuths measured in the umbral cores reflect an organization weakly influenced by Joy's law. The large selection of umbrae displays a log-normal size spectrum similar to earlier solar cycles. Influenced by the amplitude of the solar cycle and the nonlinear relationship between umbral size and core magnetic field strength, the distribution of core magnetic field strengths, fit most effectively with a skew-normal distribution, shows a weak solar cycle dependence. Yet, the mean magnetic field strength does not show a significant long term trend.

## The **Helioseismic and Magnetic Imager (HMI)** Investigation for the *Solar Dynamics Observatory (SDO)*

P.H. **Scherrer** · J. Schou · R.I. Bush · A.G. Kosovichev · R.S. Bogart · J.T. Hoeksema · Y. Liu · T.L. Duvall Jr. · J. Zhao · A.M. Title · C.J. Schrijver · T.D. Tarbell · S. Tomczyk

*Solar Phys* (2012) 275:207–227

The Helioseismic and Magnetic Imager (HMI) instrument and investigation as a part of the NASA Solar Dynamics Observatory (SDO) is designed to study convection-zone dynamics and the solar dynamo, the origin and evolution of sunspots, active regions, and complexes of activity, the sources and drivers of solar magnetic activity and disturbances, links between the internal processes and dynamics of the corona and heliosphere, and precursors of solar disturbances for space-weather forecasts. A brief overview of the instrument, investigation objectives, and standard data products is presented.

## Modeling the Effects of a Light Bridge on Properties of Magnetohydrodynamic Waves in Solar Pores

Luiz A. C. A. **Schiavo**<sup>1</sup>, Mykola Gordovskyy<sup>2</sup>, Philippa K. Browning<sup>3+++</sup>  
2024 *ApJ* 975 45

<https://iopscience.iop.org/article/10.3847/1538-4357/ad7958/pdf>

Solar pores are ideal magnetic structures for wave propagation and transport of energy radially outwards across the upper layers of the solar atmosphere. We aim to model the excitation and propagation of magnetohydrodynamic waves in a pore with a light bridge modeled as two interacting magnetic flux tubes separated by a thin, weaker-field layer. We solve the three-dimensional magnetohydrodynamic equations numerically and calculate the circulation as a measure of net torsional motion. We find that the interaction between flux tubes results in the natural excitation of propagating torsional Alfvén waves but find no torsional waves in the model with a single flux tube. The torsional Alfvén waves propagate with wave speeds matching the local Alfvén speed where wave amplitude peaks.

## Active region fine structure observed at 0.08 arcsec resolution

R. **Schlichenmaier**, O. von der Lühe, S. Hoch, [D. Soltau](#), [T. Berkefeld](#), [D. Schmidt](#), [W. Schmidt](#), [C. Denker](#), [H. Balthasar](#), [A. Hofmann](#), [K. G. Strassmeier](#), [J. Staude](#), [A. Feller](#), [A. Lagg](#), [S. K. Solanki](#), [M. Collados](#), [M. Sigwarth](#), [R. Volkmer](#), [T. Waldmann](#), [F. Kneer](#), [H. Nicklas](#), [M. Sobotka](#)  
A&A 2016

<http://arxiv.org/pdf/1607.07094v1.pdf>

The various mechanisms of magneto-convective energy transport determines the structure of sunspots and active regions. We characterise the appearance of light bridges and other fine structure details and elaborate on their magneto-convective nature. We present speckle-reconstructed images taken with the broad band imager at the 1.5 m GREGOR telescope in the 486nm and 589nm bands. We estimate the spatial resolution from the noise characteristics of the image bursts and obtain 0.08" at 589nm. We describe structure details in individual best images as well as the temporal evolution of selected features. We find branched dark lanes extending along thin (~1") light bridges in sunspots at various heliocentric angles. In thick (~2") light bridges the branches are disconnected from the central lane and have a 'Y' shape with a bright grain toward the umbra. The images reveal that light bridges exist on varying intensity levels and that their small-scale features evolve on time scales of minutes. Faint light bridges show dark lanes outlined by the surrounding bright features. Dark lanes are very common and also found in the boundary of pores. They have a characteristic width of 0.1" or less. Intergranular dark lanes of that width are seen in active region granulation. While central dark lanes in thin light bridges are elevated and associated with a density increase above upflows, the dark lane branches correspond to locations of downflows and are depressed relative to the adjacent bright plasma. Thick light bridges with central dark lanes show no projection effect. They have a flat elevated plateau that falls off steeply at the umbral boundary. There, 'Y' shaped filaments form like in the inner penumbra. This indicates the presence of inclined magnetic fields, i.e., that the umbral magnetic field wraps around the convective light bridge. 31May-14 June 2013

## Characterization of magneto-convection in sunspots

### The Gough-Taylor stability criterion in MURaM sunspot simulations★

M. **Schmassmann**<sup>1</sup>, M. Rempel<sup>2</sup>, N. Bello González<sup>1</sup>, R. Schlichenmaier<sup>1</sup> and J. Jurčák<sup>3</sup>  
A&A 656, A92 (2021)

<https://doi.org/10.1051/0004-6361/202141607>

<https://www.aanda.org/articles/aa/pdf/2021/12/aa41607-21.pdf>

Context. Observations have shown that in stable sunspots, the umbral boundary is outlined by a critical value of the vertical magnetic field component. However, the nature of the distinct magnetoconvection regimes in the umbra and penumbra is still unclear.

Aims. We analyse a sunspot simulation in an effort to understand the origin of the convective instabilities giving rise to the penumbral and umbral distinct regimes.

Methods. We applied the criterion from Gough & Tayler (1966, MNRAS, 133, 85), accounting for the stabilising effect of the vertical magnetic field, to investigate the convective instabilities in a MURaM sunspot simulation.

Results. We find: (1) a highly unstable shallow layer right beneath the surface extending all over the simulation box in which convection is triggered by radiative cooling in the photosphere; (2) a deep umbral core (beneath  $-5$  Mm) stabilised against overturning convection that underlies a region with stable background values permeated by slender instabilities coupled to umbral dots; (3) filamentary instabilities below the penumbra nearly parallel to the surface and undulating instabilities coupled to the penumbra which originate in the deep layers. These deep-rooted instabilities result in the vigorous magneto-convection regime characteristic of the penumbra; (4) convective downdrafts in the granulation, penumbra, and umbra develop at about  $2 \text{ km s}^{-1}$ ,  $1 \text{ km s}^{-1}$ , and  $0.1 \text{ km s}^{-1}$ , respectively, indicating that the granular regime of convection is more vigorous than the penumbra convection regime, which, in turn, is more vigorous than the close-to-steady umbra; (5) the GT criterion outlines both the sunspot magnetopause and peripatopause, highlighting the tripartite nature of the sub-photospheric layers of magnetohydrodynamic (MHD) sunspot models; and, finally, (6) the Jurčák criterion is the photospheric counterpart of the GT criterion in deep layers.

Conclusions. The GT criterion as a diagnostic tool reveals the tripartite nature of sunspot structure with distinct regimes of magneto-convection in the umbra, penumbra, and granulation operating in realistic MHD simulations.

## **Magnetic properties of a long-lived sunspot - Vertical magnetic field at the umbral boundary**

Markus [Schmassmann](#), [Rolf Schlichenmaier](#), [Nazaret Bello González](#)

A&A 620, A104 2018

<https://arxiv.org/pdf/1810.09358.pdf>

Context. In a recent statistical study of sunspots in 79 active regions, the vertical magnetic field component  $B_{\text{ver}}$  averaged along the umbral boundary is found to be independent of sunspot size. The authors of that study conclude that the absolute value of  $B_{\text{ver}}$  at the umbral boundary is the same for all spots.

Aims. We investigate the temporal evolution of  $B_{\text{ver}}$  averaged along the umbral boundary of one long-lived sunspot during its stable phase.

Methods. We analysed data from the HMI instrument on-board SDO. Contours of continuum intensity at  $I_c=0.5I_{qs}$ , whereby  $I_{qs}$  refers to the average over the quiet sun areas, are used to extract the magnetic field along the umbral boundary. Projection effects due to different formation heights of the Fe I 617.3 nm line and continuum are taken into account. To avoid limb artefacts, the spot is only analysed for heliocentric angles smaller than  $60^\circ$ .

Results. During the first disc passage, NOAA AR 11591,  $B_{\text{ver}}$  remains constant at 1693 G with a root-mean-square deviation of 15 G, whereas the magnetic field strength varies substantially (mean 2171 G, rms of 48 G) and shows a long term variation. Compensating for formation height has little influence on the mean value along each contour, but reduces the variations along the contour when away from disc centre, yielding a better match between the contours of  $B_{\text{ver}}=1693$  G and  $I_c=0.5I_{qs}$ .

Conclusions. During the disc passage of a stable sunspot, its umbral boundary can equivalently be defined by using the continuum intensity  $I_c$  or the vertical magnetic field component  $B_{\text{ver}}$ . Contours of fixed magnetic field strength fail to outline the umbral boundary.

## **Hot Plasma from Solar Active Region Cores: a Test of AC and DC Coronal Heating Models?**

J. T. [Schmelz](#)<sup>1</sup>, M. Asgari-Targhi<sup>2</sup>, G. M. Christian<sup>1</sup>, R. S. Dhaliwal<sup>1</sup>, and S. Pathak

2015 ApJ 806 232

Direct current (DC) models of solar coronal heating invoke magnetic reconnection to convert magnetic free energy into heat, whereas alternating current (AC) models invoke wave dissipation. In both cases the energy is supplied by photospheric footpoint motions. For a given footpoint velocity amplitude, DC models predict lower average heating rates but greater temperature variability when compared to AC models. Therefore, evidence of hot plasma ( $T > 5$  MK) in the cores of active regions could be one of the ways for current observations to distinguish between AC and DC models. We have analyzed data from the X-Ray Telescope (XRT) and the Atmospheric Imaging Assembly for 12 quiescent active region cores, all of which were observed in the XRT Be<sub>thick</sub> channel. We did Differential Emission Measure (DEM) analysis and achieved good fits for each data set. We then artificially truncated the hot plasma of the DEM model at 5 MK and examined the resulting fits to the data. For some regions in our sample, the XRT intensities continued to be well-matched by the DEM predictions, even without the hot plasma. This truncation, however, resulted in unacceptable fits for the other regions. This result indicates that the hot plasma is

present in these regions, even if the precise DEM distribution cannot be determined with the data available. We conclude that reconnection may be heating the hot plasma component of these active regions.

## **Composition of the Solar Corona, Solar Wind, and Solar Energetic Particles**

J.T. [Schmelz](#), D.V. Reames, R. von Steiger, S. Basu

E-print, 8 June 2012; ApJ

Along with temperature and density, the elemental abundance is a basic parameter required by astronomers to understand and model any physical system. The abundances of the solar corona are known to differ from those of the solar photosphere via a mechanism related to the first ionization potential of the element, but the normalization of these values with respect to hydrogen is challenging. Here we show that the values used by solar physicists for over a decade and currently referred to as the "coronal abundances" do not agree with the data themselves. As a result, recent analysis and interpretation of solar data involving coronal abundances may need to be revised. We use observations from coronal spectroscopy, the solar wind, and solar energetic particles as well as the latest abundances of the solar photosphere to establish a new set of abundances that reflect our current understanding of the coronal plasma.

## **WHAT IS THE SOURCE OF QUIET SUN TRANSITION REGION EMISSION?**

D. J. [Schmit](#)<sup>1,2</sup> and Bart De Pontieu

2016 *ApJ* **831** 158

Dating back to the first observations of the on-disk corona, there has been a qualitative link between the photosphere's magnetic network and enhanced transition-temperature plasma emission. These observations led to the development of a general model that describes emission structures through the partitioning of the atmospheric volume with different magnetic loop geometries that exhibit different energetic equilibria. Does the internetwork produce transition-temperature emission? What fraction of network flux connects to the corona? How does quiet Sun emission compare with low-activity Sun-like stars? In this work, we revisit the canonical model of the quiet Sun, with high-resolution observations from the *Interface Region Imaging Spectrograph* (IRIS) and HMI in hand, to address those questions. We use over 900 deep exposures of Si IV 1393 Å from IRIS along with nearly simultaneous HMI magnetograms to quantify the correlation between transition-temperature emission structures and magnetic field concentrations through a number of novel statistics. Our observational results are coupled with analysis of the Bifrost MHD model and a large-scale potential field model. Our results paint a complex portrait of the quiet Sun. We measure an emission signature in the distant internetwork that cannot be attributed to network contribution. We find that the dimmest regions of emission are not linked to the local vertical magnetic field. Using the MHD simulation, we categorize the emission contribution from cool mid-altitude loops and high-altitude coronal loops and discuss the potential emission contribution of spicules. Our results provide new constraints on the coupled solar atmosphere so that we can build on our understanding of how dynamic thermal and magnetic structures generate the observed phenomena in the transition region.

## **A novel metric for coronal MHD models**

[Schmit](#), D. J.; Gibson, S.; de Toma, G.; Wiltberger, M.; Hughes, W. J.; Spence, H.; Riley, P.; Linker, J. A.; Mikic, Z.

J. Geophys. Res., Vol. 114, No. A6, A06101, 2009

<http://dx.doi.org/10.1029/2008JA013732>

In the interest of quantitatively assessing the capabilities of coronal MHD models, we have developed a metric that compares the structures of the white light corona observed with SOHO LASCO C2 to model predictions. The MAS model is compared to C2 observations from two Carrington rotations during solar cycle 23, CR1913 and CR1984, which were near the minimum and maximum of solar activity, respectively, for three radial heights, 2.5 R, 3.0 R, and 4.5 R. In addition to simulated polarization brightness images, we create a synthetic image based on the field topology along the line of sight in the model. This open-closed brightness is also compared to LASCO C2 after renormalization. In general, the model's magnetic structure is a closer match to observed coronal structures than the model's density structure. This is expected from the simplified energy equations used in current global corona MHD models.

## **Design and Ground Calibration of the *Helioseismic and Magnetic Imager* (HMI) Instrument on the *Solar Dynamics Observatory* (SDO)**

J. Schou · P.H. Scherrer · R.I. Bush · R.Wachter · S. Couvidat · M.C. Rabello-Soares · R.S. Bogart · J.T. Hoeksema · Y. Liu · T.L. Duvall Jr. · D.J. Akin · B.A. Allard · J.W. Miles · R. Rairden · R.A. Shine · T.D. Tarbell · A.M. Title · C.J. Wolfson · D.F. Elmore · A.A. Norton · S. Tomczyk

*Solar Phys* (2012) 275:229–259

The Helioseismic and Magnetic Imager (HMI) investigation (*Solar Phys.* doi:10.1007/s11207-011-9834-2, 2011) will study the solar interior using helioseismic techniques as well as the magnetic field near the solar surface. The HMI instrument is part of the Solar Dynamics Observatory (SDO) that was launched on 11 February 2010. The instrument is designed to measure the Doppler shift, intensity, and vector magnetic field at the solar photosphere using the 6173 Å Fe I absorption line. The instrument consists of a front-window filter, a telescope, a set of waveplates for polarimetry, an image-stabilization system, a blocking filter, a five-stage Lyot filter with one tunable element, two wide-field tunable Michelson interferometers, a pair of 40962 pixel cameras with independent shutters, and associated electronics. Each camera takes a full-disk image roughly every 3.75 seconds giving an overall cadence of 45 seconds for the Doppler, intensity, and line-of-sight magnetic-field measurements and a slower cadence for the full vector magnetic field. This article describes the design of the HMI instrument and provides an overview of the pre-launch calibration efforts. Overviews of the investigation, details of the calibrations, data handling, and the science analysis are provided in accompanying articles.

## **The nonpotentiality of coroneae of solar active regions, the dynamics of the surface magnetic field, and the potential for large flares**

C.J. Schrijver

*ApJ* 2016

<http://arxiv.org/pdf/1602.07244v1.pdf>

Flares and eruptions from solar active regions are associated with atmospheric electrical currents accompanying distortions of the coronal field away from a lowest-energy potential state. In order to better understand the origin of these currents and their role in M- and X-class flares, I review all active-region observations made with SDO/HMI and SDO/AIA from 2010/05 through 2014/10 within approximately 40 degrees from disk center. I select the roughly 4% of all regions that display a distinctly nonpotential coronal configuration in loops with a length comparable to the scale of the active region, and all that emit GOES X-class flares. The data for 41 regions confirm, with a single exception, that strong-field, high-gradient polarity inversion lines (SHILs) created during emergence of magnetic flux into, and related displacement within, pre-existing active regions are associated with X-class flares. Obvious nonpotentiality in the active region-scale loops occurs in 6 of 10 selected regions with X-class flares, all with relatively long SHILs along their primary polarity inversion line, or with a long internal filament there.

Nonpotentiality can exist in active regions well past the flux-emergence phase, often with reduced or absent flaring. I conclude that the dynamics of the flux involved in the compact SHILs is of preeminent importance for the large-flare potential of active regions within the next day, but that their associated currents may not reveal themselves in active region-scale nonpotentiality. In contrast, active region-scale nonpotentiality, which can persist for many days, may inform us about the eruption potential other than those from SHILs which is almost never associated with X-class flaring. **01.07.2010, 15.02.11, 09.03.2011, 23.02.2011, 20.06.2011, 07.07.2011, 28.03.2012, 04.12.2011, 06.03.2012, 12.07.2012, 03.12.2012, 10.06.2013, 08.11.2013, 10.11.2013, 07.01.2014, 29.03.2014, 10.09.2014, 24.10.2014,**

**The set of 41 selected regions with 78 distinct dates is listed in Table 1.**

## **Pathways of large-scale magnetic couplings between coronal events**

C.J. Schrijver, A.M. Title, A.R. Yeates and M.L. DeRosa

E-print, May 2013, File; *ApJSS*

The high-cadence, comprehensive view of the solar corona by SDO/AIA shows many events that are widely separated in space while occurring close together in time. In some cases, sets of coronal events are evidently causally related, while in many other instances indirect evidence can be found. We present case studies to highlight a variety of coupling processes involved in coronal events. We find that physical linkages between events do occur, but concur with earlier studies that these couplings appear to be crucial to understanding the initiation of major eruptive or explosive phenomena relatively infrequently. We note that the post-eruption reconfiguration time scale of the large-scale corona, estimated from the EUV afterglow, is on average longer than the mean time between CMEs, so that many CMEs originate from a corona that is still adjusting from a previous event. We argue that the coronal field is intrinsically global: current systems build up over days to months, the relaxation after eruptions continues over many hours, and evolving connections easily span much of a hemisphere. This needs to be reflected in our modeling of the connections from the solar surface into the heliosphere to properly model the solar wind, its perturbations, and the generation and propagation of solar energetic particles. However, the large-scale field cannot be constructed reliably by currently available observational resources. We assess the potential of high-quality observations from beyond Earth's perspective and advanced global modeling to understand the couplings between

coronal events in the context of CMEs and solar energetic particle events. **2010/08/01, 2011/02/14-15, 2011/09/25-26, 2011/11/09, 2011/11/22, 2011/11/30, 2011/12/11, 2011/12/25, 2012/02/09**

## **Nonlinear Force-free Field Modeling of a Solar Active Region around the Time of a Major Flare and Coronal Mass Ejection**

C. J. **Schrijver**, M. L. DeRosa, T. Metcalf, G. Barnes, B. Lites, T. Tarbell, J. McTiernan, G. Valori, T. Wiegmann, M. S. Wheatland, T. Amari, G. Aulanier, P. Demoulin, M. Fuhrmann, K. Kusano, S. Regnier, and J. K. Thalmann

The Astrophysical Journal, Vol. 675, No. 2: 1637-1644, **2008**.

<http://www.journals.uchicago.edu/doi/pdf/10.1086/527413>

Solar flares and coronal mass ejections are associated with rapid changes in field connectivity and are powered by the partial dissipation of electrical currents in the solar atmosphere. A critical unanswered question is whether the currents involved are induced by the motion of preexisting atmospheric magnetic flux subject to surface plasma flows or whether these currents are associated with the emergence of flux from within the solar convective zone. We address this problem by applying state-of-the-art nonlinear force-free field (NLFFF) modeling to the highest resolution and quality vector-magnetographic data observed by the recently launched **Hinode** satellite on NOAA AR 10930 around the time of a powerful X3.4 flare (2006 December 10 through the second half of **2006 December 14**). We compute 14 NLFFF models with four different codes and a variety of boundary conditions. We find that the model fields differ markedly in geometry, energy content, and force-freeness. We discuss the relative merits of these models in a general critique of present abilities to model the coronal magnetic field based on surface vector field measurements. For our application in particular, we find a fair agreement of the best-fit model field with the observed coronal configuration, and argue (1) that strong electrical currents emerge together with magnetic flux preceding the flare, (2) that these currents are carried in an ensemble of thin strands, (3) that the global pattern of these currents and of field lines are compatible with a large-scale twisted flux rope topology, and (4) that the  $\sim 10^{32}$  erg change in energy associated with the coronal electrical currents suffices to power the flare and its associated coronal mass ejection.

## **NONLINEAR FORCE-FREE MODELING OF CORONAL MAGNETIC FIELDS PART I: A QUANTITATIVE COMPARISON OF METHODS**

C. J. **SCHRIJVER**, M. L. DEROSA, T. R. METCALF et al.

Solar Physics (2006) 235: 161–190, file

## **A characteristic magnetic field pattern associated with all major solar flares and its use in flare forecasting –**

Carolus J. **Schrijver**

**2007**, ApJL, 655, L117, doi: 10.1086/511857

<https://iopscience.iop.org/article/10.1086/511857/pdf>

Solar flares result from some electromagnetic instability that occurs within regions of relatively strong magnetic field in the Sun's atmosphere. The processes that enable and trigger these flares remain topics of intense study and debate. I analyze observations of 289 X- and M-class flares and over 2500 active region magnetograms to discover (1) that large flares, without exception, are associated with pronounced high-gradient polarity-separation lines, while (2) the free energy that emerges with these fibrils is converted into flare energy in a broad spectrum of flare magnitudes that may well be selected at random from a power-law distribution up to a maximum value. This maximum is proportional to the total unsigned flux  $R$  within  $\sim 15$  Mm of strong-field, high-gradient polarity-separation lines, which are a characteristic appearance of magnetic fibrils carrying electrical currents as they emerge through the photosphere. Measurement of  $R$  is readily automated, and  $R$  can therefore be used effectively for flare forecasting. The probability for major flares to occur within 24 hr of the measurement of  $R$  approaches unity for active regions with the highest values of  $R$  around  $2 \times 10^{21}$  Mx. For regions with  $R \lesssim 10^{19}$  Mx, no M- or X-class flares occur within a day.

## **On the Origin of the Photospheric Magnetic Field**

Peter W. **Schuck**<sup>1</sup>, Mark G. Linton<sup>2</sup>, Kalman J. Knizhnik<sup>2</sup>, and James E. Leake<sup>1</sup>

**2022** ApJ 936 94

<https://iopscience.iop.org/article/10.3847/1538-4357/ac739a/pdf>

This article presents results that challenge the paradigms that (1) the convection zone is the source of the radial magnetic field in the photosphere and (2) that coronal currents are neutralized from the perspective of the photosphere. We demonstrate, using a new analysis tool applied to simulations and observations, that bare or partially dressed current channels are supported by the solar corona and that fingerprints of these coronal current systems can be detected in the photosphere. These coronal current channels can be a significant source of the radial component of the magnetic field in the photosphere. The roots of these coronal current channels in the photosphere

are the source of the magnetic field component parallel to the polarity inversion line in active region NOAA 12673. These analyses and observations transform our theoretical understanding of coronal evolution and argue for a reexamination of the present paradigm in which the convection zone is the sole source of the photospheric magnetic field. **5 Sep 2017**

## **Determining the Transport of Magnetic Helicity and Free Energy in the Sun's Atmosphere**

Peter W. [Schuck](#), [Spiro K. Antiochos](#)

ApJ **882** 151 **2019**

<https://arxiv.org/pdf/1907.10598.pdf>

<https://iopscience.iop.org/article/10.3847/1538-4357/ab298a/pdf>

Direct measurements of the helicity and magnetic free energy in the coronal volume are difficult, but their values may be estimated from measurements of the helicity and free energy transport rates through the photosphere. We examine these transport rates for a topologically open system such as the corona, in which the magnetic fields have a nonzero normal component at the boundaries, and derive a new formula for the helicity transport rate at the boundaries. In addition, we derive new expressions for helicity transport due to flux emergence/submergence versus photospheric horizontal motions. The key feature of our formulas is that they are manifestly gauge invariant. Our results are somewhat counterintuitive in that only the lamellar electric field produced by the surface potential transports helicity across boundaries, and the solenoidal electric field produced by a surface stream function does not contribute to the helicity transport. We discuss the physical interpretation of this result. Furthermore, we derive an expression for the free energy transport rate and show that a necessary condition for free energy transport across a boundary is the presence of a closed magnetic field at the surface, indicating that there are current systems within the volume. We discuss the implications of these results for using photospheric vector magnetic and velocity field measurements to derive the solar coronal helicity and magnetic free energy, which can then be used to constrain and drive models for coronal activity.

## **Achieving Consistent Doppler Measurements from SDO/HMI Vector Field Inversions**

P. W. [Schuck](#), [Spiro Antiochos](#), [K.D. Leka](#), [Graham Barnes](#)

ApJ **823** 101 **2015**

<http://arxiv.org/pdf/1511.06500v1.pdf>

NASA's Solar Dynamics Observatory is delivering vector field observations of the full solar disk with unprecedented temporal and spatial resolution; however, the satellite is in a highly inclined geostationary orbit. The relative spacecraft-Sun velocity varies by  $\pm 3$  km/s over a day which introduces major orbital artifacts in the Helioseismic Magnetic Imager data. We demonstrate that the orbital artifacts contaminate all spatial and temporal scales in the data. We describe a newly-developed three stage procedure for mitigating these artifacts in the Doppler data derived from the Milne-Eddington inversions in the HMI Pipeline. This procedure was applied to full disk images of AR11084 to produce consistent Dopplergrams. The data adjustments reduce the power in the orbital artifacts by 31dB. Furthermore, we analyze in detail the corrected images and show that our procedure greatly improves the temporal and spectral properties of the data without adding any new artifacts. We conclude that this new and easily implemented procedure makes a dramatic improvement in the consistency of the HMI data and in its usefulness for precision scientific studies. **June 5-6, 2012**

## **Average motion of emerging solar active region polarities I: Two phases of emergence**

Hannah [Schunker](#), [Aaron C. Birch](#), [Robert H. Cameron](#), [Douglas C. Braun](#), [Laurent Gizon](#), [Raymond B. Burston](#)

A&A **625**, A53 **2019**

<https://arxiv.org/pdf/1903.11839.pdf>

[sci-hub.se/10.1051/0004-6361/201834627](https://sci-hub.se/10.1051/0004-6361/201834627)

Our goal is to constrain models of active region formation by tracking the average motion of active region polarity pairs as they emerge onto the surface. We measured the motion of the two main opposite polarities in 153 emerging active regions (EARs) using line-of-sight magnetic field observations from the Solar Dynamics Observatory Helioseismic Emerging Active Region (SDO/HEAR) survey (Schunker et al. 2016). We first measured the position of each of the polarities eight hours after emergence and tracked their location forwards and backwards in time. We find that, on average, the polarities emerge with an east-west orientation and the separation speed between the polarities increases. At about 0.1 days after emergence, the average separation speed reaches a peak value of  $229 \pm 11$  m/s, and then starts to decrease, and about 2.5 days after emergence the polarities stop separating. We also find that the separation and the separation speed in the east-west direction are systematically larger for active regions with higher flux. Our results reveal two phases of the emergence process defined by the rate of change of the separation speed as the polarities move apart. Phase 1 begins when the opposite polarity pairs first appear at the surface, with an east-west alignment and an increasing separation speed. We define Phase 2 to begin when the separation speed starts to decrease, and ends when the polarities have stopped separating. This is consistent with the picture of Chen, Rempel, & Fan (2017): the peak of a flux tube breaks through the surface during Phase 1. During

Phase 2 the magnetic field lines are straightened by magnetic tension, so that the polarities continue to move apart, until they eventually lie directly above their anchored subsurface footpoints.

**Table A.1.** Emerging active regions (2012-2014)

## **Switchbacks Explained: Super-Parker Fields -- the Other Side of the Sub-Parker Spiral**

[N. A. Schwadron](#), [D. J. McComas](#)

ApJ 2021

<https://arxiv.org/pdf/2102.03696.pdf>

We provide a simple geometric explanation for the source of switchbacks and associated large and one-sided transverse flows in the solar wind observed by Parker Solar Probe. The more radial, Sub-Parker Spiral structure of the heliospheric magnetic field observed previously by Ulysses, ACE, and STEREO is created within rarefaction regions where footpoint motion from the source of fast into slow wind at the Sun creates a magnetic field line connection across solar wind speed shear. Conversely, when foot-points move from the source of slow wind into faster wind, a Super-Parker Spiral field structure is formed: below the Alfvén critical point, one-sided transverse field-aligned flows develop; above the Alfvén critical point, the field structure contracts between adjacent solar wind flows, and the radial field component decreases in magnitude with distance from the Sun, eventually reversing into a switchback. The Sub-Parker and Super-Parker Spirals behave functionally as opposites. Observations from Parker Solar Probe confirm the paucity of switchbacks within rarefaction regions and immediately outside these rarefaction regions, we observe numerous switchbacks in the magnetic field that are directly associated with abrupt transients in solar wind speed. The radial component of the magnetic field, the speed gradients, radial Alfvén speed, and the ratio of the sound speed to the radial Alfvén speed all conform to predictions based on the Sub-Parker and Super-Parker Spirals within rarefaction regions and solar wind speed enhancements (spikes or jets), respectively. Critically, the predictions associated with the Super-Parker Spiral naturally explain the observations of switchbacks being associated with unexpectedly large and one-sided tangential flows. **2018-11-20-21**

## **MAGNETIC FLUX BALANCE IN THE HELIOSPHERE**

[N. A. Schwadron](#)<sup>1</sup>, [D. E. Connick](#)<sup>2</sup>, and [C. Smith](#)<sup>2</sup>

Astrophysical Journal Letters, 722:L132–L136, **2010**

Understanding the evolution of magnetic flux in the heliosphere remains an unresolved issue. The current solar minimum between cycles 23 and 24 is anomalously long, which gives rare insight into the long-term evolution of heliospheric magnetic flux when the coronal mass ejection (CME) rate and the flux emergence rate from CMEs were very low. The precipitous drop of heliospheric magnetic flux to levels lower than have ever been observed directly shows that there may be a persistent loss of open magnetic flux through disconnection, the reconnection between opposite polarity heliospheric magnetic field lines relatively near the Sun (beneath the Alfvén point). Here, we develop a model for the levels of magnetic flux in the inner heliosphere balancing new flux injected by CMEs, flux lost through disconnection, and closed flux lost through interchange reconnection near the Sun. This magnetic flux balance is a fundamental property that regulates the plasma and radiation environment of our solar system.

## **Magnetic Structures at the Boundary of the Closed Corona: A Semi-automated Study of S-Web Morphology**

[Roger B. Scott](#)<sup>1</sup>, [David I. Pontin](#)<sup>1</sup>, and [Peter F. Wyper](#)<sup>2</sup>

**2019** ApJ 882 125

<https://iopscience.iop.org/article/10.3847/1538-4357/ab364a/pdf>

Interchange reconnection is thought to play an important role in driving the dynamics of the slow solar wind. To understand the details of this process, it is important to catalog the various magnetic structures that are present at the boundary between open and closed magnetic flux. To this end we have developed a numerical method for partitioning the coronal volume into individual flux domains using volume segmentation along layers of high magnetic squashing degree ( $Q$ ). Our publicly available implementation of this method is able to identify the different magnetic structures within a coronal magnetic field model that define the open-closed boundary and comprise the so-called Separatrix-Web (S-Web). With this we test previous predictions of how different configurations of high- $Q$  arcs within the S-Web are related to coronal magnetic field structures. Here we present our findings from a survey of 11 different potential field source surface models, spanning from 2008 to 2017, which offer a representative sample of the coronal magnetic field across nearly a complete solar cycle. Two key findings of our analysis are that (i) "vertex" structures—where arcs of the S-Web meet away from the heliospheric current sheet—are associated with underlying magnetic dome structures, and (ii) that any given arc of the S-Web is almost equally as likely to be formed by a narrow corridor of open flux (corresponding to a hyperbolic flux tube) as by the separatrix surface of a magnetic null. Together, these findings highlight the importance of a variety of topological configurations for future studies of interchange reconnection and the acceleration of the solar wind.

## **Magnetic Structures at the Boundary of the Closed Corona: Interpretation of S-Web Arcs**



Roger B. [Scott](#)<sup>1</sup>, David I. Pontin<sup>1</sup>, Anthony R. Yeates<sup>2</sup>, Peter F. Wyper<sup>2</sup>, and Aleida K. Higginson  
2018 ApJ 869 60

<http://iopscience.iop.org/article/10.3847/1538-4357/aaed2b/pdf>

The topology of coronal magnetic fields near the open-closed magnetic flux boundary is important to the the process of interchange reconnection, whereby plasma is exchanged between open and closed flux domains. Maps of the magnetic squashing factor in coronal field models reveal the presence of the Separatrix-Web (S-Web), a network of separatrix surfaces and quasi-separatrix layers, along which interchange reconnection is highly likely. Under certain configurations, interchange reconnection within the S-Web could potentially release coronal material from the closed magnetic field regions to high-latitude regions far from the heliospheric current sheet, where it is observed as slow solar wind. It has also been suggested that transport along the S-Web may be a possible cause for the observed large longitudinal spreads of some impulsive, <sup>3</sup>He-rich solar energetic particle events. Here, we demonstrate that certain features of the S-Web reveal structural aspects of the underlying magnetic field, specifically regarding the arcing bands of highly squashed magnetic flux observed at the outer boundary of global magnetic field models. In order for these S-Web arcs to terminate or intersect away from the helmet streamer apex, there must be a null spine line that maps a finite segment of the photospheric open-closed boundary up to a singular point in the open flux domain. We propose that this association between null spine lines and arc termination points may be used to identify locations in the heliosphere that are preferential for the appearance of solar energetic particles and plasma from the closed corona, with characteristics that may inform our understanding of interchange reconnection and the acceleration of the slow solar wind. 2014 July 29

### **Dynamics of photospheric magnetic flux distribution and variations in solar RVs -- a study using HARPS-N solar and SDO observations**

[Anisha Sen](#), [S.P. Rajaguru](#)

ApJ 2023

<https://arxiv.org/pdf/2309.05428.pdf>

The distribution and evolution of photospheric magnetic field in sunspots, plages and network, and variations in their relative flux content, play key roles in radial velocity (RV) fluctuations observed in Sun-as-a-star spectra. Differentiating and disentangling such magnetic contributions to RVs help in building models to account for stellar activity signals in high precision RV exoplanet searches. In this work, as earlier authors, we employ high-resolution images of the solar magnetic field and continuum intensities from SDO/HMI to understand the activity contributions to RVs from HARPS-N solar observations. Using well observed physical relationships between strengths and fluxes of photospheric magnetic fields, we show that the strong fields (spots, plages and network) and the weak internetwork fields leave distinguishing features in their contributions to the RV variability. We also find that the fill-factors and average unsigned magnetic fluxes of different features correlate differently with the RVs and hence warrant care in employing either of them as a proxy for RV variations. In addition, we examine disk averaged UV intensities at 1600 Å and 1700 Å wavelength bands imaged by SDO/AIA and their performances as proxies for variations in different magnetic features. We find that the UV intensities provide a better measure of contributions of plage fields to RVs than the Ca II H-K emission indices, especially during high activity levels when the latter tend to saturate. 1 Sep 2015

### **Open and closed magnetic configurations of twisted flux tubes**

Samrat [Sen](#), [A. Mangalam](#)

ApJ 2019

<https://arxiv.org/pdf/1904.03149.pdf>

We construct two classes of magnetohydrostatic (MHS) equilibria for an axisymmetric vertical flux tube spanning from the photosphere to the lower part of the transition region within a realistic stratified solar atmosphere subject to solar gravity. We assume a general quadratic expression of the magnetic flux function for the gas pressure and poloidal current and solve the Grad-Shafranov equation analytically. The solution is a combination of a homogeneous and a particular part where the former is separable by a Coulomb function in  $r$  and exponential in  $z$ , while the particular part is an open configuration that has no  $z$  dependence. We also present another open field solution by using a self-similar formulation with two different profile functions and incorporating stratified solar gravity to maintain the magnetohydrostatic equilibria, which is a modification of earlier self-similar models with a twist. We study the admitted parameter space that is consistent with the conditions in the solar atmosphere and derive magnetic and the thermodynamic structures inside the flux tube that are reasonably consistent with the photospheric magnetic bright points (MBPs) for both open and closed field Coulomb function and self-similar models as estimated from observations and simulations. The obtained open and closed field flux tube solutions can be used as the background conditions for the numerical simulations for the study of the wave propagation through the flux tubes. The solutions can also be used to construct realistic magnetic canopies.

## **Magnetohydrostatic flux tube model in the solar atmosphere**

[S. Sen](#), [A. Mangalam](#) (Indian Institute of Astrophysics)

IAU Symposium 340

2018

<https://arxiv.org/pdf/1805.08434.pdf>

We construct two classes of the magnetohydrostatic equilibria of the axisymmetric flux tubes with twisted magnetic fields in the stratified solar atmosphere that span from the photosphere to the transition region. We built the models by incorporating specific forms of the gas pressure and poloidal current in the Grad-Shafranov equation. This model gives both closed and open field structure of the flux tube. The other open field model we construct is based on the self-similar formulation, where we have incorporated specific forms of the gas pressure, poloidal current and two different shape functions. We study the homology of the parameter space that is consistent with the solar atmosphere and find that the estimation of the magnetic structure inside the flux tubes is consistent with the observation and simulation results of the magnetic bright points.

## **Model of a flux tube with a twisted magnetic field in the stratified solar atmosphere**

[S. Sen](#), [A. Mangalam](#)

Advances in Space Research

2017

<https://arxiv.org/pdf/1705.08100.pdf>

We build a single vertical straight magnetic fluxtube spanning the solar photosphere and the transition region which does not expand with height. We assume that the fluxtube containing twisted magnetic fields is in magnetohydrostatic equilibrium within a realistic stratified atmosphere subject to solar gravity. Incorporating specific forms of current density and gas pressure in the Grad--Shafranov equation, we solve the magnetic flux function, and find it to be separable with a Coulomb wave function in radial direction while the vertical part of the solution decreases exponentially. We employ improved fluxtube boundary conditions and take a realistic ambient external pressure for the photosphere to transition region, to derive a family of solutions for reasonable values of the fluxtube radius and magnetic field strength at the base of the axis that are the free parameters in our model. We find that our model estimates are consistent with the magnetic field strength and the radii of Magnetic bright points (MBPs) as estimated from observations. We also derive thermodynamic quantities inside the fluxtube.

## **Mapping the Sun's coronal magnetic field using the Zeeman effect**

[Thomas A. Schad](#), [Gordon J.D. Petrie](#), [Jeffrey R. Kuhn](#), + + +

Science Advances, Vol. 10, no. 37, adq1604, 2024

<https://arxiv.org/pdf/2410.21568>

Regular remote sensing of the magnetic field embedded within the million-degree solar corona is severely lacking. This reality impedes fundamental investigations of the nature of coronal heating, the generation of solar and stellar winds, and the impulsive release of energy into the solar system via flares and other eruptive phenomena. Resulting from advancements in large aperture solar coronagraphy, we report unprecedented maps of polarized spectra emitted at 1074 nm by Fe+12 atoms in the active corona. We detect clear signatures of the Zeeman effect that are produced by the coronal magnetic field along the optically thin path length of its formation. Our comparisons with global magnetohydrodynamic models highlight the valuable constraints that these measurements provide for coronal modeling efforts, which are anticipated to yield subsequent benefits for space weather research and forecasting. **22 June 2023**

## **Determination of coronal magnetic fields from 10 to 26 R $\odot$ using the density compression ratios of CME-driven shocks**

[Shanmugaraju](#), A.; Suresh, K.; Moon, Y.-J.

Astrophysics and Space Science, Volume 351, Issue 1, pp.67-73, 2014; File

Recently, the estimation of coronal magnetic field using new methods, such as standoff distance method or density compression ratio method has been reported. In the present work, we utilized the density compression ratio of CME-driven shocks for 10 events at 29 different locations in the upper solar corona (10-26 R  $\odot$ ) and determined the coronal magnetic field for two different adiabatic indices ( $\gamma=4/3$  and  $5/3$ ). In addition, radial dependence of shock parameters in the corona is studied. It is found that the magnetic field estimated in the above range agree with the general trend. In addition, we obtained a radial profile of magnetic field [  $B(R)=623 R^{-1.4}$ ] in the entire upper corona (3-30 R  $\odot$ ) by combining the magnetic field estimated by Kim et al. (Astrophys. J. 746:118, 2012) in the range 3-15 R  $\odot$  and that estimated in the present study in the range (10-26 R  $\odot$ ). The power-law indices are nearly in agreement with recent results of CME-driven shocks reported in the literature. The results are discussed with the comparison of newly reported coronal magnetic field values obtained by different techniques and found that the power-law relation closely follow the literature values.

## **Dynamics of Sunspot Series on Time Scales From Days to Years: Correlation of Sunspot Births, Variable Lifetimes, and Evolution of the High-Frequency Spectral Component**

A. **Shapoval**, J.-L. Le Mouél, M. Shnirman, V. Courtillot  
JGR Volume 122, Issue 12 December 2017 Pages 11,874–11,887  
<http://sci-hub.tw/10.1002/2017JA024430>

This paper explores some features of the dynamics of daily sunspot numbers on scales from days to years. We define higher and lower frequency energy components of the series that are related to periods ranging over 1 to 6 days and 6 days to 2 years, respectively. The lower frequency component is found to follow the solar activity, but the maxima of the higher frequency component are unexpectedly lower during the last epoch of high solar activity than during the preceding epoch of low solar activity. We also consider the birthrate of sunspot groups as another indicator of quickly varying components of the solar activity and show that it is the general growth of solar activity in the 1930–1940s that drives up this birthrate. We propose an autoregressive model that captures the opposite trends exhibited by the two representatives of the high-frequency content, accurately reproduces the evolutions of the lower and higher frequency energy components, and replicates the shape of the curve representing the daily sunspot numbers. The three following hypotheses underlie the model construction: (1) proxy series of solar activity can be modeled by a random process with a modulated noise; (2) sunspot's birth and disappearance rates, both following the solar cycle, determine properties of this process; and (3) the births of sunspots are positively correlated in time during epochs of high solar activity. We find that the mean birthrate varies as a power function of the mean lifetime. Derived constraints could contribute to narrowing the choice of a proper solar dynamo model.

### **Direct observations of different sunspot waves influenced by umbral flashes**

Aishawnya **Sharma**, **G. R. Gupta**, **Durgesh Tripathi**, **V. Kashyap**, **Amit Pathak**

ApJ **850** 206 **2017**

<https://arxiv.org/pdf/1710.08438.pdf>

We report the simultaneous presence of chromospheric umbral flashes and associated umbral waves, and propagating coronal disturbances, in a sunspot and related active region. We have analyzed time-distance maps obtained using the observations from Atmospheric Imaging Assembly (AIA) on-board Solar Dynamics Observatory (SDO). These maps show the simultaneous occurrence of different sunspot oscillation and waves such as umbral flashes, umbral waves, and coronal waves. Analysis of the original light curves, i.e., without implementing any Fourier filtering on them, show that the amplitudes of different sunspot waves observed at different atmospheric layers change in synchronization with the light curves obtained from the umbral flash region, thus demonstrating that these oscillations are modulated by umbral flashes. This study provides the first observational evidence of the influence of sunspot oscillations within the umbra on other sunspot waves extending up to the corona. The properties of these waves and oscillations can be utilized to study the inherent magnetic coupling among different layers of the solar atmosphere above sunspots. **December 11, 2010**

### **The diagnostic potential of the weak field approximation for investigating the quiet Sun magnetism: the Si I 10 827 Å line**

N. G. **Shchukina**<sup>1,2,3,4</sup> and J. Trujillo Bueno<sup>4,5,6</sup>

A&A 628, A47 (2019)

[sci-hub.se/10.1051/0004-6361/201935510](http://sci-hub.se/10.1051/0004-6361/201935510)

**Aims.** We aim to investigate the validity of the weak field approximation (WFA) for determining magnetic fields in quiet regions of the solar photosphere using the polarization caused by the Zeeman effect in the Si I 10 827 Å line. **Methods.** We solved the NLTE line formation problem by means of multilevel radiative transfer calculations in a three-dimensional (3D) snapshot model taken from a state-of-the-art magneto-convection simulation of the small-scale magnetic activity in the quiet solar photosphere. The 3D model used is characterized by a surface mean magnetic field strength of about 170 G. The calculated Stokes profiles were degraded because of the atmospheric turbulence of Earth and light diffraction by the telescope aperture. We apply the WFA to the Stokes I, Q, U, V profiles calculated for different seeing conditions and for the apertures of the VTT, GREGOR, EST and DKIST telescopes. We compare the inferred longitudinal and transverse components of the magnetic field with the original vertical and horizontal fields of the 3D model.

**Results.** We find that with a spatial resolution significantly better than 0.5" the surface maps of the magnetic field inferred from the Stokes profiles of the Si I 10 827 Å line applying the WFA are close to the magnetic field of the model on the corrugated surface, corresponding to line optical depth unity at  $\Delta\lambda \approx 0.1$  Å for a disk-center line of sight. The correlation between them is relatively high, except that the inferred longitudinal and transverse components of the magnetic field turn out to be lower than in the 3D model.

**Conclusions.** The use of the WFA for interpreting high-spatial-resolution spectropolarimetric observations of the Si I 10 827 Å line obtained with telescopes like GREGOR, EST, and DKIST allows the longitudinal and transverse components of the magnetic field to be retrieved with reasonable precision over the whole quiet solar photosphere, the result being worse for telescopes of lower aperture.

## DETERMINING THE MAGNETIZATION OF THE QUIET SUN PHOTOSPHERE FROM THE HANLE EFFECT AND SURFACE DYNAMO SIMULATIONS

Nataliya [Shchukina](#)<sup>1</sup> and Javier Trujillo Bueno

2011 ApJ 731 L21

The bulk of the quiet solar photosphere is thought to be significantly magnetized, due to the ubiquitous presence of a tangled magnetic field at subresolution scales with an average strength  $B \sim 100$  G. This conclusion was reached through detailed three-dimensional (3D) radiative transfer modeling of the Hanle effect in the Sr I 4607 Å line, using the microturbulent field approximation and assuming that the shape of the probability density function of the magnetic field strength is exponential. Here, we relax both approximations by modeling the observed scattering polarization in terms of the Hanle effect produced by the magnetic field of a 3D photospheric model resulting from a (state-of-the-art) magneto-convection simulation with surface dynamo action. We show that the scattering polarization amplitudes observed in the Sr I 4607 Å line can be explained only after enhancing the magnetic strength of the photospheric model by a sizable scaling factor,  $F \sim 10$ , which implies  $B \sim 130$  G in the upper photosphere. We also argue that in order to explain both the Hanle depolarization of the Sr I 4607 Å line and the Zeeman signals observed in Fe I lines, we need to introduce a height-dependent scaling factor, such that the ensuing  $B \sim 160$  G in the low photosphere and  $B \sim 130$  G in the upper photosphere.

## Rotational Components of the Sun's Mean Field

[Neil R. Sheeley Jr](#)

ApJ 2023

<https://arxiv.org/pdf/2309.11630.pdf>

This paper uses wavelet transforms to look for the rotational frequencies of the Sun's mean line-of-sight magnetic field. For a sufficiently high wavelet frequency, the spectra of the dipole, quadrupole, and hexapole field components each show a time-dependent fine structure with periods in the range of 26.5-30 days and their harmonics. These maps confirm that a large enhancement of 30-day power occurred in the dipole field during 1989-1990, as recorded previously using Fourier techniques (Sheeley 2022). Also, during some years the maps show power at 26.5 days (or its harmonics), that is clearly distinguishable from the 26.9-27.0 day rotation period at the Sun's equator. In at least one case, the 26.5-day period was a wave phenomenon caused by the systematic eruption of active regions at progressively more western locations in the Carrington coordinate system, as if the flux were emerging from a fixed longitude in a faster rotating subsurface layer. Based on previous studies of the mean field (Sheeley et al 1985, Sheeley & DeVore 1986, Sheeley 2022), I conclude that the enhanced wavelet patterns in this paper are regions where magnetic flux is emerging in configurations that strengthen the Sun's horizontal dipole, quadrupole, and hexapole fields, and (in the case of the more slowly rotating patterns) where this flux is being transported to mid-latitudes whose rotation periods are in the range 28-30 days.

## Memorable Events During a Research Career

N. R. [Sheeley Jr.](#)

JGR [Volume 124, Issue 7](#) July 2019 Pages 4949-4959

<https://agupubs.onlinelibrary.wiley.com/doi/10.1029/2019JA026908>

In this paper, I sketch a path through my research career in solar and heliospheric physics, recalling some memorable events and discoveries that occurred along the way. This chain of events begins with an influential Time magazine article in 1955 and progresses through a summer at Bell Labs, 9 years at Caltech, 7 years at the Kitt Peak National Observatory, 43 years at the Naval Research Laboratory, and ends with a digitized map of the Sun's Ca II K-Line emission in 1919 when the AGU was born. Accidents and puzzling results are often the keys to progress and should be examined carefully.

## Tracking the Magnetic Flux in and Around Sunspots

N. R. [Sheeley Jr.](#), J. R. Stauffer<sup>1</sup>, J. C. Thomassie<sup>1</sup>, and H. P. Warren

2017 ApJ 836 144

We have developed a procedure for tracking sunspots observed by the Helioseismic and Magnetic Imager on the Solar Dynamics Observatory and for making curvature-corrected space/time maps of the associated line-of-sight magnetic field and continuum intensity. We apply this procedure to 36 sunspots, each observed continuously for nine days around its central meridian passage time, and find that the proper motions separate into two distinct components depending on their speeds. Fast ( $\sim 3-5$  km s<sup>-1</sup>) motions, comparable to Evershed flows, are produced by weak vertical fluctuations of the horizontal canopy field and recur on a timescale of 12-20 min. Slow ( $\sim 0.3-0.5$  km s<sup>-1</sup>) motions diverge from a sunspot-centered ring whose location depends on the size of the sunspot, occurring in the mid-penumbra for large sunspots and at the outer edge of the penumbra for small sunspots. The slow ingoing features are contracting spokes of a quasi-vertical field of umbral polarity. These inflows disappear when the sunspot loses its penumbra, and may be related to inward-moving penumbral grain. The slow outgoing features may have either polarity depending on whether they originate from quasi-vertical fields of umbral polarity or from the outer edge of the canopy. When a sunspot decays, the penumbra and canopy disappear, and the moat becomes filled

with slow outflows of umbral polarity. We apply our procedure to decaying sunspots, to long-lived sunspots, and to numerical simulations of a long-lived sunspot by Rempel.

## **The Recent Rejuvenation of the Sun's Large-scale Magnetic Field: A Clue for Understanding Past and Future Sunspot Cycles**

N. R. [Sheeley](#) Jr. and Y.-M. Wang

2015 ApJ 809 113

The quiet nature of sunspot cycle 24 was disrupted during the second half of 2014 when the Sun's large-scale field underwent a sudden rejuvenation: the solar mean field reached its highest value since 1991, the interplanetary field strength doubled, and galactic cosmic rays showed their strongest 27-day modulation since neutron-monitor observations began in 1957; in the outer corona, the large increase of field strength was reflected by unprecedentedly large numbers of coronal loops collapsing inward along the heliospheric current sheet. Here, we show that this rejuvenation was not caused by a significant increase in the level of solar activity as measured by the smoothed sunspot number and CME rate, but instead was caused by the systematic emergence of flux in active regions whose longitudinal distribution greatly increased the Sun's dipole moment. A similar post-maximum increase in the dipole moment occurred during each of the previous three sunspot cycles, and marked the start of the declining phase of each cycle. We note that the north–south component of this peak dipole moment provides an early indicator of the amplitude of the next cycle, and conclude that the amplitude of cycle 25 may be comparable to that of cycle 24, and well above the amplitudes obtained during the Maunder Minimum.

## **Coronal Inflows during the Interval 1996-2014**

N. R. [Sheeley](#), Jr. and Y.-M. Wang

2014 ApJ 797 10

We extend our previous counts of coronal inflows from the 5?yr interval 1996-2001 to the 18?yr interval 1996-2014. By comparing stackplots of these counts with similar stackplots of the source-surface magnetic field and its longitudinal gradient, we find that the inflows occur in long-lived streams with counting rates in excess of 18 inflows per day at sector boundaries where the gradient exceeds  $0.22\text{?G rad}^{-1}$ . These streams are responsible for the high (86%) correlation between the inflow rate and the longitudinal field gradient. The overall inflow rate was several times larger in sunspot cycle 23 than it has been so far in cycle 24, reflecting the relatively weak source-surface fields during this cycle. By comparison, in cycles 21-22, the source-surface field and its gradient had bursts of great strength, as if large numbers of inflows occurred during those cycles. We find no obvious relation between inflows and coronal mass ejections (CMEs) on timescales of days to weeks, regardless of the speeds of the CMEs, and only a 60% correlation on timescales of months, provided the CMEs are fast ( $V? > 600\text{?km?s}^{-1}$ ). We conclude that most of the flux carried out by CMEs is returned to the Sun via field line reconnection well below the  $2.0 R_{\odot}$  inner limit of the LASCO field of view, and that the remainder accumulates in the outer corona for an eventual return at sector boundaries.

## **Granular-scale Magnetic Flux Emergence and its Associated Features in an Emerging Active Region**

Jinhua [Shen](#)<sup>1,2,3</sup>, Zhi Xu<sup>4</sup>, Jianping Li<sup>3</sup>, and Haisheng Ji<sup>3</sup>

2022 ApJ 925 46

<https://iopscience.iop.org/article/10.3847/1538-4357/ac37c3/pdf>

Using the high-resolution photosphere and chromosphere observations made by the 1 m New Vacuum Solar Telescope, we studied the granular-scale magnetic flux emergence occurring in emerging active region NOAA 12579. Supplementary observations are also provided by the spacecraft Solar Dynamics Observatory. The studied granular-scale flux emergence took place at two different locations. One is completely embedded in the unipolar region of the following sunspots (Case 1), while another is located at the central part in the active region (Case 2). We find that both cases initially emerge from a dark patch like a wide intergranular lane, but showing the different subsequent features. In Case 1, the emerging granule grows in an elongated feature and reaches its maximum size of almost of  $5'' \times 3''$ , with an elongated speed of about  $2\text{--}3\text{ km s}^{-1}$ . An eruption (i.e., surge) with bright footpoints is observed after the emerging granule reaches its maximum scale. There is a time delay of more than 10 minutes between the appearance of the abnormal granule and the  $H\alpha$  surge. Furthermore, its footpoints are clearly rooted at the intergranular lane. We propose that the eruptive surge could be triggered by the reconnection between the emerging magnetic flux and the preexisting ambient field, leading to the localized heating and bidirectional flows. In Case 2, the granular cell emerging is simultaneously associated with bright points with opposite magnetic polarity, showing the separating motion between them and a bunch of newly formed arch filament systems. We infer that the bright points are due to the strong-field magnetic concentration in the dark intergranular lanes rather than the instantaneous Ellerman bombs. **2016 September 23**

## DOUBLE POWER-LAW DISTRIBUTION OF MAGNETIC ENERGY IN THE SOLAR CORONA OVER AN ACTIVE REGION

Jinhua [Shen](#)<sup>1,2,3</sup>, Haisheng Ji<sup>1</sup>, Thomas Wiegelmann<sup>2</sup>, and Bernd Inhester

2013 ApJ 764 86

In this paper, we study the magnetic energy (ME) structure contained in the solar corona over the active region NOAA 11158. The time period is chosen as from 0:00 to 06:00 UT on **2011 February 15**, during which an X-class flare occurred. The nonlinear force-free field (NLFFF) and the potential field extrapolation are carried out to model the coronal magnetic field over this active region, using high-quality photospheric vector magnetograms observed by the Helioseismic and Magnetic Imager on board the Solar Dynamics Observatory as boundary conditions. We find that the volume distribution for the density of the ME ( $B^2/8\pi$ ) and the ohmic dissipation power (ODP,  $j^2/\sigma$ ), in which  $j$  is the electric current density ( $c/4\pi\nabla \times B$ ) and  $\sigma$  is the conductivity in the corona, can be readily fitted by a broken-down double-power law. The turn-over density for the spectrum of the ME and ODP is found to be fixed at  $\sim 1.0 \times 10^4 \text{ erg cm}^{-3}$  and  $\sim 2.0 \times 10^{-15} \text{ W cm}^{-3}$  (assuming  $\sigma = 105 \Omega^{-1} \text{ m}^{-1}$ ), respectively. Compared with their first power-law spectra (fitted below the corresponding turn-over value) which remain unchanged, the second power-law spectra (fitted above the corresponding turn-over value) for the NLFFF's ME and ODP show flare-associated changes. The potential field remains steady. These results indicate that a magnetic field with energy density larger than the turn-over energy density plays a dominant role in powering the flare.

## Refinement of global coronal and interplanetary magnetic field extrapolations constrained by remote-sensing and in-situ observations at the solar minimum

[Guanglu Shi](#), [Li Feng](#), [Beili Ying](#), [Shuting Li](#), [Weiqun Gan](#)

ApJ 970 131 2024

<https://arxiv.org/pdf/2405.18665>

<https://iopscience.iop.org/article/10.3847/1538-4357/ad5200/pdf>

Solar magnetic fields are closely related to various physical phenomena on the sun, which can be extrapolated with different models from photospheric magnetograms. However, the Open Flux Problem (OFP), the underestimation of the magnetic field derived from the extrapolated model, is still unsolved. To minimize the impact of the OFP, we propose three evaluation parameters to quantitatively evaluate magnetic field models and determine the optimal free parameters in the models by constraining the coronal magnetic fields (CMFs) and the interplanetary magnetic fields (IMFs) with real observations. Although the OFP still exists, we find that magnetic field lines traced from the coronal models effectively capture the intricate topological configurations observed in the corona, including streamers and plumes. The OFP is lessened by using the HMI synoptic map instead of the GONG daily synoptic maps, and the PFSS+PFCS model instead of the CSSS model. For Carrington Rotation (CR) 2231 at the solar minimum, we suggest that the optimal parameters for the PFSS+PFCS model are  $R_{ss}=2.2\text{--}2.5 R_{sun}$  and  $R_{scs}=10.5\text{--}14.0 R_{sun}$ , as well as for the CSSS model are  $R_{cs}=2.0\text{--}2.4 R_{sun}$ ,  $R_{ss}=11.0\text{--}14.7 R_{sun}$  and  $a=1.0 R_{sun}$ . Despite the IMFs at 1 AU being consistent with the measurements by artificially increasing the polar magnetic fields, the IMFs near the sun are still underestimated. The OFP might be advanced by improving the accuracy of both the weak magnetic fields and polar magnetic fields, especially considering magnetic activities arising from interplanetary physical processes.

## 3D magnetic field configuration of small-scale reconnection events in the solar plasma atmosphere

**Review**

T. Shimizu

Physics of Plasmas 2015

<http://arxiv.org/ftp/arxiv/papers/1508/1508.05481.pdf>

The outer solar atmosphere, i.e., the corona and the chromosphere, is replete with small energy-release events, which are accompanied by transient brightening and jet-like ejections. These events are considered to be magnetic reconnection events in the solar plasma, and their dynamics have been studied using recent advanced observations from the Hinode spacecraft and other observatories in space and on the ground. These events occur at different locations in the solar atmosphere, and vary in their morphology and amount of the released energy. The magnetic field configurations of these reconnection events are inferred based on observations of magnetic fields at the photospheric level. Observations suggest that these magnetic configurations can be classified into two groups. In the first group, two anti-parallel magnetic fields reconnect to each other, yielding a 2D emerging flux configuration. In the second group, helical or twisted magnetic flux tubes are parallel or at a relative angle to each other. Reconnection can occur only between anti-parallel components of the magnetic flux tubes and may be referred to as component reconnection. The latter configuration type may be more important for the larger class of small-scale reconnection events. The two types of magnetic configurations can be compared to counter-helicity and co-helicity configurations, respectively, in laboratory plasma collision experiments.

## Generation of High-resolution Solar Pseudo-magnetograms from Ca ii K Images by Deep Learning

Gyungin [Shin](#)<sup>1</sup>, Yong-Jae Moon<sup>1</sup>, Eunsu Park<sup>2</sup>, Hyunjin Jeong<sup>1</sup>, Harim Lee<sup>2</sup>, and Sung-Ho Bae<sup>3</sup>  
2020 ApJL 895 L16

<https://doi.org/10.3847/2041-8213/ab9085>

In this Letter, we generate realistic high-resolution ( $1024 \times 1024$  pixels) pseudo-magnetograms from Ca ii K images using a deep learning model based on conditional generative adversarial networks. For this, we consider a model "pix2pixHD" that is specifically devised for high-resolution image translation tasks. We use Ca ii K 393.3 nm images from the Precision Solar Photometric Telescope at the Rome Observatory and line-of-sight magnetograms from the Helioseismic and Magnetic Imager (HMI) at the Solar Dynamics Observatory from 2011 January to 2015 June. 2465 pairs of Ca ii K and HMI are used for training except for January and July data. The remaining 436 pairs are used for an evaluation of the model. Our model shows that the mean correlation coefficient (CC) of total unsigned magnetic flux between AI-generated and real ones is 0.99 and the mean pixel-to-pixel CC after  $8 \times 8$  binning over the full disk is 0.74. We find that the AI-generated absolute magnetic flux densities are highly consistent with real ones, even to the fine scale structures of quiet regions. On the other hand, the mean pixel-to-pixel correlations of magnetic flux densities strongly depend on a region of interest: 0.81 for active regions and 0.24 for quiet regions. Our results suggest a sufficient possibility that we can produce high-resolution solar magnetograms from historical Ca ii data.

### **POLAR FIELD REVERSAL OBSERVATIONS WITH HINODE**

D. [Shiota](#)<sup>1</sup>, S. Tsuneta<sup>2</sup>, M. Shimojo<sup>2</sup>, N. Sako<sup>3</sup>, D. Orozco Suárez<sup>2,4</sup>, and R. Ishikawa  
2012 ApJ 753 157

We have been monitoring yearly variation in the Sun's polar magnetic fields with the Solar Optical Telescope aboard Hinode to record their evolution and expected reversal near the solar maximum. All magnetic patches in the magnetic flux maps are automatically identified to obtain the number density and magnetic flux density as a function of the total magnetic flux per patch. The detected magnetic flux per patch ranges over four orders of magnitude (1015-1020 Mx). The higher end of the magnetic flux in the polar regions is about one order of magnitude larger than that of the quiet Sun, and nearly that of pores. Almost all large patches ( $\geq 1018$  Mx) have the same polarity, while smaller patches have a fair balance of both polarities. The polarity of the polar region as a whole is consequently determined only by the large magnetic concentrations. A clear decrease in the net flux of the polar region is detected in the slow rising phase of the current solar cycle. The decrease is more rapid in the north polar region than in the south. The decrease in the net flux is caused by a decrease in the number and size of the large flux concentrations as well as the appearance of patches with opposite polarity at lower latitudes. In contrast, we do not see temporal change in the magnetic flux associated with the smaller patches ( $< 1018$  Mx) and that of the horizontal magnetic fields during the years 2008-2012.

### **A First Spectroscopic Measurement of the Magnetic-field Strength for an Active Region of the Solar Corona**

Ran [Si](#)<sup>1,2</sup>, Tomas Brage<sup>1</sup>, Wenxian Li<sup>1,3</sup>, Jon Grumer<sup>4</sup>, Meichun Li<sup>5,6</sup>, and Roger Hutton<sup>5</sup>  
2020 ApJL 898 L34

<https://doi.org/10.3847/2041-8213/aba18c>

For all involved in astronomy, the importance of monitoring and determining astrophysical magnetic-field strengths is clear. It is also a well-known fact that the corona magnetic fields play an important part in the origin of solar flares and the variations of space weather. However, after many years of solar corona studies, there is still no direct and continuous way to measure and monitor the solar magnetic-field strength. We present here a scheme that allows such a measurement, based on a careful study of an exotic class of atomic transitions, known as magnetic induced transitions, in Fe9+. In this contribution we present a first application of this methodology and determine a value of the coronal field strength using the spectroscopic data from Hinode.

### **Novel Approach to Forecasting Photospheric Emergence of Active Regions**

S. S. A. [Silva](#)<sup>1</sup>, M. Lennard<sup>2</sup>, G. Verth<sup>2</sup>, I. Ballai<sup>2</sup>, E. L. Rempel<sup>3,4</sup>, J. Warnecke<sup>5</sup>, H. Iijima<sup>6</sup>, H. Hotta<sup>7</sup>, S.-H. Park<sup>8</sup>, A. C. Donea<sup>9</sup>Show full author list  
2023 ApJL 948 L24

<https://iopscience.iop.org/article/10.3847/2041-8213/acd007/pdf>

One key aspect of understanding the solar dynamo mechanism and the evolution of solar magnetism is to properly describe the emergence of solar active regions. In this Letter, we describe the Lagrangian photospheric flows dynamics during a simulated flux emergence that produces an active region formed by pores. We analyze the lower photospheric flow organization prior, during and following the rise of an active region, uncovering the repelling and attracting photospheric structures that act as sources and sinks for magnetic element transport. Our results show that around 10 hr before the simulated emergence, considerable global changes are taking place on mesogranular scales indicated by an increase of the number of regions acting as a source to the multiple and scattered emergences of small-scale magnetic flux. At the location of active region's appearance, the converging flows become weaker and there is an arising of a diverging region 8 hr before the emergence time. Our study also indicates that the strong

concentration of magnetic field affects the flow dynamics beyond the area of the actual simulated pores, leading to complex and strongly diverging flows in the neighboring regions. Our findings suggest that the Lagrangian analysis is a powerful tool to describe the changes in the photospheric flows due to magnetic flux emergence.

## **DYNAMO EFFECTS NEAR THE TRANSITION FROM SOLAR TO ANTI-SOLAR DIFFERENTIAL ROTATION**

Radostin D. [Simitev](#)<sup>1,2,3</sup>, Alexander G. Kosovichev<sup>3,4</sup>, and Friedrich H. Busse  
2015 ApJ 810 80

Numerical MHD simulations play an increasingly important role for understanding the mechanisms of stellar magnetism. We present simulations of convection and dynamos in density-stratified rotating spherical fluid shells. We employ a new 3D simulation code for obtaining the solution of a physically consistent anelastic model of the process with a minimum number of parameters. The reported dynamo simulations extend into a "buoyancy-dominated" regime where the buoyancy forcing is dominant while the Coriolis force is no longer balanced by pressure gradients, and strong anti-solar differential rotation develops as a result. We find that the self-generated magnetic fields, despite being relatively weak, are able to reverse the direction of differential rotation from anti-solar to solar-like. We also find that convection flows in this regime are significantly stronger in the polar regions than in the equatorial region, leading to non-oscillatory dipole-dominated dynamo solutions, and to a concentration of magnetic field in the polar regions. We observe that convection has a different morphology in the inner and the outer part of the convection zone simultaneously such that organized geostrophic convection columns are hidden below a near-surface layer of well-mixed highly chaotic convection. While we focus our attention on the buoyancy-dominated regime, we also demonstrate that conical differential rotation profiles and persistent regular dynamo oscillations can be obtained in the parameter space of the rotation-dominated regime even within this minimal model.

## **Magnetic fields inferred by Solar Orbiter: A comparison between SO/PHI-HRT and SDO/HMI**

[J. Sinjan](#), [D. Calchetti](#), [J. Hirzberger](#), [F. Kahil](#), [G. Valori](#), [S.K. Solanki](#), et al.

A&A 673, A31 2023

<https://arxiv.org/pdf/2303.16771.pdf>

<https://www.aanda.org/articles/aa/pdf/2023/05/aa45830-22.pdf>

The High Resolution Telescope (HRT) of the Polarimetric and Helioseismic Imager on board the Solar Orbiter spacecraft (SO/PHI) and the Helioseismic and Magnetic Imager (HMI) on board the Solar Dynamics Observatory (SDO) both infer the photospheric magnetic field from polarised light images. SO/PHI is the first magnetograph to move out of the Sun-Earth line and will provide unprecedented access to the Sun's poles. This provides excellent opportunities for new research wherein the magnetic field maps from both instruments are used simultaneously. We aim to compare the magnetic field maps from these two instruments and discuss any possible differences between them. We used data from both instruments obtained during Solar Orbiter's inferior conjunction on **7 March 2022**. The HRT data were additionally treated for geometric distortion and degraded to the same resolution as HMI. The HMI data were re-projected to correct for the 3° separation between the two observatories. SO/PHI-HRT and HMI produce remarkably similar line-of-sight magnetograms, with a slope coefficient of 0.97, an offset below 1 G, and a Pearson correlation coefficient of 0.97. However, SO/PHI-HRT infers weaker line-of-sight fields for the strongest fields. As for the vector magnetic field, SO/PHI-HRT was compared to both the 720-second and 90-second HMI vector magnetic field: SO/PHI-HRT has a closer alignment with the 90-second HMI vector. In the weak signal regime (<600 G), SO/PHI-HRT measures stronger and more horizontal fields than HMI, very likely due to the greater noise in the SO/PHI-HRT data. In the strong field regime (≥600 G), HRT infers lower field strengths but with similar inclinations (a slope of 0.92) and azimuths (a slope of 1.02). The slope values are from the comparison with the HMI 90-second vector.

## **Temporal evolution of short-lived penumbral microjets**

[A. Siu-Tapia](#), [L. R. Bellot Rubio](#), [D. Orozco Suárez](#), [R. Gafeira](#)

A&A 642, A128 2020

<https://arxiv.org/pdf/2007.15926.pdf>

<https://doi.org/10.1051/0004-6361/202038370>

Context. Penumbral microjets are elongated jet-like brightenings observed in the chromosphere above sunspot penumbrae. They are transient events that last from a few seconds to several minutes and are thought to originate from magnetic reconnection processes. Previous studies have mainly focused on their morphological and spectral characteristics, and more recently on their spectropolarimetric signals during the maximum brightness stage. Studies addressing the temporal evolution of PMJs have also been carried out, but they are based on spatial and spectral time variations only.

Aims. Here we investigate the temporal evolution of the polarization signals produced by short-lived PMJs (lifetimes < 2 minutes) to infer how the magnetic field vector evolves in the upper photosphere and mid-



chromosphere.

**Methods.** We use fast-cadence spectropolarimetric observations of the Ca II 854.2 nm line taken with the CRisp Imaging Spectropolarimeter at the Swedish 1-m Solar Telescope. The weak-field approximation (WFA) is used to estimate the strength and inclination of the magnetic field vector.

**Results.** The WFA reveals larger magnetic field changes in the upper photosphere than in the chromosphere during the PMJ maximum brightness stage. In the photosphere, the magnetic field inclination and strength undergo a transient increase for most PMJs, but in 25% of the cases the field strength decreases during the brightening. In the chromosphere, the magnetic field tends to be slightly stronger during the PMJs.

**Conclusions.** The propagation of compressive perturbation fronts followed by a rarefaction phase in the aftershock region may explain the observed behavior of the magnetic field vector. The fact that such behavior varies among the analyzed PMJs could be a consequence of the limited temporal resolution of the observations and the fast-evolving nature of the PMJs. **2016 June 16**

## Superstrong photospheric magnetic fields in sunspot penumbrae

A. [Siu-Tapia](#), [A. Lagg](#), [M. van Noort](#), [M. Rempel](#), [S. K. Solanki](#)

A&A 631, A99 2019

<https://arxiv.org/pdf/1909.13619.pdf>

<https://www.aanda.org/articles/aa/pdf/2019/11/aa34083-18.pdf>

**Context.** Recently, there have been some reports of unusually strong photospheric magnetic fields (which can reach values of over 7 kG) inferred from Hinode SOT/SP sunspot observations within penumbral regions. These superstrong penumbral fields are even larger than the strongest umbral fields on record and appear to be associated with supersonic downflows. The finding of such fields has been controversial since they seem to show up only when spatially coupled inversions are performed.

**Aims.** Here, we investigate and discuss the reliability of those findings by studying in detail observed spectra associated with particularly strong magnetic fields at the inner edge of the penumbra of active region 10930.

**Methods.** We apply classical diagnostic methods and various inversions with different model atmospheres to the observed Stokes profiles in two selected pixels with superstrong magnetic fields, and compare the results with a magnetohydrodynamic simulation of a sunspot whose penumbra contains localized regions with strong fields (nearly 5 kG at  $\tau = 1$ ) associated with supersonic downflows.

**Results.** The different inversions provide different results: while the SPINOR 2D inversions consider a height-dependent singlecomponent model and return  $B > 7$  kG and supersonic positive vLOS (corresponding to a counter-Evershed flow), height-dependent 2-component inversions suggest the presence of an umbral component (almost at rest) with field strengths  $\sim 4 - 4.2$  kG and a penumbral component with vLOS  $\sim 16 - 18$  km s<sup>-1</sup> and field strengths up to  $\sim 5.8$  kG. Likewise, height-independent 2-component inversions find a solution for an umbral component and a strongly redshifted (vLOS  $\sim 15 - 17$  km s<sup>-1</sup>) penumbral component with  $B \sim 4$  kG. According to a Bayesian Information Criterion, the inversions providing a better balance between the quality of the fits and the number of free parameters considered by the models are the height-independent 2-component inversions, but they lie only slightly above the SPINOR 2D inversions. Since it is expected that the physical parameters all display considerable gradients with height, as supported by MHD sunspot simulations, the SPINOR 2D inversions are the preferred ones.

**Conclusions.** According to the MHD sunspot simulation analyzed here, the presence of counter-Evershed flows in the photospheric penumbra can lead to the necessary conditions for the observation of  $\sim 5$  kG fields at the inner penumbra. Although a definite conclusion about the potential existence of fields in excess of 7 kG cannot be given, their nature could be explained (based on the simulation results) such as the consequence of the extreme dynamical effects introduced by highly supersonic counter-Evershed flows (vLOS  $> 10$  km s<sup>-1</sup> and up to  $\sim 30$  km s<sup>-1</sup> according to SPINOR 2D), which would be much faster and more compressive downflows than those found in the MHD simulations and therefore could lead to the field intensification up to considerably stronger fields. Also, a lower gas density would lead to a deeper depression of the  $\tau = 1$  surface, making possible the observation of deeper-lying stronger fields. The superstrong magnetic fields are expected to be nearly force-free, so that they can attain much larger strengths than expected when considering only balance between magnetic pressure and the local gas pressure. **Dec 8 2006**

## Evershed and Counter-Evershed Flows in Sunspot MHD Simulations

A. L. [Siu-Tapia](#)<sup>1,2</sup>, [M. Rempel](#)<sup>3</sup>, [A. Lagg](#)<sup>1</sup>, and [S. K. Solanki](#)<sup>1</sup>

2018 ApJ 852 66

There have been a few reports in the literature of counter-Evershed flows observed in well-developed sunspot penumbrae, i.e., flows directed toward the umbra along penumbral filaments. Here, we investigate the driving forces of such counter-Evershed flows in a radiative magnetohydrodynamic simulation of a sunspot, and compare them to the forces acting on the normal Evershed flow. The simulation covers a timespan of 100 solar hours and generates an Evershed outflow exceeding 8 km s<sup>-1</sup> in the penumbra along radially aligned filaments where the magnetic field is almost horizontal. Additionally, the simulation produces a fast counter-Evershed flow (i.e., an inflow near  $\tau = 1$ ) in some regions within the penumbra, reaching peak flow speeds of  $\sim 12$  km s<sup>-1</sup>. The counter-Evershed flows are transient and typically last a few hours before they turn into outflows again. By using the kinetic energy equation

and evaluating its various terms in the simulation box, we found that the Evershed flow occurs due to overturning convection in a strongly inclined magnetic field, while the counter-Evershed flows can be well-described as siphon flows.

### **Normal and counter Evershed flows in the photospheric penumbra of a sunspot. SPINOR 2D inversions of Hinode-SOT/ SP observations**

A. [Siu-Tapia](#), [A. Lagg](#), [S. K. Solanki](#), [M. van Noort](#), [J. Jurčák](#)

A&A 607, A36 2017

<https://arxiv.org/pdf/1709.07386.pdf>

Context. The Evershed effect, a nearly horizontal outflow of material seen in the penumbrae of sunspots in the photospheric layers, is a common characteristic of well-developed penumbrae, but is still not well understood. Even less is known about photospheric horizontal inflows in the penumbra, also known as counter Evershed flows. Aims. Here we present a rare feature observed in the penumbra of the main sunspot of AR NOAA 10930. This spot displays the normal Evershed outflow in most of the penumbra, but harbors a fast photospheric inflow of material over a large sector of the disk-center penumbra. We investigate the driving forces of both, the normal and the counter Evershed flows. Methods. We invert the spectropolarimetric data from Hinode SOT/SP using the spatially coupled version of the SPINOR inversion code, which allows us to derive height-dependent maps of the relevant physical parameters in the sunspot. These maps show considerable fine structure. Similarities and differences between the normal Evershed outflow and the counter Evershed flow are investigated. Results. In both the normal and the counter Evershed flows, the material flows from regions with field strengths of the order of 1.5-2 kG to regions with stronger fields. The sources and sinks of both penumbral flows display opposite field polarities, with the sinks (tails of filaments) harboring local enhancements in temperature, which are nonetheless colder than their sources (heads of filaments). Conclusions. The anti-correlation of the gradients in the temperature and magnetic pressure between the endpoints of the filaments from the two distinct penumbral regions is compatible with both the convective driver and the siphon flow scenarios. A geometrical scale of the parameters is necessary to determine which is the dominant force driving the flows. **December 08, 2006**

### **Artifacts of SDO/HMI data and long-period oscillations of sunspots**

V. [Smirnova](#)<sup>1,2,3</sup>, V. I. Efremov<sup>2</sup>, L. D. Parfinenko<sup>2</sup>, A. Riehoainen<sup>1</sup> and A. A. Solov'ev

A&A 554, A121 (2013)

Aims. The artifacts of SDO/HMI magnetograms that may affect the low-frequency power spectrum of sunspot oscillations are analyzed.

Methods. Several examples are given that present false (artificial) harmonics, which are produced by Doppler shifts in the power spectra of long-period oscillations of sunspots. This arises from peculiarities in the orbital movements of SDO.

Results. It was found that those artifacts with periods of 12 and 24 h, as revealed even in variations of weak background magnetic fields, are actually present in SDO/HMI magnetograms. However, the quantitative impact of artifacts remains quite weak and does not change the picture of sunspot oscillations dramatically for as long as the magnetic field in the spot is less than about of 2000 Gauss. When the magnetic field strength is greater than 2000 G, the influence of these artifacts increases sharply to become the dominant factor. One can suggest that the amplification of noise components of these artifacts has a highly nonlinear character with the growth of the magnetic field, and the field strength of about 2000 G then takes on meaning of a threshold value.

### **Ti I lines at 2.2 $\mu\text{m}$ as probes of the cool parts of sunspots**

[H. N. Smitha](#), [J. S. Castellanos Durán](#), [S. K. Solanki](#), [S. K. Tiwari](#)

A&A 653, A91 2021

<https://arxiv.org/pdf/2107.01247.pdf>

<https://www.aanda.org/articles/aa/pdf/2021/09/aa41447-21.pdf>

<https://doi.org/10.1051/0004-6361/202141447>

The sunspot umbra harbors the coolest plasma on the solar surface due to the presence of strong magnetic fields. The routinely used atomic lines to observe the photosphere have weak signals in the umbra and are often swamped by molecular lines. This makes it harder to infer the properties of the umbra, especially in the darkest regions. The lines of the Ti I multiplet at 2.2  $\mu\text{m}$  are formed mainly at temperatures  $\leq 4500$  K and are not known to be affected by molecular blends in sunspots. Since the first systematic observations in the 1990's, these lines have been seldom observed due to the instrumental challenges involved at these longer wavelengths. We revisit these lines and investigate their formation in different solar features. We synthesize the Ti I multiplet using a snapshot from 3D MHD simulation of a sunspot and explore the properties of two of its lines in comparison with two commonly used iron lines at 630.25 nm and 1.5648 $\mu\text{m}$ . We find that the Ti I lines have stronger signals than the Fe I lines in both intensity and polarization in the sunspot umbra and in penumbral spines. They have little to no signal in the penumbral filaments and the quiet Sun, at  $\mu=1$ . Their strong and well-split profiles in the dark umbra are less affected by stray light. Consequently, inside the sunspot it is easier to invert these lines and to infer the atmospheric

properties, compared to the iron lines. The Cryo-NIRSP instrument at the DKIST will provide the first ever high resolution observations in this wavelength range. In this preparatory study, we demonstrate the unique temperature and magnetic sensitivities of the Ti multiplet, by probing the Sun's coolest regions which are not favourable for the formation of other commonly used spectral lines. We thus expect such observations to advance our understanding of sunspot properties.

### **Probing photospheric magnetic fields with new spectral line pairs**

H. N. [Smitha](#), [S. K. Solanki](#)

A&A 608, A111 2017

<https://arxiv.org/pdf/1709.08926.pdf>

The magnetic line ratio (MLR) method has been extensively used in the measurement of photospheric magnetic field strength. It was devised for the neutral iron line pair at 5247.1 Å and 5250.2 Å (5250 Å pair). Other line pairs as well-suited as this pair have not been reported in the literature. The aim of the present work is to identify new line pairs useful for the MLR technique and to test their reliability. We use a three dimensional magnetohydrodynamic (MHD) simulation representing the quiet Sun atmosphere to synthesize the Stokes profiles. Then, we apply the MLR technique to the Stokes V profiles to recover the fields in the MHD cube both, at original resolution and after degrading with a point spread function. In both these cases, we aim to empirically represent the field strengths returned by the MLR method in terms of the field strengths in the MHD cube. We have identified two new line pairs that are very well adapted to be used for MLR measurements. The first pair is in the visible, Fe I 6820 Å - 6842 Å (whose intensity profiles have earlier been used to measure stellar magnetic fields), and the other is in the infrared (IR), Fe I 15534 Å - 15542 Å. The lines in these pairs reproduce the magnetic fields in the MHD cube rather well, partially better than the original 5250 Å pair. The newly identified line pairs complement the old pairs. The lines in the new IR pair, due to their higher Zeeman sensitivity, are ideal for the measurement of weak fields. The new visible pair works best above 300 G. The new IR pair, due to its large Stokes V signal samples more fields in the MHD cube than the old IR pair at 1.56µm, even in the presence of noise, and hence likely also on the real Sun. Owing to their low formation heights (100-200 km above  $\tau_{5000}=1$ ), both the new line pairs are well suited for probing magnetic fields in the lower photosphere.

### **Relation between magnetic field inclination and apparent motion of penumbral grains**

Michal [Sobotka](#) (1), [Jan Jurčák](#) (1), [J. Sebastián Castellanos Durán](#) (2), [Marta García-Rivas](#)

A&A 682, A65 2024

<https://arxiv.org/pdf/2311.16820.pdf>

<https://www.aanda.org/articles/aa/pdf/2024/02/aa47979-23.pdf>

Context. Bright heads of penumbral filaments, penumbral grains (PGs), show apparent horizontal motions inwards, towards the umbra, or outwards, away from the umbra.

Aims. We aim to prove statistically whether the direction of PGs' apparent motion is related to the inclination of the surrounding magnetic field.

Methods. We use spectropolarimetric observations of five sunspot penumbrae to compare magnetic inclinations inside PGs with those in their surroundings. The data are taken by three observatories: Hinode satellite, Swedish Solar Telescope, and GREGOR solar telescope. The direction of PGs' motion is determined by feature tracking. The atmospheric conditions in PGs and their surroundings, including the magnetic field information, are retrieved by means of height-stratified spectropolarimetric inversions.

Results. On a sample of 444 inward- and 269 outward-moving PGs we show that 43% of the inward-moving PGs have magnetic inclination larger by  $8^{\circ}\pm 4^{\circ}$  than the inclination in their surroundings and 51% of the outward-moving PGs have the inclination smaller by  $13^{\circ}\pm 7^{\circ}$  than the surrounding one. The opposite relation of inclinations is observed at only one-fifth of the inward- and outward-moving PGs.

Conclusions. Rising hot plasma in PGs surrounded by a less inclined magnetic field may adapt its trajectory to be more vertical, causing an inward apparent motion of PGs. Oppositely, it may be dragged by a more horizontal surrounding magnetic field such that an outward apparent motion is observed.

### **Horizontal motions in sunspot penumbrae**

[Michal Sobotka](#), [Klaus G. Puschmann](#)

A&A 662, A13 2022

<https://arxiv.org/pdf/2205.03171.pdf>

<https://www.aanda.org/articles/aa/pdf/2022/06/aa43577-22.pdf>

High-resolution observations of horizontal motions in the penumbra are needed to complement the concept of penumbrae obtained from spectropolarimetry. Time series of intensity images of a large sunspot in AR 10634 acquired with the Swedish Solar Telescope in the G band and red continuum are analysed. The two simultaneous time series last six hours and five minutes. Horizontal motions of penumbral grains (PGs), structures in dark bodies of filaments, the outer penumbral border, and G-band bright points are measured in time slices that cover the whole width of the penumbra and the neighbouring granulation. The spatial and temporal resolutions are 90 km and 20.1 s,

respectively. In the inner penumbra, PGs move toward the umbra (inwards) with a mean speed of  $-0.7 \text{ km s}^{-1}$ . The direction of motion changes from inwards to outwards at approximately 60% of the penumbral width and the mean speed increases gradually in the outer penumbra, approaching  $0.5 \text{ km/s}$ . This speed is also typical of an expansion of the penumbra-granulation border during periods that typically last one hour and are followed by a fast contraction. The majority of the G-band bright points moves away from the sunspot, with a typical speed of  $0.6 \text{ km/s}$ . High outward speeds,  $3.6 \text{ km/s}$  on average, are observed in dark bodies of penumbral filaments. According to the model of penumbral filaments, it is suggested that the speeds detected in the dark bodies of filaments are associated with the Evershed flow and that the opposite directions of PG motions in the inner and outer penumbrae may be explained by the interaction of rising plasma in filament heads with a surrounding, differently inclined magnetic field. **18 June 2004**

## The Temperature - Magnetic Field Relation in Observed and Simulated Sunspots

Michal [Sobotka](#), [Reza Rezaei](#)

Solar Phys. 292:188 **2017**

<https://arxiv.org/pdf/1711.09821.pdf>

Observations of a relation between continuum intensity and magnetic field strength in sunspots have been made during nearly five decades. This work presents full-Stokes measurements of the full-split ( $g = 3$ ) line Fe I 1564.85 nm with spatial resolution of  $0.5''$  obtained with the GREGOR Infrared Spectrograph in three large sunspots. The continuum intensity is corrected for instrumental scattered light and the brightness temperature is calculated. Magnetic field strength and inclination are derived directly from the line split and the ratio of Stokes components. The continuum intensity (temperature) relations to the field strength are studied separately in the umbra, light bridges, and penumbra. The results are consistent with previous studies and it was found that the scatter of values in the relations increases with increasing spatial resolution thanks to resolved fine structures. The observed relations show trends common for the umbra, light bridges, and the inner penumbra, while the outer penumbra has a weaker magnetic field compared to the inner penumbra at equal continuum intensities. This fact can be interpreted in terms of the interlocking comb magnetic structure of the penumbra. A comparison with data obtained from numerical simulations was made. The simulated data have a generally stronger magnetic field and a weaker continuum intensity than the observations, which may be explained by stray light and limited spatial resolution of the observations and by photometric inaccuracies of the simulations. **11 May 2015**

## Threaded-Field-Lines Model for the Low Solar Corona Powered by the Alfvén Wave Turbulence

Igor V. [Sokolov](#), Bart van der Holst, Ward B. Manchester, Doga Can Su Ozturk, Judit Szente, Aleksandre Taktakishvili, Gabor Tóth, Meng Jin, Tamas I. Gombosi

**2016**

<http://arxiv.org/pdf/1609.04379v1.pdf>

We present an updated global model of the solar corona, including the transition region. We simulate the realistic three-dimensional (3D) magnetic field using the data from the photospheric magnetic field measurements and assume the magnetohydrodynamic (MHD) Alfvén wave turbulence and its non-linear dissipation to be the only source for heating the coronal plasma and driving the solar wind. In closed field regions the dissipation efficiency in a balanced turbulence is enhanced. In the coronal holes we account for a reflection of the outward propagating waves, which is accompanied by generation of weaker counter-propagating waves. The non-linear cascade rate degrades in strongly imbalanced turbulence, thus resulting in colder coronal holes.

The distinctive feature of the presented model is the description of the low corona as almost-steady-state low-beta plasma motion and heat flux transfer along the magnetic field lines. We trace the magnetic field lines through each grid point of the lower boundary of the global corona model, chosen at some heliocentric distance,  $R = R_b \sim (1.03 \div 1.15) R_\odot$  well above the transition region. One can readily solve the plasma parameters along the magnetic field line from 1D equations for the plasma motion and heat transport together with the Alfvén wave propagation, which adequately describe physics within the heliocentric distances range,  $R_\odot < R < R_b$ , in the low solar corona. By interfacing this threaded-field-lines model with the full MHD global corona model at  $r = R_b$ , we find the global solution and achieve a faster-than-real-time performance of the model.

## The Polarimetric and Helioseismic Imager for Solar Orbiter: SO/PHI

Sami K. [Solanki](#), Jose Carlos del Toro Iniesta, Joachim Woch, Achim Gandorfer, Johann Hirzberger, Wolfgang Schmidt, Thierry Appourchaux, Alberto Alvarez-Herrero, for the SO/PHI team

**2015** IAU Symp.

<http://arxiv.org/pdf/1502.03368v1.pdf>

The *Solar Orbiter* is the next solar physics mission of the European Space Agency, ESA, in collaboration with NASA, with a launch planned in 2018. The spacecraft is designed to approach the Sun to within  $0.28 \text{ AU}$  at perihelion of a highly eccentric orbit. The proximity with the Sun will also allow its observation at uniformly high resolution at EUV and visible wavelengths. Such observations are central for learning more about the magnetic

coupling of the solar atmosphere. At a later phase in the mission the spacecraft will leave the ecliptic and study the enigmatic poles of the Sun from a heliographic latitude of up to  $33^\circ$ .

### **The solar magnetic field** **REVIEW ARTICLE**

Sami K. **Solanki**, Bernd Inhester, and Manfred Schüssler

Rep. Prog. Phys. 69 (2006) 563-668, **File**

The magnetic field of the Sun is the underlying cause of the many diverse phenomena combined under the heading of solar activity. Here we describe the magnetic field as it threads its way from the bottom of the convection zone, where it is built up by the solar dynamo, to the solar surface, where it manifests itself in the form of sunspots and faculae, and beyond into the outer solar atmosphere and, finally, into the heliosphere. On the way it, transports energy from the surface and the subsurface layers into the solar corona, where it heats the gas and accelerates the solar wind.

### **Analytical Model of an Asymmetric Sunspot with a Steady Plasma Flow in its Penumbra**

A. A. **Solov'ev**, E. A. Kirichek

Solar Phys. Volume 291, [Issue 6](#), pp 1647-1663 **2016**

A new exact analytical solution to the stationary problem of ideal magnetohydrodynamics is derived for an unipolar asymmetric sunspot immersed in a realistic solar atmosphere. The radial and vertical profiles of pressure, plasma density, and temperature in the visible layers of the sunspot are calculated. The reduction in plasma density in the magnetic funnel of the sunspot, corresponding to the Wilson depression, is also obtained. The magnetic structure of the sunspot is given analytically in a realistic way: a part of the magnetic flux of the sunspot approaches the surrounding photosphere at the outer edge of the penumbra. The magnetic field of the sunspot is not assumed to be axially symmetric. For the first time, the angular dependence of the physical variables in this model allows us to simulate not only a deviation from the circular shape of the sunspot, but also a fine filamentary structure of the sunspot penumbra. The Alfvén Mach number (the ratio of the plasma speed to the Alfvén speed) is zero at the center of the sunspot and rises slowly toward the periphery of the sunspot; this corresponds to the structure of the Evershed flow in the penumbra. The Evershed flow in our model is mainly concentrated in dark penumbral filaments, as is observed.

### **Magnetic Relaxation Seen in a Rapidly Evolving Light Bridge in a Sunspot**

Donguk **Song**<sup>1,2</sup>, Eun-Kyung Lim<sup>1</sup>, Jongchul Chae<sup>3</sup>, Yeon-Han Kim<sup>1</sup>, Yukio Katsukawa<sup>2</sup>, and Vasyl Yurchyshyn<sup>4</sup>

**2024** ApJ 962 75

<https://iopscience.iop.org/article/10.3847/1538-4357/ad1ab0/pdf>

We report a magnetic relaxation process inside a sunspot associated with the evolution of a transient light bridge (LB). From high-resolution imaging and spectro-polarimetric data taken by the 1.6 m Goode Solar Telescope installed at Big Bear Solar Observatory, we observe the evolutionary process of a rapidly evolving LB. The LB is formed as a result of the strong intrusion of filamentary structures with relatively horizontal fields into the vertical umbral field region. A strong current density is detected along a localized region where the magnetic field topology changes rapidly in the sunspot, especially in the boundary region between the LB and the umbra, and bright jets are observed intermittently and repeatedly in the chromosphere along this region through magnetic reconnection. In the second half of our observation, the horizontal component of the magnetic field diminishes within the LB, and the typical convection structure within the sunspot, which manifests itself as umbral dots, is restored. Our findings provide a comprehensive perspective not only on the evolution of an LB itself but also on its impacts in the neighboring regions, including the chromospheric activity and the change of magnetic energy of a sunspot. **2014**

**June 5**

### **Evaluation of Coronal and Interplanetary Magnetic Field Extrapolation Using PSP Solar Wind Observation**

[Yuechun Song](#)

**2023**

<https://arxiv.org/pdf/2305.12124.pdf>

Using solar wind observation near PSP perihelions as constraints, we have investigated the parameters in various PFSS model methods. It's found that the interplanetary magnetic field extrapolation with source surface height  $R_{SS}=2R_s$  is better than that with  $R_{SS}=2.5R_s$ . HMI and GONG magnetograms show similar performance in the simulation of magnetic field variation, but the former appears to have a slight advantage in reconstruction of intensity while the latter is more adaptable to sparser grids. The finite-difference method of constructing eigenvalue problem for potential field can achieve similar accuracy as analytic method and greatly improve the computational

efficiency. MHD modeling performs relatively less well in magnetic field prediction, but it is able to provide rich information about solar-terrestrial space.

### **Three-minute Sunspot Oscillations Driven by Magnetic Reconnection in a Light Bridge**

Donguk [Song](#), [Jongchul Chae](#), [Hannah Kwak](#), [Ryouhei Kano](#), [Vasyl Yurchyshyn](#), [Yong-Jae Moon](#), [Eun-Kyung Lim](#), [Jeongwoo Lee](#)

ApJL **850** L33 **2017**

<https://arxiv.org/pdf/1711.06489.pdf>

We report a different type of three-minute chromospheric oscillations above a sunspot in association with a small-scale impulsive event in a light bridge. During our observations, we found a transient brightening in the light bridge. The brightening was composed of elementary bursts that may be a manifestation of fast repetitive magnetic reconnections in the light bridge. Interestingly, the oscillations in the nearby sunspot umbra were impulsively excited when the intensity of the brightening reached its peak. The initial period of the oscillations was about 2.3 minutes and then gradually increased to 3.0 minutes with time. In addition, we found that the amplitude of the excited oscillations was twice the amplitude of oscillations before the brightening. Based on our results, we propose that magnetic reconnection occurring in a light bridge can excite oscillations in the nearby sunspot umbra.

**November 26, 2014**

### **Chromospheric Plasma Ejections in a Light Bridge of a Sunspot**

Donguk [Song](#), [Jongchul Chae](#), [Vasyl Yurchyshyn](#), [Eun-Kyung Lim](#), [Kyung-Suk Cho](#), [Heesu Yang](#), [Kyuhyoun Cho](#), [Hannah Kwak](#)

ApJ **835** 240 **2017**

<https://arxiv.org/pdf/1701.06808v1.pdf>

It is well-known that light bridges inside a sunspot produce small-scale plasma ejections and transient brightenings in the chromosphere, but the nature and origin of such phenomena are still unclear. Utilizing the high-spatial and high temporal resolution spectral data taken with the Fast Imaging Solar Spectrograph and the TiO 7057 Å broadband filter images installed at the 1.6 meter New Solar Telescope of Big Bear Solar Observatory, we report arcsecond-scale chromospheric plasma ejections (1.7 arc) inside a light bridge. Interestingly, the ejections are found to be a manifestation of upwardly propagating shock waves as evidenced by the sawtooth patterns seen in the temporal-spectral plots of the Ca II 8542 Å and H-alpha intensities. We also found a fine-scale photospheric pattern (1 arc) diverging with a speed of about 2 km/s two minutes before the plasma ejections, which seems to be a manifestation of magnetic flux emergence. As a response to the plasma ejections, the corona displayed small-scale transient brightenings. Based on our findings, we suggest that the shock waves can be excited by the local disturbance caused by magnetic reconnection between the emerging flux inside the light bridge and the adjacent umbral magnetic field. The disturbance generates slow-mode waves, which soon develop into shock waves, and manifest themselves as the arcsecond-scale plasma ejections. It also appears that the dissipation of mechanical energy in the shock waves can heat the local corona. **2014 June 6**

### **DETECTION OF A FINE-SCALE DISCONTINUITY OF PHOTOSPHERIC MAGNETIC FIELDS ASSOCIATED WITH SOLAR CORONAL LOOP BRIGHTENINGS**

Donguk [Song](#)<sup>1</sup>, [Jongchul Chae](#)<sup>1</sup>, [Soyoung Park](#)<sup>1</sup>, [Kyung-Suk Cho](#)<sup>2</sup>, [Eun-Kyung Lim](#)<sup>2</sup>, [Kwangsu Ahn](#)<sup>3</sup>, and [Wenda Cao](#)

**2015** ApJ **810** L16

We present the transient brightening of a coronal loop and an associated fine-scale magnetic discontinuity detected in the photosphere. Utilizing the high-resolution data taken with the Fast Imaging Solar Spectrograph and InfraRed Imaging Magnetograph of the New Solar Telescope at Big Bear Solar Observatory, we detect a narrow lane of intense horizontal magnetic field representing a magnetic discontinuity. It was visible as a dark lane partially encircling a pore in the continuum image, and was located near one of the footpoints of a small coronal loop that experienced transient brightenings. The horizontal field strength gradually increased before the loop brightening, and then rapidly decreased in the impulsive phase of the brightening, suggesting the increase of the magnetic non-potentiality at the loop footpoint and the sudden release of magnetic energy via magnetic reconnection. Our results support the nanoflare theory that coronal heating events are caused by magnetic reconnection events at fine-scale magnetic discontinuities.

### **Effects of non-radial magnetic field on measuring magnetic helicity transport across solar photosphere**

[Yongliang Song](#), [Mei Zhang](#)

It is generally believed that the evolution of magnetic helicity has a close relationship with solar activity. Before the launch of SDO, earlier studies have mostly used MDI/SOHO line of sight magnetograms and assumed that magnetic fields are radial when calculating magnetic helicity injection rate from photospheric magnetograms. However, this assumption is not necessarily true. Here we use the vector magnetograms and line of sight magnetograms, both taken by HMI/SDO, to estimate the effects of non-radial magnetic field on measuring magnetic helicity injection rate. We find that: 1) The effect of non-radial magnetic field on estimating tangential velocity is relatively small; 2) On estimating magnetic helicity injection rate, the effect of non-radial magnetic field is strong when active regions are observed near the limb and is relatively small when active regions are close to disk center; 3) The effect of non-radial magnetic field becomes minor if the amount of accumulated magnetic helicity is the only concern.

## Radio remote sensing of the corona and the solar wind

Steven R. [Spangler](#) and Catherine A. Whiting

Proceedings of the International Astronomical Union / Volume 4 / Symposium S257, pp 529 – 541,

Published online: 16 May 2009

<http://journals.cambridge.org/action/displayIssue?iid=4866212>

Modern radio telescopes are extremely sensitive to plasma on the line of sight from a radio source to the antenna. Plasmas in the corona and solar wind produce measurable changes in the radio wave amplitude and phase, and the phase difference between wave fields of opposite circular polarization. Such measurements can be made of radio waves from spacecraft transmitters and extragalactic radio sources, using radio telescopes and spacecraft tracking antennas. Data have been taken at frequencies from about 80 MHz to 8000 MHz. Lower frequencies probe plasma at greater heliocentric distances. Analysis of these data yields information on the plasma density, density fluctuations, and plasma flow speeds in the corona and solar wind, and on the magnetic field in the solar corona. This paper will concentrate on the information that can be obtained from measurements of Faraday rotation through the corona and inner solar wind. The magnitude of Faraday rotation is proportional to the line of sight integral of the plasma density and the line-of-sight component of the magnetic field. Faraday rotation provides an almost unique means of estimating the magnetic field in this part of space. This technique has contributed to measurement of the large scale coronal magnetic field, the properties of electromagnetic turbulence in the corona, possible detection of electrical currents in the corona, and probing of the internal structure of coronal mass ejections (CMEs). This paper concentrates on the search for small-scale coronal turbulence and remote sensing of the structure of CMEs. Future investigations with the Expanded Very Large Array (EVLA) or Murchison Widefield Array (MWA) could provide unique observational input on the astrophysics of CMEs.

## The first light of the Solar Activity MOF Monitor Telescope (SAMM)

Roberto [Speziali](#)<sup>1\*</sup>, Andrea Di Paola<sup>1</sup>, Mauro Centrone<sup>1</sup>, Maurizio Oliviero<sup>2</sup>, Domenico Bonaccini Calia<sup>3</sup>, Luciano Dal Sasso<sup>4</sup>, Marco Faccini, Vincenzo Mauriello<sup>4</sup> and Luciano Terranegra<sup>2</sup>

J. Space Weather Space Clim. **2021**, 11, 22

<https://doi.org/10.1051/swsc/2020078>

<https://www.swsc-journal.org/articles/swsc/pdf/2021/01/swsc200068.pdf>

SAMM (Solar Activity MOF Monitor) is a ground based robotic instrument that has been developed to study and constantly monitor the magnetic activity of the Sun, focusing on Active Regions (ARs). These regions are characterized by complex magnetic structures that may result in explosive events usually associated with large amount of particle and matter ejections in the space environment. When interacting with the Earth magnetosphere they can represent a threat for our infrastructures both in space (satellites, navigation systems) and on the ground (power plants and electrical grids). Based on Sodium (Na) and Potassium (K) magneto optical filters (MOFs), SAMM provides a “tomographic” view of the magnetic structures delivering high cadence magnetograms and dopplergrams at different heights of the solar atmosphere thus providing a unique dataset with the aim to push forward the current space weather forecasting capabilities. Being able to forecast these events enough in advance (even few hours) is a fundamental task to put in place mitigation strategies to reduce the potential catastrophic impact on vital infrastructures on earth. In this scenario the SAMM observatory has been realized to be a “node” that can be replicated in a world-wide network with the aim to give a continuous coverage of the Sun situation. This project has been initially funded by the Italian Ministry of Economic Development (MiSE) in 2015 through a soft loan grant and its development and operation is carried on within a scientific collaboration between the INAF – Rome and Naples Astronomical Observatories and the Italian small enterprise (SME) Avalon Instruments. After three years of development, SAMM is in the commissioning phase. In this paper we are presenting a final instrument description along with the first light images. **Oct 10th 2019, Jan 27th 2020**

## **Analysis of BMR Tilt from AutoTAB Catalog: Hinting toward the Thin Flux Tube Model?**

Anu [Sreedevi](#)<sup>1</sup>, Bibhuti Kumar Jha<sup>2,3</sup>, Bidya Binay Karak<sup>1</sup>, and Dipankar Banerjee<sup>3,4,5</sup>

2024 ApJ 966 112

<https://iopscience.iop.org/article/10.3847/1538-4357/ad34b8/pdf>

One of the intriguing mechanisms of the Sun is the formation of bipolar magnetic regions (BMRs) in the solar convection zone (CZ), which are observed as regions of concentrated magnetic fields of opposite polarity on the photosphere. These BMRs are tilted with respect to the equatorial line, which statistically increases with latitude. The thin flux tube model, employing the rise of magnetically buoyant flux loops and their twist by Coriolis force, is a popular paradigm for explaining the formation of tilted BMRs. In this study, we assess the validity of the thin flux tube model by analyzing the tracked BMR data obtained through the Automatic Tracking Algorithm for BMRs. Our observations reveal that the tracked BMRs exhibit the expected collective behaviors. We find that the polarity separation of BMRs increases over their normalized lifetime, supporting the assumption of a rising flux tube from the CZ. Moreover, we observe an increasing trend of the tilt with the flux of the BMR, suggesting that rising flux tubes associated with lower flux regions are primarily influenced by drag force and Coriolis force, while in higher flux regions, magnetic buoyancy dominates. Furthermore, we observe Joy's law dependence for emerging BMRs from their first detection, indicating that at least a portion of the tilt observed in BMRs can be attributed to the Coriolis force. Notably, lower flux regions exhibit a higher amount of fluctuations associated with their tilt measurement compared to stronger flux regions, suggesting that lower flux regions are more susceptible to turbulent convection.

[HMI Science Nuggets](#) №201 Aug 2024 <http://hmi.stanford.edu/hminuggets/?p=4253>

## **AutoTAB: Automatic Tracking Algorithm for Bipolar Magnetic Regions**

[Anu Sreedevi](#), [Bibhuti Kumar Jha](#), [Bidya Binay Karak](#), [Dipankar Banerjee](#)

ApJS 268 58 2023

<https://arxiv.org/pdf/2304.06615.pdf>

<https://iopscience.iop.org/article/10.3847/1538-4365/acec47/pdf>

Bipolar Magnetic Regions (BMRs) provide crucial information about solar magnetism. They exhibit varying morphology and magnetic properties throughout their lifetime, and studying these properties can provide valuable insights into the workings of the solar dynamo. The majority of previous studies have counted every detected BMR as a new one and have not been able to study the full life history of each BMRs. To address this issue, we have developed an Automatic Tracking Algorithm (AutoTAB) for BMRs, that tracks the BMRs for their entire lifetime or throughout their disk passage. AutoTAB uses the binary maps of detected BMRs to automatically track the regions. This is done by differentially rotating the binary maps of the detected regions and checking for overlaps between them. In this first article of this project, we provide a detailed description of the working of the algorithm and evaluate its strengths and weaknesses. We also compare its performance with other existing tracking techniques. AutoTAB excels in tracking even for the small features and it successfully tracks 9152 BMRs over the last two solar cycles (1996-2020), providing a comprehensive dataset that depicts the evolution of various properties for each tracked region. The tracked BMRs follow familiar properties of solar cycles except for these small BMRs that appear at all phases of the solar cycle and show weak latitudinal dependency, which is represented through the butterfly diagram. Finally, we discuss the possibility of adapting our algorithm to other datasets and expanding the technique to track other solar features in the future. 15-11-2000, 3-11 Jan 2008, 3-7 Feb 2008, 17-19 Jun 2008

## **Inference of Magnetic Field in the Coronal Streamer Invoking Kink Wave Motions generated by Multiple EUV Waves**

A.K. [Srivastava](#), Talwinder Singh, Leon Ofman, B.N. Dwivedi

Mon. Not. R. Astron. Soc. 2016 File

<http://arxiv.org/pdf/1606.00337v1.pdf>

Using MHD seismology by observed kink waves, the magnetic field profile of a coronal streamer has been investigated. STEREO-B/EUVI temporal image data on 7 March 2012 shows an evolution of two consecutive EUV waves that interact with the footpoint of a coronal streamer evident in the co-spatial and co-temporal STEREO-B/COR-I observations. The evolution of EUV waves is clearly evident in STEREO-B/EUVI, and its energy exchange with coronal streamer generates kink oscillations. We estimate the phase velocities of the kink wave perturbations by tracking it at different heights of the coronal streamer. We also estimate the electron densities inside and outside the streamer using SSI of polarized brightness images in STEREO-B/COR-I observations. Taking into account the MHD theory of kink waves in a cylindrical waveguide, their observed properties at various heights, and density contrast of the streamer, we estimate the radial profile of magnetic field within this magnetic structure. Both the kink waves diagnose the exponentially decaying radial profiles of the magnetic field in coronal streamer upto 3 solar radii. Within the limit of uncertainties in the measurements, it is indicated that coronal magnetic field of the streamer varies slowly in time at various heights, although its nature always remains exponentially



decaying. It is seen that during the evolution of second kink motion in the streamer, it increases in brightness, and also in areal extent slightly, which may be associated with the decreased photospheric magnetic flux at its footpoint. As a result, the magnetic field profile produced by the second kink wave is reduced within the streamer compared to the one diagnosed by the first one. The precisely estimated magnetic field profiles with the uncertainty less than 10% match well with the empirical profile and various observational estimations of the outer coronal magnetic field.

### **On Thermal-Pulse-Driven Plasma Flows in Coronal Funnels as Observed by Hinode/EUV Imaging Spectrometer (EIS)**

A.K. [Srivastava](#), P. Konkol, K. Murawski, B.N. Dwivedi, A. Mohan  
Solar Phys., 2014

<http://arxiv.org/pdf/1407.7124v1.pdf>

Using one-arcsecond-slit scan observations from the Hinode/EUV Imaging Spectrometer (EIS) on **05 February 2007**, we find the plasma outflows in the open and expanding coronal funnels at the eastern boundary of AR 10940. The Doppler velocity map of Fe XII 195.120 Å shows that the diffuse close-loop system to be mostly red-shifted. The open arches (funnels) at the eastern boundary of AR exhibit blue-shifts with a maximum speed of about 10-15 km/s. This implies outflowing plasma through these magnetic structures. In support of these observations, we perform a 2D numerical simulation of the expanding coronal funnels by solving the set of ideal MHD equations in appropriate VAL-III C initial temperature conditions using the FLASH code. We implement a rarefied and hotter region at the footpoint of the model funnel, which results in the evolution of slow plasma perturbations propagating outward in the form of plasma flows. We conclude that the heating, which may result from magnetic reconnection, can trigger the observed plasma outflows in such coronal funnels. This can transport mass into the higher corona, giving rise to the formation of the nascent solar wind.

### **Torsional oscillations within a magnetic pore in the solar photosphere**

[Marco Stangalini](#), [Robertus Erdélyi](#), [Callum Boocock](#), [David Tsiklauri](#), ++

[Nature Astronomy](#) volume 5, pages691–696 (2021)[Cite this article](#)

<https://www.nature.com/articles/s41550-021-01354-8.pdf>

Alfvén waves have proven to be important in a range of physical systems due to their ability to transport non-thermal energy over long distances in a magnetized plasma. This property is of specific interest in solar physics, where the extreme heating of the atmosphere of the Sun remains unexplained. In an inhomogeneous plasma such as a flux tube in the solar atmosphere, they manifest as incompressible torsional perturbations. However, despite evidence in the upper atmosphere, they have not been directly observed in the photosphere. Here, we report the detection of antiphase incompressible torsional oscillations observed in a magnetic pore in the photosphere by the Interferometric Bidimensional Spectropolarimeter. State-of-the-art numerical simulations suggest that a kink mode is a possible excitation mechanism of these waves. The excitation of torsional waves in photospheric magnetic structures can substantially contribute to the energy transport in the solar atmosphere and the acceleration of the solar wind, especially if such signatures will be ubiquitously detected in even smaller structures with the forthcoming next generation of solar telescopes.

### **A novel approach to identify resonant MHD wave modes in solar pores and sunspot umbrae: B– $\omega$ analysis**

[M. Stangalini](#), [D. B. Jess](#), [G. Verth](#), [V. Fedun](#), [B. Fleck](#), [S. Jafarzadeh](#), [P. H. Keys](#), [M. Murabito](#), [D. Calchetti](#), [A. A. Aldhafeeri](#), [F. Berrilli](#), [D. Del Moro](#), [S. M. Jefferies](#), [J. Terradas](#), [R. Soler](#)

A&A 2021

<https://arxiv.org/pdf/2103.11639.pdf>

The umbral regions of sunspots and pores in the solar photosphere are generally dominated by 3~mHz oscillations, which are due to p-modes penetrating the magnetic region. In these locations, wave power is also significantly reduced with respect to the quiet Sun. However, here we study a pore where the power of the oscillations in the umbra is not only comparable, or even larger than that of the quiet Sun, but the main dominant frequency is not 3~mHz as expected, but instead 5~mHz. By combining Doppler velocities and spectropolarimetry and analysing the relationship between magnetic field strength and frequency, the resultant B– $\omega$  diagram reveals distinct ridges which are remarkably clear signatures of resonant MHD oscillations confined within the pore umbra. In addition to velocity oscillations, we demonstrate that these modes are also accompanied by magnetic oscillations, as predicted from MHD theory. The novel technique of B– $\omega$  analysis, proposed in this Letter, opens an exciting new avenue for identifying MHD wave modes in the umbral regions of both pores and sunspots. **2008 October 15**

### **Spectropolarimetric Fluctuations in a Sunspot Chromosphere**

[M. Stangalini](#), [D. Baker](#), [G. Valori](#), [D.B. Jess](#), [S. Jafarzadeh](#), [M. Murabito](#), [A.S.H. To](#), [D.H. Brooks](#), [I. Ermolli](#), [F. Giorgi](#), [C.D. MacBride](#)

<https://arxiv.org/pdf/2009.05302.pdf>

The instrumental advances made in this new era of 4-meter class solar telescopes with unmatched spectropolarimetric accuracy and sensitivity, will enable the study of chromospheric magnetic fields and their dynamics with unprecedented detail. In this regard, spectropolarimetric diagnostics can provide invaluable insight into magneto-hydrodynamic (MHD) wave processes. MHD waves and, in particular, Alfvénic fluctuations associated to particular wave modes, were recently recognized as important mechanisms not only for the heating of the outer layers of the Sun's atmosphere and the acceleration of the solar wind, but also for the elemental abundance anomaly observed in the corona of the Sun and other Sun-like stars (also known as first ionisation potential; FIP) effect. Here, we take advantage of state-of-the-art and unique spectropolarimetric IBIS observations to investigate the relation between intensity and circular polarisation (CP) fluctuations in a sunspot chromosphere. Our results show a clear link between the intensity and CP fluctuations in a patch which corresponds to a narrow range of magnetic field inclinations. This suggests the presence of Alfvénic perturbations in the sunspot. **2016-05-20**

### Propagating Spectropolarimetric Disturbances in a Large Sunspot

M. [Stangalini](#), [S. Jafarzadeh](#), [I. Ermolli](#), [R. Erdélyi](#), [D. B. Jess](#), [P. H. Keys](#), [F. Giorgi](#), [M. Murabito](#), [F. Berrilli](#), [D. Del Moro](#)

ApJ 869 110 2018

<https://arxiv.org/pdf/1810.12595.pdf>

[sci-hub.tw/10.3847/1538-4357/aaec7b](http://sci-hub.tw/10.3847/1538-4357/aaec7b)

We present results derived from the analysis of spectropolarimetric measurements of active region AR12546, which represents one of the largest sunspots to have emerged onto the solar surface over the last 20 years. The region was observed with full-Stokes scans of the Fe I 617.3 nm and Ca II 854.2 nm lines with the Interferometric Bidimensional Spectrometer (IBIS) instrument at the Dunn Solar Telescope over an uncommon, extremely long time interval exceeding three hours. Clear circular polarization (CP) oscillations localized at the umbra-penumбра boundary of the observed region were detected. Furthermore, the multi-height data allowed us to detect the downward propagation of both CP and intensity disturbances at 2.5–3-mHz, which was identified by a phase delay between these two quantities. These results are interpreted as a propagating magneto-hydrodynamic surface mode in the observed sunspot. **May 20th 2016**

### Polarised kink waves in magnetic elements: evidence for chromospheric helical waves

Marco [Stangalini](#), Fabio Giannattasio, Robertus Erdélyi, Shahin Jafarzadeh, Giuseppe Consolini, Serena Criscuoli, Ilaria Ermolli, Salvo Luigi Guglielmino, Francesca Zuccarello

ApJ 840 19 2017

<https://arxiv.org/pdf/1704.02155.pdf>

In recent years, new high spatial resolution observations of the Sun's atmosphere have revealed the presence of a plethora of small-scale magnetic elements down to the resolution limit of current cohort of solar telescopes (~100–120 km on the solar photosphere). These small magnetic field concentrations, due to the granular buffeting, can support and guide several magneto-hydrodynamics (MHD) wave modes that would eventually contribute to the energy budget of the upper layers of the atmosphere. In this work, exploiting the high spatial and temporal resolution chromospheric data acquired with the Swedish 1-meter Solar Telescope (SST), and applying the empirical mode decomposition (EMD) technique to the tracking of the solar magnetic features, we analyse the perturbations of the horizontal velocity vector of a set of chromospheric magnetic elements. We find observational evidence that suggests a phase relation between the two components of the velocity vector itself, resulting in its helical motion.

### Observational evidence for buffeting induced kink waves in solar magnetic elements

M. [Stangalini](#), G. Consolini, F. Berrilli, P. De Michelis, R. Tozzi

A&A, 2014

<http://arxiv.org/pdf/1408.3987v1.pdf>

The role of diffuse photospheric magnetic elements in the energy budget of the upper layers of the Sun's atmosphere has been the recent subject of many studies. This was made possible by the availability of high temporal and spatial resolution observations of the solar photosphere, allowing large numbers of magnetic elements to be tracked to study their dynamics. In this work we exploit a long temporal series of seeing-free magnetograms of the solar photosphere to study the effect of the turbulent convection in the excitation of kink oscillations in magnetic elements. We make use of the empirical mode decomposition technique (EMD) in order to study the transverse oscillations of several magnetic flux tubes. This technique permits the analysis of non-stationary time series like those associated to the horizontal velocities of these flux tubes which are continuously advected and dispersed by granular flows.

Our primary findings reveal the excitation of low frequency modes of kink oscillations, which are sub-harmonics of a fundamental mode with a  $7.6 \pm 0.2$  minute periodicity. These results constitute a strong case for

observational proof of the excitation of kink waves by the buffeting of the convection cells in the solar photosphere, and are discussed in light of their possible role in the energy budget of the upper Sun's atmosphere.

## **Test Problems for Potential Field Source Surface Extrapolations of Solar and Stellar Magnetic Fields**

[David Stansby](#), [Daniel Verscharen](#)

ApJ 2022

<https://arxiv.org/pdf/2201.07783.pdf>

The potential field source surface (PFSS) equations are commonly used to model the coronal magnetic field of the Sun and other stars. As with any computational model, solving equations using a numerical scheme introduces errors due to discretisation. We present a set of tests for quantifying these errors by taking advantage of analytic solutions to the PFSS equations when the input field is proportional to a single spherical harmonic. From the spherical harmonic solutions we derive analytic equations for magnetic field lines traced through the three dimensional magnetic field solution. We propose these as a set of standard analytic solutions that all PFSS solvers should be tested against to quantify their inherent errors. We apply these tests to the pfsspy software package, showing that it reproduces spherical harmonic solutions well with a slight overestimation of the unsigned open magnetic flux. It is also successful at reproducing analytic field line equations, with errors in field line footpoints typically much less than one degree.

## **Detection of Travel Time Anisotropy from Subsurface Horizontal Magnetic Fields**

[John T. Stefan](#), [Alexander G. Kosovichev](#)

ApJ 2022

<https://arxiv.org/pdf/2203.03495.pdf>

A time-distance measurement technique is derived to isolate phase travel time anisotropy caused by subsurface horizontal magnetic fields, and a method which uses the measured anisotropy to estimate the field's orientation is also derived. A simulation of acoustic waves propagating in a uniform, inclined magnetic field with solar background structure is used to verify the derived technique. Then, the procedure is applied to a numerical simulation of a sunspot, for which the subsurface state is known, to provide context for the results obtained from the study of several sunspots observed by the Helioseismic and Magnetic Imager. Significant anisotropies are detected, on the order of one minute, and the subsurface field's azimuth is estimated and compared with the azimuth of the surface magnetic field. In all cases, the subsurface azimuth is found to be well-aligned with that of the surface, and the results from the numerical simulation are used to interpret features in the detected travel time anisotropy.

## **Subsurface Structure of Pores and Sunspots**

Robert [Stein](#).

HMI Science Nugget #38, May 2015

<http://hmi.stanford.edu/hminuggets/?p=1166>

## **ON THE FORMATION OF ACTIVE REGIONS**

Robert F. [Stein](#)<sup>1</sup> and Åke Nordlund

2012 ApJ 753 L13

Magnetoconvection can produce an active region without an initial coherent flux tube. A simulation was performed where a uniform, untwisted, horizontal magnetic field of 1 kG strength was advected into the bottom of a computational domain 48 Mm wide by 20 Mm deep. The up and down convective motions produce a hierarchy of magnetic loops with a wide range of scales, with smaller loops riding "piggy-back" in a serpentine fashion on larger loops. When a large loop approaches the surface, it produces a small active region with a compact leading spot and more diffuse following spots.

## **PSP/WISPR Observations of Dust Density Depletion near the Sun. II. New Insights from within the Depletion Zone**

Guillermo [Stenborg](#)<sup>1</sup>, Russell A. Howard<sup>1</sup>, Angelos Vourlidas<sup>1</sup>, and Brendan Gallagher<sup>2</sup>

2022 ApJ 932 75

<https://iopscience.iop.org/article/10.3847/1538-4357/ac6b36/pdf>

Visible light observations from the Wide-field Imager for Solar PRobe (WISPR) aboard the Parker Solar Probe (PSP) mission offer a unique opportunity to study the dust environment near the Sun. The existence of a dust-free zone (DFZ) around stars was postulated almost a century ago. Despite numerous attempts to detect it from as close as 0.3 au, observational evidence of a circumsolar DFZ has remained elusive. Analysis of WISPR images obtained from heliocentric distances between 13.3–53.7  $R_{\odot}$  over multiple PSP orbits shows a gradually decreasing brightness gradient along the symmetry axis of the F-corona for coronal heights between 19 and 9  $R_{\odot}$ . Below 9  $R_{\odot}$ , the gradient reverses its trend, approaching the radial dependence exhibited at heights above 19  $R_{\odot}$ . After

taking into account the effects of both the electron corona background and the nonresolved starlight, the WISPR observations down to  $4 R_{\odot}$  are consistent with forward-modeling simulations of the F-corona brightness within  $[-6, 5]\%$  if a circumsolar region of depleted dust density between  $19$  and  $5 R_{\odot}$  enclosing a DFZ is considered. In addition, we show, for the first time, that the F-corona brightness inward of about  $15 R_{\odot}$  depends on the observer's location for observing distances below  $35 R_{\odot}$ . 20 Nov 2021

## History of Solar Magnetic Fields since George Ellery Hale

**Review**

Jan **Stenflo**

Space Science Reviews September 2017, Volume 210, [Issue 1–4](#), pp 5–35

<http://arxiv.org/pdf/1508.03312v1.pdf>

As my own work on the Sun's magnetic field started exactly 50 years ago at Crimea in the USSR, I have been a participant in the field during nearly half the time span since Hale's discovery in 1908 of magnetic fields in sunspots. The present historical account is accompanied by photos from my personal slide collection, which show a number of the leading personalities who advanced the field in different areas: measurement techniques, from photographic to photoelectric and imaging methods in spectro-polarimetry; theoretical foundations of MHD and the origin of cosmic magnetic fields (birth of dynamo theory); the quest for increased angular resolution from national projects to international consortia (for instruments both on ground and in space); introduction of the Hanle effect in astrophysics and the Second Solar Spectrum as its playground; small-scale nature of the field, the fundamental resolution limit, and transcending it by resolution-independent diagnostics.

## The Hanle and Zeeman polarization signals of the solar Ca II 8542 Å line

Jiří **Štěpán**, Javier Trujillo Bueno

ApJL *ApJ* **826** L10 2016

<http://arxiv.org/pdf/1606.07741v1.pdf>

We highlight the main results of a three-dimensional (3D) multilevel radiative transfer investigation about the solar disk-center polarization of the Ca II 8542 Å line. First, we investigate the linear polarization due to the atomic level polarization produced by the absorption and scattering of anisotropic radiation in a 3D model of the solar atmosphere, taking into account the symmetry breaking effects caused by its thermal, dynamic and magnetic structure. Second, we study the contribution of the Zeeman effect to the linear and circular polarization. Finally, we show examples of the Stokes profiles produced by the joint action of atomic level polarization and the Hanle and Zeeman effects. We find that the Zeeman effect tends to dominate the linear polarization signals only in the localized patches of opposite magnetic polarity where the magnetic field is relatively strong and slightly inclined, while outside such very localized patches the linear polarization is often dominated by the contribution of atomic level polarization. We demonstrate that a correct modeling of this last contribution requires taking into account the symmetry breaking effects caused by the thermal, dynamic and magnetic structure of the solar atmosphere, and that in the 3D model used the Hanle effect in forward-scattering geometry (disk center observation) mainly reduces the polarization corresponding to the zero-field case. We emphasize that, in general, a reliable modeling of the linear polarization in the Ca II 8542 Å line requires taking into account the joint action of atomic level polarization and the Hanle and Zeeman effects.

## Coronal seismology

**Stepanov**, Alexander V.; Zaitsev, Valerii V.; Nakariakov, Valery M.

Physics Uspekhi, Volume 55, Issue 9, pp. A04 (2012).

## On the diagnostics of solar small scale magnetic fields

M.I. **Stodilka**

Advances in Space Research, Volume 55, Issue 3, 1 February 2015, Pages 891–896

<http://www.sciencedirect.com/science/article/pii/S0273117714005006>

The model of small scale magnetic fields was proposed. The fields are described by two distribution functions: for unsigned magnetic field and for field vectors directions. The distribution functions were used to derive expressions for elements of the line absorption matrix and to deduce function that characterizes mutual cancellation of magnetic fields. We received the solutions for polarized radiative transfer problem within 3D MHD model of the solar photosphere and determined Stokes profiles parameters for two magnetosensitive lines Fe I  $\lambda\lambda 525.0$  nm and  $\lambda\lambda 524.7$  nm. The Stokes profiles parameters of the lines were used for further test diagnostics of small scale magnetic fields. A regression approach to diagnostics of the magnetic fields was proposed. The correlation between theoretical and reproduced parameters of small scale magnetic fields is greater than 0.95.

## **A Steady-state Supersonic Downflow in the Transition Region above a Sunspot Umbra**

Thomas **Straus**, Bernhard Fleck, Vincenzo Andretta

A&A **582, A116 2015**

<http://arxiv.org/pdf/1507.04279v1.pdf>

We investigate a small-scale ( $\approx 1.5$  Mm along the slit), supersonic downflow of about  $90 \text{ km s}^{-1}$  in the transition region above the light-bridged sunspot umbra in AR 11836. The observations were obtained with the Interface Region Spectrograph (IRIS) on 2013 September 2, from 16:40 to 17:59 UT. The downflow shows up as red-shifted "satellite" lines of the Si IV and O IV transition region lines and is remarkably steady over the observing period of nearly 80 min. The downflow is not visible in the chromospheric lines, which only show an intensity enhancement at the location of the downflow. The density inferred from the line ratio of the red-shifted satellites of the O IV lines ( $N_e = 1010.6 \pm 0.25 \text{ cm}^{-3}$ ) is only a factor 2 smaller than the one inferred from the main components ( $N_e = 1010.95 \pm 0.20 \text{ cm}^{-3}$ ). Consequently, this implies a substantial mass flux ( $\approx 5 \times 10^{-7} \text{ g cm}^{-2} \text{ s}^{-1}$ ), which would evacuate the overlying corona on time scales of the order of 10 s. We interpret these findings as evidence of a stationary termination shock of a supersonic siphon flow in a cool loop rooted in the central umbra of the spot.

## **Evolution of the flow field in decaying active regions II. Converging flows at the periphery of naked spots**

[Hanna Strecker](#), [Nazaret Bello González](#)

A&A **2022**

<https://arxiv.org/pdf/2208.14272.pdf>

In a previous work, we investigated the evolution of the flow field around sunspots during sunspot decay and compared it with the flow field of supergranular cells. The decay of a sunspot proceeds as it interacts with its surroundings. This is manifested by the changes observed in the flow field surrounding the decaying spot. We now investigate in detail the evolution of the flow field in the direct periphery of the sunspots of the same sample and aim to provide a complete picture of the role of large-scale flows present in sunspot cells. We analyse the horizontal velocity profiles of sunspots obtained from observations by the Helioseismic and Magnetic Imager (HMI) on board the Solar Dynamics Observatory (SDO). We follow their evolution across the solar disc from their stable phase to their decay and their final disappearance. We find two different scenarios for the evolution of the flow region surrounding a spot in the final stage of its decay: (i) either the flow cell implodes and disappears under the action of the surrounding supergranules or (ii) it outlives the spot. In the later case, an inwards flow towards the remaining naked spot develops in the vicinity closest to the spot followed by an outflow further out. These findings provide observational evidence to theoretical predictions by realistic magnetohydrodynamic (MHD) sunspot and moat region simulations. The Evershed flow and the moat flow, both connected to the presence of fully fledged sunspots in a spot cell, vanish when penumbrae decay. Moat flows decline into supergranular flows. The final fate of a spot cell depends on its interaction with the surrounding supergranular cells. In the case of non-imploding spot cells, the remaining naked spot develops a converging inflow driven by radiative cooling and a geometrical alignment of granules in its periphery which is similar to that observed in pores. **13 Sep 2013**

## **On the (in)stability of sunspots**

[Hanna Strecker](#), [Wolfgang Schmidt](#), [Rolf Schlichenmaier](#), [Matthias Rempel](#)

A&A **649, A123 2021**

<https://arxiv.org/pdf/2103.11487.pdf>

<https://www.aanda.org/articles/aa/pdf/2021/05/aa40199-20.pdf>

<https://doi.org/10.1051/0004-6361/202040199>

The stability of sunspots is one of the long-standing unsolved puzzles in the field of solar magnetism. We study the effects that destabilise and stabilise the flux tube of a simulated sunspot in the upper convection zone. The depth-varying effects of fluting instability, buoyancy forces, and timescales on the flux tube are analysed. The simulation was calculated with the MURaM code. The domain has a lateral extension of  $98 \text{ Mm} \times 98 \text{ Mm}$  and extends almost  $18 \text{ Mm}$  below the solar surface. The analysed data set of 30 hours shows a stable sunspot at the solar surface. We studied the evolution of the flux tube at horizontal layers by means of the relative change in perimeter and area with a linear stability analysis. We find a corrugation along the perimeter of the flux tube that proceeds fastest at a depth of about  $8 \text{ Mm}$  below the surface. Towards the surface and towards deeper layers, the decrease in compactness is damped. From the stability analysis, we find that above a depth of  $2 \text{ Mm}$ , the sunspot is stabilised by buoyancy forces. The spot is least stable at a depth of about  $3 \text{ Mm}$  because of fluting instability. The stability of the sunspot at the surface affects the behaviour of the field lines in deeper layers by magnetic tension. Therefore the fluting instability is damped at depths of about  $3 \text{ Mm}$ , and the decrease in compactness is strongest at a depth of about  $8 \text{ Mm}$ . The more vertical orientation of the magnetic field and the longer convective timescale slow down the corrugation process in layers deeper than  $10 \text{ Mm}$ . The formation of large intrusions of field-free plasma below the surface destabilises the sunspot, and eventually lead to the disruption and decay of the sunspot. This process is not visible at the surface, where the sunspot is stabilised by buoyancy forces. The onset of sunspot decay occurs in deeper layers, while the sunspot still appears stable in the photosphere.

## Evolution of the flow field in decaying active regions, Transition from a moat flow to a supergranular flow

Hanna [Strecker](#), [Nazaret Bello González](#)

A&A 620, A122 2018

<https://arxiv.org/pdf/1811.01607.pdf>

We investigate the evolution of the horizontal flow field around sunspots during their decay by analysing its extension and horizontal velocity around eight spots using SDO/HMI Doppler maps. By assuming a radially symmetrical flow field, the applied analysis method determines the radial dependence of the azimuthally averaged flow field. For comparison, we studied the flow in supergranules using the same technique. All investigated, fully fledged sunspots are surrounded by a flow field whose horizontal velocity profile decreases continuously from 881  $\text{m s}^{-1}$  at 1.1 Mm off the spot boundary, down to 199  $\text{m s}^{-1}$  at a mean distance of 11.9 Mm to that boundary. Once the penumbra is fully dissolved, however, the velocity profile of the flow changes: The horizontal velocity increases with increasing distance to the spot boundary until a maximum value of about 398  $\text{m s}^{-1}$  is reached. Then, the horizontal velocity decreases for farther distances to the spot boundary. In supergranules, the horizontal velocity increases with increasing distance to their centre up to a mean maximum velocity of 355  $\text{m s}^{-1}$ . For larger distances, the horizontal velocity decreases. We thus find that the velocity profile of naked sunspots resembles that of supergranular flows. The evolution of the flow field around individual sunspots is influenced by the way the sunspot decays and by the interplay with the surrounding flow areas. Observations of the flow around eight decaying sunspots suggest that as long as penumbrae are present, sunspots with their moat cell are embedded in network cells. The disappearance of the penumbra (and consequently the moat flow) and the competing surrounding supergranular cells, both have a significant role in the evolution of the flow field: The moat cell transforms into a supergranule, which hosts the remaining naked spot. **2 January 2013**

## Analysis methods of the flow field around decaying sunspots

Hanna [Strecker](#), [Nazaret Bello González](#)

in "Solar Polarization Workshop 8", ASP Proceedings 2018

<https://arxiv.org/pdf/1811.01621.pdf>

The moat flow, a radial outflow surrounding fully fledged sunspots, is a well characterised phenomenon. Nevertheless, its origin and especially its relation to the penumbra is still a controversial topic. We investigate the evolution of the horizontal velocity of the flow around sunspots over several days during sunspot decay. SDO/HMI Doppler maps, which allow for the continuous observation of an active regions, are used. We describe the analysis method used to retrieve the horizontal velocity of the flow field for different positions on the solar disc. For that purpose, several large and small scale flow patterns, like, e.g., differential rotation, the centre-to-limb variation in the convective blueshift and a residual pattern caused by instrumental effects, have to be taken into account in order to properly measure the horizontal velocity of the flow field surrounding the sunspots. We find that the flow field around sunspots with fully developed penumbra has a decreasing velocity profile with increasing distances to the sunspot, as already found by other authors. Most important, the velocity amplitude decreases and the profile changes as the penumbra dissolves and the sunspots decay. Our findings confirm the related disappearance of the moat flow with penumbra. Yet, we observe a remnant outflow after the penumbra disappears, which hints towards the possible overtaken of the moat flow by a supergranular flow in decaying sunspots.

## Sunspot rotation. II. Effects of varying the field strength and twist of an emerging flux tube

Z. [Sturrock](#), A. W. Hood

A&A 593, A63 2016

<http://arxiv.org/pdf/1605.07378v1.pdf>

Context. Observations of flux emergence indicate that rotational velocities may develop within sunspots. However, the dependence of this rotation on sub-photospheric field strength and twist remains largely unknown.

Aims. We investigate the effects of varying the initial field strength and twist of an emerging sub-photospheric magnetic flux tube on the rotation of the sunspots at the photosphere.

Methods. We consider a simple model of a stratified domain with a sub-photospheric interior layer and three overlying atmospheric layers. A twisted arched flux tube is inserted in the interior and is allowed to rise into the atmosphere. To achieve this, the MHD equations are solved using the Lagrangian-remap code, Lare3d. We perform a parameter study by independently varying the sub-photospheric magnetic field strength and twist.

Results. Altering the initial field strength and twist significantly affects the tube's evolution and the rotational motions that develop at the photosphere. The rotation angle, vorticity, and current show a direct dependence on the initial field strength. We find that an increase in field strength increases the angle through which the fieldlines rotate, the length of fieldlines extending into the atmosphere, and the magnetic energy transported to the atmosphere. This also affects the amount of residual twist in the interior. The length of the fieldlines is crucial as we predict the twist per unit length equilibrates to a lower value on longer fieldlines. No such direct dependence is found when we modify the twist owing to the complex effect this has on the tension force acting on the tube. However, there is still

a clear ordering in quantities such as the rotation angle, helicity, and free energy with higher initial twist cases being related to sunspots that rotate more rapidly, transporting more helicity and magnetic energy to the atmosphere.

### **Sunspot rotation. I. A consequence of flux emergence**

Z. [Sturrock](#), A. W. Hood, [V. Archontis](#), [C. M. McNeill](#)

A&A 582, A76 2015

<http://arxiv.org/pdf/1508.02437v1.pdf>

Context. Solar eruptions and high flare activity often accompany the rapid rotation of sunspots. The study of sunspot rotation and the mechanisms driving this motion are therefore key to our understanding of how the solar atmosphere attains the conditions necessary for large energy release.

Aims. We aim to demonstrate and investigate the rotation of sunspots in a 3D numerical experiment of the emergence of a magnetic flux tube as it rises through the solar interior and emerges into the atmosphere.

Furthermore, we seek to show that the sub-photospheric twist stored in the interior is injected into the solar atmosphere by means of a definitive rotation of the sunspots.

Methods. A numerical experiment is performed to solve the 3D resistive magnetohydrodynamic (MHD) equations using a Lagrangian-Remap code. We track the emergence of a toroidal flux tube as it rises through the solar interior and emerges into the atmosphere investigating various quantities related to both the magnetic field and plasma.

Results. Through detailed analysis of the numerical experiment, we find clear evidence that the photospheric footprints or sunspots of the flux tube undergo a rotation. Significant vertical vortical motions are found to develop within the two polarity sources after the field emerges. These rotational motions are found to leave the interior portion of the field untwisted and twist up the atmospheric portion of the field. This is shown by our analysis of the relative magnetic helicity as a significant portion of the interior helicity is transported to the atmosphere. In addition, there is a substantial transport of magnetic energy to the atmosphere. Rotation angles are also calculated by tracing selected fieldlines; the fieldlines threading through the sunspot are found to rotate through angles of up to 353 degrees over the course of the experiment.

### **OBSERVATIONS OF OPPOSITELY DIRECTED UMBRAL WAVEFRONTS ROTATING IN SUNSPOTS OBTAINED FROM THE NEW SOLAR TELESCOPE OF BBSO**

J. T. [Su](#)<sup>1</sup>, K. F. [Ji](#)<sup>2</sup>, W. [Cao](#)<sup>3</sup>, D. [Banerjee](#)<sup>4</sup>, T. G. [Priya](#)<sup>1</sup>, J. S. [Zhao](#)<sup>5</sup>, X. Y. [Bai](#)<sup>1</sup>, J. [Chen](#)<sup>1</sup>, M. [Zhang](#)<sup>1</sup>, and H. S. [Ji](#)

2016 ApJ 817 117

We study the umbral waves as observed by chromospheric imaging observations of two sunspots with the New Solar Telescope at the Big Bear Solar Observatory. We find that the wavefronts (WFs) rotate clockwise and form a one-armed spiral structure in the first sunspot, whereas two- and three-armed structures arise in the second sunspot where the WFs rotate anticlockwise and clockwise alternately. All the spiral arms display propagation outwards and become running penumbral waves once they cross the umbral boundaries, suggesting that the umbral and penumbral waves propagate along the same inclined field lines. We propose that the one-armed spiral structure may be produced by the WF reflections at the chromospheric umbral light bridge, and the multi-armed spirals may be related to the twist of the magnetic field in the umbra. Additionally, the time lag of the umbral oscillations in between the data of He I 10830 Å and Å is ~17 s, and it is ~60 s for that in between the data of 304 Å and Å. This indicates that these disturbances are slow magnetoacoustic waves in nature, and that they propagate upward along the inclined lines with fast radial expansions causing horizontal velocities of the running waves.

### **INTERFERENCE OF THE RUNNING WAVES AT LIGHT BRIDGES OF A SUNSPOT**

J. T. [Su](#)<sup>1</sup>, K. F. [Ji](#)<sup>2</sup>, D. [Banerjee](#)<sup>3</sup>, W. D. [Cao](#)<sup>4</sup>, T. G. [Priya](#)<sup>1</sup>, J. S. [Zhao](#)<sup>5</sup>, S. J. [Yu](#)<sup>1</sup>, H. S. [Ji](#)<sup>5</sup>, and M. [Zhang](#)<sup>1</sup>

2016 ApJ 816 30

The observations of chromospheric oscillations of two umbral light bridges (LBs) within a sunspot from NOAA Active Region 12127 are presented. It was found that the running umbral waves with periods of 2.2-2.6 minutes underwent very fast damping before approaching umbral boundaries, while those with higher periods (>2.6 minutes) could propagate outside umbrae. On two sides of each LB adjacent to umbrae, the cross-wavelet spectra displayed that the oscillations on them had a common significant power region with dominant frequencies of 2?6 minutes and phase differences of ~90?. A counterstream of two running umbral waves in the 2?6 minute frequency range propagated toward the LBs, where they encountered each other and gave rise to constructive or even destructive interference on the LBs. In addition, the velocity and density perturbations on the LBs were found in opposite phases suggesting that the perturbations were caused by the downward propagating waves.

### **Imaging Observation of Quasi-periodic Disturbances' Amplitudes Increasing with Height in the Polar Region of the Solar Corona**

J. T. [Su](#)<sup>1,2</sup>, Y. [Liu](#)<sup>3</sup>, Y. D. [Shen](#)<sup>3</sup>, and T. G. [Priya](#)

2014 ApJ 790 150.

At present, there have been few extreme ultraviolet (EUV) imaging observations of spatial variations of the density perturbations due to the slow magnetoacoustic waves (SMWs) propagating along the solar coronal magnetic fields. In this paper, we present such observations taken from the polar region of the corona with the Atmospheric Imaging Assembly (AIA) on board the Solar Dynamics Observatory and investigate the amplitude of quasi-periodic propagating disturbances that increase with height in the lower corona (0-9 Mm over the solar limb). We statistically determined the following parameters associated with the disturbances: pressure scale height, period, and wavelength in AIA 171 Å, 193 Å, and 211 Å channels. The scale height and wavelength are dependent of temperature, while the period is independent of temperature. The acoustic velocities inferred from the scale height highly correlate with the ratios of wavelength to period, i.e., phase speeds. They provide evidence that the propagating disturbances in the lower corona are likely SMWs and the spatial variations in EUV intensity in the polar region likely reflects the density compressional effect by the propagating SMWs.

### **Statistical study of free magnetic energy and flare productivity of solar active regions**

J.T. [Su](#), J. Jing, S. Wang, T. Wiegmann, H.M. Wang

ApJ 788 150, 2014

<http://arxiv.org/pdf/1405.2131v1.pdf>

Photospheric vector magnetograms from Helioseismic and Magnetic Imager on board the Solar Dynamic Observatory are utilized as the boundary conditions to extrapolate both non-linear force-free and potential magnetic fields in solar corona. Based on the extrapolations, we are able to determine the free magnetic energy (FME) stored in active regions (ARs). Over 3000 vector magnetograms in 61 ARs were analyzed. We compare FME with ARs' flare index (FI) and find that there is a weak correlation (<60%) between FME and FI. FME shows slightly improved flare predictability relative to total unsigned magnetic flux of ARs in the following two aspects: (1) the flare productivity predicted by FME is higher than that predicted by magnetic flux and (2) the correlation between FI and FME is higher than that between FI and magnetic flux. However, this improvement is not significant enough to make a substantial difference in time-accumulated FI, rather than individual flare, predictions.

#### **Table 2. Information of 61 chosen ARs**

### **Detection of emission in the Si i 1082.7 nm line core in sunspot umbrae**

D. Orozco [Suarez](#), [C. Quintero Noda](#), [B. Ruiz Cobo](#), [M. Collados Vera](#)

A&A 2017

<https://arxiv.org/pdf/1709.06773.pdf>

We analyze spectropolarimetric sunspot umbra observations taken in the near-infrared Si i 1082.7 nm line taking NLTE effects into account. The data were obtained with the GRIS instrument installed at the German GREGOR telescope. A point spread function (PSF) was constructed using prior Mercury observations with GRIS and the information provided by the adaptive optics system of the GREGOR telescope. The data were then deconvolved from the PSF using a principal component analysis deconvolution method and were analyzed via the NICOLE inversion code. The Si i 1082.7 nm line seems to be in emission in the umbra of the observed sunspot after the effects of scattered light are removed. We show how the spectral line shape of umbral profiles changes dramatically with the amount of scattered light. Indeed, the continuum levels range, on average, from 44% of the quiet Sun continuum intensity to about 20%. The inferred levels are in line with current model predictions and empirical umbral models. Current umbral empirical models are not able to reproduce the emission in the deconvolved umbral Stokes profiles. The results of the NLTE inversions suggests that to obtain the emission in the Si i 1082.7 nm line, the temperature stratification should first have a hump located at about  $\log \tau -2$  and start rising at lower heights when moving into the transition region. This is, to our knowledge, the first time the Si i 1082.7 nm line is seen in emission in sunspot umbrae. The results show that the temperature stratification of current umbral models may be more complex than expected with the transition region located at lower heights above sunspot umbrae. Our finding might provide insights into understanding why the sunspot umbra emission in the millimeter spectral range is less than that predicted by current empirical umbral models. **27 June 2014**

### **Height Variation of the Vector Magnetic Field in Solar Spicules**

D. Orozco [Suárez](#)<sup>1,2</sup>, A. Asensio Ramos<sup>1,2</sup>, and J. Trujillo Bueno

2015 ApJ 803 L18

<http://arxiv.org/pdf/1504.04637v1.pdf>

Proving the magnetic configuration of solar spicules has hitherto been difficult due to the lack of spatial resolution and image stability during off-limb ground-based observations. We report spectropolarimetric observations of spicules taken in the He i 1083 nm spectral region with the Tenerife Infrared Polarimeter II at the German Vacuum



Tower Telescope of the Observatorio del Teide (Tenerife, Canary Islands, Spain). The data provide the variation with geometrical height of the Stokes I, Q, U, and V profiles, whose encoded information allows the determination of the magnetic field vector by means of the HAZEL inversion code. The inferred results show that the average magnetic field strength at the base of solar spicules is about 80 gauss, and then it decreases rapidly with height to about 30 gauss at a height of 3000 km above the visible solar surface. Moreover, the magnetic field vector is close to vertical at the base of the chromosphere and has mid-inclinations (about 50°) above 2 Mm height. **2013 Apr 23**

### **Emission Measure Distribution for Diffuse Regions in Solar Active Regions**

Srividya [Subramanian](#), Durgesh Tripathi, James A. Klimchuk, Helen E. Mason

ApJ, **2014**

<http://arxiv.org/pdf/1409.1447v1.pdf>

Our knowledge of the diffuse emission that encompasses active regions is very limited. In the present paper we investigate two off-limb active regions, namely **AR10939** and **AR10961**, to probe the underlying heating mechanisms. For this purpose we have used spectral observations from Hinode/EIS and employed the emission measure (EM) technique to obtain the thermal structure of these diffuse regions. Our results show that the characteristic EM distributions of the diffuse emission regions peak at  $\log T = 6.25$  and the cool-ward slopes are in the range 1.4 - 3.3. This suggests that both low as well as high frequency nanoflare heating events are at work. Our results provide additional constraints on the properties of these diffuse emission regions and their contribution to the background/foreground when active region cores are observed on-disk. **2007 Jan 26, (2007 Aug 01-08, AR 10961)**

### **A Dynamic Deep-learning Model for Generating a Magnetogram Sequence from an SDO/AIA EUV Image Sequence**

Wenqing [Sun](#)<sup>1,2</sup>, Long Xu<sup>1,3</sup>, Suli Ma<sup>1</sup>, Yihua Yan<sup>1,2</sup>, Tie Liu<sup>4,5</sup>, and Weiqiang Zhang<sup>6</sup>

**2022** ApJS 262 45

<https://iopscience.iop.org/article/10.3847/1538-4365/ac85c0/pdf>

The solar magnetic field dominates solar activities in the solar atmosphere, such as solar flares and coronal mass ejections (CMEs). The Helioseismic and Magnetic Imager (HMI) on board the Solar Dynamics Observatory (SDO) has been in operation from 2010, providing a full-disk photospheric magnetogram. However, with a single view of observation, SDO/HMI cannot provide a global view of the Sun at the same time, so the farside of the Sun is blind to us. The Solar Terrestrial Relations Observatory (STEREO) provides two different views of the Sun with complementary viewing angles relative to SDO/HMI. However, it did not carry a magnetograph, but an extreme-ultraviolet (EUV) imager. Fortunately, deep learning has been proved to generate a solar farside magnetogram from STEREO farside EUV observation. Although a single generated magnetogram is morphologically very similar to ground truth, the sequence of the generated magnetogram has noticeable magnetic field fluctuation, which cannot be ignored when it is displayed as a time series, especially at an active region. This fluctuation is represented by sudden magnetic polarity reversal and drifting of magnetic field distribution. To mitigate this problem, a novel dynamic deep-learning model by integrating a convolutional gated recurrent units (convGRU) model into a pix2pix baseline is proposed in this paper. It can generate a sequence of a magnetogram with smooth transition among consecutive magnetograms by exploring spatio-temporal information of an input EUV image sequence. From both quantitative and qualitative comparisons, the proposed model can generate a magnetogram sequence more close to real observation.

### **Are the Magnetic Fields Radial in the Solar Polar Region?**

[Xudong Sun](#), [Yang Liu](#), [Ivan Milić](#), [Ana Belén Griñón Marín](#)

RNAAS 5 134 **2021**

<https://arxiv.org/pdf/2106.01461.pdf>

<https://iopscience.iop.org/article/10.3847/2515-5172/ac072c>

<https://doi.org/10.3847/2515-5172/ac072c>

We investigate the orientation of the photospheric magnetic fields in the solar polar region using observations from the Helioseismic and Magnetic Imager (HMI). Inside small patches of significant polarization, the inferred magnetic field vectors at 1'' scale appear to systematically deviate from the radial direction. Most tilt towards the pole; all are more inclined toward the plane of sky compared to the radial vector. These results, however, depend on the "filling factor"  $f$  that characterizes the unresolved magnetic structures. The default, uninformative  $f=1$  for HMI will incur larger inclination and less radial fields than  $f<1$ . The observed trend may be a systematic bias inherent to the limited resolution. **March 4, 2015**

### **Polar Field Correction for HMI Line-of-Sight Synoptic Data**

Xudong [Sun](#) (the HMI Team)

**2018** Tech notes for HMI synoptic data product

<https://arxiv.org/pdf/1801.04265.pdf>

This document provides some technical notes on the polar field correction scheme for the HMI synoptic maps and daily updated synchronic frames. It is intended as a reference for the new data products and for some minor updates on our previous scheme for MDI (Sun et al. 2011).

### **The New HMI 96-Minute Vector Magnetograms**

Xudong [Sun](#)

HMI Science Nuggets, #143, 2020 <http://hmi.stanford.edu/hminuggets/?p=3330>  
<http://jsoc.stanford.edu/data/hmi/b96m/>

### **The New HMI High-Cadence Vector Magnetograms**

Xudong [Sun](#)

HMI Science Nuggets –#67 Feb 2017  
<http://hmi.stanford.edu/hminuggets/?p=1820>  
**2011-02-15**

### **The Polar Field Reversal of Solar Cycle 24**

Xudong [Sun](#)

HMI Science Nuggets, #32, Dec 2014  
<http://hmi.stanford.edu/hminuggets/?p=1030>

HMI observations reveal a slow, north-south asymmetric polar magnetic field reversal. Cycle 24 has been weak; an even weaker Cycle 25 seems probable.

### **On Polar Magnetic Field Reversal and Surface Flux Transport During Solar Cycle 24**

Xudong [Sun](#), J. Todd Hoeksema, Yang Liu, Junwei Zhao

ApJ 2014

<http://arxiv.org/pdf/1410.8867v1.pdf>

As each solar cycle progresses, remnant magnetic flux from active regions (ARs) migrates poleward to cancel the old-cycle polar field. We describe this polarity reversal process during Cycle 24 using four years (2010.33–2014.33) of line-of-sight magnetic field measurements from the Helioseismic and Magnetic Imager. The total flux associated with ARs reached maximum in the north in 2011, more than two years earlier than the south; the maximum is significantly weaker than Cycle 23. The process of polar field reversal is relatively slow, north-south asymmetric, and episodic. We estimate that the global axial dipole changed sign in October 2013; the northern and southern polar fields (mean above 60° latitude) reversed in November 2012 and March 2014, respectively, about 16 months apart. Notably, the poleward surges of flux in each hemisphere alternated in polarity, giving rise to multiple reversals in the north. We show that the surges of the trailing sunspot polarity tend to correspond to normal mean AR tilt, higher total AR flux, or slower mid-latitude near-surface meridional flow, while exceptions occur during low magnetic activity. In particular, the AR flux and the mid-latitude poleward flow speed exhibit a clear anti-correlation. We discuss how these features can be explained in a surface flux transport process that includes a field-dependent converging flow toward the ARs, a characteristic that may contribute to solar cycle variability.

### **The CGEM Lorentz Force Data from HMI Vector Magnetograms**

Xudong [Sun](#), for the CGEM Team

2014

<http://arxiv.org/pdf/1405.7353v2.pdf>  
<http://hmi.stanford.edu/hminuggets/?p=806>

We describe a new data product from the CGEM (Coronal Global Evolutionary Model) collaboration that estimates the Lorentz force in active regions (ARs) based on HMI vector magnetogram patches. Following Fisher et al. (2012), we compute three components of the integrated Lorentz force over the outer solar atmosphere every 12 minutes throughout an AR's disk passage. These estimates, differenced during solar eruptive events, can provide valuable diagnostics on dynamic processes. We describe the pipeline modules, provide data retrieval examples, and document some systematic uncertainties that users should be aware of.

Estimates of Lorentz force acting on plasma at and above the active region photosphere are now available as a routine data product at the SDO JSOC website (<http://jsoc.stanford.edu>).

The data series `cgem.Lorentz` is generated from the vector magnetic field available in Space-weather HMI Active Region Patches (SHARPs). The series includes both indices and maps for each region every 12 minutes.

**Lorentz force estimates are based on methods described by Fisher et al. (SoPh, 277, 59, 2012) and can be useful for diagnosing eruption dynamics. Further documentation and references can be found at <http://arxiv.org/abs/1405.7353>**

### **Dynamic Evolution of an X-shaped Structure above a Trans-equatorial Quadrupole Solar Active Region Group**

J. Q. Sun<sup>1,2</sup>, X. Cheng<sup>1,2</sup>, Y. Guo<sup>1,2</sup>, M. D. Ding<sup>1,2</sup>, and Y. Li  
2014 ApJ 787 L27

In the solar corona, magnetic reconnection usually takes place at the singular configuration of the magnetic field, in particular near a magnetic null, owing to its high susceptibility to perturbations. In this Letter, we report a rare X-shaped structure, encompassing a magnetic null, above a trans-equatorial quadrupole active region group that is well observed by the Atmospheric Imaging Assembly (AIA). The observations show that this X-shaped structure is visible in all AIA EUV passbands and stably exists for days. However, possibly induced by flare activities at the northern part of the quadrupole active region group, the X-shaped structure starts to destabilize while a jet erupts near its center at ~15:05 UT on **2013 October 7**. Through nonlinear force-free field modeling, we identify a magnetic null that is above the quadrupole polarities and well corresponds to the X-shaped structure. After the jet eruption, the temperature and emission measure of the plasma near the X-shaped structure rise from ~2.3 MK and  $\sim 1.2 \times 10^{27} \text{ cm}^{-5}$  at 15:01 UT to ~5.4 MK and  $\sim 3.7 \times 10^{27} \text{ cm}^{-5}$  at 15:36 UT, respectively, revealed by the differential emission measure analysis, indicating that magnetic reconnection most likely takes place there to heat the plasma. Moreover, the height of the null increases ~10 Mm, which is most likely due to the partial opening of the field lines near the fan surface that makes the null underneath rise to seek a new equilibrium.

### **A New Method for Polar Field Interpolation**

X. Sun, Y. Liu, J. T. Hoeksema, K. Hayashi & X. Zhao  
Solar Physics, Volume 270, Number 1, 9-22, 2011

The photospheric magnetic field in the Sun's polar region is not well observed compared to the low-latitude regions. Data are periodically missing due to the Sun's tilt angle, and the noise level is high due to the projection effect on the line-of-sight (LOS) measurement. However, the large-scale characteristics of the polar magnetic field data are known to be important for global modeling. This report describes a new method for interpolating the photospheric field in polar regions that has been tested on MDI synoptic maps (1996–2009). This technique, based on a two-dimensional spatial/temporal interpolation and a simple version of the flux transport model, uses a multi-year series of well-observed, smoothed north (south) pole observations from each September (March) to interpolate for missing pixels at any time of interest. It is refined by using a spatial smoothing scheme to seamlessly incorporate this filled-in data into the original observation starting from lower latitudes. For recent observations, an extrapolated polar field correction is required. Scaling the average flux density from the prior observations of slightly lower latitudes is found to be a good proxy of the future polar field. This new method has several advantages over some existing methods. It is demonstrated to improve the results of global models such as the Wang–Sheeley–Arge (WSA) model and MHD simulation, especially during the sunspot minimum phase.

### **Evaluation of standoff distance method to determine the coronal magnetic field using CME-driven shocks**

K. Suresh, A. Shanmugaraju, M. Syed Ibrahim  
Astrophysics and Space Science November 2016, 361:360

[http://link.springer.com/article/10.1007/s10509-016-2944-4?wt\\_mc=alerts.TOCjournals](http://link.springer.com/article/10.1007/s10509-016-2944-4?wt_mc=alerts.TOCjournals)

We have analyzed the propagation characteristics of four limb coronal mass ejections (CMEs) with their shocks. These CMEs were observed in 18 frames up to 18 solar radii using LASCO white light images. Gopalswamy and Yashiro (Astrophys. J. 736:L17, 2011) introduced the standoff distance method (SOD) to find the magnetic field in the corona using CME-driven shock. In this paper, we have used this technique to determine the magnetic field strength and to study the propagation/shock formation condition of these CMEs at 18 different locations. Since the thickness of shock sheath (standoff distance or SOD) is not constant around CME, we estimate the shock parameters and their variation in large and small SOD regions of the shock. The Mach number ranges from 1.7 to 2.8 and Alfvén speed varies from  $\sim 857 \text{ km s}^{-1}$ . Finally, we estimate the magnetic field variation in the corona. The magnetic field strength ranges from 4.9 to 26.2 mG from 8.3 to 17.5 solar radii. The estimated magnetic field strength in this study is consistent with the literature value (7.6 to 45.8 mG from Gopalswamy and Yashiro (Astrophys. J. 736:L17, 2011), and 6 to 105 mG from Kim et al. (Astrophys. J. 746:118,

2012)) and it smoothly follows the general coronal magnetic field profile. **Mar 25, 2008, Aug 18, 2010, Apr 9, 2012, Apr 15, 2012, Oct 22, 2012**

## **PHYSICAL CONDITIONS OF CORONAL PLASMA AT THE TRANSIT OF A SHOCK DRIVEN BY A CORONAL MASS EJECTION**

R. [Susino](#), A. Bemporad, and S. Mancuso

2015 ApJ 812 119

We report here on the determination of plasma physical parameters across a shock driven by a coronal mass ejection using white light (WL) coronagraphic images and radio dynamic spectra (RDS). The event analyzed here is the spectacular eruption that occurred on **2011 June 7**, a fast CME followed by the ejection of columns of chromospheric plasma, part of them falling back to the solar surface, associated with a M2.5 flare and a type-II radio burst. Images acquired by the Solar and Heliospheric Observatory/LASCO coronagraphs (C2 and C3) were employed to track the CME-driven shock in the corona between 2–12  $R_{\odot}$  in an angular interval of about  $110^{\circ}$ . In this interval we derived two-dimensional (2D) maps of electron density, shock velocity, and shock compression ratio, and we measured the shock inclination angle with respect to the radial direction. Under plausible assumptions, these quantities were used to infer 2D maps of shock Mach number MA and strength of coronal magnetic fields at the shock's heights. We found that in the early phases (2–4  $R_{\odot}$ ) the whole shock surface is super-Alfvénic, while later on (i.e., higher up) it becomes super-Alfvénic only at the nose. This is in agreement with the location for the source of the observed type-II burst, as inferred from RDS combined with the shock kinematic and coronal densities derived from WL. For the first time, a coronal shock is used to derive a 2D map of the coronal magnetic field strength over intervals of 10  $R_{\odot}$  altitude and  $\sim 110^{\circ}$  latitude.

## **Calibration of the Sunspot and Group Numbers Using the Waldmeier Effect**

[Leif Svalgaard](#), [David H. Hathaway](#)

2020

<https://arxiv.org/ftp/arxiv/papers/2011/2011.01330.pdf>

The Waldmeier Effect is the observation that the rise time of a sunspot cycle varies inversely with the cycle amplitude: strong cycles rise to their maximum faster than weak cycles. The shape of the cycle and thus the rise time does not depend on the scale factor of the sunspot number and can thus be used to verify the constancy of the scale factor with time as already noted by Wolfer (1902) and Waldmeier (1978). We extend their analysis until the present using the new SILSO sunspot number (version 2) and group number and confirm that the scale factors have not varied significantly the past 250 years. The effect is also found in sunspot areas, in an EUV (and F10.7) proxy (the daily range of a geomagnetic variation), and in Cosmic Ray Modulation. The result is that solar activity reached similar high values in every one of the (17th?) 18th, 19th, and 20th centuries, supporting the finding that there has been no modern Grand Maximum.

## **Evolution and motions of magnetic fragments during the active region formation and decay: A statistical study**

Michal [Švanda](#)<sup>1,2</sup>, Michal Sobotka<sup>2</sup>, Lucia Mravcová<sup>2,1</sup> and Tatiana Výbošťoková<sup>3</sup>

A&A 647, A146 (2021)

<https://www.aanda.org/articles/aa/pdf/2021/03/aa40127-20.pdf>

<https://doi.org/10.1051/0004-6361/202040127>

Context. The evolution of solar active regions is still not fully understood. The growth and decay of active regions have mostly been studied in case-by-case studies.

Aims. Instead of studying the evolution of active regions case by case, we performed a large-scale statistical study to find indications for the statistically most frequent scenario.

Methods. We studied a large sample of active regions recorded by the Helioseismic and Magnetic Imager instrument. The sample was split into two groups: forming (367 members) and decaying (679 members) active regions. We tracked individual dark features (i.e. those that are assumed to be intensity counterparts of magnetised fragments from small objects to proper sunspots) and followed their evolution. We investigated the statistically most often locations of fragment merging and splitting as well as their properties.

Results. Our results confirm that statistically, sunspots form by merging events of smaller fragments. The coalescence process is driven by turbulent diffusion in a process similar to random-walk, where supergranular flows seem to play an important role. The number of appearing fragments does not seem to significantly correlate with the number of sunspots formed. The formation seems to be consistent with the magnetic field accumulation.

Statistically, the merging occurs most often between a large and a much smaller object. The decay of the active region seems to take place preferably by a process similar to the erosion

## **Polar Cap Magnetic Field Reversals During Solar Grand Minima: Could Pores Play a Role?**

Michal Švanda

HMI Science Nugget #48 Jan 2016

<http://hmi.stanford.edu/hminuggets/?p=1380>

## **Sunspot moats versus supergranules**

Michal Švanda<sup>1,2</sup>, Michal Sobotka<sup>1</sup>, Tomáš Bárta

HMI Science Nuggets, #28, Sept 2014

<http://hmi.stanford.edu/hminuggets/?p=974>

## **Spatial structure of resonance cavities in sunspots**

Robert Sych, Xiaoshuai Zhu, Yao Chen, Fabao Yan

MNRAS Volume 529, Issue 2, April 2024, Pages 967–978,

<https://doi.org/10.1093/mnras/stae575>

<https://academic.oup.com/mnras/article-pdf/doi/10.1093/mnras/stae575/56900200/stae575.pdf>

We present a study of wave processes in sunspots from active regions NOAA 11131 on **2010 December 10** and NOAA 12565 on **2016 July 14** observed by SDO/AIA in the 1600, 304, and 171 Å temperature channels. To study the spatial structure of the resonance cavities previously found by Jess et al., we applied spectral data processing techniques such as pixelized wavelet filtering and mode decomposition. For the first time, we found stable regions as waveguides of the oscillations in the sunspot umbra, occupying specific frequency ranges without spatial overlap. The sizes of these regions depend on the frequency oscillations, and the maximum frequency coincides with the values of the harmonics of the main oscillation mode. Frequency drifts were observed in the band occupied by these regions, with different spectral slopes depending on the location of the sources in the sunspot umbra. We suggest that the observed distribution of wave sources in the umbra is a set of resonant cavities where successive amplification of oscillations at selected multiple harmonics is observed. The distribution of sources at low frequencies indicates the influence of the atmospheric cut-off due to the inclinations of the magnetic field lines.

## **Properties of local oscillations in the lower sunspot atmosphere**

Robert Sych, Yuzef Zhugzhda, Xiaoli Yan

2020 *ApJ* 888 84

<https://arxiv.org/pdf/1910.07754.pdf>

<https://doi.org/10.3847/1538-4357/ab5a78>

We present a study of wave processes in the sunspot region NOAA 12670 on **2017 August 10** observed by the Goode Solar Telescope in the TiO 7057 Å and Ha 6563 Å spectral lines. To study the distribution of power oscillations and their dynamics, we applied the pixelized wavelet filtering (PWF) technique. For the first time, the spatial structure of oscillation sources as a footpoints of fine magnetic tubes, anchored in the sunspot umbra was obtained. We found that at the chromosphere level, emission variation is a combination of numerous independent oscillations located in the sources with small angular size. Their spatial shape varies from dots and cellular in the umbra to filaments in the penumbra. Each narrow spectrum harmonic corresponds to its source, without global correlation among themselves. There is weak background as low-frequency oscillation sources are distributed on whole umbra. At the photosphere level we found regions with co-phased broadband oscillations of the whole umbra. Their spectrum includes the ~3-min harmonic, whose maximal value is localized in umbral dots (UDs), and the low frequency part near the ~5-min period. It is shown that the oscillation sources are displaced at different heights with increasing angular size. We assume that the observed spatial distribution of wave sources indicates the existence a slow subphotosphere resonator with a vertical magnetic field in the umbra and wave cutoff frequency due to inclination of the magnetic field line in the penumbra.

## **Fine wave structure of umbral flashes**

R. Sych, M. Wang

A&A 618, A123 (2018)

<https://arxiv.org/pdf/1710.08100.pdf>

[sci-hub.tw/10.1051/0004-6361/201732139](https://sci-hub.tw/10.1051/0004-6361/201732139)

Context. Umbral flashes (UFs) are most common phenomenon of wave processes in sunspots. Studying the relationship between wave time dynamics and UF origin requires further investigating their fine spatial and height structure. Aims. We investigated the association between a short-time increase in the variations of 3-minute EUV emission at footpoints of coronal magnetic loops and the UF emergence in sunspot umbrae. Methods. We applied

the Pixelized Wavelet Filtering (PWF) technique to analyze a cube of the images obtained by SDO/AIA at 1600{\AA}, 304{\AA}, and 171{\AA} to study the spatio-temporal dynamic of oscillations in individual magnetic loops. The time-distance plots were used to obtain the wave front propagation velocity. We used the magnetic field extrapolation for SDO/HMI magnetograms to obtain localization of the magnetic loop footpoints. Results. For the first time, we obtained 2D images of fine wave processes in magnetic structures of different scales related to umbral flashes. UF sources were mainly localized at the magnetic loop footpoints anchored in an umbra. We revealed two types UFs, point and extended. The first type is related to the footpoints of open field lines, the second is associated with the closed. The time dynamics of UFs shows an increase the oscillations before the peak value within one low-frequency wave train. It is shown that the maxima of oscillation trains coincide with the peak intensity of umbral flashes. Conclusions. The sunspot wave dynamics showed a relation between the localization of oscillations power peak at the coronal magnetic loop footpoints and the UF origin. The spatial structure of the UF sources, their power and lifetime are determined by the cut-off frequency of the waves for the detected waveguides. We concluded that UFs are a process of short-time increase of the wave activity at the footpoints of magnetic loops. **December 8, 2010**

## MHD waves in sunspots

**Review**

Robert **Sych**

Chapter in AGU Monograph **2015**

<http://arxiv.org/pdf/1509.06466v1.pdf>

The review addresses the spatial frequency morphology of sources of sunspot oscillations and waves, including their localization, size, oscillation periods, height localization with the mechanism of cut-off frequency that forms the observed emission variability. Dynamic of sunspot wave processes, provides the information about the structure of wave fronts and their time variations, investigates the oscillation frequency transformation depending on the wave energy is shown. The initializing solar flares caused by trigger agents like magnetoacoustic waves, accelerated particle beams, and shocks are discussed. Special attention is paid to the relation between the flare reconnection periodic initialization and the dynamics of sunspot slow magnetoacoustic waves. A short review of theoretical models of sunspot oscillations is provided.

## Wave dynamics in a sunspot umbra

**Sych**, R., Nakariakov, V.M.

A&A, 569, A72 **2014**

[http://www2.warwick.ac.uk/fac/sci/physics/research/cfsa/people/valery/research/eprints/sych\\_nakariakov\\_2014\\_rev3\\_140814\\_Print.pdf](http://www2.warwick.ac.uk/fac/sci/physics/research/cfsa/people/valery/research/eprints/sych_nakariakov_2014_rev3_140814_Print.pdf)

<http://arxiv.org/pdf/1409.4530v1.pdf>

Context. Sunspot oscillations are one of the most frequently studied wave phenomena in the solar atmosphere. Understanding the basic physical processes responsible for sunspot oscillations requires detailed information about their fine structure. Aims. We aim to reveal the relationship between the fine horizontal and vertical structure, time evolution, and the fine spectral structure of oscillations in a sunspot umbra. Methods. The high spatial and time resolution data obtained with SDO/AIA for the sunspot in active region NOAA 11131 on **08 December 2010** were analysed with the time-distance plot technique and the pixelised wavelet filtering method. Different levels of the sunspot atmosphere were studied from the temperature minimum to the corona. Results. Oscillations in the 3 min band dominate in the umbra. The integrated spectrum of umbral oscillations contains distinct narrowband peaks at 1.9 min, 2.3 min, and 2.8 min. The power significantly varies in time, forming distinct 12?20 min oscillation trains. The oscillation power distribution over the sunspot in the horizontal plane reveals that the enhancements of the oscillation amplitude, or wave fronts, have a distinct structure consisting of an evolving two-armed spiral and a stationary circular patch at the spiral origin, situated near the umbra centre. This structure is seen from the temperature minimum at 1700? to the 1.6 MK corona at 193?. In time, the spiral rotates anti-clockwise. The wave front spirality is most pronounced during the maximum amplitude phases of the oscillations, and in the bandpasses where umbral oscillations have the highest power, 304? and 171?. In the low-amplitude phases the spiral breaks into arc-shaped patches. The 2D cross-correlation function shows that the oscillations at higher atmospheric levels occur later than at lower layers. The phase speed is estimated to be about 100 km/s. The fine spectral analysis shows that the central patch corresponds to the high-frequency oscillations, while the spiral arms highlight the lower-frequency oscillations in the 3-min band. Conclusions. The vertical and horizontal radial structure of the oscillations is consistent with the model that interprets umbral oscillations as slow magnetoacoustic waves filtered by the atmospheric temperature non-uniformity in the presence of the magnetic field inclination from the vertical. The mechanism for the polar-angle structure of the oscillations, in particular the spirality of the wave fronts, needs to be revealed.

## Emergence of non-twisted magnetic fields in the Sun: Jets and atmospheric response

Petros **Syntelis**, Vasilis Archontis, Costis Gontikakis, [Kanaris Tsinganos](#)

A&A 584, A10 **2015**

<http://arxiv.org/pdf/1509.02850v1.pdf>

<http://www.aanda.org/articles/aa/pdf/2015/12/aa23781-14.pdf>

**Aims.** We study the emergence of a non-twisted flux tube from the solar interior into the solar atmosphere. We investigate whether the length of the buoyant part of the flux tube (i.e.  $\{\lambda\}$ ) affects the emergence of the field and the dynamics of the evolving magnetic flux system. **Methods.** We perform three-dimensional (3D), time-dependent, resistive, compressible MHD simulations using the Lare3D code. **Results.** We find that there are considerable differences in the dynamics of the emergence of a magnetic flux tube when  $\{\lambda\}$  is varied. In the solar interior, for larger values of  $\{\lambda\}$ , the rising magnetic field emerges faster and expands more due to its lower magnetic tension. As a result, its field strength decreases and its emergence above the photosphere occurs later than in the smaller  $\{\lambda\}$  case. However, in both cases, the emerging field at the photosphere becomes unstable in two places, forming two magnetic bipoles that interact dynamically during the evolution of the system. Most of the dynamic phenomena occur at the current layer, which is formed at the interface between the interacting bipoles. We find the formation and ejection of plasmoids, the onset of successive jets from the interface, and the impulsive heating of the plasma in the solar atmosphere. We discuss the triggering mechanism of the jets and the atmospheric response to the emergence of magnetic flux in the two cases.

## **Effect of the Size of the Computational Domain on Spherical Nonlinear Force-Free Modeling of a Coronal Magnetic Field Using SDO/HMI Data**

Tilaye **Tadesse**, T. Wiegmann, P. J. MacNeice

Solar Phys. Volume 290, **Issue 4**, pp 1159-1171 **2015**

The solar coronal magnetic field produces solar activity, including extremely energetic solar flares and coronal mass ejections (CMEs). Knowledge of the structure and evolution of the magnetic field of the solar corona is important for investigating and understanding the origins of space weather. Although the coronal field remains difficult to measure directly, there is considerable interest in accurate modeling of magnetic fields in and around sunspot regions on the Sun using photospheric vector magnetograms as boundary data. In this work, we investigate effects of the size of the domain chosen for coronal magnetic field modeling on resulting model solutions. We applied a spherical nonlinear force-free optimization procedure to vector magnetogram data of the Helioseismic and Magnetic Imager (HMI) onboard the Solar Dynamics Observatory (SDO). We selected a particular observation in which there were four active regions observed on **9 March 2012** at 20:55 UT. The results imply that quantities such as magnetic flux density, electric current density, and free magnetic energy density of active regions of interest are significantly different from the corresponding quantities obtained in the same region with a larger computational domain. The difference is even more pronounced in the regions that are connected to the outside of the domain.

## **Comparing nonlinear force-free and potential field modeling using full-disk HMI data**

Tilaye **Tadesse**<sup>1</sup>, T. Wiegmann<sup>2</sup>, P.J. MacNeice<sup>1</sup>, B. Inhester<sup>2</sup>, K. Olson<sup>3</sup>, and A. A. Pevtsov

HMI Science Nuggets, #33, Jan **2015**

<http://hmi.stanford.edu/hminuggets/?p=1058>

We have compared the magnetic field solutions from both models. The qualitative comparison between the model magnetic field lines and the observed EUV loops indicates that the NLFFF model agrees significantly better with coronal magnetic loops as observed in SDO/AIA images (see Fig 2a,b). The study also investigated the magnetic connectivity between ARs located on either side of the solar equator (see Fig 3). For this particular observation, much of the trans-equatorial loops (TEs) connecting the active regions in the northern and southern hemispheres are potential (current-free). This indicates that the two solar hemispheres are more magnetically connected but hardly share electric currents. **9 Nov 2011**

## **Global Solar Free Magnetic Energy and Electric Current Density Distribution of Carrington Rotation 2124**

Tilaye **Tadesse**, Alexei A. Pevtsov, T. Wiegmann, P. J. MacNeice, S. Gosain

Solar Physics, November **2014**, Volume 289, Issue 11, pp 4031-4045

Solar eruptive phenomena, like flares and coronal mass ejections (CMEs), are governed by magnetic fields. To describe the structure of these phenomena one needs information on the magnetic flux density and the electric current density vector components in three dimensions throughout the atmosphere. However, current spectropolarimetric measurements typically limit the determination of the vector magnetic field to only the photosphere. Therefore, there is considerable interest in accurate modeling of the solar coronal magnetic field using photospheric vector magnetograms as boundary data. In this work, we model the coronal magnetic field for global solar atmosphere using nonlinear force-free field (NLFFF) extrapolation codes implemented to a synoptic maps of photospheric vector magnetic field synthesized from the Vector Spectromagnetograph (VSM) on Synoptic Optical Long-term Investigations of the Sun (SOLIS) as boundary condition. Using the resulting three-dimensional magnetic field, we calculate the three-dimensional electric current density and magnetic energy throughout the solar

atmosphere for Carrington rotation 2124 using our global extrapolation code. We found that spatially, the low-lying, current-carrying core field demonstrates a strong concentration of free energy in the active-region core, from the photosphere to the lower corona (about 70 Mm). The free energy density appears largely co-spatial with the electric current distribution.

### **First use of synoptic vector magnetograms for global nonlinear, force-free coronal magnetic field models**

T. [Tadesse](#)<sup>1</sup>, T. Wiegelmann<sup>2</sup>, S. Gosain<sup>3</sup>, P. MacNeice<sup>1</sup> and A. A. Pevtsov  
A&A 562, A105 (2014)

Context. The magnetic field permeating the solar atmosphere is generally thought to provide the energy for much of the activity seen in the solar corona, such as flares, coronal mass ejections (CMEs), etc. To overcome the unavailability of coronal magnetic field measurements, photospheric magnetic field vector data can be used to reconstruct the coronal field. Currently, there are several modelling techniques being used to calculate three-dimensional field lines into the solar atmosphere.

Aims. For the first time, synoptic maps of a photospheric-vector magnetic field synthesized from the vector spectromagnetograph (VSM) on Synoptic Optical Long-term Investigations of the Sun (SOLIS) are used to model the coronal magnetic field and estimate free magnetic energy in the global scale. The free energy (i.e., the energy in excess of the potential field energy) is one of the main indicators used in space weather forecasts to predict the eruptivity of active regions.

Methods. We solve the nonlinear force-free field equations using an optimization principle in spherical geometry. The resulting three-dimensional magnetic fields are used to estimate the magnetic free energy content  $E_{\text{free}} = E_{\text{nlfff}} - E_{\text{pot}}$ , which is the difference of the magnetic energies between the nonpotential field and the potential field in the global solar corona. For comparison, we overlay the extrapolated magnetic field lines with the extreme ultraviolet (EUV) observations by the atmospheric imaging assembly (AIA) on board the Solar Dynamics Observatory (SDO). Results. For a single Carrington rotation 2121, we find that the global nonlinear force-free field (NLFFF) magnetic energy density is 10.3% higher than the potential one. Most of this free energy is located in active regions.

### **A Comparison Between Nonlinear Force-Free Field and Potential Field Models Using Full-Disk SDO/HMI Magnetogram**

Tilaye [Tadesse](#), T. Wiegelmann, P. J. MacNeice, B. Inhester, K. Olson, A. Pevtsov  
Solar Physics, March 2014, Volume 289, Issue 3, pp 831-845

Measurements of magnetic fields and electric currents in the pre-eruptive corona are crucial to the study of solar eruptive phenomena, like flares and coronal mass ejections (CMEs). However, spectro-polarimetric measurements of certain photospheric lines permit a determination of the vector magnetic field only at the photosphere. Therefore, there is considerable interest in accurate modeling of the solar coronal magnetic field using photospheric vector magnetograms as boundary data. In this work, we model the coronal magnetic field above multiple active regions with the help of a potential field and a nonlinear force-free field (NLFFF) extrapolation code over the full solar disk using Helioseismic and Magnetic Imager (SDO/HMI) data as boundary conditions. We compare projections of the resulting magnetic field lines with full-disk coronal images from the Atmospheric Imaging Assembly (SDO/AIA) for both models. This study has found that the NLFFF model reconstructs the magnetic configuration closer to observation than the potential field model for full-disk magnetic field extrapolation. We conclude that many of the trans-equatorial loops connecting the two solar hemispheres are current-free.

### **Full-disk nonlinear force-free field extrapolation of SDO/HMI and SOLIS/VSM magnetograms**

T. [Tadesse](#)<sup>1,2</sup>, T. Wiegelmann<sup>3</sup>, B. Inhester<sup>3</sup>, P. MacNeice<sup>4</sup>, A. Pevtsov<sup>5</sup> and X. Sun  
A&A 550, A14 (2013)

Context. The magnetic field configuration is essential for understanding solar explosive phenomena, such as flares and coronal mass ejections. To overcome the unavailability of coronal magnetic field measurements, photospheric magnetic field vector data can be used to reconstruct the coronal field. Two complications of this approach are that the measured photospheric magnetic field is not force-free and that one has to apply a preprocessing routine to achieve boundary conditions suitable for the force-free modeling. Furthermore the nonlinear force-free extrapolation code should take uncertainties into account in the photospheric field data. They occur due to noise, incomplete inversions, or azimuth ambiguity-removing techniques.

Aims. Extrapolation codes in Cartesian geometry for modeling the magnetic field in the corona do not take the curvature of the Sun's surface into account and can only be applied to relatively small areas, e.g., a single active region. Here we apply a method for nonlinear force-free coronal magnetic field modeling and preprocessing of photospheric vector magnetograms in spherical geometry using the optimization procedure to full disk vector



magnetograms. We compare the analysis of the photospheric magnetic field and subsequent force-free modeling based on full-disk vector maps from Helioseismic and Magnetic Imager (HMI) onboard the solar dynamics observatory (SDO) and Vector Spectromagnetograph (VSM) of the Synoptic Optical Long-term Investigations of the Sun (SOLIS).

Methods. We used HMI and VSM photospheric magnetic field measurements to model the force-free coronal field above multiple solar active regions, assuming magnetic forces to dominate. We solved the nonlinear force-free field equations by minimizing a functional in spherical coordinates over a full disk and excluding the poles. After searching for the optimum modeling parameters for the particular data sets, we compared the resulting nonlinear force-free model fields. We compared quantities, such as the total magnetic energy content, free magnetic energy, the longitudinal distribution of the magnetic pressure, and surface electric current density, using our spherical geometry extrapolation code.

Results. The magnetic field lines obtained from nonlinear force-free extrapolation based on HMI and VSM data show good agreement. However, the nonlinear force-free extrapolation based on HMI data contain more total magnetic energy, free magnetic energy, the longitudinal distribution of the magnetic pressure, and surface electric current density than do the VSM data.

## **Coronal Magnetic Field Structure and Evolution for Flaring AR 11117 and Its Surroundings**

Tilaye [Tadesse](#), T. Wiegelmann, B. Inhester, A. Pevtsov

Solar Physics, November **2012**, Volume 281, Issue 1, pp 53-65

In this study, photospheric vector magnetograms obtained with the Synoptic Optical Long-term Investigations of the Sun (SOLIS) survey are used as boundary conditions to model three-dimensional nonlinear force-free (NLFF) coronal magnetic fields as a sequence of NLFF equilibria in spherical geometry. We study the coronal magnetic field structure inside an active region and its temporal evolution. We compare the magnetic field configuration obtained from NLFF extrapolation before and after the flaring event in active region (AR) 11117 and its surroundings observed on **27 October 2010**, and we also compare the magnetic field topologies and the magnetic energy densities and study the connectivities between AR 11117 and its surroundings. During the investigated time period, we estimate the change in free magnetic energy from before to after the flare to be  $1.74 \times 10^{32}$  erg, which represents about 13.5 % of the NLFF magnetic energy before the flare. In this study, we find that electric currents from AR 11117 to its surroundings were disrupted after the flare.

## **Magnetic Connectivity Between Active Regions 10987, 10988, and 10989 by Means of Nonlinear Force-Free Field Extrapolation**

Tilaye [Tadesse](#), T. Wiegelmann, B. Inhester and A. Pevtsov

Solar Physics, Volume 277, Number 1, 119-130, **2012**

Extrapolation codes for modelling the magnetic field in the corona in Cartesian geometry do not take the curvature of the Sun's surface into account and can only be applied to relatively small areas, e.g., a single active region. We apply a method for nonlinear force-free coronal magnetic field modelling of photospheric vector magnetograms in spherical geometry which allows us to study the connectivity between multi-active regions. We use Vector Spectromagnetograph (VSM) data from the Synoptic Optical Long-term Investigations of the Sun (SOLIS) survey to model the coronal magnetic field, where we study three neighbouring magnetically connected active regions (ARs 10987, 10988, 10989) observed on **28, 29, and 30 March 2008**, respectively. We compare the magnetic field topologies and the magnetic energy densities and study the connectivities between the active regions. We have studied the time evolution of the magnetic field over the period of three days and found no major changes in topologies, as there was no major eruption event. From this study we have concluded that active regions are much more connected magnetically than the electric current.

## **Nonlinear force-free field extrapolation in spherical geometry: improved boundary data treatment applied to a SOLIS/VSM vector magnetogram**

T. [Tadesse](#)<sup>1,2</sup>, T. Wiegelmann<sup>1</sup>, B. Inhester<sup>1</sup> and A. Pevtsov<sup>3</sup>

A&A 527, A30 (**2011**)

Context. Understanding the 3D structure of coronal magnetic field is important to understanding: the onset of flares and coronal mass ejections, and the stability of active regions, and to monitoring the magnetic helicity and free magnetic energy and other phenomena in the solar atmosphere. Routine measurements of the solar magnetic field are mainly carried out in the photosphere. Therefore, one has to infer the field strength in the upper layers of the solar atmosphere from the measured photospheric field based on the assumption that the corona is force-free. Meanwhile, those measured data are inconsistent with the above force-free assumption. Therefore, one has to apply some transformations to these data before nonlinear force-free extrapolation codes can be applied.

**Aims.** Extrapolation codes in Cartesian geometry for modelling the magnetic field in the corona do not take the curvature of the Sun's surface into account and can only be applied to relatively small areas, e.g., a single active region. Here we apply a method for nonlinear force-free coronal magnetic field modelling and preprocessing of photospheric vector magnetograms in spherical geometry using the optimization procedure.

**Methods.** We solve the nonlinear force-free field equations by minimizing a functional in spherical coordinates over a restricted area of the Sun. We extend the functional by an additional term, which allows us to incorporate measurement errors and treat regions lacking observational data. We use vector magnetograph data from the Synoptic Optical Long-term Investigations of the Sun survey (SOLIS) to model the coronal magnetic field. We study two neighbouring magnetically connected active regions observed on May 15 2009.

**Results.** For vector magnetograms with variable measurement precision and randomly scattered data gaps (e.g., SOLIS/VSM), the new code yields field models that satisfy the solenoidal and force-free condition significantly better as it allows deviations between the extrapolated boundary field and observed boundary data within the measurement errors. Data gaps are assigned an infinite error. We extend this new scheme to spherical geometry and apply it for the first time to real data.

## **Nonlinear force-free coronal magnetic field modelling and preprocessing of vector magnetograms in spherical geometry**

T. [Tadesse](#)<sup>1,2</sup>, T. Wiegelmann<sup>1</sup>, and B. Inhester  
A&A 508, 421-432 (2009)

*Context.* Knowledge about the coronal magnetic field is important to the understanding of many phenomena, such as flares and coronal mass ejections. Routine measurements of the solar magnetic field vector are traditionally carried out in the photosphere. We compute the field in the higher layers of the solar atmosphere from the measured photospheric field under the assumption that the corona is force-free. However, those measured data are inconsistent with the above force-free assumption. Therefore, one has to apply some transformations to these data before nonlinear force-free extrapolation codes can be applied.

*Aims.* Extrapolation codes of cartesian geometry for modelling the magnetic field in the corona do not take the curvature of the Sun's surface into account. Here we develop a method for nonlinear force-free coronal magnetic field modelling and preprocessing of photospheric vector magnetograms in spherical geometry using the optimization procedure.

*Methods.* We describe a newly developed code for the extrapolation of nonlinear force-free coronal magnetic fields in spherical coordinates over a restricted area of the Sun. The program uses measured vector magnetograms on the solar photosphere as input and solves the force-free equations in the solar corona. We develop a preprocessing procedure in spherical geometry to drive the observed non-force-free data towards suitable boundary conditions for a force-free extrapolation.

*Results.* We test the code with the help of a semi-analytic solution and assess the quality of our reconstruction qualitatively by magnetic field line plots and quantitatively with a number of comparison metrics for different boundary conditions. The reconstructed fields from the lower boundary data with the weighting function are in good agreement with the original reference fields. We added artificial noise to the boundary conditions and tested the code with and without preprocessing. The preprocessing recovered all main structures of the magnetogram and removed small-scale noise. The main test was to extrapolate from the noisy photospheric vector magnetogram with and without preprocessing. The preprocessing was found to significantly improve the agreement between the extrapolated and the exact field.

## **Reconstructing solar magnetic fields from historical observations**

### **VIII. AIA 1600 Å contrast as a proxy of solar magnetic fields**

[Ismo Tähtinen](#), [Ilpo Virtanen](#), [Alexei A. Pevtsov](#), [Kalevi Mursula](#)

A&A 2022

<https://arxiv.org/pdf/2204.13944.pdf>

The bright regions in the solar chromosphere and temperature minimum have a good spatial correspondence with regions of intense photospheric magnetic field. Their observation started more than a hundred years ago with the invention of the spectroheliograph. While the historical spectroheliograms are essential for studying the long-term variability of the Sun, the modern satellite-borne observations can help us reveal the nature of chromospheric brightenings in previously unattainable detail. Our aim is to improve the understanding of the relation between magnetic fields and radiative structures by studying modern seeing-free observations of far-ultraviolet (FUV) radiation around 1600 Å and photospheric magnetic fields. We used Helioseismic and Magnetic Imager (HMI) observations of photospheric magnetic fields and Atmospheric Imaging Assembly (AIA) observations of FUV contrast around 1600 Å. We developed a robust method to find contrast thresholds defining bright and dark AIA 1600 Å pixels, and we combine them to bright and dark clusters. We investigate the relation of magnetic fields and AIA 1600 Å radiation in bright and dark clusters. We find that the percentage of bright pixels entirely explains the observed variability of 1600 Å emission. We developed a multilinear regression model based on the percentages of

bright and dark pixels, which can reliably predict the magnitude of the disk-averaged unsigned magnetic field. We find that bright and dark clusters closely correspond respectively to the populations of moderate ( $B > 55$  G) and strong ( $B > 1365$  G) magnetic field HMI clusters. The largest bright clusters have a constant mean unsigned magnetic field, as found previously for Ca II K plages. However, the magnetic field strength of bright clusters is  $254.7 \pm 0.1$  G, which is roughly 100 G larger than found earlier for Ca II K plages.

### **CAN A NANOFLARE MODEL OF EXTREME-ULTRAVIOLET IRRADIANCES DESCRIBE THE HEATING OF THE SOLAR CORONA?**

E. [Tajfirouze](#) and H. Safari

2012 ApJ 744 113

Nanoflares, the basic units of impulsive energy release, may produce much of the solar background emission. Extrapolation of the energy frequency distribution of observed microflares, which follows a power law to lower energies, can give an estimation of the importance of nanoflares for heating the solar corona. If the power-law index is greater than 2, then the nanoflare contribution is dominant. We model a time series of extreme-ultraviolet emission radiance as random flares with a power-law exponent of the flare event distribution. The model is based on three key parameters: the flare rate, the flare duration, and the power-law exponent of the flare intensity frequency distribution. We use this model to simulate emission line radiance detected in  $171 \text{ \AA}$ , observed by Solar Terrestrial Relation Observatory/Extreme-Ultraviolet Imager and Solar Dynamics Observatory/Atmospheric Imaging Assembly. The observed light curves are matched with simulated light curves using an Artificial Neural Network, and the parameter values are determined across the active region, quiet Sun, and coronal hole. The damping rate of nanoflares is compared with the radiative losses cooling time. The effect of background emission, data cadence, and network sensitivity on the key parameters of the model is studied. Most of the observed light curves have a power-law exponent,  $\alpha$ , greater than the critical value 2. At these sites, nanoflare heating could be significant.

### **Complex Network View of the Sun's Magnetic Patches. I. Identification**

Zahra [Tajik](#)<sup>1</sup>, Nastaran Farhang<sup>2</sup>, Hossein Safari<sup>1,3</sup>, and Michael S. Wheatland<sup>2</sup>

2024 ApJS 273 1

<https://iopscience.iop.org/article/10.3847/1538-4365/ad4642/pdf>

Solar and stellar magnetic patches (i.e., magnetic fluxes that reach the surface from the interior) are believed to be the primary sources of a star's atmospheric conditions. Here, we apply the complex network approach and investigate its efficacy in the identification of these features. For this purpose, we use the line-of-sight magnetograms provided by the Helioseismic and Magnetic Imager on board the Solar Dynamics Observatory. We construct the magnetic network following a specific visibility graph condition between pairs of pixels with opposite polarities and search for possible links between these regions. The complex network facilitates the construction of node degrees and PageRank images, and applying the downhill algorithm to node-degree images allows for the grouping of pixels into features corresponding to one-to-one matches with magnetogram patches. This approach promisingly serves to identify the nontrivial morphological structure of the magnetic patches for small and large sizes. We observe that the changes in the features of the node-degree images effectively correspond to the cospatial magnetic patches over time. Through visual assessment, we estimate an average false-negative error rate of approximately 1% in identifying small-scale features (one or two pixels in size).

### **Temporal and Latitudinal Variation in Penumbra-Umbra Ratios of the Sunspots: Analyses of RGO, Kodaikanal and Debrecen Databases**

Jouni [Takalo](#)

Solar Phys. 2023

<https://arxiv.org/pdf/2305.10757.pdf>

We study the latitudinal distribution and temporal evolution of the sunspot penumbra-umbra ratio ( $q$ ) for the even and odd Solar Cycles 12-24 of RGO sunspot groups, SC21-SC24 of Debrecen sunspot groups and Kodaikanal sunspot dataset for SC16-SC24. We find that RGO even (odd) Cycles have  $q$ -values 5.20 (4.75), Kodaikanal even (odd) cycles have  $q$ -values 5.27 (5.43), and Debrecen cycles has  $q$ -value 5.74 on the average. We also show that  $q$  is at lowest around the Equator of the Sun and increases towards higher latitudes having maximum values at about 10-25 degrees. This is understandable, because smaller sunspots and groups locate nearer to Equator and have smaller  $q$ -values than larger sunspots and groups, which maximize at about 10-20 degrees at both hemispheres. The error limits are very wide and thus the confidence of this result is somewhat vague. For Debrecen dataset we find a deep valley in the temporal  $q$ -values before the middle of the cycle. We show that this exists simultaneously with the Gnevyshev gap (GG) in the graph of the total and umbral areas of the large sunspot groups. Other databases do not show GG in their  $q$ -graphs, although GG exists in their temporal total area and umbral area.

### **Numerical Study on Emergence of Kinked Flux Tube for Understanding of Possible Origin of Delta-spot Regions**

Shinsuke [Takasao](#), Yuhong Fan, Mark C. M. Cheung, and Kazunari Shibata

ApJ

2015

<http://arxiv.org/pdf/1511.02863v1.pdf>

We carried out a magnetohydrodynamics simulation where a subsurface twisted kink-unstable flux tube emerges from the solar interior to the corona. Unlike the previous expectations based on the bodily emergence of a knotted tube, we found that the kinked tube can spontaneously form a complex quadrupole structure at the photosphere. Due to the development of the kink instability before the emergence, the magnetic twist at the kinked apex of the tube is greatly reduced, although the other parts of the tube is still strongly twisted. This leads to the formation of a complex quadrupole structure: a pair of the coherent, strongly twisted spots and a narrow complex bipolar pair between it. The quadrupole is formed by the submergence of a portion of emerged magnetic fields. This result is relevant for understanding of the origin of the complex multipolar delta-spot regions that have a strong magnetic shear and emerge with polarity orientations not following Hale-Nicholson and Joy Laws.

## Coronal Heating Driven by a Magnetic Gradient Pumping Mechanism in Solar Plasmas

Baolin **Tan**

2014 ApJ 795 140

The heating of the solar corona is a longstanding mystery in astrophysics. Considering that the solar magnetic field is spatially inhomogeneous with a considerable magnetic gradient from the solar surface to the corona, this work proposes a magnetic gradient pumping (MGP) mechanism to try to explain the formation of hot plasma upflows, such as hot type II spicules and hot plasma ejections. In the MGP mechanism, the magnetic gradient may drive the energetic particles to move upward from the underlying solar atmosphere and form hot upflows. These upflow energetic particles are deposited in the corona, causing it to become very hot. Rough estimations indicate that the solar corona can be heated to above 1 million degrees, and the upflow velocity is about  $40\text{ km s}^{-1}$  in the chromosphere and about  $130\text{ km s}^{-1}$  in the corona. The solar magnetic flux tubes act as pumpers to extract energetic particles from the underlying thermal photosphere, convey them, and deposit them in the corona. The deposit of these energetic particles causes the corona to become hot, and the escape of such particles from the photosphere leaves it a bit cold. This mechanism can present a natural explanation to the mystery of solar coronal heating.

## The Extended Solar Cycle Tracked High into the Corona

S. J. **Tappin**, R. C. Altrock

Solar Physics, January 2013, Volume 282, Issue 1, pp 249-261

We present observations of the extended solar cycle activity in white-light coronagraphs, and compare them with the more familiar features seen in the Fe xiv green-line corona. We show that the coronal activity zones seen in the emission corona can be tracked high into the corona. The peak latitude of the activity, which occurs near solar maximum, is found to be very similar at all heights. But we find that the equatorward drift of the activity zones is faster at greater heights, and that during the declining phase of the solar cycle, the lower branch of activity (that associated with the current cycle) disappears at about  $3R_{\odot}$ . This implies that during the declining phase of the cycle, the solar wind detected near Earth is likely to be dominated by the next cycle. The so-called “rush to the poles” is also seen in the higher corona. In the higher corona it is found to start at a similar time but at lower latitudes than in the green-line corona. The structure is found to be similar to that of the equatorward drift.

## QSL Squasher: A Fast Quasi-separatrix Layer Map Calculator

Svetlin **Tassev**<sup>1,2</sup> and Antonia Savcheva

2017 ApJ 840 89

<http://sci-hub.cc/10.3847/1538-4357/aa6f06>

Quasi-Separatrix Layers (QSLs) are a useful proxy for the locations where current sheets can develop in the solar corona, and give valuable information about the connectivity in complicated magnetic field configurations. However, calculating QSL maps, even for two-dimensional slices through three-dimensional models of coronal magnetic fields, is a non-trivial task, as it usually involves tracing out millions of magnetic field lines with immense precision. Thus, extending QSL calculations to three dimensions has rarely been done until now. In order to address this challenge, we present QSLSquasher—a public, open-source code, which is optimized for calculating QSL maps in both two and three dimensions on graphics processing units. The code achieves large processing speeds for three reasons, each of which results in an order-of-magnitude speed-up. (1) The code is parallelized using OpenCL. (2) The precision requirements for the QSL calculation are drastically reduced by using perturbation theory. (3) A new boundary detection criterion between quasi-connectivity domains is used, which quickly identifies possible QSL locations that need to be finely sampled by the code. That boundary detection criterion relies on finding the locations of abrupt field-line length changes, which we do by introducing a new Field-line Length Edge (FLEDGE) map. We find FLEDGE maps useful on their own as a quick-and-dirty substitute for QSL

maps. QSL Squasher allows construction of high-resolution 3D FLEDGE maps in a matter of minutes, which is two orders of magnitude faster than calculating the corresponding 3D QSL maps. We include a sample of calculations done using QSL Squasher to demonstrate its capabilities as a QSL calculator, as well as to compare QSL and FLEDGE maps.

## **Bipolar solar magnetic fields**

### **Behaviors resulting from a nonlinear force-free equation**

R. C. **Tautz**<sup>1</sup> and I. Lerche

A&A 581, A6 (2015)

**Aims.** Understanding magnetic fields in the solar corona is closely related to the complex nature of the often nonlinear differential equations describing such structures. Based on the ansatz of force-free fields, a class of solutions is derived and discussed that allows for axisymmetric bipolar magnetic fields.

**Methods.** Allowed dipolar solutions for self-similar axisymmetric force-free magnetic fields use the formalism of a Grad-Shafranov equation involving the vector potential. For separable solutions involving poloidal fields decaying radially as  $r^{-n}$ , there are no dipolar field structures for the decay index  $n \geq 1$ .

**Results.** In the domain  $n < 1$  dipolar field structures are possible in restricted ranges of the angular coordinate  $\theta$  depending on the value for  $n$ . Outside of the restricted domains there are no dipolar solutions, but there can be multipole solutions. The limiting case of the parameter  $n \rightarrow 0$  has been discussed previously, so that now the full regime  $0 \leq n < \infty$  is covered.

## **Oscillations in solar Jets Observed with the SOT of Hinode: Viscous Effects during Reconnection**

Ehsan **Tavabi**, Serge Koutchmy

2014

<http://arxiv.org/pdf/1403.0814v1.pdf>

Transverse oscillatory motions and recurrence behavior in the chromospheric jets observed by Hinode/SOT are studied. A comparison is considered with the behavior that was noticed in coronal X-ray jets observed by Hinode/XRT. A jet like bundle observed at the limb in Ca II H line appears to show a magnetic topology that is similar to X-ray jets (i.e., the Eiffel tower shape). The appearance of such magnetic topology is usually assumed to be caused by magnetic reconnection near a null point. Transverse motions of the jet axis are recorded but no clear evidence of twist is appearing from the highly processed movie. The aim is to investigate the dynamical behavior of an incompressible magnetic X-point occurring during the magnetic reconnection in the jet formation region. The viscous effect is specially considered in the closed line-tied magnetic X-shape nulls. We perform the MHD numerical simulation in 2-D by solving the visco-resistive MHD equations with the tracing of velocity and magnetic field. A qualitative agreement with Hinode observations is found for the oscillatory and non-oscillatory behaviors of the observed solar jets in both the chromosphere and the corona. Our results suggest that the viscous effect contributes to the excitation of the magnetic reconnection by generating oscillations that we observed at least inside this Ca II H line cool solar jet bundle.

2007 July 08, 2009-March-14

## **Effect of Size of the Computational Domain on Spherical Nonlinear Force-Free Modeling of Coronal Magnetic Field Using SDO/HMI Data**

Tilaye **Tadesse**, Thomas Wiegelmann, Peter MacNeice

Solar Phys., 2014

<http://arxiv.org/pdf/1409.1775v1.pdf>

The solar coronal magnetic field produces solar activity, including extremely energetic solar flares and coronal mass ejections (CMEs). Knowledge of the structure and evolution of the magnetic field of the solar corona is important for investigating and understanding the origins of space weather. Although the coronal field remains difficult to measure directly, there is considerable interest in accurate modeling of magnetic fields in and around sunspot regions on the Sun using photospheric vector magnetograms as boundary data. In this work, we investigate effects of the size of the domain chosen for coronal magnetic field modeling on resulting model solution. We apply spherical Optimization procedure to vector magnetogram data of Helioseismic and Magnetic Imager (HMI) onboard Solar Dynamics Observatory (SDO) with four Active Region observed on **09 March 2012** at 20:55UT. The results imply that quantities like magnetic flux density, electric current density and free magnetic energy density of ARs of interest are significantly different from the corresponding quantities obtained in the same region within the wider field of view. The difference is even more pronounced in the regions where there are connections to outside the domain.

## **Global Solar Free Magnetic Energy and Electric Current Density Distribution of Carrington Rotation 2124**

Tilaye [Tadesse](#), Alexei A. Pevtsov, T. Wiegelmann, P. J. MacNeice, S. Gosain  
Solar Phys., 2014

Solar eruptive phenomena, like flares and coronal mass ejections (CMEs), are governed by magnetic fields. To describe the structure of these phenomena one needs information on the magnetic flux density and the electric current density vector components in three dimensions throughout the atmosphere. However, current spectro-polarimetric measurements typically limit the determination of the vector magnetic field to only the photosphere. Therefore, there is considerable interest in accurate modeling of the solar coronal magnetic field using photospheric vector magnetograms as boundary data. In this work, we model the coronal magnetic field for global solar atmosphere using nonlinear force-free field (NLFFF) extrapolation codes implemented to a synoptic maps of photospheric vector magnetic field synthesized from the Vector Spectromagnetograph (VSM) on Synoptic Optical Long-term Investigations of the Sun (SOLIS) as boundary condition. Using the resulting three-dimensional magnetic field, we calculate the three-dimensional electric current density and magnetic energy throughout the solar atmosphere for Carrington rotation 2124 using our global extrapolation code. We found that spatially, the low-lying, current-carrying core field demonstrates a strong concentration of free energy in the active-region core, from the photosphere to the lower corona (about 70 Mm). The free energy density appears largely co-spatial with the electric current distribution.

## **Reconstructing solar magnetic fields from historical observations**

### **VIII. AIA 1600 Å contrast as a proxy of solar magnetic fields**

I. [Tähtinen](#)<sup>1</sup>, I. I. Virtanen<sup>1,2</sup>, A. A. Pevtsov<sup>3</sup> and K. Mursula<sup>1</sup>  
A&A 664, A2 (2022)

<https://www.aanda.org/articles/aa/pdf/2022/08/aa41164-21.pdf>

**Context.** The bright regions in the solar chromosphere and temperature minimum have a good spatial correspondence with regions of intense photospheric magnetic field. Bright regions are visible in different emission lines and parts of the continuum. Their observation started more than a hundred years ago with the invention of the spectroheliograph. While the historical spectroheliograms are essential for studying the long-term variability of the Sun, the modern satellite-borne observations can help us reveal the nature of chromospheric brightenings in previously unattainable detail.

**Aims.** Our aim is to improve the understanding of the relation between magnetic fields and radiative structures by studying modern seeing-free observations of far-ultraviolet (FUV) radiation around 1600 Å and photospheric magnetic fields.

**Methods.** We used Helioseismic and Magnetic Imager (HMI) observations of photospheric magnetic fields and Atmospheric Imaging Assembly (AIA) observations of FUV contrast around 1600 Å. We developed a robust method to find contrast thresholds defining bright and dark AIA 1600 Å pixels, and we combine them to bright and dark clusters. We investigate the relation of magnetic fields and AIA 1600 Å radiation in bright and dark clusters.

**Results.** We find that the percentage of bright pixels (ranging from 2% to 10%) almost entirely explains the observed variability of 1600 Å emission. We developed a multilinear regression model based on the percentages of bright and dark pixels, which can reliably predict the magnitude of the disk-averaged unsigned magnetic field. We find that bright and dark clusters closely correspond respectively to the populations of moderate ( $B > 55$  G) and strong ( $B > 1365$  G) magnetic field HMI clusters. The largest bright clusters have a constant mean unsigned magnetic field, as found previously for Ca II K plages. However, the magnetic field strength of bright clusters is  $254.7 \pm 0.1$  G, which is roughly 100 G larger than found earlier for Ca II K plages.

## **Complex Network View of the Sun's Magnetic Patches: I. Identification**

[Zahra Tajik](#), [Nastaran Frahang](#), [Hossein Safari](#), [Michael S. Wheatland](#)

2023

<https://arxiv.org/pdf/2307.15523.pdf>

Solar and stellar magnetic patches (i.e., magnetic fluxes that reach the surface from the interior) are believed to be the primary sources of a star's atmospheric conditions. Hence, detecting and identifying these features (also known as magnetic elements) are among the essential topics in the community. Here, we apply the complex network approach to recognize the solar magnetic patches. For this purpose, we use the line-of-sight magnetograms provided by the Helioseismic and Magnetic Imager on board the Solar Dynamic Observatory. We construct the magnetic network following a specific visibility graph condition between pairs of pixels with opposite polarities and search for possible links between these regions. The complex network approach also provides the ability to rank the patches based on their connectivity (i.e., degree of nodes) and importance (i.e., PageRank). The use of the developed algorithm in the identification of magnetic patches is examined by tracking the features in consecutive frames, as well as making a comparison with the other approaches to identification. We find that this method could

conveniently identify features regardless of their sizes. For small-scale (one or two pixels) features, we estimate the average of 8% false-positive and 1% false-negative errors. **January 17, 2022, July 12, 2022**

## **Temporal and Latitudinal Variation in Penumbra-Umbra Ratios of the Sunspots: Analyses of RGO, Kodaikanal and Debrecen Databases**

Jouni **Takalo**

[Solar Physics](#) volume 298, Article number: 63 (2023)

<https://link.springer.com/content/pdf/10.1007/s11207-023-02161-2.pdf>

We study the latitudinal distribution and temporal evolution of the sunspot penumbra-umbra ratio ( $q$ ) for the even and odd Solar Cycles 12 – 24 of RGO sunspot groups, SC21 – SC24 of Debrecen sunspot groups and Kodaikanal sunspot dataset for SC16 – SC24. We find that RGO even (odd) Cycles have  $q$ -values 5.20 (4.75), Kodaikanal even (odd) cycles have  $q$ -values 5.27 (5.43), and Debrecen cycles have  $q$ -value 5.74 on the average.

We also show that  $q$  is at its lowest around the Equator of the Sun and increases towards higher latitudes having maximum values at about 10 – 25 degrees. This is understandable because smaller sunspots and groups locate nearer to the Equator and have smaller  $q$ -values than larger sunspots and groups, which maximize at about 10 – 20 degrees at both hemispheres. The error limits are very wide, and, thus, the confidence in this result is somewhat vague.

For the Debrecen dataset, we find a deep valley in the temporal  $q$ -values before the middle of the cycle. We show that this exists simultaneously with the Gnevyshev gap (GG) in the graph of the total and umbral areas of the large sunspot groups. Other databases do not show GG in their  $q$ -graphs, although GG exists in their temporal total area and umbral area.

## **Principal component analysis of sunspot cycle shape**

Jouni **Takalo**, [Kalevi Mursula](#)

A&A 620, A100 2018

<https://arxiv.org/pdf/1810.08583.pdf>

We study the shape of sunspot cycles using the Wolf sunspot numbers and group sunspot numbers of solar cycles 1-23. We determine the most typical "model" cycles and the most asymmetric cycles, and test the validity of the two Waldmeier rules: the anti-correlation between cycle height and the length of its ascending phase (rule 1), and between cycle height and the length of the preceding cycle (rule 2). We applied the principal component analysis to sunspot cycles and studied the first two components, which describe the average cycle shape and cycle asymmetry, respectively. We also calculated their autocorrelation in order to study their recurrence properties. The best model cycles for Wolf numbers are SC12, SC14, and SC16, the successive even cycles from a long period of rather low overall solar activity. We find that the model cycles in eight different analyses using both sunspot series are almost exclusively even cycles. Correspondingly, the most asymmetric cycles are odd cycles. We find that both Waldmeier rules are valid for the whole Wolf number series of 23 cycles. Waldmeier rule 2 is also valid for group number series although its significance is weaker. Waldmeier rule 1 is not significant for the original group number series, but becomes significant for the proxy series. For separate centuries, Waldmeier rules are not always valid for Wolf numbers and very rarely for group numbers. Our results also offer a new interpretation for the Gnevyshev gap. In addition to being a local depression of solar activity, the Gnevyshev gap is a separatrix that divides cycles into two parts whose relative intensities determine the cycle asymmetry. The Gnevyshev gap is the zero value time of PC2, located approximately 33-42% into the cycle after its start.

## **NUMERICAL STUDY ON THE EMERGENCE OF KINKED FLUX TUBE FOR UNDERSTANDING OF POSSIBLE ORIGIN OF $\delta$ -SPOT REGIONS**

Shinsuke **Takasao**<sup>1</sup>, Yuhong Fan<sup>2</sup>, Mark C. M. Cheung<sup>3</sup>, and Kazunari Shibata

2015 ApJ 813 112

<http://arxiv.org/pdf/1511.02863v1.pdf>

We carried out an magnetohydrodynamic simulation where a subsurface twisted kink-unstable flux tube emerges from the solar interior to the corona. Unlike the previous expectations based on the bodily emergence of a knotted tube, we found that the kinked tube can spontaneously form a complex quadrupole structure at the photosphere. Due to the development of the kink instability before the emergence, the magnetic twist at the kinked apex of the tube is greatly reduced, although the other parts of the tube are still strongly twisted. This leads to the formation of a complex quadrupole structure: a pair of the coherent, strongly twisted spots and a narrow complex bipolar pair between it. The quadrupole is formed by the submergence of a portion of emerged magnetic fields. This result is relevant for understanding the origin of the complex multipolar  $\delta$ -spot regions that have a strong magnetic shear and emerge with polarity orientations not following Hale-Nicholson and Joy Laws.

## **Coronal heating in multiple magnetic threads**

K. V. **Tam**, A. W. Hood, P. K. Browning, P. J. Cargill

A&A **2015**

<http://arxiv.org/pdf/1507.00259v1.pdf>

Context. Heating the solar corona to several million degrees requires the conversion of magnetic energy into thermal energy. In this paper, we investigate whether an unstable magnetic thread within a coronal loop can destabilise a neighbouring magnetic thread.

Aims. By running a series of simulations, we aim to understand under what conditions the destabilisation of a single magnetic thread can also trigger a release of energy in a nearby thread.

Methods. The 3D magnetohydrodynamics code, Lare3d, is used to simulate the temporal evolution of coronal magnetic fields during a kink instability and the subsequent relaxation process. We assume that a coronal magnetic loop consists of non-potential magnetic threads that are initially in an equilibrium state.

Results. The non-linear kink instability in one magnetic thread forms a helical current sheet and initiates magnetic reconnection. The current sheet fragments, and magnetic energy is released throughout that thread. We find that, under certain conditions, this event can destabilise a nearby thread, which is a necessary requirement for starting an avalanche of energy release in magnetic threads.

Conclusions. It is possible to initiate an energy release in a nearby, non-potential magnetic thread, because the energy released from one unstable magnetic thread can trigger energy release in nearby threads, provided that the nearby structures are close to marginal stability.

### **Stereoscopic investigation on plasma density fluctuations in the outer solar corona**

D. **Telloni**<sup>1</sup>, E. Antonucci<sup>1</sup>, S. Dolei<sup>2</sup>, P. Romano<sup>2</sup>, D. Spadaro<sup>2</sup> and R. Ventura

A&A 565, A22 (2014)

This research note extends a previous work focused on the 2D reconstruction of the spatial distribution and temporal evolution of the plasma density fluctuations in the outer solar corona and based on STEREO COR1-A white-light observations. By using the corresponding total brightness images obtained in the same observational period with the coronagraph COR1-B onboard the “Behind” twin STEREO-B spacecraft, and adopting the same methodological approach as for COR1-A data, it was possible to confirm the results of the previous work and argue for the 3D configuration of the fluctuations of the coronal plasma. This provides further evidence in support of a scenario in which the fluctuating features, which are recurrent and spatially coherent, are localized along the magnetic field lines and points out the crucial role played by the 3D magnetic field topology in the confinement and evolution of the plasma density fluctuations.

### **DETECTION OF PLASMA FLUCTUATIONS IN WHITE-LIGHT IMAGES OF THE OUTER SOLAR CORONA: INVESTIGATION OF THE SPATIAL AND TEMPORAL EVOLUTION.**

**Telloni**<sup>1</sup>, R. Ventura<sup>2</sup>, P. Romano<sup>2</sup>, D. Spadaro<sup>2</sup>, and E. Antonucci

2013 ApJ 767 138

This work focuses on the first results from the identification and characterization of periodic plasma density fluctuations in the outer corona, observed in STEREO-A COR1 white-light image time series. A two-dimensional reconstruction of the spatial distribution and temporal evolution of the coronal fluctuation power has been performed over the whole plane of the sky, from 1.4 to 4.0 R<sub>⊙</sub>. The adopted diagnostic tool is based on wavelet transforms. This technique, with respect to the standard Fourier analysis, has the advantage of localizing non-persistent fluctuating features and exploring variations of the relating wavelet power in both space and time. The map of the variance of the coronal brightness clearly outlines intermittent spatially coherent fluctuating features, localized along, or adjacent to, the strongest magnetic field lines. In most cases, they do not correspond to the visible coronal structures in the brightness maps. The results obtained provide a scenario in which the solar corona shows quasi-periodic, non-stationary density variations characterized by a wide range of temporal and spatial scales and strongly confined by the magnetic field topology. In addition, structures fluctuating with larger power are larger in size and evolve more slowly. The characteristic periodicities of the fluctuations are comparable to their lifetimes. This suggests that plasma fluctuations lasting only one or two wave periods and initially characterized by a single dominant periodicity either rapidly decay into a turbulent mixed flow via nonlinear interactions with other plasma modes, or they are damped by thermal conduction. The periodic non-stationary coronal fluctuations outlined by the closed field lines at low and mid latitudes might be associated with the existence of slow standing magneto-acoustic waves excited by the convective supergranular motion. The fluctuating ray-like structures observed along open field lines appear to be linked either to the intermittent nature of the processes underlying the generation of magnetic reconnection in the polar regions or to the oscillatory transverse displacements of the coronal ray itself.

### **Application of Kernel Based Machine Learning to Inversion Problem of Photospheric Magnetic Fields**



Fei **Teng**

Solar Phys. Volume 290, Issue 10, pp 2693-2708 **2015**

For the purpose of fast methods to handle huge amount of data coming from future solar spectropolarimeter, the statistical machine learning techniques based on Mercer's kernel have been applied to the inversion of the photospheric magnetic fields from the polarimetric data. In particular, the Regularized Neural Network and the Support Vector Machine have been tested for the data from HMI (Helioseismic and Magnetic Imager) on SDO (Solar Dynamics Observatory).

## **The Cosmic-Ray Shadow and Coronal Magnetism**

Frederik **Tenholt**

RHESSI Nuggets #351 May **2019**

[http://sprg.ssl.berkeley.edu/~tohban/wiki/index.php/The\\_Cosmic-Ray\\_Shadow\\_and\\_Coronal\\_Magnetism](http://sprg.ssl.berkeley.edu/~tohban/wiki/index.php/The_Cosmic-Ray_Shadow_and_Coronal_Magnetism)

The cosmic-ray shadow of the Sun as measured by several experiments is a relatively new, but powerful diagnostic tool for evaluating different models of the coronal magnetic field close to the Sun. An energy-dependent measurement of the shadow even further enhances the possibilities for quantitative studies.

## **INVESTIGATING THE RELIABILITY OF CORONAL EMISSION MEASURE DISTRIBUTION DIAGNOSTICS USING THREE-DIMENSIONAL RADIATIVE MAGNETOHYDRODYNAMIC SIMULATIONS**

Paola **Testa**<sup>1</sup>, Bart De Pontieu<sup>2</sup>, Juan Martínez-Sykora<sup>2,3</sup>, Viggo Hansteen<sup>3</sup>, and Mats Carlsson  
**2012 ApJ 758 54**

Determining the temperature distribution of coronal plasmas can provide stringent constraints on coronal heating. Current observations with the Extreme ultraviolet Imaging Spectrograph (EIS) on board Hinode and the Atmospheric Imaging Assembly (AIA) on board the Solar Dynamics Observatory provide diagnostics of the emission measure distribution (EMD) of the coronal plasma. Here we test the reliability of temperature diagnostics using three-dimensional radiative MHD simulations. We produce synthetic observables from the models and apply the Monte Carlo Markov chain EMD diagnostic. By comparing the derived EMDs with the "true" distributions from the model, we assess the limitations of the diagnostics as a function of the plasma parameters and the signal-to-noise ratio of the data. We find that EMDs derived from EIS synthetic data reproduce some general characteristics of the true distributions, but usually show differences from the true EMDs that are much larger than the estimated uncertainties suggest, especially when structures with significantly different density overlap along the line of sight. When using AIA synthetic data the derived EMDs reproduce the true EMDs much less accurately, especially for broad EMDs. The differences between the two instruments are due to the: (1) smaller number of constraints provided by AIA data and (2) broad temperature response function of the AIA channels which provide looser constraints to the temperature distribution. Our results suggest that EMDs derived from current observatories may often show significant discrepancies from the true EMDs, rendering their interpretation fraught with uncertainty. These inherent limitations to the method should be carefully considered when using these distributions to constrain coronal heating.

## **Flux canceling in three-dimensional radiative magnetohydrodynamic simulations**

Irina **Thaler**<sup>1,2</sup> and H. C. Spruit

A&A 601, A88 (**2017**)

We aim to study the processes involved in the disappearance of magnetic flux between regions of opposite polarity on the solar surface using realistic three-dimensional (3D) magnetohydrodynamic (MHD) simulations. "Retraction" below the surface driven by magnetic forces is found to be a very effective mechanism of flux canceling of opposite polarities. The speed at which flux disappears increases strongly with initial mean flux density. In agreement with existing inferences from observations we suggest that this is a key process of flux disappearance within active complexes. Intrinsic kG strength concentrations connect the surface to deeper layers by magnetic forces, and therefore the influence of deeper layers on the flux canceling process is studied. We do this by comparing simulations extending to different depths. For average flux densities of 50 G, and on length scales on the order of 3 Mm in the horizontal and 10 Mm in depth, deeper layers appear to have only a mild influence on the effective rate of diffusion.

## **Brightness of the Sun's small scale magnetic field: proximity effects**

I. **Thaler**, H.C. Spruit

A&A 566, A11, **2014**

<http://arxiv.org/pdf/1404.2871v1.pdf>

The net effect of the small scale magnetic field on the Sun's (bolometric) brightness is studied with realistic 3D MHD simulations. The direct effect of brightening within the magnetic field itself is consistent with measurements

in high-resolution observations. The high 'photometric accuracy' of the simulations, however, reveal compensating brightness effects that are hard to detect observationally. The influence of magnetic concentrations on the surrounding nonmagnetic convective flows (a 'proximity effect') reduces the brightness by an amount exceeding the brightening by the magnetic concentrations themselves. The net photospheric effect of the small scale field ( $\sim -0.34\%$  at a mean flux density of 50 G) is thus negative. We conclude that the main contribution to the observed positive correlation between the magnetic field and total solar irradiance must be magnetic dissipation in layers around the temperature minimum and above (not included in the simulations). This agrees with existing inferences from observations.

### **The effect of spatial resolution on magnetic field modeling and helicity computation**

[J. K. Thalmann](#), [Manu Gupta](#), [A. M. Veronig](#)

A&A 662, A3 2022

<https://arxiv.org/pdf/2204.09267>

<https://www.aanda.org/articles/aa/pdf/2022/06/aa43222-22.pdf>

Nonlinear force-free (NLFF) modeling is regularly used in order to indirectly infer the 3D geometry of the coronal magnetic field, not accessible on a regular basis by means of direct measurements otherwise. We study the effect of binning in time series NLFF modeling of individual active regions (ARs) in order to quantify the effect of a different underlying spatial resolution on the quality of modeling as well as on the derived physical parameters. We apply an optimization method to sequences of SDO/HMI vector magnetogram data at three different spatial resolutions for three solar ARs to obtain nine NLFF model time series. From the NLFF models, we deduce active-region magnetic fluxes, electric currents, magnetic energies and relative helicities, and analyze those with respect to the underlying spatial resolution. We calculate various metrics to quantify the quality of the derived NLFF models and apply a Helmholtz decomposition to characterize solenoidal errors. At a given spatial resolution, the quality of NLFF modeling is different for different ARs, as well as varies along of the individual model time series. For a given AR, modeling at a given spatial resolution is not necessarily of superior quality compared to that performed at different spatial resolutions at all time instances of a NLFF model time series. Generally, the NLFF model quality tends to be higher at reduced spatial resolution with the solenoidal quality being the ultimate cause for systematic variations in model-deduced physical quantities. Optimization-based modeling based on binned SDO/HMI vector data delivers magnetic energies and helicity estimates different by  $\lesssim 30\%$ , given that concise checks ensure the physical plausibility and high solenoidal quality of the tested model. Spatial-resolution induced differences are relatively small compared to that arising from other sources of uncertainty.

### **Magnetic helicity estimations in models and observations of the solar magnetic field. Part IV: Application to solar observations**

[J. K. Thalmann](#), [M. K. Georgoulis](#), [Y. Liu](#), [E. Pariat](#), [G. Valori](#), [S. Anfinogentov](#), [F. Chen](#), [Y. Guo](#), [K. Moraitis](#), [S. Yang](#), [A. Mastrano](#)

ApJ 2021

<https://arxiv.org/pdf/2108.08525.pdf>

In this ISSI-supported series of studies on magnetic helicity in the Sun, we systematically implement different magnetic helicity calculation methods on high-quality solar magnetogram observations. We apply finite-volume, discrete flux tube (in particular, connectivity-based) and flux-integration methods to data from Hinode's Solar Optical Telescope. The target is NOAA active region 10930 during a  $\sim 1.5$  day interval in December 2006 that included a major eruptive flare (SOL2006-12-13T02:14X3.4). Finite-volume and connectivity-based methods yield instantaneous budgets of the coronal magnetic helicity, while the flux-integration methods allow an estimate of the accumulated helicity injected through the photosphere. The objectives of our work are twofold: A cross-validation of methods, as well as an interpretation of the complex events leading to the eruption. To the first objective, we find (i) strong agreement among the finite-volume methods, (ii) a moderate agreement between the connectivity-based and finite-volume methods, (iii) an excellent agreement between the flux-integration methods, and (iv) an overall agreement between finite-volume and flux-integration based estimates regarding the predominant sign and magnitude of the helicity. To the second objective, we are confident that the photospheric helicity flux significantly contributed to the coronal helicity budget, and that a right-handed structure erupted from a predominantly left-handed corona during the X-class flare. Overall, we find that the use of different methods to estimate the (accumulated) coronal helicity may be necessary in order to draw a complete picture of an active-region corona, given the careful handling of identified data (preparation) issues, which otherwise would mislead the event analysis and interpretation.

### **On the reliability of magnetic energy and helicity computations based on nonlinear force-free coronal magnetic field models**

Julia K. [Thalmann](#), [Luis Linan](#), [Etienne Pariat](#), [Gherardo Valori](#)

ApJL 880 L6 2019

<https://arxiv.org/pdf/1907.01179.pdf>  
[sci-hub.se/10.3847/2041-8213/ab2e73](https://sci-hub.se/10.3847/2041-8213/ab2e73)

We demonstrate the sensitivity of magnetic energy and helicity computations regarding the quality of the underlying coronal magnetic field model. We apply the method of Wiegmann & Inhester (2010) to a series of SDO/HMI vector magnetograms, and discuss nonlinear force-free (NLFF) solutions based on two different sets of the free model parameters. The two time series differ from each other concerning their force-free and solenoidal quality. Both force- and divergence-freeness are required for a consistent NLFF solution. Full satisfaction of the solenoidal property is inherent in the definition of relative magnetic helicity in order to insure gauge-independence. We apply two different magnetic helicity computation methods (Thalmann et al. 2011; Valori et al. 2012) to both NLFF time series and find that the output is highly dependent on the level to which the NLFF magnetic fields satisfy the divergence-free condition, with the computed magnetic energy being less sensitive than the relative helicity. Proxies for the non-potentiality and eruptivity derived from both quantities are also shown to depend strongly on the solenoidal property of the NLFF fields. As a reference for future applications, we provide quantitative thresholds for the force- and divergence-freeness, for the assurance of reliable computation of magnetic energy and helicity, and of their related eruptivity proxies. **2011 February 12 to 16**

**Erratum:** 2020 ApJL 902 L48 <https://iopscience.iop.org/article/10.3847/2041-8213/abbfa4/pdf>

## **Temporal and spatial relationship of flare signatures and the force-free coronal magnetic field**

Julia K. **Thalmann**, Astrid M. Veronig, Yang Su

ApJ **2016**

<http://arxiv.org/pdf/1605.03703v1.pdf>

We investigate the plasma and magnetic environment of active region NOAA 11261 on **2 August 2011** around a GOES M1.4 flare/CME (SOL2011-08-02T06:19). We compare coronal emission at (extreme) ultraviolet and X-ray wavelengths, using SDO AIA and RHESSI images, in order to identify the relative timing and locations of reconnection-related sources. We trace flare ribbon signatures at ultraviolet wavelengths, in order to pin down the intersection of previously reconnected flaring loops at the lower solar atmosphere. These locations are used to calculate field lines from 3D nonlinear force-free magnetic field models, established on the basis of SDO HMI photospheric vector magnetic field maps. With this procedure, we analyze the quasi-static time evolution of the coronal model magnetic field previously involved in magnetic reconnection. This allows us, for the first time, to estimate the elevation speed of the current sheet's lower tip during an on-disk observed flare, as a few kilometers per second. Comparison to post-flare loops observed later above the limb in STEREO EUVI images supports this velocity estimate. Furthermore, we provide evidence for an implosion of parts of the flaring coronal model magnetic field, and identify the corresponding coronal sub-volumes associated to the loss of magnetic energy. Finally, we spatially relate the build up of magnetic energy in the 3D models to highly sheared fields, established due to dynamic relative motions of polarity patches within the active region.

## **Force-free field modeling of twist and braiding-induced magnetic energy in an active-region corona**

**Thalmann**, J. K., Tiwari, S. K., Wiegmann, T.

E-print, Nov **2013**; **2014** ApJ 780 102

The theoretical concept that braided magnetic field lines in the solar corona may dissipate a sufficient amount of energy to account for the brightening observed in the active-region corona, has been substantiated by high-resolution observations only recently. From the analysis of coronal images obtained with the High Resolution Coronal Imager, first observational evidence of the braiding of magnetic field lines was reported by Cirtain et al. 2013 (hereafter CG13). We present nonlinear force-free reconstructions of the associated coronal magnetic field based on vector SDO/HMI magnetograms. We deliver estimates of the free magnetic energy associated to a braided coronal structure. Our model results suggest (~100 times) more free energy at the braiding site than analytically estimated by CG13, strengthening the possibility of the active-region corona being heated by field line braiding. We were able to assess the coronal free energy appropriately by using vector field measurements and attribute the lower energy estimate of CG13 to the underestimated (by a factor of 10) azimuthal field strength. We also quantify the increase of the overall twist of a flare-related flux rope which had been claimed by CG13. From our models we find that the overall twist of the flux rope increased by about half a turn within twelve minutes. Unlike another method, to which we compare our results to, we evaluate the winding of the flux rope's constituent field lines around each other purely based on their modeled coronal 3D field line geometry - to our knowledge for the first time.

## COMPARISON OF FORCE-FREE CORONAL MAGNETIC FIELD MODELING USING VECTOR FIELDS FROM HINODE AND SOLAR DYNAMICS OBSERVATORY

J. K. [Thalmann](#), S. K. Tiwari, and T. Wiegelmann

2013 ApJ 769 59

Photospheric magnetic vector maps from two different instruments are used to model the nonlinear force-free coronal magnetic field above an active region. We use vector maps inferred from polarization measurements of the Solar Dynamics Observatory/Helioseismic and Magnetic Imager (HMI) and the Solar Optical Telescope's Spectropolarimeter (SP) on board Hinode. Besides basing our model calculations on HMI data, we use both SP data of original resolution and scaled down to the resolution of HMI. This allows us to compare the model results based on data from different instruments and to investigate how a binning of high-resolution data affects the model outcome. The resulting three-dimensional magnetic fields are compared in terms of magnetic energy content and magnetic topology. We find stronger magnetic fields in the SP data, translating into a higher total magnetic energy of the SP models. The net Lorentz forces of the HMI and SP lower boundaries verify their force-free compatibility. We find substantial differences in the absolute estimates of the magnetic field energy but similar relative estimates, e.g., the fraction of excess energy and of the flux shared by distinct areas. The location and extension of neighboring connectivity domains differ and the SP model fields tend to be higher and more vertical. Hence, conclusions about the magnetic connectivity based on force-free field models are to be drawn with caution. We find that the deviations of the model solution when based on the lower-resolution SP data are small compared to the differences of the solutions based on data from different instruments.

## Estimating the Relative Helicity of Coronal Magnetic Fields

J. K. [Thalmann](#), B. Inhester and T. Wiegelmann

Solar Physics, Volume 272, Number 2, 243-255, 2011

To quantify changes of the solar coronal field connectivity during eruptive events, one can use magnetic helicity, which is a measure of the shear or twist of a current-carrying (non-potential) field. To find a physically meaningful quantity, a relative measure, giving the helicity of a current-carrying field with respect to a reference (potential) field, is often evaluated. This requires a knowledge of the three-dimensional vector potential. We present a method to calculate the vector potential for a solenoidal magnetic field as the sum of a Laplacian part and a current-carrying part. The only requirements are the divergence freeness of the Laplacian and current-carrying magnetic field and the sameness of their normal field component on the bounding surface of the considered volume.

## First nonlinear force-free field extrapolations of SOLIS/VSM data

J. K. [Thalmann](#), T. Wiegelmann, and N.-E. Raouafi

E-print, Aug 2008; A&A Let.

We study the coronal magnetic field structure inside active regions and its temporal evolution. We attempt to compare the magnetic configuration of an active region in a very quiet period with that for the same region during a flare. Probably for the first time, we use vector magnetograph data from the Synoptic Optical Long-term Investigations of the Sun survey (SOLIS) to model the coronal magnetic field as a sequence of nonlinear force-free equilibria. We study the active region NOAA 10960 observed on **2007 June 7** with three snapshots taken during a small C1.0 flare of time cadence 10 minutes and six snapshots during a quiet period. The total magnetic energy in the active region was approximately  $3 \times 10^{25}$  J. Before the flare the free magnetic energy was about 5 % of the potential field energy. A part of this excess energy was released during the flare, producing almost a potential configuration at the beginning of the quiet period. During the investigated period, the coronal magnetic energy was only a few percent higher than that of the potential field and consequently only a small C1.0 flare occurred. This was compared with an earlier investigated active region 10540, where the free magnetic energy was about 60 % higher than that of the potential field producing two M-class flares. However, the free magnetic energy accumulates before and is released during the flare which appears to be the case for both large and small flares.

## Evolution of the flaring active region NOAA 10540 as a sequence of nonlinear force-free field extrapolations

J. K. [Thalmann](#) and T. Wiegelmann

A&A 484, 495-502 (2008)

<http://www.aanda.org/10.1051/0004-6361:200809508>

*Context.* The solar corona is structured by magnetic fields. As direct measurements of the coronal magnetic field are not routinely available, it is extrapolated from photospheric vector magnetograms. When magnetic flux emerges

from below the solar surface and expands into the corona, the coronal magnetic field is destabilized, leading to explosive phenomena like flares or coronal mass ejections.

*Aims.* We study the temporal evolution of the flaring active region NOAA 10540 and are in particular interested in the free magnetic energy available to power the flares associated with it.

*Methods.* We extrapolated photospheric vector magnetograms measured with the Solar Flare Telescope, located in Tokyo, into the corona with the help of a nonlinear force-free field model. This coronal magnetic field model is based on a well-tested multigrid-like optimization code with which we were able to estimate the energy content of the 3D coronal field, as well as an upper limit for its free magnetic energy. Furthermore, the evolution of the energy density with height and time was studied.

*Results.* The coronal magnetic field energy in active region 10540 increases slowly during the three days before an M6.1 flare and drops significantly after it. We estimated the energy that was set free during this event as  $\propto 10^{25}$  J. A sequence of nonlinear force-free extrapolations of the coronal magnetic field shows a build up of magnetic energy before a flare and release of energy during the flare. The drop in magnetic energy of the active region is sufficient to power an M6.1 flare.

## Differential Rotation of Individual Sunspots and Pores

[Andrei G. Tlatov](#), [Kseniia A. Tlatova](#)

ApJ **977** 110 **2024**

<https://arxiv.org/pdf/2411.06985>

<https://iopscience.iop.org/article/10.3847/1538-4357/ad90a0/pdf>

The analysis of the rotation rate of individual sunspots and pores was performed according to the data of the processing of observations by the Solar Dynamics Observatory/Helioseismic and Magnetic Imager (SDO/HMI) in the period 2010–2024. Sunspots stood out in the images in the continuum. To accurately track the spots, we processed 5 images for each day. To determine the polarity of the magnetic field, we superimposed the contours of sunspots on observations of magnetic fields at the same time. This made it possible to track the movement of more than 210 thousand individual sunspots and pores. It is found that the rotation rate is influenced by the rotation rate of the solar atmosphere and the systematic proper motions of the spots. Sunspots and pores of the leading polarity have a rate of meridional movement  $\approx 2.4\%$  faster than spots of the trailing polarity. We also found that regular sunspots, which have umbra and penumbra, rotate  $\approx 1.5\%$  faster than solar pores, in which penumbra is absent. The dependence of the rotation rate on these area is found. For sunspots with an area of  $S > 10 \mu\text{m}^2$ , the rotation rate is practically independent of these area. Small sunspots, with an area of lower than  $S < 10 \mu\text{m}^2$ , rotate  $\approx 1.7\%$  slower.

## Dark dots on the photosphere and counting of the sunspots index

[Andrey G. Tlatov](#)

Solar Phys. **2022**

<https://arxiv.org/pdf/2205.13142.pdf>

On modern satellite observations of the Sun in the continuum with high spatial resolution, as well as on high-quality ground observations, a large number of small dark areas can be observed. These regions have no penumbra, have a contrast of up to 20% and are similar to solar pores. The characteristic area of such structures is  $0.3 \div 5 \mu\text{m}^2$  or  $0.5 \div 5 \text{Mm}^2$ . The number of such points in one image can be several hundred. The nature of such formations remains unclear.

We have performed the selection of dark regions with a contrast of at least 3% of the level of the quiet Sun on the SDO/HMI observational data in the continuum for 2010–2020. We have studied the properties of "dark points", including the change with the cycle of activity, area distribution and contrast. We also compared such structures with the intensity of the magnetic field. We found that the number of dark dots with an area of less than  $5 \text{m}^2$ , in which the magnetic field is not significant and is less than  $|B| < 30 \text{G}$ , is from 60 to 80% of the total number of structures of this size. This means that these objects are not associated with magnetic activity. The existence of such structures can significantly affect the calculations of the sunspot index, since they can be mistaken as pores.

**2010.07.04**

## Frequently Occurring Reconnection Jets from Sunspot Light Bridges

Hui [Tian](#), [Vasyl Yurchyshyn](#), [Hardi Peter](#), [Sami K. Solanki](#), [Peter R. Young](#), [Lei Ni](#), [Wenda Cao](#), [Kaifan Ji](#), [Yingjie Zhu](#), [Jingwen Zhang](#), [Tanmoy Samanta](#), [Yongliang Song](#), [Jiansen He](#), [Linghua Wang](#), [Yajie Chen](#)

ApJ **854** 92 **2018**

<https://arxiv.org/pdf/1801.06802.pdf>

<http://sci-hub.tw/http://iopscience.iop.org/0004-637X/854/2/92/>

Solid evidence of magnetic reconnection is rarely reported within sunspots, the darkest regions with the strongest magnetic fields and lowest temperatures in the solar atmosphere. Using the world's largest solar telescope, the 1.6-meter Goode Solar Telescope, we detect prevalent reconnection through frequently occurring fine-scale jets in the

H $\alpha$  line wings at light bridges, the bright lanes that may divide the dark sunspot core into multiple parts. Many jets have an inverted Y-shape, shown by models to be typical of reconnection in a unipolar field environment. Simultaneous spectral imaging data from the Interface Region Imaging Spectrograph show that the reconnection drives bidirectional flows up to 200 km s<sup>-1</sup>, and that the weakly ionized plasma is heated by at least an order of magnitude up to  $\sim 80,000$  K. Such highly dynamic reconnection jets and efficient heating should be properly accounted for in future modeling efforts of sunspots. Our observations also reveal that the surge-like activity previously reported above light bridges in some chromospheric passbands such as the H $\alpha$  core has two components: the ever-present short surges likely to be related to the upward leakage of magnetoacoustic waves from the photosphere, and the occasionally occurring long and fast surges that are obviously caused by the intermittent reconnection jets. **2014 Oct 29**

### **High-resolution Observations of the Shock Wave Behavior for Sunspot Oscillations with the Interface Region Imaging Spectrograph**

H. [Tian](#), E. DeLuca, K. K. Reeves, S. McKillop, B. De Pontieu, J. Martínez-Sykora, M. Carlsson, V. Hansteen, L. Kleint, M. Cheung, L. Golub, S. Saar, P. Testa, M. Weber, J. Lemen, A. Title, P. Boerner, N. Hurlburt, T. D. Tarbell, J. P. Wuelser, C. Kankelborg, S. Jaeggli, S. W. McIntosh  
Astrophysical Journal, 786:137, **2014**

<http://arxiv.org/pdf/1404.6291v1.pdf>

We present the first results of sunspot oscillations from observations by the Interface Region Imaging Spectrograph. The strongly nonlinear oscillation is identified in both the slit-jaw images and the spectra of several emission lines formed in the transition region and chromosphere. We first apply a single Gaussian fit to the profiles of the Mgii 2796.35 Å, Cii 1335.71 Å, and Si iv 1393.76 Å lines in the sunspot. The intensity change is about 30%. The Doppler shift oscillation reveals a sawtooth pattern with an amplitude of about 10 km/s in Si iv. The Si iv oscillation lags those of Cii and Mgii by about 6 and 25 s, respectively. The line width suddenly increases as the Doppler shift changes from redshift to blueshift. However, we demonstrate that this increase is caused by the superposition of two emission components. We then perform detailed analysis of the line profiles at a few selected locations on the slit. The temporal evolution of the line core is dominated by the following behavior: a rapid excursion to the blue side, accompanied by an intensity increase, followed by a linear decrease of the velocity to the red side. The maximum intensity slightly lags the maximum blueshift in Si iv, whereas the intensity enhancement slightly precedes the maximum blueshift in Mgii. We find a positive correlation between the maximum velocity and deceleration, a result that is consistent with numerical simulations of upward propagating magnetoacoustic shock waves. **2013 September 2.**

### **TWO COMPONENTS OF THE SOLAR CORONAL EMISSION REVEALED BY EXTREME-ULTRAVIOLET SPECTROSCOPIC OBSERVATIONS**

Hui [Tian](#)<sup>1</sup>, Scott W. McIntosh<sup>1</sup>, Bart De Pontieu<sup>2</sup>, Juan Martínez-Sykora<sup>2,3</sup>, Marybeth Sechler<sup>1</sup> and Xin Wang  
2011 ApJ 738 18, **2011**

Recent spectroscopic observations have revealed the ubiquitous presence of blueward asymmetries of emission lines formed in the solar corona and transition region. These asymmetries are most prominent in loop footpoint regions, where a clear correlation of the asymmetry with the Doppler shift and line width determined from the single-Gaussian fit is found. Such asymmetries suggest at least two emission components: a primary component accounting for the background emission and a secondary component associated with high-speed upflows. The latter has been proposed to play a vital role in the coronal heating process and there is no agreement on its properties. Here we slightly modify the initially developed technique of red-blue (RB) asymmetry analysis and apply it to both artificial spectra and spectra observed by the Extreme-ultraviolet Imaging Spectrometer on board Hinode, and demonstrate that the secondary component usually contributes a few percent of the total emission, and has a velocity ranging from 50 to 150 km s<sup>-1</sup> and a Gaussian width comparable to that of the primary one in loop footpoint regions. The results of the RB asymmetry analysis are then used to guide a double-Gaussian fit and we find that the obtained properties of the secondary component are generally consistent with those obtained from the RB asymmetry analysis. Through a comparison of the location, relative intensity, and velocity distribution of the blueward secondary component with the properties of the upward propagating disturbances revealed in simultaneous images from the Atmospheric Imaging Assembly on board the Solar Dynamics Observatory, we find a clear association of the secondary component with the propagating disturbances.

### **UPFLOWS IN FUNNEL-LIKE LEGS OF CORONAL MAGNETIC LOOPS**

Hui [Tian](#)<sup>1,2</sup>, Eckart Marsch<sup>2</sup>, Werner Curdt<sup>2</sup>, and Jansen He<sup>2</sup>  
Astrophysical Journal, 704:883–890, **2009** October

The prominent blueshifts of Ne VIII associated with the junctions of the magnetic network in the quiet Sun are still not well understood. By comparing the coronal magnetic-field structures as obtained by a potential-field reconstruction with the conspicuous blueshift patches on the Dopplergram of Ne VIII as observed in an equatorial quiet-Sun region, we find that most of the regions with significant upflow are associated with the funnel-like legs of magnetic loops and cospatial with increments of the line width. These quasi-steady upflows can be regarded as the signatures of mass supply to coronal loops. By using the square root of the line intensity as a proxy for the plasma density, the mass flux of the upflow in each funnel can be estimated. We find that the mass flux is anti-correlated with the funnel's expansion factor as determined from the extrapolated magnetic field. One of the loop systems is associated with a coronal bright point, which was observed by several instruments and exhibited various morphologies in different wavelengths and viewing directions. A remarkable agreement between its magnetic structure and the associated EUV emission pattern was found, suggesting an almost potential-field nature of the coronal magnetic field. We also report the direct detection of a small-scale siphon flow by both *STEREO* satellites. However, this transient siphon flow occurred in a weak mixed-polarity-field region, which was outside the adjacent magnetic funnel, and thus it is perhaps not related to plasma upflow in the funnel. Based on these observations, we suggest that at upper transition region (TR) temperatures the dominant flows in quiet-Sun coronal loops are long-lasting upflows rather than siphon flows. We also discuss the implications of our results for coronal heating and unresolved magnetic structures.

### **2010 AUGUST 1-2 SYMPATHETIC ERUPTIONS. I. MAGNETIC TOPOLOGY OF THE SOURCE-SURFACE BACKGROUND FIELD**

V. S. [Titov](#)<sup>1</sup>, Z. Mikic<sup>1</sup>, T. Török<sup>1</sup>, J. A. Linker<sup>1</sup>, and O. Panasenco

2012 ApJ 759 70 [File](#)

A sequence of apparently coupled eruptions was observed on **2010 August 1-2** by Solar Dynamics Observatory and *STEREO*. The eruptions were closely synchronized with one another, even though some of them occurred at widely separated locations. In an attempt to identify a plausible reason for such synchronization, we study the large-scale structure of the background magnetic configuration. The coronal field was computed from the photospheric magnetic field observed at the appropriate time period by using the potential field source-surface model. We investigate the resulting field structure by analyzing the so-called squashing factor calculated at the photospheric and source-surface boundaries, as well as at different coronal cross-sections. Using this information as a guide, we determine the underlying structural skeleton of the configuration, including separatrix and quasi-separatrix surfaces. Our analysis reveals, in particular, several pseudo-streamers in the regions where the eruptions occurred. Of special interest to us are the magnetic null points and separators associated with the pseudo-streamers. We propose that magnetic reconnection triggered along these separators by the first eruption likely played a key role in establishing the assumed link between the sequential eruptions. The present work substantiates our recent simplified magnetohydrodynamic model of sympathetic eruptions and provides a guide for further deeper study of these phenomena. Several important implications of our results for the S-web model of the slow solar wind are also addressed.

### **Evidence of Twisting and Mixed-polarity Solar Photospheric Magnetic Field in Large Penumbra Jets: IRIS and Hinode Observations**

Sanjiv K. [Tiwari](#), [Ronald L. Moore](#), [Bart De Pontieu](#), [Theodore D. Tarbell](#), [Navdeep K. Panesar](#), [Amy R. Winebarger](#), [Alphonse C. Sterling](#)

ApJ **869** 147 **2018**

<https://arxiv.org/pdf/1811.09554.pdf>

<http://sci-hub.tw/10.3847/1538-4357/aaf1b8>

A recent study using *Hinode* (SOT/FG) data of a sunspot revealed some unusually large penumbral jets that often repeatedly occurred at the same locations in the penumbra, namely at the tail of a penumbral filament or where the tails of multiple penumbral filaments converged. These locations had obvious photospheric mixed-polarity magnetic flux in  $\lambda 5896$  NaI Stokes-V images obtained with SOT/FG. Several other recent investigations have found that extreme ultraviolet (EUV)/X-ray coronal jets in quiet Sun regions (QRs), coronal holes (CHs) and near active regions (ARs) have obvious mixed-polarity fluxes at their base, and that magnetic flux cancellation prepares and triggers a minifilament flux-ropes eruption that drives the jet. Typical QR, CH, and AR coronal jets are up to a hundred times bigger than large penumbral jets, and in EUV/X-ray images show clear twisting motion in their spires. Here, using IRIS  $\lambda 2796$  Å MgII k SJ images and spectra in the penumbrae of two sunspots we characterize large penumbral jets. We find redshift and blueshift next to each other across several large penumbral jets, and interpret these as untwisting of the magnetic field in the jet spire. Using *Hinode*/SOT (FG and SP) data, we also find mixed-polarity magnetic flux at the base of these jets. Because large penumbral jets have mixed-polarity field at their base and have twisting motion in their spires, they might be driven the same way as QR, CH and AR coronal jets. **5-Aug-2015, 15-16 Sept 2017**

Sanjiv K. **Tiwari**  
PASJ 2017

<https://arxiv.org/pdf/1712.07174.pdf>

This is a section (#7.1: Sunspot Structure) of a ~100-page review article on the "Achievements of Hinode in the First Ten Years" submitted for publication in PASJ. The invited speakers of the Hinode-10 Conference held in Nagoya, Japan, were asked to each write a section (I wrote this section for the review article early in 2017).

### **New Evidence that Magnetoconvection Drives Solar–Stellar Coronal Heating**

Sanjiv K. **Tiwari**<sup>1,2,3,4</sup>, Julia K. Thalmann<sup>5</sup>, Navdeep K. Panesar<sup>1</sup>, Ronald L. Moore<sup>1,2</sup>, and Amy R. Winebarger

2017 ApJL 843 L20

<http://iopscience.iop.org/sci-hub.cc/2041-8205/843/2/L20/>

How magnetic energy is injected and released in the solar corona, keeping it heated to several million degrees, remains elusive. Coronal heating generally increases with increasing magnetic field strength. From a comparison of a nonlinear force-free model of the three-dimensional active region coronal field to observed extreme-ultraviolet loops, we find that (1) umbra-to-umbra coronal loops, despite being rooted in the strongest magnetic flux, are invisible, and (2) the brightest loops have one foot in an umbra or penumbra and the other foot in another sunspot's penumbra or in unipolar or mixed-polarity plage. The invisibility of umbra-to-umbra loops is new evidence that magnetoconvection drives solar-stellar coronal heating: evidently, the strong umbral field at both ends quenches the magnetoconvection and hence the heating. Broadly, our results indicate that depending on the field strength in both feet, the photospheric feet of a coronal loop on any convective star can either engender or quench coronal heating in the loop's body. **2014 April 01/02, 2014 July 07**

### **Transition-Region/Coronal Signatures and Magnetic Setting of Sunspot Penumbra Jets: *Hinode* (SOT/FG), Hi-C and *SDO*/AIA Observations**

Sanjiv K. **Tiwari**, Ronald L. Moore, Amy R. Winebarger, Shane E. Alpert

ApJ 816 92 2016

<http://arxiv.org/pdf/1511.07900v1.pdf>

Penumbra microjets (PJs) are transient narrow bright features in the chromosphere of sunspot penumbrae, first characterized by Katsukawa et al (2007) using the  $\text{CaII}$  H-line filter on *Hinode*'s Solar Optical Telescope (SOT). It was proposed that the PJs form as a result of reconnection between two magnetic components of penumbra (spines and interspines), and that they could contribute to the transition region (TR) and coronal heating above sunspot penumbrae. We propose a modified picture of formation of PJs based on recent results on internal structure of sunspot penumbral filaments. Using data of a sunspot from *Hinode*/SOT, High Resolution Coronal Imager, and different passbands of the Atmospheric Imaging Assembly (AIA) onboard the *Solar Dynamics Observatory*, we examine whether PJs have signatures in the TR and corona. We find hardly any discernible signature of normal PJs in any AIA passbands, except a few of them showing up in the 1600 Å images. However, we discovered exceptionally stronger jets with similar lifetimes but bigger sizes (up to 600 km wide) occurring repeatedly in a few locations in the penumbra, where evidence of patches of opposite polarity fields at the tails of some penumbral filaments is seen in Stokes-V images. These large tail PJs do display signatures in the TR. Whether they have any coronal-temperature plasma is ambiguous. We infer that none of the PJs, including the large tail PJs, directly heat the corona in ARs significantly, but any penumbral jet might drive some coronal heating indirectly via generation of Alfvén waves and/or braiding of the coronal field. **11 July 2012**

### **Depth-dependent global properties of a sunspot observed by *Hinode* (SOT/SP)**

Sanjiv K. **Tiwari**, Michiel van Noort, [Sami K. Solanki](#), [Andreas Lagg](#)

A&A 583, A119 2015

<http://arxiv.org/pdf/1508.04830v1.pdf>

The 3D structure of sunspots has been extensively studied for the last two decades. A recent advancement of the Stokes inversion technique prompts us to revisit the problem. We investigate the global depth-dependent thermal, velocity and magnetic properties of a sunspot, as well as the interconnection between various local properties. High quality Stokes profiles of a disk centered, regular sunspot acquired by the SOT/SP (*Hinode*) are analyzed. To obtain the depth-dependent stratification of the physical parameters, we use the spatially coupled version of the SPINOR code. The vertical temperature gradient in the lower to mid-photosphere is smallest in the umbra, it is considerably larger in the penumbra and still somewhat larger in the spot's surroundings. The azimuthally averaged field becomes more horizontal with radial distance from the center of the spot, but more vertical with height. At  $\tau=1$ , the LOS velocity shows an average upflow of 300  $\text{ms}^{-1}$  in the inner penumbra and an average downflow of 1300  $\text{ms}^{-1}$  in the outer penumbra. The downflow continues outside the visible penumbral boundary. The sunspot shows a moderate negative twist of  $< 5^\circ$  at  $\tau=1$ , which increases with height. The sunspot umbra and the spines of the penumbra show considerable similarity in their physical properties albeit with some quantitative differences. The temperature shows a general anticorrelation with the field strength, with the exception of the heads of penumbral filaments,



where a weak positive correlation is found. The dependence of the physical parameters on each other over the full sunspot shows a qualitative similarity to that of a standard penumbral filament and its surrounding spines. Our results suggest that the spines in the penumbra are basically the outward extension of the umbra. The spines and the penumbral filaments are together the basic elements forming a sunspot penumbra. **5th of January 2007**

## **ON THE FORCE-FREE NATURE OF PHOTOSPHERIC SUNSPOT MAGNETIC FIELDS AS OBSERVED FROM HINODE (SOT/SP)**

Sanjiv Kumar **Tiwari**

2012 ApJ 744 65

A magnetic field is force-free if there is no interaction between it and the plasma in the surrounding atmosphere, i.e., electric currents are aligned with the magnetic field, giving rise to zero Lorentz force. The computation of various magnetic parameters, such as magnetic energy (using the virial theorem), gradient of twist of sunspot magnetic fields (computed from the force-free parameter  $\alpha$ ), and any kind of extrapolation, heavily hinges on the force-free approximation of the photospheric sunspot magnetic fields. Thus, it is of vital importance to inspect the force-free behavior of sunspot magnetic fields. The force-free nature of sunspot magnetic fields has been examined earlier by some researchers, ending with incoherent results. Accurate photospheric vector field measurements with high spatial resolution are required to inspect the force-free nature of sunspots. For this purpose, we use several vector magnetograms of high spatial resolution obtained from the Solar Optical Telescope/Spectro-Polarimeter on board Hinode. Both the necessary and sufficient conditions for force-free nature are examined by checking the global and local nature of equilibrium magnetic forces over sunspots. We find that sunspot magnetic fields are not very far from the force-free configuration, although they are not completely force-free on the photosphere. The umbral and inner penumbral fields are more force-free than the middle and outer penumbral fields. During their evolution, sunspot magnetic fields are found to maintain their proximity to force-free field behavior. Although a dependence of net Lorentz force components is seen on the evolutionary stages of the sunspots, we do not find a systematic relationship between the nature of sunspot magnetic fields and the associated flare activity. Further, we examine whether the fields at the photosphere follow linear or nonlinear force-free conditions. After examining this in various complex and simple sunspots, we conclude that, in either case, photospheric sunspot magnetic fields are closer to satisfying the nonlinear force-free field approximation.

## **EFFECT OF POLARIMETRIC NOISE ON THE ESTIMATION OF TWIST AND MAGNETIC ENERGY OF FORCE-FREE FIELDS**

Sanjiv Kumar **Tiwari** et al

ApJ 700 199-208, **2009** doi: [10.1088/0004-637X/700/1/199](https://doi.org/10.1088/0004-637X/700/1/199)

The force-free parameter  $\alpha$ , also known as helicity parameter or twist parameter, bears the same sign as the magnetic helicity under some restrictive conditions. The single global value of  $\alpha$  for a whole active region gives the degree of twist per unit axial length. We investigate the effect of polarimetric noise on the calculation of global  $\alpha$  value and magnetic energy of an analytical bipole. The analytical bipole has been generated using the force-free field approximation with a known value of constant  $\alpha$  and magnetic energy. The magnetic parameters obtained from the analytical bipole are used to generate Stokes profiles from the Unno-Rachkovsky solutions for polarized radiative transfer equations. Then we add random noise of the order of 10–3 of the continuum intensity ( $I_c$ ) in these profiles to simulate the real profiles obtained by modern spectropolarimeters such as Hinode (SOT/SP), SVM (USO), ASP, DLSP, POLIS, and SOLIS etc. These noisy profiles are then inverted using a Milne-Eddington inversion code to retrieve the magnetic parameters. Hundred realizations of this process of adding random noise and polarimetric inversion is repeated to study the distribution of error in global  $\alpha$  and magnetic energy values. The results show that (1) the sign of  $\alpha$  is not influenced by polarimetric noise and very accurate values of global twist can be calculated, and (2) accurate estimation of magnetic energy with uncertainty as low as 0.5% is possible under the force-free condition.

## **Lifetime of Sunspots and Pores**

Andrey G. **Tlatov**

[Solar Physics](#) volume 298, Article number: 93 (2023)

<https://doi.org/10.1007/s11207-023-02186-7>

The lifetime of individual sunspots and pores is analyzed according to Solar Dynamics Observatory/Helioseismic and Magnetic Imager (SDO/HMI) data from the period 2010 – 2022. It is found that the lifetime of individual sunspots and pores differs from the Gnevyshev–Waldmeier rule formulated for groups of sunspots. The dependence of the lifetime has a different pattern for different types of spots. For pores, the lifetime does not depend on the polarity of the magnetic field and has a logarithmic dependence on the area  $T_{pr}=0.24(\pm 0.01)+0.55(\pm 0.14)\log(S_{mx})$ . For regular sunspots with a developed penumbra, the dependence on the area has a linear form, but depends on the

polarity of the magnetic field. For sunspots with a magnetic field of the leading polarity  $T_{spld} = -0.62(\pm 0.2) + 0.036(\pm 0.002) S_{mx}$ . For sunspots of trailing polarity  $T_{sptr} = 0.95(\pm 0.1) + 0.01(\pm 0.001) S_{mx}$ . The decay time and the total lifetime of sunspots is related to the rate of flow in sunspots. The average vertical speed in sunspots decreases with their increasing area. Moreover, the flow rate in the sunspots of the trailing polarity is higher than in the sunspots of the leading polarity. This difference in the velocity explains the difference in the lifetime of the sunspots of the leading and trailing magnetic polarity.

## Dark Dots on the Photosphere and Their Counting in the Sunspot Index

Andrey G. **Tlatov**

[Solar Physics](#) volume 297, Article number: 67 (2022)

<https://arxiv.org/pdf/2205.13142.pdf>

<https://doi.org/10.1007/s11207-022-02002-8>

A large number of small dark areas can be observed in the continuum with high-spatial resolution in recent satellite observations of the Sun, as well as in high-quality ground-based data. These regions have no penumbra, have a contrast of up to 20% and are similar to solar pores. The characteristic area of such structures is from 0.3 to 5  $\mu\text{m}^2$  or from 0.5 to 7 Mm typical diameter. The number of such points in one image can be several hundred. The nature of such formations remains unclear.

We have performed a selection of dark regions with a contrast of at least 3% of the level of the quiet Sun using data obtained with the Helioseismic and Magnetic Imager (HMI) on board the Solar Dynamics Observatory (SDO) from 2010 to 2020. We have studied the properties of “dark dots”, including their variation with the solar cycle, area distribution, and contrast. We also studied the intensity of the magnetic field of such structures. We found that the number of dark dots with an area of less than 5  $\mu\text{m}^2$ , in which the magnetic field is not significant and is less than  $|B| < 30$  G, is from 60 to 80% of the total number of structures of this size. This means that they are not associated with magnetic activity. The existence of such structures can significantly affect the calculations of the sunspot index since they can be mistaken with pores.

## The Characteristic Sizes of the Sunspots and Pores in Solar Cycle 24

Andrey **Tlatov**, Alexandr Riehoakainen, Kseniya Tlatova

[Solar Physics](#) April 2019, 294:45

[sci-hub.se/10.1007/s11207-019-1439-1](https://sci-hub.se/10.1007/s11207-019-1439-1)

We present a comparative analysis of the size of spots in sunspot groups. For the analysis, we have used the characteristics of individual sunspots and pores according to the daily synoptic observations of the Kislovodsk Mountain astronomical station in Solar Cycle 24. We have constructed the distribution of area for the different types of the spots: pores, transitional sunspots, regular sunspots, and sunspots umbrae. We have found that the properties of the sunspots with largest area  $S_{max}$  differ from the other spots  $S_{nomax}$  in sunspot groups. In the distribution of area for  $S_{max}$  there are two local maxima  $S_{mx1} \approx 10$  msh and  $S_{mx2} \approx 130-180$  msh. The  $S_{mx1}$  is connected with the transitional spots where the penumbra is not fully developed. For sunspots with  $S_{max}$  where a penumbra is formed or the ratio  $S_{sp}/S_{um} > 3.5$ , the maximum  $S_{mx2}$  corresponds to the diameter of a round spot with  $d \approx 25$  Mm. This size is close to the size of the supergranules. In the distribution of area, the two-vertex character is absent for sunspots in the groups with the exception of the spot having the largest area. For developed sunspots with  $S_{max}$ , in the distribution of area of the sunspot's umbra we have a maximum  $S_{mxum} \approx 25$  msh. Thus, the two-vertex nature of the distribution of area is a consequence of the existence of pores and sunspots with developing penumbra.

## Bimodal Distribution of Magnetic Fields and Areas of Sunspots

Andrey G. **Tlatov** and Alexei A. Pevtsov

HMI Science Nuggets #34, Jan 2015

<http://hmi.stanford.edu/hminuggets/?p=1096>

Bimodal distribution of sunspots by their area and magnetic flux (maximum field strength) was recently noted by several researchers. Thus, for example, [4] have shown that the distribution of sunspot areas can be represented by a composite of two log-normal distributions, corresponding to “small” and “large” sunspots. They interpreted the presence of these two components as an indication of two spatially separated dynamos, with smaller sunspots forming at more shallow depths, and larger sunspots forming deeper in the solar convection zone. More recently, [5] showed that the distribution of sunspot areas can be fitted by a combination of Weibull and lognormal functions, and also interpreted this as evidence of two separate mechanisms: one directly connected to the global component of the dynamo, and the other with the small-scale component of the dynamo.

## Impact of the Large-Scale Solar Magnetic Field on the Solar Corona and Solar Wind

A.G. **Tlatov** and B.P. Filipov

**A review**

In: Exploring the Solar Wind, Ed. Marian Lazar, 2012  
<http://www.intechopen.com/books/exploring-the-solar-wind>

### **Studying the Wilson Effect from the Analysis of Averaged Sunspot Shapes.**

**Tlatova, K.A., Tlatov, A.G.**

Geomagn. Aeron. 63, 996–999 (2023).

<https://doi.org/10.1134/S0016793223070228>

Based on the method of averaging the shape of sunspots identified in the HMI/SDO images in the 2010–2022 period, an analysis was made of the relative position of sunspot nuclei during their passage across the solar disk. To do this, in different ranges of sunspot areas, we constructed averaged boundaries of the photosphere-penumbra and the core-penumbra. We then tracked changes in sunspot shape at various distances from the center of the disk in the eastern and western hemispheres. A shift of the boundary of sunspot nuclei to the western edge of the sunspot has been observed. The relative value of the shift increases with the area of sunspots. We estimated the value of the Wilson depression for sunspots of various sizes. The magnitude of the depression varies from 100 km for small sunspots to 1000 km for large sunspots. There is some imbalance of the Wilson depression near the eastern and western boundaries of the core-penumbra, depending on the area of the sunspots and their latitude.

### **Coronal Magnetic-Field Configuration Associated with Pseudostreamer and Slow Solar Wind.**

**Tokumar, M., Fujiki, K.**

Sol Phys 299, 160 (2024).

<https://doi.org/10.1007/s11207-024-02398-5>

The global distribution of the solar wind speed  $V$  is closely related to the configuration of the coronal magnetic-field, and the expansion factor  $f$  of the flux tube is known as a parameter for determining  $V$ . However, the inverse relation between  $f$  and  $V$  does not hold for pseudostreamers, which separate open-field regions with the same polarity. In the present study, we examined the magnetic-field configuration of pseudostreamers using the potential field (PF) model analysis of magnetograph observations for six Carrington rotations (CRs) in Cycle 23 and compared it with  $V$  data derived from interplanetary scintillation observations. We calculated the parameter  $S$ , which represents the relative angular distance of foot points on the photosphere magnetically connected to adjacent pixels on the source surface and  $f$  from PF model analysis and discriminated areas of helmet and pseudostreamers on the source surface by selecting large values of  $S$ . Although the overall correlation between  $S$  and  $V$  was very poor, helmet and pseudostreamers with large  $S$  values were exclusively associated with slow  $V$ . Furthermore, helmet and pseudostreamers were associated with large and small values of  $f$ , respectively. This suggests that  $S$  enables a better discrimination of slow-wind sources associated with pseudostreamers than  $f$ . We calculated the distance from the streamer boundary (DSTB) on the source surface using data of helmet and pseudostreamers to compare with  $V$  data. Calculated DSTB data exhibited significant correlations with  $V$  data except for the solar maximum period. The average of correlation coefficients between DSTB and  $V$  over five CRs excluding one at the solar maximum were 0.69, higher than that between the distance from the coronal hole boundary (DCHB) and  $V$ . This suggests that DSTB acts as a better parameter for determining  $V$  than DCHB. We demonstrated that  $f$  for pseudostreamers tended to reach a maximum at a height lower than the source surface ( $2.5 R_{\odot}$ ). This provides important insight into the formation process of the slow solar wind in pseudostreamers.

### **COSMO: The COronal Solar Magnetism Observatory,**

**Tomczyk, S., Burkepile, J., Casini, R., et al.**

2022, White Paper Submitted to the Decadal Survey for Solar and Space Physics

### **Scientific objectives and capabilities of the Coronal Solar Magnetism Observatory†**

#### **Authors**

S. **Tomczyk**, E. Landi, J. T. Burkepile, R. Casini, E. E. DeLuca, Y. Fan, S. E. Gibson, H. Lin, S. W.

McIntosh, S. C. Solomon, G. de Toma, A. G. de Wijn, J. Zhang

JGR Volume 121, Issue 8 August 2016 Pages 7470–7487 **2016**

<https://sci-hub.ru/10.1002/2016JA022871>

Magnetic influences increase in importance in the solar atmosphere from the photosphere out into the corona, yet our ability to routinely measure magnetic fields in the outer solar atmosphere is lacking. We describe the scientific objectives and capabilities of the **COronal Solar Magnetism Observatory (COSMO)**, a proposed synoptic facility designed to measure magnetic fields and plasma properties in the large-scale solar atmosphere. COSMO comprises a suite of three instruments chosen to enable the study of the solar atmosphere as a coupled system: 1) a coronagraph with a 1.5-m aperture to measure the magnetic field, temperature, density and dynamics of the corona; 2) an instrument for diagnostics of chromospheric and prominence magnetic fields and plasma properties; and 3) a white-light K-coronagraph to measure the density structure and dynamics of the corona and coronal mass ejections.

COSMO will provide a unique combination of magnetic field, density, temperature and velocity observations in the corona and chromosphere that have the potential to transform our understanding of fundamental physical processes in the solar atmosphere and their role in the origins of solar variability and space weather.

### **Comparative Study of Data-driven Solar Coronal Field Models Using a Flux Emergence Simulation as a Ground-truth Data Set**

Shin [Toriumi](#), [Shinsuke Takasao](#), [Mark C.M. Cheung](#), [Chaowei Jiang](#), [Yang Guo](#), [Keiji Hayashi](#), [Satoshi Inoue](#)

ApJ **890** 103 **2020**

<https://arxiv.org/pdf/2001.03721.pdf>

<https://doi.org/10.3847/1538-4357/ab6b1f>

For a better understanding of magnetic field in the solar corona and dynamic activities such as flares and coronal mass ejections, it is crucial to measure the time-evolving coronal field and accurately estimate the magnetic energy. Recently, a new modeling technique called the data-driven coronal field model, in which the time evolution of magnetic field is driven by a sequence of photospheric magnetic and velocity field maps, has been developed and revealed the dynamics of flare-productive active regions. Here we report on the first qualitative and quantitative assessment of different data-driven models using a magnetic flux emergence simulation as a ground-truth (GT) data set. We compare the GT field with those reconstructed from the GT photospheric field by four data-driven algorithms. It is found that, at least, the flux rope structure is reproduced in all coronal field models. Quantitatively, however, the results show a certain degree of model dependence. In most cases, the magnetic energies and relative magnetic helicity are comparable to or at most twice of the GT values. The reproduced flux ropes have a sigmoidal shape (consistent with GT) of various sizes, a vertically-standing magnetic torus, or a packed structure. The observed discrepancies can be attributed to the highly non-force-free input photospheric field, from which the coronal field is reconstructed, and to the modeling constraints such as the treatment of background atmosphere, the bottom boundary setting, and the spatial resolution.

### **Spontaneous Generation of delta-sunspots in Convective Magnetohydrodynamic Simulation of Magnetic Flux Emergence**

Shin [Toriumi](#), [Hideyuki Hotta](#)

ApJL **886** L21 **2019**

<https://arxiv.org/pdf/1911.03909.pdf>

[sci-hub.se/10.3847/2041-8213/ab55e7](https://doi.org/10.3847/2041-8213/ab55e7)

Observations reveal that strong solar flares and coronal mass ejections tend to occur in complex active regions characterized by delta-sunspots, spot rotation, sheared polarity inversion lines (PILs), and magnetic flux ropes. Here we report on the first modeling of spontaneous delta-spot generation as a result of flux emergence from the turbulent convection zone. Utilizing state-of-the-art radiative magnetohydrodynamics code R2D2, we simulate the emergence of a force-free flux tube in the convection zone that stretches down to -140 Mm. Elevated by large-scale convective upflows, the tube appears on the photosphere as two emerging bipoles. The opposite polarities collide against each other due to the subsurface connectivity, and they develop into a pair of closely-packed delta-spots. The Lorentz force drives the spot rotation and a strong counter-streaming flow of 10 km/s at the PIL in delta-spots, which, in tandem with local convection, strengthens the horizontal field to 4 kG and builds up a highly-sheared PIL. In the atmosphere above the PIL, a flux rope structure is created. All these processes follow the multi-buoyant segment theory of the delta-spot formation, and they occur as a natural consequence of interaction between magnetic flux and turbulent convection, suggesting that the generation of delta-spots and the resultant flare eruptions may be a stochastically determined process.

[HMI Science Nuggets](https://doi.org/10.3847/2041-8213/ab55e7) #134 Dec 2019 <http://hmi.stanford.edu/hminuggets/?p=3136>

### **Light Bridge in a Developing Active Region. II. Numerical Simulation of Flux Emergence and Light Bridge Formation**

Shin [Toriumi](#), [Mark C. M. Cheung](#), [Yukio Katsukawa](#)

ApJ **2015**

<http://arxiv.org/pdf/1509.00205v1.pdf>

Light bridges, the bright structure dividing umbrae in sunspot regions, show various activity events. In Paper I, we reported on analysis of multi-wavelength observations of a light bridge in a developing active region (AR) and concluded that the activity events are caused by magnetic reconnection driven by magnetconvective evolution. The aim of this second paper is to investigate the detailed magnetic and velocity structures and the formation mechanism of light bridges. For this purpose, we analyze numerical simulation data from a radiative magnetohydrodynamics model of an emerging AR. We find that a weakly-magnetized plasma upflow in the near-surface layers of the convection zone is entrained between the emerging magnetic bundles that appear as pores at the solar surface. This convective upflow continuously transports horizontal fields to the surface layer and creates a light bridge structure.

Due to the magnetic shear between the horizontal fields of the bridge and the vertical fields of the ambient pores, an elongated cusp-shaped current layer is formed above the bridge, which may be favorable for magnetic reconnection. The striking correspondence between the observational results of Paper I and the numerical results of this paper provides a consistent physical picture of light bridges. The dynamic activity phenomena occur as a natural result of the bridge formation and its convective nature, which has much in common with those of umbral dots and penumbral filaments.

### **Light Bridge in a Developing Active Region. I. Observation of Light Bridge and its Dynamic Activity Phenomena**

Shin **Toriumi**, Yukio Katsukawa, Mark C. M. Cheung

ApJ **2015**

<http://arxiv.org/pdf/1509.00183v1.pdf>

Light bridges, the bright structures that divide the umbra of sunspots and pores into smaller pieces, are known to produce wide variety of activity events in solar active regions (ARs). It is also known that the light bridges appear in the assembling process of nascent sunspots. The ultimate goal of this series of papers is to reveal the nature of light bridges in developing ARs and the occurrence of activity events associated with the light bridge structures from both observational and numerical approaches. In this first paper, exploiting the observational data obtained by Hinode, IRIS, and Solar Dynamics Observatory (SDO), we investigate the detailed structure of the light bridge in NOAA AR 11974 and its dynamic activity phenomena. As a result, we find that the light bridge has a weak, horizontal magnetic field, which is transported from the interior by large-scale convective upflow and is surrounded by strong, vertical fields of adjacent pores. In the chromosphere above the bridge, a transient brightening occurs repeatedly and intermittently, followed by a recurrent dark surge ejection into higher altitudes. Our analysis indicates that the brightening is the plasma heating due to magnetic reconnection at lower altitudes, while the dark surge is the cool, dense plasma ejected from the reconnection region. From the observational results, we conclude that the dynamic activity observed in a light bridge structure such as chromospheric brightenings and dark surge ejections are driven by magnetoconvective evolution within the light bridge and its interaction with surrounding magnetic fields.

**February 9-15, 2014**

### **Statistical Analysis of the Horizontal Divergent Flow in Emerging Solar Active Regions**

Shin **Toriumi**<sup>1</sup>, Keiji Hayashi<sup>2,3</sup>, and Takaaki Yokoyama

**2014** ApJ 794 19.

Solar active regions (ARs) are thought to be formed by magnetic fields from the convection zone. Our flux emergence simulations revealed that a strong horizontal divergent flow (HDF) of unmagnetized plasma appears at the photosphere before the flux begins to emerge. In our earlier study, we analyzed HMI data for a single AR and confirmed presence of this precursor plasma flow in the actual Sun. In this paper, as an extension of our earlier study, we conducted a statistical analysis of the HDFs to further investigate their characteristics and better determine the properties. From SDO/HMI data, we picked up 23 flux emergence events over a period of 14 months, the total flux of which ranges from 1020 to 1022 Mx. Out of 23 selected events, 6 clear HDFs were detected by the method we developed in our earlier study, and 7 HDFs detected by visual inspection were added to this statistic analysis. We found that the duration of the HDF is on average 61 minutes and the maximum HDF speed is on average 3.1 km s<sup>-1</sup>. We also estimated the rising speed of the subsurface magnetic flux to be 0.6-1.4 km s<sup>-1</sup>. These values are highly consistent with our previous one-event analysis as well as our simulation results. The observation results lead us to the conclusion that the HDF is a rather common feature in the earliest phase of AR emergence. Moreover, our HDF analysis has the capability of determining the subsurface properties of emerging fields that cannot be directly measured.

### **FAN-SPINE TOPOLOGY FORMATION THROUGH TWO-STEP RECONNECTION DRIVEN BY TWISTED FLUX EMERGENCE**

T. **Toriumi**<sup>1</sup>, G. Aulanier<sup>1</sup>, B. Schmieder<sup>1</sup>, K. K. Reeves<sup>2</sup>, and L. Golub<sup>2</sup>

Astrophysical Journal, 704:485–495, **2009** October

We address the formation of three-dimensional nullpoint topologies in the solar corona by combining *Hinode*/X-ray Telescope (XRT) observations of a small dynamic limb event, which occurred beside a non-erupting prominence cavity, with a three-dimensional (3D) zero- $\beta$  magnetohydrodynamics (MHD) simulation. To this end, we model the boundary-driven “kinematic” emergence of a compact, intense, and uniformly twisted flux tube into a potential field arcade that overlies a weakly twisted coronal flux rope. The expansion of the emerging flux in the corona gives rise to the formation of a nullpoint at the interface of the emerging and the pre-existing fields. We unveil a two-step reconnection process at the nullpoint that eventually yields the formation of a broad 3D fan-spine configuration above the emerging bipole. The first reconnection involves emerging fields

and a set of large-scale arcade field lines. It results in the launch of a torsional MHD wave that propagates along the arcades, and in the formation of a sheared loop system on one side of the emerging flux. The second reconnection occurs between these newly formed loops and remote arcade fields, and yields the formation of a second loop system on the opposite side of the emerging flux. The two loop systems collectively display an anemone pattern that is located below the fan surface. The flux that surrounds the inner spine field line of the nullpoint retains a fraction of the emerged twist, while the remaining twist is evacuated along the reconnected arcades. The nature and timing of the features which occur in the simulation do qualitatively reproduce those observed by XRT in the particular event studied in this paper. Moreover, the two-step reconnection process suggests a new consistent and generic model for the formation of anemone regions in the solar corona. **2007 April 24,**

## **Magnetic flux emergence into the solar photosphere and chromosphere**

A. [Tortosa-Andreu](#) and F. Moreno-Insertis

A&A 507, 949-967 (2009)

*Aims.* We model the emergence of magnetized plasma across granular convection cells and the low atmosphere, including layers up to the mid-chromosphere.

*Methods.* Three-dimensional numerical experiments are carried out in which the equations of MHD and radiative transfer are solved self-consistently. We use the MURaM code, which assumes local thermodynamic equilibrium between plasma and radiation.

*Results.* In the photosphere, we find good agreement between our simulation predictions and observational results obtained with the Hinode satellite for the velocity and magnetic fields. We also confirm earlier simulation results by other authors. Our experiments reveal a natural mechanism of formation of twisted magnetic flux tubes that results from the retraction of photospheric horizontal fields at new intergranular lanes in decaying granules. In the chromosphere, we present evidence for the non-radiative heating of the emerging magnetized plasma due to the passage of shocks and/or ohmic dissipation. We study the formation of high-temperature points in the magnetic domain. We detect two types of points, classified according to whether they have a photospheric counterpart or otherwise. We also find evidence of those two types in Hinode observations. Using Lagrangian tracing of a large statistical sample of fluid particles, we detect and study episodes of convective collapse of magnetic elements returning to the photosphere. On the other hand, we study the maximum heights reached by all tracers, magnetized or otherwise. Only a small fraction (1.3%) of the magnetic elements reach the mid-chromosphere ( $z > 750$  km), while virtually no unmagnetized elements in the sample rise above the level of the reverse granulation (a few 100 km above the photosphere). We find that the rise into the chromosphere occurs in the form of successive jumps with intermediate stops rather than in a smooth continuous fashion and propose a tentative explanation of this behavior. Finally, also using Lagrange tracing, we document the creation of high-temperature points in the chromosphere via rising shock fronts.

## **A data driven kinetic approach to coronal heating**

A. [Toutountzi](#)<sup>1</sup>, L. Vlahos<sup>1</sup>, H. Isliker<sup>1</sup>, K. Moraitis<sup>2</sup>, M. Georgoulis<sup>2</sup>, and G. Chintzoglou

A&A 2016

<http://arxiv.org/pdf/1603.07129v1.pdf>

*Aims.* Coronal heating through the explosive release of magnetic energy remains an open problem in solar physics. Several one-dimensional hydrodynamical models have been developed over the last decade, using simple approaches for the way energy is

deposited and transported in the coronal plasma, namely by inserting “nanoflares” in the form of “hot spots” at random sites and times. Our aim in this work is to investigate the problem from a different perspective.

*Methods.* With the help of a nonlinear force-free extrapolation method we reconstruct the coronal magnetic field of a well-studied solar active region (NOAA AR 11158) using an observed photospheric vector magnetogram of the region as the required boundary condition. We then determine the locations, energy contents, and volumes of unstable areas (i.e., areas prone to releasing energy) within the active-region corona. These areas include strong gradients in the magnetic field and are naturally connected to three-dimensional current sheets. The statistical distributions of these volumes, their fractal structure and corresponding fractal dimension as well as their electric current density distribution are then inferred. Further adopting a simple model for the resistivity, we estimate the key characteristics of the fractally distributed electric fields. We then follow the behavior of thousands of particles (electrons and ions), obeying an initial Maxwellian distribution with temperature 10 eV, monitoring their trajectories and energization obtained by encountering the electric fields enveloped by unstable volumes. For computational convenience, the spatial resolution of the magnetic field reconstruction (hundreds of km) is much coarser than the particles’ mean free path, which is 0.1 – 1 km in the low corona.

*Results.* The presence of collisions traps the bulk of the plasma around the unstable current sheets (UCS) and only a tail of the distribution of the electrons and ions gain substantial energy. Assuming that the distance between the UCS can be as small as the collisional mean free path, we find that the low active-region corona is heated to 100-200 eV, corresponding to temperatures in excess of 2 MK, within tens of seconds for electrons and thousands of seconds for ions. Our main result is that fractally distributed nanoflares inside the active region, following the statistical

properties of the extrapolated magnetic fields, can heat electrons and ions with minor enhancements of the local resistivity due to the fragmentation of electric fields inside the driven complex magnetic topology. Conclusions. The active region solar corona can be naturally heated by fractally distributed swarms of nanoflares that we simulate here as energy dissipation episodes in UCS. This could be extended for the quiet Sun corona, provided that currently undetected nanoflares are sufficient in number and occurrence frequency. **February 11-16, 2011**

## **Plasma Motions and Turbulent Magnetic Diffusivity of Active Region AR 12158 Using a Minimum Energy Functional and Non-Force-Free Reconstructions of Vector Magnetograms**

Benoit [Tremblay](#), Alain Vincent  
Solar Phys. January **2017**, 292:2

We present a generalization of the resistive minimum-energy fit (MEF-R: Tremblay and Vincent, *Solar Phys.* **290**, 437, [2015](#)) for non-force-free (NFF) magnetic fields. In MEF-R, an extremum principle is used to infer two-dimensional maps of plasma motions [ $v(x, y)$ ] and magnetic eddy diffusivity [ $\eta_{\text{eddy}}(x, y)$ ] at the photosphere. These reconstructions could be used as boundary conditions in data-driven simulations or in data assimilation. The algorithm is validated using the analytical model of a resistive expanding spheromak by Rakowski, Laming, and Lyutikov (*Astrophys. J.* **730**, 30, [2011](#)). We study the flaring Active Region AR 12158 using a series of magnetograms and Dopplergrams provided by the *Helioseismic and Magnetic Imager* (HMI) onboard the *Solar Dynamics Observatory* (SDO). The results are discussed for a non-force-free magnetic-field reconstruction [ $B_{\text{NFF}}$ ] (Hu and Dasgupta in *Solar Phys.* **247**, 87, [2008](#)). We found that the vertical plasma velocities [ $v_z(x, y)$ ] inferred using MEF-R are very similar to the observed Doppler velocities [ $v_r(x, y)$ ]. Finally, we study the potential spatial correlation between microturbulent velocities and significant values of  $\eta_{\text{eddy}}(x, y)$ . **10 September 2014**

## **ACTIVE REGION MOSS: DOPPLER SHIFTS FROM HINODE/EXTREME-ULTRAVIOLET IMAGING SPECTROMETER OBSERVATIONS**

Durgesh [Tripathi](#)<sup>1</sup>, Helen E. Mason<sup>2</sup>, and James A. Klimchuk  
**2012** ApJ 753 37

Studying the Doppler shifts and the temperature dependence of Doppler shifts in moss regions can help us understand the heating processes in the core of the active regions. In this paper, we have used an active region observation recorded by the Extreme-ultraviolet Imaging Spectrometer (EIS) on board Hinode on **2007 December 12** to measure the Doppler shifts in the moss regions. We have distinguished the moss regions from the rest of the active region by defining a low-density cutoff as derived by Tripathi et al. in 2010. We have carried out a very careful analysis of the EIS wavelength calibration based on the method described by Young et al. in 2012. For spectral lines having maximum sensitivity between  $\log T = 5.85$  and  $\log T = 6.25$  K, we find that the velocity distribution peaks at around  $0 \text{ km s}^{-1}$  with an estimated error of  $4\text{--}5 \text{ km s}^{-1}$ . The width of the distribution decreases with temperature. The mean of the distribution shows a blueshift which increases with increasing temperature and the distribution also shows asymmetries toward blueshift. Comparing these results with observables predicted from different coronal heating models, we find that these results are consistent with both steady and impulsive heating scenarios. However, the fact that there are a significant number of pixels showing velocity amplitudes that exceed the uncertainty of  $5 \text{ km s}^{-1}$  is suggestive of impulsive heating. Clearly, further observational constraints are needed to distinguish between these two heating scenarios.

## **Measurements of strong magnetic fields in umbra of sunspots: Crimea vs Mt. Wilson**

Yu.T. [Tsap](#), [V.A. Perebeynos](#), [A.V. Borisenko](#), [N.I. Lozitska](#), [N.I. Shtertser](#), [G.G. Motorina](#), [A.I. Kuleshova](#)

Astronomical and Astrophysical Transactions (AApTr) **2020**  
<https://arxiv.org/pdf/2003.12889.pdf>

The comparative analysis for 1324 measurements of the corresponding sunspot magnetic fields with  $B > 2.5 \text{ kG}$  (according to Crimean data) obtained at Crimean and Mt. Wilson observatories from 2010 to 2017 has been carried out. It has been shown that the difference between measurements can exceed  $1 \text{ kG}$  in some cases. The averaged values of the magnetic field are equal to  $2759 \text{ G}$  (Crimea) and  $2196 \text{ G}$  (Mt. Wilson). The maximum sunspot magnetic field measured at Mt. Wilson does not reach  $2.7 \text{ kG}$  while according to Crimean data it can exceed  $4.0 \text{ kG}$ . The correlation coefficient between measurements of magnetic fields in different observatories does not exceed  $0.22$ . The probable reasons of significant discrepancies are discussed. **October 22, 2014**

## **Alfvén wave phase-mixing in flows**

**Why over-dense, solar coronal, open magnetic field structures are cool**

D. [Tsiklauri](#)

## A&A 586, A95 (2016)

**Aims.** The motivation for this study is to include the effect of plasma flow in Alfvén wave (AW) damping via phase mixing and to explore the observational implications.

**Methods.** Our magnetohydrodynamic simulations and analytical calculations show that, when a background flow is present, mathematical expressions for the AW damping via phase mixing are modified by the following substitution:  $CA'(x) \rightarrow CA'(x) + V0'(x)$ , where  $CA$  and  $V0$  are AW phase and the flow speeds, and the prime denotes a derivative in the direction across the background magnetic field.

**Results.** In uniform magnetic fields and over-dense plasma structures, where  $CA$  is smaller than in the surrounding plasma, the flow, which is confined to the structure and going in the same direction as the AW, reduces the effect of phase-mixing, because on the edges of the structure  $CA'$  and  $V0'$  have opposite signs. Thus, the wave damps by means of slower phase-mixing compared to the case without the flow. This is the result of the co-directional flow that reduces the wave front stretching in the transverse direction. Conversely, the counter-directional flow increases the wave front stretching in the transverse direction, therefore making the phase-mixing-induced heating more effective. Although the result is generic and is applicable to different laboratory or astrophysical plasma systems, we apply our findings to addressing the question why over-dense solar coronal open magnetic field structures (OMFS) are cooler than the background plasma. Observations show that the over-dense OMFS (e.g. solar coronal polar plumes) are cooler than surrounding plasma and that, in these structures, Doppler line-broadening is consistent with bulk plasma motions, such as AW.

**Conclusions.** If over-dense solar coronal OMFS are heated by AW damping via phase-mixing, we show that, co-directional with AW, plasma flow in them reduces the phase-mixing induced-heating, thus providing an explanation of why they appear cooler than the background.

## Validation of the magnetic energy vs. helicity scaling in solar magnetic structures

K. [Tziotziou](#), K. Moraitis, M.K. Georgoulis, V. Archontis

A&A, 2014

We assess the validity of the free magnetic energy - relative magnetic helicity diagram for solar magnetic structures. We used two different methods of calculating the free magnetic energy and the relative magnetic helicity budgets: a classical, volume-calculation nonlinear force-free (NLFF) method applied to finite coronal magnetic structures and a surface-calculation NLFF derivation that relies on a single photospheric or chromospheric vector magnetogram. Both methods were applied to two different data sets, namely synthetic active-region cases obtained by three-dimensional magneto-hydrodynamic (MHD) simulations and observed active-region cases, which include both eruptive and noneruptive magnetic structures. The derived energy-helicity diagram shows a consistent monotonic scaling between relative helicity and free energy with a scaling index  $0.84 \pm 0.05$  for both data sets and calculation methods. It also confirms the segregation between noneruptive and eruptive active regions and the existence of thresholds in both free energy and relative helicity for active regions to enter eruptive territory. We consider the previously reported energy-helicity diagram of solar magnetic structures as adequately validated and envision a significant role of the uncovered scaling in future studies of solar magnetism.

## Energy and helicity budgets of solar quiet regions

K. [Tziotziou](#), S.-H. Park, G. Tsiropoula and I. Kontogiannis

A&A 581, A61 (2015)

**Aims.** We investigate the free magnetic energy and relative magnetic helicity injection in solar quiet regions.

**Methods.** We use the DAVE4VM method to infer the photospheric velocity field and calculate the free magnetic energy and relative magnetic helicity injection rates in 16 quiet-Sun vector magnetograms sequences.

**Results.** We find that there is no dominant sense of helicity injection in quiet-Sun regions, and that both helicity and energy injections are mostly due to surface shuffling motions that dominate the respective emergence by factors slightly larger than two. We, furthermore, estimate the helicity and energy rates per network unit area as well as the respective budgets over a complete solar cycle.

**Conclusions.** Derived helicity and energy budgets over the entire solar cycle are similar to respective budgets derived in a recent work from the instantaneous helicity and free magnetic energy budgets and higher than previously reported values that relied on similar approaches to this analysis. Free-energy budgets, mostly generated like helicity at the network, are high enough to power the dynamics of fine-scale structures residing at the network, such as mottles and spicules, while corresponding estimates of helicity budgets are provided, pending future verification from high-resolution magneto-hydrodynamic simulations and/or observations.

## Energy and helicity budgets of solar quiet regions

K. [Tziotziou](#), G. Tsiropoula, M.K. Georgoulis, I. Kontogiannis

E-print, March 2014; A&A 564, A86, 2014



<http://arxiv.org/pdf/1403.0730v1.pdf>

We investigate the free magnetic energy and relative magnetic helicity budgets of solar quiet regions. Using a novel non-linear force-free method requiring single solar vector magnetograms we calculate the instantaneous free magnetic energy and relative magnetic helicity budgets in 55 quiet-Sun vector magnetograms. As in a previous work on active regions, we construct here for the first time the (free) energy-(relative) helicity diagram of quiet-Sun regions. We find that quiet-Sun regions have no dominant sense of helicity and show monotonic correlations a) between free magnetic energy/relative helicity and magnetic network area and, consequently, b) between free magnetic energy and helicity. Free magnetic energy budgets of quiet-Sun regions represent a rather continuous extension of respective active-region budgets towards lower values, but the corresponding helicity transition is discontinuous due to the incoherence of the helicity sense contrary to active regions. We further estimate the instantaneous free magnetic-energy and relative magnetic-helicity budgets of the entire quiet Sun, as well as the respective budgets over an entire solar cycle. Derived instantaneous free magnetic energy budgets and, to a lesser extent, relative magnetic helicity budgets over the entire quiet Sun are comparable to the respective budgets of a sizeable active region, while total budgets within a solar cycle are found higher than previously reported. Free-energy budgets are comparable to the energy needed to power fine-scale structures residing at the network, such as mottles and spicules.

### **Magnetic Flux Transport and the Long-Term Evolution of Solar Active Regions**

Ignacio [Ugarte-Urra](#), Lisa Upton, Harry P. Warren, David H. Hathaway

ApJ **815** 90 2015

<http://arxiv.org/pdf/1511.04030v1.pdf>

With multiple vantage points around the Sun, STEREO and SDO imaging observations provide a unique opportunity to view the solar surface continuously. We use He II 304 Å data from these observatories to isolate and track ten active regions and study their long-term evolution. We find that active regions typically follow a standard pattern of emergence over several days followed by a slower decay that is proportional in time to the peak intensity in the region. Since STEREO does not make direct observations of the magnetic field, we employ a flux-luminosity relationship to infer the total unsigned magnetic flux evolution. To investigate this magnetic flux decay over several rotations we use a surface flux transport model, the Advective Flux Transport (AFT) model, that simulates convective flows using a time-varying velocity field and find that the model provides realistic predictions when information about the active region's magnetic field strength and distribution at peak flux is available. Finally, we illustrate how 304 Å images can be used as a proxy for magnetic flux measurements when magnetic field data is not accessible.

### **Generation of a North/South Magnetic Field Component from Variations in the Photospheric Magnetic Field**

Roger K. [Ulrich](#), Tham Tran

Solar Phys. Volume 291, Issue 4, pp 1059-1076 2016

<http://arxiv.org/pdf/1603.02697v1.pdf>

We address the problem of calculating the transverse magnetic field in the solar wind outside of the hypothetical sphere called the source surface where the solar wind originates. This calculation must overcome a widely used fundamental assumption about the source surface -- the field is normally required to be purely radial at the source surface. Our model rests on the fact that a change in the radial field strength at the source surface is a change in the field line density. Surrounding field lines must move laterally in order to accommodate this field line density change. As the outward wind velocity drags field lines past the source surface this lateral component of motion produces a tilt implying there is a transverse component to the field. An analytic method of calculating the lateral translation speed of the field lines is developed. We apply the technique to an interval of approximately two Carrington rotations at the beginning of 2011 using 2-h averages of data from the Helioseismic Magnetic Imager instrument on the Solar Dynamics Observatory spacecraft. We find that the value of the transverse magnetic field is dominated on a global scale by the effects of high latitude concentrations of field lines being buffeted by supergranular motions. **7 January - 2 March 2011**

### **THE GLOBAL SOLAR MAGNETIC FIELD—IDENTIFICATION OF TRAVELING, LONG-LIVED RIPPLES**

R. K. [Ulrich](#) and Tham Tran

2013 ApJ 768 189

We have examined the global structure of the solar magnetic field using data from the Fe I spectral line at 5250.2 Å obtained at the 150 foot tower telescope at the Mt. Wilson Observatory. For each point on the solar surface, we find the value of the magnetic field in the meridional plane,  $B_m$ , by averaging over all available observations using a cosine weighting method. We have revised our cosine weighting method by now taking into account more fully the highest latitude geometry. We use the annual variation in the latitude of the disk center,  $b_0$ , to deduce the tilt angle of the field relative to the local vertical so that we can find the radial component of the field,  $B_r$ , from  $B_m$ . We find

this tilt angle to be small except for a near-polar zone where a tilt-angle model can reduce the annual variation. The reduced annual variation in the deduced  $B_r$  allows us to study  $dB_r/dt$  and associated deviations in  $B_r$  from a smoothed  $B_r$  with a smoothing width of 2.5 yr. These functions make evident the presence of small amplitude (3-5 G) but spatially coherent ripples with a semi-regular periodicity of one to three years. At any given time, the half-wavelength (peak to trough) is between  $15^\circ$  and  $30^\circ$  of latitude. These patterns are ubiquitous and in many cases drift from near the equator to the poles over a time period of roughly two years. The drift rate pattern is not compatible with simple advection.

### **The Advective Flux Transport Model: Improving the Far-Side with Active Regions observed by STEREO 304Å**

[Lisa A. Upton](#), [Ignacio Ugarte-Urra](#), [Harry P. Warren](#), [David H. Hathaway](#)

ApJ 968 114 2024

<https://arxiv.org/pdf/2404.04280>

<https://iopscience.iop.org/article/10.3847/1538-4357/ad40a5/pdf>

Observations the Sun's photospheric magnetic field are often confined to the Sun-Earth line. Surface flux transport (SFT) models, such as the Advective Flux Transport (AFT) model, simulate the evolution of the photospheric magnetic field to produce magnetic maps over the entire surface of the Sun. While these models are able to evolve active regions that transit the near-side of the Sun, new far-side side flux emergence is typically neglected. We demonstrate a new method for creating improved maps of magnetic field over the Sun's entire photosphere using data obtained by the STEREO mission. The STEREO He II 304 Å intensity images are used to infer the time, location, and total unsigned magnetic flux of far-side active regions. We have developed an automatic detection algorithm for finding and ingesting new far-side active region emergence into the AFT model. We conduct a series of simulations to investigate the impact of including active region emergence in AFT, both with and without data assimilation of magnetograms. We find that while the He II 304 Å can be used to improve surface flux models, but care must be taken to mitigate intensity surges from flaring events. We estimate that during Solar Cycle 24 maximum (2011-2015),  $4-6 \times 10^{22}$  Mx of flux is missing from SFT models that do not include far-side data. We find that while He II 304 Å data alone can be used to create synchronic maps of photospheric magnetic field that resemble the observations, it is insufficient to produce a complete picture without direct magnetic observations from magnetographs.

### **STOCHASTIC COUPLING OF SOLAR PHOTOSPHERE AND CORONA**

Vadim M. [Uritsky](#)<sup>1</sup>, Joseph M. Davila<sup>2</sup>, Leon Ofman<sup>1</sup>, and Aaron J. Coyner

2013 ApJ 769 62

The observed solar activity is believed to be driven by the dissipation of nonpotential magnetic energy injected into the corona by dynamic processes in the photosphere. The enormous range of scales involved in the interaction makes it difficult to track down the photospheric origin of each coronal dissipation event, especially in the presence of complex magnetic topologies. In this paper, we propose an ensemble-based approach for testing the photosphere-corona coupling in a quiet solar region as represented by intermittent activity in Solar and Heliospheric Observatory Michelson Doppler Imager and Solar TERrestrial RELations Observatory Extreme Ultraviolet Imager image sets. For properly adjusted detection thresholds corresponding to the same degree of intermittency in the photosphere and corona, the dynamics of the two solar regions is described by the same occurrence probability distributions of energy release events but significantly different geometric properties. We derive a set of scaling relations reconciling the two groups of results and enabling statistical description of coronal dynamics based on photospheric observations. Our analysis suggests that multiscale intermittent dissipation in the corona at spatial scales  $>3$  Mm is controlled by turbulent photospheric convection. Complex topology of the photospheric network makes this coupling essentially nonlocal and non-deterministic. Our results are in an agreement with the Parker's coupling scenario in which random photospheric shuffling generates marginally stable magnetic discontinuities at the coronal level, but they are also consistent with an impulsive wave heating involving multiscale Alfvénic wave packets and/or magnetohydrodynamic turbulent cascade. A back-reaction on the photosphere due to coronal magnetic reconfiguration can be a contributing factor.

### **MULTISCALE DYNAMICS OF SOLAR MAGNETIC STRUCTURES**

Vadim M. [Uritsky](#)<sup>1</sup> and Joseph M. Davila

2012 ApJ 748 60

Multiscale topological complexity of the solar magnetic field is among the primary factors controlling energy release in the corona, including associated processes in the photospheric and chromospheric boundaries. We present a new approach for analyzing multiscale behavior of the photospheric magnetic flux underlying these dynamics as depicted by a sequence of high-resolution solar magnetograms. The approach involves two basic processing steps: (1) identification of timing and location of magnetic flux origin and demise events (as defined by DeForest et al.) by

tracking spatiotemporal evolution of unipolar and bipolar photospheric regions, and (2) analysis of collective behavior of the detected magnetic events using a generalized version of the Grassberger-Procaccia correlation integral algorithm. The scale-free nature of the developed algorithms makes it possible to characterize the dynamics of the photospheric network across a wide range of distances and relaxation times. Three types of photospheric conditions are considered to test the method: a quiet photosphere, a solar active region (NOAA 10365) in a quiescent non-flaring state, and the same active region during a period of M-class flares. The results obtained show (1) the presence of a topologically complex asymmetrically fragmented magnetic network in the quiet photosphere driven by meso- and supergranulation, (2) the formation of non-potential magnetic structures with complex polarity separation lines inside the active region, and (3) statistical signatures of canceling bipolar magnetic structures coinciding with flaring activity in the active region. Each of these effects can represent an unstable magnetic configuration acting as an energy source for coronal dissipation and heating.

### **Long-term trends of magnetic bright points: I. Number of MBPs at disc centre**

D. **Utz**, R. Muller, S. Thonhofer, A. Veronig, A. Hanslmeier, M. Bodnárová, M. Bárta, J. C. del Toro Iniesta

A&A A39 (2016)

<http://arxiv.org/pdf/1511.07767v1.pdf>

**Context.** The Sun shows an activity cycle that is caused by its varying global magnetic field. During a solar cycle, sunspots, i.e. extended regions of strong magnetic fields, occur in activity belts that are slowly migrating from middle to lower latitudes, finally arriving close to the equator during the cycle maximum phase. While this has been well known for centuries, much less is known about the solar cycle evolution of small-scale magnetic fields. **Aims.** To address this question, we study magnetic bright points (MBPs) as proxies for such small-scale, kG solar magnetic fields. This study is based on a homogeneous data set that covers a period of eight years. **Methods.** An automated MBP identification algorithm was applied to the synoptic Hinode/SOT G-band data over the period November 2006 to August 2014, i.e. covering the decreasing phase of Cycle 23 and the rise, maximum, and early decrease of Cycle 24. This data set includes, at the moment of investigation, a total of 4 162 images, with about 2.9 million single MBP detections. **Results.** After a careful preselection and monthly median filtering of the data, the investigation revealed that the number of MBPs close to the equator is coupled to the global solar cycle but shifted in time by about 2.5 years. Furthermore, the instantaneous number of detected MBPs depends on the hemisphere, with one hemisphere being more prominent, i.e. showing a higher number of MBPs. After the end of Cycle 23 and at the starting point of Cycle 24, the more active hemisphere changed from south to north. **Conclusions.** These findings suggest that there is indeed a coupling between the activity of MBPs close to the equator with the global magnetic field. The results also indicate that a significant fraction of the magnetic flux that is visible as MBPs close to the equator originates from the sunspot activity belts.

### **Magnetic field strength distribution of magnetic bright points inferred from filtergrams and spectro-polarimetric data**

D. **Utz**<sup>1, 2</sup>, J. Jurčák<sup>3</sup>, A. Hanslmeier<sup>2, 4</sup>, R. Muller<sup>4</sup>, A. Veronig<sup>2</sup> and O. Kühne

A&A 554, A65 (2013)

**Context.** Small scale magnetic fields can be observed on the Sun in G-band filtergrams as magnetic bright points (MBPs) or identified in spectro-polarimetric measurements due to enhanced signals of Stokes profiles. These magnetic fields and their dynamics play a crucial role in understanding the coronal heating problem and also in surface dynamo models. MBPs can theoretically be described to evolve out of a patch of a solar photospheric magnetic field with values below the equipartition field strength by the so-called convective collapse model. After the collapse, the magnetic field of MBPs reaches a higher stable magnetic field level.

**Aims.** The magnetic field strength distribution of small scale magnetic fields as seen by MBPs is inferred.

Furthermore, we want to test the model of convective collapse and the theoretically predicted stable value of about 1300 G.

**Methods.** We used four different data sets of high-resolution Hinode/SOT observations that were recorded simultaneously with the broadband filter device (G-band, Ca II-H) and the spectro-polarimeter. To derive the magnetic field strength distribution of these small scale features, the spectropolarimeter (SP) data sets were treated by the Merlin inversion code. The four data sets comprise different solar surface types: active regions (a sunspot group and a region with pores), as well as quiet Sun.

**Results.** In all four cases the obtained magnetic field strength distribution of MBPs is similar and shows peaks around 1300 G. This agrees well with the theoretical prediction of the convective collapse model. The resulting magnetic field strength distribution can be fitted in each case by a model consisting of log-normal components. The important parameters, such as geometrical mean value and multiplicative standard deviation, are similar in all data sets, so only the relative weighting of the components is different.

### **Comparison of magnetic data products from Solar Orbiter SO/PHI-FDT and SDO/HMI**

A. Moreno Vacas<sup>1,2</sup>, D. Orozco Suárez<sup>1,2</sup>, H. Strecker<sup>1,2</sup>, J. C. del Toro Iniesta<sup>1,2</sup>, J. M. +++  
A&A, 685, A28 (2024)

<https://www.aanda.org/articles/aa/pdf/2024/05/aa49096-23.pdf>

Context. The Polarimetric and Helioseismic Imager (SO/PHI), on board the Solar Orbiter mission, is the first photospheric magnetograph and tachograph to observe the Sun from outside the Sun-Earth line. The Full Disc Telescope (FDT) of SO/PHI, images the whole solar disk with a spatial resolution that varies with the distance between the Sun and the spacecraft.

Aims. We check for consistency between the magnetic field strength (B), the field inclination ( $\gamma$ ), the line-of-sight (LoS) magnetic component (BLoS) and the field azimuth ( $\phi$ ), inferred by SO/PHI-FDT and the Helioseismic and Magnetic Imager (HMI), on board Solar Dynamics Observatory (SDO), and obtain linear correlation coefficients among them.

Methods. We use data from both instruments obtained on 8 March 2022, when the angle between SDO and Solar Orbiter was  $3.4^\circ$  and the solar disk showed four developed active regions. Before comparing the magnetic field products of both instruments we perform a precise alignment of the data, including a matching of the plate scale. Further, in order to improve the homogeneity of the compared data products, the SDO/HMI data were convolved with the SO/PHI-FDT point spread function (PSF). The linear correlation coefficients are obtained through a linear regression of SDO/HMI to SO/PHI-FDT.

Results. The two instruments yield comparable magnetic field data products. The slope coefficients for a linear fit are 1.37 for B, 1.11 for  $\gamma$ , 1.35 for BLoS and 1 for the azimuth. The corresponding fit offsets are  $-94$  G,  $-9.8^\circ$ ,  $5.2$  G and  $0.1^\circ$ , respectively. The agreement between both instruments is significantly better when we take into account the different spatial resolution of both instruments. The fitting results vary slightly depending on the analyzed active region except for one of the four active regions, which shows larger differences and has been excluded from the comparison. The comparison of the LoS magnetic field products from SDO/HMI at 45 s and 720 s with SO/PHI-FDT shows a slope value of 1.17, with the offset less than 6 G, in both cases. **8 March 2022**

## **Stereoscopic disambiguation of vector magnetograms: first applications to SO/PHI-HRT data**

G. Valori, D. Calchetti, A. Moreno Vacas, É. Pariat, S.K. Solanki, +++

A&A 677, A25 2023

<https://arxiv.org/pdf/2307.09907>

Spectropolarimetric reconstructions of the photospheric vector magnetic field are intrinsically limited by the  $180^\circ$ -ambiguity in the orientation of the transverse component. So far, the removal of such an ambiguity has required assumptions about the properties of the photospheric field, which makes disambiguation methods model-dependent. The basic idea is that the unambiguous line-of-sight component of the field measured from one vantage point will generally have a non-zero projection on the ambiguous transverse component measured by the second telescope, thereby determining the "true" orientation of the transverse field. Such an idea was developed and implemented in the Stereoscopic Disambiguation Method (SDM), which was recently tested using numerical simulations. In this work we present a first application of the SDM to data obtained by the High Resolution Telescope (HRT) onboard Solar Orbiter during the March 2022 campaign, when the angle with Earth was 27 degrees. The method is successfully applied to remove the ambiguity in the transverse component of the vector magnetogram solely using observations (from HRT and from the Helioseismic and Magnetic Imager), for the first time. The SDM is proven to provide observation-only disambiguated vector magnetograms that are spatially homogeneous and consistent. A discussion about the sources of error that may limit the accuracy of the method, and of the strategies to remove them in future applications, is also presented. **17-Mar-2022**

**SO Nuggets #21 2023** <https://www.cosmos.esa.int/web/solar-orbiter/-/science-nugget-a-new-solution-to-the-ambiguity-problem>

## **Disambiguation of Vector Magnetograms by Stereoscopic Observations from the Solar Orbiter/Polarimetric and Helioseismic Imager (PHI) and the Solar Dynamic Observatory (SDO)/Helioseismic and Magnetic Imager (HMI)**

Gherardo Valori (1 and 2), Philipp Löschel (1), David Stansby (2), Etienne Pariat (3 and 4), Johann Hirzberger (1), Feng Chen (5)

Solar Phys. 297, Article number: 12 2022

<https://arxiv.org/pdf/2112.10650.pdf>

<https://link.springer.com/content/pdf/10.1007/s11207-021-01942-x.pdf>

Spectropolarimetric reconstructions of the photospheric vector magnetic field are intrinsically limited by the so-called  $180^\circ$  ambiguity in the orientation of the transverse component. The successful launch and operation of Solar Orbiter has made the removal of the  $180^\circ$  ambiguity possible using solely observations obtained from two different vantage points. While the exploitation of such a possibility is straightforward in principle, it is less so in practice and it is therefore important to assess the accuracy and limitations, as a function of both the satellites orbits and

measurement principles. In this work we present a stereoscopic disambiguation method (SDM) and discuss a thorough testing of its accuracy in applications to modeled active regions and quiet Sun observations. In a first series of tests, we employ magnetograms extracted from three different numerical simulations as test fields, and model observations of the magnetograms from different angles and distances. In these more idealized tests, the SDM is proven to reach a 100% disambiguation accuracy when applied to moderately-to-well resolved fields. Even in the case of disambiguation of quiet Sun magnetograms with significant under-resolved scale, the SDM provides an accuracy between 82% and 98% depending on the field strength. The accuracy of the SDM is found to be mostly sensitive to the variable resolution of Solar Orbiter on its highly elliptic orbit, as well as to the intrinsic scale of the observed field. Finally, as a more realistic test, we consider magnetograms that are obtained using a radiative transfer inversion code and the SOPHISM instrument simulator applied to a 3D simulation of a pore, and present a preliminary discussion of the effect of the viewing angle on the observed field.

### **Accuracy of magnetic energy computations**

G. Valori, P. Demoulin, E. Pariat, S. Masson

E-print, April 2013; A&A 553, A38 (2013)

For magnetically driven events, the magnetic energy of the system is the prime energy reservoir that fuels the dynamical evolution. In the solar context, the free energy (i.e., the energy in excess of the potential field energy) is one of the main indicators used in space weather forecasts to predict the eruptivity of active regions. A trustworthy estimation of the magnetic energy is therefore needed in three-dimensional (3D) models of the solar atmosphere, e.g., in coronal fields reconstructions or numerical simulations. The expression of the energy of a system as the sum of its potential energy and its free energy (Thomson's theorem) is strictly valid when the magnetic field is exactly solenoidal. For numerical realizations on a discrete grid, this property may be only approximately fulfilled. We show that the imperfect solenoidality induces terms in the energy that can lead to misinterpreting the amount of free energy present in a magnetic configuration. We consider a decomposition of the energy in solenoidal and nonsolenoidal parts which allows the unambiguous estimation of the nonsolenoidal contribution to the energy. We apply this decomposition to six typical cases broadly used in solar physics. We quantify to what extent the Thomson theorem is not satisfied when approximately solenoidal fields are used. The quantified errors on energy vary from negligible to significant errors, depending on the extent of the nonsolenoidal component of the field. We identify the main source of errors and analyze the implications of adding a variable amount of divergence to various solenoidal fields. Finally, we present pathological unphysical situations where the estimated free energy would appear to be negative, as found in some previous works, and we identify the source of this error to be the presence of a finite divergence. We provide a method of quantifying the effect of a finite divergence in numerical fields, together with detailed diagnostics of its sources. We also compare the efficiency of two divergence-cleaning techniques. These results are applicable to a broad range of numerical realizations of magnetic fields.

### **Comparing Values of the Relative Magnetic Helicity in Finite Volumes**

G. Valori, P. Démoulin and E. Pariat

Solar Physics, Volume 278, Number 2 (2012), 347-366

Relative magnetic helicity, as a conserved quantity of ideal magnetohydrodynamics, has been highlighted as an important quantity to study in plasma physics. Due to its nonlocal nature, its estimation is not straightforward in both observational and numerical data. In this study we derive expressions for the practical computation of the gauge-independent relative magnetic helicity in three-dimensional finite domains. The derived expressions are easy to implement and rapid to compute. They are derived in Cartesian coordinates, but can be easily written in other coordinate systems. We apply our method to a numerical model of a force-free equilibrium containing a flux rope, and compare the results with those obtained employing known half-space equations. We find that our method requires a much smaller volume than half-space expressions to derive the full helicity content. We also prove that values of relative magnetic helicity of different magnetic fields can be compared with each other in the same sense as free-energy values can. Therefore, relative magnetic helicity can be meaningfully and directly compared between different datasets, such as those from different active regions, but also within the same dataset at different times. Typical applications of our formulae include the helicity computation in three-dimensional models of the solar atmosphere, e.g., coronal-field reconstructions by force-free extrapolation and discretized magnetic fields of numerical

### **Magnetofrictional Extrapolations of Low and Lou's Force-Free Equilibria**

G. Valori · B. Kliem · M. Fuhrmann

Solar Phys (2007) 245: 263–285

<http://www.springerlink.com/content/e322435723nw2618/fulltext.pdf>

We present a careful investigation of the magnetofrictional relaxation and extrapolation technique applied to the reconstruction of two test fields. These fields are taken from the family of nonlinear force-free magnetic equilibria constructed by Low and Lou (*Astrophys.J.* **352**, 343, 1990), which have emerged as standard tests for extrapolation techniques in recent years.

## **On the Relationship Between Photospheric Footpoint Motions and Coronal Heating in Solar Active Regions**

A. A. [van Ballegoijen](#)<sup>1</sup>, M. Asgari-Targhi<sup>1</sup>, and M. A. Berger

**2014** ApJ 787 87

Coronal heating theories can be classified as either direct current (DC) or alternating current (AC) mechanisms, depending on whether the coronal magnetic field responds quasi-statically or dynamically to the photospheric footpoint motions. In this paper we investigate whether photospheric footpoint motions with velocities of 1-2 km s<sup>-1</sup> can heat the corona in active regions, and whether the corona responds quasi-statically or dynamically to such motions (DC versus AC heating). We construct three-dimensional magnetohydrodynamic models for the Alfvén waves and quasi-static perturbations generated within a coronal loop. We find that in models where the effects of the lower atmosphere are neglected, the corona responds quasi-statically to the footpoint motions (DC heating), but the energy flux into the corona is too low compared to observational requirements. In more realistic models that include the lower atmosphere, the corona responds more dynamically to the footpoint motions (AC heating) and the predicted heating rates due to Alfvén wave turbulence are sufficient to explain the observed hot loops. The higher heating rates are due to the amplification of Alfvén waves in the lower atmosphere. We conclude that magnetic braiding is a highly dynamic process.

## **Alfvén Wave Solar Model (AWSoM): Coronal Heating**

B. [van der Holst](#), I. V. Sokolov, X. Meng, M. Jin, W. B. Manchester, IV, G. Tóth, and T. I. Gombosi

**2014** ApJ 782 81

We present a new version of the Alfvén wave solar model, a global model from the upper chromosphere to the corona and the heliosphere. The coronal heating and solar wind acceleration are addressed with low-frequency Alfvén wave turbulence. The injection of Alfvén wave energy at the inner boundary is such that the Poynting flux is proportional to the magnetic field strength. The three-dimensional magnetic field topology is simulated using data from photospheric magnetic field measurements. This model does not impose open-closed magnetic field boundaries; those develop self-consistently. The physics include the following. (1) The model employs three different temperatures, namely the isotropic electron temperature and the parallel and perpendicular ion temperatures. The firehose, mirror, and ion-cyclotron instabilities due to the developing ion temperature anisotropy are accounted for. (2) The Alfvén waves are partially reflected by the Alfvén speed gradient and the vorticity along the field lines. The resulting counter-propagating waves are responsible for the nonlinear turbulent cascade. The balanced turbulence due to uncorrelated waves near the apex of the closed field lines and the resulting elevated temperatures are addressed. (3) To apportion the wave dissipation to the three temperatures, we employ the results of the theories of linear wave damping and nonlinear stochastic heating. (4) We have incorporated the collisional and collisionless electron heat conduction. We compare the simulated multi-wavelength extreme ultraviolet images of **CR2107** with the observations from STEREO/EUVI and the Solar Dynamics Observatory/AIA instruments. We demonstrate that the reflection due to strong magnetic fields in the proximity of active regions sufficiently intensifies the dissipation and observable emission. **2011- 2-16**

## **Penumbra micro-jets at high spatial and temporal resolution**

Luc Rouppe [van der Voort](#), [Ainar Drews](#)

A&A **2019**

<https://arxiv.org/pdf/1905.02981.pdf>

Sunspot observations in chromospheric spectral lines have revealed the existence of short-lived linear bright transients, commonly referred to as penumbral micro-jets (PMJs). Details on the origin and physical nature of PMJs are to large extend still unknown. We aim to characterize the dynamical nature of PMJs to provide guidance for future modelling efforts. We analyze high spatial (0.1 arcsec) and temporal resolution (1 s) Ca II H filtergram (0.1 nm bandwidth) observations of a sunspot obtained on two consecutive days with the Swedish 1-m Solar Telescope. We find that PMJs appear to be the rapid brightening of an already existing (faint) fibril. The rapid brightening is the fast increase (typically less than 10 s) in intensity over significant length (several 100s of km) of the existing fibril. For most PMJs, we cannot identify a clear root or source from where the brightening appears to originate. After the fast onset, about half of the PMJs have a top that is moving with an apparent velocity between 5 and 14 km/s, most

of them upwards. For the other PMJs, there is no significant motion of the top. For about a third of the PMJs we observe a splitting into two parallel and co-evolving linear features during the later phases of the lifetime of the PMJ. We conclude that mass flows can play only limited role in the onset phase of PMJs and that it is more likely that we see the effect of a fast heating front. **27 and 28 June 2010**

### **THE FIRST MEASUREMENT OF THE ADIABATIC INDEX IN THE SOLAR CORONA USING TIME-DEPENDENT SPECTROSCOPY OF *Hinode*/EIS OBSERVATIONS**

Tom [Van Doorselaere](#)<sup>1,4</sup>, Nick Wardle<sup>1</sup>, Giulio Del Zanna<sup>2</sup>, Kishan Jansari<sup>1</sup>, Erwin Verwichte<sup>1</sup>, and Valery M. Nakariakov<sup>1,3</sup>

*Astrophysical Journal Letters*, 727:L32 (4pp), **2011** February

We use observations of a slow magnetohydrodynamic wave in the corona to determine for the first time the value of the effective adiabatic index, using data from the Extreme-ultraviolet Imaging Spectrometer on board *Hinode*. We detect oscillations in the electron density, using the CHIANTI atomic database to perform spectroscopy. From the time-dependent wave signals from multiple spectral lines the relationship between relative density and temperature perturbations is determined, which allows in turn to measure the effective adiabatic index to be  $\gamma_{\text{eff}} = 1.10 \pm 0.02$ .

This confirms that the thermal conduction along the magnetic field is very efficient in the solar corona. The thermal conduction coefficient is measured from the phase lag between the temperature and density, and is shown to be compatible with *Spitzer* conductivity.

### **Characterizing the Motion of Solar Magnetic Bright Points at High Resolution**

Samuel J. [Van Kooten](#), [Steven R. Cranmer](#)

*ApJ* **850** 64 **2017**

<https://arxiv.org/pdf/1710.04738.pdf>

Magnetic bright points in the solar photosphere, visible in both continuum and G-band images, indicate footpoints of kilogauss magnetic flux tubes extending to the corona. The power spectrum of bright-point motion is thus also the power spectrum of Alfvén wave excitation, transporting energy up flux tubes into the corona. This spectrum is a key input in coronal and heliospheric models. We produce a power spectrum of bright-point motion using radiative magnetohydrodynamic simulations, exploiting spatial resolution higher than can be obtained in present-day observations, while using automated tracking to produce large data quantities. We find slightly higher amounts of power at all frequencies compared to observation-based spectra, while confirming the spectrum shape of recent observations. This also provides a prediction for observations of bright points with DKIST, which will achieve similar resolution and high sensitivity. We also find a granule size distribution in support of an observed two-population distribution, and we present results from tracking passive tracers which show a similar power spectrum to that of bright points. Finally, we introduce a simplified, laminar model of granulation, with which we explore the roles of turbulence and of the properties of the granulation pattern in determining bright-point motion.

### **Parameterisation of coronal heating: spatial distribution and observable consequences**

T. [van Wettum](#)<sup>1,2</sup>, S. Bingert<sup>1</sup> and H. Peter

*A&A* 554, A39 (**2013**)

**Aims.** We investigate the difference in the spatial distribution of the energy input for parameterisations of different mechanisms to heat the corona of the Sun and possible impacts on the coronal emission.

**Methods.** We use a 3D magneto-hydrodynamic (MHD) model of a solar active region as a reference and compare the Ohmic-type heating in this model to parameterisations for alternating current (AC) and direct current (DC) heating models; in particular, we use Alfvén wave and MHD turbulence heating. We extract the quantities needed for these two parameterisations from the reference model and investigate the spatial distribution of the heat input in all three cases, globally and along individual field lines. To study differences in the resulting coronal emission, we employ 1D loop models with a prescribed heat input based on the heating rate we extracted along a bundle of field lines.

**Results.** On average, all heating implementations show a rough drop of the heating rate with height. This also holds for individual field lines. While all mechanisms show a concentration of the energy input towards the low parts of the atmosphere, for individual field lines the concentration towards the foot points is much stronger for the DC mechanisms than for the Alfvén wave AC case. In contrast, the AC model gives a stronger concentration of the emission towards the foot points. This is because the more homogeneous distribution of the energy input leads to higher coronal temperatures and a more extended transition region.

**Conclusions.** The significant difference in the concentration of the heat input towards the foot points for the AC and DC mechanisms and the pointed difference in the spatial distribution of the coronal emission for these cases show that the two mechanisms should be discriminable by observations. Before drawing final conclusions, these parameterisations should be implemented in new 3D models in a more self-consistent way.

## **Tomography of the Solar Corona with the Metis Coronagraph II: Three-Dimensional Reconstructions of the Electron Density and Comparison with Reconstructions Based on LASCO-C2.**

Vásquez, A.M., Nuevo, F.A., Romoli, M. et al.  
Sol Phys 299, 165 (2024).

<https://doi.org/10.1007/s11207-024-02410-y>

We carried out tomographic reconstructions of the three-dimensional distribution of the electron density of the solar corona based on white light polarized brightness (pB) images taken by the Metis coronagraph on board the Solar Orbiter (SolO) mission. We selected three different time intervals during 2022, and further implemented independent synchronous reconstructions based on LASCO-C2 pB images for comparison purposes. The range of elongations covered by the field-of-view (FoV) of Metis considerably varies as SolO describes its highly eccentric orbit, whereas that of LASCO-C2 remains almost constant. During the selected time intervals, their FoVs partially overlap, allowing a comparison of the reconstructions within the regions in common. The shape and size of the reconstructed coronal structures, streamers and coronal holes, are consistent, demonstrating the suitability of the images of the synoptic program of Metis for tomographic reconstruction of the coronal electron density over its varying FoV. A comparison between the two tomographic reconstructions for each analyzed time interval, shows that the Metis-to-C2 ratio of reconstructed electron density has a median value of  $\approx 1.7$ . This is consistent with the observed ratio of the pB measurements of the two instruments. Our analysis thus also illustrates the value of tomography as a tool for intercalibrating solar coronagraphs irrespective of their spatial location, as long as their FoV partially overlap.

## **Seeing The Solar Corona in Three Dimensions**

Alberto Marcos Vásquez

2015

<http://arxiv.org/pdf/1503.02238v1.pdf>

The large availability and rich spectral coverage of today's observational data of the solar corona, and the high spatial and temporal resolution of many instruments, has enabled the evolution of three-dimensional (3D) physical models to a great level of detail. However, the 3D information provided by the data is rather limited as every instrument observes from a single angle of vision, or two at the most in the case of the STEREO mission. Two powerful available observational techniques to infer detailed 3D information of the solar corona from empirical data are stereoscopy and tomography. In particular, the technique known as *differential emission measure tomography* (DEMT) allows determination of the 3D distribution of the coronal electron density and temperature in the inner corona. This paper summarizes the main technical aspects of DEMT, reviews all published work based on it, and comments its future development and applications.

## **THE DYNAMICS OF THE SOLAR MAGNETIC FIELD: POLARITY REVERSALS, BUTTERFLY DIAGRAM, AND QUASI-BIENNIAL OSCILLATIONS**

A. Vecchio<sup>1,2</sup>, M. Laurenza<sup>3</sup>, D. Meduri<sup>1,4</sup>, V. Carbone<sup>1,5</sup> and M. Storini

2012 ApJ 749 27

The spatio-temporal dynamics of the solar magnetic field has been investigated by using NSO/Kitt Peak magnetic synoptic maps covering the period 1976 August-2003 September. The field radial component, for each heliographic latitude, has been decomposed in intrinsic mode functions through the Empirical Mode Decomposition in order to investigate the time evolution of the various characteristic oscillating modes at different latitudes. The same technique has also been applied on synoptic maps of the meridional and east-west components, which were derived from the observed line-of-sight projection of the field by using the differential rotation. Results obtained for the  $\sim 22$  yr cycle, related to the polarity inversions of the large-scale dipolar field, show an antisymmetric behavior with respect to the equator in all the field components and a marked poleward flux migration in the radial and meridional components (from about  $-35^\circ$  and  $+35^\circ$  in the southern and northern hemispheres, respectively). The quasi-biennial oscillations (QBOs) are also identified as a fundamental timescale of variability of the magnetic field and associated with poleward magnetic flux migration from low latitudes around the maximum and descending phase of the solar cycle. Moreover, signs of an equatorward drift, at a  $\sim 2$  yr rate, seem to appear in the radial and toroidal components. Hence, the QBO patterns suggest a link to a dynamo action. Finally, the high-frequency component of the magnetic field, at timescales less than 1 yr, provides the most energetic contribution and it is associated with the outbreaks of the bipolar regions on the solar surface.

## **Data-driven simulations of magnetic field evolution in Active Region 11429: Magneto-friction method using PENCIL code**

P. Vemareddy, Jörn Warnecke, Ph. A. Bourdin

Research in Astronomy and Astrophysics

2023

<https://arxiv.org/pdf/2312.12124.pdf>



Coronal magnetic fields evolve quasi statically over long time scales and dynamically over short time scales. As of now there exists no regular measurements of coronal magnetic fields, and therefore generating the coronal magnetic field evolution using the observations of the magnetic field at the photosphere is of fundamental requirement to understand the origin of the transient phenomena from the solar active regions. Using the magnetofriction (MF) approach, we aim to simulate the coronal field evolution in the solar active region 11429. The MF method is implemented in open source \PC along with a driver module to drive the initial field with different boundary conditions prescribed from observed vector magnetic fields at the photosphere. In order to work with vector potential and the observations, we prescribe three types of bottom boundary drivers with varying free-magnetic energy. The MF simulation reproduces the magnetic structure, which better matches to the sigmoidal morphology exhibited by AIA images at the pre-eruptive time. We found that the already sheared field further driven by the sheared magnetic field, will maintain and further build the highly sheared coronal magnetic configuration, as seen in AR 11429. Data-driven MF simulation is a viable tool to generate the coronal magnetic field evolution, capturing the formation of the twisted flux rope and its eruption. **7 Mar 2012**

## **Successive Injection of Opposite Magnetic Helicity: Evidence for Active Regions without Coronal Mass Ejections**

[P. Vemareddy](#)

MNRAS **2021**

<https://arxiv.org/pdf/2108.07741.pdf>

Magnetic helicity (MH) is a measure of twist and shear of magnetic field. MH is injected in the active region (AR) corona through photospheric footpoint motions causing twisted and sheared magnetic fields. From the conservation property of the helicity, it was conjectured that an already twisted flux rope (FR) with continuous injection of MH inevitably erupts to remove the excess accumulated coronal helicity. Therefore, understanding the nature and evolution of the photospheric helicity flux transfer is crucial to reveal the intensity of the flare/CME activity. Using the time-sequence vector-magnetograms of \textit{Helioseismic Magnetic Imager}, we study the evolution of MH injection in emerging AR 12257. The photospheric flux motions in this AR inject positive helicity in the first 2.5 days followed by negative helicity later. This successive injection of opposite helicity is consistent with the sign of mean force-free twist parameter ( $\alpha_{av}$ ), orientation of magnetic-tongues. Also, the extrapolated AR magnetic structure exhibits transformation of global-shear without a twisted FR in the core of the AR. No CMEs are launched from this AR but C-class flaring activity is observed predominantly in the second half of the evolution period. The ARs with sign reversal of the MH injection are not favorable to twisted FR formation with excess coronal helicity and therefore are important to identify CME-less ARs readily. A possible scenario in these ARs is that when one sign of helicity flux is replaced by opposite sign, the magnetic field of different connectivity with opposite shear undergoes reconnection at different scales giving rise to both intermittent flares and enhanced coronal heating. **2015 01 07-10**

## **Investigation of Helicity and Energy Flux Transport in Three Emerging Solar Active Regions**

[P. Vemareddy](#)

**2015** ApJ 806 245

We report the results of an investigation of helicity and energy flux transport from three emerging solar active regions (ARs). Using time sequence vector magnetic field observations obtained from the Helioseismic Magnetic Imager, the velocity field of plasma flows is derived by the differential affine velocity estimator for vector magnetograms. In three cases, the magnetic fluxes evolve to pump net positive, negative, and mixed-sign helicity flux into the corona. The coronal helicity flux is dominantly coming from the shear term that is related to horizontal flux motions, whereas energy flux is dominantly contributed by the emergence term. The shear helicity flux has a phase delay of 5–14 hr with respect to absolute magnetic flux. The nonlinear curve of coronal energy versus relative helicity identifies the configuration of coronal magnetic fields, which is approximated by a fit of linear force-free fields. The nature of coronal helicity related to the particular pattern of evolving magnetic fluxes at the photosphere has implications for the generation mechanism of two kinds of observed activity in the ARs.

## **Quasi-Static 3D-Magnetic Field Evolution in Solar Active Region NOAA 11166 Associated with X1.5 Flare**

[P. Vemareddy](#), and T. Wiegmann

E-print, July **2014**; ApJ

<http://arxiv.org/pdf/1406.7823v1.pdf>

We study the quasi-static evolution of coronal magnetic fields constructed from the Non Linear Force Free Field (NLFFF) approximation aiming to understand the relation between the magnetic field topology and ribbon emission during an X1.5 flare in active region (AR) NOAA 11166. The flare with a quasi-elliptical, and two remote ribbons occurred on **March 9, 2011** at 23:13UT over a positive flux region surrounded by negative flux at the center of the

bipolar AR. Our analysis of the coronal magnetic structure with potential and NLFFF solutions unveiled the existence of a single magnetic null point associated with a fan-spine topology and is co-spatial with the hard X-ray source. The footpoints of the fan separatrix surface agree with the inner edge of the quasi-elliptical ribbon and the outer spine is linked to one of the remote ribbons. During the evolution, the slow footpoint motions stressed the fieldlines along the polarity inversion line and caused electric current layers in the corona around the fan separatrix surface. These current layers trigger magnetic reconnection as a consequence of dissipating currents, which are visible as cusped shape structures at lower heights. The reconnection process reorganised the magnetic field topology whose signatures are observed at the separatrices/QSL structure both in the photosphere and corona during the pre-to-post flare evolution. In agreement with previous numerical studies, our results suggest that the line-tied footpoint motions perturb the fan-spine system and cause null point reconnection, which eventually causes the flare emission at the footpoints of the fieldlines.

## **Magnetic structure of solar active region NOAA 11158**

P. [Vemareddy](#), A. Ambastha, T. Wiegelmann

BASI 2013, Bulletin of Astronomical Society of India

<http://arxiv.org/pdf/1310.6895v1.pdf>

Magnetic fields in the solar corona are responsible for a wide range of phenomena. However, any direct measurements of the coronal magnetic fields are very difficult due to lack of suitable spectral lines, weak magnetic fields, and high temperatures. Therefore, one extrapolates photospheric field measurements into the corona. Owing to low coronal plasma  $\beta$ , we can apply a force-free model in lowest order to study the slow evolution of active region (AR) magnetic fields. On applying these models to AR 11158 and compared with coronal plasma tracers, we found that (1) the approximation of potential field to coronal structures over large length scales is a reasonable one, (2) linear force-free (LFF) assumption to AR coronal fields may not be applicable model as it assumes uniform twist over the entire AR, and (3) for modeling fields at sheared, stressed locations where energy release in the form of flares are usually observed, non-linear force free fields (NLFFF) seem to provide a good approximation. The maximum available free-energy profile shows step-wise decrease that is sufficient to power an M-class flare as observed. **2011-02-13**

## **ON THE ABSENCE OF PHOTOSPHERIC NET CURRENTS IN VECTOR MAGNETOGRAMS OF SUNSPOTS OBTAINED FROM HINODE (SOLAR OPTICAL TELESCOPE/SPECTRO-POLARIMETER)**

P. [Venkatakrisnan](#) and Sanjiv Kumar Tiwari

2009 ApJ 706 L114-L119

Various theoretical and observational results have been reported regarding the presence/absence of net electric currents in the sunspots. The limited spatial resolution of the earlier observations perhaps obscured the conclusions. We have analyzed 12 sunspots observed from *Hinode* (Solar Optical Telescope/Spectro-polarimeter) to clarify the issue. The azimuthal and radial components of magnetic fields and currents have been derived. The azimuthal component of the magnetic field of sunspots is found to vary in sign with azimuth. The radial component of the field also varies in magnitude with azimuth. While the latter pattern is a confirmation of the interlocking combed structure of penumbral filaments, the former pattern shows that the penumbra is made up of a "curly interlocking combed" magnetic field. The azimuthally averaged azimuthal component is seen to decline much faster than  $1/\varpi$  in the penumbra, after an initial increase in the umbra, for all the spots studied. This confirms the confinement of magnetic fields and absence of a net current for sunspots as postulated by Parker. The existence of a global twist for a sunspot even in the absence of a net current is consistent with a fibril-bundle structure of the sunspot magnetic fields.

## **Coronal heating in coupled photosphere-chromosphere-coronal systems: turbulence and leakage**

A. [Verdini](#)<sup>1</sup>, R. Grappin<sup>2,3</sup> and M. Velli

A&A 538, A70 (2012)

Context. Coronal loops act as resonant cavities for low-frequency fluctuations that are transmitted from the deeper layers of the solar atmosphere. These fluctuations are amplified in the corona and lead to the development of turbulence that in turn is able to dissipate the accumulated energy, thus heating the corona. However, trapping is not perfect, because some energy leaks down to the chromosphere on a long timescale, limiting the turbulent heating. Aims. We consider the combined effects of turbulence and energy leakage from the corona to the photosphere in determining the turbulent energy level and associated heating rate in models of coronal loops, which include the chromosphere and transition region.

Methods. We use a piece-wise constant model for the Alfvén speed in loops and a reduced MHD-shell model to describe the interplay between turbulent dynamics in the direction perpendicular to the mean field and propagation along the field. Turbulence is sustained by incoming fluctuations that are equivalent, in the line-tied case, to forcing by the photospheric shear flows. While varying the turbulence strength, we systematically compare the average

coronal energy level and dissipation in three models with increasing complexity: the classical closed model, the open corona, and the open corona including chromosphere (or three-layer model), with the last two models allowing energy leakage.

Results. We find that (i) leakage always plays a role. Even for strong turbulence, the dissipation time never becomes much lower than the leakage time, at least in the three-layer model; therefore, both the energy and the dissipation levels are systematically lower than in the line-tied model; (ii) in all models, the energy level is close to the resonant prediction, i.e., assuming an effective turbulent correlation time longer than the Alfvén coronal crossing time; (iii) the heating rate is close to the value given by the ratio of photospheric energy divided by the Alfvén crossing time; (iv) the coronal spectral range is divided in two: an inertial range with 5/3 spectral slope, and a large-scale peak where nonlinear couplings are inhibited by trapped resonant modes; (v) in the realistic three-layer model, the two-component spectrum leads to a global decrease in damping equal to Kolmogorov damping reduced by a factor  $u_{rms}/V_{ac}$  where  $V_{ac}$  is the coronal Alfvén speed.

### **Photospheric Magnetic Fields of the Trailing Sunspots in Active Region NOAA 12396**

[M. Verma](#), [H. Balthasar](#), [C. Denker](#), [F. Böhm](#), [C. E. Fischer](#), [C. Kuckein](#), [S. J. González Manrique](#), [M. Sobotka](#), [N. Bello González](#), [A. Diercke](#), [T. Berkefeld](#), [M. Collados](#), [A. Feller](#), [A. Hofmann](#), [A. Lagg](#), [H. Nicklas](#), [D. Orozco Suárez](#), [A. Pastor Yabar](#), [R. Rezaei](#), [R. Schlichenmaier](#), [D. Schmidt](#), [W. Schmidt](#), [M. Sigwarth](#), [S. K. Solanki](#), [D. Soltau](#), [J. Staude](#), [K. G. Strassmeier](#), [R. Volkmer](#), [O. von der Lühe](#), [T. Waldmann](#)

"Solar Polarization Workshop 8", ASP Proceedings, Luca Belluzzi (eds.)

**2018**

<https://arxiv.org/pdf/1805.07752.pdf>

The solar magnetic field is responsible for all aspects of solar activity. Sunspots are the main manifestation of the ensuing solar activity. Combining high-resolution and synoptic observations has the ambition to provide a comprehensive description of the sunspot growth and decay processes. Active region NOAA 12396 emerged on **2015 August 3** and was observed **three days later** with the 1.5-meter GREGOR solar telescope on 2015 August 6. High-resolution spectropolarimetric data from the GREGOR Infrared Spectrograph (GRIS) are obtained in the photospheric Si I  $\lambda$  1082.7 nm and Ca I  $\lambda$  1083.9 nm lines, together with the chromospheric He I  $\lambda$  1083.0 nm triplet. These near-infrared spectropolarimetric observations were complemented by synoptic line-of-sight magnetograms and continuum images of the Helioseismic and Magnetic Imager (HMI) and EUV images of the Atmospheric Imaging Assembly (AIA) on board the Solar Dynamics Observatory (SDO).

### **On the extent of the moat flow in axisymmetric sunspots**

[M. Verma](#), [P. Kummerow](#), [C. Denker](#)

Astronomische Nachrichten/Astronomical Notes

**2018**

<https://arxiv.org/pdf/1805.04356.pdf>

Unipolar, axisymmetric sunspots are figuratively called "theoretician's sunspots" because their simplicity supposedly makes them more suitable for theoretical descriptions or numerical models. On **2013 November 18**, a very large specimen (active region NOAA 11899) crossed the central meridian of the Sun. The moat flow associated with this very large spot is quantitatively compared to that of a medium and a small sunspot to determine the extent of the moat flow in different environments. We employ continuum images and magnetograms of the Helioseismic and Magnetic Imager (HMI) as well as extreme ultraviolet (EUV) images at  $\lambda$  160 nm of the Atmospheric Imaging Assembly (AIA), both on board the Solar Dynamics Observatory (SDO), to measure horizontal proper motions with Local Correlation Tracking (LCT) and flux transport velocities with the Differential Affine Velocity Estimator (DAVE). We compute time-averaged flow maps ( $\pm 6$  hours around meridian passage) and radial averages of photometric, magnetic and flow properties. Flow fields of a small- and a medium-sized axisymmetric sunspot provide the context for interpreting the results. All sunspots show the outward moat flow and the advection of moving magnetic features (MMFs). However, the extent of the moat flow varies from spot to spot but a correlation of flow properties with size is tenuous, if at all present. The moat flow is asymmetric and predominantly in the east-west direction, whereby deviations are related to the tilt angle of the sunspot group as well as to the topology and activity level of the trailing plage.

### **High-resolution imaging and near-infrared spectroscopy of penumbral decay**

[M. Verma](#), [C. Denker](#), [H. Balthasar](#), [C. Kuckein](#), [R. Rezaei](#), [M. Sobotka](#), [N. Deng](#), [H. Wang](#), [A. Tritschler](#), [M. Collados](#), [A. Diercke](#), [S.J. González Manrique](#)

A&A

**2018**

<https://arxiv.org/pdf/1801.03686.pdf>

Combining high-resolution spectropolarimetric and imaging data is key to understanding the decay process of sunspots as it allows us scrutinizing the velocity and magnetic fields of sunspots and their surroundings. Active

region NOAA 12597 was observed on **24/09/2016** with the 1.5-m GREGOR solar telescope using high-spatial resolution imaging as well as imaging spectroscopy and near-infrared (NIR) spectropolarimetry. Horizontal proper motions were estimated with LCT, whereas LOS velocities were computed with spectral line fitting methods. The magnetic field properties were inferred with the SIR code for the Si I and Ca I NIR lines. At the time of the GREGOR observations, the leading sunspot had two light-bridges indicating the onset of its decay. One of the light-bridges disappeared, and an elongated, dark umbral core at its edge appeared in a decaying penumbral sector facing the newly emerging flux. The flow and magnetic field properties of this penumbral sector exhibited weak Evershed flow, moat flow, and horizontal magnetic field. The penumbral gap adjacent to the elongated umbral core and the penumbra in that penumbral sector displayed LOS velocities similar to granulation. The separating polarities of a new flux system interacted with the leading and central part of the already established active region. As a consequence, the leading spot rotated 55-degree in clockwise direction over 12 hours. In the high-resolution observations of a decaying sunspot, the penumbral filaments facing flux emergence site contained a darkened area resembling an umbral core filled with umbral dots. This umbral core had velocity and magnetic field properties similar to the sunspot umbra. This implies that the horizontal magnetic fields in the decaying penumbra became vertical as observed in flare-induced rapid penumbral decay, but on a very different time-scale.

### **Horizontal flow fields in and around a small active region-- The transition period between flux emergence and decay**

M. **Verma**, C. Denker, H. Balthasar, C. Kuckein, S.J. González Manrique, M. Sobotka, N. Bello González, S. Hoch, A. Diercke, P. Kummerow, T. Berkefeld, M. Collados, A. Feller, A. Hofmann, F. Kneer, A. Lagg, J. Löhner-Böttcher, H. Nicklas, A. Pastor Yabar, R. Schlichenmaier, D. Schmidt, W. Schmidt, M. Schubert, M. Sigwarth, S.K. Solanki, D. Soltau, J. Staude, K.G. Strassmeier, R. Volkmer, O. von der Lühe, T. Waldmann

A&A **2016**

<http://arxiv.org/pdf/1605.07462v1.pdf>

**Aims.** Combining high-resolution and synoptic observations aims to provide a comprehensive description of flux emergence at photospheric level and of the growth process that eventually leads to a mature active region.  
**Methods.** Small active region NOAA 12118 was observed on **2014 July 18** with the 1.5-meter GREGOR solar telescope on 2014 July 18. High-resolution time-series of blue continuum and G-band images acquired in the blue imaging channel (BIC) of the GREGOR Fabry-Pérot Interferometer (GFPI) were complemented by LOS magnetograms and continuum images obtained with the HMI onboard the SDO. Horizontal proper motions and horizontal plasma velocities were computed with local correlation tracking (LCT) and the differential affine velocity estimator, respectively. Morphological image processing was employed to measure the photometric/magnetic area, magnetic flux, and the separation profile of the EFR during its evolution.  
**Results.** The computed growth rates for photometric area, magnetic area, and magnetic flux are about twice as high as the respective decay rates. The space-time diagram using HMI magnetograms of five days traces a leaf-like structure, which is determined by the initial separation of the two polarities, a rapid expansion phase, a time when the spread stalls, and a period when the region slowly shrinks again. The separation rate of 0.26 km/s is highest in the initial stage, and it decreases when the separation comes to a halt. Horizontal plasma velocities computed at four evolutionary stages indicate a changing pattern of inflows. In LCT maps we find persistent flow patterns such as outward motions in the outer part of the two major pores, a diverging feature near the trailing pore marking the site of upwelling plasma and flux emergence, and low velocities in the interior of pores. We detected many elongated rapidly expanding granules between the two major polarities.

### **Contribution of Field Strength Gradients to the Net Vertical Current of Active Regions**

P. **Vemareddy**

**2017 ApJ 851 3**

<http://sci-hub.bz/http://iopscience.iop.org/0004-637X/851/1/3/>

We examined the contribution of field strength gradients for the degree of net vertical current (NVC) neutralization in active regions (ARs). We used photospheric vector magnetic field observations of AR 11158 obtained by Helioseismic and Magnetic Imager on board SDO and Hinode. The vertical component of the electric current is decomposed into twist and shear terms. The NVC exhibits systematic evolution owing to the presence of the sheared polarity inversion line between rotating and shearing magnetic regions. We found that the sign of shear current distribution is opposite in dominant pixels (60%–65%) to that of twist current distribution, and its time profile bears no systematic trend. This result indicates that the gradient of magnetic field strength contributes to an opposite signed, though smaller in magnitude, current to that contributed by the magnetic field direction in the vertical component of the current. Consequently, the net value of the shear current is negative in both polarity regions, which when added to the net twist current reduces the direct current value in the north ( $B_z > 0$ ) polarity, resulting in a higher degree of NVC neutralization. We conjecture that the observed opposite signs of shear and twist currents are an indication, according to Parker, that the direct volume currents of flux tubes are canceled by their return currents, which are contributed by field strength gradients. Furthermore, with the increase of spatial resolution, we

found higher values of twist, shear current distributions. However, the resolution effect is more useful in resolving the field strength gradients, and therefore suggests more contribution from shear current for the degree of NVC neutralization. **13-16.02.2011**

### **High-resolution imaging and near-infrared spectroscopy of penumbral decay**

M. **Verma**<sup>1</sup>, C. Denker<sup>1</sup>, H. Balthasar<sup>1</sup>, C. Kuckein<sup>1</sup>, R. Rezaei<sup>2</sup>, M. Sobotka<sup>3</sup>, N. Deng<sup>4,5</sup>, H. Wang<sup>4,5</sup>, A. Tritschler<sup>6</sup>, M. Collados<sup>2</sup>, A. Diercke<sup>1,7</sup> and S. J. González Manrique<sup>1,8</sup>  
A&A 614, A2 (2018)

<https://www.aanda.org/articles/aa/pdf/2018/06/aa31801-17.pdf>

**Aims.** Combining high-resolution spectropolarimetric and imaging data is key to understanding the decay process of sunspots as it allows us to scrutinize the velocity and magnetic fields of sunspots and their surroundings.

**Methods.** Active region NOAA 12597 was observed on **2016 September 24** with the 1.5-meter GREGOR solar telescope using high-spatial-resolution imaging as well as imaging spectroscopy and near-infrared (NIR) spectropolarimetry. Horizontal proper motions were estimated with local correlation tracking, whereas line-of-sight (LOS) velocities were computed with spectral line fitting methods. The magnetic field properties were inferred with the “Stokes Inversions based on Response functions” (SIR) code for the Si I and Ca I NIR lines.

**Results.** At the time of the GREGOR observations, the leading sunspot had two light bridges indicating the onset of its decay. One of the light bridges disappeared, and an elongated, dark umbral core at its edge appeared in a decaying penumbral sector facing the newly emerging flux. The flow and magnetic field properties of this penumbral sector exhibited weak Evershed flow, moat flow, and horizontal magnetic field. The penumbral gap adjacent to the elongated umbral core and the penumbra in that penumbral sector displayed LOS velocities similar to granulation. The separating polarities of a new flux system interacted with the leading and central part of the already established active region. As a consequence, the leading spot rotated 55° clockwise over 12 h.

**Conclusions.** In the high-resolution observations of a decaying sunspot, the penumbral filaments facing the flux emergence site contained a darkened area resembling an umbral core filled with umbral dots. This umbral core had velocity and magnetic field properties similar to the sunspot umbra. This implies that the horizontal magnetic fields in the decaying penumbra became vertical as observed in flare-induced rapid penumbral decay, but on a very different time-scale.

### **Non-axisymmetric component of the photospheric magnetic field**

E. S. **Vernova**, **M. I. Tyasto**, **D. G. Baranov**, **O. A. Danilova**  
Solar Phys. 2019

<https://arxiv.org/pdf/1904.03034.pdf>

The longitudinal asymmetry of the photospheric magnetic field distribution is studied on the basis of the data of the Kitt Peak National Solar Observatory (synoptic maps for the period 1976 - 2016). The method of vector summing of magnetic fields is used, which allows to decrease the influence of the stochastic components uniformly distributed over the whole longitude interval, and to stress a steady non-axisymmetric component of the field. The distributions of magnetic fields of different intensity are considered separately for the strong ( $B > 50$  G), weak ( $B < 5$  G) and medium ( $50 > B > 5$  G) fields. It is shown that the longitudinal asymmetry for all groups of fields changes in phase with the 11-year cycle of solar activity. The asymmetry of strong and medium fields changes in phase with magnetic fluxes of these fields, while the asymmetry of weak fields is in antiphase with the flux of weak fields. The distributions of strong and medium magnetic fields over the longitude are similar in the shape: The maximum of distribution is located at the longitude  $\sim 180^\circ$  during the period of ascent - maximum of solar cycle and at the longitude  $\sim 360^\circ$  during the period of descent - minimum. The weak fields exhibit the opposite picture: the maximum of their distribution is always observed at the longitude, where the strong and medium fields show minimum.

### **Latitudinal profiles of the photospheric magnetic field for solar cycles 19-21**

Elena **Vernova**, Marta Tyasto, Dmitrii Barano  
2017

<https://arxiv.org/pdf/1704.02586.pdf>

For groups of photospheric magnetic fields differing in strength the time averaged synoptic maps were obtained on the basis of the National Solar Observatory Kitt Peak data (1976-2003). The latitudinal profiles of magnetic field fluxes were considered separately for each 5 G interval of the field strength  $B$ . The changes both of the profile maxima and of the latitudinal localization of these maxima were studied. The obtained results show that the latitudinal distribution of magnetic fields considerably changes at certain values of the field strength: 5 G, 15 G, and 50 G. The magnetic flux for field groups differing in strength, monotonically decreases with increase of strength for all fields with strength  $B > 5$  G. For these fields the fluxes of the southern hemisphere exceed fluxes of the northern hemisphere. A very special group is represented by the weakest fields  $B < 5$  G, which are in antiphase both in localization and in time changes with stronger fields.

## **Latitudinal Distribution of the Photospheric Magnetic Fields of Different Magnitudes**

E.S. [Vernova](#), M.I. Tyasto, D.G. Baranov

Solar Phys. Volume 291, [Issue 3](#), pp 741-750 **2015**

<http://arxiv.org/pdf/1504.02407v1.pdf>

Photospheric magnetic fields are studied using synoptic maps for 1976-2003 (NSO, Kitt Peak). Synoptic maps were averaged over the period of nearly 3 solar cycles (Solar Cycles 21-23). The change of latitudinal distribution was considered for the following groups of magnetic fields:  $B = 0-5$  G;  $B = 5-15$  G;  $B = 15-50$  G and  $B > 50$  G. Magnetic fields in each of the groups have common features of latitudinal distribution, while for different field groups these features change significantly. Each of the groups is closely related to a certain manifestation of the solar activity. Strong magnetic fields are connected with two manifestations of activity on the Sun: active regions (magnetic fields  $B > 15$  G) occupy sunspots zones and polar faculae (magnetic fields  $50 \text{ G} > B > 15 \text{ G}$ ) occupy latitudes around  $65^\circ$ - $75^\circ$ . Fields from 5 to 15 G occupy the polar regions and are connected with polar coronal holes (solar global dipole). Fields with  $B < 5$  G occupy: a) equatorial region; b) latitudes  $40^\circ$ - $60^\circ$  connected with the solar global dipole.

## **Photospheric Magnetic Field: Relationship Between North-South Asymmetry and Flux Imbalance**

E. S. [Vernova](#), M. I. Tyasto, D. G. Baranov

Solar Phys., Volume 289, Issue 8, pp 2845-2865 **2014**

Photospheric magnetic fields were studied using the Kitt Peak synoptic maps for 1976–2003. Only strong magnetic fields ( $B > 100$  G) of the equatorial region were taken into account. The north-south asymmetry of the magnetic fluxes was considered as well as the imbalance between positive and negative fluxes. The north-south asymmetry displays a regular alternation of the dominant hemisphere during the solar cycle: the northern hemisphere dominated in the ascending phase, the southern one in the descending phase during Solar Cycles 21–23. The sign of the imbalance did not change during the 11 years from one polar-field reversal to the next and always coincided with the sign of the Sun's polar magnetic field in the northern hemisphere. The dominant sign of leading sunspots in one of the hemispheres determines the sign of the magnetic-flux imbalance. The sign of the north-south asymmetry of the magnetic fluxes and the sign of the imbalance of the positive and the negative fluxes are related to the quarter of the 22-year magnetic cycle where the magnetic configuration of the Sun remains constant (from the minimum where the sunspot sign changes according to Hale's law to the magnetic-field reversal and from the reversal to the minimum). The sign of the north-south asymmetry for the time interval considered was determined by the phase of the 11-year cycle (before or after the reversal); the sign of the imbalance of the positive and the negative fluxes depends on both the phase of the 11-year cycle and on the parity of the solar cycle. The results obtained demonstrate the connection of the magnetic fields in active regions with the Sun's polar magnetic field in the northern hemisphere.

## **Model of the magnetic field in the inner heliosphere with regard to radial field strength leveling in the solar corona**

I. S. [Veselovsky](#) and A. T. Lukashenko

Solar System Research, Volume 46, Number 2, 149-159, **2012**

Astronomicheskii Vestnik, **2012**, Vol. 46, No. 2, pp. 162–172.

On the basis of experimental results from the Ulysses spacecraft, a model is proposed for calculating the magnetic field in the corona and the heliosphere in the potential approximation, which is a modification of the potential-field source-surface model. In addition to the photospheric surface and the source surface, a new demarcated spherical surface (leveling surface) is introduced in this model. The magnitude of the radial component of the magnetic field on this surface is assumed to be constant, and its sign abruptly changes from one hemisphere to another. General analytical formulas are given to calculate the potential and field for this model. Calculations are described in detail using the dipole and quadrupole harmonics as examples. Expressions are obtained for the surface currents. The results of visualization of the magnetic field for an axial dipole are discussed.

## **MODELING THE LINE-OF-SIGHT INTEGRATED EMISSION IN THE CORONA: IMPLICATIONS FOR CORONAL HEATING**

Nicholeen M. [Viall](#) and James A. Klimchuk

**2013** ApJ 771 115

One of the outstanding problems in all of space science is uncovering how the solar corona is heated to temperatures greater than 1 MK. Though studied for decades, one of the major difficulties in solving this problem has been unraveling the line-of-sight (LOS) effects in the observations. The corona is optically thin, so a single pixel measures counts from an indeterminate number (perhaps tens of thousands) of independently heated flux tubes, all along that pixel's LOS. In this paper we model the emission in individual pixels imaging the active region corona in the extreme ultraviolet. If LOS effects are not properly taken into account, erroneous conclusions regarding both

coronal heating and coronal dynamics may be reached. We model the corona as an LOS integration of many thousands of completely independently heated flux tubes. We demonstrate that despite the superposition of randomly heated flux tubes, nanoflares leave distinct signatures in light curves observed with multi-wavelength and high time cadence data, such as those data taken with the Atmospheric Imaging Assembly on board the Solar Dynamics Observatory. These signatures are readily detected with the time-lag analysis technique of Viall & Klimchuk in 2012. Steady coronal heating leaves a different and equally distinct signature that is also revealed by the technique.

## **EVIDENCE FOR WIDESPREAD COOLING IN AN ACTIVE REGION OBSERVED WITH THE SDO ATMOSPHERIC IMAGING ASSEMBLY**

Nicholeen M. [Viall](#) and James A. Klimchuk

2012 ApJ 753 35

A well-known behavior of EUV light curves of discrete coronal loops is that the peak intensities of cooler channels or spectral lines are reached at progressively later times than hotter channels. This time lag is understood to be the result of hot coronal loop plasma cooling through these lower respective temperatures. However, loops typically comprise only a minority of the total emission in active regions (ARs). Is this cooling pattern a common property of AR coronal plasma, or does it only occur in unique circumstances, locations, and times? The new Solar Dynamics Observatory/Atmospheric Imaging Assembly (SDO/AIA) data provide a wonderful opportunity to answer this question systematically for an entire AR. We measure the time lag between pairs of SDO/AIA EUV channels using 24 hr of images of AR 11082 observed on **2010 June 19**. We find that there is a time-lag signal consistent with cooling plasma, just as is usually found for loops, throughout the AR including the diffuse emission between loops for the entire 24 hr duration. The pattern persists consistently for all channel pairs and choice of window length within the 24 hr time period, giving us confidence that the plasma is cooling from temperatures of greater than 3 MK, and sometimes exceeding 7 MK, down to temperatures lower than  $\sim 0.8$  MK. This suggests that the bulk of the emitting coronal plasma in this AR is not steady; rather, it is dynamic and constantly evolving. These measurements provide crucial constraints on any model which seeks to describe coronal heating.

## **Time-Dependent Tomographic Reconstruction of the Solar Corona**

Didier [Vibert](#), Christelle Peillon, Philippe Lamy, [Richard A. Frazin](#), [Julien Wojak](#)

2016

<http://arxiv.org/pdf/1607.06308v1.pdf>

Solar rotational tomography (SRT) applied to white-light coronal images observed at multiple aspect angles has been the preferred approach for determining the three-dimensional (3D) electron density structure of the solar corona. However, it is seriously hampered by the restrictive assumption that the corona is time-invariant which introduces significant errors in the reconstruction. We first explore several methods to mitigate the temporal variation of the corona by decoupling the "fast-varying" inner corona from the "slow-moving" outer corona using multiple masking (either by juxtaposition or recursive combination) and radial weighting. Weighting with a radial exponential profile provides some improvement over a classical reconstruction but only beyond 3 R<sub>sun</sub>. We next consider a full time-dependent tomographic reconstruction involving spatio-temporal regularization and further introduce a co-rotating regularization aimed at preventing concentration of reconstructed density in the plane of the sky. Crucial to testing our procedure and properly tuning the regularization parameters is the introduction of a time-dependent MHD model of the corona based on observed magnetograms to build a time-series of synthetic images of the corona. Our procedure, which successfully reproduces the time-varying model corona, is finally applied to a set of 53 LASCO-C2 pB images roughly evenly spaced in time from **15 to 29 March 2009**. Our procedure paves the way to a time-dependent tomographic reconstruction of the coronal electron density to the whole set of LASCO-C2 images presently spanning 20 years.

## **Magnetic Rayleigh-Taylor Instability at a Contact Discontinuity With Oblique Magnetic Field**

E. [Vickers](#), [I. Ballai](#), [R. Erdélyi](#)

A&A 2019

<https://arxiv.org/pdf/1911.12734.pdf>

Aims: In the present work we investigate the nature of the magnetic Rayleigh-Taylor instability at a density interface permeated by an oblique, homogeneous magnetic field in an incompressible limit. Methods: Using the system of linearised ideal incompressible magnetohydrodynamics (MHD) equations we derive the dispersion relation for perturbations of the contact discontinuity by imposing the necessary continuity conditions at the interface. The imaginary part of the frequency describes the growth rate of waves due to instability. The growth rate of waves is studied by solving numerically the dispersion relation. Results: The critical wavenumber at which waves become unstable, present for a parallel magnetic field, disappears, due to the inclination of the magnetic field and instead waves are shown to be unstable for all wavenumbers. Theoretical results are applied to diagnose the

structure of the magnetic field in prominence threads. When applying our theoretical results to observed waves in prominence plumes, we obtain a wide range of field inclination angle; from 0.5 degrees up to 30 degrees. These results highlight the diagnostic possibility of our study.

### **The magnetic field vector of the Sun-as-a-star.**

#### **II. Evolution of the large-scale vector field through activity cycle 24**

A. A. **Vidotto** (Trinity College Dublin), [L. Lehmann](#) (St Andrews), [M. Jardine](#) (St Andrews), [A. Pevtsov](#)(NSO)

MNRAS 480, Issue 1, 11 October 2018, Pages 477–487

<https://arxiv.org/pdf/1807.06334.pdf>

[sci-hub.tw/10.1093/mnras/sty1926](http://sci-hub.tw/10.1093/mnras/sty1926)

In the present work, we investigate how the large-scale magnetic field of the Sun, in its three vector components, has evolved during most of cycle 24, from 2010 Jan to 2018 Apr. To filter out the small-scale field of the Sun, present in high-resolution synoptic maps, we use a spherical harmonic decomposition method, which decomposes the solar field in multipoles with different  $l$  degrees. By summing together the low- $l$  multipoles, we reconstruct the large-scale field at a resolution similar to observed stellar magnetic fields, which allows the direct comparison between solar and stellar magnetic maps. During cycle 24, the 'Sun-as-a-star' magnetic field shows a polarity reversal in the radial and meridional components, but not in the azimuthal component. The large-scale solar field remains mainly poloidal with  $> 70\%$  of its energy contained in the poloidal component. During its evolution, the large-scale field is more axisymmetric and more poloidal when near minima in sunspot numbers, and with a larger intensity near maximum. There is a correlation between toroidal energy and sunspot number, which indicates that spot fields are major contributors to the toroidal large-scale energy of the Sun. The solar large-scale magnetic properties fit smoothly with observational trends of stellar magnetism reported in See et al. The toroidal (Etor) and poloidal (Epol) energies are related as  $E_{\text{tor}} \sim E_{\text{pol}}^{1.38 \pm 0.04}$ . Similar to the stellar sample, the large-scale field of the Sun shows a lack of toroidal non-axisymmetric field.

**HMI Science Nuggets #106 2018** <http://hmi.stanford.edu/hminuggets/?p=2592>

### **The magnetic field vector of the Sun-as-a-star**

A. A. **Vidotto**

MNRAS 2016

<http://arxiv.org/pdf/1603.09226v1.pdf>

Direct comparison between stellar and solar magnetic maps are hampered by their dramatic differences in resolution. Here, we present a method to filter out the small-scale component of vector fields, in such a way that comparison between solar and stellar (large-scale) magnetic field vector maps can be directly made. Our approach extends the technique widely used to decompose the radial component of the solar magnetic field to the azimuthal and meridional components as well. For that, we self-consistently decompose the three-components of the vector field using spherical harmonics of different  $l$  degrees. By retaining the low  $l$  degrees in the decomposition, we are able to calculate the large-scale magnetic field vector. Using a synoptic map of the solar vector field at Carrington Rotation CR2109, we derive the solar magnetic field vector at a similar resolution level as that from stellar magnetic images. We demonstrate that the large-scale field of the Sun is not purely radial, as often assumed -- at CR2109, 83% of the magnetic energy is in the radial component, while 10% is in the azimuthal and 7% is in the meridional components. By separating the vector field into poloidal and toroidal components, we show that the solar magnetic energy at CR2109 is mainly ( $>90\%$ ) poloidal. Our description is entirely consistent with the description adopted in several stellar studies. Our formalism can also be used to confront synoptic maps synthesised in numerical simulations of dynamo and magnetic flux transport studies to those derived from stellar observations.

### **Preliminary design of the INPE's Solar Vector Magnetograph**

L. E. A. **Vieira**, A. L. Clúa de Gonzalez, A. Dal Lago, C. Wrasse, E. Echer, F.L. Guarnieri, F. Reis Cardoso, G. Guerrero, J. Rezende Costa, J. Palacios, L. Balmaceda, L. Ribeiro Alves, L. da Silva, L.L. Costa, M. Sampaio, M. C. Rabello Soares, M. Barbosa, M. Domingues, N. Rigozo, O. Mendes Jr., P. Jauer, R. Dallaqua, R.H. Branco, T. Stekel, W. Gonzalez, W. Kabata

Proceedings IAU Symposium No. 305, 2015

<http://arxiv.org/pdf/1609.00995v1.pdf>

We describe the preliminary design of a magnetograph and visible-light imager instrument to study the solar dynamo processes through observations of the solar surface magnetic field distribution. The instrument will provide measurements of the vector magnetic field and of the line-of-sight velocity in the solar photosphere. As the magnetic field anchored at the solar surface produces most of the structures and energetic events in the upper solar atmosphere and significantly influences the heliosphere, the development of this instrument plays an important role in reaching



the scientific goals of The Atmospheric and Space Science Coordination (CEA) at the Brazilian National Institute for Space Research (INPE). In particular, the CEA's space weather program will benefit most from the development of this technology. We expect that this project will be the starting point to establish a strong research program on Solar Physics in Brazil. Our main aim is acquiring progressively the know-how to build state-of-art solar vector magnetograph and visible-light imagers for space-based platforms to contribute to the efforts of the solar-terrestrial physics community to address the main unanswered questions on how our nearby Star works.

## **Numerical Simulation of a Solar Active Region. I: Bastille Day Flare**

Alain **Vincent**, Paul Charbonneau and Caroline Dubé

Solar Physics, Volume 278, Number 2 (2012), 367-391

We present three-dimensional unsteady modeling and numerical simulations of a coronal active region, carried out within the compressible single-fluid MHD approximation. We focus on AR 9077 on **14 July 2000**, and the triggering of the X5.7 GOES X-ray class “Bastille Day” flare. We simulate only the lower corona, although we include a virtual photosphere and chromosphere below. The boundary conditions at the base of this layer are set using temperature maps from line intensities and line-of-sight magnetograms (SOHO/MDI). From the latter, we generate vector magnetograms using the force-free approximation; these vector magnetograms are then used to produce the boundary condition on the velocity field using a minimum energy principle (Longcope, *Astrophys. J.* 612, 1181, 2004). The reconnection process is modeled through a dynamical hyper-resistivity which is activated when the current exceeds a critical value (Klimas et al., *J. Geophys. Res.* 109, 2218, 2004). Comparing the time series of X-ray fluxes recorded by GOES with modeled time series of various mean physical variables such as current density, Poynting energy flux, or radiative loss inside the active region, we can demonstrate that the model properly captures the evolution of an active region over a day and, in particular, is able to explain the initiation of the flare at the observed time.

## **Reconstructing solar magnetic fields from historical observations**

### **IX. The photospheric magnetic field from 1915 to 1985**

I. O. I. **Virtanen**<sup>1</sup>, A. A. Pevtsov<sup>2</sup>, L. Bertello<sup>2</sup> and K. Mursula<sup>1</sup>

*A&A* 667, A168 (2022)

<https://www.aanda.org/articles/aa/pdf/2022/11/aa44372-22.pdf>

**Context.** We apply our recently developed method to reconstruct synoptic maps of the photospheric magnetic field from observations of chromospheric plages and the magnetic polarity of sunspots. Here, we apply the method to an extended time interval from 1915 to 1985.

**Aims.** Systematic magnetographic observations of the solar photospheric magnetic field were initiated as recently as the 1970s and the lack of earlier observations limits our ability to study and understand the long-term evolution of the Solar global field. This study is aimed at creating synoptic maps of magnetic fields for the pre-magnetograph era and using these maps as input for modern simulation models to investigate the long-term (centennial) evolution of the Sun’s global magnetic fields.

**Methods.** We reconstructed active Solar regions by identifying chromospheric plages from Ca II K line synoptic maps and assigning magnetic polarities based on the observed polarity of sunspots. We used a surface flux transport (SFT) model to simulate the evolution of the photospheric magnetic field from the reconstructed active regions. We used the potential field source surface (PFSS) model to determine the amount of open magnetic flux from the reconstruction and from magnetographic observations. We also reconstructed the coronal field during two eclipses and compared the result with eclipse drawings.

**Results.** We successfully reconstructed the photospheric magnetic field from 1915 to 1985. The number and total magnetic flux of the reconstructed active regions shows a realistic cyclic behavior that mostly follows the evolution of the sunspot number, even on relatively short timescales. The polar field strengths of cycles 19 and 20 do not reflect the evolution of the sunspot number very accurately, which may be related to problems related to the calcium data during cycle 19 and the long data gap during cycle 20. The polarity of polar fields and the amount of open field both at high and low latitudes all demonstrate the expected cyclic behavior. The agreement of the modeled coronal structure with eclipse drawings in 1922 and 1923 is fair.

## **Reconstructing solar magnetic fields from historical observations**

### **VII. Far-side activity in surface flux transport simulations**

I. O. I. **Virtanen**<sup>1</sup>, A. A. Pevtsov<sup>2</sup>, I. I. Virtanen<sup>1</sup> and K. Mursula<sup>1</sup>

*A&A* 652, A79 (2021)

<https://doi.org/10.1051/0004-6361/202140656>

<https://www.aanda.org/articles/aa/pdf/2021/08/aa40656-21.pdf>

**Context.** The evolution of the photospheric magnetic field can be simulated with surface flux transport (SFT) simulations, which allow for the study of the evolution of the entire field, including polar fields, solely using

observations of the active regions. However, because only one side of the Sun is visible at a time, active regions that emerge and decay on the far-side are not observed and not included in the simulations. As a result, some flux is missed.

**Aims.** We construct additional active regions and apply them to the far-side of the Sun in an SFT simulation to assess the possible effects and the magnitude of error that the missing far-side flux causes. We estimate how taking the missing far-side flux into account affects long-term SFT simulations.

**Methods.** We identified active regions from synoptic maps of the photospheric magnetic field between 1975 and 2019. We divided them into solar cycle wings and determined their lifetimes. Using the properties of observed active regions with sufficiently short lifetimes, we constructed additional active regions and inserted them into an SFT simulation.

**Results.** We find that adding active regions with short lifetimes to the far-side of the Sun results in significantly stronger polar fields in minimum times and slightly delayed polarity reversals. These results partly remedy the earlier results, which show overly weak polar fields and polarity reversals that are slightly too early when far-side emergence is not taken into account. The far-side active regions do not significantly affect poleward flux surges, which are mostly caused by larger long-living active regions. The far-side emergence leads to a weak continuous flow of flux, which affects polar fields over long periods of time.

## **Structure and evolution of the photospheric magnetic field in 2010–2017: comparison of SOLIS/VSM vector field and Blos potential field**

Ipo I. [Virtanen](#)<sup>1</sup>, Alexei A. Pevtsov<sup>1,2,3</sup> and Kalevi Mursula<sup>1</sup>

A&A 624, A73 (2019)

<https://arxiv.org/pdf/1904.10740.pdf>

**Context.** The line-of-sight (LOS) component of the large-scale photospheric magnetic field has been observed since the 1950s, but the daily full-disk observations of the full vector magnetic field started only in 2010 using the SOLIS Vector Stokes Magnetograph (VSM) and the SDO helioseismic and magnetic imager (HMI). Traditionally, potential field extrapolations are based on the assumption that the magnetic field in the photosphere is approximately radial. The validity of this assumption has not been tested yet.

**Aims.** We investigate here the structure and evolution of the three components of the solar large-scale magnetic field in 2010–2017, covering the ascending to mid-declining phase of solar cycle 24, using SOLIS/VSM vector synoptic maps of the photospheric magnetic field.

**Methods.** We compare the observed VSM vector magnetic field to the potential vector field derived using the VSM LOS magnetic field observations as an input. The new vector field data allow us to derive the meridional inclination and the azimuth angle of the magnetic field and to investigate their solar cycle evolution and latitudinal profile of these quantities.

**Results.** SOLIS/VSM vector data show that the photospheric magnetic field is in general fairly non-radial. In the meridional plane the field is inclined toward the equator, reflecting the dipolar structure of the solar magnetic field. Rotationally averaged meridional inclination does not have significant solar cycle variation. While the vector radial component  $B_r$  and the potential radial component  $B_{PFSSr}$  are fairly similar, the meridional and zonal components do not agree very well. We find that SOLIS/VSM vector observations are noisy at high latitudes and suffer from the vantage point effect more than LOS observations. This is due to different noise properties in the LOS and transverse components of the magnetic field, which needs to be addressed in future studies.

## **Reconstructing solar magnetic fields from historical observations**

### **II. Testing the surface flux transport model**

I. O. I. [Virtanen](#)<sup>1</sup>, I. I. Virtanen<sup>1</sup>, A. A. Pevtsov<sup>2</sup>, 1, A. Yeates<sup>3</sup> and K. Mursula

A&A 604, A8 (2017)

**Aims.** We aim to use the surface flux transport model to simulate the long-term evolution of the photospheric magnetic field from historical observations. In this work we study the accuracy of the model and its sensitivity to uncertainties in its main parameters and the input data.

**Methods.** We tested the model by running simulations with different values of meridional circulation and supergranular diffusion parameters, and studied how the flux distribution inside active regions and the initial magnetic field affected the simulation. We compared the results to assess how sensitive the simulation is to uncertainties in meridional circulation speed, supergranular diffusion, and input data. We also compared the simulated magnetic field with observations.

**Results.** We find that there is generally good agreement between simulations and observations. Although the model is not capable of replicating fine details of the magnetic field, the long-term evolution of the polar field is very similar in simulations and observations. Simulations typically yield a smoother evolution of polar fields than observations, which often include artificial variations due to observational limitations. We also find that the simulated field is fairly insensitive to uncertainties in model parameters or the input data. Due to the decay term included in the model the effects of the uncertainties are somewhat minor or temporary, lasting typically one solar cycle.

## Photospheric and coronal magnetic fields in six magnetographs

### II. Harmonic scaling of field intensities

Iipo [Virtanen](#) and Kalevi Mursula

A&A 604, A7 (2017)

Context. Photospheric magnetic fields have been observed since the 1970s by several ground-based and satellite instruments. While the different instruments show a fairly similar large-scale structure and temporal evolution of the photospheric magnetic field, the magnetic field intensity varies significantly between the observations.

Aims. We introduce a new method for scaling the photospheric magnetic field in terms of the harmonic expansion.

Contrary to earlier scaling methods, the harmonic scaling method can be straightforwardly used for data sets of different resolutions.

Methods. We use synoptic maps constructed from Wilcox Solar Observatory, Mount Wilson Observatory (MWO), Kitt Peak (KP), SOLIS, SOHO/MDI and SDO/HMI measurements of the photospheric field. We calculate the harmonic expansions of the magnetic field for all these data sets (for most, up to  $n = 180$ ) and investigate the scaling of the harmonic coefficients between all possible pairs of data sets.

Results. The six data sets generally scale to one another relatively well, with the exception of even axial terms, especially the  $g_{20}$  quadrupole for a few pairs of data sets. Differences in polar field observations, pole-filling methods and possible zero-level mainly affect the scaling of even axial terms. Scaling factors typically slightly increase with harmonic order. The mutual scaling between SOLIS and HMI is very good, and one single overall coefficient of approximately 0.8 would be a reasonable choice for those data sets. Our results suggest that the KP synoptic maps are offset by a few degrees with respect to MWO and MDI. We note that the new method gives a correct scaling for the low harmonic terms that are sufficient and necessary for coronal modeling.

## Active region chromospheric magnetic fields

### Observational inference versus magnetohydrostatic modelling

G. J. M. [Vissers](#)<sup>1</sup>, S. Danilovic<sup>1</sup>, X. Zhu<sup>2,3</sup>, J. Leenaarts<sup>1</sup>, C. J. Díaz Baso<sup>1</sup>, J. M. da Silva Santos<sup>1</sup>, J. de la Cruz Rodríguez<sup>1</sup> and T. Wiegmann<sup>3</sup>

A&A 662, A88 (2022)

<https://www.aanda.org/articles/aa/pdf/2022/06/aa42087-21.pdf>

Context. A proper estimate of the chromospheric magnetic fields is thought to improve modelling of both active region and coronal mass ejection evolution. However, because the chromospheric field is not regularly obtained for sufficiently large fields of view, estimates thereof are commonly obtained through data-driven models or field extrapolations, based on photospheric boundary conditions alone and involving pre-processing that may reduce details and dynamic range in the magnetograms.

Aims. We investigate the similarity between the chromospheric magnetic field that is directly inferred from observations and the field obtained from a magnetohydrostatic (MHS) extrapolation based on a high-resolution photospheric magnetogram.

Methods. Based on Swedish 1-m Solar Telescope Fe I 6173 Å and Ca II 8542 Å observations of NOAA active region 12723, we employed the spatially regularised weak-field approximation (WFA) to derive the vector magnetic field in the chromosphere from Ca II, as well as non-local thermodynamic equilibrium (non-LTE) inversions of Fe I and Ca II to infer a model atmosphere for selected regions. Milne-Eddington inversions of Fe I serve as photospheric boundary conditions for the MHS model that delivers the three-dimensional field, gas pressure, and density self-consistently.

Results. For the line-of-sight component, the MHS chromospheric field generally agrees with the non-LTE inversions and WFA, but tends to be weaker by 16% on average than these when larger in magnitude than 300 G. The observationally inferred transverse component is systematically stronger, up to an order of magnitude in magnetically weaker regions, but the qualitative distribution with height is similar to the MHS results. For either field component, the MHS chromospheric field lacks the fine structure derived from the inversions. Furthermore, the MHS model does not recover the magnetic imprint from a set of high fibrils connecting the main polarities.

Conclusions. The MHS extrapolation and WFA provide a qualitatively similar chromospheric field, where the azimuth of the former is better aligned with Ca II 8542 Å fibrils than that of the WFA, especially outside strong-field concentrations. The amount of structure as well as the transverse field strengths are, however, underestimated by the MHS extrapolation. This underscores the importance of considering a chromospheric magnetic field constraint in data-driven modelling of active regions, particularly in the context of space weather predictions. **2018-09-30**

## Active region chromospheric magnetic fields

[G. J. M. Vissers](#), [S. Danilovic](#), [X. Zhu](#), [J. Leenaarts](#), [C. J. Díaz Baso](#), [J. M. da Silva Santos](#), [J. de la Cruz Rodríguez](#), [T. Wiegelmann](#)

A&A 2021

<https://arxiv.org/pdf/2109.02943>

Context. A proper estimate of the chromospheric magnetic fields is believed to improve modelling of both active region and coronal mass ejection evolution. Aims. We investigate the similarity between the chromospheric magnetic field inferred from observations and the field obtained from a magnetohydrostatic (MHS) extrapolation. Methods. Based Fe i 6173 Å and Ca ii 8542 Å observations of NOAA active region 12723, we employed the spatially-regularised weak-field approximation (WFA) to derive the vector magnetic field in the chromosphere from Ca ii, as well as non-LTE inversions of Fe i and Ca ii to infer a model atmosphere for selected regions. Milne-Eddington inversions of Fe i serve as photospheric boundary for the MHS model that delivers the three-dimensional field, gas pressure and density. Results. For the line-of-sight component, the MHS chromospheric field generally agrees with the non-LTE inversions and WFA, but tends to be weaker than those when larger in magnitude than 300 G. The observationally inferred transverse component is stronger, especially in magnetically weaker regions, yet the qualitative distribution with height is similar to the MHS results. For either field component the MHS chromospheric field lacks the fine structure derived from the inversions. Furthermore, the MHS model does not recover the magnetic imprint from a set of high fibrils connecting the main polarities. Conclusions. The MHS extrapolation and WFA provide a qualitatively similar chromospheric field, where the azimuth of the former is better aligned with Ca ii 8542 Å fibrils than that of the WFA, especially outside strong-field concentrations. The amount of structure as well as the transverse field strengths are underestimated by the MHS extrapolation. This underscores the importance of considering a chromospheric magnetic field constraint in data-driven modelling of active regions.

### **Non-LTE inversions of a confined X2.2 flare: I. Vector magnetic field in the photosphere and chromosphere**

[G. J. M. Vissers](#), [S. Danilovic](#), [J. de la Cruz Rodríguez](#), [J. Leenaarts](#), [R. Morosin](#), [C. J. Diaz Baso](#), [A. Reid](#), [J. Pomoell](#), [D. J. Price](#), [S. Inoue](#)

A&A 2020

<https://arxiv.org/pdf/2009.01537.pdf>

Obtaining the magnetic field vector accurately in the solar atmosphere is essential for studying changes in field topology during flares and to reliably model space weather. We tackle this problem by applying various inversion methods to a confined X2.2 flare in NOAA AR 12673 on **September 6, 2017**, comparing the photospheric and chromospheric magnetic field vector with those from two numerical models of this event. We obtain the photospheric field from Milne-Eddington (ME) and (non-)local thermal equilibrium (non-LTE) inversions of Hinode SOT/SP Fe I 6301.5Å and 6302.5Å. The chromospheric field is obtained from a spatially-regularised weak field approximation (WFA) and non-LTE inversions of Ca II 8542Å observed with CRISP at the Swedish 1-m Solar Telescope. The LTE- and non-LTE-inferred photospheric field components are strongly correlated throughout the atmosphere, with stronger field and higher temperatures in the non-LTE inversions. For the chromospheric field, the non-LTE inversions correlate well with the spatially-regularised WFA. We find strong-field patches of over 4.5 kG in the photosphere, co-located with similar concentrations exceeding 3 kG in the chromosphere. The obtained field strengths are up to 2-3 times higher than in the numerical models, with more concentrated and structured photosphere-to-chromosphere shear close to the polarity inversion line. The LTE and non-LTE Fe I inversions yield essentially the same photospheric field, while ME inversions fail to reproduce the field vector orientation where Fe I is in emission. Our inversions confirm the locations of flux rope footpoints that are predicted by numerical models. However, pre-processing and lower spatial resolution lead to weaker and smoother field in the models than what the data indicate. This emphasises the need for higher spatial resolution in the models to better constrain pre-eruptive flux ropes.

### **Evidence for a Transition Region response to penumbral microjets in sunspots**

Gregal J. M. [Vissers](#), Luc H. M. Rouppe van der Voort, Mats Carlsson

ApJL 811 L33 2015

<http://arxiv.org/pdf/1509.01402v1.pdf>

Penumbral microjets are short-lived, fine-structured and bright jets that are generally observed in chromospheric imaging of the penumbra of sunspots. Here we investigate their potential transition region signature, by combining observations with the Swedish 1-m Solar Telescope (SST) in the Ca II H and Ca II 8542Å lines with ultraviolet imaging and spectroscopy obtained with the Interface Region Imaging Spectrograph (IRIS), which includes the C II 1334/1335Å, Si IV 1394/1403Å and Mg II h & k 2803/2796Å lines. We find a clear corresponding signal in the IRIS Mg II k, C II and Si IV slit-jaw images, typically offset spatially from the Ca II signature in the direction along the jets: from base to top, the penumbral microjets are predominantly visible in Ca II, Mg II k and C

II/Si IV, suggesting progressive heating to transition region temperatures along the jet extent. Hence, these results support the suggestion from earlier studies that penumbral microjets may heat to transition region temperatures.  
**2014 September 5 and 6**

## **Sunspot Observations at the Eimmart Observatory: Revision and Supplement Research**

Mikhail [Vokhmyanin](#) & [Nadezhda Zolotova](#)

Solar Phys. volume 298, Article number: 113 (2023)

<https://link.springer.com/content/pdf/10.1007/s11207-023-02208-4.pdf>

Digital images of sunspot drawings of the archives of Georg Christoph Eimmart stored at the National Library of Russia, St. Petersburg, are analyzed to obtain sunspot-group numbers and sunspot areas as well as heliographic positions. Overall, more than a hundred drawings were processed. The impact of drawing and reproduction uncertainties and the aims of historical observations are considered. The sunspot positions are compared to those reported by contemporary observers of the Maunder minimum. The restored sunspot-group numbers and latitudes are compared to those extracted by Hoyt and Schatten (Solar Phys. 179, 189, [1998](#)) as well as Hayakawa et al. (Solar Phys. 296, 154, [2021b](#)) and Hayakawa et al. (Astrophys. J. 909, 166, [2021d](#)). The persistence of long-lived sunspots over several solar rotations is discussed.

## **Signatures of ubiquitous magnetic reconnection in the deep atmosphere of sunspot penumbrae**

[L. H. M. Rouppe van der Voort](#), [J. Joshi](#), [V. M. J. Henriques](#), [S. Bose](#)

A&A 648, A54 2021

<https://arxiv.org/pdf/2101.11321.pdf>

<https://doi.org/10.1051/0004-6361/202040171>

<https://www.aanda.org/articles/aa/pdf/2021/04/aa40171-20.pdf>

Ellerman bombs are regions with enhanced Balmer line wing emission and mark magnetic reconnection in the deep solar atmosphere in active regions and quiet Sun. They are often found in regions where opposite magnetic polarities are in close proximity. Recent high resolution observations suggest that Ellerman bombs are more prevalent than thought before. We aim to determine the occurrence of Ellerman bombs in the penumbra of sunspots. We analyze high spatial resolution observations of sunspots in the Balmer H-alpha and H-beta lines as well as auxiliary continuum channels obtained with the Swedish 1-m Solar Telescope and apply the k-means clustering technique to systematically detect and characterize Ellerman Bombs. Features with all the defining characteristics of Ellerman bombs are found in large numbers over the entire penumbra. The true prevalence of these events is only fully appreciated in the H-beta line due to highest spatial resolution and lower chromospheric opacity. We find that the penumbra hosts some of the highest Ellerman bomb densities, only surpassed by the moat in the immediate surroundings of the sunspot. Some penumbral Ellerman bombs show flame morphology and rapid dynamical evolution. Many penumbral Ellerman bombs are fast moving with typical speed of 3.7 km/s and sometimes more than 10 km/s. Many penumbral Ellerman bombs migrate from the inner to the outer penumbra over hundreds of km and some continue moving beyond the outer penumbral boundary into the moat. Many penumbral Ellerman bombs are found in the vicinity of regions with opposite magnetic polarity. We conclude that reconnection is a near continuous process in the low atmosphere of the penumbra of sunspots as manifest in the form of penumbral Ellerman bombs. These are so prevalent that they may be a major sink of sunspot magnetic energy. **29 April 2016. , 22 September 2017**

## **Reduced Microwave Brightness Temperature in a Sunspot Atmosphere due to Open Magnetic Fields**

[A. Vrublevskis](#) (1), [B. I. Ryabov](#) (1), [S. M. White](#) (2) ((1) Ventspils International Radio Astronomy Centre and Ventspils University of Applied Sciences, (2) Space Vehicles Directorate, Air Force Research Laboratory, Kirtland AFB)

Solar Phys. 2021

<https://arxiv.org/ftp/arxiv/papers/2102/2102.05476.pdf>

Motivated by dark coronal lanes in SOHO / EIT 284 Å EUV observations we construct and optimize an atmosphere model of the AR 8535 sunspot by adding a cool and dense component in the volume of plasma along open field lines determined using the Potential Field Source Surface (PFSS) extrapolation. Our model qualitatively reproduces the observed reduced microwave brightness temperature in the northern part of the sunspot in the VLA observations from **13 May 1999** and provides a physical explanation for the coronal dark lanes. We propose application of this method to other sunspots with such observed dark regions in EUV or soft X-rays and with concurrent microwave observations to determine the significance of open field regions. The connection between open fields and the resulting plasma temperature and density change is of relevance for slow solar wind source investigations.

## Validation scheme for solar coronal models -- constraints from multi-perspective observations in EUV and white-light

[A. Wagner](#), [E. Asvestari](#), [M. Temmer](#), [S.G. Heinemann](#), [J. Pomoell](#)

A&A 657, A117 2022

<https://arxiv.org/pdf/2110.01893.pdf>

<https://doi.org/10.1051/0004-6361/202141552>

<https://www.aanda.org/articles/aa/pdf/2022/01/aa41552-21.pdf>

Context: In this paper we present a validation scheme to investigate the quality of coronal magnetic field models, which is based upon comparisons with observational data from multiple sources. Aims: Many of these coronal models may use a range of initial parameters that produce a large number of physically reasonable field configurations. However, that does not mean that these results are reliable and comply with the observations. With an appropriate validation scheme the quality of a coronal model can be assessed. Methods: The validation scheme is developed on the example of the EUropean Heliospheric FORecasting Information Asset (EUHFORIA) coronal model. For observational comparison we use EUV and white-light data to detect coronal features on the surface (open magnetic field areas) and off-limb (streamer and loop) structures from multiple perspectives (Earth view and the Solar Terrestrial Relations Observatory - STEREO). The validation scheme can be applied to any coronal model that produces magnetic field line topology. Results: We show its applicability by using that validation scheme on a large set of model configurations, which can be efficiently reduced to an ideal set of parameters that matches best with observational data. Conclusions: We conclude that by using a combined empirical visual classification with a mathematical scheme of topology metrics a very efficient and rather objective quality assessment for coronal models can be performed. **01-Aug-2008, 11-Jul-2010**

## SuperSynthIA: Physics-ready Full-disk Vector Magnetograms from HMI, Hinode, and Machine Learning

Ruoyu [Wang](#)<sup>1</sup>, David F. Fouhey<sup>1,2,3</sup>, Richard E. L. Higgins<sup>3</sup>, Spiro K. Antiochos<sup>4</sup> +++

2024 ApJ 970 168

<https://iopscience.iop.org/article/10.3847/1538-4357/ad41e3/pdf>

Vector magnetograms of the Sun's photosphere are cornerstones for much of solar physics research. These data are often produced by data-analysis pipelines combining per-pixel Stokes polarization vector inversion with a disambiguation that resolves an intrinsic 180° ambiguity. We introduce a learning-based method, SuperSynthIA, that produces full-disk vector magnetograms from Stokes vector observations. As input, SuperSynthIA uses Stokes polarization images from Solar Dynamics Observatory (SDO)/Helioseismic and Magnetic Imager (HMI). As output, SuperSynthIA simultaneously emulates the inversion and disambiguation outputs from the Hinode/Solar Optical Telescope-Spectro-Polarimeter (SOT-SP) pipeline. Our method extends our previous approach SynthIA with heliographic outputs as well as using an improved data set and inference method. SuperSynthIA provides a new tool for improved magnetic fields from full-disk SDO/HMI observations using information derived from the enhanced capabilities of Hinode/SOT-SP. Compared to our previous SynthIA, SuperSynthIA provides physics-ready vector magnetograms and mitigates unphysical angle preferences and banding artifacts in SynthIA. SuperSynthIA data are substantially more temporally consistent than those from the SDO/HMI pipeline, most notably seen in, e.g., evolving active regions. SuperSynthIA substantially reduces noise in low-signal areas, resulting in less center-to-limb bias outside of strong-signal areas. We show that outputs from SuperSynthIA track the SDO/HMI-recorded evolution of the magnetic field. We discuss the limitations of SuperSynthIA that the user must understand, and we demonstrate a broad set of evaluations to test SuperSynthIA and discuss remaining known artifacts. Our tests provide both methodology and evidence that SuperSynthIA outputs are ready for use by the community, and that learning-based approaches are suitable for physics-ready magnetograms.

## Light Bridge and Magnetic Field in a Solar Active Region

Huaning [Wang](#)<sup>1,2,3,4</sup>, Changhui Rao<sup>1,2,3</sup>, Naiting Gu<sup>1,2,3</sup>, Libo Zhong<sup>1,2</sup>, and Xin Huang<sup>4</sup>

2022 ApJ 939 49

<https://iopscience.iop.org/article/10.3847/1538-4357/ac9378/pdf>

Observational data from the Helioseismic and Magnetic Imager on board the Solar Dynamics Observatory and the multiwavelength simultaneous imaging system attached to the New Vacuum Solar Telescope located at Fuxian Lake, China are employed for the study of light bridges and magnetic fields in the active region NOAA 12529. Coronal fields in this active region are computed with a boundary integration model and the field line connectivity in the dominant spot is investigated with the squashing factor  $Q$ . Quasi separatrix layer intersections in the CCD coordinate plane are determined according to values of  $Q$ . It is found that weak field lanes (WFLs) appear in the umbra and penumbra; open and closed flux systems are separated by QSLs in the dominant spot; and WFLs and QSLs look quite different from each other in the dominant spot but partially overlap in the umbra. Our study demonstrates that WFLs cannot be attributed to topological evolution of magnetic fields and might be regarded as rifts among splitting flux systems. **2016 April 12–16**

## Comparison of Two Methods for Calculating Magnetic Helicity in the Solar Corona

[Quan Wang](#), [Shangbin Yang](#), [Mei Zhang](#), [Xiao Yang](#)

ApJ 929 122 2022

<https://arxiv.org/pdf/2204.04982.pdf>

<https://iopscience.iop.org/article/10.3847/1538-4357/ac5593/pdf>

Due to the large magnetic Reynolds number, the magnetic helicity originating from the solar interior can be carried away through the photosphere into the corona. However, the relationship between the accumulated magnetic helicity flux through the photosphere and the magnetic helicity in the corona is still unclear. By selecting 36 newly emerging active regions in the 23rd solar cycle, we apply optical flow methods to derive the accumulated magnetic helicity through the photosphere (H<sub>pm</sub>) by using the sequential longitudinal magnetograms, use nonlinear force-free field extrapolation to obtain the 3D coronal magnetic field, and adopt finite volume methods to calculate the instantaneous relative magnetic helicity in the corona (H<sub>cm</sub>) by using vector magnetograms. It is found that the local correlation tracking (LCT)-based H<sub>pm</sub> is larger than H<sub>cm</sub> in 1", and that the Differential Affine Velocity Estimator-based H<sub>pm</sub> is more consistent with H<sub>cm</sub> than the LCT-based H<sub>pm</sub>. H<sub>pm</sub> is more consistent with H<sub>cm</sub> in evaluation from 2" than from 1". Moreover, H<sub>cm</sub>-H<sub>pm</sub> systematically shows consistency with the Hemispheric Helicity Rule (over 55%), no matter which resolution and method are used. These estimations suggest that the consistency of H<sub>cm</sub> and H<sub>pm</sub> is partly dependent on the resolution of the magnetograms and the calculation methods.

## Magnetograph Saturation and the Open Flux Problem

Y.-M. [Wang](#)<sup>1</sup>, R. K. Ulrich<sup>2</sup>, and J. W. Harvey<sup>4,3</sup>

2022 ApJ 926 113

<https://iopscience.iop.org/article/10.3847/1538-4357/ac4491/pdf>

Extrapolations of line-of-sight photospheric field measurements predict radial interplanetary magnetic field (IMF) strengths that are factors of ~2–4 too low. To address this open flux problem, we reanalyze the magnetograph measurements from different observatories, with particular focus on those made in the saturation-prone Fe i 525.0 nm line by the Mount Wilson Observatory (MWO) and the Wilcox Solar Observatory (WSO). The total dipole strengths, which determine the total open flux, generally show large variations among observatories, even when their total photospheric fluxes are in agreement. However, the MWO and WSO dipole strengths, as well as their total fluxes, agree remarkably well with each other, suggesting that the two data sets require the same scaling factor. As shown earlier by Ulrich et al., the saturation correction  $\delta-1$  derived by comparing MWO measurements in the 525.0 nm line with those in the nonsaturating Fe i 523.3 nm line depends sensitively on where along the irregularly shaped 523.3 nm line wings the exit slits are placed. If the slits are positioned so that the 523.3 and 525.0 nm signals originate from the same height,  $\delta-1 \sim 4.5$  at the disk center, falling to  $\sim 2$  near the limb. When this correction is applied to either the MWO or WSO maps, the derived open fluxes are consistent with the observed IMF magnitude. Other investigators obtained scaling factors only one-half as large because they sampled the 523.3 nm line farther out in the wings, where the shift between the right- and left-circularly polarized components is substantially smaller.

## Cosmic Ray Variation Lags behind Sunspot Number due to the Late Opening of Solar Magnetic Field

Yuming [Wang](#), [Jingnan Guo](#), [Gang Li](#), [Elias Roussos](#), [Junwei Zhao](#)

ApJ 2022

<https://arxiv.org/pdf/2201.01908.pdf>

Galactic cosmic rays (GCRs), the highly energetic particles that may raise critical health issues of astronauts in space, are modulated by solar activity with their intensity lagging behind the sunspot number (SSN) variation by about one year. Previously, this lag has been attributed to result of outward convecting solar wind and inward propagating GCRs. However, the lag's amplitude and its solar-cycle dependence are still not fully understood (e.g., Ross & Chaplin 2019). By investigating the solar surface magnetic field, we find that the source of heliospheric magnetic field, i.e., the open magnetic flux on the Sun, already lags behind SSN before it convects into heliosphere along with the solar wind, and the delay during odd cycles is longer than that during sequential even cycles. Thus, we propose that the GCR lag is primarily due to the greatly late opening of the solar magnetic field with respect to SSN, though solar wind convection and particle transport in the heliosphere also matters. We further investigate the origin of the open flux from different latitudes of the Sun and found that the total open flux is significantly contributed by that from low latitudes where coronal mass ejections frequently occur and also show an odd-even cyclic pattern. Our findings challenge existing theories, and may serve as the physical basis of long-term forecasts radiation dose estimates for manned deep-space exploration missions.

**Figure 6. The solar cycle variations of the CME numbers**

## Magnetograph Saturation and the Open Flux Problem

[Y.-M. Wang](#), [R. K. Ulrich](#), [J. W. Harvey](#)

2021

<https://arxiv.org/pdf/2112.09969.pdf>

Extrapolations of line-of-sight photospheric field measurements predict radial interplanetary magnetic field (IMF) strengths that are factors of  $\sim 2$ – $4$  too low. To address this "open flux problem," we reanalyze the magnetograph measurements from different observatories, with particular focus on those made in the saturation-prone Fe I 525.0 nm line by the Mount Wilson Observatory (MWO) and the Wilcox Solar Observatory (WSO). The total dipole strengths, which determine the total open flux, generally show large variations among observatories, even when their total photospheric fluxes are in agreement. However, the MWO and WSO dipole strengths, as well as their total fluxes, agree remarkably well with each other, suggesting that the two data sets require the same scaling factor. As shown earlier by Ulrich et al., the saturation correction  $\delta^{-1}$  derived by comparing MWO measurements in the 525.0 nm line with those in the nonsaturating Fe I 523.3 nm line depends sensitively on where along the irregularly shaped 523.3 nm line wings the exit slits are placed. If the slits are positioned so that the 523.3 and 525.0 nm signals originate from the same height,  $\delta^{-1} \sim 4.5$  at disk center, falling to  $\sim 2$  near the limb. When this correction is applied to either the MWO or WSO maps, the derived open fluxes are consistent with the observed IMF magnitude. Other investigators obtained scaling factors only one-half as large because they sampled the 523.3 nm line farther out in the wings, where the shift between the right- and left-circularly polarized components is substantially smaller.

**Table 1.** Photospheric Magnetic Field Maps Used in This Study

## Naked emergence of an anti-Hale active region

### I. Overall evolution and magnetic properties\*

Jincheng Wang<sup>1,2,3</sup>, Xiaoli Yan<sup>1,3</sup>, Defang Kong<sup>1,3</sup>, Zhike Xue<sup>1,3</sup>, Liheng Yang<sup>1,3</sup>, Qiaoling Li<sup>1,4</sup>, Yan Zhang<sup>1,4</sup> and Hao Li<sup>5,6</sup>

A&A 652, A55 (2021)

<https://arxiv.org/abs/2106.02786>

<https://www.aanda.org/articles/aa/pdf/2021/08/aa40685-21.pdf>

<https://doi.org/10.1051/0004-6361/202140685>

**Aims.** In order to understand the emergence of the active region, we investigate the emerging process and magnetic properties of a naked anti-Hale active region during the period between **August 24 to 25, 2018**.

**Methods.** Using the data from Helioseismic and Magnetic Imager on board the Soar Dynamic Observatory and the New Vacuum Solar Telescope, we calculated different evolving parameters (such as pole separation, tilt angle) and magnetic parameters (such as vertical electric current, force-free parameter, relative magnetic helicity) during the emergence of the active region. With these calculated parameters and some reasonable assumptions, we use two different methods to estimate the twist of the active region.

**Results.** The magnetic flux and pole separation continue increasing while the tilt angle exhibits a decreasing pattern during the emergence of the active region. The increase of the pole separation is mainly contributed as a result of the enhancement in the longitude direction. A power-law relationship between pole separation and total flux is found during the emergence of the active region. On the other hand, it is found that both the positive and negative electric currents increased equivalently and the average flux-weighted force-free parameter  $\alpha$  remains almost consistently positive, on the order of  $\sim 10$ – $8 \text{ m}^{-1}$ . The relative magnetic helicity is mainly contributed by the shear term, while the relative magnetic helicity injection flux of the shear term changes its sign at the latter stage of the emergence. The twist number of the whole active region remains on the order of  $10$ – $1$  turns during the emergence of the active region.

**Conclusions.** We find that the magnetic flux tube with low twist also could emerge into the solar atmosphere.

## Effects of erupting magnetic flux rope on running penumbral waves

Wensi Wang, Rui Liu

A&A 647, A108 2021

<https://arxiv.org/pdf/2101.04915.pdf>

<https://doi.org/10.1051/0004-6361/202039732>

<https://www.aanda.org/articles/aa/pdf/2021/03/aa39732-20.pdf>

**Context.** It is well known that solar flares have broad impacts on the low atmosphere, but it is largely unknown how they affect sunspot waves and oscillations. It is also under debate as to whether the flare-induced photospheric changes are due to the momentum conservation with coronal mass ejections or due to magnetic reconnection. **Aims.** To shed light on the so-called "back reaction" of solar eruptions, we investigated how running penumbral waves (RPWs) at one foot of an erupting magnetic flux rope (MFR) responds to the rope buildup and subsequent erosion. **Results.** During the rope-buildup stage, the western foot of the rope, which is completely enclosed by a hooked ribbon, expands rapidly and consequently overlaps a sunspot penumbra. This converts the original penumbral field into the rope field, which is associated with a transient increase in electric currents flowing through the ribbon-swept penumbral region. During the rope-erosion stage, the rope foot shrinks as the eastern section of the hooked ribbon slowly sweeps the same penumbral region, where the rope field is converted into flare loops. This conversion induces mixed effects on the photospheric field inclination but heats up the low atmosphere at the footpoints of these flare loops to transition-region temperatures, therefore resulting in the post-eruption RPWs with an enhanced contrast in the 1600Å passband and an extended bandwidth to low frequencies at 3–5 mHz, compared with the pre-



eruption RPWs that peak at 6 mHz. Conclusions. This observation clearly demonstrates that it is the magnetic reconnection in the corona that impacts the low atmosphere and leads to the changing behaviors of RPWs, which, in turn, offer a new window to diagnose flare reconnections. **2015 November 4**

### **Spatial Distributions of Sunspot Oscillation Modes at Different Temperatures**

Zhengkai Wang, [Song Feng](#), [Linhua Deng](#), [Yao Meng](#)

Research in Astronomy and Astrophysics **2019**

<https://arxiv.org/pdf/1908.04906.pdf>

Three- and five-minute oscillations of sunspots have different spatial distributions in the solar atmospheric layers. The spatial distributions are crucial to reveal the physical origin of sunspot oscillations and to investigate their propagation. In this study, six sunspots observed by Solar Dynamics Observatory/Atmospheric Imaging Assembly were used to obtain the spatial distributions of three- and five-minute oscillations. The fast Fourier transform method is applied to represent the power spectra of oscillation modes. We find that, from the temperature minimum to the lower corona, the powers of the five-minute oscillation exhibit a circle-shape distribution around its umbra, and the shapes gradually expand with temperature increase. However, the circle-shape is disappeared and the powers of the oscillations appear to be very disordered in the higher corona. This indicates that the five-minute oscillation can be suppressed in the high-temperature region. For the three-minute oscillations, from the temperature minimum to the high corona, their powers mostly distribute within an umbra, and part of them locate at the coronal fan loop structures. Moreover, those relative higher powers are mostly concentrated in the position of coronal loop footpoints. **27 Mar. 2011, 16 Mar. 2012, 17 May 2012, 15 Nov. 2013, 17 Apr. 2014, 25 Feb. 2017**

### **High-frequency Oscillations in the Atmosphere above a Sunspot Umbra**

Feng Wang<sup>1,2</sup>, Hui Deng<sup>1</sup>, Bo Li<sup>3</sup>, Song Feng<sup>1,2</sup>, Xianyong Bai<sup>4</sup>, Linhua Deng<sup>5</sup>, Yunfei Yang<sup>2</sup>, Zhike Xue<sup>5</sup>, and Rui Wang<sup>5</sup>

**2018 ApJL 856 L16**

<https://arxiv.org/pdf/1803.09046.pdf>

We use high spatial and temporal resolution observations, simultaneously obtained with the New Vacuum Solar Telescope and Atmospheric Imaging Assembly (AIA) on board the Solar Dynamics Observatory, to investigate the high-frequency oscillations above a sunspot umbra. A novel time–frequency analysis method, namely, the synchrosqueezing transform (SST), is employed to represent their power spectra and to reconstruct the high-frequency signals at different solar atmospheric layers. A validation study with synthetic signals demonstrates that SST is capable of resolving weak signals even when their strength is comparable to the high-frequency noise. The power spectra, obtained from both SST and the Fourier transform, of the entire umbral region indicate that there are significant enhancements between 10 and 14 mHz (labeled as 12 mHz) at different atmospheric layers. Analyzing the spectrum of a photospheric region far away from the umbra demonstrates that this 12 mHz component exists only inside the umbra. The animation based on the reconstructed 12 mHz component in AIA 171 Å illustrates that an intermittently propagating wave first emerges near the footpoints of coronal fan structures, and then propagates outward along the structures. A time–distance diagram, coupled with a subsonic wave speed ( $\sim 49 \text{ km s}^{-1}$ ), highlights the fact that these coronal perturbations are best described as upwardly propagating magnetoacoustic slow waves. Thus, we first reveal the high-frequency oscillations with a period around one minute in imaging observations at different height above an umbra, and these oscillations seem to be related to the umbral perturbations in the photosphere.

### **Strong Transverse Photosphere Magnetic Fields and Twist in Light Bridge Dividing Delta Sunspot of Active Region 12673**

Haimin Wang, [Vasyl Yurchyshyn](#), [Chang Liu](#), [Kwangsu Ahn](#), [Shin Toriumi](#), [Wenda Cao](#)

RNAAS **28 2018**

<https://arxiv.org/pdf/1801.02928.pdf>

<http://iopscience.iop.org/article/10.3847/2515-5172/aaa670>

Solar Active Region (AR) 12673 is the most flare productive AR in the solar cycle 24. It produced four X-class flares including the X9.3 flare on **06 September 2017** and the X8.2 limb event on 10 September. Sun and Norton (2017) reported that this region had an unusual high rate of flux emergence, while Huang et al. (2018) reported that the X9.3 flare had extremely strong white-light flare emissions. Yang et al. (2017) described the detailed morphological evolution of this AR. In this report, we focus on usual behaviors of the light bridge (LB) dividing the delta configuration of this AR, namely the strong magnetic fields (above 5500 G) in the LB and apparent photospheric twist as shown in observations with a 0.1 arcsec spatial resolution obtained by the 1.6m telescope at Big Bear Solar Observatory.

## **THE UBIQUITOUS PRESENCE OF LOOPLIKE FINE STRUCTURE INSIDE SOLAR ACTIVE REGIONS**

Y.-M. **Wang**

2016 ApJ 820 L13

Although most of the solar surface outside active regions (ARs) is pervaded by small-scale fields of mixed polarity, this magnetic "carpet" or "junkyard" is thought to be largely absent inside AR plages and strong network. However, using extreme-ultraviolet images and line-of-sight magnetograms from the Solar Dynamics Observatory, we find that unipolar flux concentrations, both inside and outside ARs, often have small, loop-shaped Fe ix 17.1 and Fe xii 19.3 nm features embedded within them, even though no minority-polarity flux is visible in the corresponding magnetograms. Such loopleftike structures, characterized by horizontal sizes of ~3–5 Mm and varying on timescales of minutes or less, are seen inside bright 17.1 nm moss, as well as in fainter moss-like regions associated with weaker network outside ARs. We also note a tendency for bright coronal loops to show compact, loopleftike features at their footpoints. Based on these observations, we suggest that present-day magnetograms may be substantially underrepresenting the amount of minority-polarity flux inside plages and strong network, and that reconnection between small bipoles and the overlying large-scale field could be a major source of coronal heating both in ARs and in the quiet Sun.

## **Correlation Between CME Occurrence Rate and Current Helicity in the Global Magnetic Field of Solar Cycle 23**

Chuanyu **Wang**, Mei Zhang

Solar Phys. 2015

We investigate the correlation between the occurrence rate of the monthly coronal mass ejection (CME) and the magnitude of the current helicity in global magnetic field on the photosphere of solar cycle 23. We used the technique introduced by Pevtsov and Latushko (Astrophys. J. 528, 999, 2000) to retrieve the vector magnetic field from longitudinal full-disk magnetograms, but applied a different method to calculate the current helicity and focused on the evolution of the magnitude of current helicity over a full solar cycle. We found that there is a close relationship between the variation of the current helicity in the global magnetic field and that of the monthly CME occurrence rate. This provides further evidence to support that helicity is an important ingredient for solar eruptions.

## **Active-Region Tilt Angles: Magnetic Versus White-Light Determinations of Joy's Law**

Y.-M. **Wang**, R. C. Colaninno, T. Baranyi, J. Li

ApJ, 798 50 2015

<http://arxiv.org/pdf/1412.2329v1.pdf>

The axes of solar active regions are inclined relative to the east–west direction, with the tilt angle tending to increase with latitude ("Joy's law"). Observational determinations of Joy's law have been based either on white-light images of sunspot groups or on magnetograms, where the latter have the advantage of measuring directly the physically relevant quantity (the photospheric field), but the disadvantage of having been recorded routinely only since the mid-1960s. White-light studies employing the historical Mount Wilson (MW) database have yielded tilt angles that are smaller and that increase less steeply with latitude than those obtained from magnetic data. We confirm this effect by comparing sunspot-group tilt angles from the Debrecen Photoheliographic Database with measurements made by Li and Ulrich using MW magnetograms taken during cycles 21–23. Whether white-light or magnetic data are employed, the median tilt angles significantly exceed the mean values, and provide a better characterization of the observed distributions. The discrepancy between the white-light and magnetic results is found to have two main sources. First, a substantial fraction of the white-light "tilt angles" refer to sunspots of the same polarity. Of greater physical significance is that the magnetograph measurements include the contribution of plage areas, which are invisible in white-light images but tend to have greater axial inclinations than the adjacent sunspots. Given the large uncertainties inherent in both the white-light and the magnetic measurements, it remains unclear whether any systematic relationship exists between tilt angle and cycle amplitude during cycles 16–23.

## **Compound Effect of Alfvén Waves and Ion-Cyclotron Waves on Heating/Acceleration of Minor Ions via the Pickup Process**

C. B. **Wang**, Bin Wang, L. C. Lee

Solar Phys., Volume 289, Issue 10, pp 3895–3916, 2014

A scenario is proposed to explain the preferential heating of minor ions and differential-streaming velocity between minor ions and protons observed in the solar corona and in the solar wind. It is demonstrated by test-particle simulations that minor ions can be nearly fully picked up by intrinsic Alfvén-cyclotron waves observed in the solar wind based on the observed wave energy density. Both high-frequency ion-cyclotron waves and low-frequency Alfvén waves play crucial roles in the pickup process. A minor ion can first gain a high magnetic moment through

the resonant wave-particle interaction with ion-cyclotron waves, and then this ion with a large magnetic moment can be trapped by magnetic mirror-like field structures in the presence of the low-frequency Alfvén waves. As a result, the ion is picked up by these Alfvén-cyclotron waves. However, minor ions can only be partially picked up in the corona because of the low wave energy density and low plasma  $\beta$ . During the pickup process, minor ions are stochastically heated and accelerated by Alfvén-cyclotron waves so that they are hotter and flow faster than protons. The compound effect of Alfvén waves and ion-cyclotron waves is important in the heating and acceleration of minor ions. The kinetic properties of minor ions from simulation results are generally consistent with in-situ and remote features observed in the solar wind and solar corona.

### **Validation of Spherically Symmetric Inversion by Use of a Tomographic Reconstructed Three-Dimensional Electron Density of the Solar Corona**

Tongjiang **Wang** and Joseph M. Devila

E-print, May 2014; Solar Phys., Volume 289, Issue 10, pp 3723-3745, 2014

<http://arxiv.org/pdf/1404.5925v1.pdf>

Determination of the coronal electron density by the inversion of white-light polarized brightness (pB) measurements by coronagraphs is a classic problem in solar physics. An inversion technique based on the spherically symmetric geometry (Spherically Symmetric Inversion, SSI) was developed in the 1950s, and has been widely applied to interpret various observations. However, to date there is no study about uncertainty estimation of this method. In this study we present the detailed assessment of this method using a three-dimensional (3D) electron density in the corona from 1.5 to 4 R<sub>sun</sub> as a model, which is reconstructed by tomography method from STEREO/COR1 observations during solar minimum in February 2008. We first show in theory and observation that the spherically symmetric polynomial approximation (SSPA) method and the Van de Hulst inversion technique are equivalent. Then we assess the SSPA method using synthesized pB images from the 3D density model, and find that the SSPA density values are close to the model inputs for the streamer core near the plane of the sky (POS) with differences generally less than a factor of two or so; the former has the lower peak but more spread in both longitudinal and latitudinal directions than the latter. We estimate that the SSPA method may resolve the coronal density structure near the POS with angular resolution in longitude of about 50 degrees. Our results confirm the suggestion that the SSI method is applicable to the solar minimum streamer (belt) as stated in some previous studies. In addition, we demonstrate that the SSPA method can be used to reconstruct the 3D coronal density, roughly in agreement with that by tomography for a period of low solar activity. We suggest that the SSI method is complementary to the 3D tomographic technique in some cases, given that the development of the latter is still an ongoing research effort. 1-8 February 2008.

### **Three-Dimensional Nonlinear Force-Free Field Reconstruction of Solar Active Region 11158 by Direct Boundary Integral Equation**

Rui **Wang**, Yihua Yan, Baolin Tan

Solar Physics, December 2013, Volume 288, Issue 2, pp 507-529

A three-dimensional coronal magnetic field is reconstructed for the NOAA active region 11158 on **14 February 2011**. A GPU-accelerated direct boundary integral equation (DBIE) method is implemented which is approximately 1000 times faster than the original DBIE used on solar non-linear force-free field modeling. Using the SDO/HMI vector magnetogram as the bottom boundary condition, the reconstructed magnetic field lines are compared with the projected EUV loop structures as observed in the front-view (SDO/AIA) and the side-view (STEREO-A/B) images for the first time; they show very good agreement three-dimensionally. A quantitative comparison with some stereoscopically reconstructed coronal loops shows that the average misalignment angles in our model are at the same order as the state-of-the-art results obtained from reconstructed coronal loops. It is found that the observed coronal loop structures can be grouped into a number of closed and open field structures with some central bright coronal loop features around the polarity inversion line. The reconstructed highly sheared magnetic field lines agree very well with the low-lying sigmoidal filament along the polarity inversion line. This central low-lying magnetic field loop system must have played a key role in powering the flare. It should be noted that while a strand-like coronal feature along the polarity inversion line may be related to the filament, one cannot simply interpret all the coronal bright features along the polarity inversion line as manifestation of the filament without any stereoscopic information.

### **On the Strength of the Hemispheric Rule and the Origin of Active-region Helicity**

Y.-M. **Wang**

2013 ApJ 775 L46

Vector magnetograph and morphological observations have shown that the solar magnetic field tends to have negative (positive) helicity in the northern (southern) hemisphere, although only ~60%-70% of active regions appear to obey this "hemispheric rule." In contrast, at least ~80% of quiescent filaments and filament channels that form during the decay of active regions follow the rule. We attribute this discrepancy to the difficulty in determining the helicity sign of newly emerged active regions, which are dominated by their current-free component; as the transverse field is canceled at the polarity inversion lines, however, the axial component becomes dominant there, allowing a more reliable determination of the original active-region chirality. We thus deduce that the hemispheric rule is far stronger than generally assumed, and cannot be explained by stochastic processes. Earlier studies have shown that the twist associated with the axial tilt of active regions is too small to account for the observed helicity; here, both tilt and twist are induced by the Coriolis force acting on the diverging flow in the emerging flux tube. However, in addition to this east-west expansion about the apex of the loop, each of its legs must expand continually in cross section during its rise through the convection zone, thereby acquiring a further twist through the Coriolis force. Since this transverse pressure effect is not limited by drag or tension forces, the final twist depends mainly on the rise time, and may be large enough to explain the observed active-region helicity.

### UTILIZATION OF MULTIPLE MEASUREMENTS FOR GLOBAL THREE-DIMENSIONAL MAGNETOHYDRODYNAMIC SIMULATIONS

A. H. [Wang](#)<sup>1</sup>, S. T. Wu<sup>1,2</sup>, E. Tandberg-Hanssen<sup>1</sup> and Frank Hill

2011 ApJ 732 19

Magnetic field measurements, line of sight (LOS) and/or vector magnetograms, have been used in a variety of solar physics studies. Currently, the global transverse velocity measurements near the photosphere from the Global Oscillation Network Group (GONG) are available. We have utilized these multiple observational data, for the first time, to present a data-driven global three-dimensional and resistive magnetohydrodynamic (MHD) simulation, and to investigate the energy transport across the photosphere to the corona. The measurements of the LOS magnetic field and transverse velocity reflect the effects of convective zone dynamics and provide information from the sub-photosphere to the corona. In order to self-consistently include the observables on the lower boundary as the inputs to drive the model, a set of time-dependent boundary conditions is derived by using the method of characteristics. We selected GONG's global transverse velocity measurements of synoptic chart CR2009 near the photosphere and SOLIS full-resolution LOS magnetic field maps of synoptic chart CR2009 on the photosphere to simulate the equilibrium state and compute the energy transport across the photosphere. To show the advantage of using both observed magnetic field and transverse velocity data, we have studied two cases: (1) with the inputs of the LOS magnetic field and transverse velocity measurements, and (2) with the input of the LOS magnetic field and without the input of transverse velocity measurements. For these two cases, the simulation results presented here are a three-dimensional coronal magnetic field configuration, density distributions on the photosphere and at 1.5 solar radii, and the solar wind in the corona. The deduced physical characteristics are the total current helicity and the synthetic emission. By comparing all the physical parameters of case 1 and case 2 and their synthetic emission images with the EIT image, we find that using both the measured magnetic field and the velocity distribution would give more cohesive results.

### ON THE WEAKENING OF THE POLAR MAGNETIC FIELDS DURING SOLAR CYCLE 23

[Y.-M. Wang](#), [E. Robbrecht](#)<sup>1</sup> and [N. R. Sheeley](#)

2009 ApJ 707 1372-1386

The Sun's polar fields are currently ~40% weaker than they were during the previous three sunspot minima. This weakening has been accompanied by a corresponding decrease in the interplanetary magnetic field (IMF) strength, by a ~20% shrinkage in the polar coronal-hole areas, and by a reduction in the solar-wind mass flux over the poles. It has also been reflected in coronal streamer structure and the heliospheric current sheet, which only showed the expected flattening into the equatorial plane after sunspot numbers fell to unusually low values in mid-2008. From latitude-time plots of the photospheric field, it has long been apparent that the polar fields are formed through the transport of trailing-polarity flux from the sunspot latitudes to the poles. To address the question of why the polar fields are now so weak, we simulate the evolution of the photospheric field and radial IMF strength from 1965 to the present, employing a surface transport model that includes the effects of active region emergence, differential rotation, supergranular convection, and a poleward bulk flow. We find that the observed evolution can be reproduced if the amplitude of the surface meridional flow is varied by as little as 15% (between 14.5 and 17 m s<sup>-1</sup>), with the higher average speeds being required during the long cycles 20 and 23.

**Is there more global solar activity on the Sun?**

J. X. **Wang**<sup>1</sup>, Y.Z. Zhang<sup>1</sup>, G.P. Zhou<sup>1</sup>, Y.Y. Wen<sup>1</sup> and J. Jiang<sup>2</sup>  
Solar and Stellar Variability: Impact on Earth and Planets, Proceedings IAU Symposium No. 264, **2009**,  
p. 251-256, A.G. Kosovichev, A.H. Andrei & J.-P. Rozelot, eds.; **File**  
Y:\obridko\otchet09

There appear indications of more global activity on the Sun which is larger, much beyond the scale of solar active regions (ARs). These indications include formation, flaring and eruption of the trans-equatorial loops seen in EUV and X-rays, formation and eruption of transequatorial filaments, global magnetic connectivity in EUV dimming associated with halo-coronal mass ejections, wide spread of radio burst sources in meter wavelength in the solar corona, and quasi-simultaneous magnetic flux emergence in both hemispheres seen during some major solar events. With examples of a few major events in the last solar cycle we discuss the possibility that there is large or global-scale activity on the Sun. Its spatial scale is many times larger than that of AR and temporal scale is over 10 hours. The exemplified trans-equatorial loops are anchored in ARs and their activity is temporally associated with flares in ARs too. In some sense the flares in ARs appear either as a part of or a precursor of the more global activity. It is likely that the combination of the flares in ARs and the associated global activity is responsible to the major solar-terrestrial events. More efforts in understanding the global activity are undertaken.

### **A Cross-Comparison of Cotemporal Magnetograms Obtained with MDI/SOHO and SP/Hinode**

D. **Wang** · M. Zhang · H. Li · H.Q. Zhang

Solar Phys (**2009**) 260: 233–244

We compared a set of cotemporal magnetograms of active regions obtained with the Michelson Doppler Imager (MDI) aboard SOHO and the Spectro-Polarimeter (SP) of the Solar Optical Telescope (SOT) on board *Hinode*. The comparison shows that even with the recent calibration of level-1.8 data, the magnetic flux density derived from the MDI data is still lower than that obtained with SP. The average ratio between current version 2008 MDI level-1.8 data and SP magnetograms is 0.71, and is 0.82 for version 2007 MDI level-1.8 data. The comparison also shows that the most recent version 2008 calibration of MDI level-1.8 data has successfully removed the center-to-limb variation, while version 2007 level-1.8 data did not, as estimated by Ulrich *et al.* (*Solar Phys.* **255**, 53, **2009**).

### **Determination of the Coronal Magnetic Field from Hot-Loop Oscillations Observed by SUMER and SXT**

Tongjiang **Wang**,<sup>1</sup> Davina E. Innes,<sup>2</sup> and Jiong Qiu<sup>1</sup>

The Astrophysical Journal, 656:598-609, 2007

### **Data-driven model of the solar corona above an active region**

J. **Warnecke** and H. Peter

A&A 623, L12 (**2019**)

<https://www.aanda.org/articles/aa/pdf/2019/04/aa35385-19.pdf>

**Aims.** We aim to reproduce the structure of the corona above a solar active region as seen in the extreme ultraviolet (EUV) using a three-dimensional magnetohydrodynamic (3D MHD) model.

**Methods.** The 3D MHD data-driven model solves the induction equation and the mass, momentum, and energy balance. To drive the system, we feed the observed evolution of the magnetic field in the photosphere of the active region AR 12139 into the bottom boundary. This creates a hot corona above the cool photosphere in a self-consistent way. We synthesize the coronal EUV emission from the densities and temperatures in the model and compare this to the actual coronal observations.

**Results.** We are able to reproduce the overall appearance and key features of the corona in this active region on a qualitative level. The model shows long loops, fan loops, compact loops, and diffuse emission forming at the same locations and at similar times as in the observation. Furthermore, the low-intensity contrast of the model loops in EUV matches the observations.

**Conclusions.** In our model the energy input into the corona is similar as in the scenarios of fieldline-braiding or flux-tube tectonics, that is, energy is transported to the corona through the driving of the vertical magnetic field by horizontal photospheric motions. The success of our model shows the central role that this process plays for the structure, dynamics, and heating of the corona. **16 August 2014**

## Current systems of coronal loops in 3D MHD simulations

J. [Warnecke](#)<sup>1</sup>, F. Chen<sup>2,1</sup>, S. Bingert<sup>3</sup> and H. Peter

A&A 607, A53 (2017)

**Aims.** We study the magnetic field and current structure associated with a coronal loop. Through this we investigate to what extent the assumptions of a force-free magnetic field break down and where they might be justified.

**Methods.** We analyze a three-dimensional (3D) magnetohydrodynamic (MHD) model of the solar corona in an emerging active region with the focus on the structure of the forming coronal loops. The lower boundary of this simulation is taken from a model of an emerging active region. As a consequence of the emerging magnetic flux and the horizontal motions at the surface a coronal loop forms self-consistently. We investigate the current density along magnetic field lines inside (and outside) this loop and study the magnetic and plasma properties in and around this loop. The loop is defined as the bundle of field lines that coincides with enhanced emission in extreme UV.

**Results.** We find that the total current along the emerging loop changes its sign from being antiparallel to parallel to the magnetic field. This is caused by the inclination of the loop together with the footpoint motion. Around the loop, the currents form a complex non-force-free helical structure. This is directly related to a bipolar current structure at the loop footpoints at the base of the corona and a local reduction of the background magnetic field (i.e., outside the loop) caused by the plasma flow into and along the loop. Furthermore, the locally reduced magnetic pressure in the loop allows the loop to sustain a higher density, which is crucial for the emission in extreme UV. The action of the flow on the magnetic field hosting the loop turns out to also be responsible for the observed squashing of the loop.

**Conclusions.** The complex magnetic field and current system surrounding it can only be modeled in 3D MHD models where the magnetic field has to balance the plasma pressure. A one-dimensional coronal loop model or a force-free extrapolation cannot capture the current system and the complex interaction of the plasma and the magnetic field in the coronal loop, despite the fact that the loop is under low- $\beta$  conditions.

## Bipolar region formation in stratified two-layer turbulence

J. [Warnecke](#)<sup>1,2</sup>, I. R. Losada<sup>2,3</sup>, A. Brandenburg<sup>2,3,4,5</sup>, N. Kleeorin<sup>6,2</sup> and I. Rogachevskii

A&A 589, A125 (2016)

**Aims.** This work presents an extensive study of the previously discovered formation of bipolar flux concentrations in a two-layer model. We interpret the formation process in terms of negative effective magnetic pressure instability (NEMPI), which is a possible mechanism to explain the origin of sunspots.

**Methods.** In our simulations, we use a Cartesian domain of isothermal stratified gas that is divided into two layers. In the lower layer, turbulence is forced with transverse nonhelical random waves, whereas in the upper layer no flow is induced. A weak uniform magnetic field is imposed in the entire domain at all times. In most cases, it is horizontal, but a vertical and an inclined field are also considered. In this study we vary the stratification by changing the gravitational acceleration, magnetic Reynolds number, strength of the imposed magnetic field, and size of the domain to investigate their influence on the formation process.

**Results.** Bipolar magnetic structure formation takes place over a large range of parameters. The magnetic structures become more intense for higher stratification until the density contrast becomes around 100 across the turbulent layer. For the fluid Reynolds numbers considered, magnetic flux concentrations are generated at magnetic Prandtl number between 0.1 and 1. The magnetic field in bipolar regions increases with higher imposed field strength until the field becomes comparable to the equipartition field strength of the turbulence. A larger horizontal extent enables the flux concentrations to become stronger and more coherent. The size of the bipolar structures turns out to be independent of the domain size. A small imposed horizontal field component is necessary to generate bipolar structures. In the case of bipolar region formation, we find an exponential growth of the large-scale magnetic field, which is indicative of a hydromagnetic instability. Additionally, the flux concentrations are correlated with strong large-scale downward and converging flows. These findings imply that NEMPI is responsible for magnetic flux concentrations.

## Towards a Quantitative Comparison of Magnetic Field Extrapolations and Observed Coronal Loops

[Harry P. Warren](#), [Nicholas A. Crump](#), [Ignacio Ugarte-Urra](#), [Xudong Sun](#), [Markus J. Aschwanden](#), [Thomas Wiegelmann](#)

ApJ 860 46 2018

<https://arxiv.org/pdf/1805.00281.pdf>

It is widely believed that loops observed in the solar atmosphere trace out magnetic field lines. However, the degree to which magnetic field extrapolations yield field lines that actually do follow loops has yet to be studied systematically. In this paper we apply three different extrapolation techniques - a simple potential model, a NLFF model based on photospheric vector data, and a NLFF model based on forward fitting magnetic sources with vertical currents - to 15 active regions that span a wide range of magnetic conditions. We use a distance metric to assess how

well each of these models is able to match field lines to the 12,202 loops traced in coronal images. These distances are typically 1-2". We also compute the misalignment angle between each traced loop and the local magnetic field vector, and find values of 5-12°. We find that the NLFF models generally outperform the potential extrapolation on these metrics, although the differences between the different extrapolations are relatively small. The methodology that we employ for this study suggests a number of ways that both the extrapolations and loop identification can be improved. **29 September 2010**

**Table 1.** Active Region Summary (2010-2011)

## **THE TEMPERATURE AND DENSITY STRUCTURE OF THE SOLAR CORONA.**

### **I. OBSERVATIONS OF THE QUIET SUN WITH THE EUV IMAGING SPECTROMETER ON *Hinode***

Harry P. [Warren](#) and David H. Brooks<sup>1</sup>

Astrophysical Journal, 700:762–773, 2009 July

Measurements of the temperature and density structure of the solar corona provide critical constraints on theories of coronal heating. Unfortunately, the complexity of the solar atmosphere, observational uncertainties, and the limitations of current atomic calculations, particularly those for Fe, all conspire to make this task very difficult. A critical assessment of plasma diagnostics in the corona is essential to making progress on the coronal heating problem. In this paper, we present an analysis of temperature and density measurements above the limb in the quiet corona using new observations from the EUV Imaging Spectrometer (EIS) on *Hinode*. By comparing the Si and Fe emission observed with EIS we are able to identify emission lines that yield consistent emission measure distributions. With these data we find that the distribution of temperatures in the quiet corona above the limb is strongly peaked near 1 MK, consistent with previous studies. We also find, however, that there is a tail in the emission measure distribution that extends to higher temperatures. EIS density measurements from several density sensitive line ratios are found to be generally consistent with each other and with previous measurements in the quiet corona. Our analysis, however, also indicates that a significant fraction of the weaker emission lines observed in the EIS wavelength ranges cannot be understood with current atomic data.

## **Observations of Umbral Dots and their Physical Models**

Hiroko [Watanabe](#)

PASJ, 2014

<http://arxiv.org/pdf/1407.4581v1.pdf>

The *Hinode* satellite opens a new era to the sunspots research, because of its high spatial resolution and temporal stability. Fine scale structures in sunspots, called umbral dots (UDs), have become one of the hottest topics in terms of the close observation of the magnetoconvection.

In this paper, a brief review of observed properties of UD is given based on the recent literature. UD born in the periphery of the umbra exhibit inward migration, and their speeds are positively correlated with the magnetic field inclination. Longer-lasting UD are tend to be larger and brighter, while lifetimes of UD show no relation with their background magnetic field strength. UD tend to disappear or stop its proper motion by colliding with the locally strong field region. The spatial distribution of UD is not uniform over an umbra but is preferably located at boundaries of cellular patterns. From our 2-dimensional correlation analysis, we measured the characteristic width of the cell boundaries (~0.5") and the size of the cells (~6").

Then we performed a simplified analysis to get statistics how the UD distribution is random or clustered using the *Hinode* blue continuum images. We find a hint that the UD become less dense and more clustered for later phase sunspots. These results may be related to the evolutionary change of the subsurface structure of a sunspot.

Based on these observational results, we will discuss their physical models by means of numerical simulations of magnetoconvection.

## **TEMPORAL EVOLUTION OF VELOCITY AND MAGNETIC FIELD IN AND AROUND UMBRAL DOTS**

Hiroko [Watanabe](#)<sup>1,2</sup>, Luis R. Bellot Rubio<sup>3</sup>, Jaime de la Cruz Rodríguez<sup>4</sup>, and Luc Rouppe van der Voort

2012 ApJ 757 49

We study the temporal evolution of umbral dots (UDs) using measurements from the CRISP imaging spectropolarimeter at the Swedish 1 m Solar Telescope. Scans of the magnetically sensitive 630 nm iron lines were performed under stable atmospheric conditions for 71 minutes with a cadence of 63 s. These observations allow us to investigate the magnetic field and velocity in and around UD at a resolution approaching 0.13. From the analysis of 339 UD, we draw the following conclusions: (1) UD show clear hints of upflows, as predicted by magnetohydrodynamic simulations. By contrast, we could not find systematic downflow signals. Only in very deep

layers, we detect localized downflows around UDs, but they do not persist in time. (2) We confirm that UDs exhibit weaker and more inclined fields than their surroundings, as reported previously. However, UDs that have strong fields above 2000 G or are in the decay phase show enhanced and more vertical fields. (3) There are enhanced fields at the migration front of UDs detached from penumbral grains, as if their motion were impeded by the ambient field. (4) Long-lived UDs travel longer distances with slower proper motions. Our results appear to confirm some aspects of recent numerical simulations of magnetoconvection in the umbra (e.g., the existence of upflows in UDs), but not others (e.g., the systematic weakening of the magnetic field at the position of UDs).

### **Cross-Calibrating Sunspot Magnetic Field Strength Measurements from the McMath–Pierce Solar Telescope and the Dunn Solar Telescope**

Fraser T. [Watson](#), Christian Beck, Matthew J. Penn, Alexandra Tritschler...

Solar Phys. Volume 290, [Issue 11](#), pp 3267-3277 2015

<http://arxiv.org/pdf/1511.07315v1.pdf>

In this article we describe a recent effort to cross-calibrate data from an infrared detector at the McMath-Pierce Solar Telescope and the Facility InfraRed Spectropolarimeter (FIRS) at the Dunn Solar Telescope. A synoptic observation program at the McMath-Pierce has measured umbral magnetic field strengths since 1998, and this data set has recently been compared with umbral magnetic field observations from SOHO MDI and SDO HMI. To further improve on the data from McMath-Pierce, we compared the data with measurements taken at the Dunn Solar Telescope with far greater spectral resolution than has been possible with space instrumentation. To minimise potential disruption to the study, concurrent umbral measurements were made so that the relationship between the two datasets can be most accurately characterised. We find that there is a strong agreement between the umbral magnetic field strengths recorded by each instrument, and we reduced the FIRS data in two different ways to successfully test this correlation further. 23 January 2013, 4 February 2013, 17–18 October 2013, 31 October 2013

### **The STARA Sunspot Catalog (the Sunspot Tracking And Recognition Algorithm)**

F. T. [Watson](#)

HMI Science Nuggets, #29, 2014

<http://hmi.stanford.edu/hminuggets/?p=981>

The STARA catalog of sunspot properties from the SOHO/MDI and SDO/HMI data is presented and discussed. For STARA, an automated detection algorithm is employed to compile the first sunspot record from space-based instruments. This catalog is publicly available at

<http://www.nso.edu/staff/fwatson/STARA>.

### **A Multi-instrument Analysis of Sunspot Umbrae**

F. T. [Watson](#), M. J. Penn, and W. Livingston

2014 ApJ 787 22

<http://arxiv.org/pdf/1511.07300v1.pdf>

The recent solar minimum and rise phase of solar cycle 24 have been unlike any period since the early 1900s. This article examines some of the properties of sunspot umbrae over the last 17 yr with three different instruments on the ground and in space: MDI, HMI and BABO. The distribution of magnetic fields and their evolution over time is shown and reveals that the field distribution in cycle 24 is fundamentally different from that in cycle 23. The annual average umbral magnetic field is then examined for the 17 yr observation period and shows a small decrease of 375 G in sunspot magnetic fields over the period 1996-2013, but the mean intensity of sunspot umbrae does not vary significantly over this time. A possible issue with sample sizes in a previous study is then explored to explain disagreements in data from two of the source instruments. All three instruments show that the relationship between umbral magnetic fields and umbral intensity agrees with past studies in that the umbral intensity decreases as the field strength increases. This apparent contradiction can be explained by the range of magnetic field values measured for a given umbral intensity being larger than the measured 375 G change in umbral field strength over time.

### **Evolution of sunspot properties during solar cycle 23**

F. T. [Watson](#)<sup>1</sup>, L. Fletcher<sup>1</sup> and S. Marshall

A&A 533, A14 (2011)



Context. The long term study of the Sun is necessary if we are to determine the evolution of sunspot properties and thereby inform modeling of the solar dynamo, particularly on scales of a solar cycle.

Aims. We aim to determine a number of sunspot properties over cycle 23 using the uniform database provided by the SOHO Michelson Doppler Imager data. We focus in particular on their distribution on the solar disk, maximum magnetic field and umbral/penumbral areas. We investigate whether the secular decrease in sunspot maximum magnetic field reported in Kitt Peak data is present also in MDI data.

Methods. We have used the Sunspot Tracking And Recognition Algorithm (STARA) to detect all sunspots present in the SOHO Michelson Doppler Imager continuum data giving us 30 084 separate detections. We record information on the sunspot locations, area and magnetic field properties as well as corresponding information for the umbral areas detected within the sunspots, and track them through their evolution.

Results. We find that the total visible umbral area is 20–40% of the total visible sunspot area regardless of the stage of the solar cycle. We also find that the number of sunspots observed follows the Solar Influences Data Centre international sunspot number with some interesting deviations. Finally, we use the magnetic information in our catalogue to study the long term variation of magnetic field strength within sunspot umbrae and find that it increases and decreases along with the sunspot number. However, if we were to assume a secular decrease as was reported in the Kitt Peak data and take into account sunspots throughout the whole solar cycle we would find the maximum umbral magnetic fields to be decreasing by  $23.6 \pm 3.9$  Gauss per year, which is far less than has previously been observed by other studies (although measurements are only available for solar cycle 23). If we only look at the declining phase of cycle 23 we find the decrease in sunspot magnetic fields to be 70 Gauss per year.

## **THE POSSIBLE IMPACT OF L5 MAGNETOGRAMS ON NON-POTENTIAL SOLAR CORONAL MAGNETIC FIELD SIMULATIONS**

Marion [Weinzierl](#)<sup>1</sup>, Duncan H. Mackay<sup>2</sup>, Anthony R. Yeates<sup>1</sup>, and Alexei A. Pevtsov

2016 ApJ 828 102

The proposed *Carrington-L5* mission would bring instruments to the L5 Lagrange point to provide us with crucial data for space weather prediction. To assess the importance of including a magnetograph, we consider the possible differences in non-potential solar coronal magnetic field simulations when magnetograph observations are available from the L5 point, compared with an L1-based field of view (FOV). A timeseries of synoptic radial magnetic field maps is constructed to capture the emergence of two active regions from the L5 FOV. These regions are initially absent in the L1 magnetic field maps, but are included once they rotate into the L1 FOV. Non-potential simulations for these two sets of input data are compared in detail. Within the bipolar active regions themselves, differences in the magnetic field structure can exist between the two simulations once the active regions are included in both. These differences tend to reduce within 5 days of the active region being included in L1. The delayed emergence in L1 can, however, lead to significant persistent differences in long-range connectivity between the active regions and the surrounding fields, and also in the global magnetic energy. In particular, the open magnetic flux and the location of open magnetic footpoints, are sensitive to capturing the real-time of emergence. These results suggest that a magnetograph at L5 could significantly improve predictions of the non-potential corona, the interplanetary magnetic field, and of solar wind source regions on the Sun.

## **A NEW TECHNIQUE FOR THE PHOTOSPHERIC DRIVING OF NON-POTENTIAL SOLAR CORONAL MAGNETIC FIELD SIMULATIONS**

Marion [Weinzierl](#)<sup>1</sup>, Anthony R. Yeates<sup>1</sup>, Duncan H. Mackay<sup>2</sup>, Carl J. Henney<sup>3</sup>, and C. Nick Arge

2016 ApJ 823 55

In this paper, we develop a new technique for driving global non-potential simulations of the Sun's coronal magnetic field solely from sequences of radial magnetic maps of the solar photosphere. A primary challenge to driving such global simulations is that the required horizontal electric field cannot be uniquely determined from such maps. We show that an "inductive" electric field solution similar to that used by previous authors successfully reproduces specific features of the coronal field evolution in both single and multiple bipole simulations. For these cases, the true solution is known because the electric field was generated from a surface flux-transport model. The match for these cases is further improved by including the non-inductive electric field contribution from surface differential rotation. Then, using this reconstruction method for the electric field, we show that a coronal non-potential simulation can be successfully driven from a sequence of ADAPT maps of the photospheric radial field, without including additional physical observations which are not routinely available.

## **Photospheric Driving of Non-potential Solar Coronal Magnetic Field Simulations**

Marion [Weinzierl](#)<sup>1</sup> and Anthony R. Yeates

HMI Science Nuggets #47 Dec 2015

<http://hmi.stanford.edu/hminuggets/?p=1367>

2014 November 1 to 2014 December 23

## **The Photospheric Imprints of Coronal Electric Currents**

[Brian T. Welsch](#)

ApJ 2022

<https://arxiv.org/pdf/2211.01911.pdf>

Flares and coronal mass ejections are powered by magnetic energy stored in coronal electric currents. Here, we explore the nature of coronal currents in observed and model active region (ARs) by studying manifestations of these currents in photospheric vector magnetograms. We employ Gauss's separation method, recently introduced to the solar physics literature, to partition the photospheric field into three distinct components, each arising from a separate source: (i) currents passing through the photosphere, (ii) currents flowing below it, and (iii) currents flowing above it. We refer to component (iii) as the photospheric imprint of coronal currents. In both AR 10930 and AR 11158, photospheric imprints exhibit large-scale, spatially coherent structures along these regions' central, sheared polarity inversion lines (PILs) that are consistent with coronal currents flowing horizontally above these PILs, similar to recent findings in AR 12673 by Schuck et al. (2022). We find similar photospheric imprints in a simple model of a non-potential AR with known currents. We find that flare-associated changes in photospheric imprints in AR 11158 accord with earlier reports that near-PIL fields become more horizontal, consistent with the "implosion" scenario. We hypothesize that this evolution effectively shortens, in an overall sense, current-carrying coronal fields, leading to decreased inductive energy (DIE) in the coronal field. We further hypothesize that, in the hours prior to flares, parts of the coronal field slowly expand, in a process we deem coronal inflation (CI) -- essentially, the inverse of the implosion process. Both of these hypotheses are testable with non-potential coronal field extrapolations. 2006/12/12, 2011/02/15

## Deriving Potential Coronal Magnetic Fields from Vector Magnetograms

Brian T. Welsch, George H. Fisher

Solar Phys. Volume 291, Issue 6, pp 1681-1710 2016

<http://arxiv.org/pdf/1503.08754v1.pdf>

The minimum-energy configuration for the magnetic field above the solar photosphere is curl-free (hence, by Ampere's law, also current-free), so can be represented as the gradient of a scalar potential. Since magnetic fields are divergence free, this scalar potential obeys Laplace's equation, given an appropriate boundary condition (BC). With measurements of the full magnetic vector at the photosphere, it is possible to employ either Neumann or Dirichlet BCs there. Historically, the Neumann BC was used, since available line-of-sight magnetic field measurements approximated the radial field needed for the Neumann BC. Since each BC fully determines the 3D vector magnetic field, either choice will, in general, be inconsistent with some aspect of the observed field on the boundary, due to the presence of both currents and noise in the observed field. We present a method to combine solutions from both Dirichlet and Neumann BCs to determine a hybrid potential field that minimizes the integrated square of the residual between the potential and actual fields, with the possibility of weighting by spatially uniform measurement uncertainties. This has advantages in both not overfitting the radial field used for the Neumann BC, and maximizing consistency with the observations. We show this with HMI vector magnetic field observations of AR 11158, and find that residual discrepancies between the observed and potential fields are significant, and imply nonzero horizontal photospheric currents. We also analyze potential fields for two other active regions observed with two different vector magnetographs, and find that hybrid potential fields have substantially less energy than the Neumann fields in every case --- by nearly  $10^{33}$  ergs in some cases. This has major implications for estimates of free magnetic energy in coronal field models, e.g., non-linear force-free field extrapolations. 2006 December 12, 27 October 2010, 2011/02/15

## Defining the Middle Corona

**Review**

[Matthew J. West](#), [Daniel B. Seaton](#), [David B. Wexler](#), [John C. Raymond](#), et al.

Working draft prepared by the middle corona heliophysics working group 2022

<https://arxiv.org/pdf/2208.04485.pdf>

The middle corona, the region roughly spanning heliocentric altitudes from 1.5 to  $6R_{\odot}$ , encompasses almost all of the influential physical transitions and processes that govern the behavior of coronal outflow into the heliosphere. Eruptions that could disrupt the near-Earth environment propagate through it. Importantly, it modulates inflow from above that can drive dynamic changes at lower heights in the inner corona. Consequently, this region is essential for comprehensively connecting the corona to the heliosphere and for developing corresponding global models. Nonetheless, because it is challenging to observe, the middle corona has been poorly studied by major solar remote sensing missions and instruments, extending back to the Solar and Heliospheric Observatory (SoHO) era. Thanks to recent advances in instrumentation, observational processing techniques, and a realization of the importance of the region, interest in the middle corona has increased. Although the region cannot be intrinsically separated from other regions of the solar atmosphere, there has emerged a need to define the region in terms of its location and extension in the solar atmosphere, its composition, the physical transitions it covers, and the underlying physics believed to be encapsulated by the region. This paper aims to define the middle corona and give an overview of the processes that occur there.

## Middle Corona Magnetic Field Strength Determined by Spacecraft Radio Faraday Rotation

David B. [Wexler](#)<sup>1</sup>, Elizabeth A. Jensen<sup>2</sup>, and Carl Heiles<sup>3</sup>

2021 Res. Notes AAS 5 165

<https://iopscience.iop.org/article/10.3847/2515-5172/ac1521>

<https://doi.org/10.3847/2515-5172/ac1521>

Faraday rotation (FR) of MESSENGER spacecraft X-band transcoronal radio transmissions were studied to evaluate the mid-coronal magnetic field strength, with the line-of-sight closest solar approach at heliocentric altitudes ranging 1.647–1.817  $R_{\odot}$ . A Community Coordinated Modeling Center (CCMC) CORHEL-MAS 3D coronal field map revealed this region to contain closed magnetic fields. By FR analysis we found a field strength of 118,000 nT at  $r = 1.647 R_{\odot}$ , with fall-off to 40,000 nT by  $r = 1.817 R_{\odot}$ . These values straddle estimates provided by the CCMC model. The mean value of 79,000 nT at  $r = 1.732 R_{\odot}$  is comparable to the value provided by an established empirical model for average coronal magnetic field strength. FR can be used to evaluate middle coronal magnetic fields, but improved methods to constrain concurrent electron column density will be needed to produce the most accurate results.

## ACHIEVING SELF-CONSISTENT NONLINEAR FORCE-FREE MODELING OF SOLAR ACTIVE REGIONS

M. S. [Wheatland](#)<sup>1</sup> and K. D. Leka

2011 ApJ 728 112

A nonlinear force-free solution is constructed for the coronal magnetic field in NOAA solar active region (AR) 10953 based on a photospheric vector magnetogram derived from Hinode satellite observations on **2007 April 30**, taking into account uncertainties in the boundary data and using improved methods for merging multiple-instrument data. The solution demonstrates the "self-consistency" procedure of Wheatland & Régnier, for the first time including uncertainties. The self-consistency procedure addresses the problem that photospheric vector magnetogram data are inconsistent with the force-free model, and in particular that the boundary conditions on vertical electric current density are overspecified and permit the construction of two different nonlinear force-free solutions. The procedure modifies the boundary conditions on current density during a sequence of cycles until the two nonlinear force-free solutions agree. It hence constructs an accurate single solution to the force-free model, with boundary values close, but not matched exactly, to the vector magnetogram data. The inclusion of uncertainties preserves the boundary conditions more closely at points with smaller uncertainties. The self-consistent solution obtained for AR 10953 is significantly non-potential, with magnetic energy  $E/E_0 = 1.08$ , where  $E_0$  is the energy of the reference potential (current-free) magnetic field. The self-consistent solution is shown to be robust against changes in the details of the construction of the two force-free models at each cycle. This suggests that reliable nonlinear force-free modeling of ARs is possible if uncertainties in vector magnetogram boundary data are included.

### A self-consistent nonlinear force-free solution for a solar active region magnetic field

M.S. [Wheatland](#) and S. Regnier

E-print, June 2009; ApJL, 700, Number 2, L88-L91, 2009.

Nonlinear force-free solutions for the magnetic field in the solar corona constructed using photospheric vector magnetic field boundary data suffer from a basic problem: the observed boundary data are inconsistent with the nonlinear force-free model. Specifically, there are two possible choices of boundary conditions on vertical current provided by the data, and the two choices lead to different force-free solutions. A novel solution to this problem is described. Bayesian probability is used to modify the boundary values on current density, using field-line connectivity information from the two force-free solutions and taking into account uncertainties, so that the boundary data are more consistent with the two nonlinear force-free solutions. This procedure may be iterated until a set of self-consistent boundary data (the solutions for the two choices of boundary conditions are the same) is achieved. The approach is demonstrated to work in application to Hinode/SOT observations of NOAA active region 10953.

### Calculating and Testing Nonlinear Force-Free Fields

M. S. [Wheatland](#), E-print, Sept 2007; Solar Phys. (2007) 245: 251–262

Improvements to an existing method for calculating nonlinear force-free magnetic fields (Wheatland 2006, Solar Phys. 238, 29) are described.

# RECONSTRUCTION OF NONLINEAR FORCE-FREE FIELDS AND SOLAR FLARE PREDICTION -- M.S. [Wheatland](#), E-print, Dec 2006

**A Fast Current-Field Iteration Method for Calculating Nonlinear Force-Free Fields**  
M. S. [Wheatland](#), Solar Physics, Volume 238 Number 1, p. 29 – 39, 2006

## Automatic Computation of Linear Magneto-Hydro-Static Equilibria

Thomas [Wiegelmann](#) & [Maria S. Madjarska](#)

[Solar Physics](#) volume 298, Article number: 3 (2023)

<https://link.springer.com/content/pdf/10.1007/s11207-022-02094-2.pdf>

Deriving the physical parameters of observed phenomena in the solar atmosphere has fundamental importance, as these parameters are then employed to constrain and validate models. Here we report the development of a new computational algorithm based on a magneto-hydro-static model that computes the magnetic field in the solar atmosphere and automatically matches individual magnetic-field lines with observed structures that appear with enhanced emission in extreme-ultraviolet (EUV) images. Presently, for the quiet-Sun regions, we can only measure the vertical photospheric magnetic field  $B_z$ , as accurate horizontal magnetic field measurements are not available. Thus, vertical photospheric magnetic-field measurements are extrapolated into the upper atmosphere, from the photosphere to the corona, with a magneto-hydro-static model. Free model parameters are then optimized with a downhill-simplex method by comparing quantitatively magnetic-field lines with the enhanced emission of loop structures composing the so-called coronal bright points recorded in EUV images taken with the Atmospheric Imaging Assembly on-board the Solar Dynamics Observatory. The algorithm will be applicable to any solar image data where individual structures with an enhanced emission can be resolved. Most importantly, the algorithm can be employed to obtain the magnetic properties of these structures above the photosphere. **15-16 Sep 2019**

## Solar force-free magnetic fields

**Review**

[Thomas Wiegelmann](#) & [Takashi Sakurai](#)

[Living Reviews in Solar Physics](#) volume 18, Article number: 1 (2021)

<https://link.springer.com/content/pdf/10.1007/s41116-020-00027-4.pdf>

<https://doi.org/10.1007/s41116-020-00027-4>

The structure and dynamics of the solar corona is dominated by the magnetic field. In most areas in the corona magnetic forces are so dominant that all non-magnetic forces such as plasma pressure gradients and gravity can be neglected in the lowest order. This model assumption is called the force-free field assumption, as the Lorentz force vanishes. This can be obtained by either vanishing electric currents (leading to potential fields) or the currents are co-aligned with the magnetic field lines. First we discuss a mathematically simpler approach that the magnetic field and currents are proportional with one global constant, the so-called linear force-free field approximation. In the generic case, however, the relationship between magnetic fields and electric currents is nonlinear and analytic solutions have been only found for special cases, like 1D or 2D configurations. For constructing realistic nonlinear force-free coronal magnetic field models in 3D, sophisticated numerical computations are required and boundary conditions must be obtained from measurements of the magnetic field vector in the solar photosphere. This approach is currently a large area of research, as accurate measurements of the photospheric field are available from ground-based observatories such as the Synoptic Optical Long-term Investigations of the Sun and the Daniel K. Inouye Solar Telescope (DKIST) and space-born, e.g., from Hinode and the Solar Dynamics Observatory. If we can obtain accurate force-free coronal magnetic field models we can calculate the free magnetic energy in the corona, a quantity which is important for the prediction of flares and coronal mass ejections. Knowledge of the 3D structure of magnetic field lines also help us to interpret other coronal observations, e.g., EUV images of the radiating coronal plasma.

## An Optimization Principle for Computing Stationary MHD Equilibria with Solar Wind Flow

[Thomas Wiegelmann](#), [Thomas Neukirch](#), [Dieter H. Nickeler](#) & [Iulia Chifu](#)

[Solar Physics](#) volume 295, Article number: 145 (2020)

<https://link.springer.com/content/pdf/10.1007/s11207-020-01719-8.pdf>

In this work we describe a numerical optimization method for computing stationary MHD equilibria. The newly developed code is based on a nonlinear force-free optimization principle. We apply our code to model the solar corona using synoptic vector magnetograms as boundary condition. Below about two solar radii the plasma  $\beta$  and Alfvén Mach number  $M_A$  are small and the magnetic field configuration of stationary MHD is basically identical to a nonlinear force-free field, whereas higher up in the corona (where  $\beta$  and  $M_A$  are above unity) plasma and flow effects become important and stationary MHD and force-free configuration deviate significantly. The new method allows for the reconstruction of the coronal magnetic field further outwards than with potential field, nonlinear force-free or magnetostatic models. This way the model might help to provide the magnetic

connectivity for joint observations of remote sensing and in-situ instruments on Solar Orbiter and Parker Solar Probe.

## Coronal Magnetic Field Models

**Review**

Thomas **Wiegmann**, Gordon J. D. Petrie, Pete Riley

Space Science Reviews 2017, Volume 210, [Issue 1–4](#), pp 249–274

<http://link.springer.com/article/10.1007/s11214-015-0178-3>

Coronal magnetic field models use photospheric field measurements as boundary condition to model the solar corona. We review in this paper the most common model assumptions, starting from MHD-models, magnetohydrostatics, force-free and finally potential field models. Each model in this list is somewhat less complex than the previous one and makes more restrictive assumptions by neglecting physical effects. The magnetohydrostatic approach neglects time-dependent phenomena and plasma flows, the force-free approach neglects additionally the gradient of the plasma pressure and the gravity force. This leads to the assumption of a vanishing Lorentz force and electric currents are parallel (or anti-parallel) to the magnetic field lines. Finally, the potential field approach neglects also these currents. We outline the main assumptions, benefits and limitations of these models both from a theoretical (how realistic are the models?) and a practical viewpoint (which computer resources to we need?). Finally we address the important problem of noisy and inconsistent photospheric boundary conditions and the possibility of using chromospheric and coronal observations to improve the models.

## Magneto-static modelling from SUNRISE/IMaX: Application to an active region observed with SUNRISE II

T. **Wiegmann**, T. Neukirch, D.H. Nickeler, S.K. Solanki, P. Barthol, A. Gandorfer, L. Gizon, J. Hirzberger, T.L. Riethmüller, M. van Noort, J. Blanco Rodríguez, J. C. Del Toro Iniesta, D. Orozco Suárez, W. Schmidt, V. Martínez Pillet, M. Knölker

ApJS 2017

<https://arxiv.org/pdf/1701.01458v2.pdf>

Magneto-static models may overcome some of the issues facing force-free magnetic field extrapolations. So far they have seen limited use and have faced problems when applied to quiet-Sun data. Here we present a first application to an active region. We use solar vector magnetic field measurements gathered by the IMaX polarimeter during the flight of the Sunrise balloon-borne solar observatory in June 2013 as boundary condition for a magneto-static model of the higher solar atmosphere above an active region. The IMaX data are embedded in active region vector magnetograms observed with SDO/HMI. This work continues our magneto-static extrapolation approach, which has been applied earlier (Paper I) to a quiet Sun region observed with Sunrise I. In an active region the signal-to-noise-ratio in the measured Stokes parameters is considerably higher than in the quiet Sun and consequently the IMaX measurements of the horizontal photospheric magnetic field allow us to specify the free parameters of the model in a special class of linear magneto-static equilibria. The high spatial resolution of IMaX (110-130 km, pixel size 40 km) enables us to model the non-force-free layer between the photosphere and the mid chromosphere vertically by about 50 grid points. In our approach we can incorporate some aspects of the mixed beta layer of photosphere and chromosphere, e.g., taking a finite Lorentz force into account, which was not possible with lower resolution photospheric measurements in the past. The linear model does not, however, permit to model intrinsic nonlinear structures like strongly localized electric currents. **2013, June 12th**

## Magneto-static modelling of the mixed plasma Beta solar atmosphere based on SUNRISE/IMaX data

T. **Wiegmann**, T. Neukirch, D.H. Nickeler, S.K. Solanki, V. Martinez Pillet, J.M. Borrero

ApJ 2015

<http://arxiv.org/pdf/1511.05568v1.pdf>

Our aim is to model the 3D magnetic field structure of the upper solar atmosphere, including regions of non-negligible plasma beta. We use high-resolution photospheric magnetic field measurements from SUNRISE/IMaX as boundary condition for a magneto-static magnetic field model. The high resolution of IMaX allows us to resolve the interface region between photosphere and corona, but modelling this region is challenging for the following reasons. While the coronal magnetic field is thought to be force-free (the Lorentz-force vanishes), this is not the case in the mixed plasma  $\beta$  environment in the photosphere and lower chromosphere. In our model, pressure gradients and gravity forces are taken self-consistently into account and compensate the non-vanishing Lorentz-force. Above a certain height (about 2 Mm) the non-magnetic forces become very weak and consequently the magnetic field becomes almost force-free. Here we apply a linear approach, where the electric current density consists of a superposition of a field-line parallel current and a current perpendicular to the Sun's gravity field. We illustrate the prospects and limitations of this approach and give an outlook for an extension towards a non-linear model.

## Magneto-static modelling from SUNRISE/IMaX: Application to an active region observed with SUNRISE II

T. [Wiegelmann](#), T. Neukirch, D.H. Nickeler, [S.K. Solanki](#), [P. Barthol](#), [A. Gandorfer](#), [L. Gizon](#), [J. Hirzberger](#), [T.L. Riethmüller](#), [M. van Noort](#), [J. Blanco Rodríguez](#), [J. C. Del Toro Iniesta](#), [D. Orozco Suárez](#), [W. Schmidt](#), [V. Martínez Pillet](#), [M. Knölker](#)

ApJS 2017 Sunrise special issue

<https://arxiv.org/pdf/1701.01458v1.pdf>

Magneto-static models may overcome some of the issues facing force-free magnetic field extrapolations. So far they have seen limited use and have faced problems when applied to quiet-Sun data. Here we present a first application to an active region. We use solar vector magnetic field measurements gathered by the IMaX polarimeter during the flight of the \sunrise{ } balloon-borne solar observatory in June 2013 as boundary condition for a magneto-static model of the higher solar atmosphere above an active region. The IMaX data are embedded in active region vector magnetograms observed with SDO/HMI. This work continues our magneto-static extrapolation approach, which has been applied earlier (Paper I) to a quiet Sun region observed with \sunrise{ } I. In an active region the signal-to-noise-ratio in the measured Stokes parameters is considerably higher than in the quiet Sun and consequently the IMaX measurements of the horizontal photospheric magnetic field allow us to specify the free parameters of the model in a special class of linear magneto-static equilibria. The high spatial resolution of IMaX (110-130 km, pixel size 40 km) enables us to model the non-force-free layer between the photosphere and the mid chromosphere vertically by about 50 grid points. In our approach we can incorporate some aspects of the mixed beta layer of photosphere and chromosphere, e.g., taking a finite Lorentz force into account, which was not possible with lower resolution photospheric measurements in the past. The linear model does not, however, permit to model intrinsic nonlinear structures like strongly localized electric currents. **2013, June 12**

## The Magnetic Field in the Solar Atmosphere **Review**

Thomas [Wiegelmann](#), Julia K. Thalmann, Sami K. Solanki

The Astronomy and Astrophysics Review, v. 22(1), Article: 78, **2014; File**

<http://arxiv.org/pdf/1410.4214v1.pdf>

This publication provides an overview of magnetic fields in the solar atmosphere with the focus lying on the corona. The solar magnetic field couples the solar interior with the visible surface of the Sun and with its atmosphere. It is also responsible for all solar activity in its numerous manifestations. Thus, dynamic phenomena such as coronal mass ejections and flares are magnetically driven. In addition, the field also plays a crucial role in heating the solar chromosphere and corona as well as in accelerating the solar wind. Our main emphasis is the magnetic field in the upper solar atmosphere so that photospheric and chromospheric magnetic structures are mainly discussed where relevant for higher solar layers. Also, the discussion of the solar atmosphere and activity is limited to those topics of direct relevance to the magnetic field. After giving a brief overview about the solar magnetic field in general and its global structure, we discuss in more detail the magnetic field in active regions, the quiet Sun and coronal holes. **June 27, 2004, August 22 to September 18, 1996, 27 May 2003, February 15 at 2011, 2012 March 9. 13 March 2012. 25 September 2007**

## Solar Force-free Magnetic Fields **Review**

Thomas [Wiegelmann](#), Takashi Sakurai

E-print, Aug **2012**; Living Reviews in Solar Physics, PUB.NO. lrsp-2012-5, sept **2012**

<http://www.livingreviews.org/lrsp-2012-5>

The structure and dynamics of the solar corona is dominated by the magnetic field. In most areas in the corona magnetic forces are so dominant that all non-magnetic forces like plasma pressure gradient and gravity can be neglected in the lowest order. This model assumption is called the force-free field assumption, as the Lorentz force vanishes. This can be obtained by either vanishing electric currents (leading to potential fields) or the currents are co-aligned with the magnetic field lines. First we discuss a mathematically simpler approach that the magnetic field and currents are proportional with one global constant, the so-called linear force-free field approximation. In the generic case, however, the relation between magnetic fields and electric currents is nonlinear and analytic solutions have been only found for special cases, like 1D or 2D configurations. For constructing realistic nonlinear force-free coronal magnetic field models in 3D, sophisticated numerical computations are required and boundary conditions must be obtained from measurements of the magnetic field vector in the solar photosphere. This approach is currently of large interests, as accurate measurements of the photospheric field become available from ground-based (for example SOLIS) and space-born (for example Hinode and SDO) instruments. If we can obtain accurate force-free coronal magnetic field models we can calculate the free magnetic energy in the corona, a quantity which is important for the prediction of flares and coronal mass ejections. Knowledge of the 3D structure of magnetic field lines also help us to interpret other coronal observations, e.g., EUV-images of the radiating coronal plasma.

## **How Should One Optimize Nonlinear Force-Free Coronal Magnetic Field Extrapolations from SDO/HMI Vector Magnetograms?**

T. [Wiegmann](#), J.K. Thalmann, B. Inhester, T. Tadesse, X. Sun, J.T. Hoeksema

E-print, Feb 2012, Solar Phys., 2012, Volume 281, Issue 1, pp 37-51

The Helioseismic and Magnetic Imager (HMI) on board the Solar Dynamics Observatory (SDO) provides photospheric vector magnetograms with a high spatial and temporal resolution. Our intention is to model the coronal magnetic field above active regions with the help of a nonlinear force-free extrapolation code. Our code is based on an optimization principle and has been tested extensively with semianalytic and numeric equilibria and applied to vector magnetograms from Hinode and ground-based observations. Recently we implemented a new version which takes into account measurement errors in photospheric vector magnetograms. Photospheric field measurements are often affected by measurement errors and finite nonmagnetic forces inconsistent for use as a boundary for a force-free field in the corona. To deal with these uncertainties, we developed two improvements: i) preprocessing of the surface measurements to make them compatible with a force-free field, and ii) new code which keeps a balance between the force-free constraint and deviation from the photospheric field measurements. Both methods contain free parameters, which must be optimized for use with data from SDO/HMI. In this work we describe the corresponding analysis method and evaluate the force-free equilibria by how well force-freeness and solenoidal conditions are fulfilled, by the angle between magnetic field and electric current, and by comparing projections of magnetic field lines with coronal images from the Atmospheric Imaging Assembly (SDO/AIA). We also compute the available free magnetic energy and discuss the potential influence of control parameters.

## **How to deal with measurement errors and lacking data in nonlinear force-free coronal magnetic field modelling?**

T. [Wiegmann](#) and B. Inhester

A&A 516, A107 (2010)

## **Solar stereoscopy – where are we and what developments do we require to progress?**

T. [Wiegmann](#)<sup>1</sup>, B. Inhester<sup>1</sup>, and L. Feng

Ann. Geophys., 27, 2925-2936, 2009; **File**

Observations from the two STEREO-spacecraft give us for the first time the possibility to use stereoscopic methods to reconstruct the 3-D solar corona. Classical stereoscopy works best for solid objects with clear edges. Consequently an application of classical stereoscopic methods to the faint structures visible in the optically thin coronal plasma is by no means straight forward and several problems have to be treated adequately: 1) First there is the problem of identifying one-dimensional structures – e.g. active region coronal loops or polar plumes- from the two individual EUV-images observed with STEREO/EUVI. 2) As a next step one has the association problem to find corresponding structures in both images. This becomes more difficult as the angle between STEREO-A and B increases. 3) Within the reconstruction problem stereoscopic methods are used to compute the 3-D-geometry of the identified structures. Without any prior assumptions, e.g., regarding the footpoints of coronal loops, the reconstruction problem has not one unique solution. 4) One has to estimate the reconstruction error or accuracy of the reconstructed 3-D-structure, which depends on the accuracy of the identified structures in 2-D, the separation angle between the spacecraft, but also on the location, e.g., for east-west directed coronal loops the reconstruction error is highest close to the loop top. 5) Eventually we are not only interested in the 3-D-geometry of loops or plumes, but also in physical parameters like density, temperature, plasma flow, magnetic field strength etc. Helpful for treating some of these problems are coronal magnetic field models extrapolated from photospheric measurements, because observed EUV-loops outline the magnetic field. This feature has been used for a new method dubbed "magnetic stereoscopy". As examples we show recent application to active region loops.

## **Can We Improve the Preprocessing of Photospheric Vector Magnetograms by the Inclusion of Chromospheric Observations?**

T. [Wiegmann](#), J. K. Thalmann, C. J. Schrijver, M. L. DeRosa and T. R. Metcalf

Solar Phys (2008) 247: 249–267

## **Nonlinear force-free modeling of the solar coronal magnetic field**

T. [Wiegmann](#)

JGR, VOL. 113, A03S02, doi:10.1029/2007JA012432, 2008

<http://www.agu.org/pubs/crossref/2008/2007JA012432.shtml>

The coronal magnetic field is an important quantity because the magnetic field dominates the structure of the solar corona. Unfortunately, direct measurements of coronal magnetic fields are usually not available. The photospheric

magnetic field is measured routinely with vector magnetographs. These photospheric measurements are extrapolated into the solar corona. The extrapolated coronal magnetic field depends on assumptions regarding the coronal plasma, for example, force-freeness. Force-free means that all nonmagnetic forces like pressure gradients and gravity are neglected. This approach is well justified in the solar corona owing to the low plasma beta. One has to take care, however, about ambiguities, noise and nonmagnetic forces in the photosphere, where the magnetic field vector is measured. **Here we review different numerical methods for a nonlinear force-free coronal magnetic field extrapolation:** Grad-Rubin codes, upward integration method, MHD relaxation, optimization, and the boundary element approach. We briefly discuss the main features of the different methods and concentrate mainly on recently developed new codes.

**Magnetic Stereoscopy -- T. [Wiegmann](#), B. Inhester, E-print, Dec 2006**

**Preprocessing of vector magnetograph data for a nonlinear force-free magnetic field reconstruction -- T. [Wiegmann](#), B. Inhester, T.Sakurai, E-print, Dec 2006**

**Testing non-linear force-free coronal magnetic field extrapolations with the Titov-Demoulin equilibrium -- T. [Wiegmann](#), B. Inhester, B. Kliem, G. Valori and T. Neukirch, , E-print, Dec 2006**

## **COMPUTING NONLINEAR FORCE-FREE CORONAL MAGNETIC FIELDS IN SPHERICAL GEOMETRY –**

Thomas [Wiegmann](#), Solar Phys., Volume 240, Number 2, Page: 227 – 239, 2007, E-print, Dec. 2006

<http://solar.physics.montana.edu/cgi-bin/eprint/index.pl?entry=2136>

## **MAGNETIC BRAIDING AND QUASI-SEPARATRIX LAYERS**

A. L. [Wilmot-Smith](#), G. Hornig, and D. I. Pontin

Astrophysical Journal, 704:1288–1295, 2009 October

The squashing factor  $Q$ , a property of the magnetic field line mapping, has been suggested as an indicator for the formation of current sheets, and subsequently magnetic reconnection, in astrophysical plasmas. Here, we test this hypothesis for a particular class of braided magnetic fields which serve as a model for solar coronal loops. We explore the relationship between quasi-separatrix layers (QSLs), that is, layer-like structures with high  $Q$  value, electric currents, and integrated parallel currents; the latter being a quantity closely related to the reconnection rate. It is found that as the degree of braiding of the magnetic field is increased, the maximum values of  $Q$  increase exponentially. At the same time, the distribution of  $Q$  becomes increasingly filamentary, with the width of the high- $Q$  layers exponentially decreasing. This is accompanied by an increase in the number of layers so that as the field is increasingly braided the volume becomes occupied by a myriad of thin QSLs. QSLs are not found to be good predictors of current features in this class of braided fields. Indeed, despite the presence of multiple QSLs, the current associated with the field remains smooth and large scale under ideal relaxation; the field dynamically adjusts to a smooth equilibrium. Regions of high  $Q$  are found to be better related to regions of high integrated parallel current than to actual current sheets.

## **Discovery of Finely Structured Dynamic Solar Corona Observed in the Hi-C Telescope**

Amy R. [Winebarger](#)<sup>1</sup>, Jonathan Cirtain<sup>1</sup>, Leon Golub<sup>2</sup>, Edward DeLuca<sup>2</sup>, Sabrina Savage<sup>1</sup>, Caroline Alexander<sup>1</sup>, and Timothy Schüle

2014 ApJ 787 L10

In the Summer of 2012, the High-resolution Coronal Imager (Hi-C) flew on board a NASA sounding rocket and collected the highest spatial resolution images ever obtained of the solar corona. One of the goals of the Hi-C flight was to characterize the substructure of the solar corona. We therefore examine how the intensity scales from AIA resolution to Hi-C resolution. For each low-resolution pixel, we calculate the standard deviation in the contributing high-resolution pixel intensities and compare that to the expected standard deviation calculated from the noise. If these numbers are approximately equal, the corona can be assumed to be smoothly varying, i.e., have no evidence of substructure in the Hi-C image to within Hi-C's ability to measure it given its throughput and readout noise. A standard deviation much larger than the noise value indicates the presence of substructure. We calculate these values for each low-resolution pixel for each frame of the Hi-C data. On average, 70% of the pixels in each Hi-C image show no evidence of substructure. The locations where substructure is prevalent is in the moss regions and in



regions of sheared magnetic field. We also find that the level of substructure varies significantly over the roughly 160 s of the Hi-C data analyzed here. This result indicates that the finely structured corona is concentrated in regions of heating and is highly time dependent.

## **Turbulence-Driven Coronal Heating and Improvements to Empirical Forecasting of the Solar Wind**

Lauren N. **Woolsey**, Steven R. Cranmer

ApJ, 787 160 2014

<http://arxiv.org/pdf/1404.5998v1.pdf>

Forecasting models of the solar wind often rely on simple parameterizations of the magnetic field that ignore the effects of the full magnetic field geometry. In this paper, we present the results of two solar wind prediction models that consider the full magnetic field profile and include the effects of Alfvén waves on coronal heating and wind acceleration. The one-dimensional MHD code ZEPHYR self-consistently finds solar wind solutions without the need for empirical heating functions. Another 1D code, introduced in this paper (The Efficient Modified-Parker-Equation-Solving Tool, TEMPEST), can act as a smaller, stand-alone code for use in forecasting pipelines. TEMPEST is written in Python and will become a publicly available library of functions that is easy to adapt and expand. We discuss important relations between the magnetic field profile and properties of the solar wind that can be used to independently validate prediction models. ZEPHYR provides the foundation and calibration for TEMPEST, and ultimately we will use these models to predict observations and explain space weather created by the bulk solar wind. We are able to reproduce with both models the general anticorrelation seen in comparisons of observed wind speed at 1 AU and the flux tube expansion factor. There is significantly less spread than comparing the results of the two models than between ZEPHYR and a traditional flux tube expansion relation. We suggest that the new code, TEMPEST, will become a valuable tool in the forecasting of space weather.

## **Propagation Properties of Sunspots Umbral Oscillations in Horizontal and Vertical Directions**

Wei **Wu**<sup>1,2</sup>, Jiang-tao Su<sup>1,2</sup>, Jie Chen<sup>2</sup>, Xiao-shuai Zhu<sup>3</sup>, and Robert Sych<sup>4</sup>

2023 ApJ 958 10

<https://iopscience.iop.org/article/10.3847/1538-4357/acf457/pdf>

We present a study on investigating the propagation characteristics of umbral oscillations in sunspots. In sunspot 1 (located in NOAA AR 12127) with four umbrae, the analysis shows that the oscillations in different umbrae are correlated. The weak correlation (<20%) is attributed to the propagation of umbral oscillations across the umbral boundary to its adjacent umbra in the horizontal direction. We speculate that oscillations in two of the umbrae have a common origin in the sub-photosphere, resulting in a stronger correlation (>30%). Additionally, utilizing the TiO (photosphere), H $\alpha$  (chromosphere) images provided by BBSO/GST, and the 304 Å (upper chromosphere and lower transition region), 171 Å (upper transition region), 193 Å (corona), and 211 Å (active region corona) images acquired by the Atmospheric Imaging Assembly on board the Solar Dynamics Observatory (SDO), we analyze the vertical propagation of oscillations in the sunspot umbra. Multi-channel observation shows that the umbral oscillations observed in the lower atmosphere of sunspot 1 cannot be detected in the upper atmosphere. However, in sunspot 2 (located in NOAA AR 12132), oscillations in the lower atmosphere can propagate to the upper atmosphere. Using photospheric magnetic field data provided by the Helioseismic and Magnetic Imager on board SDO, potential field extrapolation of the magnetic field for the two sunspots shows that open magnetic field structures allow sunspot oscillations to propagate to higher heights, while closed magnetic field structures do not.

2014 August 1, 2014 August 5

## **Observations of Energetic Particles between a Pair of Corotating Interaction Regions**

Z. **Wu**<sup>1</sup>, Y. Chen<sup>1</sup>, G. Li<sup>2</sup>, L. L. Zhao<sup>2</sup>, R. W. Ebert<sup>3</sup>, M. I. Desai<sup>3,4</sup>, G. M. Mason<sup>5</sup>, B. Lavraud<sup>6</sup>, L. Zhao<sup>7</sup>, Y. C.-M. Liu<sup>8</sup>, F. Guo<sup>9</sup>, C. L. Tang<sup>1</sup>, E. Landi<sup>7</sup>, and J. Sauvaud

2014 ApJ 781 17

We report observations of the acceleration and trapping of energetic ions and electrons between a pair of corotating interaction regions (CIRs). The event occurred in Carrington Rotation 2060. Observed by the STEREO-B spacecraft, the two CIRs were separated by less than 5 days. In contrast to other CIR events, the fluxes of the energetic ions and electrons in this event reached their maxima between the trailing edge of the first CIR and the leading edge of the second CIR. The radial magnetic field ( $B_r$ ) reversed its sense and the anisotropy of the flux also changed from Sunward to anti-Sunward between the two CIRs. Furthermore, there was an extended period of counterstreaming suprathermal electrons between the two CIRs. Similar observations for this event were also obtained with the Advanced Composition Explorer and STEREO-A. We conjecture that these observations were due to a U-shaped, large-scale magnetic field topology connecting the reverse shock of the first CIR and the forward shock of the second CIR. Such a disconnected U-shaped magnetic field topology may have formed due to magnetic reconnection in the upper corona.

## Temporal Variation of Solar Coronal Rotation

J. L. Xie<sup>1,2,3,4</sup>, X. J. Shi<sup>1,3,4</sup>, and J. Zhang

2017 ApJ 841 42

<http://sci-hub.cc/10.3847/1538-4357/aa6d7d>

In this paper, by applying the wavelet transformation analysis to the data of the daily 10.7 cm radio flux covering the period from 1947 February 14 to 2014 August 31, a significant period of about 27 days can be found, indicating the existence of rotational modulation in the temporal variation of the daily 10.7 cm radio flux. Then, the solar coronal rotation periods are obtained based on the result of the wavelet transformation analysis, and the temporal variation of the coronal rotation is revisited. We find that there exist significant periods of about 2.1, 3.0, 4.5, 6.6, 8.6, and 10.3 yr in the temporal variation of the coronal rotation. A possible period of 22.0 yr can also be found, but its statistical significance is below the 95% confidence level. The coronal rotation seems to show a weak decreasing trend during the considered time. The dependence of the coronal rotation on solar cycle phase is analyzed. The rotation periods are found to be varying with the solar cycle phase, and they are relatively longer around the minimum year of the solar cycle. The result based on the cross-correlation analysis between the rotation periods and the daily 10.7 cm radio flux indicates that there exists a phase difference of about 5.5 yr between them.

## Correction for the Weakening Magnetic Field within the Sunspot Umbra Observed by ASO-S/FMG

[Haiqing Xu](#), [Jiangtao Su](#), [Suo Liu](#), [Yuanyong Deng](#), [Xianyong Bai](#), [Jie Chen](#), [Xiaofan Wang](#), [Xiao Yang](#), [Yongliang Song](#)

Solar Phys. 299, 82 (2024)

<https://arxiv.org/pdf/2405.18699>

<https://doi.org/10.1007/s11207-024-02326-7>

The magnetic field inside the sunspot umbra, as observed by the Full-disk MagnetoGraph (FMG) onboard the Advanced Space based Solar Observatory (ASO-S), was found to be experiencing a weakening. To address this issue, we employed a method developed by Xu et al. (2021) to correct the weakening in the data of 20 active regions observed by FMG during the period spanning December 29, 2022, to July 23, 2023. Research has revealed that the onset of magnetic field weakening occurs at a minimum magnetic field strength of 705 G, with the peak strength reaching up to 1931 G. We computed the change ratio (R1) of the unsigned magnetic flux within the sunspot umbra, considering measurements both before and after correction. The change ratio (R1) spans from 26% to 124%, indicating a significant increase in the unsigned magnetic flux within sunspot umbrae observed by FMG after correction. To illustrate this, we selected four active regions for comparison with data from the Helioseismic and Magnetic Imager (HMI). After correction, it is found that the unsigned magnetic flux in sunspot umbrae measured by FMG aligns more closely with that of HMI. This supports the effectiveness of the corrective method for FMG, despite imperfections, particularly at the umbra-penumbra boundary. **2022-12-29, 2022-12-30, 2023-02-22, 2023-04-17, 2023-05-23**

**Table 1.** The information regarding the four active regions that were simultaneously observed by FMG and HMI

## Super-Resolution of SOHO/MDI Magnetograms of Solar Active Regions Using SDO/HMI Data and an Attention-Aided Convolutional Neural Network.

[Xu, C.](#), [Wang, J.T.L.](#), [Wang, H.](#) et al.

Sol Phys 299, 36 (2024).

<https://arxiv.org/pdf/2403.18302.pdf>

<https://doi.org/10.1007/s11207-024-02283-1>

Image super-resolution is an important subject in image processing and recognition. Here, we present an attention-aided convolutional neural network for solar image super-resolution. Our method, named SolarCNN, aims to enhance the quality of line-of-sight (LOS) magnetograms of solar active regions (ARs) collected by the Michelson Doppler Imager (MDI) on board the Solar and Heliospheric Observatory (SOHO). The ground-truth labels used for training SolarCNN are the LOS magnetograms collected by the Helioseismic and Magnetic Imager on board the Solar Dynamics Observatory. Solar ARs consist of strong magnetic fields in which magnetic energy can suddenly be released to produce extreme space-weather events, such as solar flares, coronal mass ejections, and solar energetic particles. SOHO/MDI covers Solar Cycle 23, which is stronger with more eruptive events than Cycle 24. Enhanced SOHO/MDI magnetograms allow for better understanding and forecasting of violent events of space weather. Experimental results show that SolarCNN improves the quality of SOHO/MDI magnetograms in terms of the structural similarity index measure, Pearson's correlation coefficient, and the peak signal-to-noise ratio.

## Transient dark ribbons at the outer boundaries of sunspot superpenumbrae in the chromosphere

Chengzhi [Xu](#), Jun Zhang and Tao Ding

A&A 678, A36 (2023)

<https://www.aanda.org/articles/aa/pdf/2023/10/aa46735-23.pdf>

Context. Although the flow of material in sunspot superpenumbrae has been studied intensively, detailed observations about the evolution of material flow at the outer boundaries of sunspot superpenumbrae are rare. Aims. We study the evolution of the flow of material at the outer boundaries of superpenumbrae.

Methods. Based on H $\alpha$  observations from the New Vacuum Solar Telescope, we tracked the evolution of the flow of material at the outer boundaries of superpenumbrae in the chromosphere. Data from the Solar Dynamics Observatory Helioseismic Magnetic Imager were employed to examine the photospheric magnetic field environment relevant to the material flow.

Results. We observed transient dark ribbons (TDRs) at the outer boundary of a sunspot superpenumbra in the chromosphere on 2018 May 12. The TDRs are located in the middle of the sunspot and a flocculus, and both of them have negative magnetic fields. While the ratio of the length and width of a TDR is greater than 8, we tracked the TDR from its formation to disappearance, so that six TDRs were studied in detail. Five TDRs were formed by the connection of several small dark sticks from end to end, and the sixth TDR was formed by the merging of two thin sticks. In the later stage of the TDR evolution, five TDRs were broken down into several small dark sticks, and the sixth TDR dissipated with oscillation. During the evolution process, no obvious flow of material along the TDRs is detected.

Conclusions. We suggest that these TDRs are an observational representation of the regular aggregation of superpenumbral fibril footpoints and adjacent solar flocculus fibril footpoints at the outer boundaries of the sunspot superpenumbrae. **2018 May 12, 2020 November 10**

## **A Method to Correct the Intensity to Polarization Crosstalk in Measuring Full-Disk Solar Photospheric Vector Magnetic Fields**

Haiqing [Xu](#), [Jiangtao Su](#), [Xianyong Bai](#), [Jie Chen](#), [Yu Gao](#), [Suo Liu](#)...

[Solar Physics](#) September 2019, 294:129

<https://link.springer.com/content/pdf/10.1007%2Fs11207-019-1463-1.pdf>  
[sci-hub.se/10.1007/s11207-019-1463-1](https://sci-hub.se/10.1007/s11207-019-1463-1)

Precise polarimetry is very important for studying the characteristics and evolution of solar magnetic fields. We focus on the intensity to linear and circular polarization crosstalk that affect polarimetric accuracy of full-disk vector magnetic-field measurements. An attempt is made to correct such crosstalk and to reconstruct full-disk vector magnetic fields from polarization data. By analyzing the data taken at 31 filter positions from  $-0.3 \text{ \AA}$  to  $0.3 \text{ \AA}$  off the spectral line Fe  $i\lambda\lambda 5324.19 \text{ \AA}$  spaced by  $0.02 \text{ \AA}$ , we estimate that the intensity to linear and circular polarization crosstalks are less than  $0.1\%$  ( $\approx 10 \text{ G}$ ) of the quiet-Sun intensity. The method, which uses background maps obtained by averaging over many Stokes  $-Q$ ,  $-U$ , and  $-V$  images to correct the crosstalks of  $I$ -to- $Q$ ,  $-U$ , and  $-V$ , is proved to be effective. **12 September 2017**

## **Sudden Penumbra Reappearance and Umbral Motion Induced by an M7.9 Solar Flare**

Zhe [Xu](#)<sup>1,2,3</sup>, Yunchun Jiang<sup>1,3</sup>, Jiayan Yang<sup>1,3</sup>, Junchao Hong<sup>1,3</sup>, and Haidong Li

**2017 ApJL 840 L21**

<http://iopscience.iop.org/sci-hub.cc/2041-8205/840/2/L21/>

The sudden flare-related changes of sunspot structures have been recognized as the photospheric responses to the solar eruptions in the corona. In this study, we report two distinctive sunspots variations associated with the flare SOL2015-06-25T08:16 (M7.9). Along the flaring polarity inversion line (PIL), the originally decayed penumbra showed a sudden reappearance, with the horizontal fields increasing in the direction of the penumbral fibrils aligned. On the other hand, the small umbra, where the reappearing penumbra rooted, had a sudden northeastward motion, toward the north part of a large sunspot located in the other side of PIL. Based on the calculation of Lorentz force changes, the area of penumbral reappearance mainly suffered a downward pressure, while the umbra region was dominated by the northeastward lateral pressure. These observations can be well understood as a result of coronal fields contraction, which can be deduced from the nonlinear force-free field extrapolation model. It also confirms the implosion idea that the restructuring of coronal fields could impact the solar surface and interior.

## **On the Origin of Differences in Helicity Parameters Derived from Data of Two Solar Magnetographs**

Haiqing [Xu](#), Hongqi Zhang, K. Kuzanyan, T. Sakurai

[Solar Phys.](#) Volume 291, Issue 8, pp 2253–2267 **2016**

We analyzed how sensitivity and accuracy in solar magnetic field measurements may affect the values of mean current helicity density  $h_{chc}$  and twist parameter  $\alpha_{av}$  by comparing these values obtained from two magnetographs (SMFT at Beijing and SFT at Mitaka, Tokyo). When we computed the helicity parameters from the SFT data, we replaced the values of the longitudinal field component, transverse field strength, and transverse field azimuth angle with those from the SMFT data and examined the differences. The results show that the correlation

coefficient and the fraction of the data that agree in signs of  $hchc$  or  $\alpha v\alpha v$  increase when an SFT parameter is substituted by the corresponding SMFT parameter because one source of discrepancy is removed. The increase in correlation coefficient is largest when the azimuthal angles and transverse field strengths are set identical in the two instruments; the correlation coefficient of  $hchc$  ( $\alpha v\alpha v$ ) increases from 0.74 (0.56) to 0.86 (0.78), respectively, indicating that the differences in the transverse field strength and its azimuthal angle are the largest source of discrepancy in the values of  $hchc$  or  $\alpha v\alpha v$ . We found a nonlinear relationship in the components of the magnetic field between the two instruments for some data samples; we conclude that this is due to the discrepancy in the calibration procedure between the two instruments. This nonlinearity can be another source of difference in determining helical parameters between the two instruments.

### Where are the solar magnetic poles?

[A. Pastor Yabar](#), [M. J. Martínez González](#), [M. Collados](#)

MNRAS Volume 453, Issue 1, 2015, p.L69-L72 2018

<https://arxiv.org/pdf/1804.09748.pdf>

Regardless of the physical origin of stellar magnetic fields - fossil or dynamo induced - an inclination angle between the magnetic and rotation axes is very often observed. Absence of observational evidence in this direction in the solar case has led to generally assume that its global magnetic field and rotation axes are well aligned. We present the detection of a monthly periodic signal of the photospheric solar magnetic field at all latitudes, and especially near the poles, revealing that the main axis of the Sun's magnetic field is not aligned with the surface rotation axis. This result reinforces the view of our Sun as a common intermediate-mass star. Furthermore this detection challenges and imposes a strong observational constraint to modern solar dynamo theories.

### Magnetic topology of the north solar pole

[A. Pastor Yabar](#), [M. J. Martínez González](#), [M. Collados](#)

A&A 616, A46 2018

<https://arxiv.org/pdf/1804.09075.pdf>

We study the polar magnetism near an activity maximum when these regions change their polarity, from which it is expected that its magnetism should be less affected by the global field. To fully characterise the magnetic field vector, we use deep full Stokes polarimetric observations of the 15648.5 Å and 15652.8 Å Fe I lines. We observe the north pole as well as a quiet region at disc centre to compare their field distributions. In order to calibrate the projection effects, we observe an additional quiet region at the east limb. We find that the two limb datasets share similar magnetic field vector distributions. This means that close to a maximum, the poles look like typical limb, quiet-Sun regions. However, the magnetic field distributions at the limbs are different from the distribution inferred at disc centre. At the limbs, we infer a new population of magnetic fields with relatively strong intensities ( $\sim 600\text{--}800$  G), inclined by 30 deg with respect to the line of sight, and with an azimuth aligned with the solar disc radial direction. We propose that this new population at the limbs is due to the observation of unresolved magnetic loops as seen close to the limb. These loops have typical granular sizes as measured in the disc centre. At the limbs, where the spatial resolution decreases, we observe them spatially unresolved, which explains the new population of magnetic fields that is inferred. This is the first (indirect) evidence of small-scale magnetic loops outside the disc centre and would imply that these small-scale structures are ubiquitous on the entire solar surface. This result has profound implications for the energetics not only of the photosphere, but also of the outer layers since these loops have been reported to reach the chromosphere and the low corona. 14 September 2013

### Three-dimensional magnetic field structure of a flux emerging region in the solar atmosphere

[Rahul Yadav](#), [J. de la Cruz Rodríguez](#), [C. J. Díaz Baso](#), [Avijeet Prasad](#), [Tine Libbrecht](#), [Carolina Robustini](#), [A. Asensio Ramos](#)

A&A 632, A112 2019

<https://arxiv.org/pdf/1910.13279.pdf>

<https://doi.org/10.1051/0004-6361/201936790>

We analyze high-resolution spectropolarimetric observations of a flux emerging region (FER) in order to understand its magnetic and kinematic structure. Our spectropolarimetric observations in the He I 1083.0 nm spectral region of a FER are recorded with GRIS at the 1.5 m aperture GREGOR telescope. A Milne-Eddington based inversion code was employed to extract the photospheric information of the Si I spectral line, whereas the He I triplet line was analyzed with the Hazel inversion code, which takes into account the joint action of the Hanle and the Zeeman effect. The spectropolarimetric analysis of Si I line displays a complex magnetic structure near the vicinity of FER. Moreover, we find supersonic downflows of 40 km/sec appears near the footpoints of loops connecting two poles of opposite polarity, whereas a strong upflows of 22 km/sec appears near the apex of the loops. Furthermore, non-force-free field extrapolations were performed separately at two layers in order to understand the magnetic field topology of the FER. We determine, using extrapolations from the photosphere and the observed chromospheric

magnetic field, that the average formation height of the He triplet line is 2 Mm from the solar surface. The reconstructed loops using photospheric extrapolations along an arch filament system have a maximum height of 10.5 Mm from the solar surface with a foot-points separation of 19 Mm, whereas the loops reconstructed using chromospheric extrapolations are around 8.4 Mm high from the solar surface with a foot-point separation of 16 Mm at the chromospheric height. The magnetic topology in the FER suggests the presence of small-scale loops beneath the large loops. Under suitable conditions, due to magnetic reconnection, these loops can trigger various heating events in the vicinity of the FER. **3 June, 2015**

### **Physical Properties of Umbral Dots Observed in Sunspots: A Hinode Observation**

Rahul [Yadav](#), Shibu K. Mathew

[Solar Physics](#) April **2018**, 293:54

Umbral dots (UDs) are small-scale bright features observed in the umbral part of sunspots and pores. It is well established that they are manifestations of magnetoconvection phenomena inside umbrae. We study the physical properties of UD in different sunspots and their dependence on decay rate and filling factor. We have selected high-resolution, G-band continuum filtergrams of seven sunspots from Hinode to study their physical properties. We have also used Michelson Doppler Imager (MDI) continuum images to estimate the decay rate of selected sunspots. An identification and tracking algorithm was developed to identify the UD in time sequences. The statistical analysis of UD exhibits an averaged maximum intensity and effective diameter of 0.26 IQSIQS and 270 km. Furthermore, the lifetime, horizontal speed, trajectory length, and displacement length (birth–death distance) of UD are 8.19 minutes, 0.5 km s<sup>-1</sup>, 284 km, and 155 km, respectively. We also find a positive correlation between intensity–diameter, intensity–lifetime, and diameter–lifetime of UD. However, UD properties do not show any significant relation with the decay rate or filling factor.

### **Investigating the relation between sunspots and umbral dots**

Rahul [Yadav](#), [Rohan E. Louis](#), [Shibu K. Mathew](#)

ApJ 855 8 **2018**

<https://arxiv.org/pdf/1802.05088.pdf>

Umbral dots (UDs) are transient, bright features observed in the umbral region of a sunspot. We study the physical properties of UD observed in sunspots of different sizes. The aim of our study is to relate the physical properties of umbral dots with the large-scale properties of sunspots. For this purpose, we analyze high-resolution G-band images of 42 sunspots observed by {em Hinode}/SOT, located close to disk center. The images were corrected for instrumental stray-light and restored with the modeled PSF. An automated multi-level tracking algorithm was employed to identify the UD located in selected G-band images. Furthermore, we employed HMI/SDO, limb-darkening corrected, full disk continuum images to estimate the sunspot phase and epoch for the selected sunspots. The number of UD identified in different umbrae exhibits a linear relation with the umbral size. The observed filling factor ranges from 3% to 7% and increases with the mean umbral intensity. Moreover, the filling factor shows a decreasing trend with the umbral size. We also found that the observed mean and maximum intensities of UD are correlated with the mean umbral intensity. However, we do not find any significant relationship between the mean (and maximum) intensity and effective diameter of umbral dots with the sunspot area, epoch, and decay rate. We suggest that this lack of relation could either be due to the distinct transition of spatial scales associated with overturning convection in the umbra or the shallow depth associated with umbral dots, or both the above.

**TABLE 1** Details of the ARs analyzed in the study (2013-2014).

### **Search for superstrong magnetic fields in active processes on the Sun using spectro-polarimetry within 15 Å around the D3 line**

[I I Yakovkin](#), [V G Lozitsky](#)

*MNRAS*, Volume 523, Issue 4, August **2023**, Pages 5812–5822,

<https://doi.org/10.1093/mnras/stad1816>

We critically review our previous results on this topic based on the following main points: (i) substantially larger wavelength range around the D3 line was investigated – up to  $\pm 15$  Å instead of  $\pm 2.5$  Å in comparison with the previous version of our study, and (ii) greater volume of observational data was analysed, including one X limb flare, additionally. Overall, our study concerns the **2004 July 12** active prominence and the **2014 June 10** limb flare of X1.5 class. For named limb flare, we found reliable and oppositely polarized secondary peaks of the V parameter located at distances of  $-4.5$  and  $+2.7$  Å from the line center. If these features are interpreted as manifestations of the magnetic splitting of the line together with its Doppler shift, then the corresponding magnetic field is  $\approx 2.2 \times 10^5$  G, and the radial velocity  $-46$  km s<sup>-1</sup>. Similar spectral manifestations were also found in the active prominence. For comparison with the theory, the spectral features of the Paschen–Back effect at magnetic fields up to 100 kG were studied too. It turned out that the theoretical width of the splitting components is relatively small, 0.3 Å, while the

width of the observed peaks is sometimes much larger. On the basis of model calculations, it is shown that in some cases an alternative explanation of the observational data is possible, which includes much weaker magnetic fields (5.5–7.1 kG), but significant macroscopic velocities of different signs, at the level of 50–60 km s<sup>-1</sup>.

### **A Data-constrained Analysis for Joule Heating as a Solar Active Region Atmosphere Heating Mechanism. I. Sunspot Umbral Light Bridge**

M. S. **Yalim**<sup>1</sup>, M. Frisse<sup>1</sup>, C. Beck<sup>2</sup>, D. P. Choudhary<sup>3</sup>, A. Prasad<sup>4</sup>, S. S. Nayak<sup>1</sup>, and G. P. Zank<sup>1,5</sup>  
2024 ApJ 973 58

<https://iopscience.iop.org/article/10.3847/1538-4357/ad5e75/pdf>

Understanding the mechanisms underlying the heating of the solar atmosphere is a fundamental problem in solar physics. The lower atmosphere of the Sun (i.e., photosphere and chromosphere) is composed of weakly ionized plasma. This results in anisotropic dissipation of electric currents by Coulomb and Cowling resistivities. Joule heating due to dissipation of currents perpendicular to the magnetic field by Cowling resistivity has been demonstrated to be the main mechanism for the heating of a sunspot umbral light bridge located in NOAA AR 12002 on **2014 March 13**. Here, we focus on the same target region and demonstrate the importance of further constraining our Joule heating model using observational data in addition to magnetic field, namely plasma temperature calculated from the inversion of spectroscopic data obtained from the Interferometric BI-dimensional Spectrometer instrument of the ground-based Dunn Solar Telescope. As a parameter in our analysis, temperature is demonstrated to have the highest sensitivity after magnetic field. We show that the heating of the light bridge is a highly dynamic event that necessitates utilization of 3D spatially resolved observational data for temperature rather than a 1D temperature stratification based on theoretical/semiempirical solar atmosphere models. Our improved data-constrained analysis using spatially resolved temperatures shows that the entire light bridge is heated by the proposed mechanism, and yields heating rate values that are consistent with our previous study.

### **A Data-Driven MHD Model of the Global Solar Corona within Multi-Scale Fluid-Kinetic Simulation Suite (MS-FLUKSS)**

Mehmet Sarp **Yalim**, Nikolai Pogorelov, Yang Liu

11th Annual International Conference on Numerical Modeling of Space Plasma Flows (ASTRONUM 2016) **2017**

<https://arxiv.org/pdf/1703.00566.pdf>

We have developed a data-driven magnetohydrodynamic (MHD) model of the global solar corona which uses characteristically-consistent boundary conditions (BCs) at the inner boundary. Our global solar corona model can be driven by different observational data including Solar Dynamics Observatory/Helioseismic and Magnetic Imager (SDO/HMI) synoptic vector magnetograms together with the horizontal velocity data in the photosphere obtained by the time-distance helioseismology method, and the line-of-sight (LOS) magnetogram data obtained by HMI, Solar and Heliospheric Observatory/Michelson Doppler Imager (SOHO/MDI), National Solar Observatory/Global Oscillation Network Group (NSO/GONG) and Wilcox Solar Observatory (WSO). We implemented our model in the Multi-Scale Fluid-Kinetic Simulation Suite (MS-FLUKSS) - a suite of adaptive mesh refinement (AMR) codes built upon the Chombo AMR framework developed at the Lawrence Berkeley National Laboratory. We present an overview of our model, characteristic BCs, and two results we obtained using our model: A benchmark test of relaxation of a dipole field using characteristic BCs, and relaxation of an initial PFSS field driven by HMI LOS magnetogram data, and horizontal velocity data obtained by the time-distance helioseismology method using a set of non-characteristic BCs.

### **PREPROCESSING MAGNETIC FIELDS WITH CHROMOSPHERIC LONGITUDINAL FIELDS**

Tetsuya T. **Yamamoto** and K. Kusano

2012 ApJ 752 126

Nonlinear force-free field (NLFFF) extrapolation is a powerful tool for the modeling of the magnetic field in the solar corona. However, since the photospheric magnetic field does not in general satisfy the force-free condition, some kind of processing is required to assimilate data into the model. In this paper, we report the results of new preprocessing for the NLFFF extrapolation. Through this preprocessing, we expect to obtain magnetic field data similar to those in the chromosphere. In our preprocessing, we add a new term concerning chromospheric longitudinal fields into the optimization function proposed by Wiegmann et al. We perform a parameter survey of six free parameters to find minimum force- and torque-freeness with the simulated-annealing method. Analyzed data are a photospheric vector magnetogram of AR 10953 observed with the Hinode spectropolarimeter and a chromospheric longitudinal magnetogram observed with SOLIS spectropolarimeter. It is found that some preprocessed fields show the smallest force- and torque-freeness and are very similar to the chromospheric longitudinal fields. On the other hand, other preprocessed fields show noisy maps, although the force- and torque-

freeness are of the same order. By analyzing preprocessed noisy maps in the wave number space, we found that small and large wave number components balance out on the force-free index. We also discuss our iteration limit of the simulated-annealing method and magnetic structure broadening in the chromosphere.

### **Polarization calibration of the Tandem Etalon Magnetograph of the Solar Magnetic Activity Research Telescope at Hida Observatory**

[Daiki Yamasaki](#), [Shin'ichi Nagata](#), [Kiyoshi Ichimoto](#)

Publications of the Astronomical Society of Japan 2022

<https://arxiv.org/pdf/2208.10696>

The Tandem Etalon Magnetograph (TEM) is one of the instruments of the Solar Magnetic Activity Research Telescope of Hida Observatory. The TEM is a partial disk (320" x240") filter magnetograph which scans the wavelength around a Fe I line at 6303 angstrom and achieves polarimetric sensitivity of  $< 5 \times 10^{-4}$  for each wavelength. To obtain the polarimeter response matrix of the instrument, we have carried out end-to-end polarization calibrations of the instrument. We have also measured the polarization characteristics of the polarization beam splitter (PBS), which is a crucial component of the instrument. As a result of end-to-end calibration, we found significant spatial variation in the response matrix across the field of view. From a laboratory test, we found that 1% of the magnitude of a circular diattenuation of the PBS was due to the retardation caused by the stress in the cube and the linear diattenuation of the film. Although the spatial variation across the field of view is more than ten times larger, to achieve the polarimetric sensitivity of  $< 5 \times 10^{-4}$ , this can be well explained by the polarization characteristic of the PBS and corrected by using the response matrix obtained in the end-to-end calibration. In addition, we also obtained the daily variation of the polarization property of the TEM. We found that the crosstalk from Stokes Q to V changes an amount comparable to the tolerance through a day. In the present configuration, we require a pixel-by-pixel calibration every 100 minutes to meet the accuracy requirement.

### **Evolution of the Non-potential Magnetic Field in the Solar Active Region 12673 Based on a Nonlinear Force-free Modeling**

[Daiki Yamasaki](#), [Satoshi Inoue](#), [Shin'ichi Nagata](#), [Kiyoshi Ichimoto](#)

ApJ 2020

<https://arxiv.org/pdf/2012.01008.pdf>

Active region (AR) 12673 produced many M-class and several X-class flares, one of which being an X9.3 flare, which is recorded as the largest solar flare in solar cycle 24. We studied the evolution of the three-dimensional flare-productive magnetic field within AR 12673, using a time series of nonlinear force-free field extrapolations of every 12 hours from September 4th 00:00 UT to 6th 00:00 UT. Our analysis found that three magnetic flux ropes (MFRs) are formed by September 4th, one of which produced the X9.3 flare on September 6th. One MFR has positive magnetic twist which is a different sign from other two MFRs. Since the temporal evolution of the magnetic flux of the MFR accumulating the positive twist is consistent with the profile of the GOES X-ray flux well observed from September 4th to 6th, we suggest that the formation of the MFR having the positive twist is closely related to the occurrence of the M-class flares including an M5.5 flare. We further found a magnetic null in the magnetic field surrounding the MFRs, in particular, above the MFR having positive twist before the M5.5 flare which is the largest M-flare observed during this period. By comparing with the AIA 1600 angstrom images, we found that the footpoints of the overlying field lines are anchored to the area where the brightening was initially observed. Therefore, we suggest that reconnection induced by the torus instability of the positively twisted MFR at the null possibly drove the M5.5 flare. **4 Sep 2017**

### **On the Coronal Magnetic Field Configuration and Solar Flare/CME Process**

Yihua [Yan](#)

Space Sci. Rev. 2006, File

The coronal magnetic field configuration is important for understanding the energy storage and release processes that account for flares and/or CMEs. Here we present a model which is based on the work for potential magnetic field problems that only applies the condition at infinity with the boundary condition on the solar surface specified. We also discuss some recent progress on general force-free field models. For some event analyses, we have employed MDI/SOHO longitudinal magnetogram inseted into the synoptic magnetogram to obtain whole boundary condition over the solar surface. Globally, the extrapolated global magnetic field structures effectively demonstrate the case for the disk signature of the radio CMEs and the evolution of the radio sources during the CME/flare processes.

### **Observing the evolution of the Sun's global coronal magnetic field over 8 months**

Zihao [Yang](#), [Steven Tomczyk](#), [...], and [Cooper Downs](#) +2 authors

Science 3 Oct 2024 Vol 386, Issue 6717 pp. 76-82

<https://doi.org/10.1126/science.ado2993>

<https://arxiv.org/pdf/2410.16555>

The magnetic field in the Sun's corona stores energy that can be released to heat plasma and drive solar eruptions. Measurements of the global coronal magnetic field have been limited to several snapshots. In this work, we present observations, using the Upgraded Coronal Multi-channel Polarimeter, that provide 114 magnetograms of the global corona above the solar limb spanning ~8 months. We determined the magnetic field distribution with altitude in the corona and monitored the evolution at different latitudes over multiple solar rotations. The field strength between 1.05 and 1.60 solar radii varies from <1 to ~20 gauss. A signature of active longitudes appears in the coronal magnetic field measurements. Coronal models are generally consistent with our observations, though they have larger discrepancies in high-latitude regions.

## **The Complexity of Emerging Magnetic Flux during the Lifetime of Solar Ephemeral Regions**

Hanlin Yang<sup>1,2,3</sup>, Chunlan Jin<sup>1,3</sup>, Zifan Wang<sup>1,3</sup>, and Jingxiu Wang<sup>1,2,3</sup>

2024 ApJ 967 59

<https://iopscience.iop.org/article/10.3847/1538-4357/ad3947/pdf>

As a relatively active region, the ephemeral region (ER) exhibits a highly complex pattern of magnetic flux emergence. We aim to study in detail the secondary flux emergences (SFEs), which we define as bipoles that appear close to ERs and finally coalesce with ERs after a period of time. We study SFEs during the whole process, from the emergence to the decay of five ERs observed by the Helioseismic and Magnetic Imager on board the Solar Dynamics Observatory. The maximum unsigned magnetic flux for each ER is around 1020 Mx. Each ER has tens of SFEs with an average emerging magnetic flux of approximately  $5 \times 10^{18}$  Mx. The frequency of normalized magnetic flux for all the SFEs follows a power-law distribution with an index of  $-2.08$ . The majority of SFEs occur between the positive and negative polarities of an ER, and their growth time is concentrated within 1 hr. The magnetic axis of SFE is found to exhibit a random distribution in the five ERs. We suggest that the relationship between SFEs and ERs can be understood by regarding the photospheric magnetic field observations as cross sections of an emerging magnetic structure. Tracking the evolution of ERs, we propose that these SFEs in ERs may have emerged consequentially from the bundle of flux tubes of ERs and that SFEs are partially emerged  $\Omega$ -loops. **2010 November 20–24**

## **Global maps of the magnetic field in the solar corona**

Zihao Yang, Christian Bethge, Hui Tian, Steven Tomczyk, Richard Morton, Giulio Del Zanna, Scott W. McIntosh, Bidya Binay Karak, Sarah Gibson, Tanmoy Samanta, Jiansen He, Yajie Chen, Linghua Wang  
Science, 369, 694 (2020)

<https://arxiv.org/ftp/arxiv/papers/2008/2008.03136.pdf>

Understanding many physical processes in the solar atmosphere requires determination of the magnetic field in each atmospheric layer. However, direct measurements of the magnetic field in the Sun's corona are difficult to obtain. Using observations with the Coronal Multi-channel Polarimeter, we have determined the spatial distribution of the plasma density in the corona, and the phase speed of the prevailing transverse magnetohydrodynamic waves within the plasma. We combine these measurements to map the plane-of-sky component of the global coronal magnetic field. The derived field strengths in the corona from 1.05 to 1.35 solar radii are mostly 1-4 Gauss. These results demonstrate the capability of imaging spectroscopy in coronal magnetic field diagnostics. **2016 October 14,**

## **Mapping the magnetic field in the solar corona through magnetoseismology**

Zihao Yang, Hui Tian, Steven Tomczyk, Richard Morton, Xianyong Bai, Tanmoy Samanta, Yajie Chen  
Sci China Tech Sci (2020)

<https://arxiv.org/pdf/2008.03146.pdf>

Magnetoseismology, a technique of magnetic field diagnostics based on observations of magnetohydrodynamic (MHD) waves, has been widely used to estimate the field strengths of oscillating structures in the solar corona. However, previously magnetoseismology was mostly applied to occasionally occurring oscillation events, providing an estimate of only the average field strength or one-dimensional distribution of field strength along an oscillating structure. This restriction could be eliminated if we apply magnetoseismology to the pervasive propagating transverse MHD waves discovered with the Coronal Multi-channel Polarimeter (CoMP). Using several CoMP observations of the Fe xiii 1074.7 nm and 1079.8 nm spectral lines, we obtained maps of the plasma density and wave phase speed in the corona, which allow us to map both the strength and direction of the coronal magnetic field in the plane of sky. We also examined distributions of the electron density and magnetic field strength, and compared their variations with height in the quiet Sun and active regions. Such measurements could provide critical information to advance our understanding of the Sun's magnetism and the magnetic coupling of the whole solar atmosphere. **Oct 14, 2016, November 3, 2016, March 20, 2017**



## Relative Magnetic Helicity Based on a Periodic Potential Field

Kai E. [Yang](#), [Michael S. Wheatland](#), [Stuart A. Gilchrist](#)

ApJ 2020

<https://arxiv.org/pdf/2004.08590.pdf>

Magnetic helicity is conserved under ideal magnetohydrodynamics (MHD) and quasi-conserved even under a resistive process. The standard definition for magnetic helicity cannot be applied directly to an open magnetic field in a volume, because it is gauge-dependent. Instead, the relative magnetic helicity is widely used. We find that the energy of a potential magnetic field in a rectangular domain with periodic lateral boundary conditions is less than that of the field with a fixed normal component on all six boundaries. To make use of this lower energy potential field in the analysis of relative magnetic helicity, we introducing a new definition for magnetic helicity for the magnetic field, which involves the periodic potential field. We apply this definition to a sequence of analytic solutions and a numerical simulation. The results show that our new gauge-invariant helicity is very close to the current-carrying part of the relative magnetic helicity of the original magnetic field. We find also that the ratio between the current-carrying helicity and the relative magnetic helicity for the original and our defined relative helicity show different behavior. It seems that the new helicity is more sensitive to the component of the field due to the electric current in the volume, which is the source for instabilities and solar eruptive phenomena.

## Scattering Matrix for the Interaction between Solar Acoustic Waves and Sunspots. II.

### Theory

Ming-Hsu [Yang](#) and Dean-Yi Chou

2020 ApJ 892 46

<https://doi.org/10.3847/1538-4357/ab72fb>

The interaction between solar acoustic waves and an isolated sunspot is a scattering problem. A common tool to study scattering problems is the scattering matrix, which is the amplitude for the transition from one mode to another after the interaction. In the previous study (Part I), the scattering matrix elements were determined with the measured scattered wavefunction of the sunspot. In this study (Part II), we obtain an analytical relation between the scattering matrix elements and the perturbed quantities of the background medium of the sunspot region. The sunspot is considered a perturbed region relative to the quiet Sun. The perturbation of the background medium includes the magnetic field, the flow velocity, and perturbed thermodynamics quantities, such as the density and pressure perturbations. Inferring these perturbed quantities from measured quantities is one of the goals of helioseismology. Here, with the help of Green's functions, the scattering matrix elements are expressed as a spatial integral, which contains these unknown perturbed quantities. This integral equation, together with the measured scattering matrix elements, could be used to infer the perturbed quantities with the forward and inversion methods. Besides the typical approximations for solar acoustic waves, two additional assumptions are made here: one is the Born approximation, and the other is that the background medium of the sunspot region does not change with time.

## Light Bridge Brightening and Plasma Ejection Driven by a Magnetic Flux Emergence

### Event

Xu [Yang](#)<sup>1,2</sup>, Vasyl Yurchyshyn<sup>2</sup>, Kwangsu Ahn<sup>2</sup>, Matt Penn<sup>3</sup>, and Wenda Cao

2019 ApJ 886 64

[sci-hub.se/10.3847/1538-4357/ab4a7d](https://doi.org/10.3847/1538-4357/ab4a7d)

Observations with the Goode Solar Telescope (GST) are presented here showing that the emergence of  $1.91 \times 10^{18}$  Mx of new magnetic flux occurred at the edge of a filamentary light bridge (LB). This emergence was accompanied by brightness enhancement of a photospheric overturning convection cell (OCC) at the endpoints of the emerging magnetic structure. We present an analysis of the origin and the dynamics of this event using high-resolution GST Fe i 1564.85 nm vector magnetic field data, TiO photospheric, and H $\alpha$  chromospheric images. The emerged structure was  $1.5 \times 0.3$  Mm in size at the peak of development and lasted for 17 minutes. Doppler observations showed presence of systematic upflows before the appearance of the magnetic field signal and downflows during the decay phase. Changes in the orientation of the associated transverse fields, determined from the differential angle, suggest the emergence of a twisted magnetic structure. A fan-shaped jet was observed to be spatially and temporally correlated with the endpoint of the OCC intruding into the LB. Our data suggest that the emerging fields may have reconnected with the magnetic fields in the vicinity of the LB, which could lead to the formation of the jet. Our observation is the first report of flux emergence within a granular LB with evidence in the evolution of vector magnetic field, as well as photosphere convection motions, and supports the idea that the impulsive jets above the LB are caused by magnetic reconnection. **2016 February 9**

## Vortex Formations and Its Associated Surges in a Sunspot Light Bridge

Heesu [Yang](#)<sup>1</sup>, Eun-Kyung Lim<sup>1</sup>, Haruhisa Iijima<sup>2</sup>, Vasyl Yurchyshyn<sup>3</sup>, Kyung-Suk Cho<sup>1</sup>, Jeongwoo Lee<sup>4</sup>, Brigitte Schmieder<sup>1,5</sup>, Yeon-Han Kim<sup>1</sup>, Sujin Kim<sup>1</sup>, and Su-Chan Bong<sup>1</sup>

ApJ 882:175 2019

<https://iopscience.iop.org/article/10.3847/1538-4357/ab36b7/pdf>

We report on the successive occurrence of  $0''.5$  wide photospheric vortices with strong transverse shear flows at the edge of a sunspot light bridge (LB), and the subsequent ejection of chromospheric surges observed using a Visible Interferometry Spectrograph, a broadband TiO filter, and a Near Infrared Imaging Spectrograph of the Goode Solar Telescope operating at Big Bear Solar Observatory. The H $\alpha$  surges ejected at the location of the vortices often appeared in a hollow cylindrical structure. We also observed quasi-periodic vortex-associated bright H $\alpha$  plasma blobs moving upward with a speed of up to 4 km s $^{-1}$ . In view of the strong shear flow at the edge of the LB, it is likely that the vortices form under the Kelvin–Helmholtz instability. The surges may result from either the magnetic tension generated after magnetic reconnection or an acoustic impulse of a fast photospheric transverse flow. Otherwise, the surges could also be associated with Alfvénic waves, in which case their origin could be torsional magnetic fields generated in the process of the vortex formation. **2016 May 5**

## **Modeling the Global Distribution of Solar Wind Parameters on the Source Surface Using Multiple Observations and the Artificial Neural Network Technique**

Yi **Yang**, Fang Shen

Solar Phys. August **2019**, 294:111

<https://link.springer.com/content/pdf/10.1007%2Fs11207-019-1496-5.pdf>  
[sci-hub.se/10.1007/s11207-019-1496-5](https://sci-hub.se/10.1007/s11207-019-1496-5)

The global distribution of magnetic field and other plasma parameters on the source surface, which we set at 2.5 solar radii, is important for coronal and heliospheric modeling. In this article, we introduce a new data-driven self-consistent method to obtain the global distribution of different parameters. The magnetic and polarized brightness (pBpB) observations are used to derive the magnetic field and electron density on the source surface, respectively. Then, an artificial neural network (ANN) machine learning technique is applied to establish an empirical relation among the solar wind velocity, the magnetic field properties, and the electron density. The ANN is trained with global observational data, and is validated to be more reliable than the Wang–Sheeley–Arge (WSA) model for reconstructing the solar wind velocity, especially at high latitudes. The plasma temperature distribution is derived by solving a simplified one-dimensional (1D) magnetohydrodynamic (MHD) equation system on the source surface. Using the method in this study we can obtain the global distribution for all the parameters self-consistently based on magnetic and polarized brightness observations. The modeling results of four Carrington rotations from different solar cycle phases are presented to validate the method.

## **Observationally quantified reconnection providing a viable mechanism for active region coronal heating**

Kai E. **Yang**, [Dana W. Longcope](#), [M. D. Ding](#), [Yang Guo](#)

**2018**

<https://arxiv.org/pdf/1802.06206.pdf>

The heating of the Sun's corona has been explained by several different mechanisms including wave dissipation and magnetic reconnection. While both have been shown capable of supplying the requisite power, neither has been used in a quantitative model of observations fed by measured inputs. Here we show that impulsive reconnection is capable of producing an active region corona agreeing both qualitatively and quantitatively with extreme-ultraviolet observations. We calculate the heating power proportional to the velocity difference between magnetic footpoints and the photospheric plasma, called the non-ideal velocity. The length scale of flux elements reconnected in the corona is found to be around 160 km. The differential emission measure of the model corona agrees with that derived using multi-wavelength images. Synthesized extreme-ultraviolet images resemble observations both in their loop-dominated appearance and their intensity histograms. This work provides compelling evidence that impulsive reconnection events are a viable mechanism for heating the corona.

## **Automated Segmentation of High-Resolution Photospheric Images of Active Regions**

Meng **Yang**, Yu Tian, Changhui Rao

[Solar Physics](#) February **2018**, 293:15

<https://link.springer.com/content/pdf/10.1007%2Fs11207-017-1236-7.pdf>

Due to the development of ground-based, large-aperture solar telescopes with adaptive optics (AO) resulting in increasing resolving ability, more accurate sunspot identifications and characterizations are required. In this article, we have developed a set of automated segmentation methods for high-resolution solar photospheric images. Firstly, a local-intensity-clustering level-set method is applied to roughly separate solar granulation and sunspots. Then reinitialization-free level-set evolution is adopted to adjust the boundaries of the photospheric patch; an adaptive

intensity threshold is used to discriminate between umbra and penumbra; light bridges are selected according to their regional properties from candidates produced by morphological operations. The proposed method is applied to the solar high-resolution TiO 705.7-nm images taken by the 151-element AO system and Ground-Layer Adaptive Optics prototype system at the 1-m New Vacuum Solar Telescope of the Yunnan Observatory. Experimental results show that the method achieves satisfactory robustness and efficiency with low computational cost on high-resolution images. The method could also be applied to full-disk images, and the calculated sunspot areas correlate well with the data given by the National Oceanic and Atmospheric Administration (NOAA). **2015-07-08, 12 Jan. 2016, 07 Oct. 2016**

### **Sunspot Light Walls Suppressed by Nearby Brightenings**

Shuhong **Yang**, Jun Zhang, Robertus Erdélyi, [Yijun Hou](#), [Xiaohong Li](#), [Limei Yan](#)

ApJL **843** L15 **2017**

<https://arxiv.org/pdf/1706.07158.pdf>

Light walls, as ensembles of oscillating bright structures rooted in sunspot light bridges, have not been well studied, although they are important for understanding sunspot properties. Using the Interface Region Imaging Spectrograph and Solar Dynamics Observatory observations, here we study the evolution of two oscillating light walls each within its own active region (AR). The emission of each light wall decays greatly after the appearance of adjacent brightenings. For the first light wall, rooted within AR 12565, the average height, amplitude, and oscillation period significantly decrease from 3.5 Mm, 1.7 Mm, and 8.5 min to 1.6 Mm, 0.4 Mm, and 3.0 min, respectively. For the second light wall, rooted within AR 12597, the mean height, amplitude, and oscillation period of the light wall decrease from 2.1 Mm, 0.5 Mm, and 3.0 min to 1.5 Mm, 0.2 Mm, and 2.1 min, respectively. Particularly, a part of the second light wall becomes even invisible after the influence of nearby brightening. These results reveal that the light walls are suppressed by nearby brightenings. Considering the complex magnetic topology in light bridges, we conjecture that the fading of light walls may be caused by a drop in the magnetic pressure, where flux is cancelled by magnetic reconnection at the site of the nearby brightening. Another hypothesis is that the wall fading is due to the suppression of driver source (p-mode oscillation), resulting from the nearby avalanche of downward particles along reconnected brightening loops. **2016 July 22, 2016 September 26**

### **Enhancement of a sunspot light wall with external disturbances**

Shuhong **Yang**, Jun Zhang, Robert Erdélyi

ApJL **2016**

<https://arxiv.org/pdf/1611.10032v1.pdf>

Based on the *Interface Region Imaging Spectrograph* observations, we study the response of a solar sunspot light wall to external disturbances. A flare occurrence near the light wall caused material to erupt from the lower solar atmosphere into the corona. Some material falls back to the solar surface, and hits the light bridge (i.e., the base of the light wall), then sudden brightenings appear at the wall base followed by the rise of wall top, leading to an increase of the wall height. Once the brightness of the wall base fades, the height of the light wall begins to decrease. Five hours later, another nearby flare takes place, a bright channel is formed that extends from the flare towards the light bridge. Although no obvious material flow along the bright channel is found, some ejected material is conjectured to reach the light bridge. Subsequently, the wall base brightens and the wall height begins to increase again. Once more, when the brightness of the wall base decays, the wall top fluctuates to lower heights. We suggest, based on the observed cases, that the interaction of falling material and ejected flare material with the light wall results in the brightenings of wall base and causes the height of the light wall to increase. Our results reveal that the light wall can be not only powered by the linkage of *p*-mode from below the photosphere, but may also be enhanced by external disturbances, such as falling material.

### **Oscillating light wall above a sunspot light bridge**

Shuhong **Yang**, Jun Zhang, Fayu Jiang, Yongyuan Xiang

ApJL **804** L27 **2015**

<http://arxiv.org/pdf/1504.03563v1.pdf>

With the high tempo-spatial *Interface Region Imaging Spectrograph* 1330 Å images, we find that many bright structures are rooted in the light bridge of NOAA 12192, forming a light wall. The light wall is brighter than the surrounding areas, and the wall top is much brighter than the wall body. The New Vacuum Solar Telescope H  $\alpha$  and the Solar Dynamics Observatory 171 Å and 131 Å images are also used to study the light wall properties. In 1330 Å, 171 Å, and 131 Å, the top of the wall has a higher emission, while in the H  $\alpha$  line, the wall top emission is very low. The wall body corresponds to bright areas in 1330 Å and dark areas in the other lines. The top of the light wall moves upward and downward successively, performing oscillations in height. The deprojected mean height, amplitude, oscillation velocity, and the dominant period are determined to be 3.6 Mm, 0.9 Mm, 15.4 km s<sup>-1</sup>, and 3.9 min, respectively. We interpret the oscillations of the light wall as the leakage of *p*-modes from below the photosphere. The constant brightness enhancement of the wall top implies the existence of some kind of atmospheric heating, e.g., via the persistent small-scale reconnection or the magneto-acoustic waves. In another

series of 1330 Å images, we find that the wall top in the upward motion phase is significantly brighter than in the downward phase. This kind of oscillations may be powered by the energy released due to intermittent impulsive magnetic reconnection. **25-Oct-2014**

### **Evolution of Relative Magnetic Helicity: Method of Computation and Its Application to a Simulated Solar Corona above an Active Region**

Shangbin **Yang**, Jörg Büchner, Jean Carlo Santos, Hongqi Zhang

Solar Physics, April **2013**, Volume 283, Issue 2, pp 369-382

For a better understanding of solar magnetic field evolution it is appropriate to evaluate the magnetic helicity based on observations and to compare it with numerical simulation results. We have developed a method for calculating the vector potential of a magnetic field given in a finite volume; the method requires the magnetic flux to be balanced on all the side boundaries of the considered volume. Our method uses a fast Laplace/Poisson solver to obtain the vector potentials for a given magnetic field and for the corresponding potential (current-free) field. This allows an efficient calculation of the relative magnetic helicity in a finite 3D volume. We tested our approach on a theoretical model (Low and Lou, *Astrophys. J.* 352, 343, 1990) and also applied our method to the magnetic field above active region NOAA 8210 obtained by a photospheric-data-driven MHD model. We found that the amount of accumulated relative magnetic helicity coincides well with the relative helicity inflow through the boundaries in the ideal and non-ideal cases. The temporal evolution of relative magnetic helicity is consistent with that of magnetic energy. The maximum value of normalized helicity,  $H m/\Phi^2=0.0298$ , is reached just before a drastic energy release by magnetic reconnection. This value is close to the corresponding value inferred from the formula that connects the magnetic flux and the accumulated magnetic helicity based on the observations of solar active regions.

### **LARGE-SCALE MAGNETIC HELICITY FLUXES ESTIMATED FROM MDI MAGNETIC SYNOPTIC CHARTS OVER THE SOLAR CYCLE 23**

Shangbin **Yang** and Hongqi Zhang

**2012** ApJ 758 61

To investigate the characteristics of large-scale and long-term evolution of magnetic helicity with solar cycles, we use the method of Local Correlation Tracking to estimate the magnetic helicity evolution over solar cycle 23 from 1996 to 2009 using 795 MDI magnetic synoptic charts. The main results are as follows: the hemispheric helicity rule still holds in general, i.e., the large-scale negative (positive) magnetic helicity dominates the northern (southern) hemisphere. However, the large-scale magnetic helicity fluxes show the same sign in both hemispheres around 2001 and 2005. The global, large-scale magnetic helicity flux over the solar disk changes from a negative value at the beginning of solar cycle 23 to a positive value at the end of the cycle, while the net accumulated magnetic helicity is negative in the period between 1996 and 2009.

### **Time-dependent MHD modeling of the global solar corona for year 2007: Driven by daily-updated magnetic field synoptic data**

**Yang**, L. P.; Feng, X. S.; Xiang, C. Q.; Liu, Yang; Zhao, Xuepu; Wu, S. T.

*J. Geophys. Res.*, Vol. 117, No. A8, A08110, **2012**

<http://dx.doi.org/10.1029/2011JA017494>

In this paper, we develop a time-dependent MHD model driven by the daily-updated synoptic magnetograms (MHD-DUSM) to study the dynamic evolution of the global corona with the help of the 3D Solar-Interplanetary (SIP) adaptive mesh refinement (AMR) space-time conservation element and solution element (CESE) MHD model (SIP-AMR-CESE MHD Model). To accommodate the observations, the tangential component of the electric field at the lower boundary is specified to allow the flux evolution to match the observed changes of magnetic field. Meanwhile, the time-dependent solar surface boundary conditions derived from the method of characteristics and the mass flux limit are incorporated to couple the observation and the 3D MHD model. The simulated evolution of the global coronal structure during 2007 is compared with solar observations and solar wind measurements from both Ulysses and spacecrafts near the Earth. The MHD-DUSM model is also validated by comparisons with the standard potential field source surface (PFSS) model, the newly improved Wang-Sheeley-Argue (WSA) empirical formula, and the MHD simulation with a monthly synoptic magnetogram (MHD-MSM). Comparisons show that the MHD-DUSM results have good overall agreement with coronal and interplanetary structures, including the sizes and distributions of coronal holes, the positions and shapes of the streamer belts, and the transitions of the solar wind speeds and magnetic field polarities. The MHD-DUSM results also display many features different from those of the PFSS, the WSA, and the MHD-MSM models.

### **Simulating the Coronal Evolution of Bipolar Active Regions to Investigate the Formation of Flux Ropes**

[Stephanie L. Yardley](#), [Duncan H. Mackay](#), [Lucie M. Green](#)

Solar Phys. **2020**

<https://arxiv.org/pdf/2012.07708.pdf>

The coronal magnetic field evolution of 20 bipolar active regions (ARs) is simulated from their emergence to decay using the time-dependent nonlinear force-free field method of Mackay et al. A time sequence of cleaned photospheric line-of-sight magnetograms, that covers the entire evolution of each AR, is used to drive the simulation. A comparison of the simulated coronal magnetic field with the 171 and 193 Å observations obtained by the Solar Dynamics Observatory (SDO)/ Atmospheric Imaging Assembly (AIA), is made for each AR by manual inspection. The results show that it is possible to reproduce the evolution of the main coronal features such as small- and large-scale coronal loops, filaments and sheared structures for 80% of the ARs. Varying the boundary and initial conditions, along with the addition of physical effects such as Ohmic diffusion, hyperdiffusion and a horizontal magnetic field injection at the photosphere, improves the match between the observations and simulated coronal evolution by 20%. The simulations were able to reproduce the build-up to eruption for 50% of the observed eruptions associated with the ARs. The mean unsigned time difference between the eruptions occurring in the observations compared to the time of eruption onset in the simulations was found to be ~5 hrs. The simulations were particularly successful in capturing the build-up to eruption for all four eruptions that originated from the internal polarity inversion line of the ARs. The technique was less successful in reproducing the onset of eruptions that originated from the periphery of ARs and large-scale coronal structures. For these cases global, rather than local, nonlinear force-free field models must be used. While the technique has shown some success, eruptions that occur in quick succession are difficult to reproduce by this method and future iterations of the model need to address this. **17-20 Mar 2012, 24 Mar 2012, 25 Feb 2013, 6-9 Dec 2014, 14-17 Nov 2015**

**Table 1.:** The 20 bipolar ARs simulated in this study (2012-2015).

### **Simulating the Coronal Evolution of AR 11437 using SDO/HMI Magnetograms**

Stephanie L. [Yardley](#), [Duncan H. Mackay](#), [Lucie M. Green](#)

ApJ **2017**

<https://arxiv.org/pdf/1712.00396.pdf>

The coronal magnetic field evolution of AR 11437 is simulated by applying the magnetofrictional relaxation technique of Mackay et al. (2011). A sequence of photospheric line-of-sight magnetograms produced by SDO/HMI are used to drive the simulation and continuously evolve the coronal magnetic field of the active region through a series of non-linear force-free equilibria. The simulation is started during the first stages of the active region emergence so that its full evolution from emergence to decay can be simulated. A comparison of the simulation results with SDO/AIA observations show that many aspects of the active region's observed coronal evolution are reproduced. In particular, it shows the presence of a flux rope, which forms at the same location as sheared coronal loops in the observations. The observations show that eruptions occur on **2012 March 17** at 05:09 UT and 10:45 UT and on **2012 March 20** at 14:31 UT. The simulation reproduces the first and third eruption, with the simulated flux rope erupting roughly 1 and 10 hours before the observed ejections, respectively. A parameter study is conducted where the boundary and initial conditions are varied along with the physical effects of Ohmic diffusion, hyperdiffusion and an additional injection of helicity. When comparing the simulations, the evolution of the magnetic field, free magnetic energy, relative helicity and flux rope eruption timings do not change significantly. This indicates that the key element in reproducing the coronal evolution of AR 11437 is the use of line-of-sight magnetograms to drive the evolution of the coronal magnetic field.

### **How good is the bipolar approximation of active regions for surface flux transport?**

A. R. [Yeates](#)

Solar Phys. **2020**

<https://arxiv.org/pdf/2008.03203.pdf>

We investigate how representing active regions with bipolar magnetic regions (BMRs) affects the end-of-cycle polar field predicted by the surface flux transport model. Our study is based on a new database of BMRs derived from the SDO/HMI active region patch data between 2010 and 2020. An automated code is developed for fitting each active region patch with a BMR, matching both the magnetic flux and axial dipole moment of the region and removing repeat observations of the same region. By comparing the predicted evolution of each of the 1090 BMRs with the predicted evolution of their original active region patches, we show that the bipolar approximation leads to a 24% overestimate of the net axial dipole moment, given the same flow parameters. This is caused by neglecting the more complex multipolar and/or asymmetric magnetic structures of many of the real active regions, and may explain why previous flux transport models had to reduce BMR tilt angles to obtain realistic polar fields. Our BMR database and the Python code to extract it are freely available.

### **The Minimal Helicity of Solar Coronal Magnetic Fields**

[A. R. Yeates](#) (Durham University, UK)

ApJL **898** L49 **2020**

<https://arxiv.org/pdf/2007.10649.pdf>  
<https://doi.org/10.3847/2041-8213/aba762>

Potential field extrapolations are widely used as minimum-energy models for the Sun's coronal magnetic field. As the reference to which other magnetic fields are compared, they have -- by any reasonable definition -- no global (signed) magnetic helicity. Here we investigate the internal topological structure that is not captured by the global helicity integral, by splitting it into individual field line helicities. These are computed using potential field extrapolations from magnetogram observations over Solar Cycle 24, as well as for a simple illustrative model of a single bipolar region in a dipolar background. We find that localised patches of field line helicity arise primarily from linking between strong active regions and their overlying field, so that the total unsigned helicity correlates with the product of photospheric and open fluxes. Within each active region, positive and negative helicity may be unbalanced, but the signed helicity is only around a tenth of the unsigned helicity. Interestingly, in Cycle 24, there is a notable peak in unsigned helicity caused by a single large active region. On average, the total unsigned helicity at the resolution considered is approximately twice the typical signed helicity of a single real active region, according to non-potential models in the literature.

## **Global Non-Potential Magnetic Models of the Solar Corona During the March 2015 Eclipse**

A. R. [Yeates](#), [T. Amari](#), [I. Contopoulos](#), [X. Feng](#), [D. H. Mackay](#), [Z. Mikić](#), [T. Wiegmann](#), [J. Hutton](#), [C. A. Lowder](#), [H. Morgan](#), [G. Petrie](#), [L. A. Rachmeler](#), [L. A. Upton](#), [A. Canou](#), [P. Chopin](#), [C. Downs](#), [M. Druckmüller](#), [J. A. Linker](#), [D. B. Seaton](#), [T. Török](#)

Space Science Reviews 214:99 2018

<https://arxiv.org/pdf/1808.00785.pdf>

Seven different models are applied to the same problem of simulating the Sun's coronal magnetic field during the solar eclipse on 2015 March 20. All of the models are non-potential, allowing for free magnetic energy, but the associated electric currents are developed in significantly different ways. This is not a direct comparison of the coronal modelling techniques, in that the different models also use different photospheric boundary conditions, reflecting the range of approaches currently used in the community. Despite the significant differences, the results show broad agreement in the overall magnetic topology. Among those models with significant volume currents in much of the corona, there is general agreement that the ratio of total to potential magnetic energy should be approximately 1.4. However, there are significant differences in the electric current distributions; while static extrapolations are best able to reproduce active regions, they are unable to recover sheared magnetic fields in filament channels using currently available vector magnetogram data. By contrast, time-evolving simulations can recover the filament channel fields at the expense of not matching the observed vector magnetic fields within active regions. We suggest that, at present, the best approach may be a hybrid model using static extrapolations but with additional energization informed by simplified evolution models. This is demonstrated by one of the models. **2015 March 20**

## **Sparse reconstruction of electric fields from radial magnetic data**

A. R. [Yeates](#)

ApJ 2017

<https://arxiv.org/pdf/1701.06780v1.pdf>

Accurate estimates of the horizontal electric field on the Sun's visible surface are important not only for estimating the Poynting flux of magnetic energy into the corona but also for driving time-dependent magnetohydrodynamic models of the corona. In this paper, a method is developed for estimating the horizontal electric field from a sequence of radial-component magnetic field maps. This problem of inverting Faraday's law has no unique solution. Unfortunately, the simplest solution (a divergence-free electric field) is not realistically localized in regions of non-zero magnetic field, as would be expected from Ohm's law. Our new method generates instead a localized solution, using a basis pursuit algorithm to find a sparse solution for the electric field. The method is shown to perform well on test cases where the input magnetic maps are flux balanced, in both Cartesian and spherical geometries. However, we show that if the input maps have a significant imbalance of flux - usually arising from data assimilation - then it is not possible to find a localized, realistic, electric field solution. This is the main obstacle to driving coronal models from time sequences of solar surface magnetic maps.

## **The global distribution of magnetic helicity in the solar corona**

A. R. [Yeates](#), G. Hornig

A&A 594, A98 2016

<http://arxiv.org/pdf/1606.06863v1.pdf>

By defining an appropriate field line helicity, we apply the powerful concept of magnetic helicity to the problem of global magnetic field evolution in the Sun's corona. As an ideal-magnetohydrodynamic invariant, the field line helicity is a meaningful measure of how magnetic helicity is distributed within the coronal volume. It may be

interpreted, for each magnetic field line, as a magnetic flux linking with that field line. Using magneto-frictional simulations, we investigate how field line helicity evolves in the non-potential corona as a result of shearing by large-scale motions on the solar surface. On open magnetic field lines, the helicity injected by the Sun is largely output to the solar wind, provided that the coronal relaxation is sufficiently fast. But on closed magnetic field lines, helicity is able to build up. We find that the field line helicity is non-uniformly distributed, and is highly concentrated in twisted magnetic flux ropes. Eruption of these flux ropes is shown to lead to sudden bursts of helicity output, in contrast to the steady flux along the open magnetic field lines.

**Erratum** A&A 603, C2 (2017)

## Filaments and Magnetic Memory in the Solar Corona

Anthony [Yeates](#)

UKSP Nugget: 47, 2014

<http://www.uksolphys.org/uksp-nugget/47-filaments-and-magnetic-memory-in-the-solar-corona/>

How time-evolution may be inescapable when computing magnetic field extrapolations

Computer modelling of the Sun's magnetic field is undergoing a quiet revolution. For half a century, we have been able to measure the magnetic field strength on the solar surface (the photosphere), and from this extrapolate the magnetic field in the overlying corona. But the traditional thinking – that one can extrapolate the coronal magnetic field using only the photospheric data at a given instant – is running into trouble. Sophisticated “force-free” models that contain free magnetic energy to power solar flares and eruptions are difficult to extrapolate uniquely from the available data. We argue that the only practical way around this problem may be to generate coronal magnetic models not by static extrapolation but by time evolution.

12 June 2013

## The coronal energy input from magnetic braiding

A. R. [Yeates](#), F. Bianchi, B. T. Welsch, P. J. Bushby

A&A, 564, A131 2014

<http://arxiv.org/pdf/1403.4396v1.pdf>

We estimate the energy input into the solar corona from photospheric footpoint motions, using observations of a plage region by the Hinode Solar Optical Telescope. Assuming a perfectly ideal coronal evolution, two alternative lower bounds for the Poynting flux are computed based on field line footpoint trajectories, without requiring horizontal magnetic field data. When applied to the observed velocities, a bound based solely on displacements between the two footpoints of each field line is tighter than a bound based on relative twist between field lines. Depending on the assumed length of coronal magnetic field lines, the higher bound is found to be reasonably tight compared with a Poynting flux estimate using an available vector magnetogram. It is also close to the energy input required to explain conductive and radiative losses in the active region corona. Based on similar analysis of a numerical convection simulation, we suggest that observations with higher spatial resolution are likely to bring the bound based on relative twist closer to the first bound, but not to increase the first bound substantially. Finally, we put an approximate upper bound on the magnetic energy by constructing a hypothetical “unrelaxed” magnetic field with the correct field line connectivity.

## Coronal Magnetic Field Evolution from 1996 to 2012: Continuous Non-potential Simulations

A.R. [Yeates](#)

Solar Physics, February 2014, Volume 289, Issue 2, pp 631-648

Coupled flux transport and magneto-frictional simulations are extended to simulate the continuous magnetic-field evolution in the global solar corona for over 15 years, from the start of Solar Cycle 23 in 1996. By simplifying the dynamics, our model follows the build-up and transport of electric currents and free magnetic energy in the corona, offering an insight into the magnetic structure and topology that extrapolation-based models cannot. To enable these extended simulations, we have implemented a more efficient numerical grid, and have carefully calibrated the surface flux-transport model to reproduce the observed large-scale photospheric radial magnetic field, using emerging active regions determined from observed line-of-sight magnetograms. This calibration is described in some detail. In agreement with previous authors, we find that the standard flux-transport model is insufficient to simultaneously reproduce the observed polar fields and butterfly diagram during Cycle 23, and that additional effects must be added. For the best-fit model, we use automated techniques to detect the latitude–time profile of flux ropes and their ejections over the full solar cycle. Overall, flux ropes are more prevalent outside of active latitudes but those at active latitudes are more frequently ejected. Future possibilities for space-weather prediction with this approach are briefly assessed.

## CHIRALITY OF HIGH-LATITUDE FILAMENTS OVER SOLAR CYCLE 23

A. R. [Yeates](#)<sup>1</sup> and D. H. Mackay

2012 ApJ 753 L34

A non-potential quasi-static evolution model coupling the Sun's photospheric and coronal magnetic fields is applied to the problem of filament chirality at high latitudes. For the first time, we run a continuous 15 year simulation, using bipolar active regions determined from US National Solar Observatory, Kitt Peak magnetograms between 1996 and 2011. Using this simulation, we are able to address the outstanding question of whether magnetic helicity transport from active latitudes can overcome the effect of differential rotation at higher latitudes. Acting alone, differential rotation would produce high-latitude filaments with opposite chirality to the majority type in each hemisphere. We find that differential rotation can indeed lead to opposite chirality at high latitudes, but only for around 5 years of the solar cycle following the polar field reversal. At other times, including the rising phase, transport of magnetic helicity from lower latitudes overcomes the effect of in situ differential rotation, producing the majority chirality even on the polar crowns at polar field reversal. These simulation predictions will allow for future testing of the non-potential coronal model. The results indicate the importance of long-term memory and helicity transport from active latitudes when modeling the structure and topology of the coronal magnetic field at higher latitudes.

## A nonpotential model for the Sun's open magnetic flux

[Yeates](#), A. R.; Mackay, D. H.; van Ballegoijen, A. A.; Constable, J. A.

J. Geophys. Res., Vol. 115, No. A9, A09112, 2010

Measurements of the interplanetary magnetic field (IMF) over several solar cycles do not agree with computed values of open magnetic flux from potential field extrapolations. The discrepancy becomes greater around solar maximum in each cycle when the IMF can be twice as strong as predicted by the potential field model. Here we demonstrate that this discrepancy may be resolved by allowing for electric currents in the low corona (below 2.5R<sub>s</sub>). We present a quasi-static numerical model of the large-scale coronal magnetic evolution, which systematically produces these currents through flux emergence and shearing by surface motions. The open flux is increased by 75%–85% at solar maximum, but only 25% at solar minimum, bringing it in line with estimates from IMF measurements. The additional open flux in the nonpotential model arises through inflation of the magnetic field by electric currents, with superimposed fluctuations due to coronal mass ejections. The latter are modeled by the self-consistent ejection of twisted magnetic flux ropes.

## Solar Cycle Variation of Magnetic Flux Ropes in a Quasi-Static Coronal Evolution Model

A.R. [Yeates](#) · J.A. Constable · P.C.H. Martens

Solar Phys (2010) 263: 121–134; [File](#)

The structure of electric current and magnetic helicity in the solar corona is closely linked to solar activity over the 11-year cycle, yet is poorly understood. As an alternative to traditional current-free “potential-field” extrapolations, we investigate a model for the global coronal magnetic field which is non-potential and time-dependent, following the build-up and transport of magnetic helicity due to flux emergence and large-scale photospheric motions. This helicity concentrates into twisted magnetic flux ropes, which may lose equilibrium and be ejected. Here, we consider how the magnetic structure predicted by this model – in particular the flux ropes – varies over the solar activity cycle, based on photospheric input data from six periods of cycle 23. The number of flux ropes doubles from minimum to maximum, following the total length of photospheric polarity inversion lines. However, the number of flux rope ejections increases by a factor of eight, following the emergence rate of active regions. This is broadly consistent with the observed cycle modulation of coronal mass ejections, although the actual rate of ejections in the simulation is about a fifth of the rate of observed events. The model predicts that, even at minimum, differential rotation will produce sheared, non-potential, magnetic structure at all latitudes.

## INITIATION OF CORONAL MASS EJECTIONS IN A GLOBAL EVOLUTION MODEL

A. R. [Yeates](#)<sup>1</sup>, D. H. Mackay

E-print, April 2009, [File](#); ApJ, 699:1024–1037, 2009 July

Loss of equilibrium of magnetic flux ropes is a leading candidate for the origin of solar coronal mass ejections (CMEs). The aim of this paper is to explore to what extent this mechanism can account for the initiation of CMEs in the global context. A simplified MHD model for the global coronal magnetic field evolution in response to flux emergence and shearing by large-scale surface motions is described and motivated. Using automated algorithms for



detecting flux ropes and ejections in the global magnetic model, the effects of key simulation parameters on the formation of flux ropes and the number of ejections are considered, over a 177-day period in 1999. These key parameters include the magnitude and sign of magnetic helicity emerging in active regions, and coronal diffusion. The number of flux ropes found in the simulation at any one time fluctuates between about 28 and 48, sustained by the emergence of new bipolar regions, but with no systematic dependence on the helicity of these regions. However, the emerging helicity does affect the rate of flux rope ejections, which doubles from 0.67 per day if the bipoles emerge untwisted to 1.28 per day in the run with greatest emerging twist. The number of ejections in the simulation is also increased by 20%-30% by choosing the majority sign of emerging bipole helicity in each hemisphere, or by halving the turbulent diffusivity in the corona. For reasonable parameter choices, the model produces approximately 50% of the observed CME rate. This indicates that the formation and loss of equilibrium of flux ropes may be a key element in explaining a significant fraction of observed CMEs.

## **INITIATION OF CORONAL MASS EJECTIONS IN A GLOBAL EVOLUTION MODEL**

A. R. [Yeates](#)<sup>1</sup>, D. H. Mackay

E-print, April 2009, *File*; ApJ, 699:1024–1037, 2009 July

Loss of equilibrium of magnetic flux ropes is a leading candidate for the origin of solar coronal mass ejections (CMEs). The aim of this paper is to explore to what extent this mechanism can account for the initiation of CMEs in the global context. A simplified MHD model for the global coronal magnetic field evolution in response to flux emergence and shearing by large-scale surface motions is described and motivated. Using automated algorithms for detecting flux ropes and ejections in the global magnetic model, the effects of key simulation parameters on the formation of flux ropes and the number of ejections are considered, over a 177-day period in 1999. These key parameters include the magnitude and sign of magnetic helicity emerging in active regions, and coronal diffusion. The number of flux ropes found in the simulation at any one time fluctuates between about 28 and 48, sustained by the emergence of new bipolar regions, but with no systematic dependence on the helicity of these regions. However, the emerging helicity does affect the rate of flux rope ejections, which doubles from 0.67 per day if the bipoles emerge untwisted to 1.28 per day in the run with greatest emerging twist. The number of ejections in the simulation is also increased by 20%-30% by choosing the majority sign of emerging bipole helicity in each hemisphere, or by halving the turbulent diffusivity in the corona. For reasonable parameter choices, the model produces approximately 50% of the observed CME rate. This indicates that the formation and loss of equilibrium of flux ropes may be a key element in explaining a significant fraction of observed CMEs.

## **Modelling the Global Solar Corona II: Coronal Evolution and Filament Chirality Comparison**

A.R. [Yeates](#) · D.H. Mackay · A.A. van Ballegooijen

*Solar Phys* (2008) 247: 103–121

<http://www.springerlink.com/content/66h3876790633575/fulltext.pdf>

14 Sept 1999

This paper considers the hemispheric pattern of solar filaments using newly developed simulations of the real photospheric and 3D coronal magnetic fields over a six-month period, on a global scale. The magnetic field direction in the simulation is compared directly with the chirality of observed filaments, at their observed locations. In our model the coronal field evolves through a continuous sequence of nonlinear force-free equilibria, in response to the changing photospheric boundary conditions and the emergence of new magnetic flux. In total 119 magnetic bipoles with properties matching observed active regions are inserted. These bipoles emerge twisted and inject magnetic helicity into the solar atmosphere. When we choose the sign of this active-region helicity to match that observed in each hemisphere, the model produces the correct chirality for up to 96% of filaments, including exceptions to the hemispheric pattern. If the emerging bipoles have zero helicity, or helicity of the opposite sign, then this percentage is much reduced. In addition, the simulation produces a higher proportion of filaments with the correct chirality after longer times. This indicates that a key element in the evolution of the coronal field is its long-term memory, and the build-up and transport of helicity from low to high latitudes over many months. It highlights the importance of continuous evolution of the coronal field, rather than independent extrapolations at different times. This has significant consequences for future modelling such as that related to the origin and development of coronal mass ejections.

## **The variation in the response of solar full-disc magnetographs**

[K. L. Yeo](#), [S. K. Solanki](#), [N. A. Krivova](#)

*A&A* 2024

<https://arxiv.org/pdf/2405.13895>

We compared magnetograms from the KPVT/SPM, SoHO/MDI, SOLIS/VSM, and SDO/HMI with the aim of probing the effect on measured solar magnetism of the variation in instrument response with time, magnetogram

signal level, and position on the solar disc. Taking near-simultaneous observations from the various instruments, we examined the surface coverage by magnetic activity and the effect of cross-calibrating the various instruments under different assumptions. By comparing the surface coverage by magnetic activity in the observations from the various instruments, we traced the effect of the time variation in instrument response on the longitudinal magnetogram signal and disc-integrated unsigned magnetic flux. This yielded evidence of acute changes in the response of MDI and VSM with certain events such as the SoHO vacation in 1998 and the upgrade of the VSM CCD camera in 2009. Excluding these changes, the effect of instrument instability on the magnetogram signal and disc-integrated magnetic flux appears to be rather benign, with an associated uncertainty of less than 2%. We determined the magnetogram signal ratio between each instrument pairing as a function of magnetogram signal level and distance from disc centre and with it cross-calibrated the various instruments. We compared the result with that from repeating the cross-calibration with the overall magnetogram signal ratio. This allowed us to estimate the uncertainty in the magnetogram signal associated with the variation in instrument response with magnetogram signal level and distance from disc centre to be about 8% to 14%. The corresponding uncertainty in the disc-integrated magnetic flux is about 7% to 23%. The results here will be useful to the interpretation of SPM, MDI, VSM, and HMI magnetograms. As examples, we applied our findings to selected results from earlier studies based on such data.

### **The relationship between bipolar magnetic regions and their sunspots**

[K. L. Yeo](#), [S. K. Solanki](#), [N. A. Krivova](#), [J. Jiang](#)

A&A 654, A28 2021

<https://arxiv.org/pdf/2109.14313.pdf>

<https://www.aanda.org/articles/aa/pdf/2021/10/aa41336-21.pdf>

<https://doi.org/10.1051/0004-6361/202141336>

The relationship between bipolar magnetic regions (BMRs) and their sunspots is an important property of the solar magnetic field, but it is not well constrained. One consequence is that it is a challenge for surface flux transport models (SFTMs) based on sunspot observations to determine the details of BMR emergence, which they require as input, from such data. We aimed to establish the relationship between the amount of magnetic flux in newly emerged BMRs and the area of the enclosed sunspots. Earlier attempts to constrain BMR magnetic flux were hindered by the fact that there is no proper database of the magnetic and physical properties of newly emerged BMRs currently available. We made use of the empirical model of the relationship between the disc-integrated facular and network magnetic flux and the total surface coverage by sunspots reported in a recent study. The structure of the model is such that it enabled us to establish, from these disc-integrated quantities, an empirical relationship between the magnetic flux and sunspot area of individual newly emerged BMRs, circumventing the lack of any proper BMR database. Applying the constraint on BMR magnetic flux derived here to an established SFTM retained its ability to replicate various independent datasets and the correlation between the model output polar field at the end of each cycle and the observed strength of the following cycle. The SFTM output indicates that facular and network magnetic flux rises with increasing sunspot magnetic flux at a slowing rate such that it appears to gradually saturate, analogous to earlier studies. The activity dependence of the ratio of facular and network flux to sunspot flux is consistent with the findings of recent studies: although the Sun is faculae-dominated, it is only marginally so as facular and network brightening and sunspot darkening appear to be closely balanced.

### **Reconstruction of Coronal Magnetic Fields Using a Poloidal–Toroidal Representation**

Sibaek [Yi](#)<sup>1</sup>, G. S. [Choe](#)<sup>1,2</sup>, [Kyung-Suk Cho](#)<sup>3</sup>, [Sami K. Solanki](#)<sup>4</sup>, and [Jörg Büchner](#)<sup>4,5</sup>

2022 ApJ 937 11

<https://iopscience.iop.org/article/10.3847/1538-4357/ac8b0e/pdf>

A new method for reconstruction of coronal magnetic fields as force-free fields (FFFs) is presented. Our method employs poloidal and toroidal functions to describe divergence-free magnetic fields. This magnetic field representation naturally enables us to implement the boundary conditions at the photospheric boundary, i.e., the normal magnetic field and the normal current density there, in a straightforward manner. At the upper boundary of the corona, a source surface condition can be employed, which accommodates magnetic flux imbalance at the bottom boundary. Although our iteration algorithm is inspired by extant variational methods, it is nonvariational and requires far fewer iteration steps than most others. The computational code based on our new method is tested against the analytical FFF solutions by [Titov & Démoulin](#). It is found to excel in reproducing a tightly wound flux rope, a bald patch, and quasi-separatrix layers with a hyperbolic flux tube.

### **Which Component of Solar Magnetic Field Drives the Evolution of Interplanetary Magnetic Field over Solar Cycle?**

[Minami Yoshida](#), [Toshifumi Shimizu](#), [Shin Toriumi](#)

ApJ 2023

<https://arxiv.org/pdf/2304.13347.pdf>

The solar magnetic structure changes over the solar cycle. It has a dipole structure during solar minimum, where the open flux extends mainly from the polar regions into the interplanetary space. During maximum, a complex

structure is formed with low-latitude active regions and weakened polar fields, resulting in spread open field regions. However, the components of the solar magnetic field that is responsible for long-term variations in the interplanetary magnetic field (IMF) are not clear, and the IMF strength estimated based on the solar magnetic field is known to be underestimated by a factor of 3 to 4 against the actual in-situ observations (the open flux problem). To this end, we decomposed the coronal magnetic field into the components of the spherical harmonic function of degree and order  $(\ell, m)$  using the potential field source surface model with synoptic maps from SDO/HMI for 2010 to 2021. As a result, we found that the IMF rapidly increased in December 2014 (seven months after the solar maximum), which coincided with the increase in the equatorial dipole,  $(\ell, m)=(1, \pm 1)$ , corresponding to the diffusion of active regions toward the poles and in the longitudinal direction. The IMF gradually decreased until December 2019 (solar minimum) and its variation corresponded to that of the non-dipole component  $\ell \geq 2$ . Our results suggest that the understanding of the open flux problem may be improved by focusing on the equatorial dipole and the non-dipole component and that the influence of the polar magnetic field is less significant.

## **Magnetic Field Extrapolation in Active Region Well Comparable to Observations in Multiple Layers**

Fu **Yu**<sup>1,2,3</sup>, Jie Zhao<sup>1,3</sup>, Yang Su<sup>1,2</sup>, Xiaoshuai Zhu<sup>3</sup>, Yang Guo<sup>4</sup>, Jinhua Shen<sup>5</sup>, and Hui Li<sup>1,2</sup>  
**2023** ApJ 951 54

<https://iopscience.iop.org/article/10.3847/1538-4357/acd112/pdf>

Magnetic field extrapolation is a fundamental tool to reconstruct the three-dimensional magnetic field above the solar photosphere. However, the prevalently used force-free field model might not be applicable in the lower atmosphere with non-negligible plasma  $\beta$ , where the crucial process of flux rope formation and evolution could happen. In this work, we perform extrapolation in active region 12158, based on a recently developed magnetohydrostatic (MHS) method that takes plasma forces into account. By comparing the results with those from the force-free field extrapolation methods, we find that the overall properties, which are characterized by the magnetic free energy and helicity, are roughly the same. The major differences lie in the magnetic configuration and the twist number of the magnetic flux rope (MFR). Unlike previous works either obtained sheared arcades or one coherent flux rope, the MHS method derives two sets of MFR, which are highly twisted and slightly coupled. Specifically, the result in the present work is more comparable to the high-resolution observations from the chromosphere, through the transition region to the corona, such as the filament fibrils, pre-eruptive braiding characteristics, and the eruptive double-J-shaped hot channel. Overall, our work shows that the newly developed MHS method is more promising to reproduce the magnetic fine structures that can well match the observations at multiple layers, and future data-driven simulation based on such extrapolation will benefit in understanding the critical and precise dynamics of flux rope before eruption. **2014 September 10**

## **Does the non-force-freeness matter for the extrapolation of solar magnetic field?**

[Fu Yu](#), [Jie Zhao](#), [Yang Su](#), [Xiaoshuai Zhu](#), [Yang Guo](#)

ApJ **2022**

<https://arxiv.org/pdf/2210.15074.pdf>

Magnetic field extrapolation is a fundamental tool to reconstruct the three-dimensional solar coronal magnetic field. However, the prevalently used force-free field model might not be applicable in the lower atmosphere, where plasma  $\beta$  is greater than 1. In this work, we perform extrapolation in active region 12158, based on an updated magnetohydrostatic (MHS) method. By comparing the results with those from the force-free field method of Current-Field Iteration in Spherical Coordinates (CFITS), we find that the overall properties, which are characterized by the magnetic free energy and helicity, are roughly the same after volume integral. The major differences lie in the magnetic configuration and the twist number of magnetic flux rope (MFR). A coherent MFR with twist around 1 is reproduced from CFITS. In another manner, two sets of MFR, which are highly twisted and slightly coupled, are derived by the MHS method. The latter one is better constrained by the high-resolution observations, such as the filament fibrils, pre-eruptive braiding characteristics and the eruptive double-J shaped hot channel. Overall, our work shows the MHS method is more promising to reproduce the magnetic fine structures that can well match the observations not only in the chromosphere but also in the corona. This initiates the necessity of reconsidering the simplification of low atmosphere for currently widely used nonlinear force-free extrapolation method, since such assumption will not only omit the magnetic structures at low atmosphere but also affect those obtained in the corona, and therefore bringing in ambiguity in interpreting the solar eruption. **2014 September 10**

## **Multilayered Kelvin–Helmholtz Instability in the Solar Corona**

Ding **Yuan**<sup>1,2,8</sup>, Yuandeng Shen<sup>3,8</sup>, Yu Liu<sup>3</sup>, Hongbo Li<sup>4</sup>, Xueshang Feng<sup>1</sup>, and Rony Keppens<sup>5</sup>  
**2019** ApJL 884 L51

<https://doi.org/10.3847/2041-8213/ab4bcd>

The Kelvin–Helmholtz (KH) instability is commonly found in many astrophysical, laboratory, and space plasmas. It could mix plasma components of different properties and convert dynamic fluid energy from large-scale structure to smaller ones. In this study, we combined the ground-based New Vacuum Solar Telescope (NVST) and the Solar

Dynamic Observatories/Atmospheric Imaging Assembly (AIA) to observe the plasma dynamics associated with active region 12673 on **2017 September 9**. In this multitemperature view, we identified three adjacent layers of plasma flowing at different speeds, and detected KH instabilities at their interfaces. We could unambiguously track a typical KH vortex and measure its motion. We found that the speed of this vortex suddenly tripled at a certain stage. This acceleration was synchronized with the enhancements in emission measure and average intensity of the 193 Å data. We interpret this as evidence that KH instability triggers plasma heating. The intriguing feature in this event is that the KH instability observed in the NVST channel was nearly complementary to that in the AIA 193 Å. Such a multithermal energy exchange process is easily overlooked in previous studies, as the cold plasma component is usually not visible in the extreme-ultraviolet channels that are only sensitive to high-temperature plasma emissions. Our finding indicates that embedded cold layers could interact with hot plasma as invisible matters. We speculate that this process could occur at a variety of length scales and could contribute to plasma heating.

### **Abnormal oscillation modes in a waning light bridge**

Ding **Yuan**, Robert W. Walsh

A&A **2016**

<http://arxiv.org/pdf/1609.00596v1.pdf>

A sunspot acts as a waveguide in response to the dynamics of the solar interior; the trapped waves and oscillations could reveal its thermal and magnetic structures. We study the oscillations in a sunspot intruded by a light bridge, the details of the oscillations could reveal the fine structure of the magnetic topology. We use the Solar Dynamics Observatory/Atmospheric Imaging Assembly data to analyse the oscillations in the emission intensity of light bridge plasma at different temperatures and investigate their spatial distributions. The extreme ultraviolet emission intensity exhibits two persistent oscillations at five-minute and sub-minute ranges. The spatial distribution of the five-minute oscillation follows the spine of the bridge; whereas the sub-minute oscillations overlap with two flanks of the bridge. Moreover, the sub-minute oscillations are highly correlated in spatial domain, however, the oscillations at the eastern and western flanks are asymmetric with regard to the lag time. In the meanwhile, jet-like activities are only found at the eastern flank. Asymmetries in forms of oscillatory pattern and jet-like activities are found between two flanks of a granular light bridge. Based on our study and recent findings, we propose a new model of twisted magnetic field for a light bridge and its dynamic interactions with the magnetic field of a sunspot.

### **Oscillations in a sunspot with light bridges**

Ding **Yuan**, Valery M. Nakariakov, Zhenghua Huang, Bo Li, Jiangtao Su, Yihua Yan, Baolin Tan

ApJ, **2014** 792 41

<http://arxiv.org/pdf/1407.1544v1.pdf>

Solar Optical Telescope onboard Hinode observed a sunspot (AR 11836) with two light bridges (LBs) on **31 Aug 2013**. We analysed a 2-hour  $\text{Ca II H}$  emission intensity data set and detected strong 5-min oscillation power on both LBs and in the inner penumbra. The time-distance plot reveals that 5-min oscillation phase does not vary significantly along the thin bridge, indicating that the oscillations are likely to originate from the underneath. The slit taken along the central axis of the wide light bridge exhibits a standing wave feature. However, at the centre of the wide bridge, the 5-min oscillation power is found to be stronger than at its sides. Moreover, the time-distance plot across the wide bridge exhibits a herringbone pattern that indicates a counter-stream of two running waves originated at the bridge sides.

Thus, the 5-min oscillations on the wide bridge also resemble the properties of running penumbral waves. The 5-min oscillations are suppressed in the umbra, while the 3-min oscillations occupy all three cores of the sunspot's umbra, separated by the LBs. The 3-min oscillations were found to be in phase at both sides of the LBs. It may indicate that either LBs do not affect umbral oscillations, or umbral oscillations at different umbral cores share the same source. Also, it indicates that LBs are rather shallow objects situated in the upper part of the umbra. We found that umbral flashes follow the life cycles of umbral oscillations with much larger amplitudes. They cannot propagate across LBs. Umbral flashes dominate the 3-min oscillation power within each core, however, they do not disrupt the phase of umbral oscillation.

### **Leakage of long-period oscillations from the chromosphere to the corona**

D. **Yuan**<sup>1</sup>, V. M. Nakariakov<sup>1,2</sup>, N. Chorley<sup>1</sup> and C. Foullon<sup>1</sup>

A&A 533, A116 (2011)

Long-period oscillations in a coronal diffuse structure are detected with the Transition Region And Coronal Explorer (TRACE). The EUV images of the NOAA active region 8253 are available in 171 Å and 195 Å bandpasses from 30 June to 4 July 1998. The average intensity variation is found to be connected with the CCD temperature, which varies with the orbital motion of the spacecraft. Hence, oscillations with the orbital period and its higher harmonics appear as artifacts in the light curves. After the exclusion of the orbital effects, we identified several long-period oscillations in the diffuse fan-like structure of the active region. Similar periodicities were detected in the

radio emission from the chromospheric part of that active region, observed with the ground-based Nobeyama Radioheliograph (NoRH) in the 17 GHz channel. It was found that 0.221, 0.312 and 0.573 mHz oscillations were present in both EUV emission lines in the corona and the radio signal from the sunspot in the chromosphere, just beneath the active region. From the frequency values, the 1st and 3rd detected oscillations could be associated with the  $l = 2, n = -3$  or  $l = 3, n = -5$  and  $l = 1$  gravity-driven solar interior modes, respectively. The appearance of these oscillations in the coronal part of the active region can be connected with the wave leakage or the evanescence of chromospheric oscillations.

## Using Potential Field Extrapolations to Explore the Origin of Type II Spicules

Vasyl Yurchyshyn<sup>1</sup>, Anneliese Schmidt<sup>2</sup>, Jiasheng Wang<sup>2</sup>, Xu Yang<sup>1</sup>, Eun-Kyung Lim<sup>3</sup>, and Wenda Cao<sup>1</sup>

2024 ApJ 961 79

<https://iopscience.iop.org/article/10.3847/1538-4357/ad0da2/pdf>

We used 29 high-resolution line-of-sight magnetograms acquired with the Goode Solar Telescope (GST) in a quiet-Sun area to extrapolate a series of potential field configurations and study their time variations. The study showed that there are regions that consistently exhibit changes in loop connectivity, whereas other vast areas do not show such changes. Analysis of the topological features of the potential fields indicates that the photospheric footprint of the separatrix between open- and closed-loop systems closely matches the roots of rapid blue- and redshifted excursions, which are disk counterparts of type II spicules. There is a tendency for the footpoints of the observed H $\alpha$  features to be cospatial with the footpoints of the loops that most frequently change their connectivity, while the area occupied by the open fields that did not show any significant and persistent connectivity changes is void of prominent jet and spicular activity. We also detected and tracked magnetic elements using the Southwest Automatic Magnetic Identification Suite and GST magnetograms, which allowed us to construct artificial magnetograms and calculate the corresponding potential field configurations. Analysis of the artificial data showed tendencies similar to those found for the observed data. The present study suggests that a significant amount of chromospheric activity observed in the far wings of the H $\alpha$  spectral line may be generated by reconnecting closed-loop systems and canopy fields consisting of "open" field lines. **2017 June 19**

## Spatial Distribution of Origin of Umbral Waves in a Sunspot Umbra

Vasyl Yurchyshyn, Ali Kilcik, Seray Sahin, Valentina Abramenko, Eun-Kyung Lim

2020 ApJ 896 150

<https://arxiv.org/pdf/2005.04202.pdf>

<https://doi.org/10.3847/1538-4357/ab91b8>

Umbral flashes (UFs) are emissions in the core of chromospheric lines caused by upward propagating waves steepening into shocks. UFs are followed by an expanding blue shifted umbral wave (UW) and red-shifted plasma returning to the initial state. Here we use 5 s cadence images acquired at  $\pm 0.04$  nm off the H $\alpha$  line center by the Visible Imaging Spectrometer (VIS) installed on the Goode Solar Telescope (GST) to detect the origin of UFs and UWs in a sunspot with a uniform umbra free of LBs and clusters of umbral dots. The data showed that UFs do not randomly originate over the umbra. Instead, they appear to be repeatedly triggered at locations with the lowest umbral intensity and the most powerful oscillations of H $\alpha$ -0.04 nm intensity. GST magnetic field measurements using Near Infra-Red Imaging Spectropolarimeter (NIRIS) also showed that the dominant location of prevalent UF origin is co-spatial associated with the strongest fields in the umbra. Interface Region Imaging Spectrograph 149.0 nm images showed that no bright UV loops were anchored in the umbra in general and near the UF patches in particular suggesting that UFs and UWs alone can not be responsible for the origin of warm coronal loops. We thus conclude that the existence of locations with prevalent origin of UFs confirms the idea that they may be driven by a sub-surface source located near the axis of a flux rope, while the presence of several UFs trigger centers may indicate the complex structure of a sunspot umbra.

## Dynamics in Sunspot Umbra as Seen in New Solar Telescope and Interface Region Imaging Spectrograph Data

Vasyl Yurchyshyn, Valentina Abramenko, Ali Kilcik

2015 ApJ 798 136

<http://arxiv.org/pdf/1411.0192v1.pdf>

We analyse sunspot oscillations using Interface Region Imaging Spectrograph (IRIS) slit-jaw and spectral data and narrow-band chromospheric images from the New Solar Telescope (NST) for the main sunspot in NOAA AR 11836. We report that the difference between the shock arrival times as measured the Mg II k 2796.35 Å and Si IV 1393.76 Å line formation levels changes during the observed period and peak-to-peak delays may range from 40 s to zero. The intensity of chromospheric shocks also displays a long term (about 20 min) variations. NST's high spatial resolution data allowed us to conclude that in this sunspot umbral flashes (UFs) appeared in the form of narrow bright lanes stretched along the light bridges and around clusters of umbral bright points. Time series also suggested that UFs preferred to appear on the sunspot-center side of light bridges, which may indicate the

existence of a compact sub-photospheric driver of sunspot oscillations. The sunspot's umbra as seen in the IRIS chromospheric and transition region data appears bright above the locations of light bridges and the areas where the dark umbra is dotted with clusters of umbral dots. Co-spatial and co-temporal data from the Atmospheric Imaging Assembly on board Solar Dynamics Observatory showed that the same locations were associated with bright footpoints of coronal loops suggesting that the light bridges may play an important role in heating the coronal sunspot loops. Finally, the power spectra analysis showed that the intensity of chromospheric and transition region oscillations significantly vary across the umbra and with height, suggesting that umbral non-uniformities and the structure of sunspot magnetic fields may play a role in wave propagation and heating of umbral loops. **2 September 2013**

### **High Resolution Observations of Chromospheric Jets in Sunspot Umbra**

**Yurchyshyn, V., Abramenko, V., Kosovichev, A., and Goode, P.**

E-print, April **2014**, ApJ, **2014**

[http://www.bbso.njit.edu/~vayur/spikes/VYurchyshyn\\_Spikes.pdf](http://www.bbso.njit.edu/~vayur/spikes/VYurchyshyn_Spikes.pdf)

<http://arxiv.org/pdf/1404.7444v1.pdf>

Recent observations of sunspot's umbra suggested that it may be finely structured at a sub-arcsecond scale representing a mix of hot and cool plasma elements. In this study we report the first detailed observations of the umbral spikes, which are cool jet-like structures seen in the chromosphere of an umbra. The spikes are cone-shaped features with a typical height of 0.5-1.0 Mm and a width of about 0.1 Mm. Their life time ranges from 2 to 3 min and they tend to re-appear at the same location. The spikes are not associated with photospheric umbral dots and they rather tend to occur above darkest parts of the umbra, where magnetic fields are strongest. The spikes exhibit up and down oscillatory motions and their spectral evolution suggests that they might be driven by upward propagating shocks generated by photospheric oscillations. It is worth noting that triggering of the running penumbral waves seems to occur during the interval when the spikes reach their maximum height. **14 June 2013**

### **Ejection of cool plasma into the hot corona ★**

**P. Zacharias<sup>1</sup> ★ ★, H. Peter<sup>2</sup> and S. Bingert**

A&A 532, A112 (**2011**)

Context. The corona is highly dynamic and shows transient events on various scales in space and time. Most of these features are related to changes in the magnetic field structure or impulsive heating caused by the conversion of magnetic to thermal energy.

Aims. We investigate the processes that lead to the formation, ejection and fall of a confined plasma ejection that was observed in a numerical experiment of the solar corona. By quantifying physical parameters such as mass, velocity, and orientation of the plasma ejection relative to the magnetic field, we provide a description of the nature of this particular plasma ejection.

Methods. The time-dependent three-dimensional magnetohydrodynamic (3D MHD) equations are solved in a box extending from the chromosphere, which serves as a reservoir for mass and energy, to the lower corona. The plasma is heated by currents that are induced through field line braiding as a consequence of photospheric motions included in the model. Spectra of optically thin emission lines in the extreme ultraviolet range are synthesized, and magnetic field lines are traced over time. We determine the trajectory of the plasma ejection and identify anomalies in the profiles of the plasma parameters.

Results. Following strong heating just above the chromosphere, the pressure rapidly increases, leading to a hydrodynamic explosion above the upper chromosphere in the low transition region. The explosion drives the plasma, which needs to follow the magnetic field lines. The ejection is then moving more or less ballistically along the loop-like field lines and eventually drops down onto the surface of the Sun. The speed of the ejection is in the range of the sound speed, well below the Alfvén velocity.

Conclusions. The plasma ejection observed in a numerical experiment of the solar corona is basically a hydrodynamic phenomenon, whereas the rise of the heating rate is of magnetic nature. The granular motions in the photosphere lead (by chance) to a strong braiding of the magnetic field lines at the location of the explosion that in turn is causing strong currents which are dissipated. Future studies need to determine if this process is a ubiquitous phenomenon on the Sun on small scales. Data from the Atmospheric Imaging Assembly on the Solar Dynamics Observatory (AIA/SDO) might provide the relevant information.

### **On the nature of the magnetic field asymmetry in magnetically coupled leading and following sunspots observed in active regions with no eruptive events**

Iu.S. **Zagainova, V.G. Fainshtein, G.V. Rudenko, V.N. Obridko**

Solar Phys. **2017**

<https://arxiv.org/pdf/1711.08895.pdf>

In this study, we investigate magnetic properties of umbra of magneto-conjugate leading and following sunspots, i.e. connected through magnetic field lines. We established dependences between individual sunspot umbra field characteristics, and between these characteristics on the umbra area ( $S$ ) separately for sunspot pairs, for which the minimal angle between the umbra magnetic field line of the leading ( $L$ ) sunspot and the positive normal line to the Sun surface is smaller, than that in the following ( $F$ ) sunspot ( $\alpha_{\min-L} < \alpha_{\min-F}$ ; such sunspot pairs are the bulk) and, on the contrary, when  $\alpha_{\min-L} > \alpha_{\min-F}$ .

The  $\alpha_{\min-L}(SL)$ ,  $\alpha_{\min-F}(SF)$ ,  $B_{\max-L}(SL)$  and  $B_{\max-F}(SF)$  dependences are shown to have similar behavior features, and are quantitatively close for two sunspot groups with a different asymmetry of the sunspot magnetic field connecting them (here,  $B_{\max-L,F}(SL)$  is the magnetic induction maximum induction in umbrae of the leading and the following sunspots). The dependence of mean values of angles within umbra  $\langle \alpha_{L,F} \rangle$  on the sunspot umbra area  $SL,F$  and on the mean value of magnetic induction in umbra  $\langle BL,F \rangle$  appeared different for two cases. Also, in the bulk of the investigated sunspot pairs, the leading sunspot was shown to appear closer to the polarity inversion line between the sunspots, than the following one. This result and the conclusion that, in the bulk of the investigated pairs of the magnetically conjugate sunspots,  $\alpha_{\min-L} < \alpha_{\min-F}$  are closely coupled.

## **Leading and following sunspots: their magnetic properties and ultra-violet emission above them**

Iu. S. **Zagainova**, V.G. Fainshtein, V.N. Obridko

**2015**

Using SDO/HMI and SDO/AIA data for sunspot groups of the 24th solar cycle, we analyzed magnetic properties and He II 304 emission in leading and following sunspots separately. Simultaneous examination of umbral magnetic properties and atmospheric characteristics above the umbrae draws on average differences in He II 304 contrast over the umbrae of leading and following spots we discovered earlier for solar cycle 23 sunspot groups based on SOHO data as well as on the hypothetical relationship between contrast asymmetry and magnetic field asymmetry in umbrae. We use a more accurate and faster algorithm for solving the pi-uncertainty problem of the transverse magnetic field direction in this research producing new results on differences in magnetic field properties between magneto-conjugated leaders and followers. We found that, in  $\sim 78\%$  of the cases, the minimum (over the umbra area) angle between the magnetic field line and the normal to the solar surface,  $\alpha_{\min}$ , is smaller in the leading spots, so the magnetic field there is more vertical than that in the counterpart following spot. It was also found that umbral area-averaged angle  $\langle \alpha \rangle$  in  $\sim 83\%$  of the spot groups examined is smaller in the leader compared to the follower and the maximum and mean magnetic flux densities inside the umbra depend on the umbral area.

## **Coronal Densities, Temperatures, and Abundances during the 2019 Total Solar Eclipse: The Role of Multiwavelength Observations in Coronal Plasma Characterization**

Giulio Del **Zanna**<sup>1</sup>, Jenna Samra<sup>2</sup>, Austin Monaghan<sup>3</sup>, Chad Madsen<sup>2</sup>, Paul Bryans<sup>3</sup>, Edward DeLuca<sup>2</sup>, Helen Mason<sup>1</sup>, Ben Berkeley<sup>3</sup>, Alfred de Wijn<sup>3</sup>, and Yeimy J. Rivera<sup>2</sup>

**2023** ApJS 265 11

<https://iopscience.iop.org/article/10.3847/1538-4365/acad68/pdf>

<https://arxiv.org/pdf/2212.11889.pdf>

The Airborne Infrared Spectrometer (AIR-Spec) offers an unprecedented opportunity to explore the near-infrared (NIR) wavelength range. It has been flown at two total solar eclipses, in 2017 and 2019. The wavelength range of the much-improved instrument on the second flight (2019 July 2) was shifted to cover two density-sensitive lines from S xi. In this paper we study detailed diagnostics for temperature, electron density, and elemental abundances by comparing results from AIR-Spec slit positions above the east and west limbs with those from Hinode/EIS, the PolarCam detector, and SDO/AIA. We find very good agreement in the electron densities obtained from the EIS EUV line ratios, those from the NIR S xi ratio, and those obtained from the polarized brightness PolarCam measurements. Electron densities ranged from  $\log N_e [\text{cm}^{-3}] = 8.4$  near the limb to 7.2 at  $R0 = 1.3$ . EIS spectra indicate that the temperature distribution above the west limb is near isothermal at around 1.3 MK, while that on the east has an additional higher-T component. The AIR-Spec radiances in Si x and S xi, as well as the AIA data in the 171, 193, and 211 Å bands, are consistent with the EIS results. EIS and AIR-Spec data indicate that the sulfur abundance (relative to silicon) is photospheric in both regions, confirming our previous results of the 2017 eclipse. The AIA data also indicate that the absolute iron abundance is photospheric. Our analysis confirms the importance of the diagnostic potential of the NIR wavelength range and that this important wavelength range can be used reliably and independently to determine coronal plasma parameters. **2019 July 2**

## **DIRECT DETECTION OF THE HELICAL MAGNETIC FIELD GEOMETRY FROM 3D RECONSTRUCTION OF PROMINENCE KNOT TRAJECTORIES**

Maciej **Zapiór** and David Martínez-Gómez

**2016** ApJ 817 123

Based on the data collected by the Vacuum Tower Telescope located in the Teide Observatory in the Canary Islands, we analyzed the three-dimensional (3D) motion of so-called knots in a solar prominence of **2014 June 9**.

Trajectories of seven knots were reconstructed, giving information of the 3D geometry of the magnetic field. Helical motion was detected. From the equipartition principle, we estimated the lower limit of the magnetic field in the prominence to  $\approx 1\text{--}3$  G and from the Ampère's law the lower limit of the electric current to  $\approx 1.2 \times 10^9$  A.

### **The excitation of 5-min oscillations in the solar corona**

T. V. [Zaqarashvili](#)<sup>1,4</sup>, K. Murawski<sup>2</sup>, M. L. Khodachenko<sup>1</sup> and D. Lee<sup>3</sup>

*A&A* 529, A85 (2011)

**Aims.** We aim to study excitation of the observed  $\sim 5$ -min oscillations in the solar corona by localized pulses that are launched in the photosphere.

**Methods.** We solve the full set of nonlinear one-dimensional Euler equations numerically for the velocity pulse propagating in the solar atmosphere that is determined by the realistic temperature profile.

**Results.** Numerical simulations show that an initial velocity pulse quickly steepens into a leading shock, while the nonlinear wake in the chromosphere leads to the formation of consecutive pulses. The time interval between the arrivals of two neighboring pulses to a detection point in the corona is approximately 5 min. Therefore, the consecutive pulses may result in the  $\sim 5$ -min oscillations that are observed in the solar corona.

**Conclusions.** The  $\sim 5$ -min oscillations observed in the solar corona can be explained in terms of consecutive shocks that result from impulsive triggers launched within the solar photosphere by granulation and/or reconnection.

### **Segmentation of photospheric magnetic elements corresponding to coronal features to understand the EUV and UV irradiance variability\***

J. J. [Zender](#)<sup>1</sup>, R. Kariyappa<sup>2</sup>, G. Giono<sup>3</sup>, M. Bergmann<sup>4</sup>, V. Delouille<sup>5</sup>, L. Damé<sup>6</sup>, J.-F.

Hochedez<sup>6,5</sup> and S. T. Kumara

*A&A* 605, A41 (2017)

**Context.** The magnetic field plays a dominant role in the solar irradiance variability. Determining the contribution of various magnetic features to this variability is important in the context of heliospheric studies and Sun-Earth connection.

**Aims.** We studied the solar irradiance variability and its association with the underlying magnetic field for a period of five years (January 2011–January 2016). We used observations from the Large Yield Radiometer (LYRA), the Sun Watcher with Active Pixel System detector and Image Processing (SWAP) on board PROBA2, the Atmospheric Imaging Assembly (AIA), and the Helioseismic and Magnetic Imager (HMI) on board the Solar Dynamics Observatory (SDO).

**Methods.** The Spatial Possibilistic Clustering Algorithm (SPoCA) is applied to the extreme ultraviolet (EUV) observations obtained from the AIA to segregate coronal features by creating segmentation maps of active regions (ARs), coronal holes (CHs) and the quiet sun (QS). Further, these maps are applied to the full-disk SWAP intensity images and the full-disk (FD) HMI line-of-sight (LOS) magnetograms to isolate the SWAP coronal features and photospheric magnetic counterparts, respectively. We then computed full-disk and feature-wise averages of EUV intensity and line of sight (LOS) magnetic flux density over ARs/CHs/QS/FD. The variability in these quantities is compared with that of LYRA irradiance values.

**Results.** Variations in the quantities resulting from the segmentation, namely the integrated intensity and the total magnetic flux density of ARs/CHs/QS/FD regions, are compared with the LYRA irradiance variations. We find that the EUV intensity over ARs/CHs/QS/FD is well correlated with the underlying magnetic field. In addition, variations in the full-disk integrated intensity and magnetic flux density values are correlated with the LYRA irradiance variations.

**Conclusions.** Using the segmented coronal features observed in the EUV wavelengths as proxies to isolate the underlying magnetic structures is demonstrated in this study. Sophisticated feature identification and segmentation tools are important in providing more insights into the role of various magnetic features in both the short- and long-term changes in the solar irradiance.

### **Origin of the Chromospheric Umbral Waves in Sunspots.**

[Zhang](#), X., Yan, X., Xue, Z. et al.

*Sol Phys* 299, 71 (2024).

<https://doi.org/10.1007/s11207-024-02323-w>

Oscillations are ubiquitous in sunspots and the associated higher atmospheres. However, it is still unclear whether these oscillations are driven by the external acoustic waves (p-modes) or generated by the internal magnetoconvection. To obtain clues about the driving source of umbral waves in sunspots, we analyzed the spiral wave patterns (SWPs) in two sunspots registered by IRIS MgII 2796 Å slit-jaw images. By tracking the motion of the SWPs, we found for the first time that two one-armed SWPs coexist in the umbra, and they can rotate either in the same or opposite directions. Furthermore, by analyzing the spatial distribution of the oscillation centers of the



one-armed SWPs within the umbra (the oscillation center is defined as the location where the SWP first appears), we found that the chromospheric umbral waves repeatedly originate from the regions with high oscillation power and most of the umbral waves occur in the dark nuclei and strong magnetic field regions of the umbra. Our study results indicate that the chromospheric umbral waves are likely excited by the p-mode oscillations.

### **A comparison of co-temporal vector magnetograms obtained with HMI/SDO and SP/Hinode**

[Mei Zhang](#), [Haocheng Zhang](#), [Chengqing Jiang](#)

RAA 2023

<https://arxiv.org/pdf/2310.04720.pdf>

An accurate measurement of magnetic field is very important for understanding the formation and evolution of solar magnetic fields. Currently there are two types of solar magnetic field measurement instruments: the filter-based magnetographs and the Stokes polarimeters. The former gives high temporal resolution magnetograms and the latter provides more accurate measurements of magnetic fields. Calibrating the magnetograms obtained by filter-based magnetographs with those obtained by Stokes polarimeters is a good way to combine the advantages of the two types. Our previous studies have shown that, compared to the magnetograms obtained by the Spectro-Polarimeter (SP) on board Hinode, those magnetograms obtained by both the filter-based Solar Magnetic Field Telescope (SMFT) of the Huairou Solar Observing Station (HSOS) and by the filter-based Michelson Doppler Imager (MDI) aboard SOHO have underestimated the flux densities in their magnetograms and systematic center-to-limb variations present in the magnetograms of both instruments. Here, using a sample of 75 vector magnetograms of stable alpha sunspots, we compare the vector magnetograms obtained by the Helioseismic and Magnetic Imager (HMI) aboard SDO with co-temporal vector magnetograms obtained by SP/Hinode. Our analysis shows that both the longitudinal and transverse flux densities in the HMI/SDO magnetograms are very close to those in the SP/Hinode magnetograms and the systematic center-to-limb variations in the HMI/SDO magnetograms are very minor. Our study suggests that using the filter-based magnetograph to construct a low spectral resolution Stokes profile, as done by HMI/SDO, can largely remove the disadvantages of the filter-type measurements and yet still possess the advantage of high temporal resolution. **2010-07-02, 2010-08-03, 2011-05-22, 2012-10-02**

### **A Babcock-Leighton-type Solar Dynamo Operating in the Bulk of the Convection Zone**

[Zebin Zhang](#), [Jie Jiang](#)

ApJ 2022

<https://arxiv.org/pdf/2204.14077>

The toroidal magnetic field is assumed to be generated in the tachocline in most Babcock-Leighton (BL)-type solar dynamo models, in which the poloidal field is produced by the emergence and subsequent dispersal of sunspot groups. However, magnetic activity of fully convective stars and MHD simulations of global stellar convection have recently raised serious doubts regarding the importance of the tachocline in the generation of the toroidal field. In this study, we aim to develop a new BL-type dynamo model, in which the dynamo operates mainly within the bulk of the convection zone. Our 2D model includes the effect of solar-like differential rotation, one-cell meridional flow, near-surface radial pumping, strong turbulent diffusion, BL-type poloidal source, and nonlinear back-reaction of the magnetic field on its source with a vertical outer boundary condition. The model leads to a simple dipolar configuration of the poloidal field that has the dominant latitudinal component, which is wound up by the latitudinal shear within the bulk of the convection zone to generate the toroidal flux. As a result, the tachocline plays a negligible role in the model. The model reproduces the basic properties of the solar cycle, including (a) approximately 11 yr cycle period and 18 yr extended cycle period; (b) equatorward propagation of the antisymmetric toroidal field starting from high latitudes; and (c) polar field evolution that is consistent with observations. Our model opens the possibility for a paradigm shift in understanding the solar cycle to transition from the classical flux transport dynamo.

### **On estimating the force-freeness based on observed magnetograms**

X. M. [Zhang](#), M. Zhang, J. T. Su

ApJ 2016

<https://arxiv.org/pdf/1611.03190v1.pdf>

It is a common practice in the solar physics community to test whether or not measured photospheric or chromospheric vector magnetograms are force-free, using the Maxwell stress as a measure. Some previous studies have suggested that magnetic fields of active regions in the solar chromosphere are close to be force-free whereas there is no consistency among previous studies on whether magnetic fields of active regions in the solar photosphere are force-free or not. Here we use three kinds of representative magnetic fields (analytical force-free solutions, modeled solar-like force-free fields and observed non-force-free fields) to discuss on how the measurement issues such as limited field of view, instrument sensitivity and measurement error could affect the estimation of force-freeness based on observed magnetograms. Unlike previous studies that focus on discussing the effect of limited field of view or instrument sensitivity, our calculation shows that just measurement error alone can significantly

influence the results of force-freeness estimate, due to the fact that measurement errors in horizontal magnetic fields are usually ten times larger than that of the vertical fields. This property of measurement errors, interacting with the particular form of force-freeness estimate formula, would result in wrong judgments of the force-freeness: a truly force-free field may be mistakenly estimated as being non-force-free and a true non-force-free field may be estimated as being force-free. Our analysis calls for caution when interpreting the force-freeness estimates based on measured magnetograms, and also suggests that the true photospheric magnetic field may be further away from being force-free than they currently appear to be. 2010 May 23: 2007 June 07:

## **Prediction of Solar Coronal Structures Using Fourier Neural Operators Based on the Solar Photospheric Magnetic Field Observation**

Jingmin Zhao, Xueshang Feng

Space Weather [Volume22, Issue5](#) May 2024 e2024SW003875

<https://doi.org/10.1029/2024SW003875>

<https://agupubs.onlinelibrary.wiley.com/doi/epdf/10.1029/2024SW003875>

This paper constructs the structures of the solar corona (SC) using Fourier neural operators (FNO) based on solar photospheric magnetic field observation. The purpose is to learn the mapping between two infinite-dimensional function spaces, which takes the photospheric magnetic field as input and the magnetohydrodynamic (MHD) solar wind plasma parameters as output, from a finite collection of input-output pairs. The FNO-SC model is established using MHD simulated results of 36 Carrington rotations (CRs) from 2008, 2009, and 2020. The performance of the FNO-SC model is tested for 6 CRs during various phases of the solar activity such as descending, minimum, and ascending phases to generate the 3D structures of the SC. With the MHD simulations as references, the average structure similarity index measure (SSIM) value for the magnetic field topology from 1 to 3Rs is around 0.88. From 1 to 20Rs, the SSIM values for the number density and radial speed surpass 0.9. Relative to OMNI observations, the mean absolute percentage error for the radial speed generated from the FNO-SC model does not exceed 0.25. These results indicate that the FNO-SC model effectively captures the solar coronal structures typical of the periods investigated, by recovering the MHD simulations as well as the observations. The FNO-SC model is further trained with enriched data from the maximum phase to assess the capability of modeling such a situation. The FNO-SC model costs 48.7 s for a single CR prediction, and thus facilitates real-time space weather forecasting.

## **Detection of Fast-moving Waves Propagating Outward along Sunspots' Radial Direction in the Photosphere**

Junwei Zhao<sup>1</sup>, Ruizhu Chen<sup>1,2</sup>, Thomas Hartlep<sup>3</sup>, and Alexander G. Kosovichev<sup>4</sup>

2015 ApJ 809 L15

<http://arxiv.org/pdf/1507.04795v1.pdf>

Helioseismic and magnetohydrodynamic waves are abundant in and above sunspots. Through cross-correlating oscillation signals in the photosphere observed by the Solar Dynamics Observatory/Helioseismic and Magnetic Imager, we reconstruct how waves propagate away from virtual wave sources located inside a sunspot. In addition to the usual helioseismic wave, a fast-moving wave is detected traveling along the sunspot's radial direction from the umbra to about 15 Mm beyond the sunspot boundary. The wave has a frequency range of 2.5–4.0 mHz with a phase velocity of 45.3 km s<sup>-1</sup>, substantially faster than the typical speeds of Alfvén and magnetoacoustic waves in the photosphere. The observed phenomenon is consistent with a scenario of that a magnetoacoustic wave is excited at approximately 5 Mm beneath the sunspot. Its wavefront travels to and sweeps across the photosphere with a speed higher than the local magnetoacoustic speed. The fast-moving wave, if truly excited beneath the sunspot's surface, will help open a new window for studying the internal structure and dynamics of sunspots.

## **The Correlation between the Magnetic and Velocity Fields on the Full Solar Disk**

M. Y. Zhao, X. F. Wang and H. Q. Zhang

Solar Physics, Volume 270, Number 1, 23-33, 2011

A possible correlation between the magnetic and velocity fields has been analyzed based on the SOHO/MDI magnetograms and Dopplergrams. It is found that the observed large-scale weak magnetic field (weaker than 50 G (gauss)) is correlated with the velocity statistically. The curves of  $u \cdot b$  with latitude, where  $u$  and  $b$  are the velocity and magnetic fields in a rectangular region ( $\pm 15^\circ$  in longitude,  $\pm 45^\circ$  in latitude) on the Sun, show the same patterns in the years 2000, 2004, and 2007. The patterns indicate that  $u$  and  $b$  are positively correlated near the equator but are anti-correlated at the middle latitudes. For a strong magnetic field between 50 G and 3000 G, the curves of  $u \cdot b$  with latitude show the same tendencies at the middle latitudes. Near the equator, however, the slope of the curve is positive in 2000 and is negative in 2004 and 2007. In addition, we give an estimation for the amplitude of the cross helicity  $h \chi$  ( $h=ub$ ) inferred from the MDI data, which is of the order of 103 G ms<sup>-1</sup> near the center of the solar disk.

## FastQSL: a fast computation method for Quasi-Separatrix Layers

[Peijin Zhang](#), [Jun Chen](#), [Rui Liu](#), [Chuanbing Wang](#)

ApJ 937 26 2022

<https://arxiv.org/pdf/2208.12569.pdf>

<https://iopscience.iop.org/article/10.3847/1538-4357/ac8d61/pdf>

Magnetic reconnection preferentially takes place at the intersection of two separatrices or two quasi-separatrix layers, which can be quantified by the squashing factor  $Q$ , whose calculation is computationally expensive due to the need to trace as many field lines as possible. We developed a method (FastQSL) optimized for obtaining  $Q$  and the twist number in a 3D data cube. FastQSL utilizes the hardware acceleration of the graphic process unit (GPU) and adopts a step-size adaptive scheme for the most computationally intensive part: tracing magnetic field lines. As a result, it achieves a computational efficiency of 4.53 million  $Q$  values per second. FastQSL is open source, and user-friendly for data import, export, and visualization.

## A Double-decker Filament Formation Driven by Sunspot Rotation and Magnetic Reconnection

Yan [Zhang](#)<sup>1,2</sup>, Xiaoli Yan<sup>1,3</sup>, Jincheng Wang<sup>1,3</sup>, Qiaoling Li<sup>4</sup>, Liheng Yang<sup>1,3</sup>, and Zhike Xue<sup>1,3</sup>  
2022 ApJ 933 200

<https://iopscience.iop.org/article/10.3847/1538-4357/ac7391/pdf>

In this paper, through analyzing data from the Solar Dynamics Observatory (SDO) and the Global Oscillation Network Group (GONG), we present a study on the formation of a double-decker filament in NOAA Active Region 12665 from **2017 July 8 to 14**. We find that magnetic reconnection occurs between two smaller filaments to form a longer filament. According to the evolution of the leading sunspot, it is obvious that the sunspot experiences a continuous rotation around its umbra. During the period from 03:00 UT on July 11 to 10:00 UT on July 14, the average speed of sunspot rotation is about  $3.7 \text{ hr}^{-1}$ . The continuous rotation of sunspot stretches the filament and results in the formation of a reversed S-shaped filament. Due to the motion of the magnetic field and internal magnetic reconnection, the filament splits into two branches and forms a double-decker filament structure. In the process of filament separation, internal magnetic reconnection can also accelerate the filament separation. Nonlinear force-free field extrapolation indicates that there are two magnetic flux ropes, which are consistent with the observed results. Eventually, the upper filament erupts and produces an M-class flare and a halo coronal mass ejection.

## Diagnostic of Spectral Lines in Magnetized Solar Atmosphere: Formation of the $H\{\eta\}$ Line in Sunspots

[Hongqi Zhang](#)

SCIENCE CHINA, Physics, Mechanics & Astronomy, November 2020 Vol. 63 No. 11: 119611

<https://arxiv.org/pdf/2009.03573.pdf>

Formation of the  $H\beta \lambda 4861.34 \text{ \AA}$  line is an important topic related to the diagnosis of the basic configuration of magnetic fields in the solar and stellar chromospheres. Specifically, broadening of the  $H\beta \lambda 4861.34 \text{ \AA}$  line occurs due to the magnetic and micro-electric fields in the solar atmosphere. The formation of  $H\beta$  in the model umbral atmosphere is presented based on the assumption of non-local thermodynamic equilibrium. It is found that the model umbral chromosphere is transparent to the Stokes parameters of the  $H\beta$  line, which implies that the observed signals of magnetic fields at sunspot umbrae via the  $H\beta$  line originate from the deep solar atmosphere, where  $|\mu\tau_c| \sim 1$  (about 300 km in the photospheric layer for our calculations). This is in contrast to the observed Stokes signals from non-sunspot areas, which are thought to primarily form in the solar chromosphere.

## From Polarimetry to Helicity: Studies of Solar Magnetic Fields at the Huairou Solar Observing Station **Review**

Hongqi [Zhang](#)

SCIENCE CHINA Physics, Mechanics & Astronomy

2019

<https://arxiv.org/pdf/1912.06557.pdf>

In this paper, we briefly introduce the basic questions in the measurements of solar magnetic fields and the possible error sources due to the approximation of the theory of radiation transfer of spectral lines in the solar atmosphere. We introduce some basic research progress in magnetic field measurement at Huairou Solar Observing Station of National Astronomical Observatories of the Chinese Academy of Sciences, especially concerning the non-potentiality in solar active regions, such as the magnetic shear, current and helicity. We also discuss some basic questions for the measurements of the magnetic fields and corresponding challenges for the future studies. **March 11, 1989, May 10 1991, 1991 June 6, June 9, 1991, 2006 April 28, 2006 May 22**

## Dark structures in sunspot light bridges

Jingwen [Zhang](#), [Hui Tian](#), [Sami K. Solanki](#), [Haimin Wang](#), [Hardi Peter](#), [Kwangsu Ahn](#), [Yan Xu](#), [Yingjie Zhu](#), [Wenda Cao](#), [Jiansen He](#), [Linghua Wang](#)

2018 *ApJ* **865** 29

<https://arxiv.org/pdf/1809.00146.pdf>

We present unprecedented high-resolution TiO images and Fe I 1565 nm spectropolarimetric data of two light bridges taken by the 1.6-m Goode Solar Telescope at Big Bear Solar Observatory. In the first light bridge (LB1), we find striking knot-like dark structures within the central dark lane. Many dark knots show migration away from the penumbra along the light bridge. The sizes, intensity depressions and apparent speeds of their proper motion along the light bridges of 33 dark knots identified from the TiO images are mainly in the ranges of 80~200-km, 30%~50%, and 0.3~1.2-km-s<sup>-1</sup>, respectively. In the second light bridge (LB2), a faint central dark lane and striking transverse intergranular lanes were observed. These intergranular lanes have sizes and intensity depressions comparable to those of the dark knots in LB1, and also migrate away from the penumbra at similar speeds. Our observations reveal that LB2 is made up of a chain of evolving convection cells, as indicated by patches of blue shift surrounded by narrow lanes of red shift. The central dark lane generally corresponds to blueshifts, supporting the previous suggestion of central dark lanes being the top parts of convection upflows. In contrast, the intergranular lanes are associated with redshifts and located at two sides of each convection cell. The magnetic fields are stronger in intergranular lanes than in the central dark lane. These results suggest that these intergranular lanes are manifestations of convergent convective downflows in the light bridge. We also provide evidence that the dark knots observed in LB1 may have a similar origin. **2015 June 20-22**

## Surge-like oscillations above sunspot light bridges driven by magnetoacoustic shocks

Jingwen [Zhang](#), [Hui Tian](#), [Jiansen He](#), [Linghua Wang](#)

*ApJ* **838** 2 2017

<https://arxiv.org/pdf/1702.08585.pdf>

High-resolution observations of the solar chromosphere and transition region often reveal surge-like oscillatory activities above sunspot light bridges. These oscillations are often interpreted as intermittent plasma jets produced by quasi-periodic magnetic reconnection. We have analyzed the oscillations above a light bridge in a sunspot using data taken by the Interface Region Imaging Spectrograph (IRIS). The chromospheric 2796-Å images show surge-like activities above the entire light bridge at any time, forming an oscillating wall. Within the wall we often see that the Mg-II 2796.35-Å line core first experiences a large blueshift, and then gradually decreases to zero shift before increasing to a red shift of comparable magnitude. Such a behavior suggests that the oscillations are highly nonlinear and likely related to shocks. In the 1400-Å passband which samples emission mainly from the Si-IV ion, the most prominent feature is a bright oscillatory front ahead of the surges. We find a positive correlation between the acceleration and maximum velocity of the moving front, which is consistent with numerical simulations of upward propagating slow-mode shock waves. The Si-IV 1402.77-Å line profile is generally enhanced and broadened in the bright front, which might be caused by turbulence generated through compression or by the shocks. These results, together with the fact that the oscillation period stays almost unchanged over a long duration, lead us to propose that the surge-like oscillations above light bridges are caused by shocked p-mode waves leaked from the underlying photosphere. **2015 September 29-30**

## ON ESTIMATING FORCE-FREENESS BASED ON OBSERVED MAGNETOGRAMS

X. M. [Zhang](#)<sup>1,2</sup>, M. Zhang<sup>1</sup>, and J. T. Su<sup>1</sup>

2017 *ApJ* **834** 80

<http://iopscience.iop.org/article/10.3847/1538-4357/834/1/80/pdf>

It is a common practice in the solar physics community to test whether or not measured photospheric or chromospheric vector magnetograms are force-free, using the Maxwell stress as a measure. Some previous studies have suggested that magnetic fields of active regions in the solar chromosphere are close to being force-free whereas there is no consistency among previous studies on whether magnetic fields of active regions in the solar photosphere are force-free or not. Here we use three kinds of representative magnetic fields (analytical force-free solutions, modeled solar-like force-free fields, and observed non-force-free fields) to discuss how measurement issues such as limited field of view (FOV), instrument sensitivity, and measurement error could affect the estimation of force-freeness based on observed magnetograms. Unlike previous studies that focus on discussing the effect of limited FOV or instrument sensitivity, our calculation shows that just measurement error alone can significantly influence the results of estimates of force-freeness, due to the fact that measurement errors in horizontal magnetic fields are usually ten times larger than those in vertical fields. This property of measurement errors, interacting with the particular form of a formula for estimating force-freeness, would result in wrong judgments of the force-freeness: a truly force-free field may be mistakenly estimated as being non-force-free and a truly non-force-free field may be estimated as being force-free. Our analysis calls for caution when interpreting estimates of force-freeness based on measured magnetograms, and also suggests that the true photospheric magnetic field may be further away from being force-free than it currently appears to be.

## **Magnetic Helicity and Energy Spectra of a Solar Active Region**

Hongqi [Zhang](#)<sup>1</sup>, Axel Brandenburg<sup>2,3</sup>, and D. D. Sokoloff

2014 ApJ 784 L45

<http://arxiv.org/pdf/1311.2432v2.pdf>

We compute for the first time the magnetic helicity and energy spectra of the solar active region NOAA 11158 during **2011 February 11-15** at 20° southern heliographic latitude using observational photospheric vector magnetograms. We adopt the isotropic representation of the Fourier-transformed two-point correlation tensor of the magnetic field. The sign of the magnetic helicity turns out to be predominantly positive at all wavenumbers. This sign is consistent with what is theoretically expected for the southern hemisphere. The magnetic helicity normalized to its theoretical maximum value, here referred to as relative helicity, is around 4% and strongest at intermediate wavenumbers of  $k \approx 0.4 \text{ Mm}^{-1}$ , corresponding to a scale of  $2\pi/k \approx 16 \text{ Mm}$ . The same sign and a similar value are also found for the relative current helicity evaluated in real space based on the vertical components of magnetic field and current density. The modulus of the magnetic helicity spectrum shows a  $k^{-11/3}$  power law at large wavenumbers, which implies a  $k^{-5/3}$  spectrum for the modulus of the current helicity. A  $k^{-5/3}$  spectrum is also obtained for the magnetic energy. The energy spectra evaluated separately from the horizontal and vertical fields agree for wavenumbers below  $3 \text{ Mm}^{-1}$ , corresponding to scales above 2 Mm. This gives some justification to our assumption of isotropy and places limits resulting from possible instrumental artifacts at small scales.

## **DISTRIBUTION OF MAGNETIC HELICITY FLUX WITH SOLAR CYCLES**

Hongqi [Zhang](#) and Shangbin Yang

2013 ApJ 763 105

It is normally believed that a magnetic field transfers helicity from the solar subatmosphere into interplanetary space. This is based on the calculation of the injected magnetic helicity near the center of the solar disk between latitude  $\pm 30^\circ$  of both solar hemispheres in the period 1996-2009. As one follows the long-term injection of magnetic helicity, one finds that the transfer of magnetic helicity does not have a monotonic sign in the northern and southern hemispheres, and that the bulk of the helicity contributed goes to the active region, while the contribution to the quiet Sun is insignificant. The consistency between the total injected magnetic helicity and the sunspot numbers has also been found statistically in the solar cycle. The estimated total injected magnetic helicity flux in our calculation is of the order of or larger than  $5.0 \times 10^{46} \text{ Mx}^2$  in the 23rd solar cycle.

## **UBIQUITOUS ROTATING NETWORK MAGNETIC FIELDS AND EXTREME-ULTRAVIOLET CYCLONES IN THE QUIET SUN**

Jun [Zhang](#)<sup>1</sup> and Yang Liu

2011 ApJ 741 L7

We present Solar Dynamics Observatory (SDO) Atmospheric Imaging Assembly (AIA) observations of EUV cyclones in the quiet Sun. These cyclones are rooted in the rotating network magnetic fields (RNFs). Such cyclones can last several to more than 10 hr and, at the later phase, they are found to be associated with EUV brightenings (microflares) and even EUV waves. SDO Helioseismic and Magnetic Imager (HMI) observations show a ubiquitous presence of RNFs. Using HMI line-of-sight magnetograms on 2010 July 8, we find 388 RNFs in an area of  $800 \times 980 \text{ arcsec}^2$  near the disk center where no active region is present. The sense of rotation shows a weak hemisphere preference. The unsigned magnetic flux of the RNFs is about  $4.0 \times 10^{21} \text{ Mx}$ , or 78% of the total network flux. These observational phenomena at small scale reported in this Letter are consistent with those at large scale in active regions. The ubiquitous RNFs and EUV cyclones over the quiet Sun may suggest an effective way to heat the corona.

## **Global analysis of active longitudes of sunspots**

L. [Zhang](#), K. Mursula, I. Usoskin and H. Wang

A&A, Volume 529, A23, May 2011

Context. Active longitudes have been found in various manifestations of solar activity. The longitudinal distribution of, e.g., sunspots and solar X-ray flares shows two persistent preferred longitudes separated by roughly 180 degrees. We previously studied solar X-ray flares using an improved version of a dynamic, differentially rotating coordinate system and found enhanced rotational asymmetry and rotation parameter values that are consistent for the three classes of X-ray flares.

Aims. We aim to find the optimal values of rotation parameters of active longitudes of sunspots for several different time intervals and separately for the two solar hemispheres.

**Methods.** We perform a global study of the longitudinal location of sunspots (all sunspots and first appearance sunspots) using a refined version of a dynamic, differentially rotating coordinate system.

**Results.** We find that the rotation parameters for sunspots are in good agreement with those obtained for X-ray flares using the same method. The improved method typically finds somewhat faster equatorial rotation with better accuracy. The improved treatment also leads to a larger non-axisymmetry. Rotation parameters for all sunspots and first appearances closely agree with each other, but non-axisymmetry is systematically larger for all sunspots than for first appearances, suggesting that strong fields follow more closely the pattern of active longitudes. The refined method emphasizes hemispheric differences in rotation. Over the whole interval, the mean rotation in the southern hemisphere is slower than in the north. We also find significant temporal variability in the two rotation parameters over the 136-year interval. Interestingly, the long-term variations (trends and residual oscillations) in solar rotation are roughly the opposite in the northern and southern hemispheres.

**Conclusions.** Rotation parameters vary differently with time in the northern and southern hemispheres. Both sunspots and flares strongly suggest that the northern hemisphere rotated considerably faster but the southern hemisphere slightly slower than the Carrington rotation rate during the last three solar cycles.

## **Large-scale Soft X-ray Loops and Their Magnetic Chirality in Both Hemispheres**

Hongqi **Zhang**, Shangbin Yang, Yu Gao, Jiangtao Su, D. D. Sokoloff, and K. Kuzanyan

**2010** ApJ 719 1955-1963

The magnetic chirality in the solar atmosphere has been studied based on soft X-ray and magnetic field observations. It is found that some of the large-scale twisted soft X-ray loop systems occur for several months in the solar atmosphere, before the disappearance of the corresponding background large-scale magnetic field. This paper provides observational evidence of the helicity of the large-scale magnetic field in the solar atmosphere and the reverse one relative to the helicity rule in both hemispheres with solar cycles. The transfer of the magnetic helicity from the subatmosphere is consistent with the formation of large-scale twisted soft X-ray loops in both the solar hemispheres.

## **A New Website Hosting HMI Time-Distance Pipeline Products**

Junwei **Zhao** & Ruizhu Chen

HMI Science Nuggets #163 September **2021**

<http://hmi.stanford.edu/hminuggets/?p=3634>

A new website was recently developed to host SDO/HMI's time-distance pipeline products, including real-time far-side images, near-real-time full-disk subsurface flow fields, synoptic subsurface flow maps, long-term near-surface zonal and meridional flows, as well as the interior meridional circulation profile. These results or data cover the period starting from 2010 May 1, when the HMI was commissioned, till the present and are ongoing. The website is at: <http://jsoc.stanford.edu/data/timed>.

## **Automatic Recognition of Sunspots in HSOS Full-Disk Solar Images**

Cui **Zhao**, GangHua Lin, YuanYong Deng, Xiao Yang

Publications of the Astronomical Society of Australia (PASA) **2016**

<http://arxiv.org/pdf/1605.01552v1.pdf>

A procedure is introduced to recognise sunspots automatically in solar full-disk photosphere images obtained from Huairou Solar Observing Station, National Astronomical Observatories of China. The images are first pre-processed through Gaussian algorithm. Sunspots are then recognised by the morphological Bot-hat operation and Otsu threshold. Wrong selection of sunspots is eliminated by a criterion of sunspot properties. Besides, in order to calculate the sunspots areas and the solar centre, the solar limb is extracted by a procedure using morphological closing and erosion operations and setting an adaptive threshold. Results of sunspot recognition reveal that the number of the sunspots detected by our procedure has a quite good agreement with the manual method. The sunspot recognition rate is 95% and error rate is 1.2%. The sunspot areas calculated by our method have high correlation (95%) with the area data from USAF/NOAA.

## **Hooked flare ribbons and flux-rope related QSL footprints**

Jie **Zhao**, Stuart A. Gilchrist, Guillaume Aulanier, Brigitte Schmieder, Etienne Pariat, Hui Li

ApJ **2014**

<http://arxiv.org/pdf/1603.07563v1.pdf>

We studied the magnetic topology of active region 12158 on **2014 September 10** and compared it with the observations before and early in the flare which begins at 17:21 UT (SOL2014-09-10T17:45:00). Our results show that the sigmoidal structure and flare ribbons of this active region observed by SDO/AIA can be well reproduced from a Grad-Rubin non linear force free field extrapolation method. Various inverse-S and -J shaped magnetic field

lines, that surround a coronal flux rope, coincide with the sigmoid as observed in different extreme ultraviolet wavelengths, including its multi-threaded curved ends. Also, the observed distribution of surface currents in the magnetic polarity where it was not prescribed is well reproduced. This validates our numerical implementation and set-up of the Grad-Rubin method. The modeled double inverse-J shaped Quasi-Separatrix Layer (QSL) footprints match the observed flare ribbons during the rising phase of the flare, including their hooked parts. The spiral-like shape of the latter may be related to a complex pre-eruptive flux rope with more than one turn of twist, as obtained in the model. These ribbon-associated flux-rope QSL-footprints are consistent with the new standard flare model in 3D, with the presence of a hyperbolic flux tube located below an inverse tear drop shaped coronal QSL. This is a new step forward forecasting the locations of reconnection and ribbons in solar flares, and the geometrical properties of eruptive flux ropes.

## **NONLINEAR DAMPING OF ALFVÉN WAVES IN THE SOLAR CORONA BELOW 1.5 SOLAR RADII**

J. S. **Zhao**<sup>1,2</sup>, Y. Voitenko<sup>3</sup>, Y. Guo<sup>4</sup>, J. T. Su<sup>2</sup>, and D. J. Wu

2015 ApJ 811 88

Nonthermal velocities measured in the solar corona imply a strong damping of upward-propagating low-frequency  $\lesssim 0.01$  Hz Alfvén waves at heliocentric distances from 1.02 to 1.4 solar radii. We propose a vector Alfvén wave decay as a feasible mechanism for the observed Alfvén wave damping. Contrary to the extensively studied scalar decay, the vector decay does not depend on the wave frequency and can be efficient for low-frequency coronal Alfvén waves. We show that the vector decay is much stronger than the scalar decay and can provide the observed damping of 0.01 Hz coronal Alfvén waves with perpendicular wavelengths of  $\sim 10^4$  km or less. Fully three-dimensional (3D) numerical simulations are needed to capture this decay, whose growth rate is proportional to the vector product of interacting wave vectors.

## **Detection of Fast-Moving Waves Propagating Outward along Sunspots' Radial Direction in the Photosphere**

Junwei **Zhao**

HMI Science Nuggets #43 Sept 2015

<http://hmi.stanford.edu/hminuggets/?p=1290>

A newly discovered, fast-moving wave propagates outward along sunspots' radial direction and may provide new diagnostics of the sunspot subsurface structure. 2011 October 8-12

## **A study of line widths and kinetic parameters of ions in the solar corona**

G. Q. **Zhao**, D. J. Wu, C. B. Wang

Astrophysics and Space Science, 2014

<http://arxiv.org/pdf/1407.5160v1.pdf>

Solar extreme-ultraviolet (EUV) lines emitted by highly charged ions have been extensively studied to discuss the issue of coronal heating and solar wind acceleration. Based on observations of the polar corona by the SUMER/SOHO spectrometer, this paper investigates the relation between the line widths and kinetic parameters of ions. It is shown that there exists a strongly linear correlation between two variables  $(\sigma/\lambda)^2$  and  $M^{-1}$ , where  $\sigma$ ,  $\lambda$  and  $M$  are the half-width of the observed line profile at  $1/e$ , the wavelength and the ion mass, respectively. The Pearson product-moment correlation coefficients exceed 0.9. This finding tends to suggest that the ions from a given height of polar corona have a common temperature and a common non-thermal velocity in terms of existing equation. The temperature and non-thermal velocity are obtained by linear least-square fit. The temperature is around 2.8 MK at heights of 57'' and 102''. The non-thermal velocity is typical 21.6 km s<sup>-1</sup> at height of 57'' and 25.2 km s<sup>-1</sup> at height of 102''.

## **Temporal Evolution of the Magnetic Topology of the NOAA Active Region 11158**

Jie **Zhao**, Hui Li, Etienne Pariat, Brigitte Schmieder, Yang Guo, Thomas Wiegelmann

2014, ApJ, 787 88

<http://arxiv.org/pdf/1404.5004v1.pdf>

We studied the temporal evolution of the magnetic topology of the active region (AR) 11158 based on the reconstructed three-dimensional magnetic fields in the corona. The non-linear force-free field (NLFFF) extrapolation method was applied to the 12 minutes cadence data obtained with the Helioseismic and Magnetic Imager (HMI) onboard the Solar Dynamics Observatory (SDO) during five days. By calculating the squashing degree factor  $Q$  in the volume, the derived quasi-separatrix layers (QSLs) show that this AR has an overall topology, resulting from a magnetic quadrupole, including an hyperbolic flux tube (HFT) configuration which is relatively stable at the time scale of the arc (1–2 hours). A strong QSL, which corresponds to some highly sheared arcades that might be related to

the formation of a ux rope, is prominent just before the **M6.6 and X2.2** ares, respectively. These facts indicate the close relationship between the strong QSL and the high are productivity of AR 11158. In addition, with a close inspection of the topology, we found a small-scale HFT which has an inverse teardrop structure above the aforementioned QSL before the X2.2 are. It indicates the existence of magnetic ux rope at this place. Even though a global con guration (HFT) is recognized in this AR, it turns out that the large-scale HFT only plays a secondary role during the eruption. In nal, we dismiss a trigger based on the breakout model and highlight the central role of the ux rope in the related eruption.

## Measurements of Sunspot Group Tilt Angles Based on SOHO/MDI and SDO/HMI Magnetograms

Shu-Guang **Zeng**<sup>1,2,3</sup>, Ao-Yu Zhao<sup>1,2</sup>, Shuang Yi<sup>1,2</sup>, Sheng Zheng<sup>1,2</sup>, Xiang-Yun Zeng<sup>1,2</sup>, Lin-Hua Deng<sup>4</sup>, and Yao Huang<sup>1,2</sup>  
2024 ApJ 975 210

<https://iopscience.iop.org/article/10.3847/1538-4357/ad7dec/pdf>

The tilt angle of sunspot groups plays a crucial role in solar dynamo models for the generation of the poloidal field, yet the statistical properties of the tilt angle are not fully comprehended. This study employs magnetograms from the Solar and Heliospheric Observatory/Michelson Doppler Imager and Solar Dynamics Observatory/Helioseismic and Magnetic Imager to measure the tilt angles of 11,373 sunspot groups over the period from 2008 to 2023. This comprehensive analysis examines the relationship between the tilt angle and latitude of the sunspot groups, as well as the correlation between the tilt angle and solar cycle strength. The methodology involves calculating tilt angles within the  $\pm 45^\circ$  central meridian distance, comparing mean-based and median-based measurements, and applying specific angular separation criteria. The findings reveal that during solar cycle 24, the tilt angles increase by approximately  $4^\circ$  for every  $10^\circ$  increase in latitude, in line with Joy's law. A significant anticorrelation is observed between the latitude-normalized tilt angle ( $\gamma/|L|$ ) and solar cycle strength. The research also uncovers a substantial hemispheric asymmetry in tilt angle parameters, with the southern hemisphere (mJoy:  $0.23 \pm 0.092 \sim 0.24 \pm 0.074$ ,  $\gamma = 8^\circ.14 \pm 0^\circ.43 \sim 9^\circ.04 \pm 0^\circ.486$ ) consistently showing larger tilt angles than the northern hemisphere (mJoy:  $0.47 \pm 0.096 \sim 0.51 \pm 0.062$ ,  $\gamma = 6^\circ.14 \pm 0^\circ.304 \sim 6^\circ.64 \pm 0^\circ.334$ ).

## Radial profile of sunspot magnetic field on the SDO data

I. **Zhivanovich**, A. A. Solov'ev, V. V. Smirnova, A. RiehoKainen, V. G. Nagnibeda  
*Astrophysics and Space Science* March 2016, 361:102

The spatial distribution of the vertical (with respect to the surface photosphere) magnetic field in a sunspot plays an important role in modeling the temperature-density characteristics of sunspot, in the calculation of its total energy, in the study of magnetic field oscillations of sunspots and in many others tasks. A number of radial field distributions, such as the Broxon's formula, is discussed in the literature, but the generally accepted, "canonical" profile of the vertical field in a sunspot does not exist on today. Magnetograms obtained with the HMI device of the Solar Dynamic Observatory (Scherrer et al. in *Sol. Phys.* 275(1–2):207–227, 2012), due to their high spatial resolution, provide a good opportunity to get closer to solving this problem. We have studied 30 regular round-shaped unipolar sunspots, situated near the center of the solar disk, without any changes of their configuration or the magnetic field strength during a day or two. Four radial cuts were taken on the magnetograms for each of these 30 sunspots. The magnetic field strength measured along a cut was normalized to the maximum value of the field in the sunspot, all distances are measured in units of the radius of the umbra of the sunspot. It is shown that the radial profile of the vertical field averaged over all studied sunspots has a smooth bell-shaped form and can be well described by the analytic formula for a magnetic monopole, with the depth of immersion into the convective zone of the Sun close to the radius of the sunspot umbra.

## The Dynamics of AR 12700 in Its Early Emerging Phase. I. Interchange Reconnection

Sihui **Zhong**<sup>1,2</sup>, Yijun Hou<sup>1,2</sup>, and Jun Zhang<sup>1,2</sup>  
2019 ApJ 876 51

<https://iopscience.iop.org/article/10.3847/1538-4357/ab1083/pdf>

The emergence of active regions (ARs) leads to various dynamic activities. Using high-resolution and long-lasting H $\alpha$  observations from the New Vacuum Solar Telescope, we report the dynamics of NOAA AR 12700 in its emerging phase on **2018 February 26** in detail. In this AR, constant interchange reconnections (IRs) between emerging fibrils and preexisting ones were detected. Driven by the flux emergence, small-scale fibrils observed in H $\alpha$  wavelength continuously emerged at the center of the AR and reconnected with the ambient preexisting fibrils, forming new longer fibrils. We investigate three IR scenarios that occurred over two hours. Specially, the third scenario of reconnection resulted in the formation of longer fibrils that show pronounced rotation motion. To derive the evolution of the magnetic structure during the reconnections, we perform nonlinear force-free field extrapolations. The extrapolated three-dimensional magnetic fields clearly depict a set of almost potential emerging loops, two preexisting flux ropes at 03:00 UT before the second reconnection scenario, and a set of newly formed loops with less twist at 03:48 UT after the third reconnection scenario. All of these extrapolated structures are



consistent with the fibrils detected at the  $H\alpha$  wavelength. The aforementioned observations and extrapolation results suggest that the constant IRs resulted in the magnetic twist being redistributed from preexisting flux ropes toward the newly formed system with longer magnetic structure and weaker twist.

## **Frozen-field Modeling of Coronal Condensations with MPI-AMRVAC I: Demonstration in two-dimensional models**

[Yuhao Zhou](#), [Xiaohong Li](#), [Rony Keppens](#)

ApJ 2024

<https://arxiv.org/pdf/2404.17056>

Large-scale coronal plasma evolutions can be adequately described by magnetohydrodynamics (MHD) equations. However, full multi-dimensional MHD simulations require substantial computational resources. Given the low plasma  $\beta$  in the solar corona, in many coronal studies, it suffices to approximate the magnetic field to remain topologically fixed and effectively conduct one-dimensional (1D) hydrodynamic (HD) simulations instead. This approach is often employed in studies of coronal loops and their liability to form condensations related to thermal instability. While 1D HD simulations along given and fixed field line shapes are convenient and fast, they are difficult to directly compare with multi-dimensional phenomena. Therefore, it is more convenient to solve volume-filling, multi-dimensional versions of the MHD equations where we freeze the magnetic field, transforming it into frozen-field HD (ffHD) equations for simulation. We have incorporated this ffHD module into our open-source MPI-AMRVAC code and tested it using a two-dimensional (2D) evaporation--condensation model to study prominence formation due to radiative losses. The 2D ffHD results are compared with those from actual 2D MHD and pseudo-2D HD simulations, analyzing the differences and their causes. Pseudo-2D studies account for the known {flux tube} expansion effects. Overall, the performance of 2D ffHD is close to that of 2D MHD and pseudo-2D HD. The 2D tests conducted in this paper will be extended in follow-up studies to 3D simulations based on analytical or observational approaches.

## **Toward a fast and consistent approach to model solar magnetic fields in multiple layers**

[Xiaoshuai Zhu](#), [Thomas Wiegelmann](#)

A&A 2021

<https://arxiv.org/pdf/2109.12789.pdf>

**Aims.** We aim to develop a fast and consistent extrapolation method to model multiple layers of the solar atmosphere.

**Methods.** The new approach combines the magnetohydrostatic (MHS) extrapolation which models the solar low atmosphere in a flat box and the nonlinear force-free field (NLFFF) extrapolation which models the solar corona with a chromospheric vector magnetogram deduced from the MHS extrapolation. We test our code with a snapshot of a radiative magnetohydrodynamic simulation of a solar flare. Comparisons are conducted by several metrics quantitatively.

**Results.** Based on a number of test runs, we find out the optimized configuration for the combination of two extrapolations with a 5.8-Mm-high box for the MHS extrapolation and a magnetogram at a height of 1 Mm for the NLFFF extrapolation. The new approach under this configuration is able to reconstruct the magnetic fields in multiple layers accurately and efficiently. Based on figures of merit that are used to assess the performance of different extrapolations (NLFFF extrapolation, MHS extrapolation, and the combined one), we find the combined extrapolation reaches accuracy of the MHS extrapolation which is better than the NLFFF extrapolation. The combined extrapolation is moderately efficient for application to magnetograms with high resolution.

## **The relationship between the 5-min oscillation and 3-min oscillations at the umbral/penumbral sunspot boundary**

Xinping [Zhou](#), Hongfei Liang

[Astrophysics and Space Science](#) March 2017, 362:46

Observations of the main sunspot of AR 11692 were carried out with the 1 m New Vacuum Solar Telescope (NVST) located on the Fuxian Solar Observatory (FSO) in  $H\alpha$  on **March 13, 2013**. The high cadence (up to 12 s)  $H\alpha$  intensity images help us to investigate the relationship between the 5-min oscillation and 3-min oscillation. It is found that running waves, periodically formed at the wave sources within umbra, propagate outward with the shape of partial arcs. The running waves run across the umbra--penumbra boundary and eventually disappear at the edge of penumbra. But there are obvious differences when we measure the period of running waves in different regions of a sunspot. The period is about 150 s when the running waves are located in umbra, which is a typical 3-min oscillation, and the period is about 300 s when the running waves are located in the penumbra, which is a typical 5-min oscillation. On the basis of time-slice images, we conclude that the waves form in the umbral region with the 5-min oscillation period, which can cause the brightness periodicity change in the umbra region with the 3-min period (in fact, is half of 5-min oscillation) and 5-min in the penumbra.

## Spectroscopic Observations of the Solar Corona during the 2017 August 21 Total Solar Eclipse: Comparison of Spectral Line Widths and Doppler Shifts Between Open and Closed Magnetic Structures

[Yingjie Zhu](#), [Shadia R. Habbal](#), [Adalbert Ding](#), [Bryan Yamashiro](#), [Enrico Landi](#), [Benjamin Boe](#), [Sage Constantinou](#), [Michael Nassir](#)

ApJ 966 122 2024

<https://arxiv.org/pdf/2403.10363>

<https://iopscience.iop.org/article/10.3847/1538-4357/ad3424/pdf>

The spectroscopic observations presented here were acquired during the 2017 August 21 total solar eclipse with a three-channel partially multiplexed imaging spectrometer (3PAMIS) operating at extremely high orders ( $> 50$ ). The  $4 R_{\odot}$  extent of the slit in the North-South direction scanned the corona starting from the central meridian out to approximately  $1.0 R_{\odot}$  off the east limb throughout totality. The line widths and Doppler shifts of the Fe X (637.4 nm) and Fe XIV (530.3 nm) emission lines, characteristic of  $1.1 \times 10^6$  K and  $1.8 \times 10^6$  K electron temperatures respectively, varied across the different coronal structures intercepted by the slit. Fe XIV was the dominant emission in the closed fields of an active region and the base of a streamer, with relatively constant 20 - 30 km s $^{-1}$  line widths independent of the height. In contrast, Fe X emission exhibited broader ( $> 40$  km s $^{-1}$ ) line widths in open fields which increased with height, in particular in the polar coronal hole. Inferences of line widths and Doppler shifts were consistent with extreme ultraviolet (EUV) observations from Hinode/EIS, as well as with the near-infrared Fe XIII 1074 nm line observed by CoMP. The differences in the spectral line widths between distinct coronal structures are interpreted as an indication of the predominance of wave heating in open structures versus localized heating in closed structures. This study underscores the unparalleled advantages and the enormous potential of TSE spectroscopy in measuring line widths simultaneously in open and closed fields at high altitudes, with minimal exposure times, stray light levels, and instrumental widths.

## Magneto-hydrostatic Modeling of the Solar Atmosphere

**Review**

[Xiaoshuai Zhu](#), [Thomas Neukirch](#), [Thomas Wiegelmann](#)

Science China Technological Sciences 2022

<https://arxiv.org/pdf/2203.15356>

Understanding structures and evolutions of the magnetic fields and plasma in multiple layers on the Sun is very important. A force-free magnetic field which is an accurate approximation of the solar corona due to the low plasma  $\beta$  has been widely studied and used to model the coronal magnetic structure. While the force-freeness assumption is well satisfied in the solar corona, the lower atmosphere is not force-free given the high plasma  $\beta$ . Therefore, a magneto-hydrostatic (MHS) equilibrium which takes into account plasma forces, such as pressure gradient and gravitational force, is considered to be more appropriate to describe the lower atmosphere. This paper reviews both analytical and numerical extrapolation methods based on the MHS assumption for calculating the magnetic fields and plasma in the solar atmosphere from measured magnetograms.

## Toward a fast and consistent approach to modeling solar magnetic fields in multiple layers

X. Zhu<sup>1</sup> and T. Wiegelmann<sup>2</sup>

A&A 658, A37 (2022)

<https://www.aanda.org/articles/aa/pdf/2022/02/aa41505-21.pdf>

<https://doi.org/10.1051/0004-6361/202141505>

**Aims.** We aim to develop a fast and consistent extrapolation method for modeling multiple layers of the solar atmosphere.

**Methods.** The new approach combines the magneto-hydrostatic (MHS) extrapolation, which models the solar low atmosphere in a flat box, together with the nonlinear force-free field (NLFFF) extrapolation, which models the solar corona with a chromospheric vector magnetogram deduced from the MHS extrapolation. We tested our code with a snapshot of a radiative magneto-hydrodynamic simulation of a solar flare and we conducted quantitative comparisons based on several metrics.

**Results.** Following a number of test runs, we found an optimized configuration for the combination of two extrapolations with a 5.8-Mm-high box for the MHS extrapolation and a magnetogram at a height of 1 Mm for the NLFFF extrapolation. The new approach under this configuration has the capability to reconstruct the magnetic fields in multi-layers accurately and efficiently. Based on figures of merit that are used to assess the performance of different extrapolations (NLFFF extrapolation, MHS extrapolation, and the combined one), we find the combined extrapolation reaches the same level of accuracy as the MHS extrapolation and they are both better than the NLFFF extrapolation. The combined extrapolation is moderately efficient for application to magnetograms with high resolution.

## Preprocessing of vector magnetograms for magneto-hydrostatic extrapolations

[Xiaoshuai Zhu](#), [Thomas Wiegelmann](#), [Bernd Inhester](#)

A&A 644, A57 2020

<https://arxiv.org/pdf/2010.06174.pdf>

<https://www.aanda.org/articles/aa/pdf/2020/12/aa39079-20.pdf>

Context. Understanding the 3D magnetic field as well as the plasma in the chromosphere and transition region is important. One way is to extrapolate the magnetic field and plasma from the routinely measured vector magnetogram on the photosphere based on the assumption of the magnetohydrostatic (MHS) state. However, photospheric data may be inconsistent with the MHS assumption. Therefore, we must study the restriction on the photospheric magnetic field, which is required by the MHS system. Moreover, the data should be transformed accordingly before MHS extrapolations can be applied.

Aims. We aim to obtain a set of surface integrals as criteria for the MHS system and use this set of integrals to preprocess a vector magnetogram.

Methods. By applying Gauss' theorem and assuming an isolated active region on the Sun, we related the magnetic energy and forces in the volume to the surface integral on the photosphere. The same method was applied to obtain restrictions on the photospheric magnetic field as necessary criteria for a MHS system. We used an optimization method to preprocess the data to minimize the deviation from the criteria as well as the measured value.

Results. By applying the virial theorem to the active region, we find the boundary integral that is used to compute the energy of a force-free field usually underestimates the magnetic energy of a large active region. We also find that the MHS assumption only requires the x-, y-component of net Lorentz force and the z-component of net torque to be zero. These zero components are part of Aly's criteria for a force-free field. However, other components of net force and torque can be non-zero values. According to new criteria, we preprocess the magnetogram to make it more consistent with the MHS system and, at the same time close, to the original data. **2013 June 12**

## **Magnetohydrostatic modeling of AR11768 based on a SUNRISE/IMaX vector magnetogram**

[Xiaoshuai Zhu](#), [Thomas Wiegelmann](#), [Sami Solanki](#)

A&A 640, A103 2020

<https://arxiv.org/pdf/2005.14332.pdf>

<https://www.aanda.org/articles/aa/pdf/2020/08/aa37766-20.pdf>

Context. High resolution magnetic field measurements are routinely done only in the solar photosphere. Higher layers like the chromosphere and corona can be modeled by extrapolating the photospheric magnetic field upward. In the solar corona, plasma forces can be neglected and the Lorentz force vanishes. This is not the case in the upper photosphere and chromosphere where magnetic and non-magnetic forces are equally important. One way to deal with this problem is to compute the plasma and magnetic field self-consistently with a magnetohydrostatic (MHS) model.

Aims. We aim to derive the magnetic field, plasma pressure and density of AR11768 by applying the newly developed extrapolation technique to the SUNRISE/IMaX data.

Methods. An optimization method is used for the MHS modeling. The initial conditions consist of a nonlinear force-free field (NLFFF) and a gravity-stratified atmosphere.

Results. In the non-force-free layer, which is spatially resolved by the new code, Lorentz forces are effectively balanced by the gas pressure gradient force and the gravity force. The pressure and density are depleted in strong field regions, which is consistent with observations. Denser plasma, however, is also observed at some parts of the active region edges. In the chromosphere, the fibril-like plasma structures trace the magnetic field nicely. Bright points in SUNRISE/SuFI 3000 {Å} images are often accompanied by the plasma pressure and electric current concentrations. In addition, the average of angle between MHS field lines and the selected chromospheric fibrils is  $11.8^\circ$ , which is smaller than those computed from the NLFFF model ( $15.7^\circ$ ) and linear MHS model ( $20.9^\circ$ ). This indicates that the MHS solution provides a better representation of the magnetic field in the chromosphere. **11-13 June 2013**

## **Testing magnetohydrostatic extrapolation with radiative MHD simulation of a solar flare**

[Xiaoshuai Zhu](#), [Thomas Wiegelmann](#)

A&A 2019

<https://arxiv.org/pdf/1910.03523.pdf>

<https://www.aanda.org/articles/aa/pdf/2019/11/aa36433-19.pdf>

Context. On the sun, the magnetic field vector is measured routinely only in the photosphere. By using these photospheric measurements as boundary condition, we developed the magnetohydrostatic (MHS) extrapolation to model the solar atmosphere. The model makes assumption about the relative importance of magnetic and non-magnetic forces. While the solar corona is force-free, this is not the case in photosphere and chromosphere.

Aim. The model has been tested with an exact equilibria in  $\backslash\text{cite}\{zw18\}$ . Here we present a more challenging and realistic test of our model with radiative MHD simulation of a solar flare.

Methods. By using the optimization method, the MHS model computes self-consistently the magnetic field, plasma pressure and density. The nonlinear force-free field (NLFFF) and gravity stratified atmosphere along the field line

are assumed as the initial condition of the optimization.

Results. Compared with NLFFF, the MHS model gives an improved magnetic field not only in magnitude and direction, but also in the magnetic connectivity. Besides, the MHS model is able to recover the main structure of the plasma in the photosphere and chromosphere.

### **On the extrapolation of magneto-hydro-static equilibria on the sun**

Xiaoshuai **Zhu**, [Thomas Wiegelmann](#)

ApJ 866,130 2018

<https://arxiv.org/pdf/1809.02168.pdf>

[sci-hub.tw/10.3847/1538-4357/aadf7f](http://sci-hub.tw/10.3847/1538-4357/aadf7f)

Modeling the interface region between solar photosphere and corona is challenging, because the relative importance of magnetic and plasma forces change by several orders of magnitude. While the solar corona can be modeled by the force-free assumption, we need to take care about plasma forces (pressure gradient and gravity) in photosphere and chromosphere, here within the magneto-hydro-static (MHS) model. We solve the MHS equations with the help of an optimization principle and use vector magnetogram as boundary condition. Positive pressure and density are ensured by replacing them with two new basic variables. The Lorentz force during optimization is used to update the plasma pressure on the bottom boundary, which makes the new extrapolation works even without pressure measurement on the photosphere. Our code is tested by using a linear MHS model as reference. From the detailed analyses, we find that the newly developed MHS extrapolation recovers the reference model at high accuracy. The MHS extrapolation is, however, numerically more expensive than the nonlinear force-free field (NLFFF) extrapolation and consequently one should limit their application to regions where plasma forces become important, e.g. in a layer of about 2 Mm above the photosphere.

### **A blow out jet caused by the eruption of a magnetic flux rope revealed by forced field extrapolation**

Xiaoshuai **Zhu**, Huaning Wang, Xin Cheng, Chong Huang

ApJL 2017

<https://arxiv.org/pdf/1703.08992.pdf>

We investigate three-dimensional (3D) magnetic structure of a blow out jet originated in the west edge of NOAA Active Region (AR) 11513 on **2012 July 02** through recently developed forced field extrapolation model. The results show that the blow out jet can be interpreted as the eruption of the magnetic flux rope (MFR) consisting of twisted and closed field lines. We further calculate the twist number  $T_w$  and squashing factor  $Q$  of the reconstructed magnetic field and find that the MFR corresponds well with the high  $T_w$  region as seen at 2D cutting plane perpendicular to the axis of the MFR. The outer boundary is also found to have very high  $Q$  values, thus may represent the bright structure at the base of the jet. The twist number of the MFR is estimated to be  $T_w = -1.54 \pm 0.67$ . The kink instability is thus considered as the initiation mechanism of the blow jet due to closing or even exceeding its theoretical threshold. Our results also show that the bright point at the decaying phase is actually comprised of some small loops that are heated by the reconnection occurred above. In summary, the blowout jet is mostly consistent with the scenario proposed by [\cite{mcs10}](#) except that the kink instability is found to be its possible trigger.

### **Forced field extrapolation of the magnetic structure of the Halpha fibrils in solar chromosphere**

Xiaoshuai **Zhu**, Huaning Wang, Zhanle Du, Han He

2016 ApJ 826 51

<http://arxiv.org/pdf/1604.00455v1.pdf>

We present a careful assess of the forced field extrapolation using Solar Dynamics Observatory/Heliioseismic and Magnetic Imager (SDO/HMI) magnetogram. The convergence property is checked by several metrics. The extrapolated field lines below 3600km appear to be aligned with most Halpha fibrils observed by New Vacuum Solar Telescope (NVST). In the region where magnetic energy far larger than potential energy, field lines computed by forced field extrapolation still consistent with the patterns of Halpha fibrils while non-linear force free field (NLFFF) results show large misalignment. The horizontal average of lorentz force ratio shows the forced region where force-free assumption is failed can reach the height of 1400–1800km. The non-force-free state of the chromosphere is also confirmed by recent radiation magnetohydrodynamics (MHD) simulation.

### **FORCED FIELD EXTRAPOLATION: TESTING A MAGNETOHYDRODYNAMIC (MHD) RELAXATION METHOD WITH A FLUX-ROPE EMERGENCE MODEL**

X. S. **Zhu**, H. N. Wang, Z. L. Du, and Y. L. Fan

2013 ApJ 768 119

We undertake an attempt to reconstruct the Sun's non-force-free magnetic field. The solar corona is often considered to be magnetohydrostatic. We solve the full MHD equations with a semi-realistic atmosphere model to attain this stationary state. Our method is tested with a Sun-like model which simulates the emergence of a magnetic flux rope passing from below the photosphere into the corona. Detailed diagnostics shows that our method can model the forced field more successfully than the optimization and potential method, but it still needs to be applied to real data.

## Subphotospheric Resonator and Local Oscillations in Sunspots

Y. Zhugzhda

[Astronomy Letters](#) May 2018, Volume 44, [Issue 5](#), pp 331–336

The conditions under which the subphotospheric slow-wave resonator can be responsible for the local oscillations in a sunspot have been determined. A rich spectrum of local 3-min oscillations can be produced by the subphotospheric resonator only if the magnetic field in the resonator magnetic flux tube is much weaker than the surrounding sunspot magnetic field. Convective upflows of hot plasma in the sunspot magnetic field satisfy this condition. Consequently, there must be a correlation between the local oscillations and umbral dots, because the latter are produced by convective flows. Various modes of operation of the subphotospheric resonator give rise to wave packets of 3-min oscillations and umbral flashes. It is shown that giant local umbral flashes can emerge under certain conditions for the excitation of oscillations in the subphotospheric resonator.

## Local sunspot oscillations and umbral dots

Y. Zhugzhda, R. Sych

Research in Astronomy and Astrophysics (RAA) 2018

<https://arxiv.org/pdf/1804.03874.pdf>

Data analysis of sunspot oscillation based on 6-hr SDO run of observation showed that low frequency ( $0.2 < \nu < 1$  mHz) oscillations are local similar to three and five minute oscillations. The oscillations in the sunspot are concentrated in cells of a few arcsec, each of which has its own oscillation spectrum. The analysis of two scenario for sunspot oscillations leads to conclusion that local sunspot oscillations occur due to subphotospheric resonator for slow mhd waves. Empirical models of sunspot atmosphere and the theory of slow waves in thin magnetic flux tubes is applied to the modeling of subphotospheric resonator. Spectrum of local oscillations consists of a great number of lines. This kind of spectrum can occur only if the subphotospheric resonator is a magnetic tube with a rather weak magnetic field. Magnetic tubes of this sort are umbral dots that appear due to the convective tongues in the monolithic sunspots. The interrelation of local oscillations with umbral dots and wave fronts of traveling waves in sunspots is discussed. **December 08, 2010**

## Spatial power spectrum of the photospheric magnetic field during solar minimum

B. Zieger<sup>1,2</sup>, I. Virtanen<sup>2</sup> and K. Mursula<sup>2</sup>

A&A 623, A51 (2019)

<https://doi.org/10.1051/0004-6361/201834216>

Context. During solar minima the spatial power spectrum of the photospheric magnetic field is dominated by the low-degree zonal (axisymmetric;  $m = 0$ ) harmonic components, reflecting the large polar coronal holes of unipolar magnetic field. However, measuring polar fields is difficult because of the unequal visibility of the two poles during most of the year and the small line-of-sight component of the roughly radial field at high solar latitudes.

Aims. In this paper we derive the spatial power spectrum of the photospheric magnetic field in terms of the harmonic coefficients of the radial component ( $B_r$ ) as well as in terms of the harmonic coefficients of the internal potential (known as Gauss coefficients). We calculate the zonal spatial power spectrum using Mount Wilson Observatory synoptic maps from 1995–1996, during the solar minimum between solar cycles 22 and 23, and investigate how filling or not filling the polar data gaps affects the zonal harmonic coefficients.

Methods. We eliminated the vantage point effect by removing the highest  $5^\circ$  of the measured magnetic field and calculating the latitudinal profile of the zonal median field over the two years, which ensured equal latitudinal data coverage of both solar hemispheres. We then derived the zonal harmonic coefficients using this latitudinal profile of  $B_r$ .

Results. We find that when the polar data gaps are left unfilled, a strong artificial power above  $l = 8$  is produced. Only the first five zonal harmonic coefficients can be considered reliable in this case. Therefore polar filling is essential to obtain a realistic spatial power spectrum. Filling the polar gap with a constant (non-zero) value yields zonal harmonics that are reliable up to  $l = 9$ . We find that the zonal octupole component contributes most to the total spatial power, more than the zonal dipole, even during the solar minimum conditions. This difference is seen more clearly in the case of polar filling. We also prove that the asymmetry of the polar fields during this solar minimum is statistically significant.

Conclusions. Our results emphasize the importance of filling the polar data gaps in order to obtain a correct estimate of the spatial power spectrum of the photospheric field. This helps in estimating the reliability of polar fields and the large-scale structure in synoptic maps of different origin. Our results also verify the asymmetric nature of the polar fields, which is important for the heliospheric magnetic field and for solar dynamo modeling.

## Evolution and Dynamics of Orphan Penumbrae in the Solar Photosphere: Analysis from Multi-instrument Observations

Francesca [Zuccarello](#)<sup>1</sup>, Salvo L. Guglielmino<sup>2,3</sup>, and Paolo Romano

2014 ApJ 787 57

We investigate the dynamics and magnetic properties of orphan penumbrae observed in the solar photosphere to understand the formation process of such structures. We observed two orphan penumbrae in active region NOAA 11089 during a coordinated observing campaign carried out in **2010 July**, involving the Hinode/Solar Optical Telescope (SOT) and Dutch Open Telescope (DOT), benefiting also from continuous observations acquired by the SDO satellite. We follow their evolution during about three days. The two structures form in different ways: one seems to break off the penumbra of a nearby sunspot, the other is formed through the emergence of new flux. Then they fragment while evolving. The SDO Helioseismic and Magnetic Imager measurements indicate the presence of strong line-of-sight motions in the regions occupied by these orphan penumbrae, lasting for several hours and decreasing with time. This is confirmed by SOT spectro-polarimetric measurements of the Fe I 630.2 nm pair. The latter also show that Stokes parameters exhibit significant asymmetries in the orphan penumbral regions, typical of an uncombed filamentary structure. The orphan penumbrae lie above polarity inversion lines, where peculiar plasma motions take place with velocities larger than  $\pm 3$  km s<sup>-1</sup>. The vector magnetic field in these regions is highly inclined, with the average magnetic field strength decreasing with time. The DOT observations in the H $\alpha$  line and SDO Atmospheric Imaging Assembly measurements in the He II 30.4 nm line indicate that there is no counterpart for the orphan penumbrae at midchromospheric heights or above. Our findings suggest that in at least one of the features investigated the emerging flux may be trapped in the low atmospheric layers by the overlying pre-existing fields, forming these filamentary structures.

## ДИФФЕРЕНЦИАЛЬНОЕ ВРАЩЕНИЕ МАГНИТНОГО ПОЛЯ СОЛНЕЧНОЙ КОРОНЫ

[Бадалян](#) О. Г., [Обридко](#) В. Н.

*«Солнечная и солнечно-земная физика – 2015»*, с. 15

We have considered the differential rotation of the solar corona at different distances from the center of the Sun. For this purpose, we calculated the magnetic field in the corona by the standard method at all latitudes up to  $\pm 75^\circ$  with a step of  $5^\circ$  at the distances from 1.0 to 2.45 solar radii for the period 1976–2004. For each day, we calculated the radial and tangential components and, then, found the field strength. The subsequent analysis was carried out using the periodogram technique. For each series of the field magnitudes, we calculated periodograms with a one-year window at a step of 3 solar rotations. Thus, we determined the rotation periods of the corona at 7 distances from the center of the Sun in the range of heliolatitudes under consideration. The results of calculations were used to map the distribution of the rotation periods of the corona at different distances from the center. The maps show how the rotation period changes depending on the distance and on the phase of the activity cycle. It is obtained that the rotation rate is the greatest (the smallest period) at the minimum of the cycle at small distances and the smallest at the middle of the ascending branch at large distances. The strongest differentiability of the rotation is observed at the minimum of the cycle, particularly, at small distances. As the distance increases, the differentiability decreases in all phases of the cycle. According to present-day theories, the rotation of the solar corona reflects the rotation of subphotospheric layers. Higher layers of the corona represent the rotation of deeper layers of the Sun. The results obtained in our work show that either the depth of generation of magnetic fields of various scales or the very process and amplitude of their generation change during an activity cycle.

## ЦИКЛИЧЕСКИЕ ИЗМЕНЕНИЯ ГЛОБАЛЬНОГО МАГНИТНОГО ПОЛЯ СОЛНЦА

[Биленко](#) И.А.

*Пулково «Солнечная и солнечно-земная физика – 2015»*, с. 23

Paper presents and discusses evolution and spatial-temporal distribution of the solar global magnetic field (GMF) and the comparison to that of active regions and radio flux at 2800 MHz during 1976–2013, cycles 21–24. The solar GMF cycle evolution reveals some magnetic structures with spatial and temporal distribution depending on a cycle phase. The results show that in different cycles and at different cycle phases the GMF on the one hand, and active regions, reflecting local magnetic field evolution and radio flux on the other hand have some common features, but at the same time they behave independently. Their interrelations are different at the rising, maximum, and declining phases. This may indicate the difference in their generation sources.

## **ДВИЖЕНИЕ МАГНИТНЫХ ОБРАЗОВАНИЙ В ПОЛУТЕНИ СОЛНЕЧНОГО ПЯТНА И ЕГО ОКРУЖЕНИИ**

**Григорьев В.М., Ермакова Л.В.**

АЖ Том: 95 Номер: 1 Год: **2018** Страницы: 88-96

Элементы магнитной структуры полутени использованы в качестве индикаторов движений в структурных образованиях полутени солнечного пятна и в ее окружении. Материалом для анализа послужили изображения в континууме и магнитограммы продольного поля активной области NOAA 11117, полученные на SDO/HMI. Структуру магнитного поля полутени в первом приближении можно рассматривать как чередование спайнов и межспайновых волокон. В картинной плоскости спайны представляют собой тонкие радиальные образования с более высокой напряженностью и меньшим наклоном вектора магнитного поля по сравнению с окружением. Подтверждено, что спайны появляются на стадии образования полутени как выступы магнитного поля тени пятна на магнитограммах продольного поля и развиваются одновременно с ростом полутени. Выход магнитных элементов из полутени в результате отделения концов спайнов начинается спустя 1 - 1.5 часа после образования спайна. В развитой полутени выход магнитных элементов носит массовый характер, и иногда групповой выход элементов поля образует структуры движущихся лент. Скорости движения магнитных элементов, отделившихся от спайнов, в 2-3 раза меньше скоростей элементов, отделившихся от межспайновых волокон. Полученные результаты согласуются с "непричесанной" моделью магнитного поля полутени.

## **Вариации фактора различия и корреляции солнечных магнитных полей в линиях Fe I 525.02 нм и Na I 589.59 нм по измерениям обсерватории Маунт-Вилсон в 2000–2012 гг.**

**Голубева Елена**

[Солнечно-земная физика \(Том 4 № 2, 2018\)](https://naukaru.ru/ru/nauka/article/20754/view)

<https://naukaru.ru/ru/nauka/article/20754/view>

На основе сопоставления одновременных измерений обсерватории Маунт-Вилсон в двух спектральных линиях анализируются 13-летние вариации фактора различия магнитных полей. Фактор различия и коэффициент корреляции вычисляются как в общем случае, так и в различных диапазонах значений магнитного поля. Рассматриваются изменения обоих параметров. Демонстрируются следующие тенденции: 1) в общем случае имеют место изменения обоих коэффициентов с циклом солнечной активности; 2) зависимости коэффициентов от величины магнитного поля представляют собой нелинейные функции времени, что особенно ярко выражено в поведении фактора различия; 3) анализ общей картины поведения фактора различия дает возможность выделить несколько характерных диапазонов величины магнитного поля. Обсуждаются соответствия между этими диапазонами и известными структурными объектами солнечной атмосферы. Это позволяет прийти к заключению, что зависимости рассматриваемых коэффициентов от величины поля и от времени определяются разнообразием структурных магнитных элементов и их циклическими перестройками. Представленные результаты могут быть полезны при решении проблем интерпретации измерений солнечных магнитных полей и для взаимной калибровки инструментов. Также они представляют интерес для задач формирования однородных продолжительных рядов солнечных магнитных полей по данным из различных источников.

## **Появление активных областей в период завершения 24-го и начала 25-го циклов активности.**

**Григорьев В.М., Ермакова Л.В., Хлыстова А.И.**

Солн.-земн. Физика [Том 8. 2022. № 4](#) С. 29–37.

<https://naukaru.ru/ru/storage/viewWindow/105299>

Изучение пространственно-временной картины появления активных областей и связи их возникновения со структурой и развитием крупномасштабного магнитного поля (КМП) проводилось в период смены 24-го и 25-го циклов солнечной активности. В этот период не отмечается бурного развития активности и поэтому динамика КМП в процессе появления новых активных областей наиболее заметна. Использовались данные SDO/HMI о продольном магнитном поле для определения времени и гелиографических координат места возникновения активной области и ежедневные карты WSO (Wilcox Solar Observatory) для сравнения со структурой КМП. Получены следующие результаты. В переходный период от одного цикла к другому новые активные области возникали в половине случаев на границе раздела полярностей КМП, причем почти исключительно на хейловских границах в соответствующих полусферах и циклах активности. В остальных случаях местом возникновения были униполярные области КМП без видимого преимущества в расположении областей поля по правилу Хейла. Образование активных областей предваряется или сопровождается изменениями в структуре КМП, при этом в тонкой структуре магнитного поля в фотосфере может наблюдаться усиление сетки магнитного поля на пространственном масштабе размера супергранул и более, а также появление малых областей нового магнитного поля обеих полярностей. Возникающие

активные области концентрировались в двух узких долготных зонах, которые покрывали обе полусферы Солнца. Новый цикл начинался в тех же долготных зонах, где затухала активность старого цикла.

### **Асимметрия в появлении лидирующей и последующей полярностей в фотосферном магнитном поле на ранней стадии образования активной области.**

**Григорьев В.М., Ермакова Л.В., Хлыстова А.И.**

Солнечно-земная физика". Т. 6, № 4, С. 3–9. 2020

<https://naukaru.ru/ru/storage/viewWindow/61999>

Эволюция магнитного поля в фотосфере на ранней стадии развития активной области изучалась по данным о продольной компоненте магнитного поля и лучевых скоростях, полученным с помощью SOHO/MDI и SDO/HMI. Визуальная инспекция 48 случаев возникновения активных областей и детальный анализ динамики потоков магнитного поля четырех активных областей показали, что в момент выхода нового магнитного поля первым в фотосфере обнаруживается поле последующей полярности. Асимметрия потоков лидирующей и последующей полярностей сохраняется несколько десятков минут. Наблюдаемая асимметрия магнитных потоков подтверждает результаты численного моделирования выхода магнитного поля активной области в верхних слоях конвективной зоны, выполненного Ремпелем и Ченгом [Rempel, Cheung, 2014].

**04.03.2012, 24.09.2014, 19.06.2018**

### **ПОДЪЕМ ВЕЩЕСТВА И ДИНАМИКА МАГНИТНОГО ПОЛЯ В ФОРМИРУЮЩЕЙСЯ ПОЛУТЕНИ СОЛНЕЧНОГО ПЯТНА**

**ГРИГОРЬЕВ В.М.1, ЕРМАКОВА Л.В.**

АЖ Том: 93Номер: 2 Год: 2016 Страницы: 240

[https://elibrary.ru/download/elibrary\\_25069211\\_36313302.pdf](https://elibrary.ru/download/elibrary_25069211_36313302.pdf)

По материалам космической обсерватории Solar Dynamic Observatory (SDO) изучалось образование полутени ведущего пятна активной области NOAA 11117. Использовались данные о продольном магнитном поле, лучевых скоростях и изображения в континууме, полученные при помощи прибора HMI. Показано, что процессу возникновения полутени предшествует появление локализованных областей подъема вещества, располагающихся между тенью и невозмущенной фотосферой. В течение нескольких минут размеры областей подъема достигают  $1.5 \times 2$  , а скорость возрастает до 1 км/с. Картина локализованных подъемов сменяется появлением области горизонтального оттока вещества из полутени (эффект Эвершеда). Впервые прослежено формирование отдельного спайна - структурного элемента магнитного поля полутени, представляющего собой тонкое радиальное образование более высокой напряженности и меньшего наклона по сравнению с окружением. Формирование спайна проявляется как возникновение области усиливающегося подъема вещества размером  $2 \times 3$  вблизи тени пятна, появление выступа в изолиниях продольного поля по одну сторону от эпицентра подъема и последующее появление магнитного полюса противоположной полярности на другой стороне области подъема. Процесс сопровождается образованием изгиба изофоты, очерчивающей границу невозмущенной фотосферы, в силу чего эпицентр подъема попадает в зону более высокой яркости. Возможная интерпретация - подъем горячей магнитной трубки. Появление и рост спайна приводит к возникновению полутени пятна.

### **ИССЛЕДОВАНИЕ ВАРИАЦИЙ МАГНИТНОГО ПОЛЯ, СОПРОВОЖДАЮЩИХ ЭРУПТИВНОЕ СОБЫТИЕ 7 ИЮНЯ 2011 Г., С ИСПОЛЬЗОВАНИЕМ НЕЛИНЕЙНОЙ БЕССИЛОВОЙ ЭКСТРАПОЛЯЦИИ ПОЛЯ**

**Егоров Я.И., Файнштейн В.Г., Мышьяков И.И., Анфиногентов С.А.,**

Руденко Г.В.

Астрономия-2018 Том 2 Солнечно-земная физика – современное состояние и перспективы Стр. 78

<http://www.izmiran.ru/library/eaas2018/eaas-2018-2.pdf>

### **МОЩНЫЕ ПОЯРЧЕНИЯ И ЛОКАЛЬНЫЕ КОЛЕБАНИЯ В СОЛНЕЧНЫХ ПЯТНАХ**

**ЖУГЖДА Ю.Д.1, СЫЧ Р.А.**

ПАЖ Том: 45 Номер: 3 Год: 2019 Страницы: 211-219

Анализ наблюдений колебаний в пятне по данным SDO AIA длительностью 6 ч показал, что мощные поярчения в пятнах возникают в ячейках локальных колебаний. Обнаружено, что спектр локальных колебаний искажается короткими импульсами, создаваемыми мощными поярчениями. Для одного из одиночных поярчений удалось выделить неискаженный спектр локальных колебаний для этой ячейки. Оказалось, что поярчение возникает на фоне локальных трехминутных колебаний. Сопоставление наблюдений в каналах 1600 А и 1700 А показало, что самые мощные поярчения возникают на уровне верхней фотосферы ниже температурного минимума. Мощные поярчения в пятнах наблюдаются в виде



одиночных или повторяющихся с интервалом порядка двадцати минут коротких импульсов. Это отличает их от давно известных менее мощных поярчений, представляющих собой цепи импульсов с интервалами порядка трех минут. Оба типа поярчений находят свое объяснение в рамках гипотезы о существовании подфотосферного резонатора на медленных волнах и различных режимах его работы.

### **Модель локальных колебаний в солнечных пятнах**

Ю. Д. Жугжда, Р. А. Сыч

Письма в Астрономический журнал, - 2014, Т. 40, #9, С. 638-656

[http://www.researchgate.net/publication/265132033\\_Model\\_of\\_Local\\_Oscillations\\_in\\_Sunspots](http://www.researchgate.net/publication/265132033_Model_of_Local_Oscillations_in_Sunspots)

Проведен анализ свойств колебаний в пятне на основе данных наблюдений SDO длительностью 6 ч. Оказалось, что спектр трехминутных колебаний состоит из десятков спектральных линий. Ширины линий находятся на пределе спектрального разрешения. Колебания в пятне разбиты на отдельные участки размером в несколько угловых секунд, каждый из которых имеет свой собственный спектр колебаний. Эти свойства колебаний не могут быть объяснены в рамках существующих моделей, основанных на предположении, что пятно колеблется как целое. Предложена модель локальных колебаний, которая объясняет сложный спектр колебаний и локальность колебаний. Показано, что кроме хромосферного резонатора существует подфотосферный резонатор для медленных МГД волн. В рамках модели Паркера наличие этого резонансного слоя позволяет объяснить локальность колебаний и их сложный спектр.

### **ИССЛЕДОВАНИЕ МАГНИТНЫХ СВОЙСТВ ТЕНИ СОЛНЕЧНЫХ ПЯТЕН**

Загайнова Ю. С., Файнштейн В. Г., Обридко В. Н., Руденко Г. В.

АЖ Том: 99Номер: 2 Год: 2022 Страницы: 100-150

Представлены результаты исследования солнечных пятен, полученные авторами обзора и другими исследователями за последние годы. В работе обсуждаются результаты исследования атмосферы над тенью пятен по данным наблюдений в спектральных линиях верхней хромосферы и нижней короны. Показано, что отдельные параметры профиля этих линий различаются в ведущих и замыкающих пятнах. Высказана и проверена гипотеза о связи параметров профилей этих спектральных линий с параметрами магнитного поля в тени пятен. Проведен сравнительный анализ магнитных свойств тени ведущих и замыкающих пятен в активных областях (АО) без взрывных процессов (ВП). Для анализа отобраны только пары магнитно-связанных ведущих и замыкающих пятен, т.е. соединенных силовыми линиями магнитного поля. Показано, что значения ряда параметров магнитного поля в тени солнечных пятен и характер связи между ними зависят от типа пятен. Так, в тени ведущих и замыкающих пятен близкой площади различаются максимальное и среднее значения магнитной индукции...

### **СРАВНЕНИЕ МАГНИТНЫХ СВОЙСТВ ВЕДУЩИХ И ЗАМЫКАЮЩИХ ПЯТЕН И УЛЬТРАФИОЛЕТОВОГО ИЗЛУЧЕНИЯ НАД НИМИ**

Загайнова Ю.С., Файнштейн В.Г., Обридко В.Н., Руденко Г.В.

АЖ Том: 94Номер: 6 Год: 2017 Страницы: 537-554

[https://elibrary.ru/download/elibrary\\_29303596\\_54755227.pdf](https://elibrary.ru/download/elibrary_29303596_54755227.pdf)

По данным инструментов SDO/HMI и SDO/AIA для 24 цикла солнечной активности с помощью более быстрого и точного метода решения проблемы  $\pi$ -неопределенности направления поперечного компонента фотосферного магнитного поля получены новые и подтверждены некоторые предыдущие результаты о магнитных свойствах ведущих и замыкающих магнитно-связанных и одиночных пятен. Показано, что в пределах тени минимальный угол наклона силовой линии поля к положительной нормали к поверхности Солнца  $\alpha_{\min}$  меньше в ведущих пятнах по сравнению с замыкающими в 78% рассмотренных пар пятен, а средний угол  $\alpha$  - в 83%. Выявлена положительная корреляция между  $\alpha_{\min}$  в ведущих и замыкающих пятнах, а также между  $\alpha$  в этих типах пятен. В среднем, в тени пятна с ростом максимума магнитной индукции  $B_{\max}$ , ее среднего значения  $B$ , площади тени  $S$ , углы  $\alpha_{\min}$  и  $\alpha$  уменьшаются в пятнах обоих типов. Подтверждено существование положительной корреляции между  $B_{\max}$  и  $S$ , и выявлена положительная корреляция между  $B$  и  $S$  в ведущих и замыкающих пятнах. Магнитные свойства тени магнитно-связанных пар пятен сопоставлены с контрастом C304 излучения в линии He II 304 над их тенью. Показано, что для пятен, удовлетворяющих определенным условиям, существует положительная корреляция между C304-L и  $\alpha_L$  для ведущих (L) пятен, и между C304-L/C304-F и  $l_L/l_F$ , где  $l_L$  ( $l_F$ ) -длина части силовой линии, соединяющей пятна, из тени ведущего (L) или замыкающего (F) пятна до вершины силовой линии.

### **ВАРИАЦИИ МАГНИТНОГО ПОЛЯ В ТЕНИ ОДИНОЧНЫХ И МАГНИТНО-СВЯЗАННЫХ ПЯТЕН ПРИ ИХ ПРОХОЖДЕНИИ ПО ДИСКУ СОЛНЦА**

Загайнова Ю.С.1, Файнштейн В.Г.2, Обридко В.Н.1,

Руденко В.Г.2, Анфиногентов С.А.2

Пулково «Солнечная и солнечно-земная физика – 2015», с.145

We study the time variations in maximum and mean values of magnetic induction as well as minimum and average angles between the field direction and the radial direction from the center of the Sun in the umbra of single sunspots and magnetically connected leaders and followers during their passage across the solar disk. Dynamics of the area of

these sunspots is also analyzed. We establish correlations between these parameters measured at different instants of time. Using the active region NOAA 11330 as an example, we show that the evolution of magnetic features of the umbra of magnetically connected leaders and followers can be complicated.

## **СРАВНИТЕЛЬНЫЙ АНАЛИЗ СВОЙСТВ МАГНИТНОГО ПОЛЯ В ВЕДУЩИХ И ЗАМЫКАЮЩИХ СОЛНЕЧНЫХ ПЯТНАХ**

**ЗАГАЙНОВА Ю.С.1, ФАЙНШТЕЙН В.Г.2, РУДЕНКО Г.В.2, ОБРИДКО В.Н.**

АЖ Том: 92 Номер: 2 Год: **2015** Страницы: 180-189

[https://elibrary.ru/download/elibrary\\_22840794\\_53955972.pdf](https://elibrary.ru/download/elibrary_22840794_53955972.pdf)

С использованием расчетов по данным SOLIS магнитного поля в потенциальном приближении, опирающихся на -технологию (Руденко, 2001), и данных SDO отобраны для периода 2010–2013 гг. пары ведущих и замыкающих солнечных пятен, тени которых соединены силовыми линиями магнитного поля. Форма силовой линии в некоторой степени отражает форму магнитной трубки, связывающей ведущие и замыкающие пятна. В тени всех отобранных пятен определены минимальный угол между силовой линией и радиальным направлением, максимальное значение магнитной индукции, длина участка силовой линии из ведущего пятна до вершины силовой линии, где радиальная компонента поля равна нулю, и длина от вершины силовой линии до ее восточного основания. Обнаружено, что в случаях минимальный угол между силовой линией и радиальным направлением в ведущем пятне меньше, чем в замыкающем. Для солнечных пятен, удовлетворяющих этому условию, между значениями этого угла в ведущих и замыкающих пятнах выявлена положительная корреляция. Показано, что зависимость угла от площади тени в ведущих и замыкающих пятнах различается. Обнаружена слабая отрицательная корреляция между значениями угла и максимальным значением магнитной индукции. Другими словами, в магнитных трубках, формирующих тени как ведущих, так и замыкающих пятен, и имеющих на уровне фотосферы более сильные поля, в среднем силовые линии оказываются более радиальными. В случаях к ведущему пятну примыкает участок силовой линии меньшей длины, чем. Похожие результаты получены для крупных одиночных пятен.

## **Наблюдательные характеристики колебательно-волновых процессов в пятне и его окрестностях. Сложности наблюдений и интерпретации.**

**Кобанов Н.И., Челпанов А.А.**

С-3 физика Том 10 № 1, 2024 С. 4–11.

<https://naukaru.ru/ru/storage/viewWindow/148029>

В настоящей статье обобщается опыт, полученный авторами в разные годы при исследовании колебательных процессов в солнечных пятнах, включая тень, полутень и ближайшие окрестности. В работе анализируется ряд факторов, затрудняющих адекватное определение некоторых характеристик распространяющихся колебаний, что может приводить к неправильной интерпретации. На примере бегущих волн полутени показано, что их распространение в строго горизонтальном направлении, сопровождаемое при этом понижением частоты, является кажущимся. Эффект вызван тем, что разные колебания распространяются вдоль разных линий магнитного поля с постепенно увеличивающимся наклоном. Это заключение справедливо и для трехминутных колебаний в хромосфере тени пятна. Изменение наклона полос на полутоновых диаграммах пространство—время, используемых для определения скорости распространения колебаний вдоль корональных петель, вызвано проекционным эффектом, а не реальным изменением скорости. Авторы предлагают использовать вспыхивающую модуляцию амплитуды собственных колебаний среды [Chelpanov, Kobanov, 2021] для устранения неопределенностей, возникающих при измерении фазовой разности одноименных сигналов, по которой судят о скорости распространения волновых возмущений в солнечной атмосфере. **2022-10-03, 2022-11-10**

## **ИНВЕРСИЯ МАГНИТНОГО ПОЛЯ СОЛНЦА В 24-М ЦИКЛЕ**

**МОРДВИНОВ А.В.1, ПЕВЦОВ А.А.2, БЕРТЕЛЛО Л.2, ПЕТРИ Г.ДЖ.Д**

С-3 физика Том: 2 Номер: 1 Год: **2016** Страницы: 3-13

[https://elibrary.ru/download/elibrary\\_26001939\\_30119759.pdf](https://elibrary.ru/download/elibrary_26001939_30119759.pdf)

Анализ синоптических данных, полученных с помощью векторного спектромагнитографа (VSM) оптических долговременных исследований Солнца (SOLIS) и НАСА/НСО спектромагнитографа на вакуумном телескопе обсерватории Китт-Пик, показывает, что инверсия магнитных полей на Солнце обнаруживают элементы стохастического процесса, который может включать развитие особых структур всплывающего магнитного потока и асимметрию активности северного и южного полушарий. Присутствие

таких неоднородностей делает моделирование и прогнозирование переполнюсовок полярного поля крайне затруднительными, если вообще возможными. В классической модели цикла солнечной активности униполярные магнитные области (УМО) с полями преимущественно хвостовой полярности двигаются по направлению к полюсу благодаря меридиональным потокам и диффузии. УМО постепенно приводят к исчезновению полярного магнитного поля предыдущего цикла и к формированию полярного поля противоположной полярности. Однако мы показываем, что эту детерминистскую картину может легко изменить развитие мощного центра активности, или всплытие сверхбольшой активной области, или образование «стратегически расположенной» корональной дыры. Мы показываем, что активность, имеющая место в 24 цикле, возможно, является результатом этой хаотичности в эволюции поверхностного магнитного поля Солнца.

## СОТНОШЕНИЕ ПЛОЩАДЕЙ СОЛНЕЧНОГО ПЯТНА И ЕГО ТЕНИ: ДВЕ ПОПУЛЯЦИИ ГРУПП СОЛНЕЧНЫХ ПЯТЕН

**НАГОВИЦЫН Ю.А.**

ПАЖ Том: 50 Номер: 5 Год: 2024 Страницы: 372-376

Рассмотрены группы солнечных пятен гринвичского типа 0 -- одиночные пятна. Показано, что, кроме ранее отмеченных свойств групп пятен, разделяющихся на две популяции: крупных долгоживущих LLG и мелких короткоживущих SSG, такие группы -- одиночные пятна -- различаются характером связи общей площади пятна с площадью тени  $U$ . Отношение  $S/U$  для всей популяции LLG этого класса может считаться постоянным и составляет  $Q_{LLG} = 5.756 \pm 0.039$ . Соотношение и для популяции SSG определяется степенным законом  $= (5.569 \pm 0.093)U^{0.8957 \pm 0.0040}$ . Различие у популяций структурных свойств пятен вместе с другими, найденными ранее различиями их физических свойств, не противоречит гипотезе о формировании магнитного потока двух разных популяций пятен в разных зонах: глубинном тахоклине и приповерхностном лептоклине.

## ОСОБЕННОСТИ ПРАВИЛА ГНЕВЫШЕВА–ВАЛЬДМАЙЕРА ДЛЯ РАЗЛИЧНЫХ ВРЕМЕН ЖИЗНИ И ПЛОЩАДЕЙ ГРУПП СОЛНЕЧНЫХ ПЯТЕН

**НАГОВИЦЫН Ю.А.** 1,2, **ИВАНОВ В.Г.**, **ОСИПОВА А.А.** 1

ПАЖ Том: 45 Номер: 10 Год: 2019 Страницы: 749-754

С использованием «Каталога солнечной деятельности» Р.С. Гневывшевой (1954–1978 гг.) правило Гневывшева–Вальдмайера исследовано по выборке из 7696 нереккуррентных и 566 рекуррентных групп солнечных пятен. Максимальное зафиксированное время жизни группы составило 160 дней. Общее для всех времен жизни правило Гневывшева–Вальдмайера имеет форму  $A_{max} = (12.1 \pm 0.70)LT$  ( $A_{max}$  - максимальная площадь группы за время существования,  $LT$  - время жизни группы). Однако оказалось, что общее правило отклоняется от полученной линейной формы для популяции короткоживущих мелких групп пятен SSG: оно имеет значимый нелинейный скейлинговый вид  $A_{max} = (8.02 \pm 0.41)LT^{(1.105 \pm 0.022)}$ . Для популяции долгоживущих крупных групп пятен LLG имеет место линейная форма  $A_{max} = (12.9 \pm 1.1)LT$ . Рассмотрение только рекуррентных групп с временами жизни больше 40 дней дает значение  $A_{max} = (13.93 \pm 0.41)LT$ .

## ДВЕ ПОПУЛЯЦИИ СОЛНЕЧНЫХ ПЯТЕН И ВЕКОВЫЕ ИЗМЕНЕНИЯ ИХ ХАРАКТЕРИСТИК

Ю. А. **Наговицын**<sup>1, 2\*</sup>, А. А. Певцов<sup>3</sup>, А. А. Осипова<sup>1</sup>,

А. Г. Тлатов<sup>1</sup>, Е. В. Милецкий<sup>1</sup>, Е. Ю. Наговицына<sup>1</sup>

ПИСЬМА В АСТРОНОМИЧЕСКИЙ ЖУРНАЛ, 2016, том 42, №10, с. 773–782

[https://elibrary.ru/download/elibrary\\_26601047\\_21072518.pdf](https://elibrary.ru/download/elibrary_26601047_21072518.pdf)

Исследуются магнитные поля и полные площади средне- и низкоширотных солнечных пятен на основе наблюдений в обсерваториях Гринвич, Кисловодск (площади пятен); Маунт-Вилсон, КрАО, Пулково, Урал, ИМИС, Уссурийск, ИЗМИРАН, Шемаха (магнитные поля). Показано, что в линейной форме зависимости логарифма полной площади пятна  $S$  от его центрального магнитного поля  $H$  коэффициенты изменяются со временем. На двумерной гистограмме встречаемости в осях  $H - \log S$  выявляются две популяции пятен: мелкие и крупные, разделенные границами  $\log S = 1.6$  ( $S = 40$  мдп) и  $H = 2050$  Гс. Рассмотрение пятенного магнитного потока выявляет с высокой степенью достоверности существование двух логнормально распределенных популяций со средней границей между ними  $\Phi = 1021$  Мх. В то же время положения максимумов встречаемости значений потока у популяций изменяются на вековой шкале: у мелких пятен в 4.5 раза, у крупных — в 1.15 раза. Подтверждено, что пятна образуют две физически различающиеся популяции, и показано, что свойства этих популяций заметно изменяются со временем. Это согласуется с гипотезой о существовании двух зон генерации пятенного магнитного поля на Солнце в свете пространственно-распределенного динамо.

## Свойства долгопериодических колебаний солнечных пятен

Ю. А. **Наговицын**, А. Л. Рыбак

Астрономический журнал, - 2014, С. 392-398

Показано, что неучет движения пятна в картинной плоскости по пикселям магнитограмм, полученных на MDI SOHO, в вертикальном направлении приводит к обнаружению ложных периодов долгопериодических колебаний магнитного поля пятен (-артефакт) с периодами 700–1300 мин вблизи центрального меридиана. Наблюдаемая мода колебаний, которую Ефремов, Парфиненко и Соловьев в опубликованной ими в 2012 г. работе считают предельной низкочастотной модой пятна, — артефакт. Предложен способ контроля этого артефакта с помощью вейвлет-преобразования, позволяющий исследовать периоды колебаний в диапазоне мин. По наблюдениям 45 пятен построена экспериментальная картина зависимости частоты колебаний магнитного поля пятна от его напряженности. Картина имеет многомодовый характер и не противоречит предыдущим данным наземных исследований. Предложена интерпретация полученной картины, основанная на существовании четырех геометрических мод колебаний, обнаруженных ранее.

## СОЛНЕЧНАЯ КОРОНА КАК ИНДИКАТОР ДИФФЕРЕНЦИАЛЬНОГО ВРАЩЕНИЯ ПОДФОТОСФЕРНЫХ СЛОЕВ

*Обридо В.Н., Бадалян О.Г.*

КОСМИЧЕСКИЕ ИССЛЕДОВАНИЯ Том: 57Номер: 6 Год: 2019 Страницы: 423-429

DOI: [10.1134/S0023420619060050](https://doi.org/10.1134/S0023420619060050)

В работах [2–4] мы предложили метод использования магнитного поля короны как неявного трассера для изучения дифференциального вращения солнечной короны. Практически, в настоящее время это единственная возможность изучения вращения Солнца на больших гелиоцентрических расстояниях вплоть до поверхности источника. В данной работе расчеты магнитного поля в короне были распространены на больший временной интервал, до 31.XII.2015. Нами показано, что солнечная корона вращается дифференциально на всех гелиоцентрических расстояниях от основания короны до поверхности источника. С увеличением расстояния степень дифференциальности уменьшается. По мере приближения к поверхности источника вращение короны постепенно приближается к твердотельному, но даже на больших расстояниях остается слабо дифференциальным. Мы предполагаем, что дифференциальное вращение короны отражает вращение глубоких подфотосферных слоев. В таком случае изменение характеристик вращения короны может быть использовано как индикатор дифференциального вращения подфотосферных слоев. Мы сопоставили изменение характеристик вращения короны с расстоянием с данными, полученными методами гелиосейсмологии. Получено удовлетворительное соответствие с данными гелиосейсмологии. Впервые изучена вариация дифференциального вращения подфотосферных слоев с фазой цикла.

## НЕОБЫЧНОЕ СВЕТЛОЕ ОБРАЗОВАНИЕ В ТЕНИ ПЯТНА NOAA 12109. НАБЛЮДЕНИЯ И ПРЕДВАРИТЕЛЬНЫЕ РЕЗУЛЬТАТЫ

О. А. **Ожогина**

ПАЖ Том: 45Номер: 9 Год: 2019 Страницы: 673-680

DOI: [10.1134/S0320010819090031](https://doi.org/10.1134/S0320010819090031)

Двенадцатого июля 2014 г. на горизонтальном солнечном телескопе Саянской обсерватории проводились наблюдения необычного светлого образования в тени пятна NOAA 12109. От традиционных светлых мостов оно отличалось тем, что находилось целиком внутри тени без видимой связи с полутенью или фотосферой. По внешнему виду наблюдавшееся светлое образование больше напоминает светлый “остров”. Проведено сканирование в двух спектральных диапазонах: ультрафиолетовом (3930–3975 Å) и инфракрасном (8490–8560 Å). По полученным спектрограммам построены изображения в обоих континуумах, двух линиях Ca II (8498 Å и 3933.6 Å) и четырех слабых линиях (3963.7 Å Cr I, 3969.3 Å Fe I, 8514.1 Å Fe I, 8556.8 Å Si I). Получено, что контраст образования зависит от спектрального диапазона и падает с высотой. В светлом образовании обнаружены восходящие лучевые скорости порядка 500 м/с по инфракрасным линиям и до 3000 м/с по ультрафиолетовым относительно тени пятна, в которой, в свою очередь, наблюдались нисходящие (до 1000 м/с) потоки относительно окружавших пятно участков спокойного солнца.

## НАБЛЮДЕНИЕ НЕОБЫЧНОГО СВЕТОВОГО ОБРАЗОВАНИЯ В ТЕНИ ПЯТНА NOAA 12109

**Ожогина**1 О.А.

Астрономия-2018 Том 2 Солнечно-земная физика – современное состояние и перспективы С.182

<http://www.izmiran.ru/library/eaas2018/eaas-2018-2.pdf>

On July 12, 2014, an unusual light structure was observed in the NOAA 12109 sunspot umbra. Unlike the well-known light bridges, it did not have an outlet to the penumbra. Spectrograms were obtained in two spectral ranges: infrared (8490 - 8550 Å) and ultraviolet (3930 - 3970 Å). Images are constructed in continua, in spectral lines and light of sight velocities. Comparison with SDO data has been made.

## ДИФФЕРЕНЦИАЛЬНОЕ ВРАЩЕНИЕ КРУПНЫХ ДОЛГОЖИВУЩИХ ГРУПП СОЛНЕЧНЫХ ПЯТЕН И ИХ МОРФОЛОГИЧЕСКАЯ СТРУКТУРА

ОСИПОВА А.А.\*<sup>1</sup>, НАГОВИЦЫН Ю.А.

ПАЖ Том: 48Номер: 11 Год: 2022 Страницы: 786-791

Наговицын и др. (2018) выявили две моды зависимости скорости вращения крупных долгоживущих групп солнечных пятен от широты, однако чем именно объясняется феномен двухкомпонентности, осталось необъясненным. В данной работе проверяется предположение о связи скорости дифференциального вращения таких групп с их морфологической структурой. Используются данные Гринвичской обсерватории за промежуток времени 1874–1976 гг. Получено, что кривая дифференциального вращения более быстрой моды крупных долгоживущих групп пятен LLG1 совпадает с кривой дифференциального вращения, полученной для групп, растянутых по долготе (streams), а кривая вращения более медленной моды LLG2 – для групп, состоящих из одного пятна или кластера пятен (singles).

### О наличии систематической ошибки в данных SDO/HMI

**Руденко** Георгий Владимирович, [Дмитриенко Ирина Сергеевна](#)

Журнал: [Солнечно-земная физика \(Том 4 № 2, 2018\)](#), 3-10

<https://naukaru.ru/ru/nauka/article/19351/view#article-info>

Показано наличие систематической ошибки в векторных магнитных данных SDO/HMI (ге-лиосейсмический и магнитный имиджер на борту Обсерватории солнечной динамики (Solar Dynamical Observatory, SDO)), обнаруживающей себя в отклонении от радиального направления узелковых магнитных полей, проявляющихся на магнитограммах в виде мелких зерен сильного магнитного поля. Величина этого отклонения характеризуется зависимостью от расстояния до центра диска, что не может быть свойством магнитного поля, а привнесено в данные искусственно. Предлагается простой способ коррекции векторных магнитограмм, устраняющий обнаруженную систематическую ошибку.

### Определение пространственной структуры коронального магнитного поля солнечных активных областей

Г. В. **Руденко**, И. И. Мышьяков, С. А. Анфиногентов

Астрономический журнал, 90(8) - 2013, С. 676-691

Показана принципиальная возможность качественного устранения возникающей при солнечных векторных магнитографических измерениях так называемой -неопределенности поперечного магнитного поля, причем вне зависимости от положения векторных магнитограмм на солнечном диске. Исправленные магнитограммы в дальнейшем используются в качестве граничных условий при восстановлении трехмерной структуры магнитного поля. Рассчитанные силовые линии хорошо согласуются с реальной непотенциальной петлевой структурой. Для устранения -неопределенности используется модифицированный алгоритм Metropolis, адаптированный для работы в сферической геометрии. Пространственная структура магнитного поля рассчитывается в нелинейном бессиловом приближении с помощью оптимизационного метода. Представлены результаты тестирования нового алгоритма решения проблемы -неопределенности на различных модельных примерах и сравнение с результатами NPFC-метода.

### Метод функции Грина для расчета потенциального магнитного поля в активных областях Солнца с учетом сферичности

В. М. **Садьков**, И. В. Зимовец

Астрономический журнал, - 2014, С. 409-416

Получена функция Грина уравнения Лапласа внешней шаровой области для нахождения градиента скалярного потенциала магнитного поля с использованием граничного условия — производной потенциала по заданному направлению. Разработан набор программ, использующих данное решение для расчета силовых линий потенциального магнитного поля в активных областях Солнца по известным граничным данным — компоненте поля по лучу зрения на уровне фотосферы. На модельных граничных данных показана правильность построенного аналитического решения и выбран оптимальный шаг построения силовых линий для реальных условий. Разработанные программы применены к четырем активным областям Солнца. В качестве граничного условия взяты фотосферные магнитограммы продольной по лучу зрения компоненты магнитного поля, полученные магнитографом HMI/SDO. Для отобранных областей восстановлены силовые линии потенциального магнитного поля в хромосфере и короне. Проведено сопоставление восстановленных силовых линий с магнитными петлями, наблюдаемыми прибором AIA/SDO в ультрафиолетовом диапазоне. На основе этого сопоставления обсуждается вопрос о применимости

потенциального приближения для описания магнитных полей для различных условий в активных областях Солнца.

## СОПОСТАВЛЕНИЕ ЗНАЧЕНИЙ МАГНИТНЫХ ПОЛЕЙ В АКТИВНЫХ ОБЛАСТЯХ НА СОЛНЦЕ, ПОЛУЧЕННЫХ РАЗЛИЧНЫМИ ИНСТРУМЕНТАМИ

СУЛЕЙМАНОВА Р.А.

Изв. КрАО Том: 118Номер: 2 Год: 2022 Страницы: 5-12

[https://www.elibrary.ru/download/elibrary\\_48749023\\_27123238.pdf](https://www.elibrary.ru/download/elibrary_48749023_27123238.pdf)

Проведено сравнение магнитных потоков в активных областях (АО), измеренных аппаратами SOHO/MDI и SDO/HMI. Получены коэффициенты перехода от HMI- к MDI-данным: 1.46 для АО, наблюдавшихся на расстоянии не более  $10^\circ$  от центрального меридиана и 1.29 для АО, наблюдавшихся на долготах  $[-60^\circ; -10^\circ]$  и  $[10^\circ; 60^\circ]$ . Были проведены сравнения значений максимального магнитного поля в пятнах, полученных в 2014 году по измерениям телескопа SDO/HMI и наземного телескопа БСТ-2 в Крымской астрофизической обсерватории РАН. Сопоставление проводилось методом ортогональной регрессии. Показано, что наилучшее соответствие между данными с двух инструментов достигается при сопоставлении крымских данных с HMI-данными о полном векторе поля (коэффициент корреляции 0.71), нежели о его продольной составляющей (коэффициент корреляции 0.66). Такой вывод свидетельствует о том, что измерения поля по сдвигу спектральной линии (метод, применяемый на БСТ-2) дают величину полного вектора поля со знаком его продольной компоненты. Результаты сопоставления свидетельствуют о возможности применять крымские данные о магнитных полях пятен, что особо ценно при изучении солнечных циклов до космической эры.

## СОПОСТАВЛЕНИЕ ЗНАЧЕНИЙ МАГНИТНЫХ ПОЛЕЙ В АКТИВНЫХ ОБЛАСТЯХ НА СОЛНЦЕ, ПОЛУЧЕННЫХ РАЗЛИЧНЫМИ ИНСТРУМЕНТАМИ

Сулейманова Р.А.

Г и А Том: 118Номер: 2 Год: 2022 Страницы: 5-12

Проведено сравнение магнитных потоков в активных областях (АО), измеренных аппаратами SOHO/MDI и SDO/HMI. Получены коэффициенты перехода от HMI- к MDI-данным: 1.46 для АО, наблюдавшихся на расстоянии не более  $10^\circ$  от центрального меридиана и 1.29 для АО, наблюдавшихся на долготах  $[-60^\circ; -100^\circ]$  и  $[100^\circ; 600^\circ]$ . Были проведены сравнения значений максимального магнитного поля в пятнах, полученных в 2014 году по измерениям телескопа SDO/HMI и наземного телескопа БСТ-2 в Крымской астрофизической обсерватории РАН. Сопоставление проводилось методом ортогональной регрессии. Показано, что наилучшее соответствие между данными с двух инструментов достигается при сопоставлении крымских данных с HMI-данными о полном векторе поля (коэффициент корреляции 0.71), нежели о его продольной составляющей (коэффициент корреляции 0.66). Такой вывод свидетельствует о том, что измерения поля по сдвигу спектральной линии (метод, применяемый на БСТ-2) дают величину полного вектора поля со знаком его продольной компоненты. Результаты сопоставления свидетельствуют о возможности применять крымские данные о магнитных полях пятен, что особо ценно при изучении солнечных циклов до космической эры.

## СОЛНЕЧНЫЙ МАГНИТОГРАФ ДЛЯ ПРОГНОЗИРОВАНИЯ КОСМИЧЕСКОЙ ПОГОДЫ

Тлатов А.Г., Березин И.А., Шрамко А.Д., Дормидонтов Д.В.

Изв. КрАО Том: 119Номер: 4 Год: 2023 Страницы: 12-16

Прогнозирование космической погоды (КП) является необходимым элементом системы обеспечения технологической безопасности для наземных и космических объектов. Наиболее перспективным на данном этапе является создание наземной наблюдательной сети. В составе такой сети должны быть солнечные магнитографы, обеспечивающие наблюдение крупномасштабных магнитных полей Солнца. Данные магнитографических наблюдений позволяют получить оценку параметров рекуррентных потоков солнечного ветра (СВ). В работе представлен проект солнечного магнитографа для обеспечения прогнозирования КП.

## “ЛОЖНЫЕ” СИГМОИДЫ В СОЛНЕЧНОЙ КОРОНЕ

ФИЛИППОВ Б.П. 1

АЖ Том: 96Номер: 9 Год: 2019 Страницы: 776-784

DOI: [10.1134/S0004629919090020](https://doi.org/10.1134/S0004629919090020)

Сигмоидальные структуры солнечной короны, то есть структуры, имеющие вид латинской буквы S или ее зеркального отображения, как правило, рассматриваются как свидетельства скрученности силовых линий магнитного поля и присутствия электрических токов в короне. Однако такие образования могут существовать и в потенциальном поле. S-образная форма солнечных волокон, например, определяется распределением фотосферных магнитных полей, которое не зависит от корональных токов. Сигмоидальные силовые линии появляются в достаточно сложном потенциальном поле в окрестностях нулевых особых точек. Причем такие линии могут демонстрировать сдвиг, тоже часто принимаемый за проявление

непотенциальности поля. Таким образом, следует относиться с осторожностью к некоторым свидетельствам непотенциальности магнитного поля в короне и исключать иные причины появления “подозрительных” структур.

### **ЭВОЛЮЦИЯ МАГНИТНЫХ ПОЛЕЙ ПЯТЕН ПО ИЗМЕРЕНИЯМ НА ТЕЛЕСКОПЕ БСТ-2 КРАО РАН В 24-ОМ ЦИКЛЕ СОЛНЕЧНОЙ АКТИВНОСТИ**

*Цап Ю.Т., Клиорин Н.И., Ахтемов З.С., Малащук В.М.*

Г и А Том: 61 Номер: 5 Год: 2021 Страницы: 555-559

DOI: 10.31857/S0016794021050151

На основе многолетних спектральных наблюдений расщепления зеемановских компонент линии FeI 630.2 нм, проводимых на Башенном солнечном телескопе БСТ-2 Крымской астрофизической обсерватории, исследована эволюция усредненных значений магнитного поля солнечных пятен с напряженностью  $\geq 1500$  Гс за период с 2010 по 2018 г. (всего 4771 измерение). Обнаружено, что в отличие от чисел Вольфа, усредненное магнитное поле пятен со временем существенно не меняется. Более того, оно очень слабо возрастает и достигает максимума к концу 24-го цикла активности Солнца. Полученные результаты свидетельствуют в пользу важной роли “отрицательного” магнитного давления в формировании пятен на малых глубинах вблизи поверхности Солнца.

### **ХАРАКТЕРИСТИКИ КОЛЕБАНИЙ В МАГНИТНЫХ УЗЛАХ СОЛНЕЧНЫХ ФАКЕЛОВ** **ЧЕЛПАНОВ А.А.1, КОБАНОВ Н.И.1, КОЛОБОВ Д.Ю.**

АЖ Том: 92 Номер: 10 Год: 2015 Страницы: 851

Проводится сравнительный анализ характеристик колебаний интенсивности, магнитного поля и доплеровской скорости в узлах концентрации магнитного поля солнечных факелов и в областях на их периферии с умеренной напряженностью магнитного поля. Исследования выполнены по изображениям полного диска в спектральных полосах Fe I 6173 А, 1700 А и He II 304 А обсерватории SDO, которые представляют нижнюю фотосферу, верхнюю фотосферу и переходную область, соответственно. В спектрах колебаний продольной напряженности поля в магнитных узлах проявляются пики с частотой около 5 мГц, которые не наблюдаются на периферии факелов. Спектральный состав фотосферных колебаний интенсивности и доплеровской скорости в магнитных узлах и в областях умеренного магнитного поля в целом схож, но мощность колебаний в узлах в  $2 \div 4$  раза ниже. В линии He II 304 А максимальные пики спектров колебаний над магнитными узлами распределены преимущественно в диапазоне  $3 \div 6$  мГц, а на периферии факела - в диапазоне  $1.5 \div 3$  мГц. Предполагается, что причиной такого распределения колебаний является конфигурация магнитного поля факелов - над узлами силовые линии близки к вертикальным, а над периферией факела они становятся наклонными.

### **О ПРИРОДЕ КОМПЛЕКСОВ АКТИВНОСТИ НА СОЛНЦЕ**

**Язев С.А.**

Астрономия-2018 Том 2 Солнечно-земная физика – современное состояние и перспективы С.274  
<http://www.izmiran.ru/library/eaas2018/eaas-2018-2.pdf>

Some properties of activity complexes (AC) on the Sun (regular ascent of the magnetic flux portions at the same place in the Carrington coordinate system) require an explanation. Three hypotheses linking the phenomenon of AC with a magnetoplasma toroid, with the magnetic tree in the convective zone and with a large-scale convective cell are considered. The argument in favor of the latter hypothesis is given.

### **КОРОНА ВО ВРЕМЯ ПОЛНОГО СОЛНЕЧНОГО ЗАТМЕНИЯ 20 МАРТА 2015 Г.И РАЗВИТИЕ 24-ГО ЦИКЛА**

**ЯЗЕВ С.А.1,2, МОРДВИНОВ А.В.2, ДВОРКИНА-САМАРСКАЯ А.А.1**

СОЛНЕЧНО-ЗЕМНАЯ ФИЗИКА Том: 2 Номер: 2 Год: 2016 Страницы: 3-11

Выполнен анализ структуры корональных образований по данным наблюдений полного солнечного затмения 20 марта 2015 г. Индекс Людендорфа, характеризующий форму короны, равен 0.09. Структура короны в северном полушарии соответствует фазе максимума цикла солнечной активности, в южном полушарии - постмаксимальной стадии. Асинхронное развитие магнитной активности в северном и южном полушариях Солнца привело к существенной асимметрии корональных структур, наблюдаемых в период смены знака полярных магнитных полей в текущем цикле. Полярные лучевые структуры в южном полушарии связаны с присутствием полярной корональной дыры, в то время как в северном полушарии полярная дыра еще не сформировалась. Выполнен анализ связи крупномасштабных магнитных полей с расположением высоких корональных структур.